HANDBOOKS

McGraw-Hill

HANDBOOK OF CERAMICS, GLASSES, AND DIAMONDS

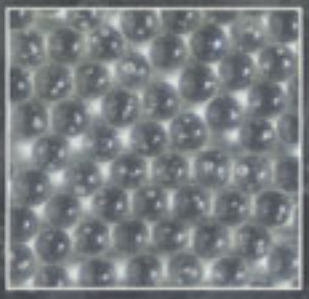

CHARLES A. HARPER

HANDBOOK OF CERAMICS, GLASSES, AND DIAMONDS

HANDBOOK OF CERAMICS, GLASSES, AND DIAMONDS

Charles A. Harper **Editor-in-Chief**
Technology Seminars, Inc., Lutherville, Maryland

McGRAW-HILL
New York Chicago San Francisco Lisbon London
Madrid Mexico City Milan New Delhi San Juan
Seoul Singapore Sydney Toronto

McGraw-Hill

A Division of The McGraw-Hill Companies

0-07-141467-3

The material in this eBook also appears in the print version of this title: 0-07-026712-X.

DOI: 10.1036/0071414673

CONTENTS

Chapter 4. Advanced Ceramics and Composites 4.1

Chapter 6. Inorganic Glasses—Commercial Glass Families, Applications, and Manufacturing Methods 6.1

PREFACE

An understanding of materials and their processing and final properties, while not always fully appreciated, is absolutely critical to the design and manufacture of products and to their performance and reliability. Although this has always been fundamentally true, the demands of modern high-technology products frequently make materials the critical limiting factor not only for success in today's products but also for success in achieving the next generation. This is, of course, a constant and continuing goal. A review of recent publications will show that modern materials technology has been well addressed for some groups of materials but not for ceramics, glasses, and diamonds. It is, therefore, the object of this handbook to present, in a single source, all the fundamental information required to understand the large number of materials and material forms, and to provide the necessary data and guidelines for optimal use of these materials and forms in the broad range of industry products. At the same time, this handbook will be invaluable to industry in acquainting its specialists with product requirements for which they must develop, manufacture, and fabricate materials and forms made with ceramics, glasses, and diamonds.

A companion to my other series handbooks, namely, *Handbook of Materials for Product Design*, *Modern Plastics Handbook*, and *Handbook of Plastics, Elastomers, and Composites*, this *Handbook of Ceramics*, *Glasses*, *and Diamonds* has been prepared as a thorough sourcebook of practical data for all ranges of interests. It contains an extensive array of property and performance data, presented as a function of the most important product variables. Further, it presents all important aspects of application guidelines, fabrication-method trade-offs, design, finishing, performance limits, and other important application considerations. It also fully covers chemical, structural, and other basic material properties. The handbook's other major features include an extensive appendix of material properties and suppliers, a thorough and easy-to-use index, and very useful end-of-chapter reference lists.

The chapter organization and coverage of the handbook is equally well suited for reader convenience. The first four chapters are devoted to ceramics, the following three to glasses, and then one chapter devoted to the important roles of ceramics and glasses in microelectronics, and a final chapter devoted to industrial diamonds. In both the ceramic and glass set of chapters, and also in the diamond chapter, the materials presented cover all areas of the subject, including fundamentals, material properties and applications, processes, and the like. As such, they are oriented to have subjects useful for all areas of interest, from research and development to processing, product design, application, and other specialist areas. Materials covered range from general purpose to advanced high-performance product applications.

As will be evident by a review of the subject and author listings, I have had the good fortune to be able to bring together a team of outstanding chapter authors, each with a great depth of experience in his or her field. Together, they offer the reader a base of knowledge as perhaps no other group could. Hence, I would like to give special credit to these authors in this preface. Also, I would like to give special credit to *Ceramic Industry Magazine*, and

Editor Christine Grahl for the material presented in the appendix. This is indeed an excellent addition to this *Handbook of Ceramics, Glasses and Diamonds*.

Reader comments will be welcomed and appreciated.

Charles A. Harper
Technology Seminars, Inc.
Lutherville, Maryland

CONTRIBUTORS

Alex E. Bailey *American Technical Ceramics, Jacksonville, Florida (CHAP. 3)*

Venkata Bhagavatula *Corning Inc., Corning, New York (CHAP. 7)*

Mark P. D'Evelyn *General Electric Company, Schenectady, New York (CHAP. 9)*

Frances Fehlner *Consultant, Corning, New York (CHAP. 7)*

Christine Grahl *Ceramic Industry Magazine, Columbus, Ohio (APPENDIX)*

Dana L. Hankey *Technology Business Development, Albuquerque, New Mexico (CHAP. 8)*

Chandra S. Khadilkar *Electronic Materials Division, Ferro Corporation, Vista, California (CHAP. 8)*

Jerry E. Sergent *TCA, Inc., Williamsburg, Kentucky (CHAP. 4)*

Thomas P. Seward III *Alfred University, Alfred, New York (CHAPS. 5, 6)*

Aziz S. Shaikh *Electronics Materials Division, Ferro Corporation, Vista, California (CHAP. 8)*

Allen B. Timberlake *Consultant, Columbia, Maryland (CHAP. 1)*

Arun Varshneya *Alfred University, Alfred, New York (CHAPS. 5, 6)*

S. Vasudevan *Electronics Materials Division, Ferro Corporation, Vista, California (CHAP. 8)*

ABOUT THE EDITOR

Charles A. Harper is President of Technology Seminars, Inc., a Lutherville, Maryland, organization that provides educational training courses in materials and electronics for industry, government, and other professional groups. Previously, he was Manager of Materials and Electronic Packaging Technologies for Westinghouse Electric Corporation in Baltimore, Maryland. Mr. Harper is also Series Editor for the McGraw-Hill Materials Science and Engineering Series, as well as the McGraw-Hill Electronic Packaging and Interconnection Series. He is a Fellow of the Society for the Advancement of Materials and Process Engineering (SAMPE) and is Past President and Fellow of the International Microelectronics and Packaging Society (IMAPS). He is a graduate of the Johns Hopkins University, Baltimore, Maryland, where he also served as Adjunct Professor. Mr. Harper is widely recognized for his teaching, writing, and editorial activities, and for his leadership role in major professional societies.

CHAPTER 1
CERAMIC MATERIALS AND PROPERTIES

Allen B. Timberlake
Consultant

1.1 INTRODUCTION

The numerous branches of ceramics technology are frequently classified as either *traditional* or *advanced*. Traditional ceramics usually include the older technologies, such as brick, china, concrete, and whiteware. Advanced ceramics, also called *fine* ceramics by Saito[1] and Norton,[2] are generally those where various methods are used to enhance the properties—to make them harder, stronger, or more chemical resistant, for example. Emphasis in this chapter is given to advanced ceramics.

This chapter is intended to provide a convenient compilation of many properties of the materials discussed in other chapters of the book. Properties of interest to workers using ceramics in structural as well as in electronic applications are listed. Several works have been used extensively, including Harrison and Moratis,[3] Mattox,[4] Schwartz,[5] Buchanan,[6] and Saito.[1] In addition, industrial sources including Coors Ceramics, Kyocera, DuPont Electronics, and Norton Diamond Film have been used.

1.1.1 Definitions of Tabulated Properties

1.1.1.1 Units and Conversion Factors.[7] The properties tabulated in this chapter are defined in this section. The units of measure used in the tables are those used in the article from which the data were taken, unless otherwise indicated. Since workers in the various branches of ceramics technology use different systems of units in their publications—e.g., cgs metric, mks metric, International (S.I.), English, or U.S. Conventional—Table 1.1 lists and defines the units of the International System. Table 1.2 provides factors for converting among the various systems.[7] In cases where it seems desirable to convert data found in a source from one system to another for consistency in a table, the converted data will be placed in brackets, { }. The properties are grouped according to whether they are mechanical, thermal, or electrical.

TABLE 1.1 Derived Units of the International System (SI)

Quantity	Name of unit	Unit symbol (if different from basic form)	Unit in terms of base units
Area	square meter		m^2
Volume	cubic meter		m^3
Density	kilogram per cubic meter		kg/m^3
Force	newton	N	$kg \cdot m/s^2$
Pressure	newton per square meter, pascal	N/m^2, Pa	$kg/(m \cdot s^2)$
Power, heat flux	watt, joule per second	W, J/s	$kg \cdot m^2/s^3$
Heat capacity	joule per kilogram per kelvin	$J/(kg \cdot K)$	$m^2/(s^2 \cdot K)$
Thermal conductivity	watt per meter per kelvin, joule-meter per second per square meter per kelvin	$W/(m \cdot K)$, $J \cdot m\ (s \cdot m^2 \cdot K)$	$kg \cdot m/(s^3 \cdot K)$

TABLE 1.2 Factors for Converting SI Units to U.S. Customary or English Units

Quantity	SI unit	U.S./English unit	To convert SI to English multiply by:	To convert English to SI, multiply by:
Area	square meter, m^2	square foot, ft^2	10.76391	0.09200304
Volume	cubic meter, m^3	cubic foot, ft^3	35.31467	2.831685×10^{-2}
Mass	kilogram, kg	pound, lb	2.204623	0.4535924
Density	kilogram per cubic meter, $kg \cdot m^{-3}$	pound per cubic foot, lb/ft^3	0.06242795	16.01847
Force	newton, N	pound force, lbf	0.2248089	4.448222
Energy	joule, J	British thermal unit, Btu	9.478172×10^{-4}	1055.056
Energy	kilowatt-hour, kwh	British thermal unit, Btu	3412.142	2.930711×10^{-4}
Pressure	Pascal, Pa	pound per square inch, lb/in^2	1.450377×10^{-4}	6894.757
Power, heat flux	watt, joule per second	Btu per hour, Btu/h	0.2939711	3.9016949
Heat capacity	joule per kilogram per kelvin	Btu per pound per Fahrenheit degree	2.389×10^{-4}	4.1868×10^3
Thermal conductivity	watt per meter per kelvin, $W/m \cdot K$	Btu-foot per hour per square foot per Fahrenheit degree, $Btuft/(h \cdot ft^2 \cdot F°)$	0.5777892	1.730735

TABLE 1.3 ASTM Property Test Methods

Properties	ASTM test methods
Physical	
Specific gravity	C-329, C-20
Porosity	C-373
Flexure strength	C-674
Hardness	C-730, E-18
Fracture toughness	
Thermal	
Expansion coefficient	F-228, C-359
Thermal conductivity	C-408, C-177
Shock resistance	D-116
Electrical	
Dielectric constant and dissipation factor	D-2149, D-150, D-2520
Dielectric strength	D-149
Electrical resistivity	D-257, D-1829

Table 1.3 lists many ASTM methods of measurement for the properties of most interest to users of ceramics.

1.1.1.2 Mechanical Properties

Density. The mass per unit volume of a material is its density. The term is often used synonymously with *specific gravity*, a unitless quantity that is the ratio of the density of the material to the density of pure water at 4°C. The two quantities are numerically identical in the SI system, but are quite different in the English system.

Elastic Modulus or Young's Modulus. When a rod of length l and cross-sectional area A is subjected to a tensile force F, the rod will undergo an increase in length Δl according to the formula

$$\Delta l = Fl/AE \tag{1.1}$$

where E is a property of the material known as *Young's modulus*. Young's modulus, then, is the relationship of stress to strain, i.e., the fractional change in dimension caused by an applied force. Young's modulus can also be determined by measuring the bending of a rod by a force applied to the midpoint of the rod supported at both ends.

Shear or Rigidity Modulus. When successive layers of material are moved or sheared by tangential surface force or a torsional force, the magnitude of strain is determined by the shear modulus or modulus of rigidity. The angular strain, θ radians, induced in a rod of radius r, length l, by a torque C is given by

$$\theta = 2Cl/\pi r^4 M \tag{1.2}$$

where M is the modulus of rigidity of the material.

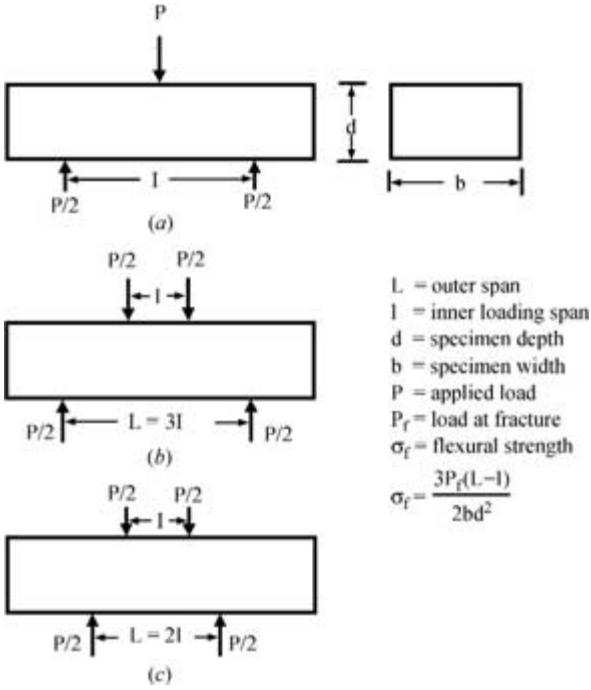

FIGURE 1.1 Schematic of flexural strength test for ceramics: (*a*) Three-point bend, (*b*) three-point loading, three-point bend, and (*c*) quarter-point loading, four-point bend.

Brittleness. The propensity of a material to chip or fracture during manufacture or handling is known as its brittleness. Although brittleness is not frequently quantified, a *brittleness index*, BI, has been defined by Lawn and Marshall,[8] as follows:

$$\text{BI} = H/K_c \tag{1.3}$$

where H is the hardness and K_c is the toughness.

Fracture Toughness. The fracture toughness, K_{Ic}, is a measure of a ceramic part's resistance to fracture. For a given part it is highly dependent on the treatment the part has experienced. Voids, inclusions, surface flaws, scratches, cracks, and other flaws seriously degrade a ceramic part's fracture toughness. Tables of fracture toughness should include a description of how the part was treated prior to testing—e.g., as-fired, polished, or etched—since the fracture toughness is significantly affected by such treatments. Fracture toughness is determined by measuring the force required to fracture a test specimen of prescribed shape in a test fixture designed for this purpose.

A frequently used fixture is shown in Fig. 1.1.[9] A test specimen is supported at the ends, and a load is imposed, equally divided on two probes placed near the center of the piece, as shown. The load is increased until the specimen fractures. Fracture toughness is calculated from the following formula[10]:

$$K_{Ic} = \sigma_c \sqrt{(\pi a) F(\zeta)} \tag{1.4}$$

where K_{Ic} = fracture toughness
σ_c = bend strength
a = flaw size
$F(\zeta)$ = constant determined by the shape of the specimen

Ceramic specimens will fail over a range of applied stresses depending on the density and types of flaws and defects as described above. In order to gain a reliable measure of the fracture toughness of a material, it is necessary to test a large number of specimens. The failures will usually follow a distribution function F, known as the Weibull function, shown in Eq. (1.5):

$$F = 1 - \exp\left\{-\int_V [(\sigma - \sigma_\mu)/\sigma_0]^m dV\right\} \tag{1.5}$$

The three parameters m, σ, and σ_0 are constants for the material; m is the Weibull modulus and σ_μ is the maximum value of stress under which the specimen will not fail, which is usually set to zero. Rearranging, setting σ equal to $\sigma_{\max}$, the largest value of stress in the specimen, setting the integral term to V_E, the effective volume, and taking logarithms of both sides reveals

$$\ln 1/(1-F) = m \ln \sigma_{\max} - \ln(\sigma_0^m / V_E) \tag{1.6}$$

A log-log plot of failure probability versus stress will have a slope of m, the Weibull modulus. Figure 1.2 shows the failure distributions of silicon carbide and silicon nitride at room and elevated temperatures.

A large value of m indicates that the all samples of the material fail over a narrow range of applied stresses. Therefore the stress required to cause failure is more predictable than it would be if the failures occurred over a wide range of applied stresses, as would be indicated by a low value of m. Saito has published several plots for specimens prepared differently, e.g., ground with different mesh abrasives, which demonstrate the sensitivity of this parameter to surface preparation. Schwartz[5] compiled data over a period of years showing how Weibull modulus and mean tensile strength depend on sample preparation.

Hardness. The resistance to indentation or deformation of a material is known as its *hardness*. There are many hardness scales and methods of measurement. Most methods involve indenting a test specimen by impressing a weighted diamond stylus of a prescribed shape on it, and measuring the area or depth of the indentation. The ratio of applied force to area of indention is defined as the hardness. The scales used most frequently for ceramic materials are Mohs, Vickers, Brinnell, Rockwell, and Knoop. These are discussed here.

1. *Mohs hardness*. For ceramic materials and minerals, which are harder than most other materials, the Mohs scale was one of the earliest measures of hardness. The Mohs scale calls for scratching the specimen with a succession of materials, with each succeeding scratch material being harder than the one that preceded it.[11] The order of the scratch material that cannot make a discernible scratch is called the *Mohs hardness* of the specimen.

   Initially 10 scratch materials were used, ranging from talc at the soft end to diamond at the hard end. The scale was later expanded to 15, with five materials added between the original numbers 9 and 10, corundum and diamond. All are listed in Table 1.4.[11] Although the Mohs scale has the advantages of simplicity and ease of use, it also has

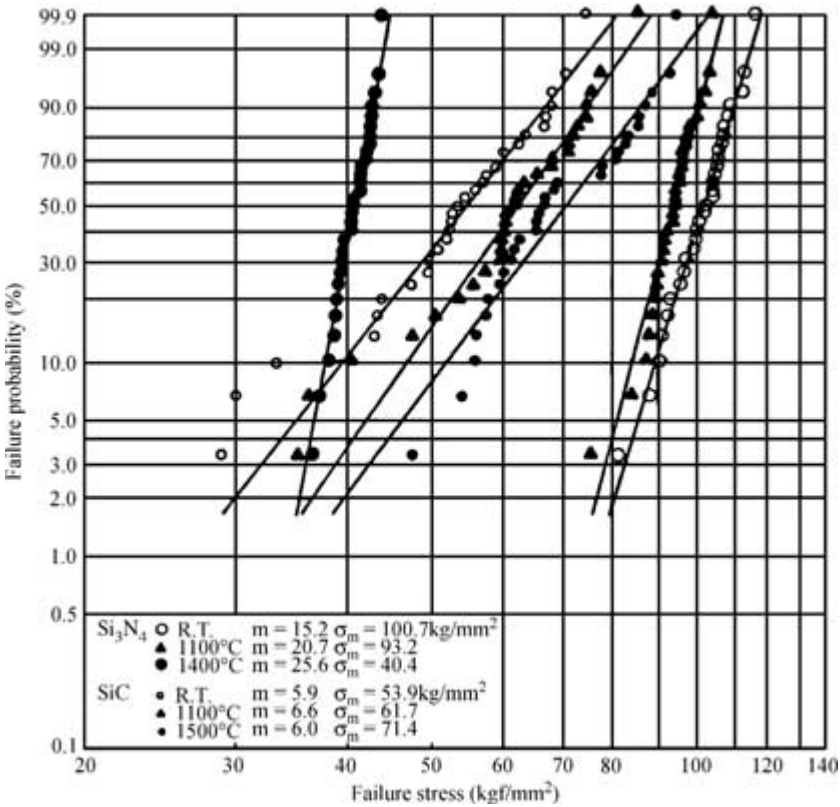

FIGURE 1.2 Weibull distribution shows spread in fracture strengths of ceramics. (*From Ref. 1.*)

several disadvantages. It is qualitative; it is not linear, in that the differences between adjacent numbers on the scale are not equal; and it does not give a value that can be expressed in terms of other physical quantities, such as force. For these reasons other methods for measuring and scaling hardness were developed.

2. *Brinnel hardness*. An indentation is made by a 10-mm-diameter hardened steel or sintered tungsten carbide ball. A load of 500 kgf is used for soft metals, and 3000 kgf for hard metals. Brinnell hardness is equal to the load in kilograms divided by the surface area in square millimeters of the impression made in the test material.
3. *Vickers hardness*. The indenter is a square-based diamond pyramid with included angle between faces of 136°. Loads of different magnitudes are used, with 10, 30, and 50 kgf in common use. The indenter makes a square indentation in the test material. Vickers hardness is defined as the load in kilograms divided by the area in square millimeters of the indentation. The area of indentation is calculated from the lengths of the diagonals.
4. *Knoop hardness*. A Knoop indenter is impressed on a specimen, and the depth of penetration determines the Knoop hardness. The Knoop indenter is a diamond pyramid with a rhombic base. The diagonals are in the ratio of 1:7, and included apical angles are 130° and 172° 30′.

TABLE 1.4 Comparison of Hardness Values of Various Ceramics on Knoop, Mohs, and Expanded Mohs Scales

Hardness number	Mohs' scale	Ridgeway's extension of Mohs' scale	Knoop hardness of expanded scale materials
1	Talc	Talc	
2	Gypsum	Gypsum	32
3	Calcite	Calcite	135
4	Fluorite	Fluorite	163
5	Apatite	Apatite	430
6	Orthoclase	Orthoclase	560
7	Quartz	Vitreous silica	—
8	Topaz	Quartz or stellite	820
9	Corundum	Topaz	1340
10	Diamond	Garnet	1360
11		Fused zirconia	—
12		Fused alumina	2100
13		Silicon carbide	2480
14		Boron carbide	2750
15		Diamond	7000

5. *Rockwell hardness*. Again, the hardness value is determined by measuring the size of an indentation caused by a point impressed on the sample under a prescribed load. The indenter can be either a $\frac{1}{16}$-, $\frac{1}{8}$-, or $\frac{1}{4}$-inch-diameter steel ball or conical diamond having an apex angle of 120° and a slightly rounded tip. Letters, with the letter indicating both the indenter and the weight of the load, designate the various scales.

Modulus of Rupture. Ordinary stress-strain testing is not generally used to test ceramic substrates since they do not exhibit elastic behavior to a great degree. An alternative test, the modulus of rupture (bend strength) test, as described in Fig. 1.1, is preferred. A sample of ceramic, either circular or rectangular, is suspended between two points, a force is applied in the center, and the elongation of the sample is measured. The stress is calculated by

$$\sigma = Mx/I \tag{1.7}$$

where σ = stress in megapascals (MPa)
M = maximum bending moment in N · m
x = distance from center to outer surface in m
I = moment of inertia in N · m^2
= $xy^3/12$ for rectangular cross section
= $\pi R^2/4$ for circular cross section

For a sample of length l, M can be shown to be $Fl/4$, where F is the applied force in newtons. When expressions for σ, M, x, and I are inserted into Eq. (1.7), the results are:

$$\sigma = 3Fl/2xy^2 \tag{1.8}$$

for rectangular cross section, and

$$\sigma = Fl/\pi r^3 \tag{1.9}$$

for circular cross section.

1.1.1.3 Thermal Properties

Thermal Conductivity. The quantity of heat a material is capable of passing per second through a specimen of unit cross-sectional area and unit length for a temperature difference of one degree is defined as the *thermal conductivity*. In the SI system heat is in joules, cross-sectional area is one square meter, length is one meter, and the temperature difference is one kelvin. In the English system the dimensions are in feet, the temperature difference is in Fahrenheit degrees, and the heat quantity is in British thermal units (Btu).

In solid materials that are not significantly electrically conductive, molecular vibrations known as *phonons* are the means of heat conduction. In metals that have "free" electrons available to conduct electric current, these same electrons provide another means of heat conduction. The electrical conductivity and *electronic component* of thermal conductivity are related by the Wiedemann-Franz-Lorenz ratio L, as shown in Eq. (1.10):

$$k/\sigma = LT \tag{1.10}$$

where k = thermal conductivity
σ = electrical conductivity
T = absolute temperature
L = Wiedemann-Franz-Lorenz constant, 2.45×10^{-8} W · Ω/K^2

This additional component of heat conduction in metals results in metals having higher thermal conductivities than most ceramics, which have virtually no electrical conductivity. Exceptions to this statement are beryllium oxide, aluminum nitride, diamond, and cubic zirconium oxide. These materials will be discussed more fully in later sections.

Figure 1.3 shows the temperature dependence of thermal conductivity of many ceramic materials and metals.[12]

Coefficient of Linear Thermal Expansion (CTE). This is the ratio of the change in length per unit length of a specimen per degree of temperature change to the length of the specimen at a reference temperature, usually room temperature. Since the changes in length per degree of temperature change are usually quite small, a fairly large temperature change is required to induce a length change that is measurable with suitable precision, even though the incremental change, hence, coefficient, around a particular temperature may be different. The coefficient is taken as an average over a specified range, assuming a linear $\Delta l/l$ relationship.

Softening or Melting Temperature. The temperature at which flow begins to take place in the absence of an applied force.

Thermal Shock Resistance. In general terms, this is the ability of a material to withstand rapid temperature change, positive or negative, without fracturing. Materials with high thermal shock resistance usually exhibit very low thermal expansion coefficient and low brittleness index.

1.1.1.4 Electrical Properties

Dielectric Constant. This quantity is defined in various ways. For the purposes of this handbook it can best be defined as the ratio of the amount of electrical charge that can be stored in a slab of material between two parallel metal plates to the amount of electrical charge that can be stored by plates of the same area and separation when the space is evacuated.

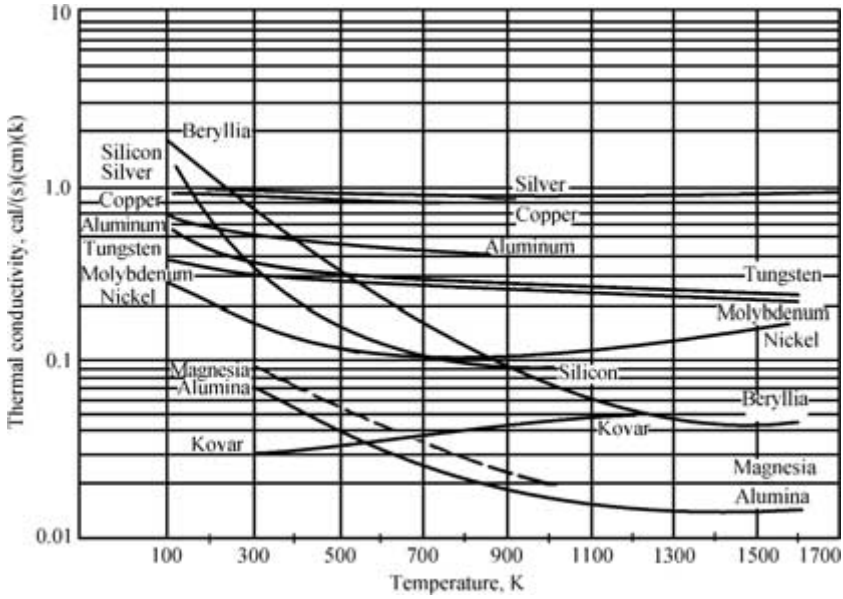

FIGURE 1.3 Temperature dependence of thermal conductivity for many materials. *Note*: 418.4 W/m · K = 1.0 cal/(s · cm · K). (*From Ref. 3, p. 3.19.*)

Dissipation Factor. An important property of dielectric materials, dissipation factor is a measure of lossiness of a dielectric. When an ac signal is impressed on a capacitor or a capacitive load, the voltage and current are ideally out of phase by 90°, and no power is dissipated in the capacitor. However, in all real capacitors the phase difference is somewhat less than 90°, and power is dissipated. The angle between the current and voltage vectors is designated δ (delta), and the tangent of delta is known as the *dissipation factor*.

Insulation Resistance. This refers to the ability of a material to isolate a part of a circuit from external electric fields.

Breakdown Voltage. The voltage at which an insulator no longer isolates conductors in different circuits. Exceeding this voltage causes an electronic avalanche, whereby electrons are accelerated enough to ionize other electrons in collisions, resulting in current that can cause damage to the parts.

1.2 CLASSES OF MATERIALS COVERED

To assist users of the information in this chapter we have divided ceramic materials including glass into six classes—following the example of Schwartz[5]—as follows:

- Minerals
- Vitreous ceramics

TABLE 1.5 Physical Properties of Minerals

Name	Formula	Crystal system	Density, g/cm^3	Mohs hardness
Albite	$NaAlSi_3O_8$	Triclinic	2.63	6.3
Aluminite	$Al_2(SO_4)(OH)_4 \cdot 7H_2O$	Monoclinic	1.74	1.5
Apatite	$Ca_5(PO_4)_3(OH, F, Cl)$	Hexagonal	3.2	5
Arsenolite	As_2O_3	Cubic	3.86	1.5
Azurite	$Cu_3(OH)_2(CO_3)_2$	Monoclinic	3.77	3.8
Beryl	$Be_3Al_2(SiO_3)_6$	Hexagonal	2.64	7.8
Beryllonite	$NaBe(PO)_4$	Monoclinic	2.81	5.8
Borax	$Na_2B_4O_7 \cdot 10H_2O$	Monoclinic	1.73	2.3
Brookite	TiO_2	Tetragonal	4.23	5.8
Claudetite	As_2O_3	Monoclinic	3.74	2.5
Cordierite	$Al_3(Mg, Fe)_2Si_5AlO_{18}$	Rhombic	2.66	7
Corundum	Al_2O_3	Hexagonal	3.97	9
Cristobalite	SiO_2	Hexagonal	2.33	6.5
Cryolite	Na_3AlF_6	Monoclinic	2.97	2.5
Diamond	C	Cubic	3.51	10
Diaspore	AlO(OH)	Orthorhombic	3.4	6.8
Dolomite	$CaMg(CO_3)_2$	Rhombic	2.86	3.5
Fluorite	CaF_2	Cubic	3.18	4
Forsterite	Mg_2SiO_4	Orthorhombic	3.21	7
Galena	PbS	Cubic	7.60	2.5
Gaylussite	$Na_2Ca(CO_3)_2 \cdot 5H_2O$	Monoclinic	1.99	2.8
Gibbsite	$Al(OH)_3$	Monoclinic	2.42	3
Gypsum	$CaSO_4 \cdot 2H_2O$	Monoclinic	2.32	2
Helvite	$Mn_4Be_3Si_3O_{12}S$	Cubic	3.32	6
Kaolinite	$Al_4Si_4O_{10}(OH)_8$	Triclinic	2.65	2.3
Kyanite	Al_2OSiO_4	Triclinic	3.59	6.3
Magnesite	$MgCO_3$	Hexagonal	3.05	4
Magnetite	Fe_3O_4	Cubic	5.17	6
Molybdenite	MoS_2	Hexagonal	5.06	1.3
Muscovite	$KAl_2Si_3AlO_{10}(OH, F)_2$	Monoclinic	2.83	2.8
Opal	$SiO_2 \cdot nH_2O$	Amorphous	1.9	5
Orthoclase	$KAlSi_3O_8$	Monoclinic	2.56	6
Periclase	MgO	Cubic	3.6	5.5
Perovskite	$CaTiO_3$	Cubic	3.98	5.5
Phosgenite	$Pb_2(CO_3)Cl_2$	Tetragonal	6.13	2.5
Pyrite	FeS_2	Cubic	5.02	6.3
Pyrochlore	$NaCaNb_2O_6F$	Cubic	5.2	5.3
Quartz	SiO_2	Hexagonal	2.65	7
Rutile	TiO_2	Tetragonal	4.23	6.2
Sapphirine	$(Mg, Fe)_2Al_4O_6SiO_4$	Monoclinic	3.49	7.5
Siderite	$FeCO_3$	Hexagonal	3.9	4.3
Spinel	$MgAl_2O_4$	Cubic	3.55	7.8
Stibnite	Sb_2S_3	Cubic	4.56	2
Talc	$Mg_3Si_4O_{10}(OH)_2$	Monoclinic	2.71	1
Thorite	$ThSiO_4$	Tetragonal	6.7	4.8
Topaz	$Al_2SiO_3(OH, F)_2$	Rhombic	3.53	8
Tourmaline	$Na(Mg, Fe, Li, Al)_3Al_6Si_6O_{18}(BO_3)_3$	Rhombic	3.14	7
Turquoise	$Cu(Al, Fe)_6(PO_4)_4(OH)_8 \cdot 4H_2O$	Triclinic	2.9	5.3

TABLE 1.5 Physical Properties of Minerals (Continued)

Name	Formula	Crystal system	Density, g/cm^3	Mohs hardness
Willemite	Zn_2SiO_4	Hexagonal	4.1	5.5
Wolframite	(Fe, Mn)WO_4	Monoclinic	7.3	4.3
Wollastonite	$CaSiO_3$	Monoclinic	2.92	4.8
Wurtzite	ZnS	Hexagonal	4.09	3.8
Zircon	$ZrSiO_4$	Tetragonal	4.6	7.5

Source: Handbook of Chemistry and Physics, 97th ed., Chemical Rubber Publishing Company, Cleveland, 1997.

- Refractory groups (including oxides, carbides, borides, and nitrides)
- Cement and concrete
- Glass
- Diamond

1.2.1 Rocks and Minerals

This group includes naturally occurring materials, used mostly in construction, such as limestone (marble), sandstone (SiO_2), and granite (aluminum silicates). These materials are cut or ground to a desired configuration after being mined from the ground. We also have included data for a small number of minerals that are used in many "fine ceramic" formulations. Table 1.5 provides chemical formulas, hardness, and density for many such materials.

1.2.2 Vitreous Ceramics

Vitreous ceramics, which derive their name from the Latin word for glass, *vitreus*, are possibly the oldest and most widely used types of ceramic materials. Marco Polo introduced them in Western Europe in the fourteenth century, and European potters strove for decades to duplicate the quality of the Chinese porcelains. In addition to porcelain they include china, pottery, and brick. Typically, they are made from clays such as hydrous aluminosilicate mixed with other inert materials.[5] Ware is formed when the clays are in the wet state, after which they are dried and fired. Various additives are used to provide desired properties.

Norton[2] has provided an excellent summary of the development of the vitreous ceramic industry in the United States and Europe.

Porcelains are the most interesting of these materials for advanced engineering applications. They are described as polycrystalline ceramic bodies containing typically more than 10 volume percent of a vitreous second phase.[6] Porcelain bodies are classified as either triaxial or nonfeldspathetic types, depending on the composition and amount of vitreous phase present. Mattox[4] has pointed out that because their compositions are greatly affected by variations in the compositions of regional clays and feldspars, there are no standard compositions. More detail of their composition is given below.

Triaxial Porcelain. These compositions are compounded from mixtures of feldspars, kaolinite clays, and flint.[4,6] Table 1.6 shows the range of compositions and formulations they utilize. Table 1.7 lists the ranges of electrical, thermal, and mechanical properties of low- and high-voltage triaxial porcelains. They exhibit fairly low mechanical strength and

TABLE 1.6 Composition and Properties of Triaxial Porcelains

		Weight percent		
		Low voltage		High voltage
Raw material	Generic	A	B	C
Kaolinite	20–35	21	25	35
Ball clay	15–30	25	20	10
Feldspar	20–35	34	33	25
Flint	20–30	20	23	25
$BaCaCO_3$	0–5	—	—	5

Property	Low voltage	High voltage
Sintering temperature	1250–1330°C	1300–1450°C
Dielectric constant	5.5–7.0	6–7
Tan δ	0.005	0.003
Loss factor	0.035	0.020

TABLE 1.7 Properties of Triaxial Porcelains

		Material	
Property	Units	Low-voltage porcelain	High-voltage porcelain
Density	g/cm^3	2.2–2.4	2.3–2.5
Water absorption	Percent	0.5–2.0	0.0
Coef. linear thermal expansion, 20–700°C	10^{-6}/°C	5.0–6.5	5.0–6.8
Safe operating temperature	°C	900	1000
Thermal conductivity	W/(cm · K)	0.016–0.021	0.0084–0.021
Tensile strength	lb/in^2	1500–2500	3000–8000
Compressive strength	lb/in^2	25,000–50,000	25,000–50,000
Impact strength, $\frac{1}{2}$-in rod	ft · lb	0.2–0.3	0.5–0.7
Modulus of elasticity	10^{-6} lb/in^2	7–10	7–14
Thermal shock resistance		Moderate	Moderately good
Dielectric constant		6.0–7.0	6.0–7.0
Power factor at 1 MHz		0.010–0.020	0.006–0.010
Resistivity, room temp.	Ω · cm	10^{12}–10^{14}	10^{12}–10^{14}

TABLE 1.8 Raw Material Compositions for Nonfeldspathic Porcelain Insulators

	Weight percent			
Raw Material	Steatite	Forsterite	Cordierite	Zircon
Talc	80–90	60–70	35–45	10–20
Kaolin/clay	5–7	5–10	40–50	10–20
$Mg(OH)_2$		20–45		
$BaCO_3$	6–7	5–7	0–2	6–8
$CaCO_3$	0–1	1–3		0–1
Zircon				55–70
Al_2O_3			12–15	
Sintering temperature, °C	1260–1300	1275–1375	1250–1350	1300–1400

thermal shock resistance. Their high-frequency electrical characteristics are generally poor, limiting their use to frequencies below 10 kHz. They are classified as *high voltage and low voltage*. High-voltage porcelains are formulated from higher purity materials and sintered to higher density than are low-voltage porcelains, and are used for high-frequency, high-voltage applications. Low-voltage porcelains have looser material composition tolerances.

Nonfeldspathic Porcelains. Because the feldspar-containing porcelains tend to be lossy because of their alkali ion content, a group known as *nonfeldspathic*, i.e., without feldspar, was developed. This group includes steatite, forsterite, cordierite, and zircon porcelain. Table 1.8 shows typical compositions of these materials. The variability in these compositions is caused by differences in the compositions of the clays used.

Properties of many widely used compositions of nonfeldspathic porcelains are presented in Table 1.9.

Steatite porcelains, with their low-loss characteristics, are attractive for high-frequency applications. Figure 1.4 shows the dielectric constant and tan δ of steatite porcelains over a wide range of frequencies and temperatures.[3] They have fair mechanical strength but rather poor thermal shock characteristics. They can be machined in the green state and fired with little dimensional change.

Forsterite can be used for high frequency and high-temperature applications. Its high thermal expansion coefficient and concomitant poor thermal shock resistance are drawbacks to its use, although the high expansion can be used to advantage when an insulator must be bonded to a high-thermal-expansion metal.[4]

Cordierite possesses very low thermal expansion coefficient and excellent thermal shock resistance.[6] Zircon porcelains have the advantage of relatively low thermal expansion coefficient, excellent dielectric properties, good thermal shock resistance, high mechanical strength, and ease of fabrication.[6] However, because of higher raw material costs, their use in electrical applications is not widespread.

1.2.3 Refractory Groups (Oxides, Nitrides, Carbides, and Borides)

Refractory ceramics are widely used in electronic, structural, and machine applications. They are characterized by high strength and fracture toughness, which are achieved in part by reducing the number and size distribution of microcracks in the finished part. Aluminas, silicon carbides and nitrides, sialons, and stabilized zirconias are the most prominent of this category. They are used in applications where heat resistance, hardness, fracture toughness,

TABLE 1.9 Properties of Nonfeldspathic Porcelains

Property	Units	Material				
		Steatite	Forsterite	Cordierite	Zircon	Alumina
Density	g/cm^3	2.5–2.7	2.7–2.9	1.6–2.1	3.5–3.8	3.1–3.9
Water absorption	%	0.0	0.0	5.0–15.0	0.0	0.0
Coef. linear thermal exp. 20–700°C	$10^{-6}/K$	8.6–10.5	11	2.5–3.0	3.5–5.5	5.5–8.1
Safe operating temp.	°C	1000–1100	1000–1100	1250	1000–1200	1350–1500
Thermal conductivity	W/(cm · K)	0.021–0.025	0.021–0.042	0.013–0.017	0.042–0.063	0.029–0.21
Tensile strength	lb/in^2	8000–10,000	8000–10,000	1000–3500	10,000–15,000	8000–30,000
Compressive strength	lb/in^2	65,000–130,000	60,000–100,000	20,000–45,000	80,000–150,000	80,000–250,000
Flexural strength	lb/in^2	16,000–24,000	18,000–20,000	1500–7000	20,000–35,000	20,000–45,000
Impact strength, ½-in rod	ft · lb	0.3–0.4	0.03–0.04	0.20–0.25	0.4–0.5	0.5–0.7
Modulus of elasticity	$10^{-6} lb/in^2$	13–15	13–15	2–5	20–30	15–52
Thermal shock resistance		Moderate	Poor	Excellent	Good	Excellent
Dielectric constant		5.5–7.5	6.2	4.5–5.5	8.0–9.0	8–9
Power factor at 1 MHz		0.0008–0.0035	0.0003	0.004–0.010	0.0006–0.002	0.001–0.002
Resistivity, room temp.	Ω · cm	10^{13}–10^{15}	10^{13}–10^{15}	10^{12}–10^{14}	10^{13}–10^{15}	10^{14}–10^{15}

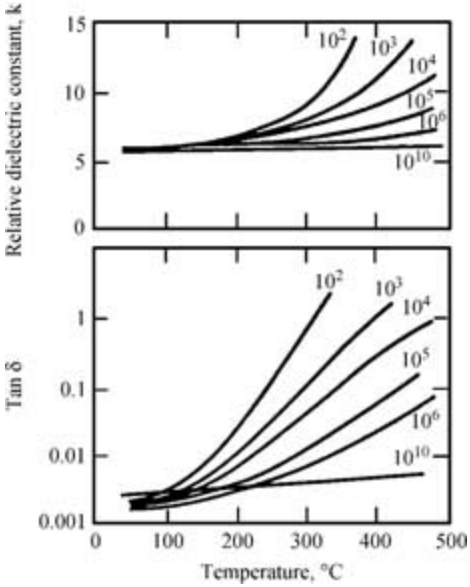

FIGURE 1.4 Dielectric constant and tan δ for steatite over a range of temperatures and frequencies. (*From Ref. 3, pp. 6–9.*)

and strength are essential, e.g., for bearings, engine and turbine parts, cutting tools, and where wear resistant surfaces are required.

1.2.3.1 Oxides. Four oxide ceramics will be discussed in this section: aluminum oxide, or alumina; beryllium oxide, or beryllia; zirconium oxide, or zirconia; and mullite, a mixture of alumina and silica.

Aluminum Oxide, Al_2O_3. Aluminum oxide, or alumina, appears in several crystalline forms, of which alpha is the most stable and most dense.[13] Alpha alumina melts at 2040°C, with creeping and sintering beginning at 1750°C. Mineralizers and fluxers permit sintering at lower temperatures.

Alumina ceramics are among the hardest of materials, and are heat resistant to approximately 2000°C. They exhibit excellent resistance to chemical attack, and find use in spark plugs, pumps, refractory lining, missile nose cones, electrical power insulators, abrasives and cutting tools, and in many ways in electronics packaging.

Native alumina is found as one of the following minerals: corundum, Al_2O_3; diaspore, $Al_2O_3 \cdot H_2O$; gibbsite, $Al_2O_3 \cdot 3H_2O$; and bauxite, an impure form of gibbsite. Corundum is a colorless, transparent crystal. The precious stones ruby and sapphire, red and blue, respectively, are forms of corundum colored by impurities.

The principal sources of purified alumina and hydrated alumina are native bauxites and laterites, from which aluminas are extracted by the *Bayer process*, in which the mineral is pulverized, melted with soda, separated, and calcined.[5] Four types of alumina are usually used in ceramic products—calcined, tabular, fused, and hydrated.

Alumina is used in ceramic products in varying amounts. However, discussion is usually limited to high alumina, which refers to those bodies containing 80 percent or more aluminum oxide. Ceramics with less than 80 percent alumina but still predominantly alumina are classified as porcelain. The most common aluminas are those containing 85, 90, 94, 96, 99, 99.8, and 99.9%. Strength and other properties improve as the alumina percentage increases, but so do cost and complexity of processing.[3] The properties are dependent not only on the alumina content, but also on microstructure and porosity.

As an alumina product approaches its theoretical density of 4.0 g/cm^3 its properties improve. Schwartz[5] has compiled an extensive list of aluminas of various compositions from a number of manufacturers. He found that flexural strength of 300 MPa and fracture toughness of 4 MPa $\cdot$ m$^{1/2}$ were typical values. Flexural strength varied from 150 to over 500 MPa, and fracture toughness ranged from 3 to 6 MPa $\cdot$ m$^{1/2}$. Weibull moduli, not frequently reported, were generally low—8 to 10.

The 85 percent grade is a general-purpose grade regarded as the workhouse of the industry. It is economical, and provides good wear resistance and strength. Parts fabricated in the 90 percent range provide good wear resistance and strength, and dielectric properties are good for some electrical applications. The 94 percent alumina is used for multilayer electronic circuits, since it is easily metallized; it sinters at about 1700°C. Grades in excess of 96 percent are usually formed from submicrometer powders, which allows them to be fired at lower temperatures. They are characterized by very smooth as-fired surfaces and exhibit high mechanical strength and excellent electrical properties.

The first step in processing alumina ceramics is to form the "green" body by compacting finely ground powders containing fluxing agents and grain growth inhibitors, at high pressures. The process used depends on the nature of the end product, and methods include dry pressing, isostatic pressing, extrusion, slip casting, injection molding, transfer molding, hot pressing, and tape casting. Since these materials are difficult to machine after firing, they are usually formed to size before firing, with allowance made for shrinkage during firing. Shrinkage can usually be controlled to about 1 percent of the nominal, which is about 17 percent. If the dimensional tolerances of the finished product are tighter than 1 percent, a grinding operation may be required, adding to the cost of the part.

The thermal and mechanical properties of most of the commercially important high alumina compositions are shown in Table 1.10. Electrical properties of the same materials are shown in Table 1.11. It can be seen that the thermal conductivity, strength, and dielectric properties of alumina are significantly affected by composition. In general, these properties improve as alumina content increases. Figure 1.5 shows how thermal conductivity increases as weight percent of alumina increases.[14] Porosity also affects the thermal conductivity dramatically[15] as shown in Fig. 1.6.

TOUGHENED ALUMINA. Numerous researchers have reported that the addition of a second phase, a process referred to as *toughening*, can increase the strength and toughness of alumina. Schwartz discusses the properties of alumina toughened by additions of various forms of zirconia, and by additions of silicon carbide. Saito[1] discusses alumina toughened by addition of titanium carbide, TiC.

The fracture strength and toughness of alumina can be increased by additions of yttria and zirconia.[5] Zirconia-toughened alumina ZTA consists of an alpha-alumina matrix with a dispersion of ZrO_2 particles. The resultant product is dependent on the structure of the zirconia particles. ZTAs containing primarily monoclinic (m) zirconia will have excellent fracture toughness and thermal shock resistance, but will be weak. Those containing primarily triclinic (t) zirconia will have excellent strength but only moderate toughness and

TABLE 1.10 Thermal and Mechanical Properties of Aluminum Oxide Ceramics

		Aluminum Oxide, weight percent as indicated					
Property	Units	85	92	94	96	99.5	99.9
Density	gm/cm^3	3.41	3.6	3.62	3.72	3.89	3.96
Water absorption	%	0	0	0	0	0	0
Coef. linear thermal expansion							
25–200°C	10^{-6}/K	5.3	6.5*	6.3	6.0	7.1	6.5
25–800°C		6.9	7.5	7.6	8.0	8.0	7.8
25–1200°C		7.5		8.1	8.4		8.3
Maximum service temp.	°C	1400	1500	1700	1700	1750	1900
Thermal conductivity	W/(cm · K)						
20°C		0.15	0.16	0.18	0.26	0.36	0.39
100°C		0.12		0.14	0.20	0.26	0.28
400°C		0.067		0.079	0.12	0.12	0.13
Tensile strength							
25°C	10^3lb/in^2	22		28	28	38	45
1000°C				15	14		32
Compressive strength	10^3lb/in^2						
25°C		280		305	300	380	550
1000°C				50			280
Flexural strength							
25°C	10^3lb/in^2	43	46	51	52	55	80
1000°C		25		20	25		60
Modulus of elasticity	10^6lb/in^2	32	39	41	44	54	56
Shear modulus	10^6lb/in^2	14		17	18	22	23
Hardness	R45N	73		78	78	83	90
Thermal shock resistance		Moderate			Poor	Excellent	Good

*Measured from 20–400°C.

thermal shock resistance. According to Schwartz, most ZTAs contain both zirconia phases. Table 1.12 shows several examples of such toughening.

ALUMINA FOR ELECTRONIC PACKAGING AND INTERCONNECTION. Most freestanding alumina substrates for electronic applications, wherein conductive films are applied by thick or thin film processes, are 96 or 99.5 percent alumina. The 99.5 percent substrates are usually used for high-frequency applications, since their higher purity improves dielectric loss characteristics. They may also have better as-fired flatness and smoother surfaces than the lower alumina varieties, also desirable attributes for high-frequency operation.[16,17] Fine-grained 99.5 percent alumina will have an as-fired surface finish of 1- to 2-μin centerline average (CLA), compared to 8- to 10-μin CLA for coarse-grained alumina.[15]

TABLE 1.11 Electrical Properties of Aluminum Oxide Ceramics

		Aluminum Oxide Content, Weight Percent as Indicated					
Property	Units	85	92	94	96	99.5	99.9
Dielectric constant	None						
1 kHz		8.2	8.5	8.9	9.0	9.8	9.8
1 MHz		8.2		8.9	9.0	9.7	9.7
100 MHz		8.2		8.9	9.0		
Dissipation factor	None						
1 kHz		0.0014		0.0002	0.0011	0.0002	0.0020
1 MHz		0.0009	0.0025	0.0001	0.0001	0.0003	0.0002
100 MHz		0.0009		0.0005	0.0002		
Resistivity							
25°C	$\Omega \cdot$ cm	$>10^{14}$		$>10^{14}$	$>10^{14}$	$>10^{14}$	$>10^{14}$
1000°C				5.0×10^5	1.0×10^6		1.1×10^7

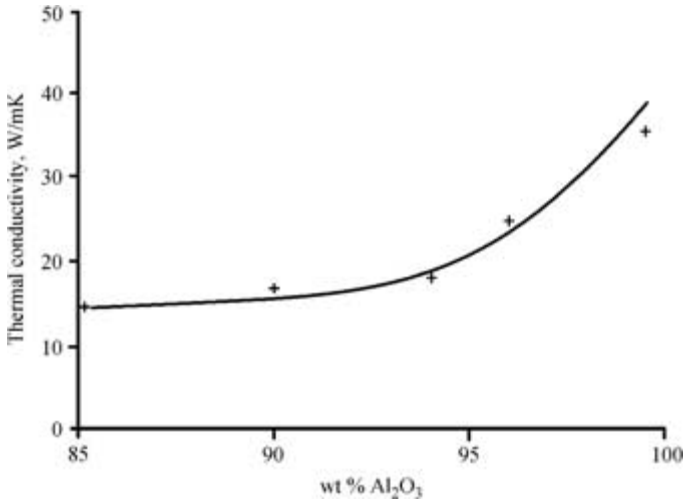

FIGURE 1.5 Thermal conductivity of alumina compositions increases as alumina content increases. (*From Ref. 14, p. 3.12.*)

Tape casting technology is used to fabricate three-dimensional alumina structures in a wide variety of shapes, thickness, and configurations.[4,18] The starting material here is "green" alumina tape, usually 92 percent, which is cast from slurry in a doctor blade process. Slurry consists of alumina powder, sintering agents, organic binders, and solvent that is cast onto a plastic sheet with the thickness controlled by a doctor blade. The slurry dries after a brief time into a flexible tape that is easily removed from the plastic sheet. The tape is cut to size, or blanked. The blanks are punched with an array of holes, or vias, in a precise pattern with a hardened tool steel punch. For prototype work a single punch programmed to locate the vias in the desired pattern may be used. These holes will be filled with a metallic paste in a screen or stencil-printing process and will be used to make electrical connection between layers. It is desirable for reasons of promoting circuit density to make

TABLE 1.12 Properties of Toughened Alumina

Property	Units	Material		
		99.9% Al_2O_3	Al_2O_3 + 30% TiC (from Ref. 1)	Zirconia-toughened alumina
Density	g/cm^3	3.96	4.25	
Flexural strength	MPa	550	670	Up to 850
Fracture toughness	$MPa \cdot m^{1/2}$	4–5	7.12	Up to 8.5
Weibull modulus		8–10	5.4	
Coef. thermal exp.	$10^{-6}/K$	6.5	7.9	
Thermal conductivity, 25°C	$W/(m \cdot K)$	39	21	

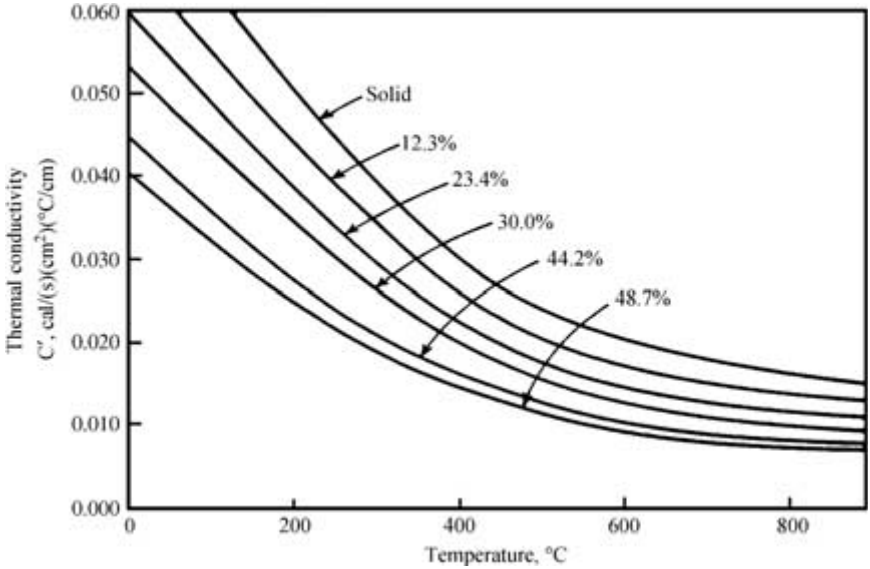

FIGURE 1.6 Thermal conductivity of alumina decreases as porosity increases over a wide range of temperatures. (*From Ref. 15, pp. 6–11.*)

the vias as small as possible: typically 10 mil (250 μm), with 5 mil-inches (125 μm) a practical minimum at the present time. The blanks are then printed with a metallic pattern appropriate for the layer—i.e., signal, ground, power, or device attachment. When all layers for an interconnection board are completed with vias punched and filled, and conductor patterns printed, the layers are laminated under pressure of several hundred psi. The laminated parts are then fired in an appropriate atmosphere at a temperature high enough to promote sintering, typically 1700°C. After firing, the exposed conductors are plated with a solderable or wire-bondable metal.

The high temperature required to sinter the ceramic requires that the conductors be refractory metals. Tungsten or a mixture of molybdenum and manganese, "moly-manganese," is used. These metals have an electrical resistance approximately 3 times that of copper, gold,

or silver used in thick-film substrates. Hence the need for an additional plated layer after the final firing.

The tape casting technology also forms the basis for construction of hermetic ceramic packages for integrated circuit chips. Such a package, in its simplest form, consists of a base layer on which the chip is mounted, a second level that forms a border around the chip mounting area, and a seal ring to which a metal cover is soldered. The second layer consists of an array of metallized fingers that in the final product run to the outside of the package. The base layer and the seal ring are also metallized. After firing the exposed metal layers, tungsten at this point, are plated with metallization that can be wire-bonded or soldered to. The integrated circuit chip makes contact with external circuitry through an electrical path consisting of 1-mil gold or aluminum wire from the chip to the package pad, and the tungsten path passing between the ceramic layers to the outside wall of the package. Electrical contact from the package to the mounting board is made by one of two ways. In the most widely used technique, a plated-metal lead frame is brazed to the metallized surface of the package, and the leads are soldered to pads or through-holes on the board. The less widely used alternative is to use a leadless chip carrier, where a solderable pad is plated to the bottom surface of the package, and all the pads are simultaneously soldered to mating pads on the board.

Substrates made by the multilayer process from tape cast alumina have received considerable attention in recent years for multichip module (MCM) applications.[19] An MCM consists of an array of closely packed chips on an interconnect board several inches on a side. Cofired ceramic is attractive relative to organic laminates because its thermal conductivity is almost 2 orders of magnitude higher, an important consideration in high-density circuitry. In addition both alumina and aluminum nitride ceramics are more closely matched to silicon in CTE than are organic boards. For similar reasons, alumina and AlN are attractive for ball grid array (BGA) mounting of chips.[20]

LOW TEMPERATURE COFIRED CERAMIC (LTCC). A logical extension of the discussion of cofired alumina is a brief discussion of a recently developed technology: low temperature cofired ceramic. A comprehensive discussion of this technology is contained in numerous sources, including a companion to this work, *Electronic Packaging and Interconnection Handbook*.[21] The information presented in that work is summarized here.

LTCC technology is similar in most respects to the high temperature cofired technology (HTCC) discussed above. The principal difference is in the material. HTCC is based on alumina or aluminum nitride, which require firing temperatures of 1700°C or higher. Consequently, conductors used with HTCC must be refractory—tungsten or moly-manganese—and have relatively high electrical resistance. LTCC, on the other hand, uses materials having high glass content in addition to the ceramic, thereby permitting firing temperatures lower than 1000°C. Thus, conductor layers can be gold, silver, or copper, with much lower track resistance than permitted by the refractory metals. The reduced firing temperature makes shrinkage much more predictable. Firing can be accomplished in a conventional thick-film belt furnace, since the firing temperatures of LTCC are similar to those of thick film. Thus, productivity is improved as well.

The advances made in LTCC technology have been presented elsewhere, e.g., Ref. 21, and will not be detailed here. Rather, some of the major milestones will be presented.

DuPont Electronic Materials Division and Hughes Aircraft introduced the first LTCC materials system at the 1983 ISHM Conference in Philadelphia.[22] DuPont then marketed a complete line of tapes and conductor systems with which to build complete systems.[23] Solderable conductors and screened resistor inks soon followed.[24] The properties of these DuPont materials are shown in Table 1.13. It can be seen that their properties are similar to those of alumina and thick film dielectrics.

TABLE 1.13 Properties of Commercial Low Temperature Cofired Ceramics

		DuPont			Ferro
Property	Units	851	951	943	A6
Density	g/cm^3	3.02	3.1	3.2	1.8
TCE (25 to 200°C)	$10^{-6}/K$	7.9	5.8	5.3	7.7
Dielectric constant					
1 MHz		7.9	7.8	7.5	5.8
10 GHz					
Loss tangent			.0015	0.0009	0.002
1 MHz					
10 GHz					
Volume resistivity, 25°C	$\Omega \cdot$ cm		$>10^{12}$		
Flexural strength	MPa	207	320		130
Thermal conductivity	$W/(m \cdot K)$	2	3.0		

In the late 1980s many potential users experimented with LTCC, considering it an advance in the state of the art of thick film.[25–27] Ferro Electronic Materials entered the market in the late 1980s, and offered a tape with a crystallizable component which offered low dielectric loss at high frequencies.[28] Properties of this tape are included in Table 1.13.

In addition to the LTCC systems made available by the material producers, manufacturers of electronic systems were developing tapes to meet their own requirements. Mattox[29] has described both the requirements that were driving the developments, the tradeoffs these requirements imposed, and many of the programs engaged in by electronic system manufacturers to meet the requirements. In most cases, these requirements include being able to operate at computer clock speeds in excess of 100 MHz; matched in CTE to alumina, silicon, or GaAs; and capable of achieving high circuit density.

Table 1.14 presents the results of the various manufacturers' tape system development programs.

Nishigaki et al.[27] at Narumi China Corporation, Nagoya, Japan, described an LTCC tape system that included ruthenium oxide resistors, silver conductors, and postfired copper conductors. The tape was composed of 40 percent alumina and 60 percent alumina-silica-calcia-boron oxide glass, and had dielectric constant of 7.7. Thermal conductivity of the fired tape was approximately 2.5 $W/(m \cdot K)$. Westinghouse Electronic Systems Group, Baltimore, and Westinghouse Systems and Technology Center, Pittsburgh, under contract with the Naval Ocean Systems Command, San Diego, developed a tape system with dielectric constant of 4.1.[30] The tape was compatible with DuPont inner layer gold and solderable top layer platinum gold. On the same program, a low-dielectric-constant thick-film dielectric was also developed and has been marketed by DuPont.

IBM Corporation, which had used an alumina cofired ceramic modules in its System 360 in the early 1980s, developed an LTCC system to replace the alumina-based system.[31] The history of this development is well documented in Ref. 31. Salient features of the IBM system are as follows:

- Copper metallization, inner and outer layers
- Dielectric constant of 5
- Thermal expansion matched to silicon (3.0×10^{-6}/°C)
- Each substrate 127.5 mm square, 60 metallized layers

TABLE 1.14 Properties of System Manufacturers' Low Temperature Cofired Ceramics

Property	Units	Westinghouse/ NOSC[30]	Narumi China[27]	NGK[35]	IBM[31]	NEC
Density	g/cm^3	2.3	2.9		2.62	
TCE (25 to 200°C)	10^{-6}/K	6.8	5.5	5.1	3.0	5.0
Dielectric constant						
1 MHz		4.5	7.7	7.0	5.0	7.1
10 GHz		4.1 (1 GHz)				7.1
Loss tangent						
1 MHz		0.001	0.0003	0.001		0.002
10 GHz		0.005 (1 GHz)				0.005
Volume resistivity, 25°C	Ω · cm		10^{14}			$>10^{14}$
Flexural strength	MPa	200		380	210	280
Thermal conductivity	W/(m · K)	1.5	2.5	3	<4	

- Mechanical strength: 210 MPa (30,000 lb/in^2)
- Number of vias increased from 350,000 to 2,000,000
- Polyimide-copper thin-film redistribution

This substrate development was incorporated into the IBM System/390-ES/9000 family of computers. Although IBM did not offer these materials for sale, it is understood that they would license the technology.

Other developments were taking place among LTCC merchants. Hartmann and Booth[32] announced a low-*K* crystallizable dielectric tape that could be cofired with copper. Properties are shown in Table 1.13. Alexander described a tape with similar characteristics, although it was not cofirable with copper.[27] Gupta discussed the issues involved in the synthesis of a low-firing tape system that offered low dielectric constant, low loss, and CTE matched to silicon.[33] A later paper described the results of his research.[34]

Researchers at NGK Spark Plug[35] developed an LTCC system for MCMs directed toward the personal computer market. Their material, with dielectric constant of 7.0, had sufficient strength to be brazed to Kovar and Alloy 42, a nickel-iron alloy similar to Kovar. The dielectric is a mixture of alumina, CaO, B_2O_3, and a small amount of zirconia. Varying the alumina content affected the flexural strength and CTE. Flexural strength maximized at 4.0 weight percent alumina. CTE was varied from 4.5 to 6.5, as alumina content varied from 2.0 to 5.0.

To summarize LTCC, it offers systems designers a tool of considerable flexibility for packaging electronic systems. The potential for integrating passive components to save space and to tailor dielectric constant and expansion coefficient are a few of the possibilities this technology offers.

Beryllium Oxide (BeO). Beryllium oxide, or beryllia, has many characteristics that make it desirable for numerous applications.[36–38] Foremost among these are applications where high thermal conductivity and electrical isolation are required. As can be seen in Table 1.15, which shows the electrical, mechanical, and thermal properties of beryllium oxide, pure beryllia exhibits a thermal conductivity higher than that of all metals except silver, gold, copper, and high-purity aluminum. In addition, beryllia has excellent dielectric properties; outstanding resistance to wetting and corrosion by many metals and chemicals; mechanical properties comparable to those of the higher aluminas; valuable

TABLE 1.15 Properties of Beryllium Oxide, BeO

Property	Units	Value	
		96% BeO	99.5% BeO
Density	g/cm^3	2.85	2.9
Hardness	Knoop 1000 g, kg/mm^2		9.8
	Rockwell R45N	64	67
Melting point	°C		2570
Modulus of elasticity	lb/in^2	44×10^6	51×10^6
Compressive strength	MPa		1550
Poisson's ratio			0.26
Thermal conductivity	$W/(m \cdot K)$		
20°C		159	281
100°C		134	201
400°C		67	84
Specific heat	$W \cdot s/(g \cdot K)$		
25°C			
100°C		1.26	1.3
Thermal coef. of expansion	$10^{-6}/K$		
25 to 200°C		6.3	6.4
25 to 500°C		7.5	7.7
25 to 800°C		8.4	8.5
25 to 1000°C		8.9	8.9
Dielectric constant			
1 MHz			6.7
10 GHz			6.8
Loss tangent			
1 MHz		0.0007	0.001
10 GHz		0.003	0.003
Volume resistivity	$\Omega \cdot cm$		
25°C		$>10^{17}$	$>10^{17}$
500°C		1×10^{13}	5.0×10^{13}
1000°C		4×10^7	7×10^7

nuclear properties, including an extremely low thermal neutron cross section; and the ability to be metallized by thick- and thin-film technology.

Most beryllia used today is of purity greater than 99.4 percent, since thermal conductivity drops rapidly as purity decreases. Figure 1.7 shows how thermal conductivity falls off as beryllia content decreases from 99.9 to 88 percent.

Major applications for BeO ceramics include microwave tube parts; substrates and mounting platforms for power transistors; crucibles for melting uranium, thorium, and beryllium; and numerous uses in the nuclear reactor industry because of beryllia's high thermal conductivity and ability to moderate fast neutrons.

For electronic packaging, beryllia is available in the forms of flat substrates for subsequent thick- or thin-film metallization. Most paste manufacturers offer pastes especially formulated for BeO. Beryllia also exists in green tape form, and can be used for cofired multilayer substrates. Hermetic packages are also available.

Despite its favorable properties, use of beryllia is limited because it is toxic for approximately 1 percent of the populace when submicrometer-size particles are ingested into the lung.[39,40] There is no test for an individual's susceptibility to the resultant condition, berylliosis, and no known cure. Thus, users must take stringent precautions to filter out dust

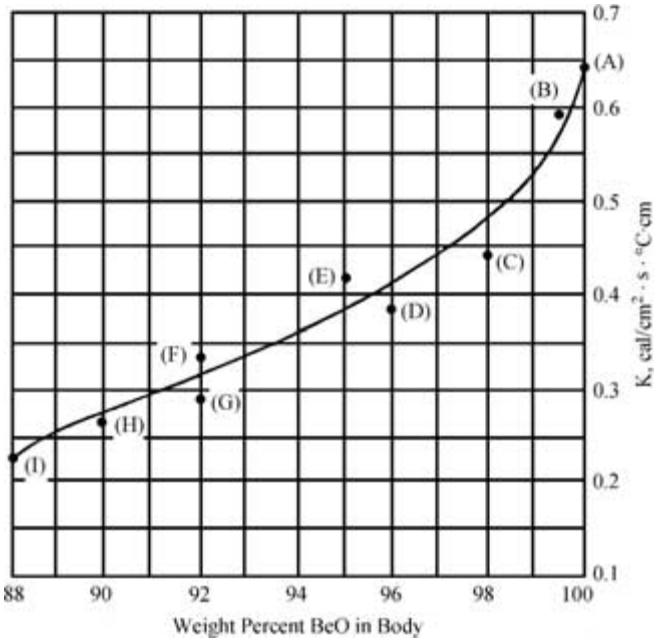

FIGURE 1.7 Thermal conductivity of BeO decreases rapidly as BeO content is decreased from 99.9 to 88 percent.

particles from cutting and grinding operations in order to prevent exposure of workers to beryllia dust. Powers[39] and Foley and Rees[40] have performed numerous tests to measure beryllia dust accumulation at workstations as a result of various processing operations, including laser trimming of resistors. Their work has shown that with proper precautions, BeO dust accumulation resulting from these operations can be reduced below detectable limits. Such measures entail additional costs that may be enough to cause users to select other materials.

Zirconia, ZrO_2. Although zirconia has been used in the refractories industry for close to a century, only recently has advanced, stabilized, fine-grained zirconia come into widespread use.[41,42] The combination of hardness, good thermal insulation, chemical inertness, high density, low coefficient of friction, expansion coefficient close to that of steel, and high fracture toughness has made various forms of zirconia attractive for many applications.

Zirconia is usually produced from zircon, $ZrSiO_4$.[42] The first step is to convert zircon to zirconyl chloride by melting the zircon with sodium hydroxide to form Na_2ZrO_3. This compound is then treated with HCl to form zirconyl chloride, $ZrOCl_2 \cdot 8H_2O$. Two methods are used to make zirconia from zirconyl chloride: thermal decomposition and precipitation. The thermal decomposition method is the less costly of the two, but the resulting material is not usually of as high a purity and fine particle size as that produced by precipitation. The precipitation method uses chemical reactions to obtain the zirconia hydroxides as an intermediate material. A final calcination process results in zirconia powder. By controlling the precipitation and calcination conditions, it is possible to achieve desired particle size and shape, grain size, and specific surface area.

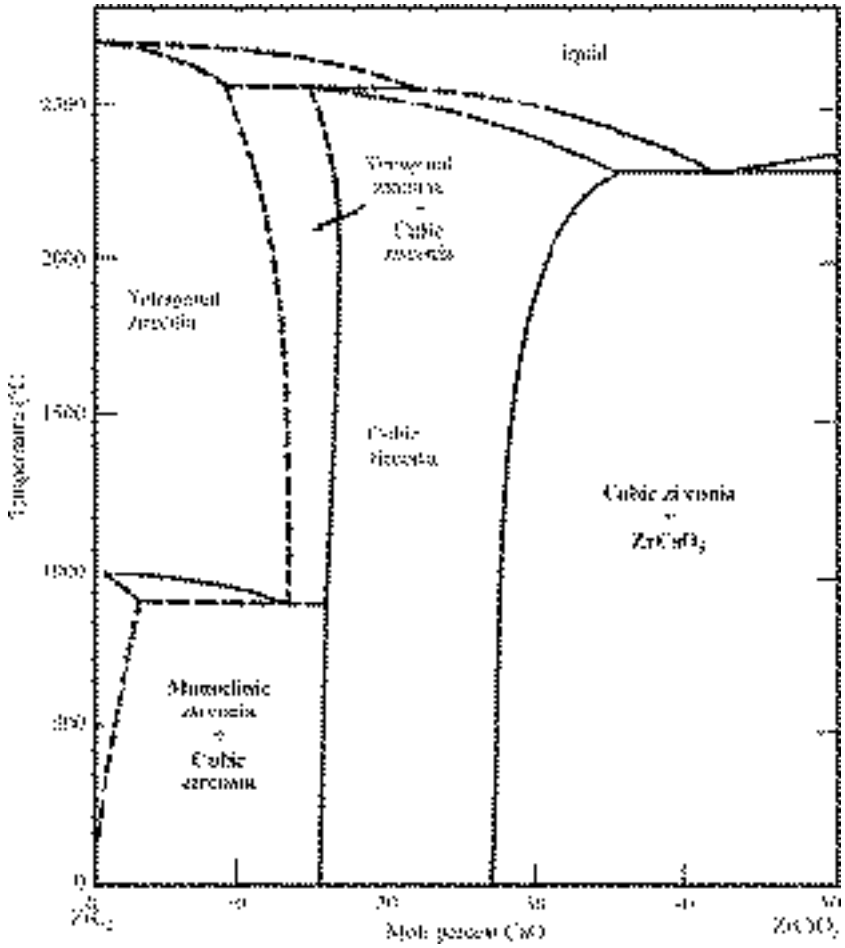

FIGURE 1.8 Phase diagram of calcia-stabilized zirconia.[42]

Zirconia exists in three crystalline forms: monoclinic, tetragonal, and cubic. Figure 1.8 is a phase diagram for calcia-stabilized zirconia. The structure is monoclinic (m) from room temperature to 1170°C, at which point it transforms to tetragonal (t). It remains tetragonal until about 2370°C, when it converts to cubic[43] (c). In the pure material the cubic phase exists only above 2370°C and is not encountered in sintered products, which are processed at much lower temperatures. Pure ZrO_2 sintered above 1170°C spontaneously disintegrates during cooling because of the triclinic to monoclinic transformation[42] that involves an increase in density from 5.7 to over 6 g/cm^3. For applications involving temperatures over 1000°C, zirconia must be stabilized to prevent the phase inversion, which is usually destructive. The stabilization may be either partial or full, depending on the amount of stabilizer added. This process is discussed more fully below. The properties of several forms of zirconia are given in Table 1.16.

TABLE 1.16 Properties of Zirconia, Partially Stabilized Zirconia, and Toughened Zirconia

Properties	Units	Monoclinic zirconia ZrO_2 (m)[a]	Partially stabilized zirconia (PSZ)		Transformation Toughened	
			ZrO_2 (c)[a] + 2.65 mol% MgO	ZrO_2 (c)[a] + 5.1 mol% Y_2O_3	Zycron L[b]	Zycron H[6]
Density	g/cm^3	5.7	5.8	6	5.7	5.6
Coef. of linear thermal expansion	$10^{-6}/K$	6.5		9.6	9.8	2.4
Maximum service temp.	°C	<1000	>2200	>2200		
Thermal conductivity, 20°C	W/(m · C)			3	2	2
Tensile strength, 25°C	MPa				414	248
Compressive strength, 25°C	10^3 lb/in^2				285	285
	MPa				1965	1965
Modulus of rupture	MPa		687 MPa		621	414
Modulus of elasticity	GPa			200	248	221
Hardness	As indicated			>10 GPa	RA 85	RA83
Fracture toughness	MPa · $m^{1/2}$		9	8	13	7
Weibull modulus	None				12	14

[a]Indicates monoclinic structure.
[b]Trademark Zircoa Corporation, Solon, OH.
[c]Indicates cubic structure.

PURE ZIRCONIA. Pure, or unstabilized zirconia, has many uses despite the phase-transformation phenomenon described. Its density, 6.05 g/cm^3, makes it valuable as a grinding medium. Added to alumina or magnesia it promotes sinterability and enhances strength and other properties, as discussed above under "Toughened alumina." It is an important constituent of ceramic colors, and a component of lead-zirconia-titanate–based electronic ceramic devices such as capacitors. But its uses increase dramatically as a result of a process known as stabilization, which is discussed in the following sections.

FULLY STABILIZED ZIRCONIA. To prevent the destructive monoclinic-to-tetragonal phase inversion during firing and subsequent cooling, stabilizers such as CaO, MgO, and Y_2O_3 are added to the mixture. The composition, called *stabilized zirconia*, retains the cubic structure without the destructive inversion during cooling. For zirconia to be fully stabilized, more than 16 mol% CaO, 16 mol% MgO, or 8 mol% Y_2O_3 must be added. The structure is then a cubic solid solution, and has no phase transformation from room temperature to about 2500°C.

PARTIALLY STABILIZED ZIRCONIA (PSZ). Partially stabilized zirconia contains an insufficient amount of calcia, magnesia, or yttria stabilizing compound to achieve formation of a stable cubic phase. A cubic plus metastable tetragonal ZrO_2 is obtained, and the resulting zirconia is known as *partially stabilized*. Partially stabilized zirconia has been found to have higher strength and toughness. The partially stabilized zirconia, being a mixture of tetragonal and cubic phases, is also known as *tetragonal zirconia polycrystal* (TZP). Transformation toughened zirconia can be fabricated by using a cubic matrix with 20 to 50% tetragonal added.

The physical properties of several formulations of zirconia are presented in Table 1.16

Mullite. A mixture of alumina and silica, mullite is valuable because of its low thermal expansion and resistance to spalling and deformation under load. The specific composition of a given specimen depends on the method of synthesis. The theoretical composition is 71.8 percent alumina and 28.2 percent silica, but alumina content can range as high as 77 percent or as low as 62.6 percent.

Mullite was used originally as a spark plug insulator. In recent years it has found extensive use in kiln furniture applications, and as liner material in tube-type furnaces.

The properties of mullite are given in Table 1.17. The data are taken from different sources, which are identified in the table. Differences are presumed to be a result of somewhat different final compositions due to different source materials and different manufacturing procedures.

1.2.3.2 Nitrides. Three nitrides will be discussed in this section: aluminum nitride, which has become an important substrate material in the past decade; silicon nitride; and two forms of boron nitride—cubic and hexagonal. The characteristics of these materials are discussed in the following sections.

Aluminum Nitride. Aluminum nitride, AlN, has generated a great deal of interest in the past 15 years[44–47] because of its high thermal conductivity, which is 5 times that of alumina at room temperature, and above 200°C is higher than that of beryllia. Mechanical strength is comparable to that of alumina. Its thermal expansion coefficient of 4.7 parts per million (ppm) per °C is better matched to that of silicon, 3.0 ppm/°C, than is that of alumina, making it advantageous for use in high-power circuitry.

The properties of substrate-grade aluminum nitride are presented in Table 1.18.

TABLE 1.17 Properties of Mullite

Property	Units	Kyocera dense, K635	Coors	Materials Engineering
Density	g/cm^3	2.6	2.82	3.0–3.3
Water absorption	%	None	None	None
Coef. linear thermal expansion	$10^{-6}/K$			
25–200°C		4.6*	3.7	4.9–5.4§
25–800°C		4.8‡	4.8	
25–1000°C			5.0	
Maximum service temperature	°C	1110	1700 (no load)	1650–1700
Thermal conductivity	W/(m · K)			
20°C				
400°C		2.1†	4.1	2.39–2.51†
800°C				
Tensile strength	10^3 lb/in^2			
25°C				
1000°C				
Compressive strength	MPa (10^3 lb/in^2)			
25°C				
1000°C		(98)	551	(100–150)
Flexural strength	MPa (10^3 lb/in^2)			
25°C		(20)	186	
1000°C			151	
Modulus of elasticity	GPa		155	

*40–400°C.
†Values were converted to SI from English.
‡40–800°C.
§68–212°F.

When AlN was introduced for electronic packaging applications in 1985 it was considered inconsistent in properties. This inconsistency was due to problems with the AlN powders used to make sintered products.[47] The powders were made by either of two methods: direct nitridation of aluminum metal in a nitrogen gas atmosphere or carbothermal reduction of alumina, which involves the decomposition of the reaction product of aluminum trichloride with ammonia. The first process was cheaper, but the resultant powders were not especially well suited to materials for electronic applications. The carbothermal process produces powders of greater uniformity and purity, with greater control over size and shape, than the nitridation process, and is the more widely used process today.[48]

Pure AlN powders are sintered with sintering agents, typically oxides of yttrium or calcium. These additions degrade the thermal conductivity. In addition, moisture and many chemicals attack pure AlN substrates. As protection against these elements, and to promote adhesion to thick-film inks, a thin oxide layer is usually grown on the surface. Consequently, the thermal conductivity of AlN can vary widely from its maximum value, reported to be 320 W/(m · K),[45,46] and is typically in the range of 170 to 200 W/(m · K). B. B. Poole of Carborundum Corporation[49] published results of a program carried out there to improve the mean value and reduce the variability of the thermal conductivity of their substrates. As a result of their effort the mean thermal conductivity of AlN substrates manufactured by their process was improved from 172 W/(m · K), with standard deviation of 19.6 W/(m · K), to mean of 192 and standard deviation of 3.0 W/mK.

TABLE 1.18 Properties of Aluminum Nitride (Highest Grade)

Property	Units	Value
Density	g/cm^3	3.27
Hardness	Knoop 100 g	1200
Melting point	°C	2232
Modulus of elasticity	GPa	300
Compressive strength	MPa	2000
Poisson's ratio		0.23
Thermal conductivity	W/(m · K)	
25°C		270
150°C		195
Specific heat	W · s/(g · K)	
25°C		0.76
150°C		0.94
Coef. linear thermal expansion		
25–400°C	10^{-6}/K	4.7
Dielectric constant		
1 MHz		8.9
10 GHz		9.0
Loss tangent		
1 MHz		0.0004
10 GHz		0.0004
Volume resistivity	Ω · cm	
25°C		$>10^{12}$
500°C		2×10^8

During the decade of the 90s the uses of aluminum nitride have expanded almost exponentially. Although its room temperature thermal conductivity is lower than that of beryllia, 170–190 w/(m·K) vs. 250 w/(m·K), as temperature increases their respective thermal conductivities become closer. Above approximately 200°C, aluminum nitride's thermal conductivity is higher than beryllia's, as shown in Fig. 1.9.

Aluminum nitride has been demonstrated to be suitable for blank substrates for high power and high frequency applications. Substrates from many sources are available for thick or thin film metallization.[50–53] Thick film paste manufacturers now supply pastes formulated for aluminum nitride. The multilayer process described in the previous section has also been adapted for aluminum nitride.[54,55] Both multilayer substrates and packages are available commercially.

In addition to uses in electronic packaging, aluminum nitride is valuable wherever high strength and high thermal conductivity are needed. Examples are as crucibles for aluminum melting, for ballistic armor, and for aluminum resistant refractory ware.

Boron Nitride. Boron nitride is a highly refractory material with physical and chemical properties similar to those of carbon. Known polymorphs of BN are graphite-like, wurtzite, and zinc blend, corresponding to the graphite (hexagonal) and diamond (cubic) structures. These two forms of boron nitride, hexagonal and cubic, have attracted the attention of potential users because of high thermal conductivity,[38,56,57] hardness, compatibility with other materials, and other features. Both forms have properties that make manufacture of finished parts difficult. However, progress is being reported for both materials, and they are finding their way into wider usage. Both materials are discussed briefly below.

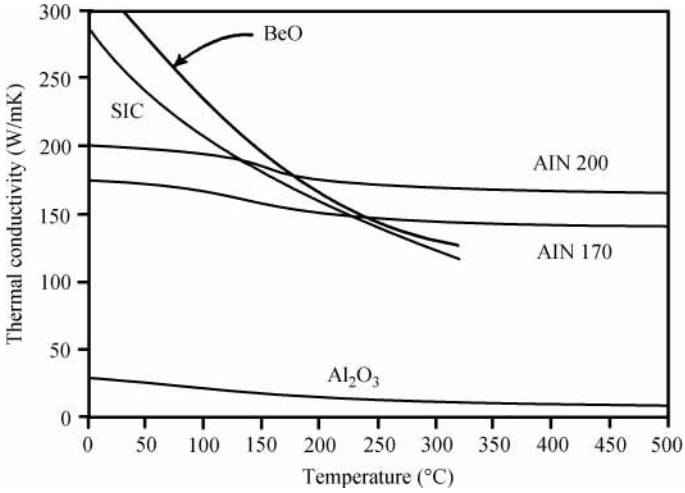

FIGURE 1.9 Aluminum nitride exhibits thermal conductivity comparable to that of beryllia and silicon carbide. (*From Ref. 4, p. 3.13.*)

HEXAGONAL BORON NITRIDE (HBN). Hexagonal boron nitride is a soft, graphite-like material. It can be hot-pressed into a wide variety of shapes, which can then be machined to final dimensions. It is available as powder that has excellent lubricating properties for applications such as a mold release medium. When mixed with epoxies or mold compounds, its high thermal conductivity, 55 W/(m · K), greatly enhances the thermal conductivity of the body. Thus, hBN-filled adhesives can be used for mounting semiconductor chips in high-power circuitry without compromising circuit performance. Lelonis[56] reports that boron nitride–filled epoxy molding compounds reduced thermal resistance of a 176-lead integrated circuit package from 20°C/W to 11°C/W. Boron nitride–filled epoxy demonstrated higher thermal conductivity than epoxies filled with aluminum oxide, aluminum nitride, or silica, over the 35 to 60 percent fill range. This result, along with its low thermal expansion and high electrical resistance make hBN an attractive filler material.

Several techniques for hot pressing of hBN have been developed that result in materials of very desirable properties. Union Carbide Corporation reports three grades that have different ranges of usefulness. First, HBN grade, pressed with a boron oxide binder, can be used at temperatures up to 550–850°C in an oxidizing atmosphere, and up to 1600°C in vacuum. Because boron oxide is attacked by water, another grade using a calcium borate binder, HBR, is available. HBR has a maximum service temperature of 1600°C. A third material that does not use any binder, HBC, can be used at temperatures up to 3000°C. Hexagonal BN is chemically inert and is not wetted by most metals. The properties of several configurations of hBN are presented in Table 1.19. It can be seen that many of the properties are sensitive to pressing direction.

CUBIC BORON NITRIDE (CBN). As has been reported, cBN is difficult to manufacture, requiring use of pressures of 6 GPa and temperatures in the neighborhood of 1500°C, similar to the technology for fabricating synthetic diamond. Like diamond, cBN has two properties that set it apart from almost all other materials: high thermal conductivity and

TABLE 1.19 Properties of Hexagonal and Cubic Boron Nitride (BN)

Property	Units	Values			
		hBN*	HBN†	HBR†	Cubic
Binder		None	Boron oxide	Calcium borate	
Density	g/cm^3	2.08‡			
Hardness	Knoop 100g	2.7		205	Vickers 7500
Binder melting point	°C	NA	550	1150	
Maximum service temperature	°C				
Oxidizing atmosphere			550–850	850	1400 (air)
Inert atmosphere				1150–1600	
Young's modulus	GPa	43			
Compressive strength					
Parallel	10^3 lb/in^2	11.7	11	6	
Perpendicular§		13.9	13	7.5	
Thermal conductivity, 25°C	W/(m · K)				~1300
Parallel		22.8	59	55	
Perpendicular			33	33	
Coef. thermal expansion, 20–300°C	10^{-6}/K				
Parallel		2.0	1.2	1.0	
Perpendicular		4.1	3.2	2.0	
Dielectric constant		4.1	4.3–4.7	4.2–4.6	
Volume resistivity, 25°C	Ω · cm	10^{13}	10^{13}	10^{13}	

*96% BN.
†Designation of Union Carbide Corporation.
‡Theoretical density.
§Relative to pressing direction.

hardness. Since these properties are required attributes for abrasives and cutting tools, cBN is naturally a competitor for diamond in those markets. The cubic form is reported to have thermal conductivity approximately the same as that of diamond—1400 W/(m · K). Hardness is lower than that of diamond, 7500 kg/cm^2 Vickers microhardness versus 9000 for diamond. Although on these bases diamond would appear to be the abrasive of choice, cBN has several features that make it more desirable in certain applications. First, it does not react with ferrous materials. Second, it is stable in air up to 1400°C, it is tough, and is available in a variety of grain sizes.

The properties of cBN have not been widely reported. Table 1.19 presents many mechanical and thermal properties.

Silicon Nitride and Sialon. In this section we discuss both silicon nitride and sialon, a material with similar properties. Silicon nitride, Si_3N_4, exhibits very high resistance to heat and corrosion, and is exceptionally strong. Sialon, a family of silicon-aluminum-silica oxynitrides, has properties comparable to those of silicon nitride, and is much easier to manufacture and form into complex shapes.

SILICON NITRIDE. Because pure Si_3N_4 powders are difficult to sinter, several methods are used to achieve finished parts of desired size and shape, and the processing technology used has a significant affect on the physical properties of the finished part. These processing

TABLE 1.20 Properties of Silicon Nitride (Si_3N_4)

Property	Units	Hot Pressed (HPSN)*	Sintered (SSN)	Reaction bonded (RBSN)
Density	g/cm^3	3.10 (3.07–3.37)	3.13 (2.8–3.4)	2.4 (2.0–2.8)
Hardness	Knoop 100 g	2200 (k100)		900 (VHN, 0.5 kg)
Coef. thermal expansion, 20–1000°C	10^{-6}/K	3.3 (3.0–3.9)	3.5	2.9 (2.5–3.1)
Young's modulus, 20°C	GPa	300 (250–325)	245 (195–315)	175 (100–220)
Young's modulus, 1400 °C	GPa	175 (175–250)		155 (120–200)
Flexure strength, 20°C	MPa	750 (450–1100)	415 (275–840)	200 (50–300)
Flexure strength, 1400°C	MPa	300 (0–600)	70 (0–700)	250 (0–400)
Fracture toughness	$MPa \cdot m^{1/2}$	4.8 (2.8–6.6)	4.3 (3.0–5.6)	3.6
Coefficient of thermal expansion, 20–1000°C	10^{-6}/°C	3.3 (3.0–3.9)	3.5	2.9 (2.5–3.1)
Thermal conductivity, 25°C	$W/(m \cdot K)$	32		8–12
Maximum service temp.	°C	1300		1300

*The numbers in parentheses in many cells are the ranges of values observed by Schwartz for a particular property.

technologies are[5] (1) reaction bonding, (2) hot pressing, and isostatically hot pressing, and (3) sintering and gas-pressure-assisted sintering. Schwartz[5] has provided a comprehensive description of the details of these processes and the reasons for using them in particular situations. This discussion will not be repeated here, but an attempt will be made to summarize the properties achieved by each method.

Schwartz[59] compiled a list of 51 silicon nitrides from different suppliers with their mechanical properties as provided by the manufacturers. Table 1.20 gives typical properties and ranges of the three classifications of silicon nitride.

SIALON. Sialon[59] is synthesized by reacting together silicon nitride, silica, alumina, and aluminum nitride. Sialon exists in three forms: β' based on β silicon nitride; α' based on α silicon nitride, and O′ sialon, which has the crystal structure of silicon oxynitrides and obeys the formula $Si_zAl_{2-z}O_{3-z}N_z$, with z taking values in the range of 1.3 to 2. Materials based on β' sialon or a mixture of α and β' sialons are well suited for high-temperature and high-stress applications.

Table 1.21 compares the properties of sialon with one formulation of hot-pressed silicon nitride.

1.2.3.3 Silicon Carbides. Silicon carbide is a widely used ceramic characterized by high hardness, high strength at elevated temperatures, good thermal shock resistance resulting from its good thermal conductivity, and relatively low thermal expansion. In recent years it

TABLE 1.21 Properties of Sialon (typical) Compared to HP Silicon Nitride

Property	Units	Sialon	Si_3N_4
Density	g/cm^3	3.25	3.2
Hardness	Knoop, k100	1800	2200
Melting point	°C		
Modulus of elasticity	GPa	0.28	0.31
Compressive strength	MPa	>3500	>3500
Toughness	$MPa \cdot m^{1/2}$	7.7	5
Weibull modulus		11–15	10–15
Poisson's ratio		0.23	0.27
Thermal conductivity at 25°C	$W/(m \cdot K)$	21.3	25
Specific heat at 25°C	$Cal/g \cdot K$	0.15	0.17
TCE (0 to 1000°C)	$10^{-6}/K$	3.04	3.2

has gained attention, although not widespread usage, as an electronic packaging material because of its good thermal expansion match to silicon in addition to its favorable properties already cited.[46,60,61]

Silicon carbide exists in a cubic form, beta silicon carbide, and in several noncubic forms lumped under the term *alpha silicon carbide*.

Silicon carbide is produced most often by the Acheson process, discovered in 1891 by Edward Goodrich Acheson. Later in 1891 he formed Carborundum Corporation to manufacture SiC abrasives. In this process current is passed through a mixture of carbon and sand causing the reaction $SiO_2 + 3C \rightarrow SiC + 2CO$. When carried out at 2600°C or higher the result is alpha; the beta form can be achieved at 1500 to 1600°C.[5]

As with silicon nitride, solid forms of silicon carbide are made by one of three processes: sintered, hot-pressed, or reaction-sintered. Sintering requires use of an additive such as alumina, carbon, or boron to promote liquid-phase sintering. Hot pressing is done at 2000°C and results in a very hard, dense material. Reaction sintering occurs when a mixture of SiC powder and carbon is heated in contact with molten silicon. The reaction results in a nearly complete conversion to SiC, although according to Schwartz, most materials made by this process contain an excess of carbon or silicon.[59]

The properties of silicon carbide are summarized in Table 1.22.

1.2.4 Concrete

Concrete[62] is an exceptionally versatile engineering material consisting of a hydraulic cementing substance such as portland cement, aggregates (sand, gravel, or stones), water, reinforcing materials, and other additives to supply desired properties. Concretes are similar in composition to mortars that are used to bond masonry, except that mortars have only sand as the aggregrate, whereas concrete has much larger aggregates, and as a result is much stronger.

Portland cement is a generic name for hydraulic, or water-setting, cement. It is composed of high-limed calcium silicates that are ground together with a small amount of gypsum to a fine powder. During hardening the calcium compounds chemically combine with water to produce the hard, finished product. The portland cement–water hydration product becomes the binder, which joins sand and stone in mortar and concrete to produce a monolithic product.

Since concrete is initially plastic, it can be molded into an almost infinite variety of shapes, and is used in construction on an enormous scale. Applications include pavements, footings, pipes, unit masonry, floor slab, beams, columns, dams, and tanks. A concrete mix

TABLE 1.22 Properties of Silicon Carbide

Property	Units	Value
Density	g/cm^3	3.21
Hardness	Knoop 100g	27.5
Melting point	°C	
Modulus of elasticity	GPa	407
Flexure strength	MPa	450
Poisson's ratio		
Thermal conductivity	W/(m · K)	
25°C		70
150°C		
Specific heat	W · s/g · K	
25°C		
150°C		
TCE (room temp. to 400°C)	10^{-6}/K	3.8
Dielectric constant		
1 MHz		40–79
10 GHz		
Loss tangent		
1 MHz		0.050
10 GHz		
Volume resistivity	Ω · cm	
25°C		$>10^{13}$
500°C		

is designed to provide characteristics that are needed in the particular application, such as strength, durability, or low cost.

Concrete is classified as either flexible or rigid. Mainly the cementitious materials used to bond the aggregates determine these characteristics.

Flexible Concrete. Flexible concrete is used mainly for pavements. It has a bituminous, asphaltic binder that must be heated to achieve enough plasticity for application. It is applied and rolled to a desired thickness. When the mix cools it hardens enough to withstand heavy loads.

Rigid Concrete. Ordinary rigid concretes are those made as described previously: mixtures of portland cement, sand, larger aggregate, and water, which hydrates the cement to bond the aggregates into a solid mass. Various admixtures may be added to the mix to impart specific properties to it or to the hardened concrete. Types of rigid concrete include nailable; insulating; heavyweight; lightweight; fiber-reinforced, in which steel or fiberglass fibers are imbedded to impart resistance to tensile stresses; and others.

Stress and Reinforcement. Ordinary concrete, like most ceramic materials, is much weaker in tension than in compression. Use of unreinforced concrete is limited to structures in which the tensile stresses will be small, such as massive dams and heavy foundations. In applications requiring additional strength, the concrete is prestressed with a stronger material such as steel, which places the body in compression. Steel bars or rods or structural steel shapes may be incorporated in the concrete. Prestresses to offset tensile stresses may be applied at specific locations by permanently installed compressing jacks, high-strength steel bars, or steel strands. Prestresses may also be distributed throughout a concrete component by embedded pretensioned steel elements. Another option is to use

cement that tends to expand on curing but is prevented from doing so by enclosures, thus forcing the concrete into compression.

Aggregates. Aggregates used for concrete should be inert, dimensionally stable, hard, tough, and approximately round or cubical in shape. They should be free of clay, organic matter, silt, and salts. Aggregates that cause a deleterious reaction with cement should be avoided.

Coarse and fine aggregates are typically used. The coarse material, usually crushed gravel or stone, is sized by retention on a No.4 sieve [4.75 mm (0.019 in) openings]. Fine aggregates, usually sand, are retained by a No. 200 [75 μm (0.003 in) openings] sieve.

Mix Design and Concrete Properties. To achieve desired properties the concrete mixture should meet certain specifications. Principal among these are the ratios of (1) water to cement, (2) cement to aggregates, and (3) fine to coarse aggregates. The greater the cement-to-water ratio the greater the strength. Excessive water may leave voids and cracks.

Conventional concrete usually weighs about 150 lb/ft^3, or 2400 kg/m^3. Values differ for heavier- and lighter-weight concretes. The thermal expansion coefficient of concrete averages about 10^{-5}/°C, or 5.5×10^{-6}/°F.

Admixtures. Materials known as admixtures are added to the mix to impart particular properties. The American Society for Testing and Materials (ASTM) specifies several types of admixtures, as follows:

Type A reduces the quantity of mixing water that would normally be required to produce a concrete with a certain strength and consistency.

Type B slows the setting of the concrete.

Type C accelerates the setting and promotes early development strength.

Type D reduces water requirements and delays setting.

Type E decreases water requirements and hastens setting.

Type F reduces water requirements by more than 12 percent to achieve a desired strength and consistency.

Type G acts much like Type F but in addition retards the setting of the concrete.

In addition to these admixtures others have been developed, including air-entraining, waterproofing, pozzolans, superplasticizers, and pigments.

Other Types of Concrete. There are many varieties of concrete that can be achieved by selection of the materials in the mixture.

Lightweight concretes, made by using lightweight aggregates or by expanding concrete mixes, bring appreciable savings in weight, improved thermal and sound insulation, and improved fire resistance.

Heavyweight concretes can weigh up to 385 lb/ft^3 (6170 kg/m^3), and are used for shielding nuclear reactors. The increased weight is achieved by using such heavyweight aggregates as barite, limonite, magnetite, steel punchings, and steel shot.

Polymer concretes are those in which polymers are either impregnated in hardened concrete, incorporated in the mix, or replace portland cement. Impregnated polymers can double compressive strength and elastic modulus, decrease creep, and improve resistance to freezing and thawing. They are used in concrete road surfaces. Polymers added to the mix are used for resurfacing roads. They hasten cure time. Polymer concretes in which a

polymer replaces portland cement are similar to those with impregnated polymers. These also feature much shorter cure times, thus enabling faster return of roads to service.

High-tensile-strength concretes are made by using an organic admixture that fills the voids in concrete. As a result the concrete develops a tensile strength up to 20 times that of ordinary concrete.

Silica-fume concretes incorporate silica fume, or microsilica, as a partial replacement for portland cement. Strength increases of 25 percent may result without use of any other admixtures.

It can be seen that concrete exists in too many varieties to be covered adequately in a handbook such as this. The American Concrete Institute (ACI), ASTM, and the American Association of State Highway and Transportation Officials (AASHTO) publicize recommended practices for manufacturing, testing, and using concrete.

1.2.5 Glasses

Glass has been used for centuries for structural applications such as windows, packaging such as bottles, and ware such as drinking glasses and goblets. In the twentieth century the inventions of radio, television, and advanced electronics created numerous new applications for glass, and resulted in many new compositions with superior electrical properties. Glasses have an amorphous structure and a wide range of compositions. Oxide-based glasses can be classified as silicates, borates, phosphates, or germanates, depending on which of the glass-forming oxides (SiO_2, B_2O_3, P_2O_5, or GeO_2) make up the structure.[63]

Because three later chapters of this handbook are devoted to glass, the subject will be dealt with only briefly here. The intent will be to show how glasses and ceramics compare in their various characteristics.

Tables 1.23 and 1.24, taken from Mattox,[63] show the properties and compositions of the most widely used glasses. Two points regarding the data in the tables need to be made: (1) Thermal expansion data are for temperatures well below the softening temperature. Glasses undergo an abrupt increase in thermal expansion within 20 to 50°C of the softening temperature. This effect is illustrated in Fig. 1.10. If a process calls for glass to be raised to that temperature, this sharp change should be taken into consideration. (2) the four temperature points cited, strain, softening, annealing, and working, are defined as follows: *Strain* and *annealing* refer to the temperatures at which strain is relieved by viscous flow. *Softening* is the temperature at which a fiber will deform under its own weight. *Working* is the temperature at which the viscosity is low enough for the glass to be moved around or flowed.

1.2.6 Diamond

Diamond has been much sought after for centuries for its brilliance and beauty as a gem. In the last 50 years it has demonstrated other outstanding characteristics, principally exceptional hardness and the highest thermal conductivity of any known material, that make it highly desirable in many industrial applications. Natural diamond being prohibitively expensive for practical applications, scientists have tried for over a century to create synthetic diamond by a variety of techniques.[64] General Electric Corporation scientists were successful in this effort in 1955, using a high-pressure, high-temperature, technique. The availability of synthetic diamond crystal enabled workers to understand more of the thermodynamics of diamond formation and thereby improve the process. However, temperatures of over 3000 K and pressures over 100 kbar were required, and apparatus capable of these conditions large enough to form diamond at a rate acceptable for commercial

TABLE 1.23 Properties of Commercial Glasses

Property	Units	Glass code and type							
		0010 Potash soda lead	0080 Soda lime	7052 Boro-silicate	7570 High lead	7740 Boro-silicate	7900 96% silica	7940 Fused silica	9010 Potash soda barium
Density	g/cm^3	2.86	2.47	2.28	5.42	2.23	2.18	2.20	2.64
TCE (0 to 300°C)	$10^{-6}/K$	93	92	46	84	33	8	5.5	89
Strain point	°C	395	470	435	340	515	820	990	405
Annealing point	°C	435	510	480	365	565	910	1050	445
Softening point	°C	625	695	710	440	820	1500	1580	650
Working point	°C	985	1005	1115	560	1245	—	—	1010
Young's modulus	$10^6 lb/in^2$	8	10.0	8.2	8.0	9.1	10.0	10.5	9.8
Poisson's ratio		0.21	0.24	0.22	0.28	0.20	0.19	0.16	0.21
Dielectric constant									
1 kHz		6.63	7.2	4.9	15.0	4.6	3.85	3.8	6.3
1 MHz		6.7					3.8		
25 GHz		5.87					3.82		
Loss factor, 1 MHz	%	1.0	6.5	1.3	3.3	2.6	0.10	0.0038	1.1
Volume resistivity	$\log_{10} \Omega \cdot cm$								
25°C		17.+	12.4	17.0	—	15.0	17.0	—	—
250°C		8.9	6.4	9.2	10.6	8.1	9.7	11.8	8.9
350°C		7.0	5.1	7.4	8.7	6.6	8.1	10.2	7.0

Source: Mattox, Ref. 63.

TABLE 1.24 Estimated Commercial Glass Compositions

Glass code*	Type	Thermal expansion 0–300°C, 10^{-7}/°C	Viscosity data, °C				Density, g/cm^3	Young's modulus, 10^6 lb/in^2	Poisson's ratio	$\log_{10}$ of volume resistivity			Dielectric properties at 1 MHz and 20°C		
			Strain point	Annealing point	Softening point	Working point				25°C	250°C	350°C	Power factor, %	Dielectric constant	Loss factor, %
0010	Potash soda lead	93	395	435	625	985	2.86	8	0.21	17.+	8.9	7.0	0.16	6.7	1
0080	Soda lime	92	470	510	695	1005	2.47	10.0	0.24	12.4	6.4	5.1	0.9	7.2	6.5
7052	Borosilicate	46	435	480	710	1115	2.28	8.2	0.22	17.0	9.2	7.4	0.26	4.9	1.3
7570	High lead	84	340	365	440	560	5.42	8.0	0.28	—	10.6	8.7	0.22	15.0	3.3
7740	Borosilicate	33	515	565	820	1245	2.23	9.1	0.20	15.0	8.1	6.6	0.50	4.6	2.6
7900	96% silica	8	820	910	1500	—	2.18	10.0	0.19	17.0	9.7	8.1	0.05	3.8	0.019
7940	Fused silica	5.5	990	1050	1580	—	2.20	10.5	0.16	—	11.8	10.2	0.001	3.8	0.0038
9010	Potash soda barium	89	405	445	650	1010	2.64	9.8	0.21	—	8.9	7.0	0.17	6.3	1.1

*Corning Glass Works.
Source: Mattox, Ref. 63.

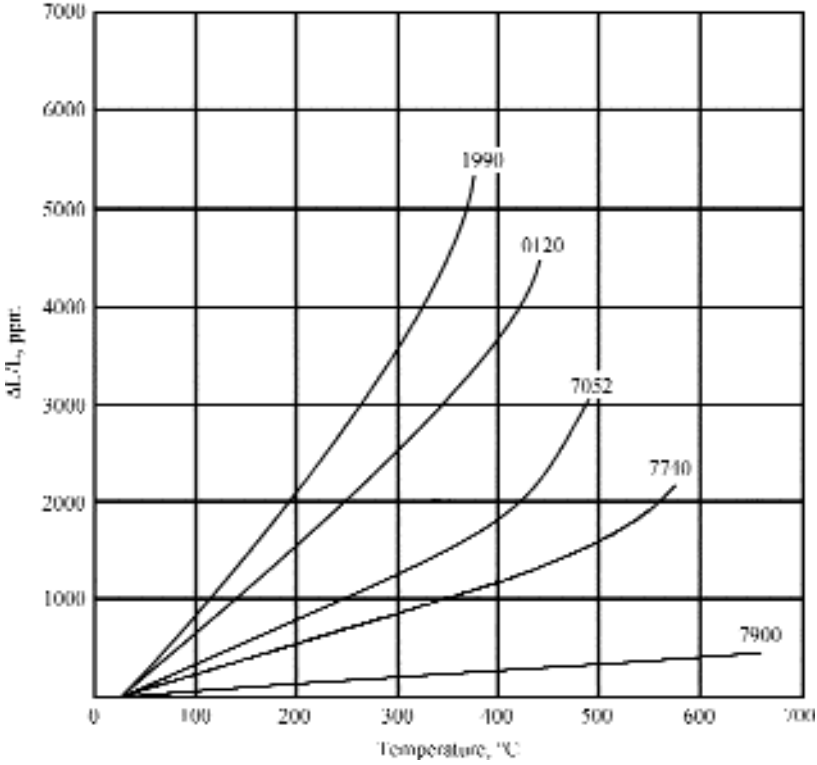

FIGURE 1.10 Thermal expansion characteristics of glass show abrupt increases as temperature approaches melting point. (*From Ref. 63, Fig. 3.9.*)

applications was not feasible. Bovenkerk and coworkers found that catalysts from group VIII metals greatly accelerated the rate of formation of diamond,[64] making possible the commercial production of industrial diamond without prohibitively costly high-pressure apparatus.

Following these developments Japanese scientists discovered two processes for deposition of diamond by chemical vapor deposition.[65,66] CVD diamond, as it is known, has made diamond substrates with outstanding thermal, mechanical, and electrical properties available for metal shaping, bearing, and electronic applications. The following sections discuss these developments

1.2.6.1 CVD Diamond. CVD diamond has been the subject of numerous journal articles in recent years. The outstanding properties of single-crystal diamond are repeated without much degradation in CVD diamond. Kempfer, in a 1990 review article, described the effort being put into CVD diamond and diamond-like coatings.[67] Research on CVD substrates, heat sinks, and windows at six US corporations was reported.

Applications of CVD diamond include substrates and heat sinks for electronic packaging; hardened surfaces for cutting tools and abrasives, hardened surfaces for bearings and wear components, and windows for radar and infrared systems.[68]

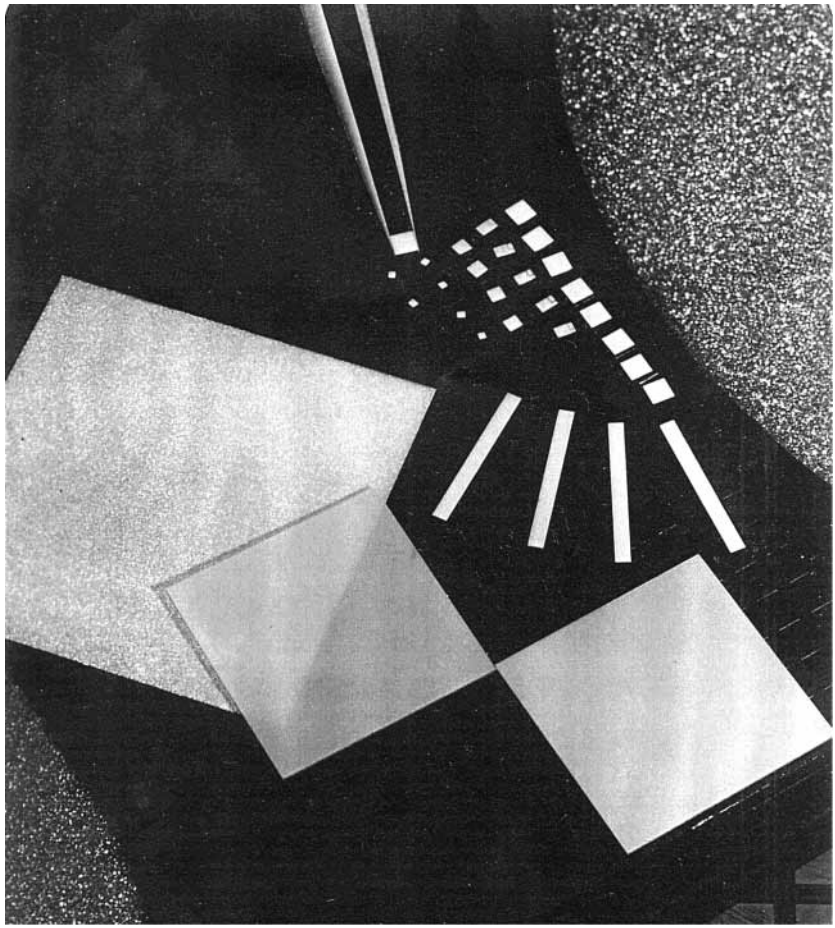

FIGURE 1.11 Free-standing CVD diamond substrates as large as 7 in on a side are commercially available. (*Photo provided by Norton Diamond Film, Northborough, Massachusetts.*)

The use of CVD diamond for electronic packaging was reported in *Electronic Packaging and Interconnection Handbook*.[69] The efforts of numerous companies to use diamond substrates, and the successes and problems, were reported. Norton Diamond Film marketed substrates as large as 6 in in diameter and 1 mm thick, shown in Fig. 1.11. Researchers at several companies, including Raytheon, GE, and the University of Arkansas, demonstrated that circuitry could be fabricated on CVD diamond substrates, and major improvements in thermal management were achieved in the process.[70–72]

These papers and others[73,74] show the efficiency of CVD diamond substrates in removing heat from high-power modules. Its use as a heat sink or heat spreader seems to be feasible in most situations. Problems may occur because of its exceptionally low CTE, since it will eventually interface with a metal or printed wiring board having much higher CTE. It also would usually need to be polished before use as a circuit-bearing substrate, as opposed to

TABLE 1.25 Properties of CVD Diamond

Property	Units	Norton[a] ET 100	P1 Limited[c]	Raytheon[72]	Diamonex, Inc.[d]	Single crystal
Density	g/cm^3	3.51	3.51	3.5		
Coefficient of thermal expansion (Range,°C)	10^{-6}/K	1.2 (25–400)	1.0	3 (25–200)	2 (25–200)	1.2
Hardness	10^4 kg/mm^2		1.0	9–10		7–12,000
Modulus of elasticity	GPa	1140	1200	1143		
Flexural strength	MPa	900				7000[b]
Poisson's ratio		0.09	0.2			
Thermal conductivity	W/(m · K)					
25°C		1200	500–1200, temp. not specified	1600[e]	>1300	18–2200
150°C		1000				
Specific heat	W · s/(g · K)					
25°C		0.52				
150°C						
log volume resistivity, 25°C	Ω · cm	10	Up to 16	>12		15–17
Dielectric constant		5.6[f]	5.7	5.6	5.7	
Loss tangent		0.0001[f]	$<4 \times 10^{-4}$	< 0.001[f]	>0.0005 at 1.5 GHz	

[a]Norton Diamond Film, Northboro, MA.
[b]Vickers.
[c]P1 Limited, Mountain View, CA.
[d]Diamonex, Inc., Allentown, PA.
[e]In plane.
[f]45 MHz to 20 GHz.

a heat sink. The only metallizing option appears to be a thin-film process such as sputtering or evaporation, or the High Density Interconnect (HDI) decal described by DeKenipp.[73]

Kerns et al.[75] have described results obtained with a newly developed composite of copper and micrometer-size Type I diamond powder called Dymalloy. Although the thermal conductivity is considerably lower than that of CVD diamond substrates—420 compared to 1200 W/(m · K)—its thermal expansion coefficient can be tailored to match that of a semiconductor die mounted on it.

The thermal conductivity of CVD diamond substrates can vary by as much as 50 percent, apparently depending on deposition conditions. Table 1.25 shows the properties of CVD diamond available from various suppliers.

1.2.6.2 Diamond-Like Carbon. Diamond-like Carbon (DLC) is a film deposited by a technique similar in many ways to the CVD techniques used to produce diamond substrates. The main difference is that the deposition is carried out at a substrate temperature of about 150°C, rather than the 1000°C typical of CVD. Thus DLC can be deposited on many materials that cannot withstand the higher deposition temperature. The film is amorphous, with no long-range order. Small sp2 bonded graphitic domains are cross-linked by a small number of diamond-like sp3 bonds. The properties of the film depend on the growth conditions that determine the proportion of sp2 to sp3 bonds. DLC films are much less expensive than CVD films, and do not possess all of the exceptional characteristics. Thermal conductivity, for example, is reported to be in the neighborhood of 75 W/(m · K), compared to values of 1200 and greater for

TABLE 1.26 Properties of Diamond-Like Coating

Property	Units	DLC	CVD diamond
Hardness	kg/mm^2	3–5000	7–12,000
Friction coefficient		0.09–0.29	0.05–0.15
Internal stress		Compressive	Tensile

CVD diamond. DLC films possess the desirable attributes of hardness, resistance to wear, low friction, and resistance to most chemicals and acids. They are finding application as optical coatings and coatings on thin-film magnetic disks for wear resistance.

The properties of diamond film are presented in Table 1.26.

1.3 SUMMARY

The mechanical, thermal, and electrical properties of numerous ceramic materials have been presented in this chapter. Neither the number of materials nor the properties cited more than scratch the surface of data that are available, either in the literature or from numerous databases that are accessible through the Internet. Later chapters of this handbook, and publications referred to in the text, should be consulted if in-depth coverage is needed. It is hoped that enough data have been presented in this chapter to provide a guide for deeper investigations as needed.

REFERENCES

1. S. Saito, in *Fine Ceramics,* S. Saito (ed.), Elsevier Science Publishing, New York, 1988.
2. F. H. Norton, in *Fine Ceramics Technology and Applications,* McGraw-Hill, 1970.
3. D. E. Harrison and C. J. Moratis, in *Handbook of Materials and Processes for Electronics,* C. A. Harper (ed.), McGraw-Hill, New York, 1970.
4. D. M. Mattox, in *Electronic Materials and Processes Handbook,* 2d ed., C. A. Harper and R. M. Sampson (eds.), McGraw-Hill, New York, 1994.
5. M. M. Schwartz, *Handbook of Structural Ceramics,* McGraw-Hill, New York, 1992, pp. 1.1–2.35.
6. R. C. Buchanan, *Ceramic Materials for Electronics,* Marcel Dekker, New York, 1986, pp. 1–66.
7. *McGraw-Hill Encyclopedia of Science and Technology,* vol. 4, 8th ed., 1997, pp. 114 ff., McGraw-Hill, New York.
8. B. R. Lawn and D. B. Marshall, *J. Am. Ceram. Soc.,* vol. 62, pp. 347–350, 1979.
9. MIL-STD 1942A, Fig. 1.
10. S. Saito, in *Fine Ceramics,* S. Saito (ed.), Elsevier Science Publishing, New York, 1985, p. 222.
11. *Van Nostrand's Scientific Encyclopedia,* 8th ed., p. 1451, Van Nostrand Rheinhold, New York.
12. D. E. Harrison and C. J. Moratis, in *Handbook of Materials and Processes for Electronics,* C. A. Harper (ed.), McGraw-Hill, New York, 1970, p. 3.19.
13. "Materials Handbook," *Ceramic Industry,* January 1989, pp. 21 ff. Corcoran Communications, Solon, Ohio.
14. D. M. Mattox, in *Electronic Materials and Processes Handbook,* 2d ed., C. A. Harper and R. M. Sampson (eds.), McGraw-Hill, New York, 1994, Fig. 3.4.

15. D. E. Harrison and C. J. Moratis, in *Handbook of Materials and Processes for Electronics,* C. A. Harper (ed.), McGraw-Hill, New York, 1970, Fig. 10.
16. W. H. Class, "Thin Film Processing on Dielectric Substrates," *Solid State Technology,* August 1974, pp. 32–36.
17. J. R. Bosnell and K. H. Lloyd, "Substrate Composition and High Microwave Performance," *Electronic Packaging and Production,* November 1972, pp. 31–36.
18. R. E. Mistler, D. J. Shanefield, and R. B. Runk, "Tape Casting of Ceramics," in *Ceramic Processing Before Firing,* G. Y. Onoda, Jr., and L. L. Hench (eds.), Wiley, New York, 1978, pp. 411–448.
19. B. M. Hargis, "Increase MCM Yields," *Advanced Packaging,* Summer, 1993, pp. 30–33.
20. J. U. Knickerbocker, "Ceramic BGA," *Advanced Packaging,* January/February 1995, pp. 20–25.
21. *Electronic Packaging and Interconnection Handbook,* 3d ed., C. A. Harper (ed.), McGraw-Hill, 2000, pp. 1.88–1.93.
22. W. A. Vitriol and J. I. Steinberg, "Development of a Low Temperature Cofired Multilayer Ceramic Technology," *Proc. 1983 Int. Symp. on Microelectronics,* 1983, pp. 593–598.
23. J. I. Steinberg, S. J. Horowitz, and R. J. Bacher, "Low Temperature Co-Fired Tape Dielectric Material Systems for Multilayer Interconnections," *Solid State Electronics,* pp. 97–101, January 1986.
24. H. T. Sawhill, A. L. Eustice, S. J. Horowitz, J. Gar-El, and A. R. Travis, "Low Temperature Cofirable Ceramics with Co-Fired Resistors," *Proc. 1986 Int. Symp. on Microelectronics,* 1986, pp. 473–481.
25. R. G. Pond and W. A. Vitriol, "Custom Packaging in a Thick Film House Using Low Temperature Cofired Multilayer Ceramic Technology," *Proc. 1984 Int. Symp. on Microelectronics,* 1984, pp. 268–271.
26. R. G. Pond, C. J. Sabo, W. A. Vitriol, and R. L. Brown, "Processing and Reliability of Resistors Incorporated Within Low Temperature Co-Fired Ceramic Structures," *Proc. 1986 Int. Symp. on Microelectronics,* 1986, pp. 461–472.
27. S. Nishigaki et al., "A New Low Temperature Fireable Ag Multilayer Ceramic Having Post-Fired Cu Conductor (LFC-2)," *Proc. 1986 Int. Symp. on Microelectronics,* 1986, pp. 429–449.
28. J. H. Alexander et al., "A Low Temperature Cofiring Tape System Based on a Crystallizing Glass," *Proc. 1991 Int. Conf. on Microelectronics,* 1991, pp. 414–417.
29. D. M. Mattox, "New Choices for Electronic Packaging," *J. Proc. Int. SAMPE Elec. Conf.,* 1992, pp. 659–671.
30. D. M. Mattox, S. R. Gurkovich, J. A. Olenick, and K. M. Mason, "Low Dielectric Constant Alumina-Compatible Co-Fired Multilayer Substrate," *Ceramic Eng. Sci. Proc.,* vol. 9, no. 11–12, 1998, pp. 1567–1568.
31. R. R. Tummala et al., "High-Performance Glass-Ceramic/Copper Multilayer Substrate with Thin Film Redistribution," *IBM J. Res. Develop.,* vol. 36, no. 5, September 1992, pp. 889–902.
32. H. S. Hartmann and C. L. Booth, "Development of a Crystallizable, Low-*K*, Low-Loss, Low Temperature Multilayer Interconnection System," *Proc. Int. Microelectronics Conference,* May 1990.
33. T. K. Gupta, "In Search of Low Dielectric Constant Ceramic Materials for Electronic Packages," *Int. J. Microcircuits and Elec. Packaging,* vol. 17, no. 1, first quarter 1994, pp. 80–98.
34. J. H. Jean and T. K. Gupta, "Properties of a Cristobalite-Free Low-*K* Silica Dielectric," *Int. J. Microcircuits and Elec. Packaging,* vol. 17, no. 2, second quarter 1994, pp. 169–175.
35. K. Miura et al., "Characteristics of Low Temperature Firing Ceramic and Its Application to MCM," *Int. J. Microcircuits and Elec. Packaging,* vol. 18, no. 4, fourth quarter 1995, pp. 336–342.
36. "MCM Process Combines Beryllia Substrate," *Electronic Packaging and Production,* August 1996, p. 81.
37. R. E. Holmes, "Choices Widen for Ceramic Substrates," *Electronic Packaging and Production,* July 1991, pp. 56–58.

38. "Beryllia vs. Boron Nitride: The Heat is On," *Ceramic Industry,* vol. 132, no. 7, July 1989, pp. 34–35.

39. M. B. Powers, "Potential Beryllium Exposure While Processing Beryllia Ceramics for Electronic Applications," Brush-Wellman Engineered Materials, Ceramics Division.

40. E. Foley and G. Rees, "Preliminary Investigation of Potential Beryllium Exposure While Laser Trimming Resistors on Beryllia Substrates," Brush Wellman Corp., TR-8007.

41. B. H. Neimeier, "Zirconia Finds Diverse Applications in Manufacturing," *Ceramic Industry,* vol. 137, no. 5, October 1991, pp. 27–31.

42. "Applications and Preparation of Zirconia and Stabilized Zirconia Powders," Technical Support Team, Stanford Materials Company, San Mateo, California, (http://www.stanfordmaterials.com/zro2.html).

43. D. S. Saito, in *Fine Ceramics,* S. Saito (ed.), p. 172, Elsevier Science Publishing, New York.

44. Y. Kurokawa, K. Utsumi, H. Takamizawa, T. Kamata, and S. Noguchi, "AlN Substrates with High Thermal Conductivity," *IEEE Trans. on Comp., Hybrids, and Man. Technology,* vol. CHMT 8, no. 2, June 1985, pp. 247–252.

45. Y. Kurokawa, H. Hamaguchi, Y. Shimada, K Utsumi, H. Takamizawa, ST. Kamata, and S. Noguchi, "Development of Highly Thermal Conductive AlN Substrates by Green Sheet Technology," *IEEE Trans. On Comp., Hybrids, and Man. Technology,* vol. CHMT 9, no. 2, 1986, pp. 412–418.

46. E. S. Dettmer and H. K. Charles, "Fundamental Characterization of Aluminum Nitride and Silicon Carbide for Hybrid Substrate Applications," *Int. J. Hybrid Microelectron.,* vol. 10, no. 2, 2d quarter 1987, pp. 9–18.

47. P. A. Janeway, "Aluminum Nitride: Making the Grade in Demanding Electronic Applications," *Ceramic Industry,* vol. 137, no. 1, July 1991, pp. 2532.

48. "Aluminum Nitride Plant to be Built by Dow Chemical," *Bull. Am. Ceram. Soc.,* vol. 72. no.10, October 1993, pp. 26–27.

49. B. B. Poole, "Aluminum Nitride Thermal Conductivity: Statistical Analysis of Manufactured Product," *Proc. Int. Symp. Hybrid. Microelectronics,* 1991.

50. Barnewell, P., Brakspear, S., and Cen, Y., "Thick Film Substrates," *Advanced Packaging,* vol. 3, no. 2, March/April 1994, pp. 18–23.

51. B. Van Rees, A. Wohlert, and J. Blum, "Aluminum Nitride Improves MMIC Assembly Efficiency," *Microwaves and RF,* July 1990, pp. 81–86.

52. M. B. Healy and R. Spivey, "Reliable Metallization of Aluminum Nitride," *Electronic Packaging and Production,* vol. 34, no. 11, November 1994, pp. 8–9.

53. "AN 175 Aluminum Nitride Substrates," Intertec Southwest, Inc., Tucson, Arizona.

54. E. Luh, J. W. Lau, D. Horn, and W. Minehan, "Current Processing Capabilities for Multilayer Aluminum Nitride," *Int. J. Microcircuits and Electronic Packaging,* vol. 16, no. 2, 2d quarter 1993.

55. W. Minehan, W. Weidner, R. Jensen, R. Spielbelberger, and W. Jacobsen, "Fabrication, Assembly, and Characterization of Stacked Multichip Modules Using Hot Pressed, Co-fired Aluminum Nitride," *Int. J. Microcircuits and Electronic Packaging,* vol. 17, no. 4, 4th quarter 1994.

56. D. A. Lelonis, "Boron Nitride Tackles the Tough Ones," *Cer. Ind.,* vol. 132, no. 4, April 1989, pp. 57–60.

57. S. Fehr and R. Hill, "Boron Nitride Fillers," *Advanced Packaging,* vol. 6, no. 4, July/August 1997, pp. 44–46.

58. G. T. Hilda, "Sialon, an Alternative to Silicon Nitride," *Cer. Ind.,*vol. 139, no. 7, December 1992, pp. 42–46.

59. M. M. Schwartz, in *Handbook of Structural Ceramics,* McGraw-Hill, New York, 1992, pp. 3.20–3.28.

60. M. Ura and O. Asai, "Development of SiC Ceramics Having High Thermal Conductivity and Electrical Resistivity," *F.C. Report,* vol. 1, no. 4, Japan Fine Ceramics Association, Tokyo.

61. S. Fuchs and P. G. Barnwell, "A Review of Substrate Materials for Power Hybrid Circuits," *Int. J. Microcircuits and Electron. Packaging,* vol. 20, no. 1, 1st quarter 1997, pp. 61–67.

62. *McGraw-Hill Encyclopedia of Science and Technology,* vol. 4, 8th ed., McGraw-Hill, New York, 1997.

63. D. M. Mattox, Sec. 3.4 in *Electronic Materials and Processes Handbook,* 2d ed., C. A. Harper and R. M. Sampson (eds.), McGraw-Hill, New York, 1994.

64. S. Saito, in *Fine Ceramics,* S. Saito (ed.), Elsevier Science Publishing, New York, 1988, pp. 3–9.

65. M. Matsumoto, Y. Sato, Y. Kamo, and N. Setaka, "Vapor Deposition of Diamond Particles from Methane," *Japan. J. Appl. Phys.,* vol. 21, L183, 1982.

66. M. Kamo, Y. Sato, S. Matsumoto, and N. Setaka, "Diamond Synthesis from Gas Phase in Microwave Plasma," *J. Cryst. Growth,* vol. 62, 1983, pp. 642–644.

67. L. Kempfer, "Diamond: A Gem of a Coating," *Materials Engineering,* May 1990, pp. 26–29.

68. "Diamond Coatings Come Out of the Rough," *Design Engineering,* January 1991, pp. 72–78.

69. *Electronic Packaging and Interconnection Handbook,* 3d ed., C. A. Harper, ed., McGraw-Hill, New York, 2000, pp. 1.88–1.93.

70. H. A. Naseem, I. Meyyappan, C. S. Prasad, and W. D. Brown, "Au-Based Metallizations on Diamond Substrates for Multichip Module Applications," *Int. J. of Microcircuits and Electronic Packaging,* vol. 16, no. 4, 4th quarter 1993, pp. 257–270.

71. L. M. Napolitano, Jr., E. Meeks, J. E. Robles, et al., "Development of a Power Electronics Multichip Module on Synthetic Diamond Substrates," op. cit., Ref. 51, pp. 271–278.

72. C. Iacovangelo and E. Jerabek, "Metallizing CVD Diamond for Electronic Applications," *Int. J. Microelectronics and Packaging,* vol. 17, no. 3, 3d quarter 1994, pp. 252–258.

73. R. J. DeKenipp, B. W. Chignola, W. E. Wesolowski, C. W. Ho, and W. E. Johns, "Design, Build, and Characterization of HDI-on-Diamond MCMs," *Int. J. of Microcircuits and Electronic Packaging,* vol. 18, no. 4, pp. 401–409.

74. D. Peterson, J. Sweet, D. Andaleon, R. Renzi, and D. Johnson, "Demonstration of a High Heat Removal CVD Diamond Substrate Edge-Coated Multichip Module," *Int. J. of Microcircuits and Electronic Packaging,* vol. 17, no. 4, 4th quarter 1994, pp. 383–391.

75. J. Kerns, N. Colella, D. Makowiecki, and H. Davidson, "Dymalloy: A Composite Substrate for High Power Density Electronic Components," *Int. J. of Microcircuits and Electronic Packaging,* vol. 19, no. 3, 3d quarter 1996.

CHAPTER 2
CERAMICS, GLASSES, AND MICAS FOR ELECTRICAL PRODUCTS

Don E. Harrison and Christy J. Moratis
Consultants
Pittsburgh, Pennsylvania

2.1 INTRODUCTION

This chapter was written from the viewpoint of the materials technologist. Its aim is to provide the electrical or electronics design engineer with a concise description of the more important electrical and magnetic characteristics of ceramics, glasses, and micas. The contents are divided into four principal sections, namely, insulators, dielectrics, piezoelectrics, and ceramic magnets. For our purposes, we classify materials with permittivities under 12 as *insulators* and those with values over 12 as *dielectrics*. Since the most important application of high-dielectric-constant materials is for capacitive devices, the section on dielectrics is devoted entirely to capacitors. The sections on piezoelectrics and ceramic magnets give descriptions of the phenomena and the extent to which they are affected by the crystal chemistry and the microstructure of the ceramic. In addition to these four topics, reference to some of the more common measuring and testing techniques is given as well. The symbols used are listed in Table 2.1.

We are indebted to the literature generously supplied by the companies cited in the text. In particular, we wish to acknowledge Mr. T. I. Procopowicz of the Sprague Electric Company for supplying us with much unpublished data on ceramic capacitors and for reviewing the section on capacitors, Dr. H. W. Stetson of the Western Electric Company for giving us information on ceramic substrates, and finally from the Westinghouse Research Laboratories thanks are due Dr. A. I. Braginski for reviewing the section on ceramics, and Dr. G. Mott and Mr. J. H. Thompson.

TABLE 2.1 Symbols Used in Test

Symbol	Meaning	Practical units		
		mks	cgs	English
ac	Alternating current			
Å	Angstrom			
AV	Anion vacancies			
B	Magnetic induction	webers/meter^2	gauss	lines/in.^{2}
B_{max}	Maximum magnetic induction	webers/meter^2	gauss	lines/in.^{2}
B_r	Residual induction	webers/meter^2	gauss	lines/in.^{2}
B_dH_d	Peak energy product	(webers)(amp-turns)/meters^3	gauss-oersteds	(lines)(amp-turns)/in.^{3}
c_{ij}	Elastic stiffness constant	newtons/meter^2	dynes/cm^2	lb weight/in.^{2}
C'	Thermal conductivity	cal/(sec)(meter)(°C)	cal/(sec)(cm)(°C)	Btu/(sec)(in.)(°F)
C	Capacitance	farads	farads	farads
CV	Cation vacancies			
d, t	Thickness	meter	cm	in.
D_{ij}	Piezoelectric strain constants	meters/volt = coul/newton	10^7 cm/volt = coul/dyne	in./volt = 0.113 coul/lb weight
d_p	Planar piezoelectric strain constant	meters/volt = coul/newton	10^7 cm/volt = coul/dyne	in./volt = 0.113 coul/lb weight
d_h	Hydrostatic piezoelectric strain constant	meters/volt = coul/newton	10^7 cm/volt = coul/dyne	in./volt = 0.113 coul/lb weight
dc	Direct current			
D	(superscript) At constant electric displacement			
D, D_1 D_3	Electric displacement and its components	coul/meter^2	coul/cm^2	coul/in.^{2}
$D = \tan \delta$	Dissipation factor			
e	Charge on electron	coul	coul	coul
E	(superscript) At constant electric field			
ϵ_r''	Relative loss factor			
E, E_1 E_3	Electric field intensity and its components	volts/meter	volts/cm	volts/in.
E, Y_{ij}	Young's modulus	kg/meter^2	g/cm^2	lb weight/in.^{2}
E	Energy	joules	ergs	ft-lb weight
f, Hz, ω	Frequency	Hz	Hz	Hz

g	Landé g factor			
g_{ij}	Piezoelectric "voltage" constant; electric field/stress at constant charge or strain/ charge density at constant stress	volt-meters/newton = meters^2/coul	volt-cm/dyne = 10^7 cm^2/coul	volt-in./lb weight = 8.85 in.^{2}/coul
g_p	Planar piezoelectric voltage constant	volt-meters/newton = meters^2/coul	volt-cm/dyne = 10^7 cm^2/coul	volt-in./lb weight = 8.85 in.^{2}/coul
g_h	Hydrostatic piezoelectric voltage constant	volt-meters/newton = meters^2/coul	volt-cm/dyne = 10^7 cm^2/coul	volt-in./lb weight = 8.85 in.^{2}/coul
ΔH	Resonance absorption line width	amp-turns/meter	oersteds	amp-turns/in.
H	Magnetic field strength	amp-turns/meter	oersteds	amp-turns/in.
H_c	Magnetic coercive force	amp-turns/meter	oersteds	amp-turns/in.
H_i	Internal magnetic field	amp-turns/meter	oersteds	amp-turns/in.
H_θ^a	Magnetic anisotropy field	amp-turns/meter	oersteds	amp-turns/in.
H_a	Applied magnetic field	amp-turns/meter	oersteds	amp-turns/in.
J	Magnetic moment	amp/meter^2	amp/cm^2	amp/in.^{2}
k_{31}	Transverse coupling factor			
k_{33}	Longitudinal coupling factor			
k_{15}	Shear coupling factor			
k_t	Thickness coupling factor			
k_p	Planar coupling factor			
K_1, K_2	Magnetic anisotropy constants			
L	Angular momentum	(kg)(meter^2)/sec	(g)(cm^2)/sec	(lb weight)(in.^{2})/sec
L	Inductance	henrys	henrys	henrys
m	Mass of electron	kg	grams	lb weight
M	Magnetization	webers/meter^2	gauss	lines/in.^{2}
M_s	Magnetic saturation	webers/meter^2	gauss	lines/in.^{2}
$N_{x,\,y,\,z}$	Demagnetization coefficients			
P	Electric polarization	coul/meter^2	coul/cm^2	coul/in.^{2}
P.F.	Power factor			
Q	Mechanical quality factor			
R''	Thermal stress or shock resistance	cal/(sec)(meter)(°C)^2	cal/(sec)(cm)(°C)^2	Btu/(sec)(in.)(°F)^2

(*Continued*)

TABLE 2.1 Symbols Used in Test (Continued)

Symbol	Meaning	Practical units		
		mks	cgs	English
R	Resistance of sample	ohms	ohms	ohms
R_s	Magnetic squareness ratio			
rf	Radio frequency			
s_{ij}	Elastic compliance constants	meters^2/newton	cm^2/dyne	in.^{2}/ft-lb weight
S	(superscript) At constant strain			
S	Spin momentum	(kg)(meter^2)/sec	(gram)(cm^2)/sec	(lb weight)(in.^{2})/sec
T	(superscript) At constant stress			
T_c	Curie temperature	°C	°C	°F
VHF	Very high frequency	cycles/sec	cycles/sec	cycles/sec
Z	Impedance	ohms	ohms	ohms
α	Linear thermal expansion coefficient	per °C	per °C	per °F
γ	Gyromagnetic ratio			
γ	Surface energy	joules/meter^2	ergs/cm^2	lb-weight/in.^{2}
δ	Loss angle			
ϵ:	Permittivity of free space	farads/meter	farads/cm	farads/in.
ϵ	Permittivity of medium	farads/meter	farads/cm	farads/in.
ϵ_r, K	Relative permittivity or dielectric constant	farads/meter	farads/cm	farads/in.
ϵ_r^*	Complex dielectric constant ($\epsilon_r^* = \epsilon_r' - j\epsilon_r''$)	farads/meter	farads/cm	farads/in.
ϵ, ϵ_{ij}	Strain			
θ	Phase angle			
λ_{ijk}	Magnetostrictive linear dialation	meters	cm	in.
μ_0	Permeability of free space	henrys/meter	gauss/oersted	lines/(amp-turns)(in.)
μ	Permeability of medium	henrys/meter	gauss/oersted	lines/(amp-turns)(in.)
μ_r	Relative permeability			
μ_r^*	Complex relative permeability ($\mu_r^* = \mu_r' - j\mu_r''$)			
tan δ_m	Magnetic dissipation factor			
ρ	Density	kg/meter^2	g/cm^3	lb/in.^{3}
ρ	Electrical resistivity	ohm-meters	ohm-cm	ohm-in.
σ_{ij}	Stress	newtons/meter^2	dynes/cm^2	lb weight/in.^{2}
χ	Susceptibility	henrys/meter	gauss/oersted	lines/(amp-turns)(in.)

2.2 ELECTRICAL TESTS AND MEASUREMENTS

The properties of ceramics, glasses, and micas that are of most interest to the electrical or electronics design engineer include resistivity, dielectric constant, dielectric loss, dielectric strength, and magnetic permeability. The manner in which these properties vary as a function of temperature, frequency, and electric or magnetic field determines the suitability of materials for specific applications. A description of the more common measuring and testing methods is given in the following references:

2.2.1 Resistivity

Guard electrode: ASTM D 257.[2]

Electrode materials: ASTM D 257,[2] Sauer and Flaschen,[3] Landis.[4]

Measuring circuits:

Voltmeter-Ammeter (V-I) Method: ASTM D 257.[2]

Comparison Method: ASTM D 257.[2]

Wheatstone Bridge: Sauer and Shirk.[5]

2.2.2 Dielectric Constant

Dielectric measurements:

Electrodes: ASTM D 150.[6]

Two-terminal System: ASTM D 150.[6]

Three-terminal System: ASTM D 150.[6]

Micrometer-Electrode System: ASTM D 150.[6]

Dielectric constant test methods:

Frequency Range (10^0 to 10^7 Hz): ASTM D 150,[6] Von Hippel.[7]

Frequency Range (10^4 to 10^8 Hz): ASTM D 150,[6] Von Hippel,[7] ASTM C 525-63T.[8]

2.2.3 Microwave Properties

Saturation magnetization: ASTM C 527-63T, Foner.[1]

Spin-wave line width: Ollom, Von Aulock.[149]

Complex dielectric constant: ASTM C 525-63T.[8]

Line width and gyromagnetic ratio: ASTM C 524-63T.

2.2.4 Dielectric Strength

Short-time test; slow-rate-of-rise test; step-by-step test: ASTM D 149-64.

Effect of specimen thickness: Comeforo.[71]

Testing frequency: Frisco.[9]

2.2.5 Magnetic Properties

Magnetizing force H: ASTM Publication 371, Magnetic Testing.

Magnetic flux density B: ASTM Publication 371, Magnetic Testing.

Hysteresis curves: Storm.[10]

2.2.6 Piezoelectric Properties

Piezoelectric constants: IRE Standards on Piezoelectric Crystals.[11]

2.3 INSULATORS

The properties of inorganic materials with dielectric constants less than 12 are described in this section under the headings of Ceramics, Glasses, Micas, Substrates, Glass-Ceramics, and Thick Films. Since micas and glasses are also used as dielectrics, the properties associated with capacitor applications are discussed in the section on Dielectrics.

2.3.1 Ceramics

Ceramic materials offer mechanical and electrical properties that make them especially suitable for the electrical and electronics industries. The bulk of electrical ceramics are used either as insulators or as dielectrics. Electrical grade ceramics have more exacting property requirements than the ceramics used for refractory or structural purposes. Properties such as dielectric strength, dielectric constant, dissipation factor, and thermal and electric conductivity are closely related to microstructure as well as to composition and processing.

In common with other insulating materials, ceramic insulators must have low dielectric constants so as to avoid capacitance effects, adequate dielectric strength to withstand the applied voltage without breakdown, low dissipation in order to avoid excessive electrical losses, and mechanical strength sufficient to withstand service conditions.

Oxide ceramics are characterized by their chemical inertness, oxidation resistance, moderately high refractoriness (see Fig. 2.1) and resistivity (see Fig. 2.2), and by their low thermal expansions (see Fig. 2.3), thermal conductivities (see Fig. 2.4), and densities (see Fig. 2.5). Both the electrical resistivity and the thermal conductivity of oxide ceramics decreases with increasing temperature.

Ceramics are subject to failure by thermal shock due to the disruptive stresses that result from the differential dilation between the surface and core of a body. With the relatively slow cooling rates usually encountered in most electrical and electronic applications and with the exception of materials with very low thermal expansion coefficients, the thermal conductivity usually determines the resistance of a ceramic to failure by thermal shock. Listed in Table 2.2 are the thermal stresses or shock resistances of several ceramics as derived from the relation $R'' = C'\sigma/\alpha E$, where C' is the thermal conductivity, σ is the tensile strength, α is the coefficient of thermal expansion, and E is Young's modulus.

2.3.1.1 Electrical Porcelain. A typical electrical porcelain body consists of approximately 50 percent clay [$Al_2Si_2O_5(OH)_4$] and 25 percent each of flint (SiO_2) and of feldspar ($KAlSi_3O_8$). The high clay content gives the green body plasticity, which facilitates easy

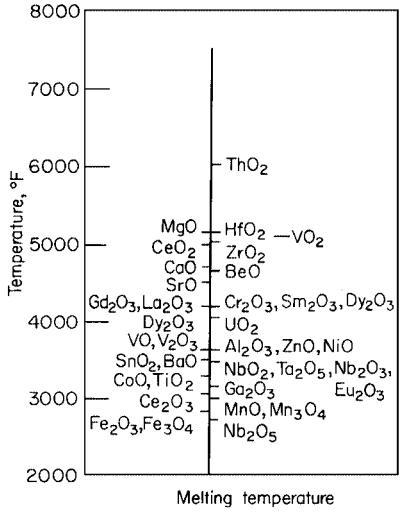

FIGURE 2.1 Melting temperatures of typical oxide ceramics.[65]

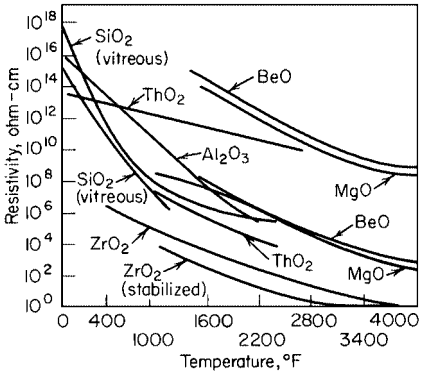

FIGURE 2.2 Relationship between resistivity and temperature of typical oxide ceramics.[66]

fabrication. Feldspar reacts with the clay at high temperatures (1200 to 1300°C) to give mullite and a viscous liquid phase. Solution of flint (1300 to 1400°C) increases the viscosity of the liquid phase and helps to maintain the shape of the body during firing. These compensating changes give porcelain an unusually long firing range and a great tolerance for compositional variations.[16]

The high-loss factor of porcelain is due to the large glass content and to the high mobility of the alkali ions. These ions also cause porcelain to have a relatively low resistivity (see Fig. 2.6). The electrical properties can be improved by replacing the alkali ions with larger and less mobile alkaline-earth ions (Ca^{2+}, Mg^{2+}, Ba^{2+}) and by lowering the glass content. High-alumina porcelains have a dielectric constant nearly constant through the temperature range of most interest (−50 to +250°C) in electronic device application (see Fig. 2.7).

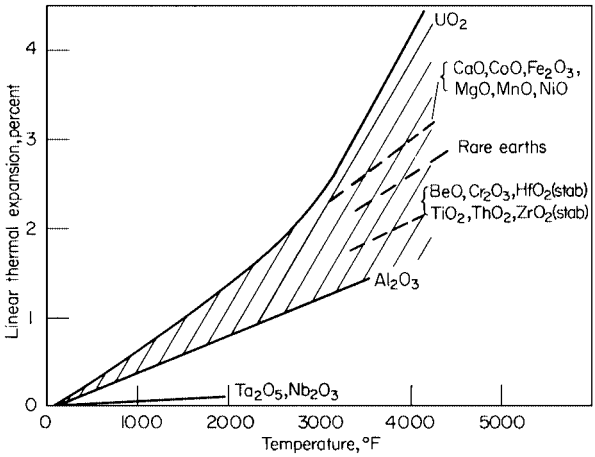

FIGURE 2.3 Linear thermal expansion of typical oxide ceramics.[65]

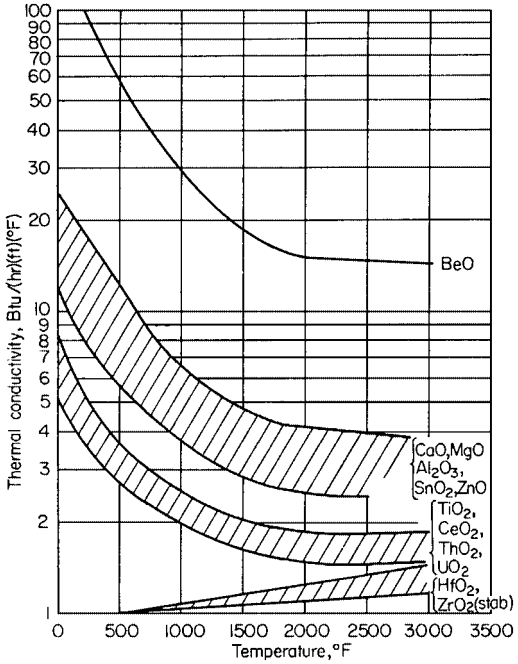

FIGURE 2.4 Thermal conductivities of oxide ceramics.[65]

TABLE 2.2 Thermal Stress Resistance Factor R'' for Various Materials, Calculated from Published Values of C', α, γ, and E[67]

Material	C', cgs	$\alpha \times 10^{-6}$	σ, psi	E, psi $\times 10^{-6}$	$R'' = C'\sigma/\alpha E$
Beryllium oxide	0.53	9.0	10,000	40.0	14.7
Fused silica	0.004	0.5	15,500	10.9	11.4
Pyroceram 9605†	0.01	1.4	20,000*	20.0	7.0*
Sapphire (Linde)	0.065	6.7	35,000	50.0	6.8
Coors AI200	0.05	6.7	26,000	40.2	4.8
Zircon (Coors Z14)	0.009	3.36	11,500	19.4	1.6
Pyroceram 9606†	0.007	5.7	20,000*	18.0	1.36*
Aluminosilicate glass (Corning 1723)	0.005*	4.6	10,000	6–13	1.1*
Steatite (AlSiMag 228‡)	0.006	6.4	10,000	10*	0.94*
Forsterite (AlSiMag 243‡)	0.008	9.1	10,000	10*	0.88*
Soda-lime-silica glass	0.004	9.0	10,000	9.5	0.47
Fireclay	0.0027	5.5	750	2.3	0.16

*Estimated values.
†Trademark of Corning Glass Works, Corning, N.Y.
‡Trademark of American Lava Corp, Ridgefield, N.J.

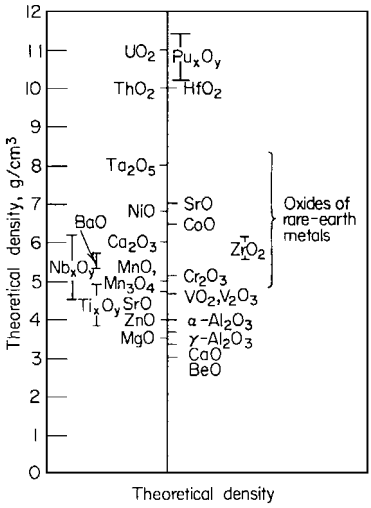

FIGURE 2.5 Density of oxide ceramics.[65]

2.3.1.2 Steatite. Steatite porcelains are low-loss materials that are widely used as components for variable capacitors, coil forms, electron tube sockets and general structural insulation (bushings, spacers, support bars, etc.). These bodies can be manufactured to close dimensional tolerances using automatic dry pressing and extrusion methods. Unlike clay-flint-feldspar porcelains, steatite bodies require close control of the firing temperature, since the firing range is short to obtain vitrified materials. Commercial steatite compositions are

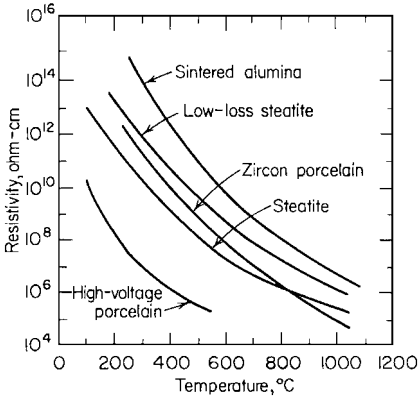

FIGURE 2.6 Decrease in resistivity with temperature for some typical oxide ceramics.[68]

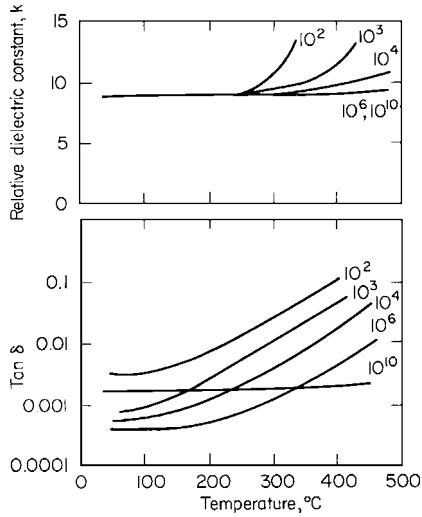

FIGURE 2.7 Dielectric constant and tan δ for an alumina porcelain over a range of temperatures and frequencies.[69]

based on 90 percent talc [$Mg_3Si_4O_{10}(OH)_2$] plus 10 percent clay. Feldspar additions greatly extend the firing range, but they degrade the electrical properties because of the introduction of alkali ions. Low-loss steatite compositions use additional magnesia to combine with the excess silica, and barium oxide as the fluxing agent. The fired body consists of enstatite ($MgSiO_3$) crystals bonded together by a glassy matrix.[16]

Steatite is characterized by a dielectric constant and a dissipation factor that increase with temperature at low frequencies, but are relatively independent of temperature at microwave frequencies (see Fig. 2.8). The physical properties of steatite are listed in Table 2.3.

2.3.1.3 Cordierite. The low thermal expansion coefficient, and consequently the high thermal shock resistance, makes cordierite ($Mg_2Al_4Si_5O_{18}$) bodies useful for electric heater

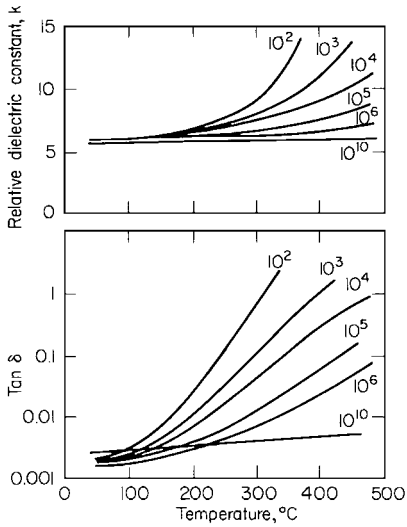

FIGURE 2.8 Dielectric constant and tan δ for a steatite ceramic over a range of temperatures and frequencies.[69]

plates, resistor cores, thermocouple insulators, and burner nozzles. Like steatite, vitrified bodies are difficult to make because of the short firing range. When the intended use is for other than electrical applications, feldspar is added as the fluxing agent in order to increase the firing range. Typical physical properties are listed in Table 2.3.

2.3.1.4 Forsterite. In contrast to either steatite or cordierite, forsterite (Mg_2SiO_4) bodies present few firing problems. The absence of alkali ions in the vitreous phase give forsterite insulators a higher resistivity (see Fig. 2.9) and a lower electric loss with increasing temperature than steatite bodies. Since these low-loss dielectric properties persist at high frequencies, forsterite is used for small microwave tubes such as nuvistors.[17]

The high thermal expansion coefficient makes forsterite suitable for ceramic-to-metal seals, but it also causes the material to have poor thermal shock resistance. Table 2.3 lists the physical properties of forsterite.

2.3.1.5 Alumina. The desirable electrical and mechanical properties possessed by alumina (Al_2O_3) make it suitable for a wide variety of applications. The high strength and refractoriness of alumina permit it to be used for spark-plug insulators, power resistor cores, and missile nose cones. Because of its high dielectric strength (200 volts/mil) and resistivity ($>10^{14}$ Ω-cm), alumina is used for bushings, insulators, and circuit-breaker components. The relatively low dielectric constant (see Fig. 2.7) and the low-loss factor over a wide frequency range make alumina suitable for radome housings, microwave windows, and electron-tube spacers and envelopes.

The dielectric constant and the loss tangent of alumina are affected by impurities, e.g., Si, Ti, Mg, and Ca.[18] Substitution of either Si^{4+} or Ti^{4+} for Al^{3+} in alumina creates donor levels at the impurity sites and acceptor levels at the compensating cation vacancies. Conversely, the substitution of either Mg^{2+} or Ca^{2+} for Al^{3+} creates acceptor levels at the impurity sites and donor levels at the compensating interstitials. These donors and acceptors contribute charge carriers which affect the dielectric and loss characteristics of alumina. Since the solubility of Si^{4+} in Al_2O_3 is limited, excess SiO_2 leads to the formation of a glassy phase at the grain boundaries, and to ionic conduction.

TABLE 2.3 Typical Physical Properties of Ceramic Dielectrics[70]

	Vitrified products						
	1	2	3	4	5	6	7
Material	High-voltage porcelain	Alumina porcelain	Steatite	Forsterite	Zircon porcelain	Lithia porcelain	Titania, titanate ceramics
Typical applications	Power-line insulation	Spark-plug cores, thermocouple insulation, protection tubes	High-frequency insulation, electrical appliance insulation	High-frequency insulation, ceramic-to-metal seals	Spark-plug cores, high-voltage high-temperature insulation	Temperature-stable inductances, heat-resistant insulation	Ceramic capacitors, piezoelectric ceramics
Specific gravity, g/cm^3	2.3–2.5	3.1–3.9	2.5–2.7	2.7–2.9	3.5–3.8	2.34	3.5–5.5
Water absorption, %	0.0	0.0	0.0	0.0	0.0	0.0	0.0
Coefficient of linear thermal expansion, at 20–700°C, 10^{-6} in./(in.) (°C)	5.0–6.8	5.5–8.1	8.6–10.5	11	3.5–5.5	1	7.0–10.0
Safe operating temperature, °C	1,000	1,350–1,500	1,000–1,100	1,000–1,100	1,000–1,200	1,000	—
Thermal conductivity, (cal/cm^2)/(cm)(sec)(°C)	0.002–0.005	0.007–0.05	0.005–0.006	0.005–0.010	0.010–0.015	—	0.008–0.01
Tensile strength psi	3,000–8,000	8,000–30,000	8,000–10,000	8,000–10,000	10,000–15,000	—	4,000–10,000
Compressive strength, psi	25,000–50,000	80,000–250,000	65,000–130,000	60,000–100,000	80,000–150,000	60,000	40,000–120,000
Flexural strength, psi	9,000–15,000	20,000–45,000	16,000–24,000	18,000–20,000	20,000–35,000	8,000	10,000–22,000
Impact strength ($^1/_2$-in. rod), ft-lb	0.2–0.3	0.5–0.7	0.3–0.4	0.03–0.04	0.4–0.5	0.3	0.3–0.5
Modulus of elasticity, psi × 10^{-6}	7–14	15–32	13–15	13–15	20–30	—	10–15
Thermal shock resistance	Moderately good	Excellent	Moderate	Poor	Good	Excellent	Poor
Dielectric strength ($^1/_4$-in.-thick specimen), volts/mil	250–400	250–400	200–350	200–300	250–350	200–300	50–300
Resistivity at room temperature, ohm/cm^3	10^{12}–10^{14}	10^{14}–10^{15}	10^{13}–10^{15}	10^{13}–10^{15}	10^{13}–10^{15}	—	10^3–10^{15}
Te value, °C	200–500	500–800	450–1,000	above 1,000	700–900	—	200–400
Power factor at 1 MHz	0.006–0.010	0.001–0.002	0.0008–0.0035	0.0003	0.0006–0.0020	0.05	0.0002–0.050
Dielectric constant	6.0–7.0	8–9	5.5–7.5	6.2	8.0–9.0	5.6	15–10,000
L grade (JAN Spec. T-10)	L-2	L-2–L-5	L-3–L-5	L-6	L-4	L-3	—

	Semivitreous and refractory products			
	8	9	10	11
Material	Low-voltage porcelain	Cordierite refractories	Alumina, aluminum silicate refractories	Massive fired talc, pyrophyllite
Typical applications	Switch bases, low-voltage wire holders, Light receptacles	Resistor supports, burner tips, heat insulation arc chambers	Vacuum spacers, high-temperature insulation	High-frequency insulation, vacuum-tube spacers, ceramic models
Specific gravity, g/cm^3	2.2–2.4	1.6–2.1	2.2–2.4	2.3–2.8
Water absorption, %	0.5–2.0	5.0–15.0	10.0–20.0	1.0–3.0
Coefficient of linear thermal expansion, at 20–700°C, 10^{-6} in./(in.) (°C)	5.0–6.5	2.5–3.0	5.0–7.0	11.5
Safe operating temperature (°C)	900	1,250	1,300–1,700	1,200
Thermal conductivity, (cal/cm^2)/(cm)(sec)(°C)	0.004–0.005	0.003–0.004	0.004–0.005	0.003–0.005
Tensile strength (psi)	1,500–2,500	1,000–3,500	700–3,000	2,500
Compressive strength, psi	25,000–50,000	20,000–45,000	15,000–60,000	20,000–30,000
Flexural strength psi	3,500–6,000	1,500–7,000	1,500–6,000	7,000–9,000
Impact strength (^{1}/2-in. rod), ft-lb	0.2–0.3	0.2–0.25	0.17–0.25	0.2–0.3
Modulus of elasticity, psi $\times 10^{-6}$	7–10	2–5	2–5	4–5
Thermal shock resistance	Moderate	Excellent	Excellent	Good
Dielectric strength (^{1}/4-in.-thick specimen), volts/mil	40–100	40–100	40–100	80–100
Resistivity at room temperature, ohm/cm^3	10^{12}–10^{14}	10^{12}–10^{14}	10^{12}–10^{14}	10^{12}–10^{18}
Te value, °C	300–400	400–700	400–700	600–900
Power factor at 1 MHz	0.010–0.020	0.004–0.010	0.0002–0.010	0.0008–0.016
Dielectric constant	6.0–7.0	4.5–5.5	4.5–6.5	5.0–6.0
L grade (JAN Spec. T-10)	—	—	—	—

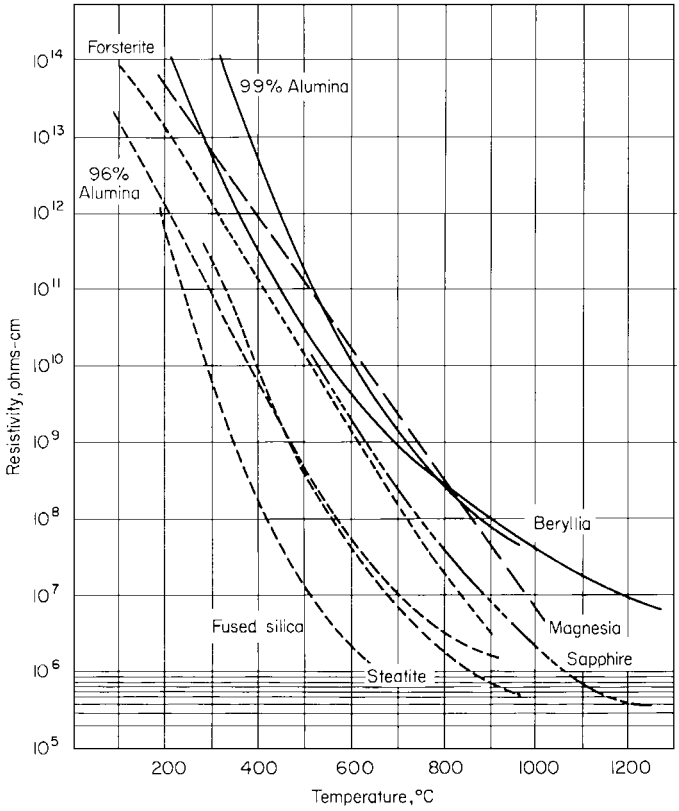

FIGURE 2.9 Change in volume resistivity for various ceramics as a function of temperature.[71]

Ultra-low-loss alumina can be made by eliminating the glassy phase. This is accomplished by sintering pure, fine-grained powder at high temperatures (1800 to 1900°C) to produce a low-porosity body having very small grain size. The problem of residual porosity in Al_2O_3 ceramics affects both the thermal and the optical properties. Below a red heat, thermal conductivity decreases with increasing porosity, since the pores act as a thermal impedance (see Fig. 2.10).[19] The effect of even a small amount of porosity on the optical transmission of Al_2O_3 is drastic (see Fig. 2.11), and emphasizes the difficulty involved in making a translucent ceramic. High-density polycrystalline alumina bodies have been made with sufficient translucency to be used as envelopes for high-intensity lamps.[20]

Alumina ceramics have high elastic moduli ($\sim 50 \times 10^6$ psi) and high strengths (bend strength 20 to 40×10^3 psi), giving them the highest fracture strength among the refractory oxides. In common with other oxide ceramics, the strength begins to decrease rapidly above 1000°C.

Alumina is stable in air, vacuum, water vapor, hydrogen, carbon monoxide, nitrogen, and argon at temperatures up to 1700°C. Hydrogen fluoride will react with alumina. At high temperatures (~1700°C) alumina will vaporize as Al_2O in the presence of either water vapor or reducing atmospheres.[21] A compilation of the electrical and physical properties of alumina is listed in Table 2.4.

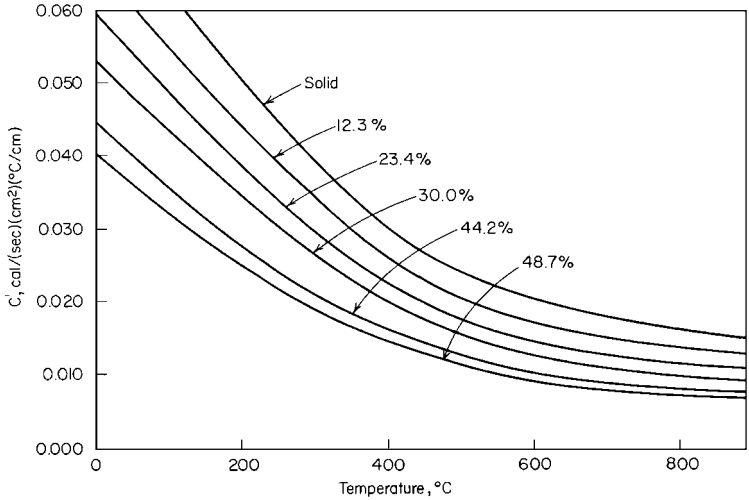

FIGURE 2.10 Thermal conductivity of Al_2O_3 with various amounts of porosity.[19]

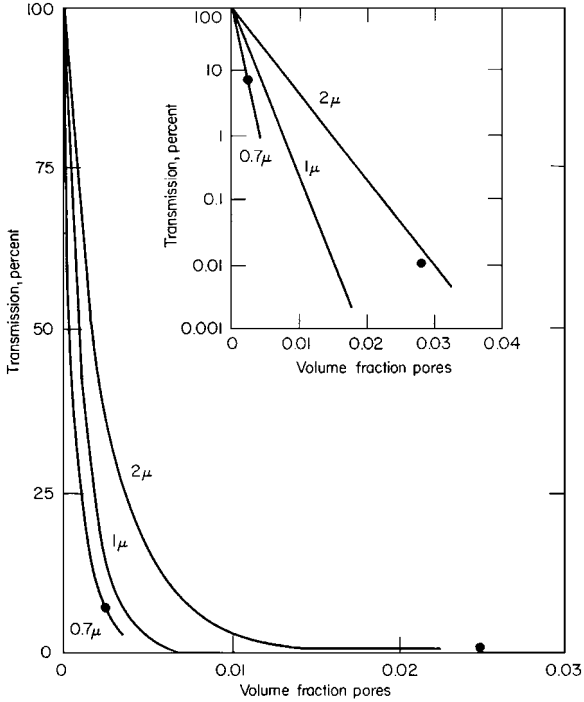

FIGURE 2.11 Transmission of polycrystalline alumina containing small amounts of residual porosity.[72]

TABLE 2.4 Mechanical, Thermal, and Electrical Properties of Coors Alumina and Beryllia Ceramics

Property*	Test	(1) AD-85	(2) AD-90	(3) AD-94	(4) AD-96
Specific gravity:					
Typical	ASTM C 20-46	3.42	3.58	3.62	3.72
Minimum	ASTM C 20-46	3.37	3.53	3.57	3.67
Hardness (typical), Rockwell 45N	ASTM E 1867	75	79	78	78
Surface finish, μin. (arithmetic avg.):					
Typical, as fired	Profilometer (0.030-in. cutoff)	65	65	65	65
Typical, ground	Profilometer (0.030-in. cutoff)	45	40	50	50
Ultimate, lapped	Profilometer (0.030-in. cutoff)	13	3	10	10
Crystal size, microns:					
Range		2–12	2–10	2–25	2–20
Average		7	4	12	11
Water absorption	ASTM C 373-56	None	None	None	None
Gas permeability†		None	None	None	None
Color		White	White	White	White
Compressive strength (typical) psi $\times 10^{-3}$:					
At 25°C	ASTM C 528-63T	280	360	305	300
At 1000°C	ASTM C 528-63T	—	75	50	—
Flexural strength, psi $\times 10^{-3}$:					
At 25°C:					
Typical	ASTM C 369-56 (1/2-in.-diam. rods)	43	49	51	52
Minimum†	ASTM C 369-56 (1/2-in.-diam. rods)	39	44	46	47
At 1000°C:					
Typical	ASTM C 369-56 (1/2-in.-diam. rods)	25	—	20	25
Minimum‡	ASTM C 369-56 (1/2-in.-diam. rods)	20	—	17	20
Tensile strength (typical), psi $\times 10^{-3}$:		22	32	28	28
At 25°C	Brazil test				
At 1000°C	Brazil test	—	15	15	14
Modulus of elasticity, psi $\times 10^{-6}$	Sonic method	33	39	41	44
Shear modulus, psi $\times 10^{-6}$	Sonic method	13	16	17	18
Bulk modulus, psi $\times 10^{-6}$	Sonic method	20	23	24	25
Sonic velocity, 10^3 m/sec	Sonic method	8.2	8.7	8.9	9.1
Poisson's ratio	Sonic method	0.22	0.22	0.21	0.21
Maximum use temperature, °C(°F)		1400 (2550)	1500 (2725)	1700 (3100)	1700 (3100)

Thermal coefficient of linear expansion, 10^{-6} cm/(cm)(°C):		°C	°F	°C	°F	°C	°F	°C	°F		
–200 to 25°C	ASTM C 372-56	3.4	1.3	3.4	1.9	3.4	1.9	3.4	1.9		
25 to 200°C		5.3	3.0	6.1	3.4	6.3	3.5	6.0	3.3		
25 to 500°C		6.2	3.5	7.0	3.9	7.1	3.9	7.4	4.1		
25 to 800°C		6.9	3.8	7.7	4.3	7.6	4.2	8.0	4.4		
25 to 1000°C		7.2	4.0	8.1	4.5	7.9	4.4	8.2	4.6		
25 to 1200°C		7.5	4.2	8.4	4.7	8.1	4.5	8.4	4.7		
Thermal conductivity, cal/(sec)(cm^2) (°C/cm):											
20°C	ASTM C 408-58		0.035		0.040		0.043		0.043		
100°C			0.029		0.032		0.035		0.035		
400°C			0.016		0.017		0.017		0.017		
800°C			0.010		0.010		0.010		0.010		
Specific heat at 100°C, cal/(g)(°C)	ASTM C 351-61		0.22		0.22		0.21		0.21		
Dielectric strength, volts/mil (avg. rms values)		AC	DC	AC	DC	AC	DC	AC	DC		
Specimen thickness, in.:											
0.250	ASTM D 116-69	240	—	235	—	220	—	210	—		
0.125		340	940	320	920	300	1050	275	740		
0.050		440	1250	450	1100	425	1100	370	840		
0.025		550	1550	580	1300	550	1140	450	900		
0.010		720	1750	760	1600	720	1150	580	980		
Dielectric constant:		25°C	500°C	25°C		25°C	500°C	800°C	25°C	500°C	800°C
1 kHz	ASTM D 150-65T	8.2	13.9	8.8		8.9	11.8	—	9.0	10.8	—
1 MHz		8.2	8.9	8.8		8.9	9.7	—	9.0	9.6	—
100 MHz		8.2	—	8.8		8.9	—	—	9.0	—	—
1 GHz		8.2	—	—		8.9	—	—	8.9	—	—
10 GHz		8.2	8.3	8.7		8.9	9.1	9.4	8.9	9.4	9.9
50 GHz		—	—	—		8.7	—	—	8.7	—	—

(*Continued*)

*Footnotes are on page 2.25.

TABLE 2.4 Mechanical, Thermal, and Electrical Properties of Coors Alumina and Beryllia Ceramics (Continued)

Property	Test	(1) AD-85		(2) AD-90	(3) AD-94			(4) AD-96		
Dissipation factor:										
1 kHz	ASTM D 150-65T	0.0014	0.580	0.0006	0.0002	0.215	—	0.0011	0.200	—
1 MHz		0.0009	0.024	0.0004	0.0001	0.008	—	0.0001	0.0039	—
100 MHz		0.0009	—	0.0004	0.0005	—	—	0.0002	—	—
1 GHz		0.0014	—	—	0.0008	—	—	0.0001	—	—
10 GHz		0.0019	0.003	0.0009	0.0010	0.002	0.004	0.0006	0.0009	0.0028
50 GHz		—	—	—	0.0021	—	—	0.0068	—	—
Loss index:										
1 kHz	ASTM #??	0.011	8.06	0.005	0.002	2.54	—	0.010	2.16	—
1 MHz		0.007	0.214	0.004	0.001	0.078	—	0.001	0.037	—
100 MHz		0.007	—	0.004	0.004	—	—	0.002	—	—
1 GHz		0.011	—	—	0.007	—	—	0.001	—	—
10 GHz		0.016	0.025	0.008	0.009	0.018	0.038	0.005	0.008	0.028
50 GHz		—	—	—	0.018	—	—	0.059	—	—
Volume resistivity, ohm/cm^2/cm:										
25°C	ASTM D 1829-66	$>10^{14}$		$>10^{14}$	$>10^{14}$			$>10^{14}$		
300°C		4.6×10^{10}		1.4×10^{11}	9.0×10^{11}			3.1×10^{11}		
500°C		4.0×10^{8}		2.8×10^{8}	2.5×10^{9}			4.0×10^{9}		
700°C		7.0×10^{6}		7.0×10^{6}	5.0×10^{7}			1.0×10^{8}		
1000°C		—		8.6×10^{6}	5.0×10^{5}			1.0×10^{6}		
Te value, °C		850		960	950			1000		

Specific gravity:				
Typical	ASTM C 20-46	3.83	3.84	3.82
Minimum	ASTM C 20-46	3.78	3.80	3.78
Hardness, typical Rockwell 45N	ASTM E 1867	80	81	79
Surface finish, μin. (arithmetic avg.):				
Typical, as fired	Profilometer (0.030-in. cutoff)	55	55	—
Typical, ground	Profilometer (0.030-in. cutoff)	35	35	—
Ultimate, lapped	Profilometer (0.030-in. cutoff)	3	3	—
Crystal size, microns:				
Range		5–50	10–50	10–35
Average		22	20	12
Water absorption	ASTM C 373-56	None	None	None
Gas permeability[†]		None	None	None
Color		White	Pink	Ivory
Compressive strength (typical), psi $\times 10^{-3}$:				
At 25°C	ASTM C 528-63T	345	330	320
At 1000°C	ASTM C 528-63T	130	140	—
Flexural strength, psi $\times 10^{-3}$:				
At 25°C:				
Typical	ASTM C 369-56 ($^1/_2$-in.-diam. rods)	48	45	48
Minimum[‡]	ASTM C 369-56 ($^1/_2$-in.-diam. rods)	45	40	43
At 1000°C:				
Typical	ASTM C 369-56 ($^1/_2$-in.-diam. rods)	30	33	28
Minimum[‡]	ASTM C 369-56 ($^1/_2$-in.-diam. rods)	25	28	—
Tensile strength (typical), psi $\times 10^{-3}$:				
At 25°C	Brazil test	31	28	—
At 1000°C	Brazil test	12	15	—
Modulus of elasticity, psi $\times 10^{-6}$		50	52	50
Shear modulus, psi $\times 10^{-6}$	Sonic method	21	22	21
Bulk modulus, psi $\times 10^{-6}$	Sonic method	29	30	—
Sonic velocity, 10^3 m/sec	Sonic method	9.4	9.7	9.4
Poisson's ratio	Sonic method	0.21	0.21	0.21
Maximum use temperature, °C(°F)		1725 (3140)	1750 (3180)	1950 (3540)

(*Continued*)

*Footnotes are on page 2.25.

TABLE 2.4 Mechanical, Thermal, and Electrical Properties of Coors Alumina and Beryllia Ceramics (Continued)

Property*	Test	(5) AD-99		(6) AD-995		(7) AD-998	
Thermal coefficient of linear expansion, 10^{-6} cm/(cm)(°C):		°C	°F	°C	°F	°C	°F
−200 to 25°C	ASTM C 372-56	3.4	1.9	3.4	1.9	3.4	1.9
25 to 200°C		6.3	3.5	6.3	3.5	6.7	3.7
25 to 500°C		7.3	4.0	7.3	4.1	7.3	4.1
25 to 800°C		7.9	4.4	7.8	4.4	7.8	4.4
25 to 1000°C		8.2	4.6	8.1	4.5	8.0	4.5
25 to 1200°C		8.4	4.7	8.3	4.6	8.3	4.6
Thermal conductivity, cal/(sec)(cm^2) (°C/cm):							
20°C	ASTM C 408-58	0.070		0.075		0.070	
100°C		0.055		0.065		0.055	
400°C		0.025		0.028		0.025	
800°C		0.015		0.017		0.015	
Specific heat at 100°C, cal/(g)(°C)	ASTM C 351-61	0.21		0.21		0.21	
Dielectric strength, volts/mil (avg. rms values): Specimen thickness, in.:		AC	DC	AC	DC		
0.250	ASTM D 116-69	215	—	225	—		
0.125		290	800	310	840		
0.050		390	900	450	1050		
0.025		480	980	550	1150		
0.010		600	1100	625	1300		
Dielectric constant:		25°C	500°C	800°C	25°C	500°C	800°C
1 kHz	ASTM D 150-65T	9.4	11.3	—	9.4	—	—
1 MHz		9.4	10.0	—	9.4	10.3	—
100 MHz		—	—	—	—	—	—
1 GHz		9.4	10.0	10.5	9.4	10.4	11.0
10 GHz		9.4	10.0	10.4	9.4	9.8	10.2
50 GHz		—	—	—	—	—	—

Dissipation factor:							
1 kHz	ASTM D 150-65T	0.0042	0.1500	—	0.0004	—	—
1 MHz		0.0002	0.0047	—	0.0001	0.0023	—
100 MHz		—	—	—	—	—	—
1 GHz		0.0002	0.0003	0.0005	0.0001	0.0002	0.0003
10 GHz		0.0002	0.0002	0.0006	0.0001	0.0003	0.0006
50 GHz		—	—	—	—	—	—
Loss index:							
1 kHz	ASTM #??	0.040	1.70	—	0.004	—	—
1 MHz		0.002	0.047	—	0.001	0.024	—
100 MHz		—	—	—	—	—	—
1 GHz		0.002	0.003	0.005	0.001	0.002	0.003
10 GHz		0.002	0.002	0.006	0.001	0.003	0.006
50 GHz		—	—	—	—	—	—
Volume resistivity, ohm/cm^2/cm:							
25°C	ASTM D 1829-66		$>10^{14}$			$>10^{14}$	$>10^{14}$
300°C			1.0×10^{13}			1.5×10^{11}	$>10^{13}$
500°C			6.3×10^{10}			1.4×10^{9}	6.3×10^{11}
700°C			5.0×10^{8}			4.0×10^{7}	3.4×10^{9}
1000°C			2.0×10^{6}			8.0×10^{5}	7.8×10^{6}
Te value, °C			1050			980	1140

(*Continued*)

*Footnotes are on page 2.25.

TABLE 2.4 Mechanical, Thermal, and Electrical Properties of Coors Alumina and Beryllia Ceramics (Continued)

Property*	Test	(8) AD-999	(9) Vistal	(10) BD-995-2
Specific gravity:				
Typical	ASTM C 20-46	3.96	3.99	2.90
Minimum		3.94	3.98	2.86
Hardness (typical), Rockwell 45N	ASTM E 1867	90	85	67
Surface finish, μin. (arithmetic avg.):				
Typical, as fired	Profilometer (0.030-in. cutoff)	20	25	22
Typical, ground		35	35	20
Ultimate, lapped		<1	<1	—
Crystal size, microns:				
Range		1–6	50–45	10–40
Average		3	20	24
Water absorption	ASTM C 373-56	None	None	None
Gas permeability†		None	None	None
Color		Ivory	Translucent white	White
Compressive strength (typical), psi $\times 10^{-3}$:				
At 25°C	ASTM C 528-63T	550	370	310
At 1000°C		280	70	40
Flexural strength, psi $\times 10^{-3}$:				
At 25°C:				
Typical	ASTM C 369-56 ($^1/_2$-in.-diam. rods)	95	41	40
Minimum‡		89	—	35
At 1000°C:				
Typical		70	25	—
Minimum‡		65	—	—
Tensile strength (typical), psi $\times 10^{-3}$:				
At 25°C	Brazil test	48	30	20
At 1000°C		32	15	5
Modulus of elasticity, psi $\times 10^{-6}$	Sonic method	56	57	51
Shear modulus, psi $\times 10^{-6}$		23	23.5	20
Bulk modulus, psi $\times 10^{-6}$		—	—	—
Sonic velocity, 10^3 m/sec		9.9	9.9	11.1
Poisson's ratio		0.22	0.22	0.26
Maximum use temperature, °C(°F)		1900 (3450)	1900 (3450)	1850 (3360)

		°C	°F	°C	°F	°C	°F
Thermal coefficient of linear expansion, 10^{-6} cm/(cm)(°C):							
−200 to 25°C	ASTM C 372-56	3.6	2.0	3.4	1.9	2.4	1.3
25 to 200°C		6.5	3.6	6.5	3.6	6.4	3.6
25 to 500°C		7.4	4.1	7.4	4.1	7.7	4.3
25 to 800°C		7.8	4.3	7.8	4.3	8.5	4.7
25 to 1000°C		8.0	4.5	8.0	4.5	8.9	4.9
25 to 1200°C		8.3	4.6	8.3	4.6	9.4	5.2

Thermal conductivity, cal/(sec)(cm^2) (°C/cm):					
20°C	ASTM C 408-58	0.074	0.095	0.67	
100°C		0.055	0.070	0.48	
400°C		0.031	0.030	0.20	
800°C		—	—	0.07	
Specific heat at 100°C, cal/(g)(°C)	ASTM C 351-61	0.21	0.21	0.31	

		AC	DC	AC	AC	DC
Dielectric strength, volts/mil (avg. rms values): Specimen thickness, in.:						
0.250	ASTM D 116-69	240	—	230	260	—
0.125		325	920	340	340	830
0.050		460	1050	510	490	—
0.025		590	1200	650	610	—
0.010		800	1450	—	800	—

		25°C	500°C	800°C	25°C	25°C
Dielectric constant:						
1 kHz	ASTM D 150-65T	9.9	—	—	10.1	6.8
1 MHz		9.8	—	—	10.1	6.8
100 MHz		—	—	—	10.1	6.8
1 GHz		—	—	—	—	6.8
10 GHz		9.8	10.3	10.7	10.1	6.7
50 GHz		—	—	—	—	—

(*Continued*)

TABLE 2.4 Mechanical, Thermal, and Electrical Properties of Coors Alumina and Beryllia Ceramics (Continued)

Property	Test	(8) AD-999			(9) Vistal	(10) BD-995-2
Dissipation factor:						
1 kHz	ASTM D 150-65T	0.002	—	—	0.0005	0.001
1 MHz		0.0002	—	—	0.00004	0.0003
100 MHz		—	—	—	0.00006	0.0006
1 GHz		—	—	—	—	0.0006
10 GHz		0.00006	0.0003	0.0008	0.00009	0.0003
50 GHz		—	—	—	—	—
Loss index:						
1 kHz	ASTM #??	0.020	—	—	0.005	0.007
1 MHz		0.002	—	—	0.0004	0.002
100 MHz		—	—	—	0.0006	0.004
1 GHz		—	—	—	—	0.004
10 GHz		0.0006	0.003	0.009	0.001	0.002
50 GHz		—	—	—	—	—
Volume resistivity, ohm/cm^2/cm:						
25°C	ASTM D 1829-66		$>10^{15}$		—	$>10^{17}$
300°C			1.0×10^{15}		—	$>10^{15}$
500°C			3.3×10^{12}		—	5.0×10^{13}
700°C			9.0×10^{9}		—	1.5×10^{10}
1000°C			1.1×10^{7}		—	7.0×10^{7}
Te value, °C			1170		—	1240

Footnotes to Table 2.4

*Ceramic property values vary somewhat according to method of manufacture, size, and shape of part. Closer control of values is possible.

†No helium leak through a 1-in.-diameter plate, 0.001 in. thick, measured at 3×10^{-7} torr vacuum versus approximately 1 atm helium pressure for 15 sec at room temperature.

‡Minimum flexural strength is a minimum mean for a sample of 10 specimens.

(1) AD-85: Nominally 85% Al_2O_3. A good all-round high-alumina ceramic for both electrical and mechanical applications.

(2) AD-90: Nominally 90% Al_2O_3. A tough, fine-grained alumina ceramic especially well suited for demanding mechanical applications.

(3) AD-94: Nominally 94% Al_2O_3. A very good alumina ceramic for metallizing; ideal for all but the most critical electrical and mechanical applications.

(4) AD-96: Nominally 96% Al_2O_3. An excellent alumina ceramic for special electronic applications and many mechanical applications.

(5) AD-99: Nominally 99% Al_2O_3. A very strong, impervious alumina ceramic designed for virtually all kinds of critical electrical and mechanical applications.

(6) AD-995: Nominally 99.5% Al_2O_3. An extremely low-loss alumina ceramic used widely in many electronic applications and some mechanical applications.

(7) AD-999: Nominally 99.9% Al_2O_3. The hardest, strongest, purest alumina ceramic available; recommended for use in ultrasevere mechanical applications and/or highly hostile environments.

(8) Vistal: Registered trademark. Nominally 99.9% Al_2O_3. A translucent, high-purity alumina ceramic for highly critical electrical and electronic applications; strong, excellent resistance to chemical attack.

(9) BD-995-2: Nominally 99.5% BeO. A much-improved beryllia ceramic possessing low dielectric loss, high electrical resistivity, good dielectric strength; meant for use where high thermal conductivity is required.

General Notes:

All measurements are typical for the materials shown. For some specific applications it may be necessary to measure values for use in design formulas. Dielectric constant specifically can be controlled.

Dashes (—) and blank spaces indicate values not measured at this time. All values shown are measured at room temperature unless otherwise specified. All data are typical unless otherwise specified.

Composition Control: alumina and beryllia contents of Coors ceramics are controlled using chemical, spectrographic, and x-ray fluorescent methods for quantitative determination of minor ingredients.

Chemical Resistance: Coors sintered alumina and beryllia ceramics are highly resistant to chemical attack and corrosion. For optimum material selection, it is recommended that specific data on chemical resistance be obtained for particular applications.

Source: Coors Porcelain Company.

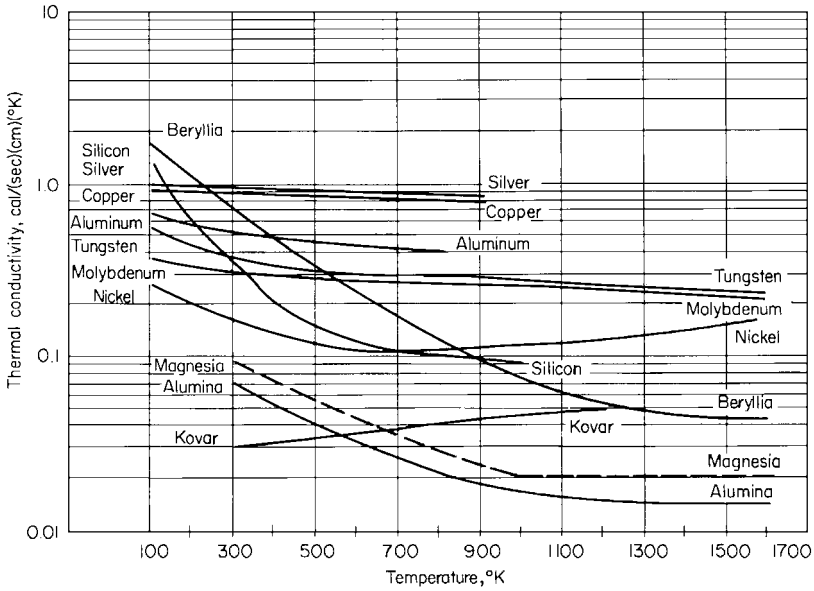

FIGURE 2.12 Thermal conductivity as a function of temperature for various materials.[71]

2.3.1.6 Beryllia. BeO offers the unusual combination of high thermal and high electric conductivity. At room temperature, the thermal conductivity is about one-half that of copper, but with increasing temperature the conductivity of beryllia decreases much more rapidly than that of copper (see Fig. 2.12). The high strength and the high thermal conductivity gives BeO good thermal shock resistance.

Beryllia is stable in air, vacuum, hydrogen, carbon monoxide, argon, and nitrogen at temperatures up to 1700°C.[22] Of all the oxides in contact with graphite at high temperatures, BeO is the most stable, and it is resistant to corrosion by liquid alkali metals. Beryllia will react with water vapor above 1650°C to form volatile $Be(OH)_2$, and it will decompose in atmospheres containing halogens or sulfur.

BeO has lower dielectric constant than alumina, but one with about the same temperature dependence (see Fig. 2.13). The temperature dependence of the resistivity of BeO is again similar to that of Al_2O_3 (see Fig. 2.9).

The high cost of BeO has limited its use to critical applications. It is employed for structural and insulating members in electron and traveling-wave tubes, microwave windows in high-power klystrons, and heat sinks for transistors.[23]

In massive form, BeO is not dangerous; however, in the form of powder or dust, beryllia is hazardous to health.[24]

2.3.1.7 Magnesia. MgO is a better electrical insulator than Al_2O_3, particularly at high temperatures. Because of its high thermal expansion (see Fig. 2.3) and low strength, it has poor thermal shock resistance. Although MgO shows little tendency to hydrate in large masses, it will hydrate in powdered form. The combination of high thermal and low electric conductivity makes MgO suitable for insulating thermocouple leads and for heating-core elements.

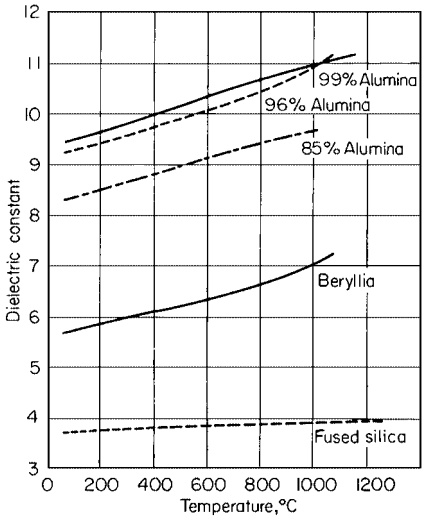

FIGURE 2.13 Dielectric constant as a function of temperature measured at a test frequency of 4 GHz.[71]

2.3.1.8 Zirconia. Dense, crack-free zirconia (ZrO_2) ceramics are difficult to produce because of the disruptive volume change (~10 percent) that occurs during the tetragonal to monoclinic phase transformation at 1000°C. This disruptive phase change is eliminated by stabilizing the cubic form of zirconia with solid solutions of CaO, Y_2O_3, Yb_2O_3, Nd_2O_3, or Sc_2O_3. Stabilized ZrO_2 has relatively poor thermal resistance because of its high thermal expansion coefficient [$\sim 11 \times 10^{-6}$ cm/(cm) (°C), about $1\frac{1}{2}$ times that of alumina] and its relatively low thermal conductivity [0.004 cal/(sec) (cm^2) (°C/cm), about one-fourth that of alumina].

The electrical resistivity of yttria- and calcia-stabilized ZrO_2 decreases with temperature (see Fig. 2.14), primarily owing to the increase in the oxygen ion diffusion rate.[25] This property has led to use of stabilized ZrO_2 for the electrolyte in high-temperature fuel cells.[26] At temperatures between 400 and 1000°C, oxygen ions diffuse through the ceramic electrolyte, whereas gases such as hydrogen, nitrogen, carbon dioxide, carbon monoxide, and water vapor cannot penetrate the zirconia electrolyte. Electronic conduction is negligible under these conditions. A sensitive oxygen detector system operating in the range of 10^{-4} to 10^{+3} torrs and using a stabilized zirconia electrolyte is shown in Fig. 2.15. When the electrolyte is maintained at 850°C, the electric output as a function of pressure follows the relation, emf = 0.056 log (0.2/p), where p in torrs is the oxygen pressure to be measured. Sintered zirconia ceramic heating elements containing up to 15 mole percent MgO have been operated as high as 2000°C. The resistivity of this ceramic decreases from 10^4 ohm-cm at 600°C to 6 ohm-cm at 1200°C.[27]

2.3.1.9 Carbides. Compounds in this group are among the most refractory materials known (see Fig. 2.16). Most carbides are easily oxidized; therefore, they require protective atmospheres at high temperatures (>1000°C). Silicon carbide, on the contrary, has excellent oxidation resistance because of the formation of a protective surface layer of silica. Maximum reported working temperatures for SiC are approximately 1700°C in oxidizing atmospheres and 2200°C in neutral atmospheres.[28]

Silicon Carbide. SiC heating elements are made by pressing rods of granular SiC with a temporary binder and firing at 2000 to 2500°C. After sintering, the bulk resistance of the

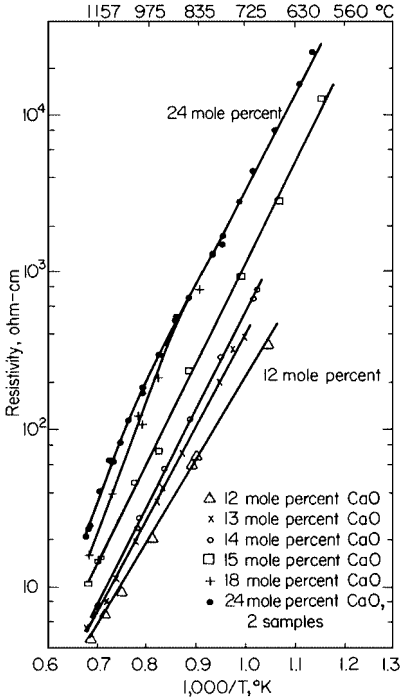

FIGURE 2.14 Temperature-dependent resistivities of zirconia-calcia solutions.[73]

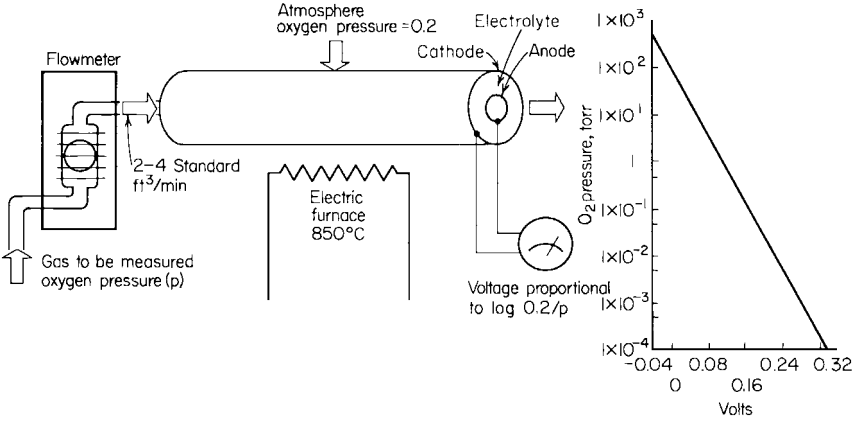

FIGURE 2.15 Oxygen detector using a stabilized zirconia electrolyte.[74] To detect oxygen, gas to be measured is passed through heated fuel cell. Voltage generated by cell is displayed on the voltmeter.

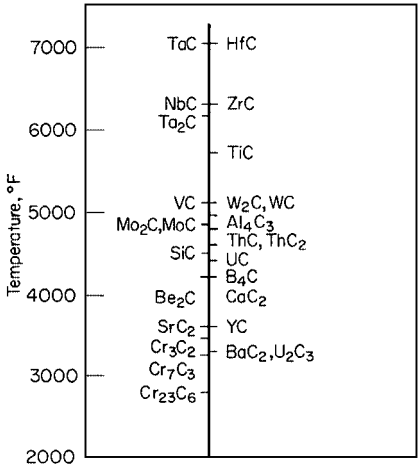

FIGURE 2.16 Melting or decomposition temperature of various carbides.[65]

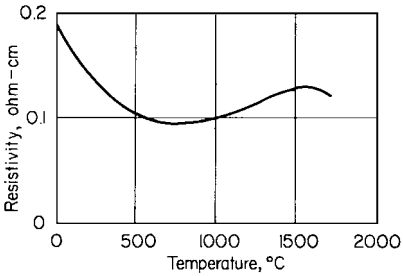

FIGURE 2.17 Resistivity as a function of temperature for a typical SiC heating element.[29]

body is essentially the same as that of the individual grains. A typical resistivity of these rods at room temperature is 0.2 ohm-cm; this decreases to 0.1 ohm-cm at 1000°C (see Fig. 2.17). In the low-temperature region (0 to 750°C), the number of conducting electrons increases progressively with increasing temperature as more and more electrons are released by thermal excitation from impurity centers. Between 750 and 1500°C, thermal vibration decreases the mobility of the conduction electrons, which in turn causes higher resistance. Above 1500°C, intrinsic conduction becomes significant, and the resistivity falls abruptly with increasing temperature.

Nonlinear Silicon Carbide. Nonlinear electrical grade SiC is used for lightning arrestors and in voltage-limiting resistor applications. Practically the entire voltage drop in SiC occurs at the interface between the grains, and it is described by the relation. $V = KI^n$, where K is a constant depending on the geometry of the body, and n is a constant determined by the manufacturing process. The exponent n generally varies from 0.1 to 0.35. The high resistance of nonlinear SiC is attributed to a grain-boundary barrier, which has been given several explanations. One is that the barrier is a layer of silica or silaceous material; another one is that the barrier results from the distribution of space charges in the SiC lattice.[29] The typical relationship between voltage and current in SiC (see Fig. 2.18) shows that an ohmic or linear relationship exists at both very low and very high voltages. In the intermediate voltage range, the *V-I* relationship is nonlinear.

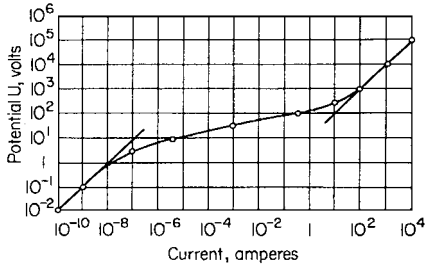

FIGURE 2.18 Voltage-current characteristic of nonlinear SiC.[75]

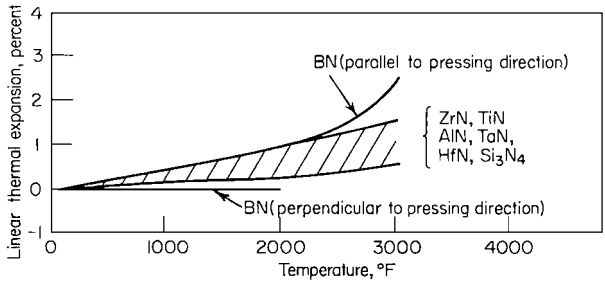

FIGURE 2.19 Linear thermal expansion of various nitrides.[65]

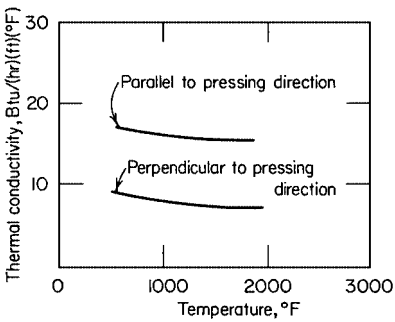

FIGURE 2.20 Thermal conductivity of boron nitride.[65]

2.3.1.10 Nitrides. Nitride ceramics have both low thermal expansions and low thermal conductivites (see Figs. 2.19 and 2.20). Several nitride ceramics have high melting points (see Fig. 2.21); however, they are not oxidation-resistant and are not recommended for use above 1100°C.

Boron Nitride. Massive boron nitride (BN) is made by hot pressing at 2000°C and 1,000 psi. It can be easily machined by conventional edge-cutting methods. Unreacted B_2O_3 will hydrate during exposure to moist air, and it may cause BN to exhibit erratic electrical behavior and spalling during rapid heating. These difficulties can be avoided by thoroughly dehydrating BN at 350°C.

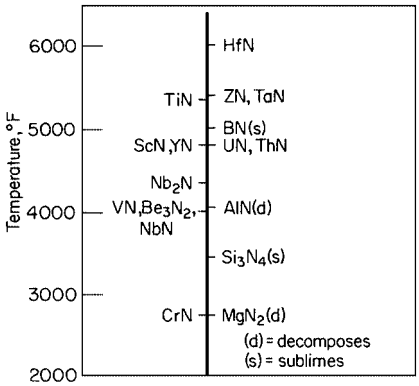

FIGURE 2.21 Melting or decomposition temperature of various nitrides.[65]

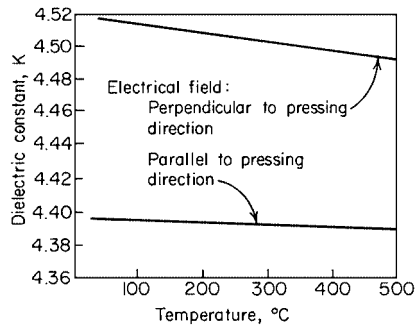

FIGURE 2.22 Dielectric constant of hot-pressed BN over a range of temperatures—test frequency 8.5×10^9 Hz.[76]

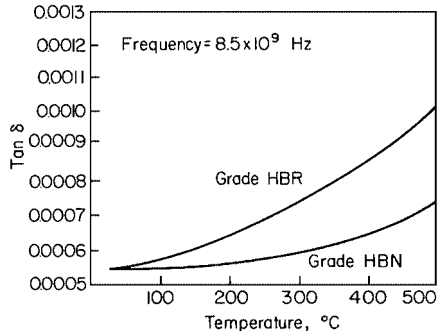

FIGURE 2.23 Loss tangent of hot-pressed BN over a range of temperatures—test frequency 8.5×10^9 Hz.[76]

The dielectric constant and loss tangent of hot-pressed BN are relatively low at microwave frequencies (10^9 Hz) and fairly independent of temperature between 25°C and 500°C (see Figs. 2.22 and 2.23). By careful control of the microstructure, the anistropy in the dielectric constant can be as little as 2 percent. BN has good arc-tracking characteristics,[30] although its electrical resistance is two decades lower than that of alumina (see Fig. 2.24). Hot-pressed BN is used for high-temperature insulation in plasma-arc heaters,

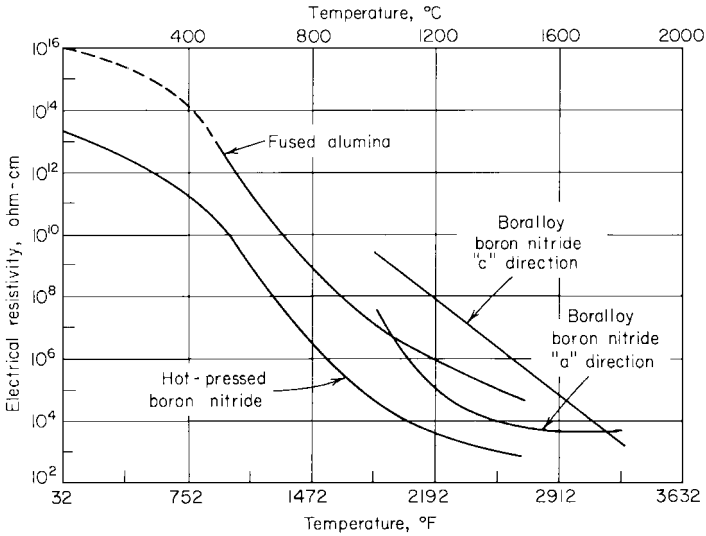

FIGURE 2.24 Electrical resistivity of hot-pressed and pyrolytic (Boralloy) BN.[77] (Boralloy is trademark of Union Carbide Corp.)

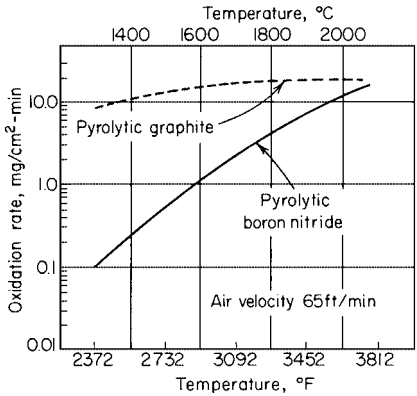

FIGURE 2.25 Oxidation rate of pyrolytic forms of BN and graphite.[77]

refractories for magnetohydrodynamic generators and electric furnaces, heat sinks, and high-temperature capacitors.

Pyrolytic BN in the form of a pure, dense, anistropic film can be deposited at high temperatures from a mixture of ammonia and boron halide. It has a higher electrical resistivity than hot-pressed BN (see Fig. 2.24), but its dielectric constant and loss tangent are about the same. The dielectric strength of BN is rated at 4,000 volts/mil at room temperature, which makes it an excellent insulator. As is illustrated in Fig. 2.25, the oxidation rate of pyrolytic BN is significantly less that that of pyrolytic graphite below 2000°C.

Silicon Nitride. Si_3N_4 is characterized by high resistivity (>10^{12} ohm-cm at 200°C), high strength (>25,000 psi at 1200°C), excellent thermal shock resistance, and chemical

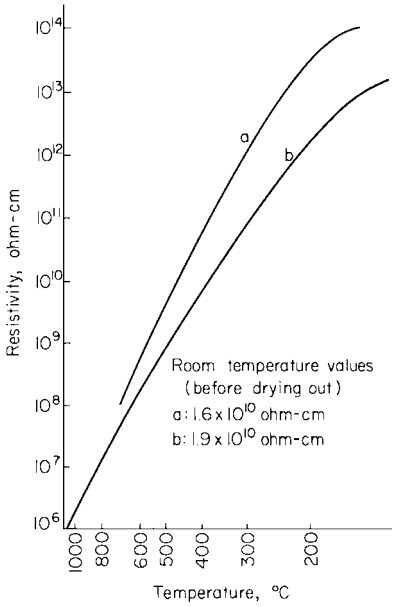

FIGURE 2.26 Electrical resistivity of silicon nitride.[31]

inertness. High-purity Si_3O_4 powder cannot be sintered or hot pressed. However, silicon powder can be nitrided in situ by heating it in nitrogen at between 1250 and 1450°C.[31] Partially nitrided material can be worked by conventional edge-cutting tools. Since little volume change (~1 percent) occurs on nitriding, intricate shapes having close dimensional tolerances can be produced. The porosity of these reaction-sintered bodies depends on the density of the compacted silicon powder, and it is rarely less than 20 percent because of the absence of sintering. Silicon nitride can be hot pressed to theoretical density by using small additions of MgO. As shown in Fig. 2.26, Si_3N_4 has high electrical resistivity; however, unreacted silicon degrades the electrical properties severely.

Pure silicon nitride in the form of a thin, dense electrically insulating layer can be pyrolytically deposited on molybdenum or graphite by heating the substrate to 1000°C in ammonia and passing over it silicon tetrachloride vapors in a nitrogen carrier gas.

2.3.2 Glass

Reproducible electrical properties, ease of fabrication into complex shapes, and low cost are the principal reasons why glass is used in many electrical and structural applications in the electrical industry, e.g., tube envelopes, capacitor dielectrics, and substrates. On the order of 500 to 600 varieties of glass are commercially available, covering a wide range of electrical properties. Silicate glasses exhibit dielectric constants ranging from 3.8 for pure silica to 10 for high-lead glasses and to as much as 25 for certain tellurium- and barium-oxide glasses. Loss factors vary from a tan δ of approximately 0.0009 for vitreous silica to about 0.009 at 60 Hz for soda-borosilicate glasses. At room temperature, most glasses are good electrical insulators (resistivity $>10^{14}$ ohm-cm); however, certain ones are poor insulators with resistivities between 10^2 and 10^9 ohm-cm, and others are semiconductors.

TABLE 2.5 Chemical Compositions (percent by weight) of Some Typical Commercial Glasses[12]

	Soda-lime-silica glasses		Borosilicate glasses			Lead glass	Alkali-free aluminosilicate glasses	
Constituent oxide	Soft soda glass for lamp and valve envelopes	Sheet glass	Chemical and heat resisting glass	A glass for sealing to Kovar	A glass for sealing to tungsten	Glass for lamp and valve pinches	Glass for high-pressure mercury vapor lamps	Electrical fiber glass
SiO_2	70.5	72.8	80.0	65.0	74.6	56.5	54.5	53.5
Al_2O_3	1.8	1.4	2.1	2.3	1.0	1.0	21.1	14.5
B_2O_3	—	—	13.2	24.0	18.0	—	7.4	10.0
CaO	6.7	8.1	—	—	0.3	—	13.3	17.5
MgO	3.4	3.8	—	—	—	—	—	4.5
BaO	—	—	—	—	—	—	3.5	
PbO	—	—	—	—	—	30.0		
Na_2O	16.7	12.8	4.1	4.0	4.2	5.1		
K_2O	0.8	0.7	0.2	4.2	1.7	7.2		

Glass is made up of randomly crosslinked networks of polyhedra, e.g., SiO_4^{-4}, BO_3^{-3}, PO_4^{-3}. In order to lower the vicosity and softening range of pure oxide glasses, alkalies and alkaline-earth oxides are added to the melt. As a result of making the glass structure more open, these ions are able to migrate more freely through the polyhedra and produce ionic conductivity. Thus, if an alkali metal is used as the fluxing agent, potassium is preferred to sodium since it has a lower mobility because of its larger size. The properties of a glass, therefore, can be altered substantially by making the appropriate additions, e.g., Al_2O_3 to improve the strength, PbO to improve the optical quality, and B_2O_3 to increase the resistance to thermal shock.

2.3.2.1 Commercial Glasses. Typical compositions are listed in Table 2.5. The general types of commercial glasses and some of their applications include: (1) soda-lime glasses: inexpensive; used for lamp envelopes, bottles, and window glazing; (2) borosilicate glasses: inexpensive; used for sealing to Kovar* and tungsten, and for ultraviolet transmission and chemical glassware; (3) high-silica glasses: expensive; used for ultrasonic devices, antenna shields, missile nose cones, and high-temperature-service chemical glassware; (4) high-lead glasses: moderately expensive; used for electric-light bulb stems, neon sign tubing, optical devices, quality glassware, and radiation shields for absorbing x-rays and gamma rays; and (5) alkali-free aluminosilicate glasses: moderately expensive; possessing properties similar to those of high-silica glasses; used in high-performance, high-power electron tubes; and in optical-quality aluminosilicate glass employed for electron-tube faceplates and for space-vehicle windows.

2.3.2.2 Electrical Resistivity. Because of its high resistivity, glass is widely used for electrical insulation (see Fig. 2.27). Resistivity is largely determined by the composition of the glass; however, it is affected by temperature, moisture, and structural defects. Since the factors that affect volume and surface resistivity are somewhat different, these properties are treated separately.

* Trademark, Sprague Electric Co.

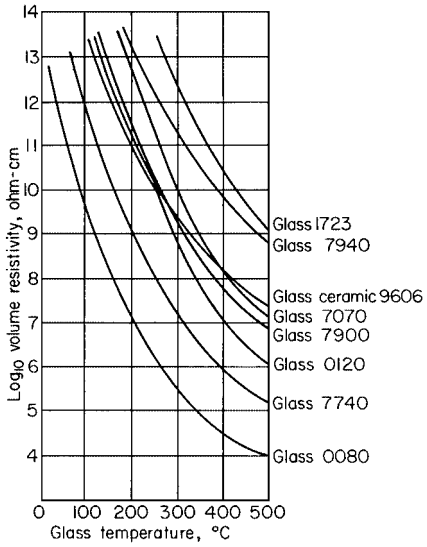

FIGURE 2.27 Volume resistivity as a function of temperature for several Corning glasses.[78]

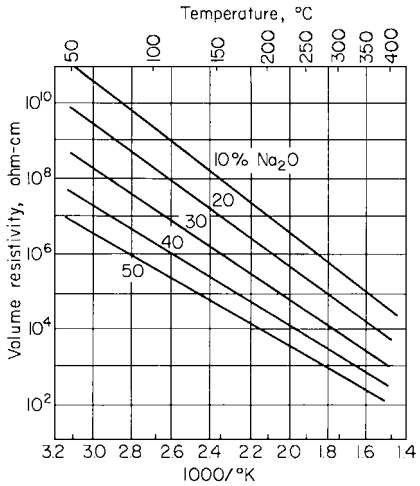

FIGURE 2.28 Effect of increasing the amount of Na_2O in a soda-silica glass on volume resistivity.[79]

2.3.2.3 Volume Resistivity. Electric conductivity in most oxide glasses occurs by ion transport under the influence of an electric field. Because ions such as Li^{1+} and Na^{1+} are relatively small, they can easily move through the glass structure. The K^{1+}, Mg^{2+}, Ca^{2+}, Pb^{2+}, and Ba^{2+} ions, however, are larger and less mobile and, therefore, less able to contribute to the electric conductivity. With increasing alkali content, the degree of crosslinking in the network polyhedra is lowered; consequently, the volume resistivity is decreased in proportion to the alkali content (see Fig. 2.28).

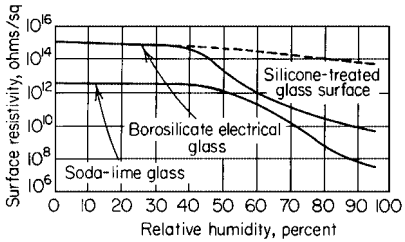

FIGURE 2.29 Effect of relative humidity on surface resistivity of several glasses.[78]

Semiconducting glasses exhibit electronic rather than ionic conductivity. Glasses with resistivities in the range of 10^2 to 10^9 ohm-cm have been reported in the Ge-P-V oxide system[32,33] and in the elemental glasses of either S, Se, or Te combined with one or more of the elements Si, Ge, P, As, Th, and Pb.[34] Electronic devices are described that use semiconducting glasses as the solid-state switch or memory component.[35,36]

Temperature. With increasing temperature, the volume resistivity of oxide glasses decreases (see Fig. 2.27) because of the thermal weakening or breakdown of the bonds between the individual polyhedra. This causes the volume of the interstices to increase, which in turn permits higher mobility of the modifying cations. At the melting temperature, the resistivity of the glass decreases to as low as 10^1 to 10^2 ohm-cm, thereby making it possible to use the glass itself as the electric conductor for melting and sealing operations.

2.3.2.4 Surface Resistivity. The relatively low surface resistivity exhibited by glass under certain conditions is usually caused by either adsorbed moisture of electrolytic substances in the surface.

Moisture. The effect of atmospheric moisture becomes pronounced above 50 percent relative humidity (see Fig. 2.29). Below 50 percent, the surface water does not form a coherent monolayer; therefore, it does not provide an electrical path for conduction. Treating the glass with water-repellent materials such as silicones will lessen the effect of humidity on surface resistivity.

Electrolytic Effects. The chemical resistance of a glass determines its stability in the presence of moisture. Glasses with loosely bound ions, e.g., Na^{1+}, Li^{1+}, will give up these ions to surface moisture and in that way contribute to the surface conductivity. This condition can be avoided by selecting glasses with low alkali contents, e.g., high-silica or aluminosilicate glasses, and by rinsing the surface with a mineral acid to remove surface impurities.[37]

Techniques for Lowering the Surface Resistance. By applying a thin film of either a semiconductor or a metal to the glass, the surface resistivity can be deliberately lowered so as to either eliminate a static charge or to give the desired resistance to the surface. For example, SnO can be applied on glass as an optically transparent conductive coating by hydrolysis of stannic chloride at elevated temperatures. Defrostable aircraft windshields are made by this process.

The surface resistance of high-lead glass can be lowered by a thermal treatment in hydrogen (see Fig. 2.30). This process forms a surface layer of metallic lead approximately 100 Å thick having a resistivity of 800 ohms/sq or greater.[38]

2.3.2.5 Dielectric Strength. A practical requirement of a dielectric is that it be able to withstand the applied voltage stress. Dielectric breakdown can occur by thermal and intrinsic processes. Thermal breakdown is due to localized heating caused by inhomogeneities in the electric field and in the dielectric itself. With increasing temperature, dielectric

TABLE 2.6 Dielectric Strength of Alumina at Several Temperatures[71]

Ceramic	Volts/mil at 60 Hz			
	25°C	400°C	800°C	1000°C
Alumina porcelain (0.125 in. thick)	400	200	50	30–40
Alumina, 99% (electrode spacing 0.038 in.)	450	180	55	35
	(250)*	(70)*	(35)*	(17)*

*Safe maximum values; sample withstood 2,000 hr at these voltages.

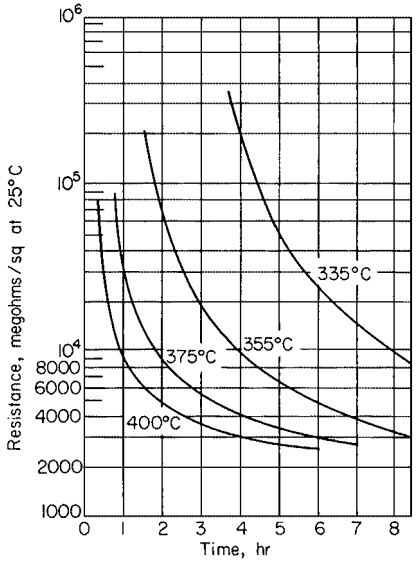

FIGURE 2.30 Surface resistivity of a Ba-Pb-Si oxide glass at room temperature after heating at 335 to 400°C in hydrogen for various periods of time.[38]

strength of typical alumina ceramics decreases by about 40 to 50 volts/ml per 100°C (See Table 2.6). If thermal heating is permitted to increase without limit, chemical breakdown of the dielectric will result in the passage of even higher currents, which in turn leads to fusion, vaporization, and finally puncture of the dielectric.

Intrinsic or electronic breakdown occurs when conduction electrons are accelerated to sufficiently high energies by local field gradients to liberate valence electrons by collision. This avalanche effect continues at an accelerating rate until finally dielectric breakdown results. The dielectric strength of various materials at several frequencies is given in Table 2.7.

The effect of the testing medium on the dielectric strength is shown in Fig. 2.31. The intrinsic breakdown strengths of borosilicate glass *A* and soda-lime-silicate glass *B* are both very high and linearly dependent on the specimen thickness. When these glasses are tested in various mediums, e.g., insulating and semiconducting oils, the breakdown strengths are much lower and nonlinearly related to specimen thickness. A carefully designed glass insulator can have an impulse-voltage strength of 1.7×10^6 volts/cm in air.[39]

Temperature and Time. The dielectric strength of glass decreases with increasing temperature because of the greater ionic conductivity at the higher temperatures (see Fig. 2.32). Regions of instability due to the channeling of the current and the formation of hot spots result in dielectric breakdown by the puncture of the dielectric material.

TABLE 2.7 Dielectric Strengths of Various Insulating Materials at Frequencies from 60 Hz to 100 MHz (rms volts/mil)[80]

Material	Thickness, mils	60 Hz	1 kHz	38 kHz	180 kHz	2 MHz	18 MHz	100 MHz
Polystyrene (unpigmented)	30	3174	2400	1250	977	725	335	220
Polyethylene (unpigmented)	30	1091	965	500	460	343	180	132
Polytetrafluoroethylene (Teflon*)	30	850	808	540	500	375	210	143
Monochlorotrifluoroethylene (Kel-F)‡	20	2007	1478	1054	600	354	129	29†
Glass-bonded mica	32	712	643	—	360	207	121	76
Soda-lime glass	32	1532	1158	—	230	90	55	20†
Dry-process porcelain	32	232	226	—	90	83	71	60†
Steatite	32	523	427	—	300	80	58	56†
Forsterite, (AlSiMag-243)	65	499	461	455	365	210	112	74
Alumina, 85% (AlSiMag-576§)	55	298	298	253	253	178	112	69

*Trademark of E. I. du Pont de Nemours & Co., Inc., Wilmington, Del.
†Puncture with attendant volume heating effect.
‡Trademark of Minnesota Mining and Manufacturing Co., St. Paul, Minn.
§Trademark of American Lava Corp., Ridgefield, N.J.

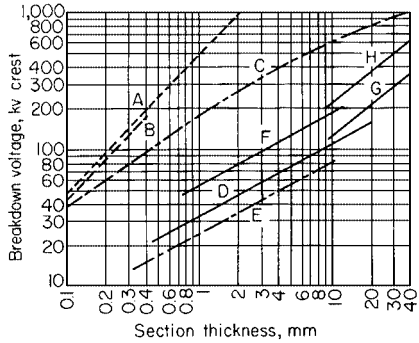

FIGURE 2.31 Breakdown voltage versus thickness of glass for different conditions at room temperature—60-Hz voltage raised continuously. *A*, Intrinsic dielectric strength of borosilicate glass. *B*, Intrinsic dielectric strength of soda-lime glass. *C*, Highest test values available for borosilicate glass. *D*, Borosilicate glass plate immersed in insulating oil. *E*, Soda-lime glass plate immersed in insulating oil. *F*, Borosilicate glass plate immersed in semiconducting oil. *G*, Borosilicate glass power-line insulator immersed in insulating oil. *H*, Borosilicate glass power-line insulator immersed in semiconducting oil.[81]

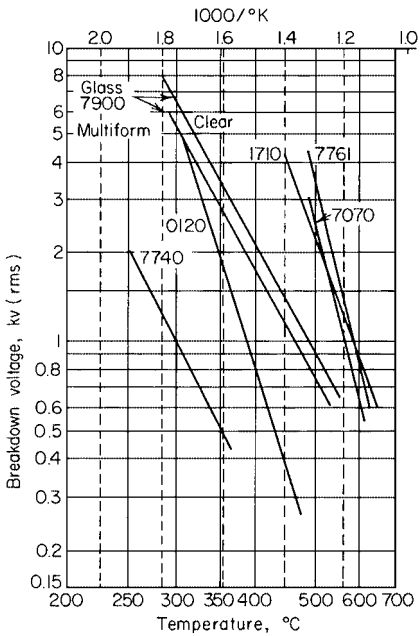

FIGURE 2.32 Dielectric breakdown of several Corning glasses at higher temperature—1-min breakdown for thickness of 2 mm at 60 Hz.[8]

The combined effects of temperature and duration of applied voltage stress on Pyrex* glass are shown in Fig. 2.33. Below −50°C, the breakdown strength is quite high and independent of both temperature and duration of applied voltage stress. Above room temperature, however, the combined effects of higher temperatures and longer testing times do cause a decrease in the dielectric strength.

Frequency. The dielectric strength of glass is lowered at higher frequencies by dipole relaxation processes (see Fig. 2.34). Data listed in Table 2.8 indicate that the dielectric strength of ordinary glass at 100 MHz is 2 to 5 percent of the corresponding value measured at 60 Hz.

2.3.2.6 Dielectric Constant. The dielectric constants of the more common types of glass (silicates, phosphates, borosilicates, and aluminosilicates) vary from a low of 3.8 for fused silica to 8 to 10 for high-lead glasses (see Fig. 2.35). The high polarizability of the Pb^{2+} ion gives rise to the high dielectric constant of high-lead glasses, whereas the absence of such ions in fused quartz accounts for the low permittivity. Tellurium- and barium-oxide glasses with dielectric constants of 25 are reported.[40]

High-dielectric-constant glass-ceramic capacitors are made by crystallizing a ferroelectric phase from the glass.[41] This process requires careful control of the nucleation and growth steps in order to obtain the required electrical properties.

Temperature. The dielectric constant of glass increases with rising temperature in proportion to the polarizability of the medium. When stability of the dielectric properties is required, glasses with rigid structures, e.g., fused silica and high-silica glasses, are used.

*Trademark of Corning Glass Works, Corning, N.Y.

TABLE 2.8 Dielectric Breakdown of Ordinary Glass as a Function of Frequency[84]

	Breakdown voltage, rms kv	
Frequency	0.030 in. thick	0.125 in. thick
60 Hz	38.2	38.4
1 kHz	28.3	
14 kHz	21	
150 kHz	7.5	
2 MHz	2.65	9.25
4.2 MHz	2.0	
9.8 MHz	1.7	
18 MHz	1.7	3.4
100 MHz	0.63	1.9

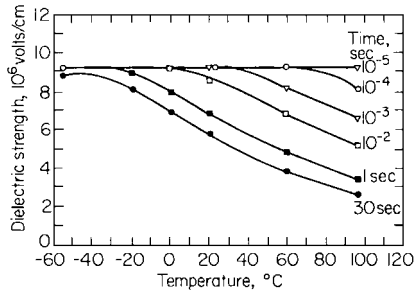

FIGURE 2.33 Effect of test temperature and test duration on the breakdown strength of a Pyrex glass.[82]

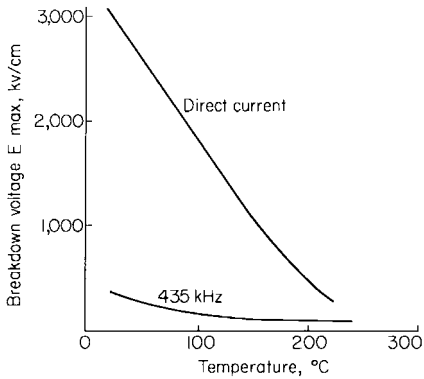

FIGURE 2.34 Breakdown voltage in air for lime glass as a function of temperature for direct current and for 435-KHz alternating current.[83]

Frequency. The dielectric constant of glass decreases very slightly with increasing frequency (see Fig. 2.36). At frequencies above 50 Hz, the relatively long relaxation times typical of silicate glass structures prevents an increase in the dielectric constant. Table 2.9 lists the dielectric constants at several frequencies for a number of commercial glasses.

2.3.2.7 Dielectric Loss. The total dielectric loss in glass is the sum of four different loss mechanisms, namely, conduction, dipole relaxation, vibration, and deformation losses. As

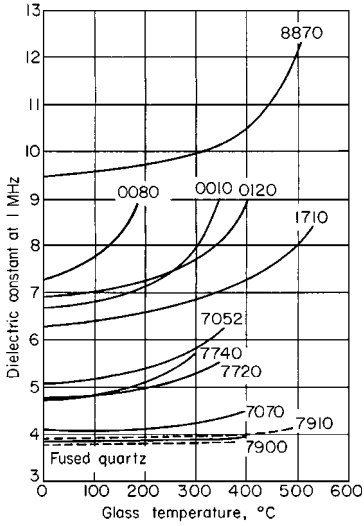

FIGURE 2.35 Dielectric constants of several Corning glasses at 1 MHz as a function of temperature.[81]

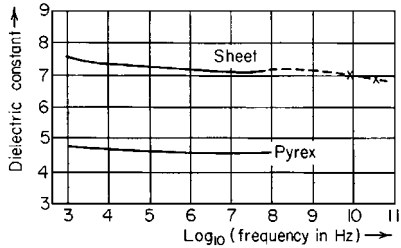

FIGURE 2.36 Dielectric constant as a function of frequency for sheet and Pyrex glasses.[85]

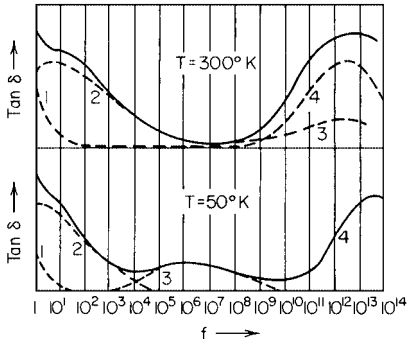

FIGURE 2.37 The general shape of tan δ as a function of the frequency at 300 and 50°K. The fully drawn curves give the total losses. The sum of four different contributions: (1) the conduction losses, (2) the dipole relaxation losses (sometimes called relaxation losses), (3) the vibration losses, (4) the deformation losses.[87]

shown in Fig. 2.37, the magnitude of each of these loss mechanisms varies with frequency and temperature. Conduction and dipole relaxation losses (1 and 2) are the predominant loss mechanisms at low frequencies; whereas vibration and deformation losses (3 and 4) are the controlling mechanisms at high frequencies. These losses generally increase with rising temperature.

Conduction Losses. This loss mechanism is important only at frequencies less than about 50 Hz, where it is described by the relation, $\tan \delta = (2\pi f \rho \epsilon' \epsilon_0)^{-1/2}$. Since the conductivity $1/\rho$

TABLE 2.9 Dielectric Properties of Several Commercial Glasses[86]

Glass	Composition	Temperature, °C	Dielectric properties at: 60 Hz	1 kHz	1 MHz	100 MHz	3 GHz*	25 GHz*	60 Hz	1 kHz	1 MHz	100 MHz	3 GHz*	25 GHz*
			Dielectric constant						Dissipation factor					
Corning 0010	Soda-potash-lead silicate ~20% lead oxide	24	6.70	6.63	6.43	6.33	6.10	5.87	0.0084	0.00535	0.00165	0.0023	0.0060	0.0110
Corning 0120	Soda-potash-lead silicate	23	6.76	6.70	6.65	6.65	6.64	6.51	0.0050	0.0030	0.0012	0.0018	0.0041	0.0127
Corning 1990	Iron-sealing glass	24	8.41	8.38	8.30	8.20	7.99	7.84	—	0.0004	0.0005	0.0009	0.00199	0.0112
Corning 1991		24	8.10	8.10	8.08	8.00	7.92	—	0.0027	0.0009	0.0005	0.0012	0.0038	
Corning 7040	Soda-potash-borosilicate	25	4.85	4.82	4.73	4.68	4.67	4.52	0.0055	0.0034	0.0019	0.0027	0.0044	0.0073
Corning 7050	Soda-borosilicate	25	4.90	4.84	4.78	4.75	4.74	4.64	0.0093	0.0056	0.0027	0.0035	0.0052	0.0083
Corning 7060 (Pyrex)	Soda-borosilicate	25	—	4.97	4.84	4.84	4.82	4.65	—	0.0055	0.0036	0.0030	0.0054	0.0090
Corning 7070	Low-alkali potash-lithia-borosilicate	23	4.00	4.00	4.00	4.00	4.00	3.9	0.0006	0.0005	0.0008	0.0012	0.0012	0.0031
Corning 7720	Soda-lead borosilicate	24	4.75	4.70	4.62	—	4.60	—	0.093	0.0042	0.0020			
Corning 7750	Soda-borosilicate ~80% silicon dioxide	25	—	4.42	4.38	4.38	4.38	—	—	0.0033	0.0018	—	0.0043	
Corning 7900	96% silicon dioxide	20	3.85	3.85	3.85	3.85	3.84	3.82	0.0006	0.0006	0.0006	0.0006	0.00068	0.0013
Fused silica 915c	Silicon dioxide	25	—	3.78	3.78	3.78	3.78	—	—	0.00026	0.00001	0.00003	0.0001	
Quartz (fused)	100% silicon dioxide	25	3.78	3.78	3.78	3.78	3.78	3.78	0.0009	0.00075	0.0001	0.0002	0.00006	0.00025

*GHz = giga Hertz = 10^9 Hz.

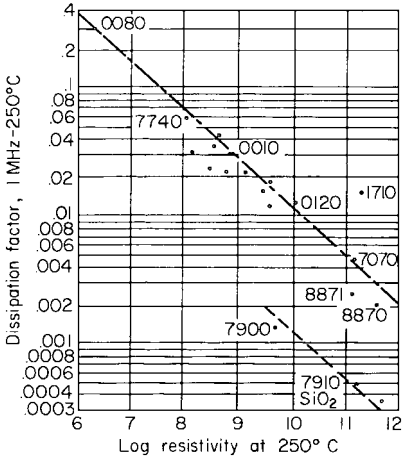

FIGURE 2.38 Relationship between log dissipation factor and log resistivity of several Corning glasses at 250°C.[81]

of glass increases with rising temperature, so also does the conduction loss. Likewise, alkali-rich glasses exhibit greater conduction losses than high-silica glasses.

Dipole Relaxation Losses. Up to about 10^6 Hz, dipole relaxation losses are important. They result from the energy that is given up by mobile ions as they jump over small distances in the network. Dipole losses are greatest when the frequency of the applied field is equal to the relaxation time of the dipole. At frequencies either far above or far below the resonant frequency, the losses are the least. Because of its random structure, glass has more than one relaxation time. This results in a broad distribution of dipole relaxation losses with frequency, rather than one discrete loss peak (see curve 2 in Fig. 2.37).

The dissipation factor at 1 MHz and 250°C for various commercial glasses (see Fig. 2.38) reveals a correlation between high resistivity and low dielectric losses. This is further illustrated in Fig. 2.39 by glasses with low alkali content, having not only lower losses but also showing greater temperature stability. Above 200°C losses become excessive in practically all glasses because of increased ionic conduction.

Deformation Losses. Relaxation and deformation losses are similar in that they are associated with small displacements of ions in the glass network. Deformation losses involve smaller ion movements than do either conduction or dipole relaxation loss mechanisms, and they occur in the region of 10^3 Hz at room temperature (see curve 4 in Fig. 2.37).

Vibration Losses. These losses occur by a resonance phenomena involving both the network-forming ions and the network-modifying ions. As shown in Fig. 2.37 (curve 3), vibration losses take place over a broad frequency range because of the variation in both the mass and the location of the different ions in the glass network. The resonant frequency of this loss mechanism is given by $f_{res} = (A/M)^{1/2}$, where A is a constant relating the displacement and the restoring force, and M is the mass of the ion.

In general, heavy ions, Pb^{2+} or Ba^{2+}, will decrease the resonant frequency of the network whereas lighter ions will shift it to higher frequencies. This is shown in Fig. 2.40 where glass 7910, a high-silica glass, has a slowly increasing dissipation factor at 10^{10} Hz whereas glass 8870, a high-lead glass, has a rapidly increasing loss factor at this frequency.

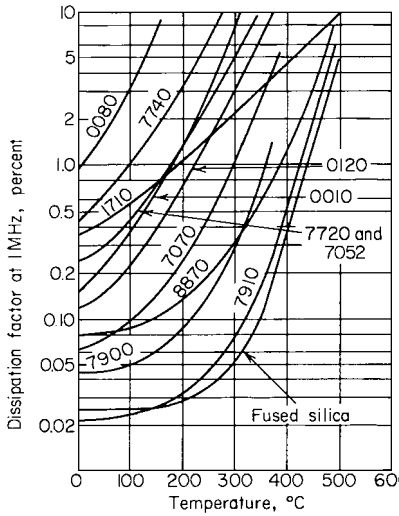

FIGURE 2.39 Dissipation factors of several Corning glasses at 1 MHz as a function of temperature.[81]

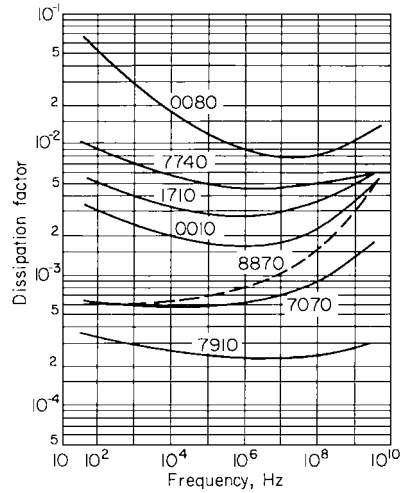

FIGURE 2.40 Dissipation factors at room temperature over a range of frequencies for several Corning glasses.[81]

2.3.3 Mica

Mica is used in the electrical industry as a dielectric in capacitors and as an electrical insulator in motors, electron tubes, transistors, and appliances such as toasters and flatirons. Commercially important mica is a naturally occurring form of a potassium-alumina-silicate mineral. Muscovite or ruby mica [$KAl_3Si_3O_{10}(OH)_2$] is the most desirable form for capacitor use because of its low dissipation factor and high dielectric strength. Phlogopite or amber mica [$KMg_3AlSi_3O_{10}(OH)_2$] has better resistance at high temperature than muscovite, but its

TABLE 2.10 ASTM Specifications and Methods of Test for Mica and Mica Products

D 748-59	Natural block mica and mica films suitable for use in fixed mica-dielectric capacitors
D 351-62	Natural muscovite mica based on visual quality
D 2131-65T	Natural muscovite mica splittings
D 352-63	Pasted mica used in electrical insulation
D 1082-54	Power factor and dielectric constant natural mica
D 1677-62	Untreated mica paper used for electrical insulation sampling and testing
D 374-57T	Thickness of solid electrical insulation
D 1039-65	Testing glass-bonded mica used as electrical insulation
F 12-64T	Mica bridges for electron tubes
F 48-64T	Dimensioning mica bridges
F 652-61T	Measuring mica stampings or substitutes used in electron devices and lamps

electrical properties are not so well suited for use as capacitor dielectrics. Phlogopite mica is used, however, to insulate motor and generator commutator segments, as well as flatiron and toaster heater elements. Fluorophlogopite is a synthetic form of mica ($KMg_3AlSi_3O_{10}F_2$), where the hydroxyl ions have been replaced by fluorine ions. The absence of water in the synthetic composition has resulted in a form of mica that is more stable at elevated temperatures. Other types of commercial mica include glass-bonded mica and ceramoplastic and reconstituted mica.

Mica has a unique combination of electrical properties not available in other materials. The relatively stable dielectric constant, the low-loss tangent, and the high dielectric strength of mica are used to form stable and reliable capacitors for critical circuit applications. Disadvantages of mica are its small capacitance-to-volume ratio and its high cost in the form of large natural sheets. A listing of ASTM specifications and methods of testing mica and mica products is given in Table 2.10.

2.3.3.1 Muscovite—Ruby Mica. Muscovite is chemically inert when in contact with the chemicals typically used in electrical insulation. It is attacked by HF and H_2SO_4 but it is resistant to other acids, solvents, and alkalies. Unless precautions are taken, liquids such as water or oil can work their way in between the laminae of mica by capillary action. Water lowers the electrostatic force of attraction between the layers of mica by an exchange mechanism of hydroxyl for potassium ions.

Outgassing becomes intense above 600°C (Fig. 2.41), and prolonged exposure at higher temperatures results in further release of water and finally in decomposition of the mica.[42] For this reason, mica spacers and insulators should be outgassed before being used in vacuum tubes or other devices where outgassing is a problem.

Muscovite is easily split into thin uniform sheets because of its planar cleavage habit. Efforts to mechanize the splitting process have not been successful, and splitting is still a hand operation.

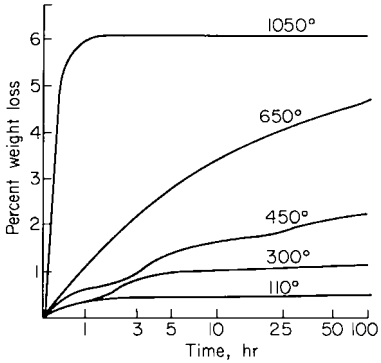

FIGURE 2.41 Change of total percentage weight loss as a function of time for pulverized muscovite held at various temperatures in air.[42]

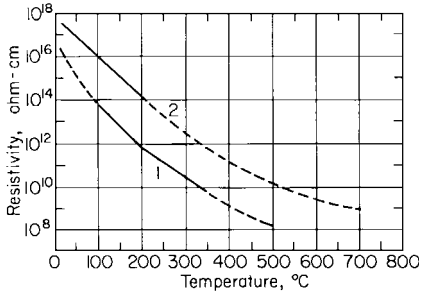

FIGURE 2.42 Electrical resistivity of muscovite mica as a function of temperature.[88]

The electrical resistivity of muscovite decreases with increasing temperature, as shown in Fig. 2.42. Because of the removal of moisture from the surface as well as from between the exfoliated layers, the electrical resistivity of the degassed mica is higher than that of the untreated material.

Muscovite has a high dielectric strength that averages between 3,000 and 6,000 volts/mil at 60 Hz for specimens 1 to 3 mils thick. It has a relatively stable dielectric constant over a wide frequency range, as is shown in Fig. 2.43. Muscovite also has a dissipation factor (tan δ) that decreases with frequency. This makes ruby mica an especially useful dielectric for high-frequency applications.

2.3.3.2 Phlogopite—Amber Mica. Phlogopite is more stable at higher temperatures (850 to 1000°C) than muscovite. However, the higher dissipation factor and lower dielectric strength of phlogopite prevents it from being used in capacitor applications. Phlogopite is used mainly for insulation in transformers, motors, and soldering irons, and as insulating washers or disks. The thermal conductivity of phlogopite is about the same as that of muscovite.

2.3.3.3 Synthetic Mica—Fluorophlogopite. A synthetic form of mica is made by heating a mixture of silica, alumina, magnesia, and fluoride compounds. Fluorophlogopite mica has better temperature-resistance properties than muscovite mica (Table 2.11) because the structure contains no water.

TABLE 2.11 Properties of Mica[13]

Property	Natural mica		Synthetic mica
	Muscovite	Phlogopite	Fluorophlogopite
Volume resistivity, ohm-cm:			
At 20°C	10^{16}–10^{14}	Lower than muscovite at low temperature	10^{16}–10^{17}
At 500°C	10^{8}–10^{10}	Higher at high temperatures	
Dielectric strength (1–3-mil specimen), volts/mil	3,000–6,000	3,000–4,000	2,000–3,000
Dielectric constant:			
At 100 Hz	5.4		
At 1 MHz	5.4	6	5–6
At 100 MHz	5.4		
Dissipation factor:			
At 100 Hz	0.0025		
At 1 MHz	0.0003	0.001–0.01	0.0004–0.0007
At 100 MHz	0.0002		
Safe operating temperature, in vacuo, °C	350–450	—	1,000
Water absorption	Practically zero	Practically zero	Practically zero
Compressive strength, psi	25,000	15,000	

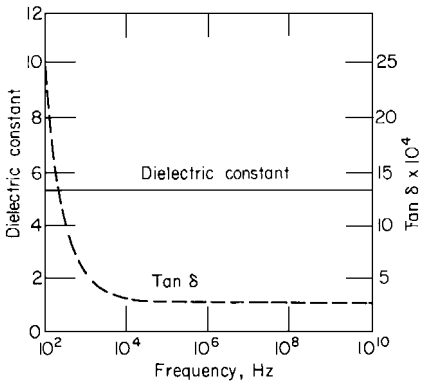

FIGURE 2.43 Dielectric constant and tan δ for muscovite mica over a range of frequencies.[89]

The cleavage of synthetic mica is similar to that of natural mica. Synthetic fluorophlogopite has a lower dielectric strength than natural muscovite (Fig. 2.44). However, it can be used at a much higher operating temperature than muscovite. A method of obtaining single-crystal sheets of fluorophlogopite up to 3 in. in diameter and 3 to 10 mils thick has been developed.[43]

2.3.3.4 Reconstituted Mica. Reconstituted mica is a sheet material made from thin flakes of either natural or synthetic mica that have been ground up, pressed into sheet form, and heated under pressure to bond the tiny mica flakes together. Reconstituted natural mica

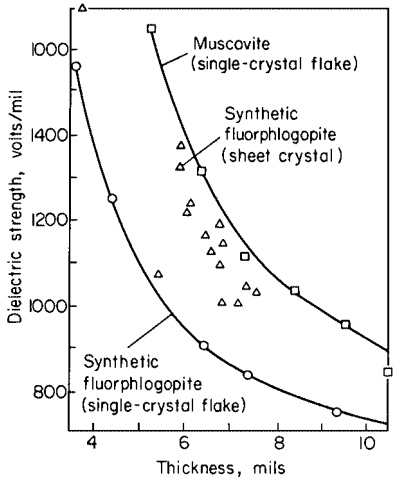

FIGURE 2.44 Relationship between dielectric strength and thickness of mica specimens.[43]

evolves more gas than natural mica, up to 500°C.[44] At 800°C, however, natural mica becomes more gassy than reconstituted mica. Reconstituted mica is available in tape and sheet form, and it is used as insulation for motors, generators, and transformers. A dielectric strength of approximately 450 to 900 volts/mil for the synthetic material is somewhat lower than that of natural mica. The properties of reconstituted mica are highly reproducible in sheet form.

2.2.3.5 Glass-Bonded Mica (Ceramoplastics). Glass-bonded mica consists of fine particles of either natural or synthetic mica mixed with low-melting glass powder. The glass must become plastic at temperatures below the decomposition temperature of the mica. An advantage of this material is that it can be formed into various shapes by either compression or injection molding. It can be molded or machined to close tolerances, which makes it useful for components such as bases and sockets for electronic tubes, coil supports, brush holders, switchboard panels, washers, and spacers. Since the thermal expansion rate of glass-bonded mica is identical to that of mild steel, metal inserts can be attached directly to it. Glass-bonded mica is easily outgassed thereby making it especially useful for structural members in vacuum tubes,[45] as well as for high-temperature vacuum-tight windows.[46] Techniques for attaching metal gasket seals to glass-bonded mica are available.[47]

Electrical properties of a commercially available glass-bonded mica with respect to temperature frequency and humidity are shown in Figs. 2.45 to 2.48. The low dissipation factor and relatively stable dielectric constant at high frequencies persist to fairly high temperatures. Engineering properties of glass-bonded mica are listed in Table 2.12.

2.3.4 Ceramic and Glass Substrates

The demand for miniaturization and for increased reliability of electronic equipment is responsible for the increased use of ceramic and glass substrates. These materials serve as the base upon which electrical components such as resistors, capacitors, and conductors are

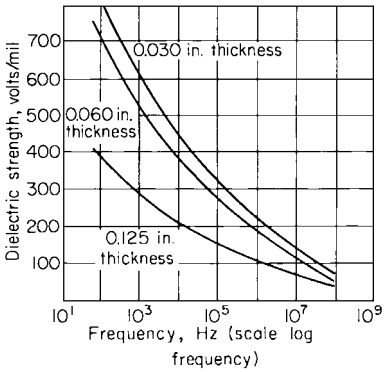

FIGURE 2.45 Relationship between dielectric strength and frequency for three thicknesses of Mycalex 400. (*Mycalex Corp. of America.*)

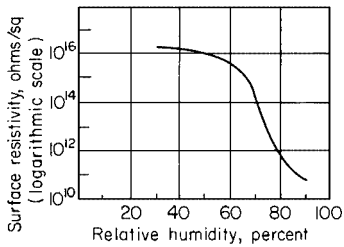

FIGURE 2.46 Variation of surface resistivity of Mycalex 400 with relative humidity. (*Mycalex Corp. of America.*)

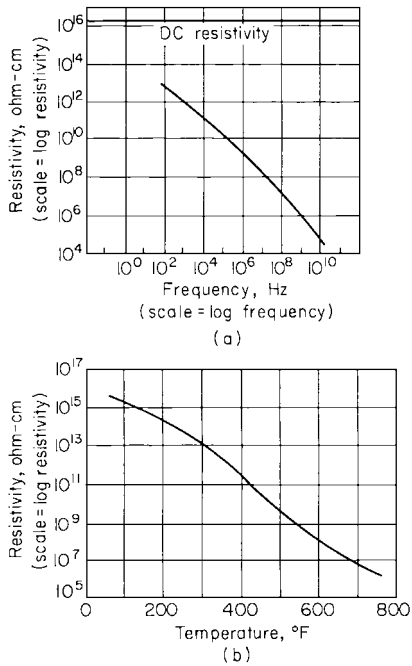

FIGURE 2.47 Variation of volume resistivity of Mycalex 400 with (*a*) frequency and (*b*) temperature. (*Mycalex Corp. of America.*)

TABLE 2.12 Properties of Glass-bonded Mica[13]

Property	Moldable grade (injection-molded)	Machinable grade (compression-molded)
Volume resistivity, ohm-cm:		
At 20°C	10^{14}–10^{16}	10^{17}–10^{18}
At 500°C	10^{8}	10^{7}
Dielectric strength, volts/mil	270–400	250–500
Dielectric constant at 1 MHz	6.7–8.8	6.8–6.9
Dissipation factor at 1 MHz	0.0014–0.0023	0.0013–0.0020
Maximum temperature endurance (unstressed), °C	345–650	370–845
Thermal expansion coefficient at 20–300°C, 10^{-7}in./(in.)(°C)	94–114	112–120
Compression strength, psi	25,000–40,000	35,000–40,000
Impact strength (Charpy), ft-lb/in.^{2}	1.2–2.0	1.2–2.4
vacuum tightness (He leakage rate), cm^3/sec	Less than 2×10^{-10}	

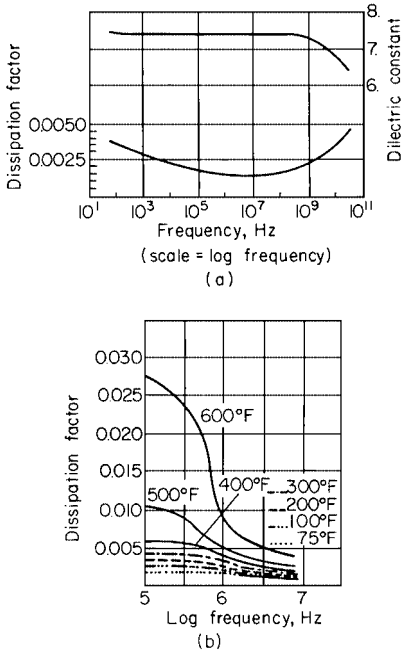

FIGURE 2.48 Variation of dissipation factor and dielectric constant of Mycalex 400 with (*a*) frequency and (*b*) frequency at several temperatures. (*Mycalex Corp. of America.*)

deposited by silk screening, vacuum depositing, sputtering, and painting processes. Discrete components can be attached to the substrate by either soldering or compression welding.

A substrate must be physically, electrically, and chemically compatible with the material deposited on it, and in particular it should be selected on the basis of the following properties:

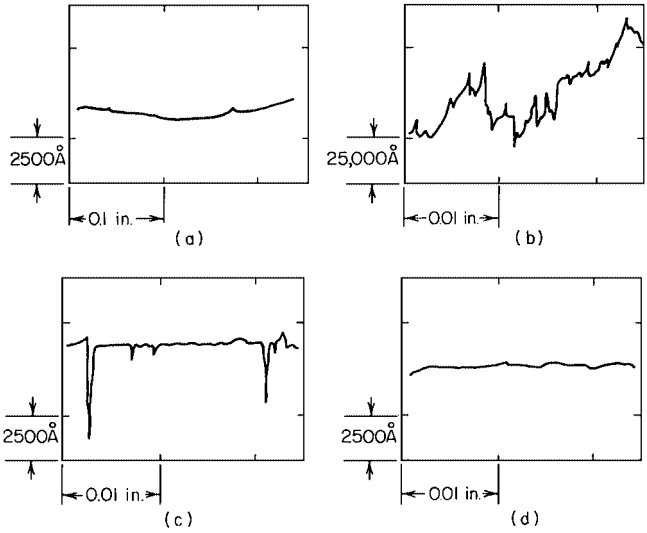

FIGURE 2.49 Stylus instrument traces of substrate surfaces. (*a*) Glazes and drawn glasses, (*b*) as-fired, large-grain polycrystalline ceramic, (*c*) polished, large-grain polycrystalline ceramic, and (*d*) polished, small-grain polycrystalline ceramic.[49]

2.3.4.1 Surface Smoothness. The surface finish requirements for thick-film deposition ($\sim 10^{-3}$ cm) are not as stringent as those for thin-film deposition ($\sim 10^{-6}$ cm). Consequently, either a glass or a glazed ceramic is required for thin-film deposition, whereas an "as-fired" ceramic substrate is satisfactory for thick-film deposition.

The smoothness of a ceramic depends upon its microstructure and density. A high-density body composed of small grains will form a smoother substrate than a ceramic consisting of larger grains (see Fig. 2.49). As-fired alumina substrates with a 2 μin. surface finish are reported,[48] and glass substrates with a surface smoothness of $^1/_4$ μin. (60 Å) are commercially available (Corning 7059).

Glazed ceramic substrates have somewhat lower thermal conductivities than as fired ones, but compared to glass substrates they have good thermal conductivities. Glazed ceramic substrates, therefore, combine the properties of surface smoothness and good thermal conductivity. Ceramic substrates having a glaze several mils thick and a surface finish of approximately one microinch are reported.[49]

2.3.4.2 Electric Conductivity. Both the volume and the surface resistance of a substrate must be high in order that leakage currents are minimized either through the bulk of the substrate or along the surface between the components. Alkali-metal ions, especially Na^+, should be avoided in the substrate as well as in the deposited material.[50,51] This ionic species migrates relatively easily under the influence of an electric field. Furthermore, it has a high thermal diffusion coefficient, which can lead to device degradation.

The aging effect of tantalum nitride resistors deposited on substrates containing differing amounts of sodium is shown in Fig. 2.50. Although the glazed alumina with 3 percent Na_2O contains more alkali than the 7059 glass, the glazed alumina body is still more stable than the glass substrate. This is because the thermal conductivity of the alumina is greater

TABLE 2.13 Effect of Alumina Content on the Thermal Conductivity of Alumina Substrates

% Alumina	Thermal conductivity cal/(sec)(cm^2)(°C/cm)	% change in thermal conductivity
99	0.070	
98	0.061	–13
96	0.043	–39
85	0.035	–50

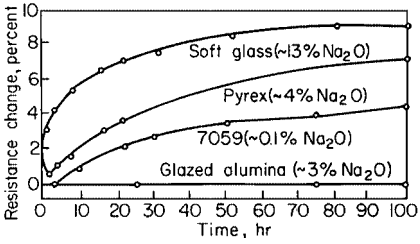

FIGURE 2.50 Effect of substrate alkali content on overload testing of tantalum nitride resistors.[90]

than that of the glass; therefore, both the temperature of the alumina substrate and the Na^+ ion diffusion rate are lower than in the 7059 glass.

2.3.4.3 Thermal Conductivity. Substrates with high thermal conductivities permit greater component packing density since surface temperatures can be lowered and the danger of hot spots minimized through the use of heat sinks. Since ceramics have higher thermal conductivities than glasses, glazing ceramic substrates to improve their surface finish will decrease their thermal conductivities. For example, the thermal resistance of 1 ml of glaze is equivalent to that of 30 mils of Al_2O_3 or 190 mils of BeO.

A high alumina content is required to achieve a high thermal conductivity in alumina-based substrate. This effect is illustrated by the data in Table 2.13, which shows that the thermal conductivity decreases by 13 percent when the alumina content is lowered from 99 to 98 percent, and by 50 percent when the alumina content is lowered to 85 percent.

BeO has a higher thermal conductivity than Al_2O_3; however, the conductivity of Al_2O_3 is adequate for most applications, and alumina is much less expensive than beryllia.

2.3.4.4 Thermal Shock Resistance. This property is important particularly as it affects the ability of a substrate to withstand soldering and joining operations. For the heat transfer rates usually encountered in electronic packaging operations, thermal conductivity, thermal expansion, and strength largely determine the ability of a substrate to withstand thermal shock. The high thermal shock resistance of BeO is due to its high thermal conductivity, whereas that of fused silica is due to its low rate of thermal expansion (see also Table 2.2).

2.3.4.5 Differential Thermal Expansion. To help assure long device life, the thermal expansion mismatch between substrate and components, interconnections, and seals should be as small as possible so as to minimize residual stresses.

TABLE 2.14 Properties of Ceramic Substrates and Glazes[91]

Material	Tensile strength, psi	Expansion coefficient, 10^{-6} in./(in.) (°C)	Coefficient of heat transfer, (watts) (in.)/(in.^{2}) (°C)	Dielectric properties at 1 MHz and 25°C		Volume resistivity at 150°C, ohm-cm $\times 10^{-12}$
				Relative dielectric constant	% dissipation factor	
Alumina	25,000	6.4	~0.89	9.2	0.03	>100
Beryllia	15,000	6.0	5.8	6.4	0.01	>100
Corning 7059 glass	~10,000	4.6	~0.03	5.8	0.1	>100
Modified $BaTiO_3$	4,000	9.1	0.007	6,500	1.8	0.2
Modified TiO_2	7,500	8.3	0.017	80	0.03	0.5
Glaze for alumina:						
2.5% sodium oxide	~10,000	5.5	~0.03	6.3	0.16	>100
Alkali-metal-free	~10,000	5.3	~0.03	7	0.2	>100

2.3.4.6 Dielectric Constant. At high frequencies, the dielectric constant of the substrate is especially important. A substrate with a high dielectric constant may have a sufficiently high capacitive reactance to be no problem at low frequencies, whereas at higher frequencies low reactance paths may develop. Ceramic and glass substrates are available with dielectric constants in the range from 4 to 9 (see Tables 2.14 and 2.15). In substrate form, $BaTiO_3$ can have a dielectric constant of 6,500; however, it also has a higher dissipation factor and a lower volume resistivity than other substrate materials.

2.3.4.7 Fabrication. The higher thermal conductivity and strength of ceramic over glass substrates permits them to be processed by automatic machinery. Holes, perforations, and scribed lines (to facilitate breaking) can be easily made while the ceramic is in the "green" or unfired state. In contrast to this, it is difficult to put holes in a glass substrate during the drawing operation when the smooth surface is formed. Critical applications requiring a substrate with both high thermal conductivity and surface smoothness use single-crystal sapphire.[52]

2.3.5 Glass-Ceramics

The advantage that a glass-ceramic offers over either glass or ceramic materials is the combination of easy fabrication and outstanding mechanical properties. Before the crystallization process, the glassy body is worked by conventional glass-forming methods, i.e., blowing, pressing, drawing, and rolling. After the forming operation, the glass is cooled to approximately 100°C above the annealing temperature for a time sufficiently long to allow stable nuclei to separate from the vitreous phase. After nucleation, the body is heated to approximately 100°C below the softening point of the glass for rapid crystallization. Nucleating agents commonly used include TiO_2, Au, Ag, ZrO_2, Cr_2O_3, and NiO.[53] Several glass compositions and the precipitating crystalline phases are listed in Table 2.16. Since glass-ceramic bodies have zero porosity and submicron grains, they are mechanically stronger than many conventional glass and ceramic bodies. The mechanical properties of several glass-ceramic, glass, and ceramic materials are listed in Table 2.17.

TABLE 2.15. Properties of Glass Substrate Materials[147]

Glass Code Number	0080	0211	1715	1723	7059	7740	7900	7940
Glass type	Soda lime	Alkali zinc boro-silicate	Lime alumino-silicate, alkali-free	Lime alumino-silicate, alkali-free	Barium alumino-silicate, alkali-free	Alkali boro-silicate	96% silica	Fused silica
Dielectric constant:								
At 100 Hz:								
25°C	8.3	6.8	6.0	6.4	5.9	4.9	3.9	3.9
200°C	—	—	6.1	6.6	6.1	—	4.1	3.9
400°C	—	—	7.2	7.3	7.4			
At 1 MHz:								
25°C	6.9	6.6	5.9	6.4	5.8	4.6	3.9	3.9
200°C	9.3	7.4	6.1	6.5	5.9	5.1	3.9	3.9
400°C	—	—	6.3	6.7	6.1	—	3.9	3.9
Loss tangent:								
At 100 Hz:								
25°C	0.078	0.01	0.0018	0.0008	0.0011	0.027	0.0006	0.00006
200°C	—	—	0.0047	0.0024	0.0062	—	0.07	0.0003
400°C	—	—	0.2	0.09	0.19			
At 1 MHz:								
25°C	0.01	0.0047	0.0024	0.0013	0.0011	0.0062	0.0006	0.00002
200°C	0.17	0.032	0.0028	0.0014	0.0018	0.03	0.001	0.00002
400°C	—	—	0.0061	0.0034	0.0071	—	0.026	0.0003
Viscosity data, °C:								
Annealing point	512	542	866	710	650	565	910	1050
Softening point	696	720	1060	910	872	820	1500	1580
Linear coefficient of thermal expansion at 0–300°C, 10^{-7} in./(in.)(°C)	92	72	35	46	45	32.5	8	5.6
Density, g/cm^3	2.47	2.57	2.48	2.63	2.76	2.23	2.18	2.20
Volume resistivity ($\log_{10}$) ρ, ohm-cm:								
At 250°C	6.4	8.3	13.6	14.1	13.5	8.1	9.7	11.8
At 350°C	5.1	6.7	11.3	11.8	11.3	6.6	8.1	10.2
Thermal conductivity, cal/(sec)(°C)(cm)								
At 25°C	0.0025	0.002	0.002	0.0032	0.0030	—	—	0.0035
At 300°C	0.0032	—	—	—	0.0036	—	—	0.0042

TABLE 2.16 Some Representative Glass-Ceramic Composition Fields[53]

Glass	Crystal phases	Catalysts
$MgO\text{-}Al_2O_3\text{-}SiO_2$	$2MgO\text{-}2Al_2O_3\text{-}5SiO_2$	TiO_2
$Li_2O\text{-}Al_2O_3\text{-}SiO_2$	$Li_2O\text{-}Al_2O_3\text{-}2SiO_2$	TiO_2
	$Li_2O\text{-}Al_2O_3\text{-}4SiO_2$	TiO_2
	$LiO\text{-}Al_2O_3\text{-}6SiO_2$	TiO_2
	$Li_2O\text{-}SiO_2$	Au, Ag, Cu,Pt
	$Li_2O\text{-}2SiO_2$	Au, Ag, Cu,Pt
$Na_2O\text{-}BaO\text{-}SiO_2$	$BaO\text{-}2SiO_2$	Au, Ag, Cu,Pt

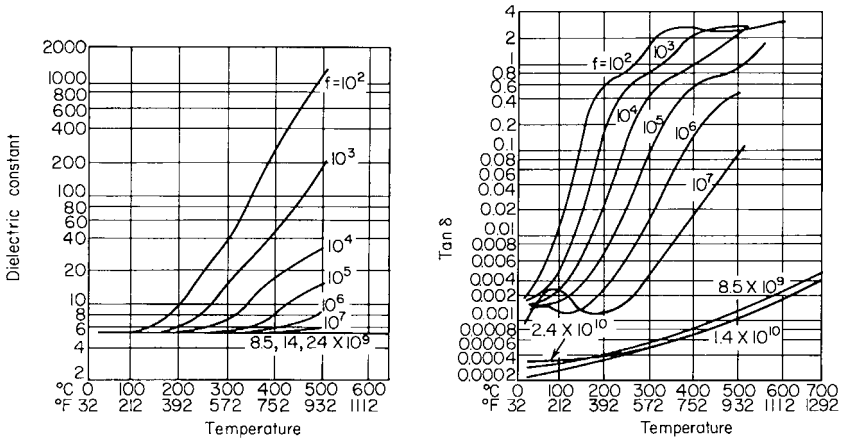

FIGURE 2.51 Dielectric constant and loss tangent of Pyroceram 9606 glass as a function of temperature at various frequencies. (*Corning Glass Works.*)

Certain glass-ceramic compositions are used in microwave applications because of their low dissipation factors ($\tan \delta = 0.0003$) at high frequencies (10 MHz), as shown in Fig. 2.51.

2.3.6 Seals

2.3.6.1 Glass-to-Metal Seals. Incandescent and vapor lamps and electron tubes are some of the many applications that use glass-to-metal seals for the combination of either optical or insulating qualities and metallic conductivity. The requirements for bonding glass and metal are: (1) The glass must be wet and adhere to the metal, and (2) the thermal expansions of the glass and metal should closely match over the temperature range of intended use. Glasses suitable for sealing to various metals are given in Table 2.18.

2.3.6.2 Bonding. In order to form a strong glass-to-metal bond, an oxide layer is needed on the surface of the metal. Ideally, the metal oxide will diffuse into the molten glass to form the bond. Bonding, therefore, depends on how well the molten glass wets the metal (see Fig. 2.52). The degree of wetting is described by the wetting or contact angle θ, which is related to the energy between the solid-liquid, the solid-vapor, and the liquid-vapor interfaces by the

TABLE 2.17 Comparison of Properties of Pyroceram, Glass and Ceramic[13]

	Pyroceram*		Glass				Ceramic		
Property	9606	9608	Fused silica 7940	Vycor* 7900	Pyrex* 7740	Lime glass 0080	High-purity alumina (93%+)	Steatites $MgO\text{-}SiO_2$	Forsterite $2MgO\text{-}SiO_2$
Specific gravity at 25°C	2.61	2.50	2.20	2.18	2.23	2.47	3.6	2.65–2.92	2.9
Water absorption, %	0.00	0.00	0.00	0.00	0.00	0.00	0.00	0–0.03	0–0.01
Gas permeability	0	0	0	0	0	0	0	—	0
Thermal:									
Softening temperature, °C[†]	—	—	1584	1500	820	696	1700	1349	1349
Specific heat (25°C)	0.185	0.190	0.176	0.178	0.186	0.200	0.181	—	—
Specific heat mean (25–400°C)	0.230	0.235	0.223	0.224	0.233	0.235	0.241	—	—
Thermal conductivity, cgs, at 25°C mean temperature	0.0087	0.0047	0.0032	0.0036	0.0026	0.0025	0.042–0.086[¶]	0.0062–0.0065	0.010
Linear coefficient of thermal expansion at 25–300°C, 10^{-7} in./(in.)(°C)	57	4–20[‡]	5.5	8	32	92	73(20–500°C)	81.5–99. (20–500°C)	99. (20–500°C)
Mechanical:									
Modulus of elasticity, psi × 10^{-6}	17.1	12.5	10.5	10.0	9.1	10.2	40–50	15	20
Poisson's ratio	0.25	0.25	0.17	0.19	0.20	0.22	0.21		
Modulus of rupture (abraded), psi × 10^{-3}	18–20	12–14	5–9	5–9	6–10	6–10	50[§]	20[§]	19[§]
Knoop hardness:									
100 g	657	593	—	463	418	—	1850	—	—
500 g									
Electrical:									
Dielectric constant:									
At 1 MHz:									
25°C	5.58	6.78	3.78	3.8	4.6	7.2	8.81	5.9	6.3
300°C	5.60	—	—	3.9	5.9				
500°C	8.80	—	—	—	—	—	9.03		

At 10 GHz:									
25°C	5.45	6.54	3.78	3.8	4.5	6.71	8.79	5.8	5.8
300°C	5.51	6.65	3.78						
500°C	5.53	6.78	3.78	—	—	—	9.03		
Dissipation factor:									
At 1 MHz:									
25°C	0.0015	0.0030	—	0.0005	0.0046	0.009	0.00035	0.0013	0.0003
300°C	0.0154	—	—	0.0042	0.0130				
500°C	—	—	—	—	—	—	0.012		
At 10 GNz:									
25°C	0.00033	0.0068	—	0.0009	0.0085	0.017	0.0015	0.0014	0.0010
300°C	0.00075	0.0115	—						
500°C	0.00152	0.040	—	—	—	—	0.0021		
Loss factor:									
At 1 MHz:									
25°C	0.008	0.02	—	0.0019	0.0212	0.065	0.0031	0.0077	0.0019
300°C	0.086	—	—	0.0164	0.0566				
500°C	—	—	—	—	—	—	0.108		
At 10 GHz:									
25°C	0.002	0.045	—	0.0036	0.0382	0.114	0.0132	0.0082	0.0058
300°C	0.004	0.077							
500°C	0.008	0.27	—	—	—	—	0.019		
Volume resistivity ($\log_{10}$), ohm-cm:									
At 250°C	10	8.1	12.0	9.7	8.1	6.4	14.0(100°C)	14(20°C)	14(20°C)
At 350°C	8.6	6.8	9.7	8.1	6.6	5.1	12.95(300°C)		

*Trademarks of Corning Glass Works, Corning, N.Y.
†Softening temperature; method of evaluation: (*a*) glass: ASTM C 338-54T; (*b*) ceramics: ASTM C 24–56.
‡Expansion coefficients depend on heat treatment.
§Unabraded values.
¶99.5% pure; 98.0% dense.

TABLE 2.18 Glass-Metal Combinations for Seals[92]

Metal or alloy	Trade name or type	Thermal conductivity cal/(sec)(cm)(°C)	Electrical resistivity at 20°C, ohm-cm × 10^{-6}	Matching glass		Remarks
				Corning	Other	
Cold-rolled steel, SAE 1010, AlSi C1010	Other grades of soft steel or iron also used	0.108	18	1990 1991	 5643[a]	Tends to oxodize excessively. Plating with Cu, Cr, or Ag often used to prevent this. External rings of iron are frequently sealed to Pt-sealing glasses.
17% chrome iron, A151 430A	Allegheny Telemet[c]			0129 9019	3720[a]	Used in metal TV picture tube as a ring seal outside a glass plate of lower expansion, putting glass in compression.
28% chrome iron	Allegheny Sealment-1[c] Ascaloy 446[d] Carpenter-27	0.06	72	9012	K-51[b]	Used in TV tubes. Pt-sealing glasses can also be used under certain conditions and types of seals. Alloy should be preoxidized in wet H_2 gas.
Platinum	—	0.165	10.6	0010	R-5[b] R-6[b]	Now used mainly for scientific apparatus. Preoxidizing unnecessary.
Composite material: core, 42 Ni, 58 Fe Sheath, Cu	Dumet[d]	0.04	4–6	0080 0120 7570	KG-12[b]	Copper sheath bonded to core. Surface usually coated with borax to reduce oxidation. Expansion: Radial, 90×10^{-7} per °C. Axial, 63×10^{-7} per °C. Wire size usually limited to 0.020 in. D.
Nickel–chrome iron: 42 Ni, 6	Sylvania 4 Allegheny Sealmet HC-4	0.032	34	 8160		Matches Pt-sealing glasses. Relatively large seals can be made beween this alloy and suitable glasses. Pre-treatment in H_2 atmosphere furnace essential.

Cr, 52 Fe	Carpenter 426			9010			
Nickel-cobalt iron:	Kovar[d]	0.046	47	7040		K-650[b]	Low-expansion sealing alloy. Should be annealed after cold working and pretreated in H_2 atmosphere furnace.
28 Ni, 18	Fernico[e]				7055		
CO, 53 Fe				7050		K-704[b]	
					8830		
	Rodar[f]			7052		K-705[b]	
Molybdenum	—	0.35	5.7	7040	1720		Metal rods usually ground and sometimes polished. Surfaces should be cleaned in fused nitrite and not overoxidized.
				7052			
Tungsten	—	0.38	5.5	3320	7050	K-772[b]	Same as for molybdenum.
				7720	8830		
Copper	OFHC grade (oxygen-free high-conductivity)	0.92	1.75	Most glasses			Copper-glass seals are made with Housekeeper technique with thin metal sections. Care must be taken to prevent overoxidation of copper.

Physical properties of metals and alloys from Monack and Partridge.
[a] Trademarks of Pittsburgh Plate Glass Company, Pittsburgh, Pa.
[b] Trademarks of Kimble Glass Division, Owens-Illinois Glass Company, Montclair, N.J.
[c] Trademark of Allegheny Ludlum Steel Corp., Windsor, Conn.
[d] Trademark of Westinghouse Electric Corporation, Pittsburgh, Pa.
[e] Trademark of General Electric Company, Schenectady, N.Y.
[f] Trademark of Wilbur B. Driver Co., Newark, N.J.

TABLE 2.19 Stresses in Glass Parts of Seals—Metal Rod or Wire Surrounded by Glass

Type of stress	Glass contraction greater than metal	Glass contraction less than metal
Axial	Tensile	Compressive
Tangential	Tensile	Compressive
Radial	Compressive	Tensile

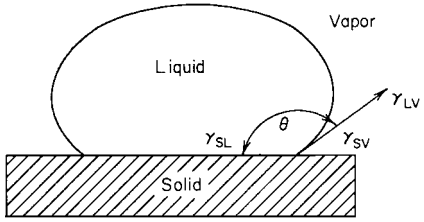

FIGURE 2.52 Relationship between interfacial energy and contact angle of a sessile drop.

relation $\cos\theta = (\gamma_{sv} - \gamma_{sl})/\gamma_{lv}$, where γ is the surface energy. When $\theta < 90°$, the liquid partially wets the surface; when $\theta > 90°$, the liquid is nonwetting; and when $\theta = 0°$, the liquid completely wets the surface.

The surface energy of a liquid or solid arises from the unsatisfied bonds of the surface atoms. Since these atoms are more strongly bound by internal forces, work (surface free energy) must be done against the internal forces to bring additional atoms to the surface and create new surface area.

The strongest glass-to-metal bond results when the interfacial energy is lowered. This occurs when the metal ions from the metal oxide interdiffuse with the oxygen ions of the glass. If the metal oxide layer is dissolved or is very thin, a weaker (van der Waals) bond is produced.[54]

2.3.6.3 Stresses. The stresses that develop in a glass-to-metal seal are proportional to the differential contraction between the two materials. When molten glass is first joined to a metal, no stresses develop until the glass becomes rigid. Glass is considered rigid at its setting point, which is approximately 20°C below its annealing temperature. Below the setting point, the differential contraction rate of the metal and the glass will determine the stresses in the seal (see Table 2.19). Tangential stresses in annealed tubular joints can be calculated from the relation $\sigma_t = \bar{E}\,\Delta L/2L$, where σ_t is the tangential stress, $\bar{E}$ is the average of the elastic moduli for the two materials, and $\Delta L/L$ is the differential contraction between the two materials at the setting point of the glass, or if two glasses are joined at the lower setting point. Stresses from 0.5 to 1.5 kg/mm^2 can be tolerated in tubular butt seals, depending on the size and quality of the seal. A method for measuring residual stresses in cylindrical metal-to-glass seals is given in ASTM Standard F 218-50.

A useful guide for evaluating combinations of sealing materials is given in Tables 2.20 and 2.21 in terms of the differential expansion between glasses, ceramics, or metals. The following general rules apply: (1) Differential expansions <100 ppm provide very good sealing conditions, (2) differential expansions between 100 and 500 ppm satisfy conditions for medium-size seals, and (3) differential expansions between 500 and 1,000 ppm are tolerable for either small seals of short length or seals in which the critical stresses are compressive.

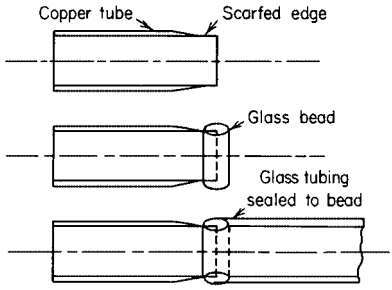

FIGURE 2.53 Housekeeper type of seal, and procedure for making it.[92]

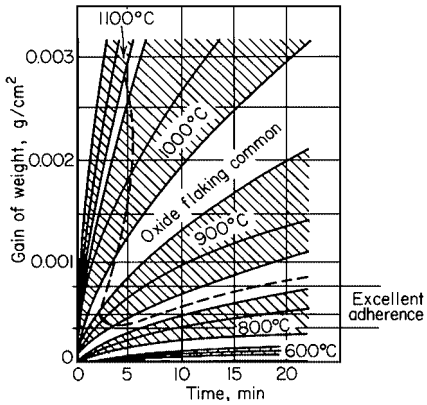

FIGURE 2.54 Oxidation of Kovar: Areas inside V-shaped dotted curve indicate conditions under which greatest tendency for oxide flaking exists.[54]

Housekeeper Seals. Seals of this type are used to join relatively soft metals (e.g., copper) that have high rates of thermal expansion to glasses that have low rates of thermal expansion. The seal is made by forming a taper or feather edge on the metal, and then sealing the glass to the taper (see Fig. 2.53.) Mismatch between the expansion rates of the metal and glass is equalized by the flexibility of the thin taper. This seal was originally developed for high-power water-cooled radio tubes.

Kovar Seals. Kovar is a Fe-Ni-Co alloy with a thermal expansion rate which matches that of several hard- or low-expansion glasses such as Corning 7052 and 7040. It is available as a powder as well as in tube, sheet, and rod stock form. An advantage of Kovar seals is that they can be fired in air since the oxidation rate of Kovar is low compared to the softening rate of hard glass (see Fig. 2.54). The problem of power losses at high frequencies and the resultant heating of the glass-metal joint can be overcome by plating the Kovar with silver, gold, or chromium, to lower its effective resistance.[55] Kovar seals are used extensively in vacuum technology and in packaging of solid-state components.

Fused Silica-to-Metal Seals. The high viscosity of fused silica makes it particularly suitable for glass-to-metal seals for high-temperature applications, e.g., seals for mercury-arc lamps. Since fused silica has a very low thermal expansion rate, special attention is given to minimizing the strain between the metal and glass. These techniques include using an intermediate glass between the fused silica and metal and making the metal leads very thin. The intermediate glass method can be used to seal tungsten rods as large as 3 mm in diameter to fused silica.[56]

Because of its low dielectric losses at microwave frequencies, fused silica is used for microwave windows. By first metallizing the silica with TiH_2 and a solder containing In, Sn,

TABLE 2.20 Differential Expansion between Glasses, Ceramic, or Metals[148]—Low Expansion Range (differential in ppm)

Metal	Glass code no.	7761	7070	7740	7760	1715	7720	Tungsten	7251	5420	9700	7780	9741	3320	7750	1720	7331	1723	7052	7050	Molybdenum	7040	1826	8830	7510	Kovar	7055	7056	8800	7520	7280	7340	Alumina	7530	42 Ni-Fe	46 Ni-Fe	7550
	7761	0	380	50	210	230	400	630	210	260	180	470	850	400	770	640	610	740	—	890	—	—	—	—	980	—	—	—	—	—	—	—	—	—	—	—	—
	7070	380	0	290	160	130	20	290	150	100	150	50	680	60	520	300	230	390	730	500	690	700	—	630	650	770	690	690	—	—	—	—	—	—	—	—	—
	7740	50	290	0	180	90	470	550	220	310	140	400	690	440	630	580	690	680	880	820	—	940	—	960	970	—	—	—	—	—	—	—	—	—	—	—	—
	7760	210	180	180	0	30	230	400	0	50	50	260	630	180	550	420	390	510	750	690	820	820	—	830	860	—	910	910	—	—	—	—	—	—	—	—	—
	1715	230	130	90	30	0	310	330	80	150	40	230	550	310	480	860	570	980	720	660	—	770	—	830	810	—	910	920	—	—	—	—	—	—	—	—	—
	7720	400	20	470	230	310	0	120	270	220	330	90	530	90	450	130	140	240	680	520	530	660	950	670	560	880	700	700	980	980	—	—	—	—	—	—	—
Tungsten		630	290	550	400	330	120	0	360	250	410	180	180	130	80	350	120	440	320	250	X	370	610	420	390	X	490	490	—	—	—	—	X	—	X	X	—
	7251	210	150	220	0	80	270	360	0	50	80	250	570	190	510	380	390	480	760	680	800	850	—	840	790	—	900	910	—	—	—	—	—	—	—	—	—
	5420	260	100	310	50	190	220	250	50	0	180	200	550	150	470	290	330	390	710	630	700	750	—	790	740	—	850	830	—	—	—	—	—	—	—	—	—
	9700	180	150	140	50	40	330	410	80	180	0	270	580	310	500	430	530	560	750	680	870	860	—	880	840	—	940	940	—	—	—	—	—	—	—	—	—
	7780	470	50	400	260	230	90	180	250	200	270	0	530	50	430	190	150	290	660	430	580	640	960	590	520	730	620	620	970	970	—	—	—	—	—	—	—
	9741	860	680	690	630	550	550	180	570	550	580	550	0	400	220	190	240	120	40	110	170	10	130	40	60	0	100	100	470	470	630	730	830	940	490	980	—
	3320	400	60	440	180	310	90	130	190	150	310	50	400	0	320	170	180	260	580	480	570	650	850	630	610	—	710	720	—	—	—	—	—	—	—	—	—
	7750	770	520	630	550	480	450	80	510	470	500	430	220	320	0	80	140	10	190	50	290	160	540	180	180	230	240	240	620	620	810	910	—	—	—	—	—
	1720	640	300	580	420	890	150	350	380	290	450	190	150	170	80	0	80	110	320	240	290	380	620	400	370	—	480	480	—	—	—	—	—	—	—	—	—
	7331	610	250	690	390	570	140	120	390	330	550	150	240	180	140	80	0	20	380	290	330	410	670	440	400	890	510	510	890	890	—	—	—	—	—	—	—
	1723	740	390	680	510	980	240	440	480	390	560	290	120	260	10	110	20	0	240	150	190	270	540	310	280	—	380	390	—	—	—	—	—	—	—	—	—
	7052	+	730	880	790	720	680	320	760	710	750	660	40	560	190	320	380	240	0	200	50	50	350	40	60	20	0	0	390	390	590	690	850	900	640	—	—
	7050	890	500	820	690	660	520	250	680	630	690	450	110	480	30	240	290	150	200	0	180	190	510	150	90	270	180	180	530	530	730	840	940	—	960	—	—

Molybdenum		+	690	+	820	+	550	×	800	700	870	580	170	570	290	290	330	190	50	160	0	20	$\overline{250}$	$\overline{10}$	30	×	$\overline{50}$	$\overline{50}$	$\overline{710}$	$\overline{710}$	$\overline{950}$	—	×	—	×	×	—
	7040	+	700	940	820	770	690	370	800	750	800	640	$\overline{10}$	600	160	360	410	270	$\overline{50}$	190	$\overline{20}$	0	$\overline{380}$	40	70	$\overline{70}$	$\overline{10}$	$\overline{10}$	$\overline{380}$	$\overline{380}$	$\overline{580}$	$\overline{650}$	$\overline{800}$	$\overline{900}$	$\overline{720}$	—	—
	1826	+	+	+	+	+	990	610	+	+	+	960	120	850	540	620	670	540	350	510	250	380	0	350	360	320	300	300	$\overline{80}$	$\overline{80}$	$\overline{280}$	$\overline{380}$	$\overline{480}$	$\overline{550}$	$\overline{270}$	$\overline{680}$	$\overline{920}$
	8830	+	650	990	850	830	670	420	840	790	860	590	40	640	180	400	440	310	$\overline{40}$	150	10	$\overline{40}$	$\overline{350}$	0	70	$\overline{140}$	$\overline{30}$	$\overline{30}$	$\overline{370}$	$\overline{370}$	$\overline{570}$	$\overline{650}$	$\overline{800}$	$\overline{910}$	$\overline{840}$	—	—
	7510	980	600	970	800	810	560	390	790	740	840	520	60	610	180	370	400	280	$\overline{60}$	90	$\overline{30}$	$\overline{70}$	$\overline{360}$	$\overline{70}$	0	$\overline{280}$	$\overline{120}$	$\overline{120}$	$\overline{430}$	$\overline{450}$	$\overline{630}$	$\overline{760}$	$\overline{870}$	$\overline{950}$	—	—	—
Kovar		+	770	+	+	+	860	×	+	+	+	730	0	+	230	+	890	+	20	270	×	70	$\overline{320}$	140	280	0	130	130	30	30	260	$\overline{260}$	×	$\overline{570}$	×	×	—
	7055	+	690	+	910	910	700	490	900	860	940	620	100	710	240	480	510	380	0	180	80	10	$\overline{300}$	30	120	$\overline{130}$	0	0	$\overline{320}$	$\overline{320}$	$\overline{520}$	$\overline{630}$	$\overline{750}$	$\overline{860}$	$\overline{840}$	—	—
	7056	+	690	+	910	920	700	490	910	850	940	620	100	720	240	480	510	390	0	180	80	10	$\overline{300}$	30	120	$\overline{130}$	0	0	$\overline{320}$	$\overline{320}$	$\overline{520}$	$\overline{630}$	$\overline{740}$	$\overline{870}$	$\overline{850}$	—	—
	8800	+	+	+	+	+	980	+	+	+	+	970	470	+	620	+	890	+	390	530	710	380	80	370	450	$\overline{30}$	320	320	0	0	$\overline{10}$	$\overline{290}$	$\overline{270}$	$\overline{610}$	$\overline{810}$	—	—
	7520	+	+	+	+	+	980	+	+	+	+	970	470	+	620	+	890	+	390	530	710	380	80	370	450	$\overline{30}$	320	320	0	0	$\overline{10}$	$\overline{290}$	$\overline{270}$	$\overline{610}$	$\overline{810}$	—	—
	7280	+	+	+	+	+	+	+	+	+	+	+	650	+	810	+	+	+	590	730	950	580	280	570	630	$\overline{260}$	520	520	10	10	0	$\overline{330}$	$\overline{180}$	$\overline{530}$	—	—	$\overline{950}$
	7340	+	+	+	+	+	+	+	+	+	+	+	750	+	910	+	+	+	690	840	+	680	380	680	760	260	630	630	290	290	330	0	80	$\overline{310}$	$\overline{530}$	$\overline{750}$	$\overline{800}$
Alumina		+	+	+	+	+	+	×	+	+	+	+	830	+	+	+	+	+	800	940	×	800	480	800	870	×	750	740	270	270	160	$\overline{80}$	0	$\overline{300}$	×	×	$\overline{730}$
	7530	+	+	+	+	+	+	+	+	+	+	+	940	+	+	+	+	+	900	+	+	900	580	910	990	570	860	870	610	610	550	310	300	0	$\overline{210}$	$\overline{450}$	$\overline{530}$
42 Ni-Fe		+	+	+	+	+	+	×	+	+	+	+	490	+	+	+	+	+	640	960	×	720	270	840	+	×	840	850	810	810	+	530	×	210	0	×	$\overline{330}$
46 Ni-Fe		+	+	+	+	+	+	×	+	+	+	+	960	+	+	+	+	+	+	+	×	+	680	+	+	×	+	+	+	+	+	750	×	450	×	0	$\overline{50}$
	7550	+	+	+	+	+	—	+	+	+	+	+	+	+	+	+	+	+	+	+	+	+	920	+	+	+	+	+	+	+	990	800	730	530	330	80	0
	0280	+	+	+	+	+	—	+	+	+	+	+	+	+	+	+	+	+	+	+	+	+	+	+	+	+	+	+	+	+	+	+	950	750	570	320	250
Platinum		+	+	+	+	+	—	×	+	+	+	+	+	+	+	+	+	+	+	+	×	+	+	+	+	×	+	+	+	+	+	+	×	780	×	×	320
	7570	+	+	+	+	+	—	+	+	+	+	+	+	+	+	+	+	+	+	+	+	+	+	+	+	+	+	+	990	990	840	770	720	620	+	560	360

Note: Expansion differentials between Corning glasses and metals or ceramics in parts per million are given at the setting point of the glass for glass-to-metal (or ceramic) seals, and at the setting point of the softer glass for glass-to-metal seals. The setting point is arbitrarily chosen as lying 5°C above the strain point of the glass. A minus sign above a number indicates that for this combination of materials, the one on the ordinate has a lower effective expansion than the one on the abscissa. So too, a large plus or minus sign indicates that the effective expansion is in excess of 1,000 ppm.

TABLE 2.21 Differential Expansion between Glasses, Ceramic, or Metals[148]—High Expansion Range (differential in ppm)

Metal	Glass code no.	7340	Alumina	7530	42 Ni Fe	46 Ni Fe	7550	0280	Platinum	7570	0041	7560	0281	28% Cr steel	0122	9010	Sylvania no. 4	0120	8161	9361	8870	0050	8160	0081	0010	52 Ni Fe	0080	0088	9823	9821	8361	0128	430 Ti steel	9019	0129	8871	7290	1010 steel	1990
	8800	250	270	610	810	—	—	—	—	950	—	—	—	—	—	—	—	—	—	—	—	—	—	—	—	—	—	—	—	—	—	—	—	—	—	—	—
	7520	290	270	610	810	—	—	—	—	990	—	—	—	—	—	—	—	—	—	—	—	—	—	—	—	—	—	—	—	—	—	—	—	—	—	—	—
	7280	330	160	530	—	—	990	—	—	840	—	—	—	—	—	—	—	—	—	—	—	—	—	—	—	—	—	—	—	—	—	—	—	—	—	—	—
	7340	0	80	310	530	750	800	—	—	770	970	—	—	—	—	—	—	—	—	—	—	—	—	—	—	—	—	—	—	—	—	—	—	—	—	—	—
Alumina		80	0	300	X	X	730	950	X	720	880	—	—	X	970	—	X	—	950	—	—	—	—	—	—	X	—	—	—	—	—	X	—	—	—	X	—
	7530	310	300	0	210	430	530	750	780	620	780	—	—	—	870	900	—	890	840	980	930	950	960	—	970	—	—	—	—	—	—	—	—	—	—	—	—	—
42 Ni Fe		530	X	210	0	X	330	570	X	—	—	860	970	X	—	—	X	—	—	—	—	—	—	—	—	X	—	—	—	—	—	X	—	—	—	X	—
46 Ni Fe		750	X	450	X	0	80	320	X	550	720	660	680	X	830	880	X	850	820	890	900	910	930	870	940	X	930	940	X	850	980	—	X	—	—	—	X	—
	7550	800	730	530	330	80	0	250	320	360	450	540	610	—	550	590	—	590	540	640	640	630	660	780	660	570	830	850	850	750	920	—	—	—	—	—	—	—
	0280	+	950	750	570	320	250	0	110	240	280	300	380	860	400	440	—	440	390	470	490	480	510	580	520	350	630	630	700	560	680	820	—	920	980	920	—	—	—
Platinum		+	X	780	X	X	320	110	0	60	30	130	160	X	60	120	X	130	80	160	180	170	200	300	210	X	370	380	410	340	510	520	X	620	680	610	—	X	—
	7570	770	720	620	+	560	360	240	60	0	120	120	50	480	40	10	30	70	10	80	130	70	100	60	110	250	110	110	170	80	210	210	610	300	320	620	—	—	—
	0041	970	880	780	+	720	450	280	30	120	0	110	30	630	210	230	380	270	210	180	320	250	340	110	350	210	170	190	250	180	290	410	860	510	550	780	—	—	—
	7560	+	+	+	860	600	540	300	130	120	110	0	120	620	230	270	740	290	240	300	340	330	360	330	370	70	410	390	500	300	380	640	860	730	790	780	—	—	—
	0281	+	+	+	970	680	610	380	160	50	50	120	0	570	170	200	620	220	160	220	270	250	290	220	300	0	320	290	400	180	290	530	800	630	700	710	—	—	—
28% Cr. steel		+	X	+	X	X	+	860	X	480	630	620	570	0	470	450	X	410	470	450	350	390	340	410	330	X	330	330	270	390	240	130	X	40	20	170	880	X	—
	0122	+	970	870	+	830	550	400	90	40	210	250	170	470	0	10	130	60	30	20	180	90	180	40	170	100	20	30	120	0	130	200	630	310	350	700	—	—	—
	9010	+	+	900	+	880	590	440	120	10	230	270	200	450	10	0	130	60	0	0	130	70	140	60	150	70	0	10	100	20	120	190	600	300	330	640	—	—	—

Sylvania no. 4		+	×	+	×	×	+	+	×	−50	380	740	620	×	150	130	0	60	130	220	−30	60	−20	410	−30	×	310	350	180	460	360	−30	×	90	−180	−670	—	×	—
	0120	+	+	890	+	860	590	440	130	70	270	290	220	−410	90	60	−60	0	60	30	−70	−10	−70	80	−80	−60	30	20	−60	50	−100	−140	−570	−230	−280	−580	—	—	—
	8161	+	950	840	+	820	540	390	80	10	210	240	160	−470	30	0	−130	−60	0	−20	−140	−70	−140	30	−150	−120	−30	−40	120	0	−130	−200	−620	−320	−340	−650	—	—	—
	9361	+	+	980	+	890	640	470	160	80	180	300	220	−430	20	0	−230	−30	20	0	−90	−60	−110	80	−120	−20	0	0	−110	30	−110	−240	−630	−340	−350	−580	—	—	—
	8870	+	+	930	+	900	640	490	180	130	320	340	270	−350	180	150	30	70	140	90	0	70	10	140	0	−20	80	80	0	110	−40	−70	130	−500	−180	−220	−530	—	—
	0050	+	+	950	+	910	630	480	170	70	290	330	250	−350	90	70	−60	10	70	60	−70	0	−70	120	−80	−30	60	40	−40	80	−70	−120	−540	−240	270	590	—	—	—
	8160	+	+	960	+	930	660	510	200	100	340	360	290	−340	160	140	20	70	140	110	−10	70	0	160	−10	0	100	−90	10	120	−30	−60	−500	−180	−220	−550	—	—	—
	0081	+	+	+	+	870	780	560	300	60	110	330	220	−410	−40	−60	−410	−80	−30	−80	−140	−120	−160	0	−160	180	−100	−60	−230	30	−90	−390	−620	−480	−540	−600	—	—	—
	0010	+	+	970	+	940	660	520	210	110	350	370	300	−350	170	−50	30	80	150	120	0	80	10	160	0	10	110	100	20	130	−20	−30	−480	170	−200	−540	—	—	—
52 Ni Fe		+	×	+	×	×	570	330	×	260	210	70	0	×	100	70	×	60	120	20	20	30	0	−180	−10	0	−230	−260	270	190	−310	−350	×	−480	−520	−410	—	×	—
	0080	+	+	+	+	950	850	630	370	110	170	410	320	−330	20	0	−310	−30	30	0	−80	−60	−100	100	−110	230	0	50	−140	110	−10	−320	−550	−400	−480	550	—	—	—
	0088	+	+	+	+	940	850	630	380	110	190	390	290	−330	30	10	−350	−20	40	0	−80	−40	−90	60	−100	260	−30	0	−130	100	−20	−310	−520	−440	−480	−550	—	—	—
	9823	+	+	+	+	+	890	700	410	170	290	500	400	−270	120	100	−180	60	120	110	0	40	−10	230	−20	270	140	150	0	210	70	−190	−470	−270	−330	−490	—	—	—
	9821	+	+	+	+	860	790	560	340	80	160	300	180	−350	0	−20	−450	−50	0	−30	−110	−80	−120	−30	−130	190	−110	−100	−210	0	−110	−330	−620	−440	−500	−570	—	—	—
	8361	+	+	+	+	980	920	680	510	210	290	380	290	−240	150	120	−360	100	150	110	40	70	30	90	20	310	10	20	−70	110	0	−210	−480	−310	−370	−440	—	—	—
	0128	+	+	+	+	+	+	820	520	210	410	640	550	−130	200	190	30	140	200	240	70	120	60	390	50	350	320	310	190	350	210	0	−310	−70	−130	−440	—	—	—
430 Ti steel		+	×	+	×	×	+	+	×	610	800	860	800	×	630	600	×	570	620	620	−130	540	500	620	480	×	550	550	470	620	480	310	0	230	170	−30	−720	×	−770
	9019	+	+	+	+	+	+	920	620	300	510	730	630	−40	310	300	90	250	320	340	500	240	180	480	170	460	400	400	270	440	310	70	−230	0	−70	−340	—	—	—
	0129	+	+	+	+	+	+	980	680	320	550	790	700	20	350	330	160	280	340	390	180	270	220	540	200	520	460	460	330	500	370	130	−170	70	0	−320	—	—	—
	8871	+	+	+	+	+	+	920	610	620	780	780	710	170	700	640	670	580	650	580	220	590	550	600	540	410	550	550	490	570	440	440	30	340	320	0	−500	−790	−810
	7290	+	+	+	+	+	+	+	+	+	+	+	+	880	+	+	+	+	+	+	530	+	+	+	+	+	+	+	+	+	+	+	720	+	+	500	0	−220	−330
1010 steel		+	×	+	×	×	+	+	×	+	+	+	+	×	+	+	×	+	+	+	+	+	+	+	+	×	+	+	+	+	+	+	×	+	+	790	220	0	−30
	1990	+	+	+	+	+	+	+	+	+	+	+	+	+	+	+	+	+	+	+	+	+	+	+	+	+	+	+	+	+	+	+	770	+	+	810	330	30	0

Note: Expansion differentials between Corning glasses and metals or ceramics in parts per million are given at the setting point of the glass for glass-to-metal (or ceramic) seals, and at the setting point of the softer glass for glass-to-metal seals. The setting point is arbitrarily chosen as lying 5°C above the strain point of the glass. A minus sign above a number indicates that for this combination of materials, the one on the ordinate has a lower effective expansion than the one on the abscissa. So too, a large plus or minus sign indicates that the effective expansion is in excess of 1,000 ppm.

and Pb, which are needed to form an adherent alloy, the silica can be sealed to metallic waveguides. In this process, the metallized silica is clamped to the metal part, which must be coated with either Ag or Au, and then the combination is heat treated to produce a diffusion joint.[57]

2.3.6.4 Ceramic-to-Metal Seals. These seals are commonly used in vacuum tubes, semiconductor devices, feed-through insulators, bushings, and transformer and capacitor terminals. They are particularly useful in operation either at high temperatures or in corrosive atmospheres. Properties that often dictate the use of ceramic-to-metal rather than glass-to-metal seals are greater strength, better dielectric ratings, greater refractoriness, and better thermal shock resistance. The principal disadvantages are opacity to most radiations and high cost when compared to glass-to-metal seals.

2.3.6.5 Bonding. The mechanism of ceramic-to-metal bonding depends on the sealing technique that is used, and it may be due to chemical reaction between the seal members, mechanical interlocking of microscopically rough surfaces, interfacial diffusion, or interpenetration of glassy phases.

Molybdenum-Manganese Process. The sintered-metal-powder process is used to form very high strength seals for klystrons, traveling-wave tubes, and large feed-through insulators. A slurry, which can be deposited by spraying, painting, or silk screening, is made from powdered molybdenum and manganese, with small additions of Fe, Si, TiO_2, Al_2O_3, and CaO. The bond is formed between the ceramic and metal parts by heating them to between 1300 and 1500°C in a wet hydrogen atmosphere. At these temperatures, the oxides form a eutectic melt that reacts with the ceramic and the oxide on the metal and with the sintered molybdenum and manganese to form the bond. Low-purity alumina (94 to 96 percent Al_2O_3) will usually yield a stronger bond than high-purity alumina (99 percent Al_2O_3) because of the larger amount of eutectic melt formed by the impurities in the former. Evidence indicates that the bond strength of alumina-to-metal seals increases with the average grain size of the alumina ceramic (see Fig. 2.55).[58]

Active-Metal Process. This process is based on the ability of Ti and Zr metals to adhere to the oxide surfaces of the parts to be joined without the assistance of a fluxing phase. It is accomplished at a lower temperature than the moly-manganese process; however, the bond strength is slightly lower as well. With this technique, seals can be made between different ceramics, or ceramics and metals, or different metals. For example, the ceramic and metal parts can be coated with a slurry of TiH_2 or ZrH_2 in nitrocellulose and bonded together by heating to 900°C in vacuum to decompose the hydrate and release the free metal. In metal-to-metal joining, the seal is formed by the alloying effect of the Ti or Zr, whereas in either metal-to-ceramic or ceramic-to-ceramic joining, it is formed by chemical reaction.[59]

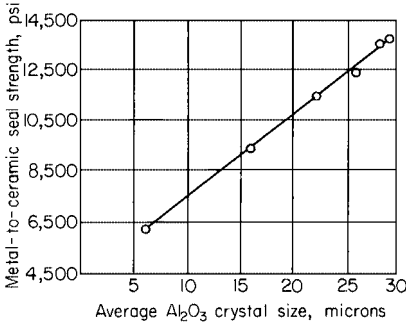

FIGURE 2.55 Effect of alumina crystal size on metal-to-ceramic bond strength when metallized at 1550°C.[58]

TABLE 2.22 Comparison of Printed-film Resistor Systems[91]

Property	Carbon	Metal	Cermet
Resistivity range (sheet)	100 ohms–20 megohms	1 ohm–15 kilohms	2–50 kilohms
Tolerance, %	±10	±0.5	±0.5
Temperature coefficient, ppm per °C	–2,000	±500	±150
Voltage coefficient, ppm/volt	500	30	20
Noise, μv/volt per frequency decade	2	0.1	0.5
Typical load life*	–7	+0.25 (+ 0.025% on alkali-metal free underglaze)	+0.25

*1,000 hr at 85°C with 0.2 watt on a 0.050- by 0.150-in. resistor.

2.3.7 Thick-Film Components

Circuit networks can be built up by depositing resistors, capacitors, and interconnectors in the form of films on insulating substrates. Thick films are usually made by silk screening, brushing, dipping, or spraying, whereas thin films are made by vacuum deposition, sputtering, or chemical deposition. The temperature of the substrate depends on the number of resistors, the power dissipation per unit area, and the cooling method. Techniques for optimizing the thermal conditions by the correct placement of the resistors and various cooling techniques are available.[69] This section describes several of the materials used in making thick-film components.

2.3.7.1 Resistors. Thick-film resistor technology can be divided into three areas, namely, carbon, cermet, and precious metal films. A general comparison of their electrical properties is given in Table 2.22.

Carbon. One of the materials first used for thick-film resistors was carbon. Early carbon-film resistors had a negative coefficient of resistance (NTC) from 0.01 to 0.05 percent per °C, whereas later resistors had an NTC from 0.005 to 0.02 percent per °C.[61] This improvement in performance was achieved by adding boron to help prevent oxidation of the carbon. A metallic dispersion in the carbon film also improves the temperature coefficient; the NTC of the carbon is balanced by the PTC of the metallic dispersion. Carbon and boron-carbon films have the highest electrical noise level of the film-type resistors. Noise is generated by the small fluctuations in the resistance caused by imperfections, variations in the particle-to-particle contact, and hot spots.

Cermets. Resistor films of this type are usually either mixtures of precious metals (e.g., Ag or Au) and glass frit or mixtures of PdO and glass frit. Cermet resistive inks are made by mixing a cermet powder with an organic vehicle of suitable viscosity. This mixture can be screened onto a substrate and cured by firing. Resistor films are typically 0.25 to 2.0 mils thick, and usually they do not require an overglaze for protection. Cermet films are sufficiently hard and abrasion resistant to be used as slide resistors in potentiometers. Since thick cermet films are not very sensitive to substrate surface roughness, special surface preparation usually are not necessary.

The resistance of a cermet film is determined by the metal-to-glass ratio. For example, the resistance of lead-borosilicate glass and either Ag or Au changes by five orders of magnitude with a few percent change in metal content (see Fig. 2.56), whereas either Pd or Pd + Ag glass mixtures are much less sensitive; therefore, they are more easily reproduced on a production basis. The addition of silver to palladium improves the temperature coefficient of resistance and decreases the electrical noise and resistivity of the films (see Table 2.23).

TABLE 2.23 Effect on Temperature Coefficient of Resistance and Noise of Silver Content in Palladium-Lead Borosilicate Compositions[93]

Silver, %	Resistivity, ohms/mil^2	TCR at 25–105°C, ppm per °C	Noise, db/decade
0	200,000	+1720	+22
10	7,300	+440	+12
20	400	+380	+4
30	20	+175	−8
40	0.5	+320	−4

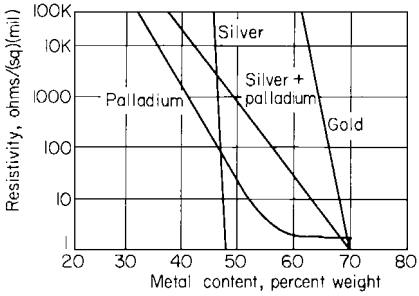

FIGURE 2.56 Relationship between resistivity and concentrations of metal powders in PbO-B_2O_3-SiO_2 frit.[93]

A casting method of forming Pd-Ag-glass resistor films was developed that is less wasteful of material than either the screening or the brushing process.[62] In the casting method, cermet powder is made into a slurry and cast into a continuous flexible sheet, which can be stored indefinitely before being applied to the substrate. With this technique, any resistance value between 50 ohms and 1 megohm can be made by fusing together a maximum of four films, each having a different resistivity.

The conductivity mechanism in cermet films is not well understood; however, the available evidence indicates that conduction occurs by chains or networks of touching conductive particles embedded in an insulating matrix. In these films, the temperature coefficient of resistance varies from negative at low temperatures to positive at high temperatures.

Metal Films. Resistors of this type are made by depositing a layer of metal on a glazed substrate and then overglazing the film for protection (see Fig. 2.57). The glaze should be alkali-free in order to prevent ionic conduction and degradation. Both the underglaze, which provides a smooth surface for deposition, and the overglaze, which encapsulates and protects the resistor, should be in slight compression after firing, to lessen the effects of thermal and mechanical shock. The temperature coefficient of resistance changes from negative and nonlinear to zero, and finally to positive and linear as the film thickness increases and the resistivity decreases (see Fig. 2.58).

2.3.7.2 Dielectrics. Techniques for forming dielectric films are similar to those used to form resistive ones. Films used for capacitor applications should have high dielectric constants, whereas those used for either insulator or crossover functions should have low dielctric constants in order to minimize both capacitance effects and crosstalk or coupling between components. By using various materials, e.g., glasses, titanates, niobates, and stannates, capacitors can be made with values form 6,500 to 150,000 pf/in.^{2} with a dielectric

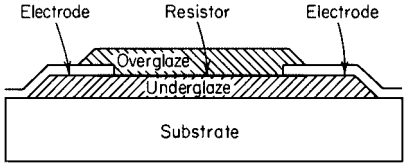

FIGURE 2.57 Precious metal film-resistor structure.[94]

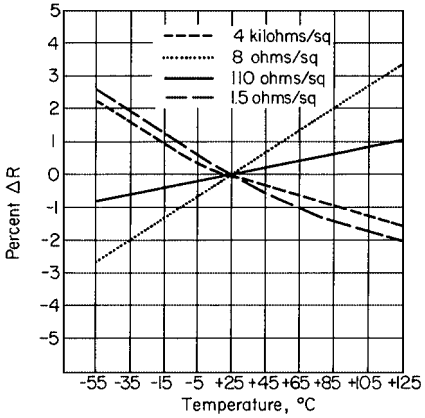

FIGURE 2.58 Relationship between resistivity and temperature of films having different resistivities.[94]

strength of 500 dc volts/mil.[63] Dielectric constants between 20 and 400 can be obtained by varying the degree of crystallization in a ferroelectric glass-ceramic. Higher-dielectric-constant films (400 to 1,200) can be obtained by crystallizing $BaTiO_3$ from the glassy phase.[64]

REFERENCES

1. Foner, S.: Versatile and Sensitive Vibrating-sample Magnetometer, *Rev. Sci. Instrum*., vol. 30, pp. 548–557, 1959.
2. *ASTM Designation* D 257–66, D-C Resistance or Conductance of Insulating Materials.
3. Sauer, H. A. and S. S. Flaschen: Positive Temperature Coefficient of Resistance Thermistor Materials for Electronic Applications, *Proc. 1956 Elec. Comput. Conf.,* pp. 41–46, 1956.
4. Landis, H. M.: Electrodes for Ceramic $BaTiO_3$ Type Semiconductors, *J. Appl. Phys.,* vol. 36, no. 6, p. 2000, June, 1965.
5. Sauer, H. A. and W. H. Shirk: A D-C Wheatstone Bridge for Multi-terohm Measurements with High Accuracy Capability, *IEEE Commun. and Electron.,* March, 1964.
6. *ASTM Designation* D 150, Tests for Dielectric Constant of Electrical Insulation.
7. Von Hippel, A. R.: "Dielectric Materials and Applications," Technology Press of MIT and John Wiley & Sons, Inc., New York, 1954.
8. *ASTM Rep*. C 525-63T, Test for Complex Dielectric Constant of Nonmetallic Magnetic Materials at Microwave Frequencies.
9. Frisco, L. J.: Frequency Dependence of Electric Strength, *Electro-Technol.,* vol. 68, pp. 110–116, August, 1961.
10. Storm, H. F.: "Magnetic Amplifiers," pp. 53–58, John Wiley & Sons, Inc., New York, 1955.

11. IRE Standards on Piezoelectric Crystals: Measurements of Piezoelectric Ceramics, *1961 Proc. IRE,* vol. 49, no. 7, pp. 1162–1169, July, 1961; vol. 46, no. 4, pp. 764–778, April, 1958.
12. Birks, J. B., Modern Dielectric Materials, p. 19, Heywood and Co., London, England, 1960.
13. Kohl, W. H.: "Handbook of Materials and Techniques for Vacuum Devices," p. 586, Reinhold Publishing Corp., New York, 1967. Copyright 1967 by Reinhold Publishing Corp., by permission of Van Nostrand Reinhold Co.
14. Mason, W. P. and H. Jaffe: Methods for Measuring Piezoelectric, Elastic, and Dielectric Coefficients of Crystals and Ceramics, *Proc. IRE,* vol. 42, pp. 921–930, June, 1954.
15. Von Hippel, A. R.: "Dielectrics and Waves," p. 1, John Wiley & Sons, Inc., New York, 1954.
16. Kingery, W. D.: "Introduction to Ceramics," pp. 420–426, John Wiley & Sons, Inc., New York, 1960.
17. Kohl, *op. cit*. p. 77.
18. Atlas, N. M. and H. H. Nakamura: Control of Dielectric Constant and Loss in Alumina Ceramics, *J. Amer. Ceram. Soc.,* vol. 45, no. 10, pp. 467–471, October, 1962.
19. Francl, J. and W. D. Kingery: Thermal Conductivity: IX, Experimental Investigation of Effect of Porosity on Thermal Conductivity, *J. Amer. Ceram. Soc.,* vol. 37, no. 2, pp. 99–107, February, 1954.
20. Coble, R. L.: Transparent Alumina and Method of Preparation, U.S. Patent 3,026,210, March, 1962.
21. Kingery, W. D.: "Oxides for Higher Temperature Applications," pp. 76–89, McGraw-Hill Book Company, New York, 1960.
22. Smith, R. and J. P. Howe: Beryllium Oxide, *Proc. 1st Int. Conf. on BeO,* North-Holland Publishing Company, Amsterdam, 1964.
23. McPhee, K. H.: Cooling Transistors with Beryllia Heat Sinks, *Electron.,* vol. 34, pp. 76–78, May 5, 1961.
24. Kohl, *op. cit*. p. 89.
25. Strickler, D. W. and W. G. Carlson: Ionic Conductivity of Cubic Solid Solutions in the System CaO-Y_2O_3-ZrO_2, *J. Amer. Ceram. Soc.,* vol. 47, no. 3, pp. 122–127, March, 1964.
26. Weissbart, J. and R. Ruka: A Solid Electrolyte Fuel Cell, *J. Electrochem. Soc.,* vol. 109, no. 8, pp. 723–726, 1962.
27. Keler, E. K. and E. N. Nitikiv: High Temperature Ceramic Heaters, *J. Appl. Chem. (USSR)* (English Transl.), vol. 32, no. 9, pp. 2033–2036, 1959; *Ceram. Abstr*. p. 140f, June, 1962.
28. Pearl, H. A., J. M. Nowak and H. G. Deban: Mechanical Properties of Selected Alloys at Elevated Temperatures: II, Design Criteria of SiC, *WADC-TR-702 Tech. Rep*., Contract AF-33(616)–5760, March, 1960.
29. Fetterly, G. H.: Electrical Conduction in SiC, *J. Electrochem. Soc*., vol. 104, no. 5, pp. 322–327, May, 1957.
30. Shepard, C. E., V. R. Watson, and H. A. Stine: Evaluation of a Constricted-arc Supersonic Jet, *NASA Tech. Note* D-2066, January, 1964.
31. Popper, P. and S. N. Ruddlesden: The Preparation, Properties and Structure of Silicon Nitride, *Trans. Brit. Ceram. Soc*., vol. 60, pp. 603–626, 1961.
32. Janakirama-Rao, B. H. V.: Structure and Mechanism of Semiconductor Glasses, *J. Amer. Ceram. Soc*., vol. 48, no. 6, pp. 311–319, June, 1965.
33. Mackenzie, J. D.: Semiconducting Oxide Glasses: General Principles of Preparation, *J. Amer. Ceram. Soc*., vol. 47, no. 5, pp. 211–214, May, 1964.
34. Owen, A. E.: Electronic Conduction Mechanisms in Glasses, *The Glass Industry,* part I, pp. 637–642, November, 1967; part II, pp. 695–699, December, 1967.
35. Sideris, G.: Transistors Face an Invisible Foe, *Electronics,* vol. 39, pp. 191–195, Sept. 19, 1966.

36. Perschy, J. A.: On the Threshold of Success: Glass Semiconductor Circuits, *Electron.,* vol. 40, pp. 74–84, July 24, 1967.
37. Kohl, *op. cit.,* pp. 34–35.
38. Blodgett, K. B.: Surface Conductivity of Lead Silicate Glass after Hydrogen Treatment, *J. Amer. Ceram. Soc.,* vol. 34, no. 1, pp. 14–27, January, 1951.
39. Birks, *loc. cit.,* p. 218.
40. Stanworth, J. E.: Telluride Glasses, *J. Soc. Glass Technol.,* vol. 38, no. 183, pp. 425–435, August, 1954.
41. Corning Glass Works: Glass-K Capacitors, Ref. file CE-1.02, December, 1966.
42. Roy, R.l: Decomposition and Resynthesis of the Micas, *J. Amer. Ceram. Soc.,* vol. 32, no. 6, pp. 202–209, June, 1949.
43. Levine, A. K. and S. Nathansohn: Growth of Sheet Crystals of Fluoropholgopite, *Amer. Ceram. Soc. Bull.,* vol. 45, no. 3, pp. 307–311, March, 1966.
44. Crawford, S. C. and J. C. Hickle: Electrical Quality Classification of the Suitability of Reconstituted Mica Paper for Use as Receiving Tube Spacers, in D. Slater (ed.), "Advances in Electron Tube Techniques," *Proc. 5th Nat. Conf.,* 1960, Pergamon Press, New York, 1961.
45. Hatch, R. A.: Synthetic Mica Investigation: IX, Review of Progress from 1947–1955, *Bur. Mines, Rep. of Invest*. 5337, June, 1957.
46. Gould, L.: Improved Keep-alive Design for TR Tubes, *Proc. IRE,* vol. 45, no. 4, pp. 530–533, April, 1957.
47. Lindsay, W. C.: Improved Demountable High Temperature Mica Vacuum Windows, *Rev. Sci. Instrum.,* vol. 32, no. 6, pp. 748–749, June, 1961.
48. Stetson, H. W. and W. J. Gyurk: Development of Two Micro-inch (CLA) As-fired Alumina Substrates, presented at American Ceramic Society Meeting, New York, May, 1967.
49. Brown, R.: Substrates for Tantalum Thin-film Circuits, *Amer. Ceram. Soc. Bull.,* vol. 45, no. 8, pp. 720–726, August, 1966.
50. Cox, S. M.: Ion Migration in Glass Substrates for Electronic Components, *Phys. Chem. Glasses,* vol. 5, no. 6, pp. 161–165, December, 1964.
51. Mackenzie, J. D.: Fine Structure in Glass from Ionic and Volumetric Considerations, *Proc. VII Int. Congr. Glass,* paper No. 22, Brussels, June, 1965.
52. Cramer, H. A., W. R. Johnston, and D. W. Callaway: Industrial Sapphire: a Key to Reliable Microelectronics, *IEEE Trans. Component Parts,* vol. CP11, no. 2, pp. 120–128, June, 1964.
53. Stookey, S. D. and R. D. Maurer: Catalyzed Crystallization of Glass: Theory and Practice, *Progr. Ceram. Sci.* vol. 2, pp. 77–102, Pergamon Press, New York, 1962.
54. Pask, J. A.: New Techniques in Glass-to-Metal Sealing, *Proc. IRE.,* vol. 36, pp. 286–289, February, 1948.
55. Dusing, W.: Seal Metals with Precious Metal Coatings for Microwave Tubes, *Glastech. Ber.,* vol. 31, pp. 137–142, April, 1958.
56. Dalton, R. H.: How to Design Glass-to-Metal Joints, *Prod. Eng.,* vol. 36, pp. 62–69, April, 1965.
57. Bondley, R. J.: Quartz-Metal Seals, *Proc. Int. Congr. on Microwave Tubes,* pp. 598–601, Academic Press, Inc., New York, 1961.
58. Floyd, J. R.: Effect of Composition and Crystal size of Alumina Ceramics on Metal-to-Ceramic Bond Strength, *Amer. Ceram. Soc. Bull.,* vol. 42, no. 2, pp. 65–70, February, 1963.
59. Wisser, G. R. and M. W. Hagadorn: An Improved Nickel-Titanium Ceramic-to-Metal Seal, *Gen. Tel. & Elec. Res. & Develop. J.,* vol. 1, pp. 43–46, January, 1961.
60. Hatzipangos, D. and J. H. Power: Thermal Characteristics of Film Resistor Modulus, *Proc. IEEE Electron. Components Conf.,* pp. 69–78, Washington, D. C., 1968.

61. "Reference Data for Radio Engineers," 4th ed., pp. 79–83, International Telephone & Telegraph Corp., American Book-Stratford Press, Inc., New York, 1961.
62. Buzard, J. B.: Cermet Resistor Process for Commercial Applications, *Proc. IEEE Electron. Components conf.,* pp. 79–83, Washington, D. C., 1968.
63. Asher, J. W. and C. P. Pratt: Screen-printed Ferro-electric Glass-Ceramic Capacitors, *Proc. IEEE Electron. Components Conf.,* pp. 239–245, Washington, D.C., 1968.
64. Herczog, A.: Microcrystalline $BaTiO_3$ by Crystallization from Glass, *J. Amer. Ceram. Soc.,* vol. 47, no. 3, pp. 107–115, March, 1964.
65. Hague, J. R., J. F. Lynch, A. R. Rudnick, F. C. Holden, and W. H. Duckworth: "Refractory Ceramics for Aerospace," published by American Ceramic Society, 1964.
66. Ceramic Parts, *Mater. Des. Eng.,* Manual 239, November, 1966.
67. Priest, D. H. and R. Talcott: Thermal Stresses in Ceramic Cylinders Used in Vacuum Tubes, *Amer. Ceram. Soc. Bull.,* vol. 38, no. 3, pp. 99–105, March, 1959.
68. Kingery, W. D.: "Introduction to Ceramics," John Wiley & Sons, Inc., New York, p. 682, 1960.
69. *Ibid.,* pp. 723–724.
70. Von Hippel, ref. 7, p. 181.
71. Comeforo, J. E., Properties of Ceramics for Electronic Applications, *Electron. Eng.,* April, 1967.
72. Kingery, W. D.: "Introduction to Ceramics," p. 534, John Wiley & Sons, Inc., New York, 1960.
73. Dixon, J. M., L. D. LaGrange, U. Merten, C. F. Miller, and J. T. Porter: Electrical Resistivity of Stabilized Zirconia at Elevated Temperatures, *J. Electrochem. Soc.,* vol. 110, no. 4, pp. 276–280, April, 1963.
74. Hickman, W. M. and J. F. Zamaria: Furnace Control by Fuel Cell, *Instrum. and Contr. Syst.,* vol. 40, p. 87, August, 1967.
75. Goffaux, R.: Electrical Properties of SiC Varistors, *Proc. Symp. on SiC: A High Temperature Semicond.,* pp. 462–481, Pergamon Press, New York, 1960.
76. Fredrickson, J. E. and W. H. Redanz: Boron Nitride for Aerospace Applications, Carbon Products Div., Union Carbide Corp.
77. *Union Carbide Bull*. 713–204 EF.
78. "Engineering with Glass," Corning Glass Works, Library of Congress Catalog Card No. 62-19567.
79. Sedden, E., E. J. Tippett, and W. E. S. Turner: The Electrical Conductivity of Sodium Metasilicate–Silicate Glasses, *J. Soc. Glass Technol.,* vol. 16, pp. 450T–477T, 1932. Kohl, *op. cit.,* p. 30.
80. Frisco, L. J.: Frequency Dependence of Electric Strength, *Electro-Technol.,* vol. 68, pp. 110–116, August, 1961. Kohl, *op. cit.,* p. 587.
81. Shand, E. B.: "Glass Engineering Handbook," 2d ed., pp. 67–90, McGraw-Hill Book Company, New York, 1958.
82. Vermeer, J.: The Impulse Breakdown Strength of Pyrex Glass, *Physica,* vol. 20, pp. 313–325, 1954.
83. Guyer, E. M.: Electrical Glass, *Proc. IRE,* vol. 32, pp. 743–750, December, 1944.
84. Chapman, J. J. and L. J. Frisco: *Elec. Mfg.,* vol. 53, p. 136, May, 1959; Shand, *op. cit.,* p. 79.
85. Birks, *op. cit.,* p. 214.
86. "Reference Data for Radio Engineers," 4th ed., p. 64, International Telephone & Telegraph Corp., American Book–Stratford Press, Inc., New York, 1961.
87. Stevels, J. M.: "Electrical Properties of Glass," *Handb. Phys.,* vol. 20, pp. 350–391, 1957.
88. Kohl, *op. cit.,* p. 121.
89. Von Hippel, ref. 7, p. 313.
90. McLean, D. A., N. Schwartz, and E. D. Tidd: Tantalum Film Technology, *Proc. IEEE* (Special Issue on Integrated Electronics), vol. 52, no. 12, pp. 1450–1462, December, 1964.

91. Martin, J. H.: The Manufacture of Ceramic-based Microcircuits, *Sprague Tech. Paper* TP-66-10, Sprague Electric Co., North Adams, Mass.

92. Shand, *op. cit.,* pp. 123–126.

93. Hoffman, L. C.: Precision Glaze Resistors, *Amer. Ceram. Soc. Bull.,* vol. 42, no. 9, pp. 490–493, September, 1963.

94. Burks, D. P. and B. Greenstein: Screened Thick Film Resistors, *Sprague Tech. Paper* TP-67-2.

CHAPTER 3
ELECTRONIC CERAMICS

Alex E. Bailey
LTCC Technology Manager
American Technical Ceramics
Formerly, Fellow Engineer
Northrop Grumman Corporation

3.1 PROPERTIES OF ELECTRONIC MATERIALS

The dielectric constant and dielectric susceptibility of a material are parameters that describe how the material interacts with an applied electric field. Dielectrics contain charge carriers that are displaced by an applied field, setting up dipole moments. When an electric field is applied to a dielectric, charges within the dielectric act to partially neutralize the applied field. This neutralizing, bound charge is the mechanism for charge storage in capacitors. The polarization is a measure of the surface charge density of this bound charge. The ratio of the resulting electric flux density D for an applied field E is the permittivity of the material, $\varepsilon' = D/E$. The ratio of the material permittivity relative to that of free space is the relative permittivity, or dielectric constant, of the material:

$$K = \varepsilon_r = \varepsilon'/\varepsilon_0 \tag{3.1}$$

where ε_0 is 8.854×10^{-12} F/m.

The electric flux density in the material is the sum of the flux density from the applied field and the polarization, or dipole moment per unit volume, of the material:

$$D = \varepsilon_0 E + P = \varepsilon E \tag{3.2}$$

Therefore,

$$P = D - \varepsilon_0 E = \varepsilon_0(\varepsilon_r - 1)E \tag{3.3}$$

Dielectric susceptibility is a measure of the polarization per applied field or the ratio of the bound charge density to the free charge density:

$$X = P/\varepsilon_0 E = K - 1 \tag{3.4}$$

The polarization is equal to the dipole moment times the number of dipoles per unit volume. That is, $P = N\mu$ where μ is equal to the polarizability times the local electric field. The local electric field is the sum of the applied electric field plus fields resulting from aligned

dipoles in the localized material:

$$P = N\alpha E_{\text{local}}$$

The dielectric constant of a material depends on contributions to the polarizability by

$$\frac{N\alpha}{3\varepsilon_0} = \frac{K-1}{K+2} \tag{3.5}$$

where α = polarizability
N = number of molecules per unit volume
ε_0 = permittivity of free space

Mechanisms of polarization include electronic, ionic, dipole, and space charge contributions. Electronic polarization is due to shifting of electron clouds as a result of applied fields. Materials containing large ions with more loosely bound outer-shell electrons generally have higher electronic polarizability. Ionic polarization arises from the displacement of ions of opposite charge from their normal lattice position under an applied field. Dipole polarization arises from the alignment of preexisting dipoles with the applied field. Space charge polarization is a result of mobile charges that are displaced but trapped in the material.

In real materials, the movement of charges in response to an applied field requires time, therefore, as the frequency is increased, polarization mechanisms can no longer respond to the rapidly changing field. The contributors to polarizability exhibit associated response times and are, therefore, frequency dependent as shown in Fig. 3.1.

In real materials, there is a response time for polarization, which acts as an internal resistance causing a phase lag δ of the charging current. The phase lag between applied voltage and charging current results in input power dissipated as heat. The portion of the current vector in phase with the voltage, loss current, is given by tan δ, also called the *dissipation factor*. The energy loss per second is given by

$$P = \pi v \epsilon V_{\text{max}^2} \tan\delta \tag{3.6}$$

where v is the frequency and V_{max} is the maximum voltage.

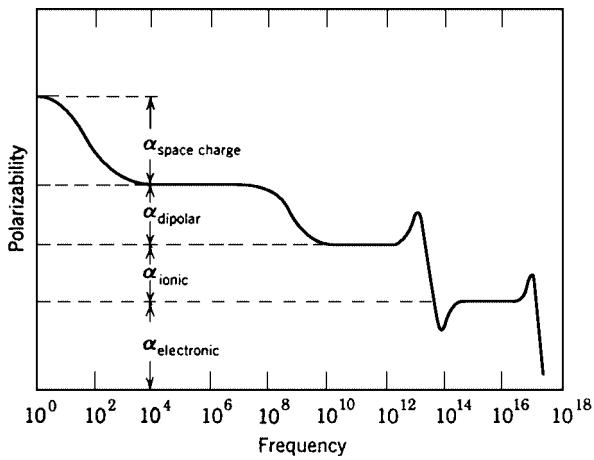

FIGURE 3.1 Frequency dependence of polarization mechanisms.[20]

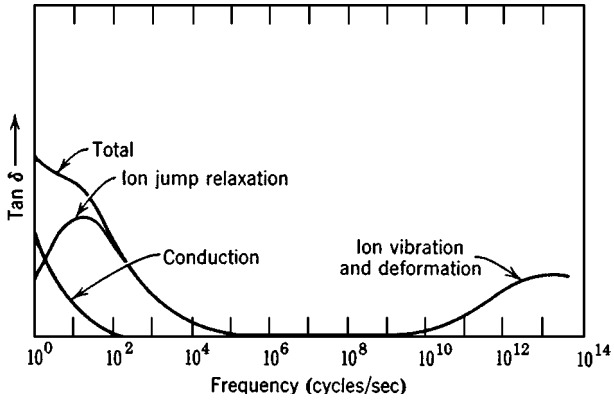

FIGURE 3.2 Frequency dependence of loss mechanisms.[20]

Losses in ceramic dielectrics may arise from ion migration, ion vibration and deformation, and electronic polarization. Figure 3.2 shows the loss contributions as a function of frequency for a lossy material.

3.1.1 Electrical Conductivity

For pure insulating ceramic materials, the electronic band gap is sufficiently large that any conduction is a result of charged ion movement. However, there may be both ionic and electronic contributions to conduction in common ceramic materials. The electrical conductivity of a material is defined as the charge flux density, j[C/(m^2·s)] for a given applied electric field E(V/m). That is,

$$\sigma = j/E = (nze)v/E \tag{3.7}$$

where n (m^{-3}) is the number of charged particles per unit volume having a drift velocity v(m/s), and ze (coulombs, C) is the charge per particle. The electrical conductivity is proportional to the concentration (nze) times the mobility (v/E) of the charge carriers. Table 3.1 shows the resistivity of a variety of conductors, semiconductors, and insulators.

The Nerst-Einstein relationship shows the temperature dependence of conductor mobility.

$$\sigma = j/E = (nze)v/E = (nze)(eza^2n/kT)\exp(-DG/kT) \tag{3.8}$$

where a = jump distance
n = jump frequency
k = Boltzmann's constant
DG = activation energy for ion mobility

Figure 3.3 shows the effect of charge carriers in insulating materials. The higher-purity silicas have considerably higher resistivities than those containing alkali metals such as

TABLE 3.1 Electrical Resistivity of Various Materials

Material	Electrical resistivity, $\Omega \cdot$ cm
Conductors:	
Copper	1.7×10^{-6}
Gold	2.3×10^{-6}
Molybdenum	5.2×10^{-6}
Tungsten	5.5×10^{-6}
ReO_2	2×10^{-6}
CrO_2	30×10^{-6}
Platinum	10.5×10^{-6}
Palladium	11×10^{-6}
Semiconductors (pure):	
Silicon	$>10^2$
Germanium	40
SiC	10
Insulators:	
Low-voltage porcelain	10^{12}–10^{14}
SiO_2 glass	$>10^{14}$
Al_2O_3	$>10^{15}$
Soda-lime-silica glass	10^5

soda-lime-silica glass. As temperature increases, the mobility of charge carriers increases, reducing the resistivity of the material. Impurity concentration can have a substantial effect on the electrical resistivity, since impurities generally raise the amount of charge carriers in a material, both through mobile ions and electronic conduction as a result of lattice defects (acceptor or donor sites). Acceptor sites are formed when an ion of lower valence is substituted on a lattice site. Typically, oxygen vacancies form as compensation for charge imbalance. Donor sites, formed from substitutions of higher-valence ions, result in excess electrons.

Measured values of electrical resistivity vary somewhat since the levels of impurities vary considerably from starting material sources, and compositions are often modified with additives to promote densification. In some systems, the impurities tend to collect as a glassy phase at the grain boundaries. The electrical resistivity of the material is then a composite of the two phases.

The insulator materials listed in Table 3.2 possess common features such as high electrical resistivity, high dielectric strength, low dielectric constant, and relatively low dielectric loss. Electrical resistivity is affected by a number of factors such as purity, porosity, and multiple phases. Note, for instance, the difference between fused quartz glass and general glass containing more mobile alkaline ions. The higher-purity, less ionic, materials such as Al_2O_3 and SiO_2 possess considerably higher electrical resistivities. Increasing porosity has the effect of increasing electrical isolation nearly linearly at low volume porosity levels. See Fig. 3.4.

While high electrical resistivity is the fundamental property of ceramics in electronic applications, superconductors being the exception, much of the development effort is involved in improving secondary properties, such as low dielectric constant, low electrical loss, good thermal conduction for heat dissipation, low density for weight savings, and good mechanical strength.

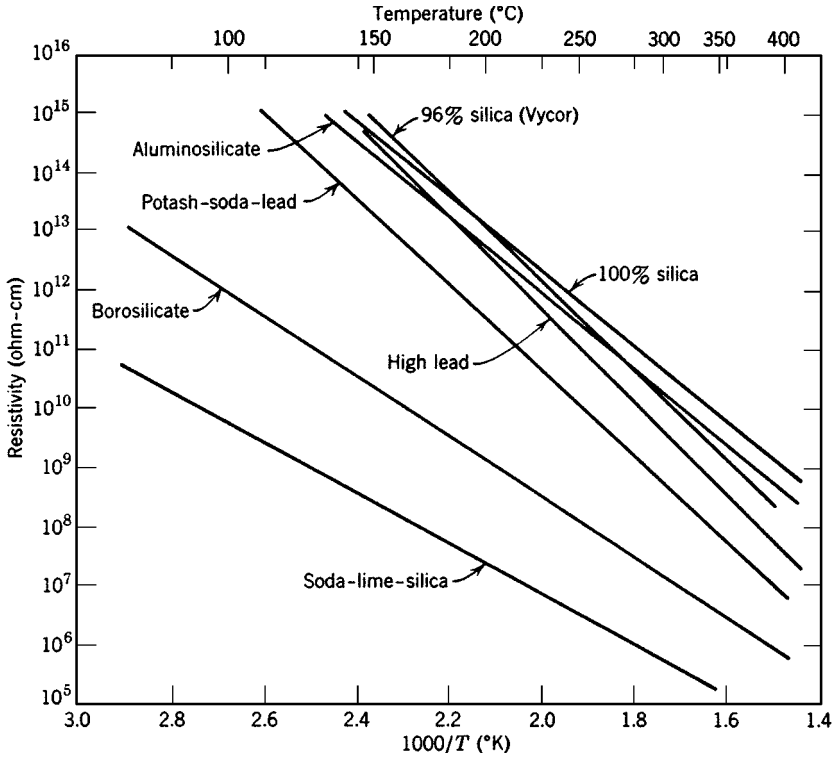

FIGURE 3.3 Effect of charge carriers on resistivity of glasses.[20]

3.1.2 Thermal Expansion

Thermal expansion of any material depends on the crystal structure, bond strength, density, phase transitions, and heat capacity. For instance, Al_2O_3 has a relatively high density because of its hexagonal-close-packed oxygen ions, whereas the silicates have lower densities because of the relatively open network structures resulting from the low coordination number of the silicon ion. The more open structure of the silicates is more accommodating to increased thermal vibrations, and therefore they expand less than alumina. Glass phases have more open networks and, therefore, even lower densities and lower thermal expansion than corresponding crystalline phases. Comparing amorphous fused silica (TCE = 0.5 ppm/°C) to crystalline quartz (TCE = 11 ppm/°C) is a good example. There are some unique crystalline phases, such as spodumene, that have an open structure and therefore a much lower thermal expansion.

Thermal expansion coefficient is inversely proportional to the bond strength of the compound. Strong covalent bonded materials, such as SiC and BN, and diamond have lower thermal expansion coefficients. These compounds require significantly more thermal energy to increase the amplitude of atomic vibrations, resulting in increased volume than a more weakly bonded material. For electronic insulators, engineers are most often concerned with thermal expansion coefficients near room temperature; however, it is important to remember that thermal expansion is not constant with temperature. In general, expansion increases

TABLE 3.2 Properties of Dielectric Insulators

Material	Thermal expansion, ppm/°C	Dielectric constant	Dielectric loss	Thermal conductivity, W/(m · K)	Flexural strength, MPa	Density, g/cm^3
96% Al_2O_3	7.4–8.2	9.5	0.0004	26	400	3.75
99.5% Al_2O_3	7.5–8.3	9.9	0.0002	35	552	3.90
Mullite	3.7–5.3	5.4–6.8	0.003	4–6.7	186	2.82–3.1
AlN	4.3–4.6	8.6–10.0	0.0002–0.001	140–220	207–345	3.25–3.30
BeO	7.5–8.8	6.5–6.7	0.0003	260	207	2.85
Steatite	4.2–7.2	5.7	0.0007–0.001	2.5	170–200	2.7
Fosterite	9.8–10.7	6.2	0.0002–0.0005	3.3–4.6	170–210	2.9–3.22
Spinel	7.0–8.8	6.6–8.3		7.6–15	200	3.6
Cordierite	1.4–2.5	4.5–5.7	0.004–0.008	2.5	120–245	2.0–2.53
Cristobalite	3.8	50.0				2.27–2.32
Spodumene	2.0	6.0				
Porcelain	5.0	6.5		2.0	140	2.4
Si_3N_4	2.0–3.5	6.0–8.1		21–43	150–1200	3–3.18
SiC	3.1–4.7	40		36–270	230–860	3.2
a-quartz	11.2	3.8		2.0	180	2.2
BN	3.8	4.1		60(cubic)–1300(hex)	110–150	2.2
Diamond	1.1	5.5		2000	1400	3.5
Lead borosilicate glass	7.0	7.0	0.004	2.5	320	3.1
Borosilicate glass	3.1	4.1	0.0006	2.0	150	2.3
Fused quartz	0.5	3.8	0.00004	1.6	80	2.2

with temperature and is proportional to the heat capacity of the material. This is important to consider in applications that may have broader temperature excursions or for device fabrication processes, such as soldering, brazing, or cofiring, that may involve bonding of dissimilar materials at temperatures significantly higher than room temperature. Heat capacity, the energy required to raise the temperature of a material, increases with temperature up to the Debye temperature, at which point there is little change with increasing temperature. The Debye temperature depends on crystal properties such as bond strength and elastic constants. The relationship between heat capacity and thermal expansion is as follows:

$$C_p - C_v = (dH/dT)_p - (dE/dT)_v = \alpha^2 V_0 T/B \tag{3.9}$$

where $\alpha = dv/v\,dT$ is the thermal expansion. Figure 3.5 shows the relationship between heat capacity and thermal expansion.

3.1.3 Thermal Conductivity

Thermal conductivity of a material is a measure of the quantity of heat transferred, Q, through a given cross section A for a temperature gradient ΔT across a thickness t. Thermal conductivity is defined as:

$$Q = kt/A\Delta T \tag{3.10}$$

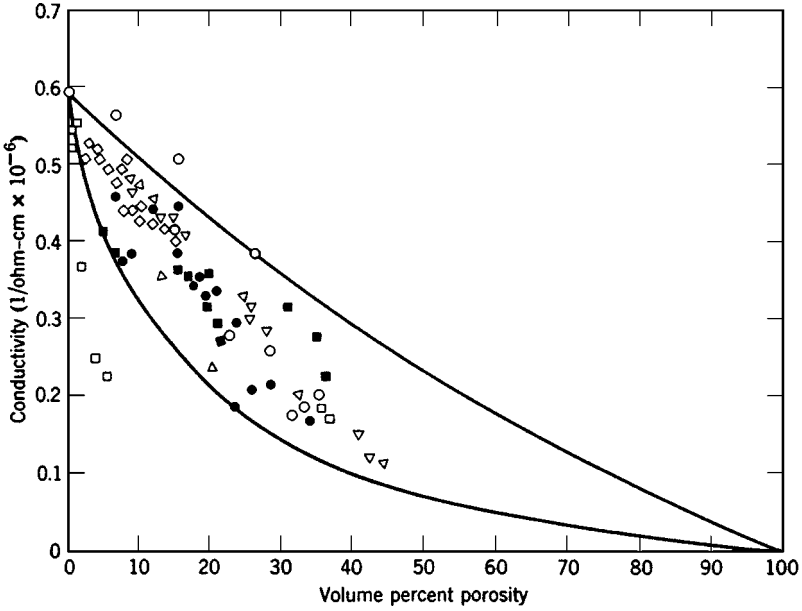

FIGURE 3.4 Porosity effect on electrical conductivity.[20]

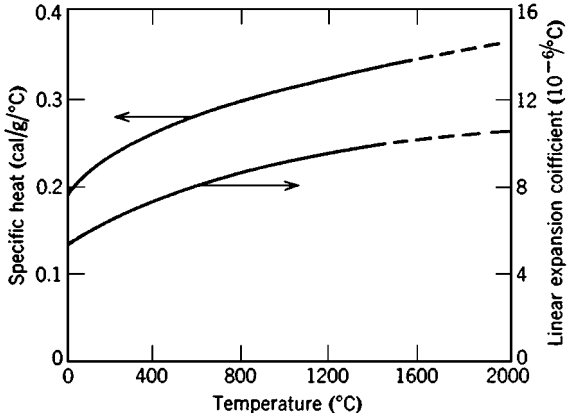

FIGURE 3.5 Relationship between heat capacity and thermal expansion of Al_2O_3.[20]

and is typically expressed in terms of W/(m · K) [or W/(m · C°)] or Btu/(h · ft · F°). The thermal conductivity of various materials is shown in Table 3.3.

Thermal conductivity is strongly influenced by such factors as crystal structure, atomic weights, grain size, and porosity. Figure 3.6 illustrates how thermal conductivity is affected by differences in atomic weights of constituent atoms. The greater

TABLE 3.3 Thermal Conductivity of Various Materials

Material	Thermal conductivity Wm · K
Diamond	2000
BN	1300
Ag	419
Cu	395
Au	298
BeO	242
SiC	270
AlN	230
Al	120–218
Si	118
Al_2O_3	25
Si_3N_4	3.0
α-SiO_2	2
Air	0

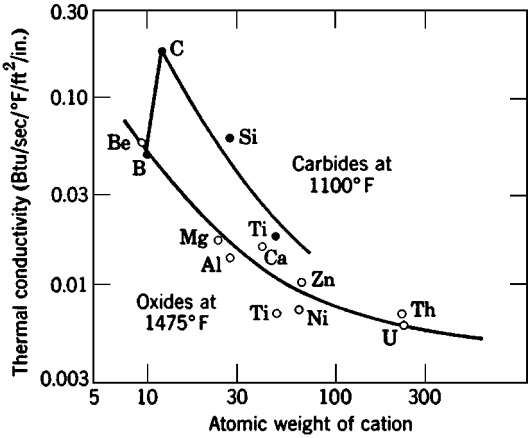

FIGURE 3.6 Effect of atomic weight on thermal conductivity.[20]

the difference, the more anharmonic the lattice vibrations, resulting in lower phonon conduction. This results in materials such as BeO, SiC, and AlN having very high thermal conductivity while materials such as cordierite and porcelains have considerably lower conductivity. Phonon scattering occurs at boundaries between grains, dissimilar materials, lattice imperfections, or at porosity interfaces. Figure 3.7 shows how the absence of grain boundaries in single crystals results in higher thermal conductivity than polycrystalline phases.

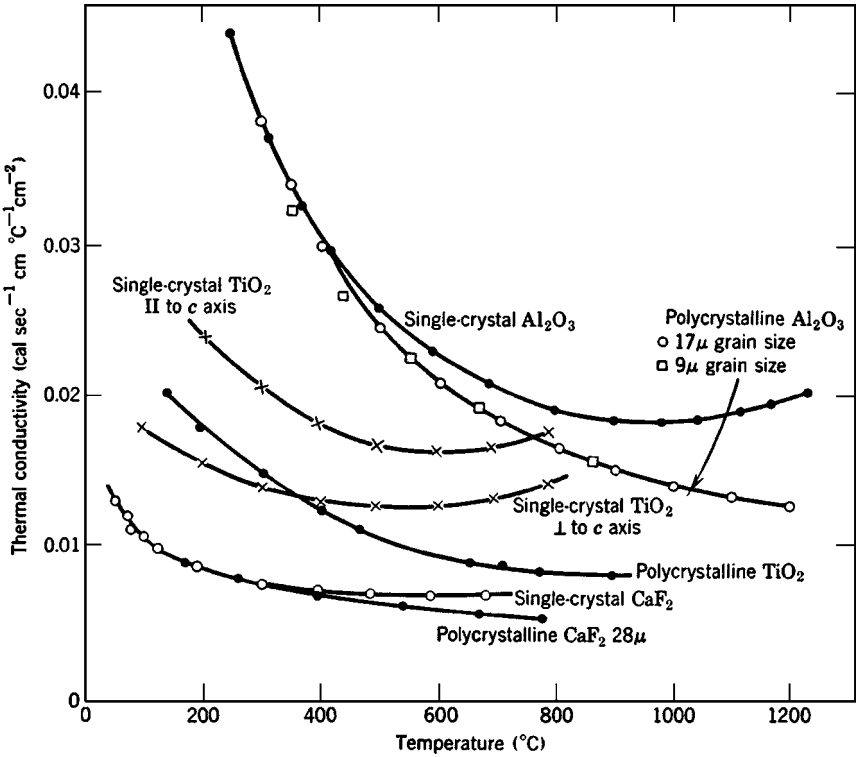

FIGURE 3.7 Thermal conductivity dependence on microstructure.[20]

3.2 DIELECTRIC INSULATORS

The general grouping of dielectric insulators covers a wide range of applications, from porcelains used for power line insulators to the most complex microelectronics packaging applications. Traditional ceramic insulators are made from materials that can be easily fabricated from abundant raw material sources, such as porcelains and glasses. Porcelains, consisting primarily of clay materials, have been in use since the fourth century B.C. and used in electronic insulator applications since the nineteenth century. In recent years, more refined insulators have been developed, which can generally be grouped into oxides, borides, nitrides, and carbides.

3.2.1 Oxides

Porcelains, $(K, Na, Ca)_2O \cdot Al_2O_3 \cdot SiO_2$, have traditionally been used since the advent of electricity for low-frequency insulator applications. Porcelains typically consist of polycrystalline materials containing greater than 10 volume percent of a glassy phase. The glassy phase aids in densification and to a large degree determines the resultant dielectric

and mechanical properties. Porcelains are typically composed of 40 to 60 percent clays, such as kaolinite, $Al_2Si_2O_5(OH)_4$, or montmorillonites, $Al_2Si_4O_{10}(OH)_2$. These fine platelet clays provides the main body for the ceramic. It also provides the main crystalline phase, mullite, which develops during firing.

Typically, 25 to 35 percent of the porcelain is composed of alkaline oxide fluxes, such as feldspars, (K, Na, Ca)$AlSi_3O_8$. The feldspar provides the main flux phase, which aids in densification of the structure. The amount of feldspars added determines the resultant properties. The alkaline elements in the feldspar lower the temperatures at which liquid phases form during firing and thus aid in sintering. On cooling, these liquid phases solidify as amorphous material.

The third ingredient in porcelain is 20 to 30 percent crystalline filler such as alumina (Al_2O_3), quartz (SiO_2), or zircon ($ZrSiO_4$). These refractory fillers are added to porcelains as a particulate reinforcement for attaining higher strength. The more commonly used quartz is partially dissolved on firing, increasing the viscosity of the liquid phase, which aids in maintaining shape during firing.

Low-voltage porcelains generally contain more feldspar phase and, therefore, densify at lower temperatures, 1000 to 1320°C. Because of the additional alkaline content, they are generally more lossy and yield lower breakdown strengths, 40 to 100 V/mil. These porcelains are used for low-voltage, low-frequency applications such as light receptacles, switch bases, fuse holders, tubes, bushings, and hot plate and toaster insulation.

High-voltage porcelains contain higher clay content and densify at higher temperature, 1350 to 1450°C, because of the lower alkaline content. These compositions yield better dielectric properties and are used in high-voltage applications. Breakdown strength for these compositions is higher because of the lower mobile ion content in the 250- to 400-V/mil range. Applications as power line (suspension) insulators and high-voltage circuit breakers are common.

Low porosity (less than 4 percent) is required for electronics applications to minimize moisture penetration and maintain good breakdown strengths. In many applications, particularly outdoor uses such as transmission line insulators, the porcelains are glazed to improve surface resistivity.

The properties of porcelains vary considerably general classifications were defined by Von Hippel as displayed in Table 3.4. Figure 3.8 shows the dielectric behavior as a function of temperature and frequency.

Corundum, α-Al_2O_3, is the most common electrical insulator material in the microelectronics industry. Its combination of low loss (less than 0.005), high electrical resistance (less than $10^{14}\ \Omega \cdot$ cm), and good thermal conduction (25 to 35 W/(m · K) makes it an excellent candidate for use in electronic packaging. Hexagonal α-alumina is fabricated by decomposition of hydrates of alumina, bauxite ($Al_2O_3 \cdot 2H_2O$). The strong covalent bonding of the Al and O ions result in a highly stable compound with a high melting point, 2050°C, excellent mechanical strength (350 MPa), and the highest hardness of any oxide material. This enables uses in harsh conditions such as spark plug insulators where temperatures and pressures can reach 900°C and 10 MPa. The volume resistivity of high-purity alumina is greater than $10^{15}\ \Omega \cdot$ cm, making it suitable for high power applications such as insulators in klystrons and magnetrons. Its transparency at microwave frequencies and good thermal conduction and hermeticity enable its use as microwave windows. The properties of alumina are largely dependent on the levels of impurities and additions of sintering aids. Firing temperatures range from 1500 to 1600°C, depending on the amount of sintering aids. Alumina is widely used as substrate in thick- and thin-film hybrid circuitry. It is also widely used in multilayer form, cofired with refractory metallizations in microelectronic packaging applications. An example of this application is the Intel 486 and Pentium microprocessor packaging.

TABLE 3.4 Properties of Porcelains

Material	1 High-voltage porcelain	2 Alumina porcelain	3 Stealite	4 Forsterite	5 Zircon porcelain	6 Lithia porcelain	7 Titania, titanate ceramics
Typical applications	Power line insulation	Spark plug cores, thermocouple insulation, protection tubes	High-frequency insulation, electrical appliance insulation	High-frequency insulation, ceramic-to-metal seals	Spark plug cores, high-voltage high-temperature insulation	Temperature-stable inductances, heat-resistant insulation	Ceramic capacitors, piezolectric ceramics
Specific gravity, g/cm^3	2.3–2.5	3.1–3.9	2.5–2.7	2.7–2.9	3.5–3.8	2.34	3.5–5.5
Water absorption, %	0.0	0.0	0.0	0.0	0.0	0.0	0.0
Coefficient of linear thermal expansion, at 20–700°C, 10^{-6} in/(in · °C)	5.0–6.8	5.5–8.1	8.6–10.5	11	3.5–5.5	1	7.0–10.0
Safe operating temperature, °C	1,000	1,350–1,500	1,000–1,100	1,000–1,100	1,000–1,200	1,000	
Thermal conductivity, cal/(s · cm · °C)	0.002–0.005	0.007–0.05	0.005–0.006	0.005–0.010	0.010–0.015	—	0.008–0.01
Tensile strength, lb/in^2	3,000–8,000	8,000–30,000	8,000–10,000	8,000–10,000	10,000–15,000	—	4,000–10,000
Compressive strength, lb/in^2	25,000–50,000	80,000–250,000	65,000–130,000	60,000–100,000	80,000–150,000	60,000	40,000–120,000
Flexural strength, lb/in^2	9,000–15,000	20,000–45,000	16,000–24,000	18,000–20,000	20,000–35,000	8000	10,000–22,000
Impact strength ($^1/_2$-in rod), ft · lb	0.2–0.3	0.5–0.7	0.3–0.4	0.03–0.04	0.4–0.5	0.3	0.3–0.5
Modulus of elasticity, 10^{-6} lb/in^2	7–14	15–52	13–15	13–15	20–30	—	10–15
Thermal shock resistance	Moderately good	Excellent	Moderate	Poor	Good	Excellent	Poor
Dielectric strength ($^1/_4$-in-thick specimen), V/mil	250–400	250–400	200–350	200–300	250–350	200–300	50–300
Resistivity at room temperature, Ω/cm^3	10^{12}–10^{14}	10^{14}–10^{15}	10^{13}–10^{15}	10^{13}–10^{15}	10^{13}–10^{15}	—	10^3–10^{15}
T_e value,* °C	200–500	500–800	450–1,000	above 1,000	700–900	—	200–400
Power factor at 1 MHz	0.006–0.010	0.001–0.002	0.0008–0.0035	0.0003	0.0006–0.0020	0.05	0.0002–0.050
Dielectric constant	6.0–7.0	8–9	5.5–7.5	6.2	8.0–9.0	5.6	15–10,000
L grade (JAN Spec. T-10)	L-2	L-2–L-5	L-3–L-5	L-6	L-4	L-3	—

*Temperature at which resistivity is 1 MΩ · cm.

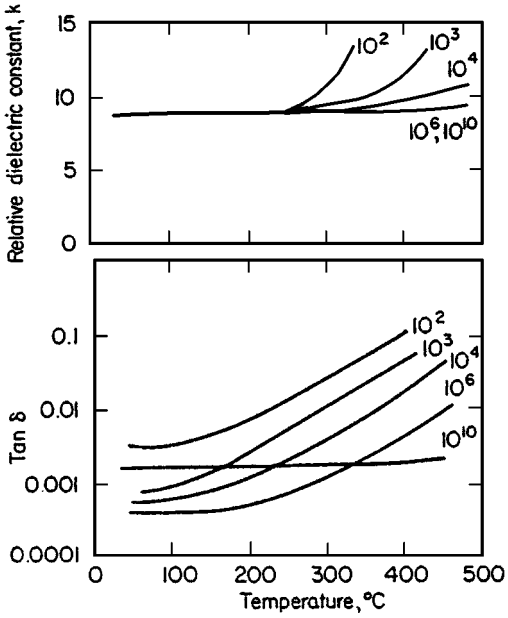

FIGURE 3.8 Electrical properties of porcelain as a function of temperature and frequency.[18]

The quartz form of SiO_2 is a commonly used packaging material, primarily for its high resistivity and low losses, particularly at high frequencies. Difficulties in fabricating high-quality polished substrates results in relatively high cost and therefore limits its applications. The thermal and electrical properties of crystalline quartz is highly anisotropic. The thermal conductivity at 400 K is 7.9 W/(m · K) perpendicular to the *c* axis and 4.8 W/(m · K) parallel to the *c* axis. The coefficient of thermal expansion increases up to 40 ppm/°C perpendicular to the *c* axis and 23 ppm/°C parallel to the *c* axis. The liquid phase of SiO_2 tends to have very high viscosity and readily forms a glass phase on cooling. SiO_2 is commonly used in its glass form, fused silica. The thermal conductivity for bulk silica glass is 1.5 W/(m · K). The thermal expansion of fused silica is considerably lower, 0.5 ppm/°C, than the crystalline phase because of the lower density of the glass structure. Fused quartz is more commonly used in insulators, but its low thermal expansion limits its use as a packaging material.

Beryllia, BeO, is commonly used as a substrate material in electronic packaging as a result of its low dielectric loss (0.02 percent) and combined high electrical and low thermal resistivities. Its electrical and thermal properties are somewhat better than those of alumina. This material is relatively easily sintered into dense substrates. Beryllia is higher in cost than alumina because of the higher cost of its raw materials and its higher-temperature fabrication (T_{melt} = 2570°C). The limiting factor keeping it from widespread use is the toxicity of Be-base powders. Beryllia has been used in klystron devices and power diodes.

Magnesia, MgO, not commonly used as a substrate material because its high sintering temperatures result in low-density ceramics. Some more recent cryogenic applications as substrates for superconductor substrates have emerged as a result of its thermal expansion match to high-temperature superconductor (HTS) materials.

Zirconia, ZrO_2, is used in applications where high fracture toughness is needed. Partially stabilized zirconia (PSZ) is formed with additions of Ca and Y oxides.

Spinel, $MgAl_2O_4$, is not commonly used because of difficulty in fabrication. Limited applications take advantage of its high thermal expansion, 8 ppm/°C, or its high use temperature, above 1900°C.

Mullites, $Si_2Al_6O_{13}$, have a low thermal expansion and are more thermal-shock-resistant than alumina. Typical processing results in an amorphous grain boundary that leads to low strength (less than 200 MPa) and low fracture toughness (1 to 2 MPa $\cdot$ $m^{1/2}$).

Steatite, $MgO\text{-}SiO_2$, ceramics are primarily used for high-frequency insulators because of their low losses at high frequency and high resistivity. Talc, $Mg_3Si_4O_{11} \cdot H_2O$, is the typical raw material used to form steatite ceramics. Typical firing temperatures are in the range of 1300°C. Figure 3.8 shows the dielectric behavior as a function of temperature and frequency. Abundance of raw materials and ease of fabrication were its key attributes in early application. It could rather easily be die-pressed into shapes with tight dimensional control without the use of inorganic additives. Steatite has fair mechanical strength relative to porcelains because of the lower vitreous phase content. The high thermal expansion and fair mechanical strength results in poor thermal shock resistance. The first electronics applications came in the 1920s for radio transmitters, which required the low loss properties of steatite. The first true ceramic substrate applications used steatite material in the mid-1950s.

Forsterite, $2MgO \cdot SiO_2$, ceramics are easier to fire than steatite or cordierite and have low dielectric losses, even to microwave frequencies. Their high thermal expansion limits their use as substrate materials and results in poor thermal shock resistance. Forsterite ceramics are used in high-power applications such as ceramic vacuum tube envelopes.

Cordierite, $Mg_2Al_4Si_5O_{18}$, has slightly higher losses than steatite or fosterite but has very low thermal expansion coefficient and good thermal shock resistance. Cordierite is typically formed from clays and talc. Typical firing temperatures are 1150 to 1400°C. The commonly used form of cordierite is hexagonal, which has anisotropic thermal expansion. Negative expansion in the *c* axis is offset by low positive expansion perpendicular to the *c* axis, resulting in a low volume expansion, about 2 ppm/°C. This low thermal expansion is a result of a ring structure accommodating thermal expansion through rotation and twisting. Cordierite is used primarily in applications where good thermal shock resistance is needed, such as catalytic substrates in diesel engines, fuse holders, electric heater plates, thermocouple insulation, radomes, and spark plug insulators.

Spodumene, $Li_2O \cdot Al_2O_3 \cdot SiO_2$, has low net shrinkage during sintering because of expansion of the B phase. This material has a near zero or negative thermal expansion coefficient, resulting in excellent thermal shock resistance.

3.2.2 Nitrides and Carbides

Si_3N_4 is primarily used in structural applications; however, it possesses low dielectric loss, thermal expansion match to silicon, and high thermal conductivity, making it an exceptional candidate for substrate applications. The relatively high fabrication costs and difficulty of fabrication, sintering, or hot pressing above 1700°C limit its potential.

BN has a hexagonal structure that can be easily machined. BN has relatively high thermal conduction and good thermal shock resistance.

AlN has received considerable attention in recent years because of its excellent dielectric properties, high thermal conduction, and high strength, outperforming Al_2O_3. AlN is formed by nitriding aluminum powder and must be fired in a nitrogen atmosphere to avoid oxidation. As with all the nitrides, high sintering temperatures (greater than 1800°C) are

needed for fabrication. Sintering aids or hot pressing is necessary to achieve high densities. AlN has strength similar to that of alumina, due to the strong covalent Al-N bond. Toshiba Ceramics has a version that is hot-pressed above 1600°C. As a result of its excellent properties and good thermal expansion match to silicon, AlN is often used in microelectronics substrates and multilayer packaging. The multilayer versions are typically hot-pressed in a vacuum atmosphere to nitriding the refractory metallizations, such as tungsten.

SiC has high strength and thermal conductivity, but its semiconducting properties limit its use as a substrate material.

3.3 ELECTRONIC PACKAGING

The microelectronics era began in 1955 with the development of diodes and transistors. The first ceramic substrates, in the mid-1950s, were made from steatite that fires in the range of 1200 to 1350°C. These packages were subsequently metallized with gold, silver, platinum, or palladium, pastes. These substrates were used for mounting resistors, capacitors, conductors, and vacuum tubes. The steatites were eventually replaced by 96 percent Al_2O_3. Alumina had been developed as a spark plug insulator in the 1940s because of its superior dielectric and thermal properties. Because of the high firing temperatures, over 1600°C, refractory metallizations such as W, Mo, and W-Mo pastes were developed for cofiring with the alumina substrate. The first multilayer ceramic package was developed in 1960 by engineers at RCA as a package for quartz crystal oscillators. This was the first laminated ceramic package formed from tapecast alumina and Mo-Mn metallization.

There are three primary classifications of interconnect technology:

- Laminated polymers [multichip module L (MCM-L)]
- Ceramic (MCM-C)
- Deposited polymers (MCM-D)

Each of these systems continues to be thoroughly exploited to meet the more demanding packaging requirements. The demand for higher-performance packaging technologies requires higher circuit density, faster transmission, lower transmission loss, and greater reliability. These requirements translate to finer and tighter circuit geometry using high-conductivity metallization in a low-dissipation, low-dielectric-constant medium. Also, the materials must be mechanically and chemically stable and thermally matched to surrounding materials. As semiconductor chip size continues to increase, the need for thermal expansion matching is greater. Manufacturing engineers strive to optimize and automate processing to minimize costs. Some of these requirements are mutually exclusive; ultimately engineers must make tradeoff in selecting the appropriate material system.

MCM-L will continue to have significant market share because of its maturity and low cost; however, it will likely lose market share to the greater circuit density capabilities of MCM-D and -C. The area with highest growth potential is MCM-D, where significantly higher circuit densities and I/O count are achievable. Table 3.5 shows the current tradeoff between input/output (I/O) capacity for the three different categories of packaging.

The key advantage of laminated polymer technology is generally considered to be low cost. While it does involve etching and plating processes, the materials are very low cost (Cu metallization, epoxy glass, or polyimide), and the processes are very mature. The ceramic packaging offers higher circuit density, better thermal conductivity, higher potential for three-dimensional (3-D) packaging, integration of passive components, and hermeticity over that of deposited polymer packages. The ceramic packaging technology is less mature and

TABLE 3.5 Comparison of Interconnect Densities

Technology	Connection density, in/in^2/per layer	Signal layers (total layers)	Total length, in/in^2	Via density per in^2
PC boards (3 tracks, 0.100-in pitch)	30	12 (12)	360	100
Multilayer ceramic (1 track, 0.020-in pitch)	50	20 (42)	1000	2,500
Cu/PI thin film (2 tracks, 140-μm pitch)	350	4 (8)	1400	33,000

Source: Ref. 12.

currently has higher associated materials and manufacturing costs; however, there is now considerable effort to bring lower-cost metal systems and manufacturing systems into higher-volume production. For an increasing number of electronic systems, the circuit or I/O density is overwhelmingly the most critical factor in choosing a packaging technology. The more recently developed deposited-polymer packaging offers the significant advantage of higher circuit density than any other packaging technology. Because it is a less mature technology, the current associated costs are high.

There are efforts to combine features and processes of these different packaging approaches, such as multilayer ceramic with surface thin-film or photoimaged circuitry or multilayer polymer on ceramic combinations. While there are significant advantages and disadvantages to each of these packaging technologies, each will continue to possess significant market share for years to come.

3.3.1 Ceramic Packaging

Ceramic interconnect technology offers significant benefits in terms of design flexibility, density, and reliability. These advantages, inherent in the ceramic materials themselves, often make this material the preferred alternative for high-density, high-reliability applications. The ceramic packaging can be categorized as thin-film, thick-film, and multilayer.

Table 3.5 compares various ceramic substrate materials. If one were to design the ultimate substrate material, a thermal expansion matched to that of the semiconductor chips (3.5 ppm/°C for Si, 7.5 ppm/°C for GaAs) would be desirable to improve reliability, particularly as chip sizes continue to grow. Low dielectric loss is desirable, as it has a direct impact on the transmission losses of the thin- or thick-film circuits. Usually high thermal conductivity is desired, particularly in power devices, to conduct heat away from the chips. Thermal management is a key element in mechanical design of today's advanced electronics. The trend to high circuit densities within ICs and the packaging lead to higher heat densities, and component failure rates increase exponentially as temperature is increased. High mechanical strength is desirable for mechanical stability and reliability. Low-density materials are typically desired for lightweight systems. The desired dielectric constant may vary, depending on the application. Lower dielectric constant generally allows closer spacing of signal lines and higher transmission speeds. In some devices, such as resonators or filters, higher dielectric constants result in reduced feature dimensions.

Speed of data transmission in semiconductor devices has been the focal point of development; however, the levels of packaging materials, through which the signals must eventually pass, have not kept pace, and packaging has become one of the limiting factors

in the speed of transmission of microelectronic devices. The transmission time delay is related to the dielectric constant of the packaging material by

$$\tau_d = K^{1/2} l/c \tag{3.11}$$

where l = length of the circuit
c = speed of light
K = dielectric constant of the transmission media

Therefore, it is desirable to design in low dielectric constant media, such as the silicates. For instance, silica with a relative permittivity of about 4 would yield a transmission delay about twice that of pure vacuum ($\varepsilon_r = 1$), whereas alumina with a relative permittivity of about 10 would yield about 3 times the delay. The lowest dielectric constant ceramic packaging is silica based, such as quartz or Northrop Grumman's low-K LTCC. Higher dielectric constants also contribute to the losses of the material. Power absorption P is related to both the dielectric loss and dielectric constant of the material by

$$P = p\varepsilon_0 V^2 \nu K \tan\delta \tag{3.12}$$

where V is the applied voltage and ν is the operating frequency.

3.3.1.1 Thin Film. Thin-film metallization on ceramic substrates was developed to take advantage of high circuit density and tight dimensional tolerances of deposited and etched metals and the high thermal conduction and mechanical stability of ceramic substrates. Typically the substrate used is high-purity alumina (99.5 to 99.6 percent), polished to fine surface finish and good flatness. However, thin-film circuitry has been used on a wide variety of ceramics, including glasses, multilayer ceramics, and magnetic ceramics as a method of forming surface features with tight dimensional control and fine-line resolution (about 0.5- to 1-mil lines and spaces). Standard grain size for the 99.5 percent alumina is about 2 to 2.5 μm, yielding a surface finish of less than 0.15 μm (less than 6 μin). The more expensive 99.6 percent alumina substrates are used in applications for very fine line depositions, since they are generally more defect-free and have finer surface finish. Thin-film metallization is applied to a suitable substrate by a variety of deposition methods such as evaporation, sputtering, plating, or chemical vapor deposition (CVD). The metallization is generally deposited over the entire substrate surface and then photoimaged and etched to the desired circuit pattern.

All of the desirable high-conductivity metallizations—Au, Cu, Ag, Al—can be deposited as thin films. Additionally, thin-film resistors of materials such as tantalum nitride (TaN or Ta_2N) or nickel chrome (NiCr) are used. Materials such a silicon oxides or nitrides have been deposited to serve as passivation and capacitor dielectrics. The evaporation method is a vacuum deposition process where a source metal is heated to its vaporization temperature under high vacuum (10^{-5} to 10^{-6} torr). Figure 3.9 shows the schematic for a typical vacuum evaporator. Sputtering involves bombardment of a metal target with an ion plasma. The metal target is used as the cathode; the substrate to be plated is the anode. When a high electric field is applied between the electrodes in an evacuated chamber, argon purge gas is ionized. The Ar^+ ion is then accelerated by the electric field into the metal cathode. The high-energy collisions sputter ions of the target metal, forming a plasma, which then deposits on the substrates at the anode. Figure 3.10 shows a schematic of a sputtering system. Since the material is depositing at high kinetic energy, the sputtered film is typically better adhered and more dense than evaporated films.

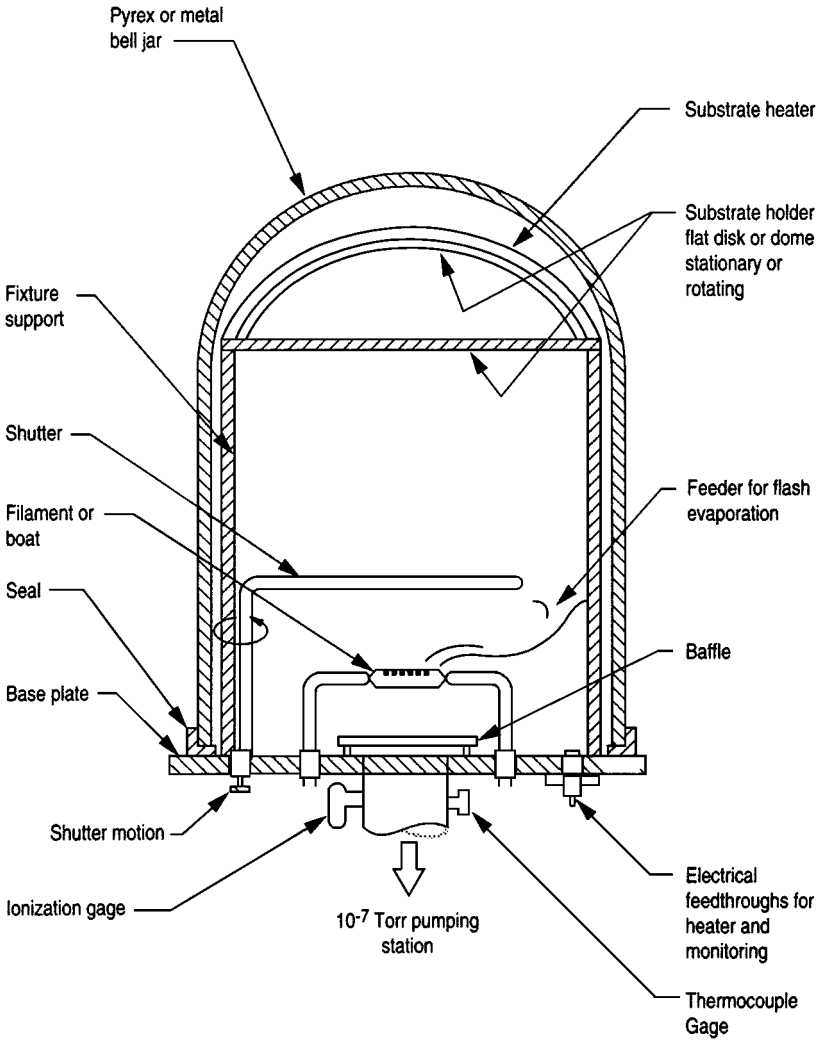

FIGURE 3.9 Schematic for vacuum evaporator.[18]

The properties of deposited films are highly dependent on the processing conditions and substrate properties such as surface chemistry and finish. Typically, a thin adhesion layer, such as Cr, Ti, NiCr, or TaN, is first deposited onto the substrate. This is followed by the high-conductivity metallization layer. Sometimes it is necessary to apply a final barrier layer over the metallization to prevent oxidation.

3.3.1.2 Thick Film. In its simplest form, thick-film technology involves the deposition of metal circuitry on a dense ceramic substrate by screen-printing technology.

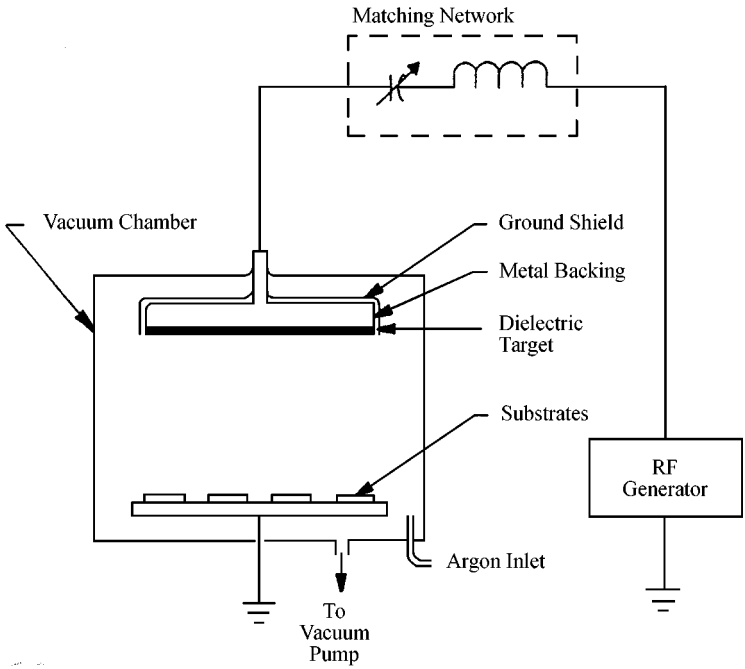

FIGURE 3.10 Schematic for RF sputtering unit.[18]

The metallizations are formulated with glasses and oxides to aid in densification of the metal and adhesion to the substrate at relatively low temperatures (600 to 950°C). The ability to build up multiple layers of circuitry by using insulating dielectric layers is a key advantage of this technology. Successive layers are printed, dried, and fired to build up a multilayer structure on a rigid ceramic or metal base. The substrate material is widely varying; thick-film metallization is used in nearly all forms of electronic ceramics, including magnetic, electrooptic, and superconductor substrate ceramics. Thick-film circuits are often used as hybrid packaging, that is, as a method to interconnect active ICs and passive components, such as capacitors, resistors, and inductors. In packaging applications, those materials listed in Table 3.2 are often used as the base substrate, 96 percent Al_2O_3 being most common. Special pastes for deposition of inductors, capacitors, and resistors have been developed, greatly expanding the capabilities of the technology. Thick film has been in use in various forms since the 1920s and is one of the longest-running commodity markets in the electronics industry.

These pastes are designed for thermal expansion matching to the semiconductor chips and the base substrate. The metal, dielectric, resistor, and ferrite pastes consist of the organic vehicle, the metal or oxide powders, and a glass frit. The organic vehicle consists of a solvent, dispersants, and a binder system. The binder system is used to hold the fine inorganic particles together and form a temporary bond with the underlying substrate prior to the firing process. The organic binder resin can be dissolved in solvents and easily decomposed in air or nitrogen atmosphere. The solvents and dispersants are used with the binder and inorganic particles to form a paste that can be deposited onto substrates with a rubber squeegee.

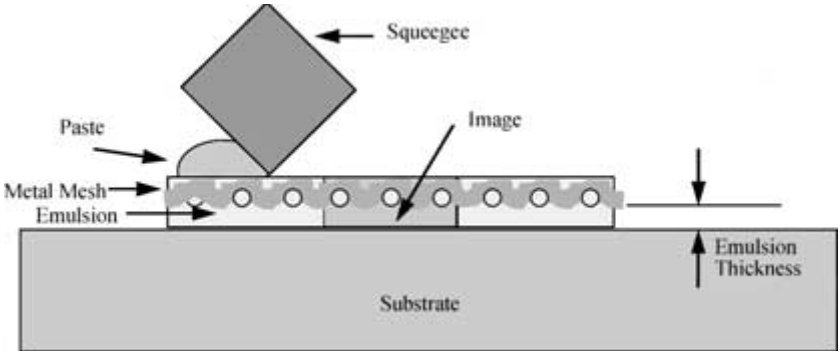

FIGURE 3.11 Screen printing schematic.

Glass frit and/or bismuth or copper oxides are added to promote adhesion to the substrate. Typically, the frit consists of high-lead or -bismuth glasses and is added to conductor paste blends to aid in adhesion. Glasses are chosen whose melting point is about 200°C lower than the firing temperature of the paste.

Figure 3.11 shows the basis of the thick-film process, screen printing. In screen printing a rubber squeegee is used to force a thick paste through a stainless steel mesh screen, imaged for the circuit features, onto the substrate material. Typically, stainless steel mesh screens are used. The mesh of the screen is filled with a UV light–curable emulsion. Normally the emulsion is thicker than the metal mesh, flush with the mesh on the squeegee surface and extending beyond the mesh on the substrate side of the screen. Emulsions typically extend beyond the thickness of the wires by several ten-thousandths of an inch. This additional emulsion is used to control print thickness and prevent the mesh patterns from being transferred to the printed features. The circuit patterns to be printed are imaged into the screen emulsion by using positive image artwork on Mylar film or glass plates. Those areas exposed to the UV light are cured. The noncured emulsion is water soluble and is washed away, leaving the open stainless steel mesh through which the thick-film pastes will be deposited. Screen parameters such as mesh, emulsion thickness, wire diameter, and mesh angle determine the thickness and quality of the printed circuits. Screen meshes range from 200 to 400 mesh (wires per inch), but 325 mesh is most common. In general, finer wire diameters are desirable but the fineness is limited by the tensile strength of stainless steel; 0.0006- to 0.002-in. wires are used. Equipment parameters such as squeegee pressure, speed and angle, snap-off, and down-stop also impact print quality. Also, material parameters such as paste rheology and control, and substrate surface finish, porosity, and flatness impact print quality and variability.

Typically, two prints are used for each dielectric layer to avoid pin holes, which would result in shorts between layers. The two dielectric layers are applied in print-dry-fire-print-dry-fire or print-dry-print-dry-fire fashion. As shown in Fig. 3.12, openings of about 10 mils are designed into the dielectric layers to be filled with conductive pastes on subsequent processing. These metallized "vias" serve as the interconnect between the layers of circuitry. As increasing numbers of layers are applied, the substrate surface becomes less planar. Nonplanar surfaces can result in difficulties in automated assembly of components to the package. This limits the number of circuit layers that can be applied by thick-film technology to about seven to eight layers. The screen printing operation limits the resolution of thick-film circuitry to about 4-mil lines and spaces in volume production; 6- and 8-mil lines

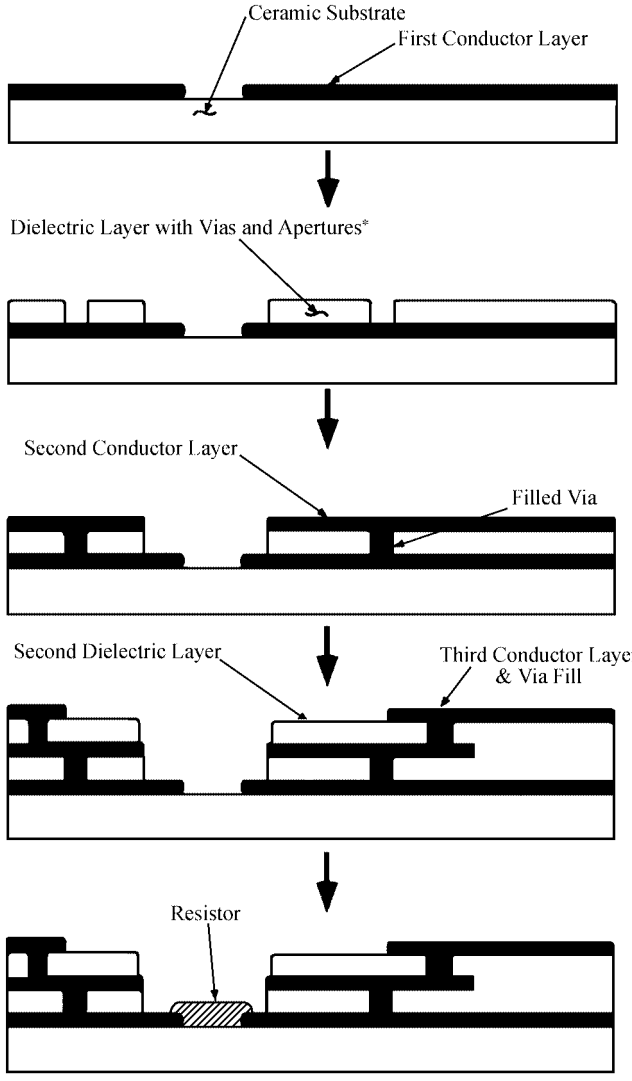

FIGURE 3.12 Thick-film multilayer fabrication steps.[18]

are more common. Other technologies are being developed to expand the capabilities of thick-film processes. Direct writing machines, such as the Micropen, print circuitry through a dispensing nozzle. This system is capable of writing 3- to 4-mil lines with fine spaces (1 to 2 mils) over nonplanar surfaces and in cavities. Photoimageable and etchable thick-film systems have been developed to improve the circuit resolution of thick-film. DuPont's Fodel and Herneus' KQ systems are examples. Some systems involve polymerization of

TABLE 3.6 High-Conductivity Metallizations

	Au wire bonding	Al wire bonding	Eutectic bonding	Sn/Pb solder	Epoxy bonding
Au	Y	N	Y	N	Y
Pd/Au	N	Y	N	Y	Y
Pt/Qu	N	Y	N	Y	Y
Ag	Y	N	N	Y	Y
Pd/Ag	N	Y	N	Y	Y
Pt/Ag	N	Y	N	Y	Y
Pt/Pd/Ag	N	Y	N	Y	Y
Cu	N	Y	N	Y	N

the pastes by exposure to a UV light through a photonegative mask. The paste containing uncured polymer is washed away. This process of photoimaging results in finer circuit features, such as via diameters down to 100 μm. This allows for more densely packed circuitry. Etchable thick-film metallizations have also been developed. The substrate is covered with a thick-film layer of fired gold, rather than deposited metal as in thin-film. This metal can then be processed through subsequent thin-film photoresist and etching processes to form fine-resolution circuits, compatible with subsequent thick-film printing and firing processes.

One of the key advantages of thick-film is the use of high-conductivity metallizations such as Au-, Ag-, and Cu-based systems, as shown in Table 3.6. The choice of metal systems is based on cost, package assembly, and performance requirements. Thick-film may be Au and Al wire bondable, low-temperature solderable, or high-temperature brazeable. Gold is often used for its noble metal properties, that is, its inertness to oxidation, migration, and chemical reaction. Gold circuits have excellent thermocompression bonding and high-temperature brazing (with Au-Sn, Au-Ge) properties, but are not well suited for soldering because of gold's poor leach resistance. Adding Pt and Pd to Au forms solid solutions that are more leach resistant, but less conductive. The need for lower cost drove the development of Ag- and Cu-based conductors. Silver (1.5 to 3 mΩ/square) and Cu (2 to 4 mΩ/square) have better conductivity than Au (3 to 5 mΩ/square) and are dramatically lower in cost, but they are prone to oxidation during firing. Silver also has problems with migration, especially in humid conditions. Silver-palladium alloys help to reduce Ag migration. Copper has excellent stability and solderability but must be fired in an inert atmosphere to avoid oxidation. The metal powders typically have spherical morphology. Flake-shaped particles are sometimes used for improving particle contact.

3.3.1.3 Multilayer. The multilayer ceramic technology allows multiple circuits to be handled in a single, self-contained, hermetic package. Structures incorporating buried components allow increased design flexibility by providing a mechanism for establishing both stripline and microstrip within the same medium. The ability to integrate digital, analog, radio-frequency (RF), microwave, and buried passive components in this manner reduces assembly complexity and improves overall component and system reliability by reducing part count and interconnections.

The multilayer systems use low-dielectric-constant materials similar to traditional ceramic substrates for dielectric layers and an internal circuit metallization designed to be cofired with the ceramic dielectric. Cofiring of metallization with a ceramic dielectric required development of compatible systems which would have matching shrinkage onsets, shrinkage rates, and total volumetric shrinkage. Since the metal thermal expansions are

considerably higher than that of the ceramic matrix, the metal must be compliant or have additives to make its thermal expansion more closely match that of the ceramic. Additionally, the thick-film pastes must be formulated with solvents and binder systems that are compatible with the ceramic green tape. Additives to the metallization, in the form of glass frits or oxide bonding agents, are added to promote adhesion of the metal to the ceramic. Since these additives increase the resistivity of the metallization, the amount of additives are limited.

High Temperature Cofired Ceramics (HTCC). The most common multilayer packaging technology uses alumina-based material (90 to 94 percent) with silica and alkaline fluxes, such as MgO and CaO, added as sintering aids. The small amount of glass that forms is needed to improve the densification behavior of the dielectric and achieve better adhesion to the metallization. HTCC was first developed by IBM for use in mainframe computers. In the early 1980s IBM developed a multilayer tape-casting process for fabrication of a 33-layer, cofired Mo metallization package housing 100 bipolar chips. The relatively high firing temperature of alumina-based ceramics, about 1600°C, requires the use of more refractory metallizations for cofired internal circuitry. Since these metals possess high electrical resistivities, about 4 times that of gold, the electrical losses are higher than in other ceramic packaging technologies.

Figure 3.13 shows the fabrication process for HTCC packaging. The ceramic powders are dispersed in a solvent mixture with binder and plasticizers. The slurry is cast into thin tape form by a doctor blade process. The thin (0.5- to 10-mil) tape is heated during a continuous casting operation to dry off the solvents, leaving behind a thin flexible ceramic-organic composite. These flexible sheets allow low-cost assembly of very complex packages by forming the three-dimensional structure in the green state.

The thin sheets are cut to standard processing sizes. The circuit connections between layers (vias) are formed by programmable pneumatic punches or hard dies. The vias are filled with conductive metallization by using stencils in a screen printing process. The unique internal circuits are printed on the individual tape layers. Three-dimensional cavity patterns are formed by cutting the patterns in individual layers by punches, cutting dies, routing, and laser cutting. The layers are stacked and registered relative to one another.

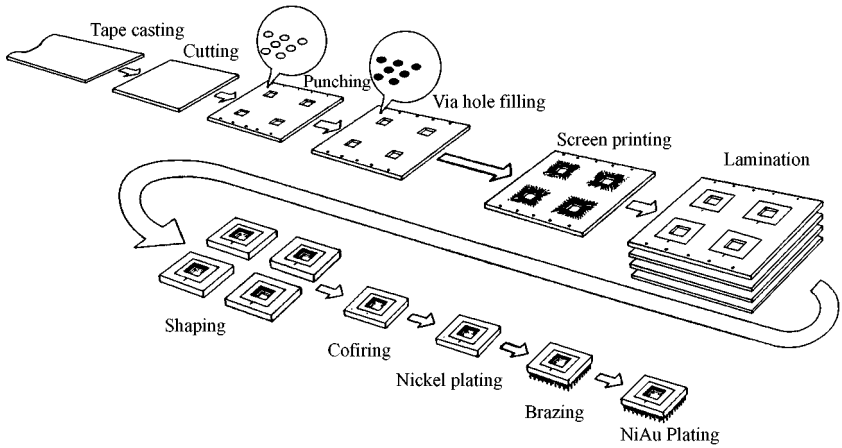

FIGURE 3.13 HTCC multilayer fabrication steps.[17]

The individual layers are laminated together by heated hydraulic presses. Typically, isostatic pressure is achieved on the three-dimensional pattern with isostatic pressing or through the use of molds or conformal bladders or bags. Finally, the laminates are green cut to final or near-net expanded dimensions. The multilayer parts are then heated in a burnout and firing process to remove organics and densify the ceramic and metal materials.

The cofirable metal systems based on W, Mo, and Mn are not able to be interconnected with traditional methods, that is they are not wettable with solder systems or wire- or ribbon-bondable. Therefore, these packages require postfire plating, electrolytic or electroless, with a Ni base layer followed by a thin Au layer to provide solder-wettable and wire-bondable terminations for interconnection. Electrolytic plating requires electrical connection to all pads requiring plating. The electroless systems plate all exposed metal surfaces.

HTCC is in widespread use for military, computer, and telecommunication applications.

Low Temperature Cofired Ceramics (LTCC). Low temperature cofired ceramic is a glass ceramic composite that provides highly integrated, high-performance electronic packaging. LTCC utilizes material technologies and manufacturing processes developed for two very mature systems: high temperature cofired ceramic (HTCC) and multilayer thick-film substrates. The LTCC material system consists of a low-firing-temperature ceramic with the multilayering capability of HTCC and the high conductivity metals (gold, silver, and copper) used in the thick film process. This combination of material technologies allows for low-temperature (less than 1000°C) processing of three-dimensional packages and the use of conventional chip and wire technologies for the fabrication of various complex LTCC packages. Traditional LTCC materials are glass-based systems that undergo devitrification to a crystalline phase during the firing process or consist of a glass matrix with crystalline filler.

Figure 3.14 shows the microstructure of an LTCC material with crystalline filler and partial devitrification. Since the glass phase of a material behaves as a supercooled liquid, it will densify at lower temperatures than the crystalline phase. The crystalline filler is added for thermal expansion match to the semiconductor chip, to control the densification behavior of the LTCC, and to achieve specific electrical performance. Figure 3.15 shows the effect of crystalline filler on TCE of a glass matrix LTCC. The crystalline phase is used for thermal expansion match to other components. The key discriminating feature of LTCC is the low firing temperature, which enables the use of high-conductivity metallizations in multilayer structures. This technology allows the high density and resolution circuitry of HTCC in complex three-dimensional structures but uses the low firing temperature and, therefore, more highly conductive metallizations. The lower dielectric constants allow circuits with finer spacing without signal coupling.

Unlike the thick-film process, where successive lamination and firing steps cause bowing and line degradation at high layer counts, the single-step lamination and firing of LTCC produces a flat substrate with fine, high-quality line definition. In addition, the elimination of costly repeated firings greatly increases the number of conductive layers achievable. The ability to form complex three-dimensional structures with multilayer ceramic technologies offers a significant advantage in integrating multiple functions into a single cofired structure. That is, analog and digital signals from dc through microwave frequencies can be channeled through one package, with isolation of one section from another. Typically, ground via fences are used in the wall dividing various devices to achieve a high degree of electrical isolation.

The current state of LTCC technology allows high-density circuitry (as fine as 0.003-in lines and spaces) interconnected with conductive vias (as fine as 0.0035-in diameter). Figure 3.16 shows a comparison of packaging technologies in terms of circuit density. The wide range in available dielectric constants in LTCC increases design flexibility. Dielectric constants as low as 3.8 are particularly well suited for high-speed digital applications. Moderate dielectric constants ranging from 6 to 80 are well suited for higher-frequency applications.

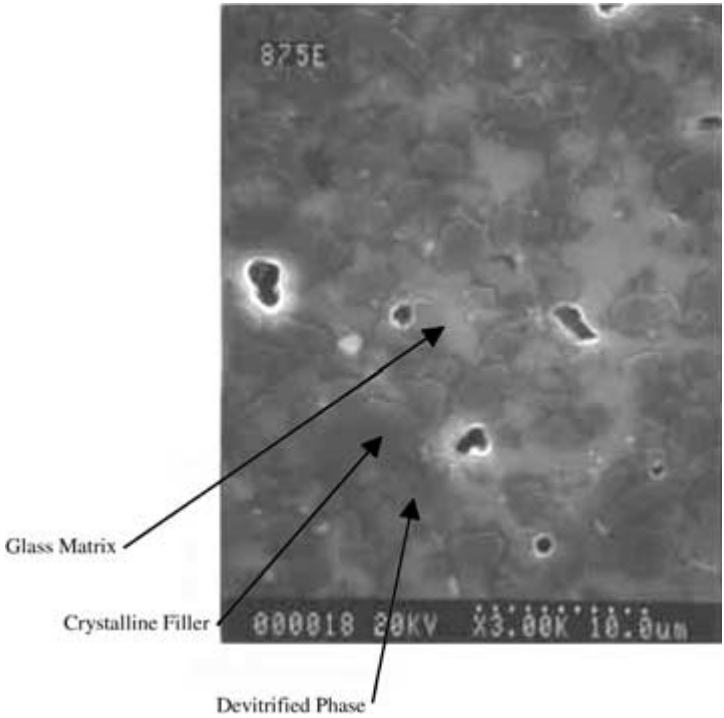

FIGURE 3.14 LTCC microstructure. (*Courtesy of DuPont.*)

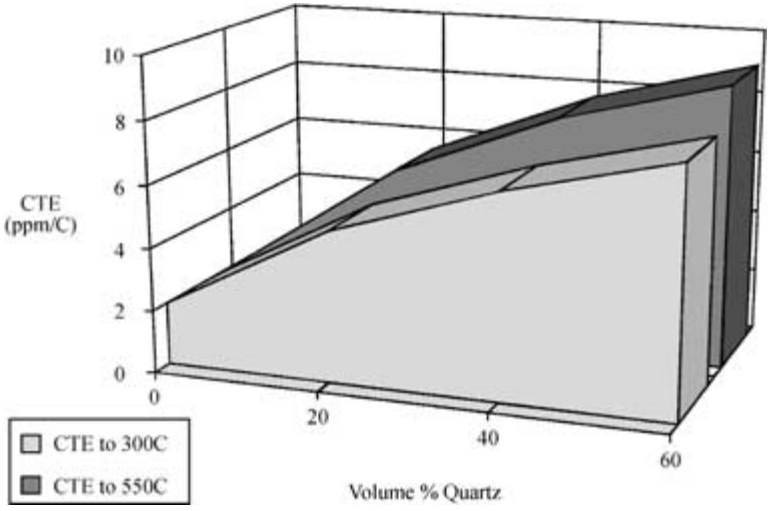

FIGURE 3.15 Effect of crystalline filler additions on thermal expansion of LTCC.

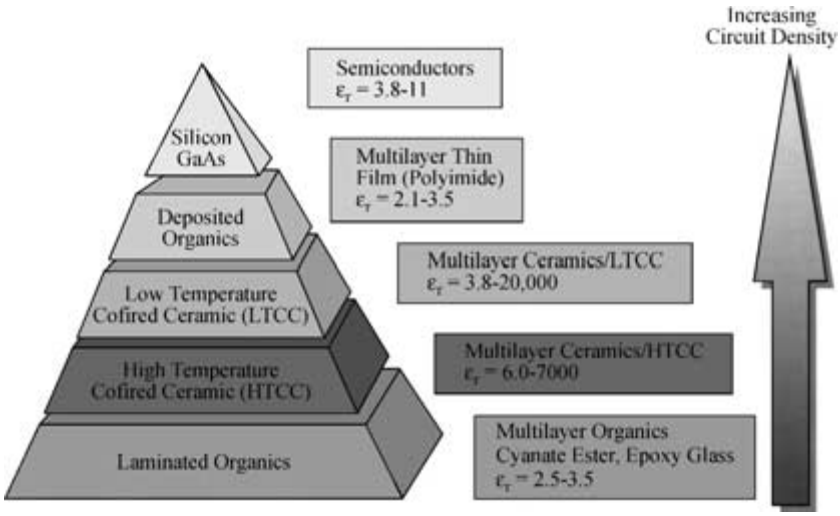

FIGURE 3.16 General comparison of circuit densities for packaging technologies.

The availability of high dielectric constants (up to 5000) allows integration of capacitor devices into the multilayer structure. Resistor pastes are available that can be printed on internal layers of circuitry and cofired into the structure. This integration of passive components reduces the number of surface mount components, reducing the number of solder and wirebond connections, and thereby increasing reliability. The ability to form complex three-dimension structures with multilevel cavities and the ability to form grounded "walls" of conductive vias provides considerable isolation potential. This isolation allows multiple signals to be handled in one cofired package, reducing the number of substrates required, reducing interconnections, and thereby improving reliability. Devices such as controllers and voltage regulators can be shared, reducing volume. The fact that there are fewer exterior walls or housings when multiple circuits are contained in the same package also contributes to a reduction in volume compared to individually packaged modules. Fewer modules results in fewer signals needing to be routed through small areas at the ends of the modules.

Figure 3.17 shows an example of eight integrated transmit/receive (T/R) channels containing digital, analog, and RF functions combined into one cofired package. The reduced part count leads to reduced labor hours in package manufacturing and assembly and therefore reduces costs. The reduction in the number of interconnections realized by combining functions or passive components into one package dramatically improves the reliability of the system.

A comparison of the electrical properties at high frequencies for several LTCC systems is shown in Figs. 3.18 and 3.19. Table 3.7 shows a comparison of properties for various LTCC and HTCC systems.

Figure 3.20 depicts the core processing steps in the LTCC manufacturing process flow. The nine basic processes in the fabrication of an LTCC device are blanking, via formation, via filling, circuit printing, cavity formation, layup, lamination, firing, and postprocessing.

Blanking is the process by which sections of green tape of an appropriate size for processing are stripped from the Mylar carrier film and stabilized to remove residual stresses from the tape-casting process. Thermal and electrical vias for interconnection between layers

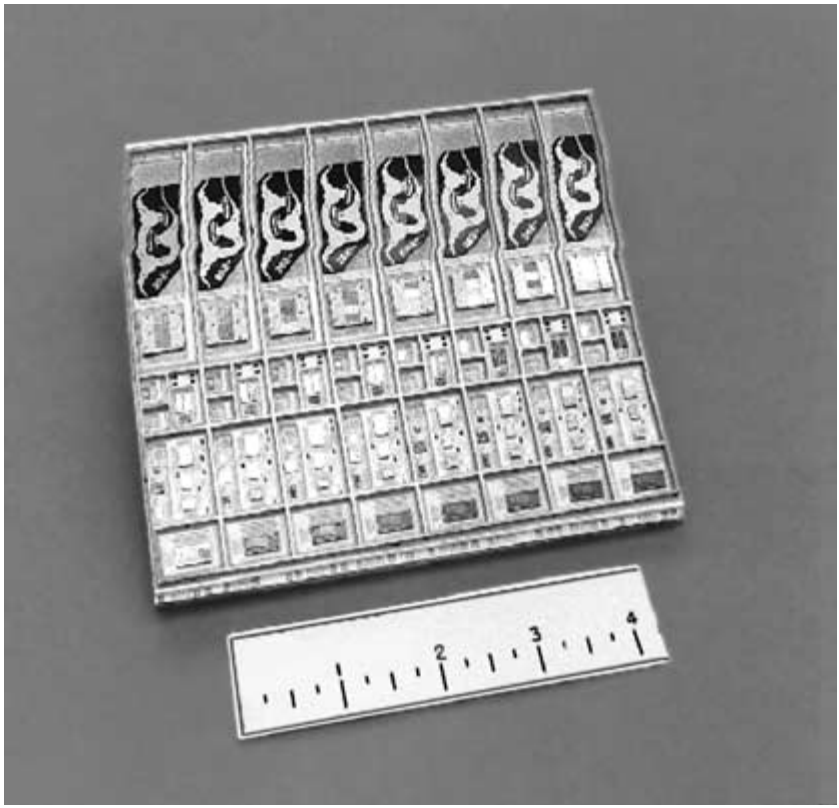

FIGURE 3.17 Northrop Grumman's eight-channel transmit-receive module in LTCC.

of circuitry (diameters ranging from 0.002 to 0.020 in) are formed in the appropriate layers of unfired tape by pneumatic punching equipment with more than 10,000 vias per layer. In high volumes, specialized gang punches or fixed die sets are used to form large patterns of vias simultaneously.

Vias are subsequently filled with a specially formulated conductive material applied through a stencil in a screen printing process. The stencil is made from 0.002- to 0.003-in-thick brass or stainless steel containing etched or punched vias of the same pattern as the tape. The stencil and punched tape are typically optically aligned before printing the conductive pastes into the vias. Quality factors are completeness of fill, without overfill, and accuracy of placement of the fill material.

Conductor patterns are printed on the green tape by the process used for printing thick-film conductors. In general, printing on green tape is of better quality and higher resolution than that possible on a thick-film substrate for two reasons: The printing is always done on a flat surface without the warping and topography characteristics of multilayer thick film, and the paste is deposited on a porous surface that inhibits the tendency of the paste to spread.

The three-dimensional cavity structure is formed by cutting the patterns in each layer of tape in the required location by die punching, mechanical machining, or carbon dioxide laser cutting.

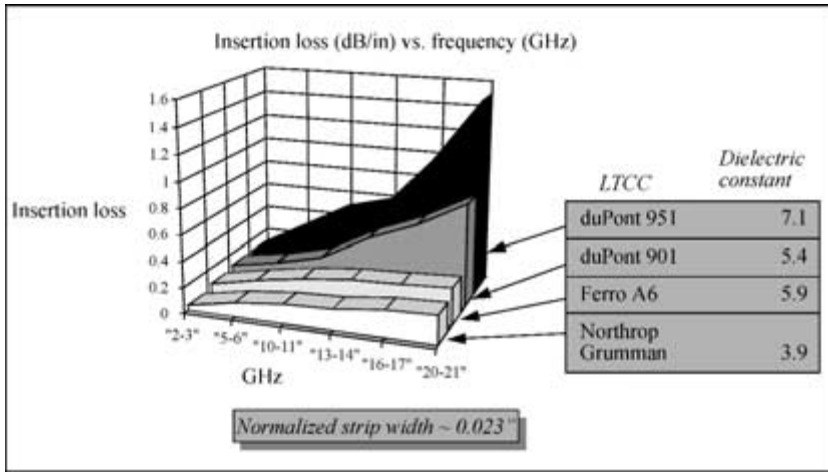

FIGURE 3.18 Attenuation versus frequency for several LTCC systems using gold metallization in microstrip configuration.

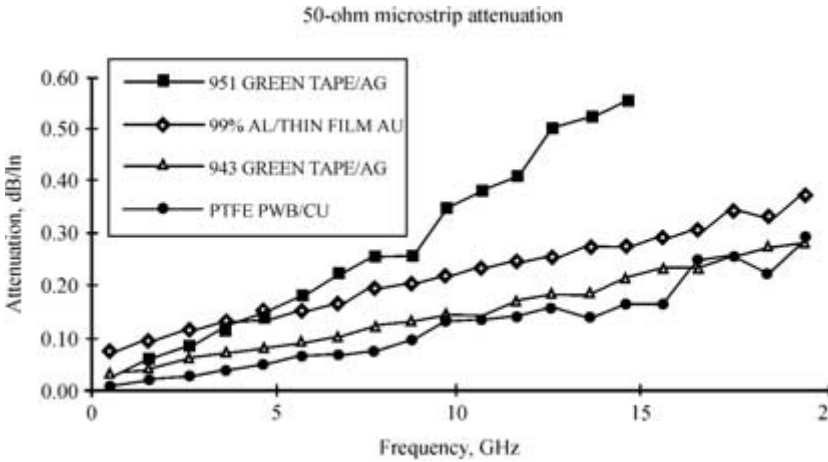

FIGURE 3.19 Attenuation versus frequency for DuPont LTCC with silver conductor versus thin film and PTFE printed wiring board.

The individual sheets of processed tape used in a substrate are collated and aligned by using tooling holes aligned to the via and circuit pattern in each layer of tape. The multilayer stack is then laminated under elevated temperature (70 to 90°C) and pressure (2000 to 6000 lb/m^2) to bond the individual layers into one cohesive stack. Two distinct methods of lamination are used: isostatic and uniaxial. Isostatic lamination is used to laminate substrates containing cavities since it is critical to attain uniform applied pressure to surfaces as well as bottoms of cavities. Uniaxial lamination is used for flat substrate designs.

TABLE 3.7 Properties of Multilayer Ceramic Packaging

Material	Primary phase	Thermal expansion, ppm/°C	Dielectric constant	Dielectric loss	Thermal conductivity, W/(m · K)	Flexural Strength, MPa	Density, g/cm^3
HTCC	Al_2O_3	7.1	9.5	0.0004	25	420	3.9
Kyocera	Al_2O_3	7.0	10	0.002	18	275	3.6
NTK	>92% Al_2O_3	6.8	9.4		17		
IBM	92% Al_2O_3	6.5	9.5		20	275	
NTK	Mullite	4	6.6		5		
Kyocera	Mullite	4.2	6.4	0.002	5	196	2.9
ALN	ALN	4.4	8.9	0.0004	175	320	3.3
NTK	AlN		8.9		170		
Kyocera	AlN	4.6	8.5	0.0004	150	343	3.4
Kyocera	SiC	3.7	45		270	441	
LTCC	glass matrix, crystallized	3–7	3.9–7.5	0.0002–0.003	2	180–210	2.25–3
NTK	Crystallized glass	3	4.9–5.6		3		
IBM	Cordierite	3	5.3–5.7		5		
IBM	Spodumene	2.8	5.65				
DuPont 951	*Pb-BSG + $CaZrO_3$ + Al_2O_3	7	7.1	0.007	3	206	
DuPont 943	Crystallized glass + Al_2O_3	5.3	7.5	0.001	3.0	230	3.2
Ferro A6	Crystallized Ca-BSG	3	5.9	0.002	2		2
Northrop	*BSG + Quartz	6.8	3.9	0.0008	2	100	2.3
Fujitsu	*BSG + Al_2O_3	4	5.7		2.5	200	
NEC	*Pb-BSG + Al_2O_3	7.9	7.8	0.003		343	
Kyocera	Glass-ceramic	7.9	7.9	0.003	2	196	2.8
Kyocera	Glass-ceramic	4.0	5.0	0.0029	2	186	2.5
Murata		8.0	6.1	0.0007	4.2	196	

*BSG: borosilicate glass.

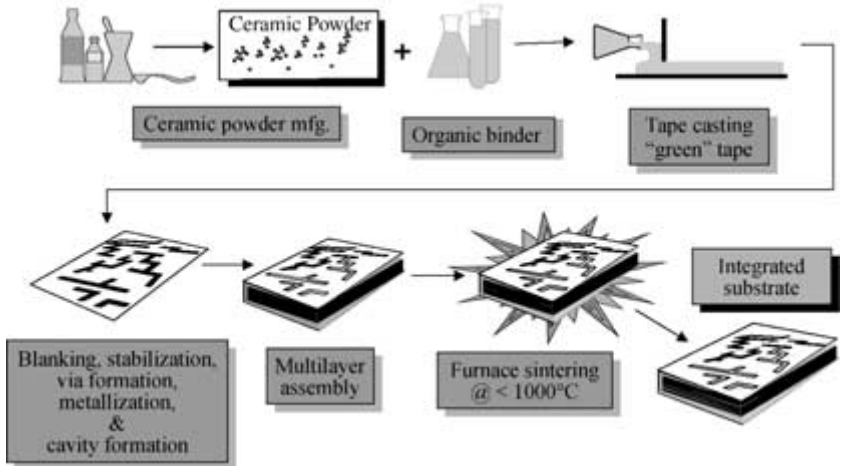

FIGURE 3.20 LTCC multilayer fabrication steps.

Laminated stacks are fired in belt or box furnaces to burn out organic binders and densify the ceramic and metallic constituents. Burnout and firing can be accomplished in one continuous operation so that the part does not experience thermal gradients from end to end as temperature is changed. Finished parts may be metallized with either a screen-printed thick film or sputtered and etched thin-film conductor.

The reduced weight of LTCC packages and the low-loss characteristics of the dielectrics and conductors make this packaging technology useful in high-performance commercial and military electronic systems.

3.4 CAPACITORS

Capacitors are essential components in most electronic circuits. Capacitors function as devices for energy storage, current blocking, electrical noise filtering, high-frequency tuning devices, etc. Since the first demonstration of the energy storage capability of a capacitor device in 1745 by Leyden, with a glass as the dielectric, capacitors have taken on a wide variety of designs. In the early 1900s, the first practical capacitor devices were fabricated from steatite porcelains, paper, and mica. Lower-loss porcelains were developed in the 1920s, followed by higher-dielectric-constant TiO_2-based ceramics in the 1930s. In 1942, researchers at the American Lava Co. discovered the ferroelectric behavior of $BaTiO_3$. $BaTiO_3$ has been modified over the years, by forming solid solutions with other perovskites and doping with various ions. $BaTiO_3$ remains the most widely used material in the ceramic capacitor industry today. Process improvements have contributed to dramatic improvements in capacitor performance through the years. The development of tape casting and cofired metallizations made possible the fabrication of multilayer capacitors with extremely high capacitance density. Chemical synthesis techniques have led to fine-particle dielectric powders that densify at lower temperatures and have better breakdown strengths.

The capacitance of a device is a measure of the charge stored per applied voltage and is measured in units of farads, or $s^2 \cdot C/kgm^2$. In its simplest form, a capacitor consists of two parallel electrodes separated by a dielectric medium. The capacitance of such a device, in units of farads, is given by

$$C = A\varepsilon_r\varepsilon_0/t \tag{3.13}$$

where A = effective area of electrode plates
ε_0 = permittivity of free space
ε_r = relative permittivity (dielectric constant) of the material
t = separation distance between electrodes

The intrinsic volumetric energy density U of a parallel plate capacitor, in units of J/cm^3, is given by

$$U_{\text{vol}} = \int E\, dP \tag{3.14}$$

where P is the polarization resulting with an applied electric field E. For an ideal dielectric where ε_r is independent of applied field, this relationship reduces to

$$U_{\text{vol}} = \frac{1}{2}\varepsilon_r\varepsilon_0 E^2 \tag{3.15}$$

TABLE 3.8 Alternative Capacitor Materials Designs

Type	Materials	Operating frequency, Hz	Benefits
Polymer film	Polystyrene, polypropylene, polyester, polycarbonate, PVD, PVDF, paper	$0–10^{10}$	High voltage, high energy density, self-healing
Electrolytic	Aluminum foil electodes with electrolyte-impregnated paper dielectric	$0–10^{4}$	High capacitance
Tantalum	Porous Ta with MnO_2 or wet electrolyte	$0–10^{4}$	Stable
Mica	Mica plates clamped in multilayer stack	$10^{3}–10^{10}$	Low cost, one of the first capacitor materials
Ceramic	Ferroelectric perovskites	$10^{2}–10^{10}$	High capacitance
Multilayer ceramic	Tape-cast ferroelectric dielectrics cofired with internal electrodes	$10^{2}–10^{10}$	High energy density, very high capacitance
Thick film	Usually $BaTiO_3$-based paste with glass adhesion promoters fired onto substrate	$10^{2}–10^{10}$	Embedded passives in hybrid circuits
Thin film	Dielectrics such as SiO_2 or TiO_2 deposited on a substrate	$10^{2}–10^{10}$	Embedded passives in hybrid circuits

Substituting Eq. 3.13 gives the electrical energy stored, in units of Joules (W · s), in a capacitor:

$$U_{\text{device}} = \frac{1}{2} CV^2 \tag{3.16}$$

where V is the applied voltage. These relationships show the energy density could be maximized by increasing the permittivity, the applied electric field, or both.

While all capacitors are based on metal electrodes separated by a dielectric material, they come in many different forms. Table 3.8 gives a list of various capacitor materials and designs. Ceramic capacitors alone come in a wide variety of forms, some containing only one dielectric layer, others containing many thin layers of dielectric separated by interdigitated metal electrodes. The capacitance per unit volume of a device can be increased by increasing the area/thickness ratio or using higher-permittivity materials. The development of the cofired multilayer process in the 1950s allowed fabrication of thin dielectric layers mechanically stacked in series and electrically connected in parallel. High-permittivity materials will raise capacitance values, but, in general, with higher permittivity comes higher loss.

Polymer-film capacitors are fabricated by interleaved polymer sheets and aluminum electrodes. The electrodes consist of either aluminum foil or evaporated metal. The dielectric thickness is typically several micrometers; therefore, relatively high capacitive densities can be achieved. The use of thin layers of oil-impregnated polymer dielectrics with low permittivities, $\varepsilon_r = 3$ to 10, has made possible operation at fields up to 300 MV/m, yielding energy densities as high as 3 J/cm^3. Ceramic capacitors have significantly higher permittivities (up to about 25,000); however, ceramic dielectrics have not realized their full potential because of a reduction in permittivity and resistivity at high fields and, therefore, low breakdown strengths. Recent improvements in ceramic processing and materials

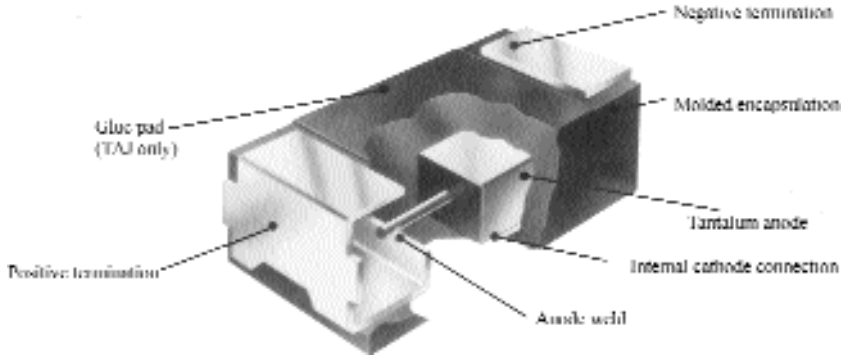

FIGURE 3.21 Tantalum capacitor design.[5]

properties are rivaling the state-of-the-art polymer capacitors. Polymer-film capacitors currently hold at least 25 percent of the market.

Electrolytic capacitors consist of aluminum foil electrodes separated by a thin sheet of porous paper and wound into a cylindrical shape. The paper is impregnated with an electrolyte solution. These capacitors are relatively inexpensive to fabricate and allow very high capacitance values. The drawbacks to electrolytics are that they are polar and operate only at lower frequencies (less than 10 kHz).

Tantalum capacitors, as shown in Fig. 3.21, are formed by sintering Ta metal powder around a Ta lead wire to form a porous body that serves as the anode. The porous Ta is then coated with a semiconductive MnO_2 layer, and coated with carbon and silver paints to form the cathode. A supporting T bar is then welded to the lead wire and the assembly is encapsulated. A wet electrolyte may be used in place of the MnO_2. Tantalum capacitors are very stable over time and temperature.

Mica capacitors consist of mica, $KAl_2(Si_3Al)O_{10}(OH)_2$, plates with fired-on silver electrodes. The metallized plates are stacked together in a multilayer fashion. Mica capacitors are extremely stable over time, have low thermal coefficient of capacitance, and have relatively low loss.

Ceramic capacitors are fabricated in four general processes: thin-film, thick-film, single layer, and multilayer. Thin-film capacitors were developed out of a need to embed passive components into electronic packaging in hybrid circuits. Dielectrics such as SiO, SiO_2, Ta_2O_3, TiO_2, titanates, and aluminosilicates can be vacuum deposited with a variety of electrode metallizations.

Thick-film hybrid packaging consists of layers of screen-printed/fired dielectric and circuit layers. Here again, the desire to embed passive devices into the substrate drove the development of thick-film capacitors. The screen-printed pastes consist of a high-*K* dielectric, usually $BaTiO_3$-based, a glass binder, and organic constituents such as binder, dispersant, and solvent. The glass is needed to bond the crystalline dielectric particles together and achieve good adhesion to the substrate and metal electrodes.

Single-layer capacitors represent the simplest form of ceramic capacitors. These capacitors use a single layer of dielectric ceramic between two metal electrodes. The dielectric may be in the form of a disk, cylinder, or rectangular plate. Typically, the shapes are formed by die pressing or extrusion.

In general, capacitors are designed to take advantage of the material and geometric contributions to the capacitance. However, there are secondary properties of capacitors that drive

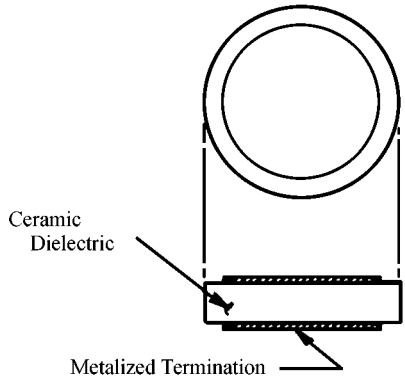

ASSEMBLED DISC CAPACITOR

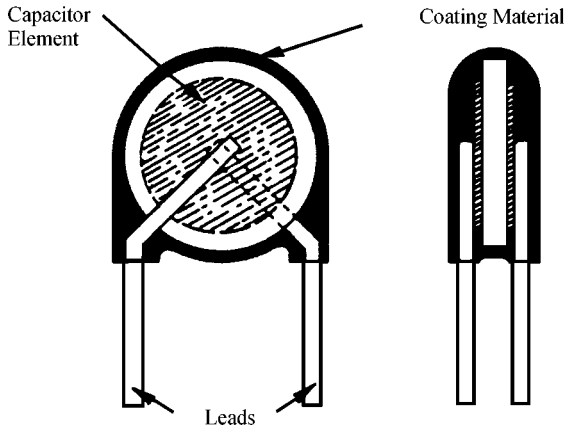

FIGURE 3.22 Simple disk capacitor design.[21]

the design. For example, high-permittivity materials are desired to maximize the energy density per unit volume, but the material must also exhibit some specified temperature response and possess low dielectric loss. For this reason, the material selection for a specific application is generally a compromise. Since capacitance is additive when individual capacitors are placed in parallel, it is desirable to use multilayer devices with interdigitated electrodes. In order to take advantage of the inverse relationship to dielectric thickness there is a drive to improve processes and powder characteristics to achieve thinner dielectric layers.

Figure 3.22 shows the simple disk capacitor structure containing one layer of ceramic dielectric. This structure was the standard for ceramic capacitors for many years. The development of multilayer capacitors has eroded the market for single-layer discrete capacitors. The most efficient way to maximize capacitance is to stack many thin layers of dielectric

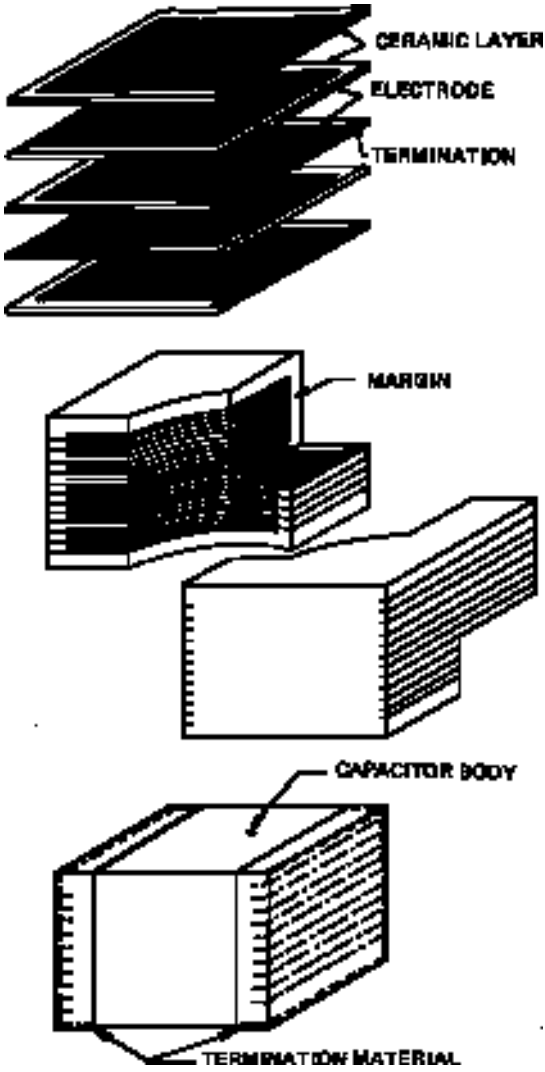

FIGURE 3.23 Multilayer capacitor design.[21]

in series and connect them electrically in parallel as shown in Fig. 3.23. When capacitors are connected electrically in parallel, $C_{\text{total}} = C_1 + C_2 + C_3 + \cdots$.

Two processes for forming multilayer capacitors (MLCs) are shown in Fig. 3.24. In both processes, the dielectric powders are mixed in a solvent solution with dispersant, organic binders, and plasticizers. In the tape process, the slurry is de-aired and cast into thin sheets using a doctor blade. The tape-casting process is shown schematically in Fig. 3.25. The slurry is typically pumped into a reservoir. The leading edge of the reservoir has a small,

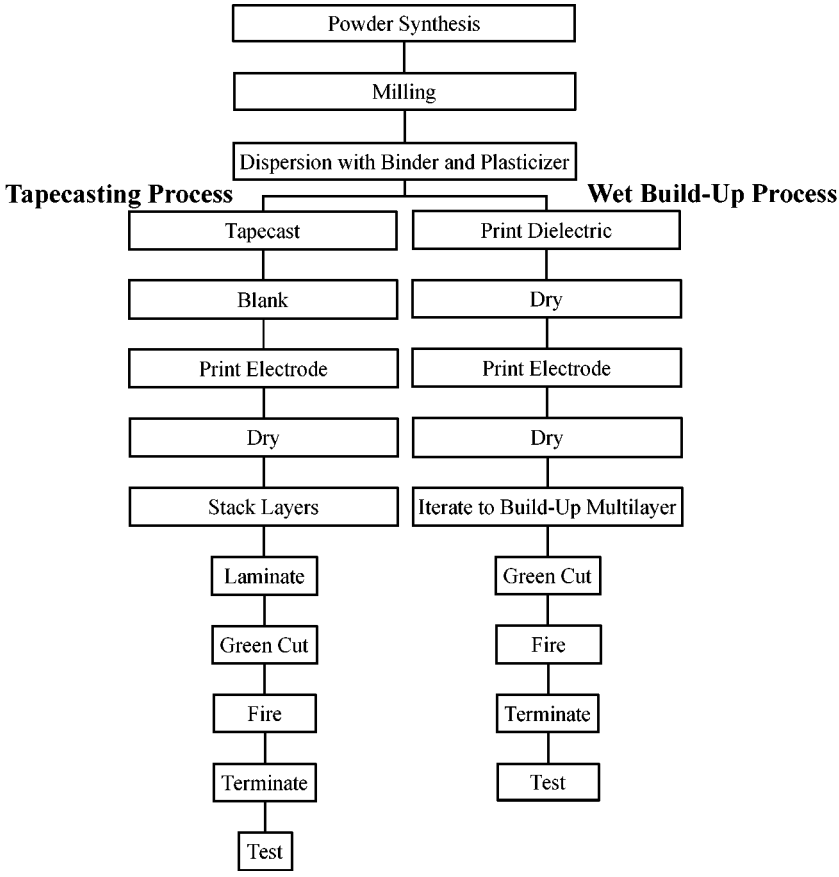

FIGURE 3.24 Multilayer capacitor fabrication steps.

adjustable gap. A metal belt or polymer film moves under the reservoir and doctor blade. As it does so, a thin film of slurry is carried along the belt. The thin film continues to move through a heated bed that gradually drives off solvents, leaving a flexible ceramic-binder film, called *green tape*. The end of the caster is typically equipped with a spooler so that the casting is a continuous process. The green tape is typically 50 to 60 vol% ceramic, 25 to 30 vol% percent organic binder. Dielectric sheets 15 to 100 micrometer thick are typical. Sheets of the green tape are printed with a metal-organic paste, typically Ag– or Ag-Pd–based, by a screen printer, to form the pattern of the internal electrodes. The pastes are dried and the printed sheets are stacked and laminated at elevated pressure (1 to 4 klb/in^2) and temperature (50 to 90°C). Individual capacitors are diced from the laminated block prior to firing by a hot knife or gang saws.

For thinner dielectric layers, 10 to 25 μm, a wet laydown process is used. The wet laydown process differs from the tape process in that the multilayer structure is built up through a successive printing and drying process. Here the slurry is printed onto a carrier plate in very thin layers. The printed dielectric is dried and the process repeated to avoid

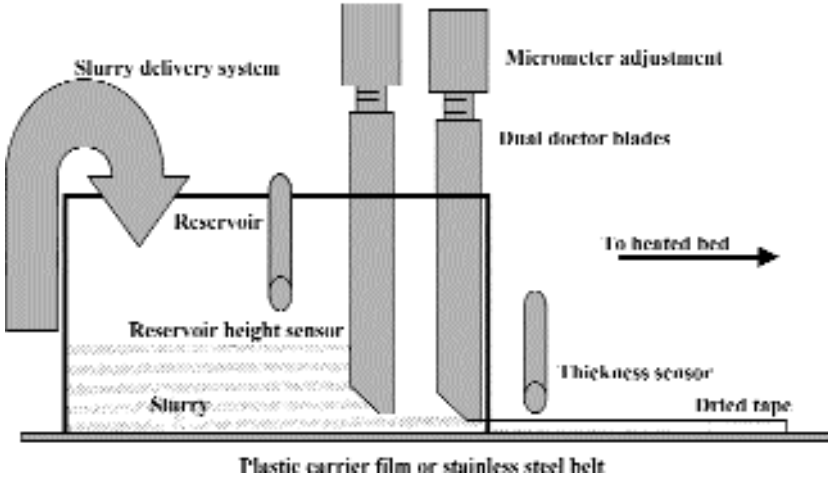

FIGURE 3.25 Schematic of tape-casting process.

pinholes. The electrode print is applied to the dried dielectric layer. This process is repeated to build up the multilayer structure. The capacitors are fired in a variety of methods, but all go through some method of binder decomposition followed by sintering of the metal and ceramic particles. The fired capacitors are then terminated on two sides to achieve electrical connection to alternate layers.

3.4.1 Material Classification

The Electronic Industries Association (EIA) has specified a method of classifying capacitors based on their capacitance value and temperature sensitivity. Class 1 capacitors are highly stable with respect to temperature and time (i.e., no aging) and have low loss. Typically these capacitors are made with titanates or tantalum. Class 2 capacitors are significantly more affected by temperature, time, and frequency; however, they are made from materials with much higher dielectric constants. Class 2 capacitors are typically made with ferroelectric materials and possess various ranges of stability. Therefore, EIA also set categories for temperature stability, outlined in Table 3.9. The classifications of Class 2 capacitors are expressed in terms of three-symbol codes. The first symbol represents the lower operating temperature, the second represents the upper operating temperature, and the third represents the change in capacitance over the operating temperature range.

NP0s (negative-positive 0 ppm/°C) are Class 1 dielectrics typically based on rutile TiO_2. These compositions can contain up to 50 percent $BaTiO_3$, which raises the dielectric constant and balances the negative temperature coefficient of rutile as shown in Table 3.9. Class 1 dielectrics are necessary for applications where a high degree of stability is necessary, as shown. Figure 3.26 shows the temperature stability for various classes of capacitors.

Class 2 capacitors are based on ferroelectric materials with considerably higher dielectric constants such as those listed in Table 3.10. These materials exhibit shifts in dielectric constant as a function of time (aging). This phenomenon is a result of ferroelectric domain movement over time. A typical aging curve is shown in Fig. 3.27. The application of heat,

TABLE 3.9 Electronic Industries Association (EIA) Capacitor Classifications and Examples

EIA code	Temperature range, °C	Change in capacitance, %	Typical dielectric constant	Typical dielectric loss, %
X7	−55 to +125			
X5	−55 to +85			
Y5	−30 to +85			
Z5	+10 to +85			
D		± 3.3		
E		± 4.7		
F		± 7.5		
P		± 10		
R		± 15		
S		± 22		
T		+22 to −33		
U		+22 to −56		
V		+22 to −82		
Examples:				
X7R	−55 to +125	± 15	3000–4000	<2.5
Z5U	+10 to +85	+22 to −56	8000–10,000	<4.0
Y5U	−30 to +85	+22 to −56	12,000–20,000	<4.0
Y5V	−30 to +85	+22 to −82	12,000–25,000	<4.0
COG (NP0)	−55 to +125	30 ppm/°C	Up to 100	<0.1

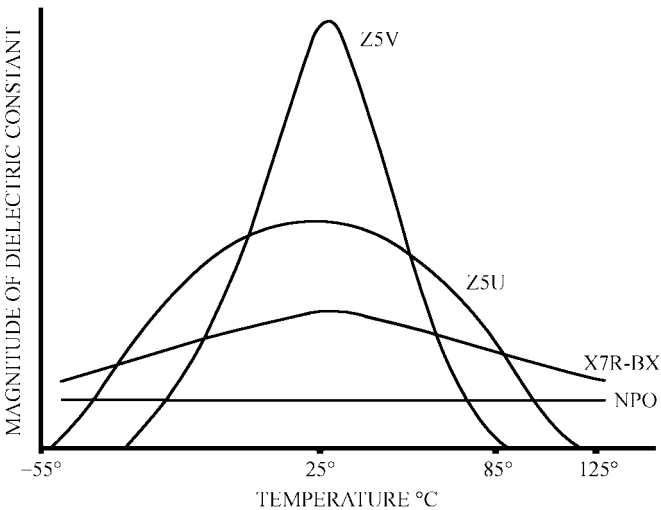

FIGURE 3.26 Temperature dependence of capacitance for various dielectrics.[21]

TABLE 3.10 Ceramic Capacitor Materials

Material	Relative permittivity	Dissipation factor, %
TiO_2	110	0.02–0.04
$SrTiO_3$	285	<0.1
$CaTiO_3$	130	<0.1
$MgTiO_3$	16	0.01–0.03
Al_2O_3	10	0.04
MgO	10	<0.1
Steatite	6	0.03–0.1
$BaTi_4O_9$	40	0.01–0.03
$BaTiO_3$ (BT)	14,000	1–3
BT + $CaZrO_3$	5700–7000	<3
$BaSrCaZrTiO_3$	11,500–14,000	<3
$Ba(TiZr)O_3$	10,000	<3
PMN-PT*	20,000–28,000	<3
PFN-PFW†	24,000	<3

*PMN-PT = $Pb(Mg_{1/3}Nb_{2/3})O_3$–$PbTiO_3$.
†PFN-PFW =

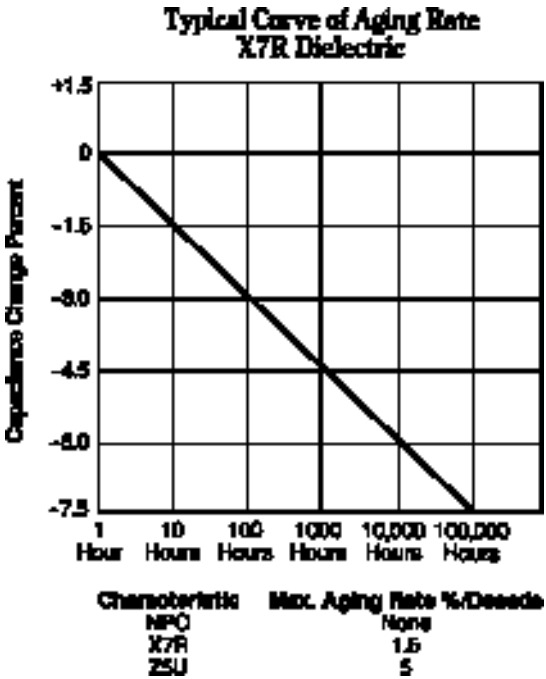

FIGURE 3.27 Aging behavior of various dielectrics.[5]

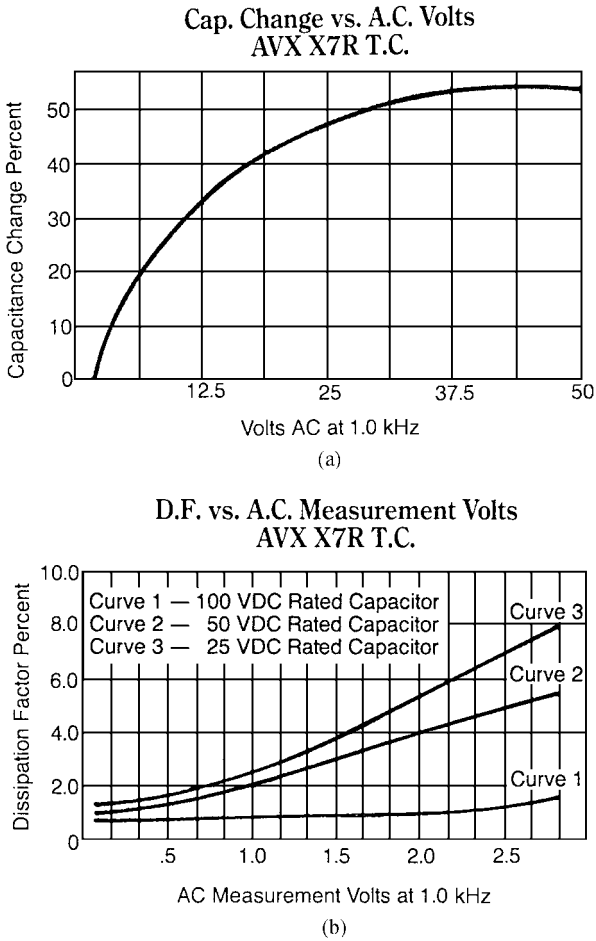

FIGURE 3.28 Effect of dc and ac voltages on capacitance and dissipation factor.[5]

voltage, or stress to the material will have a de-aging effect. Increasing frequency will result in reduced dielectric constant and increased dissipation factor in Class 2 dielectrics.

Applying dc voltage to a Class 1 dielectric results in a decreased capacitance and dissipation factor. AC voltages tend to raise the dielectric constant and dissipation factor. See Fig. 3.28.

Figure 3.29 shows the basic perovskite structure of $BaTiO_3$. Paraelectric perovskite is cubic and has an ABO_3 form with one formula unit per unit cell. The A site is at the corners of the unit cell, the B site is at the unit cell center, and the oxygen is at the unit cell face centers. Ferroelectric perovskite phases have the same arrangement as the cubic phase but the unit cell is slightly distorted into a tetragonal, rhombohedral, or orthorhombic structure. The A site atoms are coordinated by 12 O^{-2} atoms and the B site atoms are coordinated by six O^{-2} atoms (Table 3.11).

TABLE 3.11 Ionic Radii for Constituent and Dopant Ions

Ion	Site	Coordination number	Ionic Radii, Å
Pb^{2+}	A	12	1.63
Ba^{2+}	A	12	1.74
Sr^{2+}	A	12	1.6
Ca^{2+}	A	12	1.34
Zn^{2+}	B	6	0.89
Nb^{5+}	B	6	0.78
Ti^{4+}	B	6	0.745
Li^{+}	B	6	0.88
Mg^{2+}	B	6	0.86
Fe^{3+}	B	6	0.785
Ta^{5+}	B	6	0.83
Sb^{5+}	B	6	0.75
W^{6+}	B	6	0.74

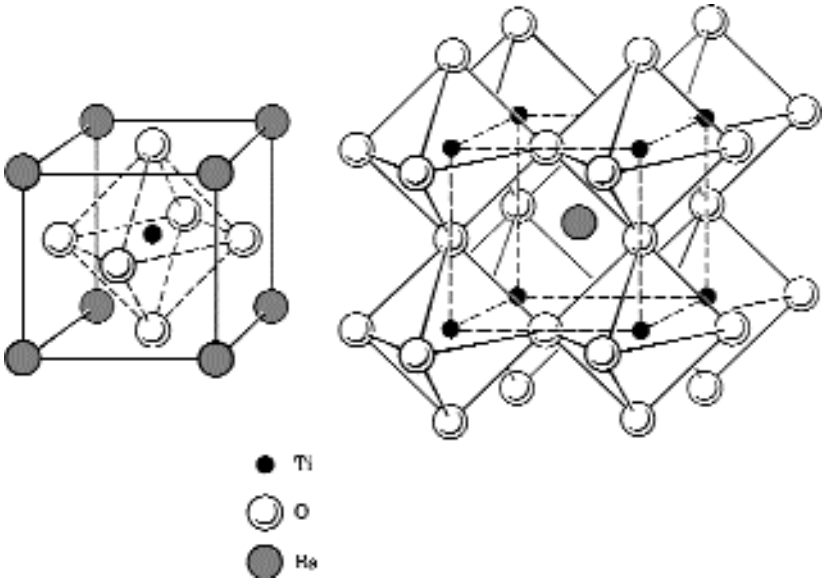

FIGURE 3.29 Perovskite $BaTiO_3$ structure.[20]

$BaTiO_3$ is the most common ceramic capacitor material as a result of its high permittivity, stability, and ease of doping. Figure 3.30 shows the unit cell dimensional change and associated dielectric constant change for $BaTiO_3$ as a function of temperature. The diagram shows that stoichiometric $BaTiO_3$ undergoes several phase transitions on cooling from high temperature. At about 110°C the high-temperature cubic phase converts from a paraelectric cubic phase to tetragonal ferroelectric phase. Cooling further results in conversion to an orthorhombic phase at about −10°C and a rhombohedral phase at about −100°C. At high temperatures, the lattice is expanded sufficiently to allow the B site ion to

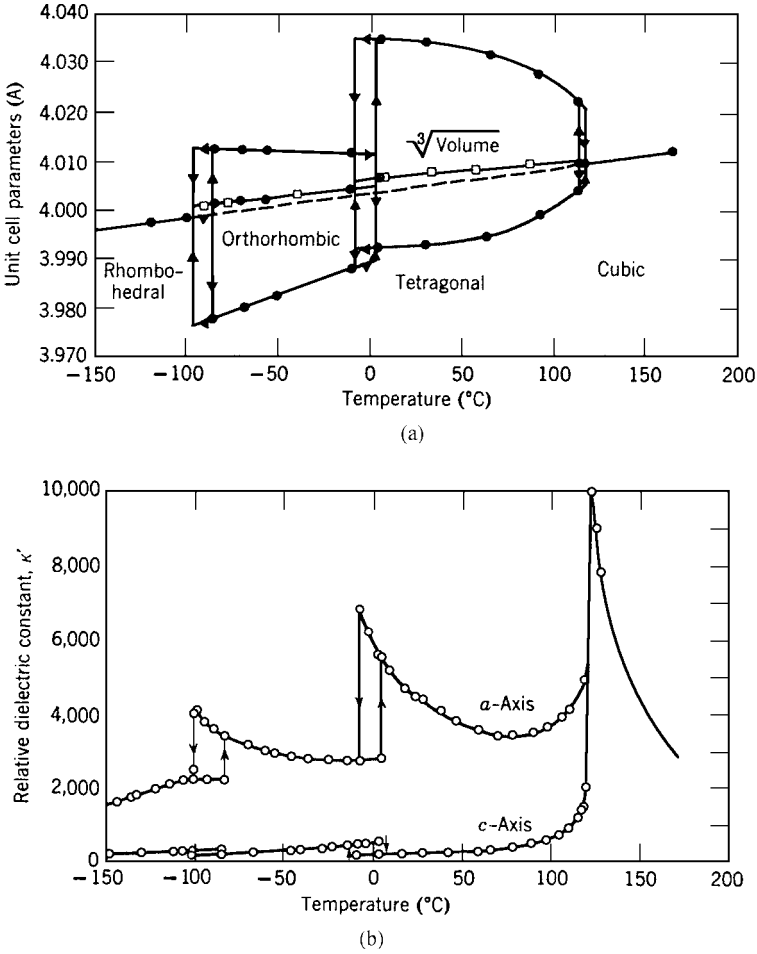

FIGURE 3.30 Unit cell dimensional and associated dielectric constant change for $BaTiO_3$ as a function of temperature.[20]

be centered in the cubic structure. As the material is cooled, the B site ion is shifted off center, creating a permanent dipole.

Perovskite, $SrTiO_3$ (ST), is also a base capacitor material with a dielectric constant of approximately 300 at room temperature. Pure $SrTiO_3$ is paraelectric with a transition temperature near 0°K. $SrTiO_3$ is frequently used in high-voltage applications because its dielectric constant is relatively independent of electric field, it shows virtually no electrostrictive strain at high field, and it maintains high resistivity at high fields and is, therefore, resistant to voltage breakdown. See Figs. 3.31 and 3.32. Commercial $SrTiO_3$ compositions are typically donor doped to reduce oxygen vacancies and improve resistivities.

Calcium titanate, $CaTiO_3$ (CT), is used in applications similar to those of ST; however, the dielectric constant is roughly half that of ST, as shown in Fig. 3.31. $CaTiO_3$ has a

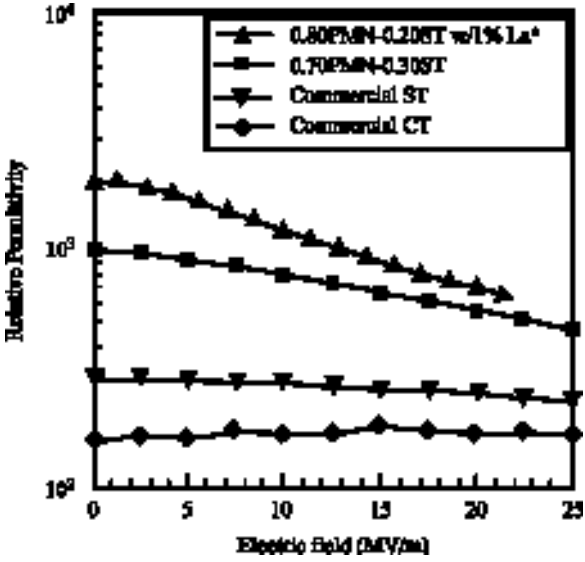

FIGURE 3.31 Permittivity versus dc field for doped PMN, ST, and CT dielectrics.[7]

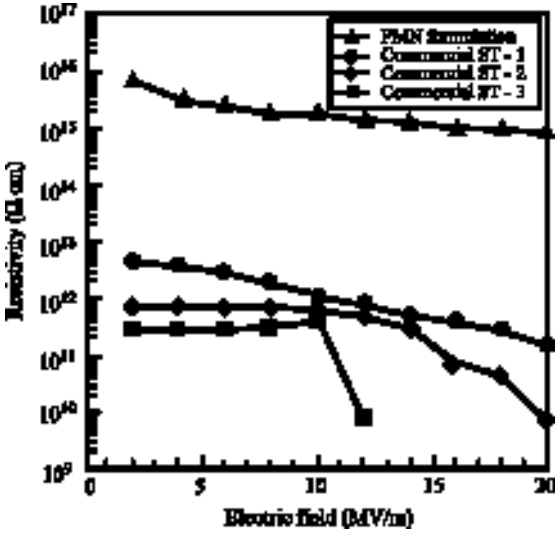

FIGURE 3.32 Resistivity versus field for doped PMN and ST dielectrics.[7]

relatively flat dielectric constant over temperature and field. Both ST and CT are used in solid solutions with higher permittivity materials to improve temperature and field stability.

Magnesium titanate, $MgTiO_3$ (MT), is an ilmenite-structure material with a low but stable dielectric constant ($K = 16$). MT meets the EIA requirements for an NPO capacitor formulation of <30 ppm/°C over −55 to 125°C.

Lead titanate, $PbTiO_3$ (PT), is a ferroelectric perovskite material with a Curie temperature near 490°C. PT is used extensively as a piezoelectric material; however, it is often used in solid solutions with other perovskites to improve capacitance and stabilize the perovskite phase. Modification of PT with Sr^{2+} substitutions for Pb^{2+} and W^{6+} and Mg^{2+} substitutions for Ti^{+4} yield excellent capacitor formulations with $K = 5000$ at room temperature.

Lead magnesium niobate, $Pb(Mg_{1/3}Nb_{2/3})O_3$, is a ferroelectric relaxor material which is paraelectric at room temperature. The perovskite phase is typically modifield with addition of lead titanate or barium titanate, which raises the Curie temperature to near room temperature. Very high dielectric constants can be achieved, >20,000, but at the expense of temperature stability.

3.4.1.1 Effect of Additives. The sharp changes in dielectric properties as a function of temperature are generally impractical. The properties of perovskites such as $BaTiO_3$ can easily be modified by additions of materials that form solid solutions in the perovskite structure. Isovalent substitutions on both the A and B site can be used to the transition temperature of perovskite materials. The ionic radii for the constituent and dopant ions are shown in Fig. 3.11 for the perovskite structure. In $BaTiO_3$, Pb^{2+}, Ca^{2+}, Sr^{2+}, Cd^{2+} are substituted on the larger A site (1.3 to 1.6). Pb^{2+} raises the phase transition (Curie) temperature, T_C Sr^{2+} lowers T_C, and Ca^{2+} broadens the transition. These effects are predictable if one considers these substitutions as solid solutions in titanate form. For example, $PbTiO_3$ has a higher (500°C) Curie point than $BaTiO_3$, and $SrTiO_3$ is near 0°K. Therefore, one would expect Pb^{2+} additions to raise the Curie point and Sr^{2+} additions to drop the transition temperature. Hf^{4+}, Zr^{4+}, and Sn^{4+} can be used to substitute for Ti^{4+} on the smaller B site (0.6 to 0.75) of the perovskite structure. Isovalent substitutes have quite high solubility in the perovskite structures. Figure 3.33 shows the effect of isovalent substitutions on the transition temperature.

The effects of acceptor and donor ion substitutions in the perovskite structure was described by Jaffe, Cook, and Jaffe,[19] as outlined in Table 3.12. Ion valences of the acceptor-type impurity atoms are lower than those of the constituent atoms. Oxygen vacancies are introduced to maintain charge balance. A decrease in dc resistivity has been attributed to the presence of charge carriers such as oxygen vacancies in the lattice. The decrease in resistivity ultimately leads to dielectric breakdown, but many ceramics fail because of the presence of voids or microcracks, which serve as initiation points for breakdown. Acceptor solubility is generally limited to <5mol%. In $BaTiO_3$, acceptor dopants such as, $Mn^{2+,3+}$, $Co^{2+,3+}$, $Fe^{2+,3+}$, Ni^{2+}, and Zn^{2+} are substituted on the B site. The advantage of acceptor substitutions is that they lead to lower dissipation factors and inhibited grain growth. The distortion in the smaller unit cell caused by oxygen vacancies is believed to be the primary cause of such properties. Grain growth inhibition is attributed to decreased diffusion during firing as a result of the lattice shrinkage.

The ion valence of donor-type impurity atoms is higher than that of the constituent atoms, and A site vacancies are introduced. In perovskite $BaTiO_3$, donor atoms are known to suppress the peak dielectric and piezoelectric properties. This is believed to be due to a compensating valence change of some of the Ti^{+4} to Ti^{+3} since Ba is not volatile. In lead perovskites, such as lead zirconate titanate (PZT) or lead titanate (PT), it is believed that the excess lead created by the vacancies is allowed to leave the structure because of its high

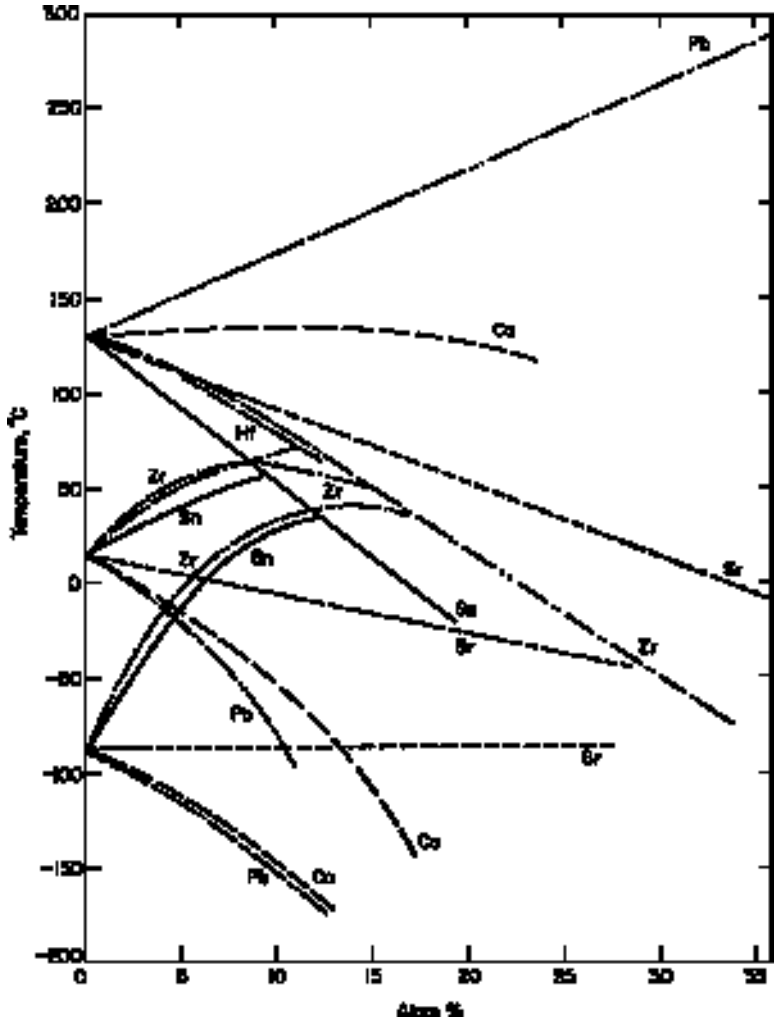

FIGURE 3.33 Effect of isovalent substitutions on the transition temperature of $BaTiO_3$ ceramic.[19]

volatility, so the stoichiometry corrects itself. In these compounds the peak dielectric constant and the piezoelectric properties are higher. In $BaTiO_3$, Nb^{5+}, Ta^{5+}, and W^{6+} are substituted on the B site. Bi^{3+}, La^{3+}, or Nd^{3+} is used on the A site. The properties in this case are generally explained by increased domain wall motion due to the A site vacancy. The ease with which these domains will switch results in (1) low coercive field to switch polarity and (2) a reduced mechanical quality factor because the domains will also move to cancel a small applied stress. The increased dielectric losses are also due to increased domain wall losses. Lower aging rates are attributed to low residual stress as a result of the

TABLE 3.12 Substitution Effects on Dielectric and Piezoelectric Properties

Property	Isovalent substitution	Acceptor substitution	Donor substitution
Curie temperature	Lower	Higher	Lower
Dielectric constant	Higher	Lower	Higher
Dielectric loss	Lower	Lower	Higher
Electrical resistivity		Lower	Higher
Coercive force		Higher	Lower
Remnant polarization		Lower	Higher
Piezoelectric coefficient		Lower	Higher
Aging	Higher	Lower	Lower
Coupling coefficient		Lower	Higher
Mechanical quality factor		Higher	Lower
Elastic compliance	Lower	Lower	Higher
Strain hysteresis		Lower	Higher
Hysteresis squareness	Lower	Lower	Higher

TABLE 3.13 Formulations for NPO Capacitors

	Composition, wt%		
	1	2	3
$BaTiO_3$	41–49	39–47	15–21
TiO_2	48–54	41–47	26–34
ZrO_2		8–13	
$Nd(CO_3)_4$			59–45
Other	3–7	2–5	Small
k'(25°C, 1 kHz)	35	30	62
tan δ	<0.002	<0.002	<0.002

TABLE 3.14 Formulations for X7R Capacitors

	Composition, wt%			
	1	2	3	Comment
$BaTiO_3$	90–97	85–92	86–94	Base material
$CaZrO_3$	2–5	4–8		Shifter
$BaCO_3$	0–5			Stoichiometry adjustment
$SrTiO_3$		3–6		Shifter
Bi_2O_3			5–10	Depressor, flux
Other	2–5	1–4	2–6	
k' (25°C, 1 kHz)	1600–2000	1800	1400–1500	
tan δ	<0.025	<0.025	<0.015	

ease of domain wall movement. The higher dc resistivity is due to the excess electrons countering p-type conduction.

The decrease in permittivity at high electric fields, dielectric saturation, is especially problematic in Class 2 dielectrics containing ferroelectric phases. It occurs because the ionic lattice distortion that produces the polarization has its limits. Tables 3.13 to 3.15 show

TABLE 3.15 Formulations for 25μ Capacitors

	Composition, wt%			
	1	2	3	Comment
$BaTiO_3$	84–90	65–80	72–76	Base material
$CaZrO_3$	8–13			Shifter
$MgZrO_3$	0–3			Depressor
$SrTiO_3$		7–11	5–8	Shifter
$CaTiO_3$		7–11	4–6	Depressor
$BaZrO_3$		7–11	7–10	Shifter
$CaSnO_3$			2–4	Shifter
Other	1–3	8–13	0–3	
k'(25°C, 1 kHz)	5700–7000	5500–6500	11,500–13,000	
tan δ	≤ 0.03	≤ 0.03	≤ 0.03	

typical capacitor formulations that are used to achieve NPO, X7R, and Z5U performance, respectively.

3.5 ELECTROMECHANICAL MATERIALS

Electromechanical materials are an interesting family of materials used for their ability to generate an electrical signal from a mechanical stimulation (passive devices) or generate mechanical displacements from electrical inputs (active devices). Passive devices are sensors such as sonar hydrophones, which give electrical signals as the sensor is stressed by sound waves. Advanced materials have been developed with very high electromechanical coefficients, resulting in high-sensitivity devices. New manufacturing processes allow complex arrays, composites, and multilayer stacks to be fabricated, further improving signal resolution. Other passive applications for electromechanical materials are ultrasonic sensors in medical devices and sensors in vibration cancellation devices such as active suspensions in automobiles.

Active applications include microdisplacive devices and sonic projectors, which output mechanical displacements as a result of applied electrical inputs. The high displacements coupled with the high stiffness of ceramic electromechanical materials allows generation of high forces. This allows vibration cancellation of relatively massive structures or generation of significant sonar source levels. Other active applications for electromechanical materials are actuators used for precision positioning; pumps; vibration cancellation; loudspeakers, resonators, and filters for radios and televisions; and ultrasonic generators for medical devices, milling, and cleaning. These applications range from semiconductor-processing-scale devices for electromechanical switches or miniature arrays to several-ton transducer arrays for active sonar.

3.5.1 Piezoelectrics

The piezoelectric effect was first discovered late in 1880 by Pierre and Jacques Curie. The effect was found in naturally occurring crystals, including quartz and Rochelle salt. Near the turn of the century, Woldemar Voight determined which of the 32 crystal structures have the potential for piezoelectric behavior. Of the 32 symmetry point groups, 21 are noncentrosymmetric and possibly piezoelectric. Of these, 20 groups are polarized with applied stress, i.e., are piezoelectric. Ten of these polar groups exhibit spontaneous polarization and

pyroelectric behavior. If the polar axis is switchable along more than one direction, the material is also ferroelectric. Of the 20 groups that are possibly piezoelectric, only those which are ferroelectric are available in polycrystalline ceramic form.

The first significant application for piezoelectrics occurred during World War I when Langevin developed a means of generating acoustic waves in water for signaling and detection of German submarines. These early forms of active sonar employed piezoelectric quartz. In 1920, ferroelectric behavior was discovered in Rochelle salt by Valasek. Rochelle salt became used for its large piezoelectric effect for microphones, phonographs, loudspeakers, recorders, and oscillographs. In 1930, Sawyer and Tower developed a circuit to record the hysteresis behavior of this ferroelectric. The first polycrystalline piezoelectrics, based on $BaTiO_3$, were discovered by Von Hippel and others in the mid-1940s. R. B. Gray and S. Roberts were among the first to develop piezoelectric ceramics by "poling" ferroelectrics. The ferroelectric behavior of lead titanate was discovered in 1950. In 1952, piezoelectric behavior was discovered in tungsten-bronze–structure lead niobate. In the mid-1950s, PZT (lead zirconate titanate) was developed and became the most widely used piezoelectric ceramic to date. The first piezoelectric polymer, polyvinyledene fluoride, was developed in 1969 by stretching it under high fields. More recently, a variety of complex niobate-based piezoelectrics with very high piezoelectric coefficients have been developed. Multilayer and thin-film processing have dramatically expanded the applications of this important group of materials.

3.5.2 Ferroelectrics

Polycrystalline piezoelectric materials exhibiting ferroelectric behavior are the center of attention, since they can be readily formed into various shapes and sizes by conventional processing. Ferroelectricity is the spontaneous alignment of dipoles as a result of their mutual interaction. At lower temperatures, the electric dipoles in a ferroelectric material create a local field stronger than the thermal energy required for randomization and spontaneous polarization results. Without external applied forces, the dipoles align in regions or domains. The various domains are then oriented along different crystallographic directions resulting in the lowest (strain) energy state and a net zero polarization for the fired ceramic. Compounds of the perovskite structure shown in Fig. 5.30, such as $Pb(Zr,Ti)O_3$ (PZT), $BaTiO_3$, $Pb(Mg_{1/3}\,Nb_{2/3})O_3$ (PMN), $Pb\,(Zn_{1/3}\,Nb_{2/3})O_3$ (PZN), and tungsten-bronze structure, such as $(Sr, Ba)Nb_2O_6$, $PbNb_2O_6$, and $LiNb_2O_6$, are often ferroelectric.

These compounds are typically cubic and, therefore, paraelectric at high temperature. As the material is cooled a phase change to a ferroelectric phase occurs at the Curie temperature T_C, and spontaneous polarization results. The perovskite ferroelectric phase is typically tetragonal or rhombohedral. Most of the perovskite compounds readily form solid solutions with one another, allowing substantial substitution to achieve optimum performance. Often, solid solutions are formed with perovskites of different crystal structures, resulting in a composition range where two different ferroelectric phases are present, the morphotropic phase boundary. Figure 3.34[19] shows the effect of solid solutions between ferroelectric $PbTiO_3$ and antiferroelectric $PbZrO_3$. It is generally desirable to develop compositions near the morphotropic phase boundary because at this region the dielectric and piezoelectric properties are maximized, as shown in Fig. 3.35.

The critical temperature below which the spontaneous polarization occurs is given by the Curie-Weiss law:

$$\chi = K' - 1 = P/\varepsilon_0 E = 3T_C/(T - T_C) \tag{3.17}$$

where χ is the electric susceptibility and T_C is the critical, or Curie, temperature. Equation (3.17) shows that as the Curie temperature is approached the resulting polarization for a

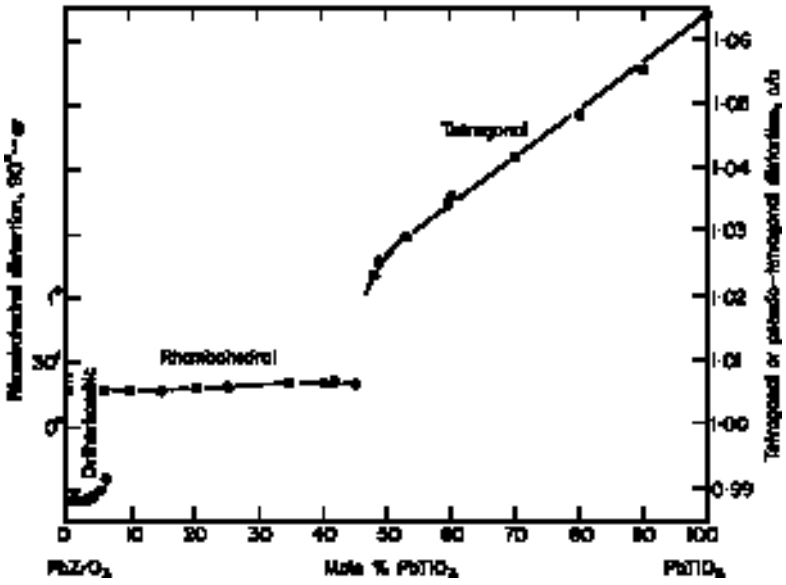

FIGURE 3.34 Unit cell dimension change versus temperature in the PZT system.[19]

given field is greater. The added thermal energy aids in shifting of domain walls. For this reason, it is typical for ferroelectrics to be cooled from elevated temperatures while high electric fields are applied to create the remnant dipolar orientation in the polycrystalline piezoelectric ceramics, i.e., poling. When a ferroelectric is cooled through its Curie region, the cubic lattice deforms to a polar phase. The polarization orients into regions, or domains, in order to minimize intergranular stresses. The dipoles of adjacent domains align along crystallographic axes.

Figure 3.36 shows how polarization changes with applied field in a ferroelectric material. At low initial fields, polarization increases nearly linearly with field. As higher fields are applied, the domains begin to align with the field, and grow. The polarization increases more rapidly. Ultimately, a significant portion of the domains are aligned with the field, and little additional polarization results as the field is raised. The highest polarization achieved at high fields (>2 MV/m) with all dipoles aligned is the saturation polarization P_S. When the external electric field is released most of the dipole alignment remains and there is a remnant polarization P_R. The domain alignment can again be randomized to a net zero polarization by reversing the polarity of the field. The field required to achieve this is the coercive field E_C. As fields of opposite polarity are increased, the domains again align with the field, resulting in polarization of opposite polarity. This behavior under applied ac fields results in the hysteresis loop shown in Fig. 3.36. The hysteresis in the *P-E* relationship indicates energy lost in moving domain boundaries. The process of applying a high electric field to a polycrystalline ferroelectric to obtain a high remnant polarization, poling, is necessary to achieve strong piezoelectric behavior.

Table 3.16 gives a generalized comparison of piezoelectric and electrostrictive materials. The piezoelectric expansion or contraction in the direction of an applied field results from alignment and stretching of dipoles in the material with the applied field. The expansion is linear and directly proportional to the magnitude and polarity of the applied field.

TABLE 3.16 Electromechanical Ceramics

Property	Hard piezoelectrics	Soft piezoelectrics	Electrostrictors
Modulus	High	Moderate	High
Strain/energy density	Low	Moderate	High
Strain response	Linear	Linear	Quadratic
Temperature sensitivity	Low	Low	Moderate–high
Hysteresis	Moderate	High	Low
Pressure sensitivity	Moderate	Pressure depoling	Low
Bias	None	None	Electric

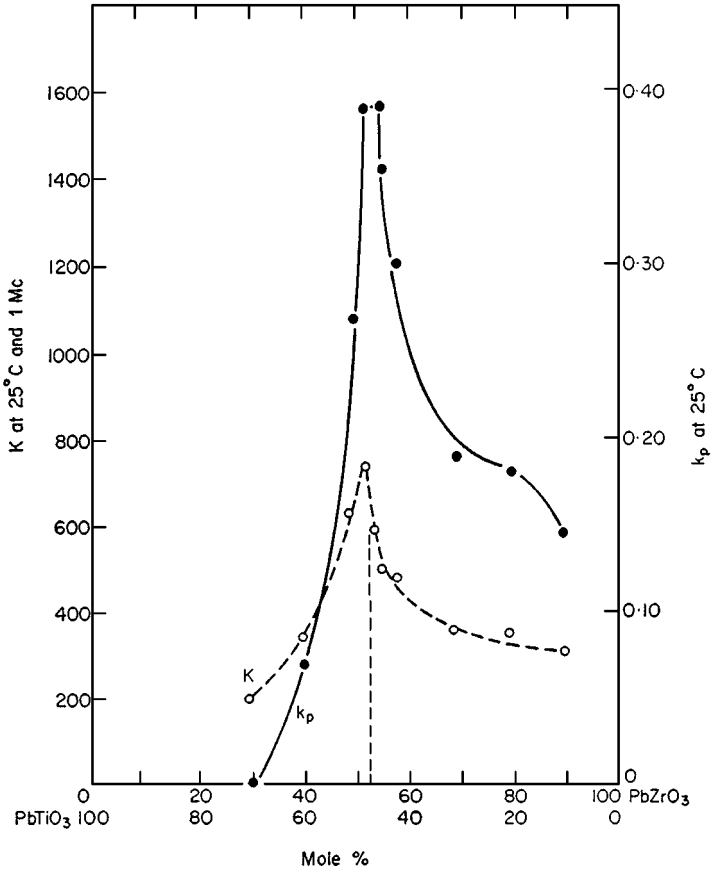

FIGURE 3.35 Dielectric constant and planar piezoelectric coupling coefficient for compositions near the morphotropic phase boundary in PZT.[19]

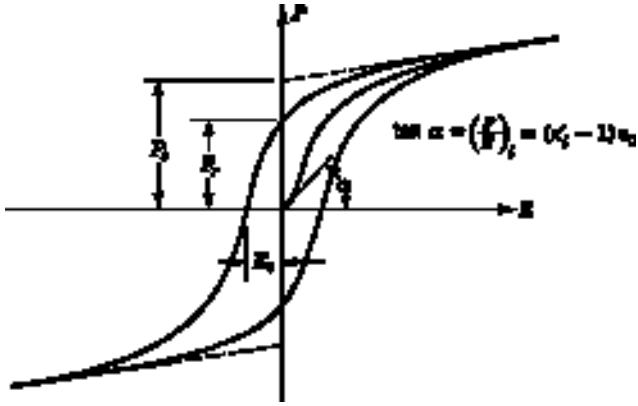

FIGURE 3.36 Electronic polarization versus field for a ferroelectric material.[20]

Piezoelectric ceramics have reorientable dipoles; therefore, dipolar reorientation may occur if energy is added to by the electric fields, heat, or pressure. Reorientation by field—i.e., poling—is an integral part of the fabrication of a piezoelectric ceramic. Poling creates the initial remnant dipolar orientation in the material. Since all of the reorientation mechanisms involve energy inputs, there is an intrinsic energy loss during any reorientation: This energy loss is proportional to the hysteresis.

3.5.3 Electrostrictors

More recent development of complex perovskite structures has resulted in a new class of electromechanical materials, *electrostrictors*. Purely electrostrictive materials are paraelectric and centrosymmetric; that is, they do not possess a polar axis and are typically cubic. The electrostrictive materials of most interest are ferroelectrics that are operated above or near their transition temperatures. The electrostrictive effect is a second-order phenomenon whereby an applied electric field results in a lattice distortion and mechanical distortion in the material.

The weak-field dielectric properties of a typical relaxor electrostrictor show a transition region above which electrostrictive properties predominate (correlated with low dielectric loss and reduced strain) and below which piezoelectric properties predominate (increased dielectric loss and reduced strain) (Figs. 3.37 and 3.38). The optimum tradeoff among maximum strain, minimum hysteresis, and minimum temperature dependence occurs within the transition zone ("fuzzy" region); however, the position of the zone is dependent on composition, frequency, and likely drive conditions.

During the 1980s, substantial research on electrostrictive materials, particularly PMN-based materials, occurred in the United States and Japan [PMN is $Pb(Mg_{1/3}Nb_{2/3})O_3$]. Significant improvements in electrostrictive materials were made, achieving a pyrochlore-free perovskite near the morphotropic phase boundary. Researchers at Martin Marietta Laboratories[4] formed the perovskite phase using a sol-gel process and a mixed oxide process with barium titanate (BT) and strontium titanate (ST) additions. In particular, the base composition $0.855Pb(Zn_{0.33}Nb_{0.67})$-$0.195PbTiO_3$-$0.05BaTiO_3$, has yielded some of the

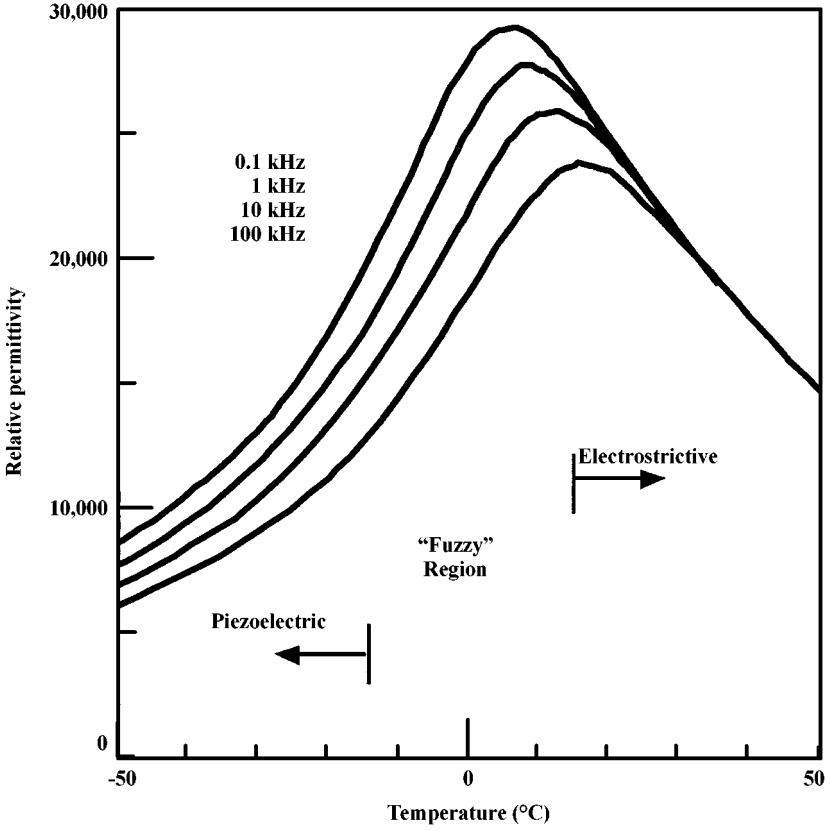

FIGURE 3.37 Weak-field dielectric properties for a relaxor ferroelectric.[30]

highest effective piezoelectric coefficients available (i.e., low-field $d_{33} = 500$ to 750 pC/N). The dielectric properties are very high ($K < 18{,}000$) near the Curie temperature ($T_C = 146°C$). The piezoelectric properties are very high but relatively soft—soft meaning the ferroelectric domains are rather easily realigned (at relatively low coercive fields).

The field-induced strain in piezoelectric and electrostrictive materials is on the order of 10^{-4} to 10^{-3}. The induced strain in a material is a function of applied mechanical stresses, electric fields, and thermal expansion. Under isothermal conditions, the net elastic strain in a material is given by

$$\varepsilon_{ij} = s_{ijkl}\sigma_{ij} + g_{ijk}P_k + Q_{ijkl}P_kP_l + \cdots \tag{3.18}$$

where the $s_{ijkl}\sigma_{ij}$ term describes the mechanically induced strain, the $g_{ijk}P_k$ term describes the first-order piezoelectric response, and the second-order $Q_{ijkl}P_kP_l$ term describes the electrostrictive contributions. The P term refers to the field-induced polarization of the material, where P is directly proportional to the applied field:

$$P_i = \varepsilon_0\chi_{ij}E_j \tag{3.19}$$

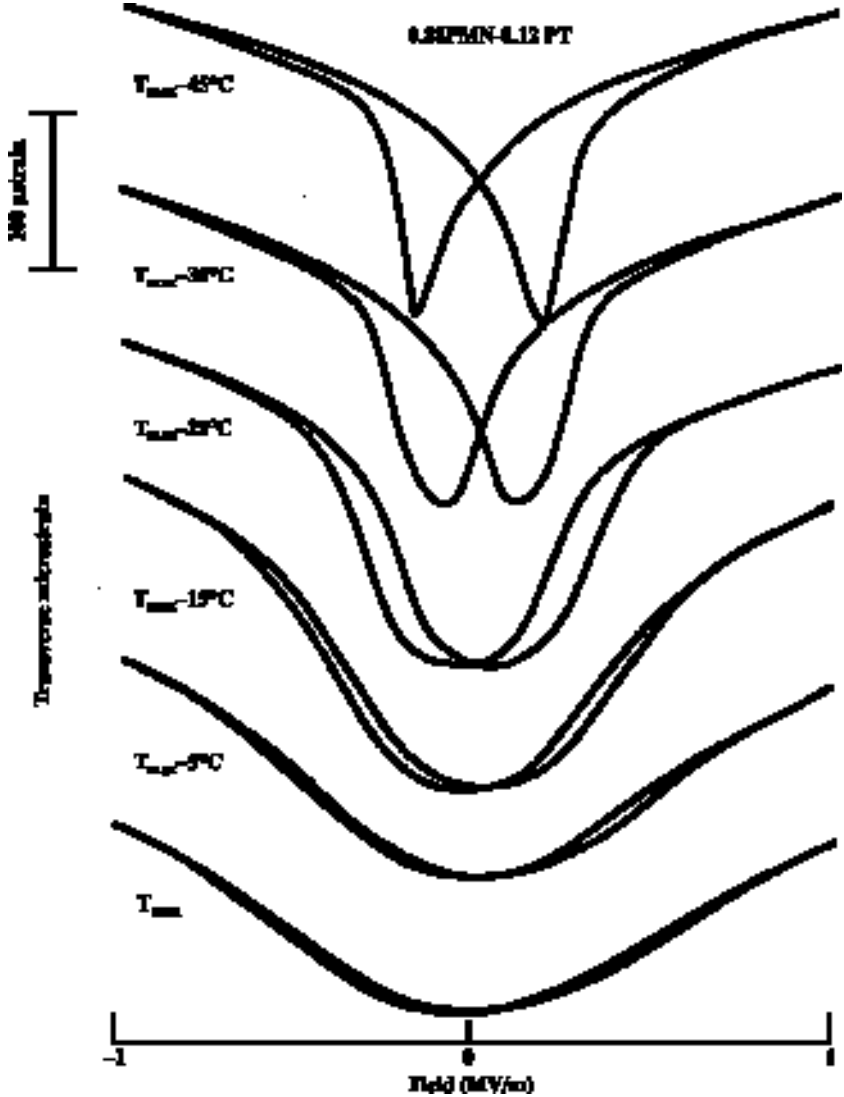

FIGURE 3.38 Strain versus field and temperature for a ferroelectric, showing piezoelectric response well below T_C and a more quadratic electrostrictive response as T_C is approached.[30]

where χ_{ij} is the dielectric susceptibility. Therefore, Eq. (3.18) can be expressed in terms of applied fields as

$$\varepsilon_{ij} = s_{ijkl}\sigma_{ij} + d_{ijk}E_k + M_{ijkl}E_kE_l + \cdots \tag{3.20}$$

In general, most electromechanical materials have contributions from both effects. However, typically one effect is significantly more dominant than the other. All materials

TABLE 3.17 Piezoelectric Standards and Properties of Selected Materials

Powder	Curie temp., °C	Room temp. permittivity	Aging rate	d_{33} or effective d_{33}, pC/N	Hysteresis,* %
Navy standards:					
Type I	325	1275 ± 12.5%	–4.5 ± 2.0%	290 ± 15%	1–3
Type II	350	1725 ± 12.5%	–1.5 ± 0.7%	390 ± 15%	
Type III	325	1025 ± 12.5%	–4.0 ± 1.5%	215 ± 15%	
Type IV	115	1275 ± 12.5%	–1.5 ± 0.5%	140 ± 15%	
Type V	240	2500 ± 12.5%	–2.0 ± 1.0%	495 ± 15%	
Type VI	180	3250 ± 12.5%	–2.0 ± 1.0%	180 ± 15%	
MMC (129) PMN	25	23,000		760	1–4
MMC (100) PMN	33	18,000		850–1000	1–3
MMC PZN-PT-BT	144	3000–3500		650	10–11
0.91PZN-0.09PT single crystal	178	2200–4100		1500	
$BaTiO_3$	120	1400–2000		191	
$PbTiO_3$	500				
$Pb(Ti_{0.48}Zr_{0.52})O_3$				223	
U5H-32† PZT	195	2500		600	1–12

*Measurement taken at 20°C.
†Ultrasonics Corp., South Plainfield, N.J.

have some degree of electrostriction, although in many cases the Q and M coefficients may be near zero or the dielectric permittivity is so low that no significant polarization results. Only materials with a unique polar axis will exhibit the piezoelectric response.

Figure 3.37 shows the transition region for a typical polycrystalline ferroelectric material. The material is cubic, paraelectric, and exhibits purely electrostrictive behavior well above the transition region and piezoelectric, rhombohedral, or tetragonal, below the transition. In the transition region, polarization is maximized as demonstrated in Eq. (3.17).

Observing the strain response as a function of the applied field across the transition region shows quadratic, low hysteresis behavior at higher temperatures (Fig. 3.38). The dielectric permittivity is maximized at the transition region along with the dielectric loss. The polarization versus field plots show no hysteresis and no remnant polarization well above T_C. In pure electrostrictors, the first-order strain term in Eq. (3.20) becomes negligible and the relation of strain to polarization or field becomes quadratic (at low fields). Electrostrictive strain is a result of a lattice distortion with the applied field. Expansion of the material is observed in the direction of the applied field, regardless of the field polarity. Increasing polarization, strain, and hysteresis is observed as the material is cooled. Polarization and field-induced strain are maximized near the transition region. Ultimately, significant effects of the polar axis switching are observed, that is, large hysteresis and contraction with alternating fields (the butterfly response). Piezoelectrics expand under fields of the same polarity as the poling field, but also contract under negative fields. Table 3.17 shows the properties of piezoelectric standards as well as common piezoelectric and electrostrictive materials.

3.5.4 Materials

Figure 3.39 shows the strain versus field relationship of various types of electromechanical ceramics. "Hard" piezoelectric materials, Types I to IV, are typically formulated to operate well below the transition region. The piezoelectric phase is highly stable and typically formulated for high coercive force and minimal domain wall movement (minimal

aging). This results in a material where the *d* coefficient is lower but the hysteresis is relatively small because of minimal domain wall movement. This type of material is the most common electromechanical material, used in passive and active sonar as well as many commercial applications where high induced force and stable response is needed.

"Soft" piezoelectrics, Types V and VI, are formulated to operate closer to the transition region, achieving higher strains with higher polarization. Typically this results in corresponding higher hysteresis and dielectric losses and more susceptibility to pressure depoling and aging. These materials are attractive for high-sensitivity passive transducers and actuator applications where high-field-induced strains are desired.

Soft electrostrictors operate just above the transition region where strains are maximized by contributions of both piezoelectric and electrostrictive effects. This combined effect results in materials that achieve the highest electromechanical energy density and possess the highest degree of sensitivity. However, these materials are highly temperature sensitive and require high-power drivers in active roles because of the corresponding high capacitance and power dissipation.

Hard electrostrictors are formulated for low hysteresis and, therefore, operate well above the transition region where pure electrostrictive behavior is observed. These materials have excellent "shape memory" because of their low hysteresis and are well suited for precision positioning applications such as deformable mirrors.

Lead zirconate titanate (PZT) is perhaps the most well known piezoelectric material. Perhaps the most promising group of piezoelectric materials is the family of complex niobates that have a perovskite or tungsten-bronze structure.

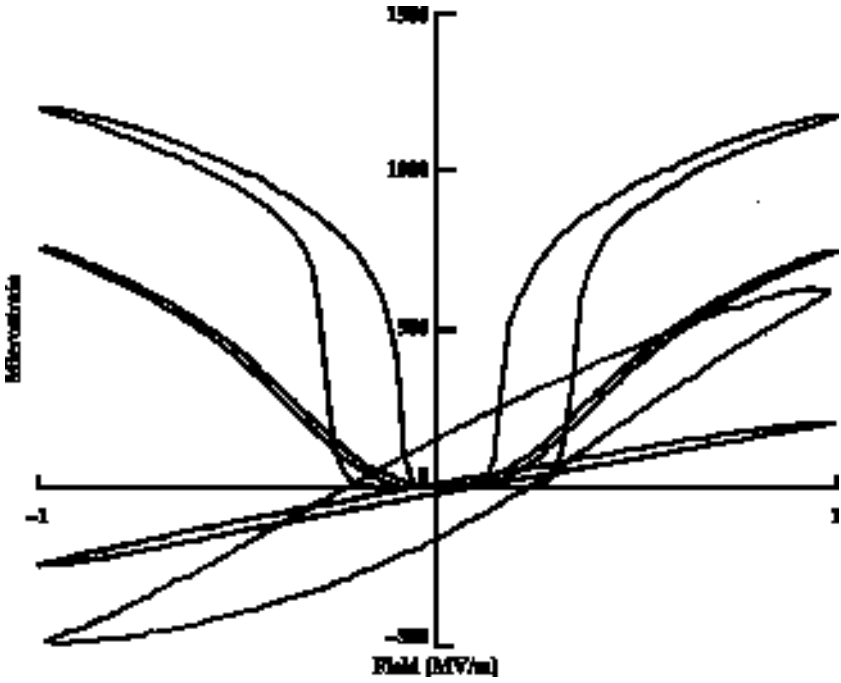

FIGURE 3.39 Strain versus field relationship for various electromechanical ceramics.[30]

TABLE 3.18 Properties of Piezoelectric Transducer Materials

Material	Dielectric constant	d_{33}, pC/N	d_{31}, pC/N	g_{33}, 10^3 m^2/C	$d_h g_h$	k_p
$PbNb_2O_6$	225	85	–10		2300	
$Pb_{0.5}Ba_{0.5}Nb_2O_6$		220	–90			
$PbTiO_3$		51	–4			
$BaTiO_3$		190	–79	13		0.36
PZT		223	–93.5			0.52
PZT	1800	450	–205		100	
0.855PZN-0.095PT-0.05BT	3000–3500	540	–228		279	
0.873PZN-0.097PT-0.03BT	1825	440	–196		143	
PLZT 2/65/35		150		23		0.45
PLZT 7/60/40		710		22		0.72
PLZT 7/55/45		405		15		0.56

Table 3.18 shows the properties of various piezoelectric transducer materials. Generally, those materials with lower piezoelectric coefficients have significantly higher coercive fields, resulting in a more stable piezoelectric response.

In most electromechanical materials, dopants are used to tailor the properties for specific applications. Isovalent substitutions are often used to modify the dielectric properties of these materials—for instance, Ba^{2+} or Sr^{2+} substitution for Pb^{2+} in perovskite and tungsten-bronze structures or Sn^{4+} for Zr^{4+} in PZT. The perovskite and tungsten-bronze structures will allow significant substitution with isovalent ions of similar size.

The $Pb(Zn_{1/3}Nb_{2/3})O_3$ (PZN) materials are cubic above the transition temperature T_C, 140°C, and undergo a diffuse phase transition to rhombohedral as they are cooled below T_C. PT is cubic above its Curie temperature of 490°C and undergoes a diffuse phase transition to tetragonal as it is cooled below T_C. The resulting solid solution of these materials results in a morphotropic phase transition between the rhombohedral and tetragonal phases at 9 percent PT. Additions of barium titanate (BT) to PZN-PT allow formation of pure perovskite near the morphotropic phase boundary where properties are maximized. Figure 3.40 shows a ternary compositional diagram. Increased amounts of PT or BT yield pure perovskite; however, there is a coincidental drop in properties due to shifting from the phase boundary at 0.91PZN-0.09PT where properties are a maximum. Smaller amounts of BT result in some amount of pyrochlore formation.

A typical PZN-PT-BT composition reacts to form 100 percent pyrochlore after an 800°C calcination, and perovskite becomes stable at higher temperatures (950°C), i.e., during sintering. The perovskite structure can then decompose to pyrochlore if the atmosphere is not controlled to reduce lead loss during sintering. The presence of both the rhombohedral and tetragonal phases is expected in a diffuse transition, because of slight variations in composition resulting in microregions of rhombohedral and tetragonal phases. The PZN-based compositions are dielectric relaxors as well. Figure 3.41 shows a dielectric constant versus temperature plot for the PZN-PT-BT composition at various frequencies. The relative shape of the curve and response with frequency are typical of relaxor behavior. It is generally believed that compositional variations in the microscopic level in the disordered perovskite structure accounts for the decrease in permittivity with increasing frequency in the ferroelectric region (below T_C) and the convergence of permittivity in the paraelectric region (above T_C). Disordered relaxors, such as PZN, also exhibit a shift in T_C to higher temperatures with increasing frequency.

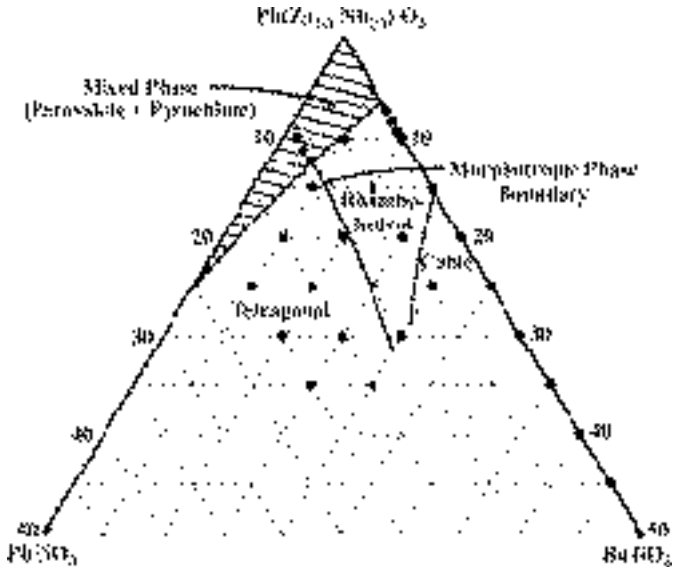

FIGURE 3.40 Phase diagram for the PZN-PT-BT system.[16]

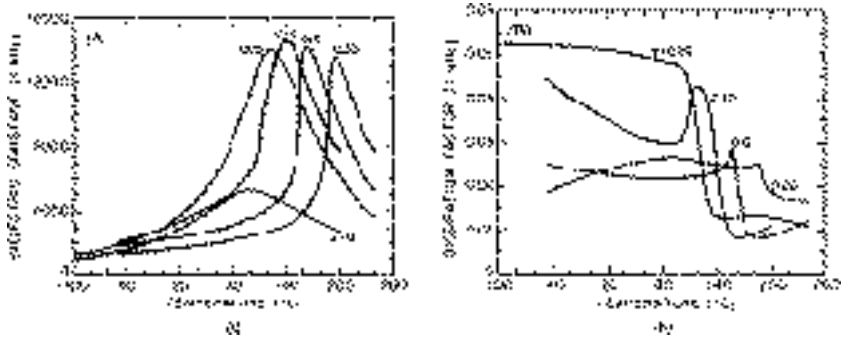

FIGURE 3.41 Dielectric constant and dissipation factor (1 kHz) versus temperature for (1−*x*)PZN-0.05BT-*x*PT ceramics.[16]

The ferroelectric phase of tungsten-bronze structure $PbNb_2O_6$ is metastable; that is, it normally exists only at high temperatures, greater than 1200°C. However, by doping and rapidly cooling from high temperature the ferroelectric tetragonal phase can be retained to low temperatures.

Piezoelectrics have been the sensing and broadcasting element of underwater acoustics since its inception. Passive sensors are designed to detect acoustic signals by converting pressure waves or vibrations into electrical signals. Ignoring temperature, bias stress, and electrostrictive effects, Eqs. (3.18) and (3.20) reduce to:

$$\varepsilon_{ij} = g_{ijk} P_k \tag{3.21}$$

and

$$\varepsilon_{ij} = d_{ijk} E_k \tag{3.22}$$

for a pure piezoelectric material.

where ε_{ij} = strain
P_k = dielectric polarization vector
E_k = electric field vector
g_{ijk}, d_{ijk} = piezoelectric coefficients

The piezoelectric charge coefficients d_{ijk} are generally expressed by using condensed subscripts, such as d_{33} and d_{31}, where the first subscript refers to the electric field direction or direction of polarization and the second subscript refers to the stress or strain direction. The piezoelectric charge coefficients g_{ijk} are also expressed in condensed form and are related to the charge coefficients via the dielectric constant K,

$$g_{ij} = d_{ij}/K\varepsilon_0 \tag{3.23}$$

When a piezoelectric transducer is stressed, charge of opposite polarity is generated on the electroded surfaces (the direct piezoelectric effect). That is,

$$P_i = d_{ijk}\sigma_{ij} \tag{3.24}$$

As an electric field is applied a mechanical strain develops (the converse piezoelectric effect), as in Eq. (3.22). The charge generated on electroded surfaces when an external stress is applied is

$$Q = -d(F/A\hat{F})A_e \tag{3.25}$$

where d = piezoelectric strain coefficient (C/N, m/V)
$F/A\hat{F}$ = applied force per unit area
A_e = area of conductive electrodes

The charge that accumulates as a result of applied voltage is given by

$$Q = K\varepsilon_0 A_e V/t \tag{3.26}$$

where K = dielectric constant of the material
$\varepsilon_0 = 8.854 \times 10^{-12}$ F/m, the permittivity of free space
V = applied voltage
t = parallel electrode spacing

The strain resulting from both applied force and voltage is

$$\varepsilon = dE - s(F/A\hat{F}) \tag{3.27}$$

where E is the applied electric field and s is the material compliance.

3.5.5 Applications

By definition, electromechanical materials provide a coupling between electrical and mechanical energy. While the mechanical displacements are relatively small, these materials can generate significant electrical and mechanical forces.

Multilayer ceramic actuators are finding practical uses in systems for adaptive optics, vibration damping, active sonar, and micropositioning uses such as proportional valve control. They are filling the void between low stiffness/high displacement/low voltage devices such as bimorphs and high stiffness/low displacement/high voltage monolithic ceramics. Practical uses of actuators in these systems require:(1) selection of optimal electrostrictive or piezoelectric compounds with consideration of the tradeoff in field-induced strains, hysteresis, temperature dependence, pressure dependence, frequency response, and mechanical properties and (2) design and fabrication of multilayer actuators that have demonstrated reliability and satisfy performance objectives.

Acoustic transducers convert electrical inputs into acoustic signals, i.e., *projectors*, or convert acoustic signals into electrical signals, i.e., *sensors*. Underwater acoustics applications have driven the development of piezoelectric ceramics. Hydrophones are the passive sensing device in underwater acoustic applications. Hydrophones take advantage of the direct piezoelectric effect; that is, acoustic inputs in the form of pressure changes result in a electrical output. Hydrophones are designed for collecting inputs from a broad frequency band, 0.1 to 100 kHz. The higher frequencies allow higher resolution but are rapidly dissipated in water. Lower frequencies are therefore used for longer-range detection.

When piezoelectrics are used in hydrostatic pressure conditions, such as hydrophone applications, the hydrostatic piezoelectric coefficient determines performance. The hydrostatic coefficients take into account the transverse piezoelectric effect from directions orthogonal to the poling axis. They are the hydrostatic strain coefficient

$$d_h = d_{33} - 2d_{31} \tag{3.28}$$

and the hydrostatic voltage coefficient

$$g_h = d_h/\varepsilon_0 K \tag{3.29}$$

The hydrophone figure of merit is the product $d_h g_h$. When the piezoelectric has a high K, inexpensive preamplifiers can be used. The open-circuit hydrophone sensitivity is expressed as output voltage per input plane wave pressure:

$$V_0/P = A_e d/C \tag{3.30}$$

where A_e = electrode area
d = piezoelectric coefficient
C = device capacitance

Reducing the capacitance by increasing electrode separation or lowering the dielectric constant increases the open-circuit sensitivity. However, in hydrophone circuits a larger capacitance is needed to drive the electronics that amplify and transmit the signal to processors. Given the hydrostatic pressure condition of a hydrophone, cylindrical shells can be used to maximize the device performance. The configurations shown in Fig. 3.42 minimize the impact of the transverse effect in hydrostatic environments. The sensitivity of the design is improved to

$$V_0/P = r_0\left[\frac{d_{33}t}{\varepsilon(r_0 + r_i)} + \frac{d_{31}}{\varepsilon}\right] \tag{3.31}$$

for the radial mode and to

$$V_0/P = 2\pi r_0/N \ln\left(\frac{r_0}{r_i}\right)\left[\frac{d_{31}t}{\varepsilon(r_0 + r_i)} + \frac{d_{33}}{\varepsilon}\right] \tag{3.32}$$

for the tangential mode,

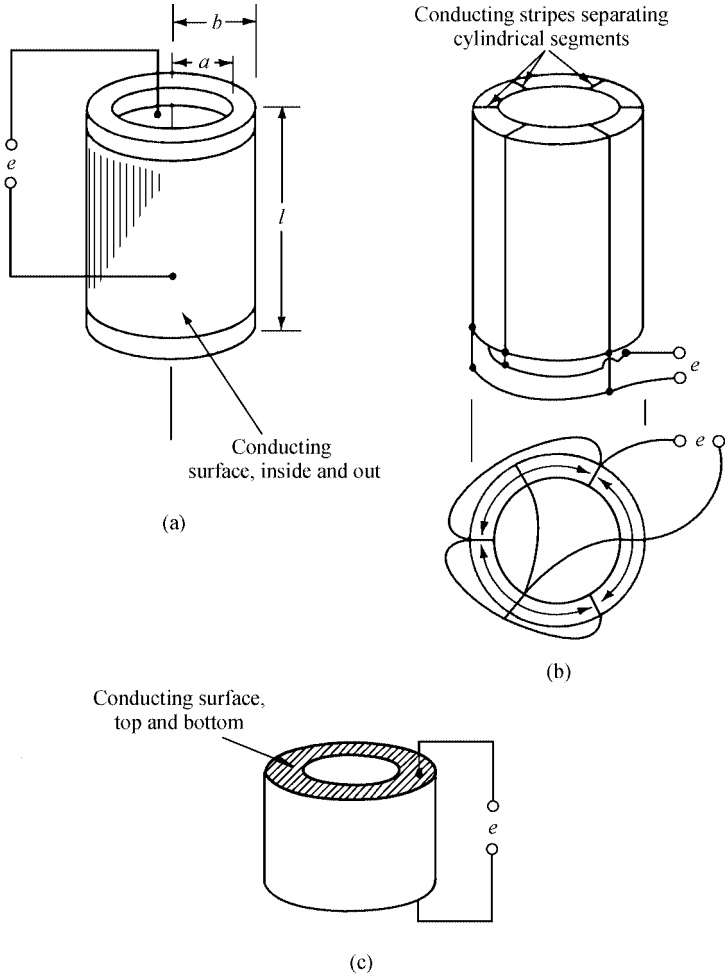

FIGURE 3.42 Ceramic cylindrical hydrophones: (*a*) radial mode, (*b*) tangential mode, and (*c*) longitudinal mode.[9]

where r_0 = outer cylinder radius
r_i = inner radius
t = cylinder wall thickness
ε = material permittivity
N = number of segments in the tangential mode hydrophone.

The radial mode design significantly increases the sensitivity in hydrostatic conditions and possesses higher capacitance than simple parallel plate slabs. The tangential mode design yields even higher sensitivity, but generally has much lower capacitance because of the large spacing between electrodes.

In sonar projector applications, acoustic power is applied to the water by an active surface. Most often in active sonar applications the device operates at a natural resonant frequency in order to minimize the power requirements for large displacements. Projectors are the active device for sound generation in underwater acoustics. Sonar projectors take advantage of the converse piezoelectric effect by converting large electrical signal inputs into mechanical outputs in the form of pressure changes, or sound waves. Projectors are typically designed to operate at resonance for maximum source level, therefore, the operating frequency band of individual devices is narrow. Often arrays of projectors operating at different frequencies are used to produce broadband acoustic sources.

Two types of sonar projectors are shown in Fig. 3.43. The Tompilz projector uses a stack of longitudinally poled piezoelectric slabs. The slabs are doughnut shaped so that a center bolt can be used to connect the head mass to the tail mass and prestress the multilayer ceramic stack. The slabs typically are metallized with thick-film fired-on metals, with thicker metal shims separating slabs for better current-carrying capability. The multilayer stack is electrically connected in parallel.

Flextensional transducers also contain a longitudinally poled stack of piezoelectric slabs, electrically parallel connected, inserted into an elliptical metal ring. The metal ring is designed to have a center opening somewhat smaller than the ceramic stack so that the metal ring must be compressed to insert the stack. This is an effective method for prestressing the multilayer stack. The approximately 3:1 aspect ratio of the flextensional transducer amplifies the mechanical displacement along the minor axis. The flextensional transducer obeys conservation of energy laws so that the 3:1 amplitude improvement is at the expense of a 3:1 reduction in the force generated along the minor axis direction.

The hard PZT piezoelectrics are the most common in sonar applications.

The field of electromechanical actuators has seen significant growth in the past 2 decades. Actuators generate mechanical displacements with electrical inputs for applications that include precision positioning devices, miniature motors, fuel injectors, printer heads, precision machining devices, noise cancellation devices, and optical devices such as deformable mirrors. A variety of methods have been developed to achieve practical displacements with practical drive voltages. The practical maximum displacement for an electromechanical ceramic is 0.1 percent at fields of 1 to 2 MV/m. Therefore, 1 mm of material is needed to achieve a displacement of 1 μm. A monolithic block of material would require 1 to 2 kV to achieve this displacement. Multilayer actuators use ceramic capacitor processing and designs to reduce voltage requirements. The drive voltage required for a multilayer design is reduced by a factor equal to the number of layers. For instance, if the 1-mm-thick actuator consisted of ten 0.1-mm layers, the drive voltages for the 1-μm displacement would be reduced to 100 to 200 V. Figure 3.44 shows a variety of actuator electrode designs aimed at minimizing tensile stresses that develop in inactive regions. This type of design is capable of generating relatively high displacements with substantial forces. Cofired actuators as long as 2 in with up to 2 mils displacement have been produced in this fashion. Figure 3.45 shows examples of Lockheed Martin actuators with typical displacements versus applied voltage. Longer actuators are fabricated by building stacked pucks.

Toyota's electronically modulated suspension (TEMS) uses piezoelectric sensors and actuators in a vibration cancellation role (Fig. 3.46). The system senses the road vibrations with a five-layer piezoelectric sensor. When rough roads or hard turns are encountered, the sensor is stressed and outputs an electronic signal. The signal is amplified by a control unit, which outputs a voltage to the 88-layer piezoelectric actuator. The actuator expands up to 50 μm on a hydraulic motion amplifier, which expands to 2 mm. This displacement stiffens the damping force of the shock absorbers, all within a 20-ms period.

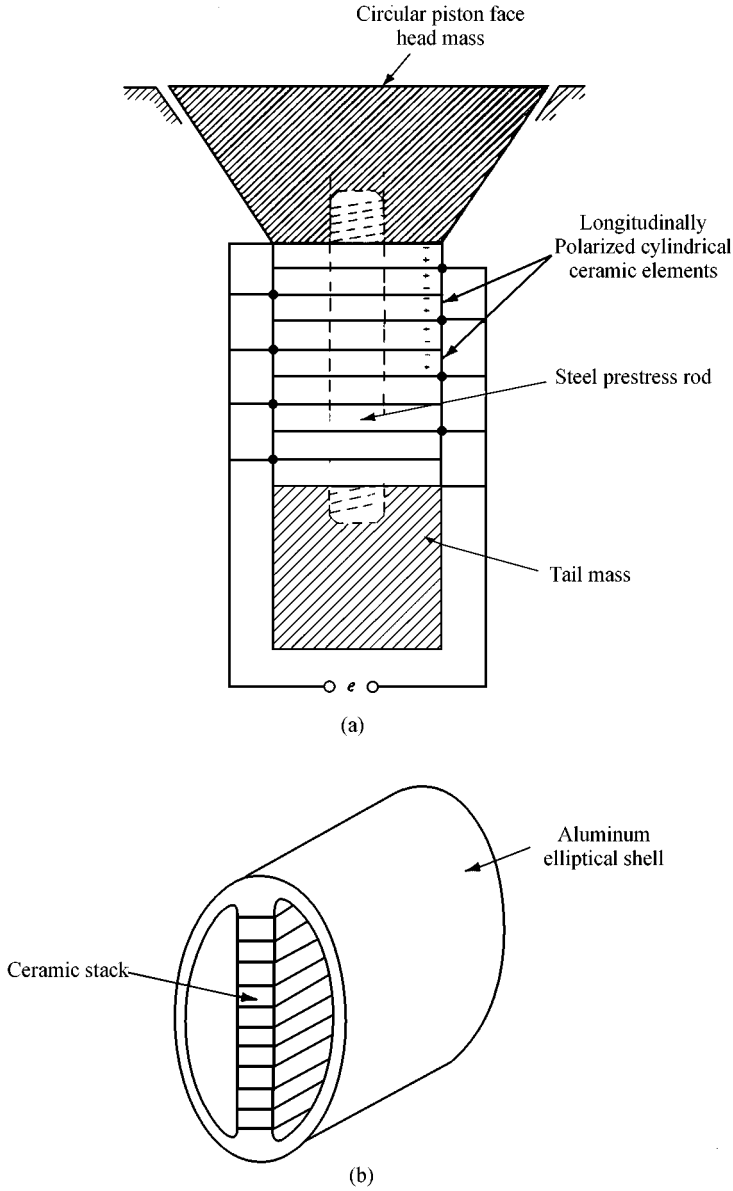

FIGURE 3.43 Active sonar projectors: (*a*) Tompilz projector and (*b*) Flextensional transducer.

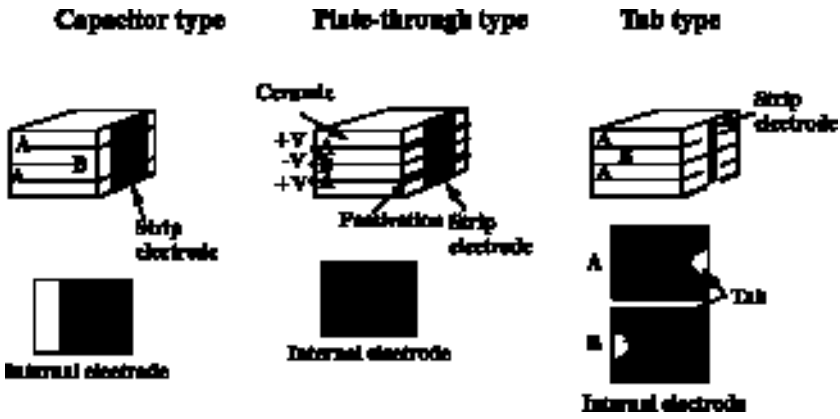

FIGURE 3.44 Actuator electrode and termination configurations.[9]

Ultrasonic transducers for medical imaging utilize piezoelectric ceramics and composites to generate an ultrasonic beam that can penetrate soft tissue. The same transducer then picks up the reflections off internal structure, organs, fetus, etc. These transducers most often consist of square-cross-section piezoelectric rods in a polymer matrix. These are formed by a dice-and-fill process. Figure 3.47 shows various piezoelectric-polymer composites used to optimize the performance for various applications. The diced 1-3 composite is typically used in ultrasonic transducer applications.

Deformable mirrors are used to correct the phase of incident light distorted by atmospheric conditions. The mirrors generally consist of an array of actuators that change the shape of a mirror.

Linear and rotational motors, Fig. 3.48, are designed to use surface wave vibrations generated by piezoelectrics.

3.6 ELECTROOPTIC MATERIALS

The electrooptic effect is simply the change in an optical property, namely refractive index, with an applied field. Changes in refractive indices are relatively small, on the order of 10^{-4}; however, this is sufficient to modulate the phase or intensity of transmitted light. A half-wavelength change in phase is sufficient to modulate polarized light from 0 to 100 percent transmission.

The first observation of natural optical anisotropy was made in 1669 by Bartolinius in calcite crystals, in which light travels at different velocities depending on the direction of propagation relative to the crystal structure. The electrooptic effect, electric-field-induced anisotropy, was first observed in glass in 1875 by J. Kerr. Kerr found a nonlinear dependence of refractive index on applied electric field. The term *Kerr effect* is used to describe the quadratic electrooptic effect observed in isotropic materials. The linear electrooptic effect was first observed in quartz crystals in 1883 by W. Rontgen and A. Kundt. Pockels broadened the analysis of this relationship in quartz and other crystals, which led to the term *Pockels effect* to describe linear behavior. In the 1960s several developments

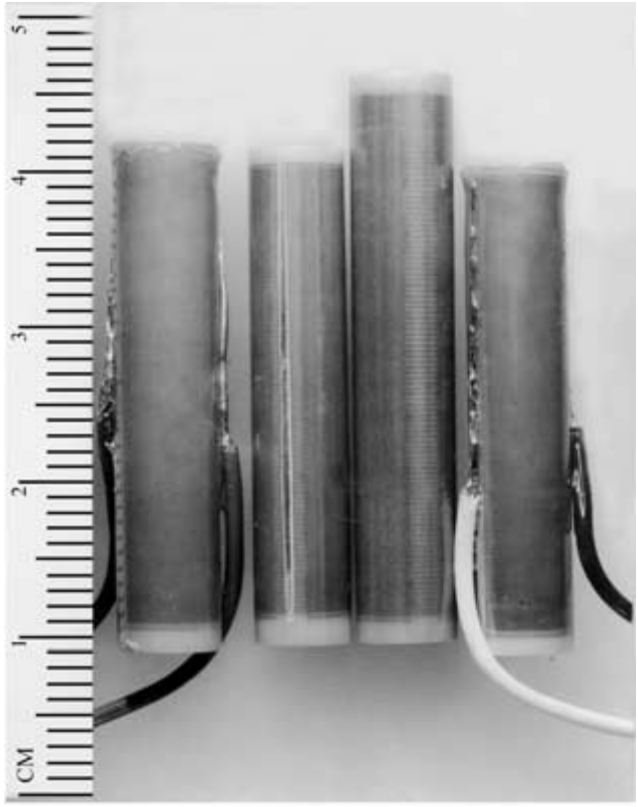

(a)

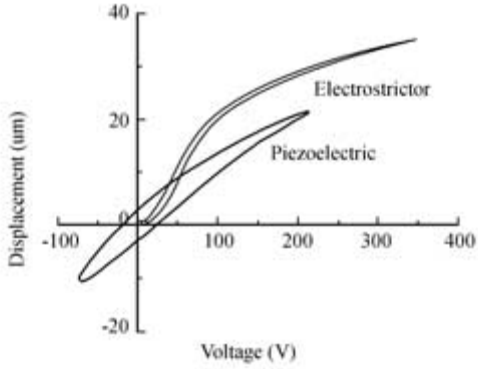

(b)

FIGURE 3.45 Multilayer actuators (*a*) may have many hundreds of active layers and (*b*) produce tens of millimeters displacement with several hundred volt drive. The response is distinctly different for piezoelectric and electrostrictive materials.[30]

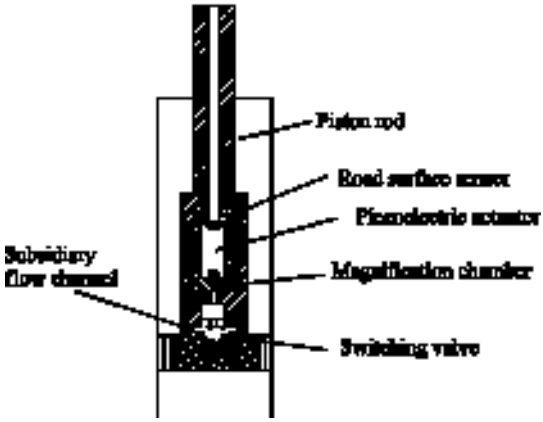

FIGURE 3.46 Schematic of Toyota electronically modulated suspension (TEMS) shock absorber.[29]

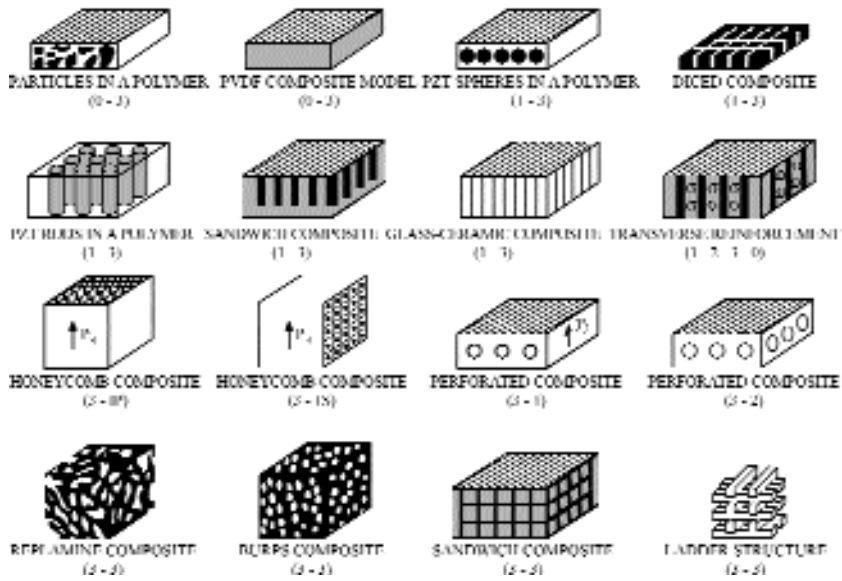

FIGURE 3.47 Piezoelectric-polymer composite configurations used to optimize ultrasonic transducer and hydrophone performance.[21]

in the areas of materials and processing lead to the concept of electrooptic ceramics. The development of hot-pressing techniques enabled the fabrication of fully dense ceramic bodies with a high degree of transparency. The first electrooptic ceramics developed at Sandia National Laboratories were based on the solid solution of lead zirconate–lead titanate (PZT). By 1969, the first transparent ceramics of lanthanum-doped PZT (PLZT)

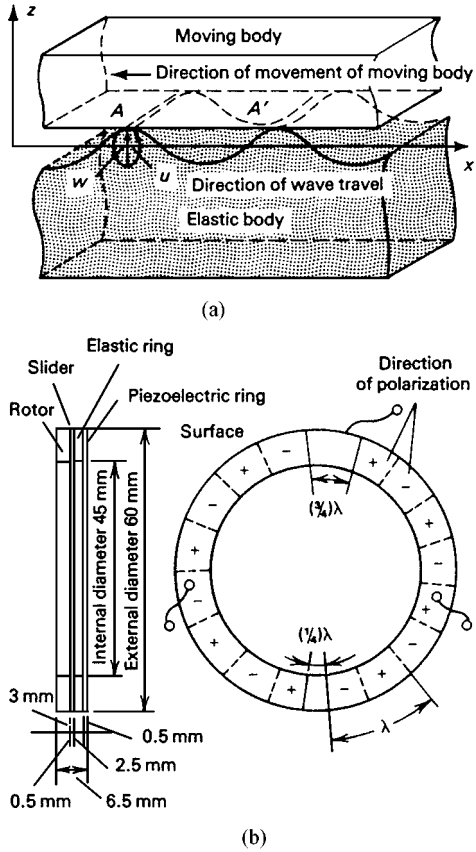

FIGURE 3.48 (*a*) Operating principle of surface wave linear motor (transverse propagating wave exciting an elastic body); (*b*) a structural example of a surface wave rotational device.[3]

were fabricated. G. Hartling and C. Land have extensively studied the electrooptic properties of PLZT and defined the composition dependence. The first single crystals of $Sr_xBa_{1-x}Nb_2O_6$ were fabricated in 1966 by A. Ballman and H. Brown. The large electrooptic coefficients were attractive for applications in laser modulation and deflection devices.

In order to sufficiently describe this effect, a review of optical properties of materials is necessary. The refractive index n of a material is a measure of the reduction in the speed of light as it travels through a transparent material; that is,

$$n = c/c_{\text{matl}} \tag{3.33}$$

where c is the speed of light in vacuum, 3×10^8 m/s, and c_{matl} is the speed of light in the material. Since $\lambda = c\nu$, a reduction in the speed of light results in a reduction in wavelength λ.

TABLE 3.19 Index of Refraction for Various Transparent Materials

Material	Refractive index
Air	1.003
Soda-lime-silica glass	1.52
Fused quartz	1.46
Quartz	1.5–1.6
Calcite, $CaCO_3$	1.56–1.74
ZnSe	2.62
$SrTiO_3$	2.49
SBN	
KDP	
PLZT	2.50
$BaTiO_3$	2.40
$LiNbO_3$	2.31

PLZT = lanthanum-doped lead zirconate–lead titanate.

The speed of light is affected as a result of the interaction with the electronic structure of the medium in which it is traveling. Materials containing large ions or negatively charged ions whose outer electrons are not so tightly bound, i.e., those having high polarizability, have a stronger interaction with electromagnetic waves. In general, materials with more dense crystal structures lower the speed of light and result in higher refractive indices. The index of refraction of various transparent materials is shown in Table 3.19. Refractive index is somewhat dependent on the wavelength of the incident light. Typically there is an increase in index at low wavelengths and reduction at high wavelengths. Figure 3.49 shows the variation in refractive index for a variety of optical materials as a function of wavelength. The amount of light reflected or refracted at the interface between two different materials is determined by their refractive indices. The amount of light R reflected at an angle equal to the incident angle is given by Fresnel's formula:

$$R = \left(\frac{n-1}{n+1}\right)^2 \tag{3.34}$$

for reflection in air.

The degree of refraction at the interface due to the change in light velocity is given by Snell's law:

$$\frac{\sin\phi_i}{\sin\phi_r} = \frac{n_2}{n_1} \tag{3.35}$$

where n_2 is the refractive index of the material through which the light is refracted.

Unpolarized white light contains randomly oriented electric field vectors, phases, and wavelengths. Both the reflected and refracted light undergo polarization of the electric field component vibrations. When unpolarized light contacts an interface, the reflected wave will have an electric field component whose vibrations tend to polarize perpendicular to the plane of incidence. This is illustrated in Fig. 3.50. The refracted wave vibrations tend to polarize parallel to the plane of incidence.

The direction of polarization in an isotropic material is always parallel to the applied field. The velocity of light traveling in an anisotropic material is dependent on both the direction of polarization and that of propagation. The optic axis is the crystallographic direction in which light will propagate at a speed independent of the polarization plane.

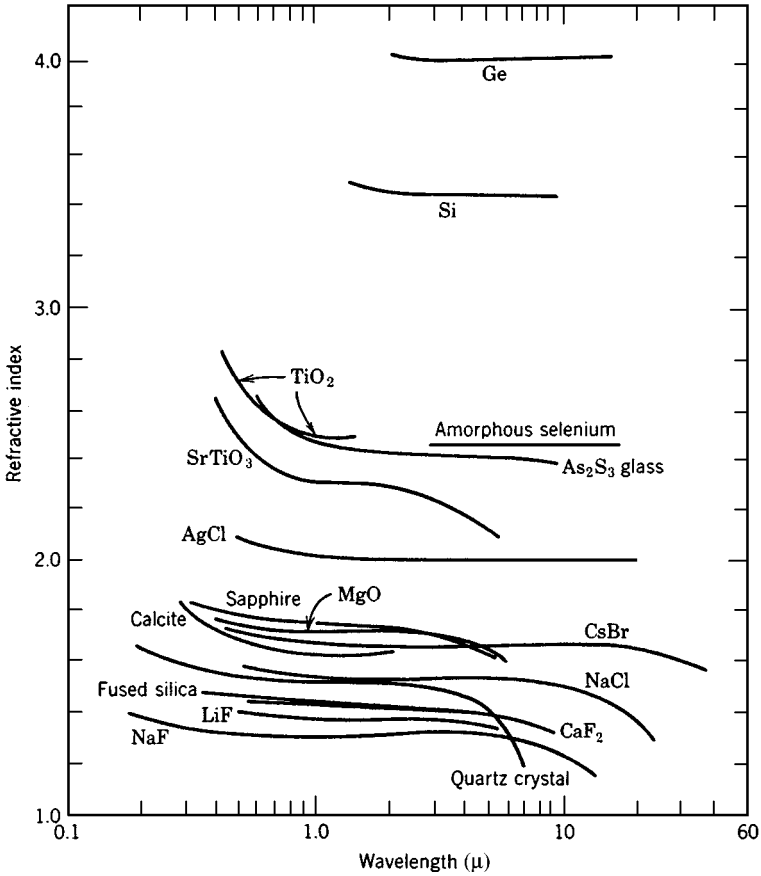

FIGURE 3.49 Change in refractive index with wavelength for several crystals and glasses.[20]

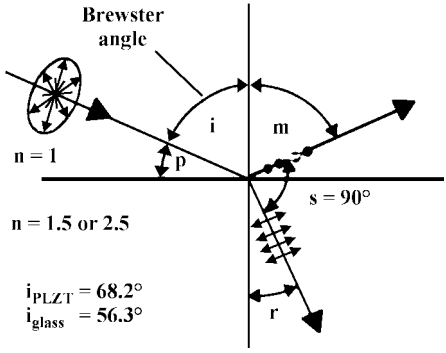

FIGURE 3.50 Polarization effects in unpolarized light on reflection and refraction.[21]

When the electric displacement component of light vibrates at right angles to the optic axis, regardless of direction, the ray is called *ordinary*. For those rays that vibrate parallel to the optic axis, extraordinary waves, the speed depends on the direction. The difference in refractive index between that of the ordinary wave, n_0, and the extraordinary wave, n_e, is the birefringence Δn. Birefringence is a measure of the phase difference between the ordinary and extraordinary waves. The relative impermeability of a material is given by

$$B_{ij} = 1/\varepsilon_r = 1/n^2 \tag{3.35a}$$

where ε_r is the relative permittivity and n is the refractive index for the material.

B_{ij} is a symmetrical tensor; therefore,

$$B_{ij} x_i x_j = 1 \tag{3.36}$$

In reference to the principal axes of a crystal, the relation becomes

$$x_1^2/n_1^2 + x_2^2/n_2^2 + x_3^2/n_3^2 = 1, \tag{3.37}$$

which is called the *optical indicatrix*.

Application of field causes a distortion of ΔB_{ij} in the optical indicatrix. The electrooptic effect can be described in terms of the dependence of the relative impermeability ΔB_{ij} on applied field,

$$\Delta B_{ij} = r_{ijk} E_k + R_{ijkl} E_k E_l \tag{3.38}$$

or, in terms of induced polarization,

$$\Delta B_{ij} = f_{ijk} P_k + g_{ijkl} P_k P_l \tag{3.39}$$

where r_{ijk} and f_{ijk} are the linear Pockels electrooptic coefficients and R_{ijk} and g_{ijkl} are the quadratic Kerr electrooptic coefficient.

The relation between these coefficients is:

$$f_{ijk} = \frac{r_{ijk}}{\varepsilon_k - \varepsilon_0} \tag{3.40}$$

$$g_{ijkl} = \frac{R_{ijk}}{(\varepsilon_k - \varepsilon_0)(\varepsilon_l - \varepsilon_0)} = \frac{R_{ijk}}{(K_l \varepsilon_0)^2} \tag{3.41}$$

where ε_k and ε_l are permittivity values in the direction of applied field.

When a field is applied to an anisotropic crystal, the relative impermeability relation reduces to

$$(B_{ij} + \Delta B_{ij}) x_i x_j = 1 \tag{3.42}$$

where $\Delta B_{ij} = r_{ijk} E_k$. Through crystal symmetry considerations, this relationship reduces to

$$\Delta n = \frac{-n^3 r_c E}{2} \tag{3.43}$$

where $r_c = r_{33} - n_0^3 r_{13}/n_e^3$ in reduced tensor notation. These relationships describe the linear Pockels electrooptic effect.

When a field is applied to an isotropic crystal, the relative impermeability relation reduces to

$$B_{ij} + \Delta B_{ij} = 1 \tag{3.44}$$

where $\Delta B_{ij} = R_{ijkl} E_k E_l$. Through crystal symmetry considerations this relationship reduces to

$$\Delta n = \frac{-n^3 (R_{11} - R_{12}) E^2}{2} \tag{3.45}$$

These relationships describe the quadratic Kerr electrooptic effect.

In anisotropic materials, the polarization depends on the direction and magnitude of the applied electric field. That is,

$$D_i = \varepsilon_{ij} E_j \tag{3.46}$$

and

$$P_i = D_i - \varepsilon_0 E_j = \varepsilon_0 (\varepsilon_r - 1) E_j = \varepsilon_0 (X_{ij_1} E_j + X_{ij_2} E_j E_k + \cdots) \tag{3.47}$$

Just as the permittivity and polarization of a dielectric is dependent on the applied field, so is the refractive index; that is

$$n = n_0 + aE_0 + bE_0^2 + \cdots \tag{3.48}$$

The refractive index at no applied field is represented by n_0. The aE_0 component represents the linear behavior between the refractive index and applied electric field for materials that are noncentrosymmetric. The quadratic relationship between refractive index and applied field, the term, bE_0^2 is seen in glasses and isotropic materials. In isotropic materials, the refractive index is the same regardless of the direction of light propagation, and the polarization state of the incident light remains unchanged. As an electric field is applied there is distortion of the electronic structure of the crystal and the material will then exhibit different refractive indices. Therefore, light passing through the material will split into two rays having different velocities. As the rays recombine on exiting the material, there is interference resulting in a rotation of the polarization direction. The phase shift, or retardation, Γ is given by

$$\Gamma = \Delta n t \tag{3.49}$$

where t is the thickness of the electrooptic material through which the light propagates.

3.6.1 Materials

All electrooptic materials are ferroelectric; that is, they exhibit a spontaneous polarization below T_C. The material of greatest importance is La-doped $Pb(Zr_zTi_{1-z})O_3$ (PLZT). The phase diagram for PLZT is shown in Fig. 3.51. La^{+3} substitutes on the A site of the perovskite structure in place of Pb^{+2}, acting as an electron donor. Charge neutrality is maintained by the formation of A or B site vacancies. While the exact lattice configuration is still unknown, experimental results by Hartling, et al., have shown a significant number of lattice vacancies exist when PZT is doped with La. The result is a reduction in the *c*/*a* ratio

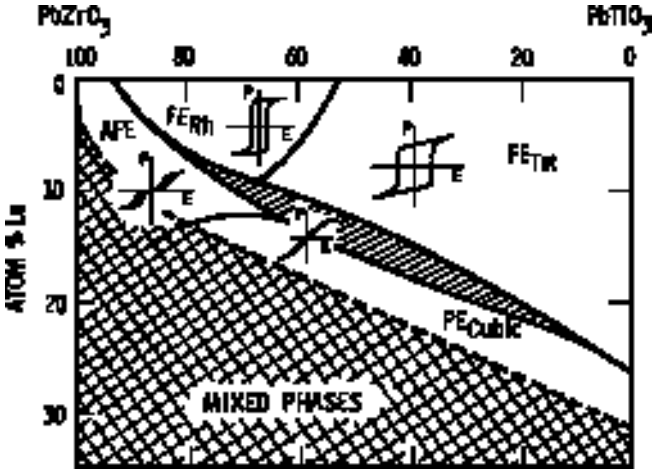

FIGURE 3.51 Room temperature phase diagram of the PLZT system illustrating the phases present and typical hysteresis loops associated with each phase.[21]

and a drop in the T_C. As T_C is approached in a ferroelectric, the domain structure is more easily realigned; i.e., low coercive fields exist. PLZT compositions used in electrooptic applications are nearly cubic; the *c*/*a* ratio is about 1.01. Most often, compositions are chosen that lie close to the morphotropic phase boundary between tetragonal and rhombohedral phases where properties are maximized. Compositions on the tetragonal side of the boundary tend to be hard ferroelectrics, i.e., have higher coercive fields. Compositions on the rhombohedral side are softer, i.e., have lower coercive fields. Table 3.20 shows the electrooptic coefficients for some common electrooptic materials.

Transparency is a key requirement of electrooptic materials. Light scattering will occur at discontinuities such as porosity, phase boundaries, and grain boundaries. The best transmission is usually observed in isotropic materials that are single phase with a high degree of homogeneity and fully dense. The amount of transmitted light to incident light can be determined from Rayleigh's equation,

$$I_t / I_0 = 1 + \frac{\cos^2 \theta r^6 (n_p - n_m)^2}{x^2 \lambda^4 n_m^2} \tag{3.50}$$

While the properties of single-crystal electrooptic materials are superior to those of ceramics, because of scattering mechanisms in ceramics, polycrystalline ceramics have a number of advantages over single crystals. Process complexity and cost is perhaps the greatest advantage. Single crystals are typically grown from a molten bath and are limited in size. Polycrystalline materials can be formed in large sizes and complex shapes at relatively low cost. In order to approach the properties of single-crystal specimens, electrooptic ceramics are typically hot pressed to achieve full densification. Improvements in homogeneity have occurred with the adoption of wet chemistry methods, such as sol-gel and precipitation, for preparation of the ceramic powders.

TABLE 3.20 Electrooptic Properties of Various Materials

Material (single crystals)	T_C, °C	R, m^2/V^2	R_c, m/V	E_c, kV/cm
$BaTiO_3$	130		19–23	
$LiNbO_3$			17.5	
$LiTaO_3$			22	
2/65/35	320	10^{-16}		13.7
7/65/35	150	10^{-16}		5.3
8/65/35	65	10^{-16}		3.6
8.5/65/35		38.6×10^{-16}		
9/65/35	5	3.8×10^{-16}		0
9.5/65/35	–10	1.5×10^{-16}		0
10/65/35	–25	0.80×10^{-16}		0
11/65/35		0.32×10^{-16}		0
12/65/35		0.16×10^{-16}		0
8/90/10		10^{-16}		0
8/70/30	20	11.7×10^{-16}		0
8/40/60	240		1.0	
8/10/90	355			37.5
12/40/60			1.2	
$Sr_{0.5}Ba_{0.5}Nb_2O_6$			2.10	
$Sr_{0.75}Ba_{0.25}Nb_2O_6$			14.0	
KH_2PO_4			0.52	
$LiNbO_3$			0.17	
$LiTaO_3$			0.22	

3.6.2 Applications

Electrooptic behavior falls into three categories: memory, linear, and quadratic. Figure 3.52 shows the characteristic polarization versus field behavior and the change in refractive index with applied field. Devices using the quadratic configuration are based on isotropic compositions with no applied field, such as 8 to 12 percent La additions in $Pb(Zr_{0.65}Ti_{0.35})O_3$. As field is applied, a ferroelectric-type state is induced. These materials exhibit the quadratic, Kerr, dependence of birefringence on electric field:

$$\Delta n = -n^3 RE^2/2 = -n^3 gP^2/2 \tag{3.51}$$

Linear characteristics are achieved by forming compositions that are hard ferroelectrics, i.e., in the tetragonal phase region of PLZT, where the coercive fields are large (about 1.5 to 2 MV/m). Typically, compositions for linear behavior are based on 8 to 12 percent La–doped $Pb(Zr_{0.40}Ti_{0.60})O_3$. To achieve the desired linear characteristics (Pockels behavior), the material must first be poled to achieve high remnant polarization.

Memory characteristics include soft ferroelectric behavior. Compositions exhibiting low coercive forces, less than 1 MV/m, near the morphotropic phase boundary are typical, such as $Pb(Zr_{0.65}Ti_{0.35})O_3$ doped with less than 8 percent La. Typically a large field is applied to achieve a large remnant polarization. Intermediate polarization states can be obtained by applying voltages.

Optical shutters utilize the properties of quadratic electrooptic materials as shown in Fig. 3.53. Switching from zero field to the field required for half-wave retardation results in a light shutter. If the electrooptic material is placed between crossed polarizers, polarized

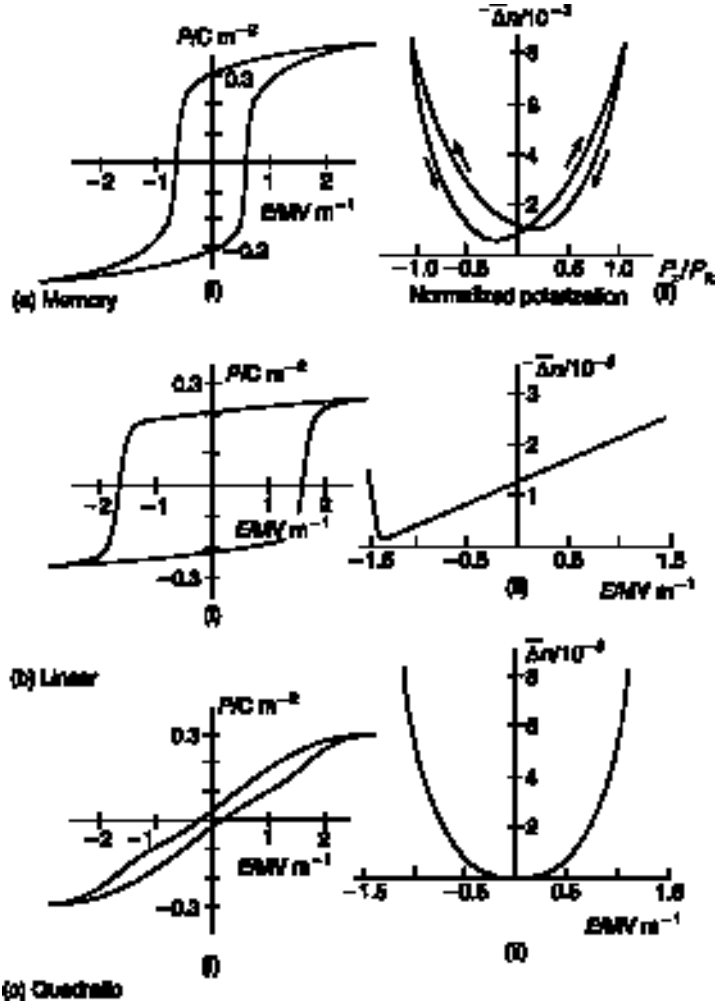

FIGURE 3.52 Hysteresis and electrooptic characteristics of the three main types of PLZT: (*a*) memory, (*b*) linear, and (*c*) quadratic.[24]

light is transmitted through the first polarizer. None of the polarized light is transmitted through the second crossed polarizer at zero applied field. Applying sufficient field causes birefringence and a net rotation of 90° of polarized light passing through the second crossed polarizer, as shown in Fig. 3.53.

The voltage required to achieve 90° rotation of one-wave component relative to the other is given by

$$V = \frac{\lambda t_{\text{field}}}{R t_{\text{prop}}} \tag{3.52}$$

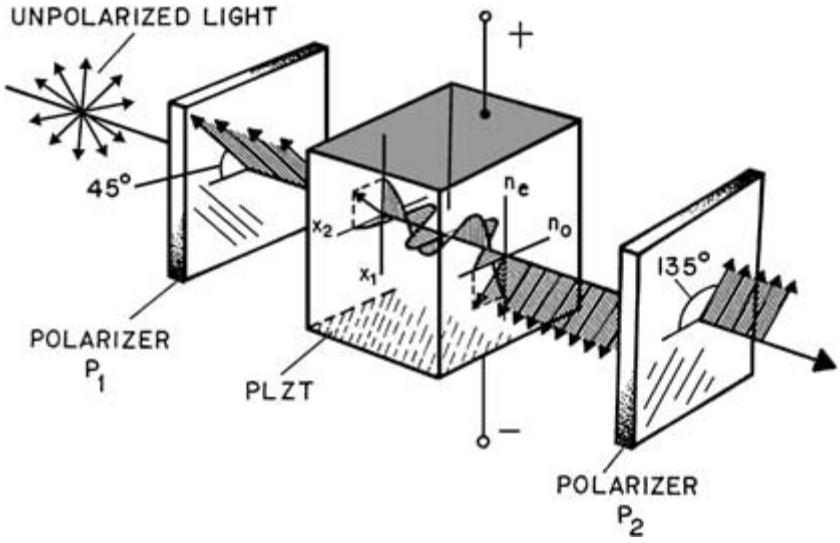

FIGURE 3.53 Optical phase retardation in an activated PLZT electrooptic ceramic; the open state at half-wave voltage is shown for a crossed polarizer configuration.[21]

where λ = wavelength of the incident light
t_{field} = thickness across which an electric field is applied
t_{prop} = propagation distance

The voltage required can be reduced by increasing the electrooptic coefficient, reducing the material thickness in the applied field direction, or increasing the propagation distance.

The ratio of transmitted light to incident light in a cross-polarized light shutter is given by

$$I_t/I_i = \sin^2(\Delta n\pi/\lambda) \tag{3.53}$$

for monochromatic light of wavelength λ.

However, when the incident light is white light there is a retardation of different wavelengths as the electric field is increased. Figure 3.54 is the Kerr optical interference color chart, showing transmitted wavelengths and, therefore, colors with applied field for various material birefringence and thickness values.

Electrooptic thin-film devices are of two types: one in which the propagation of light is along the plane of the film (optical waveguides) and the other in which the light passes through the film (optical memory and displays). An optical waveguide controls the propagation of light in a transparent material (ferroelectric thin film) along a certain path. For the waveguide to work properly, the refractive index of the film should be higher than that of the substrate. For light to propagate in the waveguide, the thin film should be optically transparent. A great deal of work has been done on making ferroelectric thin film waveguides from $LiNbO_3$ and $Li(Nb,Ta)O_3$ using liquid-phase epitaxy (LPE), EGM, and molecular beam epitaxy (MBE) methods. PZT and PLZT thin films are even better candidates for optical waveguide applications because of their large electrooptic coefficients.

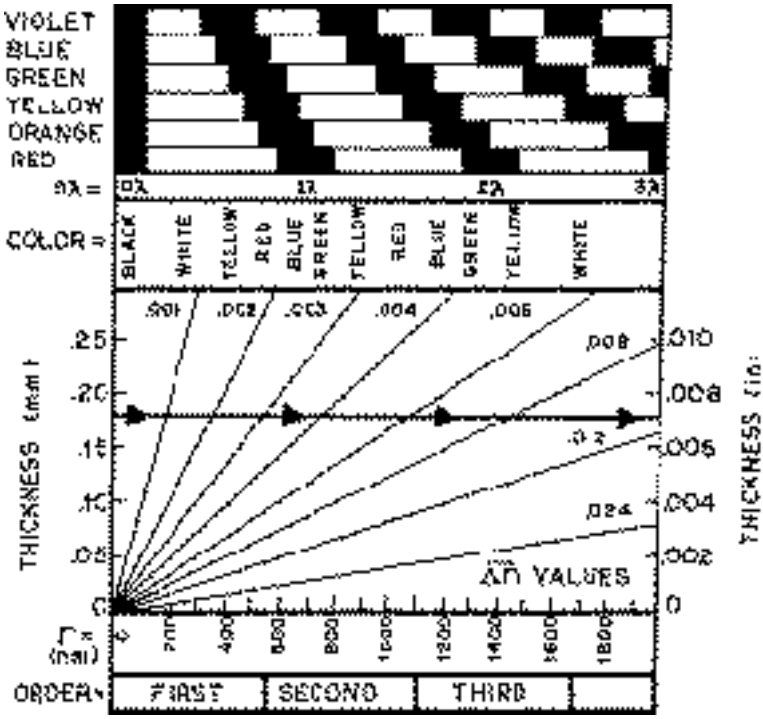

FIGURE 3.54 A Kerr retardation chart showing the origin of the Newton color orders.[21]

Ferroelectric thin films may replace PLZT bulk ceramics for optical memory and display applications. The advantages offered by thin films for display applications include a simplification of the display device design and lower operating voltages compared to PLZT ceramic devices. Optical memories using PLZT thin films will also need lower operating voltages.

3.7 SUPERCONDUCTIVE CERAMICS

The electric current density J is a measure of the charge moving through an area of material over a given time:

$$J = nzev \tag{3.54}$$

where n = number of charged particles per unit volume
e = electronic charge
z = valence (in the case of ionic conduction)
v = drift velocity in units of cm/s

The ratio of the drift velocity to the local electric field, v/E, is defined as the charge mobility, μ, in units of $cm^2/(V \cdot s)$.

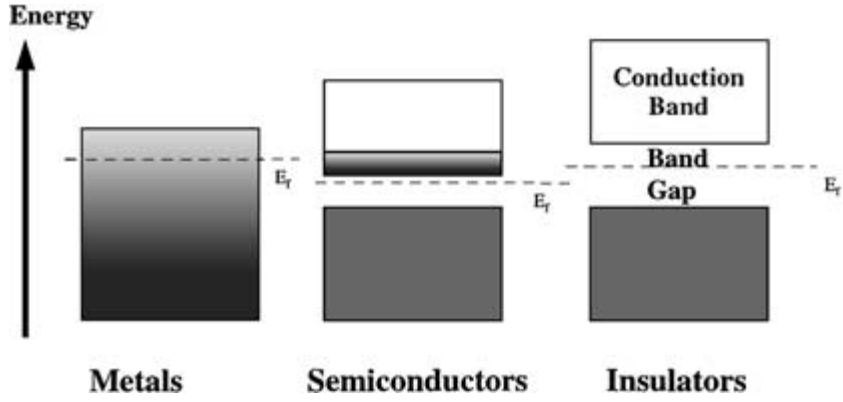

FIGURE 3.55 Electronic band structure for metals, semiconductors, and insulators.

Electrical conductivity σ is a measure of the current density, J with an applied electric field E:

$$\sigma = J/E = nze\,(v/E) = nze\mu \tag{3.55}$$

As shown in Fig. 3.55, metals always have a concentration of electrons in the conduction band. Semiconductors have small band gaps and the concentration of electrons in the conduction band depends on the composition and temperature, and insulators have such a wide band gap that there are no electrons in the conduction band under normal conditions. Introduction of oxygen interstices in insulators results in cation vacancies or holes, leading to p-type conduction; likewise, oxygen vacancies result in excess electrons, leading to n-type conduction.

3.7.1 Materials

The phenomenon of superconductivity was first discovered in 1911 by K. Onnes in mercury metal shortly after his development of a process for forming liquid helium. He found that resistance dropped sharply to an infinitesimal value at a temperature of 4.2 K (–269°C). The development of liquid helium enabled the discovery of superconductivity in many compounds since it allows the cooling of materials to near absolute zero temperature (0 K). Meissner, in 1933, showed that superconductors exhibit not only zero electrical resistance but also diamagnetic behavior. Diamagnetic materials have electronic interactions that produce a net zero magnetic moment. If a magnetic field is applied to these materials, a magnetic moment is induced that is oriented opposite to the applied field. These materials, which typically have closed electron shells, have negative magnetic susceptibilities, on the order of 10^{-5} to 10^{-6}. The generation of the opposing magnetic field is the driving force for the high surface current (screening current) flow in the material.

When a magnetic field is applied to a superconductor below the critical superconducting transition temperature T_c, electric currents flow in the material without resistance, creating a magnetic field opposing the applied field (the Meissner effect). There is a critical current density J_c above which superconduction halts. Also, there is a maximum magnetic field H_c above which superconduction ceases. In general, as the temperature is

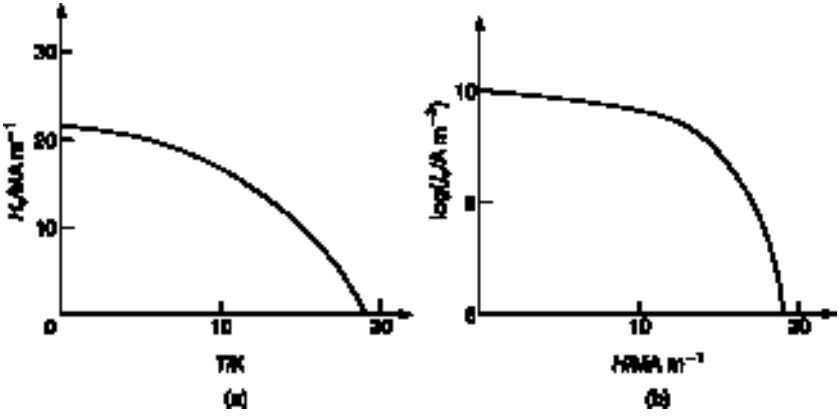

FIGURE 3.56 (*a*) Critical magnetic field H_c as a function of temperature for Nb_3Sn; (*b*) critical current density J_c as a function of magnetic field at 4.2 K for Nb_3Sn.[24]

raised to T_c, J_c and H_c decrease as shown in Fig. 3.56 for Nb_3Sn. The desirable properties of a superconducting material are a high T_C, high critical current density, a high critical magnetic field H_c, low cost, reliability, and manufacturablity. J_c is the highest current density exhibited with infinitesimal resistance. H_c is the highest magnetic field that can be applied to a superconductor.

In Type I superconductors, all magnetic flux is contained in a surface layer of the material, the London penetration depth. Metallic superconductors are Type I. In Type II superconductors, magnetic flux penetrates the interior of the material at a critical magnetic field. If the flux lines are not pinned, there is resistive energy loss and the current density at which the magnetic flux moves into the interior determines J_c. If the flux lines are pinned along controlled crystalline defects such as impurity inclusions or second phases, higher magnetic fields can be tolerated, leading to higher current density. The high-temperature superconductor (HTS) ceramics are Type II and are capable of withstanding much higher magnetic fields.

In the 1950s, Frohlich and J. Bardeen theorized that superconduction is a result of electron-phonon interactions that couple electron pairs. This pairing up can occur only at low temperatures where thermally induced motions of the electrons are sufficiently reduced. Later, L. N. Cooper showed how an electron pair (a Cooper pair), would have a combined energy level lower than conduction electrons in the highest energy state, the Fermi level. In 1957, Bardeen, L. N. Cooper, and J. R. Schrieffer further theorized the large-scale interaction of Cooper pairs, the Bardeen-Cooper-Schrieffer (BCS) theory. The BCS theory describes how electron pairs in a superconducting metal interact such that their combined momenta are unchanged. Conduction scattering mechanisms, such as phonon interactions, have equal and opposite effects on each of the paired electrons. Therefore, there is no change in momentum and no resistance to the conduction of electron pairs. In 1950, B. T. Matthias attempted to establish criteria for good superconductors. Material requirements included a high concentration of Fermi level electrons, the presence of soft phonons, and the proximity to a metal-insulator transition.

The quest for a room temperature superconductor has spurred the development of thousands of compounds incrementally driving the critical temperature for superconduction to higher values. Table 3.21 shows various superconducting materials with corresponding

TABLE 3.21 Transition Temperatures for Superconducting Materials

Element/compound	T_c, K
$SrTiO_{3-x}$	0.5
Sn	3.7
Hg	4.2
Pb	7.2
Nb	9.2
$BaPb_{1-x}Bi_xO_3$ ($x \approx 0.25$)	13
$Li_{1+x}Ti_{2-x}O_4$ ($0 < x < 1/3$)	14
Nb_3Sn	18
$Nb_3Al_{0.5}Ge_{0.2}$	20.9
Nb_3Ge	23
BaKBiO	30
$La_{2-x}Ba_xCuO_{4-y}$	35
PbSrCaLaCuO	55
$YBa_2Cu_3O_{7-x}$	93
$Bi_2Sr_2Ca_2Cu_3O_x$	110
$Bi_{1.5}Pb_{0.5}Sr_2Ca_2Cu_3O_x$	110
BiAlCaSrCuO	114
TlCaBaCuO	100–125
$HgBa_2Ca_2Cu_3O_8$	133 (150–160 pressurized)

transition temperatures below which the resistivity falls to infinitesimal levels. At this point in time, the highest temperature for the onset of superconductivity is about 130°C.

In 1966, the first superconducting ceramic was discovered in the perovskite structure $SrTiO_{3-x}$ with a T_c of 0.5 K. The oxygen deficiency results in lattice vacancies, which aid in the n-type conduction. Johnson et al., in 1973, documented the superconducting behavior of $Li_{1+x}Ti_{2-x}O_4$ ($0 < x < 1/3$) at about 14 K. In 1986, J. G. Bednorz and K. A. Muller received the Nobel prize for their discovery of the superconducting behavior of perovskite-like $La_{2-x}\,Ba_x\,CuO_{4-y}$ with a T_c of 35 K. The crystal structure consists of layers of perovskite formed by Cu-O separated by layers of rock-salt crystal structure formed by (La, Ba)-O ions. Their data, shown in Fig. 3.57*a*, sparked a significant amount of research in cuprate superconductors, where Cu^{2+} and Cu^{3+} can coexist. Soon thereafter, Wu and Chu discovered compositions of $YBa_2Cu_3O_{7-x}$, the 123-cuprate material shown in Fig. 3.57*b*, with a transition temperature well above the 77K boiling point of nitrogen, at about 93K. Superconductors that operate above liquid nitrogen temperatures allow the fabrication of practical devices cooled by much cheaper liquid N_2. These 123-cuprates are of the layered-perovskite type crystal structure shown in Fig. 3.58. Again, the superconducting behavior results from the existence of multivalence copper ions mixed with oxygen ions, forming planar arrays separated by perovskite layers. The perovskite structure favors the existence of soft-mode phonons as evident in its instability and morphotropic phase boundaries, one of the Matthias's criteria. The presence of multivalence ions and oxygen vacancies seems to favor superconductivity. The Cu-O distance is dependent on the oxidation state of the copper. Therefore, as an electron is transferred, the oxidation state of the copper changes, resulting in a lattice displacement. This is theorized to be the mechanism for the electron-phonon interaction described in the BCS theory.

In 1988, Maeda et al. discovered superconducting phases in the Bi-Sr-Ca-Cu-O system. Similarly, Sheng and Hermann discovered high T_c in the Tl-Ba-Ca-Cu-O system. The compounds contain Cu-O sheets interleaved with Tl-O or Bi-O sheets. The Bi-Sr-Ca-Cu-O

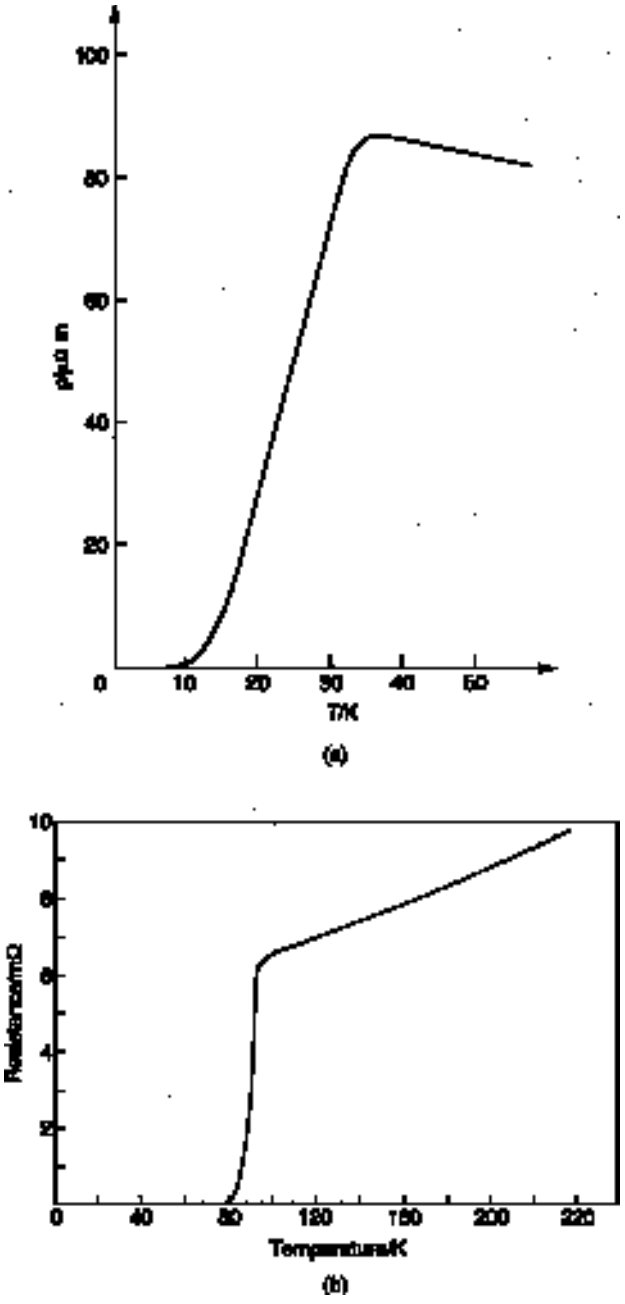

FIGURE 3.57 (*a*) Superconductivity in $(La, Ba)_2CuO_4$ and (*b*) $YBa_2Cu_3O_{7-\delta}$.[24]

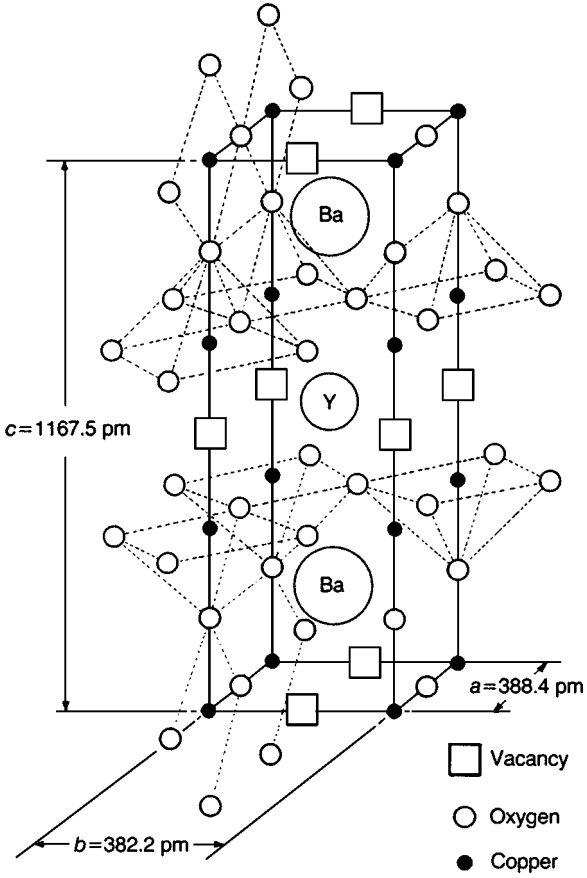

FIGURE 3.58 123-cuprate layered perovskite structure.[24]

system has three superconducting phases, $(BiO)_2Sr_2Ca_{n-1}Cu_nO_{2n+2}$, where $n = 1, 2, 3$. Their respective critical temperatures are 7, 80, and 110 K. Deficiencies on any of the cation sites, creating hole conduction, have been found to significantly increase the critical current density. Figure 3.59 shows the change in conductivity as a function of oxygen atmosphere during processing for a 123-cuprate superconductor. In 1993, the discovery of a series of mercury-based compounds with high critical temperatures sparked a new level of interest. The layered structure of $HgBa_2Ca_2Cu_3O_8$ has been shown to have a T_c of about 130 K, 164 K under high-pressure conditions.

Fabrication of these materials in large volumes with homogeneous phase and consistent properties has been a primary focus of superconductor research. Low critical current density J_c and poor mechanical properties have been the key problem areas. For most superconducting applications, a J_c of 10^5 to 10^6 A/cm^2 is required. The J_c of polycrystalline ceramics is generally much lower than that of single crystals because of high resistivity phases, microcracks, and changes in crystal orientation at the grain boundaries. Polycrystalline materials with J_c as high as 5×10^3 A/cm^2 have been reported.

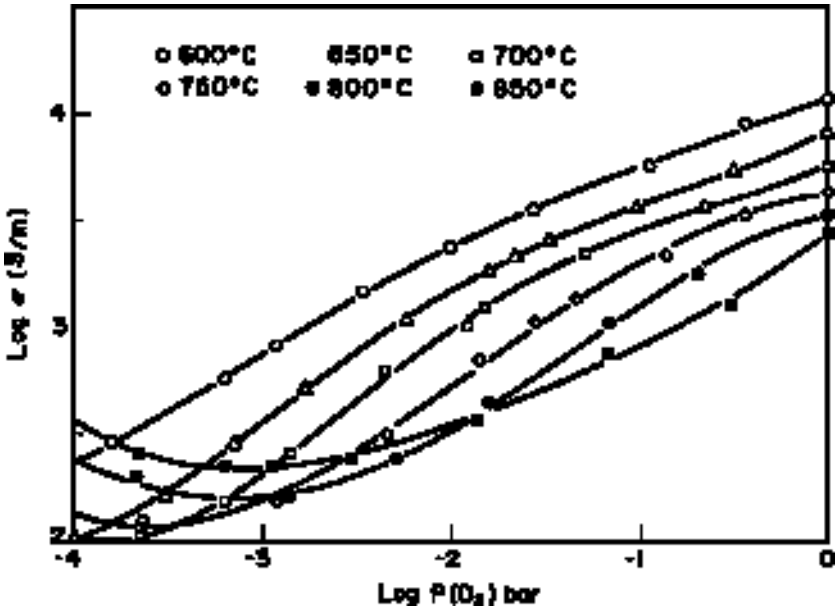

FIGURE 3.59 The equilibrium conductivity of $YBa_2Cu_3O_x$ as a function of oxygen activity in the temperature range 600 to 850°C.[26]

The highest-current-density materials have been fabricated in single-crystal or thin-film form. Critical current densities greater than 10^6 A/cm^2 have been achieved in single crystals and epitaxially grown thin films. Oak Ridge National Laboratory (ORNL) has demonstrated Y-Ba-Cu-O–coated conductor with the ability to produce 1- to 2-cm long, 0.3-cm-wide conductors with critical current densities up to 3×10^6 A/cm^2 at 77 K. Midwest Superconductivity Inc. (MSI) has produced high J_c results by using chemical vapor deposition (MOCVD) for Y-Ba-Cu-O deposition on a substrate produced by ORNL resulting in a short sample with J_c of 6.4×10^5 A/cm^2.

The properties of ceramic superconductors are highly dependent on the concentration of charge carriers. Therefore, the properties are determined by the phase purity, crystal structure, composition, and defect structure of the material. The final oxidation state of these oxide superconductors is critical to achieving maximum performance and maximize T_c. Most device fabrications include an anneal in oxidizing atmospheres. A significant amount of research is focused on processing methodologies, final chemistry, and phase relations in order to achieve the desirable phase stability and purity. Polycrystalline ceramic superconductors are typically prepared by solid-state calcination of oxide, nitrate, or carbonate precursors. Multiple milling steps are incorporated to promote homogeneity. Chemical synthesis routes using organometallic, salts, and metal alkoxide precursors such as sol-gel, precipitation, and decomposition processing have also been used to achieve a high degree of homogeneity. For thin-film superconductors, a variety of processes have had some degree of success including: chemical vapor deposition (CVD), spin coating, plasma spraying, molecular beam epitaxy, magnetron sputtering, laser ablation, and laser evaporation.

Grain-orienting processing techniques have been used to achieve anisotropic single-crystal behavior in polycrystalline ceramics. Current flows more easily perpendicular to the

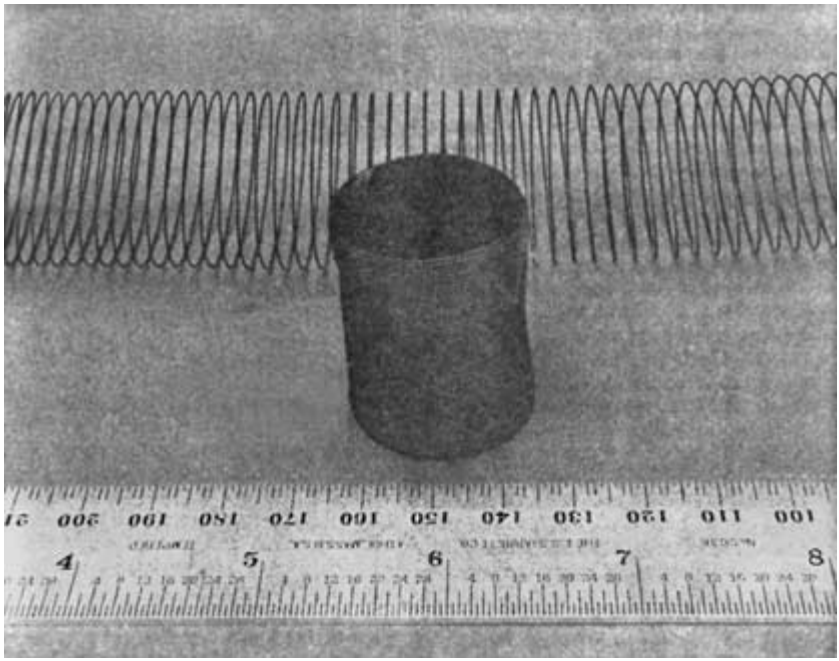

FIGURE 3.60 YBCO coils after heat treatment. Precipitates of Y_2BaCuO_5 are dispersed in a matrix of $YBa_2Cu_3O_x$.[3]

C axis of the crystals, therefore, a larger J_c and low onset resistivity is observed. Hot forging is a process similar to hot pressing; however, the material is unconstrained in the plane of the platens. The material is forced to densify or deform under a constant strain. Manufacturers of superconducting devices continue to strive for practical methods for forming useful superconducting circuits. The simple fact that the high-temperature superconductors are ceramic is a significant obstacle to forming wiring. However, processes such as plastic extrusion and tape casting are being used to fabricate superconducting coils such as those shown in Figs. 3.60 and 3.61. The wires are formed by extruding lengths of calcined powders mixed with organic binders. The extruded wires are wrapped around mandrels to form coils and fired. In composite structures like that in Fig. 3.61, the insulating phase isolates the coil turns, preventing short circuits, while the metal layer improves the flexibility, alleviates stresses form shrinkage and CTE mismatches during firing, and provides a good thermal conductor in operational conditions. Polycrystalline wire formed by placing 123-cuprate in silver metal tubing is used to achieve current densities in the 2 to 3×10^3 A/cm^2 range.

3.7.2 Applications of Superconductors

Superconductor materials are being used in an increasing number of applications. Most applications fall into one of three categories of functions: for low-loss transmission electronics, high-magnetic-field generation, or high-current-carrying conductors for power delivery. Up to 15 percent of electrical power is lost to transmission line resistance between

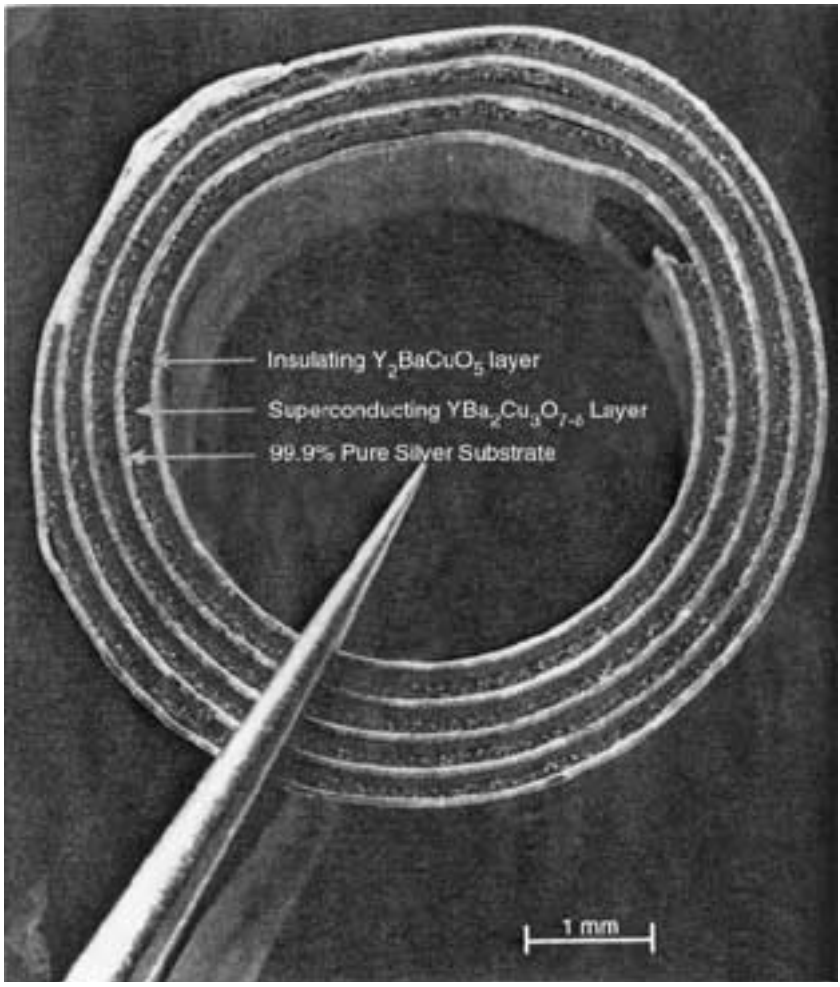

FIGURE 3.61 Prototype multilayer superconducting coil.[3]

the power source and the end user; superconducting transmission wires have the potential to eliminate this energy loss. The high current densities attained with superconducting coils allows the generation of large magnetic fields. Large magnetic field generation is required in medical diagnostic equipment, particle accelerators in nuclear energy research, and fusion containment magnets. Nuclear magnetic resonance (NMR) and magnetic resonance imaging (MRI) equipment use superconductors for generation of the large magnetic fields needed in these imaging systems. Efficient superconducting magnets are used to create magnetic fields as high as 20 T. No-loss electrical transmission and high-speed signal processing have generated interest in the area of digital processing. Because of the diamagnetic behavior of superconducting materials (the Meissner effect), they are being used in

magnetic-field-shielding applications. Superconductors allow fabrication of highly efficient motors and generators. Magnetic levitation for efficient high-speed trains is now a possibility.

A superconducting quantum interference device (SQUID) is a superconducting device capable of detecting minute changes in magnetic fields. SQUID sensors can detect weak magnetic fields, as low as 10^{-15} T. SQUID sensors have medical applications where magnetic fields resulting from electrical currents flowing in the human brain can be detected. Other applications include geological research and military applications such as submarine detection.

In 1962, B. D. Josephson predicted that Cooper pairs in superconductors could tunnel through an insulating barrier without encountering electrical resistance, the Josephson effect. A Josephson junction allows current to flow with no resistance with no applied field. However, at a critical voltage level, the Cooper pairs split up and normal quantum-mechanical tunneling occurs with resistive losses. The Josephson effect allows the fabrication of microelectronic switches and transistors that operate faster and with lower power loss than semiconductor devices.

In planar conductors, the surface impedance is calculated by

$$Z_s = (1 + j)(\bar{\omega}\mu / 2\sigma)^{0.5} \tag{3.56}$$

where $\bar{\omega}$ is the frequency, μ is the permeability, and σ is the conductivity. This shows that the loss of the conductor increases with the square root of the frequency. Impedance changes with frequency because of conduction electrons moving through thinner surface layers of material as the frequency increases (the skin effect). Surface roughness can have a significant impact on impedance since it effectively increases the surface conduction path because of the surface irregularities.

In high-temperature superconductors, the BCS theory does not seem to apply. A currently in-fashion idea is that high-temperature superconductors are the first "d wave." For alternating current, resistance increases slowly with increasing frequency. However, even at microwave frequencies, the resistance of a superconductor is approximately 1/1000 the resistance of copper or silver.

An example of high-current transmission lines is shown in Figs. 3.62 and 3.63, the warm dielectric cable and cryogenic dielectric cable fabricated by American Superconductor Corporation.

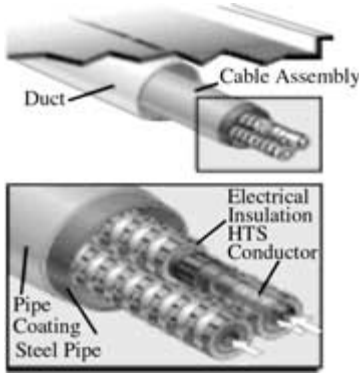

FIGURE 3.62 High-current transmission line, warm dielectric cable, from American Superconductor Corp.[1]

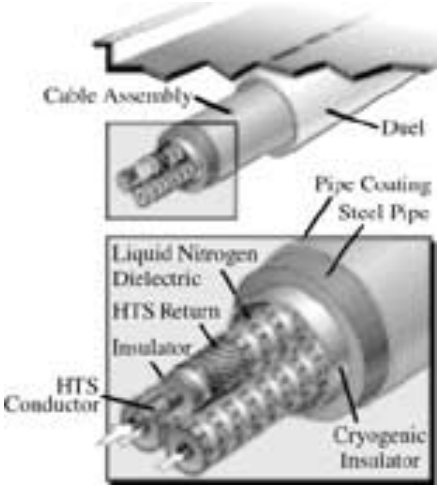

FIGURE 3.63 High-current transmission line, cryogenic dielectric cable, from American Super-conductor Corp.[1]

These power transmission cables consist of high-temperataure superconductor (HTS) wires wound around a hollow core through which liquid nitrogen flows for cooling below T_c. The conductor is surrounded by conventional dielectric insulation. The efficiency of this design reduces losses. The cryogenic dielectric is a coaxial configuration comprising an HTS conductor cooled by liquid nitrogen flowing through a flexible hollow core and an HTS return conductor, providing even greater current capacity, further reducing losses and entirely eliminating the need for dielectric fluids.

Motors and generators using HTS windings have twice the efficiency of conventional copper wire motors. Major motor applications include pumps, fans, and compressors as well as handling and processing manufactured materials. According to the Department of Energy, this energy accounts for 70 percent of all the energy consumed by the manufacturing sector and over 55 percent of the total electric energy generated in the United States.

Conductus Inc. fabricates high-performance radio-frequency (RF) filters and filter subsystems based on HTS technology for the telecommunications market. The ClearSite® line of front-end receiver subsystems for cellular and PCS base stations manufactured by Conductus contain microwave filters with as many as 19 poles made from thin-film HTS superconductors. See Fig. 3.64. Conventional filters are significantly larger than HTS filters, more inefficient, and can support no more than 9 poles, all of which limits their filtering capability. Conductus products are based primarily on YBaCuO thin films synthesized through sputtering, pulsed laser deposition, and coevaporation.

IGC–Advanced Superconductors manufactures superconductive wire, cable, and tape for MRI diagnostic systems, high-energy physics, and fusion power research. Products are based on NbTi, Nb_3Sn, BSCCO (Bi-Sr-Ca-Cu-O) 2212/Ag, and BSCCO 2223/Ag multifilament wire and tape.

Superconductor Technologies Inc. (STI) manufactures SuperFilter® Systems based on thin-film superconductor receiver filter systems for use in wireless base stations.

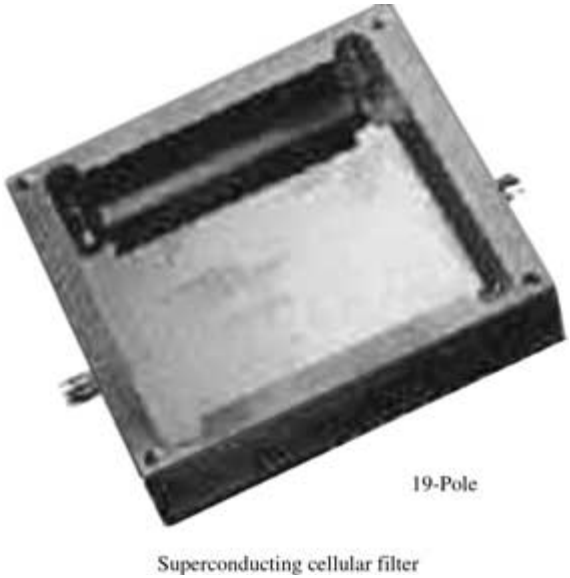

FIGURE 3.64 Conductus Inc. 19-pole superconducting cellular filter.[11]

3.8 MAGNETIC CERAMICS

Magnetic ceramics are an important category of electronic materials. They are used extensively as inductor and transformer cores, recording devices, bubble memory cores, permanent magnets, microwave circulators, isolators, and phase shifters. Magnetic ceramics differ from magnetic metals in that they are oxides having lower magnetic moments, high resistivities, and a greater dependency of properties on microstructure; some types of magnetic ceramics, ferro- and ferrimagnetic materials, exhibit remnant induction behavior. Magnetite (Fe_3O_4) is a naturally occurring magnetic material (lodestone) that was used in primitive magnets thousands of years ago. Magnetite belongs to the spinel family of minerals, having the general formulation MFe_2O_4, where M is typically a transition metal ion. Other important crystal structures in magnetic ceramics are iron garnets, $M_3Fe_5O_{12}$, and magnetoplumbite, $MFe_{12}O_{19}$.

Investigations into the magnetic properties of various spinels began in the early 1900s (Hilpert). Throughout the 1930s, '40s, and '50s there was increasing interest in developing ferrite materials as magnetic cores. These investigations led to the discovery of ferromagnetism by Neel in 1948, permanent magnet hexaferrites in 1951 by Went, and ferromagnetic behavior in other structures such as orthoferrites and garnets. Magnetic garnets were discovered in the mid-1950s by Bertaut and Forrat. Volume production of Cu-Zn ferrite materials for magnetic core applications began in the 1930s. Applications for ferrite ceramics has expanded with the rapid growth of the electronics industry to include inductors, transformers, permanent magnets, magnetooptical devices, electromechanical devices, and microwave electronics devices.

A magnetic moment results from current loops. In a magnetic material this can result from electrons orbiting atomic nuclei, electrons spinning on their own axis, and nuclei contributions. Nuclear magnetic moments are very small and typically ignored. The magnetic

moment contributions from electron orbit and spin can be calculated by considering the magnetic moment μ created by a moving charged particle:

$$\mu = ia = Q\rho/2m \tag{3.57}$$

where i is the current and ρ is the angular momentum for a particle of charge Q and mass m circling an area a.

The Bohr theorem states that orbital angular momentum ρ is quantized in units of $h/2\pi$, where h is Plank's constant (6.623×10^{-34} J/s). For an electron circling a nucleus, a magnetic moment of

$$\mu = -eh/4\mu m_e \tag{3.58}$$

is produced.

The magnitude of magnetic moment for an orbiting electron is a Bohr magneton,

$$\mu_B = \frac{eh}{4\pi m_e} = \frac{(1.602\times10^{-19}\text{C})(6.623\times10^{-34}\text{ J/s})}{4\pi(9.109\times10^{-31}\text{ kg})}$$

$$= 9.274\times10^{-24}\text{ A}\cdot\text{m}^2/\text{electron}\ (9.274\times10^{-21}\text{ erg/Oe})$$

In addition to orbital magnetic moment, there is a component of magnetic moment due to electrons spinning on their own axes. In an unmagnetized state, the electrons spin moments are randomly oriented so that no net moment results. As an external magnetic field is applied, the magnetic moments begin to orient in the direction of the applied field. The magnitude of the spin moment is nearly exactly equal to 1 Bohr magneton. As a result of the spin angular momentum, $s = \pm 1/2$ (from the Pauli exclusion principle), the electron also has a component of magnetic moment of $2s\mu_B$ in the magnetic field direction.

Electrons are oriented in four types of orbitals, s, p, d, and f, for which the space quantum number ℓ equals 0, 1, 2, and 3, respectively. The orbital quantum number for all the electrons in an ion is equal the sum of the space quantum numbers, $L = \Sigma\ell$. The space quantum number is equal to $-\ell$, $-\ell+1$,$-\ell+2$,$-\ell+3$,$\cdots+\ell$ for the number of electrons in each orbital. The spin quantum number for all the electrons in an ion, S, is equal to Σs. Hund's rules can be used to determine the total magnetic moment for a given atom or ion. Hund's rules state:

1. The number of unpaired spins is a maximum.

2. The L value is the maximum allowed.

3. $J = |L - S|$ when the shell is less than half filled.
$J = |L + S|$ when the shell is more than half filled.
$J = S$ when the shell is half filled.

An electron with an orbital quantum number ℓ possesses a total orbital magnetic moment of $[\ell(\ell+1)]^{1/2}\mu_B$. With an applied magnetic field, the total spin magnetic moment $\mu = 2[s(s+1)]^{1/2}\mu_B$. The total angular momentum of the electrons in an ion is

$$\rho = [J(J+1)]^{1/2}h \tag{3.59}$$

and the total magnetic moment for the ion is

$$\mu = e\rho/2m_e = 2[J(J+1)]^{1/2}\mu_B \tag{3.60}$$

This relationship can be used to calculate the magnetic moments of various ions in a solid.

In most ferrites, the electronic interaction in bonding is such that there is little electron orbital momentum (orbital quenching). The main contribution to magnetic moment is from electron spins, which are free to orient with an applied field. Pauli exclusion principles allow only two electrons to occupy an energy level. These electrons will have opposite spins, which cancel their magnetic moments ($s = +1/2$, $s = -1/2$). Permanent magnetic moments are found in solids containing ions with unpaired electrons, such as those containing conduction band electrons; an odd number of electrons; or transition, rare-earth, or actinide elements (because of their incompletely filled inner shells). The bulk magnetization M can be calculated by the formula:

$$M = n\mu_B N_0 d / A \tag{3.61}$$

where n = number of unpaired electron spins/atom
N_0 = Avagadro's number (6.023×10^{23} atoms/mole)
d = density
A = atomic weight

Experimental data, in general, closely match the magnetization calculated by determining the number of unpaired spins per formula unit.

Diamagnetic materials have electronic interactions that produce a net zero magnetic moment. If a magnetic field is applied to these materials, a small magnetic moment is induced, which orients opposite to the applied field. These materials, which have closed electron shells, have negative susceptibilities, on the order of 10^{-5} to 10^{-6}. Diamagnetic materials include most ceramics and metals with closed electron shells, organics, and inert gases.

Materials containing ions with odd numbers of electrons, such as those from the rare earth and transition series, possess a net magnetic moment. In the absence of an applied magnetic field, the orientation of these moments is random with no mutual interaction, resulting in a net zero magnetism. If a magnetic field is applied, the individual moments tend to align their polarity with the field, creating a net magnetism. Paramagnetic materials have a permanent magnetic moment with a positive but small susceptibility (10^{-3} to 10^{-6}). Thermal energy opposes this effect.

Ferromagnetic materials have large magnetization due to strong magnetic dipole interaction, spontaneously aligning without an applied field in small volumes of material. The magnetic dipole interaction is a result of electron exchange between O^{2-} ions and neighboring Fe^{3+} ions. These small volumes of material with aligned dipoles (Weiss domains) tend to randomly orient to the lowest energy state in the absence of an applied field. The result is a material without a net magnetic moment on a macroscopic level. Under applied field, those domains oriented in the direction of the applied field grow at the expense of oppositely oriented or perpendicular domains. The spontaneous magnetization is typically several orders of magnitude greater than the applied field, resulting in very high permeability.

Antiferroelectric materials have an exchange interaction between unpaired electrons that results in antiparallel alignment of electron spins. The magnetic moments of ions in adjacent planes are equal in magnitude, aligned, but in opposite polarity; therefore, the result is no net magnetization. A few materials such as FeO, MnO, NiO, and CoO exhibit this behavior.

It is more common for materials to exhibit antiparallel alignment between two sublattices. These different sublattices have unequal numbers of antiparallel moments, resulting in a net magnetic moment for the crystal. These ferrimagnetic materials (ferrites) are the most broadly used magnetic material group. Both ferromagnetic and ferrimagnetic materials possess Weiss domain regions where there is a strong mutual interaction between magnetic moments and spontaneous magnetization occurs. However, the net

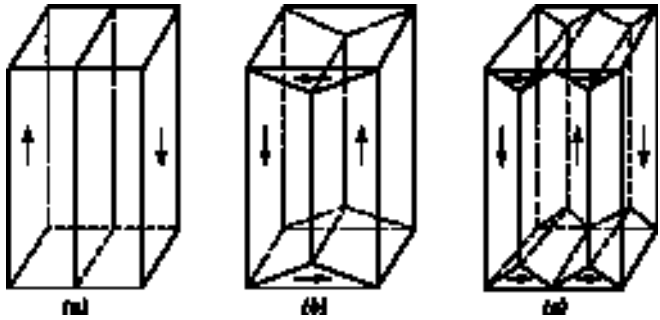

FIGURE 3.65 Several domain structures of a solid, each having a zero net magnetization but progressively lower energy.[20]

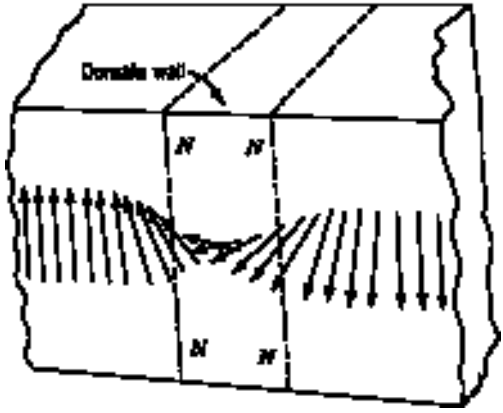

FIGURE 3.66 Change in magnetic moment through a domain wall.[20]

magnetization for the bulk material is zero because of random orientation of the magnetization vectors between domains. This spontaneous magnetization occurs along specific crystallographic directions which minimize the free energy of the material. Figure 3.65 shows how the successive breakup of magnetic domains keeps the magnetic flux within the material and lowers the energy level of the material. The boundary between adjacent domains has a finite width (approximately 1 μm) and consists of a gradual change in magnetic moment from one orientation to the other, which minimizes the boundary energy. See Fig. 3.66.

Figure 3.67 shows the behavior of a ferro- or ferrimagnetic material as the magnetic field is applied. The magnetic moments begin to align with the field; domain boundaries move so that domains aligned with the field grow at the expense of others. This alignment results in increased magnetization as higher fields are applied. The ratio of the change in magnetic induction with applied field is the magnetic permeability; that is,

$$\mu = \Delta B/\Delta H \tag{3.62}$$

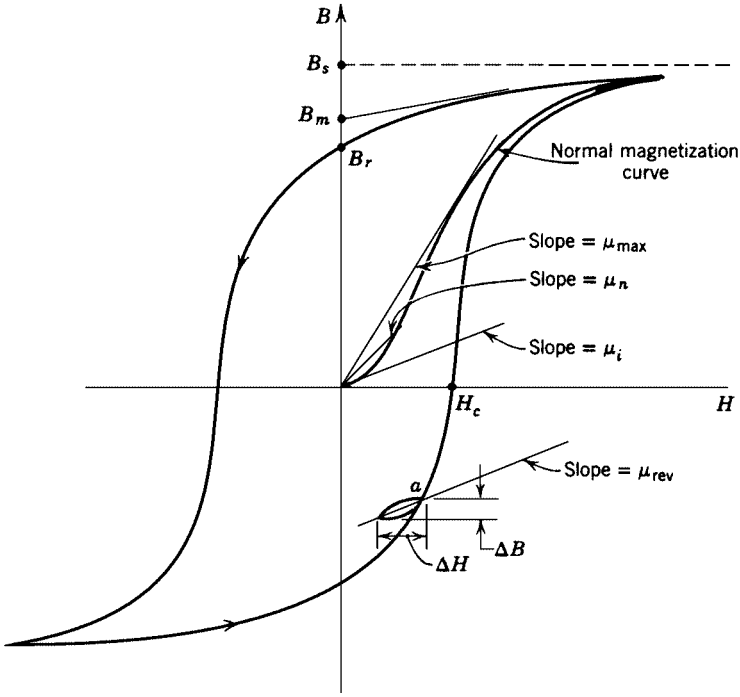

FIGURE 3.67 Magnetic induction versus magnetic field for a ferrite.[20]

At high fields, the magnetization saturates (magnetization = B_s) as nearly all the material aligns with the field. If the field is removed, a significant portion of the domain alignment remains, creating a remnant magnetization (induction), B_r. If a reversed field is applied, the remnant induction is reduced. The field required to completely reverse the induced magnetization is the coercive field H_c. If a large enough reverse field is applied, the domains will align in the opposite direction and ultimately saturate with reverse polarity. This cyclical behavior (hysteresis) is characteristic of ferro-/ferrimagnetic materials. The nonreversible *B-H* behavior represents an energy loss, in the form of heat, as a result of moving domain boundaries.

An applied magnetic field on a ferromagnetic material causes alignment of the magnetization vectors in the direction of the field. The magnetization M is the magnetic moment per unit volume and has units of teslas (Wb/m^2). Analogous to dielectric relationships, the relative permeability μ_r can be defined as μ'/μ_0. The magnetic susceptibility X_m is defined as the amount of magnetization for an applied magnetic field,

$$X_m = M/H = \mu_r - 1 \tag{3.63}$$

Ferro- and ferrimagnetic materials obey the Curie-Weiss law; that is, magnetization drops as temperature increases because of the randomization of magnetic moments caused by the increased thermal energy. At the Curie temperature, spontaneous magnetization goes

to zero and the material becomes paramagnetic:

$$\frac{1}{X} = \frac{1}{C(T - T_C)} \tag{3.64}$$

where C is the Curie-Weiss constant and T_C is the Curie temperature.

The resultant magnetic induction (or magnetic flux density) B as a result of a current loop on a nonmagnetic material is $B = \mu_0 nI$, where μ_0 is the magnetic permeability of vacuum, $4\pi \times 10^{-7}$ H/m (1 G/Oe); n is the number of turns; and I is the current. If a coil is wound on magnetic material, amperian currents (I_a) result from electron orbits and spin; this results in an additional contribution to the magnetic induction. The total magnetic induction (magnetic flux density) on a magnetic material is the sum of the magnetization and the external magnetic field:

$$B = \mu_0 nI + \mu_0 I_a = \mu_0 (H + M) = \mu_0 (H + X_m H) = \mu_0 \mu_r H = \mu' H \tag{3.65}$$

where μ is the permeability of the material.

When an external field is applied to a ferrite shape, the material aligns to oppose the applied field and magnetic poles are formed at the surfaces. The shape of the ferrite determines the magnitude of the field within the material. This internal field, H_i, is related to the applied field H_a and the demagnetizing field H_D by

$$H_i = H_a - H_D = H_a - N_D M \tag{3.66}$$

where N_D is the demagnetizing factor, dependent on the device shape, and M is the magnetization. If a uniform sphere of material is assumed, N_D is equal to $^1/_3$ and the magnetic induction and will equal 4π, then

$$B = H + 4\pi M \tag{3.67}$$

Typically, the total induction is expressed with the field subtracted out to equal $4\pi M_s$. In materials where saturation can be reached at relatively low fields, the saturation induction is equal to $4\pi M_s$. Therefore, the total magnetic induction in a material is given by:

$$B = H + 4\pi M_s \tag{3.68}$$

In soft ferrites, the peak induction approaches the $4\pi M_s$ value. Ferrites have lower saturation magnetization and higher resistivities than magnetic metals, primarily because of the amount of large, nonmagnetic oxygen ions.

The magnetic moments in ferrite materials are a result of electron spins that are not canceled by antiparallel spins on other sublattices. Ions whose inner electron shells are not full have unpaired spins that contribute to the magnetic moment of a ferrite material. The Aufbau chart in Fig. 3.68 shows the order in which electrons fill electron orbitals in an atom or ion. The superscript represents the number of electrons in each orbital. For instance, oxygen has eight electrons and, therefore, has the electronic configuration of $1s^2 2s^2 2p^4$ and the O^{2-} ion has the configuration $1s^2 2s^2 2p^6$. Table 3.22 shows the electron configuration of ions in ferrite materials. Notice the unfilled 3d orbital for the transition metal ions. These unfilled orbitals result in the unpaired electron spins that contribute to the magnetic moment of the material.

TABLE 3.22 Electron Configuration of Ferrite Constituent Ions

Ion	Electrons	Electron configuration	Unpaired electrons
O^{2-}	10	$1s^2 2s^2 2p^6$	0
Fe^{2+} (Fe^{3+})	24 (23)	$1s^2 2s^2 2p^6 3s^2 3p^6 3d^6 (3d^5)$	4 (5)
Mg^{2+}	10	$1s^2 2s^2 2p^6$	0
Al^{3+}	10	$1s^2 2s^2 2p^6$	0
Li^{+}	2	$1s^2$	0
Zn^{2+}	28	$1s^2 2s^2 2p^6 3s^2 3p^6 3d^{10}$	0
Cd^{2+}	46	$1s^2 2s^2 2p^6 3s^2 3p^6 4s^2 4p^6 4d^{10}$	0
Mn^{2+} (Mn^{3+}) (Mn^{4+})	23 (22) (21)	$1s^2 2s^2 2p^6 3s^2 3p^6 3d^5 (3d^4)$ $(3d^3)$	5 (4) (3)
Cr^{2+} (Cr^{3+})	22 (21)	$1s^2 2s^2 2p^6 3s^2 3p^6 3d^4$ $(3d^3)$	4 (3)
Co^{2+} (Co^{3+})	25 (24)	$1s^2 2s^2 2p^6 3s^2 3p^6 3d^7$ $(3d^6)$	3 (4)
Ni^{2+}	26	$1s^2 2s^2 2p^6 3s^2 3p^6 3d^8$	2
Cu^{+} (Cu^{2+})	28 (27)	$1s^2 2s^2 2p^6 3s^2 3p^6 3d^{10} (3d^9)$	0 (1)

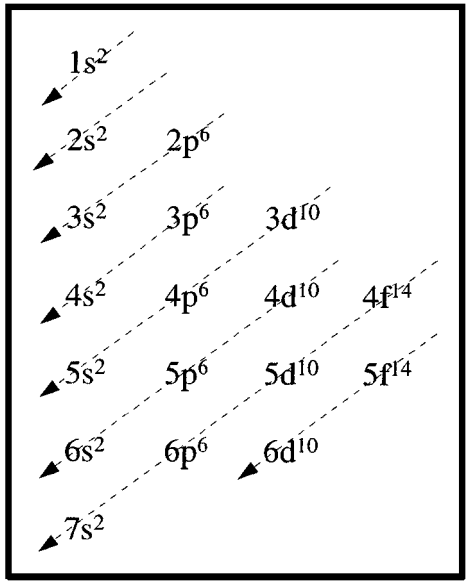

FIGURE 3.68 Aufbau chart showing the order of electron orbital filling.

3.8.1 Spinels

Spinels have the general chemical formula, MFe_2O_4, where M is typically a metal ion such as Li^{+}, Mg^{2+}, Mn^{3+}, Cr^{3+}, Co^{3+}, Al^{3+}, Ga^{3+}, Ni^{2+}, Zn^{2+}, or Cu^{2+}. The unit cell of the spinel crystal structure is composed of eight formula units, with the oxygen ions forming a cubic close-packed array as shown in Fig. 3.69. The oxygen array contains 64 tetrahedral (A sites) and 32 larger octahedral (B sites) coordinated interstices. Eight of the tetrahedral A sites

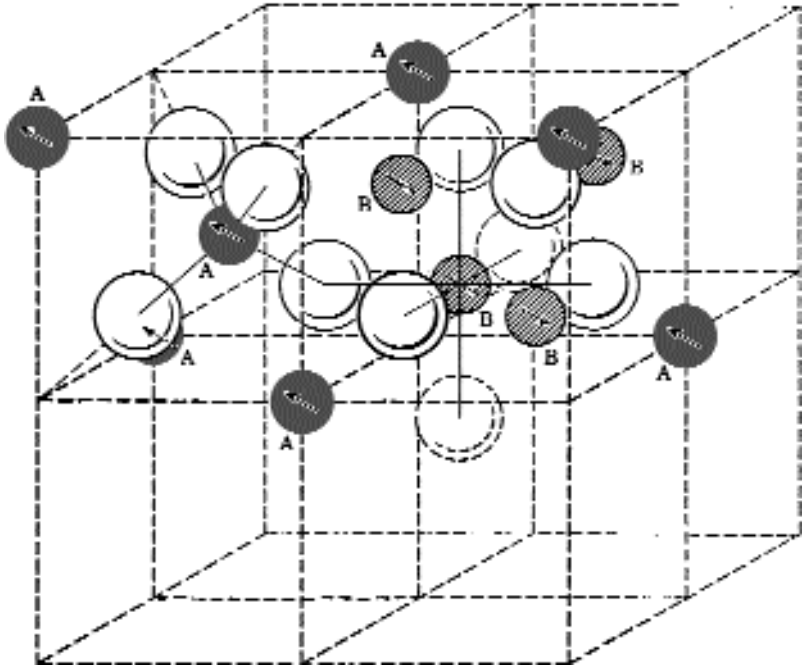

FIGURE 3.69 The crystal structure of spinel, AB_2O_4.[20]

and 16 of the octahedral B sites are filled; that is, 1 tetrahedral and 2 octahedral sites per formula unit are filled. The electronic spins of the ions on the A and B sites, and therefore their magnetic moments, are set up in opposing directions (antiferroelectric). In normal spinel, such as $MgFe_2O_4$, $CdFe_2O_4$, or $ZnFe_2O_4$, divalent ions occupy all 8 of the available A sites and trivalent Fe ions occupy the available B sites, the chemical formula is $(M^{2+}O)Fe^{3+}{}_2O_3$. The tetrahedral site (0.55 to 0.67 Å) is smaller than the octahedral site (0.72 to 0.78 Å) and can more readily accommodate the smaller trivalent ions.

In inverse spinels, such as Fe_3O_4 or $CoFe_2O_4$, all the A sites and half the available B sites are filled with trivalent ions; the remaining 8 B sites are occupied by divalent ions. The chemical formula of Fe^{3+} $(Fe^{3+}$ $M^{2+})$ O_4. The O^{2-} ions have a full $2p$ shell; the 6 electrons pair off with opposing spins, which cannot contribute to a magnetic moment. Each Fe^{3+} ion has 5 unpaired $3d$ shell electrons whose spins are parallel and can contribute to a magnetic moment. In these antiferromagnetic materials, the unpaired electronic spins of the trivalent ions (Fe^{3+}) on A site ions are antiparallel to those on the B site, canceling their magnetic moments. The net moment is a result of the remaining 8 divalent ions on the B site. In $NiFe_2O_4$, the Fe^{3+} ions on the A site align antiparallel to those on the B site and mutually cancel. The net moment is due to the remaining Ni^{2+} ions on the B site.

For a divalent M ion from the transition series with n electrons in the d shell, the magnetic moment for the ferrite is

$$\begin{aligned} \mu_m &= n\mu_B \quad \text{if } n < 6 \\ \mu_m &= (10-n)\mu_B \quad \text{if } n > 5 \end{aligned} \tag{3.69}$$

All of the metal atoms in the A and B sites will orient in the minimum energy configuration. Some ferrite formulations result in structures that are not fully inverse or normal, depending on the metal ion size, heat treatment and atmosphere. If x is the fraction of divalent ions on the B site, then

$$\mu_m(\text{A site}) = (1-x)n\mu_B + x5\mu_B \tag{3.70}$$

$$\mu_m\,(\text{B site}) = (1-x)5\mu_B + 5 + xn\mu_B \tag{3.71}$$

$$\mu_m\,(\text{net}) = \mu_m(\text{A site}) - \mu_m(\text{B site}) \tag{3.72}$$

Manganese ferrite is about 80 percent normal spinel and is not influenced much by heat treatment. Nickel ferrite is about 80 percent inverse and also is not affected by heat treatment. In general, ferrites shift to the normal structure at higher temperatures. Magnesium and copper ferrite are normal spinel at high temperature; if quenched, the normal spinel structure is retained. If slowly cooled, the spinel transforms to the inverse spinel structure.

Lithium ferrite, $Li_{0.5}Fe_{2.5}O_4$, requires an excess of Fe^{3+} ions to maintain charge balance with Li^+. Four of the 16 occupied octahedral sites are filled by Li^+. Gamma ferric oxide, γ-Fe_2O_3, is a special case of the spinel structure containing no divalent ions. For charge balance, only two-thirds of the normally occupied octahedral sites are filled with Fe^{3+}. This leads to an imbalance in the magnetic spins on the A and B sites, resulting in a net magnetic moment. Table 3.23 shows the magnetic moments for various ferrites calculated in this manor versus measured values. The differences are primarily due to variability in ion location from the prediction, minor contributions from orbital momentum, and spin directions not being perfectly parallel.

The saturation magnetization can be calculated from the magnetic moment, since

$$M_S = \text{magnetic moment/unit volume}$$

where unit volume is the unit cell volume.

Table 3.24 shows the range of properties for ferrite materials.

Zinc substitutions for magnetic divalent ions can be used to raise the magnetic moment of the material. Zn^{2+} ions enter the tetrahedral A sites with no magnetic moment to orient antiparallel to the B site moments. The result is a larger uncanceled moment from the B site that contributes to the net magnetic moment. Figure 3.70 shows the measured effect of Zn additions to various ferrite.

Since Fe^{3+} and Mn^{2+} have the highest magnetic contribution of any ion, $5\mu_B$, they have the highest potential contribution to the magnetization of a ferrite. Materials for

TABLE 3.23 Measured versus Calculated Values for Magnetic Moments of Ferrites

	Density, g/cm^3	T_C, °C	μ_m	M_s	B_s
$FeFe_2O_4$	5.24	585	4	480	6000
$ZnFe_2O_4$	5.33	N/A	0		
$MgFe_2O_4$	4.52	440	0	110	1500
$NiFe_2O_4$	5.38	585	2	270	3400
$CuFe_2O_4$	5.42	455	1	135	1700
$Li_{0.5}Fe_{2.5}O_4$	4.75	670	2.5	310	3900
$MnFe_2O_4$	5.00		5	400	6000
$CoFe_2O_4$	5.29	520	3	425	5300

TABLE 3.24 Properties of Commercially Available Mircowave Ferrites (Measurements Made at X Band)

Major composition	Saturation magnetization $4\pi M_s$, G	Curie temperature T_C, K	Resonance line width ΔH, Oe	Lande g factor	Coercive force H_c, Oe	Dielectric constant ε	Dielectric loss factor tan δ_ε	Dielectric density, g/cm^3
Y	1800	575	60					
Y	1780	555	45	2.00			<0.00025	5.06
Y	1780	555	55	2.01	0.75	16.0	<0.00025	
Y	1750	555	60	2.0		15	0.0005	
Y	1750	555	35	2.01		16.3		5.08
Y	1750	550	50			16.2	0.0005	
Y	1740	550	60	2.0				5.1
YGd	1600	540	60	2.0	1.1	16.0	<0.00025	
YAl	1540	550	50			14.8	0.0005	
YGd	1520	555	55	2.01			<0.00025	5.26
YAl	1470	525	40	2.01			<0.00025	5.04
YGd	1300	555	70	2.03			<0.00025	5.42
YAl	1220	515	55			14.6	0.0005	
YGd	1220	525	100	2.0		15	0.0005	
YGd	1200	555	85	2.00	0.75	15	<0.00025	
YAl	1200	535	60	1.99	0.5	15.5	<0.00025	
YGdAl	1200	525	55			14.8	0.0005	
YAl	1150	500	60	2.0				5.0
YAl	1120	485	40	2.01			<0.00025	5.03
YGd	1000	555	130	2.05			<0.00025	5.68
YGd	1000	555	120	2.00	0.8	15.5	<0.00025	
YAl	1000	525	60	1.99	1.2	15.0	<0.00025	
YAl	990	485	55			14.4	0.0005	
YAl	850	455	40	2.01			<0.00025	5.00
YGd	850	555	160	2.00	1.0	15.5	<0.00025	
YGd	840	525	200	2.0		15	0.0005	
YAl	800	505	65	2.00	1.2	15.0	<0.00025	
YGdAl	800	525	110			15.0	0.0005	

(*Continued*)

TABLE 3.24 Properties of Commercially Available Mircowave Ferrites (Measurements Made at X Band) (Continued)

Major composition	Saturation magnetization $4\pi M_s$, G	Curie temperature T_C, K	Resonance line width ΔH, Oe	Lande g factor	Coercive force H_c, Oe	Dielectric constant ε	Dielectric loss factor tan δ_ε	Dielectric density, g/cm^3
YGdAl	750	525	80			15.0	0.0005	
YGd	750	555	200	2.08			<0.00025	5.85
YGd	725	555	220	2.03	1.0	15.5	<0.0005	
YAl	680	475	70	2.00	1.2	15.0	<0.00025	
YAl	680	455	45	2.00	1.0	14.5	<0.00025	
YGdAl	675	475	120	2.0				5.1
YGdAl	660	525	210	2.05			<0.00025	5.73
YAl	650	445	40	2.02			<0.00025	5.00
YAl	600	430	60	2.0		15	0.0005	
YAl	600	445	40			14.3	0.0005	
YAl	550	435	75	2.00	1.2	14.0	<0.00025	
YAl	475	430	50			14.0	0.0004	
YAl	400	405	45	2.01	1.0	14.0	<0.00025	
YAl	400	405	45			13.8	0.0005	
YAl	370	400	40			14.0	0.0005	
YGdAl	340	475	310	2.10			<0.00025	5.63
YAl	300	400	40	2.02	0.4	14.0	<0.00025	
YAl	290	390	40			13.4	0.0005	
YAl	240	370	40	2.03	1.0	14.0	<0.00025	
YAl	225	380	35			13.8	0.0004	

Nickel ferrites								
NiZn	5000	650	135	2.08	0.9	12.5	0.001	
Ni	3000	850	350	2.3				5.1
NiCo	3000	860	350	2.21	12	13.0	0.0025	
NiCo	3000	865	200	2.2		13	0.0005	
Ni	3000	865	500	2.3		12	0.0005	
NiCoAl	2440	826	260	2.33			<0.0005	5.05
NiTiAl	2200	825	500	2.45		12.0	0.002	4.80
NiAl	2000	835	450	2.31	4	12.8	0.001	
NiCoAl	1800	820	1000	2.55	36	9.0	0.0015	
NiCoAl	1800	775	800	2.55	21	9.5	0.002	
NiAl	1600	755	450	2.53		11.3	0.0003	
NiCoAl	1600	725	330	2.45	6.5	12.0	0.001	
Ni	1500	850	800	2.42		9.4	0.0017	
NiAl	1450	715	275	2.5				4.7
NiAl	1450	715	300	2.5				4.7
NiCoAl	1400	700	200	2.38	14	12.5	0.001	
NiCoAl	1240	699	360	2.57			<0.0005	5.04
NiAl	1000	675	300	2.7	7	12.0	0.001	
NiCoAl	800	642	600	2.94			<0.0005	4.97
NiAl	500	435	155	1.54	5.5	9.0	0.005	
NiAl	420	430	225	1.4				4.8
NiAl	350	555	225	1.46		8.2	0.0003	4.8

(Continued)

TABLE 3.24 Properties of Commercially Available Mircowave Ferrites (Measurements Made at X Band) (Continued)

Major composition	Saturation magnetization $4\pi M_s$, G	Curie temperature T_C, K	Resonance line width ΔH, Oe	Lande g factor	Coercive force H_c, Oe	Dielectric constant ε	Dielectric loss factor tan δ_ε	Dielectric density, g/cm^3
				Magnesium ferrites				
MgMn	2220	585	500	2.07			<0.00025	4.20
MgMn	2150	595	540	2.10	2.5	13.0	<0.00025	
MgMn	2100	575	425	2.0		12	0.0005	
MgMn	2000	555	350	2.0				4.3
MgMn	2000	575	400	2.07		12	0.0008	4.3
MgMn	1950	515	150	2.0				4.3
MgMn	1780	595	380	2.06	1.4	12	0.0005	4.15
MgMnAl	1760	565	490	2.11	2.1	12	0.0005	4.10
MgMnAl	1700	500	225	2.00	1.0	12.0	<0.00025	
MgMn	1650	575	650	2.0				4.3
MgMnAl	1550	515	375	2.0				4.3
MgMnAl	1250	439	155	2.00	0.4	11.5	<0.00025	
MgMnAl	1250	475	300	2.0				4.2
MgMnAl	1140	425	165	2.02				4.10
MgMnAl	1110	415	220	2.04	0.8	12	0.0003	3.95
MgMnAl	730	375	120	2.00	0.7	12	0.0004	3.90
MgMnAl	680	375	120	2.02	1.2	11.5	<0.00025	

Source: *Handbook of Microwave Ferrite Materials*, W. H. von Aulock, ed. Academic Press, Orlando, 1965, pp. xviii–xxi. Copyright: Academic Press, Orlando, Florida.

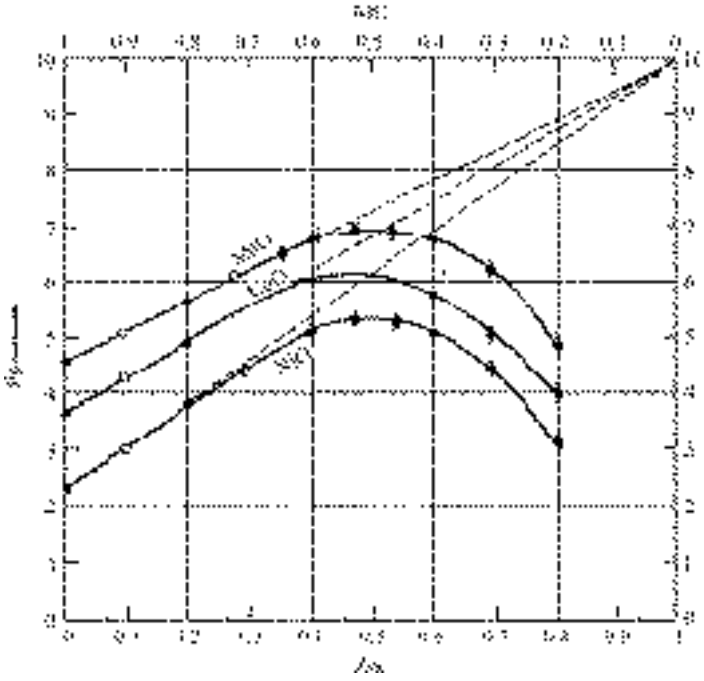

FIGURE 3.70 Effect of zinc substitutions on magnetic moments of various ferrites.[15]

applications where the highest magnetic moments are needed typically contain Mn^{2+} or uncompensated Fe^{3+} additions. The magnetostriction coefficient for ferrous ferrite is positive; therefore, addition of Fe^{3+} ions also reduces the magnitude of electrostriction in most ferrites. Replacing some of the Mn^{2+} ions in $MnFe_2O_3$ with Fe^{3+} ions has the effect of reducing the magnetic anisotropy to zero, raises the permeability, and decreases the resistivity. Additions of Co in most ferrites has the effect of making anisotropy more positive. Co is also added to improve power handling in ferrites.

Zn substitution in Mn and Ni ferrites increases the magnetic moments but also reduces the Curie temperatures, resulting in lower saturation induction values. Zinc addition also lowers magnetostriction and magnetocrystalline anisotropy. Figure 3.71 shows the effect of Zn additions on anisotropy for commercial ferrites. Most commercial ferrites are solid solutions of different ferrites (mixed ferrites) to optimize the properties for a particular application. $NiFe_2O_4$ and $MgFe_2O_4$ have lower magnetic moments, but have higher resistivities, which are well suited for high-frequency applications.

The size and orientation of the magnetic domains depend on minimization of magnetostatic, magnetocrystalline anisotropy, magnetostrictive, and domain wall energies.

When a magnetic field is applied to a ferrite material, the magnetic domains align with the field. This alignment causes a lattice distortion, called *magnetostriction*, that is generally in the direction of the applied field. Conversely, when a mechanical stress is applied to a magnetic material, the magnetic domains align parallel or perpendicular to the direction of the stress. The magnetostrictive energy is given by

$$E_m = 3/2\lambda\sigma \tag{3.73}$$

TABLE 3.25 Direction Cosines and Anisotropy Energies for Magnetization Directions in Cubic Spinel

Direction	$\alpha_1(x)$	$\alpha_2(y)$	$\alpha_3(z)$	E_k
(100)	1	0	0	0
(110)	$1/\sqrt{2}$	$1/\sqrt{2}$	0	$1/4K_1$
(111)	$1/\sqrt{3}$	$1/\sqrt{3}$	$1/\sqrt{3}$	$K_1/3 + K_2/27$

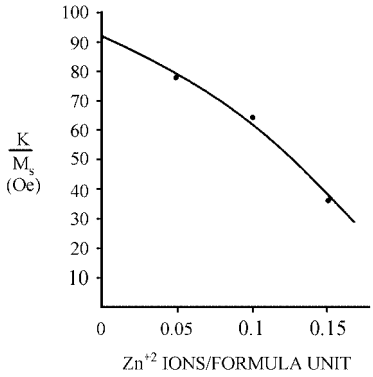

FIGURE 3.71 Anisotropy versus zinc concentration in 400-G $4\pi Ms$ lithium titanium ferrites.[25]

where λ is the magnetostrictive constant and σ is the applied stress. Most device manufacturing involves machining of the fired material to some extent. The stresses from the machining operation will have some effect on the domain alignment.

Typically, the magnetic domains will align along one of the main crystallographic directions to reduce free energy; this is called the *easy direction* of magnetization. To achieve alignment along other directions requires more energy. The energy required to shift the direction of magnetization from the easy direction to another is the magnetocrystalline anisotropy energy. The magnetostrictive anisotropy energy is given by

$$E_k = K_1(\alpha_1^2\,\alpha_2^2 + \alpha_2^2\,\alpha_3^2 + \alpha_3^2\,\alpha_1^2) + K_2(\alpha_1^2\,\alpha_2^2\,\alpha_3^2 + \cdots) \tag{3.74}$$

where the α's are the direction cosines. The direction cosines and anisotropy energies for other magnetization directions for cubic materials such as spinels are shown in Table 3.25. When K_1 is positive, the (100) direction will be the easy direction of lowest energy. If K_1 is negative, which is most common in ferrites, the 111 direction will be the preferred direction of magnetization.

The magnetostatic energy is a measure of the work needed for magnetic poles in the material; it is highly dependant on the geometry. Geometries that have longer flux paths outside the magnetic material have higher magnetostatic energies. The magnetostatic energy is given by

$$E_p = \text{constant} \times dM_s^2 \tag{3.75}$$

where d is the domain width. This energy can be minimized by the formation of 180° domains, which reduce the magnetic flux path and decrease the domain width.

The domain wall energy is given by:

$$E_d = 2(K_a T_C / a)^{1/2} \tag{3.76}$$

where a = interatomic spacing
K_a = magnetocrystalline anisotropy constant
T_C = Curie temperature

Lower Curie temperatures and greater atomic spacing (greater domain wall width) reduces the domain wall energy.

In alternating currents, the complex permeability μ^* can be defined as

$$\mu^* = \mu' + j\mu''$$

where μ' represents the real part indicating energy stored and μ'' represents the imaginary part. The ratio $\mu''/\mu' = \tan \delta$ represents the energy dissipated from the result of hysteresis and eddy current losses.

3.8.2 Garnets

Garnets have the general structure $M_3Fe_5O_{12}$, $(3M_2O_3)(2Fe_2O_3)(3Fe_2O_3)$, where M is a trivalent rare-earth or yttrium ion. The crystal structure is cubic, containing 8 formula units per unit cell. Figure 3.72 shows the garnet crystal structure. The oxygen array forms 24 tetrahedral (D site), 16 octahedral (A site), and 16 dodecahedral (C site) coordination

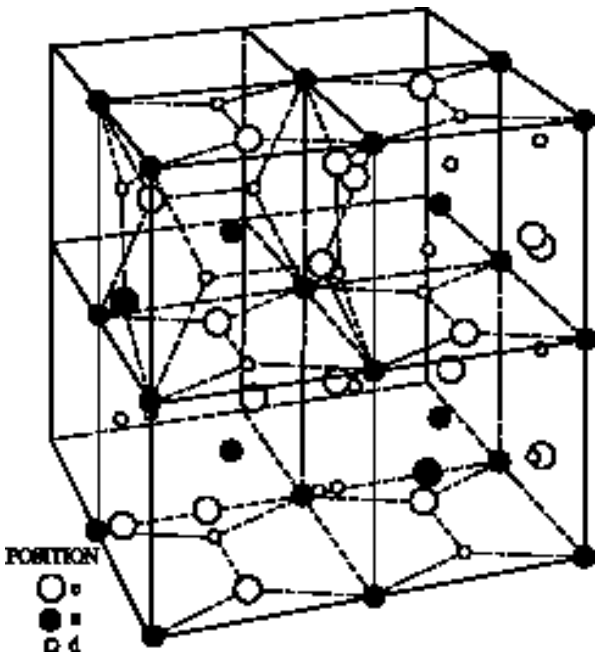

FIGURE 3.72 Unit cell of a rare-earth garnet.[15]

interstices per unit cell. The Fe^{3+} ions occupying the tetrahedral are aligned antiparallel to the A and C sites. The net magnetic moment per unit cell is given by

$$\mu_m(\text{net}) = \mu_m(\text{A site}) + \mu_m(\text{C site}) - \mu_m(\text{D site}) \tag{3.77}$$

The rare earth ions are large and, therefore, occupy the large dodecahedral sites. Since there are three D site Fe^{3+} for each two A site Fe^{3+} and three C site M^{3+} ions and the moment for each Fe^{3+} ion is 5 μ_B, the equation shortens to

$$\mu_m(\text{net}) = 2\mu_m(2\text{Fe}_\text{A}^{3+}) + 3\mu_m(2\text{M}_\text{C}^{3+}) - 3\mu_m(2\text{Fe}_\text{D}^{3+}) = 3\mu_m(2\text{M}_\text{C}^{3+}) - 10\mu_B \tag{3.78}$$

The Y^{3+} ion has no magnetic moment since it has no unpaired spins (i.e., $4s^2 4p^6$), so the magnetic moment is due to the Fe^{3+} ions only. The rare-earth ions have unpaired 4*f* electrons that contribute to the magnetic moment. However, estimating the magnetic moment for garnets in this manner has some error because of an electron spin-orbital coupling. This is due to the 4*f* orbital surrounding full 5*s*, 5*p*, and 5*d* orbitals.

Substitutions are sometimes made for the Fe^{3+} ions to modify the properties of a garnet. Smaller ions, such as Al^{3+}, will occupy the smaller tetrahedral sites. This decreases the moment of the tetrahedral site and, therefore, the net moment of the garnet. Larger ions, such as In^{3+} and Sc^{3+}, occupy the larger octahedral sites. Again these substitutions will decrease the moment for the site; however, the difference in the moment between the octahedral and tetrahedral sites is greater. These substitutions result in a higher net moment for the crystal.

3.8.3 Perovskites

The general formula for perovskite ferrites is $MFeO_3$, where M is a rare-earth or Y^{3+}, La^{3+}, Ca^{2+}, Sr^{2+}, or Ba^{2+} ion. The crystal structure is orthorhombic with face-centered oxygen ions thus the name *orthoferrites*. See Fig. 3.73. The A and B site moments are aligned antiparallel; however, there is a slight canting leading to a small net magnetic moment.

3.8.4 Hexagonal Ferrites

Hexagonal ferrites have the general formula $MFe_{12}O_{19}$ where M is Ba^{2+}, Sr^{2+}, or Pb^{2+}. The crystal structure shown in Fig. 3.74, magnetoplumbite, consists of a hexagonal close-packed array of oxygen ions with 2 formula units per unit cell. The oxygen layers contain

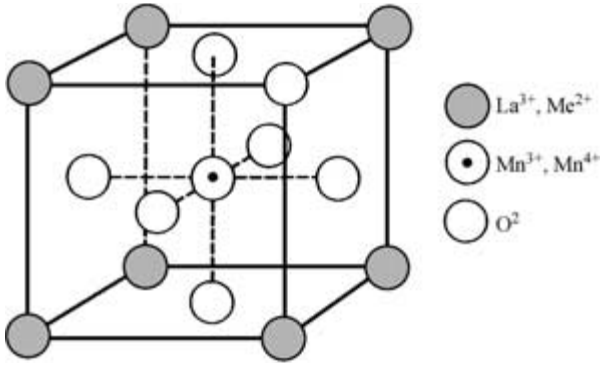

FIGURE 3.73 Unit cell of perovskite orthoferrite.[15]

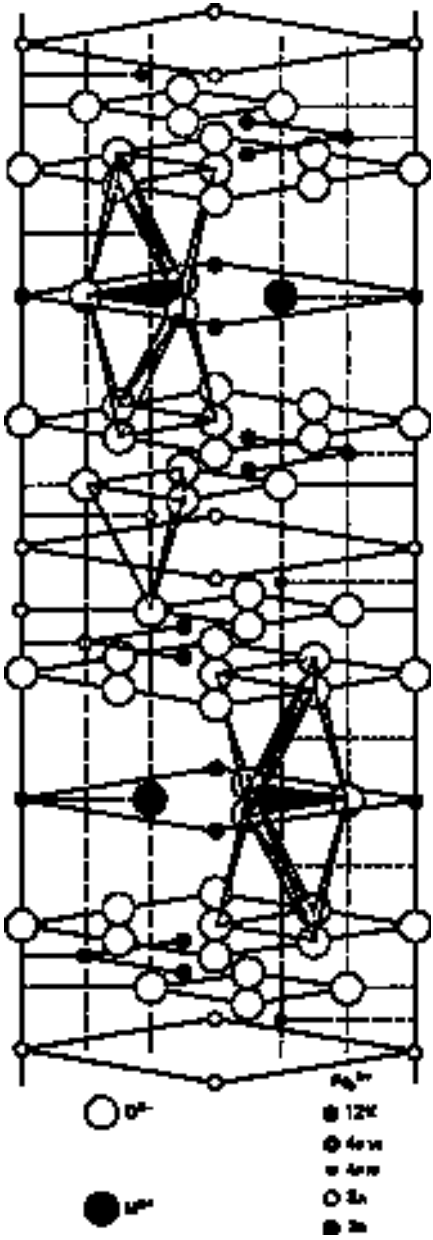

FIGURE 3.74 Unit cell structure of magnetoplumbite (hexagonal) ferrite, $M^{2+}Fe_{12}O_{19}$.[8]

the M^{2+} ions, which can substitute for oxygen sites. The unit cell consists of 10 O^{2-} layers with M^{2+} replacing O^{2-} on every fifth layer. Two layers contain M^{2+} ions, four layers contain four O^{2-} ions, one layer contains 3 O^{2-} with one M^{2+}, four layers contain all O^{2-} ions, and one layer contains 3 O^{2-} with one M^{2+}. The Fe^{3+} ions occupy 2 tetragonal sites, 9 octahedral sites, and 1 five coordination site. All of the tetragonal sites and 2 of the octahedral sites are aligned antiparallel to the remaining sites. This leaves 4 sites where the moments are not canceled by antiparallel alignment. The net moment is $4 \times 5\mu_B$ (Fe^{3+}).

Hexagonal ferrite is used as a permanent magnet because of its high magnetocrystalline anisotropy and high coercive fields. The easy direction of magnetization is the *c* axis (001).

3.8.5 Applications

Phase shifters are the enabling component for electronically scanned array radars (ESAs). In this application a time delay in an RF signal is achieved by propagating through a magnetized waveguide or in transverse electromagnetic mode (TEM) through conductors embedded in the magnetic material. The degree of phase shift is controlled by varying the current applied to coil loops around the magnetic materials.

Magnetic garnets can be epitaxially grown in thin-film form on nonmagnetic substrates. CTE differences result in a preferred magnetization direction perpendicular to the substrate. Magnetic domains with spins up and spins down form. These domains appear as bubbles in polarized light. These bubble domains provide binary inputs for digital computers (bubble memory).

Magnetic field strength and flux density are measured in terms of gauss or oersteds (1 Oe = 79.7 A/m, 1 G = 10^{-4} Wb/m^2, 1 Wb/m^2 = 1 tesla = 796 emu/cm^3). Permeability is given in terms of H/m or erg/Oe. The elementary unit of magnetic moment, the Bohr magneton, μ_B, is 9.27×10^{-24} A · m^2/electron = 9.27×10^{-21} erg/G.

REFERENCES

1. American Superconductor Corporation. www.nmsupr.com.
2. Argentina, G. M. and P. D. Baba, "Microwave Lithium Ferrites: An Overview," *IEEE Transactions on Microwave Theory and Techniques,* vol. MTT-22, no. 6, June 1974, pp. 652–658.
3. ASM International Handbook Committee, *Ceramics and Glasses,* vol. 4, ASM International, Materials Park, Ohio, 1991.
4. ASM International Handbook Committee. *Packaging,* vol. 1, ASM International, Materials Park, Ohio,1989.
5. AVX Corporation Product Catalog, "Tantalum Capacitors," p. 6.
6. A. S. Bhalla, E. M. Vogel, K. M. Nair (eds.), *Electro0Optics and Nonlinear Optic Materials*. vol. 14. Westerville, Ohio: The American Ceramic Society, 1990.
7. Bailey, Bridger.
8. R. C. Buchanan, *Ceramic Materials for Electronics,* Marcel Dekker, New York, 1986.
9. W. S. Burdic, Underwater Acoustic Systems Analysis, Prentice-Hall, Englewood Cliffs, N.J., 1984.
10. David E. Clark, Wayne R. Tinga, and Joseph R. Laia, Jr., (eds.), *Microwaves: Theory and Application in Materials Processing II,* vol. 36, American Ceramic Society, Westerville, Ohio, 1993.
11. Conductus Inc.
12. Philip E. Garrou and Iwona Turlik, *Multichip Module Technology Handbook,* McGraw-Hill, New York, 1998.

13. Bhaskar B. Ghate and John J. Simmons (eds.), *Magnetic Ceramics,* vol. 47, American Ceramic Society, Westerville, Ohio, 1994.
14. Edward A. Giess, King-Ning Tu, and Donald R. Uhlmann (eds.), *Electronic Packaging Materials Science,* vol. 40, Materials Research Society, Pittsburgh, 1985.
15. A. Goldman, *Modern Ferrite Technology,* Van Nostrand Reinhold, New York, 1990.
16. A. Halliyal, U. Kumar, R. E. Newnham, and L. E. Cross, "Dielectric and Ferroelectric Properties of Ceramics in the Pb(Zn1/3Nb2/3)O3-BaTiO3-PbTiO3 System," *J. Am. Ceram. Soc,* vol. 70, 1987, pp. 119–124.
17. Charles A. Harper (ed.), *Electronic Packaging and Interconnection Handbook,* 2d ed., McGraw-Hill, New York, 1997.
18. Charles A. Harper, Ronald N. Sampson (eds.), *Electronic Materials and Processes Handbook,* 2d ed., McGraw-Hill, New York, 1994.
19. Bernard Jaffe, William R. Cook, Jr., and Hans Jaffe, *Piezoelectric Ceramics,* Academic Press, New York, 1971.
20. W. D. Kingery, H. K. Bowen, and D. R. Uhlmann, *Introduction to Ceramics,* 2d ed., John Wiley & Sons, New York, 1976.
21. Lionel M. Levinson (ed.), *Electronic Ceramics: Properties, Devices and Applications,* Marcel Decker, New York, 1988.
22. Hung C. Ling and Man F. Yan (eds.), *Ceramic Dielectrics: Composition, Processing and Properties,* vol. 8, American Ceramic Society, Westerville, Ohio, 1990.
23. The Materials Information Society, *Ceramics and Glasses,* vol. 4, ASM International, Materials Park, Ohio, 1991.
24. A. J. Moulson and J. M Herbert, *Electroceramics: Materials, Properties, Applications,* Chapman & Hall, New York, 1996.
25. K. M. Nair, U. Balachandran, Y.-M. Chiang, and A. S. Bhalla (eds.), *Superconductivity and Ceramic Superconductors II.* vol. 18, American Ceramic Society, Westerville, Ohio, 1991.
26. K. M. Nair and E. A. Giess (eds.), *Superconductivity and Ceramic Transducers,* vol. 13, American Ceramic Society, Westerville, Ohio, 1991.
27. K. M. Nair, J. P. Guha, and A. Okamoto (eds.), *Dielectric Ceramics: Processing, Properties and Applications,* vol. 32, The American Ceramic Society, Westerville, Ohio, 1993.
28. K. M. Nair, R. Pohanka, and R. C. Buchanan (eds.), *Materials and Processes for MicroElectronic Systems,* vol. 15, American Ceramic Society, Westerville, Ohio, 1990.
29. R. E. Newnham and G. R. Ruschau, "Smart Materials," *Earth and Mineral Sciences,* vol. 60, pp. 27–31, Pennsylvania State University, State College, Pennsylvania.
30. A. P. Ritter, A. E. Bailey, F. Poppe, and J. Galvagni, "Fabrication of Multilayer Ceramic Actuators," *Active Materials and Adaptive Structures,* IOP Publishing Ltd., 1992, pp. 693–696.
31. B. W. Wessels and G. Y. Chin (eds.), *Advances in Electronic Materials.* American Society of Materials, Metals Park, Ohio, 1984.

CHAPTER 4
ADVANCED CERAMICS AND COMPOSITES

Dr. Jerry E. Sergent
Director of Technology
TCA, Inc.

4.1 INTRODUCTION

Ceramics are crystalline in nature, with a dearth of free electrons. They have a high electrical resistivity, are very stable, chemically and thermally, and have a high melting point. They are formed by the bonding of a metal and a nonmetal and may exist as oxides, nitrides, carbides, or silicides. An exception is diamond, which consists of pure carbon subjected to high temperature and pressure. Diamond substrates meet the criteria for ceramics and may be considered as such in this context.

The primary bonding mechanism in ceramics is ionic bonding. An ionic bond is formed by the electrostatic attraction between positive and negative ions. Atoms are most stable when they have eight electrons in the outer shell. Metals have a surplus of electrons in the outer shell, which are loosely bound to the nucleus and readily become free, creating positive ions. Similarly, nonmetals have a deficit of electrons in the outer shell, and readily accept free electrons, creating negative ions. Figure 4.1 illustrates an ionic bond between a magnesium ion with a charge of +2 and an oxygen ion with a charge of −2, forming magnesium oxide (MgO). Ionically bonded materials are crystalline in nature, and have both a high electrical resistance and a high relative dielectric constant. Because of the strong nature of the bond, they have a high melting point and do not readily break down at elevated temperatures. By the same token, they are very stable chemically and are not attacked by ordinary solvents and most acids.

A degree of covalent bonding may also be present, particularly in some of the silicon and carbon-based ceramics. The sharing of electrons in the outer shell forms a covalent bond. A covalent bond is depicted in Fig. 4.2, illustrating the bond between oxygen and hydrogen to form water. A covalent bond is also a very strong bond, and may be present in liquids, solids, or gases.

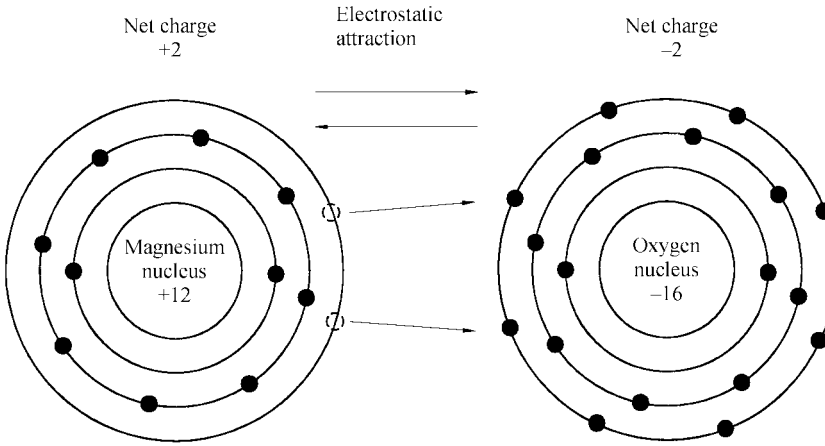

FIGURE 4.1 Magnesium oxide ionic bond.

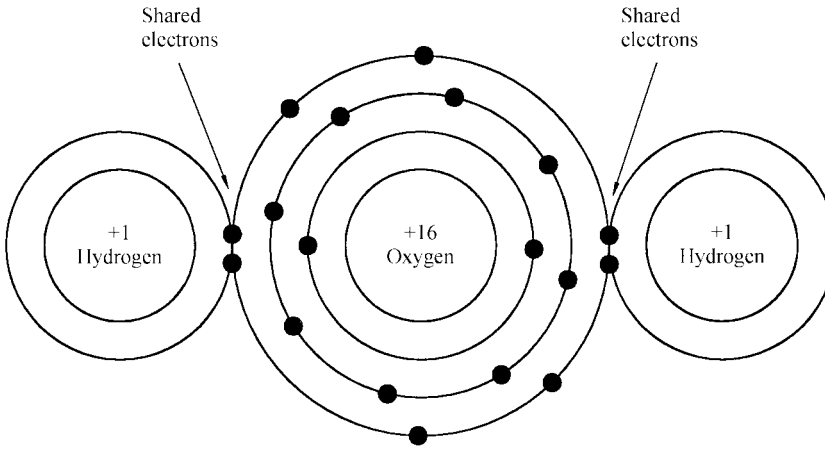

FIGURE 4.2 Covalent bond between oxygen and hydrogen to form water.

4.1.1 Composites

A composite is a mixture of two or more materials that retain their original properties, but, in concert, offer parameters that are superior to either. Composites in various forms have been used for centuries. Ancient peoples, for example, used straw and rocks in bricks to increase their strength. Modern structures use steel rods to reinforce concrete. The resulting composite structure combines the strength of steel with the lower cost and weight of concrete.

Ceramics are commonly used in conjunction with metals to form composites for electronic applications, especially thermal management. Ceramic-metal (cermet) composites typically have a lower temperature coefficient of expansion (TCE) than metals, a higher

thermal conductivity than ceramics, and are more ductile and more resistant to stress than ceramics. These properties combine to make cermet composites ideal for use in high-power applications where heat removal and TCE matching are critical.

This chapter considers the properties of ceramics used in microelectronic applications, including aluminum oxide (alumina, Al_2O_3), beryllium oxide (beryllia, BeO), aluminum nitride (AlN), boron nitride (BN), diamond (C), and silicon carbide (SiC). Several composite materials, aluminum silicon carbide (AlSiC) and Dymalloy®, a diamond/copper structure, are also described. Although the conductive nature of these materials prevents them from being used as a conventional substrate, they have a high thermal conductivity and may be used in applications where their relatively low electrical resistance is not a consideration.

4.2 CERAMIC FABRICATION

It is difficult to manufacture ceramic substrates in the pure form. The melting point of most ceramics is very high, as shown in Table 4.1, and most are also very hard, limiting the ability to machine the ceramics. For these reasons, ceramic substrates are typically mixed with fluxing and binding glasses, which melt at a lower temperature and make the finished product easier to machine.

4.2.1 Manufacturing Process

The manufacturing processes for Al_2O_3, BeO, and AlN substrates are very similar. The base material is ground into a fine powder, several micrometers in diameter, and mixed with various fluxing and binding glasses, including magnesia and calcia, also in the form of powders. An organic binder, along with various plasticizers, is added to the mixture and the resultant slurry is ball-milled to remove agglomerates and to make the composition uniform.

The slurry is formed into a sheet, the so-called green state, by one of several processes, as shown in Fig. 4.3[1], and sintered at an elevated temperature to remove the organics and to form a solid structure. Following are the steps in the process.

Roll compaction. The slurry is sprayed onto a flat surface and partially dried to form a sheet with the consistency of putty. The sheet is fed through a pair of large parallel rollers to form a sheet of uniform thickness.

Tape casting. The slurry is dispensed onto a moving belt that flows under a knife edge to form the sheet. This is a relatively low pressure process compared to the others.

TABLE 4.1 Melting Points of Selected Ceramics

Material	Melting point, °C
SiC	2700
BN	2732
AlN	2232
BeO	2570
Al_2O_3	2000

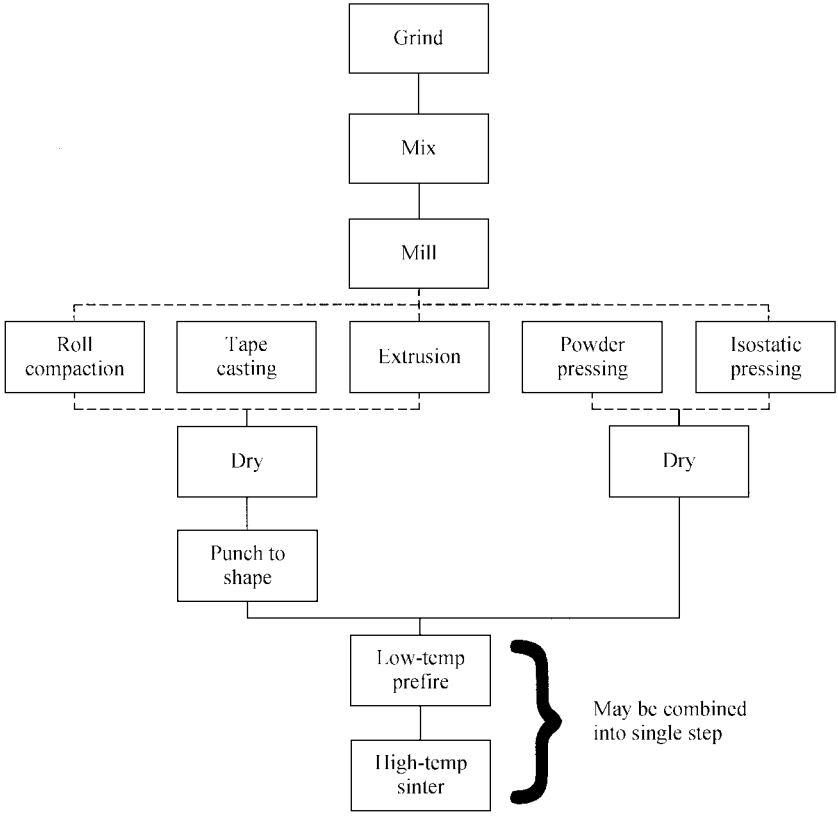

FIGURE 4.3 Flowchart for ceramic substrate processing.[1]

Powder Pressing. The powder is forced into a hard die cavity and subjected to very high pressure (up to 20,000 lb/in^2) throughout the sintering process. This produces a very dense part with tighter as-fired tolerances than other methods, although pressure variations may produce excessive warpage.

Isostatic powder pressing. This process utilizes a flexible die surrounded with water or glycerin, compressed up to 10,000 psi. The high pressure is more uniform and produces a part with less warpage.

Extrusion. The slurry, less viscous than for other processes, is forced through a die. Tight tolerances are hard to obtain, but the process is very economical and produces a thinner part than is attainable by other methods.

In the green state, the substrate is approximately the consistency of putty and may be punched to the desired size. Holes and other geometries may also be punched at this time.

Once the part is formed and punched, it is sintered at a temperature above the glass melting point to produce a continuous structure. The temperature profile is critical, and the process may actually be performed in two stages: one stage to remove the volatile organic

materials and a second stage to remove the remaining organics and to sinter the glass/ceramic structure. The peak temperature may be as high as several thousand degrees celsius and may be held for several hours, depending on the material and the type and amount of binding glasses. For example, pure alumina substrates formed by powder processing with no glasses are sintered at 1930°C.

It is essential that all the organic material be removed prior to sintering. Otherwise, the gases formed by the organic decomposition may leave serious voids in the ceramic structure and cause serious weakening. The oxide ceramics may be sintered in air. In fact, it is desirable to have an oxidizing atmosphere to aid in removing the organic materials by allowing them to react with the oxygen to form CO_2. The nitride ceramics must be sintered in the presence of nitrogen to prevent oxides of the metal from being formed. In this case, no reaction of the organics takes place; they are evaporated and carried away by the nitrogen flow.

During sintering, a degree of shrinkage takes place as the organic material is removed and the fluxing glasses activate. Shrinkage may be as low as 10 percent for powder processing to as high as 22 percent for sheet casting. The degree of shrinkage is highly predictable and may be considered during design.

Powder pressing generally forms boron nitride substrates. Various silica and/or calcium compounds may be added to lower the processing temperature and improve machinability. Diamond substrates are typically formed by chemical vapor deposition (CVD). Composite substrates, such as AlSiC, are fabricated by creating a spongy structure of SiC, and forcing molten aluminum into the crevices.

4.3 SURFACE PROPERTIES OF CERAMICS

The surface properties of interest, surface roughness and camber, are highly dependent on the particle size and method of processing. Surface roughness is a measure of the surface microstructure, and camber is a measure of the deviation from flatness. In general, the smaller the particle size, the smoother will be the surface.

4.3.1 Surface Roughness

Surface roughness may be measured by electrical or optical means. Electrically, surface roughness is measured by moving a fine-tipped stylus across the surface. The stylus may be attached to a piezoelectric crystal or to a small magnet that moves inside a coil, inducing a voltage proportional to the magnitude of the substrate variations. The stylus must have a resolution of 25.4 nm (1 μin) in order to read accurately in the most common ranges. Optically, a coherent light beam from a laser diode or other source is directed onto the surface. The deviations in the substrate surface create interference patterns that are used to calculate the roughness. Optical profilometers have a higher resolution than the electrical versions and are used primarily for very smooth surfaces. For ordinary use, the electrical profilometer is adequate and is widely used to characterize substrates in both manufacturing and laboratory environments.

The output of an electrical profilometer is plotted as shown in schematic form in Fig. 4.4 and in actual form in Fig. 4.5. A quantitative interpretation of surface roughness can be obtained from the plot in one of two ways: by the root mean square (rms) value and by the arithmetic average.

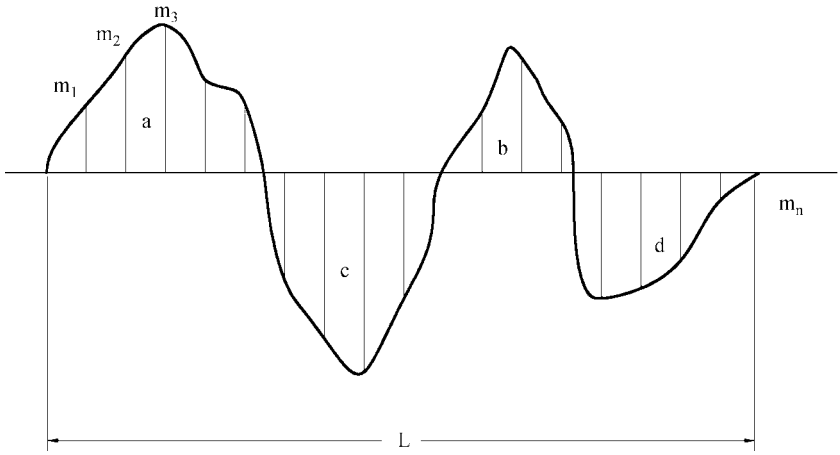

FIGURE 4.4 Schematic of surface trace.

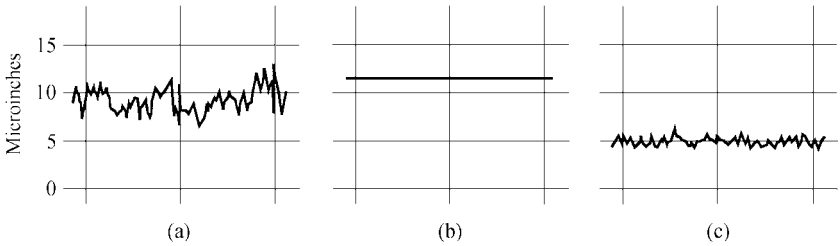

FIGURE 4.5 Surface trace of three substrate surfaces. (a) 23 μin surface; (b) 0.3 μin surface; (c) 7 μin surface.

The rms value is obtained by dividing the plot into n small, even increments of distance and measuring the height m at each point, as shown in Fig. 4.4. The rms value is calculated by

$$\text{rms} = \sqrt{\frac{m_1^2 + m_2^2 + \cdots + m_n^2}{n}} \tag{4.1}$$

and the average value [usually referred to as the *center line average* (CLA)] is calculated by

$$\text{CLA} = \frac{a_1 + a_2 + a_3 + \cdots + a_n}{L} \tag{4.2}$$

where a_1, a_2, a_3, ... = areas under the trace segments (Fig. 4.4) and L = length of travel. For systems where the trace is magnified by a factor M, Eq. (4.2) must be divided by the same factor.

For a sine wave, the average value is 0.636 × peak and the rms value is 0.707 × peak, which is 11.2 percent larger than the average. The profilometer trace is not quite sinusoidal in nature. The rms value may be greater than the CLA value by 10 to 30 percent.

Of the two methods, the CLA is the preferred method of use because the calculation is more directly related to the surface roughness, but it also has several shortcomings:

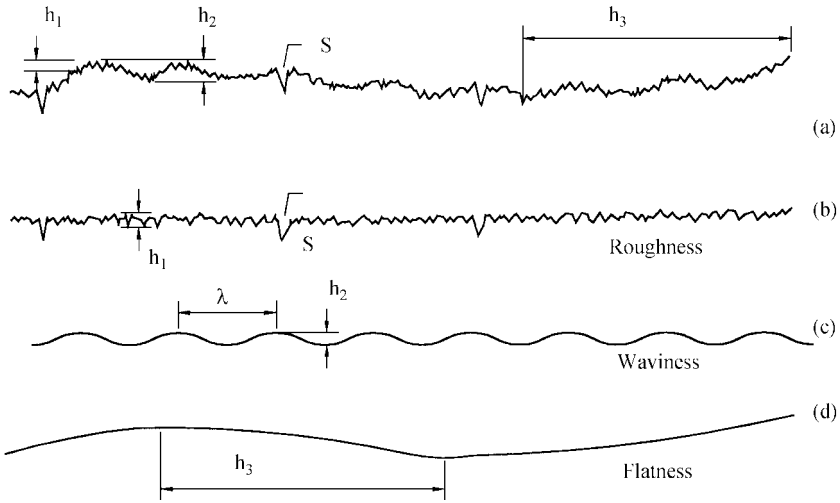

FIGURE 4.6 Surface characteristics.

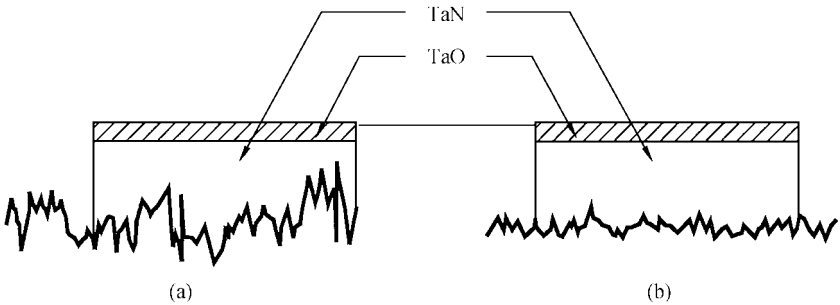

FIGURE 4.7 Tan resistor with TaO passivation on substrates with different surface roughness: (*a*) 5 microinch surface; (*b*) 1 microinch surface.

- The method does not consider surface waviness or camber, as shown in Fig. 4.6.[2]
- Surface profiles with different periodicities and the same amplitudes yield the same results, although the effect in use may be somewhat different.
- The value obtained is a function of the tip radius.

Surface roughness has a significant effect on the adhesion and performance of thick- and thin-film depositions. For adhesion purposes, it is desirable to have a high surface roughness to increase the effective interface area between the film and the substrate. For stability and repeatability, the thickness of the deposited film should be much greater than the variations in the surface. For thick films, which have a typical thickness of 10 to 12 μm, surface roughness is not a consideration, and a value of 25 μin (625 nm) is desirable. For thin films, however, which may have a thickness measured in angstroms, a much smoother surface is required. Figure 4.7 illustrates the difference in a thin film of tantalum nitride (TaN) deposited on both a 1-μin surface and a 5-μin surface. Tantalum nitride is commonly used to fabricate

resistors in thin-film circuits and is stabilized by growing a layer of tantalum oxide, which is nonconductive, over the surface by baking the resistors in air. Note that the oxide layer in the rougher surface represents a more significant percentage of the overall thickness of the film in areas where the surface deviation is the greatest. The result is a wider variation in both the initial and poststabilization resistor values and a larger drift in value with time.

4.3.2 Camber

Camber and waviness are similar in form in that they are variations in flatness over the substrate surface. Referring to Fig. 4.6, camber can be considered an overall warpage of the substrate, while waviness is more periodic in nature. Both of these factors may occur as a result of uneven shrinkage during the organic removal/sintering process or as a result of nonuniform composition. Waviness may also occur as a result of a "flat spot" in the rollers used to form the green sheets.

Camber is measured in units of length/length, interpreted as the deviation from flatness per unit length, and is measured with reference to the longest dimension by placing the substrate through parallel plates set a specific distance apart. Thus, a rectangular substrate would be measured along the diagonal. A typical value of camber is 0.003 in/in (also 0.003 mm/mm), which for a 2×2-in substrate represents a total deviation of $0.003 \times 2 \times 1.414 = 0.0085$ in. For a substrate that is 0.025 in thick, a common value, the total deviation represents a third of the overall thickness!

The nonplanar surface created by camber adversely affects subsequent metallization and assembly processes. In particular, screen printing is made more difficult because of the variable snap-off distance. Torsion bar printing heads on modern screen printers can compensate to a certain extent, but not entirely. A vacuum holddown on the screen printer platen also helps, but only flattens the substrate temporarily during the actual printing process. Camber can also create excessive stresses and a nonuniform temperature coefficient of expansion. At temperature extremes, these factors can cause cracking, breaking, or even shattering of the substrate.

Camber is measured by first measuring the thickness of the substrate and then placing the substrate between a series of pairs of parallel plates set specific distances apart. Camber is calculated by subtracting the substrate thickness from the smallest distance that the substrate will pass through and dividing by the longest substrate dimension. A few generalizations can be made about camber:

- Thicker substrates will have less camber than thinner.
- Square shapes will have less camber than rectangular.
- The pressed methods of forming will produce substrates with less camber than the sheet methods.

4.4 THERMAL PROPERTIES OF CERAMIC MATERIALS

4.4.1 Thermal Conductivity

The thermal conductivity of a material is a measure of the ability to carry heat and is defined as

$$q = -k \frac{dT}{dx} \tag{4.3}$$

where k = thermal conductivity in W/(m · °C)
q = heat flux in W/cm^2
dT/dx = temperature gradient in °C/m in steady state

The negative sign denotes that heat flows from areas of higher temperature to areas of lower temperature.

There are two mechanisms that contribute to thermal conductivity: the movement of free electrons and lattice vibrations, or phonons. When a material is locally heated, the kinetic energy of the free electrons in the vicinity of the heat source increases, causing the electrons to migrate to cooler areas. These electrons undergo collisions with other atoms, losing their kinetic energy in the process. The net result is that heat is drawn away from the source toward cooler areas. In a similar fashion, an increase in temperature increases the magnitude of the lattice vibrations, which, in turn, generate and transmit phonons, carrying energy away from the source. The thermal conductivity of a material is the sum of the contributions of these two parameters:

$$k = k_p + k_e \tag{4.4}$$

where k_p = contribution due to phonons and k_e = contribution due to electrons.

In ceramics, the heat flow is primarily due to phonon generation, and the thermal conductivity is generally lower than that of metals. Crystalline structures, such as alumina and beryllia, are more efficient heat conductors than amorphous structures such as glass. Organic materials used to fabricate printed circuit boards or epoxy attachment materials are electrical insulators and highly amorphous, and tend to be very poor thermal conductors.

Impurities or other structural defects in ceramics tend to lower the thermal conductivity by causing the phonons to undergo more collisions, lowering the mobility and lessening their ability to transport heat away from the source. This is illustrated by Table 4.2, which lists the thermal conductivity of alumina as a function of the percentage of glass. Although the thermal conductivity of the glass binder is lower than that of the alumina, the drop in thermal conductivity is greater than would be expected from the addition of the glass alone. If the thermal conductivity is a function of the ratio of the materials alone, it follows the rule of mixtures:

$$k_T = P_1 k_1 + P_2 k_2 \tag{4.5}$$

where k_T = net thermal conductivity
P_1 = volume percentage of material 1 in decimal form

TABLE 4.2 Thermal Conductivity of Alumina Substrates with Different Concentrations of Alumina

Volume percentage of alumina	Thermal conductivity, W/(m · °C)
85	16.0
90	16.7
94	22.4
96	24.7
99.5	28.1
100	31.0

k_1 = thermal conductivity of material 1
P_2 = volume percentage of material 2 in decimal form
k_2 = thermal conductivity of material 2

In pure form, alumina has a thermal conductivity of about 31 W/(m · °C), and the binding glass has a thermal conductivity of about 1 W/(m · °C). Equation (4.5) and the parameters from Table 4.2 are plotted in Fig. 4.8.

By the same token, as the ambient temperature increases, the number of collisions increases, and the thermal conductivity of most materials decreases. A plot of the thermal conductivity versus temperature for several materials is shown in Fig. 4.9[3] One material not plotted in this graph is diamond. The thermal conductivity of diamond varies widely with composition and the method of preparation, and is much higher than those materials listed. Diamond will be discussed in detail in a later section. Selected data from Fig. 4.9 was analyzed and extrapolated into binomial equations that quantitatively describe the thermal conductivity versus temperature relationship. The data are summarized in Table 4.3.

4.4.2 Specific Heat

The specific heat of a material is defined as

$$c = \frac{dQ}{dT} \tag{4.6}$$

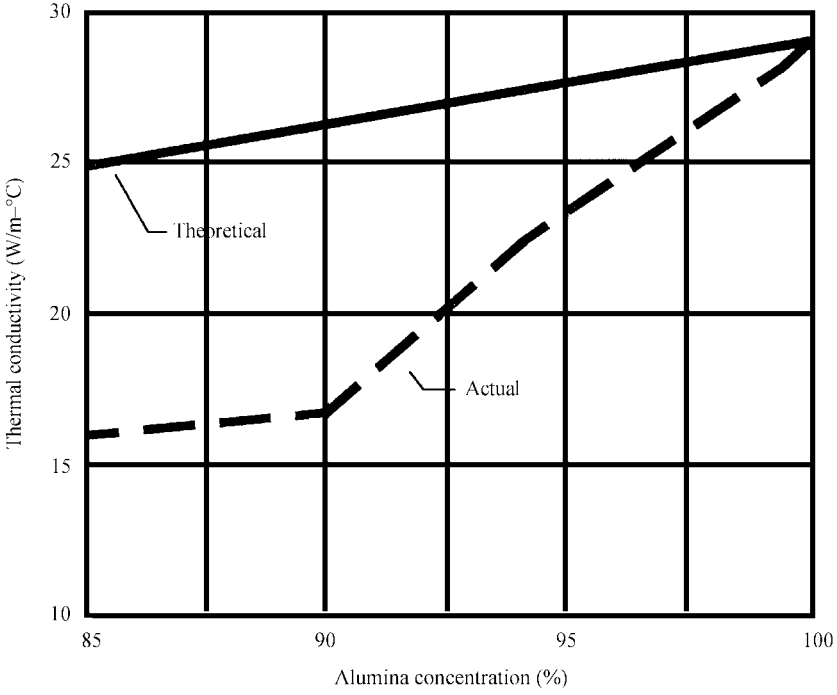

FIGURE 4.8 Thermal conductivity of alumina versus concentration, theoretical and actual.

TABLE 4.3 Approximate Thermal Conductivity versus Temperature for Selected Ceramic Materials (Binomial Relationship)

Material	Constant	T Coefficient	T^2 Coefficient
SiC	285	−1.11	1.55×10^{-3}
BeO	275	−1.10	1.06×10^{-3}
AlN (pure)	271	−0.60	3.81×10^{-4}
AlN (grade 1)	210	−1.39	3.45×10^{-3}
AlN (grade 2)	185	−1.37	4.40×10^{-3}
BN (perpendicular)	73	−0.06	2.17×10^{-4}
Al_2O_3 (99%)	34	−0.12	2.00×10^{-4}
Al_2O_3 (96%)	17	−0.07	5.70×10^{-5}

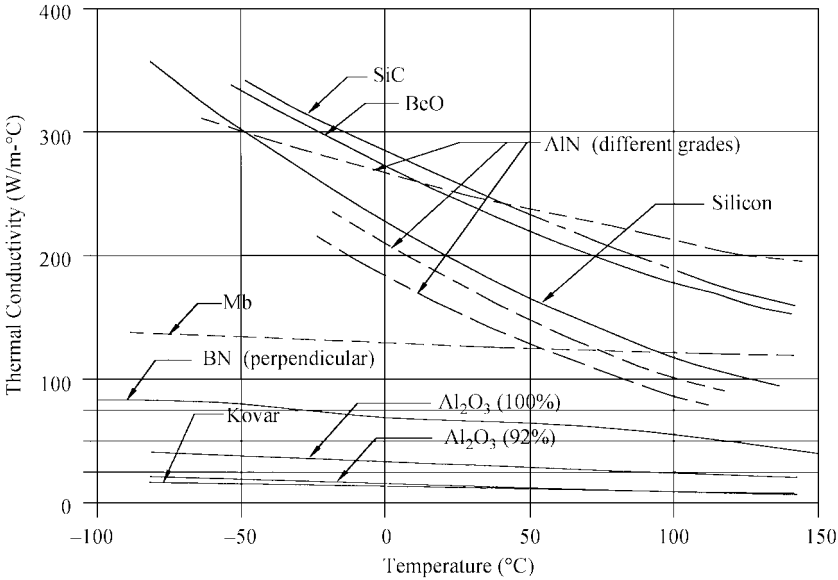

FIGURE 4.9 Thermal conductivity versus temperature for selected materials.[3]

where c = specific heat, W · s/(g · °C)
Q = energy, W · s
T = temperature, °C

The specific heat c is defined in a similar manner and is the amount of heat required to raise the temperature of one gram of material by one degree celsius with units of W · s/(g · °C). The term *specific heat* in this context refers to the quantity c_V, which is the specific heat measured with the volume constant, as opposed to c_P, which is measured with the pressure constant. At the temperatures of interest, these numbers are nearly the same for most solid materials. The specific heat is primarily the result of an increase in the vibrational energy of the atoms when heated, and the specific heat of most materials increases with temperature up to a point called the *Debye temperature*, where it becomes essentially independent of temperature. The specific heat of several common ceramic materials as a function of temperature is shown in Fig. 4.10.

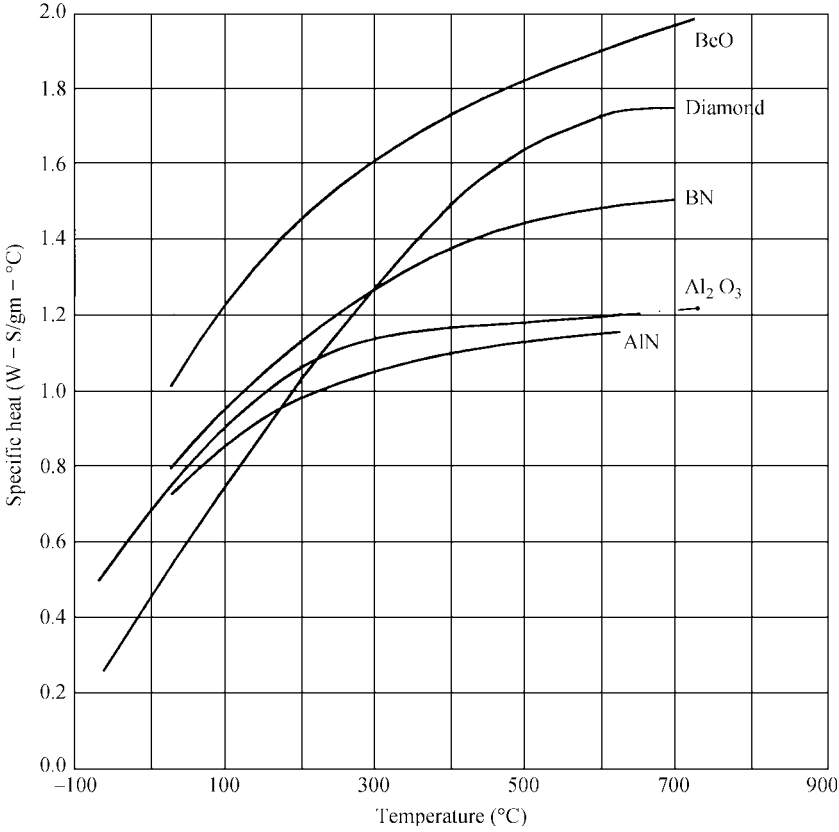

FIGURE 4.10 Specific heat versus temperature for selected ceramic materials.

The heat capacity C is similar in form, except that it is defined in terms of the amount of heat required to raise the temperature of a mole of material by one degree celsius and has the units of W · s/(mol · °C).

4.4.3 Temperature Coefficient of Expansion

The temperature coefficient of expansion (TCE) arises from the asymmetrical increase in the interatomic spacing of atoms as a result of increased heat. Most metals and ceramics exhibit a linear, isotropic relationship in the temperature range of interest, while certain plastics may be anisotropic in nature. The TCE is defined as

$$\alpha = \frac{l_{T2} - l_{T1}}{l_{T1}\,(T_2 - T_1)} \tag{4.7}$$

TABLE 4.4 Temperature Coefficient of Expansion of Selected Ceramic Substrate Materials

Material	TCE, ppm/°C
Alumina (96%)	6.5
Alumina (99%)	6.8
BeO (99.5%)	7.5
BN	
Parallel	0.57
Perpendicular	−0.46
Silicon carbide	3.7
Aluminum nitride	4.4
Diamond, Type IIA	1.02
AlSiC (70% SiC loading)	6.3

where α = temperature coefficient of expansion, ppm/°C
T_1 = initial temperature
T_2 = final temperature
l_{T1} = length at initial temperature
l_{T2} = length at final temperature

The TCE of most ceramics is isotropic. For certain crystalline or single-crystal ceramics, the TCE may be anisotropic, and some may even contract in one direction and expand in the other. Ceramics used for substrates do not generally fall into this category, as most are mixed with glasses in the preparation stage and do not exhibit anisotropic properties as a result. The temperature coefficient of expansion of several ceramic materials is shown in Table 4.4.

4.5 MECHANICAL PROPERTIES OF CERAMIC SUBSTRATES

The mechanical properties of ceramic materials are strongly influenced by the strong interatomic bonds that prevail. Dislocation mechanisms, which create slip mechanisms in softer metals, are relatively scarce in ceramics, and failure may occur with very little plastic deformation. Ceramics also tend to fracture with little resistance.

4.5.1 Modulus of Elasticity

The temperature coefficient of expansion (TCE) phenomenon has serious implications in the applications of ceramic substrates. When a sample of material has one end fixed, which may be considered to be a result of bonding to another material that has a much smaller TCE, the net elongation of the hotter end per unit length, or *strain* (E), of the material is calculated by

$$E = \text{TCE} \times \Delta T \tag{4.8}$$

where E = strain in length/length and ΔT = temperature differential across the sample.

TABLE 4.5 Mechanical Properties of Selected Ceramics

Material	Modulus of elasticity, GPa	Tensile strength, MPa	Compressive strength, MPa	Modulus of rupture, MPa	Flexural strength, MPa	Density, g/cm^3
Alumina (99%)	370	500	2600	386	352	3.98
Alumina (96%)	344	172	2260	341	331	3.92
Beryllia (99.5%)	345	138	1550	233	235	2.87
Boron nitride (normal)	43	2410	6525	800	53.1	1.92
Aluminum nitride	300	310	2000	300	269	3.27
Silicon carbide	407	197	4400	470	518	3.10
Diamond (Type IIA)	1000	1200	11000	940	1000	3.52

Elongation develops a stress S per unit length in the sample, as given by Hooke's Law:

$$S = EY \tag{4.9}$$

where S = stress, lb/in^2 per inch (N/m^2 per meter) and Y = modulus of elasticity, lb/in^2 (N/m^2).

When the total stress, as calculated by multiplying the stress per unit length by the maximum dimension of the sample, exceeds the strength of the material, mechanical cracks will form in the sample that may even propagate to the point of separation. The small elongation that occurs before failure is referred to as *plastic deformation*. This analysis is somewhat simplistic, but serves as a basic understanding of the mechanical considerations. The modulus of elasticity of selected ceramics is summarized in Table 4.5, along with other mechanical properties.

4.5.2 Modulus of Rupture

Ordinary stress-strain testing is not generally used to test ceramic substrates since they do not exhibit elastic behavior to a great degree. An alternative test, the modulus of rupture (bend strength) test, as described in Fig. 4.11, is preferred. A sample of ceramic, either circular or rectangular, is suspended between two points, a force is applied in the center, and the elongation of the sample is measured. The stress is calculated by

$$\sigma = \frac{Mx}{I} \tag{4.10}$$

where σ = stress, Mpa
M = maximum bending moment, N · m
x = distance from center to outer surface, m
I = moment of inertia, N · m^2

The expressions for σ, M, x, and I are summarized in Table 4.6. When these are inserted into Eq. (4.10), the result is

$$\sigma = \frac{3FL}{2xy^2} \qquad \text{(rectangular cross section)} \tag{4.11a}$$

$$\sigma = \frac{FL}{\pi R^3} \qquad \text{(circular cross section)} \tag{4.11b}$$

TABLE 4.6 Parameters of Stress in Modulus of Rupture Test[5]

Cross section	M	c	I
Rectangular	$\frac{FL}{4}$	$\frac{y}{2}$	$\frac{xy^3}{12}$
Circular	$\frac{FL}{4}$	R	$\frac{\pi R^2}{4}$

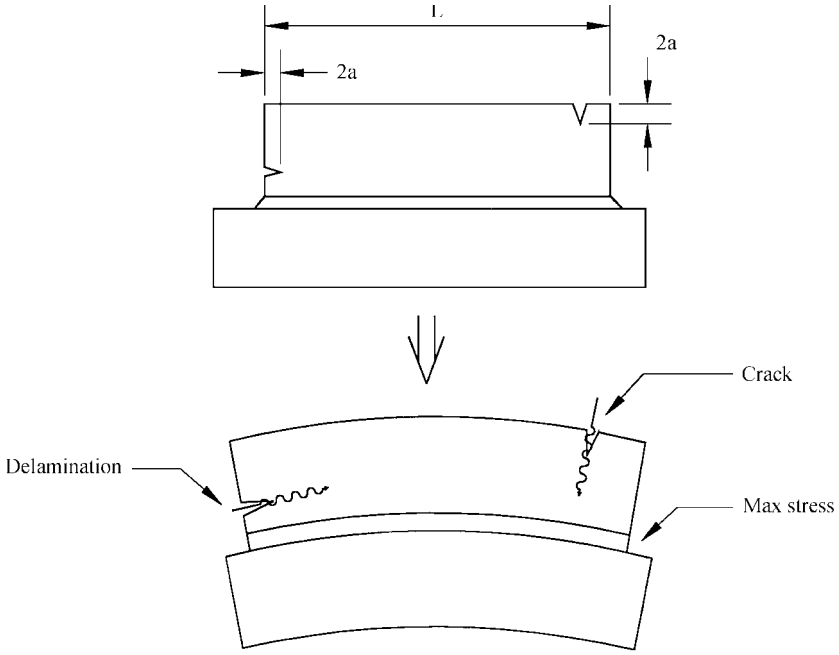

FIGURE 4.11 Cracks and chip-outs in substrates.[4]

where F = applied force in newtons
x = long dimension of rectangular cross section, m
y = short dimension of rectangular cross section, m
L = length of sample, m
R = radius of circular cross section, m

The modulus of rupture is the stress required to produce fracture and is given by

$$\sigma_r = \frac{3F_r L}{2xy^2} \qquad \text{(rectangular)} \tag{4.12a}$$

$$\sigma_r = \frac{F_r L}{\pi R^3} \qquad \text{(circular)} \tag{4.12b}$$

where σ_r = modulus of rupture, n/m^2, and F_r = force at rupture.

The modulus of rupture for selected ceramics is shown in Table 4.5.

4.5.3 Tensile and Compressive Strength

A force applied to a ceramic substrate in a tangential direction may produce tensile or compressive forces. If the force is tensile, in a direction such that the material is pulled apart, the stress produces plastic deformation as defined in Eq. (4.9). As the force increases past a value referred to as the *tensile strength*, breakage occurs. Conversely, a force applied in the opposite direction creates compressive forces until a value referred to as the *compressive strength* is reached, at which point breakage also occurs. The compressive strength of ceramics is, in general, much larger than the tensile strength. The tensile and compressive strength of selected ceramic materials is shown in Table 4.5.

In practice, the force required to fracture a ceramic substrate is much lower than predicted by theory. The discrepancy is due to small flaws or cracks residing within these materials as a result of processing. For example, when a substrate is sawed, small edge cracks may be created. Similarly, when a substrate is fired, trapped organic material may outgas during firing, leaving a microscopic void in the bulk. The result is an amplification of the applied stress in the vicinity of the void that may exceed the tensile strength of the material and create a fracture. If the microcrack is assumed to be elliptical with the major axis perpendicular to the applied stress, the maximum stress at the tip of the crack may be approximated by[4]

$$S_M = 2S_0 \leq \left(\frac{a}{\rho_t}\right)^{1/2} \tag{4.13}$$

where S_M = maximum stress at the tip of the crack
S_0 = nominal applied stress
a = length of the crack as defined in Fig. 4.11
ρ_t = radius of the crack tip

The ratio of the maximum stress to the applied stress may be defined as

$$K_t = \frac{S_M}{S_0} = 2\left(\frac{a}{\rho_t}\right)^{1/2} \tag{4.14}$$

where K_t = stress concentration factor. For certain geometries, such as a long crack with a small tip radius, K_t may be much larger than 1, and the force at the tip may be substantially larger than the applied force.

From this analysis, a material parameter called the *plain strain fracture toughness*, a measure of the ability of the material to resist fracture, can be defined as

$$K_{IC} = ZS_C\sqrt{\pi a} \tag{4.15}$$

where K_{IC} = plain strain fracture toughness, psi · $\text{in}^{1/2}$ or Mpa · $\text{m}^{1/2}$
Z = dimensionless constant, typically 1.2 (Ref. 4)
S_C = critical force required to cause breakage

From Eq. (4.15), the expression for the critical force can be defined as

$$S_C = Z\frac{K_{IC}}{\sqrt{\pi a}} \tag{4.16}$$

TABLE 4.7 Fracture Toughness for Selected Materials

Material	Fracture toughness, $MPa \cdot m^{1/2}$
Silicon	0.8
Alumina (96%)	3.7
Alumina (99%)	4.6
Silicon carbide	7.0
Molding compound	2.0

TABLE 4.8 Knoop Hardness for Selected Ceramics

Material	Knoop hardness (100 g)
Diamond	7000
Aluminum oxide	2100
Aluminum nitride	1200
Beryllium oxide	1200
Boron nitride	5000
Silicon carbide	2500

When the applied force on the die due to TCE or thermal differences exceeds this figure, fracture is likely. The plain strain fracture toughness for selected materials is presented in Table 4.7. It should be noted that Eq. (4.16) is a function of thickness up to a point, but is approximately constant for the area-to-thickness ratio normally found in substrates.

4.5.4 Hardness

Ceramics are among the hardest substances known, and their hardness is correspondingly difficult to measure. Most methods rely on the ability of one material to scratch another and the measurement is presented on a relative scale. Of the available methods, the Knoop method is the most frequently used. In this approach, the surface is highly polished and a pointed diamond stylus under a light load is allowed to impact on the material. The depth of the indentation formed by the stylus is measured and converted to a qualitative scale called the *Knoop* or *HK scale*. The Knoop hardness of selected ceramics is given in Table 4.8.

4.5.5 Thermal Shock

Thermal shock occurs when a substrate is exposed to temperature extremes in a short period of time. Under these conditions, the substrate is not in thermal equilibrium, and internal stresses may be sufficient to cause fracture. Thermal shock can be liquid to liquid or air to air, with the most extreme exposure occurring when the substrate is transferred directly from one liquid bath to another. The heat is more rapidly absorbed or transmitted, depending on the relative temperature of the bath, because of the higher specific heat of the liquid as opposed to air.

The ability of a substrate to withstand thermal shock is a function of several variables, including the thermal conductivity, the coefficient of thermal expansion, and the specific

TABLE 4.9 Thermal Endurance Factor for Selected Materials at 25°C

Material	Thermal endurance factor
Alumina (99%)	0.640
Alumina (96%)	0.234
Beryllia (99.5%)	0.225
Boron nitride (*a* axis)	648
Aluminum nitride	2.325
Silicon carbide	1.40
Diamond (Type IIA)	30.29

heat. Winkleman and Schott[5] developed a parameter called the *coefficient of thermal endurance* that qualitatively measures the ability of a substrate to withstand thermal stress.

$$F = \frac{P}{\alpha Y}\sqrt{\frac{k}{\rho c}} \tag{4.17}$$

where F = coefficient of thermal endurance
P = tensile strength, MPa
α = thermal coefficient of expansion, 1/K
Y = modulus of elasticity in MPa
k = thermal conductivity, W/(m · K)
ρ = density, in kg/m^3
c = specific heat, W · s/(kg · K)

The coefficient of thermal endurance for selected materials is shown in Table 4.9. The phenomenally high coefficient of thermal endurance for BN is primarily a result of the high tensile strength to modulus of elasticity ratio compared to other materials. Diamond is also high, primarily because of its high tensile strength, high thermal conductivity, and low TCE.

The thermal endurance factor is a function of temperature in that several of the variables, particularly the thermal conductivity and the specific heat, are functions of temperature. From Table 4.9, it is also noted that the thermal endurance factor may drop rapidly as the alumina-to-glass ratio drops. This is due to the difference in the thermal conductivity and TCE of the alumina and glass constituents that increase the internal stresses. This is true of other materials as well.

4.6 ELECTRICAL PROPERTIES OF CERAMICS

The electrical properties of ceramic substrates perform an important task in the operation of electronic circuits. Depending on the applications, the electrical parameters may be advantageous or detrimental to circuit function. Of most interest are the resistivity, the breakdown voltage, or dielectric strength, and the dielectric properties, including the dielectric constant and the loss tangent.

4.6.1 Resistivity

The electrical resistivity of a material is a measure of the ability of that material to transport charge under the influence of an applied electric field. More often, this ability is presented in the form of the electrical conductivity, the reciprocal of the resistivity as defined in Eq. (4.18).

$$\sigma = \frac{1}{\rho} \tag{4.18}$$

where σ = conductivity in siemens/unit length and ρ = resistivity in ohm-unit length.

The conductivity is a function primarily of two variables; the concentration of charge and the mobility, the ability of that charge to be transported through the material. The current density and the applied field are related by the expression

$$J = \sigma E \tag{4.19}$$

where J = current density, amperes/unit area, and E = electric field in volts/unit length.

It should be noted that both the current density and the electric field are vectors since the current is in the direction of the electric field.

The current density may also be defined as

$$J = nv_d \tag{4.20}$$

where n = free carrier concentration in coulombs/unit volume and v_d = drift velocity of electrons in unit length/second.

The drift velocity is related to the electric field by

$$v_d = \mu E \tag{4.21}$$

where μ = mobility in length^2/volt-second.

In terms of the free carrier concentration and the mobility, the current density is

$$J = n\mu E \tag{4.22}$$

Comparing Eq. (4.17) with Eq. (4.21), we can define the conductivity as

$$\sigma = n\mu \tag{4.23}$$

The free carrier concentration may be expressed as

$$n = n_t + n_i \tag{4.24}$$

where n_t = free carrier concentration due to thermal activity and n_i = free carrier concentration due to field injection.

The thermal charge density n_t in insulators is a result of free electrons obtaining sufficient thermal energy to break the interatomic bonds, allowing them to move freely within the atomic lattice. Ceramic materials characteristically have few thermal electrons as a result of the strong ionic bonds between atoms. The injected charge density n_i occurs when a potential is applied and is a result of the inherent capacity of the material. The injected charge density is given by

$$n_i = \varepsilon E \tag{4.25}$$

where ε = dielectric constant of the material in farads/unit length.

TABLE 4.10 Electrical Properties of Selected Ceramic Substrates

Material	Property			
	Electrical resistivity, $\Omega \cdot$ cm	Breakdown voltage, ac kV/mm	Dielectric constant	Loss tangent at 1 MHz
Alumina (96%)				
25°C	$>10^{14}$		9.0	
500°C	4×10^{9}	8.3	10.8	0.0002
1000°C	1×10^{6}			
Alumina (99.5%)	$>10^{14}$			
25°C	2×10^{10}	8.7	9.4	0.0001
500°C	2×10^{6}		10.1	
1000°C				
Beryllia				
25°C	$>10^{14}$	6.6	6.4	0.0001
500°C	2×10^{10}		6.9	0.0004
Aluminum nitride	$>10^{13}$	14	8.9	0.0004
Boron nitride	$>10^{14}$	61	4.1	0.0003
Silicon Carbide*	$>10^{13}$	0.7	40	0.05
Diamond (Type II)	$>10^{14}$	1000	5.7	0.0006

*Depends on method of preparation. May be substantially lower.

Inserting Eqs. (4.25) and (4.24) into Eq. (4.22) gives

$$J = \mu n_t E + \mu \varepsilon E^2 \tag{4.26}$$

For conductors, $n_t >> n_i$ and Ohm's law applies. For insulators, $n_i >> n_t$, and the result is a square law relationship between the voltage and the current:[6]

$$J = \mu \varepsilon E^2 \tag{4.27}$$

The conductivity of ceramic substrates is extremely low. In practice, it is primarily due to impurities and lattice defects, and may vary widely from batch to batch. The conductivity is also a strong function of temperature. As the temperature increases, the ratio of thermal to injected carriers increases. As a result, the conductivity increases and the *V-I* relationship follows Ohm's law more closely. Typical values of the resistivity of selected ceramic materials are presented in Table 4.10.

4.6.2 Breakdown Voltage

The term *breakdown voltage* is very descriptive. While ceramics are normally very good insulators, the application of excessively high potentials can dislodge electrons from orbit with sufficient energy to allow them to dislodge other electrons from orbit, creating an *avalanche effect*. The result is a breakdown of the insulation properties of the material, allowing current to flow. This phenomenon is accelerated by elevated temperature, particularly when mobile ionic impurities are present.

The breakdown voltage is a function of numerous variables, including the concentration of mobile ionic impurities, grain boundaries, and the degree of stoichiometry. In most applications,

the breakdown voltage is sufficiently high as to not be an issue. However, there are two cases where it must be a consideration:

1. At elevated temperatures created by localized power dissipation or high ambient temperature, the breakdown voltage may drop by orders of magnitude. Combined with a high potential gradient, this condition may be susceptible to breakdown.
2. The surface of most ceramics is highly "wettable," in that moisture tends to spread rapidly. Under conditions of high humidity, coupled with surface contamination, the effective breakdown voltage is much lower than the intrinsic value.

4.6.3 Dielectric Properties

Two conductors in proximity with a difference in potential have the ability to attract and store electric charge. Placing a material with dielectric properties between them enhances this effect. A dielectric material has the capability of forming electric dipoles, displacements of electric charge, internally. At the surface of the dielectric, the dipoles attract more electric charge, thus enhancing the charge storage capability, or capacitance, of the system. The relative ability of a material to attract electric charge in this manner is called the *relative dielectric constant*, or *relative permittivity*, and is usually given the symbol *K*. The relative permittivity of free space is 1.0 by definition and the absolute permittivity is

$$\varepsilon_0 = \text{permittivity of free space}$$

$$\varepsilon_0 = \frac{1}{36\pi} \times 10^{-9} \frac{\text{farads}}{\text{meter}} \tag{4.28}$$

The relationship between the polarization and the electric field is

$$\overline{P} = \varepsilon_0 (K-1)\overline{E} \frac{Q}{m^2} \tag{4.29}$$

where P = polarization, C/m^2, and E = electric field, V/m.

There are four basic mechanisms that contribute to polarization:

1. *Electronic polarization*. In the presence of an applied field, the cloud of electrons is displaced relative to the positive nucleus of the atom or molecule, creating an induced dipole moment. Electronic polarization is essentially independent of temperature and may occur very rapidly. The dielectric constant may therefore exist at very high frequencies, up to 10^{17} Hz.
2. *Molecular polarization*. Certain molecule structures create permanent dipoles that exist even in the absence of an electric field. These may be rotated by an applied electric field, generating a degree of polarization by orientation. Molecular polarization is inversely proportional to temperature and occurs only at low to moderate frequencies. Molecular polarization does not occur to a great extent in ceramics, and is more prevalent in organic materials and liquids, such as water.
3. *Ionic polarization*. Ionic polarization occurs in ionically bonded materials when the positive and negative ions undergo a relative displacement to each other in the presence of an applied electric field. Ionic polarization is somewhat insensitive to temperature and occurs at high frequencies, up to 10^{13} Hz.

4. *Space charge polarization.* Space charge polarization exists as a result of charges derived from contaminants or irregularities that exist within the dielectric. These charges exist to a greater or lesser degree in all crystal lattices and are partly mobile. Consequently, they will migrate in the presence of an applied electric field. Space charge polarization occurs only at very low frequencies.

In a given material, more than one type of polarization can exist and the net polarization is given by

$$\overline{P}_t = \overline{P}_e + \overline{P}_m + \overline{P}_i + \overline{P}_s \tag{4.30}$$

where P_t = total polarization
P_e = electronic polarization
P_m = molecular polarization
P_i = ionic polarization
P_s = space charge polarization

Normally, the dipoles are randomly oriented in the material and the resulting internal electric field is zero. In the presence of an external applied electric field, the dipoles become oriented as shown in Fig. 4.12.

There are two common ways to categorize dielectric materials: as polar or nonpolar, and as paraelectric or ferroelectric. Polar materials include those that are primarily molecular in nature, such as water, and nonpolar materials include both electronically and ionically polarized materials. Paraelectric materials are polarized only in the presence of an applied electric field and lose their polarization when the field is removed. Ferroelectric materials retain a degree of polarization after the field is removed. Materials used as ceramic substrates are usually nonpolar and paraelectric in nature. An exception is silicon carbide, which has a degree of molecular polarization.

In the presence of an electric field that is changing at a high frequency, the polarity of the dipoles must change at the same rate as the polarity of the signal in order to maintain the dielectric constant at the same level. Some materials are excellent dielectrics at low frequencies, but the dielectric qualities drop off rapidly as the frequency increases. Electronic polarization, which involves only displacement of free charge and not ions, responds more rapidly to the changes in the direction of the electric field, and remains viable up to about 10^{17} Hz. The polarization effect of ionic displacement begins to fall off at about 10^{13} Hz, and molecular and space charge polarizations fall off at still lower frequencies. The frequency response of the different types is shown in Fig. 4.13, which also illustrates that the dielectric constant decreases with frequency.

Changing the polarity of the dipoles requires a finite amount of energy and time. The energy is dissipated as internal heat, quantified by a parameter called the *loss tangent* or *dissipation factor*. Further, dielectric materials are not perfect insulators. These phenomena may be modeled as a resistor in parallel with a capacitor. The loss tangent, as expected, is a strong function of the applied frequency, increasing as the frequency increases.

In alternating current applications, the current and voltage across an ideal capacitor are exactly 90° out of phase, with the current leading the voltage. In actuality, the resistive component causes the current to lead the voltage by an angle less than 90°. The loss tangent is a measure of the real or resistive component of the capacitor and is the tangent of the difference between 90° and the actual phase angle.

$$\text{Loss tangent} = \tan(90° - \delta) \tag{4.31}$$

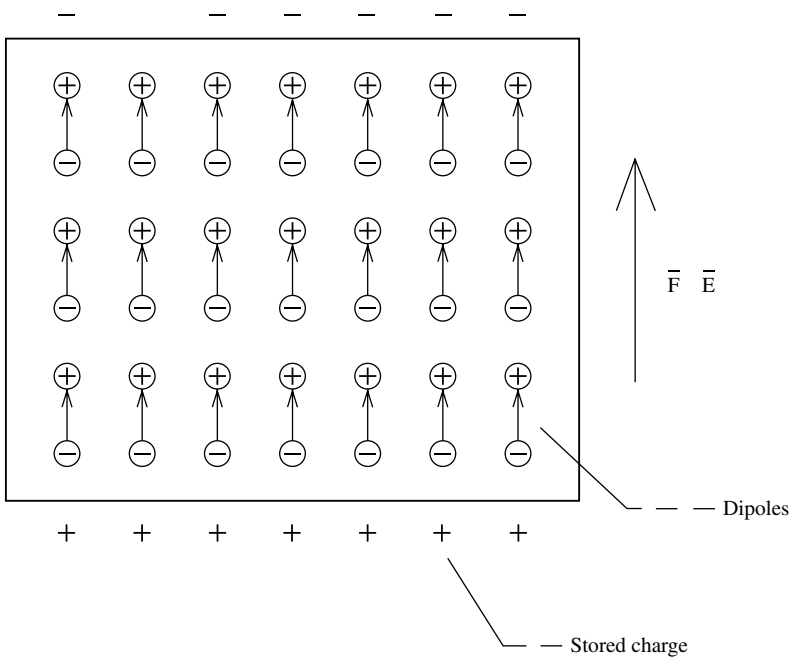

FIGURE 4.12 Orientation of dipoles in an electric field.[1]

where δ = phase angle between voltage and current. The loss tangent is also referred to as the *dissipation factor* (DF).

The loss tangent may also be considered a measure of the time required for polarization. It requires a finite amount of time to change the polarity of the dipole after an alternating field is applied. The resulting phase retardation is equivalent to the time indicated by the difference in phase angles.

4.7 METALLIZATION OF CERAMIC SUBSTRATES

There are three fundamental methods of metallizing ceramic substrates: thick film, thin film, and copper, which includes direct bond copper (DBC), plated copper, and active metal braze (AMB). Not all of these processes are compatible with all substrates. The selection of a metallization system depends on both the application and the compatibility with the substrate material.

4.7.1 Thick Film

The thick-film process is an additive process by which conductive, resistive, and dielectric (insulating) patterns in the form of a viscous paste are screen printed, dried, and fired onto a ceramic substrate at an elevated temperature to promote the adhesion of the film. In this

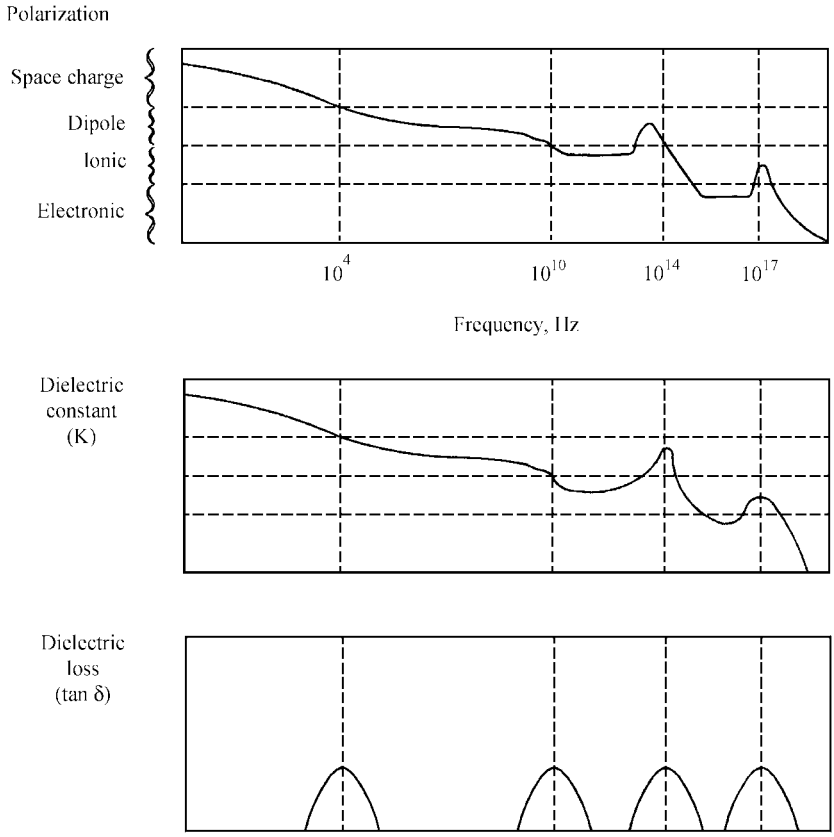

FIGURE 4.13 Frequency effects on dielectric materials.

manner, by depositing successive layers, as shown in Fig. 4.14, multilayer interconnection structures can be formed, which may contain integrated resistors, capacitors, or inductors.

The initial step is to generate 1:1 artworks corresponding to each layer of the circuit. The screen is a stainless steel mesh with a mesh count of 80 to 400 wires/inch. The mesh is stretched to the proper tension and mounted to a cast aluminum frame with epoxy. It is coated with a photosensitive material and exposed to light through one of the artworks. The unexposed portion is rinsed away, leaving openings in the screen mesh corresponding to the pattern to be printed.

Thick-film materials in the fired state are a combination of glass ceramic and metal, referred to as *cermet* thick films, and are designed to be fired in the range 850 to 1000°C. A standard cermet thick-film paste has four major ingredients:

- An active element, which establishes the function of the film
- An adhesion element, which provides the adhesion to the substrate and a matrix which holds the active particles in suspension

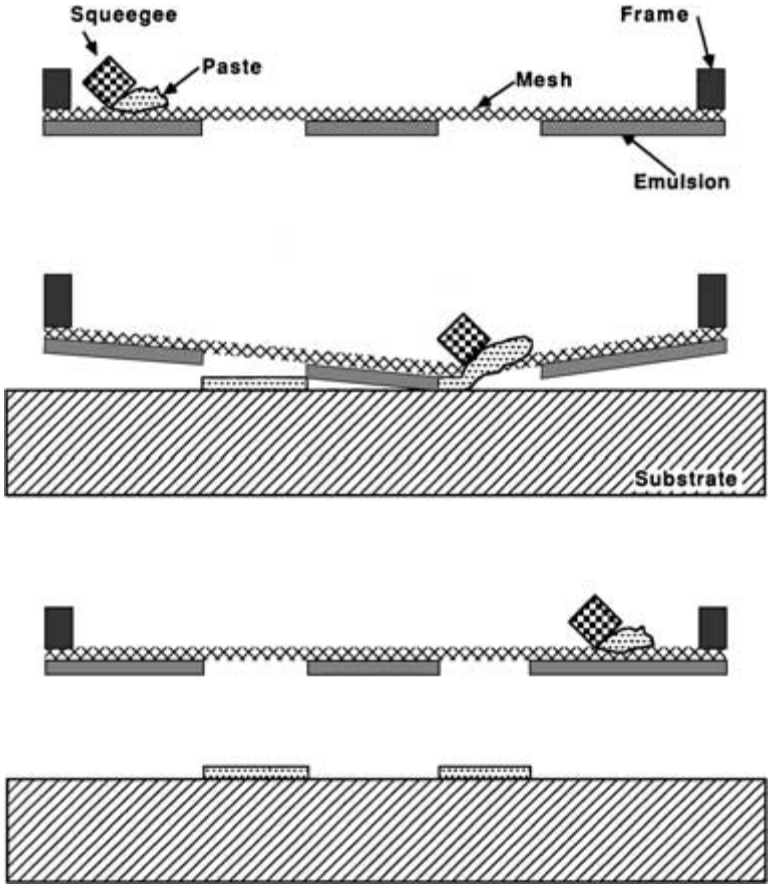

FIGURE 4.14 Screen printing process for material deposition onto a substrate.

- An organic binder, which provides the proper fluid properties for screen printing
- A solvent or thinner, which establishes the viscosity of the vehicle phase.

4.7.1.1 The Active Element. The active element within the paste dictates the electrical properties of the fired film. If the active element is a metal, the fired film will be a conductor; if it is a conductive metal oxide, a resistor; and, if it is an insulator, a dielectric. The active element is most commonly found in powder form ranging from 1 to 10 μm in size, with a mean diameter of about 5 μm.

4.7.1.2 The Adhesion Element. There are two primary constituents used to bond the film to the substrate: glass and metal oxides, which may be used singly or in combination. Films that use a glass, or frit, are referred to as fritted materials, and have a relatively low

melting point (500 to 600°C). There are two adhesion mechanisms associated with the fritted materials: a chemical reaction and a physical reaction. In the chemical reaction, the molten glass chemically reacts with the glass in the substrate to a degree. In the physical reaction, the glass flows into and around the irregularities in the substrate surface. The total adhesion is the sum of the two factors. The physical bonds are more susceptible to degradation by thermal cycling or thermal storage than the chemical bonds, and are generally the first to fracture under stress. The glass also creates a matrix for the active particles, holding them in contact with each other to promote sintering and to provide a series of three-dimensional continuous paths from one end of the film to the other. Principal thick-film glasses are based on B_2O_3-SiO_2 network formers with modifiers such as PbO, Al_2O_3, Bi_2O_3, ZnO, BaO, and CdO added to change the physical characteristics of the film, such as melting point, viscosity, and coefficient of thermal expansion. Bi_2O_3 also has excellent wetting properties, both to the active element and to the substrate, and is frequently used as a flux. The glass phase may be introduced as a prereacted particle or formed in situ by using glass precursors such as boric oxide, lead oxide, and silicon. Fritted conductor materials tend to have glass on the surface, making subsequent component assembly processes more difficult.

A second class of materials utilizes metal oxides to provide the adhesion to the substrate. In this case, a pure metal, such as copper or cadmium, is mixed with the paste and reacts with oxygen atoms on the surface of the substrate to form an oxide. The conductor adheres to the oxide and to itself by sintering, which takes place during firing. During firing, the oxides react with broken oxygen bonds on the surface of the substrate, forming a Cu or Cd spinel structure, such as $CuAl_2O_4$. Pastes of this type offer improved adhesion over fritted materials, and are referred to as *fritless*, *oxide-bonded*, or *molecular-bonded* materials. Fritless materials typically fire at 900 to 1000°C, which is undesirable from a manufacturing aspect. Ovens used for thick-film firing degrade more rapidly and need more maintenance when operated at these temperatures for long periods of time.

A third class of materials utilizes both reactive oxides and glasses. The oxides in these materials react at lower temperatures, but are not as strong as copper. A lesser concentration of glass than found in fritted materials is added to supplement the adhesion. These materials, referred to as *mixed bonded* systems, incorporate the advantages of both technologies and fire at a lower temperature.

The selection of a binding material is strongly dependent on the substrate material. For example, the most common glass composition used with alumina is a lead/bismuth borosilicate composition. When this glass is used in conjunction with aluminum nitride, however, it is rapidly reduced at firing temperatures.[1] Alkaline earth borosilicates must be used with AlN to promote adhesion.

4.7.1.3 Organic Binder. The organic binder is generally a thixotropic fluid and serves two purposes: It holds the active and adhesion elements in suspension until the film is fired, and it gives the paste the proper fluid characteristics for screen printing. The organic binder is usually referred to as the nonvolatile organic since it does not evaporate, but begins to burn off at about 350°C. The binder must oxidize cleanly during firing, with no residual carbon, which could contaminate the film. Typical materials used in this application are ethyl cellulose and various acrylics.

For nitrogen-firable films, where the firing atmosphere can contain only a few parts per million of oxygen, the organic vehicle must decompose and thermally depolymerize, departing as a highly volatile organic vapor in the nitrogen blanket provided as the firing atmosphere, since oxidation into CO_2 or H_2O is not feasible because of the oxidation of the copper film.

4.7.1.4 Solvent or Thinner. The organic binder in the natural form is too thick to permit screen printing, and the use of a solvent or thinner is necessary. The thinner is somewhat more volatile than the binder, evaporating rapidly above about 100°C. Typical materials used for this application are terpineol, butyl carbitol, and certain of the complex alcohols into which the nonvolatile phase can dissolve. The low vapor pressure at room temperature is desirable to minimize drying of the pastes and to maintain a constant viscosity during printing. Additionally, plasticizers, surfactants, and agents that modify the thixotropic nature of the paste are added to the solvent to improve paste characteristics and printing performance.

To complete the formulation process, the ingredients of the thick-film paste are mixed together in proper proportions and milled on a three-roller mill for a sufficient period of time to ensure that they are thoroughly mixed and that no agglomeration exists.

Thick-film conductor materials may be divided into two broad classes: air firable and nitrogen firable. Air-firable materials are made up of noble metals that do not readily form oxides, gold and silver in the pure form, or alloyed with palladium and/or platinum. Nitrogen-firable materials include copper, nickel, and aluminum, with copper being the most common.

Thick-film resistors are formed by adding metal oxide particles to glass particles and firing the mixture at a temperature/time combination sufficient to melt the glass and to sinter the oxide particles together. The resulting structure consists of a series of three-dimensional chains of metal oxide particles embedded in a glass matrix. The higher the metal oxide to glass ratio, the lower the resistivity and vice versa. The most common materials used are ruthenium-based, such as ruthenium dioxide, RuO_2, and bismuth ruthenate, $BiRu_2O_7$.

Thick-film dielectric materials are used primarily as insulators between conductors, either as simple crossovers or in complex multilayer structures. Small openings, or *vias*, may be left in the dielectric layers so that adjacent conductor layers may interconnect. In complex structures, as many as several hundred vias per layer may be required. In this manner, complex interconnection structures may be created. Although the majority of thick-film circuits can be fabricated with only three layers of metallization, others may require several more. If more than three layers are required, the yield begins dropping dramatically, with a corresponding increase in cost.

Dielectric materials used in this application must be of the *devitrifying* or *recrystallizable* type. Dielectrics in the paste form are a mixture of glasses that melt at a relatively low temperature. During firing, when they are in the liquid state, they blend together to form a uniform composition with a higher melting point than the firing temperature. Consequently, on subsequent firings they remain in the solid state, providing a stable foundation for firing sequential layers. By contrast, vitreous glasses always melt at the same temperature and would be unacceptable for layers to either "sink" and short to conductor layers underneath, or "swim" and form an open circuit.

Additionally, secondary loading of ceramic particles is used to enhance devitrification and to modify the temperature coefficient of expansion (TCE).

Dielectric materials have two conflicting requirements in that they must form a continuous film to eliminate short circuits between layers and, at the same time, they must maintain openings as small as 0.010 in. In general, dielectric materials must be printed and fired twice per layer to eliminate pinholes and prevent short circuits between layers.

The TCE of thick-film dielectric materials must be as close as possible to that of the substrate to avoid excessive *bowing*, or warpage, of the substrate after several layers. Excessive bowing can cause severe problems with subsequent processing, especially where the substrate must be held down with a vacuum or where it must be mounted on a heated stage. In addition, the stresses created by the bowing can cause the dielectric material to

crack, especially when it is sealed within a package. Thick-film material manufacturers have addressed this problem by developing dielectric materials that have an almost exact TCE match with alumina substrates. Where a serious mismatch exists, matching layers of dielectric must be printed on the bottom of the substrate to minimize bowing, which obviously increases the cost.

4.7.2 Thin Film

The thin-film technology is a subtractive technology in that the entire substrate is coated with several layers of metallization and the unwanted material is etched away in a succession of selective photoetching processes. The use of photolithographic processes to form the patterns allows much finer and more well-defined lines than can be formed by the thick-film process. This feature promotes the use of the thin-film technology for high-density and high-frequency applications.

Thin-film circuits typically consist of three layers of material deposited on a substrate. The bottom layer serves two purposes: It is the resistor material and it also provides the adhesion to the substrate. The adhesion mechanism of the film to the substrate is an oxide layer that forms at the interface between the two. The bottom layer must therefore be a material that oxidizes readily. The most common types of resistor material are nichrome (NiCr) and tantalum nitride (TaN). Gold and silver, for example, are noble metals and do not adhere well to ceramic surfaces.

The middle layer acts as an interface between the resistor layer and the conductor layer, either by improving the adhesion of the conductor or by preventing diffusion of the resistor material into the conductor. The interface layer for TaN is usually tungsten (W), and for NiCr, a thin layer of pure Ni is used.

Gold is the most common conductor material used in thin-film circuits because of the ease of wire and die bonding to it and the high resistance of the gold to tarnish and corrosion. Aluminum and copper are also frequently used in certain applications. It should be noted that copper and aluminum will adhere directly to ceramic substrates, but gold requires one or more intermediate layers since it does not form the necessary oxides for adhesion.

The term *thin film* refers more to the manner in which the film is deposited onto the substrate than to the actual thickness of the film. Thin films are typically deposited by one of the vacuum deposition techniques, sputtering or evaporation, or by electroplating.

4.7.2.1 Sputtering. Sputtering is the prime method by which thin films are applied to substrates. In ordinary dc triode sputtering, as shown in Fig. 4.15, a current is established in a conducting plasma formed by striking an arc in an inert gas, such as argon, with a partial vacuum of approximately 10 μm pressure. A substrate at ground potential and a target material at high potential are placed in the plasma. The potential may be ac or dc. The high potential attracts the gas ions in the plasma to the point where they collide with the target with sufficient kinetic energy to dislodge microscopically sized particles with enough residual kinetic energy to travel the distance to the substrate and adhere.

The adhesion of the film is enhanced by presputtering the substrate surface by random bombardment of argon ions prior to applying the potential to the target. This process removes several atomic layers of the substrate surface, creating a large number of broken oxygen bonds and promoting the formation of the oxide interface layer. The oxide formation is further enhanced by the residual heating of the substrate as a result of the transfer of the kinetic energy of the sputtered particles to the substrate when they collide.

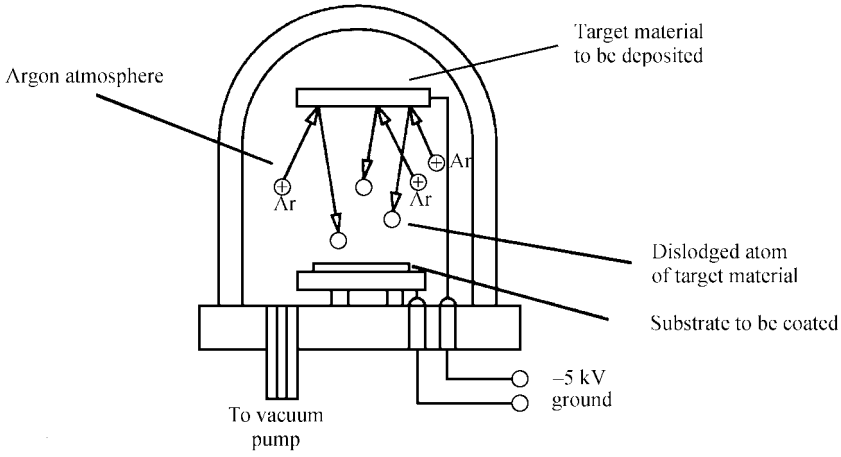

FIGURE 4.15 A DC sputtering chamber.

DC triode sputtering is a very slow process, requiring hours to produce films with a usable thickness. By utilizing magnets at strategic points, the plasma can be concentrated in the vicinity of the target, greatly speeding up the deposition process. In most applications, an RF potential at a frequency of 13.56 MHz is applied to the target. The RF energy may be generated by a conventional electronic oscillator or by a magnetron. The magnetron is capable of generating considerably more power, with a correspondingly higher deposition rate.

By adding small amounts of other gases, such as oxygen and nitrogen, to the argon, it is possible to form oxides and nitrides of certain target materials on the substrate. It is this technique, called *reactive sputtering*, that is used to form tantalum nitride, a common resistor material.

4.7.2.2 Evaporation. Evaporation of a material into the surrounding area occurs when the vapor pressure of the material exceeds the ambient pressure and can take place from either the solid state or the liquid state. In the thin-film process, the material to be evaporated is placed in the vicinity of the substrate and heated until the vapor pressure of the material is considerably above the ambient pressure. The evaporation rate is directly proportional to the difference between the vapor pressure of the material and the ambient pressure and is highly dependent on the temperature of the material.

There are several techniques by which evaporation can be accomplished. The two most common of these are resistance heating and electron-beam (E-beam) heating.

Evaporation by resistance heating, as depicted in Fig. 4.16, usually takes place from a boat made with a refractory metal, a ceramic crucible wrapped with a wire heater, or a wire filament coated with the evaporant. A current is passed through the element and the heat generated heats the evaporant. It is somewhat difficult to monitor the temperature of the melt by optical means because of the propensity of the evaporant to coat the inside of the chamber, and control must be done by empirical means. There exist closed-loop systems that can control the deposition rate and the thickness, but these are quite expensive. In general, adequate results can be obtained from the empirical process if proper controls are used.

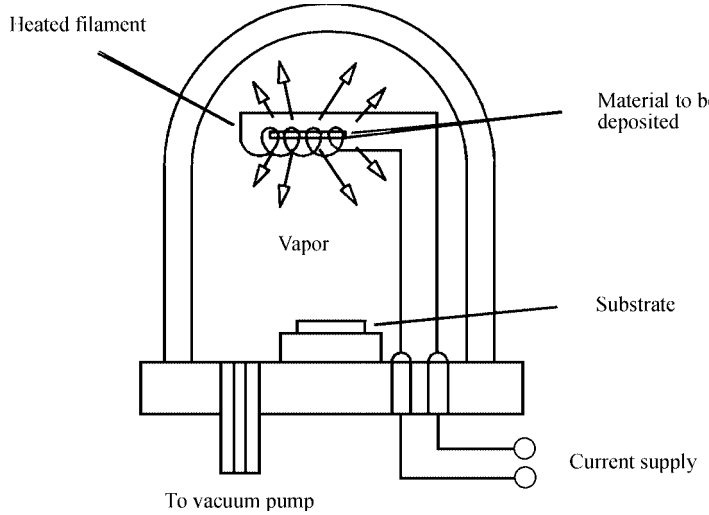

FIGURE 4.16 A thermal vacuum evaporation system.

The E-beam evaporation method takes advantage of the fact that a stream of electrons accelerated by an electric field tends to travel in a circle when entering a magnetic field. This phenomenon is utilized to direct a high-energy stream of electrons onto an evaporant source. The kinetic energy of the electrons is converted into heat when they strike the evaporant. E-beam evaporation is somewhat more controllable since the resistance of the boat is not a factor and the variables controlling the energy of the electrons are easier to measure and control. In addition, the heat is more localized and intense, making it possible to evaporate metals with higher 10^{-2}-torr temperatures and lessening the reaction between the evaporant and the boat.

While evaporation provides a more rapid deposition rate, there are certain disadvantages compared with sputtering.

1. It is difficult to evaporate alloys such as nichrome (NiCr) because of the difference between the 10^{-2}-torr temperatures. The element with the lower temperature tends to evaporate somewhat faster, causing the composition of the evaporated film to be different from the composition of the alloy. To achieve a particular film composition, the composition of the melt must contain a higher portion of the material with the higher 10^{-2}-torr temperature and the temperature of the melt must be tightly controlled. By contrast, the composition of a sputtered film is identical to that of the target.
2. Evaporation is limited to the metals with lower melting points. Refractory metals, ceramics, and other insulators are virtually impossible to deposit by evaporation.
3. Reactive deposition of nitrides and oxides is very difficult to control.

4.7.2.3 Electroplating. Electroplating is accomplished by applying a potential between the substrate and the anode, which are suspended in a conductive solution of the material to be plated. The plating rate is a function of the potential and the concentration of the solution. In this manner, most metals can be plated to a metal surface.

In the thin-film technology, it is a common practice to sputter a film of gold a few angstroms thick and to build up the thickness of the gold film by electroplating. This is

considerably more economical and results in much less target usage. For added savings, photoresist can be applied to the substrate and gold electroplated only where actually required by the pattern.

The interconnection and resistor patterns are formed by selective photoetching. The substrate is coated with a photosensitive material exposed to ultraviolet light through a pattern formed on a glass plate. The photoresist may be of the positive or negative type, the positive type being prevalent because of its inherently higher resistance to the etchant materials. The unwanted material that is not protected by the photoresist may be removed by *wet* (chemical) etching or by *dry* (sputter) etching.

In general, two masks are required: one corresponding to the conductor pattern and one corresponding to a combination of both the conductor and resistor patterns, generally referred to as the *composite* pattern. As an alternative to the composite mask, a mask that contains only the resistor pattern plus a slight overlap onto the conductor to allow for misalignment may be used. The composite mask is preferred since it allows a second gold etch process to be performed to remove any bridges or extraneous gold that might have been left from the first etch.

Sputtering may also be used to etch thin films. In this technique, the substrate is coated with photoresist and the pattern exposed in exactly the same manner as with chemical etching. The substrate is then placed in a plasma and connected to a potential. In effect, the substrate acts as the target during the sputter etching process, with the unwanted material being removed by the impingement of the gas ions on the exposed film. The photoresistive film, being considerably thicker than the sputtered film, is not affected.

4.7.3 Copper Metallization Technologies

The thick-film and thin-film technologies are limited in their ability to deposit films with a thickness greater than 1 mil (25 μm). This factor directly affects the ohmic resistance of the circuit traces and affects their ability to handle large currents or high frequencies. The copper metallization technologies provide conductors with greatly increased conductor thickness that offer improved circuit performance in many applications. There are three basic technologies available to the hybrid designer; direct bond copper (DBC), active metal braze (AMB), and the various methods of plating copper directly to ceramic.

4.7.3.1 Direct Bond Copper. Copper may be directly bonded to alumina ceramic by placing a film of copper in contact with the alumina and heating to about 1065°C, just below the melting point of copper, 1083°C. At this temperature, a combination of 0.39 percent O_2 and 99.61 percent Cu form a liquid that can melt, wet, and bond tightly to the surfaces in contact with it when cooled to room temperature. In this process, the copper remains in the solid state during the bonding process and a strong bond is formed between the copper and the alumina with no intermediate material required. The metallized substrate is slowly cooled to room temperature at a controlled rate to avoid quenching. To prevent excessive bowing of the substrate, copper must be bonded to both sides of the substrate to minimize stresses due to the difference in TCE between copper and alumina.

In this manner, a film of copper from 5 to 25 mils thick can be bonded to a substrate and a metallization pattern formed by photolithographic etching. For subsequent processing, the copper is usually plated with several hundred microinches of nickel to prevent oxidation. The nickel-plated surface is readily solderable, and aluminum wire bonds to nickel is one of the most reliable combinations.[7] Aluminum wire bonded directly to copper is not as reliable and may result in failure on exposure to heat and/or moisture.[8]

Multilayer structures of up to four layers have been formed by etching patterns on both sides of two substrates and bonding them to a common alumina substrate. Interconnections between layers are made by inserting oxidized copper pellets into holes drilled or formed in the substrates prior to firing. Vias may also be created by using one of the copper plating processes.

The line and space resolution of DBC is limited because of the difficulty of etching thick layers of metal without substantial undercutting. Special design guidelines must be followed to allow for this factor.[1] While the DBC technology does not have a resistor system, the thick-film technology can be used in conjunction with DBC to produce integrated resistors and areas of high-density interconnections.

Aluminum nitride can also be used with copper, although the consistency of such factors as grain size and shape are not as good as aluminum oxide at this time. Additional preparation of the AlN surface is required to produce the requisite layer of oxide necessary to produce the bond. This can be accomplished by heating the substrate to about 1250°C in the presence of oxygen.

4.7.3.2 Plated Copper Technology. The various methods of plating copper to a ceramic all begin with the formation of a conductive film on the surface. This film may be vacuum deposited by thin-film methods, screen printed by thick-film processes, or deposited with the aid of a catalyst. A layer of electroless copper may be plated over the conductive surface, followed by a layer of electrolytic copper to increase the thickness.

A pattern may be generated in the plated surface by one of two methods. Conventional photolithographic methods may be used to etch the pattern, but this may result in undercutting and loss of resolution when used with thicker films. To produce more precise lines, a dry film photoresist may be utilized to generate a pattern on the electroless copper film that is the negative of the one required for etching. The traces may then be electroplated to the desired thickness using the photoresist pattern as a mold. Once the photoresist pattern is removed, the entire substrate may be immersed in an appropriate etchant to remove the unwanted material between the traces. Plated copper films created in this manner may be fired at an elevated temperature in a nitrogen atmosphere to improve the adhesion.

4.7.3.3 Active Metal Brazing Copper Technology. The active metal brazing (AMB) process utilizes one or more of the metals in the IV-B column of the periodic table, such as titanium, hafnium, or zirconium, to act as an activation agent with ceramic. These metals are typically alloyed with other metals to form a braze that can be used to bond copper to ceramic. One such example is an alloy of 70Ti/15Cu/15Ni that melts at 960 to 1000°C. Numerous other alloys can also be used.[2]

The braze may be applied in the form of a paste, a powder, or a film. The combination is heated to the melting point of the selected braze in a vacuum to minimize oxidation of the copper. The active metal forms a liquidus with the oxygen in the system that acts to bond the metal to the ceramic. After brazing, the copper film may be processed in much the same manner as DBC.

4.8 CERAMIC MATERIALS

The characteristics of various substrate materials have been summarized in previous sections. However, there may be substantial variations in the parameters due to processing, composition, stoichiometry, or other factors. This section covers the materials in more detail and also describes some common applications.

4.8.1 Aluminum Oxide

Aluminum oxide, Al_2O_3, commonly referred to as *alumina*, is by far the most common substrate material used in the microelectronics industry because it is superior to most other oxide ceramics in mechanical, thermal, and electrical properties. The raw materials are plentiful, low in cost, and amenable to fabrication by a wide variety of techniques into a wide variety of shapes.

Alumina is hexagonal close-packed with a corundum structure. Several metastable structures exist, but they all ultimately irreversibly transform to the hexagonal alpha phase.

Alumina is stable in both oxidizing and reducing atmospheres up to1925°C. Weight loss in vacuum over the temperature range 1700°C to 2000°C ranges from 10^{-7} to 10^{-6} g/(cm^2 · s). It is resistant to attack by all gases except wet fluorine to at least 1700°C. Alumina is attacked at elevated temperatures by alkali metal vapors and halogen acids, especially the lower-purity alumina compositions that may contain a percentage of glasses.

Alumina is used extensively in the microelectronics industry as a substrate material for thick- and thin-film circuits, for circuit packages, and as multilayer structures for multichip modules. Compositions exist for both high- and low-temperature processing. High temperature cofired ceramics (HTCC) use a refractory metal, such as tungsten or molybdenum/manganese, as a conductor and fire at about 1800°C. The circuits are formed as separate layers, laminated together, and fired as a unit. Low temperature cofired ceramics (LTCC) use conventional gold or palladium silver as conductors and fire as low as 850°C. Certain power MOSFETs and bipolar transistors are mounted on alumina substrates, which act as electrical insulators and thermal conductors.

The parameters of alumina are summarized in Table 4.11.

4.8.2 Beryllium Oxide

Beryllium oxide (BeO, beryllia) is cubic close-packed and has a zinc blend structure. The alpha form of BeO is stable to above 2050°C. BeO is stable in dry atmospheres and is inert to most materials. It hydrolyzes at temperatures greater than 1100°C with the formation and volatilization of beryllium hydroxide. BeO reacts with graphite at high temperature, forming beryllium carbide.

Beryllia has an extremely high thermal conductivity, higher than aluminum metal, and is widely used in applications where this parameter is critical. The thermal conductivity drops rapidly above 300°C, but is suitable for most practical applications.

Beryllia is available in a wide variety of geometries formed by a variety of fabrication techniques. While beryllia in the pure form is perfectly safe, care must be taken when machining BeO, as the dust is toxic if inhaled.

Beryllia may be metallized with thick film or thin film, or by one of the copper processes. However, thick-film pastes must be specially formulated to be compatible. Laser or abrasive trimming of BeO must be performed in a vacuum to remove the dust.

The properties of 99.5 percent beryllia are summarized in Table 4.12.

4.8.3 Aluminum Nitride

Aluminum nitride is covalently bonded with a wurtzite structure and decomposes at 2300°C under 1 atm of argon. In a nitrogen atmosphere of 1500 lb/in^2, melting may occur in excess of 2700°C. Oxidation of AlN in even a low concentration of oxygen (less than 0.1 percent) occurs at temperatures above 700°C. A layer of aluminum oxide protects the nitride to a temperature of 1370°C, above which the protective layer cracks, allowing oxidation to

TABLE 4.11 Typical Parameters of Aluminum Oxide

			Percentage, %			
Parameter	Units	Test	85	90	96	99.5
Density	g/cm^3	ASTM C20	3.40	3.60	3.92	3.98
Elastic modulus	GPa	ASTM C848	220	275	344	370
Poisson's ratio		ASTM C848	0.22	0.22	0.22	0.22
Compressive strength	MPa	ASTM C773	1930	2150	2260	2600
Fracture toughness	$Mpa \cdot m^{1/2}$	NOTCHED BEAM	3.1	3.3	3.7	4.6
Thermal conductivity	$W/(m \cdot °C)$	ASTM C408	16	16.7	24.7	31.0
TCE	$10^{-6}/°C$	ASTM C372	5.9	6.2	6.5	6.8
Specific heat	$W \cdot s/(g \cdot °C)$	ASTM E1269	920	920	880	880
Dielectric strength	ac Kv/mm	ASTM D116	8.3	8.3	8.3	8.7
Loss tangent (1 MHz)		ASTM D2520	0.0009	0.0004	0.0002	0.0001
Volume resistivity	$\Omega \cdot cm$	ASTM D1829				
25°C			$>10^{14}$	$>10^{14}$	$>10^{14}$	$>10^{14}$
500°C			4×10^8	4×10^8	4×10^9	2×10^{10}
1000°C				5×10^5	1×10^6	2×10^6

continue. Aluminum nitride is not appreciably affected by hydrogen, steam, or oxides of carbon to 980°C. It dissolves slowly in mineral acids and decomposes slowly in water. It is compatible with aluminum to 1980°C, gallium to 1300°C, iron or nickel to 1400°C, and molybdenum to 1200°C.

Aluminum nitride substrates are fabricated by mixing AlN powder with compatible glass powders containing additives such as CaO and Y_2O_3, along with organic binders, and casting the mixture into the desired shape. Densification of the AlN requires very tight control of both atmosphere and temperature. The solvents used in the preparation of substrates must be anhydrous to minimize oxidation of the AlN powder and prevent the generation of ammonia during firing.[9] For maximum densification and maximum thermal conductivity, the substrates must be sintered in a dry reducing atmosphere to minimize oxidation.

Aluminum nitride is primarily noted for two very important properties; a high thermal conductivity and a TCE closely matching that of silicon. There are several grades of aluminum nitride with different thermal conductivities available. The prime reason for the differences is the oxygen content of the material. It is important to note that even a thin surface layer of oxidation on a fraction of the particles can adversely affect the thermal conductivity. Only with a high degree of material and process control can AlN substrates be made consistent.

The thermal conductivity of AlN does not vary as widely with temperature as that of BeO. For the highest grade of AlN, the crossover temperature is about 20°C. Above this temperature, the thermal conductivity of AlN is higher; below, 20°C, that of BeO is higher.

TABLE 4.12 Typical Parameters for 99.5% Beryllium Oxide

Parameter	Units	Value
Density	g/cm^3	2.87
Hardness	Knoop 100 g	1200
Melting point	°C	2570
Modulus of elasticity	GPa	345
Compressive strength	MPa	1550
Poisson's ratio		0.26
Thermal conductivity	$W/(m \cdot K)$	
25°C		250
500°C		55
Specific heat	$W \cdot s/(g \cdot K)$	
25°C		1.05
500°C		1.85
TCE	$10^{-6}/K$	7.5
Dielectric constant		
1 MHz		6.5
10 GHz		6.6
Loss tangent		
1 MHz		0.004
10 GHz		0.004
Volume resistivity	$\Omega \cdot cm$	
25°C		$>10^{14}$
500°C		2×10^{10}

The TCE of AlN closely matches that of silicon, an important consideration in mounting large power devices. The second level of packaging is also critical. If an aluminum nitride substrate is mounted directly to a package with a much higher TCE, such as copper, the result can be worse than if a substrate with an intermediate, although higher, TCE were used. The large difference in TCE builds up stresses during the mounting operation that can be sufficient to fracture the die and/or the substrate.

Thick-film, thin-film, and copper metallization processes are available for aluminum nitride. Certain of these processes, such as direct bond copper (DBC), require oxidation of the surface to promote adhesion. For maximum thermal conductivity, a metallization process should be selected that bonds directly to AlN to eliminate the relatively high thermal resistance of the oxide layer.

Thick-film materials must be formulated to adhere to AlN. The lead oxides prevalent in thick-film pastes that are designed for alumina and beryllia oxidize AlN rapidly, causing blistering and a loss of adhesion. Thick-film resistor materials are primarily based on RuO_2 and MnO_2.

Thin-film processes available for AlN include NiCr/Ni/Au, Ti/Pt/Au, and Ti/Ni/Au.[10] Titanium in particular provides excellent adhesion by diffusing into the surface of the AlN. Platinum and nickel are transition layers to promote gold adhesion. Solders, such as Sn60/Pb40 and Au80/Sn20 can also be evaporated onto the substrate to facilitate soldering.

Multilayer circuits can be fabricated with W or MbMn conductors. The top layer is plated with nickel and gold to promote solderability and bondability. Ultrasonic milling may be used for cavities, blind vias, and through vias. Laser machining is suitable for through vias as well.

Direct bond copper may be attached to AlN by forming a layer of oxide over the substrate surface, which may require several hours at temperatures above 900°C. The DBC

TABLE 4.13 Typical Parameters for Aluminum Nitride (Highest Grade)

Parameter	Units	Value
Density	g/cm^3	3.27
Hardness	Knoop 100 g	1200
Melting point	°C	2232
Modulus of elasticity	GPa	300
Compressive strength	MPa	2000
Poisson's ratio		0.23
Thermal conductivity	$W/(m \cdot K)$	
25°C		270
150°C		195
Specific heat	$W \cdot s/(g \cdot K)$	
25°C		0.76
150°C		0.94
TCE	$10^{-6}/K$	4.4
Dielectric constant		
1 MHz		8.9
10 GHz		9.0
Loss tangent		
1 MHz		0.0004
10 GHz		0.0004
Volume resistivity	$\Omega \cdot cm$	
25°C		$>10^{12}$
500°C		2×10^8

forms a eutectic with aluminum oxide at about 963°C. The layer of oxide, however, increases the thermal resistance by a significant amount, partially negating the high thermal conductivity of the aluminum nitride. Copper foil may also be brazed to AlN with one of the compatible braze compounds. Active metal brazing (AMB) does not generate an oxide layer. The copper may also be plated with nickel and gold.

The properties of aluminum nitride are summarized in Table 4.13.

4.8.4 Diamond

Diamond substrates are primarily grown by chemical vapor deposition (CVD). In this process, a carbon-based gas is passed over a solid surface and activated by a plasma, a heated filament, or a combustion flame. The surface must be maintained at a high temperature, above 700°C, to sustain the reaction. The gas is typically a mixture of methane (CH_4) and hydrogen (H_2), with 1 to 2 percent CH_4 by volume.[11] The consistency of the film in terms of the ratio of diamond to graphite is inversely proportional to the growth rate of the film. Films produced by plasma have a growth rate of 0.1 to 10 μm/h and are very high quality, while films produced by combustion methods have a growth rate of 100 to 1000 μm/h and are of lesser quality.

The growth begins at nucleation sites and is columnar in nature, growing faster in the normal direction than in the lateral direction. Eventually, the columns grow together to form a polycrystalline structure with microcavities spread throughout the film. The resulting substrate is somewhat rough, with a 2 to 5 μm surface variation. This feature is detrimental to the effective thermal conductivity, and the surface must be polished for optimum

results. An alternative method is to use an organic filler[12] on the surface for planarization. This process has been shown to have a negligible effect on the overall thermal conductivity from the bulk, and dramatically improves heat transfer. Substrates as large as 10 cm^2 and as thick as 1000 μm have been fabricated.

Diamond can be deposited as a coating on refractory metals, oxides, nitrides, and carbides. For maximum adhesion, the surface should be a carbide-forming material with a low TCE.[13]

Diamond has an extremely high thermal conductivity, several times that of the next highest material. The primary application is, obviously, in packaging power devices. Diamond has a low specific heat, however, and works best as a heat spreader in conjunction with a heat sink. For maximum effectiveness,[13]

$$0.5\, r_k \le t_d \le r_h$$
$$r_D = 3\, r_h$$

where t_D = thickness of diamond substrate
r_h = radius of heat source
r_D = radius of diamond substrate

Applications of diamond substrates include heat sinks for laser diodes and laser diode arrays. The low dielectric constant of diamond coupled with its high thermal conductivity makes it attractive for microwave circuits as well. As improved methods of fabrication lower the cost, the use of diamond substrates is expected to expand rapidly.

The properties of diamond are summarized in Table 4.14.

TABLE 4.14 Typical Parameters for CVD Diamond

Parameter	Units	Value
Density	g/cm^3	3.52
Hardness	Knoop 100 g	7000
Modulus of elasticity	GPa	1000
Compressive strength	MPa	11,000
Poisson's ratio		0.148
Thermal conductivity	W/(m · K)	
Normal		2200
Tangential		1610
Specific heat	W · s/(g · K)	
25°C		0.55
150°C		0.90
TCE	10^{-6}/K	1.02
Dielectric constant		
1 MHz		5.6
10 GHz		5.6
Loss tangent		
1 MHz		0.001
10 GHz		0.001
Volume resistivity	Ω · cm	
25°C		$>10^{13}$
500°C		2×10^{11}

4.8.5 Boron Nitride

There are two basic types of boron nitride (BN). Hexagonal (alpha) BN is soft and is structurally similar to graphite. It is sometimes called *white graphite* for its color. Cubic (beta) BN is formed by subjecting hexagonal BN to extreme heat and pressure, as in the process used to fabricate synthetic industrial diamonds. Melting of either phase is possible only under nitrogen at high pressure.

Hot-pressed BN is very pure (greater than 99 percent), the major impurity being boric oxide (BO). Boric oxide tends to hydrolyze in water, degrading the dielectric and thermal shock properties. Calcium oxide (CaO) is frequently added to tie up the BO to minimize the water absorption. When exposed to temperatures above 1100°C, BO forms a thin coating on the surface, slowing further oxide growth.

Boron nitride in the hot-pressed state is easily machinable and may be formed into various shapes. The properties are highly anisotropic and vary considerably in the normal and tangential directions of the pressing force. The thermal conductivity in the normal direction is very high and the TCE is very low, making BN an attractive possibility for a substrate material. However, it has not yet been proved possible to metallize BN,[14] and the range of applications is therefore limited. It can be used in contact with various metals, including, copper, tin, and aluminum, and may be used as a thermally conductive electrical insulator. Applications of BN include microwave tubes and crucibles.

The properties of boron nitride are summarized in Table 4.15.

TABLE 4.15 Typical Parameters for Boron Nitride

Parameter	Units	Value
Density	g/cm^3	1.92
Hardness	Knoop 100 g	5000
Modulus of elasticity	GPa	
Normal		43
Tangential		768
Compressive strength	MPa	
Normal		110
Tangential		793
Poisson's ratio		0.05
Thermal conductivity	$W/(m \cdot K)$	
Normal		73
Tangential		161
Specific heat	$W \cdot s/(g \cdot K)$	
25°C		0.84
150°C		1.08
TCE	$10^{-6}/K$	
Normal		0.57
Tangential		–0.46
Dielectric constant		
1 MHz		4.1
Loss tangent		
1 MHz		0.0003
Volume resistivity	$\Omega \cdot cm$	
25°C		1.6×10^{12}
500°C		2×10^{10}

4.8.6 Silicon Carbide

Silicon carbide (SiC) has a tetrahedral structure and is the only known alloy of silicon and carbon. Both elements have four electrons in the outer shell, with an atom of one bonded to four atoms of the other. The result is a very stable structure not affected by hydrogen or nitrogen up to 1600°C. In air, SiC begins decomposing above 1000°C. As with other compounds, a protective oxide layer forms over the silicon, reducing the rate of decomposition. Silicon carbide is highly resistant to both acids and bases. Even the so-called white etch (hydrofluoric acid mixed with nitric and sulfuric acids) has no effect.

Silicon carbide structures are formed by hot pressing, dry and isostatic pressing (preferred), CVD, or slip casting. Isostatic pressing using gas as the fluid provides optimum mechanical properties.

Silicon carbide in pure form is a semiconductor, and the resistivity depends on the impurity concentration. In the intrinsic form, the resistivity is less than 1000 $\Omega \cdot$ cm, which is unsuitable for ordinary use. The addition of a small percentage (less than 1 percent) of BeO during the fabrication process[15] increases the resistivity to as high as 10^{13} $\Omega \cdot$ cm by creating carrier-depleted layers around the grain boundaries.

Both thick and thin films can be used to metallize SiC, although some machining of the surface to attain a higher degree of smoothness is necessary for optimum results. The two parameters that make SiC attractive as a substrate are its exceptionally high thermal conductivity, second only to diamond, and its low TCE, which matches that of silicon to a higher degree than any other ceramic. SiC is also less expensive than either BeO or AlN. A possible disadvantage is the high dielectric constant, 4 to 5 times higher than other substrate materials. This parameter can result in cross-coupling of electronic signals or in excessive transmission delay.

The parameters of SiC are summarized in Table 4.16.

TABLE 4.16 Typical Parameters for Silicon Carbide

Parameter	Units	Value
Density	g/cm^3	3.10
Hardness	Knoop 100 g	500
Modulus of elasticity	GPa	407
Compressive strength	MPa	4400
Fracture toughness	$MPa \cdot m^{1/2}$	7.0
Poisson's ratio		0.14
Thermal conductivity	$W/(m \cdot K)$	
25°C		290
150°C		160
Specific heat	$W \cdot s/(g \cdot K)$	
25°C		0.64
150°C		0.92
TCE	$10^{-6}/K$	3.70
Dielectric constant		40
Loss tangent		0.05
Volume resistivity	$\Omega \cdot$ cm	
25°C		$>10^{13}$
500°C		2×10^9

4.9 COMPOSITE MATERIALS

Composite materials have been in use for thousands of years. Ancient peoples used straw and rocks to strengthen adobe bricks for building shelters, and concrete reinforced with steel rods is used extensively in the construction industry. Only recently have composites been introduced into electronic applications. In particular, the demands for improved thermal management and higher packaging density have driven the development of composite materials. Today, several composite materials are available to meet the needs of electronic packaging engineers.

A two-component composite consists of a matrix and a filler, which may be in the form of long or short fibers, large or small particles, or laminates. The theory of composite materials is well documented. For this discussion it is sufficient to simply describe composites by the so-called *rule of mixtures*, stated as

$$P_C = P_M V_{fM} + P_F V_{fF} \tag{4.32}$$

where P_C = parameter of the composite
P_M = parameter of the matrix
V_{fM} = volume fraction of the matrix
P_F = parameter of the filler
V_{fF} = volume fraction of the filler

The degree to which the composite will obey the rule of mixtures depends on a number of factors, including the size and orientation of the filler and the extent of the interaction between the matrix and the filler. Consider the structure in Fig. 4.17, consisting of

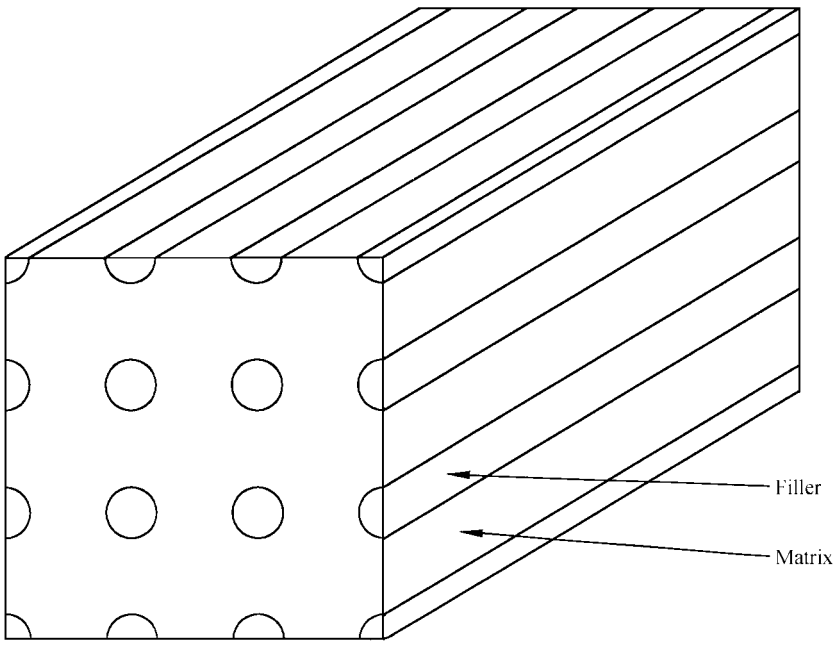

FIGURE 4.17 Matrix with continuous filler.

continuous fibers uniformly dispersed in a matrix. Assuming that no slippage between the two occurs, the strain E, as defined in Eq. (4.8) is the same for both materials when a longitudinal force is applied. For this case,

$$E_C = E_M = E_F = \frac{\Delta L}{L_0} \tag{4.33}$$

where E_C = strain in composite
E_M = strain in matrix
E_F = strain in filler
ΔL = change in length
L_0 = initial length

A structure of this type will closely approximate the rule of mixtures. Where the filler is not uniformly distributed as in Fig. 4.17, a critical length may be defined as

$$L_C = \frac{D_F S_{\text{MAX}}}{2\sigma_M} \tag{4.34}$$

where L_C = critical length
D_F = diameter of filler
S_{MAX} = maximum shear strength of filler
σ_M = shear strength of matrix

To be effective, the filler must have a diameter greater than the critical length.

The rule of mixtures may also be used to approximate other parameters, as illustrated in Eq. (4.5) to calculate the thermal conductivity of a glass-alumina matrix.

It is possible to tailor composite materials to obtain desirable properties superior to either component for specific applications. Composite materials may be divided into several categories according to the nature of the matrix and the filler, as described in Secs. 4.9.1 to 4.9.5.

4.9.1 Organic-Organic Composites

Composites composed of organic materials typically use an epoxy as the matrix and a variety of organic fibers as the filler. The epoxy may be in the liquid or powder form. For example, nylon-reinforced plastics are commonly used to mold plastic parts for a number of applications.

4.9.2 Organic-Ceramic/Glass Composites

Organic-ceramic composites may use an epoxy as the matrix and glass or ceramic powder as the filler. A common example is the fiberglass-reinforced epoxy used as a printed circuit laminate. An epoxy substrate filled with alumina and carbon black has also been developed.[14] By weight, the composition is 10.8 percent epoxy resin, 89 percent alumina, and 0.2 percent carbon black. This material has a thermal conductivity of 3.0 to 4.0 W/(m · K), compared to both glass-epoxy printed circuit material [0.2 W/(m · K)] and glass-alumina low temperature cofired substrates [2.5 W/(m · K)]. The TCE (17 ppm/°C) is substantially below that

of PCB material (25 to 50 ppm/°C). This composite can be utilized to make multilayer interconnection structures. Organic-ceramic composites are also commonly used as materials for housings for electronic systems. Glass-reinforced plastics, for example, are very strong and are capable of withstanding considerable mechanical shock without breaking.

4.9.3 Ceramic-Ceramic Composites

Ceramic-based composites are somewhat difficult to fabricate because of their high melting point. Lawrence Berkeley National Laboratory[15] has developed a method of coating platelets of silicon carbide with alumina and forming them into a composite matrix with exceptional fracture strength and fracture toughness. This approach was demonstrated by coating alpha SiC platelets with about 2 μm of alumina and combining them with a matrix of beta SiC. The coating prevents the alpha SiC from being assimilated into the beta SiC during processing and diverts cracks to the perimeter of the particles rather than through the body. The result is a SiC-SiC composite ceramic that is 2 to 3 times stronger than conventional SiC.

4.9.4 Ceramic-Glass Composites

In all but the simplest electronic circuits, it is necessary to have a method for fabricating multilayer interconnection structures to enable all the necessary points to be connected. The thick film technology is limited to three layers for all practical purposes because of yield and planarity considerations, and thin-film multilayer circuits are quite expensive to fabricate. The copper technologies can produce only a single layer because of processing limitations.

Ceramic-glass composite materials may be used to economically fabricate very complex multilayer interconnection structures. The materials in powder form are mixed with an organic binder, a plasticizer, and a solvent and formed into a slurry by ball or roll milling. The slurry is forced under a doctor blade and dried to form a thin sheet, referred to as *green tape* or *greensheet*. Further processing depends on the type of material. There are three basic classes of materials: high temperature cofired ceramic (HTCC), low temperature cofired ceramic (LTCC), and aluminum nitride.

4.9.4.1 High Temperature Cofired Ceramic (HTCC). HTCC multilayer circuits are primarily alumina based. The green tape is blanked into sheets of uniform size, and holes are punched where vias and alignment holes are required. The metal patterns are printed and dried next. Despite their relatively high electrical resistance, refractory metals such as tungsten and molybdenum are used as conductors because of the high firing temperature. Via fills may be accomplished during conductor printing or during a separate printing operation. The process is repeated for each layer.

The individual layers are aligned and laminated under heat and pressure to form a monolithic structure in preparation for firing. The structure is heated to approximately 600°C to remove the organic materials. Carbon residue is removed by heating to approximately 1200°C in a wet hydrogen atmosphere. Sintering and densification take place at approximately 1600°C.

During firing, HTCC circuits shrink anywhere from 14 to 17 percent, depending on the organic content. With careful control of the material properties and processing parameters, the shrinkage can be controlled to within 0.1 percent. Shrinkage must be taken into

TABLE 4.17 Properties of Multilayer Ceramic Materials

	Low temperature cofired ceramic (LTCC)	High temperature cofired ceramic (HTCC)	Aluminum nitride
Material	Cordierite MgO, SiO_2, Al_2O_3 Glass filled composites SiO_2, B_2O_3, Al_2O_3 PbO, SiO_2, CaO, Al_2O_3 Crystalline-phase ceramics Al_2O_3, CaO, SiO_2, MgO, B_2O_3	88–92% alumina	AlN, yttria, CaO
Firing temperature	850–1050°C	1500–1600°C	1600–1800°C
Conductors	Au, Ag, Cu, PdAg	W, MoMn	W, MoMn
Conductor resistance	3–20 mΩ/square	8–12 mΩ/square	8–12 mΩ/square
Dissipation factor	$15–30 \times 10^{-4}$	$5–15 \times 10^{-4}$	$20–30 \times 10^{-3}$
Relative dielectric constant	5–8	9–10	8–9
Resistor values	0.1 Ω–1 MΩ	N/A	N/A
Firing shrinkage			
x,y	12.0 ± 0.1%	12–18%	15–20%
z	17.0 ± 0.5%	12–18%	15–20%
Repeatability	0.3–1%	0.3–1%	0.3–1%
Line width	100 μm	100 μm	100 μm
Via diameter	125 μm	125 μm	125 μm
Number of metal layers	33	63	8
CTE	3–8 ppm/°C	6.5 ppm/°C	4.4 ppm/°C
Thermal conductivity	2–6 W/(m · °C)	15–20 W/(m · °C)	180–200 W/(m · °C)

consideration during the design, punching, and printing processes. The artwork enlargement must exactly match the shrinkage factor associated with a particular lot of green tape.

Processing of the substrate is completed by plating the outer layers with nickel and gold for component mounting and wire bonding. The gold is plated to a thickness of 25 μin for gold wire and 5 μin for aluminum wire. Gold wire bonds to the gold plating, while aluminum wire bonds to the nickel underneath. The gold plating in this instance is simply to protect the nickel surface from oxidation or corrosion.

The properties of HTCC materials are summarized in Table 4.17

4.9.4.2 Low Temperature Cofired Ceramic (LTCC). LTCC circuits consist of alumina mixed with glasses that can simultaneously sinter and crystallize.[17] These structures are often referred to as glass-ceramics. Typical glasses are listed in Table 4.17. The processing steps are similar to those used to fabricate HTCC circuits with two exceptions;[16] the firing temperature is much lower, 850 to 1050°C, and the metallization is gold based or silver based thick film formulated to be compatible with the LTCC material. Frequently, silver based materials are used in the inner layers with gold on the outside for economic reasons. Special via fill materials are used between the gold and the silver layers to prevent electrolytic reaction.

The shrinkage of LTCC circuits during firing is in the range of 12 to 18 percent. If the edges are restrained, the lateral shrinkage can be held to 0.1 percent with a corresponding increase in the vertical shrinkage.

One advantage that LTCC has over the other multilayer technologies is the ability to print and fire resistors. Where trimming is not required, the resistors can be buried in intermediate layers with a corresponding saving of space. It is also possible to bury printed capacitors of small value.

4.9.4.3 Aluminum Nitride. Aluminum nitride multilayer circuits are formed by combining AlN powder with yttria or calcium oxide.[17] Glass may also be added. Sintering may be accomplished in three ways;

1. Hot pressing during sintering.
2. High-temperature (greater than 1800°C) sintering without pressure
3. Low-temperature (greater than 1650°C) sintering without pressure

Tungsten or molybdenum pastes are used to withstand the high firing temperatures. Control of the processing parameters during sintering is critical if optimum properties are to be attained. A carbon atmosphere helps in attaining a high thermal conductivity by preventing oxidation of the AlN particles. Shrinkage is in the range of 15 to 20 percent.

The properties of aluminum nitride multilayer materials are summarized in Table 4.17.

4.9.5 Metal-Ceramic Composites

Metal-ceramic composites are primarily formed by one of two methods. One is to form in situ, whereby the filler and the matrix are mixed and fused together by a combination of heat and pressure. A more common approach is to form the filler into a porous shell and subsequently fill the shell with the matrix material in the molten state.

Ceramics typically have a low thermal conductivity and a low TCE, while metals have a high thermal conductivity and a high TCE. It is a logical step to combine these properties to obtain a material with a high thermal conductivity and a low TCE. The ceramic in the form of particles or continuous fibers is mixed with the metal to form a structure with the desirable properties of both. The resultant material is referred to as a *metal matrix composite* (MMC). MMCs are primarily used in applications where thermal management is critical.

The most common metals used in this application are aluminum and copper, with aluminum being more common because of lower cost. Fillers include SiC, AlN, BeO, graphite, and diamond. Compatibility of the materials is a prime consideration. Graphite, for example, has an electrolytic reaction with aluminum but not with copper.[16]

Two examples will be described here: AlSiC, a composite made up of aluminum and silicon carbide, and Dymalloy®, a combination of copper and diamond.

Aluminum silicon carbide (AlSiC) is produced by forcing liquid aluminum into a porous SiC preform. The preform is made by any of the common ceramic processing technologies, including dry pressing, slip molding, and tape casting. The size and shape of the preform is selected to provide the desired volume fraction of SiC. The resulting combination has a thermal conductivity almost as high as that of pure aluminum, with a TCE as low as 6.1 ppm/°C. AlSiC is also electrically conductive, prohibiting its use as a conventional substrate.

The mechanical properties of the composite are determined by the ratio of SiC to aluminum, as shown in Fig. 4.18.[18] A ratio of 70 to 73 percent of SiC by volume provides the optimum properties for electronic packaging.[16] This ratio gives a TCE of about 6.5 ppm/°C,

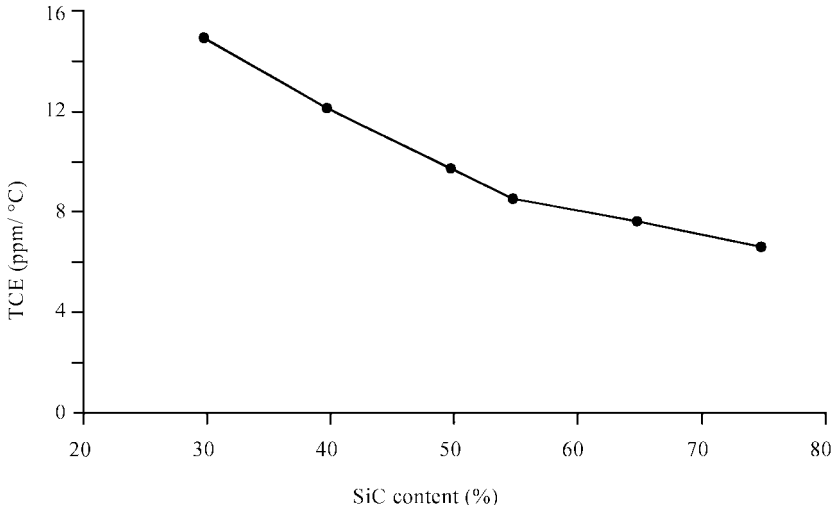

FIGURE 4.18 TCE vs. SiC content for AlSiC.

which closely matches that of alumina and beryllia. This allows AlSiC to serve as a baseplate for ceramic substrate, so that its high thermal conductivity can be used to maximum advantage.

AlSiC, being electrically conductive, may be readily plated with aluminum to provide a surface for further processing. The aluminum coating may be plated with nickel and gold to permit soldering, or may be anodized where an insulating surface is required.[21] An alternative approach is to flame-spray the AlSiC with various silver alloys for solderability.

Two other advantages of AlSiC are strength and weight. The aluminum is somewhat softer than SiC and reduces the propagation of cracks. The density is only about one-third that of Kovar®, and the thermal conductivity is over 12 times greater.

AlSiC has been used to advantage in the fabrication of hermetic single-chip and multichip packages and as heat sinks for power devices and circuits. While difficult to drill and machine, AlSiC can be formed into a variety of shapes in the powder state. It has been successfully integrated with patterned AlN to form a power module package.[21]

The TCE linearly increases with temperature up to about 350°C, and then begins to decrease. At this temperature, the aluminum matrix softens and the SiC matrix dominates. This factor is an important feature for power packaging.

The parameters of AlSiC are summarized in Table 4.18, along with those of aluminum and silicon carbide. Table 4.18 provides an interesting comparison of how the properties of a composite compare to those of the constituents.

Dymalloy is a matrix of Type I diamond and Cu20/Ag80 alloy.[22] The diamond is ground into a powder in the 6- to 50-μm range. The powder is coated with W74/Rh26 to form a carbide layer approximately 100 Å thick followed by a 1000-Å coating of copper. The copper is plated to a thickness of several micrometers to permit brazing.

The powder is packed into a form and filled in a vacuum with Cu20/Ag80 alloy, which melts at approximately 800°C. This material is selected over pure copper, which melts at a much higher temperature, to minimize graphitization of the diamond. The diamond loading is approximately 55 percent by volume.

The parameters of Dymalloy are summarized in Table 4.19.

TABLE 4.18 Typical Parameters for AlSiC (70% SiC by volume), SiC, and Aluminum

Parameter	Units	AlSiC	SiC	Al
Density	g/cm^3	3.02	3.10	2.70
Modulus of elasticity	GPa	224	407	69
Tensile strength	MPa	192	See note.	55
Thermal conductivity (25°C)	$W/(m \cdot K)$	218	290	237
TCE	$10^{-6}/K$	7.0	3.70	23
Volume resistivity (25°C)	$\mu\Omega \cdot cm$	34	$>10^{13}$	2.8

Note: Depends on method of preparation and number/size of defects.

TABLE 4.19 Typical Parameters for Dymalloy (55% Diamond by Volume)

Parameter	Units	Value
Density	g/cm^3	6.4
Tensile strength	Mpa	400
Specific heat (25–75°C)	$W \cdot s/(g \cdot °C)$	$0.316 + 8.372 \times 10^{-4}\ T$
Thermal conductivity	$W/(m \cdot K)$	360
TCE (25–200°C)	$10^{-6}/K$	$5.48 + 6.5 \times 10^{-3}\ T$

REFERENCES

1. Jerry Sergent and Charles Harper, *Hybrid Microelectronics Handbook*, 2d ed., McGraw-Hill, New York, 1995.
2. Richard Brown, "Thin Film Substrates," in *Handbook of Thin Film Technology*, Leon Maissel and Reinhard Glang (eds.), McGraw-Hill, New York, 1971.
3. Philip Garrou and Arne Knudsen,"Aluminum Nitride for Microelectronic Packaging," *Advancing Microelectronics*, vol. 21, no. 1, January–February 1994.
4. C. G. M. Van Kessel, S. A. Gee, and J. J. Murphy, "The Quality of Die Attachment and Its Relationship to Stresses and Vertical Die-cracking," *Proc. IEEE Components Conf.*, 1983.
5. A. Winkleman and O. Schott, *Ann. Phys. Chem*., vol. 51, 1984.
6. Jerry Sergent and H. Thurman Henderson, "Double Injection in SemiInsulators," *Proceedings, Solid State Materials Conference*, 1973.
7. George Harman, "Wire Bond Reliability and Yield," ISHM Monograph, 1989.
8. Craig Johnston, Robin A. Susko, John V. Siciliano, and Robert J. Murcko, "Temperature Dependent Wear-Out Mechanism for Aluminum/Copper Wire Bonds," *Proceedings, ISHM Symposium*, 1991.
9. Ellice Y. Yuh, John W. Lau, Debra S. Horn, and William T. Minehan, "Current Processing Capabilities for Multilayer Aluminum Nitride," *International Journal of Microelectronics and Electronics Packaging*, vol. 16, no. 2, 2d quarter, 1993.
10. Nobuyiki Karamoto, "Thin Film and Co-Fired Metallization on Shapal Aluminum Nitride," *Advancing Microelectronics*, vol. 21, no. 1, January/February, 1994.
11. Paul W. May, "CVD Diamond—A New Technology for the Future?" *Endeavor Magazine*, vol. 19, no. 3, 1995.
12. Ajay P. Malshe, S. Jamil, M. H. Gordon, H. A. Naseem, W. D. Brown, and L. W. Schaper, "Diamond for MCMs," *Advanced Packaging*, September/October, 1995.

13. Thomas Moravec and Arjun Partha, "Diamond Takes the Heat," *Advanced Packaging*, special issue, October 1993.
14. Koichi Hirano, Seiichi Nakatani, and Jun'ichi Kato, "A Novel Composite Substrate with High Thermal Conductivity for CSP, MCM, and Power Modules," Proceedings, *International Microelectronic and Packaging Society*, 1998.
15. C. De Johghe, T. Mitchell, W. J. Moberly-Chan, and R.O. Ritchie, "Silicon Carbide Platelet/Silicon Carbide Composites," *Journal American Ceramics Society*, 1994.
16. S. Fuchs and P. Barnwell, "A Review of Substrate Materials for Power Hybrid Circuits," *IMAPS Journal of Microcircuits and Electronic Packaging*, vol. 20, no. 1, 1st quarter, 1997.
17. Mitsuru Ura and Osami Asai, Internal Report, Hitachi Research Laboratory, Hitachi Industries, Ltd.
18. Jerry E. Sergent, "Materials for Multichip Modules," *Electronic Packaging and Production*, December 1996.
19. Philip E. Garrou and Iwona Turlik, *Multichip Module Technology Handbook*, McGraw-Hill, New York, 1998.
20. M. K. Premkumar and R. R. Sawtell, "Alcoa's AlSiC Cermet Technology for Microelectronics Packaging," *Advancing Microelectronics*, July/August, 1995.
21. M. K. Premkumar and R. R. Sawtell, "Aluminum-Silicon Carbide," *Advanced Packaging*, September/October 1996.
22. J. A. Kerns, N. J. Colella, D. Makowiecki, and H. L. Davidson, "Dymalloy: A Composite Substrate for High Power Density Electronic Components," *International Journal of Microcircuits and Electronic Packaging*, vol. 19, no. 3, 3d quarter, 1996.

CHAPTER 5

INORGANIC GLASSES—STRUCTURE, COMPOSITION AND PROPERTIES

Arun K. Varshneya and Thomas P. Seward III
New York State College of Ceramics
Alfred University
Alfred, New York

5.1 FUNDAMENTALS OF THE GLASSY STATE

5.1.1 Definitions of Glass

The origin of the word *glass* is the late Latin term *glæsum* used to refer to a lustrous and transparent or translucent body. Glassy substances are also called *vitreous*, originating from the word *vitrum*, again denoting a clear, transparent body. Although glass became a popular commodity in the growth of civilization, perhaps because of its transparency, luster (or shine), and durability, the current understanding of glass no longer requires any of these characteristics to distinguish it from other substances. Glass can be inorganic (non-carbon-based) as well as organic (carbon-based), and fusion is not the only method to make a glass. Thus, the old ASTM definition that *glass is an inorganic product of fusion which has been cooled to a rigid condition without crystallizing* is not appropriate. The current chapter, however, is limited to inorganic oxide glasses made by fusion techniques only, which form the bulk of the commercial tonnage.

According to Zachariasen,[1] glass is a *substance [which] can form extended three-dimensional networks lacking periodicity with an energy content comparable with that of the corresponding crystal network*. In essence, the *density* and the mechanical properties of glass are solid-like; however, the atoms form a continuous random network such that *the unit cell* (in crystal structure terminology) *is infinitely large, containing an infinite number of atoms*. Thus a working definition of glass is that *it is a solid with a liquid-like structure*.

Unlike a crystal, glass may not be represented by a simple chemical formula. There are no restrictions with regard to the relative numbers of chemically different atoms other than the fact that the valences and/or coordination requirements may need to be satisfied. Unlike a crystal, glass does not have a sharp melting point when heated. The seemingly rigid solid gradually softens and flows at higher temperatures. At ambient temperatures, however, the

viscosity of glass may be sufficiently high that measurable flow does not occur over millennia—certainly not over practical time scales in typical laboratory experiments. It is doubtful that glass windows in building structures of the middle ages have flowed to become thicker at the bottom. Chunks of glass do not have habit planes. Nor does glass have identifiable cleavage planes. In the absence of externally applied mechanical, electrical, thermal, magnetic, and gravitational fields, *the properties of glass are essentially isotropic like those of a typical liquid*.

In principle, glasses and *amorphous solids* make up a class of substances called *noncrystalline solids.* Both glass and amorphous solids are "x-ray amorphous." The distinction from an amorphous solid is made to recognize the smooth transition of glass to liquid state on heating; amorphous solids appear to crystallize before transformation to the liquid state. Care should, however, be taken in not confusing glass with an *amorphous powder*, a term commonly used to refer to a random assemblage of finely divided crystals.

5.1.2 Methods of Making Inorganic Glasses

The most common method for making glass is to:

1. Fuse various raw materials in appropriate proportions together with the application of heat,
2. Gather and form into useful products,
3. Cool subsequently at a rate fast enough to avoid distortion of the shape yet slow enough to avoid cracking.

In reality, a substance may, however, be brought to a glassy state or amorphous state from any of the three equilibrium states of matter—solid, liquid, or gas. A crystal can be made glassy by the passage of the shock wave that follows, for instance, a meteoritic impact. Some minerals have natural radioactivity with heavy particle emission. Such emitted particles may have sufficient momentum to displace the host crystal atoms from their regular periodic locations. Over geological times, such minerals undergo amorphization, and are called *metamict* solids. Vapors of many substances when allowed to condense on a cold substrate often yield an amorphous structure. The structure may be a glass or an amorphous solid depending on experimental parameters. Inorganic glasses may also be obtained by

1. Hydrolyzing an alcoholic solution of an organometallic compound,
2. Stirring the hydrolyzed product to allow rapid chelation to a *gel* state,
3. Drying the gel mass to drive off the organics,
4. Sintering at an elevated temperature to obtain a compact.

This method, called the *sol-gel route* to glassmaking, is often used to deposit thin films such as *antireflection coatings.*

5.1.3 The Volume-Temperature Diagram

For a more in-depth reading on this subject, see Varshneya in the Bibliography. From a thermodynamic viewpoint, *glass is not the fourth state of matter.* This may be understood by examining the volume-temperature (*V-T*) relationship of a typical glass-forming melt upon cooling, as shown in Fig. 5.1.

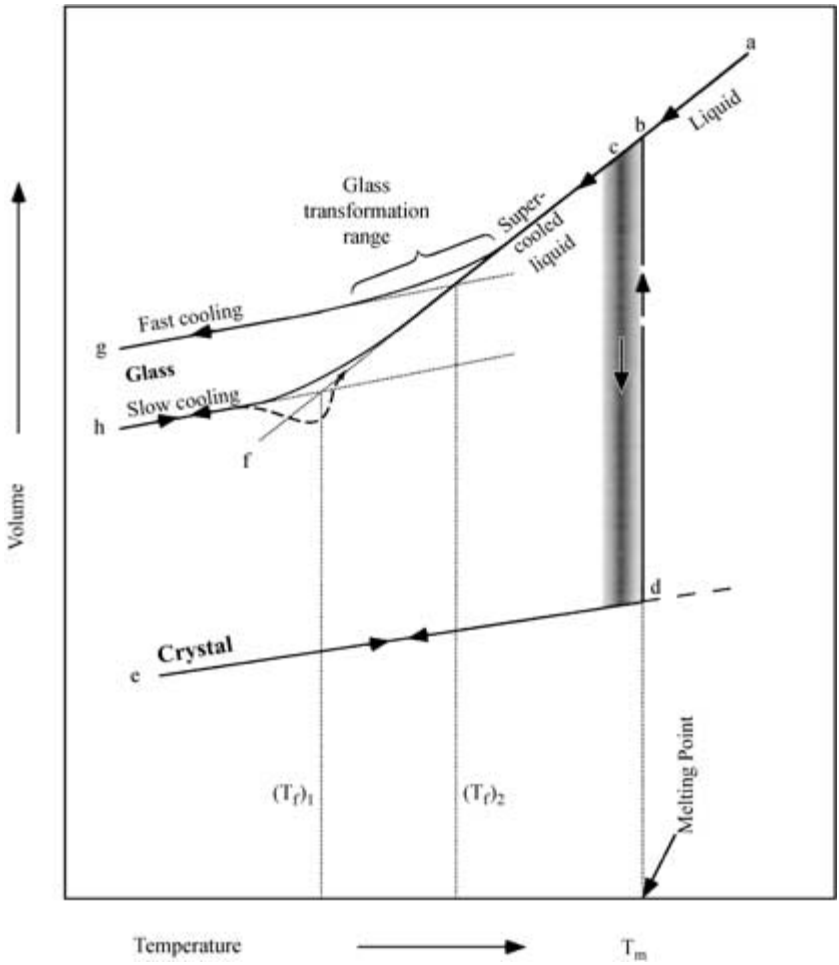

FIGURE 5.1 The volume-temperature diagram. (*After A. K. Varshneya, Fundamentals of Inorganic Glasses, Fig. 2-1, p. 15, Academic Press, 1994.*)

When a melt is cooled from a high temperature state, point *a*, the volume *V* typically shrinks along the line *ab*. Although *b* is the thermodynamic freezing point of the melt (or the thermodynamic melting point T_m of a crystal of the same composition), crystallization may only occur if, and only if, (1) there is sufficient *nucleation* rate *I* followed by (2) a significant *crystal growth rate u*. The dependence of the nucleation *rate I* and the crystal growth rate *u* with temperature *T* is shown in Fig. 5.2. Note that both the rates are zero at T_m, hence no crystallization is expected at T_m. With increasing *supercooling* (also referred to as *undercooling*), the two rates begin to increase at varying rates. There may be some overlap in the curves, shown hatched in Fig. 5.2, leading to crystallization over a range of temperatures, shown shaded in Fig. 5.1, with *c* being the location with the highest probability of crystallization. On crystallization at some point in the shaded region in Fig. 5.1,

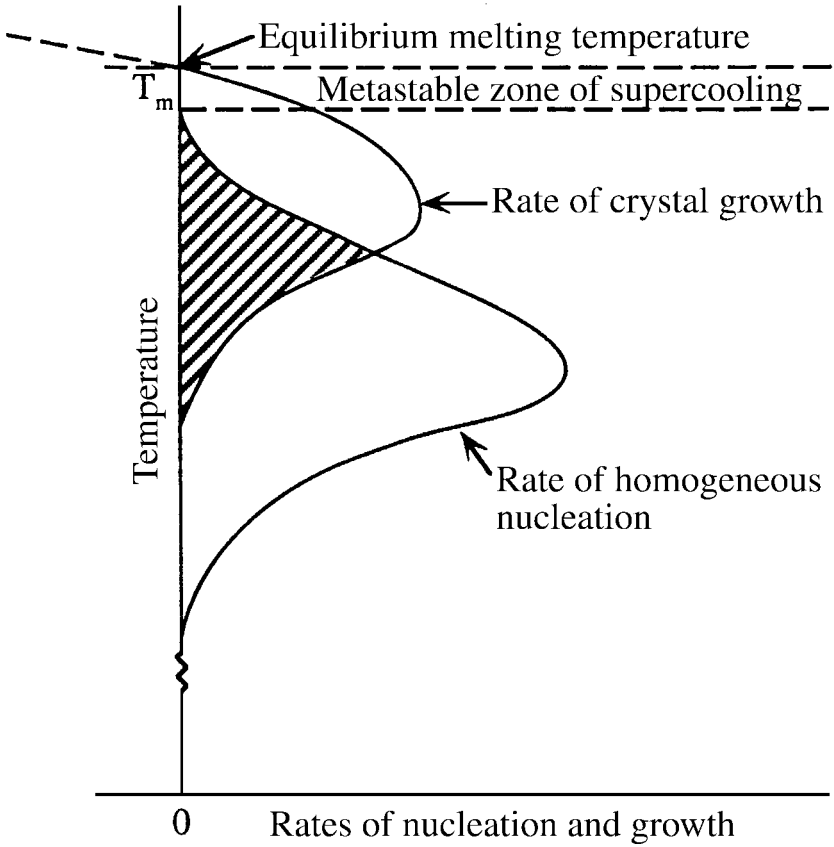

FIGURE 5.2 Plot of nucleation and crystal growth rates as a function of temperature.

the mass shrinks in volume discontinuously without changing its temperature (a *first-order thermodynamic transition*), followed by shrinkage along the crystal state line *de* on further cooling. (There are some exceptions, for instance, water near the ice point, where the liquid actually expands on cooling and on crystallization). In the absence of a significant overlap between the nucleation and the crystal growth rate curves, the liquid at *b* passes monotonically into a *supercooled liquid* state without the appearance of crystals. Further cooling brings about increases of viscosity at exponential rates such that the atomic configurations of the liquid are increasingly unable to redistribute themselves into a volume required by the equilibrium equation of state for the liquid. This implies that the state begins to depart from the extrapolated line *bcf*, and generates smooth curves of the type *bcg* or *bch*, depending on the cooling rate. The extent of departure per incremental cooling increases until the state line becomes nearly parallel to the crystal line. For most practical purposes, *the material now appears solid-like.* The contraction of volume corresponds essentially to the interatomic separation. *This is the beginning of the glassy state.* The mass, when cooled faster, is brought to a glass at point *g* having a volume higher (again, with some exceptions) than that at *h*, which was attained using a slower cooling rate. The curved region joining the glassy state and the supercooled liquid state is called the *glass transformation range* or the

transition range. The transition from the supercooled liquid to glassy state does not occur at a sharp temperature; rather it occurs smoothly over a range of temperatures. It is, however, customary to locate a *glass transition temperature* T_g in the transformation range at the intersection of the glass line with a tangent to the steepest portion of the transition curve.

The temperature T_f corresponding to the intersection of the extrapolated glassy state line and the supercooled liquid state line is called the *fictive temperature*. It may be assumed that the liquid structure at T_f is instantly frozen into the solid glass. To describe this approximately, one may say that the structure of the liquid relaxes rapidly at first, the rate of such *relaxation* slowing down exponentially because of exponentially increasing viscosity with falling temperatures. The structure ultimately freezes at T_f into the glassy state. In reality, the structure at room temperature is a manifestation of the entire cooling history (called the *thermal history*); hence a single fictive temperature as an *internal order parameter* to uniquely describe the structure of glass is only approximate. No further structural relaxation occurs in the glassy state. In the liquid state, the atomic motions are fast enough to bring about changes in configurations extremely rapidly (in milli-, micro-, or nanoseconds). In the solid state, structural changes are so sluggish that no perceptible changes are expected to occur even over millennia. Thus, the glass transition range is characterized as the region of temperatures where the structure of the mass is continuously relaxing to greater equilibrium as we observe it. We may say that *glass is in unstable equilibrium with respect to the supercooled liquid, which itself is in metastable equilibrium with respect to the corresponding crystal.* Whereas both the crystal and the liquid (including the supercooled liquid) can be treated thermodynamically as *equilibrium states* in terms of three state parameters—pressure P, volume V, and temperature T—of which only two are independent, it takes at least one more "structural order" parameter, such as the fictive temperature, to attempt a thermodynamic equation of state for the "unstable" glassy state.

The irreversibility of time forces glass to continuously approach the liquid and not vice versa. Thus, reheating the glass from h causes the state to reproduce the glass line only through relatively low temperatures where the mass is a solid. On heating to a point where perceptible viscous flow (actually, structural change) may occur, the state moves to reduce the disparity between itself and its corresponding supercooled liquid state. In Fig. 5.1, this behavior is shown by the dashed curve heading downward, overshooting the extrapolated liquid line, and ultimately recovering to merge into it at higher temperatures. The volume of glass generally shrinks somewhat as it heats through the lower regions of the transition range. It should be emphasized that glass during reheating may *never* reproduce its cooling path regardless of any practical rates.

The volume of glass is that occupied by the crystalline lattice plus a *free volume* corresponding to the need of a long-range disorder. Heating of glass allows the atoms to occupy other "disordered" sites with gradually expanding free volume and rapidly increasing fluidity. *On reaching the "equilibrium" supercooled liquid state, all thermal history is wiped out.*

Although the second-derivative thermodynamic properties such as *heat capacity, thermal expansion coefficient*, and *isothermal compressibility* display steep changes at the transition (shown in subsequent sections), *it is generally agreed that the glass transition is not a second-order thermodynamic transition, and is best referred to as a "freezing-in" transition.* A residual entropy at 0 K is expected; it does not violate the third law of thermodynamics on grounds that glass is not an equilibrium substance.

In multicomponent systems, the temperature T_m is generally identified as the *liquidus temperature.* At temperatures above the liquidus, the system is completely liquid. Growth of one crystalline phase may occur just below the liquidus. As the temperature is lowered further, more crystalline phases may grow. Experimental measurement of the liquidus temperature is often desirable for large-scale glass manufacturing to avoid problems due to *devitrification* in the glass tank delivery system, or in the finished product, where they

appear as inclusions often termed *stones*. A convenient method is described in ASTM C829-81, where grains of glass are placed in a suitable boat and heated inside a gradient furnace for a desired period of time. Liquidus temperature is located by visually judging the demarcation between clear glass and the appearance of opacity.

5.2 GLASS FORMATION

5.2.1 Structural Concepts of Glass Formation

A variety of materials form glass readily by cooling from the molten state. Some of these are listed in Table 5.1 (purely organic glasses are excluded from this table). Many of these require quenching (such as splat cooling). It may be recognized that the glass formation range is quite extensive. Many other materials, on the other hand, form a noncrystalline solid only when special techniques, such as cooling from the vapor state, are used. A prime example of this is a-Si:H (amorphous hydrogenated silicon), used extensively for solar cell applications. It is not clear whether most of these amorphous solids are, in fact, glassy solids with a thermodynamic continuity to a supercooled liquid state.

The question of what characteristics make a substance a ready glass former has been the subject of intense research. These are discussed in detail in Ref. 2. Historically, the most prevalent thoughts were advanced by Zachariasen, who suggested four rules for an oxide, A_mO_n, to form a glass readily:

1. The oxygen is linked to no more than two atoms of A.

2. Coordination of the oxygen about A is small, say 3 or 4.

3. Oxygen polyhedra share corners, and not edges or faces.

4. At least three corners are shared.

Application of the above "random network theory" concepts suggests why oxides such as SiO_2, GeO_2, and B_2O_3, where the oxygen formed tetrahedra or triangles, are ready glass formers, and why compounds such as A_2O and AO have to be ruled out. Figure 5.3 shows a two-dimensional representation of the atomic arrangements in an A_2O_3 glass versus its corresponding crystalline form. (The figure may also correspond to AO_2, where A is tetrahedrally bonded to oxygens, the fourth oxygen being out of the plane of the paper.) Whereas the local oxygen coordination is almost the same as that in a corresponding crystalline solid, the intermediate range order described by ring structures clearly differs considerably between the crystalline and the glassy forms. The glass network consists of holes that are larger than those in the crystal. (The aggregate of the holes yields the free volume discussed above.) When a compound such as Na_2O is introduced in silica, the arrangement of atoms in a two-dimensional plane is believed to look somewhat like that in Fig. 5.4. Those oxygens, which connect two silicon tetrahedra at corners, are called *bridging oxygens* (BOs). Some oxygens are linked to only one silicon; these are called the *nonbridging oxygens* (NBOs). Since oxygen is a bivalent ion, its connection to only one silicon ion leaves one negative charge, which is satisfied by a univalent positive sodium ion in the interstitial spaces.

Much of the early criticism of Zachariasen was based on the discussion of how random is random and, of course, the observation that elements such as S and Se make good glasses yet they did not fit Zachariasen's criteria. Electron microscopy of several otherwise transparent glasses has shown that glass may not be as random as Zachariasen thought and that some type of phase segregation exists in many glasses.

TABLE 5.1 Glasses Formed by Cooling from the Liquid

Elements
P, S, Se, Te(?)
Oxides
B_2O_3, SiO_2, GeO_2, P_2O_5 (primary glass formers)
Borates, silicates, phosphates, germanates, etc.
(compounds of the primary glass formers with a wide range of oxides including those of alkalis, alkaline earth, water, rare earths, and actinides)
By splat cooling: As_2O_3, Sb_2O_3, In_2O_3, Tl_2O_3, SnO_2, PbO_2, SeO_2, V_2O_5
Conditional (require small amounts of other oxides to stabilize the structure):
TiO_2, TeO_2, SeO_2, Al_2O_3, Ga_2O_3, MoO_3, WO_3, Bi_2O_3, Nb_2O_3, SO_3
Sulfides, selenides, tellurides (chalcogenides)
various compounds with Group 13, 14, and 15 elements
Halides
BeF_2, AlF_3, $ZnCl_2$, Ag(Cl/Br/I), Pb(Cl_2/Br_2/I_2), and mixtures
$BiCl_3$-KCl
Heavy metal fluoride glasses (HMFG):
Mixtures of ZrF_4/HfF_4 (major constituent), BaF_2, LaF_3, YF_3, AlF_3, NaF
Chalcohalides and chalcooxides
mixtures of chalcogenides (major constituent) with halides and oxides
Halooxides
(Li/Na/K)F-(Mg/Ca)O
CaF_2-(Zr/Th)O_2
Na_2BeF_4-Ca_2SiO_4
15%(Cl/Br) in borosilicates
Nitrates
KNO_3-$Ca(NO_3)_2$ and similar binary mixtures
Sulfates
$KHSO_4$, K_2SO_4-$CoCl_2$
Carbonates
K_2CO_3-$MgCO_3$
Complex oxyflurophosphates
$NH_4H_2PO_4$-PbF_2-SnF_2-SnO_2
Acetates, formates, and thiocyanates
(K/Na/Li)CH_3COO-(Pb/Zn/Cd/Ca)$(CH_3COO)_2$
$NaHCO_2$
$Ca(SCN)_2$-KSCN
Dichromates
20-40%$Li_2Cr_2O_7$-$Na_2Cr_2O_7$; 40-50%$Li_2Cr_2O_7$-$K_2Cr_2O_7$
Hydrates
$Ca(NO_3)_2 \cdot 4H_2O$
$(Ca/Cd)(NO_3)_2 \cdot 4H_2O$-(Li/Na/K/Rb/Cs/$NH_4$)$NO_3$
$Ca(NO_3)_2 \cdot 4H_2O$-(Zn/Co/Ni)Cl_2
$Ca(NO_3)_2 \cdot 4H_2O$-KCNS
Aqueous salt solutions
KOH, LiCl, (Be/Ca/Mg/Zn/Co/Ni/Cu/Mn)$(NO_3)_2$
Glassy metals (by splat cooling only)
$(Au/Pd)_4Si$, Ni_4P, Nb_3Ni_2, W_9Fe_{11}, $Zr_{76}Fe_{24}$
$Fe_{40}Ni_{40}P_{14}B_6$
$CoGd_2$, $MgCa_2$, Al_3La_7, Cr_3U_7

Source: Compiled from R. H. Doremus, *Glass Science*, p. 12, Wiley-Interscience, New York, 1973, and N. J. Kreidl in *Glass Science and Technology*, vol. 1, pp. 105–299, D. R. Uhlmann and N. J. Kreidl, (eds.) Academic Press, New York, 1983.

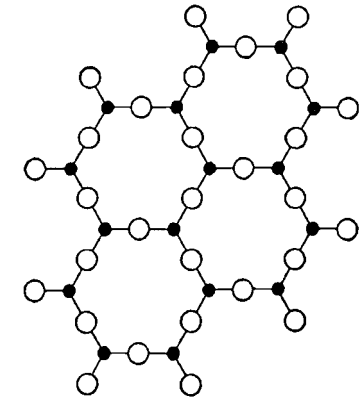

(a)

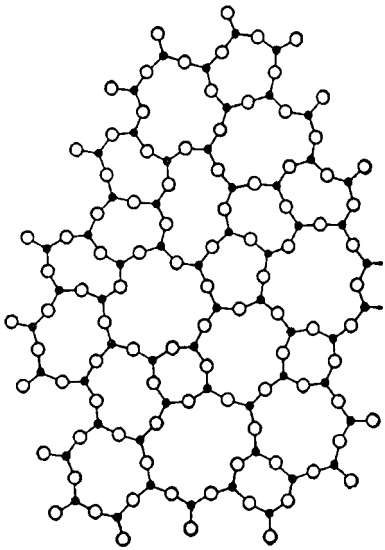

(b)

FIGURE 5.3 A two-dimensional representation of A_2O_3: (*a*) crystal and (*b*) glass.

On the basis of the calculation of single bond strengths in an oxide AO_x, Sun suggested that oxides such as B_2O_3, SiO_2, GeO_2, P_2O_5, V_2O_5, and As_2O_5 should be classified as *glass network formers* (NWFs), as they ought to be able to form the glass skeleton on their own. Oxides such as Li_2O, Na_2O, K_2O, CaO, BaO, ZnO, CdO, Ga_2O_3, In_2O_3, and PbO_2 were classified as glass *network modifiers* (NWMs); the cations of these oxides occupied the interstitial spaces in the network formed by the NWF oxides and, hence, acted as network

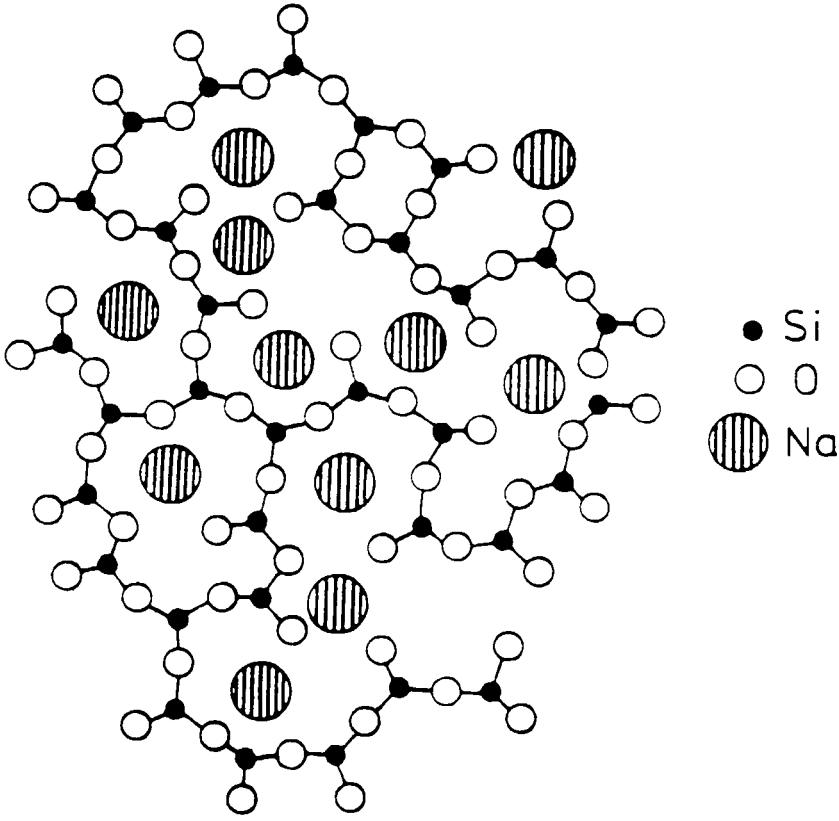

FIGURE 5.4 A two-dimensional representation of a sodium silicate glass.

modifiers only. Oxides such as BeO, Al_2O_3, TiO_2, ThO_2, and ZrO_2 were termed *intermediates*; these did not make glass readily on their own, but did make a glass when present in large quantities mixed with the NWF or NWM oxides.

It has also been recognized that glass formation in multicomponent mixtures is easier when the composition is near the eutectic region on the phase diagrams.

5.2.2 Kinetic Considerations

It is now acknowledged that *any substance may be brought to glassy state provided that its melt is cooled at a rate exceeding the critical cooling rate*, as shown in the *time-temperature transformation* (T-T-T) diagram, Fig. 5.5. This is the kinetic theory of glass formation. Figure 5.5 is constructed by computing the time needed to develop an experimentally discernible amount of crystals (typically 1 ppm) in a molten mass in which the nucleation and crystal growth curves are given by Fig. 5.2. A nose-type curve develops. The critical cooling rate is the line drawn sloping downward from T_m that is tangent to the nose at T_n. If experimental cooling is fast enough, i.e., if the line is steep enough, then it may stay to the

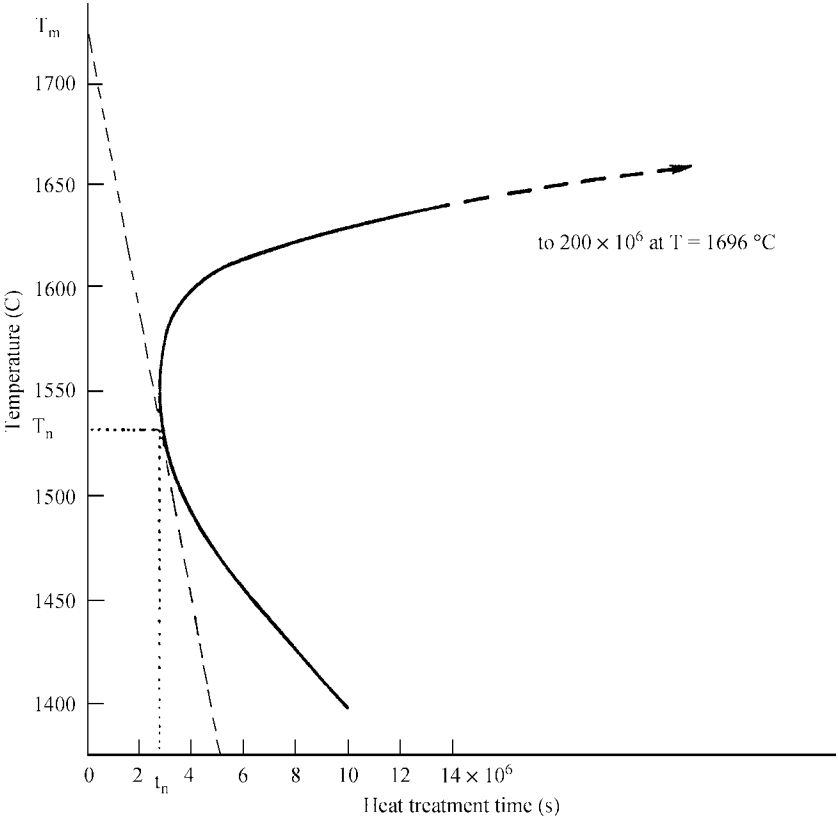

FIGURE 5.5 A typical time-temperature-transformation (T-T-T) diagram for glass formation. (*After D. Uhlmann, J. Non-Cryst. Sol., vol. 7, 1972, p. 337.*)

left of the nose and perceptible crystallization may not develop. On the other hand, the cooling line corresponding to a slowly cooled mass would intersect the nose, and crystallization (or *devitrification*) would occur. Critical cooling rates, given by the slope $(T_m - T_n)/t_n$, where t_n is the time corresponding to T_n, for some substances are shown in Table 5.2. Note that even metals could be brought to a glassy state by cooling at sufficiently fast rates. The critical cooling rates are affected greatly by the presence of foreign contamination such as crucible walls.

5.2.3 Ranges of Glass Formation

Some of the materials that are able to form glass are summarized in Tables 5.1 and 5.2. Ranges of ready glass formation in several binary systems are shown in Table 5.3. Nearly all of these glasses have little commercial use, primarily because of poor chemical durability. More than 90 percent of the commercial tonnage is oxide silicate glasses, which are generally multicomponent. These systems are high-silica glasses (including vitreous silica,

TABLE 5.2 Examples of Critical Cooling Rates (°C/s) for Glass Formation

Material	Homogeneous nucleation	Heterogeneous nucleation contact angle (degrees)		
		100	60	40
SiO_2 glass	9×10^{-6}	10^{-5}	8×10^{-3}	2×10^{-1}
GeO_2 glass	3×10^{-3}	3×10^{3}	1	20
$Na_2O \cdot 2SiO_2$ glass	6×10^{-3}	8×10^{-3}	10	$3 \times 10^{+2}$
Salol	10			
Water	10^{7}			
Ag	10^{10}			
Typical metal	9×10^{8}	9×10^{9}	10^{10}	5×10^{10}

After P. I. K. Onorato and D. R. Uhlmann, *J. Non-Cryst. Sol.*, vol. 22, no. 2, 1976, pp. 367–378.

TABLE 5.3 Range (mol %) of Glass Formation in Binary Systems

	SiO_2	B_2O_3	P_2O_5
Li_2O	0–46	0–44	0–40
Na_2O	0–58	0–38; 66.5–71.5	0–60
K_2O	0–42	0–38	0–47
Rb_2O	0–32		
Cs_2O	0–46		
Tl_2O	0–55	0–45	
MgO		43–44	0–60
CaO	40–58	28–41	0–56
SrO	20–40	24–43	0–56
BaO	28–40	17–40	0–58
ZnO		44–63.6	0–64
PbO	20–75	20–76.5	0–62
Al_2O_3	0–24		
B_2O_3	0–100		
Bi_2O_3	25–65	22–65.3	
GeO_2	0–100		
TiO_2	2.4–9		
P_2O_5	17.4–64.2		

Silicate data compiled from N. Bansal and R. H. Doremus, *Handbook of Glass Properties*, Academic Press, Orlando, 1986.

Borate and phosphate data compiled from M. Imaoka, in *Advances in Glass Technology*, Part 1, pp. 149–164, Plenum Press, New York, 1962.

which is the only single-component system), *soda lime silicates*, *sodium borosilicate*, *aluminosilicates*, and *lead silicate/borates.* The balance tonnage comprises borate and *phosphate glasses* and several nonoxide glasses such as *heavy metal fluorides, glassy metals, chalcogenides*, and *amorphous semiconductors.* Commercial silicate glasses are discussed in Chap. 6.

5.3 THE MICROSTRUCTURE OF GLASS

5.3.1 Phase Separation and Liquid Immiscibility

Even the most transparent-appearing glasses may possess a phase-separated structure on a scale of a few tens to hundreds of angstroms (tens of nanometers). Electron microscopy replicas of freshly fractured multicomponent glass surfaces shows that, instead of the generally featureless image expected for single-component glasses, two different-appearing types of microstructure are often found, as shown in Fig. 5.5. In Fig. 5.6*a*, the glass consists of small, nearly spherical droplets of a particular composition dispersed in a matrix of seemingly homogeneous material. In reality, the composition of the matrix surrounding the droplets varies during early stages of phase separation until the growth of the droplets is complete and the matrix no longer maintains a concentration gradient. Often, however, the growth is incomplete because of the continuous cooling of the melt during the glass manufacturing process.

In Fig. 5.6*b*, the microstructure appears in the form of two highly intertwined worm-like matrices of relatively uniform dimensions (widths on the micrograph). The compositional differences between adjacent "worms" grow with time until equilibrium compositions (those having the lowest free energy) are achieved, or until the phase separation is arrested by the cooling process.

The driving forces for the observed phase separation are believed well understood in terms of the thermodynamics of mixing. When the heat of mixing of the individual components is positive, there exists a region of metastable (or sometimes stable) liquid-liquid *immiscibility* on the phase diagram, Fig. 5.7. The boundary is shown as the *immiscibility dome*.

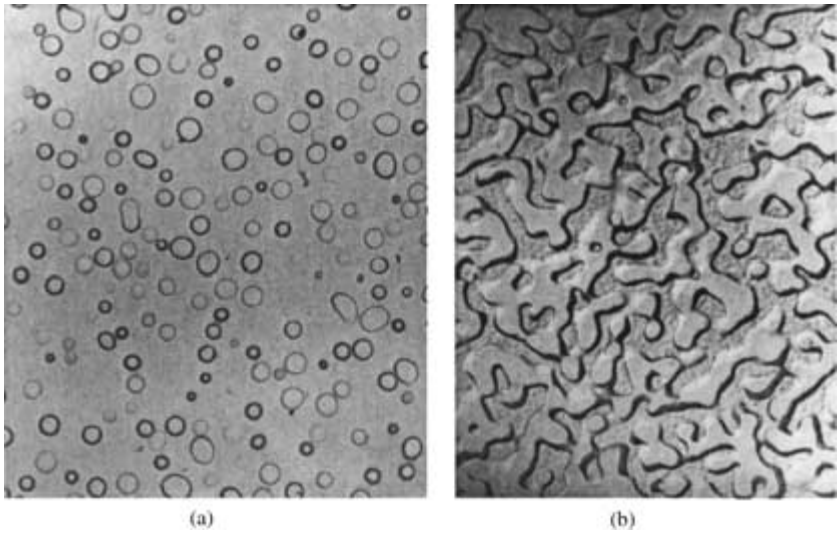

FIGURE 5.6 Observed microstructures in glass: (*a*) nucleated growth type phase separation; (*b*) phase separation by the spinodal mechanism. (*After H. Rawson, Properties and Applications of Glass, Fig. 10, Elsevier Science Publishers, Netherlands, 1980.*)

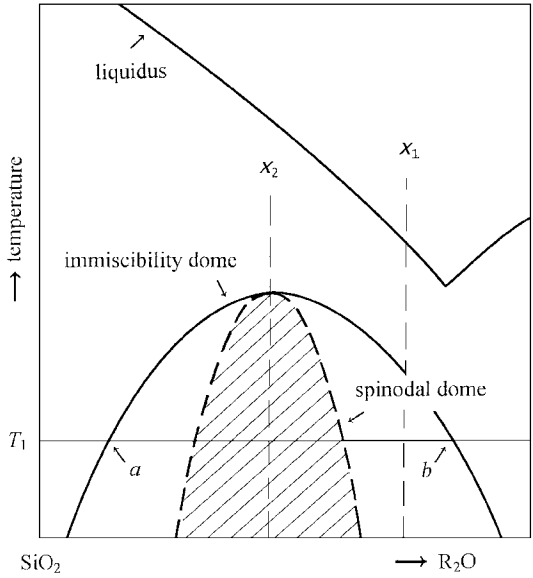

FIGURE 5.7 Location of immiscibility and spinodal domes in phase diagrams.

Within the immiscibility dome, there exists another dome called the *spinodal region*, or *spinodal dome*. Phase separation by a nucleation-and-growth (*droplet*) mechanism takes place when the composition X_1 of the parent liquid mass and the temperature T_1 of heat treatment are such that the system lies between the two domes, giving rise to discrete second-phase particles of composition *a* while the matrix moves towards *b*.

Worm-like configurations appear when the system lies inside the spinodal dome. At least two possibilities exist for how such microstructure might develop. First, nucleation and growth of very small droplets begins as the system cools through the immiscibility dome, but before it reaches the spinodal region. As the system cools further and enters the spinodal region, the droplets grow and connect to each other as dictated by occupied volume considerations. (If the system composition X_2 lies close to that of the immiscibility dome peak, the volume ratio will be about 50:50.) According to the second possibility, the true spinodal mechanism, the separation begins everywhere essentially simultaneously, with the composition differences between worm-like regions beginning as infinitesimal wave-like composition fluctuations, and growing with time until the equilibrium compositions are reached. Both mechanisms can explain the observed microstructure, and from a practical (commercial) viewpoint, the consequences are the same.

The temperature range for liquid-liquid phase separation (metastable immiscibility) in glass is generally below the liquidus temperature and above the glass transition. Immiscibility in glass is a widely occurring behavior; the microstructure can clearly affect the way glass will behave, for instance, with respect to corrosive media. Both types of phase separation behavior are easily observed in alkali borosilicate glasses. The phase diagram for sodium borosilicate system is shown in Fig. 5.8. The top of the immiscibility dome is located at

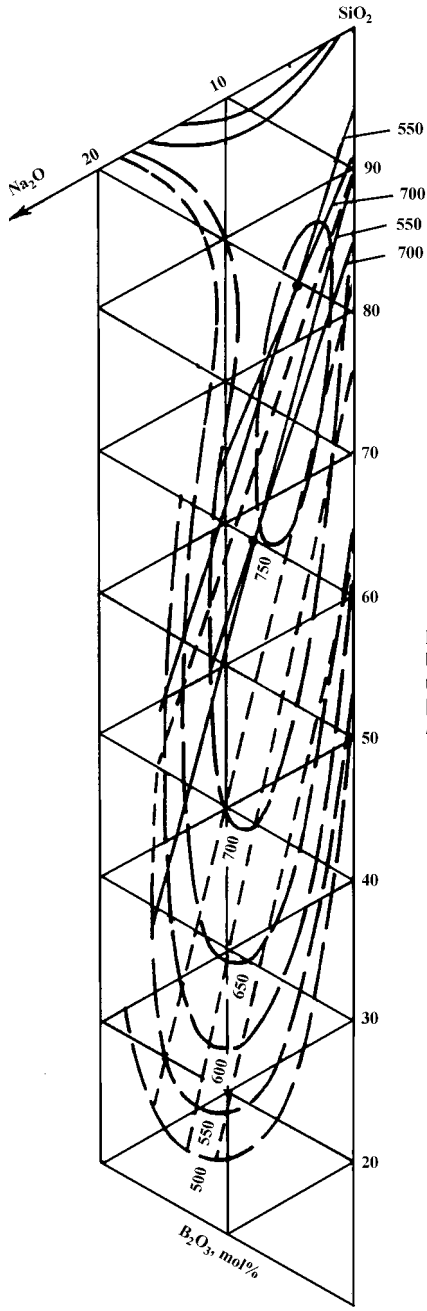

FIGURE 5.8 Liquid immiscibility in the sodium borosilicate system. Curves are isothermal sections of the immiscibility dome at temperatures marked in °C. [*After O. V. Mazurin, Phase Separation in Glass, Fig. 59. Elsevier Science Publishers, Netherlands, 1984.*]

around $5Na_2O \cdot 23B_2O_3 \cdot 72SiO_2$ (mol%) composition with a critical temperature of 765°C. Compositions within the spinodal dome [5–10 $Na_2O \cdot$ 20–35 $B_2O_3 \cdot$ 55–75 SiO_2 (mol%)] separate at 500 to 600°C into two continuous intertwined matrices, one of which is a 96 percent silica and the other a sodium borate. The latter is dissolved away by using acid (for instance, 3N H_2SO_4 at 90°C), which leaves behind the porous silica skeleton. The "thirsty silica" thus produced may be used as a molecular sieve, or as a time-release encapsulating container. Upon sintering, one obtains a dense glass sold under the trade name Vycor® by Corning Inc. Heat-resistant Pyrex® glasses of the borosilicate type have a highly dispersed separation of tiny sodium borate droplets, with the matrix made silica-rich after separation. The increase in the matrix silica actually raises the chemical durability; hence, these glasses are often utilized for chemical laboratory glassware.

5.3.2 Controlled Crystallization of Glass

It may be noted in Fig. 5.2 that the nucleation rate curve has been drawn at temperatures lower than those for crystal growth rate. This is close to the reality. It is possible for the two curves to be separated enough such that there is little overlap, and hence little chances of crystallization during the first cool-down (since, nucleation must precede crystal growth). The cooled mass, however, does have nuclei grown within the bulk, and a reheat to the crystal growth regions can readily bring about crystallization. Such material is termed *glass-ceramic*. In reality, the mass may be mostly crystalline ceramic particles surrounded by a vitreous layer. The process yields essentially monosized crystals randomly distributed through the volume with a high number density. These facts, combined with the absence of porosity, yield a mass that has exceptional strength characteristics. A typical time-temperature cycle to form a glass-ceramic is shown in Fig. 5.9. Often, the nucleation step is aided by the presence of small amounts of nucleating agents such as TiO_2, P_2O_5, ZrO_2, and $ZrO_2.SiO_2$. Several quite successful commercial products are now available that utilize this controlled crystallization technique; Corningware® and Visionware® are two examples. Because of the large increase in viscosity after the "ceramming" step, crystallizable (or devitrifiable) sealing glass is quite useful. The front panel of a television is usually sealed to the back funnel by a devitrifiable sealing glass, which enables an important baking step to be carried out after the sealing. Some of the glass-ceramic products are discussed in Sec. 6.2.7 (Chap. 6).

5.4 ATOMIC ARRANGEMENTS IN GLASS

5.4.1 Structure of Silica Glass

As indicated above, the atomic arrangements in glass are similar to those in a solid except that there is no long-range order. Some similarity to a crystalline type of order, perhaps out to about 10 to 20 Å, is actually expected in most multicomponent glasses. Figure 5.10 shows the arrangement of atoms in fused silica glass in a "pancaked" version. The building block (Fig 5.10*a*) is an SiO_4 tetrahedron comprising a silicon ion bonded to four oxygens. One negative charge of each of the four oxygens satisfies the four positive charges on the silicon, which leaves each oxygen to form a corner shared with an adjacent tetrahedron, thus acting as a bridging oxygen (BO). Corner sharing allows three angles, shown

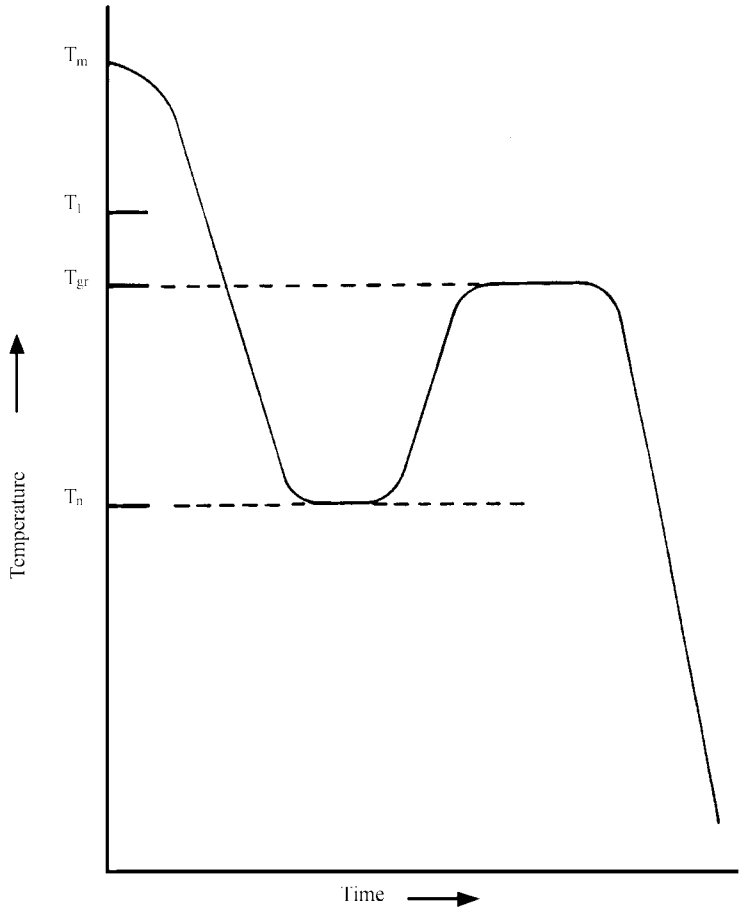

FIGURE 5.9 A typical time-temperature curve for forming a glass-ceramic.

in Fig 5.10*b*—the bond angle -Si-O-Si-, the azimuthal angle α_1, and the twist angle α_2—to assume random values over a large range. Variations in these angles create a random, three-dimensional, structure lacking long-range periodicity, as shown in Fig 5.10*c*. Randomness is described in terms of the ring statistic, which is the number of silicon atoms contacted when a spider takes the shortest path to come back to its origin atom. Much of the randomness is believed to arise from variations in the three angles shown in Fig. 5.10*b*. The tetrahedron does not itself have to be deformed significantly. A typical radial distribution function for silica glass obtained by using x-ray diffraction is shown in Fig. 5.11. The peak locations yield the most probable distances between atomic pairs; the number of atom centers within a coordination shell may be calculated from the area under the peak (defined with some arbitrary cutoff radial distance limits on the left and right). The first peak, at 1.62 Å, corresponds to the shortest distance, which is the Si-O distance. The area corresponds to, more or less, four oxygen atoms, confirming a tetrahedral coordination for Si.

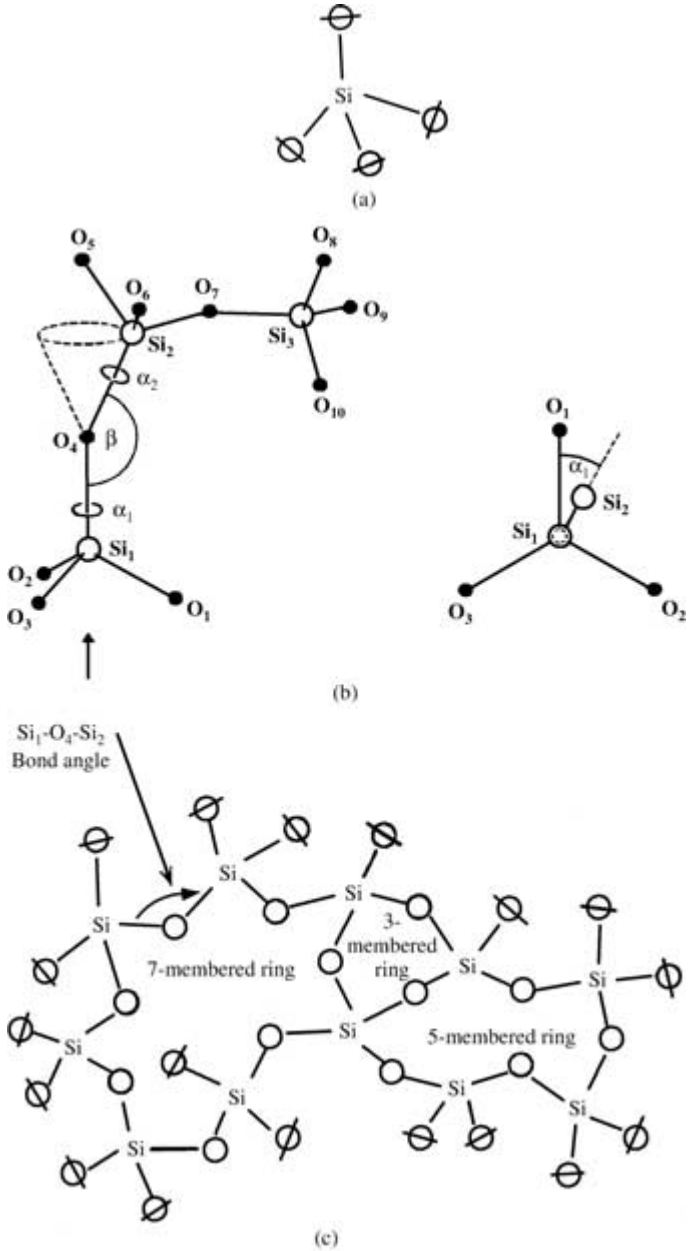

FIGURE 5.10 Silica glass structures: (*a*) the SiO_4 building block—line through the oxygen implies a bridging end; (*b*) intermediate range structures in silica glass; (*c*) A two-dimensional representation of silica glass structure. (Part *b after A. C. Wright, G. A. N. Connell, and J. W. Allen, J. Non-Cryst. Sol. vol. 42, 1980, p. 69*).

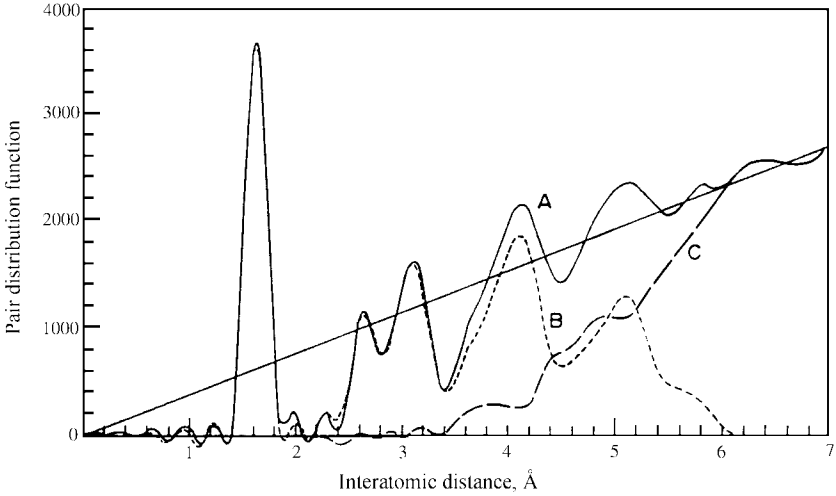

FIGURE 5.11 Radial distribution function for silica glass. Curve *A* is the function measured by x-ray diffraction. Curve *B* is the sum of calculated peaks for Si_1-O_1, O_1-O_2, Si_1-Si_2, Si_1-O_6, O_1-O_6, and Si_1-Si_3. Curve *C* is the difference.

The second nearest distance is 2.65 Å, corresponding to the tetrahedral O-O edge distance. Other computed distances are 3.12 Å for Si-Si, 4.15 Å for Si–second O, about 5.0 Å for O–second O, and about 5.0 Å for Si–second Si. The Si-O-Si bond angles are continuously distributed randomly between 120 and 180° and have a maximum probability at 144°. Physical models made with balls and sticks and computer simulations using molecular dynamics generally support the structure of silica glass as presented in Figs. 5.10*c* and 5.11. Disagreements tend to be limited to the description of ring statistics.

5.4.2 Structure of Alkali Silicate Glass

The addition of one molecule of sodium oxide (Na_2O) to silica glass breaks up a bridge and creates two *nonbridging oxygens* (NBO) as follows:

$$[O]_3Si\text{-}O\text{-}Si[O]_3 + Na_2O = [O]_3Si\text{-}O^-Na^+ + Na^+\ ^-O\text{-}Si[O]_3 \qquad (5.1)$$

Each added sodium ion is attached more or less ionically to one nonbridging oxygen. The overall electrical neutrality of the structure is thus maintained. (The reader should note that each BO is counted as a half and each NBO is counted full, and thus mass balance exists between the two sides of the above equation.) If the oxygen bridges are broken up, the structure begins to lose connectivity and, as a result, becomes more fluid relative to the fully connected silica glass at comparable temperatures. The schematics of the atomic arrangements in alkali silicate glass are shown in Fig. 5.4. The range of relatively easy glass formation (by ordinary melt cooling techniques) in alkali silicate glasses is shown in Table 5.3.

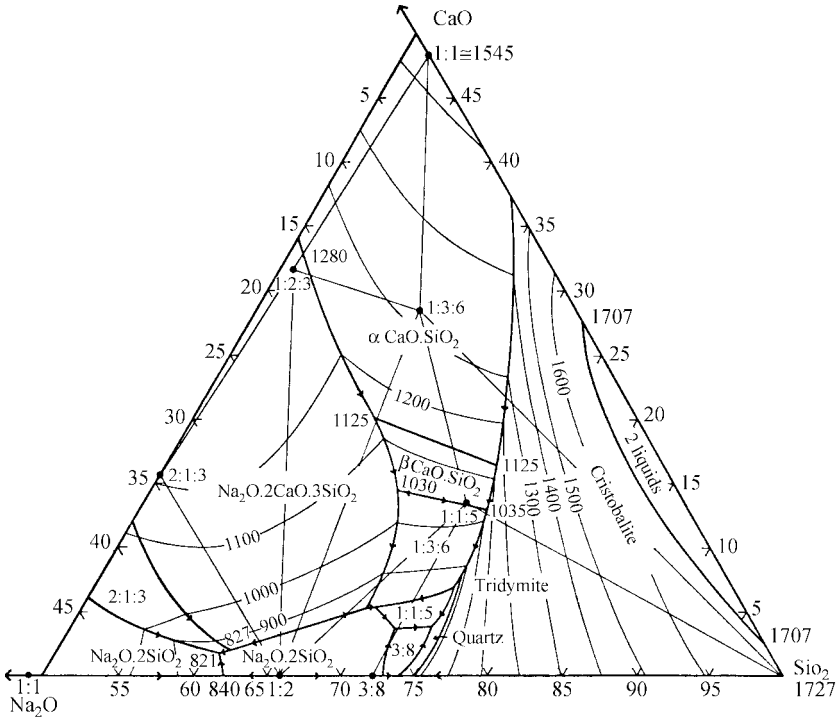

FIGURE 5.12 Phase equilibria and glass formation region in the soda-lime-silica system. *(After K. A. Shahid and F. P. Glasser, "Phase equilibria in the system Na_2O-CaO-SiO_2," Phys. Chem. Glasses, vol. 12, 1971, p. 50.)*

5.4.3 Structure of Alkali-Alkaline Earth-Silicate Glass

When an alkaline earth ion containing oxide, such as CaO, is added to silica, the bivalent alkaline earth ion is attached to two NBOs. The bridge via the Ca^{++} ion is not as strong as the direct -O- bridge, but is not as weak as the broken bridge with alkalis. The increased stability of a soda lime silica glass relative to the sodium silicate glass may be explained in such qualitative terms. Excellent glasses are formed in the $Na_2O \cdot 3CaO \cdot 6SiO_2$ primary phase field (shown as 1:3:6) around the $15Na_2O \cdot 10CaO \cdot 75SiO_2$ composition in the soda-lime-silica phase equilibrium diagram (Fig. 5.12). These form the basis of most of the commercial container, flat, and household lamp (both incandescent and fluorescent) glass industry. Typical compositions are shown in Table 6.1 in Chap. 6.

5.4.4 Structure of Boric Oxide, Borate, and Borosilicate Glasses

Pure boric oxide is perhaps the best glass former (even better than silica). Crystals of B_2O_3 are hard to obtain from a melt at the slowest cooling rates. (All of the commercially sold anhydrous boric oxide is actually boric oxide glass.) The structure is composed of fully connected BO_3 triangles with the boron atoms slightly out of the plane formed by the oxygens.

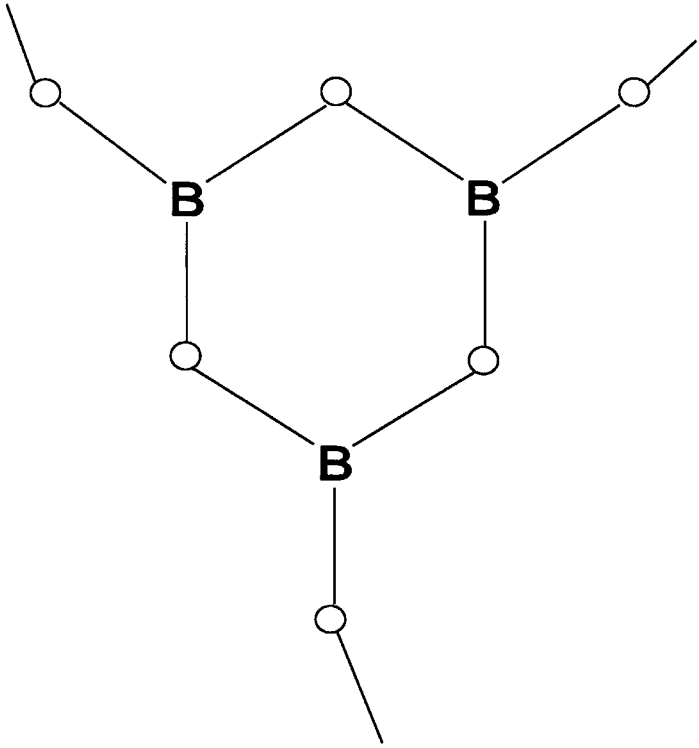

FIGURE 5.13 The boroxol building block in B_2O_3 glass.

According to current beliefs, a significant fraction of the triangles make up a boroxol unit shown in Fig. 5.13. Variation in the three bridging oxygen bond angles at the ends provides most of the randomness. The amount of these units decreases with increases in temperature. Addition of an alkali ion, M^+, to boric oxide brings about two possibilities, as shown in Fig. 5.14:

1. Each sodium ion converts one bridging oxygen to one nonbridging oxygen (NBO) and attaches itself to the NBO as in silicate glasses.
2. One triangularly coordinated boron (B_3) is converted to a tetrahedrally coordinated boron (B_4). Since boron is a trivalent ion, the presence of four oxygens leaves the BO_4 group with one net negative charge, which is satisfied by the univalent alkali ion bonded loosely to the group. Conversion of B_3 to B_4 yields a greater level of network connectivity (without the creation of any NBO), resulting in increasing glass transition temperature and decreasing thermal expansion coefficient.

It has been suggested that the addition of alkali to boric oxide proceeds through option 2 initially up to about 33 mol% added alkali oxide, corresponding to about 50 percent B_4 conversion. Continuing additions of alkali subsequently create NBO through option 1. Thus, it is also agreed that the appearance of extrema in physical properties such as

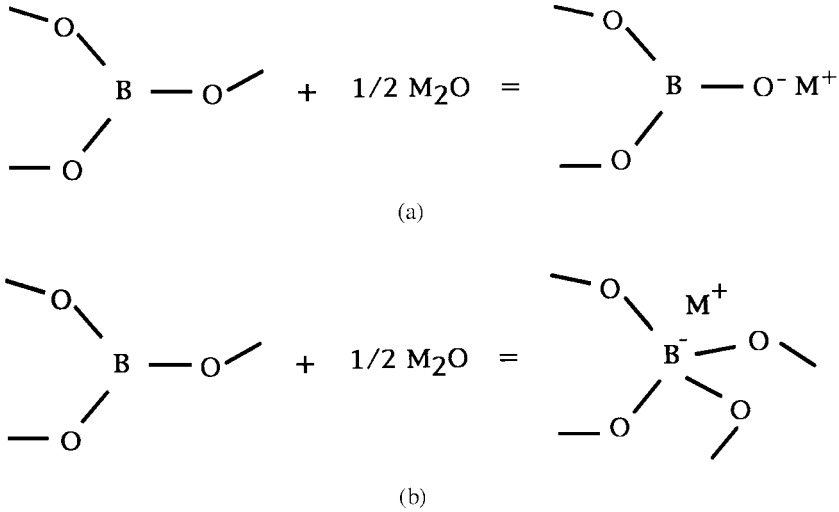

FIGURE 5.14 Structural changes in B_2O_3 on alkali addition: (*a*) formation of nonbridging oxygen; (*b*) conversion of triangularly coordinated boron to tetrahedrally coordinated boron.

the thermal expansion coefficient at 13 to 17 mol% alkalis in alkali borate glasses (see Sec. 5.11.4), otherwise known as the *boric oxide anomaly*, has little to do with the stopping of the B_3 to B_4 conversion, earlier thought to occur in the anomalous region. The range of glass formation in an alkali borate system is shown in Table 5.3.

In alkali borosilicate glasses, the alkali is believed to prefer its association with boron; thus, no NBOs are present in the structure for mol $Na_2O/B_2O_3 < 0.5$. Thereafter, the alkalis are distributed between borons and silicons, depending on the composition and temperature.

5.4.5 Structure of Alkali Aluminosilicate Glasses

In alkali aluminosilicate system, it is believed that the Al^{3+} ion initially goes into the network as a former creating AlO_4 tetrahedra. Like the boron ion, the trivalency then forces the alkali ion M^+ to be loosely connected to the AlO_4 group. Such is the case for mol $Al_2O_3/M_2O < 1$. On further addition, the Al^{3+} ion enters the network as a network modifier with an octahedral coordination of oxygens. There are other suggestions based upon steric considerations, and supported by molecular dynamic simulations in recent years, that argue against the need for an octahedral coordination of Al at $Al_2O_3/M_2O > 1$. An oxygen atom may be shared between three tetrahedra of SiO_4 and AlO_4, forming a tricluster arrangement. Possibilities also exist that all the three tetrahedra could be either AlO_4 or SiO_4, leading to a phase-separated structure.

5.4.6 Structure of Phosphate Glasses

In phosphate glasses, the network is composed of PO_4 tetrahedra. Since P is a pentavalent ion, only three of the four oxygens are corner-shared with adjacent tetrahedra. The fourth oxygen is attached to the P with a double bond to satisfy charge neutrality and acts

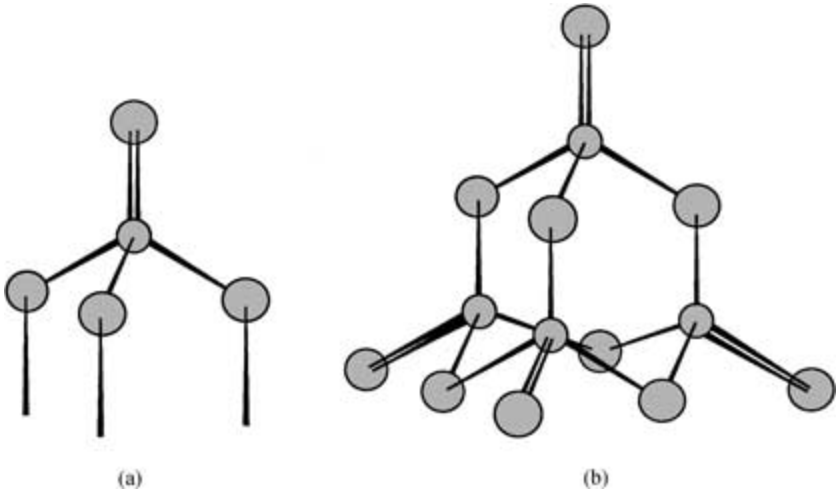

FIGURE 5.15 Structures in P_2O_5 glasses: (*a*) PO_4 tetrahedron; (*b*) P_4O_{10} molecule.

as a terminator. Pure P_2O_5 glass may contain isolated P_4O_{10} molecules (Fig. 5.15) with van der Waals forces between the molecules. With additions of network modifiers, such as Na_2O and CaO, the molecules begin to break up to form linear chains and sheet-like structures. Glass structures are, therefore, not as rigid and stable as those of the silicates, and may readily crystallize or be attacked by chemical media. The range of glass formation in some phosphate systems is shown in Table 5.3.

5.4.7 Structure of Lead and Zinc Silicate Glasses

Although classified by Sun as an NWM, PbO can go into the network as both a former and a modifier. Pure PbO does not make a glass; however, glasses with as high as 90 wt% PbO can be made. It is possible that two SiO_4 tetrahedra are joined via a Pb atom. Another suggestion has been the formation of twisted PbO_4 pyramids with a Pb atom sitting at the apex. Similar considerations hold for ZnO, though not as strongly.

5.5 COMPOSITION-STRUCTURE-PROPERTY RELATIONSHIPS

5.5.1 Presentation of Glass Formulas

As stated above, the entire body of a glass is a single unit cell. Hence, the chemical formula for glass need not be simple. The various component oxides that constitute traditional oxide glasses may be written as mol%, mol fraction, weight % (abbreviated wt%), and

weight fraction. As a convention, the various NWM oxides in increasing order of cation valency precede the NWF. Minor constituents, generally less than 1 percent, added with a specific purpose (for instance, for coloring) are written at the end. Thus, a traditional amber bottle glass composition is a soda lime silicate glass, written usually as $13.5Na_2O$, 8CaO, 3MgO, $2Al_2O_3$, $73.3SiO_2$, $0.25Fe_2O_3$ (wt%). Note that the valence state of the colorant is often not known accurately, hence, summing up to 100 percent may not be an easy task. (If chemical analysis is presented for the most oxidized state, then it may even be possible for the oxide percentages to add up to greater than 100 percent.)

When the number of components is small, for instance in research projects, it may be possible to reduce mol% presentation to a molar formula. For example, $20Na_2O$, 20CaO, $60SiO_2$ (mol%) may simply be presented as $Na_2O \cdot CaO \cdot 3SiO_2$. Like the oxides, the chalcogenide glasses are written usually in atom% or atom fraction, with the chain-forming chalcogen parent at the end. For instance, a germanium-antimony-selenium glass may be written as $28Ge \cdot 12Sb \cdot 60Se$ or as $Ge_{28} \cdot Sb_{12} \cdot Se_{60}$. There are no set conventions for presenting other nonoxide glasses.

5.5.2 Interdependence of Glass Composition, Structure, and Properties

The atomic arrangements in glass are more or less random. Hence, *the physical properties of glass are, in general, isotropic like those of liquids*. There may exist local point defects such as wrong coordinations or missing atoms (or electronic defects); however, there are no such things as dislocations in glass. Hence, *observations of ductility in glass are rare and fracture in glass, for the most part, is brittle. Plastic deformation may occur at extremely high-point loading* and involves a considerable amount of bond bending and local cooperative bond rearranging rather than the large-scale dislocation motion or grain boundary sliding typical of metals.

Viscosity of glasses is expected to increase with network connectivity. Thus, the tetrahedrally coordinated SiO_2 glass has the highest viscosity at any temperature among commercial glasses of practical interest; the triangularly connected B_2O_3 glass has the lowest. Conversion of triangular boron to tetrahedral boron increases connectivity, and hence raises the viscosity. Likewise, creation of NBO in glasses increases fluidity.

Increase in the NBO content generally raises the thermal expansion coefficient. This is because the average atomic separation between the NBO and the ionically bonded interstitial cation increases with temperature more readily.

The openness of the structure allows permeation of inert gases through the network much like a sieve. Thus, the SiO_2 glass has one of the highest permeation rates for gases. Introduction of network-modifying cations in the structure plugs the interstitial spaces and thereby reduces permeability.

Often glass acts like a solution. Each component contributes to a property an amount proportional to its mol or weight fraction in the glass. *The total property, then, is a linear sum of the additivity factors multiplied by the mol or weight fraction.* Such additivity factors work well over a narrow range of compositions. Density, *refractive index, elastic moduli*, and to some extent, thermal expansion and viscosity are a few of those properties where the additivity factors have found considerable use. Nonlinearities are most pronounced in electrical conductivity of alkali glasses, particularly when more than one alkali ion is present. The dramatic nonlinearity observed in ionic conductivity in mixed alkali glasses (discussed later) is called the *mixed alkali effect.* Caution against nonlinearity is also to be taken in thermal expansion and viscosity.

5.6 DENSITY AND MOLAR VOLUME

5.6.1 Introduction

Density ρ is defined as mass per unit volume. Appropriate units are g/cm^3 (or g/cc) in the cgs system and kg/m^3 in the SI system. Relative density is defined as density with respect to water at 4°C and is, hence, unitless. Because the density is inversely proportional to the volume, a change ΔT in temperature changes the density by $-3\alpha\,\Delta T$, where α is the linear thermal expansion coefficient. *Molar volume* V_M is the volume of one mole formula weight and is computed by

$$V_M = M/\rho \tag{5.2}$$

where M is the mol weight in grams with the formula of glass *expressed on a one-molecule basis* (or on a one-atom basis for elemental glasses, such as the chalcogenides). Thus, a glass of the formula $Na_2O \cdot Al_2O_3 \cdot 6SiO_2$ should be first written as $1/8Na_2O \cdot 1/8Al_2O_3 \cdot 6/8SiO_2$ to obtain the value of M. Likewise, $Na_2B_4O_7$ glass should be written as $1/3Na_2O \cdot 2/3B_2O_3$. *Over a limited range of compositions, the molar volume may be considered as composed of additive contributions from the different constituting species*, i.e.,

$$V_M = n_1 v_1 + n_2 v_2 + n_3 v_3 + \cdots \tag{5.3}$$

where v_i is the *partial molar volume* of species i and n_i is its molar concentration. Consideration of partial molar volumes is important in understanding the role of specified ions or atoms within the structure.

5.6.2 Measurement of Density

Density is traditionally measured with a pyknometer, which allows the measurement of volume of a known mass of the specimen. Commercially available gas pyknometers measure the volume by measuring gas pressure changes in a compartment with and without the specimen. Using Archimedes's principle, one may measure the specimen volume as the buoyancy (the decrease in weight) when the specimen is immersed in 4°C water. The buoyancy equals the weight in grams of the displaced fluid, which for water equals the volume in cm^3 (see ASTM C693-93). If the glass is attacked by water, then it is advisable to use odorless kerosene as the immersion fluid, and multiply by the density of kerosene to obtain the specimen density.

A method commonly used to measure density in the glass industry is the sink-float technique. (See ASTM Standard C729-75.) The unknown specimen is gently lowered into a tube containing a slightly denser fluid, prepared by mixing a heavy organic liquid such as *sym*-tetrabromoethane (density = 2.96 g/cm^3) or methylene iodide (density = 3.32 g/cm^3) with a light miscible liquid such as isopropyl salicylate (density = 1.1 g/cm^3). The temperature around the tube is gradually increased until the previously floating specimen begins to sink. The known temperature dependence of the liquid's density yields the density of the specimen.

Perhaps the most rapid technique is the use of a gradient column, which consists of a long (generally about 1 m) one-end-closed glass tube having a vertically standing liquid column with a density gradient. The column is prepared by pouring, first, a heavy liquid such as *sym*-tetrabromoethane. Next, a light liquid is poured on the top without causing turbulence. A continuous gradient establishes itself over a short period of time. The density of

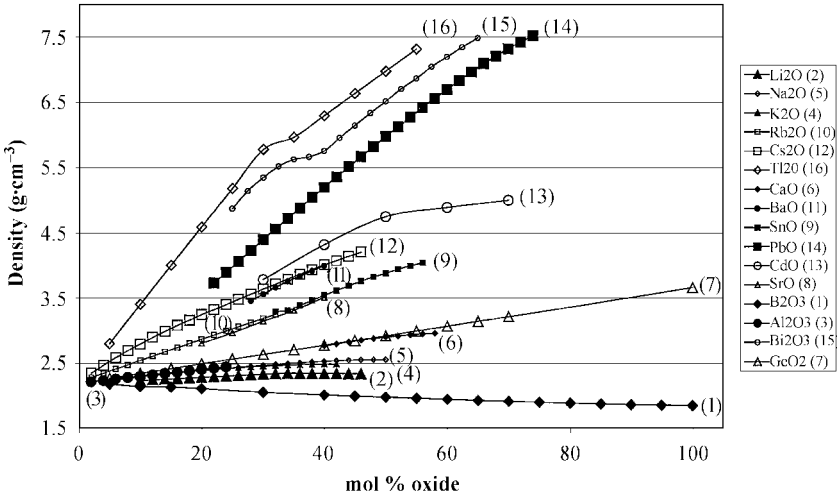

FIGURE 5.16 Density of binary silicate glasses.

an unknown specimen is obtained by noting its floatation level against a scale calibrated by density standards lowered into the column. The column may remain useful for several weeks.

5.6.3 Dependence on Composition

Density of silica glass is 2.20 g/cm^3 at room temperature. There is no detectable difference observed in density of silica regardless of the different methods of production. Of the various forms of crystalline silica, the density of silica glass is closest to that of β-cristobalite (high-temperature form), which is 2.25 g/cm^3. Since the density of α-quartz is 2.65 g/cm^3, it is apparent that large structural changes occur during the melting of sand. Addition of alkalis to silica increases the density steadily: The alkali ions go inside the interstices as NWM, taking up holes. Heavier alkali ions generally are more effective in increasing the density, as is shown in Fig. 5.16. Likewise, heavy elements such as Ba, Cd, Pb, and Bi bring large increases in the density.

Because density can be measured readily and accurately to the third decimal place, and because it is extremely sensitive to composition, *density charts are often used to control the quality of glass production in a commercial environment.*

5.7 ELASTIC PROPERTIES

5.7.1 Introduction

For a semiempirical description of elastic properties consistent with the various types of engineering experiments, it is customary to define stress as the force per unit area of application and strain as the relative deformation in a particular dimension. On the application of a stress, the body may instantaneously deform. *An elastic body recovers deformation instantaneously and completely on the removal of the stress if the yield point has not been exceeded.*

Plastic bodies are those in which the applied shear stress has exceeded the yield point. Under these conditions, the *deformation of the plastic body is progressive with time until, at some point, it is able to sustain a constant applied shear stress.* On the removal of the shearing stress, any elastic component of the total strain is recovered; however, the plastic component of the strain is not recovered. When the body deforms over a measurable period of time, i.e., *flows* under the action of a constant stress, one speaks of *creep* occurring. *An elastic-plastic body having a near-zero yield point can be called a viscous body.* Such a body can not sustain shear stress over a finite period of time, since the stress relaxes with time; in other words, the *body flows to relieve shear stresses.* At constant strain, the stress could initially build up instantaneously as an elastic response, however, *such stress would ultimately decay through internal relaxation mechanisms.* If the externally applied stress is maintained, the deformation will continue to occur with time, since the applied stress is never balanced. The slower the rate of stress relaxation, the more viscous the body is.

We normally ascribe elastic and plastic behavior to be typical of the solid state, and the viscous behavior to that of the liquid state. It should, however, be understood that the real distinctions between a solid state and a liquid state are truly subtle. A liquid has near-absence of a shear stress yield point and a real-time-measurable shear stress relaxation rate. The drift of continents over millennia is one such thought-provoking example. Should the continents be classified as solids or as liquids?

Since externally applied stresses generally cause small strains in solids, the relationship between stress below certain "elastic limits" and the strain is often linear and is a statement of *Hooke's law*. Actually, the body may still be considered elastic so long as the recovery on the removal of stress is complete—it simply displays *non-Hookean elasticity* at large strains. In the linear region, the constants of linearity are called the *moduli of elasticity.* (Because force is a vector and the area is represented by its normal vector, stress is a second rank tensor requiring six components in a 3×3 matrix representation according to the formal phenomenology of elasticity. Likewise, strain is also a second-rank tensor. The stress components with two indices and the strain components, also with two indices, are then related through elastic constants, which are a fourth-rank tensor. In the discussion that follows, such phenomenology is abandoned in favor of the semiempirical approach, which reflects easy correspondence to experimental measurements.)

The application of a uniaxial stress σ_x (simplified representation of σ_{xx}) develops a uniaxial extensional strain e_x, such that

$$\sigma_x = Ee_x \tag{5.4}$$

where E is called *Young's modulus* (Fig. 5.17*a*). (A stress is tensile or positive if it produces an elongation in the applied direction.) Accompanying this elongation in the x direction, there will be a shrinkage in the y and z directions such that

$$e_y = e_z = -\nu e_x \tag{5.5}$$

The ratio ν of transverse strain to the longitudinal strain is called *Poisson's ratio*. Under a two-dimensional state of pure shear (Fig. 5.17*b*), the ratio G of the shear stress σ_{xy} to the shear strain e_{xy} is called the *shear modulus* or *rigidity*. Its reciprocal is called the *shear compliance J*. A special situation arises when the three components of a triaxial stress system are exactly equal (Fig. 5.17*c*), i.e.,

$$\sigma_x = \sigma_y = \sigma_z = -p \tag{5.6}$$

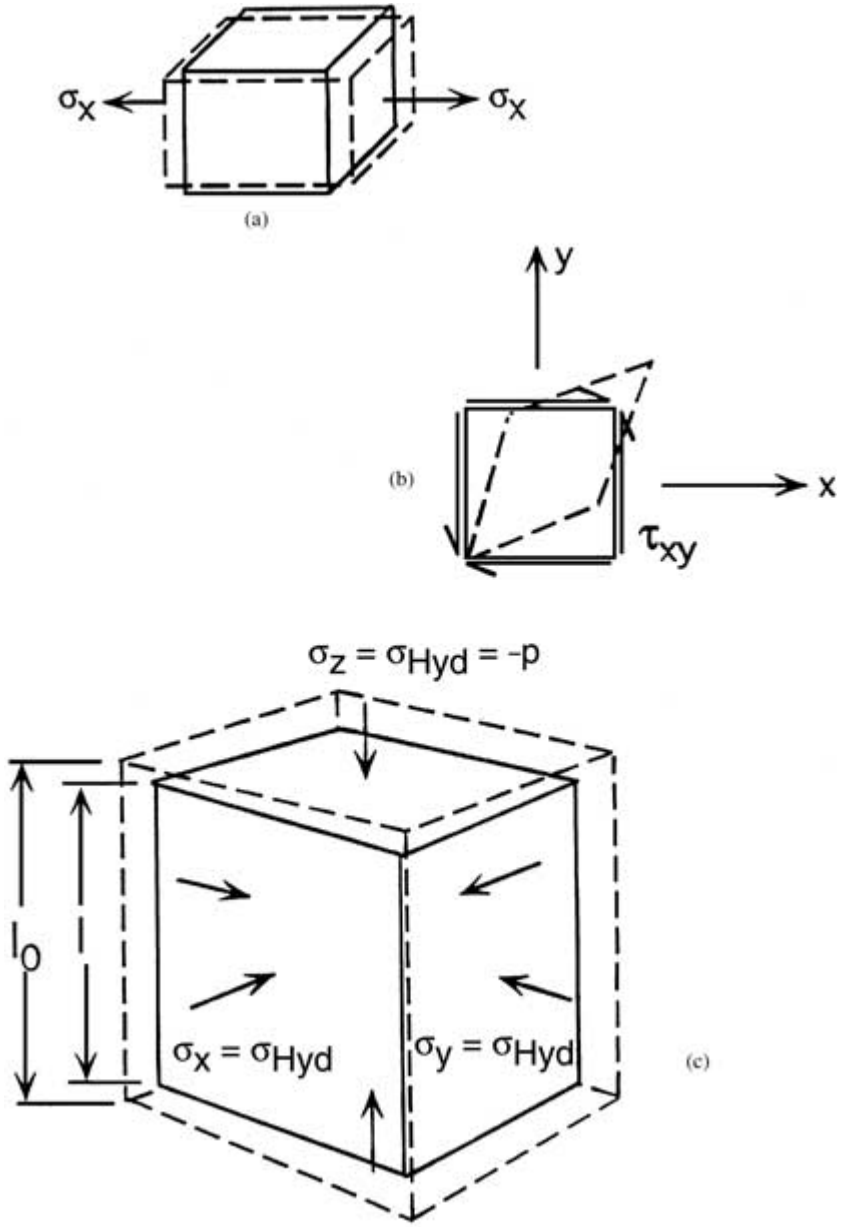

FIGURE 5.17 Description of *E*, *v*, and *K*.

This *hydrostatic* application of stress $-p$, where p is called the *pressure*, generates a volumetric strain (dilatation) e_m

$$e_m = e_x + e_y + e_z \tag{5.7}$$

where the extensional strains $e_x = e_y = e_z$, and the shear strains $e_{xy} = e_{yz} = e_{zx} = 0$. The pressure is related to the dilatation by

$$-p = K e_m \tag{5.8}$$

where K is called the *bulk modulus*. Although experiments are readily designed to measure each of the four moduli of elasticity for glass, only two of the four are actually independent, since glass is basically isotropic. Stress is generally measured in units of megapascals (MPa) in the SI system (1 Pa = 1 newton/m^2; 1 GPa = 1000 MPa = 10^9 Pa), dynes per square centimeter (dyn/cm^2) in the cgs system, and pounds per square inch (psi or lb/in^2) in the English system (1 MPa = 10^7 dyn/cm^2 $\approx$ 145 lb/in^2). Strain is unitless. Elastic moduli are, therefore, expressed in the units used for stress.

5.7.2 Methods of Measuring Elastic Moduli

Young's modulus may be measured by a beam-bending technique with a universal mechanical testing machine. For a three-point centrally loaded uniform beam, the elastic deflection δ is related to the load F and the beam geometry through the relation

$$\delta = FL^3/48EI \tag{5.9}$$

where L is the beam length between the two support pegs and I is the geometric moment of inertia; $I = bh^3/12$ for a beam having a rectangular cross section of width b and height h, and $I = \pi a^4/4$ for a circular rod of radius = a. Because of the errors associated with slippage at the supports and because linear elastic theory is applicable only to small deflections of the beam ($\delta < h/2$), such methods have given way to pulse-echo techniques based on ultrasonics. In a pulse-echo technique, an ultrasonic pulse is sent through the medium (about 1 cm diameter by 2 to 4 mm thick) by a suitable transducer (generally 2 to 10-MHz frequency) affixed by using couplers such as honey. The same transducer records the arrival of the echo reflected from the other end of the specimen. The time of flight measurement by an oscilloscope can be related to an appropriate elastic modulus of the medium. Use of separate longitudinal and transverse wave transducers allows one to measure v and G, generally in the same setup. The major source of errors in these measurements is the presence of bubbles, crystals, or internal cracks, which tend to reflect the echo prematurely. Elastic moduli may also be calculated from the resonance frequencies of defined geometry specimens in longitudinal or transverse modes (see ASTM C623-92).

5.7.3 Composition Dependence of Elastic Moduli

Elastic moduli of glasses do not change dramatically with composition. Values for fused silica glass are often quoted as $E = 70$ GPa, $K = 37$ GPa, $G = 30.5$ GPa, and $v = 0.17$. Presence of heavy elements decreases the Young's modulus because of a decreased interatomic attractive force due to increased separation. Glasses containing Li_2O, BeO, and Al_2O_3, therefore, tend to have the larger Young's moduli. Variation of E and v in the Na_2O-xMO-$5SiO_2$ glasses as a function of x, where M = Be, Mg, Ca, Sr, Ba, Zn, Cd, and Pb is shown in Fig. 5.18. Young's modulus generally increases from 65 GPa to 85 GPa with the added M except for PbO additions. Poisson's ratio increases from 0.22 to about 0.27.

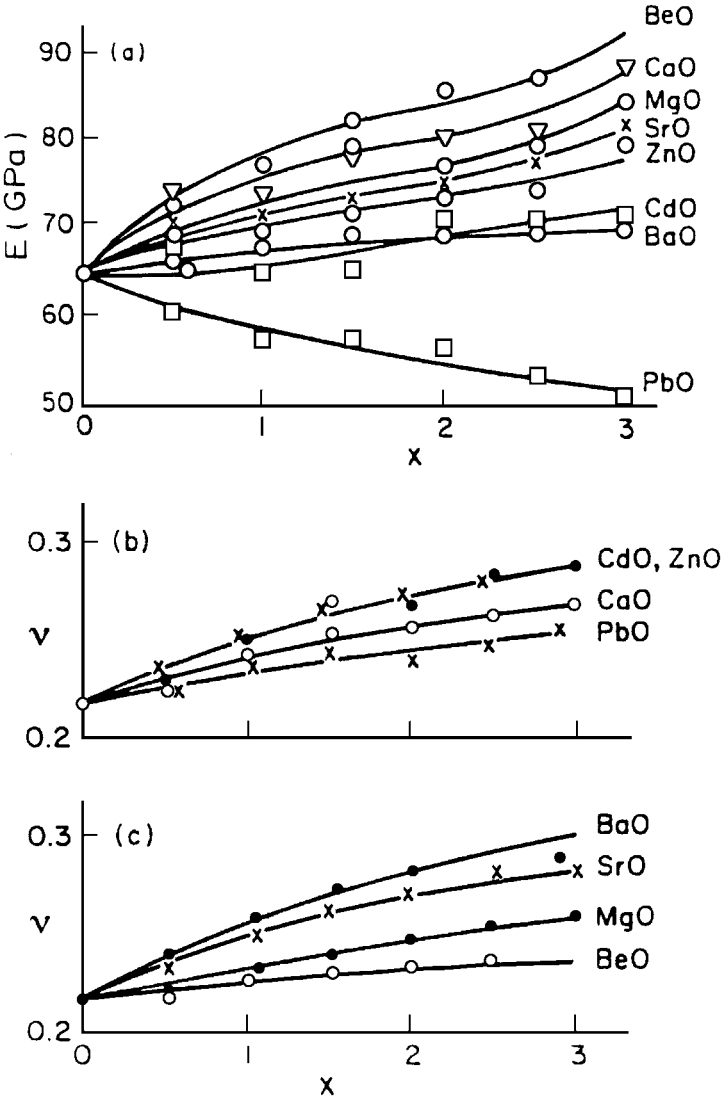

FIGURE 5.18 Variation of E and ν in Na_2O-xMO-5SiO_2 glasses. (*Figure 10.4 in N. P. Bansal and R. H. Doremus, Handbook of Glass Properties, Academic Press, Orlando 1986.*)

Young's modulus E may be calculated by using Makishima and Mackenzie's additivity factors[3]:

$$E\ (\text{GPa}) = 8.36[(\rho/M)\Sigma V_i p_i][\Sigma F_i p_i] \tag{5.10}$$

where ρ is the density (g/cm^3), M is the effective molecular weight ($= \Sigma M_i p_i$), p_i is the mole fraction of the ith component oxide, and the values of the packing factor V_i and the dissociation

TABLE 5.4 Dissociation Energy F_i per Unit Volume and Packing Factor V_i of Oxides

Oxide	F_i, kcal/cm^3	V_i
Al_2O_3	32	21.4
BeO	30.0	7.0
ZrO_2	23.2	15.1
TiO_2	20.7	14.6
Sc_2O_3	20.2	23.6
Mgo	20.0	7.6
ThO_2	19.3	28.5
Li_2O	19.2	8.0
B_2O_3	18.6	20.8
Y_2O_3	17.7	24.8
Ga_2O_3	17.1	21.9
La_2O_3	16.2	28.4
CaO	15.5	9.4
SiO_2	15.4	14.0
P_2O_5	15.0	34.8
As_2O_5	13.1	36.2
SnO_2	12.9	17.4
SrO	11.6	10.5
ZnO	9.9	7.9
BaO	9.7	13.1
PbO_2	9.1	15.3
Na_2O	8.9	11.2
CdO	7.6	9.2
In_2O_3	6.7	23.5
K_2O	5.6	18.8
Pb_2O	4.5	9.9
PbO	4.2	11.7
Cs_2O	3.4	31.2

energy F_i (kcal/cm^3) are listed for several oxides in Table 5.4. Makishima and Mackenzie suggest that a glass based on the system BeO-Al_2O_3-ZrO_2 should have an E value of roughly 160 GPa.

5.8 MICROHARDNESS OF GLASS

5.8.1 Introduction

Microhardness represents the ability of a material to resist abrasion or scratching when mechanically rubbed against another material. Harder substances resist penetration or erosion by sharp projectiles of another. On an atomic scale, the pointed object first deforms the target elastically and subsequently plastically after reaching the *yield point* of the target. Whereas glasses are generally regarded as brittle solids, the atomic network is able to yield (bend, fold, or rearrange) when concentrated forces are applied over regions no more than a few micrometers in size. (Application over a larger area would most certainly result in

fracture.) *Under the immediate region of contact, glass is densified to some extent, and displaced into folds at the perimeter.* Thus, in a microhardness experiment, glass not only undergoes elastic deformation, it displays *volume plasticity* (densification) as well as *shear plasticity* (permanent shape change). Volume plasticity involves *volume viscosity* which is treated in Sec. 5.9, "Viscosity of Glass."

5.8.2 Measurement of Microhardness

The scratching ability of solids is ranked using the *Mohs scale* of hardness from 1 to 10, with 10 being diamond. Most glasses fall between 5 (apatite) and 7 (crystalline quartz). In a laboratory environment, it is now customary to measure the hardness on a scale of microns using a square pyramid-shaped (*Vickers*), or an elongated pyramid-shaped (*Knoop*) diamond indenter (Fig. 5.19). A loaded indenter is lowered against a polished flat surface of the test specimen for a specified period of contact time and retracted automatically afterwards. During loading, the indenter penetrates into the glass and, on retracting, leaves a permanent pyramidal (square or elongated) indentation. The diagonal length of the impression is measured by using a filar eyepiece. For most glasses, with a 10- to 200-g load, the indentation is generally of the order of 5 to 25 micrometers. For a Vickers microindenter, the *Vickers hardness number* (VHN) is given by:

$$\text{VHN} = 1.8544F/D^2 \tag{5.11}$$

where F is the force in kg and D is the average diagonal length of the impression in mm. Implied units of VHN are kgf/mm^2. (*Note:* 1 kgf/mm^2 = 9.81 MPa.)

For a Knoop indenter, the *Knoop hardness number* (KHN) is written as (see ASTM C730-85):

$$\text{KHN} = 14.23F/L^2 \tag{5.12}$$

where L is the length (mm) of the long diagonal.

Because of elastic recovery on load removal, the static measurements of the impression diagonal in a Vickers experiment yield an apparently higher value of microhardness. (The error is reduced in the Knoop experiment, since the elastic recovery is confined mostly to the short diagonal in this case). A relatively newer method to measure "instantaneous" microhardness during loading is to use the *recording microindenter*, where penetration h

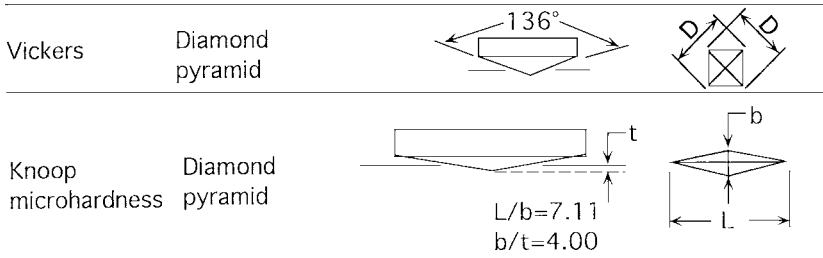

FIGURE 5.19 Vickers and Knoop indenters.

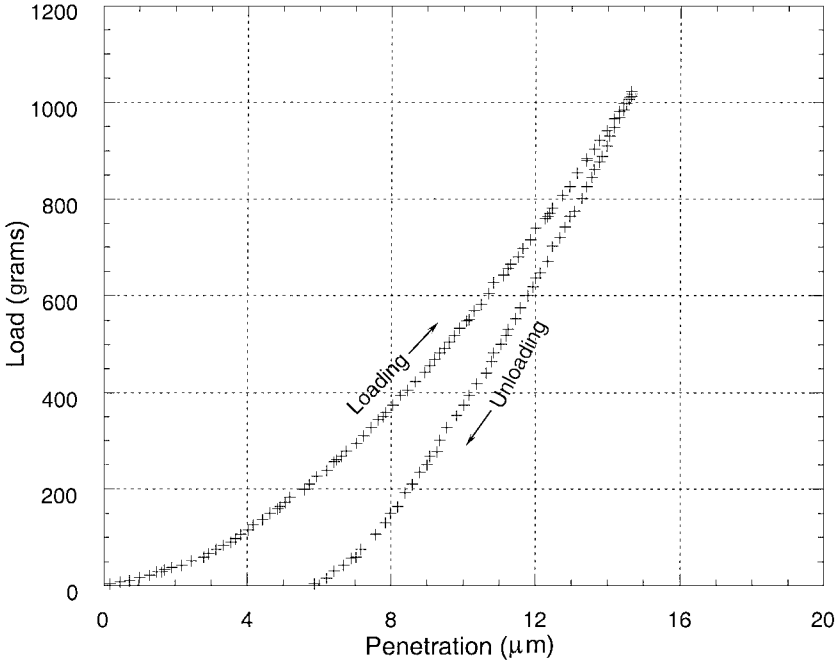

FIGURE 5.20 Load versus penetration curves in a recording microhardness indenter.

is measured concurrently with increasing load. A load-versus-penetration plot during loading as well as during unloading is obtained (Fig. 5.20). The *F*-*h* plot is fitted to a polynomial of the type:

$$F = a_1 h + a_2 h^2 = F_1 + F_2 \tag{5.13}$$

where the constants a_1 and a_2 are computed from the fit. A load-independent hardness number F_2HN is defined as:

$$F_2HN = a_2/K^* \tag{5.14}$$

where K^* is the indenter geometry constant. The area integrated under the loading curve represents the energy needed to carry out the indentation, whereas the area under the unloading curve is the elastically recovered energy.

It must be recognized that the stress developed under an indentation load is generally very high (even though the loads are only 100 g or so). Fracture may generally develop along median planes of the indentation, propagating downward during loading, or at the apices, propagating radially outward during unloading. Since the development of fracture represents consumption of energy, loads used during a measurement of microhardness must be small enough to avoid any cracking. It will, however, be shown in Sec. 5.19.6, "Measurement of Glass Strength and Toughness," that indentation experiments involving deliberate cracking are useful in estimating the toughness of the material.

5.8.3 Composition Dependence

The VHN of fused silica is generally quoted at about 630 kgf/mm^2 (6.18 GPa) and that of B_2O_3 glass at about 205 kgf/mm^2. The addition of alkalis decreases the connectivity in silica and hence the hardness. Microhardness decreases to 330 kgf/mm^2 at the $K_2O \cdot 2SiO_2$ glass composition. On the other hand, since alkalis added to B_2O_3 increase connectivity (from 3 coordination to 4 coordination), the microhardness of alkali borate glasses typically increases. Common soda-lime-silica glasses have a microhardness of around 550 kgf/mm^2.

5.9 VISCOSITY OF GLASS

5.9.1 Introduction

As indicated in Sec. 5.7.1, viscosity is a property typical of the liquid state describing its flow due to externally applied stresses. In normal discussion, it is the shear viscosity that is of concern. Analogously to Hooke's law for elasticity, an externally applied shear stress and the developed shear strain rate are related through *Newton's law of viscosity*:

$$\sigma_{xy} = \eta \, de_{xy}/dt \tag{5.15}$$

where η is called the *coefficient of viscosity* (or simply the *viscosity*) and has the units *P* (*poise* in the cgs system) and Pa · s (*pascal-seconds* in the SI system), where 1 Pa · s = 10 P. Viscosity is the reciprocal of fluidity. Much like non-hookean behavior of solids at large shear strains, it is possible for a liquid to become non-newtonian at high shear strain rates. It is useful to draw an elasticity-viscosity analogy that the deformation of an elastic solid under the action of a given shear stress can be translated to a deformation rate for the same body, but now a viscous liquid, by substituting η for G (shear modulus) in the elasticity solutions. A further assumption of incompressibility ($\nu = 0.5$) allows the replacement of G by $E/3$ in the elasticity solution, where E is the Young's modulus.

5.9.2 Viscosity-Temperature Dependence

Viscosity is the single most important physical property that allows continuous glass forming on an industrial scale. *Viscosity increases steeply and monotonically with temperature from about 10^2 poise to greater than 10^{22} poise*. Hence, glassmaking involves melting the glass in a suitable continuous feed container, transporting the molten glass stream to a forming machine and, after forming a desired product, extracting heat out of the formed product in a controlled but continuous manner till the body is rigid. The viscosity-temperature dependence of glass-forming melts is generally of the Arrhenius form:

$$\eta = \eta_0 \exp(\Delta H/RT) \tag{5.16}$$

where R is the gas constant, T the absolute temperature (kelvin scale), ΔH is the activation energy for viscous flow, and η_0 is the preexponential. However, this equation does not fit well over the entire temperature range of practical interest. Apparently, a superior empirical fit to inorganic silicate melt viscosity data is given by the Vogel-Fulcher-Tammann relation (the *VFT relation*, also called the *Fulcher relation*):

$$\log \eta = -A + B/(T - T_0) \tag{5.17}$$

where A, B, and T_0 are empirically determined constants. This relationship suggests that the glass viscosity tends to infinity as the temperature approaches T_0 from above. Glass manufacturers often tabulate the values of A, B, and T_0 for their product literature. The various steps of glass forming are essentially determined by using the η-T curve. Four viscosity reference temperatures are used as guidelines:

Working point is the temperature at which the viscosity is 10^4 poise. This is the viscosity at which a machine is able to work on glass without losing control.

Softening point is the temperature at which the viscosity is $10^{7.6}$ poise. This is the approximate viscosity at which a glass will deform under its own weight on the time scale of manufacturing operations. Glass temperature must be lower than this before the glass leaves the forming machine.

Annealing point is the temperature at which the viscosity is 10^{13} poise. Stresses that form in the glass object are relieved at this viscosity in a matter of minutes.

Strain point is the temperature at which the viscosity is $10^{14.5}$ poise. Stresses that form in the glass object are relieved at this viscosity in a matter of hours.

The latter two viscosity reference points are roughly in the lower half of the glass transition range, and are of interest for practical *annealing* of glass products, a subject that is covered in Chap. 6, "Inorganic glasses—commercial glass families, applications, and manufacturing methods."

In addition, some industrial consultants use *melting point* (viscosity = 100 poise) and *flow point* (viscosity = 10^5 poise). To obtain a feeling for these viscosities, the reader should bear in mind that water at room temperature has a viscosity of 0.01 poise, glycerine has a viscosity of 1 poise, and hot molasses (if you were in the moonshine business, you should have no problem recognizing this one) has a viscosity of about 100 poise.

Viscosity-temperature dependence of a typical soda-lime-silicate glass is shown in Fig. 5.21. Glass is melted at around 1450°C, delivered to a forming machine around 1000°C, placed on a conveyor belt as a formed product at temperatures lower than about 700°C, and annealed between 530°C and 480°C.

5.9.3 Measurement of Viscosity

It is not possible to measure the viscosity of glass over the entire 20-decade range using a single instrument. Often a variety of methods are employed. In the fluid range, a rotating viscometer or a falling sphere method is used. There are two versions of the rotating viscometer technique (see ASTM C965-96). In one, molten glass is placed in a platinum crucible having a concentric inner platinum spindle. The rotation of the outer crucible at a fixed velocity causes the inner spindle to show a twist, which is measured. In the second version, the inner spindle is rotated by applying a constant torque, and the resulting speed of the spindle is measured. In the falling sphere method, which is based on Stokes' law, the velocity of a descending platinum ball is measured. (The vertical column containing the melt should have a transparent window.) Softening point, sometimes called the *Littleton softening point*, is traditionally measured using a fiber elongation technique (see ASTM C338-93). A round fiber, nominally 0.65 mm (0.55 to 0.75 mm) in diameter, 23.5 cm long, is suspended in a prescribed furnace, which heats the top 10 cm of the fiber at a rate of 5°C per minute. The temperature at which the rate of sagging of the lower end of the fiber is 1 mm/minute is reported as the softening point.

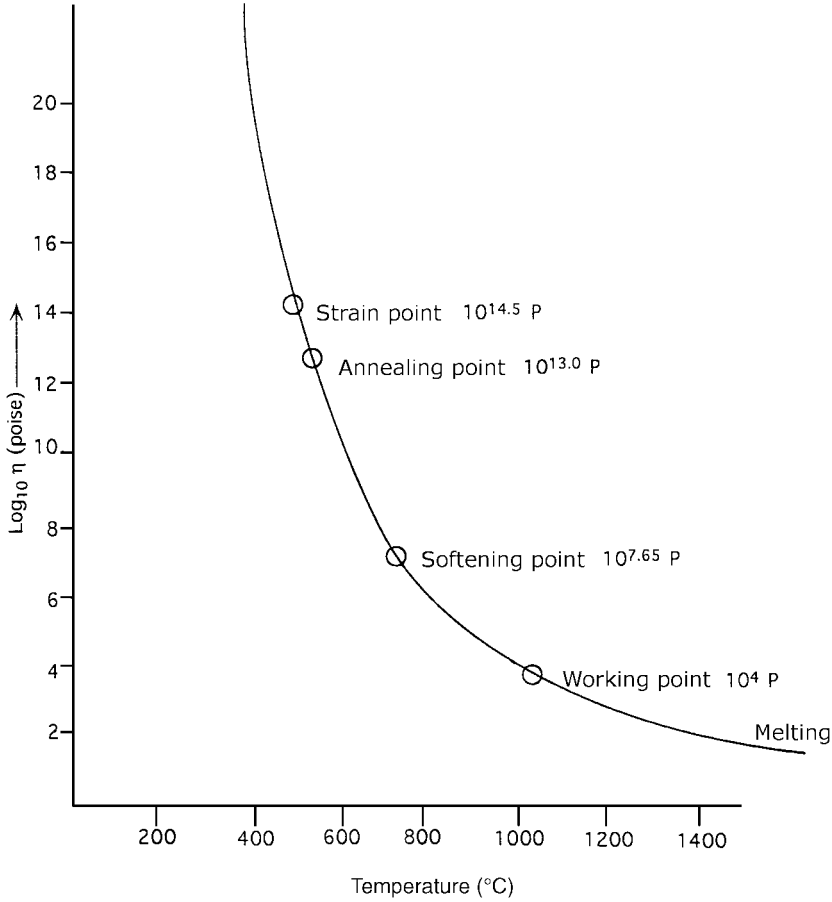

FIGURE 5.21 Viscosity η versus temperature for a typical soda-lime-silicate glass.

A rapid technique used for determining softening point in the industry is the penetration viscometer. In this technique, the temperature at which the penetration of a platinum ball in the heated glass reaches up to a specified depth is reported as the softening point. Viscosities near the softening point may also be measured using a type of cone/cup arrangement, where the glass occupying the annular space between the inside cone and the outside cup is sheared.

Somewhat higher viscosities, up to 10^{11} poise or so, are measured using a parallel plate viscometer (see ASTM C1351M-96). In the parallel plate viscometer, a suitably sized disk (about 8 mm in diameter by 3 to 6 mm thick) of glass is sandwiched between two parallel plates (inconel plates covered with platinum foil or thin alumina substrates). The top plate is loaded with known weights. Viscosity can be calculated by measuring the rate of decrease in the thickness of the specimen with a linear variable differential transformer (LVDT) device.

Higher viscosities, those corresponding to the annealing point and the strain point, may be measured by a centrally loaded beam-bending method (see ASTM C598-93 and ASTM

C1350M-96) or by elongation of a loaded fiber (see ASTM C336-71). The calculation of viscosity in both these techniques utilizes the elasticity-viscosity analogy discussed above (Sec. 5.9.1). One merely writes an appropriate equation for the elastic deflection (involving Young's modulus E) of an incompressible body and replaces E by 3η, and the deflection by the rate of deflection. Very high viscosities are generally measured by using a vertically loaded fiber.

One must recognize, however, that unless the structure of glass has been stabilized, the measured glass viscosity in the glass transformation range continues to drift generally to higher values. The time required for stabilization is minutes at the annealing point, hours at the strain point, and increases by decades as the viscosity increases (see Sec. 5.14.3, "Relaxation of Properties"). Thus, direct measurements of viscosities exceeding about 10^{19} poise ($= 10^{18}$ Pa · s) are not practical. An example of the controversy surrounding very high viscosities is the apparently larger thickness observed in the lower regions of vertically mounted windows in old European churches. Earlier beliefs that glass collected at the bottom because of flow over a thousand years have been refuted, and ascribed to the way the windows were made in the first place (*broad glass* process), and their biased mounting by a carpenter subsequently.

5.9.4 Composition Dependence of Viscosity

Viscosities of some single glass formers as a function of the reciprocal of absolute temperature are shown in Fig. 5.22. Of all the glasses of commercial and scientific interest, silica glass perhaps has the highest viscosity. OH-free silica generally has an annealing point around 1130°C and a softening point around 1550°C. No doubt, the high viscosity is due

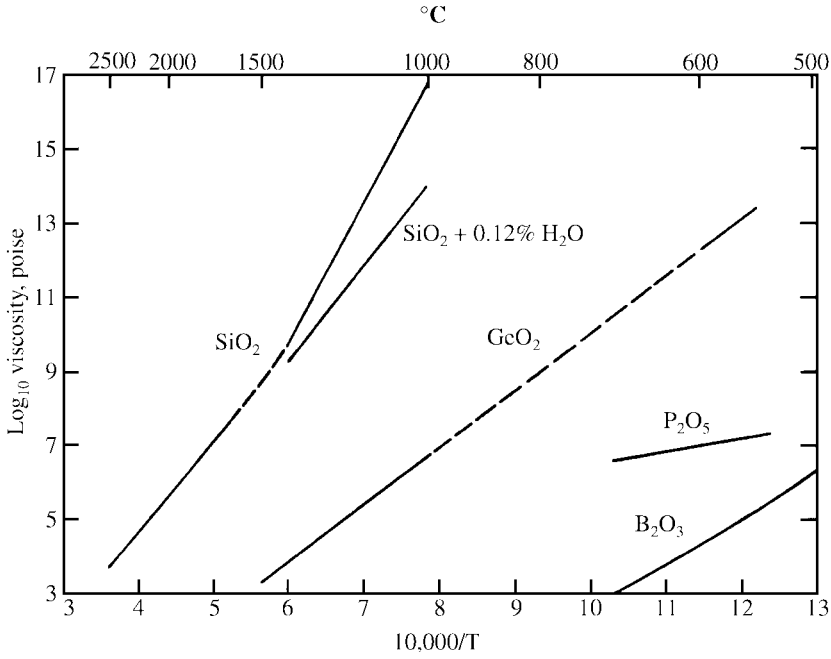

FIGURE 5.22 Log η versus $1/T$ (K) for single glass formers. (*After R. H. Doremus, Glass Science, Fig.2, Wiley & Sons, New York, 1973.*)

primarily to the high tetrahedral connectivity of the network. B_2O_3 glass, which has only triangularly coordinated structures, has an annealing point as low as about 230°C. Although the cation polyhedra in P_2O_5 and GeO_2 glasses are tetrahedal, the linkages are not symmetrically three-dimensional. The presence of hydroxyls (for instance, in hydroxylated-vapor-phase-produced silica) greatly decreases the annealing point, to as low as 1000°C. Likewise, additions of alkali decrease the viscosity (Fig. 5.23). As little as 5 mol% addition of Na_2O to silica glass decreases the viscosity of silica by about 5 decades around the softening point. However, one must recognize that, relatively speaking, OH still has the most profound influence in decreasing the viscosity. Replacement of alkali by alkaline earth oxides and alumina increases the viscosity (Fig. 5.24). In alkali borate glasses, the initial additions of alkali to the B_2O_3 glass actually increase the viscosity and further additions decrease it after about 13 to 17 mol% alkali—an observation discussed earlier as the B_2O_3 anomaly.

Viscosity additivity factors to fit into a Fulcher equation to describe the temperature dependence of soda-lime-silicate glasses are given by Lakatos et al.[4] These factors are:

$$\begin{aligned} B &= -6039.7Na_2O - 1439.6K_2O - 3919.3CaO + 6285.3MgO + 2253.4Al_2O_3 + 5736.4 \\ A &= -1.4788Na_2O + 0.8350K_2O + 1.6030CaO + 5.4936MgO - 1.5183Al_2O_3 + 1.4550 \\ T_0 &= -25.07Na_2O - 321.0K_2O + 544.3CaO - 384.0MgO + 294.4Al_2O_3 + 198.1 \end{aligned} \tag{5.18}$$

where the various oxide symbols represent the mole oxide ratio to mole of SiO_2.

The T_g of alkaline earth aluminosilicate glasses of the type used for halogen headlamp inner bulb application may be estimated by the relation:

$$T_g\ (°C) = 1130 - 13.7CaO - 13.4BaO + 1.6Al_2O_3 + 6.0ZrO_2 \tag{5.19}$$

where the oxide formulas represent wt% composition, and SiO_2 is assumed to be the balance.

5.9.5 Strong and Fragile Liquids

Compositional modifications that lead to the breaking up of structural units apparently cause the viscosity-temperature dependence to become more and more non-Arrhenius. This is shown in Fig. 5.25, where $\log_{10}$ (viscosity) is plotted normalized against T_g/T for a variety of glasses. Glass-forming melts such as SiO_2 that fall close to the diagonal line (describing an Arrhenius dependence) are called *strong liquids*. The addition of alkali to silica causes the dependence to become more and more curve-shaped, presumably because such melts have a larger number of unconstrained conformations capable of being rearranged in the vicinity of T_g. Such liquids are called *fragile*. Other examples of fragile liquids are the heavy-metal fluoride glasses.

5.9.6 Non-Newtonian Viscosity

Non-Newtonian flow occurs when the coefficient of viscosity depends on the magnitude of the applied strain rate. *The most common non-Newtonian effect observed in glass melts is shear-thinning, where the coefficient of viscosity decreases at high shear strain rates*. This is shown for a soda lime glass in Fig. 5.26 for fiber elongation and cone/cup measurements.

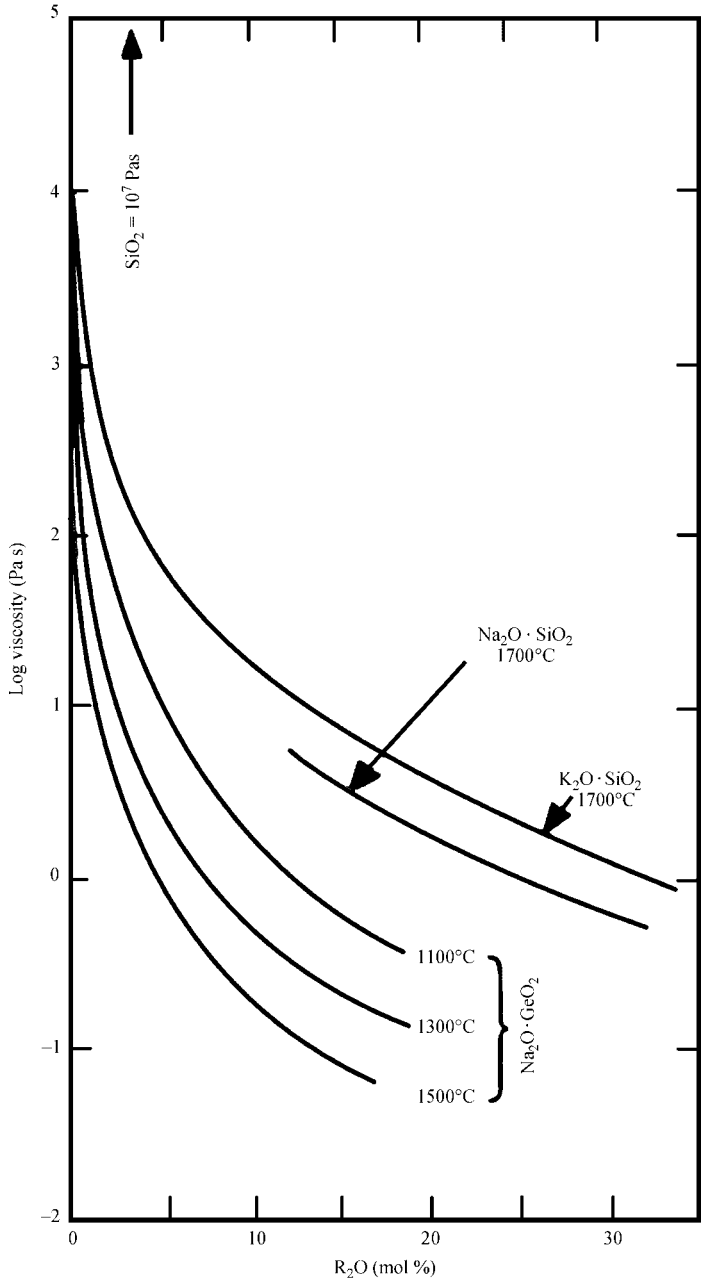

FIGURE 5.23 Viscosity decrease in SiO_2 and GeO_2 glasses due to R_2O addition.

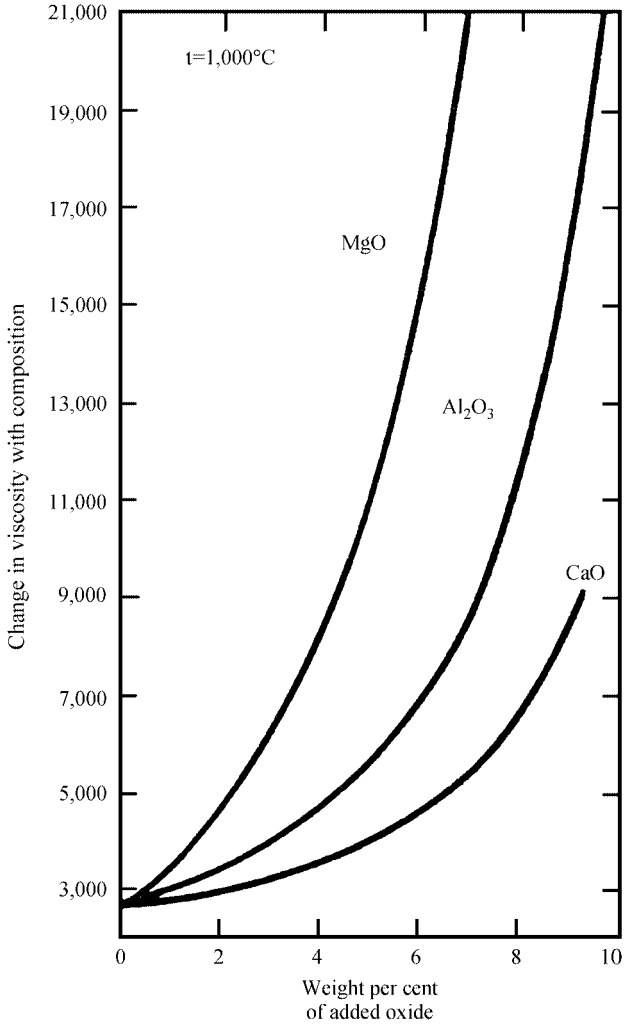

FIGURE 5.24 Effect of CaO, MgO, and Al_2O_3 replacing Na_2O on the viscosity of $Na_2O \cdot 3SiO_2$ glass at 1000°C. (*After S. English, J. Soc. Glass Technol., vol. 8, p. 205, 1924.*)

It has been observed that the onset of non-Newtonian viscosity may occur at a strain rate as low as 5×10^{-6} s^{-1} at 530°C, whereas viscosity remains Newtonian up to a strain rate of 40 s^{-1} at 900°C. Non-Newtonian behavior of glass melts is of great commercial importance in high speed-glass forming processes. Much of the glass pressing operations and fiber drawing operations critically depend on the melt viscosity.

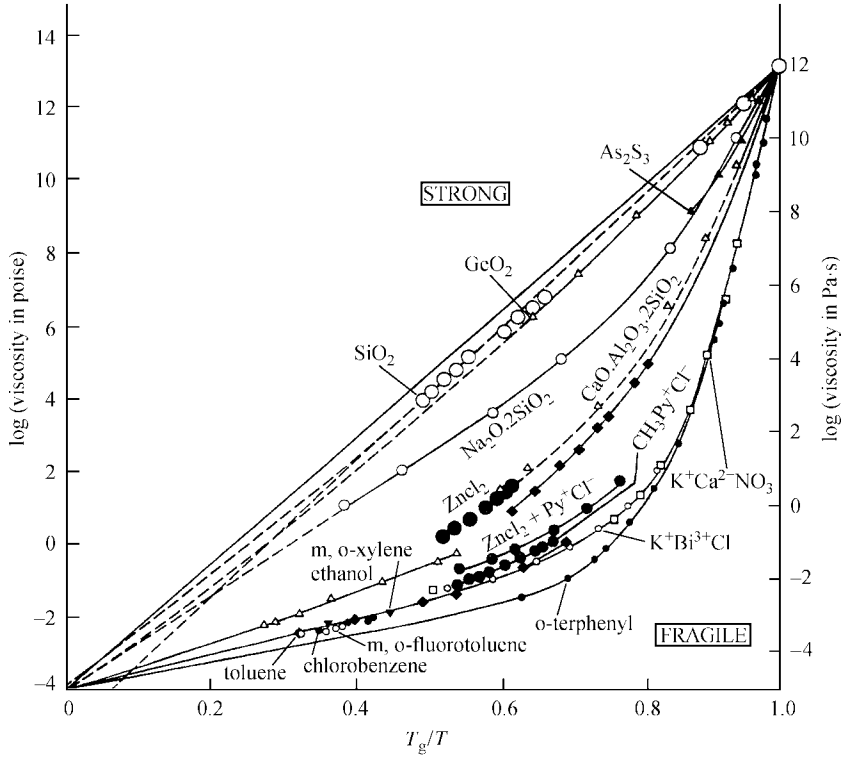

FIGURE 5.25 Strong and fragile liquids. (*After C. A. Angell and W. Sichina, Ann. N.Y. Acad. Sci., vol. 484, p. 241, 1986.*)

5.10 SURFACE ENERGY

5.10.1 Introduction

Similar atomic sites that are located deep in the interior of a body may experience a potential that is periodic over these sites. We may call these sites essentially equivalent. However, on approaching a surface, the sites begin to lose their equivalency because the distribution of atoms is no longer spherically symmetric. The atoms, which are exactly on the surface, have the maximum difference in potential energy. We may consider the surface region as that for which the potential energy is distinguishable from its "bulk" periodic value. The difference of the potential energy integrated over all of the atoms residing in a 1-m^2 cross-section area of the surface region constitutes *surface energy* γ and has the units of J/m^2 in the SI system (or $ergs/cm^2$ in the cgs system). Surface energy is the reversible work in creating a unit area of the surface. The reversible work is equal to the change in Helmholtz free energy, if we ignore changes in atomic concentration in the surface brought about by adsorption while creating the surface. (This is generally true for single-component systems.)

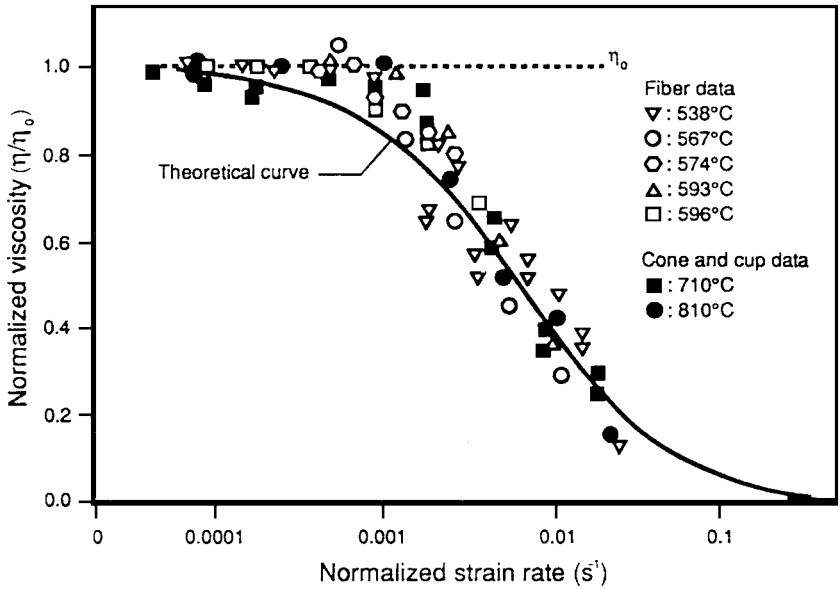

FIGURE 5.26 Nonlinear viscosity. (*After J. H. Simmons and C. J. Simmons, Cer. Bull., vol. 68, no. 11, p. 1949, 1989.*)

Surface energy may also be considered as a force per unit length (N/m or dyn/cm), called *surface tension*, in the surface plane acting perpendicular to the boundary (hence tending to contract the surface). The surface tension of fluid glass is important in most glass-forming processes. Particular attention must be paid to surface tension of glass in the glass-forming processes, for instance, in glass blowing, and drawing processes such as those for tubing, float glass and fiberglass. In addition, the wetting behavior of molten glass on other substrates such as metals and ceramics is critically controlled by surface tension.

5.10.2 Measurement of Surface Tension

For glass melts that are fairly fluid, methods such as the drop-weight technique or the bubble pressure technique are satisfactory. In the former, the melt is allowed to drip out of a platinum tube of radius r having a sharp-cut end. If the weight of the drop is W, then

$$\gamma = W/2\pi r \tag{5.20}$$

with the assumption that the drop separates at the same diameter as the tube opening. Often this assumption is not true and a correction must be applied.[5] In the bubble pressure method, air pressure is applied through a platinum tube dipped in the melt. Again, assuming that the air bubble detaches itself at the same radius as that of the tube,

$$\gamma = r(p - l\rho g)/2 \tag{5.21}$$

where p is the air pressure, l is the length to which the tube is immersed, ρ is the density of the melt, and g is the acceleration due to gravity. For higher viscosities, a fiber method has been found satisfactory. A suspended glass fiber is heated at a point along its length. The hanging length of the fiber below the point of heating will cause the bottom end of the fiber to either extend downward or contract upward. If l is the length such that it neither extends nor shrinks, then

$$\gamma = rl\rho g \tag{5.22}$$

5.10.3 Composition and Temperature Dependence

Since surface energy results from the asymmetry of forces on an atom, it may be readily understood that weakly bonded or highly polarizable ions and atoms contribute less to the surface energy. One expects to have the highest surface energy in vacuum—exposure to atmosphere causes gas or other impurity atoms to be adsorbed or attached to the surface, thereby reducing the surface energy. The surface tension of pure silica melts at 1200°C is about 280×10^{-3} N/m; that for B_2O_3 is only about 80×10^{-3} N/m at 900°C. As shown in Fig. 5.27 for binary silicate melts at 1300°C, γdoes not change much with the added Na_2O. The addition of K_2O decreases γ, whereas Li_2O increases γ. The effect of adding various

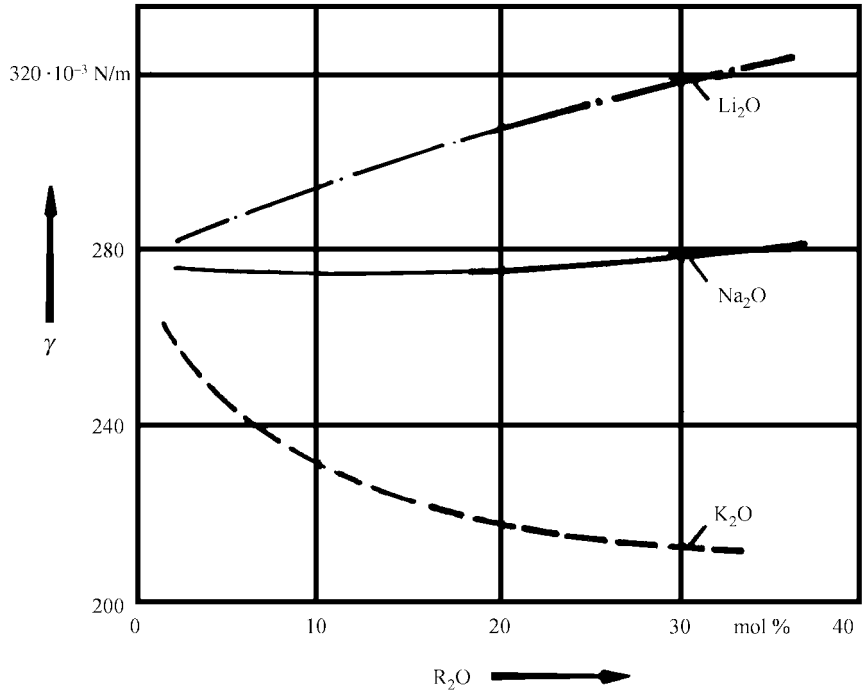

FIGURE 5.27 Surface energy of binary silicates. (*After L. Shartsis and S. Spinner, J. Res. Nat. Bur. Stand., vol. 46, p. 385, 1951.*)

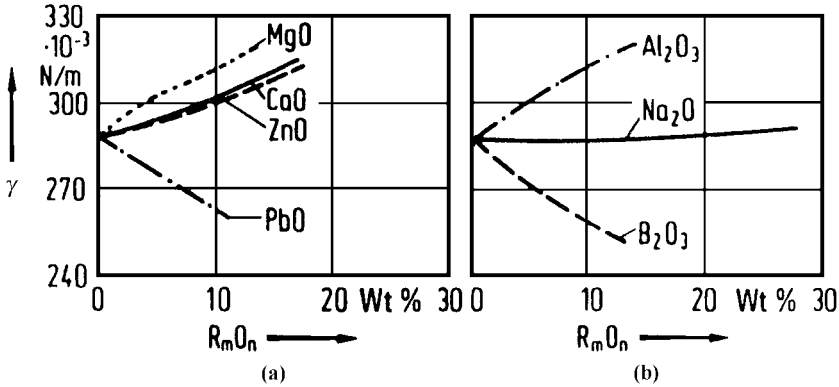

FIGURE 5.28 Surface energy of ternary glasses. (*After L. Shartsis, S. Spinner, and A. W. Smock, J. Amer. Ceram. Soc., vol. 31, p. 23, 1948.*)

other oxides to a $20Na_2O \cdot x\,R_mO_n \cdot (80 - x)\,SiO_2$ (wt%) glass at 1400°C is shown in Fig. 5.28. Surface energy γ(N/m) for silicate melts may be written as:

$$\gamma(1200°C) = [489.2 - 12.5p(Na_2O) - 33.0p(K_2O) + 2.75p(MgO) + 2.33p(CaO) + 1.4p(Al_2O_3) + 3.33p(Fe_2O_3)] \times 10^{-3}\ \text{N/m}$$

$$\gamma(1400°C) = [371 - 6.0p(Na_2O) - 20.0p(K_2O) + 4.0p(MgO) - 1.33p(CaO) + 1.6p(Al_2O_3) - 8.89p(Fe_2O_3)] \times 10^{-3}\ \text{N/m} \quad (5.23)$$

where $p(R_mO_n)$ is the wt% of the oxide, and the SiO_2 contribution is already figured in (see Scholze, in the Bibliography).

Since the bond strength weakens with temperature, the surface tension decreases. In silicate and borate glasses, the surface tension decreases by about 4 to 10×10^{-3} N/m per 100 K increase in temperature.

5.11 THERMAL EXPANSION

5.11.1 Introduction and Definitions

When heat is given to a body, it normally expands. Thermal expansion is the relative change in a given dimension when the body is heated. For instance, $\Delta L/L_0$ is the linear expansion. Thermal expansion is important in determining the suitability of using a variety of materials particularly involving a glass in a restrained condition, e.g., when sealed. On cooling of a glass-sealed assembly, the differential "free" (incompatible) contraction of the various materials generates stresses in the assembly, which may cause glass fracture if the stresses in glass are tensile and their magnitude exceeds the engineering strength of the glass (strength in the presence of flaws, see Sec. 5.19, "Mechanical Strength"). Likewise, when products containing a glass component are suddenly subjected to a rapid temperature change, tensile

stresses may result in glass because of its usually low thermal conductivity. As before, this may lead to glass fracture. The resistance to sudden temperature change, otherwise called *thermal shock resistance* or *thermal endurance*, is determined primarily by the thermal expansion coefficient and the thickness dimension of the product in the direction of the heat flow.

The addition of thermal energy causes a pair of atoms to acquire a larger mean interatomic separation (based on residence time) because of the asymmetric potential well about each atom. In network systems, such as glasses, the variation in polyhedra-connecting bond angles provides yet another mechanism for expansion. Thus, although fused silica is structurally similar to β-cristobalite, the two have widely different thermal expansion.

The linear thermal expansion coefficient (often called as TEC or TCE in industry) α is obtained by dividing thermal expansion by the change in temperature; i.e.,

$$\alpha = \Delta L/L_0\, \Delta T \tag{5.24}$$

Because thermal expansion coefficient usually varies with temperature, an *average thermal expansion coefficient* α_m over the temperature range T_1 to T_2 is obtained as

$$\alpha_m = (L_2 - L_1)/L_0(T_2 - T_1) \tag{5.25}$$

and the *true expansion coefficient* α_T at temperature T as

$$\alpha_T = dL/L\, dT \tag{5.26}$$

Appropriate units for thermal expansion coefficient are /°C or cm/cm/°C. (The reader is cautioned about the use of /°F as is common in U.S. industry. Also, thermal expansion coefficient of glasses is often written in terms of $\times 10^{-7}$/°C, as opposed to $\times 10^{-6}$/°C or ppm/°C for metals. The corresponding volume expansion coefficients β are obtained by substituting V for L in the expressions. For most solids with small expansion coefficients, $\beta = 3\alpha$.

5.11.2 Measurement of Thermal Expansion

Thermal expansion of glasses is often measured by commercially available pushrod dilatometers (see ASTM E228 and ASTM C372-94). The system consists of a spring-loaded pushrod that pushes the ends of a specimen (usually 1.00 inch long) against the flat wall of a tube, generally made out of alumina or fused silica. The measuring tube is inside a temperature-programmed furnace. The expansion of the specimen relative to the tube is measured by an LVDT device. It is important that the specimen should have flat ends perpendicular to the length dimension. For superior accuracy, it is strongly recommended that a double pushrod system be used, where the second pushrod presses against a standard platinum rod specimen, and the differential expansion with respect to platinum is recorded. Glass specimens should be heated at a rate of about 3°C/min, held near the low end of the transition range for about 10 minutes and, subsequently, cooled to room temperature at 3°C/min. Care must be taken during the heating segment to stop at the approach of the transition range (noted by rapid change in length). An accuracy of about 1 percent is expected.

A typical dilatometric expansion curve for a glass is shown in Fig. 5.29. At the onset of the glass transition range, a specimen that had been cooled rapidly in the past tends to shrink, whereas a well-annealed specimen shrinks little. Both of the specimens would expand at a rapid rate on further heating and develop a hook, marking the *dilatometric softening point* T_d. At this point, the specimen becomes soft enough that the pushrod actually begins to penetrate into it, countering any expansion. The furnace should be stopped from

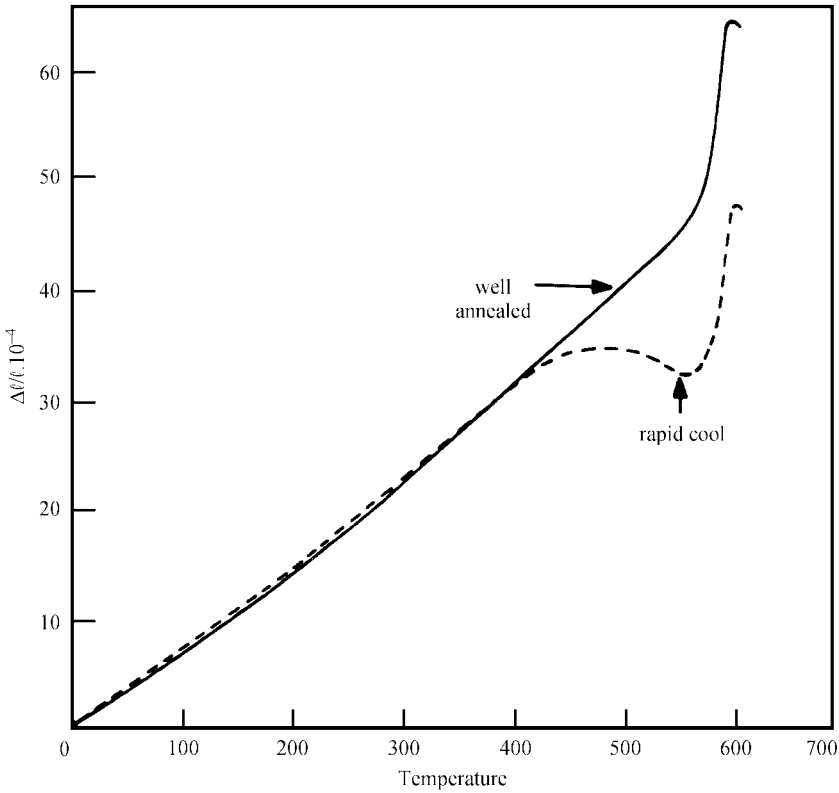

FIGURE 5.29 Typical dilatometric curve of a glass.

further heating at this point. During the isothermal coasting segment, the specimen may shrink further (with continuing push of the pushrod), and would then contract along a different path during the cooling segment. The dimensional changes essentially constitute the volume-temperature diagram (Fig. 5.1), and hence, it must be clearly understood that *the thermal expansion of a glass from room temperature to its glass transition range is different from its thermal contraction from the transition range to the room temperature*.

5.11.3 Expansion Mismatch Consideration for Glass-to-Metal Seals

In glass-to-metal sealing, the glass is typically heated to a flowing condition and fused subsequently to a metal. Since shear stresses begin to set in the transition range during cooling, *the linear thermal contraction curves are more important for glass sealing applications.* The glass contraction curve is overlaid on the metal contraction curve (which is usually the same as its expansion curve) and vertically displaced (see Fig. 5.30) to have the curves coincide at the *set point*, which is often taken as somewhere between the strain point and the annealing point of glass. The offset on the y-axis then yields ε, the *differential contraction*

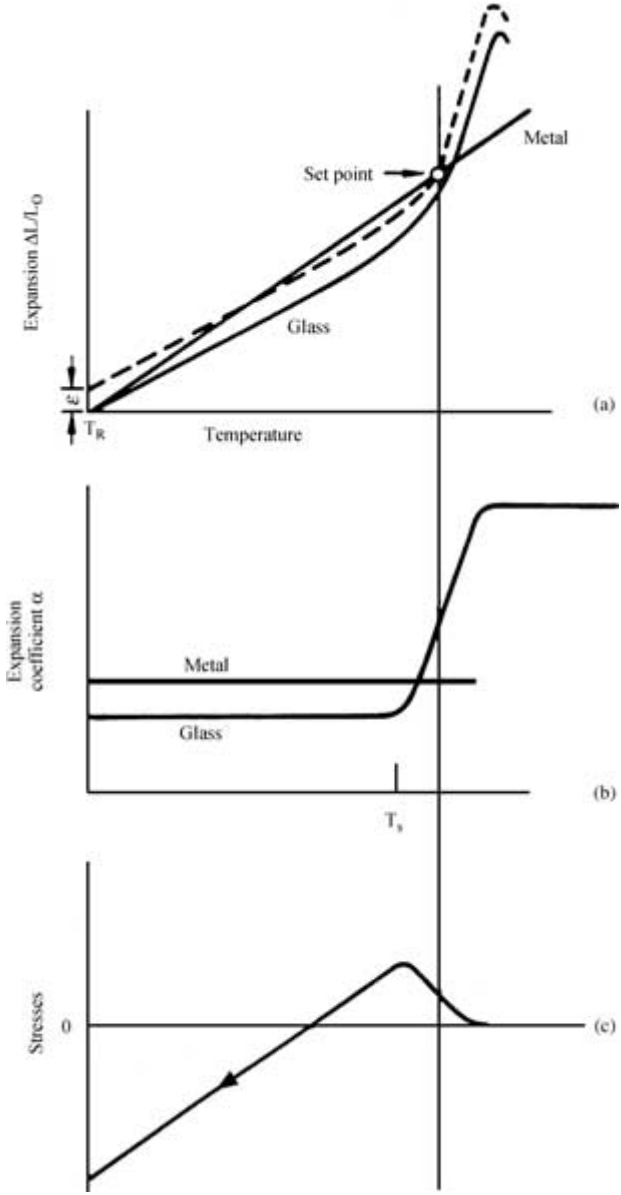

FIGURE 5.30 Set point of glass. (*a*) The expansion curves of the glass and the metal are matched at the set point. (*b*) Because of the variation in the expansion coefficients, stresses develop (*c*) whose magnitude at room temperature corresponds to the mismatch ε shown in (*a*). (*After A. K. Varshneya, J. Amer. Ceram. Soc., vol. 63, no. 5-6, pp. 311–315, 1980.*)

or the *mismatch*, which is to be used in stress calculations. For a low-failure-risk glass-to-metal, glass-to-ceramic, or glass-to-glass seal, a rule of thumb is that $\varepsilon < 500$ ppm for low annual production volume and <200 ppm for high-volume production. A convenient way of measuring ε experimentally is to make a sandwich seal against a known standard (see ASTM F144-80), measuring the stress birefringence by optical means, and correlating the stress so obtained to the ε using equations appropriate for the seal configuration [see, for example, Ref. 6]. For a glass-to-glass seal, ε can be measured by a composite fiber technique. In this method, rods of the two glasses, with similar diameters, are held in both hands and heated at the ends to softening. On sufficient softening, they are allowed to lay on each other, pressed, and resoftened a little to assure good contact. The composite is then gently drawn to obtain a uniform fiber, 0.3 to 0.8 mm in diameter and 10 to 20 cm long. The fiber is then snapped off the residual rods. If the thermal contraction coefficients are different, then the composite develops into the form of a curved segment. This segment is laid over a scale to measure the height h of the segment. The thermal contraction difference is calculated by the formula

$$\varepsilon = (\alpha_1 - \alpha_2)\Delta T = 5dh/(a^2 + 4h^2) \tag{5.27}$$

where d is the average diameter of the composite fiber and a is the length of the cord.

5.11.4 Temperature and Composition Dependence of Thermal Expansion Coefficient

Since the volume generally increases rapidly, with a few exceptions, at the onset of the glass transition range during heating, it is expected that the thermal expansion coefficient would increase rapidly around T_g. Researchers have often wondered if the increase in thermal expansion coefficient, which is a second-derivative thermodynamic property, at the T_g is discontinuous, suggesting that glass transition may be a second-order thermodynamic transition. It is now established that the change in thermal expansion coefficient at the glass transition while transforming from the glassy state to the liquid state can be positive or negative, and is rapid, but not discontinuous. Even while heating in the glassy state, most silicate glasses display rapid increase in the linear expansion coefficient. (Hence, the reader is again cautioned, particularly for glass sealing applications, against the indiscriminate use of glass suppliers' published data, which is usually quoted for the 0 to 300°C range.)

Fused silica and some other single-component glasses such as $Zn(PO_3)_2$, BeF_2, and GeO_2 display anomalous negative thermal expansion coefficient in the vicinity of absolute zero temperature. The exact cause of this behavior is not clearly understood.

Between 20°C and 1000°C, a value of 5.5×10^{-7}/°C is often quoted as the linear thermal expansion coefficient for fused silica, making it one of the lowest for silicate glasses and enables silica glass products to be extremely resistant to thermal shock. Addition of alkali and alkaline earths, which act to convert bridging oxygens to nonbridging, resulting in a decreased connectivity, causes a steady increase in α. In general, the larger the NWM ion concentration the larger the α (see Fig 5.31). On the other hand, the addition of alkali to B_2O_3 glass increases the connectivity by converting triangularly coordinated boron atoms to tetrahedral coordination. This increased connectivity results in a decrease in α down to 13 to 17 mol% added alkali and increasing subsequently because of steric influences. The variation of α with the added alkali is shown in Fig 5.32 (see also the discussion of the boric oxide anomaly in Sec. 5.4.4).

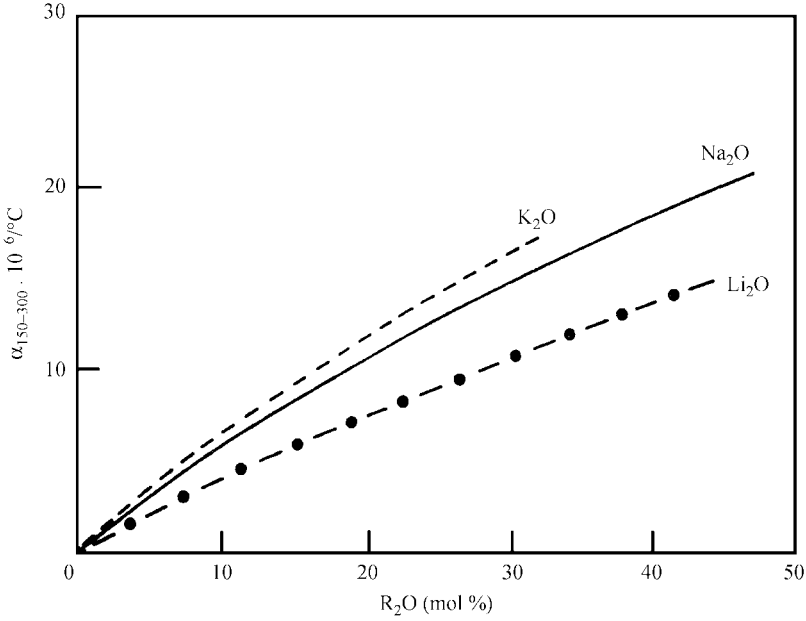

FIGURE 5.31 Thermal expansion of R_2O-SiO_2 glasses.

The addition of TiO_2 lowers the expansion coefficient of silica glass. A $7.5TiO_2$-$92.5SiO_2$ (wt%) glass, made by a vapor-phase process, has an α of $0 \pm 0.3 \times 10^{-7}$/°C over the 5 to 35°C range, and is sold under the trade name ULE® (ultralow expansion) glass by Corning Inc. (see Chap. 6). The ultralow expansion is very desirable for earth-based and deep-space-based telescope mirror applications. Thermal expansion coefficients for several commercial glass compositions are listed in Table 6.2 (Chap. 6). The soda-lime glasses generally have α in the range of 85 to 95×10^{-7}/°C, which is "high" for a glass, making it quite susceptible to thermal shock. The soft potash-soda-lead glasses also have similar values of α, making them and soda-lime glasses a near-ideal pair to produce several glass products having complex-shaped parts at an optimized lower total cost. (As an example, a common household incandescent lamp shell is made out of soda-lime glass to which the filament assembly is fused via a potash-soda-lead glass mount structure.) Between the large-expansion soda-lime glasses or the lead glasses and the low-expansion silica glasses are the borosilicates (α values in the range of 33 to 55×10^{-7}/°C) and the alkaline earth aluminosilicates (α values in the range of 40 to 60×10^{-7}/°C).

To calculate α_m for soda-lime-silicate glasses, Lakatos et al.[7] have suggested the use of the following expression:

$$\alpha_m = (51.3 + 210.864Na_2O + 275.584K_2O + 13.8887CaO - 23.93MgO - 88.638Al_2O_3) \times 10^{-7}/°C \quad (5.28)$$

where the oxide formulas represents the number of moles of the oxide per mole of silica in the glass composition.

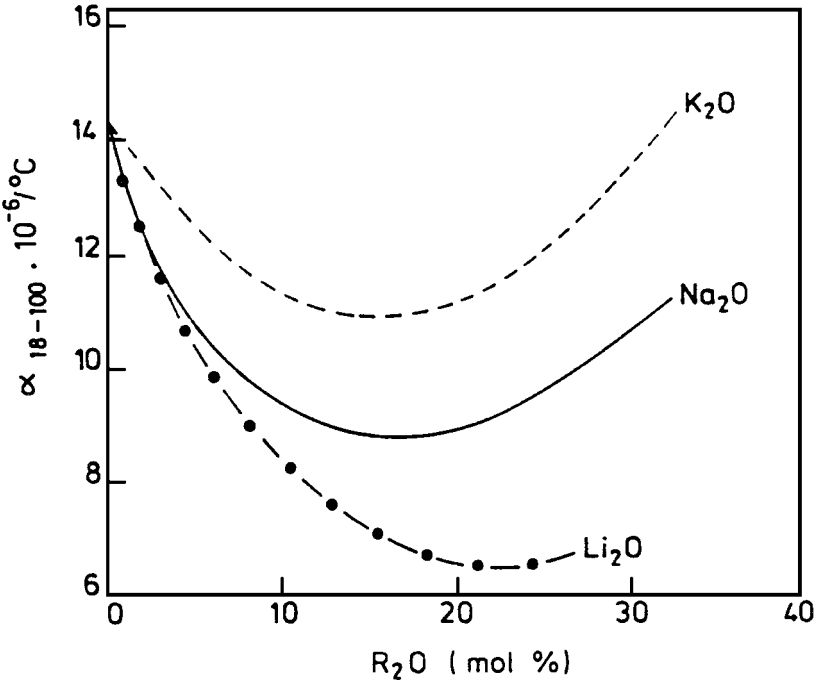

FIGURE 5.32 Thermal expansion of R_2O-B_2O_3 glasses.

The thermal contraction coefficient from T_g to room temperature of alkaline earth aluminosilicate glasses of the type used in halogen headlamp inner bulb application may be estimated using the relation:

$$\alpha_{T_g-20C} = (12.63 + 2.4\text{CaO} + 1.4\text{BaO} - 0.185\text{Al}_2\text{O}_3 + 0.48\text{ZrO}_2) \times 10^{-7}/^{\circ}\text{C} \quad (5.29)$$

where the oxide formulas represent wt% composition and SiO_2 is assumed to be the balance.

5.11.5 Thermal Shock Resistance

When a glass plate has a temperature gradient that is a function of the thickness direction z only, then it may be shown that planar stresses σ_x or σ_y are given by

$$\sigma_x = \sigma_y = -\left(\frac{E}{1-v}\right)\alpha(T - T_a) \quad (5.30)$$

where T_a is the average temperature across the thickness. This implies that a biaxial tensile stress develops wherever the temperature is less than the average and a compressive stress develops where the temperature is higher than the average. In either case, the magnitude of the stress is directly proportional to the thermal expansion coefficient. The biaxial stress

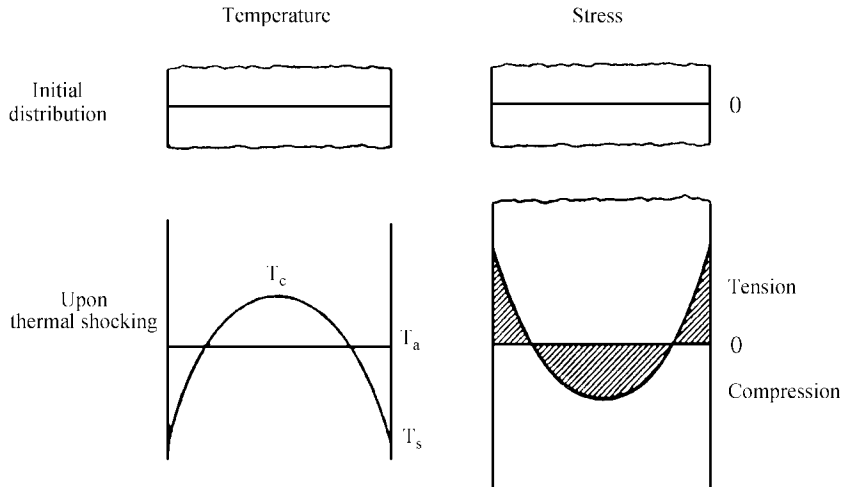

FIGURE 5.33 Development of stresses across a wall due to thermal shock.

has the same mathematical form as the temperature distribution. Hence, when the plate has a parabolic temperature distribution with center temperature T_c and surface temperature T_s (such as that obtained in normal cooling from both sides (see Fig. 5.33), a parabolic stress distribution is expected, with outside surface having a tensile stress of the magnitude

$$\sigma_x = \sigma_y = 2\left(\frac{E}{1-v}\right)\alpha\left(\frac{T_c - T_s}{3}\right) \tag{5.31}$$

and the center having a compressive stress of the magnitude

$$\sigma_x = \sigma_y = -\left(\frac{E}{1-v}\right)\alpha\left(\frac{T_c - T_s}{3}\right) \tag{5.32}$$

Because of a high probability of flaws on the surface, glass fracture may result. The term $(T_c - T_s)$ clearly depends on several parameters such as the *thermal diffusivity* (defined in Sec. 5.13, "Heat Transfer") and the thickness in the direction of the heat flow. A thermal shock test is conducted (see ASTM C149-86) by soaking a lot of product, generally no less than 20 in number, in a rack inside a hot oven, and then quickly immersing the rack into ice water, counting the failures, and repeating the remainder lot to higher and higher oven temperatures. Thermal endurance parameter ΔT_E is computed as that temperature interval at which the lot has a 50 percent survival probability. Because glass strength is sensitive to the environment of immersion and stressing rate, and the rate of heat transfer to a fluid is sensitive to its viscosity (hence, its temperature), thermal shock experiments must be carried out consistently, and should not be compared from one medium to another, or from one temperature range to another. To test the strength of an internal surface, for instance, a glass-to-metal interface, it may be desirable to design upshock experiments, i.e., taking the

product out of a low-temperature bath and immersing it into a high-temperature bath. Empirically it has been observed that

$$\Delta T_E = m/\alpha L^{1/2} \tag{5.33}$$

where m is a constant. Thus, the thermal endurance is increased by reducing the thermal expansion coefficient or by reducing the thickness L of the glassware.

5.12 HEAT CAPACITY

The amount of thermal energy needed to raise the temperature of a unit mass of the substance is called its *heat capacity*, denoted generally by C_p when the measurement is made at constant pressure (for instance, under laboratory atmosphere) or by C_v when the measurement is made at constant volume. Appropriate units are cal/(g · °C) in conventional cgs units or J/(kg · K) in SI units. Heat capacity is conveniently measured by using a differential scanning calorimeter (DSC), in which the rate of heat input to raise the temperature of a small known mass of the substance, say 50 mg, at a specified rate is measured and compared to that of the empty pan. A typical heat capacity versus temperature curve for a soda lime silicate glass is shown in Fig. 5.34. In the solid state, the heat capacity C_{pg} increases slowly, and is limited to $3R$ per gram-atom (R = gas constant) by the *DuLong and Petit law* for vibrational heat capacity. Thus the solid-state heat capacity of most silicate glasses is about 0.3 cal/(g · °C). At the onset of the glass transition, heat capacity rises steeply because of added

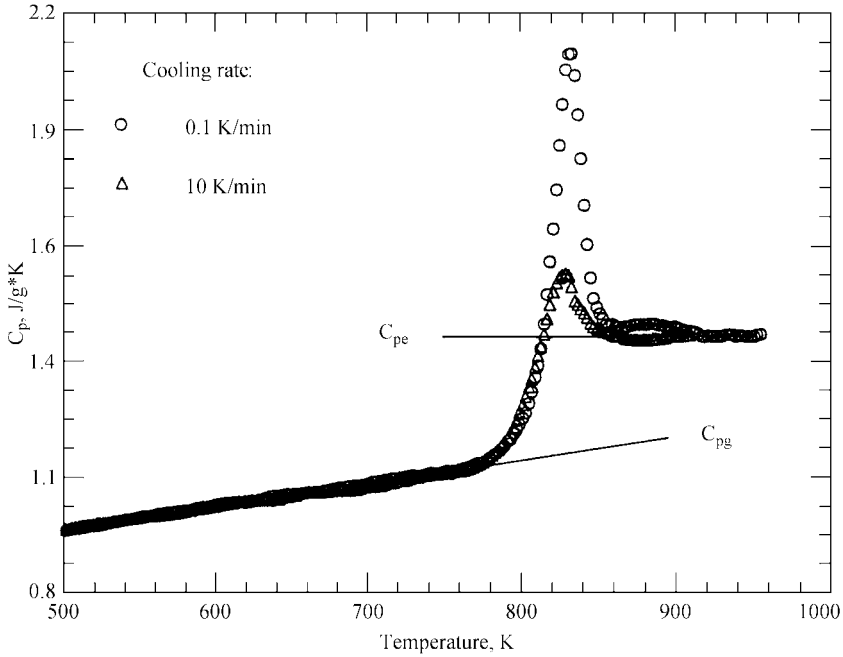

FIGURE 5.34 Thermal history dependence of heat capacity of glass showing steep rise in the transition range. (*After C. T. Ho, Ph. D. thesis, Alfred University.*)

TABLE 5.5 Factor for Calculation of Mean Specific Heat of Glass from the Composition

Oxide	*a*	*c*
SiO_2	0.000468	0.1657
Al_2O_3	0.000453	0.1765
CaO	0.000410	0.1709
MgO	0.000514	0.2142
Na_2O	0.000829	0.2229
SO_3	0.00083	0.189
K_2O	0.000445	0.1756
B_2O_3	0.000598	0.1935
Fe_2O_3*	0.000380	0.1449
Mn_3O_4	0.000294	0.1498

*Good only at 600°C.

Source: After D.E. Sharp and L.B. Ginther, *J. Amer. Ceram. Soc.,* vol. 34, pp. 260–271, 1951.

contribution from the various configurations that the structure is able to achieve. When the supercooled liquid state is reached, the heat capacity, denoted as C_{pe} in Fig. 5.34, once again levels to steadier values (and may even decrease at higher temperatures). Since heat capacity is the first derivative of the molar enthalpy and the second derivative of the molar Gibbs free energy, and since the variation in enthalpy is often similar to the variation in volume, the temperature dependence of heat capacity is often similar to the slope of the volume-temperature curves (Fig. 5.1). This implies that when a glass is heated, depending on the thermal history (prior cooling history) of the specimen, (1) there is often a decrease in heat capacity as the glass approaches the transition, (2) the jump at the glass transition is not sharp, and (3) there is an overshoot at the onset of the transition range as seen in Fig. 5.34. A slower-cooled glass shows a higher amount of overshoot for the same reheating rate in the DSC instrument (see thermal history effects in Sec. 5.14.4, "Relaxation of Properties").

Moore and Sharp[8] have found that the mean heat capacity C_m (cal/g) for various silicate glasses in the solid state fits the equation:

$$C_m = \frac{T\Sigma p_i a_i + \Sigma p_i c_i}{0.00146T + 1} \tag{5.34}$$

where p_i is the weight fraction, a_i and c_i are the additivity factors for each oxide, and T is the temperature in °C. Values of a_i and c_i are given in Table 5.5. The $\Sigma p_i c_i$ term essentially gives the mean heat capacity at 0°C.

5.13 HEAT TRANSFER

Transfer of thermal energy occurs via three basic mechanisms: *conduction, convection*, and *radiation.* Conduction of heat in metallic solids occurs via electrons. When one end of a metallic rod is heated, the excited electrons essentially run to the other end conducting the heat. In opaque, nonmetallic solids, heat is conducted via the excitation of lattice waves, or vibrations, which exchange quantized packets of energy, called *phonons*, with each other.

In fluids, the atoms and molecules may themselves migrate and set up convection currents or flow. Radiative heat transfer, on the other hand, requires no medium for transport. Thermal energy is carried with light-wave packets, called *photons*, and heats up the body when the body absorbs the photons. Whereas the phonon conductivity dominates heat transfer in the glassy state, transfer of heat in molten glass tanks is mostly due to radiative transfer and to some extent by convective and conductive transfer.

Thermal conductivity K of a solid is written according to *Fourier's law* in one dimension (x) as

$$Q = -KA\, dT/dx \tag{5.35}$$

where Q is the quantity of heat current (flux per unit time), A is the cross-sectional area, and T is the temperature. The negative sign implies that heat flows in the direction of decreasing temperatures. Appropriate units for K are cal/(cm · °C · s) in the cgs system, and W/(m · K) in the SI system. [*Note*: 1 W/(m · K) = 2.388×10^{-3} cal/(cm · °C · s)]. Thermal conductivity of insulating solids in the low-temperature range may be measured by a method described in ASTM C408-88, where heat flux is introduced into a cylindrical specimen, (about 1 cm dia × 1 cm thick) via an upper thermode, and a steady state of heat flow into a lower thermode is achieved. For transient heat flow conditions without an internal generation of heat, the application of the conservation of heat yields

$$dT/dt = \kappa d^2T/dx^2 \tag{5.36}$$

where κ is called the *thermal diffusivity* and is equal to $K/\rho C_p$, ρ being the density. Equations of heat transfer and mass transfer are analogous; one merely needs to substitute concentration C in place of the temperature T, and mass diffusivity D in place of κ. Thermal diffusivity may be measured by commercially obtainable laser instruments.

Values of K for most silicate glasses in the range 25 to 500°C are of the order of 2.5×10^{-3} cal/(cm · °C · s) or about 1 W/(m · K), and do not change much with the temperature. As temperature increases, a "clear" glass body acts as a *diathermanous* solid; i.e., it emits as well as transmits radiated energy. It is possible to show that the *hemispherical radiative conductivity* K_R of such a body is given by:

$$K_R = 16n^2\sigma T^3/3\alpha \tag{5.37}$$

where n is the refractive index for the wavelength transmitted, σ is Stefan's constant, and α is the *absorption coefficient* (see Sec. 5.20.3, "Transmission and Absorption") for the same wavelength. A plot of K_R versus temperature is shown in Fig. 5.35. It may be noted that, whereas the phonon conductivity contribution remains roughly 0.0025 cal/(cm ·°C · s), the K_R rises steeply above 500°C to 0.175 at 1400°C for clear glasses, which is about one-fifth the conductivity of copper. In a glass-melting tank, all of the radiation that is of greater than 4.5 μm wavelength gets absorbed in the top few micrometers of the molten glass, causing the surface to heat up. Shorter wavelengths are able to penetrate into the glass and be absorbed by deeper layers. The heated surface subsequently emits radiation, of which the long wavelength portion heats the layer immediately underneath and the short wavelength portion heats layers much deeper. This high rate of heat transfer by radiation, absorption, transmission, reradiation, and reabsorption, in cascade from the furnace crown, sidewalls, burner flames, and the hot glass eventually heats as much as 4- to 5-ft depths in a clear glass melting tank. Because of the high absorption coefficient, particularly around the 1-μm wavelength, colored glasses do not transfer heat as readily. Tanks for melting colored glasses based on fossil fuel energy, hence, must be quite shallow to avoid cold, virtually immobile glass at the bottom. The usual recommendation in such cases is to provide an auxiliary electric heating boost from the bottom of the tank.

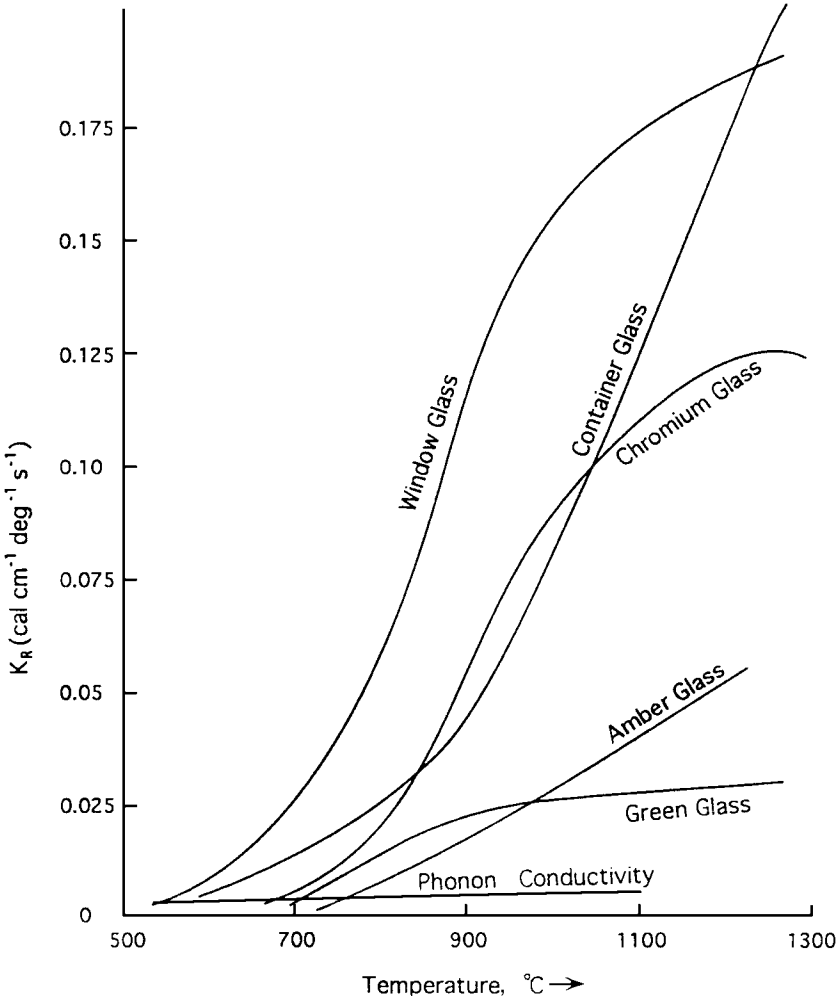

FIGURE 5.35 Radiative heat transfer in glass.

5.14 GLASS TRANSFORMATION RANGE BEHAVIOR

5.14.1 Introduction

In the glass transformation range, the volume of the mass smoothly departs from that of the equilibrium supercooled liquid line *bcf* as shown in Fig. 5.1. This is because the molecular units within the material are no longer able to relax to their equilibrium structure within the available time. Holding the mass isothermally at any temperature within the transformation

range causes the glass structure to approach equilibrium. This is termed *stabilization* or *relaxation*. Hence, the magnitude of glass properties varies with the time of holding within the transformation range.

5.14.2 Measurement of Glass Transition Temperature T_g and the Fictive Temperature T_f

Glass transition temperature T_g is defined as the temperature corresponding to the intersection of the glassy state line with the tangent to the steepest portion in the transition range on the calorimetric curve. Instead of the calorimetric curve, one may use a dilatometric curve. It must, however, be understood that there is no specific temperature at which the supercooled liquid transforms into a glass.

The fictive temperature T_f is represented by the temperature corresponding to the intersection of the glassy state line with the extrapolation of the supercooled liquid line. The understanding here is that the structure of the glass is identical to the structure of the liquid at T_f. Thus, T_f is determined by an area matching technique as discussed by Moynihan et al.[9]

5.14.3 Relaxation of Properties

The simplest expression describing the relaxation of properties during an isothermal hold for time t is *Maxwell's relationship*:

$$p_t = p_0 \exp(-t/\tau) \tag{5.38}$$

where p_t = value of the property p at time t
p_0 = value at time $t = 0$
τ = relaxation time

The relaxation time is usually estimated from the relation:

$$\tau = \eta/M \tag{5.39}$$

where η is the viscosity and M is a modulus of elasticity (generally taken as the shear modulus G, since shear relaxation is the more common situation). It has been found that a more suitable expression for relaxation is the *Kohlrausch-Williams-Watts* (KWW) power-law relationship:

$$p_t = p_0 \exp - (t/\tau)^n \tag{5.40}$$

where the KWW exponent n is 0.5 for shear relaxation and about 0.68 for volume relaxation. Having $n < 1$ causes the relaxation to be considerably slower than that predicted by the simple Maxwell relation. Mathematically, the KWW expression is equivalent to a linear sum of weighted Maxwell terms (5 to 10 terms are generally sufficient) with a spectrum of relaxation times.

It may be readily recognized that, at the annealing point viscosity of 10^{12} Pa · s (= 10^{13} poise) and a shear modulus of roughly 10^{10} Pa, the time for 90% relaxation (about $5\eta/M$) is of the order of a few minutes. At the strain point, where the viscosity is $10^{13.5}$ Pa · s, relaxation requires as much as 4 to 6 hours. One may also realize that the time for relaxation (or stabilization) of glass could increase to well beyond several decades at temperatures where

viscosities exceed 10^{18} Pa · s (see also Sec. 5.9.3). Since viscosities for most commercial glasses at room temperatures are well beyond measurable or meaningful values (>> 10^{20} Pa · s), the stabilization of glass would require millennia!

Glass at room temperature behaves as if it had the characteristics of the structure at the fictive temperature T_f. The density and the viscosity of glass should increase; the electrical conductivity and the permeability to inert gases should decrease with time in the transformation range, since the T_f gradually decreases causing the volume to shrink (Sec. 5.1.3). A fast-cooled glass having a higher T_f would be expected to relax faster relative to a slow-cooled glass when both are held at an identical temperature in the transformation range. These concepts must, however, be treated as a very basic description only. As indicated already in Sec. 5.1.3, glass actually accumulates an entire thermal history during cooling; hence, a single fictive temperature concept is not adequate. Additionally, continuing relaxation occurs in glass during reheating through the transition range (Sec. 5.1.3). After the initial solid-state expansion, the volume relaxes toward the equilibrium supercooled liquid line (or its extrapolation), the rate of such relaxation being dependent on the heating rate and the thermal history. An overshoot is generally noted (dashed line, Fig. 5.1). The more rapid the heating rate, the larger is the overshoot. Note that *glass never retraces its cooling path regardless of the heating rate*. The thermal history continues to accumulate until such time that the glass is once again brought to the equilibrium liquid line, at which point the thermal history is wiped clean.

5.15 DIFFUSION AND PERMEATION

5.15.1 Introduction

At essentially all temperatures, atoms are vibrating; they vibrate more vigorously at higher temperatures. Occasionally, their thermal energy is sufficient to cause them to overcome a potential barrier experienced by them and jump to a neighborhood site. Even in the absence of a chemical potential gradient (such as that caused by a concentration gradient) and external fields (such as electric, magnetic, or gravitational), atoms are able to move about from site to site via what is called a *random walk*. If r is an average jump distance and ν the frequency of successful jumps in one dimension, then the *self-diffusion coefficient*, or the *diffusivity*, D_i is defined as

$$D_i = r^2\nu/2 \tag{5.41}$$

Appropriate units of D are cm^2/s or m^2/s.

Diffusion is the underlying basis of mass transfer properties such as *permeation, electrical conduction, dielectric loss, viscosity*, and *chemical durability*.

5.15.2 Measurement of Diffusion

Although there is no net transfer of mass during self-diffusion, it should be apparent that a diffusivity can be measured by allowing a labeled isotope, either radioactivated or having a slightly different mass, to undergo random walk over a period of time and obtaining the distribution of the labeled isotope, subsequently, by methods such as sequential etching or slicing.

The presence of a chemical potential gradient and/or external force fields biases such motion to cause a net mass transfer across an imaginary plane. Such diffusion is broadly categorized as *chemical diffusion*. In a special case where the chemical diffusion of one species causes the counterflow of a second species, such a situation may be termed *interdiffusion*. An *ion exchange* reaction occurs when a diffusing ion exchanges sites with another ion on a no net transfer of charge basis. The various coefficients of chemical diffusion are generally quite different in magnitude from the self-diffusion coefficients. Chemical diffusion along a concentration gradient can be conveniently measured by instruments such as the electron microprobe or the energy dispersive spectrometer (EDS).

5.15.3 Temperature Dependence of Diffusion

All of the mass transfer properties, being thermally activated, follow an Arrhenius relation of the type

$$D = D_0 \exp(-\Delta H/RT) \tag{5.42}$$

where ΔH is the activation energy for diffusion (units: kcal/mol or kJ/mol), R is the gas constant, T is the absolute temperature, and D_0 is simply a preexponential factor. The diffusivity increases exponentially with temperature, and plots of log D (and ln D) versus $1/T$ are straight lines sloping downward.

In silicate glasses, ionic motion is the dominant diffusion phenomenon. The activation energy for ionic diffusion is generally written in terms of the electrostatic binding energy for the ion to detach itself from the present site plus a strain energy to push the ion through an interstitial "doorway." As the size of the ion increases, so does the strain energy, and hence the activation energy.

5.15.4 Composition Dependence of Diffusion

Alkali ions, particularly Na^+ and Li^+, are among the most mobile species. Diffusion of water as H^+ and H_3O^+ (hydronium ion) is also quite rapid, and is of interest to understanding chemical durability of glass. Plots of the self-diffusion coefficient of Na in vitreous silica and binary sodium silicates are shown in Figs. 5.36 and 5.37. Values of diffusivity vary in the 10^{-5} to 10^{-10} cm^2/s range from about 400° to 900°C. Some breaks in otherwise Arrhenius behavior are observed in binary silicates, particularly around the glass transition range. Typical activation energies for Na^+ ion in silicate glasses are about 20 kcal/mol, or about 80 kJ/mol.

5.15.5 Permeation

Permeation is the motion of an inert atom or molecule through the glass network without making a chemical bond with any of the constituents. While permeating, some of the mass may be left behind in the network, i.e., physically dissolve in it. Permeability K of a gas is defined as

$$K = DS \tag{5.43}$$

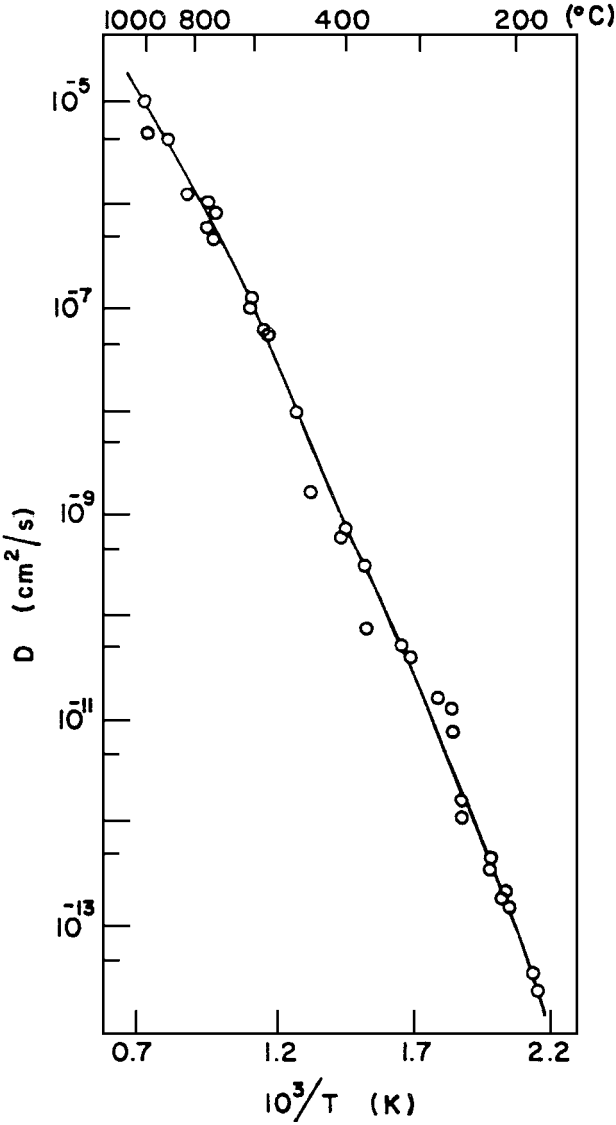

FIGURE 5.36 Self-diffusion coefficient of sodium in silica glass. (*After G. H. Frischat, J. Amer. Ceram. Soc., vol. 51, p. 528, 1968.*)

where S is the solubility. The solubility itself is defined here as

$$S = c_i/c_g \tag{5.44}$$

where c_i is the concentration in glass and c_g is the concentration in the gas phase. Since S is unitless, the units for permeability are the same as those for the diffusivity. The diffusing

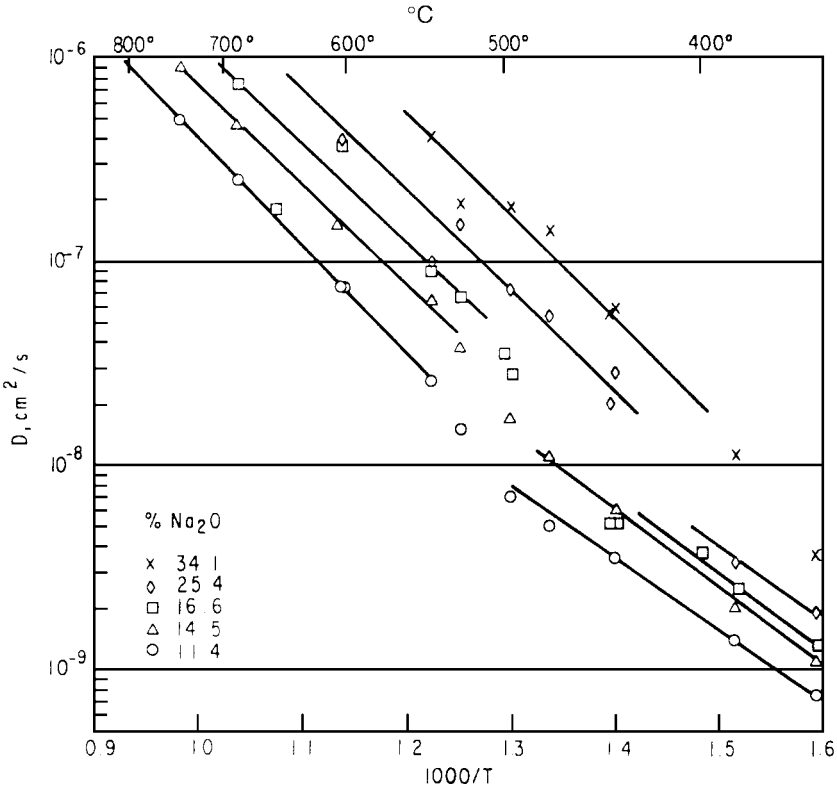

FIGURE 5.37 Self-diffusion coefficient of sodium in Na_2O-SiO_2 glasses.

species essentially squeezes through the network as if the network were a sieve—the larger the open area the higher the permeability, or conversely, the larger the size of the species the lower the permeability. One may think of an inert species as experiencing a frictional force, much like that due to viscosity, during permeation through the glass. The diffusivity may be related to the viscosity through the *Stokes-Einstein relation*:

$$D = k_B T/6\pi\eta r \tag{5.45}$$

where k_B is the Boltzmann constant and η the viscosity of the medium. Examples of permeation would be the motion of He atoms, or N_2 molecules, through glass. Gas permeability is generally measured by obtaining the mass of gas permeated across a thin membrane of glass while maintaining a known gas pressure on the other side of the membrane.

A plot of log K versus $1000/T$ for helium permeation through various glasses is shown in Fig. 5.38. Note that the permeation also follows Arrhenius behavior quite well, and that the more open-structured glasses are the more permeable. Permeability decreases rapidly with increasing size of the permeating atom.

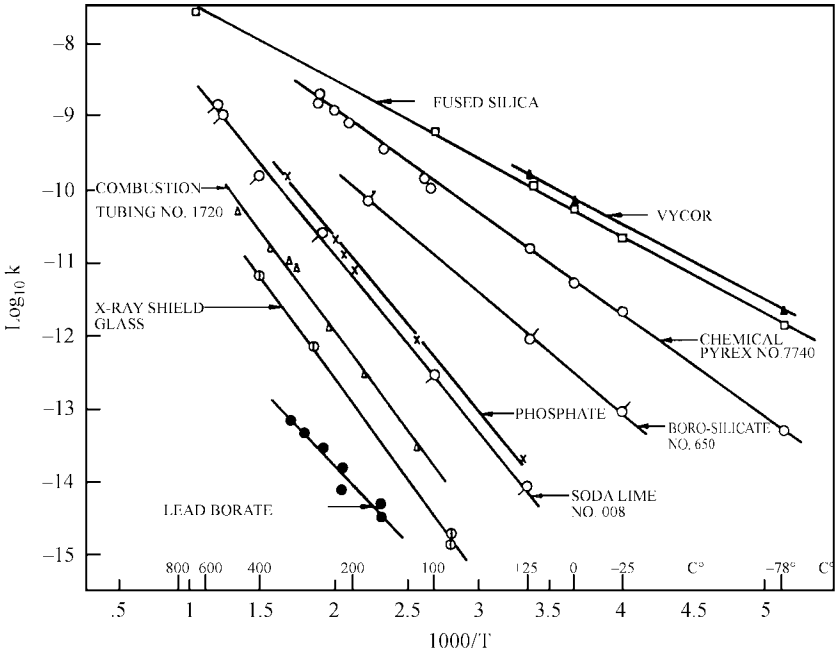

FIGURE 5.38 Logarithm of the permeability of helium gas versus 1000/*T* for various glasses. (*After F. J. Norton, J. Amer. Ceram. Soc., vol. 36, p. 90, 1953.*)

5.16 ELECTRICAL CONDUCTION

5.15.1 Introduction

As stated in the earlier section, ionic motion is the dominant diffusion phenomenon in silicate glasses. Of these, conduction by alkali ions makes up 99 percent or better of the electrical transport in common silicate glasses. Hence, ions are the most mobile charge carriers. Since ions are less mobile than electrons, the silicate glasses are basically electrical *insulators* relative to the metals, where electrons are the dominant charge carriers. There is some electronic conduction in silicate glasses, particularly in those that have a significant amount of transition metals, such as Fe, Mn, and V, displaying multivalency in glass. Electronic conduction is predominant in elemental glasses, such as silicon, germanium, and the chalcogenides, where such conduction is, in fact, responsible for the semiconductor properties, and, perhaps, for much of the modern electronic industry. Glasses containing fluoride ions display anionic conduction based on the transport of F^-. Some silver- and copper-containing glasses display fast ion conduction based on transport of charge by Ag^+ and Cu^+ ions.

The basic equation describing electrical conduction is *Ohm's law*, according to which the resistance R_e (ohms) is given by

$$R_e = V/I \tag{5.46}$$

V is the electrical potential (volts) applied across the conductor and I is the current (in amperes) that flows. The resistance for a conductor having a cross-sectional area A and length L is given by

$$R_e = \rho L/A \tag{5.47}$$

where ρ is called the *resistivity*. Appropriate units for ρ are $\Omega \cdot$ cm (in cgs) or $\Omega \cdot$ m (in SI). Conductivity σ is the reciprocal of resistivity; the units are often written as mho/cm or S/m (siemens per meter). Conductivity is related to the diffusivity through the Nernst-Einstein relation:

$$\sigma = \frac{n(ze)^2 D}{H_R k_B T} = \frac{z^2 F^2 DC}{H_R RT} \tag{5.48}$$

where n is the number of charge carriers per unit volume, e is the electronic charge, z is the valency, k_B is the Boltzmann constant, R is the gas constant, C is the concentration in mols/volume, and F is the Faraday unit of charge. H_R is the *Haven ratio*, which correlates charge conduction to the atomic motion in successive jumps. Often D/H_R is written as D_σ. The value of the Haven ratio for diffusion by a vacancy mechanism may be shown to be approximately 0.4.

5.15.2 Temperature Dependence

The temperature dependence of resistivity is given by the empirically obtained *Rasch-Hinrichsen equation*, which is

$$\log r_\rho = A + [B/T] \tag{5.49}$$

where A and B are constants. The equation is essentially the Arrhenius equation of the form valid for diffusion. For conductivity

$$\sigma \cong \sigma_0 \exp(-\Delta H/RT) \tag{5.50}$$

where the activation energy ΔH is essentially the same as that for diffusion.

5.15.3 Application of DC Potential across Glass

When a dc potential is applied across a thin disk of a silicate glass, the mobile alkali cations (e.g., Na^+) migrate from the anode region to the cathode region. The two nonbridging oxygen anions, to which the two Na^+ were attached, recombine to form one bridging oxygen and release one O^{2-}, which moves toward the anode. Glass is thus gradually electrolyzed. The electrode reactions are

$$\begin{aligned} &\text{Cathode region:} \quad 2Na^+ + 2e \rightarrow 2Na^0 \\ &\text{Anode region:} \quad O^{2-} \rightarrow 2e + \frac{1}{2}O_2 \uparrow \end{aligned} \tag{5.51}$$

Thus, metallic sodium is deposited on the cathode plate and oxygen is outgassed from the anode region. The depletion of ions near each electrode builds a *polarization field*, which causes a rapid decrease of current. In time, the current stops flowing. Oxygen outgassing

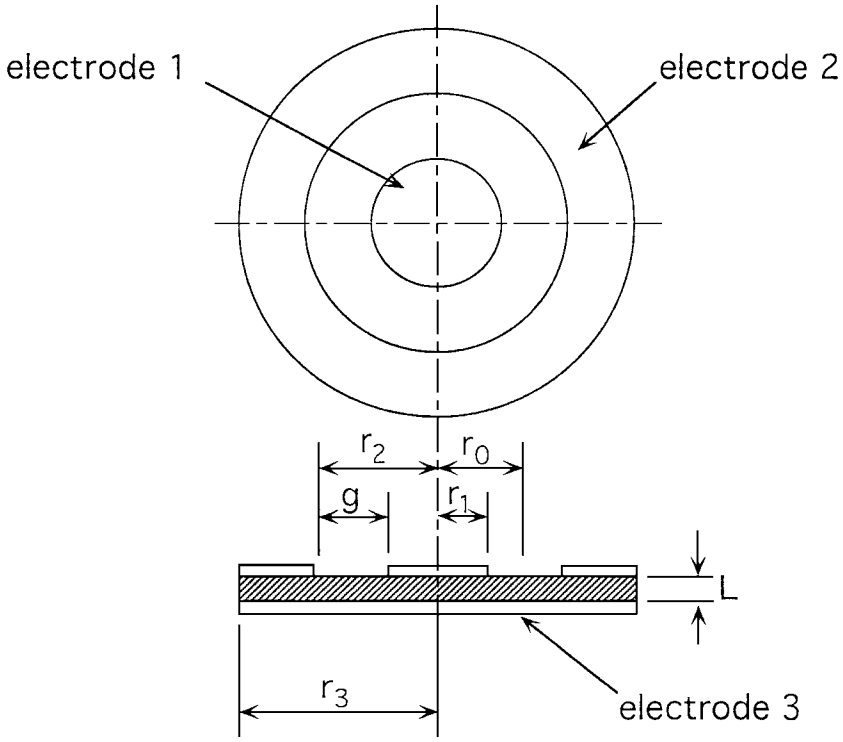

FIGURE 5.39 Guard ring arrangement to measure dc conductivity.

and the motion of alkali ions, both under the influence of electric field, are a serious problem when glass is bombarded by charged particles, such as electrons in a television picture tube or in instruments such as an electron microscope or an electron probe analyzer.

5.15.4 Measurement of Electrical Conductivity

Electrical conductivity of a glass may be measured by using a "guard ring" arrangement (see ASTM C657-93) and an ac bridge circuit. Metallic electrodes, often as thin as approximately 300 Å, are vacuum deposited on both sides of a glass disk. On one of the sides, the deposition is carried out by using a ring mask—the outer ring thus acts as a guard against surface conduction along the edge surface (see Fig. 5.39). Both the center and the guard ring are held at the same potential (voltage), but the current is measured only through the center electrode. Use of the alternating current in place of the direct current avoids the electrode polarization effects mentioned above. One measures the complex impedance (Z^*) of the specimen as a function of the ac frequency. The plot of the imaginary part (Z'') of the complex impedance against the real part (Z') generally has the shape of a semicircular arc. The intercept of the arc (or its extrapolation) with the Z' axis directly yields the dc resistance. Since the electrodes do not provide a supply of the ions into glass, such a method is often termed the *blocking electrode* method.

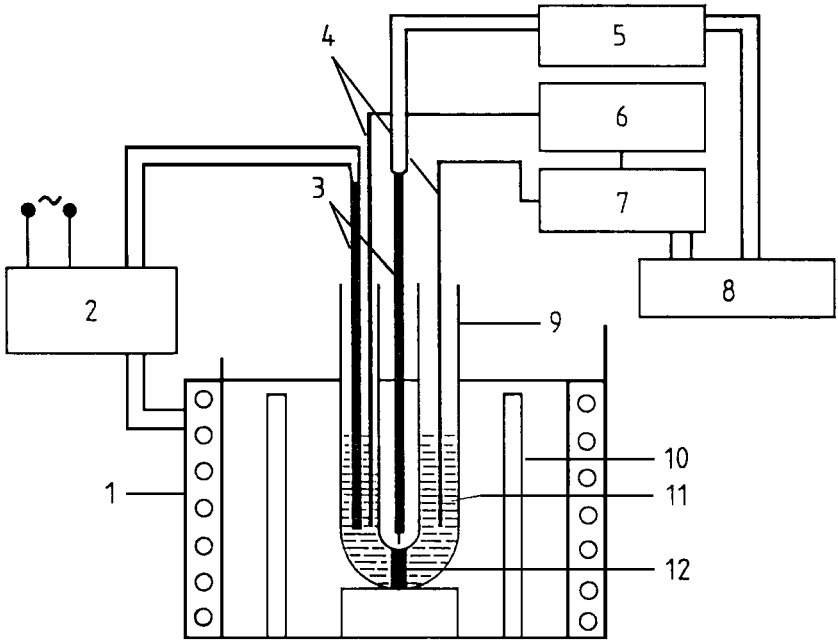

FIGURE 5.40 Nonblocking electrode method to measure dc conductivity. *1* = furnace, *2* = controller, *3* = thermocouple, *4* = platinum electrodes, *5* = thermometer, *6* = dc power supply, *7* = ammeter, *8* = recorder, *9* = U-tube, *10* = steel shield, *11* = fused salt, *12* = specimen. (*After V. Jain, A. Varshneya, and P. Bihuniak, Glastech. Ber. vol. 61, p. 321, 1988.*)

For a *nonblocking electrode* method, the disk of glass may be sealed into a tube in a way that separates the two arms of a glass U tube (of matching thermal expansion coefficient, so that fusion is successful). Alkali salts, e.g., $NaNO_3$, are filled into the arms of the tubes and the tube is placed in a vertical orientation inside a furnace. After a sufficiently high temperature is reached, platinum electrodes are inserted into the arms, a dc potential applied, and the current is measured with a sensitive electrometer (see Fig. 5.40).

Surface conductivity of glass or of thin films on glass is often measured in terms of sheet resistance R_{sh} (ohms per square, or $\Omega/\square$) using a four-point probe technique. Electrically contacting point probes are placed at the four corners of a square on the surface or the film. A current I is allowed to pass through two adjacent probes, and the potential difference V developed across the other two probes is measured. Sheet resistance in this arrangement is calculated as

$$R_{sh} = \left(\frac{2\pi}{\ln 2}\right)\left(\frac{V}{I}\right) \tag{5.52}$$

5.15.5 Composition Dependence

Electrical conductivity of silicate glasses is extremely sensitive to chemical composition. In general, the higher the Na and Li content, the higher the conductivity. As expected, conductivity increases rapidly with increasing temperatures, closely following the Arrhenius relation, with an activation energy of about 20 kcal/mol (80 kJ/mol), the same as that for

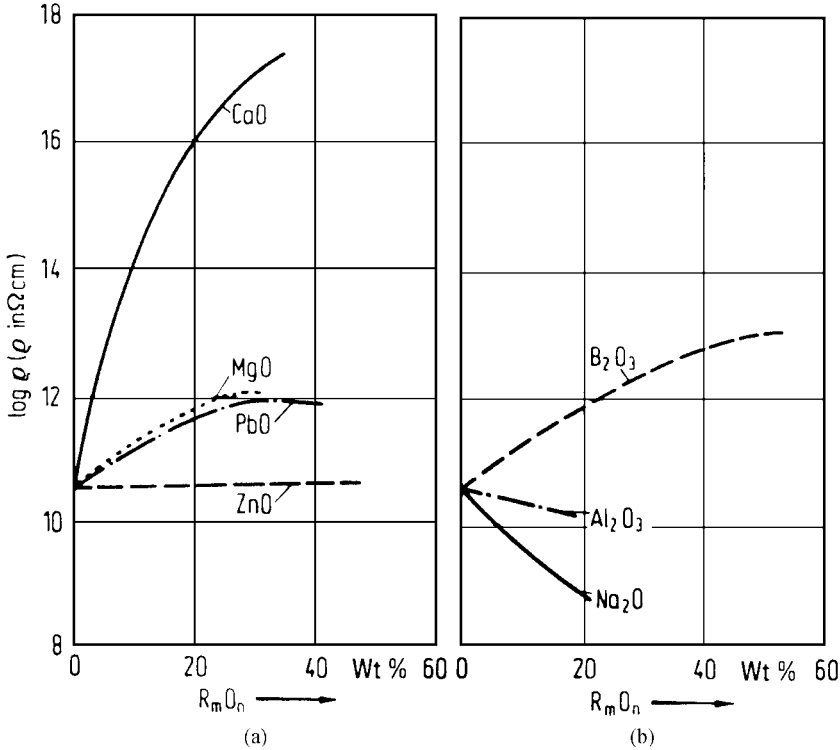

FIGURE 5.41 Variation of dc resistivity at 25°C of $15Na_2O \cdot 85SiO_2$ (wt%) glass with progressive replacement of SiO_2.

the sodium ion diffusivity. The effect of replacing silica by other oxides on resistivity at 25°C in a $15Na_2O \cdot 85SiO_2$ (wt%) glass is shown in Fig. 5.41. Addition of CaO and B_2O_3 appears to raise resistivity greatly. Dependence on the cationic radius of the added oxide is indicated in Fig. 5.42. Shown in Table 6.2 (Chap. 6) are values of the electrical resistivity of some commercial compositions at 25°C. Šašek and Knotek[10] have offered the following additivity calculations for the soda-lime-silicate glasses:

$$\sigma = \Sigma \sigma_i p_i / 100 \tag{5.53}$$

where p_i is the wt% of the oxide and σ_i is the factor given in Table 5.6 at three different temperatures. The reader must, however, be cautioned against using additivity factors to calculate the electrical conductivity. The most dramatic departures from the additivity relationship are displayed by diffusivity and ionic conductivity in mixed alkali glasses. This is shown, for instance, in Fig. 5.43 for Na^+ and Cs^+ ions in mixed Na_2O-Cs_2O-SiO_2 glasses at 480°C as a function of the mixed alkali ratio. It is noted that the self-diffusivity of Na^+ ions (measured by tracer isotopes) decreases dramatically with increasing Cs content and actually becomes lower than that of the Cs^+ in the pure Cs_2O-SiO_2 glass. Likewise, the self-diffusivity of Cs^+ ions decreases with increasing Na content and crosses over to unmeasurable values. *The measured conductivity is far from being the linear sum of the conductivities in the end compositions*: It shows a dramatic negative deviation, *4 orders of magnitude difference*, from an additivity behavior. The minimum in conductivity is not at

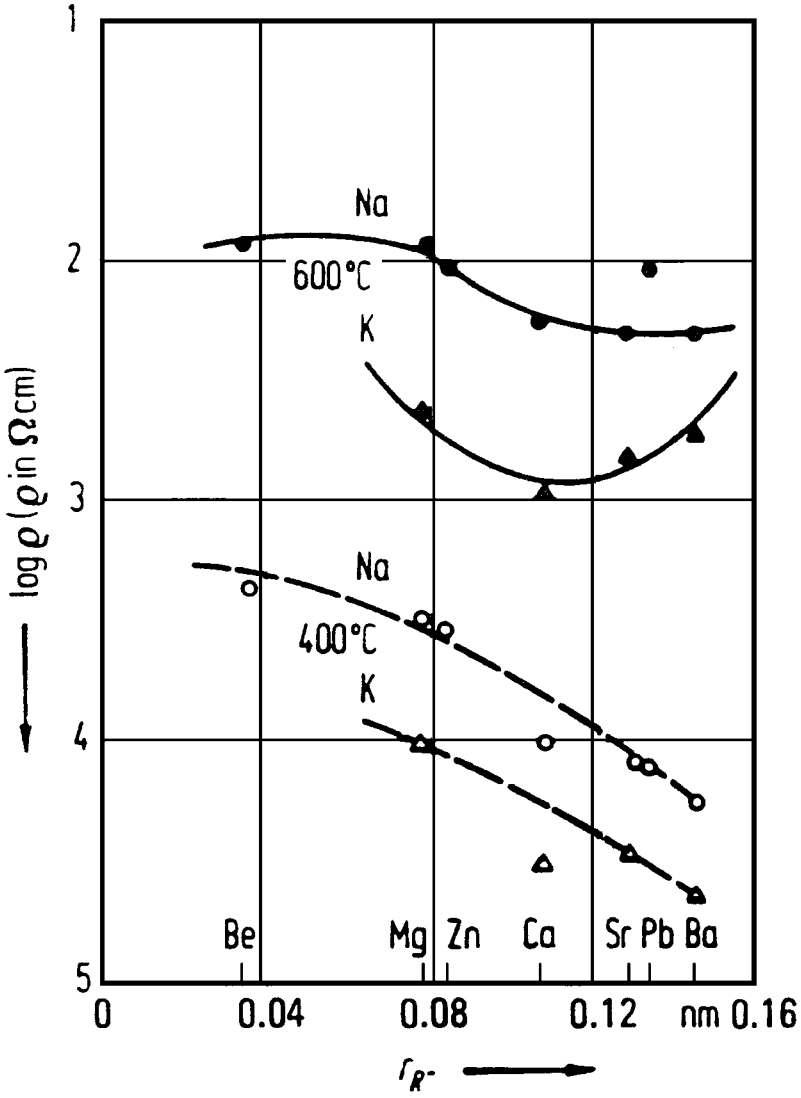

FIGURE 5.42 DC resistivity of $2R'_2O{\cdot}R''O{\cdot}7SiO_2$ as a function of alkaline earth ionic radius $r_{R''}$. (*After H. Wakabayashi, R. Terai, and H. Watanabe, J. Ceram. Soc. Japan, vol. 94, p. 677, 1986; vol. 94, p. 948, 1986.*)

the diffusivity crossover; rather it is a bit toward the more mobile cation (around the 0.6 mixed alkali ratio). In glass science, this phenomenon is called the *mixed-alkali effect*, and remains the most intriguing of all the unsolved mysteries. (One may not be called a glass scientist if one did not indulge in trying to unravel at least some aspect of it.) It does appear that *one alkali somehow affects the motion of the other.* From a practical application point of view, the mixed alkali effect has been beneficially utilized in developing very low electrical

TABLE 5.6 Factors σ_i for Determining Electrical Conductivity (in S/cm) of Soda-Lime-Silicate Glass Melts at Different Temperatures

	σ_i for T in °C		
Oxide	1200	1320	1400
SiO_2	−0.413	−0.576	−0.701
Al_2O_3	−0.654	−0.908	−1.10
Fe_2O_3	−0.311	−0.439	−0.537
MgO	−0.168	−0.100	−0.019
CaO	−0.243	−0.088	−0.087
Na_2O	+3.61	+4.93	+5.92
K_2O	−0.582	−0.458	−0.282

Source: After L. Šaˇsek and M. Knotek, *Chem. Technol. Silik.*, vol. L13, pp. 91–106, 1985.

conductivity glasses to insulate current leads in high-wattage lamps. The mixed alkali effect is of concern in properties other than electrical conductivity as well. For instance, the mixed alkali effect has been shown responsible for the undesirable drift in mercury-glass thermometers during a temperature measurement (otherwise known as the *thermometer effect*). Hence, precision glass thermometers are now made out of single-alkali glasses.

5.17 DIELECTRIC PROPERTIES

When a dc voltage V is applied to a large parallel plate capacitor having a narrow vacuum gap d between the plates, then the plates are charged with ^{+}q and ^{-}q charges per unit area immediately. The electric displacement flux D_0 that develops may be given by:

$$D_0 = q \tag{5.54}$$

The electric field strength E is defined by

$$D_0 = \varepsilon_0 E \qquad \text{and} \qquad E = V/d \tag{5.55}$$

where ε_0 is called the absolute permittivity (*dielectric constant*) of the free space, and has a value 8.854×10^{-12} F/m. The capacitance C_0 per unit area between the parallel plates is given by

$$C_0 = \varepsilon_0/d \tag{5.56}$$

If we replace vacuum by a dielectric such as glass, the new capacitance C and electric displacement are given by

$$C = \varepsilon_s C_0 \qquad \text{and} \qquad D = \varepsilon_s D_0 \tag{5.57}$$

where ε_s is called the *static relative permittivity* (or the relative dielectric constant). Thus,

$$D = \varepsilon_s \varepsilon_0 E = \varepsilon E \tag{5.58}$$

where ε is called the *electric permittivity* of the medium.

In an alternating field, we may write

$$D^* = \varepsilon^* \varepsilon_0 E^* \tag{5.59}$$

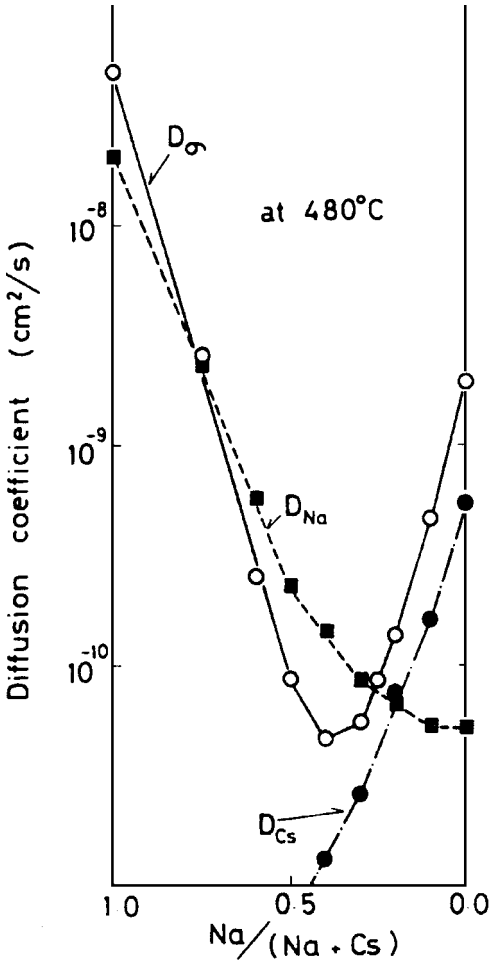

FIGURE 5.43 Diffusivity and electrical conductivity in Na_2O-Cs_2O-SiO_2 glasses at 480°C. D_σ is the diffusivity calculated from the measured conductivity by the Nernst-Einstein relation. The deep minimum in D_σ (actually the electrical conductivity) represents the mixed-alkali effect. (*After R. Terai, J. Non-Cryst. Sol., vol. 6, no. 2, p. 121, 1971.*)

where the asterisk is used to represent complex numbers. Thus, the complex dielctric constant has the form

$$\varepsilon^* = \varepsilon' - j\varepsilon'' \tag{5.60}$$

where $j = (-1)^{1/2}$. The real part ε' is the dielectric constant, and the imaginary part ε'' is the dielectric loss factor. The ratio

$$\varepsilon''/\varepsilon' = \tan \delta \tag{5.61}$$

is termed the *loss angle*, where δ is the phase difference angle between the electric field E^* and the electric displacement flux D^*. Dielectric properties are measured as a function of the applied frequency by ac bridges or other electronic equivalents.

All dielectrics suffer from breakdown when the applied voltage exceeds the dielectric strength. The breakdown usually results in a changeover from an insulating to a conducting behavior, often because of a large dielectric loss factor. Dielectric constants are important for many applications. Large capacitors require high dielectric constants. On the other hand, in integrated circuit applications, the substrates are required to have low dielectric constants to allow a high interconnect signal speed.

The dielectric constant of glasses is generally 4 to 11 at 1 MHz and 20°C. Typical values for soda-lime-silicates are 7 to 9. Some internally nucleated glass-ceramics in the B_2O_3-P_2O_5-SiO_2 system have values as low as 3.8 to 4.5, suggesting potential applications as microelectronic substrates, replacing alumina for which the dielectric constant is 9. The loss angle, tan δ, is strongly related to the conductivity σ. Values are generally 10^{-3} and increase with the amount of alkali ions, again mitigated by the mixed-alkali effect. Presence of heavy metal ions, such as Pb, causes a decrease in tan δ.

5.18 CHEMICAL DURABILITY

5.18.1 Introduction

The high chemical durability or the resistance of glass to a large number of corrosive media has been one the primary reasons why glass is a preferred material in a variety of applications. Glasses are preferred over plastics for beverage containers primarily because the sintering aids used in the manufacture of the latter impart undesirable taste to the contained fluid. Plastics also adsorb some of the taste-generating organics in the beverages. (Additionally, the permeation of oxygen through most plastics causes the oxidation of alcohols to aldehydes and ketones, which has also been deemed undesirable.) However, glasses are not altogether inert to most fluids. Even water attacks glass gradually over long periods, causing it to develop a white surface deposit. Silicate glasses are readily dissolved by hydrofluoric acid (HF). Phosphoric acid (H_3PO_4) attacks most silicate glasses at temperatures exceeding about 200°C. Caustic alkalis are also able to attack most silicates, albeit generally slowly.

There are two primary mechanisms of chemical attack on silicate glasses:

1. *Leaching*, where the mobile alkali ions such as Na^+ in the glass interstices are gradually leached out and replaced by H^+ (or the hydronium ion, H_3O^+) on a no net transfer of charge basis. The reaction may be represented by

$$Si\text{-}O^-Na^+ + H^+OH^- \rightarrow Si\text{-}O^-H^+ + Na^+OH^- \tag{5.62}$$

   which is an interdiffusion reaction. The extracted mass of alkali is directly proportional to the square root of time.

2. *Dissolution*, where the corrosive medium attacks the Si-O primary bond and may be represented by

$$Si\text{-}O\text{-}Si + Na^+OH^- \rightarrow Si\text{-}O^-Na^+ + HO\text{-}Si \tag{5.63}$$

   The result is the breakup of a bridging bond to form a more gel-like structure. With time, more and more of the bridging bonds are broken, causing the network to essentially fall apart. The extent of corrosion generally increases linearly with time.

The leaching mechanism operates primarily in media having pH = 7 or less (water or acidic). On the other hand, when pH > 7, i.e., in alkaline solutions, the corrosion is primarily due to the network dissolution. Since both the mechanisms are thermally enhanced, chemical durability of glass decreases at elevated temperatures.

The leaching mechanism is the underlying science in *weathering* of glass. The extracted alkali reacts with CO_2 in the air and deposits white, opaque layers of sodium carbonate and bicarbonate on the surface. Inexpensive glassware often undergoes this weathering reaction after repeated dishwashing cycles. Likewise, window glasses develop the white carbonate layer over a period of time because of reaction with atmospheric humidity and CO_2. Over long periods of time of storage, hard liquors and wines extract Pb from lead crystal glass containers, which may be a health risk. Glass enamels containing PbO and CdO which have been applied to the rim and the lip areas of hollow ware for decorative purposes may also pose a health risk (see ASTM C927-80 for the determination of Pb and Cd extraction by acetic acid from glass tumblers).

5.18.2 Measurement of Chemical Durability

Methods of measuring chemical resistance of glass are generally simple. A weighed quantity of glass (with a known surface area) either in bulk form or in a pulverized form is allowed to react with a known quantity of fluid (see ASTM C225-85). The reaction is carried out at controlled temperature with gentle stirring without changing the fluid or by replenishing it periodically (flowing condition). After a known amount of time, the amount of metal elements extracted in the leachate is analyzed by standard methods such as an atomic absorption (AA) spectrophotometer, or an induction-coupled plasma (ICP) unit. Since the surface of most glass products is generally somewhat different in composition from the bulk, the preference would be to use the as-manufactured bulk product. However, because of the low surface area, such tests could take significant amounts of time. The degree of chemical attack on decorations may be judged visually by the appearance of a stain, iridescence, matte, or gross discoloration (see ASTM C724-91 for acid resistance of decorations on architectural glass, C735-93 for acid resistance of decorations on glass containers, C675-91 for alkali resistance of decorations on glass containers, C676-93 for detergent resistance of decorations on tableware, and C777-93 for sulfide resistance of ceramic decorations on glass), or by weight loss (see ASTM C1203-91 for alkali resistance of glass enamels). When the leachate is not replenished, it is expected that the pH of the attacking medium will continuously change over the test interval. A number of specialized tests have been developed for durability measurements on optical and ophthalmic glasses. These tests include ISO 8424 for acid resistance (SR test), ISO 9689 for phosphate resistance (PR test) and ISO DIS 10629 for alkali resistance (AR test). A climate resistance test (CR test) has also been proposed to ISO. Before these standardized tests became available, most optical manufacturers had their own specific test procedures.

The testing of chemical durability for products that are disposed into landfills is often carried out using the toxicity characteristic leaching test (TCLP) set forth by the Environmental Protection Agency (EPA) method 1311 in the United States.

5.18.3 Composition Dependence

Higher-alkali-containing glasses tend to be less durable. Figure 5.44 shows a qualitative representation of the chemical resistance of some commercial silicate glass families. Note that silica glass, having very few mobile ions, is the most durable, followed by alkaline earth silicates and sodium borosilicates. For a sheet glass composition, the quantity W_e (mg of Na_2O)

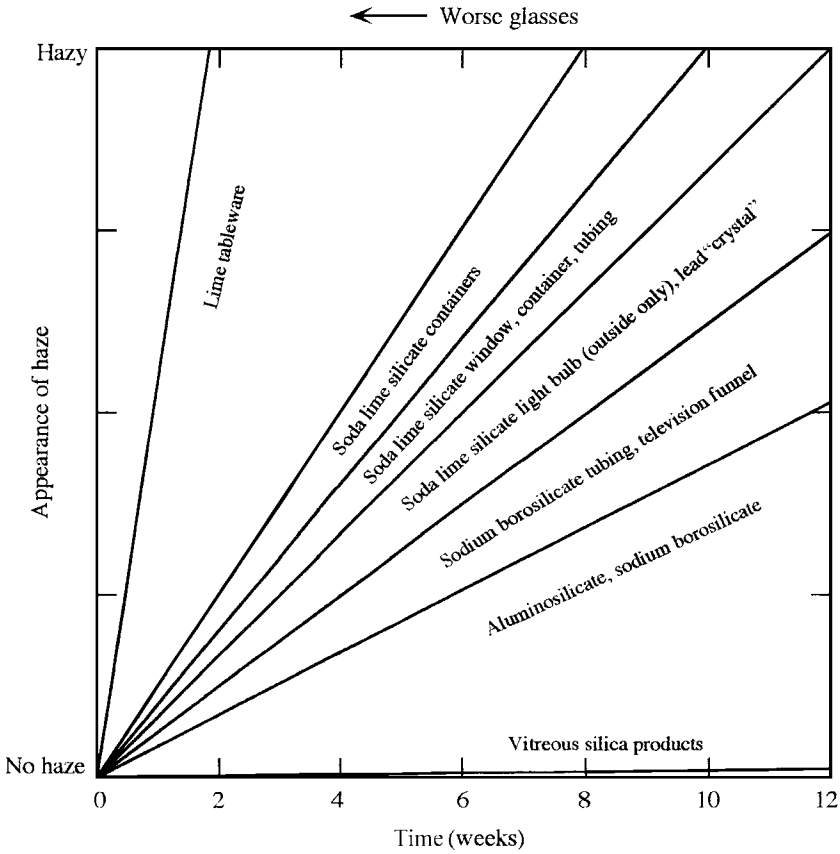

FIGURE 5.44 Chemical durability of commercial glasses. (*Adapted from H. V. Walters and P. B. Adams, J. Non-Cryst. Sol., vol. 19, p. 198, 1975.*)

extracted from a 2-g quantity of pulverized glass by 50 mL of water may be estimated from the formula:

$$W_e = -1 + 0.135\ Na_2O + 0.164K_2O - 0.023MgO - 0.021CaO - 0.1Al_2O_3 - 0.002Fe_2O_3 \quad (5.64)$$

where the various oxides are expressed in wt%. Perhaps the most sophisticated model for predicting the durability is based on estimating the free energy of hydration. It was developed by Jantzen et al.[11] in reference to high-radioactivity-level nuclear waste immobilization. In the model, the composition data are first assembled to predict the extent of phase separation (extent of heterogeneity), which is subsequently utilized to properly locate the dependence between the weight-averaged free energy of hydration and the mass loss in a standardized test.

5.18.4 Methods of Improving Chemical Durability

Chemical durability of silicate glasses is generally improved by any technique that renders the surface richer in silica. The foremost of these is *firepolishing*, which causes surface alkali to volatilize, leaving the surface silica-rich. Treatment of soda-lime-silicate glass products in SO_2/SO_3 gas laden with water vapor is also able to extract the surface alkali. This is sometimes referred to as *dealkalization* of the glass surface. The sodium sulfate on the surface appears as a bloom, which is then washed away. Surface coatings such as those of lacquer or acrylates reduce the activity of water on the glass surface, hence improve the durability.

5.19 MECHANICAL STRENGTH

5.19.1 Introduction

It is a common observation that glass products fracture readily at stress levels as low as about 5000 lb/in^2 (about 35 MPa). Freshly formed glass products often withstand 20,000 lb/in^2. A thermally tempered product (such as a bathroom sliding door, cooking oven transparency, or automobile side window) is able to withstand 20,000 to 30,000 lb/in^2. Aircraft windshields, are chemically strengthened to have strengths of the order of 65,000 lb/in^2 in order to withstand the impact of birds flying at as much as 400 knots. Glass fibers for optical telecommunication have a strength specification of no less than 100,000 lb/in^2 in bending. The rather large variation in glass strengths is a result of the random atomic structure of glass, which excludes the existence of line defects such as dislocations found typically in metals and which provide a predictable "yield" strength.

Under ordinary application of a tensile stress, glass acts like a brittle solid. There is no observable plasticity unless the stress is highly concentrated in a localized region, such as when a microindenter is used. It may be shown that the strength σ_m of a brittle solid, i.e., the tensile stress required to separate two atoms a distance a_0 apart initially, is given by

$$\sigma_m = (E\gamma_f / a_0)^{1/2} \tag{5.65}$$

where E is Young's modulus and γ_f is the fracture surface energy. (γ_f should not be confused with γ, which is the interfacial surface energy discussed in Sec. 5.10. Some energy is dissipated as heat and acoustic energy during fracture as well as in creating two new surfaces, hence $\gamma_f > \gamma$.) Using $E = 70$ GPa and $\gamma_f = 3.5$ J/m^2, $a_0 = 0.2$ nm for a typical silicate glass, we get $\sigma_m = 35$ GPa (about 5,000,000 lb/in^2). This value of theoretical strength makes a silicate glass the strongest material. Specially processed silica fibers have been obtained that approach about one-fifth of this value. Most bulk glass specimens, however, have surface flaws that reduce the engineering strength to a value σ_f given by

$$\sigma_f = \frac{1}{2}(E\gamma_f / c)^{1/2} \tag{5.66}$$

where c is the length of the flaw (simulated by a semielliptical hole whose semimajor axis is c). In theory, the applied stress σ_a is magnified at the tip of the flaw by a factor of $2(c/a_0)^{1/2}$. *Failure occurs when the magnified stress at the tip approaches* σ_m, i.e., when $c = c^*$, a critical length. The engineering strength of glass, thus, may be as little as a few megapascals

in tension, depending on the severity of the flaws. It should be borne in mind that, under the application of a pure compression, glass undergoes densification—the bonds fold upon each other to reduce the interstitial space.

5.19.2 Slow Crack Growth

How an ordinary flaw of length c becomes a critical flaw of length c^* is explained by slow crack growth arguments of fracture mechanics. It is customary to define stress intensity factor K as

$$K = \sigma_a(\pi c)^{1/2} \tag{5.67}$$

A plot of the crack velocity versus the stress intensity factor for a range of humidity levels is shown in Fig. 5.45. Note that, in region I, the *(subcritical) crack growth* velocity increases with the magnitude of K and the humidity. In region II, the velocity is independent of K. In the final stage, region III, the (subcritical) crack grows rapidly to critical length with K, but now independent of the humidity level. Failure of the specimen is imminent in region III. It may also be readily argued that the subcritical growth of the initial crack length c also increases K, thus causing the velocity to follow the curve until failure (unstable crack propagation). The instant at which failure occurs may be called the *critical stress intensity factor* $K_c = \sigma_a(\pi c^*)^{1/2}$. In addition to the effect of the medium, the crack growth velocity also increases with the ambient temperature as shown in Fig. 5.46.

Brittle solids fail in one of three possible modes, shown in Fig. 5.47. In mode I (the *opening mode*), both the crack plane and the direction of propagation are normal to the applied tension. In mode II (the *sliding mode*), a tensile shear acts to slide the fracture planes over each other in the direction of stress. Mode III (the *tearing mode*) is also a shear failure, except that the shear causes the fracture to propagate normal to the stress. Corresponding to these three modes, a material has three critical values of the stress intensity factor $K_{\mathrm{I}c}$, $K_{\mathrm{II}c}$, and $K_{\mathrm{III}c}$ (pronounced K-one-cee, etc.), and it is generally recognized that K_{ic} is characteristic of the material. In a generalized stress application, most brittle materials fail in the $K_{\mathrm{I}c}$ mode: Both the fracture plane and the direction of fracture propagation are perpendicular to the principal tension.

Since cracks grow with time, glass fails at lower stresses when subjected to sustained loads for long times. This is often termed *static fatigue*. Likewise, the strength of glass may be higher at higher stressing rates. (This effect is called *dynamic fatigue.*) It may, however, be noted in Fig. 5.45 that there perhaps is a threshold for K below which crack growth is essentially nonexistent. This low limit is called the *fatigue limit*, which for silicate glasses is generally around 0.3 MPa $\cdot$ m$^{1/2}$. The relationship between the crack velocity V and K_{I} is often written in terms of a power law as

$$V = A(K_{\mathrm{I}})^n \tag{5.68}$$

where A and n are constants; n is called the *stress-corrosion susceptibility coefficient* or the *crack-growth exponent* and ranges between 12 and 35 for most glasses.

5.19.3 Toughness

Toughness, by definition, is the amount of work needed to create fracture. It is the area under the stress-strain curve until the point of fracture. If glass undergoes a pure brittle fracture (perfectly elastic until failure) then there is no energy dissipation, and the development of a crack releases all the energy applied till that point. The strain energy release rate $G_{\mathrm{I}c}$

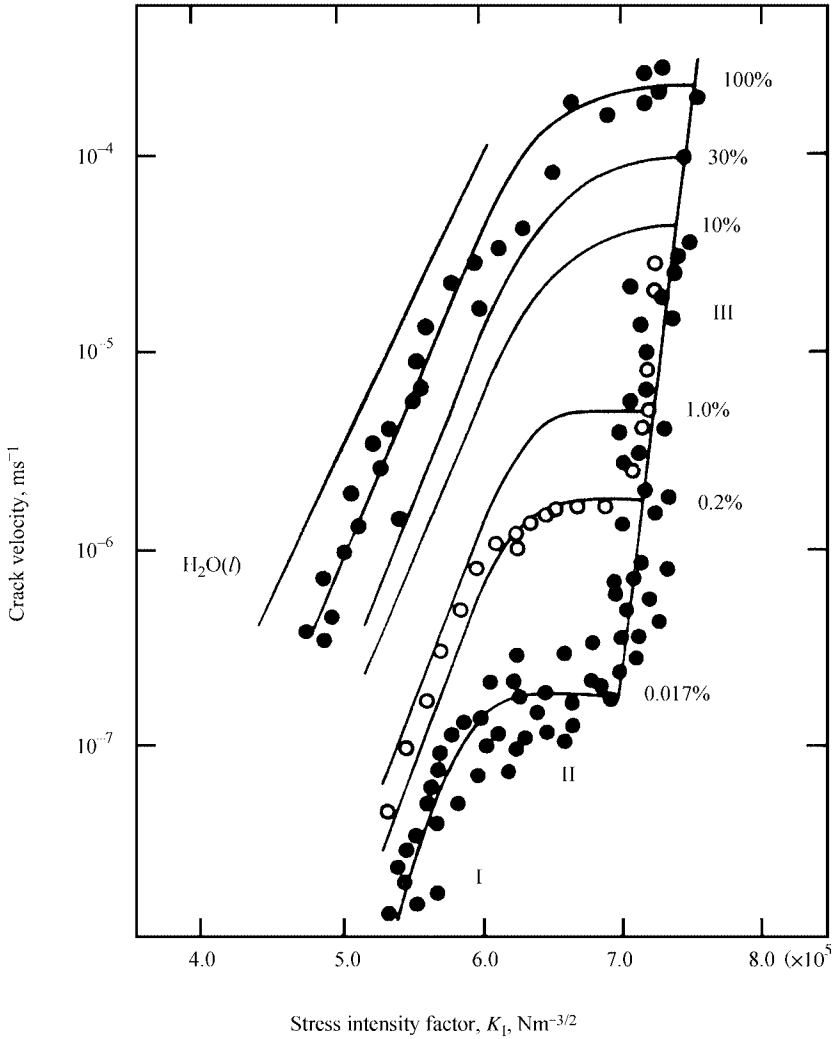

FIGURE 5.45 Variation of crack velocity with stress intensity factor and relative humidity. (*After S.M. Wiederhorn, J. Amer. Ceram. Soc., vol. 50, pp. 407–414, 1967.*)

corresponding to mode I failure under plain stress conditions is given by

$$G_{Ic} = K_{Ic}^2/E \tag{5.69}$$

Thus, the critical stress intensity factor K_{Ic} is a sufficient measure of the toughness and, hence, is also called the *fracture toughness*. Units of fracture toughness are MPa · $m^{1/2}$.

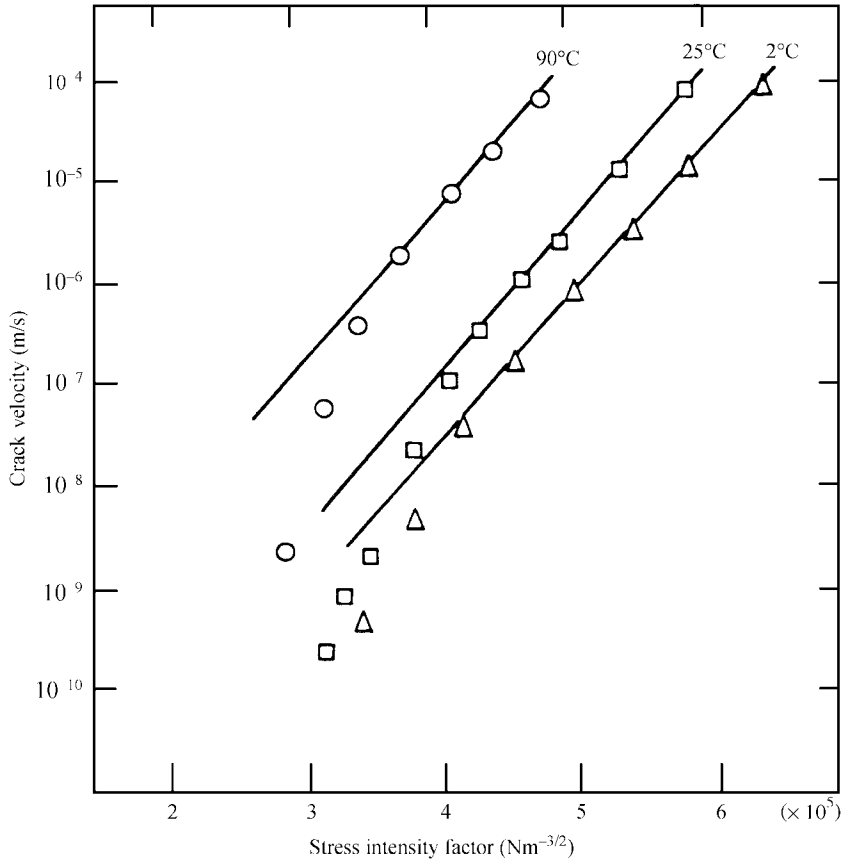

FIGURE 5.46 Variation of crack velocity with temperature. (*After S. M. Wiederhorn and C. H. Bolz, J. Amer. Ceram. Soc., vol. 53, pp. 545–548, 1970.*)

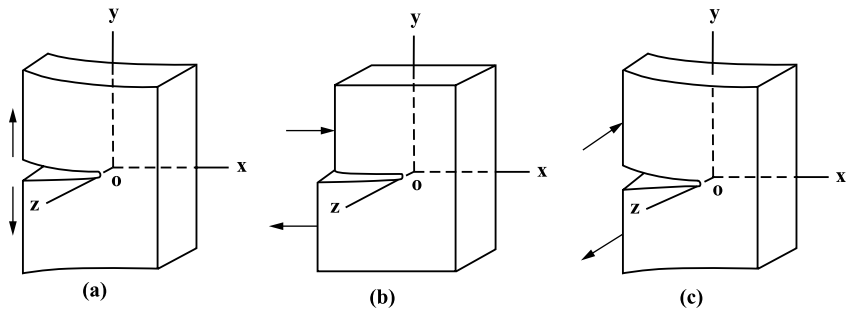

FIGURE 5.47 Three modes of failure in brittle materials: (*a*) opening, (*b*) sliding, (*c*) tearing.

5.19.4 Statistics of Strength Distribution

The severity of the flaws present on the surface of glass is distributed statistically. The flaw population due to common glass-forming and handling situations may be normally distributed. It is entirely possible that a problematic machine generates a given type of flaw through the forming/handling process. It is reasonable to assume that glass fracture would occur when the tensile stress at any defect site is sufficient to cause unstable crack propagation. This is the weakest-link argument and generally leads to a *Weibull distribution* of strengths. The cumulative probablity P of failure due to a stress σ applied uniformly over the tested area is given by:

$$P = 1 - \exp - \left(\frac{\sigma_a - \sigma_u}{\sigma_0} \right)^m \tag{5.70}$$

where σ_u is a stress corresponding to the fatigue limit, σ_0 is a normalizing stress and m is called the *Weibull modulus*. If we assume $\sigma_u = 0$, then a plot of ln ln[1/(1 − P)] versus ln σ_a yields a straight line, the slope of which is m (see Fig. 5.48). Clearly, for product reliability, one likes to have as high a value for m as possible (giving a very narrow range of strength distribution). For most commercial glass products, m = 5 to 15. Low values of m tend to give a *low-strength tail*, which is quite undesirable in large-volume production.

5.19.5 Life Prediction

If a crack velocity V versus K_I curve is available, then life prediction at constant applied stress may be made by stepwise integration of the entire curve using small time steps Δt. The value of V at some applied stress intensity factor causes the crack to grow Δc, where $\Delta c/\Delta t = V$. A new K_I corresponding to the length $c + \Delta c$ is read off. This then determines the new (and increased) V, and so on. The integrated time till c equals the specimen length gives the life expectancy.

In the absence of the V versus K_I curve, one needs to measure the failure time t_f for at least two values of the applied stress σ_a (generally different from the stress during service). Application of static fatigue principles allows one to write

$$\log t_f = -n \log \sigma_a + C \tag{5.71}$$

where n is the stress-corrosion susceptibility coefficient [see Eq. (5.68)] and C is a constant. Both the constants can be determined if t_f for two different values of σ_a are known. A superior procedure for life prediction involving the same parameters is to use proof testing, where the time to failure t_f is determined for *proof stresses* (σ_P) higher than the expected service stress σ_a. The survival of the specimens at σ_P guarantees that K_I at the tip of the most severe flaw is less than K_{Ic}. The minimum time to failure t_{min} is given by

$$t_{\min} = \frac{2(\sigma_P/\sigma_a)^{n-2}}{K_{Ic}^{n-2}\sigma_a^2 A Y^2 (n-2)} \tag{5.72}$$

where Y is a geometry parameter (= $\pi^{1/2}$, for a slit crack in an infinite plate).

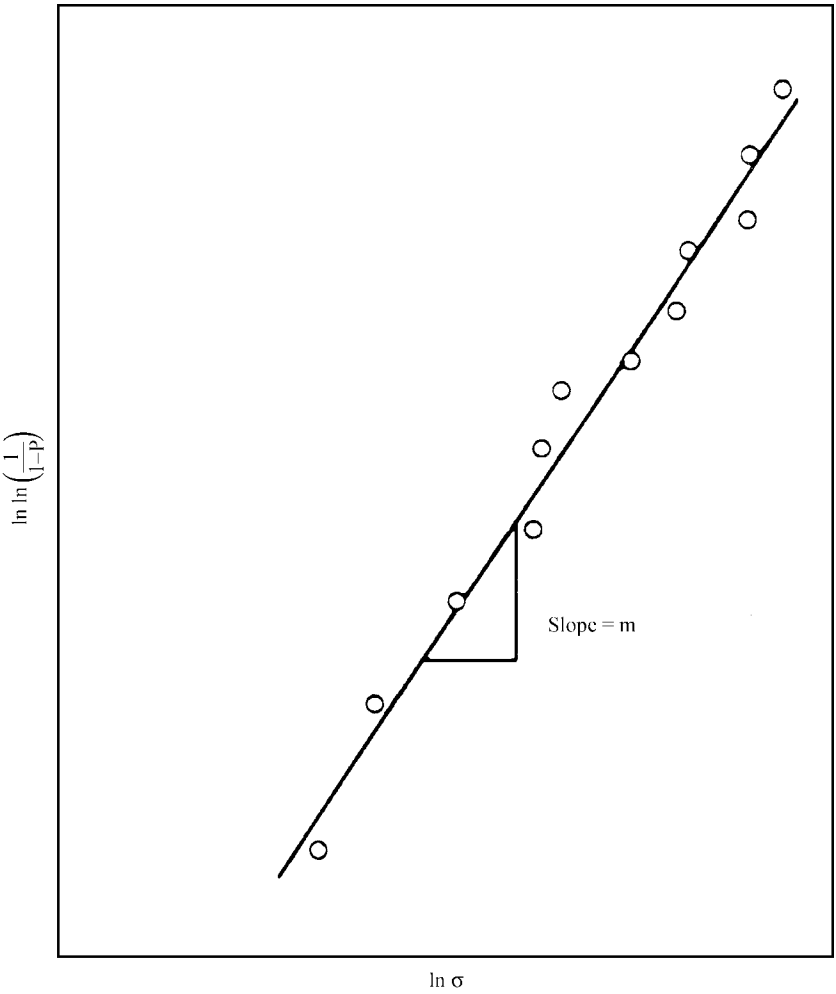

FIGURE 5.48 Weibull plot showing the probability of failure versus applied stress.

5.19.6 Measurement of Glass Strength and Toughness

Strength of glass is traditionally measured by using a three-point or four-point beam bending method in a universal mechanical tester (see ASTM C158-95). The maximum stress at the point of failure is calculated and reported as the *modulus of rupture* (MOR). It is necessary to use a large sample, generally not less than 20 specimens (maybe more), and to obtain the mean strength, the standard deviation, and (for comfort purposes) the lowest value observed. In a three-point bend strength measurement, the maximum stress is obtained below the central peg on the convex side. On the other hand, in a four-point bend test, the region within the inner pegs is subjected to the maximum stress. Since the

sampling of the flaws is done over a much larger area in the four-point bend test, the average strength obtained in this test must be smaller than that in the three-point bend test. In both the tests, care must be taken to avoid edge-originated fracture. (It is advisable to determine the origin of fracture in failed specimens by *fractographic analysis*; see ASTM C1256-93 for the interpretation of fracture markings.) Hence, circular cross-section glass rods having as-formed smooth surfaces should be used instead of cut or ground beam specimens. To test the strength of plate specimens, it is recommended to carry out ball-on-ring or ring-on-ring tests (preferred for reasons similar to those for four-point versus three-point bend testing). A ball pressing centrally against specimen supported on a "ring" formed by three other balls is described in ASTM F394-78. Occasionally, it is beneficial to abrade the surface by standardized abrasion techniques (such as dropping silicon carbide grit through a narrow orifice from a known height, sandblasting (see ASTM C158-95 Appendix A2), or placing microhardness indentations). This allows any preexisting flaw population to be replaced by a known, uniform flaw population. Glass containers are often tested by bursting by the application of internal pressure (see ASTM C147-86).

Glass toughness is most readily measured as *indentation toughness* by using loading that develops cracks during microhardness indentation. It was mentioned in Sec. 5.8.2 that loads for microhardness measurement must be small enough to avoid cracking from the median planes or the apices of the indentation. To measure toughness, sufficiently large loads are used such that the radial cracks produced are much longer than the indentation diagonal itself. According to Antsis et al.,[12] the fracture toughness may be calculated from the expression

$$K_{Ic} = \Omega P(E/H)^{1/2} c_0^{-3/2} \tag{5.73}$$

where $\Omega = 0.016$ (a material-dependent constant for Vickers-produced cracks), P is the applied load in newtons, E = Young's modulus (MPa), H = Vickers hardness (MPa), and $2c_0$ is the postindentation equilibrium length of the radial cracks on the surface from end to end (>3 times the indentation diagonal).

5.19.7 Methods of Improving Glass Strength

Glass products may be permanently strengthened by one of several techniques; the most commonly used are (1) thermal tempering and (2) chemical strengthening. These are discussed in Sec. 6.2.8, "Strengthened Glasses."

5.20 OPTICAL PROPERTIES OF GLASS

While many optical properties of materials are of interest to scientists, engineers, and technologists, those generally of greatest concern to users of glass include *refraction*, *reflection*, and *transmission* of light, and the wavelength dependence of those properties.

5.20.1 Refraction and Dispersion

A light beam is bent or *refracted* as it obliquely enters or leaves a piece of glass, such as a lens or a prism. The angle of incidence and angle of refraction are related by *Snell's law*:

$$\frac{\sin i}{\sin r} = \frac{n_2}{n_1}$$

where i and r are the angles of incidence and refraction (relative to the surface normal), n_2 is the *refractive index* of the glass, and n_1 is the refractive index of the surrounding medium (usually air, sometimes another glass, and sometimes another material such as water).

The refractive index n of a glass is a measure of the speed of light traveling through the glass, and is expressed as $n = c/v$, where c is the velocity of light in vacuum and v is the velocity in the glass. The refractive index of most glasses is greater than about 1.4. The refractive index generally depends on the wavelength of light at which it is being measured. This is because the speed of light is affected by the motions of the electrons within the glass in response to the light. These motions themselves vary depending on the wavelength of light, some electrons moving more actively at one wavelength and less at others. Optical glasses are often described in terms of their refractive index n_d at the wavelength of the helium d line, 587.6 nm.

Dispersion characterizes how the refractive index of a particular glass varies with wavelength. This is clearly an important specification for optical glasses. In general, the index of glass decreases with increasing wavelength in an armchair shape. Refractive index increases dramatically as one approaches the ultraviolet transmission limit of the glass and dramatically decreases as one approaches the infrared region. One measure of dispersion is the ν value, or *Abbe number*, which for the helium d line can be defined as $\nu_d = (n_d - 1)/(n_F - n_C)$, where n_F is the refractive index at the hydrogen F line (486.1 nm) and n_C is the refractive index at the hydrogen C line (656.3 nm). The quantity $(n_F - n_C)$ is sometimes referred to as the *principal dispersion*. It can be seen that the higher the ν value, the lower the dispersion (lower the variation in index with wavelength).

Refractive indices of optical glasses range from about 1.4 to 2.4 and ν_d values between about 15 and 100, although not all combinations are possible. In fact, low index in combination with high dispersion (low ν value) is difficult to achieve and high index in combination with low dispersion (high ν value) is presently essentially impossible in silicate glasses. The range of refractive indices and dispersions (Abbe numbers) available in various categories of optical glass is shown in Fig. 5.49.

5.20.2 Reflection

Also important to the application of glass is the reflection of light when the light beam is incident on a surface. *Reflection is not determined by the glass alone, but rather depends on the nature of the interface between that glass and the surrounding medium, such as air or vacuum*. For light arriving perpendicularly to a flat, well-polished glass surface, the fraction reflected is, to a good approximation, described by the simple Fresnel formula

$$R = \frac{(n_g - n_a)^2}{(n_g + n_a)^2} \tag{5.74}$$

where n_g and n_a are the refractive indices of the glass and the surrounding medium, respectively. However, when light arrives obliquely to a glass surface, the reflectivity depends on both the angle of incidence and the state of polarization of the light, and can be calculated by using a more general form of the Fresnel equations. In all cases, the angle of incidence and angle of reflection are equal and lie in a plane containing the normal to the glass surface. This is commonly referred to a *specular reflection*.

However, if the glass surface is not a smooth plane, such as a ground glass surface, some of the light will be scattered diffusely, rather than reflected in a single direction. For this

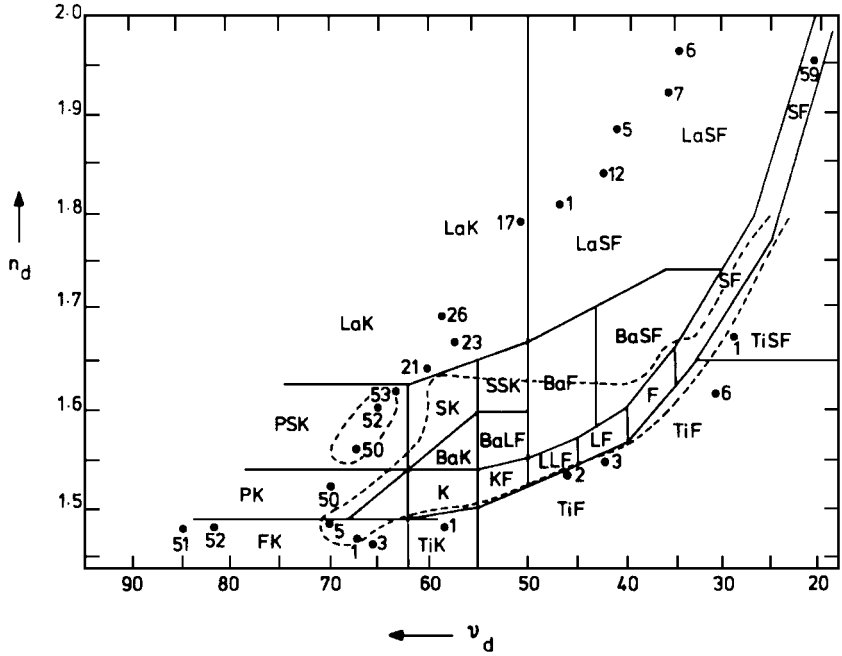

FIGURE 5.49 Refractive index and dispersion values of optical glasses.

case, referred to as *diffuse* (or *nonspecular*) *reflection*, calculations of amounts and directions become much more complicated.

If a glass is not homogeneous, but rather contains a dispersion of very small particles of refractive index different from that of the glass matrix, internal reflections and backscattering of light can occur, giving the glass a translucent or even an opaque appearance. The glass will appear white or colored. To be colored, either the matrix glass, or the dispersed particles, or both, must be colored. If the glass surface is well polished, it is possible to have a portion of the light specularly reflected from the surface, and a portion diffusely reflected from below the surface.

For specular reflection of light passing perpendicularly through a sheet of window glass (refractive index about 1.5), about 4 percent of its intensity will be lost by reflection at each surface (front and back), as calculated by the simple Fresnel formula given above, leaving only about 92 percent transmitted.

5.20.3 Transmission and Absorption

Transparency (or *absorption* as its inverse) is one of the more important properties of glass for its application. Light travels through oxide glasses essentially unimpeded because the energy of the light is ineffective in exciting structural vibrations or causing changes in electronic energy states within the glass, either of which would result in the light being absorbed. Oxide glasses can be considered to be wide-band-gap insulators. Silica glass, for example,

has an energy band gap of about 8.5 eV, which means that the energy difference for electrons between the highest occupied bonding orbital and the first unoccupied nonbonding orbital is about 8.5 eV. The photon energy 8.5 eV corresponds to a wavelength of about 145 nm. [For conversion, 1 eV = 1239.8/λ (λ in nm).] Only light of wavelength shorter than about 150 to 160 nm has sufficient photon energy to excite electrons from the valence band to the conduction band. Hence, the energy band gap provides the short wavelength limit to a glass's transmission range.

At much longer wavelengths, transmission is limited because the electric field of the light can excite energy-quantized vibrations of the atoms that make up the structure of the glass. These quantized vibrations are called *phonons*. The absorption in this region is referred to as *multiphonon absorption*, since one photon of light has sufficient energy to excite two or more phonons. For pure silica, this long-wavelength, multiphonon absorption becomes significant only at wavelengths around 4 to 5 μm and greater. Hence silica is transparent throughout the entire range of the visible spectrum, plus the near infrared (IR) and much of the ultraviolet (UV) spectral regions. Figure 5.50 shows the transmittance versus wavelength curve for a popular synthetic fused silica, Corning code 7940.

If network modifiers, for example alkali or alkaline earth oxides, are added to silica, NBOs (nonbridging oxygens) are created. Recall that an NBO consists of an oxygen atom bonded to only one silicon. As such, it contains an unpaired valence electron that creates an electron energy state or level within the insulator's band gap, thus causing absorption of light at a wavelength corresponding to the energy needed to excite this electron into the conduction band. The addition of network modifiers to silica thereby shifts the absorption edge to longer wavelengths. Transition metal ions, such as iron, which is almost universally present as an impurity in most commercial glassmaking raw materials, are capable of absorbing light through electronic transitions of inner core electrons between energy levels whose differences correspond to wavelengths in the ultraviolet, visible, or near-infrared regions. As discussed in Sec. 5.20.3.2, "Color," this is one of the dominant mechanisms of producing color in glass.

Absorption of light is also possible by transfer of charges (electrons) from electron shells of one ion to unfilled shells of another ion located in sufficiently close spatial proximity. The spectral absorption bands resulting from such interionic transitions are sometimes called *charge transfer* bands. The participating ions may be major or minor components of the glass. Electron transfer between multivalent transition element ions, such as Fe^{2+}-Fe^{3+} pairs, are examples of the latter.

5.20.3.1 Transmittance and Absorption Coefficient. When a beam of light impinges on and passes through a piece of glass, some portion is reflected back from each surface of the glass, some is absorbed within, and the rest is transmitted. The fraction of the light that is reflected at each surface is characterized by the reflection coefficient R, discussed in Sec. 5.20.1. The amount of light absorbed by each volume element within the glass is proportional to the intensity of the light, the proportionality constant being called the *linear absorption coefficient* α. The *internal transmittance* $T_{\text{int}} = I_{\text{out}}/I_{\text{in}} = e^{-\alpha t}$, where I_{in} is the intensity of the light entering through the front surface of the glass, I_{out} is the intensity reaching the back surface, and t is the thickness of the glass.

Internal transmittance, a material property of the glass, is difficult to measure directly. Rather, the *overall transmittance* of the glass, T, is generally measured as I/I_0, where I_0 is the intensity of the light impinging on the front surface of the glass and I is the intensity of the light exiting the back surface. The two transmittances are related by

$$T = (1 - R_f)T_{\text{int}}(1 - R_b) \tag{5.75}$$

where R is reflectivity coefficient and the subscripts f and b refer to the front and back

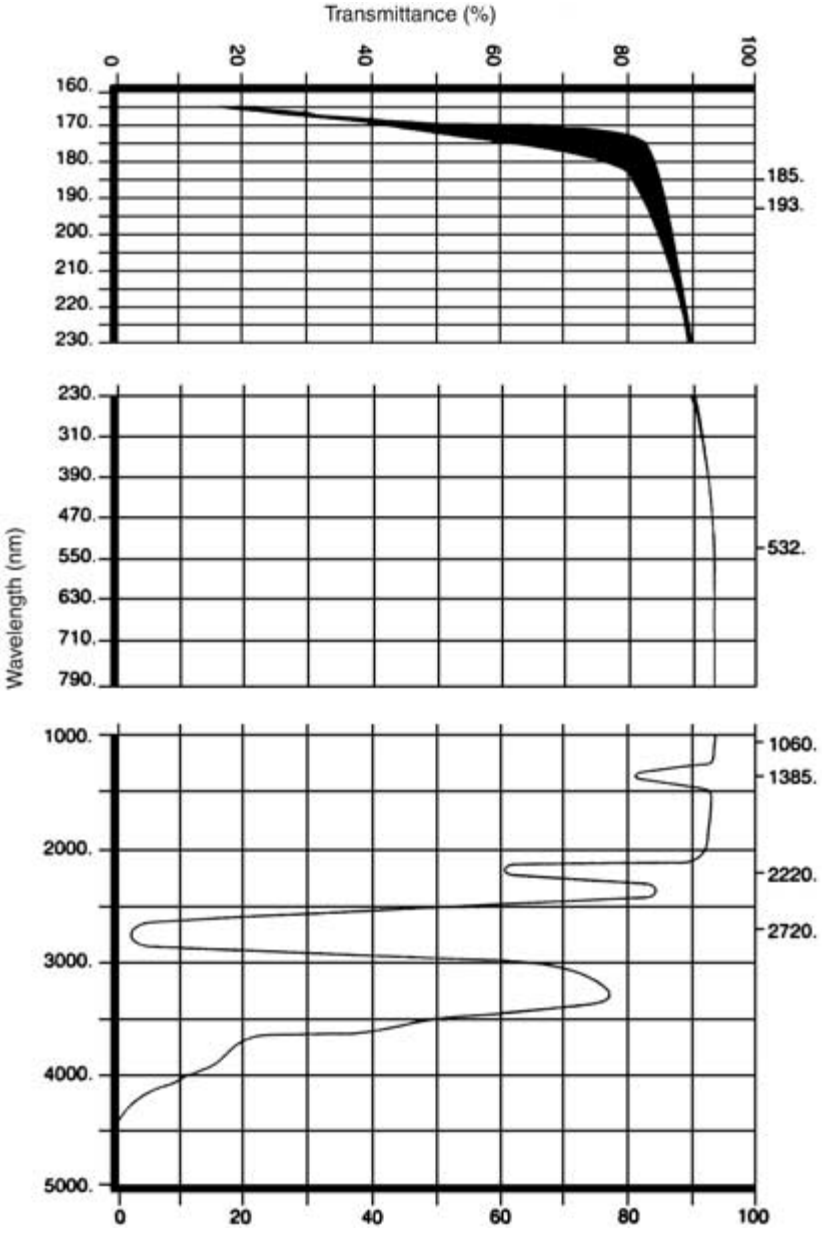

FIGURE 5.50 Wavelength dependence of transmission for fused silica glass.

surfaces of the glass respectively. If both surfaces are identically prepared, the two reflectivity coefficients are equal. Thus,

$$T = (1 - R)^2 T_{\text{int}} \tag{5.76}$$

For a glass of refractive index $n = 1.5$, $R = 0.04$ from Eq. (5.75) and $(1 - R)^2 = 0.922$. This means that even pure silica, whose linear absorption coefficient is so small as to be practically immeasurable at visible wavelengths, is only 92 percent transmitting when viewed through two free surfaces. [To approximate the effects of multiple reflections within the glass, the factor $(1 - R)^2$ should be replaced by the factor $(1 - R)^2/[1 - (T_{\text{int}} R)^2] = 0.923$ for $n = 1.5$ and $T_{\text{int}} = 1.0$, not much of a difference for most applications.]

Absorption coefficient should not be confused with *absorbance A*, a quantity defined as $\log_{10}(1/T)$ and often measured automatically on a spectrophotometer. Accordingly, $T = 10^{-A}$ and $A = 0.434\alpha t$. (Also, for conversion: αt = absorbance × 2.303.)

One sometimes speaks of absorption in terms of *optical density* (OD). Optical density is numerically equivalent to absorbance, except that optical density is often defined as an average over some specified wavelength region whereas absorbance is generally quoted at specified wavelengths. Each unit increase in absorbance, or OD, gives an order of magnitude decrease in transmittance.

In communications (telephone, radio, television, and data transmission), the equivalent of optical density, or absorbance, is transmission loss, or signal attenuation, expressed in units of bels or, more often, tenths of bels (decibels, abbreviated dB), named after the inventor of the telephone, Alexander Graham Bell. An attenuation of 1 bel, an absorbance of 1, and an optical density of 1 all refer to the output having only one-tenth the signal intensity of the input. For optical communication over low-loss-glass optical fiber this nomenclature has been retained. The optical signal attenuation rates are specified in terms of dB/km (decibels of attenuation per kilometer of fiber). This attenuation rate and linear absorption coefficient are related as follows:

$$\text{Loss (dB)} = 4.343\ \alpha t$$

For $\alpha = 1\ \text{cm}^{-1}$,

$$\text{Loss} = 4.343 \times 10^5\ \text{dB/km}$$

For loss = 1 dB/km,

$$\alpha = 2.303 \times 10^{-6}\ \text{cm}^{-1}$$

An absorption coefficient as small as $0.001\ \text{cm}^{-1}$ is thus equivalent to an optical loss rate of 434.3 dB/km, which is extremely high from a long-distance communication point of view. (See Sec. 6.7, "Optical Communications Fiber".)

5.20.3.2 Color. If the absorbance (or, inversely, the transmittance) of a glass varies with wavelength through some portion of the visible spectrum, the glass appears colored. For example, if the green and red portions of the spectrum are more strongly absorbed, then when viewed in white light, the glass will appear blue. This is sometimes referred to as *subtractive coloration*. Color in glass is usually caused by the intentional, or sometimes unintentional, inclusion of absorbing ions, *which are generally transition metal ions*, in the composition. Since the absorbed wavelength corresponds to the electron transitions allowed, the resulting color produced is a function of the oxidation state of the transition

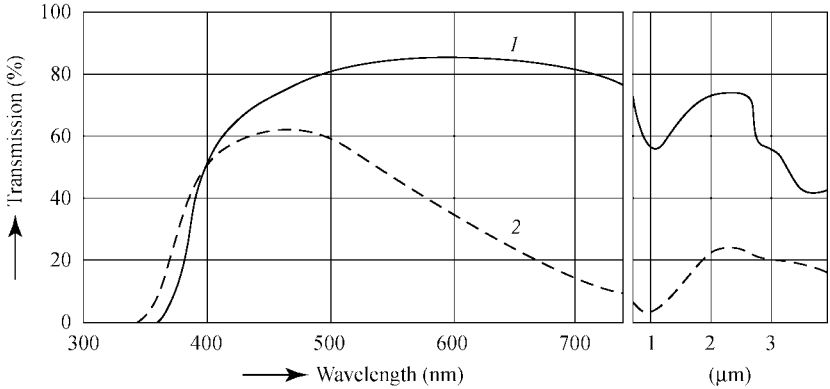

FIGURE 5.51 Absorption due to iron in glass.

metal ion. The bluish-green color noted in a piece of window glass viewed through its edge is primarily due to an absorption at 1.1-μm wavelength by Fe^{2+} iron present as an impurity in most commercial glass-making raw materials. By melting the glass in a more oxidizing atmosphere, some of the Fe^{2+} converts to Fe^{3+}. The absorption due to a charge transfer between Fe^{2+} and Fe^{3+} is in the ultraviolet, tailing into the visible region. This results in a straw-yellow color. By a judicious control of the Fe^{3+}/Fe^{2+} ratio, the straw-yellow color due to $Fe^{3+} \Leftrightarrow Fe^{2+}$ and the bluish-green color due to Fe^{2+} complement each other to bring about *decolorization* of glass (see Sec. 6.3.2, "Colored and Opal Glasses"). Absorption due to the iron impurity in glass is shown in Fig. 5.51. Figure 5.52 shows absorption spectra due to a few other transition metal ions of interest.

As described in Secs. 5.20.4.2, 5.20.7, and 5.20.8 and in Chap. 6, dispersing colloidal-sized particles, or pigments, within the glass can also produce color. These pigments can be oxide, semiconductor or metal, and can be mixed into the glass, as with some types of vitreous glazes, or chemically precipitated after having been put into solution at high temperatures in the melt. The red color obtained as a result of the presence of approximately 200-Å gold particles in glass is shown in Fig. 5.53. Practical colors are discussed further in Chap. 6. A partial listing of "practical" colors that can be generated in glass by the various schemes is given in Table 6.13.

5.20.3.3 Optical Absorption by Water in Glass. Water (H_2O) is to some extent chemically incorporated into the structure of all glasses during their manufacture. For high-purity fused silica for long-distance optical fiber communication, the water content is often maintained below 10 parts per billion, by weight, while for more traditional commercial glasses, manufactured in modern glass melters directly fired by gas-oxygen burners, the level can reach a few hundredths of a percent.

The presence of water can affect physical properties such as viscosity, but we mention it in this section because of its important optical effects; in particular, it produces strong absorption bands in the near-infrared spectral region. Avoidance of the absorption bands due to water in silica is one of the key reasons the wavelength locations of the two current long-distance optical communications wavelength bands, at 1.31 and 1.55 μm, were chosen. For other glasses, measurement of the intensities of the near-infrared water bands allows a quantitative determination of the amount of water in the glass; i.e., it provides an analytical technique.

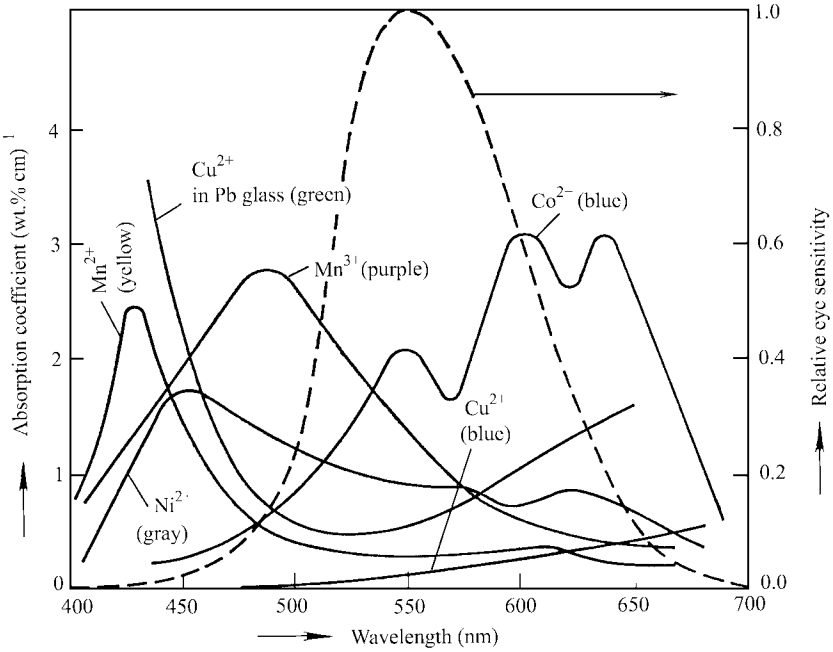

FIGURE 5.52 Absorption due to other transition metal ions in glass. (*After W. D. Kingery, H. K. Bowen, and D. R. Uhlmann, Introduction to Ceramics, 2d ed., Wiley & Sons, New York, 1976, p. 683.*)

Water is chemically incorporated into silicate and other oxide glasses as oxygen-hydrogen (O-H) bonds, generally by replacing an Si-O-Si network bond by two Si-O-H nonnetwork bonds. There is no direct linkage between the OH groups; they act as local terminations of the network. These Si-O-H entities are infrared-active; i.e., they absorb in the infrared region.

In fused silica, OH absorption bands occur at about 2.73, 3.6, and 4.2 μm (Fig. 5.50). The 2.73-μm band corresponds to the fundamental O-H stretching vibration. If this band is particularly strong, overtone bands can be seen at about 1.38 and 0.945 μm. The bands at 2.6, 3.8, and 4.4 μm are ascribed to stretching vibrations, which occur if other network oxygens lie within a distance of about 0.25 nm of the proton (H). Again, an overtone band is sometimes seen at about 2.2 μm. The Si-O-H bending vibration occurs at much longer wavelengths and is not seen in silicate glasses because it is hidden by the strong multiphonon infrared absorptions.

The relative strengths of these OH infrared bands depend somewhat on the overall composition of the glass, so for quantitative analysis, the appropriate molar extinction coefficients must be determined for each type of glass being analyzed. The molar extinction coefficient, at any wavelength, is defined as the extinction coefficient (in units of cm^{-1}) that would result from 1 mole of a solute being dissolved in 1 liter of solution—in the present case, 1 mole of water dissolved in 1 liter (1000 cm^3) of glass. With this information, and the measured absorption coefficient for the glass at that wavelength, the concentration of water in the glass can be determined. However, since one molecule of dissolved water produces two OH bonds in the glass, one must be careful when converting to concentrations in weight percentages.

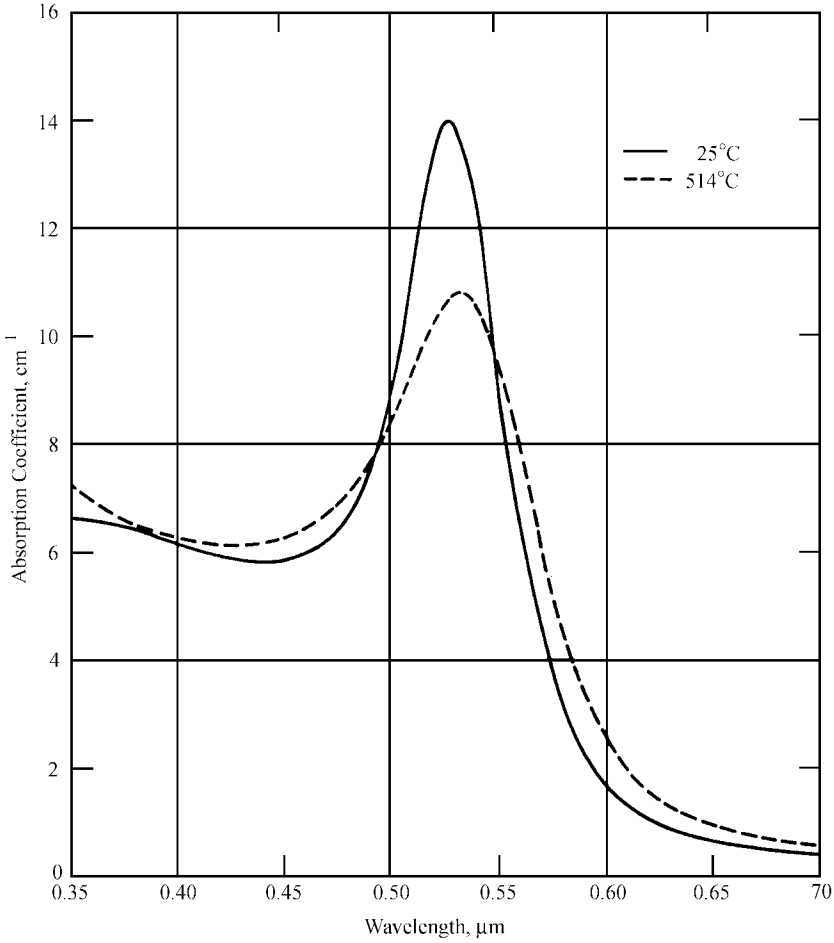

FIGURE 5.53 Absorption due to approximately 200-Å gold particles in glass. (*After R. H. Doremus, J. Chem. Phys., vol. 40, no. 8, p. 2389, 1964.*)

5.20.4 Light Scattering Losses

When light travels through a tangible medium (as compared to a vacuum) it interacts with all the electric charges present in the medium. This interaction causes the light to change its speed of travel and gives rise to the concept of refractive index, which was discussed in Sec. 5.20.1. Any variation in refractive index from position to position within the glass is called *optical inhomogeneity*. If the material is inhomogeneous on a scale similar to the wavelength of the light, the light is scattered to a small or great extent, depending on a variety of conditions. If the *scattering* is significant, the linear absorption coefficient, discussed above, should be replaced by an *extinction coefficient* consisting of two terms: one representing the absorption losses α, in which light energy is truly absorbed by the glass, and a

second, the *scattering coefficient* γ, which accounts for the amount of light scattered away from the forward direction.

There are many sources of inhomogeneity in glass that give rise to light scattering, only some of which are amenable to quantitative mathematical analysis or description by techniques currently available. Fortunately, some of the more simple cases are the most technologically important. We describe two here.

5.20.4.1 Rayleigh Scattering. In the Rayleigh approximation, the scattering regions are considered to be of dimensions much smaller than the wavelength of light (diameter $d << \lambda$, or at least $d < \lambda/4\pi$), to be randomly distributed throughout the glass, to be noninteracting, and to be dielectric in nature. The assumption of small size allows the regions to be treated as simple dipole radiators. (Hence, Rayleigh scattering is sometimes referred to as *dipole scattering*.) The assumption of random distribution and noninteraction means that light scattered from different regions will not interfere (neither constructively nor destructively), so that the scattered intensities from each region can be summed together.

In this approximation, for spherical scatterers of natural (nonpolarized) light, the ratio of scattered to incident intensities, at a given angle θ, is given by

$$I(\theta)/I_0 = \left(\frac{9\pi^2 NV^2}{2d^2\lambda^4}\right)\left(\frac{n^2-1}{n^2+2}\right)^2 (1+\cos^2\theta) \tag{5.77}$$

where N = number of scattering centers per unit volume
V = volume of each center
n = refractive index of the center relative to the surrounding glass
λ = wavelength of light being scattered
d = distance from the sample to the observer
θ = angle of observation relative to the forward direction

A key point is the inverse dependence on the fourth power of the wavelength; shorter wavelengths scatter much more intensely than longer ones. (This is the explanation for the blue color of the daytime sky, where all the air molecules act as Rayleigh/dipole scatterers.) The total intensity scattered out of the forward direction is obtained by integrating this equation over 4π steradians of surface at the distance d. It should be noted that if the distance d is not sufficiently large relative to the pupil diameter of the observer's eye, or the acceptance aperture of the measuring instrument, some small forward region of the surface must be excluded from the integration.

Even the most pure, well-prepared glasses exhibit some inhomogeneity and consequent scattering losses. At high temperatures, thermal density fluctuations naturally exist in the melt. These translate into refractive index fluctuations. (The refractive index is roughly proportional to the number of atoms per unit volume.) Both the temperature and the compressibility of the melt dictate the extent of these fluctuations. As the glass is cooled through the glass transition temperature, these fluctuations are frozen into the system. The scattering coefficient contributed by such fluctuations can be described by

$$\gamma = \frac{8\pi^3(n^2-1)^2\beta k_B T_f}{3\lambda^4} \tag{5.78}$$

where β is the isothermal compressibility, k_B is the Boltzmann constant, and T_f is the fictive temperature of the glass (see Sec. 5.1.3). There are some variations on this relationship

reported in the literature, but for all, low refractive index, low compressibility, and low fictive temperature yield a low scattering coefficient. (It should be noted that because refractive index is a function of wavelength, as discussed in Sec. 5.20.1, extinction due to scattering in glass is not precisely inversely related to the fourth power of the wavelength.) For pure fused silica glass, the extinction coefficient is almost entirely due to scattering, which is less than 10^{-4}/cm at the center of the visible spectrum (500 nm).

For a multicomponent glass, thermal composition fluctuations exist at temperatures above the glass transition. These tend to be frozen in on cooling. The loss contribution due to scattering from such fluctuations can be described by terms proportional to

$$\left(\frac{dn}{dc_i}\right)^2 \frac{\langle \Delta c_i^2 \rangle}{\lambda^4}$$

where dn/dc_i describes the differential dependence of refractive index on composition component i and $\langle \Delta c_i^2 \rangle$ is an appropriate mean square composition fluctuation. In practice, the scattering losses are difficult to predict theoretically because the extent of the composition fluctuations cannot be independently calculated. For a phase-separable system, quenched from slightly above the maximum immiscibility temperature, the fluctuations can be quite large (critical opalescence); other glass compositions exhibit very little tendency for anything but a uniform spatial distribution of all the elements. Most glasses are believed to lie somewhere between these extremes. (Again because of the wavelength dependence of the refractive index, the inverse proportionality to the fourth power of the wavelength is not strictly observed and depends on the composition of the glass. For optical glasses, exponents ranging between 3.5 and 4.8 have been reported.)

While the scattering losses of chemically homogeneous, single-phase glasses are not a concern for most applications, they are truly significant for optical communications, as will be discussed in later chapters of this handbook.

5.20.4.2 Absorbing Particles. Some colored glasses contain many very small particles of highly light absorbing materials such as semiconductors or metals. For these materials the refractive index and the dielectric constant of the particle must be described by complex numbers n^* and ε^*, respectively,

$$n^* = n_0 + jk \qquad \text{and} \qquad \varepsilon^* = \varepsilon' + j\varepsilon'' \tag{5.79}$$

where n_0 and k are the real and imaginary parts of the refractive index, ε' and ε'' are the real and imaginary parts of the dielectric constant, and $j = (-1)^{1/2}$. The two quantities for nonferromagnetic materials are related by

$$\varepsilon^* = n^{*2}$$

In the Rayleigh approximation, valid for very small conducting particles, the scattering coefficient for spherical particles is given by

$$\gamma = \frac{18\pi N V n^3 \varepsilon''}{\lambda[(\varepsilon' + 2n^2)^2 + \varepsilon''^2]} \tag{5.80}$$

where n is the refractive index (real) of the host glass.

Similarly, simple exact solutions can be obtained for small ellipsoidal particles of any arbitrary axial ratio. Such solutions have been found extremely useful in explaining the colors produced by colloidal metal particles suspended in glass, the coloration and polarizing effects found in *photochromic* glasses, and the color and performance possibilities of

metal-particle-containing polarizing glasses. In all these cases, the extinction is predominantly absorptive, and results from a *plasma resonance* of the highly conductive electrons in the metal particles.

5.20.4.3 Mie Scattering. In cases where the scattering regions are particles of sizes comparable to, or greater than, the wavelength of light, the particles cannot be considered as simple dipoles; the scattering from each region of the particle must be considered separately and the total scattering from the particle calculated by combining the scattering from the individual parts, taking into account constructive and destructive wave interference. The particles themselves, however, are considered to scatter independently, so that the total scattering is again the simple sum of the scattering from all the particles in a given volume. Solutions to this problem are complex. A useful approach due to Mie involves mathematical series expansions, for which the Rayleigh extinction coefficients are merely the first terms. Scattering from such large particles is often referred to as *Mie scattering*. Further discussions of this type of scattering are beyond the scope of this handbook.

5.20.5 Birefringence

Well annealed, homogeneous glasses are isotropic in the absence of external and internal force fields, meaning their properties are independent of the direction of measurement. Related to light, this means that for a given wavelength, the speed of light through the glass is independent of the direction of travel. Further, the speed is independent of the state of polarization of the light. If the light is linearly polarized, meaning that the light entering the glass has its electric field (E vector) oriented in a single, fixed direction, it will travel through the glass at the same speed as light having its electric field oriented in any other direction.

However, if the glass is stressed so as to develop a strain field within the glass, or in the presence of annealed internal stresses, the electric fields about the atoms become distorted in one direction more than others and the glass structure is no longer isotropic. This gives rise to *double refraction*, or *birefringence*, the condition where light of one polarization may travel more rapidly than light of a different polarization. Perpendicularly (orthogonally) polarized rays of light that are initially in phase develop a phase difference and, equivalently, an optical path difference or retardation with respect to each other. For a uniaxially applied stress σ_{33}, the glass develops two refractive indices, n_1 and n_3 (hence the term *double refraction*, or *birefringence*). The optical path difference δ between light oriented with its electric field in the x_3 direction and that with its electric vector oriented in the x_1 direction, when viewed along the x_2 axis, is given by the *stress-optic relation*:

$$\sigma_{33} = \delta / B_\lambda d \tag{5.81}$$

where d is the thickness of the specimen and B is called the *stress-optical coefficient* or *Brewster's constant*. (δ, the optical path difference, is the product of the physical path length times the difference in effective refractive index for each polarization of light, and describes the retardation one polarized beam will experience relative to the other. The subscript λ is used to indicate that B may vary with the wavelength.) When stress is written in terms of bars (1 bar = 10^6 dyn/cm^2 ≈ 14.5 lb/in^2), thickness is written in cm, and d is measured in nm, then the unit of B is the brewster (1 brewster = 10^{-13} cm^2/dyn = 10^{-12} Pa^{-1} = 1 TPa^{-1}). *The sign of the observed birefringence, or retardation, depends on whether the stress is compressive or tensile*. Values of B for several glasses are listed in Chap. 6. These generally vary between 2.4 to 3.1 for most glasses. Of particular note, however, are the high

PbO-containing glasses where the increase in the PbO content leads to a decrease in B; a glass containing about 80 mol% PbO has a negative value of B.

We should note that since stress is related to strain, birefringence effects could also be described in terms of strain-optical, or elastooptical, coefficients. Collectively, these are sometimes referred to as *Pockels coefficients*.

A variety of electrooptic (*Kerr effect*) and stress-optic (piezooptic) devices have been built on the relatively simple concept of birefringence developed in a glass under applied stress. The full mathematical analysis of the effects and device performance, however, requires rather complicated tensor analysis. Stress-induced birefringence is useful for measuring the amount of residual stress in a glass, for example, after annealing or after rapid cooling, or in a glass-to-metal seal or a glass-to-glass seal, as described in Sec. 6.5, "Annealing and Tempering."

Glasses also show birefringence when placed in a strong magnetic field. When the direction of the magnetic field is transverse to the direction of travel of the light, the effect is the magnetic equivalent of the Kerr effect. If, however, the direction of the magnetic field is in the same direction the light is traveling, circular birefringence results. In this case, circularly polarized light of clockwise rotation will travel at a different speed than that with counterclockwise rotation. Since linearly polarized light may be considered as composed of two circularly polarized beams of opposite rotation, by using this effect it is possible to rotate, in a controlled manner, the orientation of linearly polarized light passing through the glass. This is known as the *Faraday effect*. The degree of circular birefringence is proportional to the strength of the magnetic field, the proportionality constant being known as the *Verdet constant*. For most silicate optical glasses measured at 633 nm, the Verdet constant ranges between 4 and 30 rad/(T · m), where T indicates magnetic field in teslas. The positive values indicate diamagnetic behavior. Verdet constants for special terbium- (Te) and cerium- (Ce) doped silicate and phosphate glasses are negative (paramagnetic). Values from –20 to –70 rad/(T · m), at 633 nm and room temperature, have been reported. Verdet constants of the paramagnetic glasses increase with decreasing temperature, whereas for the diamagnetic materials they are practically independent of temperature. In both cases, the absolute magnitude of Verdet constant increases approximately hyperbolically as the wavelength approaches the short-wavelength fundamental absorption edge.

5.20.6 Nonlinear Effects

Nonlinear optical properties are those for which the inherent nature of the effect depends upon the intensity of the light that causes the effect. There are several such effects known and others likely to be discovered. A complete discussion of such phenomena is beyond the scope of this handbook, but we will give two examples. For light of any given wavelength, the refractive index of a given glass is generally considered to be a constant. However, at very high light intensities (of the order of megawatts per square centimeter) the refractive index is observed to actually increase. Among other things, this can cause wanted or unwanted self-focusing when high-intensity lasers are directed through the glass. Generally this effect is more pronounced for glasses of higher refractive index, where highly polarizable ions tend to contribute most to the effect.

The second example: As described in Sec. 5.20.3, the amount of light absorbed by a glass is proportional to the intensity of the light traveling through it, the proportionality constant being the absorption coefficient. However, for very high light intensities, such as can be generated by pulsed lasers, the absorption coefficient itself may increase with the intensity of light, leading to an enhanced absorption.

5.20.7 Radiation Effects

Irradiation of glass by electromagnetic radiation (light, x-ray, and gamma-ray photons, for example), high-energy atomic particles such as electrons or neutrons, or even highly accelerated atoms and ions, can cause transient and/or permanent changes in the optical properties. Electrons can generate light (*cathodoluminescence*), as can x-rays and ultraviolet light (*photoluminescence*). If the light emitted by the glass persists long after the exciting radiation ceases, the luminescence is referred to as *phosphorescence*.

Such forms of irradiation can also cause coloration of glass. For example, sunlight, especially unfiltered sunlight possessing a large ultraviolet component, can gradually color windows and other glass products. This effect is called *solarization*. It results from the trapping of photoexcited electrons in energy states located within the energy band gap described in Sec. 5.20.3. These trapped electrons are then able to absorb light in the visible portion of the spectrum, imparting color to the glass. The trapping sites are often associated with impurity species in the glass composition. The effect is sometimes countered during manufacture by adding cerium oxide, which provides competing electron traps whose absorption spectra lie outside the visible region (in the ultraviolet). Similarly, the electron beam in a cathode-ray tube (CRT) can cause *electron browning* of the face plate, if appropriate glass compositions are not chosen.

Irradiation by ultraviolet light, or shorter-wavelength electromagnetic radiation, or fast neutrons has been shown to cause permanent density changes in glass. This has become of particular interest in recent years for at least two reasons. First, we mention a concern. For fused silica lenses in the photolithography stepper cameras used for semiconductor manufacture, such density changes, even if only a few parts per million and developed over long service life, could adversely affect image quality. Hence, for this application it is an effect to be minimized. Second, an opportunity. By exposing a silica-based optical communications fiber to very intense monochromatic ultraviolet light through suitable photomasks, or by interfering two coherent beams from a laser, it is possible to develop periodic refractive index variations within the core that can act as Bragg gratings to selectively reflect certain wavelengths of light. Applications of this useful effect will be discussed further in Chap. 7, "advanced applications of glass."

5.20.8 Photosensitive Glasses

The noble metals gold, silver, and copper can be dissolved in their oxidized state into sufficiently oxidized silicate glass melts as network-modifying ions. In this state, the metal ions give the glass no visible color. On cooling of the melt, under certain conditions, these noble metal ions may become reduced to neutral atoms, whereupon they may precipitate from the melt as uniformly dispersed colloidal-sized particles of metal, via a nucleation and growth process. As such, the metals give the glass color: Gold produces red, purple, or blue; silver produces yellow, orange, or red-brown; copper produces red. The actual color given by each metal depends on the size, shape, and concentration of the particles in the glass, as is discussed in Chap. 6. With skill, a glassmaker can learn to develop copper- or gold-containing red glass appearing remarkably like the ruby gemstone, called copper or gold ruby glass. During cooling, the nucleation and growth of the particles can occur quite abruptly, with the color almost suddenly appearing. This is often referred to as *striking* or *striking in* the color.

The control of the reduction of the ionic metals as the glass cools is sometimes a skilled art. Among the chemical tools available are the multivalent ions tin and antimony. If included in the glass composition at concentrations somewhat greater than the gold, silver, or copper, and if the overall oxidation state of the glass melt at its highest temperatures is controlled to keep the noble metals oxidized, but the tin or antimony is at least partly

reduced, then on cooling, the tin or antimony is available to chemically reduce the noble metals, as by the following reaction for silver and tin:

$$Ag^{+} + Sn^{+} \Leftrightarrow Ag^{0} + Sn^{2+} \qquad \text{(reversible at about 900°C)}$$

In the late 1930s researchers at Corning Glass Works developed and patented a methodology to photosensitively control this striking in of color. In this method, ions such as Ce^{3+}, Cu^{+}, and Eu^{2+}, which absorb in the ultraviolet spectral region, serve as electron donors when excited by ultraviolet light. The released electrons serve to reduce the noble metal ions to the atomic state prior to their precipitation. For gold, one can express this chemically as

$$Au^{+} + Ce^{3+} + h\nu \Rightarrow Au^{+} + Ce^{4+} + e^{-} \Rightarrow Au^{0} + Ce^{4+}$$

where $h\nu$ represents a photon of ultraviolet light and e^{-} an electron.

In practice, the clear glass is cooled to room temperature for the exposure. On exposure, the photogenerated electrons are trapped locally within the glass structure, perhaps at nonbridging oxygens (NBOs). The glass is then reheated to a temperature near the softening point, where the electrons and noble metal ions are able to react and the resulting atoms are sufficiently mobile to nucleate and grow the metal particle colorants.

By exposing the glass to the ultraviolet light through a suitable photomask (generally a negative photomask), or by direct writing with an ultraviolet light beam, it is possible to produce controlled patterns of color or photographic images within the glass by this photosensitive mechanism.

The solarization process described in Sec. 5.20.7 is also a type of photosensitivity, which could be controlled through the use of a suitable photomask if so desired.

A third type of photosensitivity valuable to glass workers is the photosensitive control of crystallization within glass. It was found, again by researchers at Corning, that photosensitively generated nanometer-sized metal particles, particularly of gold and silver, can act as sites on which crystalline material can subsequently heterogeneously nucleate and grow within the glass. Again, if suitable photomasks are used, the patterns of crystallization may be controlled. Such techniques are used for the photosensitive glass-ceramics and polychromatic glasses described in Chap. 6.

5.20.9 Measurement of Optical Properties

5.20.9.1 Transmission. Transmittance and absorbance, as functions of wavelength, are generally measured by using a variety of commercial spectrophotometers. The sample specimens are usually flat plates, although pressed KBr pellets containing fine particles of the specimen are sometimes used at mid-IR and longer wavelengths. Sample preparation is especially important for high-transmittance, low-absorbance materials, where poor surface finish can give surface scattering losses comparable to or exceeding the losses inherent in the glass. It is also important that the major surfaces of the specimen be flat and parallel; any wedge or lens effect can displace the spectrophotometer beam on its detector, producing an erroneous increase or decrease in signal relative to the open beam condition (no sample in place).

5.20.9.2 Refractive Index and Dispersion. Refractive index, as a function of wavelength, can be measured by a variety of techniques, the difficulty of which depends on the precision required of the measurement.

Approximate measurements of refractive index may be made by the Becke line technique. With this, a small chip of glass having a sharp edge is immersed in standardized refractive index oil on the stage of a transmission optical microscope illuminated by a monochromatic light source. The distance between the microscope objective and the

specimen is gradually increased from the focused condition. A bright diffraction line contouring the specimen, called the *Becke line*, moves from the medium of lower refractive index into the medium of higher index. The measurement is repeated successively with different index oils until the movement of the Becke line becomes difficult to discern. The precision of the measurement is on the order of ±0.01. The accuracy depends of course on the quality of the index standard.

More precise measurements can be obtained with commercial refractometers, such as an Abbe or Pulfrich. Both refractometers are based on measuring the critical angle of incidence between the specimen and a standard prism. The sample consists of a flat plate with one surface and an adjacent vertical edge well polished. The contact between the polished sample and the prism is enhanced with an approximately matching index oil. A split image is adjusted to coincide, and the refractive index is read directly. The precision here is generally of the order $\pm 10^{-5}$.

The most precise measurements of refractive index are made by determining the angle of minimum deviation of a light beam with the specimen being used as a prism on a goniometer stage. This procedure, often called the *minimum angle of deviation* technique, is capable of index measurements to $\pm 10^{-6}$. For this precision, the specimen must be in the form of an accurately manufactured prism, of excellent quality glass (homogeneous, no *striae*), having excellent surface flatness and polish. The specimen preparation is generally by far the most expensive part of the measurement. This is a relative measurement, since the refractive index is almost always measured in air. The refractive index of the laboratory air, which is a function of temperature, pressure, and relative humidity (H_2O content), must be known to convert the relative measurement to absolute.

Interference techniques are sometimes used to measure glass homogeneity in terms of the refractive index. While not absolute, they can measure relative refractive index differences on the order of $\pm 10^{-7}$.

Refractive index may also be measured by using an ellipsometer, which analyzes the polarization state of reflected light. Application of the general Fresnel equations for reflection from a plane surface, which give the relative intensities of the two perpendicular components of the reflected polarized light, as a function of angle of reflection and refractive indices of air and glass, enable one to calculate the refractive index. This technique is most often used for thin films, coatings, and layers which are not amenable to other techniques. When applied to bulk specimens of glass, one must remember, the technique is only measuring the refractive index of the surface and subsurface layers.

The accuracy of all the measurements above, of course, depends on the accuracy to which the wavelength of the light source is known. Table 5.7 lists the wavelength sources used in the optical glass industry. It should be noted that none of the lines are truly monochromatic (all have some finite spectral width) and some consist of doublet and triplet lines, which may not be resolvable with all instruments.

5.20.9.3 Measurement of Color. For many glass applications, consistent color matching of different lots of product, often to a well-defined specification, is required. Here the science of colorimetry is important. The perception of color is a psychophysical phenomenon; stimulation of three different sets of sensor cells (cones) located in the retina of the eye is interpreted as color sensation by the brain. The observed color of an object depends on the emission spectrum of the illuminating source, the transmittance and/or reflectance spectra of the material composing the object, and the spectral sensitivity of the sensor cells in the eyes of the observer. For example, the color observed for a red traffic light signal depends on the emission spectrum of the hot incandescent lamp filament behind the lens, the transmittance spectrum of the red glass filter lens, and the human observer. If the red traffic light was illuminated by a blue-white mercury arc lamp, or was observed by a color-blind person, it would not appear the appropriate red color.

TABLE 5.7 Wavelengths of Sources Used in the Glass Industry

Wavelength, nm	Line designation	Spectral line description
1013.9800	t	infrared hydrogen (H) line
852.1101	s	infrared cesium (Cs) line
706.5188	r	red helium (He) line
656.2725	C	red hydrogen (H) line
643.8469	C′	red cadmium (Cd) line
632.8	None	heliom-neon (He-Ne) gas laser
589.2938	D	yellow sodium (Na) line
587.5618	d	yellow helium (He) line
546.0740	e	green mercury (Hg) line
486.1327	F	blue hydrogen (H) line
479.9914	F′	blue cadmuim (Cd) line
435.8343	g	blue mercury (Hg) line
404.6561	h	violet mercury (Hg) line
365.0146	i	ultraviolet mercury (Hg) line

In 1931, to make the measurement of color both quantitative and standardized, the CIE (Commission Internationale de l'Eclairage—International Commission on Illumination) defined and adopted spectral sensitivity data for "standard" observers in terms of three sets of stimuli, red, blue, and green, called the *tristimulus values*. These data are available as tables or graphs showing the tristimulus values for monochromatic (spectral) light of equal intensity as functions of wavelength. For example, the CIE tristimulus values for monochromatic green light of 500-nm wavelength are $\underline{\underline{x}} = 0.0049$, $\underline{\underline{y}} = 0.3230$ and $\underline{\underline{z}} = 0.2720$. (One should note that the curves are normalized to make the maximum value of y = unity.) The tristimulus values X, Y, and Z for any light reaching the eyes of a standard observer can be obtained by multiplying together, as a function of wavelength, the emission spectrum of the light source, the transmittance spectrum of the glass (or reflectance spectrum, if the glass is viewed in reflection) and the CIE tristimulus values for the standard observer, and integrating the product over the full wavelength range of 400 to 700 nm. For example,

$$X = \frac{\int \underline{\underline{x}}(\lambda)P(\lambda)T(\lambda)d\lambda}{\int \underline{\underline{y}}(\lambda)P(\lambda)d\lambda}$$

$$Y = \frac{\int \underline{\underline{y}}(\lambda)P(\lambda)T(\lambda)d\lambda}{\int \underline{\underline{y}}(\lambda)P(\lambda)d\lambda}$$

$$Z = \frac{\int \underline{\underline{z}}(\lambda)P(\lambda)T(\lambda)d\lambda}{\int \underline{\underline{y}}(\lambda)P(\lambda)d\lambda}$$

where $P(\lambda)$ is the energy distribution of the source and $T(\lambda)$ is the transmittance at wavelength λ.

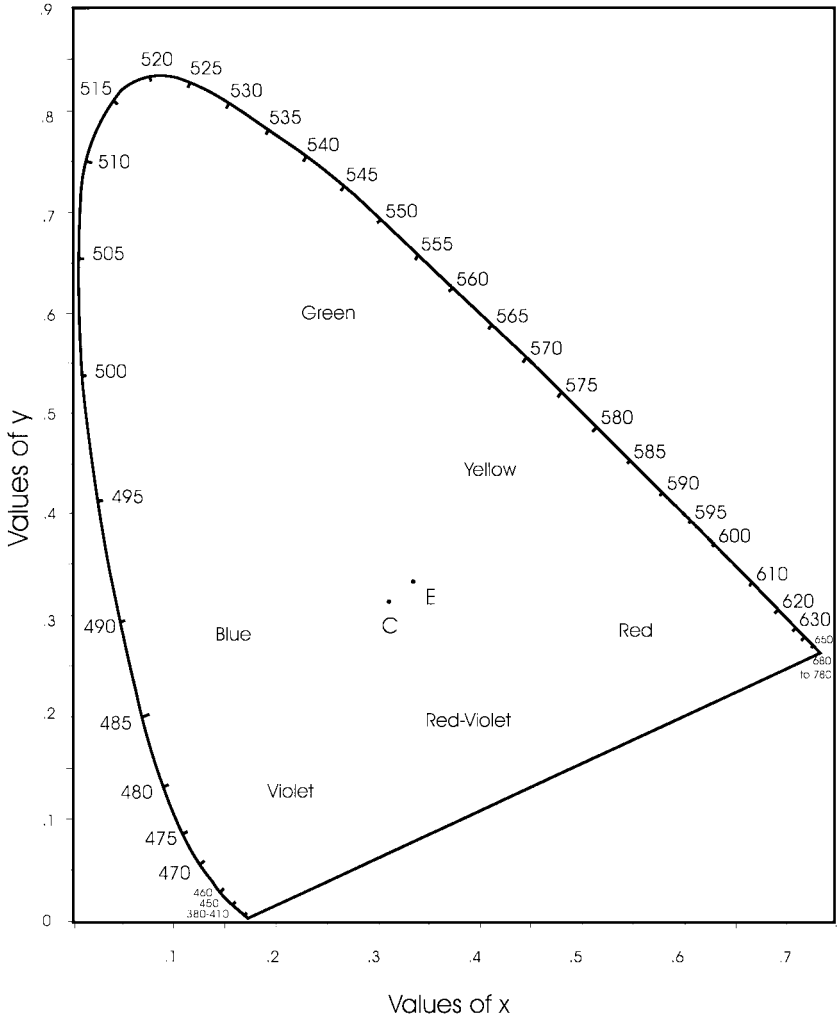

FIGURE 6.54 Chromaticity diagram.

From these values, the *trichromatic coefficients* x, y, and z may be calculated to give an unambiguous definition of the perceived color as

$$x = \frac{X}{X+Y+Z} \qquad y = \frac{Y}{X+Y+Z} \qquad z = \frac{Z}{X+Y+Z}$$

The trichromatic coefficents x and y, often referred to as the color coordinates "little x" and "little y," can be plotted on a *chromaticity diagram* such as shown in Fig. 5.54. The horseshoe-shaped curve is the locus of the color coordinates of the spectral wavelengths.

Point E ($x = 0.333$, $y = 0.333$) represents the chromaticity of equal-energy spectral radiation (all wavelength intervals $d\lambda$ having the same intensity) and point C represents the standard "illuminant C," a good representation of average mid-day daylight.

As an alternative to making the spectral measurements and performing mathematical calculations as described above, instruments can be designed for specific applications that will measure a specimen and interpret the results in terms of color coordinates. Such instruments, called *colorimeters*, are extremely useful for manufacturing products that require careful matching of color as part of their quality control. Of course, for some applications, one can also rely on a non-color-biased person, using an appropriate light source, to judge production samples against standardized "limit" samples.

5.20.9.4 Measurement of Other Optical Properties. Measurement of other optical properties such as strain-, electro-, magneto-, and acoustooptical effects involve specialized techniques beyond the scope of this chapter. The same is true for measurements of transmittance, refractive index profile, dispersion, and other important properties of optical communications fiber. Birefringence and strain-optical measurements will, however, be discussed in Chap. 6, in relationship to annealing and strengthening of glass.

BIBLIOGRAPHY

Arun K. Varshneya, *Fundamentals of Inorganic Glasses*, Academic Press New York, 1994.

J. Zarzycki, *Glasses an d the Vitreous State*, English edition, Cambridge University Press, Cambridge, U.K., 1991.

S. J. Schneider, Jr. (ed.), *Engineered Materials Handbook*, vol 4, *Ceramics and Glasses*, ASM International, Metals Park, Ohio, 1991.

H. Scholze, *Glass*, translated into English by M. Lakin, Springer-Verlag, New York, 1991.

N. P. Bansal and R. H. Doremus, *Handbook of Glass Properties*, Academic Press, Orlando, 1986.

H. Bach and N. Neuroth (eds.), *The Properties of Optical Glass*, Springer-Verlag. New York, 1998.

A. Paul, *Chemistry of Glasses*, 2d ed., Chapman and Hall, London, 1990.

D. R. Uhlmann and N. J. Kreidl (eds.), *Glass Science and Technology*, vols. 1, 2, 3, 5, Academic Press, New York, 1980–1985.

M. Tomozawa and R. H. Doremus (eds.), *Treatise on Materials Science and Technology*, vol. 12 (*Glass I,* 1977), vol. 17 (*Glass II,* 1979), vol. 22 (*Glass III,* 1982), vol. 26 (*Glass IV,* 1985), Academic Press, New York.

Computerized databases of several glass properties have been compiled in the form of "SciGlass" software by SciVison Corp., Burlington, Mass. and as "InterGlad" by New Glass Forum, Tokyo.

REFERENCES

1. W. H. Zachariasen, "The atomic arrangements in glass," *J. Amer. Chem. Soc*., vol. 54, 1932, pp. 3841–3851.
2. H. Rawson, "Inorganic Glass-Forming Systems," Academic Press, London, 1967.
3. A. Makishima and J. D. Mackenzie, "Direct calculation of Young's modulus of glass," *J. Non-Cryst. Sol*., vol. 12, no. 1, 1973, pp. 35–45.
4. T. Lakatos, L.-G. Johansson, and B. Simminsköld, "Viscosity-temperature relations in the glass system SiO_2-Al_2O_3-Na_2O-K_2O-CaO-MgO in the composition range of technical glasses," *Glass Technol*., vol. 13, pp. 88–95, 1972.

5. P. R. Rao and N. Subramanian, "Effect of viscosity in the determination of surface tension by the drop-weight method," *J. Sci. Ind. Res*., vol. 18B, pp. 402–404, 1959.

6. A. K. Varshneya, "Stresses in glass-to-metal seals," in M. Tomozawa and R. Doremus (eds.), *Treatese on Materials Science and Technology*, vol. 22, Glass III, Academic Press, New York, 1982.

7. T. Lakatos, L.-G. Johansson, and B. Simminsköld, *Glastek. Tidsk*., vol. 28, pp. 69–73, 1973.

8. J. Moore and D. E. Sharp, "Note on Calculation of Effect of Temperature and Composition on Specific Heat of Glass," *J. Amer. Ceram. Soc*., vol. 41, pp. 461–463, 1958.

9. C. T. Moynihan, A. J. Esteal, J. Wilder, and J. Tucker, *J. Phys. Chem*., vol. 78, p. 2673, 1974.

10. L. Šašek and M. Knotek, "Determination of factors for the calculation of electrical conductivity of silicate glass melts," *Chem. Technol. Silik*., vol. L 13, pp. 91–106, 1985.

11. C. M. Jantzen, J. B. Pickett, K. G. Brown, and T. B. Edwards, "Method of determining glass durability," U.S. Patent 5, 846, 278, December 8, 1998.

12. G. R. Antsis, P. Chantikul, B. R. Lawn, and D. B. Marshall, *J. Amer. Ceram. Soc.,* vol. 64, p. 533, 1981.

CHAPTER 6

INORGANIC GLASSES—COMMERCIAL GLASS FAMILIES, APPLICATIONS, AND MANUFACTURING METHODS

Thomas P. Seward III and Arun K. Varshneya
New York State College of Ceramics, Alfred University, Alfred, New York

6.1 COMMERCIAL GLASS FAMILIES

6.1.1 Introduction

Historically, development of glasses of many different compositions and properties was based on product (end use) needs and manufacturing capabilities. Composition inventions and process inventions went hand in hand. This is still true today, but now employee safety and environmental concerns have considerable impact on development as well. Among other things, this chapter will show how glass composition and manufacturing processes are interrelated, through chemistry and physics, and how both must be considered when selecting or developing a glass for a particular application.

Viscosity reigns supreme. We say this because almost every process step in glass manufacturing is performed most effectively within a certain range of melt viscosity. For example, melting of batch raw materials is generally performed best at a temperature where the melt has a viscosity of about 100 poises (P). On the other hand, pressing of molten glass into metal molds is most effective at viscosities in the range from 1000 to 10,000 P. Figure 6.1 shows the useful viscosity ranges for a number of process steps that will be described later in this chapter.

Another key factor is the viscosity of the melt at the liquidus temperature. The liquidus temperature of a melt is defined thermodynamically as the temperature above which the melt is stable as a liquid. Whether this liquid is very fluid or very viscous is not of thermodynamic importance. At temperatures below the liquidus temperature, the melt begins to devitrify (i.e., develop crystals); the extent of devitrification depends on the glass chemical composition, the temperature and the time allowed.

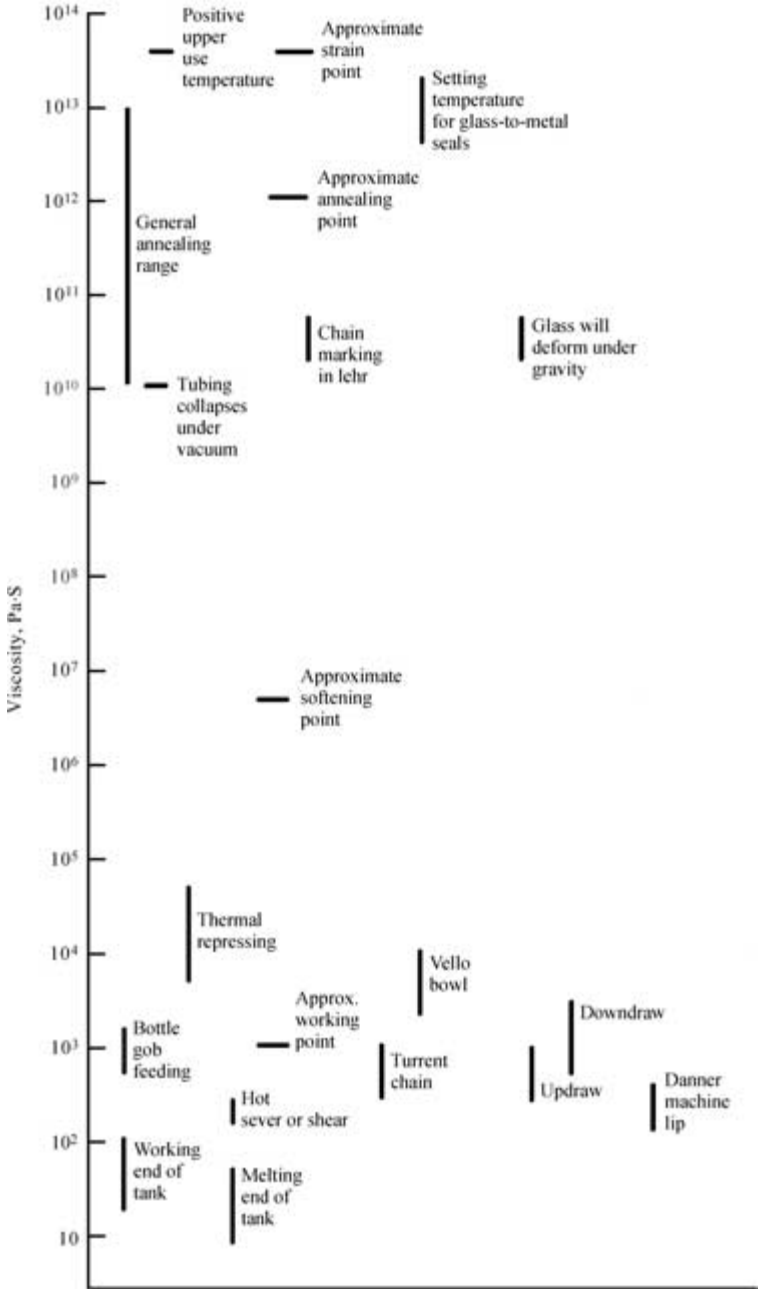

FIGURE 6.1 Approximate viscosity values for forming and processing methods (Pa · s × 10 = P). (*Courtesy of Corning Incorporated.*)

If, in order to operate a certain manufacturing process at the required viscosity, the glass temperature has to be decreased below the liquidus temperature, then there is the risk that, given enough time, the molten glass will crystallize. (See also the sections on kinetics of glass formation and TTT diagrams in Chap. 6.) So, for any melting and forming process, the glass composition must be designed so that the liquidus temperature is less than any processing temperature at which some or all of the molten glass will be held for long periods of time.

It is customary in glass science and technology to refer to glasses as *soft* or *hard*, not in terms of physical hardness, but rather in terms of the temperatures required to soften the glass and make it flow. Soft and hard are relative terms; one glass is harder than another if one must heat it to higher temperatures to make it flow. Nevertheless, on a technology scale, some glasses are considered "soft" and others "hard." Additionally, glasses are called *long* or *short*, depending on the slope of the viscosity curve (versus temperature) within the working range, the temperature interval between the softening and working points. The terms short and long thus refer to the relative amount of time available to work the glass as it cools. The wide variety of viscosity-temperature relationships exhibited by commercial glasses is illustrated in Figure 6.2. The glass code numbers shown in the figure correspond to those of glass compositions listed in Tables 6.1 and 6.2.

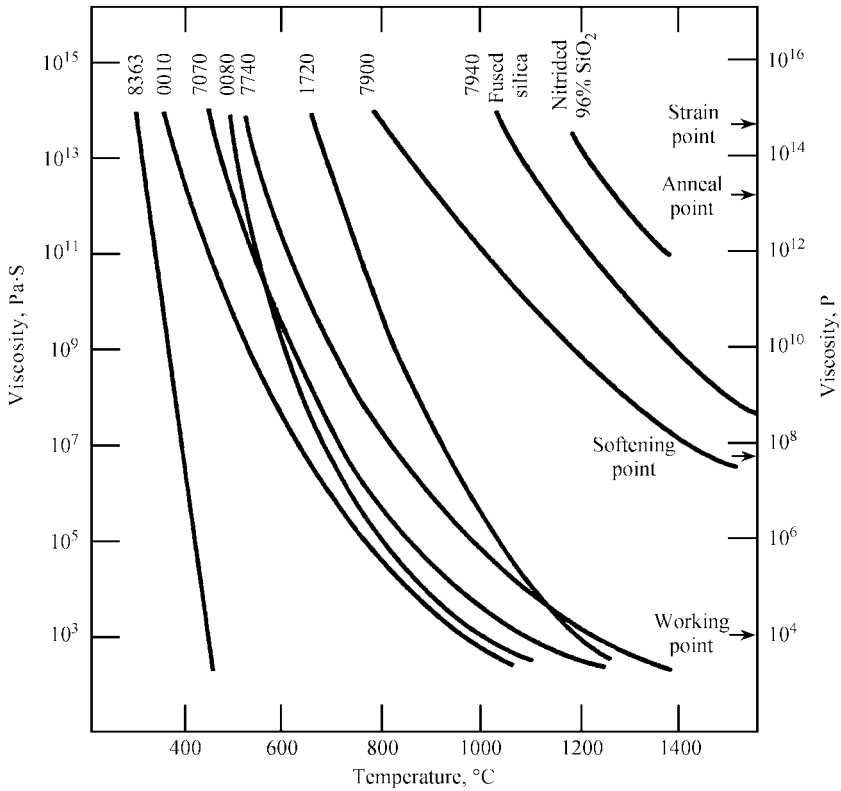

FIGURE 6.2 Viscosity versus temperature for some commercial glasses designated by glass codes (see Tables 6.1 and 6.2). (*Courtesy of Corning Incorporated.*)

TABLE 6.1 Glass Compositions—Listed by Glass Type, wt%

Glass identification	Description/use	SiO_2	Al_2O_3	B_2O_3	Li_2O	Na_2O	K_2O	MgO	CaO	SrO	BaO	PbO	ZnO	Other	References
Soda-lime glasses															
Typical generic	Multipurpose	73	2			15			10						
Corning 0070	Elect./lamp tubing	71	3			13	1	5	7						Boyd et al.[9]
Corning 0080	Lamp bulbs	73	1			17		4	5						Boyd et al.[9]
Corning 0091	Elect./lamp bulbs	73.5	1			15	0.5	4	6						Boyd et al.[9]
Typical container	Green tinted	73	0.5			16			9.3					$Fe_2O_3 = 0.5$; $Cr_2O_3 = 0.2$; $SO_2 = 0.5$	
Typical flat glass	Clear float	73.1	0.1			13.7	0.1	3.8	8.9					$Fe_2O_3 = 0.5$; $TiO_2 = 0.5$; F = 0.2	
Lead glasses															
Corning 0010	Lamp tubing	63	1			8	6					22			Boyd et al.[9]
Corning 0120	Lamp tubing	56	2			4	9					29			Boyd et al.[9]
Corning 8160	Electron tubes (discontinued)	56	2			3	10		1		5	23		Some F	Hutchins et al.[9a]
Corning 8161	Electron tubes (discontinued)	40					5				2	51		$Rb_2O = 2$	Hutchins et al.[9a]
Corning 8363	Radiation shielding	5	3	10								82			Hutchins et al.[9a]
Corning 8871	Capacitors	42			1	2	6					49			Hutchins et al.[9a]
Lead sealing															
Corning 1990	To iron	41			2	5	12					40			Boyd et al.[9]
Corning 7570	Solder sealing	3	11	12								74			Boyd et al.[9]

TABLE 6.1 Glass Compositions—Listed by Glass Type, wt% (Continued)

Glass identification	Description/use	SiO_2	Al_2O_3	B_2O_3	Li_2O	Na_2O	K_2O	MgO	CaO	SrO	BaO	PbO	ZnO	Other	References
Lead TV glasses															
Corning 0120	Stem tubing	56	2			4	9					29		$Sb_2O_3 = 0.5$	Connelly et al. in Schneider[7]
Corning 0137	Neck tubing	52.5	1			0.8	12			5		28		$Sb_2O_3 = 0.5$	Connelly et al.[7]
Corning 0138	Funnel	54	2			6	8	2.5	3.5			23		$Sb_2O_3 = 0.1$	Connelly et al.[7]
Corning 7580	Sealing frit	2	0.1	8.4							1.9	75.4	12.2		Connelly et al.[7]
Borosilicate glasses															
Corning 0211	Microsheet	65	2	9		7	7						7	$TiO_2 = 3$	Boyd et al.[9]
Corning 7070	Low-loss electrical	72	1	25	0.5	0.5	1								Boyd et al.[9]
Corning 7251	Sealed beam lamps	82	2	12		4									Boyd et al.[9]
Corning 7740	General purpose	81	2	13		4									Boyd et al.[9]
Kimble KG33	Laboratory ware	81	2	13		4									Boyd et al.[9]
Corning 7720	Tungsten sealing	74	1	15		4						6			Boyd et al.[9]
Corning 7760	General purpose	78	2	15		3	1							$As_2O_3 = 1$	Boyd et al.[9]
Corning 9741	UV transmitting	65	5	27	1	2								Some F	Boyd et al.[9]
Aluminoborosilicates															
Corning 7059	Electronic display substrates	49	10	15							25			$As_2O_3 = 1$	Boyd et al.[9]

TABLE 6.1 Glass Compositions - Listed by Glass Type, wt% (Continued)

Glass identification	Description/use	SiO_2	Al_2O_3	B_2O_3	Li_2O	Na_2O	K_2O	MgO	CaO	SrO	BaO	PbO	ZnO	Other	References
Aluminosilicates															
Corning 1720	Ignition tubes	62	17	5		1		7	8						Boyd et al.[9]
Corning 1723	Electron tubes, spacecraft windows	57	16	4				7	10	6					Boyd et al.[9]
Corning 6720	Tableware (opal)	60	10	1		8	2		5				10	F = 4	Boyd et al.[9]
Corning 6750	Lighting ware	61	11			15					9			F = 3	Boyd et al.[9]
Corning 0317	Ion exchange strengthened	61.4	16.8			12.7	3.6	3.7	0.2					TiO_2 = 0.8	Dumbaugh in Boyd[5]
E-type fiberglass	Continuous textile fiber—typical	54	14	10				4.5	17.5						Boyd et al.[9]
S-type fiberglass	High-strength continuous textile fiber	65	25					10							Aubourg and Wolf in Boyd[5]
High-silica glasses															
Typical fused quartz	Fused quartz	>99.9													
Typical synthetic	Synthetic fused silica	>99.9													
Corning 7940	Synthetic fused silica	>99.9												H_2O = 0.08	Corning prod. lit.
Corning 7980	Synthetic fused silica	>99.9												H_2O = 0.08	Corning prod. lit.
Corning 7913	Vycor brand 96% silica	96.5	0.5	3											Corning prod. lit.
Corning 7971	ULE brand (ultralow expansion)	93												TiO_2 = 7	Corning prod. lit.

TABLE 6.2 Glass Physical Properties Listed by Glass Type

Glass identification	Description/use	Density, g/cm^3	CTE, 0 to 300°C 10^{-7}/°C	Strain point, °C	Annealing point, °C	Softening point, °C	Working point, °C	Young's modulus, GPa	Poisson's ratio	Refractive index	Resistivity at 350°C log(Ω · cm)	References
Soda-lime glasses												
Typical generic	Multipurpose											
Corning 0070	Elect./lamp tubing	2.5	91	487	527	715				1.513		Boyd et al.[9]
Corning 0080	Lamp bulbs	2.47	93.5	473	514	696	1005	70	0.22	1.512	5.1	Boyd et al.[9]
Corning 0091	Elect./lamp tubing	2.48	91	485	523	705						Boyd et al.[9]
Lead glasses												
Corning 0010	Lamp tubing	2.79	93.5	395	435	628	985	62	0.21	1.54	7	Boyd et al.[9]
Corning 0120	Lamp tubing	3.05	89.5	395	435	630	985	59	0.22	1.56	8.1	Boyd et al.[9]
Corning 8160	Electron tubes (discontinued)	2.98	91	395	435	630	975			1.553	8.4	Hutchins et al.[9a]
Corning 8161	Electron tubes (discontinued)	4.00	90	400	435	600	860	54	0.24	1.659	9.9	Hutchins et al.[9a]
Corning 8363	Radiation shielding	6.22	104	300	315	380	460	51	0.27	1.97	7.5	Hutchins et al.[9a]
Corning 8871	Capacitors	3.84	102	350	385	525	785	58	0.26		8.8	Hutchins et al.[9a]
Lead sealing												
Corning 1990	To iron	3.5	124	340	370	500	756	58	0.25		7.7	Boyd et al.[9]
Corning 7570	Sealing frit	5.42	84	342	363	440	558	55	0.28	1.86	8.7	Boyd et al.[9]
Lead TV glasses												
Corning 0120	Stem tubing	3.05	89.5	395	435	630	986	59	0.22	1.56	8	Connelly et al. in in Schneider[7]
Corning 0137	Neck tubing	3.18	97	436	478	661	978	65	0.24	1.55	8.3	Connelly et al.[7]
Corning 0138	Funnel	2.98	97	435	474	654	965	69	0.23	1.565	7.6	Connelly et al.[7]
Corning 7580	Sealing frit	6.47	98	293	311	374	890		0.25	1.65	8.2	Connelly et al.[7]

TABLE 6.2 Glass Physical Properties Listed by Glass Type (Continued)

Glass identification	Description/use	Density, g/cm^3	CTE, 0 to 300°C 10^{-7}/°C	Strain point, °C	Annealing point, °C	Softening point, °C	Working point, °C	Young's modulus, GPa	Poisson's ratio	Refractive index	Resistivity at 350°C log(Ω · cm)	References
Borosilicate glasses												
Corning 0211	Microsheet	2.57	74	508	550	720	1008	74	0.21	1.52		Boyd et al.[9]
Corning 7070	Low-loss dielectric	2.13	32	456	496		1068	51	0.22	1.469	9.1	Boyd et al.[9]
Corning 7251	Sealed beam lamps	2.26	36.5	521	565	808	1192	64	0.19	1.476	6.5	Boyd et al.[9]
Corning 7740	General purpose	2.23	32.5	510	560	821	1252	63	0.2	1.474	6.6	Boyd et al.[9]
Kimble KG33	Laboratory ware	2.23	32	513	565	827	1240			1.47	6.6	Boyd et al.[9]
Corning 7720	Tungsten sealing	2.35	36	484	523	755	1146	63	0.2	1.487	7.3	Boyd et al.[9]
Corning 7760	General purpose	2.24	34	478	523	780	1198	62	0.2	1.473	7.7	Boyd et al.[9]
Corning 9741	UV transmitting	2.16	39.5	408	450	705	1161	49	0.23	1.468	7.6	Boyd et al.[9]
Aluminoborosilicates												
Corning 7059	Electronic display substrates	2.76	46	593	639	844	1160	68	0.28	1.53	11	Boyd et al.[9]
Aluminosilicates												
Corning 1720	Ignition tubes	2.52	42	667	712	915	1202	87	0.24	1.53	9.5	Boyd et al.[9]
Corning 1723	Electron tubes, spacecraft window	2.64	46	665	710	908	1168	86	0.24	1.547	11.3	Boyd et al.[9]
Corning 6720	Tableware (opal)	2.58	78.5	505	540	780	1023	70	0.21	1.507		Boyd et al.[9]
Corning 6750	Lighting ware	2.59	88	447	485	676	1040			1.513		Boyd et al.[9]
Corning 0317	Ion-exchange strengthenable	2.46	88	576	622	870		72	0.22	1.506	5.5 @ 250°C	Corning prod. lit.
E-type fiberglass	Typical	2.62	54	615	657	846		72		1.562		Auborg et al. in Boyd and MacDowell[5]
S-type fiberglass	Typical	2.50	16	760	810	970		89		1.525		Auborg et al.[5]
High-silica glasses												
Typical fused quartz	Ranges			1040–1108	1585–1625	1582–1813						
Typical synthetic	Ranges			987–1020	1075–1120	1585–1625						
Corning 7940	Synth. fused silica	2.202	5.6	990	1075	1585		73	0.17	1.459	10.5	Boyd et al.[9]
Corning 7980	Synth. fused silica	2.202	5.6	990	1075	1585		73	0.17	1.459	10.5	Corning prod. lit.
Corning 7913	Vycor® brand	2.18	7.5	890	1020	1530		68	0.19	1.458	8.1	Boyd et al.[9]
Corning 7971	ULE™ brand	2.21	0.5	890	1000	1500		68	0.17	1.484	10.1	Boyd et al.[9]

In the following sections we present several families of glasses, generally progressing from the softer to the harder. We discuss each family, giving examples and ranges of useful compositions. We also list key properties of importance, current commercial applications, and some manufacturing processes used to form articles from those glasses. Applications and processes are discussed more thoroughly in later sections of the chapter.

6.1.2 Soft Glasses

6.1.2.1 Soda-Lime-Silica Glass

Brief History. Soda-lime-silica glass, sometimes called simply *soda-lime* glass, is the generic name for a family of glass compositions based on the network former silica (SiO_2) and modified by soda (Na_2O) and lime (CaO). It is the oldest commercial type of glass and has roots with the earliest commercial glasses developed in the Middle East thousands of years B.C. Silica is too refractory a material to be melted and formed as a glass by wood or fossil fuel fires. However, it was discovered that additions of soda ash (Na_2CO_3) and limestone ($CaCO_3$) to silica sand (crystalline quartz) acted as fluxes to help melt the sand over simply fueled fires. The resulting melt was sufficiently fluid that it could be worked to form useful objects.

The relative ease of discovery and manufacture are key to the almost universal use of soda-lime-silica glass products. For example, sand was plentiful and at the outset contained sufficient calcium oxide as impurities (often as calcium carbonate from shell fragments) that when combined with soda and potash from wood and plant fires allowed the discovery of good stable glasses that could be melted over wood fires. The fluxing agent magnesia (MgO) was also present as a minor component in the ash. The relatively low cost (compared to most other commercial glass compositions) and the relatively low required melting temperatures (about 1150°C) combined with physical and chemical properties acceptable for a wide variety of applications continue to make it the major type of glass manufactured today in terms of volume.

Most commercial soda-lime glass compositions are based on a eutectic composition in the Na_2O-CaO-SiO_2 phase diagram located at about 22 percent Na_2O, 5 percent CaO, and 73 percent SiO_2, by weight. The more useful compositions are higher in CaO and lower in Na_2O for several reasons, one of which is improved chemical durability. A typical composition is $15Na_2O \cdot 10CaO \cdot 2Al_2O_3 \cdot 73SiO_2$ (wt%), the alumina (Al_2O_3) being present in part to help improve chemical durability and in part to decrease the tendency for crystallization. This composition lies in the thermodynamic stability field of the mineral devitrite ($Na_2O \cdot 3CaO \cdot 6SiO_2$). While the term devitrification is applied to all families of glasses to describe the process whereby the molten glass gradually crystallizes if held at temperatures somewhat below the liquidus, the name devitrite is reserved for devitrification in this particular soda-lime-silica composition field.

In commercial glass compositions, one often finds other alkali oxides substituted for some of the Na_2O and magnesia (MgO) substituted for some of the lime. This is in part to provide more desirable properties, including higher viscosities at the liquidus temperature, and sometimes, especially in the case of the magnesia, because of more economically available raw materials. Typical composition ranges for soda-lime-silica glasses and representative commercial glass compositions are given in Table 6.1. Properties for those glasses are given in Table 6.2.

Chemistry and Properties. This section, and similar sections in the discussions of other glass families, contains a synopsis of the types of chemical components used in typical glass

compositions and the properties or performance characteristics that depend on them.

Glass former. SiO_2

Modifiers. Alkali and alkaline earth oxides.

Intermediates. Alumina.

Alkalis. They act as fluxes, making the glass easier to melt. The melt viscosity is greatly decreased relative to that of silica at all temperatures. This makes melting and forming easier. Hence, alkali-containing glass is more economic as a product. Among adverse effects are lower use temperatures (deformation temperatures), increased thermal expansion coefficient [about 5 points (5×10^{-7}/°C) per 1 percent soda], which is frequently undesirable, and greatly decreased chemical durability (attack by aqueous solutions). Further, since the alkali ions are somewhat mobile within the glass network (see Chap. 5), the glass becomes more electrically (ionically) conductive, especially as temperature increases, thus decreasing its effectiveness as an insulator. (This, however, can be an advantage in electrically boosted melting.)

Soda, Na_2O (from soda ash and/or nitre). The most important alkali for glass making.

Lithia, Li_2O (from lithium carbonate). A better flux than soda, provides slightly better durability, but is much more expensive.

Potassia, K_2O (from potash and/or potassium nitrate). Has a larger ionic size, so is less mobile and therefore better for electrical insulation properties, but not quite as good a flux as soda.

Alkaline earths. They also provide fluxing action (but not as good as the alkalis). They are significantly better than alkalis for chemical durability, and for dielectric properties (i.e., the electrical conductivity of alkaline earth ions is less than alkalis; they have a double ionic charge, thus are less mobile).

Lime, CaO (from limestone). The most important alkaline earth for glass making.

Magnesia, MgO. Often present with CaO in natural batch materials, for example in dolomite [$MgCa(CO_3)_2$] or dolomitic limestone.

Alumina, Al_2O_3 (generally from feldspar or nepheline syenite). Alumina can be considered a network modifier, but is often a network former, especially if present in amounts less than the alkalis. It improves chemical durability and generally decreases the tendency for crystallization (devitrification). Rarely is alumina included in the batch as the oxide, but rather as a compound containing two or more of the major glass components.

Key Characteristics. Soda-lime silicates are generally useful glasses: Density is about 2.3 g/cm^3. Typically, they are hard (5 to 7 on the Mohs scale), stiff (Young's modulus about 70 GPa, 10^7 lb/in^2) and strong (design strength above 7MPa, 1000 lb/in^2). They are transparent, with refractive index about 1.51 to 1.53. They are electrical insulators with good dielectric strength. They have a dielectric constant of about 7 and a dielectric loss of about 7 percent at 1 MHz. They are chemically durable against water and acid, and have fairly good weathering resistance. However, they have high thermal expansion (about 90×10^{-7}/°C) and only fair upper use temperature (softening point about 700°C; strain point about 475°C). They provide benchmarks against which all property improvements may be judged.

Advantages. A general, all-around glass; easy to melt; perhaps the least expensive and most widely used family of glasses.

Disadvantages. Because of their high thermal expansion, soda-lime-silica glasses are prone to thermal shock failure, and because of their relative softness, they have limited

high-temperature usefulness relative to the harder families of glasses to be discussed later. They are somewhat inferior electrically (have high dielectric loss).

Applications

Architectural glazing (windows and spandrels)

Automotive glazing (flat glass and reshaped glass)

Lighting (household lamp and fluorescent tubing envelopes, tubing for neon lighting)

Electrical (radio tube envelopes—a reemerging application)

Containers (bottles, drinkware, tableware)

Decorative and art

Variations—tempered (thermal and chemical), coated, laminated

For each of these applications one could list all the required glass properties to see why soda-lime glass is suited to the application. We will do this just for the lighting application. Some of the key glass requirements are that it:

- Transmit light and other wavelength radiation
- Be impervious to gas diffusion
- Be readily degassed in a vacuum
- Be hermetically sealable to other glass and metal parts
- Be relatively chemically durable
- Withstand the high temperatures generated by the light source
- Have good dielectric properties
- Be easily fabricated into shapes suitable for the product application

Soda-lime glass satisfactorily meets all these requirements for incandescent and fluorescent lamp applications (but not for halogen cycle and arc lamp applications) and is inexpensive compared to higher-temperature (harder) glasses. This explains its almost universal use in these applications. Glass compositions and properties of soda-lime-silica glasses used for some of the above applications are given in Tables 6.3 through 6.6.

Forming Processes. Pressing, blowing, casting, rolling, tube drawing, sheet drawing, floating on a tin bath. (These processes and others are described in Sec. 6.3, "Glassmaking I—Glass Melting.")

6.1.2.2 Lead Silicate Glasses

Brief History. The first commercial use of lead oxide as a major glass component was by George Ravenscroft in seventeenth century England. For many reasons, the supply of glass from continental Europe had become unreliable, as had the importing of plant ashes for soda. Ravenscroft developed high-quality potassia-lead-silica glasses. The glass was exceptionally brilliant in appearance. Ravenscroft called it *crystal* and kept secret the fact that lead was the key ingredient; so did his successor. The glass was also called *flint* glass because the silica came from flint nodules found in the chalk deposits of southeast England. This source of silica was highly pure, a key factor in the clarity and brilliance of Ravenscroft's products. The term *flint* glass is still used today in two contexts: (1) for high-dispersion optical glasses, often containing lead oxide, and

TABLE 6.3 Glass Compositions for Laboratory, Electric Lighting, and Container Applications, wt%

Glass identification	Description	SiO_2	Al_2O_3	B_2O_3	Li_2O	Na_2O	K_2O	MgO	CaO	SrO	BaO	PbO	ZnO	Other	References
Laboratory glassware															
Borosilicate	Typical, low TCE	81	2	13		4									Bardhan et al. in Schneider[7]
	Corning 7740	81	2	13		4									Boyd et al.[9]
Aluminoborosilicate	Jena G20	75.7	5.1	6.9		6.2	1.2		1.3		3.6				Hutchins et al.[9a]
	O-I N-51a	74.7	5.6	9.6		6.4	0.5		0.9		2.2				Hutchins et al.[9a]
	Typical	72	6	11		7	1		1						Bardhan et al.[7]
Soda-lime	Typical	73	2			14		4	7						Bardhan et al.[7]
Zinc-titania cover glass	Typical	65	2	9		7	7						7	$TiO_2 = 3$	Bardhan et al.[7]
High silica	Corning 7913	96.5	0.5	3											Boyd et al.[9]
Electric lighting															
Soda-lime	Typical	72	2			16	1	4	3						Van Reine et al. in Boyd[5]
Lead	Typical	63	2			7	7					21			Van Reine et al.[7]
Borosilicate	Typical	78	2	15		5									Van Reine et al.[7]
Aluminosilicate	Typical	61	16	1					10		12				Van Reine et al.[7]
	Corning 1720	62	17	5		1		7	8						Schneider[7]
	Osram 742a	51.3	25.3	1				4.2	8.3		5.3			$P_2O_5 = 4.6$	Dumbaugh et al.[5]
	AEI C37	55.8	23	5.1					13		3.1				Dumbaugh et al.[5]
	GEC H.26	54	21	8					14		3				Dumbaugh et al.[5]
High silica	Corning 7913	96.5	0.5	3											Boyd et al.[9]
Fused silica/ fused quartz	Typical	>99.9													Van Reine et al.[7]
Container															
Soda-lime	Typical	74.1	1.3			13.5	0.3		10.5	Tr.	Tr.				
Borosilicate	Typical	80.5	2.2	12.9		3.8	0.4								Vergano[7]
Pharmaceutical	Corning 7800	72	6	11		7	1		1		2				Boyd et al.[9]

Tr = Trace, <<1.0%

TABLE 6.4 Physical Properties of Glasses for Laboratory, Electric Lighting, and Container Applications

Glass identification	Description	Density, g/cm^3	CTE, 0 to 300°C, 10^{-7}/°C	Strain point, °C	Annealing point, °C	Softening point, °C	Working point, °C	Young's modulus, GPa	Refractive index,	Resistivity 350°C, log (Ω · cm)	References
Laboratory glassware											
Borosilicate	Typical, low TCE	2.23	32.5	510	570	821	1252	63	1.474		Bardhan et al in Schneider[7]
	Corning 7740	2.23	32.5	510	560	821	1252	63	1.474	6.6	Boyd et al.[9]
Aluminoborosilicate	Jena G20	2.39		524	569	794	1190	71		6	Hutchins et al.[9a]
	O-I N51a	2.36		540	580	795	1175		1.49	5.6	Hutchins et al.[9a]
	Typical	2.36	50	533	576	795	1189		1.491		Bardhan et al.[7]
Soda-lime	Typical	2.4	89	511	545	724			1.515		Bardhan et al.[7]
Zinc-titania cover glass	Typical	2.57	74	508	550	720		74	1.52		Bardhan et al.[7]
High silica	Corning 7913	2.18	7.5	890	1020	1530		68	1.458	8.1	Boyd et al.[9]
Electric lighting											
Soda-lime	Typical	2.5	94	490	520	700	1015	72		5	van Reine et al. in Schneider[7]
Lead	Typical	2.8	93	410	445	635	1000	61		7	van Reine et al.[7]
Borosilicate	Typical	2.3	40	520	570	800	1200	64		7	van Reine et al.[7]
Aluminosilicate	Typical	2.6	45	770	810	1025	1250	88		11	van Reine et al.[7]
	Corning 1720	2.52	42	667	712	915	1202	87	1.53	9.5	Dumbaugh et al. in Boyd[5]
	Osram 742a	2.62	31								Dumbaugh et al.[5]
	AEI C37	2.55	42.5		760						Dumbaugh et al.[5]
	GEC H.26		43		760						Dumbaugh et al.[5]
High silica	Corning 7913	2.18	7.5	890	1020	1530		68	1.458	8.1	Boyd et al.[9]
Fused silica/ fused quartz	Typical	2.2	5.5	1070	1140	1670		73	1.459	10	van Reine et al.[7]
Container											
Soda-lime	Typical	(see laboratory glassware, above)									
Borosilicate	Typical, low TCE	(see laboratory glassware, above)									
Pharmaceutical	Corning 7800	2.36	50	533	576	795	1189		1.491	5.7	Boyd et al.[9]

TABLE 6.5 Glass Compositions for Houseware Applications, wt%

Glass identification	Description	SiO_2	Al_2O_3	B_2O_3	Li_2O	Na_2O	K_2O	MgO	CaO	SrO	BaO	PbO	ZnO	As_2O_3	Sb_2O_3	F^-	Other	References
Tableware—glass																		
Durand table	NaF opal	71.5	5.6			13					6.3					3.7		Fine in Schneider[7]
Durand Arcopal	Glass-glass opal	75.3	3.2	13.5		6.6			0.7							0.8		Fine[7]
Corning 6720	CaF_2 opal	58.9	10.5	1.4		8.4			5.8				8.7			4.2		Fine[7]
Durand soda-lime	Soda-lime	71.1	1.6			14.2	0.5	1.1	9.8									Fine[7]
Corning corelle—a glass-glass laminate	Borosilicate (skin)	58	15	6				6	15							3		Fine[7]
	CaF_2 opal (core)	64	6	5		3	3	1	15									
Tableware—glass-ceramic																		
Corning 9609 (Pyroceram)	Nephelene	43.3	29.8	5.5		14								0.9			$TiO_2 = 6.5$	Fine[7]
Corning 0308 (Pyroceram)	Potassium-richterite	67.1	1.8	0.3	0.8	3	4.8	14.3	4.7						0.2	3.5	$P_2O_5 = 1$	Fine[7]
Drinkware																		
Durand	Lead crystal	59.9				3.3	10.3		1.3			24.4						Fine[7]
Libbey	Soda-lime	72.6	1.3			13.5		4.3	6.8									Fine[7]
Schott	Alkaline earth silicate	68.4	0.2	0.8		10.6	5.5		10		4.5							Fine[7]
Rosenthal	Alkaline earth silicate	69.4	0.6			10.7	7.2	1.2	4.9		6							Fine[7]
Bormioli	Alkaline earth silicate	69.4	1.4	0.7		9.8	5.6		7.6		5.7							Fine[7]
Anchor/Libbey/Durand/Pasabache	Soda-lime range	72–73.1	1.1–1.5			13.5–14.4	Tr.–0.28	1.0–3.4	8.5–11.3	0–0.2							$Fe_2O_3 < 0.03$; $SO_3 = 0.2$–0.3	McGaughey[12]
Ovenware—glass																		
Anchor Hocking	Tempered borosilicate	76.4	1.8	14.7		5.4			0.7					0.4				Fine[7]
Corning 0281	Tempered soda-lime	74	2	0.5		13.5			10						0.2			Fine[7]
Corning 7251	Tempered borosilicate	82	2	12		4												Fine[7]

TABLE 6.5 Glass Compositions for Houseware Applications, wt% (Continued)

Glass identification	Description	SiO_2	Al_2O_3	B_2O_3	Li_2O	Na_2O	K_2O	MgO	CaO	SrO	BaO	PbO	ZnO	As_2O_3	Sb_2O_3	F^-	Other	References
Ovenware—glass-ceramic																		
Corning Ware	β-spodumene s.s.	69.7	17.8		2.8			2.6					1	0.6			$TiO_2 = 4.7$	Fine[7]
Corning Visions	β-quartz s.s.	68.8	19.2		2.7	0.2	0.1	1.8			0.8		1	0.8			$TiO_2 = 2.7$; $ZrO_2 = 1.8$	Fine[7]
Durand Arcoflam—Clear Line	β-quartz s.s.	66.1	20.2		3.9	0.4		1			1.8		1	1			$TiO_2 = 3.0$; $ZrO_2 = 1.7$	Fine[7]
Tableware (dinnerware) glazes																		
Semivitreous lead-free		59.09	13.53	4.3	0.51	1.81	3.92	0.96	11.76	4.12								Fine[7], Eppler in Boyd[5]
Vitreous lead-free		55.79	7.37	5.47		1.81	2.71	0.62	9.16	3.07	2.5		10.94				$ZrO_2 = 0.57$	Fine[7], Eppler in Boyd[5]
Leaded		55.88	9.57	6.04		3.06	1.72		7.65			16.08						Fine[7], Eppler[5]
Leaded, low-temperature (Cone 06)		42.45	7.04	8.93		2.46			3.09			35.3					$ZrO_2 = 0.72$	Fine[7], Eppler[5]

s.s. = Solid solution.

TABLE 6.6 Physical Properties of Glasses for Houseware Applications

Glass identification	Description	CTE 25–300°C, 10^{-7}/°C	Softening point, °C	References
Tableware—glass				
Durand table	NaF opal	75	715	Fine in Schneider[7]
Durand Arcopal	Glass-glass opal	44	764	Fine[7]
Corning 6720	CaF_2 opal	80	792	Fine[7]
Durand soda-lime	Soda-lime			Fine[7]
Corning Corelle—glass-glass laminate	Borosilicate (skin) CaF_2 opal (core)	48 71	890	Fine[7]
Tableware—glass-ceramic				
Corning 9609 (Pyroceram)	Nephelene	95	NA (crystallized)	Fine[7]
Corning 0308 (Pyroceram)	Potassium-richterite	118	NA (crystallized)	Fine[7]
Drinkware				
Durand	Lead crystal	89	647	Fine[7]
Libbey	Soda-lime	86	736	Fine[7]
Schott	Alkaline earth silicate	98	695	Fine[7]
Rosenthal	Alkaline earth silicate	99	682	Fine[7]
Bormioli	Alkaline earth silicate	89	704	Fine[7]
Anchor/Libbey/Durand/Pasabache	Soda-lime range			McGaughey[12]
Ovenware—glass				
Anchor Hocking	Tempered borosilicate			Fine[7]
Corning 0281	Tempered soda-lime	86		Fine[7]
Corning 7251	Tempered borosilicate	37		Fine[7]
Ovenware—glass-ceramic				
Corning Corning Ware	β-spodumene s.s.	4–20	NA (crystallized)	Fine[7]
Corning Visions	β-quartz s.s.	5–7		Fine[7]
Durand Arcoflam—Clear Line	β-quartz s.s.	1		Fine[7]

(2) for clear (uncolored) beverage bottles, generally made of soda-lime-silica glass containing no lead at all.

Chemistry/Properties

Glass former. SiO_2.

Modifiers. Alkali, alkaline earth, and lead oxide.

Intermediates. Alumina

Lead oxide, PbO. At low molar compositions it acts as a network modifier. It is a good flux. Like alkaline earth oxides, it has less adverse effect on thermal expansion or chemical durability than alkalis. It significantly increases the refractive index and elastic modulus.

It increases the working range (*long* glass, see Sec. 6.1.1). A typical composition (alkali lead silicate with intermediate lead concentration) is $30PbO \cdot 9K_2O \cdot 4Na_2O \cdot 2Al_2O_3 \cdot 55SiO_2$ (wt%). On a mole percent basis, this composition would look similar to a mixed alkali-lime-silica glass, with lead oxide substituted for calcium oxide.

At high lead concentrations, say greater than 50 percent PbO by weight, lead can be a network former. This is especially true in binary lead silicates, borate glasses and phosphate glasses, which will be discussed in later sections. Up to 70 wt% lead oxide is used in high-refractive-index optical glasses and in radiation-shielding windows. Typical composition ranges for lead silicate glasses and example commercial glass compositions are given in Table 6.1. Properties for those glasses are given in Table 6.2.

Key Characteristics. The main characteristics of lead silicate glasses are high expansion, long working range, good dielectric properties, high refractive index in combination with high dispersion, and fairly good chemical durability.

Advantages. Glasses containing lead are generally easy to melt. Compared to soda-lime glasses of similar softening points, they have a longer working range, higher refractive index, better electrical resistivity, and lower dielectric loss, but are more expensive than soda lime. Lead provides x-ray absorption in television cathode-ray tube (CRT) bulbs.

Disadvantages. Lead oxide is considered to be a health and environmental concern. It is especially so in the glass-manufacturing environment where particles of lead oxide may be airborne. Once incorporated into a commercial glass product, the concern is less, unless the glass itself is ground into a fine powder, as in sawing, grinding, and engraving operations.

Applications. Major uses are

Glass tubing (e.g., neon sign tubing)

Electric filament mount structures (incandescent and fluorescent lamps)

Cathode-ray tubes (television bulb neck and funnel, radar screens)

Optical/ophthalmic (refractive index adjustment)

Solder glass and frits (for relatively low temperature joining or sealing of glass/metal, glass/ceramic, and glass/glass; conductive, resistive, and dielectric pastes in electronic circuits; decorative enamels)

Drink ware (“hollow ware”)

Decorative and art glass

Radiation shielding (nuclear “hot” labs)

Glass compositions and properties of lead-silicate glasses used for some of the above applications are given in Tables 6.3 through 6.10. Two example applications are discussed below.

Cathode-Ray Tube Application. The construction of a color television bulb is illustrated in Fig. 6.3. Several different glass components are involved; panel, funnel, neck tubing, electron gun mount, and evacuation tube. Some key design requirements of the glasses are as follows:

Strength: The bulbs are designed to withstand 3 atmospheres of external pressure.

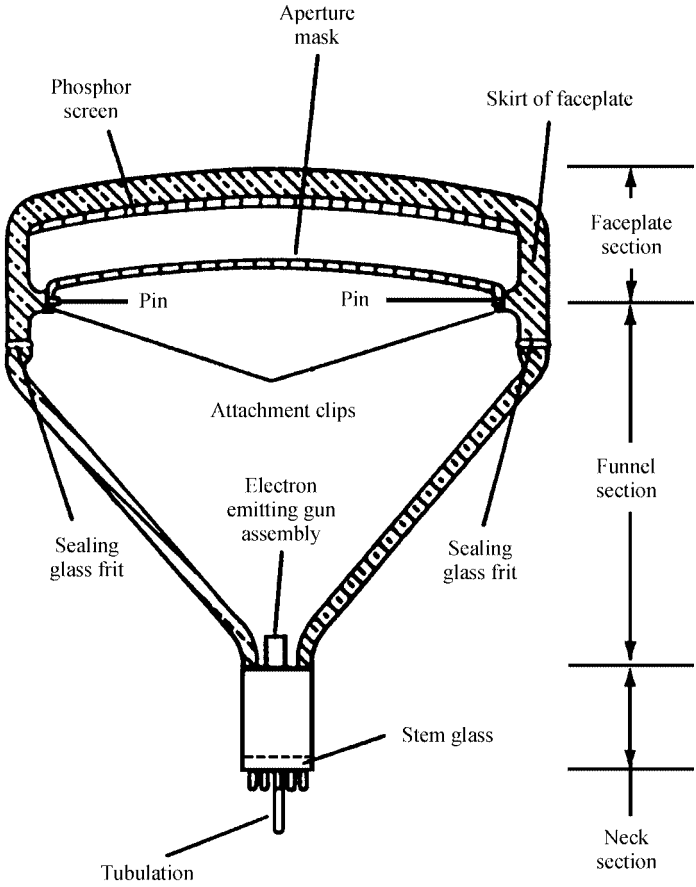

FIGURE 6.3 Schematic showing cross section of components of a conventional color television tube. The glass envelope consists of a funnel section, a faceplate section, and a neck section. The tubulation is used to evacuate the tube and is removed after vacuum processing. (*From J. H. Connelly and D. J. Lopata, Ref. 7.*)

X-ray absorption: Assembled tubes must have sufficiently high x-ray absorption to meet federal standards. Lead is generally used in neck and funnel glass for good electrical properties as well as radiation absorption (see Sec. 6.2.3.5, "Radiation-absorbing glasses"); it is not used as much in the panel glass (screen) because it "browns" under irradiation.

Radiation damage: The panel glass must not change color or "brown" under x-ray or electron irradiation. Since the presence of lead promotes electron browning, only small amounts of lead can be used in a panel glass. Cerium oxide is often added to the composition to help minimize the browning. Cerium ions act as electron traps that do not absorb light in the visible portion of the spectrum.

TABLE 6.7 Glass Compositions for Television Applications, wt%

Glass identification	Description	SiO_2	Al_2O_3	B_2O_3	Li_2O	Na_2O	K_2O	MgO	CaO	SrO	BaO	PbO	ZnO	As_2O_3	Sb_2O_3	TiO_2	ZrO_2	CeO_2	Other	References
Lead TV glasses																				
Corning 0120	Stem tubing	56	2			4	9					29			0.5					Connelly et al. in Schneider[7]
Corning 0137	Neck tubing	52.5	1			0.8	12			5		28			0.5					Connelly et al.[7]
Corning 0138	Funnel	54	2			6	8	2.5	3.5			23			0.1					Connelly et al.[7]
Corning 7580	Sealing frit	2	0.1	8.4							1.9	75.4	12.2							Connelly et al.[7]
Television panel glasses																				
Corning 9008	Panel—B&W	55.1	3.6		0.5	6.8	6.4				12	1.7		0.2	0.4				F = 1	Connelly et al.[7]
Corning 9039	Panel—projection	57.5	1.7		1	6.3	5.8			8.7	15				0.4		3	0.7		Connelly et al.[7]
Corning 9061	Panel—color	62	2			7	9	0.7	1.7	10.3	2.4	2.2		0.2	0.4	0.5		0.2	F = 0.3*	Connelly et al.[7]
Corning 9068	Panel—color	62.9	2.1			6.99	8.9	0.85	1.79	10.31	2.37	2.31		0.16	0.38	0.52		0.21	F = 0.29*	Connelly et al.[7]
Owens Illinois TL-28	Panel—color	64.39	1.31			7.59	8.08	0.05	2.8	9.42	2.09	2.84		0.15	0.4	0.47		0.22	F = 0.26*	Connelly et al.[7]
RCA/TCE G999	Panel—color	62.61	1.83			7.81	7.92	1.53	2.21	10.13	2.03	2.48		0.31	0.43	0.42		0.25	*	Connelly et al.[7]
Schott 8051	Panel—color	62.16	2.1			7.7	7.85	0.56	0.84	9.99	7.38	0.05		0.01	0.6	0.48		0.25	*	Connelly et al.[7]
NEG PT-28C	Panel—color	61.43	2.06			7.48	7.58	0.03	0.12	9.61	8.71	0.04	0.49	0.01	0.32	0.51	1.28	0.29	*	Connelly et al.[7]
Asahi 5008	Panel—color	59.48	2.27		0.19	7.96	6.77	0.52	2.44	7.93	8.8	0.05		0.01	0.31	0.39	2.58	0.26	*	Connelly et al.[7]
Samsung Corn. 9075	Panel—color	61.3	2.06		0.46	8.43	6.69	0.04	1.88	9.51	5.51	0.05		0.22	0.4	0.51	2.59	0.31	*	Connelly et al.[7]
NEG (Nd_2O_3)	Panel—color	62.6	1		0.5	7.2	7.2	0.5	0.5	9	7.2	0.5	1			0.3	1	0.5	Nd_2O_3 = 1.00*	Connelly et al.[7]

*Typical colorant levels for contrast enhancement are Fe_2O_3 = 0.04, NiO = 0.012, Co_3O_4 = 0.002, and Cr_2O_3 = 0.0006.

TABLE 6.8 Physical Properties of Glasses for Television Applications, wt%

Glass identification	Application	Density, g/cm^3	CTE, 0 to 300°C, 10^{-7}/°C	Strain point, °C	Annealing point, °C	Softening point, °C	Working point, °C	Young's modulus, GPa	Poisson's ratio	Refractive index	Resistivity, 350°C, log (Ω · cm)	Absorption at 0.06 nm, cm^{-1}	References
Lead TV glasses													
Corning 0120	Stem tubing	3.05	89.5	395	435	630	986	59.6	0.22	1.56	8	75	Connelly et al.[7]
Corning 0137	Neck tubing	3.18	97	436	478	661	978		0.23	1.55	8.3	90	Connelly et al.[7]
Corning 0138	Funnel	2.98	97	435	474	654	965		0.24	1.565	7.6	62	Connelly et al.[7]
Corning 7580	Sealing frit	6.47	98	293	311	374	890		0.25	1.65	8.2	40	Connelly et al.[7]
Television panel glases													
Corning 9008	Panel—B&W	2.64	89	406	444	646	1004		0.24	1.506	7.4	20	Connelly et al.[7]
Corning 9039	Panel—projection	2.9	96.4	458	500	680	983		0.24	1.553	7.7	35	Connelly et al.[7]
Corning 9061	Panel—color	2.7	99	460	501	689	1000		0.23	1.518	7.5	28	Connelly et al.[7]
Corning 9068	Panel—color	2.696	98.5–99.5	455–470	510–525	685–755					>7	29.1	Connelly et al.[7]
Owens Illinois TL-28	Panel—color	2.696	98.5–99.5	455–470	510–525	685–755					>7	28.4	Connelly et al.[7]
RCA/TCE G999	Panel—color	2.708	98.5–99.5	455–470	510–525	685–755					>7	29.2	Connelly et al.[7]
Schott 8051	Panel—color	2.77	98.5–99.5	455–470	510–525	685–755					>7	29.3	Connelly et al.[7]
NEG PT-28C	Panel—color	2.769	98.5–99.5	455–470	510–525	685–755					>7	29.4	Connelly et al.[7]
Asahi 5008	Panel—color	2.797	98.5–99.5	455–470	510–525	685–755					>7	29	Connelly et al.[7]
Samsung Corn. 9075	Panel—color	2.759	98.5–99.5	455–470	510–525	685–755					>7	28.9	Connelly et al.[7]
NEG (Nd_2O_3)	Panel—color		98.5–99.5	455–470	510–525	685–755					>7	29	Connelly et al.[7]

TABLE 6.9 Sealing and Solder Glass Compositions, wt%

Glass identification	Application	SiO_2	Al_2O_3	B_2O_3	Li_2O	Na_2O	K_2O	BaO	PbO	ZnO	Other	References
Sealing glasses												
Lead glasses												
Corning 1990	To iron	41			2	5	12		40			Boyd et al.[9]
Corning 7570	Solder sealing	3	11	12					74			Boyd et al.[9]
Corning 7575		X		X					X	X		Corning prod. lit.
Corning 7580	Sealing frit	2	0.1	8.4				1.9	75.4	12.2		Connelly et al. in Schneider[7]
Corning 7583		X		X					X	X		Corning prod. lit.
Corning 7593				X					X		TiO_2	Corning prod. lit.
Borosilicate glasses												
Corning 3320	To tungsten	76	2	15		4	2				$U_3O_8 = 1$	Boyd et al.[9]
Corning 7040	To Kovar	67	3	23		4	3					Boyd et al.[9]
Corning 7050	Miscellaneous	68	2	24		6						Boyd et al.[9]
Corning 7052	To Kovar	64	8	19	1	2	3	3			Some F	Boyd et al.[9]
Corning 7056	To Kovar	68	3	18	1	1	9					Boyd et al.[9]
Corning 7070	Low-loss (elect.)	72	1	25	0.5	0.5	1					Boyd et al.[9]
Corning 7720	To tungsten	74	1	15		4			6			Boyd et al.[9]
Corning 7723		X		X					X			Corning prod. lit.
Corning 8830	To Kovar	65	5	23		7						Boyd et al.[9]
Corning 7574		X		X						X		Corning prod. lit.

Note: X = components present but amounts not indicated by manufacturer.

TABLE 6.10 Physical Properties of Sealing and Solder Glasses

Glass identification	Application	Density, g/cm^3	CTE, 0–300°C, 10^{-7}/°C	CTE, 25°C to set point, 10^{-7}/°C	Strain point, °C	Annealing point, °C	Softening point, °C	Working point, °C	Young's modulus, Gpa	Poisson's ratio	Refractive index	Resistivity, 350C log (Ω · cm)	References
Sealing glasses													
Lead glasses													
Corning 1990	To iron	3.5	124	136	340	370	500	756	58	0.25		7.7	Boyd et al.[9]
Corning 7570	Solder sealing	5.42	84	92	342	363	440	558	55	0.28	1.86	8.7	Boyd et al.[9]
Corning 7575		3.80	89				380		51	0.25		8.6*	Corning prod. lit.
Corning 7580	Sealing frit	6.47	98		293	311	374	890		0.25	1.65	8.2	Connelly et al. in Schneider[7]
Corning 7583		6.00	84				370					8.5*	Corning prod. lit.
Corning 7593													Corning prod. lit.
Borosilicate glasses													
Corning 3320	To tungsten	2.27	40	43	493	540	780	1171	65	0.19	1.481	7.1	Boyd et al.[9]
Corning 7040	To Kovar	2.24	47.5	54	449	490	702	1080	59	0.23	1.48	7.8	Boyd et al.[9]
Corning 7050	Miscellaneous	2.24	46	51	461	501	703	1027	60	0.22	1.479	6.8	Boyd et al.[9]
Corning 7052	To Kovar	2.27	46	53	436	480	712	1128	57	0.22	1.484	7.4	Boyd et al.[9]
Corning 7056	To Kovar	2.29	51.5	56	472	512	718	1058	64	0.21	1.487	8.3	Boyd et al.[9]
Corning 7070	Low-loss (elect.)	2.13	32	39	456	496		1068	51	0.22	1.469	9.1	Boyd et al.[9]
Corning 7720	To tungsten	2.35	36	43	484	523	755	1146	63	0.20	1.487	7.3	Boyd et al.[9]
Corning 7723		2.90	35		480	522	770				1.548	12.1*	Corning prod. lit.
Corning 8830	To Kovar	2.24	49.5		460	501	708	1042	56	0.22		6.3	Boyd et al.[9]
Corning 7574		3.78	42.2		537	560	644		63		1.668	13.7*	Corning prod. lit.

*at 250°C.

Electrical properties: High bulk electrical resistivity (excellent insulator); high dielectric strength to resist electrical puncture or discharge through the glass under high potential gradients (anode voltage can exceed 25 kV for color television).

Optical properties: The luminous transmittance and chromaticity of screen is specified and varies among TV set designers and manufacturers (absorption of light is needed to improve viewing contrast); doping elements used for tinting include Ni, Co, Cr, and Fe.

Viscosity: A working range that allows forming into large sizes.

Thermal expansion: All parts (panel, funnel, neck, solder glass, and shadow mask metal alignment pins) must match fairly closely, 90 to 100 $\times$ 10^{-7}/°C.

Compositions and properties of lead-containing glasses useful for television bulb manufacture are given in Tables 6.7 and 6.8.

Drinkware ("Hollow Ware") and Art Glass Applications of Lead Glass. Historically the term *crystal* has been used for any clear glass of high transparency, especially when cut so that it has many light-reflecting surfaces, as in crystal chandeliers. We should note here that this use of the term crystal indicates nothing about the atomic level structure of the material. As is true for all the glasses in this section, the structure is amorphous, not crystalline.

ASTM defines crystal as "(1) colorless, highly transparent glass, which is frequently used for art or tableware. (2) colorless, highly transparent glass historically containing lead oxide." In Europe, *lead crystal* must contain at least 24 wt% PbO and *full lead crystal* at least 30 wt%. Steuben™ glass has traditionally contained about 30 wt% PbO.

Attributes of lead crystalware are brilliance, clarity, sonority (acoustic resonance), density, meltability, and workability. Brilliance is related to the refractive index, transmittance, and degree that surface polish is maintained. Sonority is related to the high elastic modulus and low internal friction (acoustic damping) of the glass, a function of the mixed alkalis present. Lead is not an absolute requirement for any of these attributes. A negative: high-lead glasses are more easily scratched or abraded. Most lead crystal manufacturers are developing non-lead compositions for at least some of their products.

Forming Processes. Pressing, blowing, tube drawing, casting, centrifugal casting, and fritting, but not limited to these.

6.1.3 Hard Glasses

6.1.3.1 Borosilicate Glasses

Brief History. Boric oxide was used as a fluxing agent in glass compositions in Europe in the eighteenth century. Michael Faraday used it as a component in his pioneering optical glass developments in the mid-nineteenth century. Beginning in the 1880s, Otto Schott and Ernst Abbe developed boron-containing optical glasses including borate crowns, borosilicate crowns, and borate flints. (See Sec. 6.2.4, "Optical Glass," for definitions of the terms *crown* and *flint*.) Schott was perhaps the first to recognize the usefulness of boric oxide additions to silicate glasses for the purpose of reducing their thermal expansion, which led to Schott's development of thermal-shock-resistant borosilicate laboratory ware. However, it was Corning Glass Works' development of chemically durable, low-thermal-expansion borosilicate glasses during the first two decades of the twentieth century that opened the way for wide commercialization of borosilicate glasses. Between 1908 and 1912,

Corning developed a soft, lead-containing, low-expansion borosilicate glass in response to the practical problem of thermal shock breakage of railroad lantern globes and lenses. The uncolored version, Nonex™ (for nonexpanding glass), was also used for battery jars and even baking dishes. A harder, lead-free version, first introduced in 1915 as a heat-resistant glass under the trade name Pyrex™, soon became the standard for laboratory ware and oven-safe baking ware throughout the world.

Typical composition ranges for borosilicate glasses and example commercial glass compositions are given in Table 6.1. Properties for those glasses are given in Table 6.2.

Chemistry/Properties

Glass formers. SiO_2 and B_2O_3 [B_2O_3 from hydrated sodium tetraborate (borax), boric acid, or other boron oxide containing compounds; rarely from anhydrous B_2O_3].

Modifiers. Alkali, alkaline earth, and lead oxides.

Intermediates. Alumina.

Boron oxide. B_2O_3—a network former. Alone, it readily forms a soft glass, having low deformation temperature, high thermal expansion, and good electrical properties. Pure B_2O_3 glass is very hygroscopic, even *soluble* in water; it is usually used in combination with silica, SiO_2.

In borosilicate glasses, B_2O_3 acts as a flux for silica, and when combined with alkali oxides, the thermal expansion can be controlled to match various materials. Alkali borosilicates tend to phase-separate. Alumina helps to reduce this tendency. A typical composition (alkali borosilicate) is $81SiO_2 \cdot 13B_2O_3 \cdot 4Na_2O \cdot 2Al_2O_3$ (wt%). This is close to that of Corning code 7740, used for Pyrex™ brand products. Its approximate properties are listed in Table 6.2.

Key Characteristics. Low expansion (can be tailored over a range by varying the ratio of triangularly coordinated boron to the tetrahedrally coordinated silicon), moderately hard (higher deformation temperatures than soda-lime-silica glasses, several hundred degrees higher melting temperature), good electrical properties, and excellent chemical durability when the composition is not phase separated.

Advantages. Thermal expansion can be tailored over a wide range by suitable composition changes. This allows excellent thermal shock resistance and excellent chemical durability to be combined for a product application. It also allows for designing glasses that can be sealed directly to certain metals such as tungsten, molybdenum, and Kovar™. Many borosilicate glasses have higher use temperatures than do soda-lime-silica glasses. Borosilicates are perhaps the second most widely used family of glasses.

Disadvantages. More expensive than soda-lime glasses. This is primarily due to costs associated with melting at higher temperatures and to the price of boron-containing raw materials.

Low-alkali, low-alumina borosilicate glasses are subject to phase separation when held for prolonged periods of time above their glass transformation range (say between the annealing and softening points). This can lead to decreased chemical durability and sometimes to haziness or opacity of the glass. However, the manufacture of some commercial products (e.g., Vycor™ brand 96 percent silica glass and controlled-pore-size porous glass) is based on the phase separation phenomenon. This will be discussed in Sec. 6.2.9.2, "Porous and 'Reconstructed' High-Slica Glasses."

Applications. Major uses are chemical ware, pharmaceutical ware, cosmetic containers, housewares, optical and ophthalmic lenses, photochromic glass, lighting and electrical applications, telescope and other mirror substrates, solar energy systems, flat panel display

substrates. Glass compositions and properties of borosilicate glasses used for some of these applications are given in Tables 6.3 through 6.6, 6.9, and 6.10. Borosilicate glasses for fiberglass applications are discussed in Sec. 6.6, "Glass Fiber."

Forming Processes. Important forming processes are casting, pressing, blowing, tube drawing, rolling, and sheet drawing, but processes are not limited to these. Borosilicates are a very versatile family of glass.

6.1.3.2 Aluminosilicate Glasses

Chemistry/Properties

Glass formers. SiO_2, B_2O_3, and sometimes Al_2O_3.

Modifiers. Alkali, alkaline earth, and lead oxides.

Intermediates. Al_2O_3.

Alumina (aluminum oxide, Al_2O_3). This is a very refractory oxide, even more so than silica. It has a very high Al-O bond strength. When incorporated in the glass network, it makes the glass more refractory (harder in glassmakers' terms).

Aluminosilicates typically (not always) contain boron oxide, but are termed *aluminosilicate* if they contain more alumina than boron oxide, on a molar basis. Generally, they are the most refractory (high-temperature) of glasses containing alkali and alkaline earth modifiers. They have a relatively steep ("short") viscosity-temperature curve giving high annealing and strain points, but are still meltable in conventional furnaces. A typical composition (lime aluminosilicate): $58SiO_2 \cdot 20Al_2O_3 \cdot 16CaO \cdot 5B_2O_3 \cdot 1Na_2O$ (wt%).

The *molar ratio of alumina to alkali modifiers* is key to the glass properties. At ratios less than 1, alumina tends to enter the glass network, replacing the NBOs (nonbridging oxygens) caused by the presence of the alkalis. Many glass properties are sensitive to this ratio, including density, viscosity, thermal expansion, internal friction, Knoop hardness, electrical conductivity, and ionic diffusion. For example, adding aluminum oxide to alkali silicate glasses increases the viscosity.

Composition ranges for aluminosilicate glasses and examples of commercial glass compositions are given in Table 6.2. Properties for those glasses are given in Table 6.1.

Key Characteristics. Very hard (high deformation temperature) glasses, but still meltable at reasonable temperatures, good dielectric properties, high elastic moduli, good resistance to chemical attack (particularly to caustic alkalis), useful for high temperature applications. The alkali aluminosilicates can be readily strengthened chemically by ion exchange (see Sec. 6.5.8, "Chemical Strengthening of Glass").

Advantages. All characteristics listed above are advantages for some applications. Ready availability of alkali-free compositions is important for electronic applications where the presence of alkali would degrade silicon semiconductor device performance.

Disadvantages. The required higher melting temperatures and more costly batch materials make these glasses more expensive to produce, relative to soda-lime-silica and some borosilicates.

Applications. Major uses are electrical and electronic insulators and dielectrics, aircraft and spacecraft windows, top-of-stove cooking ware, high-temperature lamp envelopes, chemically strengthened frangible components, chemical apparatus, glass electrodes, load-bearing members in fiberglass-reinforced plastics (E glass and S glass). An important emerging area

of application is as substrate glass for flat panel active-matrix liquid crystal displays (AMLCDs). See Chapter 7, "Advanced Application of Glass." Compositions and properties of aluminosilicate glasses used for some of the above applications are given in Tables 6.3 through 6.6, 6.9, and 6.10.

Alkali aluminosilicates are used for ion-selective electrodes, chemically strengthened (ion-exchanged) glass and nuclear waste fixation.

Chemical (ion exchange) strengthening of glass is discussed in Sec. 6.5.8. Examples of chemically strengthenable aluminosilicate glasses are Corning codes 0317, 0331, and 0417 and PPG 947M. The composition of 0317 is listed in Table 6.11.

Calcium-based alkaline earth aluminosilicate 0317 is the most important commercially. Eutectic compositions in the calcia-alumina-silica system have been the basis for a number of commercial glasses. The eutectic at 1170°C ($62.1SiO_2 \cdot 14.6Al_2O_3 \cdot 23.3CaO$ wt%) was the basis for the original OCF (Owens Corning Fiberglas) E-glass fiber, tungsten-halogen lamp envelopes, space shuttle window inner panes, and the cladding glass for Corning's Corelle™ tableware. Some of the lower-silica eutectics ($31.7SiO_2 \cdot 29.1Al_2O_3 \cdot 27.1CaO$ wt% and $7SiO_2 \cdot 43.4Al_2O_3 \cdot 49.6CaO$ wt%) provided the basis for infrared-transmitting glasses at 4- 5-μm wavelengths.

Eutectic compositions are further modified by additions of other network modifiers and boron oxide. For high-temperature lamp applications, such as the tungsten-halogen lamp ampoule in automobile headlamps, the thermal expansion is matched to that of molybdenum, the electric lead wire metal.

Typical types are 1710 (once used for top-of-stove ware), 1720 (ignition furnace tubes), 1723 (spacecraft windows), and 1724 (halogen headlight inner bulb). Compositions and properties of these glasses are given in Tables 6.1 and 6.2. Aluminosilicate glasses for fiberglass applications (for example, E glass and S glass are discussed in Sec. 6.6).

Liquid Crystal Display Applications. These applications and their glass property requirements are discussed in more detail in Chap. 7. We list some of the key requirements here for the AMLCD application:

- Thin (less than 1.0 mm)
- Flat (low warp and bow)
- Smooth surface (low roughness)
- Excellent dimensional tolerances
- High strain point (600 to 800°C)
- Low thermal shrinkage (often called *compaction*) during customer's processing
- "Zero" alkali (avoids contamination of silicon electronics; no need for barrier layers)
- Defect-free (interior and at the surface)
- Excellent chemical durability (resistant to etchants)
- Preferred thermal expansion match to silicon (less than 40×10^{-7}/°C)

Corning codes 7059 (aluminoborosilicate), 1729, 1733, 1737, 2000 and other manufacturers' glasses are used (See Table 6.12.).

Glass-Ceramics. Lithium aluminosilicate and magnesium aluminosilicate glass compositions form the bases for several families of commercially important glass-ceramic products, as described in Sec. 6.2.7.

Forming Processes. Important forming processes are pressing, blowing, downdraw from a slot, "fusion" (Corning's overflow sheet drawing process, see Sec. 6.4, "Glassmaking II—Glass forming"), minifloat, redraw, and others.

TABLE 6.11 Ion Exchange Strengthenable Glass Compositions, wt%

Glass identification	Description	SiO_2	Al_2O_3	B_2O_3	Li_2O	Na_2O	K_2O	MgO	CaO	BaO	PbO	ZnO	Other	Typical exchange bath	References
Aluminosilicate	Corning 0317	61.4	16.8			12.7	3.6	3.7	0.2				TiO_2 = 0.8	KNO_3	Dumbaugh and Danielson in Boyd[5]
Borosilicate															
Photochromic base	Ophthalmic	56.5	6.2	18.2	1.8	4.1	5.7						ZrO_2 = 5.0 TiO_2 = 2.1	60% KNO_3/40% $NaNO_3$ (wt)	Borrelli and Seward in Schneider[7]
Photochromic base	Ophthalmic	55.9	9	16.2	2.6	1.9				6.7	5.1		ZrO_2 = 2.3 Other = 0.3	60% KNO_3/40% $NaNO_3$ (wt)	Kozlowski and Chase[13]
Photochromic base	Sheet glass	60.4	11.8	17.7	2.1	5.9	1.6				0.3		Other 0.2	60% KNO_3/40% $NaNO_3$ (wt)	Borrelli and Seward[7]
Pharmaceutical	Corning 7800	72	6	11		7	1		1	2				KNO_3	Boyd et al.[9]
Ophthalmic crown	Corning 8361	68.3	2			8	9.4		8.4			3.5	Other = 0.4	KNO_3	Kozlowski and Chase[13]

TABLE 6.12 Physical Properties of LCD Substrate Glasses

Glass identification	Description	Density, g/cm^3	CTE 0 to 300°C, 10^{-7}/°C	Strain point, °C	Annealing point, °C	Softening point, °C	Working point, °C	Young's modulus, GPa	Poisson's ratio	Refractive index	Resistivity at 350°C log(Ω · cm)	References
Display manufacturing temperature <350C												
Corning 0211	Alkali-zinc borosilicate	2.57	74	508	550	720		74.5	0.22	1.523	6.7	Bocko & Whitney in Schneider[7]
Corning 7740	Soda borosilicate	2.23	32.5	510	560	821		62.7	0.20	1.473	6.6	Bocko & Whitney [7]
Asahi AS	Soda-lime silicate	2.49	81*	511	554	740		71.7	0.21	1.52	5.9	Bocko & Whitney [7]
Asahi AX	Borosilicate	2.42	49*	522	568	789		68.9	0.18	1.5		Bocko & Whitney [7]
NEG BLC	Alkali borosilicate	3.36	51†	535	575	775				1.493		Bocko & Whitney [7]
Display manufacturing temperature <450C												
Corning Code 7059	Barium aluminosilicate	2.76	46‡	593	639	844	1160	68	0.28	1.53	11	Boyd et al[9]
Hoya NA 45	Barium aluminosilicate	2.78	46	610	658	859		68.9	0.24	1.533		Bocko & Whitney [7]
Schott AF 45	Barium borosilicate	2.72	45	627	663	876		66	0.235	1.5276	11.5	Bocko & Whitney [7]
Asahi AN635	Alkaline-earth aluminosilicate	2.77	48	635				73				Nakao[14]
Corning Code 1733	Alkaline-earth boroaluminosilicate	2.49	37	640	689	928		66.9	0.235	1.516	11.4	Bocko & Whitney [7]
Display manufacturing temperature <550C												
NEG OA2	Alkaline-earth aluminosilicate	2.76	47†	650	700					1.54	12.5	NEG Product into sheet 11/96
NH Techno NA35	Alkaline-earth boroaluminosilicate	2.49	37‡	650	705			70.2	0.24	1.516		Hoya product info sheet, 1993
Hoya NA 40	Alkaline-earth zinc lead aluminosilicate	2.87	43‡	656				92.4	0.26	1.574		Bocko & Whitney [7]
Corning Code 1737	Alkaline-earth boroaluminosilicate	2.54	37.6	666	721	975	1312	69.9	0.22	1.5186	11.4	Corning info sheet 1/99
Corning Code 2000	Alkaline-earth aluminosilicate	2.37	31.8	666	722	985	1321	69.2	0.23	1.5068	10.5	Corning info sheet 8/00
Asahi AN100	Alkaline-earth boroaluminosilicate	2.51	38	670				77.4				Nakao[14]
Corning Code 1724	Alkaline-earth boroaluminosilicate	2.64	44	674	726	926		82.7		1.54	11.6	Bocko & Whitney [7]
Display manufacturing temperature <750C												
Corning Code 1729	Alkaline-earth aluminosilicate	2.56	35	799	855	1107		80.6	0.216	1.52	11	Bocko & Whitney [7]
Display manufacturing temperature <950C												
Corning Code 7940	Synthetic fused silica	2.2	5.6	990	1075	1585		72.4	0.16	1.458	10.7	Bocko & Whitney [7]

*50–200°C.
†30–380°C.
‡100–300°C.
§at 300°C.

6.1.4 Fused Silica and High-Silica Glasses

Fused silica (fused quartz) is the glassy form of the chemical compound SiO_2. Its natural raw materials include quartz sand and the mineral quartzite. However, because of its very high viscosity and high volatility at the temperatures required to melt the raw materials (1723°C is the melting point of cristobalite, the high-temperature crystalline form of silica), silica cannot be melted to form good quality products by conventional, large-scale glass melting techniques. (Most commercial glasses are melted at temperatures corresponding to a viscosity of about 100 P; the viscosity of silica at 1725°C is about 10^7 P, 5 orders of magnitude greater.) Consequently specialized small-scale melting techniques have been devised. Fused silica can also be prepared by high-temperature synthesis from silicon- containing halide or metal-organic precursors. These specialized manufacturing techniques will be discussed in Sec. 6.2.9, "High-Silica Glasses," as will techniques for manufacturing special high-silica (greater than 90 wt%) glasses.

Key Characteristics. The most refractory glass (annealing point greater than 1000°C, depending on purity and thermal history), very high thermal shock resistance (due to the low thermal expansion, 5.5×10^{-7}/°C), high chemical durability (water, acid, base resistance), high optical transparency, very broad spectral transmittance range (deep UV to near IR, approximately 170- to 3500-nm wavelength), good radiation damage resistance, low dielectric constant, and low electrical loss tangent.

Transport properties of fused silica (for example, viscosity and electrical conductivity) are controlled by the purity of the silica, in part as a result of NBOs (nonbridging oxygens) introduced into the glass network by the impurities. Values for these properties in absolutely pure silica have probably never been measured. The reported values depend on the method of manufacture (as described in Sec. 6.2.9). Table 6.2 shows the range of viscosity- related properties reported for commercial fused silica glasses.

Advantages. Each of the key characteristics listed above give silica glass different advantages over other types of glass, depending on the application.

Disadvantages. One of the main advantages of silica glass is also its main disadvantage. As described above, the refractoriness (high softening point) makes melting of the raw material, crystalline quartz, extremely difficult, specialized, and hence expensive. Further, silica glass is not easily worked in a flame to change its shape. These difficulties cause silica products to be rather expensive compared to other glasses. Silica is used only when the applications warrant the cost.

Applications. Major applications are lighting (high-intensity-discharge lamp envelopes), semiconductor industry (crucibles, substrates, coatings, and annealing furnace tubing and "furniture"), optical (lenses, prisms, windows, mirrors, fiber-optic and photonic devices for communications), high-energy laser optics, spacecraft windows, other (labware, furnace and other tubing, specialty fiber and wool).

Some Properties. See Sec. 6.2.9, "High-Silica Glasses," for a further discussion of silica properties.

6.1.5 Borate, Phosphate, Aluminate, and Germanate Glasses

6.1.5.1 Borate Glasses

As noted in Sec. 6.1.3.1, pure B_2O_3 glass is very hygroscopic, even *soluble* in water. The same is true for many binary alkali and alkaline earth borate glasses. The solubility of sodium borate glasses has been utilized to prevent rot in telephone poles and fence poles.

When inserted in the wood below ground level, the glass slowly dissolves, producing a fungicidal solution. An older, perhaps archaic application, is the Lindeman glass (B_2O_3 + Li_2O + BeO) developed in the early days of radiography as an x-ray transmitting window.

Rare earth borate glasses of high refractive index (e.g., lanthanum borates) have unusually low dispersions, making them very useful optical glasses. These glasses are much more chemically durable. There are also useful chemically stable aluminum borate optical glasses.

Other commercial applications of boric oxide include the lead and zinc borosilicate solder glasses discussed in Secs. 6.1.2.2 and 6.2.2, which are quite chemically durable. Boric oxide is also used in many fiberglass compositions, discussed in Sec. 6.6, "Glass Fiber."

6.1.5.2 Phosphate Glasses

P_2O_5 is deliquescent (dissolves in absorbed atmospheric moisture), so phosphates are noted for their lack of durability. The structure of P_2O_5 is characterized by rings, chains, and sheets of PO_4 tetrahedra as discussed in Chap. 5.

Some Commercial Applications. "Slow-release" phosphate glasses are used for treating mineral deficiencies in ruminant animals and as fertilizer. A general composition range for animal treatment is 28–50$Na_2O \cdot$ 0–28$CaO \cdot$ 0–28$MgO \cdot$ 28–50P_2O_5 (mol%) and 0.1 to 20 percent of required nutrient elements, e.g., cobalt, copper, selenium, iodine.

Bioactive and bioresorbable glasses are a recent development. Since the middle of this century, biologically inert materials such as surgical stainless steel, certain organic polymers, and alumina ceramics have been used to repair or replace damaged body parts such as bones, bone joints, and teeth. Such materials, while stable and nontoxic in the body environment, are not truly inert. They are gradually encapsulated by a thin, nonadherent fibrous layer, which progressively loosens the implant and limits its useful lifetime. In the late 1960s, Hench and coworkers at the University of Florida discovered that glasses within a certain composition range of the soda-lime-phosphate-silica system developed mechanically strong chemical bonding to bone surface. Such glasses are now called *bioactive glasses*, and some have been manufactured under the trademark Bioglass™. Phosphate glass compositions have also been discovered that bond to soft tissue. Applications include prostheses to replace bones in the middle ear and roots of teeth and materials to repair damaged or diseased jawbone. More recently, compositions have been developed that are gradually absorbed by the body as they catalyze the regeneration of the bone they replaced. These discoveries have opened up major new areas for biomedical materials science and engineering.

Al_2O_3 and P_2O_5 can combine to give *aluminophosphates*, an $AlPO_4$ structural unit isomorphous to $SiSiO_4 = 2(SiO_2)$. $AlPO_4$ alone does not produce a glass, but when combined with suitable modifiers yields good glasses (higher temperature capability and improved chemical durability compared to the straight phosphates).

Heat-absorbing glasses are made from iron-doped aluminophosphates. (In phosphate glasses, the iron ion absorption bands, located in the UV and IR regions, are much sharper than they are in silicate glasses. Hence almost clear glasses containing several percent of iron are possible.) HF acid–resistant glasses have been made from zinc aluminophosphates.

Laser host glasses are typically neodymium-doped aluminum phosphates. An example is 12$Na_2O \cdot$ 10$Al_2O_3 \cdot$ 6$La_2O_3 \cdot$ 2$Nd_2O_3 \cdot$ 70P_2O_5 (mol%). An advantage over silicate-based glass is a high solubility for platinum. Glasses that are melted in platinum for purity dissolve some platinum during melting. Some of the dissolved platinum precipitates in silicate glasses on cooling, causing the glass to fracture because of heat generated during the lasing action, rendering the silicate glasses less desirable.

Fluorophosphates are used as specialized optical glasses. For example, fluorophosphate glasses, such as those designated FK-5 or FK-50 by Schott have very low optical dispersion.

Silicophosphates are also used as optical glasses. An example is ophthalmic crowns: $20P_2O_5 \cdot 21SiO_2 \cdot 22Al_2O_3 \cdot 12B_2O_3$ (wt%) plus alkali and alkaline earth oxides; $n = 1.523$.

Possible Emerging Applications. Low-temperature zinc-alkali-phosphate glasses for polymer-glass melt blends are being developed by Corning. Key characteristics are glass transitions near 325°C and water durability comparable to or exceeding common soda-lime glass. Most durable compositions lie in the orthophosphate and pyrophosphate regions.

Nonlead solder glasses for use in color TV tube assembly, based on $SnO\text{-}ZnO\text{-}P_2O_5$, have been patented, tested, and found suitable for the application. The cost is higher, and so unless absolutely required by environmental legislation, commercialization may be difficult.

6.1.5.3 Aluminate Glasses. Al_2O_3 does not form a glass (other than by vapor deposition processes). However, it can make a major contribution to the glass network structure as in the aluminosilicates (Sec. 6.1.3.2) and the aluminophosphate glasses discussed above. It can even be the primary network former, and as such has found several commercial applications: Calcium aluminate glasses are used as IR-transmitting glasses, boroaluminates have been used as optical glasses and as nondiscoloring envelopes for sodium vapor lamps, and "Cabal" (calcium boroaluminates) have electrical resistivities greater than silica.

6.1.5.4 Germanate Glasses. Germanate glasses are useful as IR-transmitting glasses. As such, they are of considerable interest in heat-seeking missile applications.

6.1.6 Nonoxide Glasses

Other commercial glass systems include fluoride-based glasses; chalcogenide and chalcohalide glasses; the amorphous semiconductors, silicon and germanium; and glassy metals.

In fluoride glasses, fluorine rather than oxygen is the primary glass network anion. BeF_2 (beryllium fluoride), alone and in combination with alkali fluorides, has sometimes been considered a low-temperature model for silica. Those glasses transmit even farther into the ultraviolet region, and have lower refractive index and lower dispersion than silica, but because of health hazards associated with handling beryllium compounds and the difficulty of producing high-purity melts, these glasses have seen little commercialization. Heavy metal fluoride (HMF) glasses also transmit farther into the infrared region than silica and can be produced with sufficiently high purity that they have found optical applications, including optical fiber (mostly for short hauls and sensors).

The chalcogen elements, sulfur (S), selenium (Se), and tellurium (Te), are elements from group 16 (previously called VI-A) of the chemical periodic table. Sulfur and selenium themselves form glasses. All three, in combination with certain group 14 (IV) and group 15 (V) elements, such as arsenic (As) and antimony (Sb), form glasses over considerably broad composition ranges. When modified by adding halogens, the materials are known as chalcohalides. The major interest in these glasses is for their semiconducting, photoconducting, and IR-transmitting properties. The photoconductivity of amorphous selenium was the historical basis for the xerographic approach to photocopying.

Although these materials are generally opaque to visible light, their IR-transmitting capabilities, in some cases extending to 18-μm wavelength, or more, are unique among glasses, and have made them candidates for optic-fiber transmission of high-intensity CO_2 laser light (10.6-μm wavelength) for laser-assisted surgery. (See Sec. 6.6.3, "Traditional Fiber Optics.")

Amorphous silicon, in thin-film form, is a widely used electronic semiconductor. Its excellent photovoltaic properties, grain-boundary-free structure, and relative ease of fabrication have made it widely used for solar energy conversion (solar cells) and as the thin-film transistor (TFT) switching elements in active-matrix liquid crystal display (AMLCD) television screens and computer monitors, particularly portable units. (This application will be discussed further in Chap. 7.) Chalcogenides and amorphous semiconductors have been considered for other electronic and electrooptic applications such as computer memories.

Glassy metals, which are essentially metals, metal alloys, or metals in combination with metalloid elements, having a glass-like atomic structural arrangement, are generally prepared by extremely rapid quenching (10^5 to 10^8°C/s) from the molten state. While they are of commercial value for their significantly enhanced electrical, magnetic, and structural strength aspects, a full discussion of these materials is beyond the scope of this chapter.

Oxyhalide, oxynitride, and oxycarbide glasses have also been made and studied. The high anionic electrical conductivity observed for some oxyhalides has raised interest in them as possible solid electrolytes.

For the glasses described in this section (6.1.6), the glass manufacturing processes described in Sec. 6.3 (glass melting), and many described in Sec. 6.4 (glass forming), will not be applicable.

6.2 SPECIAL GLASSES

6.2.1 Introduction

In this section we group together some glasses that are somewhat special, either because of their unique chemical, physical, or optical properties, or because they have been developed for specific applications requiring special combinations of properties.

6.2.2 Sealing Glasses and Solder Glasses

Sealing glasses, as the name implies, are used to form a seal with (or to) another material, such as electrical wires entering a glass light bulb envelope. Typically, the seal must be mechanically strong and hermetic, requiring that the thermal expansions of the glass and the material sealed to match over the temperature range between the set point of the glass and the use temperature of the seal, which is generally room temperature. Because some mismatch in thermal contraction between the sealed components from the set-point to room temperature and/or the use temperature is inevitable, the process of sealing leaves both components in a stressed condition. A risk of glass fracture exists when tensile stresses so produced in one of the glass components exceed the engineering strength of the glass. An often-used design criterion is to ensure that the mismatch is no greater than 200×10^{-6} cm/cm ($\Delta L/L$). Modification of these stresses by a suitable annealing schedule may be helpful

(see Sec. 6.5.4, "Annealing Practices"). Be it glass-to-metal or glass-to-glass, if a sufficiently close match in expansion is not directly possible, a graded seal utilizing a zone containing one or more glass layers of intermediate thermal expansion is sometimes used.

When two dissimilar glasses or other materials are joined using a layer of glass, that sealing glass is sometimes called a *solder glass*. However, the term *solder glass* is generally reserved for sealing glasses used at relatively low temperatures when parts that are being sealed or encapsulated would be damaged if subjected to higher temperatures. Solder glasses are used for integrated circuit (IC) packaging, color TV picture tube assembly, and other mechanical seals, coatings, and wire feed-through seals.

Sealing glasses are available in two forms: vitreous and devitrifying. Vitreous sealing glasses are thermoplastic materials (glasses) which soften and flow at the same temperatures each time they are processed. A seal may sometimes be undone (unsoldered) by heating it to temperatures at or slightly above those used to make the seal. Devitrifying sealing glasses are thermosetting materials that crystallize according to a designed time-temperature relationship. Because of the crystalline nature, the devitrified sealing glass has a thermal, and often chemical, stability greater than that of the parent glass. Seals using devitrifying glasses cannot be undone by reheating to their sealing temperature. Devitrifying sealing glasses are a type of glass-ceramic material that is discussed more fully in Sec. 6.2.7, "Glass-Ceramics."

Vitreous sealing glasses are available with softening points between 330 and 770°C and coefficients of thermal expansion between 35 and 125 $\times$ 10^{-7}/°C. For devitrifying sealing glasses, softening points range from 310 to 645°C and expansion from 42 to 100 $\times$ 10^{-7}/°C. Thermal expansion of sealing glasses is often modified by use of low-expansion fillers (fine particles of low expansion crystals or glasses). Compositions and properties of some commercial sealing glasses are given in Tables 6.9 and 6.10.

Typically, sealing glasses are supplied as a 100-mesh powder (passes through screen of 100 mesh/inch), called *frit*, which is mixed with an organic vehicle and applied like paint, paste, or slurry before firing.

Generally lead borate–based glasses are used for low-sealing-temperature vitreous sealing glasses and lead-zinc borates for the devitrifying type. Because of environmental and workplace health concerns, non-lead-based sealing glasses are being developed.

6.2.3 Colored and Opal Glasses

6.2.3.1 Overview and Applications. Glasses based on the glass formers SiO_2, B_2O_3, and P_2O_5 generally transmit light well across a broad spectral region extending from within the ultraviolet region to well within the near-infrared region. Thus they are inherently clear, "water-white" materials. Certain impurities and intentionally added network modifying components can alter this situation, giving color, grayness, and sometimes dullness to the glass as an unintended and undesired consequence. Other constituents can be added to the glass to color or opacify it to produce specific effects for intended applications.

Generally, a glass is considered "colored" if it absorbs some portions of the visible spectrum more than it does others. For example, a glass that preferentially absorbs light in the blue and green regions of the spectrum is colored red.

For many applications, particularly the more scientific or technical, detailed knowledge of the full transmittance and reflectance spectra of the glass may be important. Such information can be obtained by using UV, visible, and infrared spectrophotometers. For other applications, consistent color matching of different lots of product, often to a well-defined target, is sufficient. Here the science of colorimetry is important. The observed color of an

object depends on the emission spectrum of the illuminating source, the transmittance and/or reflectance spectra of the material composing the object, and the spectral sensitivity of the eyes of the observer. The science of colorimetery and methods for characterizing and measuring color are described in Chap. 5, Sec. 5.20.

Applications include:

Colored lenses and filters (e.g., traffic lights, sunglasses, photography, scientific applications)

Color television panel glass (gray color for screen contrast enhancement)

Decorative/art glass

Bottles and other containers

Drinkware, tableware, and cookware

Automotive and architectural glazing

6.2.3.2 Glasses Colored by Transition Metal and Rare Earth Ions. Probably the most common method of imparting color to glass is to include various multivalent ions, such as transition metal and lanthanide series metal ions, in the glass composition, as discussed in Chap. 5 (Sec. 5.20.3.2). The coloration results from light absorption that occurs when electrons are excited from one energy state to another, either within a single ion or between pairs of ions. The color depends on the wavelength dependence of these absorption processes. Colors resulting from some common coloring ions are shown in Table 6.13.

It must be emphasized that the electronic energy levels of a given ion, and consequently the color it imparts, are dependent on both the valence state of the ion and the static electric field at the ion produced by surrounding ions, generally oxygen ions. This electric field is often referred to as the *ligand field*, where ligand is another name for near neighbor. For any coloring ion, the ligand fields depend on the internal atomic structure of the glass and consequently on its chemical composition and thermal history. Thus colors produced by a given ion will vary from glass system to glass system. The colors will also vary somewhat depending on the size and valence of the network-modifying ions used to make the glass. For example, progressively interchanging the alkali ions from lithium to sodium to potassium in a series of alkali borosilicate glasses containing nickel as a colorant will change the color from a straw yellow color due predominantly to Ni^{++} ions to a purple color due predominantly to Ni^{+} ions. The Ni^{++}/Ni^{+} equilibrium is shifted by the change in alkali ion size.

Coloration due to chromium ions in certain borosilicate glasses illustrates the effect of thermal history on color. Chromium enters the glass structure in a Cr^{+3}/Cr^{+6} equilibrium. Cr^{+6} is tetrahedrally coordinated with oxygen, giving the glass a yellow color; Cr^{3+} is octahedrally coordinated, producing an emerald green color. Heat treatment of certain rapidly cooled borosilicate glasses at temperatures somewhat above their annealing point will shift the chromium ion equilibrium toward Cr^{3+}, giving the glass a more green color. Whether this is related to phase separation (Sec. 5.3.1) within the glass or merely to an overall change in oxygen coordination of the boron within the glass has been debated.

Zinc oxide is often used as a major component in colored glasses. Structurally ZnO is an RO-type modifier oxide similar in behavior to PbO, whereby at high concentrations it acts more as a network former (like silica) than a modifier (like lime). Zinc-containing batch

TABLE 6.13 Glass Colorants

Color effect	Colorant	Typical additive
UV absorbing	Ce^{3+} and Ce^{4+} ions	CeO_2
	Ti^{4+} ion	TiO_2
	Fe^{2+} ion	Fe_2O_3 in P_2O_5 glasses
	Cu^{2+} ion	CuO
Blue/turquoise	Co^{2+} ion	Co_3O_4
	Cu^{2+} ion	Cu^2 + CuO
Purple/violet	Mn^{3+} ion	Mn_2O_3
	Ni^{2+} (tetrahedral)	NiO in potassium borosilicates
	Nd^{3+} ion	Nd_2O_3
	Ti^{3+} ion	
Green	Cr^{3+} ion	Cr_2O_3
	Fe^{3+} ion	$Fe_2O_3 + Cr_2O_3 + CuO$
	V^{5+} ion	V_2O_3
		CuO
	Pr^{3+} ion	
	Sm^{2+} ion	
Brown	Mn^{2+} ion	MnO (reducing conditions)
	Ion complex	$MnO + Fe_2O_3$
	Ion complex	$TiO_2 + Fe_2O_3$
	Ni^{2+} ion	NiO
		$MnO + CeO_2$
	Eu^{2+} ion	
Amber	FeS_x	Na_2S with Fe_2O_3
	Ionic complex	$Fe_2O_3 + TiO_2$
Pale yellow	V^{5+} ion	
	Cr^{6+} ion	
Yellow	Colloidal CdS	CdS
	$Ce^{4+} + Ti^{4+}$	$CeO_2 + TiO_2$
	Colloidal Ag	$AgNO_3 + SnO_2$
	U^{6+} ion	UO_3
Orange	Colloidal CdS:Se	
Red	Colloidal CdS:Se	
	Colloidal Au	$AuCl + SnO_2$
	Colloidal Cu	CuO
Pink	Er^{3+} ions	
	Se^{2-} ions	
Gray and black	Co^{2+} + other ions	Co_3O_4 + Mn, Ni, Fe, Cu and Cr oxides
	PbS, FeS, $CoSe_x$	Various sulfides and selenides
Near IR (heat) absorbing	Fe^{2+} ion	FeO

Source: Taken in part from "Glass," D. C. Boyd, P. S. Danielson, and D. A. Thompson, in *Kirk-Othmer Encyclopedia of Chemical Technology*, 4th ed., vol. 12, John Wiley & Sons, New York, 1994, p. 591.

materials are generally more expensive than their calcium or lead counterparts, hence it tends to be little used commercially. One exception is in the manufacture of colored glass, especially color filter glasses for scientific/technical use. For example, to get a good purple color using NiO as the coloring agent, the nickel must occupy a network-forming position rather than act as a network modifier. (As a network modifier, Ni^{++}, it gives a yellow color, as discussed above.) When used in combination with relatively high concentrations of ZnO instead of CaO as the chemically stabilizing flux oxide, the nickel seems to enter the network positions along with the zinc. Similar ZnO-containing glasses are also used for cobalt-containing blue filters and cadmium sulfoselenide–containing sharp-cutoff red and orange filter glasses. The latter will be discussed in Sec. 6.2.3.3.

Because of impurities in commercial glass-making batch materials, iron is commonly present at sufficient concentrations to color the resulting glass. When the iron impurity is small (up to about 0.075%), a judicious control of the Fe^{2+}/Fe^{3+} ("redox" control, see Section 6.3.2.2, "Processes occurring within the melter") can bring about decolorization. The two oxidation states of iron ion provide complimentary colors. Selenium (1 to 5 ppm) which provides a pink color in the metallic form, often mixed with cobalt oxide (Se:CoO = about 1:3), nickel oxide, or cerium oxide are added to bring about decolorization when larger amounts of the iron impurity are present in the batch. (Older use of MnO_2 has now been abandoned because of Mn solarization, see Section 5.20.7). Decolorization produces a more neutral colored, but somewhat less brilliant glass because of overall transmission decrease in glass. The more brilliant, higher transmission, glasses are made by using iron-free raw materials.

6.2.3.3 Glasses Colored by Precipitated Colloidal Particles. Glasses may also be colored by creating a dispersion of colloidal-sized particles of some light-absorbing pigment within the glass. Such colloidal colorants include semiconducting particles such as CuCl/CuBr and CdS/CdSe solid solutions and the noble metals copper, silver, and gold. The colors produced by these colorants are listed in Table 6.13. They tend to be relatively independent of the base glass structure and composition.

Colloidal-sized particles cannot simply be added to a glass batch with the expectation that they will survive the melting process. Rather, the chemical components are added to the batch and the particles generated within the glass melt by nucleation and growth processes. Sometimes the precipitation is controlled by rapidly cooling the melt to a rigid state without particle precipitation occurring, followed by a reheating to temperatures above the annealing point to nucleate and grow the particles. Occasionally the precipitation is allowed to occur during the initial cooling of the melt. Such types of processing can result in very uniform dispersions of particles within the glass with consequent uniform coloration. The color often appears very rapidly during the cooling or reheating process step, leading to the terms *striking* or *striking-in* of the color. Sharp cutoff orange and red color filter glasses are produced in this manner by precipitating cadmium sulfo-selenide solid-solution particles; ruby red colors are often produced using gold or copper metal particles. Alkali-zinc borosilicate base glass composition have been found particularly useful for such filters, e.g., Corning code 2405 [$1Al_2O_3 \cdot 12B_2O_3 \cdot 5Na_2O \cdot 11ZnO \cdot 70SiO_2$ (wt%)] with small amounts of CdS and Se added. An important application for colloidal-particle colored glasses is red and yellow traffic light lenses.

Colloidal metal coloration generally requires careful control of the overall oxidation state of the glass throughout the process. The melt must be kept sufficiently oxidized at the melting temperatures to keep the metal dissolved in its oxidized state until the melt is cooled, then it must be made sufficiently reduced to allow precipitation of the metal particles. [The metal must transform from the +1 oxidation state to the neutral (metallic) oxidation state as

the glass cools.] The oxidation state is generally controlled by incorporating multivalent noncoloring ions such as tin or antimony in the batch. As the glass cools, these ions become more oxidized at the expense of the noble metals, which become reduced. (Such oxidation-state changes of antimony and tin are key to their roles as glass fining agents, as will be discussed in Sec. 6.3.2, "Steps in Glass Melting").

6.2.3.4 Light-Polarizing, Dichroic Glasses. If a glass containing nonspherical, non-equiaxed light-absorbing particles of refractive index different from the glass matrix is illuminated by polarized white light, each of the particles will absorb light to a different degree, and generally with a different wavelength dependence, depending on the polarization orientation of the light. If most of the particles within the glass are aligned along a common axis, the glass itself will be a light polarizer. The glass will also be dichroic; it will show different colors, depending on the polarization of the light with which it is viewed. The effectiveness of the polarizer will depend on the effectiveness of the individual particles to absorb light of one polarization orientation in comparison to the other, on the degree of their common alignment, and on the concentration of the particles in the glass. Submicrometer-sized elongated particles of silver metal have been found most effective for this purpose. Elongated particles of copper-doped silver halide have provided glasses that are both photochromic and polarizing (see Sec. 6.2.5, "Photochromic and Polarizing Glasses").

6.2.3.5 Radiation-Absorbing Glasses

X-Ray Absorbing. In color television (CTV) picture tubes, electrons hitting the aperture mask or screen have about 25 keV of kinetic energy. Some of this energy is converted to x-rays, 0.5 Å (angstrom) or greater wavelength, as the electrons are scattered or absorbed. The x-rays can be effectively absorbed by the neck, funnel, and panel glasses of the picture tube by incorporating heavy metal (high atomic number) elements such as strontium, barium, zirconium, and lead into the compositions. While x-ray absorption generally increases with the atomic number of the element, the wavelength locations of the K and L absorption edges vary from element to element and must be taken into consideration in seeking the most effective elements for absorption of specific x-ray wavelength ranges. In Fig. 6.4 we show the mass absorption coefficient as a function of wavelength for these elements.

We note here that CTV neck and funnel glasses often contain between 20 and 30 wt% PbO. Because of the tendency for electron browning mentioned in Sec. 6.1.2.2, current panel glasses contain less than 5 percent PbO, and sometimes none. Barium oxide (BaO), strontium oxide (SrO), and zirconium oxide (ZrO_2) provide the required magnitude of x-ray absorption. Tables 6.7 and 6.8 show compositions and properties for several commercial TV panel glasses.

Ultraviolet Absorbing. UV-absorbing species such as cerium oxide (CeO_2) are used as glass composition additives to reduce the amount of UV radiation transmitted by the glass. Mixed semiconductor precipitates of CuCl/CuBr provide a sharp cutoff of short wavelength radiation. The spectral cutoff wavelength region can be tailored by adjusting the chlorine/bromine ratio to provide good UV absorption while maintaining a clear "white" appearance of the glass.

Heat (Infrared) Absorbing. Most silicate glasses are naturally opaque at wavelengths longer than about 4.5 micrometers and so are inherently good absorbers for mid- and long-wavelength infrared heat radiation. Infrared-absorbing species, such as

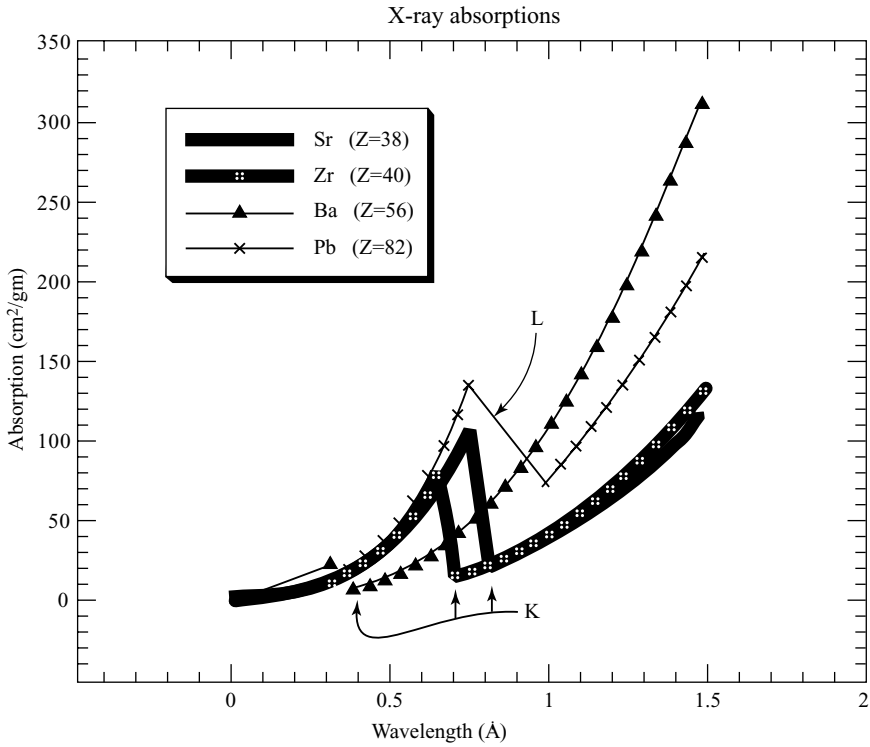

FIGURE 6.4 X-ray absorption versus wavelength for several chemical elements. (Constructed by authors from data in International Critical Tables.)

ferrous oxide (FeO), which absorb in the near-infrared spectral region, are used to make so-called heat-absorbing glass. Phosphate glasses are particularly effective because the absorption of the ferrous ion in phosphate glasses is less strong in the visible region than it is in silicates, thus providing good near-IR absorption without adding significant coloration to the glass.

Hot cell windows. Large concentrations (high-weight fractions) of PbO have been used to make radiation shielding glass for use in nuclear "hot cells," primarily as viewing windows behind which mechanical and chemical operations are conducted with radioactive components. An example is Corning code 8363 glass ($3Al_2O_3 \cdot 10B_2O_3 \cdot 82PbO \cdot 5SiO_2$ wt%) shown in Tables 6.1 and 6.2.

6.2.3.6 Opal Glasses. Opal glasses are characterized by their milky appearance. They range from translucent (light is transmitted but visual images are not) to fully opaque. The opal nature arises from light scattering due to the presence of inhomogeneities or inclusions within the glass. Generally the inclusions themselves transmit light, but are of different refractive index from the matrix glass. Thus the inclusions scatter the light, but absorb relatively little of it. If there is a high concentration of scatterers, or if the glass is very thick, it will be opaque because most of the light is scattered back toward the source.

Examples of such opalizing or opacifying agents are TiO_2, NaF, or CaF_2 crystallites, or glassy phase-separated particles such as sodium-borate glass particles in a sodium borosilicate glass matrix. If either the particulate phase or the matrix phase is colored, the opal product appears colored, although generally only with low color saturation, that is, pastel-like, because most of the incoming light is scattered from the glass before much wavelength-selective absorption can occur. (Examples of CaF_2-based white opal glass compositions are the Corning code 6720 and Corelle body glass dinnerware opals shown in Tables 6.5 and 6.6.)

6.2.4 Optical Glass

6.2.4.1 Introduction. Broadly defined, an optical glass could be any glass used in an optical device, instrument, or system. However, as used by the optical glass industry (and in this chapter section), the terminology refers to glasses designed for use in optical imaging systems, such as microscopes, telescopes, and a wide variety of camera types. Properties important for optical glasses, in addition to light transmittance, refractive index, dispersion, and birefringence (discussed in Chap. 5), are temperature dependence of the refractive index, chemical durability of the glass, and glass quality, especially homogeneity of refractive index and birefringence throughout the body of the glass. All these factors affect image quality. Often the refractive index is specified to four or more decimal places and for most applications birefringence must be extremely low. These quality requirements necessitate careful melting and annealing of the glass during manufacture.

To obtain the required ranges of refractive indices and dispersions, optical glass compositions sometimes contain heavy batch ingredients that tend to settle toward the bottom of the melt and volatile species that tend to evaporate from the surface of the melt. The melts often are corrosive, gradually dissolving (into the melt) the refractory container used for melting them. While these phenomena occur to some extent during the melting of all glasses (see Sec. 6.3), the strict homogeneity requirements of optical glass make its manufacture a greater challenge.

For a given glass composition, the refractive index of the glass depends on its density, which in turn depends on its thermal history, particularly how rapidly it has been cooled through its glass transformation range. Careful annealing of the glass is a must, especially when the refractive index must be held within tolerances to the fourth or higher decimal place. Much of what we understand today about the fine annealing and volume-temperature relationships of glass was learned because of the striving for higher quality optical glass for sight telescopes and other military optics during the World Wars.

The design and manufacture of optical glass and the techniques for generating and polishing precision lens and mirror surfaces comprise some of the more technically sophisticated areas of glass science and technology. Many treatises and books have been written on those subjects, so the coverage in this chapter can be only superficial.

6.2.4.2 Brief History. Glass has been an important element for optical devices since its first use as spectacle lenses to aid aging eyes in Italy around the year 1280. Magnifying glasses came into use about that same time. It has been said that these two inventions or discoveries contributed to the widespread use of the printed word that followed the invention of the printing press in 1450. Galileo Galilei invented, or reinvented, the two-lens-element telescope in the summer of 1609. Advances in optical instruments depended on developments in optical glass light-refracting properties and manufacturing quality, and

on advances in the techniques for grinding and polishing the glass to the required lens shapes. Pierre-Louis Guinand (1803) pioneered mechanical stirring of melts for improved homogeneity. Michael Faraday (1820s) is credited with the development of glasses with different refractive indices and dispersions, and use of platinum crucibles for increased homogeneity. William Vernon Harcourt (1870s) explored the effects of many elements, including phosphorus, boron, tin, and zinc, on the properties of glasses. He melted in platinum and worked with combustion-gas-free atmospheres above the melts. Ernst Abbe and Otto Schott (1880s) are credited with the development of a wide variety of glass compositions and first attempts to scientifically define composition factors that affect glass properties. Corning Glass Works (1940s) developed continuous melting of optical glass in platinum-lined melters incorporating platinum finers and stirrers. Annealing schedules were developed at the U.S. National Bureau of Standards and Corning Glass Works from the 1920s through the 1950s.

6.2.4.3 Applications of Optical Glass. Lenses, prisms, windows (for instruments), and mirrors are typical major applications.

While glass remains the material of choice for most imaging applications, many other applications for glass in the fields of optics and optoelectronics have emerged during the past half-century. Some have matured, others are growing, and yet others are just now emerging. Some of the currently most active developmental areas include UV-transmitting glasses, IR-transmitting glasses, laser glasses, ophthalmic glasses, and special glasses for atomic and nuclear technology applications.

UV-Transmitting Glasses. The trend of the semiconductor industry (electronics) to more and therefore smaller features on a semiconductor computer chip (memory chips or microprocessors) has driven the designs to submicrometer feature sizes. The optical lithography techniques involved require imaging wavelengths in the near and deep UV regions. While pure borosilicate crown glasses and special fluorophosphate glasses have been applied to lens systems operating at wavelengths longer than 300 nm, only high-purity fused silica is capable of meeting all lens design needs at shorter wavelengths, specifically 248 nm and 193 nm, which are the emission wavelengths of the KrF and ArF pulsed excimer laser, respectively. Some fluoride glasses transmit at wavelengths shorter than 250 nm, but the percent transmittance of these glasses is not yet sufficient for these applications because of difficulties in manufacturing them at sufficient purity. To move to wavelengths shorter than about 185 nm will be a serious challenge for transmissive optical materials, glass or otherwise.

IR-Transmitting Glasses. Glasses that transmit well in various spectral regions throughout the infrared are needed for thermography, pyrometry, IR spectroscopy, sensing, and a variety of specialized military applications. The wavelength limits for transmission depend, of course, on the thickness of the glass, since there are no sharp cutoff edges to the absorption spectra. However, one can say that, in general, pure silica has a long wavelength limit of about 4.5 μm. Heavy metal oxide (HMO) glasses extend this into the 6- to 9-μm range, with refractive indices reaching 2.4. Heavy metal fluoride glasses are good to about 8 μm. Some chalcogenide glasses can transmit to about 25 μm, and have refractive indices as high as about 3.

Laser Glass. For some applications, glass has an advantage over crystals as a host for the "lasing" ions: It can be produced in large volumes and large sizes with high homogeneity and free of absorbing particles or other absorbing defects. The concentration of active ions in glass can often be greater than in crystals. Also, adverse nonlinear refractive index effects can be kept low in glass. Glass lasers are used in industrial applications, mostly for materials processing. Neodymium-doped glasses have been chosen for the large

multilaser systems being developed for inertial confinement nuclear fusion energy studies in the United States and Europe. Erbium-doped silica core glasses are used in optical fiber amplifiers (OFAs) operating in the 1.55-μm communications band, and other lasing core glasses are being developed for the 1.31-μm band.

Ophthalmic Glasses. The term *ophthalmic* here refers to glasses made for spectacles (eyeglasses) intended for vision correction, as opposed to nonprescription sunglasses. Trends in recent decades have been to "smart" photochromic glasses (as described in Sec. 6.2.5), and to lighter weight. The lighter weight has been achieved by using higher-refractive-index glass, which allows thinner lenses, a particular advantage for "strong" corrections, and by using glass compositions with lower mass densities. To further lower the mass density will be a continuing challenge because of the conflicting need to maintain high index, which itself requires the presence of heavy, highly electrically polarizable atoms. Ophthalmic glasses are discussed in more detail in Sec. 6.2.4.5.

Atomic and Nuclear Glasses. In the atomic and nuclear technology area, special glasses are used as particle detectors, dosimeters, x-ray imaging screens, and radiation-absorbing windows that shield against nuclear and x-radiation.

6.2.4.4 Characteristics, Properties, and Qualities. As discussed in Chap. 5, the key property of optical glass that relates to its refractive (light-bending) ability is the refractive index. The higher the index, the more light is refracted for a given lens geometry. Complex lens designs call for glasses with a variety of refractive indices. With any optical material, the refractive index varies with the wavelength of light, the phenomenon known as dispersion. This means light of different wavelengths focuses differently through the same lens. To develop achromatic lens systems, ones that focus all wavelengths, or at least several widely spaced wavelengths, equally, combinations of lenses of different refractive indices and complementary dispersive ability are needed. Much effort has been expended in developing a wide range of suitable optical glass compositions. An equally great effort went into developing methods for melting the glasses from raw materials that would ensure the homogeneity of properties over a volume large enough for the required lens. Since refractive index is a sensitive measure of density of the glass, careful annealing of optical glasses is needed to assure uniform density and refractive index.

Glass Compositions and Nomenclature. Glass composition is key to generating the variety of required refractive indices and dispersions needed by lens designers. Figure 6.5 shows the historical evolution of the range of refractive properties. Glasses at the upper right are alkali-lead silicates and alkali-barium-lead silicates; glasses at the lower left tend to be fluorosilicates with high fluorine or P_2O_5 content. Fluoride-based glasses tend to have low index and low dispersion (high Abbe number, ν_d, as described in Sec. 5.20.1). Heavy metal– and rare earth lanthanum–borate glasses tend to have high index and medium to high dispersion (low to medium Abbe number).

Historically, optical glasses have been classified as either flint or crown according to the following criteria: All glasses with a refractive index n_d less than 1.60 and a ν value of 55 or greater (low index, low dispersion) are called *crown*. Glasses with an index greater than 1.60 are also considered as crown, provided the ν value is at least 50. All glasses with a ν value less than 50 (high dispersion) are called *flint*. The line of demarcation between crown and flint glasses is shown in Fig. 6.5. Alphanumeric labels such as K 3 or BK 7 have for a long time been used to identifiy optical glasses; K stood for crown (die Krone or das Kronglas in German) and B for boron. Hence BK 7, a widely used glass, is a particular boron crown glass whose properties can be found in manufacturers' tables; these include n_d = 1.517 and ν_d = 64.2. Another system of nomenclature more recently developed is based

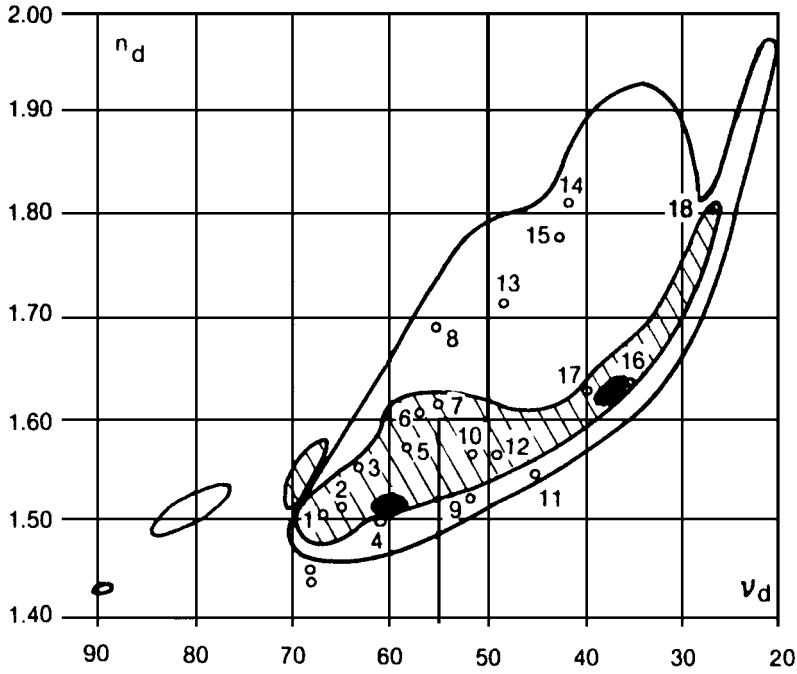

FIGURE 6.5 Representation of optical glasses in the $\{n_d, \nu_d\}$ plane. Glasses listed by numbers correspond approximately to nominal compositions given in Table 6.5 and 6.6; 0 = fused silica. Solid dividing line separates crowns (left) and flints (right). Diagram also contains historically significant boundaries: solid areas = 1870, hatched area = 1920, solid boundaries only = 1984. (*From E. W. Deeg, Ref. 5.*)

on the actual refractive index and dispersion of the glass. The scheme uses the first three digits after the decimal point in refractive index followed by the first three digits of the Abbe value, ignoring the decimal points. So BK 7 becomes 517642. Actually, the latter nomenclature provides a broader definition since it specifies only index and dispersion; the former often specifies chemical composition and properties such as physical density and transmittance ranges. There are more than 750 different optical glass types, from five major manufacturers, listed in a recent compilation by Schott Glas of Germany (see Ref. 11). Some typical optical glass compositions are shown in Table 6.14.

The refractive index of glass changes with temperature, a factor that must be considered when designing lenses that operate over a range of temperature. Stress and strain also affect optical properties. Generally any nonhydrostatic stress develops birefringence in the glass (see Sec. 6.20.5), the refractive index for light of one polarization orientation being different than that of another. The proportionality coefficients for stress birefringence differ, depending on glass composition. Stress birefringence provides an optical method for determining stress within a body of glass, but the analysis can sometimes be quite complicated. Minimization of birefringence is another reason for careful annealing during manufacture of optical glasses (see Sec. 6.5, "Annealing and Tempering").

TABLE 6.14 Optical and Ophthalmic Glass Compositions, wt%

Generic type	Description	Fig. 6.5 designation	SiO_2	Al_2O_3	B_2O_3	Li_2O	Na_2O	K_2O	MgO	CaO	SrO	BaO	PbO	ZnO	TiO_2	ZrO_2	La_2O_3	Other	References
Optical crown glasses																		*	
PK	Phosphorous crown	1	68		14		8	8				1							Deeg[5]
BK	Boron crown	2	72		12		4	8				1		2					Deeg[5]
PSK	Dense phosphorus crown	3	55	2	12		5	4				22							Deeg[5]
K	Crown	4	75	1			9	11		4									Deeg[5]
BaK	Barium crown	5	48	1	4		1	7				29		9					Deeg[5]
SK	Dense crown	6	41	2	5							42		9					Deeg[5]
SSK	Extra-dense crown	7	37	2	6							40	4	8					Deeg[5]
LaK	Lanthanum crown	8	6		40					17						6	30		Deeg[5]
Optical flint glasses																		†	
KF	Crown flint	9	67				16						13	3					Deeg[5]
BaLF	Barium light flint	10	54				2	9				14	11	10					Deeg[5]
LLF	Extra-light flint	11	61				5	8					26						Deeg[5]
BaF	Barium flint	12	56				2	13				12	17						Deeg[5]
LaF	Lanthanum flint	13	4		32					14		8	6	12		6	19		Deeg[5]
LaSF	Dense lanthanum flint	14	6		17							11		4		6	24	$WO_3 = 7$ $Ta_2O_5 = 8$ $CdO = 14$	Deeg[5]
LF	Light flint	15	53				4	7					34						Deeg[5]
F	Flint	16	44				2	7					46						Deeg[5]
BaSF	Dense barium flint	17	42				1	7				11	34	5					Deeg[5]
SF	Dense flint	18	27				1	1					71						Deeg[5]

*Additional oxides found in crowns include P_2O_5, CeO_2, TiO_2, MgO, SrO, and Li_2O.
†Additional oxides found in optical flints include P_2O_5, Nb_2O_5, TiO_2, Al_2O_3, Sb_2O_3, and Li_2O.
‡Sb_2O_3 and As_2O_3 are often used in small quantities as fining agents and the halides CaF_2, KHF_2, NaCl, KBr, and NH_4Cl in small amounts as fluxes.

TABLE 6.14 Optical and Opthalmic Glass Compositions, wt% (Continued)

Generic type	Description	Fig. 6.5 designation	SiO_2	Al_2O_3	B_2O_3	Li_2O	Na_2O	K_2O	MgO	CaO	SrO	BaO	PbO	ZnO	TiO_2	ZrO_2	La_2O_3	Other	References
Ophthalmic crowns																			
Refractive index = 1.523 for all			67	2			7	11	< 1	9				2	< 1				Deeg[5]
			68	2			8	9		9				3	< 1				Deeg[5]
			70				9	8		6				5	1				Deeg[5]
			56	9	16	3	2					7	6			2			Deeg[5]
			21	22	12	< 1	2	7	< 1	3		9			< 1	2		P_2O_5 = 20	Deeg[5]
	Corning code 8361		68.3	2			8	9.4		8.4				3.5				Others total 0.4	Kozlowski & Chase[b]
	photochromic		56.46	6.19	18.15	1.81	4.08	5.72							2.07	4.99		Ag = 0.21; Cl = 0.17; Br = 0.14; CuO = 0.006	Borrelli & Seward[7]
Ophthalmic flints																			
Refractive index = 1.59			47	1	5		6	7		4		22		2	3	2			Deeg[5]
= 1.60			48		4		7	2		6	< 1	13	14		4				Deeg[5]
= 1.62			45	1			3	8					40		1	1			Deeg[5]
= 1.66			39		2		6	1		6		19	16		4	6			Deeg[5]
= 1.68			34		6		8	< 1		8	< 1	14	18		7	5			Deeg[5]

Chemical durability of optical glasses is an important design factor. Some optical glasses, especially those containing large amounts of alkali oxides, P_2O_5, B_2O_3, or fluorides, have rather poor durability and can be used only in protected environments. Others, while generally considered chemically durable, will suffer gradual degradation of their optical surface properties in acidic or alkaline environments.

The optical materials discussed in this section are all passive or static materials; their properties normally remain constant in use. As mentioned in Sec. 6.2.4.1, modern optics has evolved to use many nonstatic, or active, properties developed in certain glasses. Important effects of this type include the ability to amplify light (laser glasses), the ability to change refractive index as a function of light intensity (nonlinear optics), and the ability to change optical properties as a function of externally applied electric or magnetic fields. These properties and effects are mentioned in Chap. 7 in relationship to optical communication of digital information (as opposed to lens systems that communicate or transfer images directly), and will not be covered here.

6.2.4.5 Ophthalmic Glass. Ophthalmic glass refers to glass used for prescription eyeglasses, or "spectacles." While often considered optical glass, ophthalmic glasses are not manufactured to as tight tolerances as those discussed above. Corrective lens prescriptions are not determined by the physician to less than $^1/_4$ diopter, and often $\pm^1/_4$ diopter differences cannot be perceived by the wearer. [Diopter D is a measure of the magnification power of a lens. It is the inverse of the focal length measured in meters. For a thin lens it can be calculated as $D = 1/f = (n - 1)(1/R_1 - 1/R_2)$, where f is the focal length, n is the refractive index, and R_i are the radii of curvature of the lens surfaces.] Homogeneity is important, but considerable gradual index variations across a lens can be tolerated, as evidenced by the popularity of the "progressive" type lenses that many wearers prefer to multifocal (bifocal and trifocal) lenses.

Refractive indices of ophthalmic lenses have been standardized at about six levels. 1.523 being the lowest and most popular, and ranging to 1.9. The higher indices allow "stronger" prescriptions without requiring great differences between front and back lens surface curvatures and the consequent thick (and heavy) lenses. The glasses are generally manufactured to a three decimal place tolerance, but tighter tolerances are specified for fused multifocal segment glasses described below. Dispersion is generally not a very important consideration for ophthalmic lenses, but ranges between 50 and 60 for the 1.523 index "white crown" glass. The composition of a typical chemically (ion-exchange) strengthenable white crown ophthalmic glass is given in Table 6.14.

Multifocal eyeglasses may be made by generating (grinding) different curvatures into the upper and lower portions of the lenses. Alternatively, a glass of different composition and refractive index (the segment glass) can be fused into the lens blank (major glass) onto which a single lens curvature may be generated, the different index regions producing different magnifications at the same curvature. Design of such "fused" multifocal lenses require matching of thermal expansion to prevent residual stress after sealing, which could lead to debonding of the seal, or fracture of the lens.

6.2.5 Photochromic and Polarizing Glasses

Photochromic glasses are glasses that darken, or decrease their transmittance, when exposed to light, particularly ultraviolet light or light in the violet and blue spectral regions. These glasses generally recover their high transmittance when removed from the darkening radiation, an effect often called *clearing* or *fading*. The speed of recovery depends on the particular glass design and on temperature; higher temperatures yield faster clearing.

The degree of darkening is not linear with light intensity, which partly explains the limited commercial applications for this material other than as eyeglasses, including prescription and nonprescription sunglasses. For prescription eyewear, the photochromic glasses must meet all the requirements described above for ophthalmic glass (Sec. 6.2.4.5).

Commercial photochromic glasses depend for their behavior on many very small crystallites (about 10 nm) of copper-doped silver chloride/bromide, uniformly dispersed throughout their volume. The components for the crystals are dissolved in the glass melt during manufacture and are precipitated as molten silver halide droplets by heat treatment of the resulting glass. The droplets crystallize as the glass is cooled to room temperature. The darkening results from a process similar to latent image formation in silver halide-based photographic emulsions. The light in a sense decomposes some of the silver halide to produce metallic silver, which absorbs visible light. Because each silver halide crystal is trapped in a small cavity within the glass, all the reaction products are available to recombine when the light source is removed. (This photochromic process is similar to that of latent image formation in silver-based photography, but in photography, some of the reaction products are lost in the organic emulsion, rendering the process irreversible. Photochromic plastics, on the other hand, rely on reversible photochemical reactions of organic dye molecules captured within their structure.)

The performance of photochromic glass strongly depends on the size, concentration, and composition of the silver halide particles dispersed within the glass. These factors in turn depend on the overall composition of the glass and the heat treatment used to precipitate the particles. The glass is often formed as a homogeneous glass, followed by a special heat treatment, which sometimes includes separate particle nucleation and growth steps, at temperatures somewhat above the glass transition temperature (usually between the softening and annealing point temperatures). Borosilicate glasses are especially useful for preparing photochromic glasses because they show a large difference between the high- and low-temperature solubility of silver chloride; this difference results from a change of boron-oxygen coordination with temperature. Borosilicate glasses with the required refractive indices for ophthalmic (prescription) eyeglasses have been developed, as have ion-exchange strengthenable glasses for both prescription eyewear and for sunglasses. Two such compositions are shown in Table 6.14.

Light-polarizing materials (Sec. 6.2.3.4), in the context we use here, are materials that preferentially transmit light of one linear polarization compared to light of a different polarization. A sheet of such material, when rotated in a beam of linear polarized light, will have an orientation of maximum transmittance and, at 90° from that, an orientation of minimum transmittance. The effectiveness of the polarizer can be characterized by the difference in these two transmittances; the greater the difference, the better the polarizer. (Or if one considers optical absorption, the greater the ratio of the two absorbances, the more effective the polarizer.) Commercially produced polarizing glass, developed by Corning Incorporated and sold as Polarcor^{TM}, is made by stretching photochromic-type glass at a very high viscosity, using redraw techniques described in Sec. 6.4.5, so as to elongate and align the silver halide particles within the glass. The stretched glass is then treated in a hydrogen or forming gas (H_2-N_2) atmosphere at temperatures below the melting point of the silver halide crystals to chemically reduce the silver halide to silver metal. The polarizing efficiencies of these glasses tend to be greater in the near infrared than in the visible portions of the spectrum and have found applications in photonic devices. In particular, they have become key components in optical isolators used in optical-fiber communications.

Glasses containing precipitated particles of silver or other metals can also be deformed to produce polarizing glass; silver gives the best performance. In all cases, since the size of the precipitated particles are small, surface tension forces work to keep the particles spherical throughout the manufacturing process. Thus it is necessary to redraw (or extrude) the glasses under conditions that provide viscous elongation forces sufficiently great to overcome the surface tension effects.

6.2.6 Photosensitive Glass

Photosensitive is a more general term than *photochromic*. Photochromic glasses are certainly sensitive to light, but the term photosensitive is more commonly used to describe glasses in which a latent image can be produced in the glass by selective exposure to ultraviolet light, such as through a suitable photomask or other imaging system. Once the latent image is recorded, subsequent heat treatment can generate colored patterns or opal patterns. Commercial products made this way are the Corning Polychromatic™ and Fotalite™ glasses. Another photosensitive glass, in which the opal regions can be dissolved in mineral acids to make intricate mechanical parts, was developed by Corning and sold under the trade name Fotoform™, but is now produced by other manufacturers. Some photosensitive glass compositions are shown in Table 6.15.

Commercial photosensitive glasses typically have compositions near $17Na \cdot 7Al_2O_3 \cdot 5ZnO \cdot 71SiO_2$ (wt%) with 0.2 Sb_2O_3, 0.01 to 0.1 Ag, and 0.05 CeO_2 added in excess of 100 percent. The cerium ions absorb the sensitizing ultraviolet radiation and release electrons to reduce the silver to the metallic state needed to grow the silver colloidal particles. The antimony oxide helps establish the appropriate oxidizing-reducing conditions in the glass. Exposure is generally done at room temperature, but heating at temperatures above about 500°C is required to grow (develop) the metallic colloids that color the glass. Gold, or gold in combination with palladium, can be substituted for the silver. Such photosensitive glasses produce monochrome photographic images.

Overall glass composition is important because it controls the glass structure and the photosensitivity. Generally a significant number of NBOs (nonbridging oxygens), such as found in the above soda-zinc-aluminosilicate glasses, must be present for effective photosensitivity. It has been suggested that these NBOs act as deep hole traps to prevent premature recombination of the photoelectrons with the cerium ions from which they were released. No commercially successful photosensitive glasses have been made in the borosilicate glass system, presumably because they lack sufficient concentrations of NBOs.

If fluorine is added to the above composition at about the 2 to 3 percent level, sodium fluoride crystals can nucleate and grow on the metal colloids to give the glass opacity in a pattern controlled by the initial exposure. Such glasses are referred to as photo-opals. One version was sold by Corning Glass Works under the trade name Fotalite™. If, in addition, bromine is added, a second exposure and heat treatment can impart a wide variety of low-saturation colors to the glass, again in patterns controlled by the exposure. Such a glass, developed by Stookey, was briefly marketed by Corning Glass Works under the trade name Polychromatic™ glass.

Crystallization in certain glass-ceramics (see Sec. 6.2.7) can be controlled photosensitively to create patterns to close dimensional tolerance. In the Fotoform brand products briefly described above, lithium disilicate crystals grow on photosensitively generated colloidal silver nuclei. A typical Fotoform-type glass composition is discussed in Sec. 6.7.2.

6.2.7 Glass-Ceramics

Glass-ceramics can be described as polycrystalline materials formed by the controlled crystallization of glass. Internally nucleated glass-ceramics were discovered at Corning Glass Works in the late 1950s by Stookey. For the purposes of this section, we will define a glass-ceramic as a material or product that has been manufactured and/or formed as a glass,

TABLE 6.15 Photosensitive Glass Compositions, wt%

Type	Description	SiO_2	Al_2O_3	Li_2O	Na_2O	K_2O	ZnO	SnO	Sb_2O_3	CeO_2	Other (as excess over 100%)	References
Typical photosensitive glasses												
Colored	Monochrome	71	7		17		5	0.05	0.2	0.05	Ag = 0.01 to 0.1	Borrelli & Seward in Schneider[7]
Opal	(White)	71	7		17		5	0.05	0.2	0.05	F = 2.5; Ag = 0.1	
Colored	Polychrome	71.6	7.1		16.3		5	0.05	0.2	0.05	F = 2.3; Ag = 0.1; Br = 1	
Photosensitive glass-ceramics												
Fotoform	Corning code 8603	79.6	4	9.3	1.6	4.1		0.003	0.4	0.014	Ag = 0.11; Au = 0.001	Beall in Boyd and MacDowell[5]

using typical, often highly automated, glass-forming techniques, and subsequently, using a suitable heat treatment, caused to crystallize in a controlled manner (see Sec. 5.3.2). The resulting product consists of a fully dense (no pores or voids) ceramic body, often of a shape that cannot be easily obtained by normal ceramic processing techniques. Some definitions of glass-ceramic require that the final product be at least 50 percent crystalline; often the percentage exceeds 90 percent. For our definition we require only that the properties of the product be significantly determined or controlled by the crystals that are present. This being said, however, the overall glass composition is important for glass formation, workability, and control of nucleation, and that of the residual glassy phase after processing is important for chemical durability.

Because of the requirements of various glass-forming processes that the molten glass be stable against crystallization during the forming steps, not every ceramic composition can be formed as a glass. Perhaps the most notable example is alumina (Al_2O_3), which cannot be formed from the melt as a glass even under conditions of extremely rapid quenching.

Glass-ceramics can also be formed by powder processing methods in which glass frits are sintered and crystallized. This procedure somewhat extends the range of possible glass-ceramic compositions. It also allows for surface as well as internal nucleation. The devitrifying solder glasses of Sec. 6.2.2 are examples of powder-processed glass-ceramics.

In general, efficient bulk (internal) nucleation is necessary for fine, uniform grain size in the final product. The role of nucleation and growth in the controlled crystallization of glass is discussed in Sec. 5.3.2. Nucleation can occur heterogeneously (on a nucleation-catalyzing surface, such as another previously precipitated crystalline phase) or homogeneously (spontaneously throughout the volume of the glass). Homogeneous nucleation is sometimes preceded by a fine-scale glass-in-glass phase separation, in which one of the separated phases is more unstable with respect to nucleation and growth of the desired crystalline phase than was the parent glass.

Thermal, Mechanical, and Optical Properties. The unusual and in some cases unique thermal, mechanical, and optical properties of glass-ceramics have contributed much to their commercial success. Almost all of these properties relate to the characteristics of the crystalline phases, and to their microstructural arrangement.

Low coefficient of thermal expansion and the consequent resistance to thermal shock arises when the thermal expansion of the crystalline phase is very low. In the lithium-alumina silicate system described in Table 6.16, the crystals are either β-quartz or β-spodumene solid solutions that have very low, or even negative, volume thermal expansion. [Expansion is positive along one crystal axis (c) and negative along the other two (a and b).] These properties led to applications as varied as cookware, stovetops and stove windows, and giant (8-meter-diameter) earth-based telescope mirror substrates.

The strength and fracture toughness of a glass-ceramic depends very much on the size and shape of the crystallites within the manufactured body. Crack propagation generally follows the intercrystalline grain boundaries, regions that often contain a glassy phase. If the crystallite size is small, say less than 100 nm, the cracks do not deviate much from a plane surface and propagate much as they would within a homogeneous glass. For much larger grain sizes, the cracks deviate around the crystals, giving the crack significantly greater surface area and requiring a higher energy for fracture. In glass-ceramics composed of three-dimensional network-type crystal structures (sometimes referred to as *framework-type structures*), such as the lithium-aluminosilicate spodumene and quartz solid solutions, the crystallites grow in an approximately equiaxed manner (all crystal growth directions having similar dimensions). However, growth of sheet-silicate crystal structures, such as fluorine-substituted micas and clays, tends to be nonequiaxed, almost two-dimensional. Here the internal microstructure of a glass-ceramic often resembles a "house of cards" structure. Fracture toughness for these materials is generally much

TABLE 6.16 Glass-Ceramics by Primary Crystal Type

Network crystals (framework silicates)	Description
1. Lithium aluminosilicates (Li_2O-Al_2O_3-SiO_2)	- Based on stuffed β-quartz or β-spodumine (keatite) solid solutions - Three-dimensional crystalline phases - Nucleated by TiO_2 and ZrO_2 - Low thermal expansion (< 0 to 12×10^{-7}/°C) - Somewhat expensive because of lithium content
a. β-quartz isomorphs (solid solutions), sometimes referred to as "stuffed" β-quartz	- $(Li_2,R)O \cdot Al_2O_3 \cdot nSiO_2$, with n between 2 and 10 (commercially between 6 and 8) and R = divalent cations such as Mg^{2+} or Zn^{2+} - 3-dimensional, hexagonal crystal structure - $ZrTiO_4$ common nucleating agent - Unstable above 900°C, therefore heat-treated <900°C - Transparent material when crystal sizes <100 nm, sometimes <50 nm - Tends to be brownish in color because of nucleating agents - Can have very low thermal expansions, near zero, or even negative - High chemical durability - Applications include: transparent cookware (Visions™, thermal expansion = 7×10^{-7}/°C), optical materials (e.g., ring-laser gyroscopes), telescope mirror blanks (Zerodur™), infrared-transmitting electric range tops, wood-stove windows, fire door glazing
b. β-spodumene (keatite) solid solutions	- 3-dimensional, tetragonal crystal structure - $Li_2O \cdot Al_2O_3 \cdot nSiO_2$, with n between 4 and 10 - Generally nucleated by TiO_2 - Crystallized at temperatures between 1000°C and 1200°C - Opaque white (or tinted with colorants); opacity aided by crystalline anatase or rutile coming from the TiO_2 nucleating agent - Low in thermal expansion (about 12×10^{-7}/°C) - High chemical durability - Strong and tough; toughness aided by the larger crystal size (1–2 μm) and resulting tortuous paths for crack propagation - Applications: cookware (e.g., Corning Ware™, Neoceram), opaque cooking range tops, building wall cladding, laboratory bench tops, ceramic regenerators in turbine engines
2. Magnesium aluminosilicates (MgO-Al_2O_3-SiO_2)	- Based on hexagonal crystal, cordierite ($Mg_2Al_4Si_5O_{18}$) - Nucleated by TiO_2 - Other crystals present: spinel ($MgO \cdot Al_2O_3$), stuffed β-quartz, quartz, cristobalite - Excellent dielectric properties, transparent to radar - Good thermal stability and shock resistance, moderate thermal expansion (45×10^{-7}/°C) - Applications: cooking ware, radomes (e.g., Corning code 9606)
3. Lithium silicates	
a. Photosensitivity nucleated	- Basis for Fotoform/Fotoceram™ "chemically machined" (etched) products

TABLE 6.16 Glass-Ceramics by Primary Crystal Type (Continued)

Network crystals (framework silicates)	Description
	- Nucleated by gold and/or silver nanoparticles, themselves photonucleated with the aid of UV-absorbing cerium (3^+) ions Crystallized (at about 600°C) to dendritic form of lithium metasilicate (Li_2SiO_3), which is soluble in HF acid - Photonucleation plus heat treatment at higher temperatures (850°C) produces stable lithium disilicate ($Li_2Si_2O_5$) and α-quartz - Applications include: fluidics devices (fluid amplifiers), electronic components, magnetic recording head and inkjet printer head components, SMILE™ microlens arrays
b. Nucleated via glass-in-glass phase separation	- Additional components present to improve the chemical durability of the glass-ceramic via the glass matrix phase - Applications: dental prosthesis (inlays, onlays, crowns, bridges); example—IPS Empress 2 (Ivoclar)
4. Calcium silicates	- Based on blast furnace slag, chiefly in eastern Europe (referred to as slag-sitall in the former Soviet Union) - Crystal phases: diopside ($CaMgSi_2O_6$) and wollastonite ($CaSiO_3$), nucleated by sulfides of Zn, Mn, and Fe present in the slag - Inexpensive, high hardness (abrasion resistance), good chemical durability - Applications: interior and exterior wall cladding and tile
5. Sodium aluminosilicates	- Based on soda nephelene ($NaAlSiO_4$) - High in thermal expansion (about 95×10^{-7}/°C) - Can be glazed with lower expansion (e.g., 65×10^{-7}/°C) glaze to provide additional strength - Applications: institutional (hotels, restaurants, etc.) tableware (the original Pyroceram™ and Centura™ brand products)
Sheet silicates*	**Description**
1. Fluorophlogopite solid solutions	- Based on the trisilicic fluorophlogopite ($KMg_3AlSi_3O_{10}F_2$) - Other components (B_2O_3 and excess SiO_2) added to form the glass - Other minor crystals present: mullite ($3Al_2O_3 \cdot 2SiO_2$) - Tough, machinable (with conventional metalworking tools) - House of cards structure, only local mechanical damage - Applications: precision dielectric components, electrical insulators, high-vacuum components, other electronic and mechanical parts - Example: Macor™ (Corning code 9658)
2. Tetrasilicic fluormicas	- Based on the tetrasilicic fluormica $KMg_{2.5}Si_4O_{10}F_2$ - Tough, translucent, very chemically durable - Application: dental restorations (inlays, crowns, etc.) - Cerium oxide added to simulate fluorescent character of natural teeth - Example: Dicor™ (Dentsply)

TABLE 6.16 Glass-Ceramics by Primary Crystal Type (Continued)

Chain silicates†	Description
1. Potassium fluorrichterite	- Principal phase: potassium fluorrichterite ($KNaCaMg_5Si_8O_{22}F_2$), an amphibole - Minor additions such as Al_2O_3, P_2O_5, Li_2O, and BaO in some combination with excess SiO_2 are needed to form the glass - Random acicular (rod-like) structure - Strong and tough (cracks must follow very tortuous path) - Commercial compositions also contain minor amounts of cristobalite - Thermal expansion $\approx 115 \times 10^{-7}$/°C - Articles can be strengthened with a compressive glaze - Applications include high-performance institutional tableware (latest version of Pyroceram™) and cups for the Corelle™ line of tableware
2. Fluorcanasite	- Principal phase: $Ca_5K_{2-3}Na_{3-4}Si_{12}O_{30}F_2$ - Can be synthesized from glasses close to this stoichiometry - Structure characterized by four silicate chains running parallel to the *b* axis to form a tubular unit - CaF_2 crystallites act as nuclei - Very fine grained, strong, and tough - Thermal expansion about 125×10^{-7}/°C - Potential applications: architectural building cladding, thin tableware, magnetic memory substrates

*Fluormica crystals composed of 2-dimensional tetrahedral-silica layers. The OH in the natural mica structure is replaced by F in these synthetic materials.

†Crystals in which single or higher order chains of silica tetrahedra form the structural backbone, like natural nephrite jade. The crystals tend to grow in acicular (needle-like) form in the glass.

greater than for homogeneous glass, as illustrated in Table 6.18. This is due in part to the extremely tortuous path the fracture surface must follow. This effect can be even more pronounced in glass-ceramics containing crystals of chain-silicate-type structure. The structure of these glass-ceramics resembles tightly interwoven arrays of acicular or fiber-like crystals. Glass-ceramics of the chain-silicate types have shown the highest body strengths and fracture toughness of any glass-ceramic. A limit to the advantage of the tortuous fracture surface along the crystallite boundaries is reached in each case at some crystallite size where it becomes easier (requires less energy) for the crack to propagate through the crystallites, rather than around them.

As discussed in Secs. 5.20 and 6.2.3.6, glasses tend to be cloudy or even opaque because of light-scattering effects when they contain many small particles of refractive index different from that of the matrix glass. The smaller the size and concentration (number per unit volume) of the particles, the less the effect. Crystallites within glass-ceramics behave as such light-scattering particles. The difference between a very transparent manufactured body and an extremely opaque one of the same composition is often only a matter of crystallite size, as is discussed below for the lithium-aluminosilicate glass-ceramic composition systems. Extremely bright "white" opaque bodies often result when crystalline phases of very high refractive index, such as zirconia and titania phases, are present. So, the presence of titania and zirconia is important not only for their role as nucleating agents, but also as opacifiers.

It has recently been found that if the crystallite sizes are small, even with considerable difference in refractive indices between the crystals and the residual glass, transparency is often preserved even at very high concentrations of the crystalline phase. This would be surprising in view of the mathematical descriptions of light scattering presented in Chap. 5, but those descriptions strictly apply only to materials in which the particles scatter independently of each other. For highly concentrated systems, different mathematics applies. In these cases, it can be shown that for sufficiently small particle sizes, there is a range of concentrations for which the material behaves as a transparent body with a refractive index equal to an appropriately weighted average of the indices of the two phases. Materials of this type that contain microcrystalline host phases for lasing ions are finding interest for photonic devices.

Commercial Compositions and Applications. Many glass-ceramics have been produced in university and industrial laboratories, but only a few have so far found commercial applications. Those that have can be grouped according to their type of crystal structure as shown in Table 6.16. Commercial applications for each type are listed in the table.

Applications. The wide variety of applications include electric range tops, wood stove windows, telescope mirrors, cooking utensils, dinnerware, building facing materials, radomes, precision electronic parts, fluid amplifiers, inkjet printer heads, dental prostheses, and many more.

Manufacturing Considerations. To obtain uniformity of the microstructure throughout the glass, objects are generally formed and cooled sufficiently rapidly to produce a homogeneous glass body. This body is then subjected to a controlled heat treatment at temperatures between the annealing and softening points. This heat treatment generally consists of two or more sequential steps at progressively higher temperatures, the first to generate a uniform dispersion of crystal nuclei throughout the glass, then a second at a higher temperature during which the final crystalline assemblage grows on these nuclei to achieve the desired crystal sizes. The composition of the nuclei may bear little resemblance to the major glass-ceramic phase. Sometimes the preferred nuclei are noble metal particles, sometimes very refractory materials like titania and zirconia, and sometimes very small particles of the final crystal phase itself. The latter is referred to as *homogeneous nucleation*, the first two examples as heterogeneous nucleation. For some compositions and products the growing crystals pass through a series of phases (differing in both crystal structure and composition) before reaching the final goal. Often, the temperature or sequence of temperatures chosen for the crystal growth stage must be high enough to maintain sufficient fluidity in the composite structure to relax any strains generated by volume changes during crystallization, but low enough that the product is sufficiently viscous to maintain its shape (viscosity = 10^{10} to 10^{12} poise).

Forming Methods. Common forming methods include rolling, pressing, blowing, and casting. Some glass-ceramics are not suitable for forming processes such as sheet and tube drawing, because the required forming viscosities occur at temperatures below the liquidus temperature of the melt, leading to uncontrolled crystallization during the forming operations.

Dental and Bioactive Applications. In addition to the fluormica and lithium disilicate materials shown in Tables 6.16 through 6.18, glass-ceramic dental restoratives based on the systems SiO_2-Al_2O_3-Na_2O-K_2O-CaO-P_2O_5-F (leucite and apatite phases), SiO_2-Li_2O-ZrO_2-P_2O_5, and SiO_2-Li_2O-ZnO-K_2O-P_2O_5 have been developed by Ivoclar in Liechtenstein. Others based on CaO-P_2O_5-Al_2O_3 have been developed in Japan (Kyushu Refractories Co.). See Table 6.18.

As discussed in Sec. 6.1.5.2, CaO and P_2O_5 are key components in bioactive glasses. Correspondingly, bioactive glass-ceramics have been developed. Ceravital™ is a bioactive glass-ceramic containing crystalline apatite [$Ca_5(PO_4)_3(OH, F)$], Cerabone™ A-W contains the

TABLE 6.17 Glass-Ceramic Compositions, wt%

Glass identification	Description	SiO_2	Al_2O_3	B_2O_3	P_2O_5	Li_2O	Na_2O	K_2O	MgO	CaO	BaO	ZnO	TiO_2	ZrO_2	As_2O_3	F	Other	References
Aluminosilicates:																		
Transparent	β-quartz solid solutions																	
Corning Visions		68.8	19.2			2.7	0.2	0.1	1.8		0.8	1.0	2.7	1.8	0.8		$Fe_2O_3 = 0.1$	Pinckney[7], Beall[5]
Schott Zerodur		55.5	25.3		7.9	3.7	0.5		1.0			1.4	2.3	1.9	0.5		$Fe_2O_3 = 0.03$	Pinckney[7], Beall[5]
Shott Ceran		63.4	22.7		N.A	3.3	0.7	N.A	N.A		2.2	1.3	2.7	1.5	N.A	N.A	N.A	Pinckney [7]
Nippon Electric Narumi		65.1	22.6		1.2	4.2	0.6	0.3	0.5				2.0	2.3	1.1	0.1	$Fe_2O_3 = 0.03$	Pinckney[7], Beall[5]
Aluminosilicates:																		
Opaque																		
Corning 9608 (Corning Ware)	β-spodumene solid solutions	69.7	17.8			2.8	0.4	0.2	2.6			1.0	4.7	0.1	0.6		$Fe_2O_3 = 0.1$	Pinckney[7], Beall[5]
Corning 9606	Cordierite	56.1	19.8						14.7	0.1			8.9		0.3		$Fe_2O_3 = 0.1$	Pinckney[7], Beall[5]
Corning 9609 (Pyroceram)	Nephelene	43.3	29.8				14.0				5.5		6.5		0.9			Beall[5]
Lithium disilicates:																		
Fotoform/ Fotoceram	Corning 8603	79.6	4			9.3	1.6	4.1									Ag = 0.11, Au = 0.001, $CeO_2 = 0.014$, $SnO_2 = 0.003$, $Sb_2O_3 = 0.4$	Beall[5]
Ivoclar Empress 2		57–80	0–5		0–11	11–19		0–13	0–5			0–8					$La_2O_3 = 0.1$ to 6, + others	Holand[15]
Sheet silicates:	fluoromicas																	
Corning Macor	Corning 9658	47.2	16.7	8.5				9.5	14.5							6.3		Pinckney[7], Beall[5]
Dentsply Dicor		56–64	0–2					12–18	15–20					0–5		4–9	$CeO_2 = 0.05$	Pinckney[7], Beall[5]
Chain silicates:																		
Slagsital	White (Russia) Wollastonte	55.5	8.3				5.4	0.6	2.2	24.8		1.4					MnO = 0.9, $Fe_2O_3 = 0.3$, S = 0.4	Pinckney[7], Beall[5]
Minelbite	Gray (Hungary) diopside	60.9	14.2				3.2	1.9	5.7	9.0							MnO = 2.0, $Fe_2O_3 = 2.5$, S = 0.6	Pinckney[7], Beall[5]
K-richterite	Corning	67.3	1.8		1.0	0.8	3.0	4.8	14.3	4.7	0.3					3.5		Pinckney[7]
Canasite	Corning	54–62	1–4				6–10	6–12	0–2	17–25		0–2				4–8		Pinckney[7]
Other																		
Calcium aluminophosphate	Kyushu Refractories		10		70					20								Abe[16]

NA = Data not available.

TABLE 6.18 Glass-Ceramic Properties

Glass identification	Description	Modulus of rupture, MPa	Young's Modulus, GPa	Hardness, HK_{100}	Fracture toughness $MPa \cdot m^{1/2}$	Fracture energy, $J \cdot m^2$	CTE, 10^{-7}/°C	References
Aluminosilicates:								
Transparent	β-quartz solid solutions							
Corning Visions								
Schott Zerodur								
Shott Ceran								
Nippon Electric Narumi								
Aluminosilicates:								
Opaque								
Corning 9608 (Corning Ware)	β-spodumene solid solutions	100	81	660			12 (0–500°C)	Pinckney[7]
Corning 9606 (Cercor)	Cordierite	250	120	700	2.2		45 (0–700°C)	Pinckney[7]
Corning 9609 (Pyroceram)	Nephelene							
Lithium disilicates:								
Fotoform/Fotoceram Empress 2—Ivoclar		350 ± 50			3.2 ± 0.3		106 ± 5	Holand[d]
Sheet silicates:	fluoromicas							
Corning Macor	Corning 9658	100	65	250		8.2	129 (25–600°C)	Pinckney[7]
Corning/Dentsply Dicor		152	70.3	362	2.5		72 (25–600°C)	Pinckney[7], Abe[16]
Chain silicates:								
Slagsital	White (Russia)	65–100	75– 88	590–700			91–95 (0–500°C)	Pinckney[7]
	Gray (Hungary)	80–120	88–108	640–740			72–76 (0–500°C)	Pinckney[7]
K-richterite	Corning	150–200	87–95		3.2	60	115 (0–300°C)	Pinckney[7], Beall[23]
Canasite	Corning	250–300	80–82	500	4–5	150	125 (0–300°C)	Pinckney[7], Beall[23]
Other								
Calcium aluminophosphate	Kyushu Refractories	160–230	80		2.7		118	Abe[e]
For comparison								
Ion-exchanged	Soda-lime-silica	170	70		0.5	2		Beall[23]
Corning code 0313*	Aluminosilicate	340	70		0.5	2		Beall[23]

*Code 0313 is an ion exchanged product made from code 0317 glass.

crystals apatite and wollastonite ($CaSiO_3$), and Biovert™ contains apatite and fluorphlogopite. All have been shown to bond with human bone; some are in clinical use as bone-repairing materials. Note that hydroxyapatite [$Ca_5(PO_4)_3OH$] is the major mineral constituent of bone.

Photonic Applications. Several areas of application of glass-ceramic materials are emerging in the photonic and optical communications fields. These include lasers and frequency up-conversion devices in which the optical advantages of fluorescent rare-earth ions in crystalline host materials are combined with manufacturing and structural advantages of glass. Their technical importance and commercial impact is not yet clear.

The ability to make a structurally stable material with a designed thermal expansion is being applied to temperature-compensating substrates for coupling and decoupling (mixing) devices in wavelength-division-miltiplexed (WDM) communications systems. For this application, a stuffed β-eucryptite ($Li_2O{:}Al_2O_3{:}SiO_2 = 1{:}1{:}2.5$) with a thermal expansion of about -7×10^{-6}/°C (note negative expansion coefficient) has been proposed.

6.2.8 Strengthened Glasses

6.2.8.1 Introduction. As discussed in Sec. 5.19, the strength of glass tends to be limited by the presence of surface flaws that, when stressed in tension, propagate as cracks that lead to fracture of the glass. The generally accepted approaches to improving the use strength of glass include fire polishing to remove mechanical surface flaws; acid polishing and/or etching to remove surface flaws or make the crack tips more blunt; coating the newly formed pristine glass surface with a protective coating, such as the multilayer polymer coatings applied to optical communications fiber; and providing a compressively stressed layer at and beneath the glass surface whose effects must be overcome when the glass is stressed in tension during use.

Strengthening by removal of surface flaws can only be temporary; it is generally limited to an in-process step.

Many ways have been demonstrated for effectively generating surface compressive layers, some of which have been applied commercially. These include thermal tempering, ion exchange at temperatures either above or below the glass transition, surface crystallization, lamination, and glazing.

Thermal tempering and ion exchange strengthening will be discussed along with annealing in Sec. 6.5.

6.2.8.2 Glazed and Cased Glasses. Crystalline ceramic articles may be strengthened considerably by "glazing" them with a glassy coating of lower thermal expansion than the bulk ceramic body. This process has also been used to strengthen glass and glass-ceramic commercial products. The glaze is applied as a glass frit in a suitable binder that is then fired to give a smooth glassy coating. Glass objects can also be clad with a lower expansion layer during their manufacturing process. This is a relatively old technique. In its earliest hand shop versions, the gob of glass on the end of the blowing iron would be dipped into a pot containing the cladding glass, which would leave a layer covering the entire surface of the glass when it was removed from the pot. After blowing, the cladding glass formed a continuous layer over the surface of the object. If this cladding glass was colored, it was often referred to as *cased* glass; if thin and colored it was sometimes referred to as *flashed*. If the thermal expansion of the glass closely matched that of the body glass, little strengthening would result, but the colored surface glass could be cut away to give decorative patterns of colored and clear regions.

6.2.8.3 Laminated and Wired Glasses. A variation on cased glass has been commercialized by Corning Incorporated in the form of products made from laminated glass sheet. In the Corning process, molten core (body) and skin glasses, prepared in separate melters, are brought together in a special laminating delivery orifice from which the core glass flows as a wide ribbon, simultaneously clad on both sides by the skin glass. This ribbon is fed between counterrotating rollers to generate a sheet of controlled thickness, which is then fed onto a special machine consisting of a hublike device that serves to vacuum-form articles of various shapes. For its Corelle™ line of tableware products, the Corning Consumer Products Company uses a special combination of glasses for laminating: an opal core glass, containing calcium fluoride microcrystals as the opacifying agent, and a clear, lower-expansion skin glass. Examples of these compositions are shown in Table 6.6. Although the difference in thermal expansion between the core and skin glass provides improved strength, Corelle products are additionally strengthened by thermal tempering of the laminated glass.

Sheets of glass are sometimes sealed together by a polymer adhesive interlayer to form "safety" and other products. A polyvinyl butyral (PVB) elastomeric sheet is often used to seal together sheets of annealed, partially tempered, or fully tempered glass to produce versions of safety glass. While this approach does not directly reduce the probability of surface flaws leading to fracture, the PVB layer does add several safety features: (1) it adds toughness to the composite; (2) on fracture of the product, the PVB layer keeps the fracture-produced shards from flying about, or from having their sharp edges readily accessible to cause injury to humans; (3) it serves as a restraint to prevent objects from being propelled through the glass from inside or outside a room or vehicle. This is one form of "safety" glass used for automobile windshields and in earlier times for side windows as well. It is both "antilacerative" and passenger restraining.

Such laminated glass is gaining acceptance as safety and security glazing for buildings, the intent being to prevent shards of glass being propelled into the interior of buildings during hurricanes or following nearby bomb blasts. A simpler laminate consisting of a single sheet of annealed glass coated on one side (the inside) by retrofitted polymer films is also gaining popularity. These films are sometimes known as *shatter-resistant window film* (SRWF) and *fragment retention film* (FRF).

More complex versions of laminated glass, consisting of multiple, thick alternating layers of glass and polymer (plastic) are used as a type of transparent armor, most commonly called *bulletproof glass*. Such armor is inherently thick and heavy, thus providing an opportunity for future weight-reduction methods research. Aircraft windshields, which are designed to withstand a 400-knot bird impact, are typically composed of two or three layers of chemically strengthened glass laminated with PVB interlayers.

Wired glass (or wire glass) consists of a metallic *chicken wire–type* mesh imbedded along its center plane (see Sec. 6.4.7.) It is often seen in skylights or fire doors. The purpose of the wire is not to increase breaking strength, but rather to prevent the fractured glass from falling out of the frame, an especially important function in preventing the spread of a building fire.

6.2.9 High-Silica Glasses

6.2.9.1 Fused Silica

Manufacturing History. As pointed out in Sec. 6.1.4, because of the high viscosity and high volatility of silica (SiO_2) at the temperatures needed to melt its crystalline phases, specialized techniques are required to prepare silica glass products. Some key highlights in process evolution include:

- Nineteenth century. The introduction of oxygen-injected or oxygen/fuel (as opposed to air/fuel) burners and torches allowed sufficient energy concentration to melt crystalline quartz.
- 1899–1910. Commercial development began in England, France, and Germany. Key issues were purity and continuous fabrication.
- Early twentieth century. Carbon arc and carbon resistance electric heating methods were developed.
- 1930s. Hyde (Corning Glass Works) first prepared silica glass by flame hydrolysis of $SiCl_4$. His U.S. patent, issued in 1942, became the basis for all synthetic fused silica processes used commercially today.

Classifications of Fused Silica and Methods of Manufacture. Methods of manufacture that involve gas-oxygen combustion as a heat source allow considerably more water vapor (a product of combustion) to be incorporated within the glass structure as hydroxyl ions than do electric melting methods. Synthetic precursors, as opposed to naturally occurring minerals, allow greater chemical purity. These two factors, heat source and raw material source (natural versus synthetic) have lead to a commonly accepted classification of fused silica types (after Heatherington et al.[19] and Bruckner[20]):

TYPE I

- Produced from natural quartz
- Electric fusion (arc or resistance heating) under vacuum or inert gas
- Sometimes using tungsten or molybdenum containers
- "Dry"—contains less than 5 ppm OH
- Contains the metallic impurities present in the raw materials and the furnace refractories, e.g., 100 ppm Al, 5 ppm Na, etc.
- Examples: Infrasil (Heraeus), IR-Vitreosil (TSL), GE codes 105, 124, 201, and 214

TYPE II

- Produced from crystalline quartz powder by oxy-hydrogen flame fusion (similar to Verneuille crystal growth process)
- "Wet"—contains 150 to 400 ppm OH from combustion products
- Less metallic impurities than Type I
- Examples: Herasil, Homosil, Optosil (Heraeus), OG Vitreosil (TSL), GE 104
- Special oxygen treatment can improve UV transmittance; example: Ultrasil (Heraeus)

TYPE III

- "Synthetic" fused silica produced by flame hydrolysis of $SiCl_4$ in oxy-hydrogen flame (variations: other chemical precursors; natural gas (methane)–oxygen flame)
- "Wet"—contains OH up to 1200 ppm
- Very few metallic impurities, few ppm or less
- With $SiCl_4$ precursor, about 100 ppm Cl retained
- Examples: Suprasil (Heraeus), Spectrosil (TSL), and Corning 7940 and 7980

TYPE IV

- "Synthetic" fused silica produced from $SiCl_4$ (or other precursors) in water-free plasma oxidation torch
- Like Type III, but "dry," containing <5 ppm OH
- Examples: Suprasil W (Heraeus) and Spectrosil WF (TSL)

TYPE IVA

- Not a traditional classification; coined here by Seward
- Synthetic, like Types III and IV
- Made by a two-step synthetic process: Step 1, deposition of a porous synthetic preform; Step 2, drying and consolidation under flow of gases, often chlorine (for drying) and helium (for completeness of densification)
- "Very dry," OH measured in ppb
- "Very pure," impurities measured in ppb

TYPE V

- Sol-gel derived silica
- Classification V introduced by Sempolinski and Schermerhorn
- Many processing variations exist
- Glass properties depend on the process techniques

Types I and II are often referred to as *fused quartz* and Types III and IV as *synthetic fused silica*, although this nomenclature is not always adhered to. Table 6.19 shows some of the current commercially available fused silicas on a process method/purity matrix.

Process Methods.

ELECTRIC ARC MELTING (TYPE I) In this process grains of crystalline quartz are fed into an electric arc. They soften and fall onto a heated rotating surface, where they form a dense glassy body by fluid flow (continuous viscous sintering).

The portion of the process in which the molten glass particles drop and are collected and consolidated in a layer of previously deposited material to eventually build up a large mass of glass is called the *boule* process, the mass of solid glass produced being called a *boule*. After the initial layers of glass are deposited, the glass is no longer in contact with any supporting refractory materials, so the boule process is in a sense a containerless process, without the inherent contamination that comes from melting in a container.

Often the raw materials are beneficiated to improve purity. Beneficiation steps include:

- Quartz crystals extracted from the earth
- Hand sorted for defects (contaminants)
- Rinsed in dilute HF
- Calcined at 800°C
- Water quenched
- HF acid washed

TABLE 6.19 Vitreous Silica—Purity and Manufacturing Methods

Process		Raw material, increasing purity → Sand (Alk ≈ 50, M ≈ 400, Al ≈ 200)	Crystal (Alk ≈ 5, M < 10, Al ≈ 10–50)	Beneficiated sand (Alk ≈ 5, M < 10, Al ≈ 20)	Synthetic (Alk ≈ 1, M ≈ 1, Al ≈ 1
Flame Fusion: Decreasing OH^-	$CH_4,H_2/O_2$		OH^- ≈ 200 H/A—TO8, Ultrasil, Homosil TSL/TAFQ—Vltreosil 055		OH^- ≈1000 Cl^- ≈ 100 CGW–7940, 7980, ULE (*d*) Dynasil 1000
			TOS–T1030, 1070, 1130(*d*), 1170(*d*) Q/S—981		GE(WQS)—Synsil H/A—Suprasil TSL/TAFQ—Spectrosil TOS–T–4040 Q/S—Tetrasil A,B
	Plasma				OH^- < 10 Cl^- < 200 H/A—Suprasil W TSL/TAFQ—Spectrosil WF TOS–T–4042 Q/S—Tetrasil SE
Electric Fusion:	Arc atmosphere			OH^- ≈ 30 GE–510 GTE crucibles QSI crucibles	
Decreasing OH^-	Resistance/induction atmosphere	OH^- ≈ 200 GE–318 H/A—Rotosil TSL/TAFQ—Vitreosil TOS–T100, 200, 800 Q/S—opaque		OH^- ≈ 30 GE–511 Pyro crucibles	
			OH^- ≈ 30 TOS–T–2030	OH^- ≈ 30 GE–124,214	
	Vacuum Rebake		Q/S–453, Purposil, Pursil, Germiosil(*d*), 676	OH^- < 5 GE–214, 982, 219(*d*) GTE–SG 255C TOS–T–7082	

Alk = alkali content, ppmw total; M = transition metal content, ppmw; A = aluminum metal content, ppmw; GTE = Sylvania; QSI = Quartz Scientific Inc.; Q/S = Quartz et Silice; H/A = Heraeus, Amersil; TSL = Thermal Syndicate Ltd.; TAFQ = Thermal American Fused Quartz; TOS = Toshiba; GE = General Electric; WQS (West Deutsche Quarzschmelze); CGW = Corning Inc.; and *d* = doped. ***Source***: After Bihuniak in Ref. 5.

RESISTANCE ELECTRIC HEATING (TYPE I) In one version, crushed quartz crystals are continuously fed into the top of an electrically heated graphite or refractory metal crucible (Ta, W, or Mo), enclosed by an inert gas atmosphere. The molten glass is drawn from the bottom through a refractory graphite or metal die to continuously form solid rod. (If tubing is needed, a suitable core with flowing inert gas can be inserted within the orifice. See Sec. 6.4.5. for a discussion of tube drawing techniques.) These techniques are used to make silica rods and tubing for a variety of applications. In more recent versions, radio-frequency (RF) induction heating of the crucible has been used.

Type I processes are used by GE, Nippon Silica Glass, Shin-Etsu, Heraeus, Heraeus Amersil, TSL, Toshiba, and Quartz et Silice.

FLAME FUSION (TYPE II) This also is a boule process. The fine grains of crystalline quartz are fed into the flame of a hydrogen-oxygen burner to soften and drop onto the surface of a rotating rod or boule, where they flow and merge. This approach was developed by Heraeus and is presently used by that company.

FLAME HYDROLYSIS (TYPES III AND IVA) In this process, in its simplest form, a liquid silica precursor such as $SiCl_4$ is volatilized and entrained in a suitable carrier gas, such as oxygen or helium, and fed into a specially designed high-temperature gas-oxygen burner. In the resulting burner flame the precursor reacts to form SiO_2 molecules as described by the following chemical equations:

$$SiCl_4 + H_2O \Rightarrow SiO_2 + 4HCL$$
$$SiCl_4 + O_2 \Rightarrow SiO_2 + 2Cl_2$$

The first process is called *flame hydrolysis*, the second *flame oxidation*. Because of the high concentrations of water vapor generated by the combustion process, the first reaction, flame hydrolysis, dominates.

The gas phase within the flame becomes supersaturated with respect to solid SiO_2, which precipitates as molten droplets of transparent soot, approximately 10 nm in diameter. These droplets are subsequently expelled from the flame. (If the expelled soot is given sufficient room to cool to the solid state, it can be collected as a fine white powder, called *fumed* silica, such as is sold under the trade name Cab-O-Sil™.) In the Type III silica processes, the silica soot is deposited on a hot (greater than 1600°C) surface where it continuously consolidates to produce a homogeneous boule.

Figure 6.6 shows schematically the deposition process whereby Corning deposits boules of its codes 7940 and 7980 fused silica exceeding 5 feet in diameter and approximately 1 foot thick.

Heraeus, Shin-Etsu, and Nippon Silica Glass employ variations of this process called *vapor axial deposition* (VAD), whereby the silica soot is deposited on the end of a continuously withdrawing rotating mandrel and is consolidated to full density in a separately heated zone of the processing apparatus. This process is illustrated in Fig. 6.7.

In the Type IVa process, the soot is deposited on a relatively cool substrate (near the annealing point) so that the arriving soot particles bond to the layer of particles beneath them, but do not sinter to full density. This intermediate product has about 20 to 30 percent porosity, which allows it to be reacted at high temperatures with suitable gaseous drying agents such as Cl_2, HCl, thionyl chloride ($SOCl_2$), or ammonia diluted with nitrogen. The dry porous body is subsequently consolidated to full density at temperatures greater than 1400°C in vacuum or in a flowing helium atmosphere. Such drying and consolidation leads to incorporation of either chlorine or ammonia ions within the glass structure. It is a variation of this Type IVa process that is used in the outside vapor deposition (OVD) process for optical communications fiber manufacture described in Sec. 6.7.

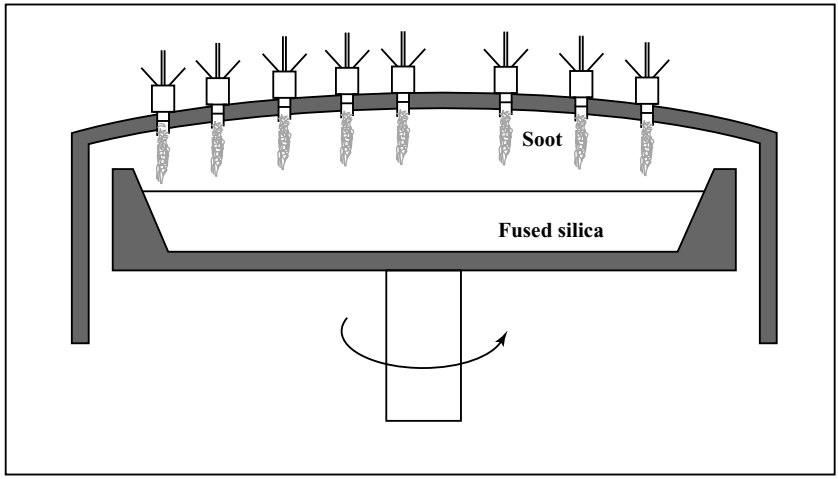

FIGURE 6.6 Corning Code 7940 synthetic fused silica process. (*Illustration courtesy John Rowe, Corning Incorporated, ca. 1993.*)

In summary, these processes consist of the steps:

- Vapor generation
- Chemical reaction using specialized burners
- Generation of soot particles
- Deposition of particles
- Consolidation (sintering/densification)

PLASMA TORCH (TYPE IV) In this synthetic process, the precursor chemical vapor stream is fed into the high-temperature flame of an oxygen gas plasma, generated by microwave energy. The chemical precursors react via the flame oxidation reaction described above. (There is no water vapor present to promote flame hydrolysis.) A dry silica soot is generated and collected on a hot boule rotating below. Heraeus Amersil, TSL, Toshiba, and Quartz et Silice use these techniques.

SOL-GEL TECHNIQUES (TYPE V) Sol-gel methods for glassmaking consist of chemical and thermal processes conducted at temperatures considerably less than those required for melting glass from crystalline raw materials. They involve solution chemistry processes, sometimes augmented by traditional ceramic processing techniques. The steps for most methods include, in this sequence,

1. Preparation of a solution or sol
2. Casting in a mold
3. Gelation (formation of a colloidal gel network)
4. Drying (formation of a three-dimensional porous solid)
5. Consolidating (sintering) to fully dense glass

Gelation can be produced by destabilization of colloidal silica sols wherein the colloidal size can range between 1 and 1000 nm. Alternatively, polymeric gels can be produced by the hydrolysis of metal-organic compounds in solution.

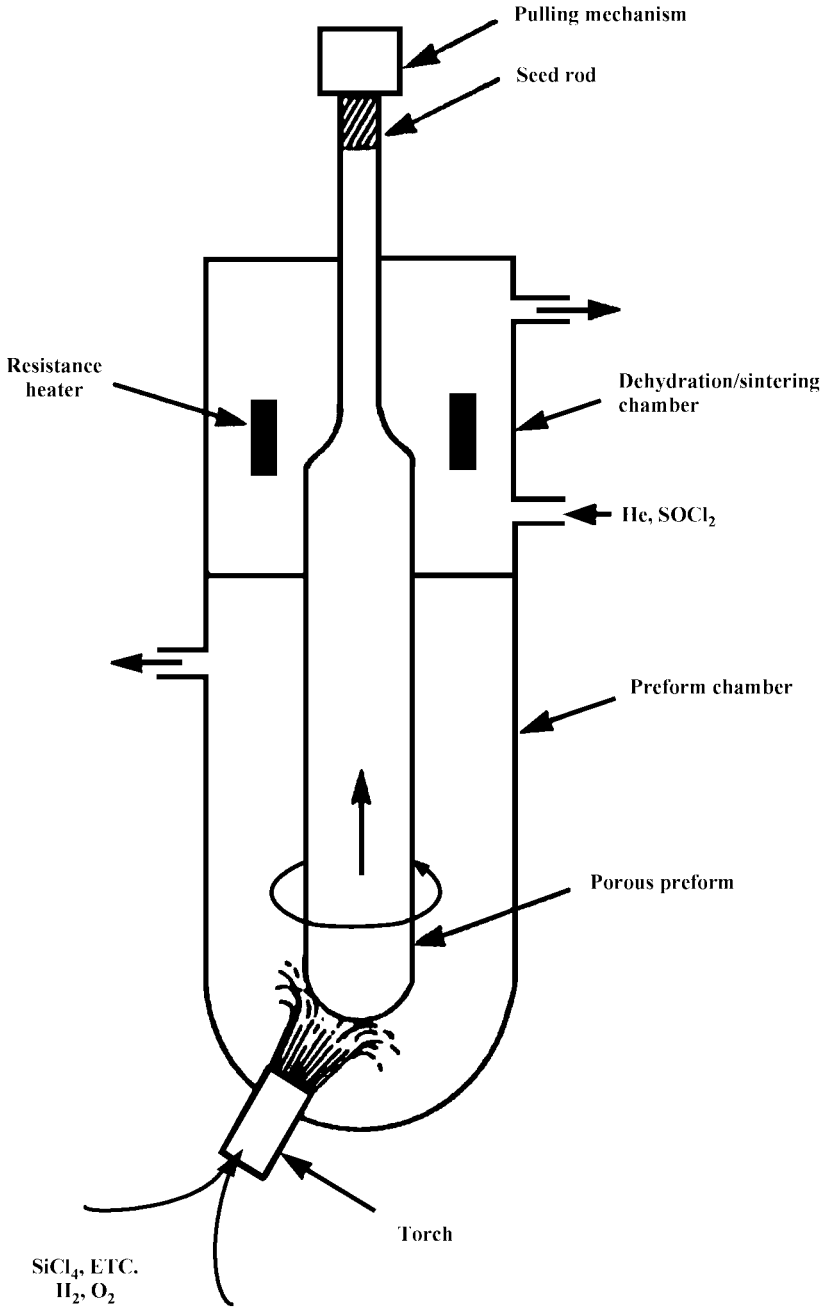

FIGURE 6.7 Vapor axial deposition (VAD) process for synthetic fused silica. (*From "Optical Fiber Waveguides" by R. M. Klein in Glass: Science and Technology, Vol. 2, Processing, edited by D. R. Uhlmann and N. J. Kreidl, copyright © 1983 by Academic Press, reproduced by permission of the publisher.*)

The sol-gel concepts have been known since the late nineteenth century, but have been intensively investigated since the 1970s, a motivator having been global concerns over high quantities of energy consumed in traditional glass manufacture. Although multicomponent glasses can be produced by sol-gel techniques, the greatest commercial successes have been with silica and high-silica glasses; maintaining chemical homogeneity in multicomponent glasses adds to the complexity and expense of the processing. While energy savings are still of interest, the ability to generate highly pure silica glass in "near net shape" form, albeit with high degrees of dimensional shrinkage, have been strong drivers for sol-gel processing of silica. While purity of the precursors is key to the purity of the product, the fact that the gels can be dried and consolidated at relatively low temperatures lessens the likelihood of contamination from the furnace refractories and crucibles. The various forms of sol-gel-derived silica have been collectively termed Type V silica.

Drying of the gel to produce a porous solid is perhaps the most challenging part of any sol-gel process. The small pore sizes of the gels can generate great internal capillary forces that in turn can lead to cracking and destruction of the dried porous structure unless very tedious or expensive techniques, such as supercritical drying or special drying control chemical additives (DCCA), are employed. In general, the larger the gel pore sizes the easier the drying and sintering. We can correspondingly classify silica sol-gel preparation techniques in the order of increasing pore size, depending on the solution or sol precursor used:

- *Polymerizing gel routes.* Precursor: metal organic compounds, e.g., alkoxides such as TEOS (tetraethylorthosilicate). Process: acid catalyzed hydrolysis and condensation reactions to form gel. Pore sizes: 1 to 5 nm.
- *Colloid particle routes.* Precursor: colloidal silica sol. Process: flocculation of silica particles, sometimes with chemically induced bonding. Pore sizes: 100 to 250 nm.
- *Dispersion processing (aqueous or nonaqueous).* Precursor: fumed silica/silica soot dispersed in polymerizing gels or potassium silicate aqueous solutions; colloidal silica for dispersion can be prepared from aerosols as soot or "fumed silica" by flame hydrolysis, or other suitable methods. Examples of fumed silica are Cab-O-Sil™ (Cabot Corp.) and Aerosil OX-50 (Degussa Corp.). Process pore sizes: 100 to 300 nm.
- *Alkoxide-derived gel*. The gel is dried rapidly to form high surface area particles, reheated, and milled in water to form slurries that are cast, dried, and consolidated.

Consolidation (sintering) can be performed at temperatures less than 1200°C for pore sizes less than 10 nm; 1400°C is generally required for pore sizes greater than 100 nm. Prior to consolidation, the porous body can be treated in Cl_2 gas to remove residual OH, dechlorinated by heating in O_2, and consolidated to full density in He or under vacuum. Details of the various sol-gel methods are beyond the scope of this handbook.

Applications of sol-gel-derived fused silica include thin films (thickness less than 1 μm), coatings, controlled-size spherical particles, fibers, and bulk silica glass. Among product examples for bulk silica glasses are lightweight space-based telescope mirror blanks (Corning), optical components (Corning and GelTech, Alachua, Florida), integrated circuit photomask substrates (Seiko-Epson, Japan), and outer cladding layers of optical telecommunications fiber preforms (AT&T/Lucent Technologies).

6.2.9.2 Porous and "Reconstructed" High-Silica Glasses. In the 1930s a technique was developed by Corning Glass Works for making high-silica glass that did not require the high melting temperatures described above. It is based on the principles of phase separation described in Sec. 5.3. An alkali borosilicate glass of appropriate composition is melted, formed into a desired shape, and heat-treated to generate the two intertwining matrix phases, one very high in silica content, the other high in boron oxide. This two-phase product is then

leached in a hot dilute acid (such as nitric acid), rinsed, and carefully dried, yielding a porous material having very high silica content. Several products have resulted including:

Porous Glass. By careful control of the initial glass composition, heat treatment, and chemical leaching, glass products having uniform interconnected (open) porosity can be made with a wide selection of pore sizes, generally less than 5 nm diameter (common range 4 to 6 nm), although by special processing pore sizes of 20 nm have been achieved. When dry, these materials display a strong tendency to absorb water from the atmosphere because of their very high internal surface area (up to approximately 300 m^2/g), giving them the name "thirsty glass." Applications include drying agents, salt bridges for electrochemistry, filtration media, catalyst supports (including immobilization of enzymes), and adsorption chromatography substrates. For these latter two applications, the porous glass has been generated in the form of granules with pore sizes available in the range of about 7 to 300 nm and is often referred to as *controlled pore glass* (CPG). Potential applications include time release "capsules" used to enclose drugs, vaccines, and fertilizer.

96 Percent Silica (Vycor™ Brand Products)

- Made by phase separating alkali borosilicate glass, chemically leaching out nonsilica phase, and consolidating to a fully dense body, approximately 96 wt% SiO_2, 3 percent B_2O_3 and less than 0.5 percent alkali.
- Consolidated by firing in vacuum at about 1200°C.
- Unlike fused silica, it can be produced by standard glass forming methods like tube draw, pressing, blowing, and rolling.
- Example: Corning code 7900 glass.

Primarily because of the slow leaching and rinsing times required (hours to days), the process is generally applicable only to relatively thin walled bodies, usually less that 10 mm thick, although 25 mm has been achieved when the cost of the slow chemical processing was justified.

Near-IR transmitting properties can be improved by drying the porous glass with special treatments, such as flowing chlorine gas at high temperatures, to remove the hydroxyl ions, just prior to consolidation.

Colored glass can be made by impregnating the porous glass with aqueous or organic solutions containing suitable coloring ions (e.g., nitrate or chloride salt in water), then heating to drive off the carrier media (evaporate the water, evaporate or oxidize the organic materials) leaving the coloring ions to be incorporated into the glass structure during consolidation. A variation is to impregnate only a surface layer so as to produce a product with a clear body and colored surface layer. These techniques are used for certain high-temperature lamp envelopes.

Properties. Similar to fused silica, but not quite as refractory. Continuous use at 900°C, intermittent at up to about 1200°C. Coefficient of thermal expansion is 7.5×10^{-7}/°C. See Tables 6.1 and 6.2.

Applications. Defroster tubes (refrigerators), radiant electric heater substrates, lab ware, high-temperature furnace/stove windows, UV-transmitting windows, UV lamps. These are examples only; many specialized applications exist.

6.2.9.3 Ultralow Expansion (ULE™) Glass. When TiO_2 (titania) is substituted into the structure in amounts less than about 15 wt%, it enters into the glass network. An unusual property, not yet fully explained on a theoretical basis, is that the glass has a region of negative thermal expansion extending from cryogenic temperatures to above room temperature, the upper limit of the range depending on the concentration of the titania. At about 7.5 percent TiO_2, the expansion changes from negative to positive somewhere between about 0 and 30°C,

being near zero over most of that range. Large pieces of such titania-doped silica can be made by the Type III synthetic process, described above, by feeding suitable concentrations of titania precursors (e.g., $TiCl_4$) into the burner along with the silica precursors. Corning Incorporated sells such glass products under the ULE trade name, glass code 7971.

Properties. Thermal expansion near zero from 5 to 35°C, thus it can be fusion welded at room temperature, enabling fabrication of complex structures having extreme dimensional stability. (See Tables 6.1 and 6.2.)

Applications. Telescope mirrors (currently up to 8 m diameter), lightweight mirrors (for space deployment), precision instrument stages, temperature-inert mountings

6.2.9.4 Doped Silica for Optical Communications (Fiber and Planar Waveguides). This is a very specialized, highly technical topic. It will be expanded on in Sec. 6.7 and in Chap. 7. The desired optical properties of the various optical system components are often produced by a controlled geometrical distribution of dopant ion concentrations in the glass. Here we briefly discuss the needs for such doping and methods for achieving it.

Communications at Optical Wavelengths. Transmission of data at higher rates is possible by using the higher frequencies (shorter wavelengths) of light radiation than is possible with radio or television frequencies. What is needed is a transmission medium (other than air or vacuum) having low loss. An early threshold target for long distance communication was 20 dB/km loss (equivalent to 1 percent transmission through 1 km of fiber), consistent with an economical number of electronic repeaters (amplifiers) along the path. This was achieved using glass waveguides made from high-purity synthetic silica, now called *optical communications fiber*, or just *optical fiber*.

Lightguiding over optical fiber requires that the fiber have a higher refractive index at its core and a lower refractive index at its outer surface, often referred to as the *cladding*. This can be achieved by doping the silica core regions to increase the index, by doping the silica cladding regions to decrease the index, or by doing both. For success, one must dope with components that (1) will not produce optical absorption in the glass at the transmitted wavelengths (specifically near 1.31 μm and 1.55 μm), (2) can be incorporated synthetically by the vapor phase route along with the silica, and (3) are available with sufficiently high purity. This limits the choices to glass-forming oxides (boron, phosphorus, and germanium), fluorine (which can substitute for oxygen in the network), and possibly titania and alumina. It is advantageous from a strength point of view to use dopants that give the core a slightly higher thermal expansion than the cladding. Figure 6.8 shows the effects various concentrations of these components have on the refractive index of silica.

Synthetic silicas can be doped during manufacture by incorporating appropriate precursors, along with the silica precursor in the vapor stream fed to the deposition burners. Methods for doing so are described in Sec. 6.7.4. Example precursors include the chlorides $GeCl_4$, BCl_3, and $POCl_3$, the fluoride SiF_4, and the solid $AlCl_3$, which can be delivered by subliming at high temperatures.

Fiber Amplifiers and All-Optical Systems. The future directions of optical communication are toward all-optical systems. That is, to utilize optical signal processing (coupling/splitting, switching, amplifying) rather than converting light signals to electronic signals, processing electronically, then converting back to light signals. Such signal processing can be done with fiber devices (constructed from optical fiber) or planar devices (constructed by building optical paths on flat substrates using patterned layers of different refractive index glass, generally doped silica, often in combination with vapor-deposited conducting and semiconducting films).

Light amplifiers are essential to all-optical systems (no electronic repeaters, no light-to-electronic conversion) since they compensate for optical losses within the fibers and the associated connectors, couplers, and switches. They are achieved by doping the fiber core with fluorescent lasing ions such as erbium or neodymium, and "pumping" using laser diodes.

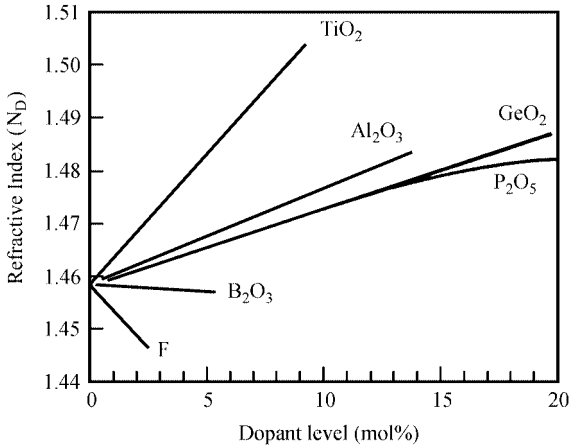

FIGURE 6.8 Dependence of silica refractive index on dopant concentration. [*A. J. Bruce, in Infrared Fiber Optics, J. S. Sanghera and I. D. Aggarwal, eds., CRC Press, Boca Raton, Fla., 1998, p. 40; his references 21 and 22 are: P. I. Schultz, Wiss. Z. Friederich-Schiller-Univ. Jena, Math. Naturwiss. Reihe, vol. 32, 215 (1983) and H. Takahashi, A. Oyobe, M. Kosuge, and R. Setaka, Tech. Dig., ECOC '86, vol. 3 (1986).*]

The operation of the erbium optical fiber amplifier (OFA) is based on the lasing action at 1.55 μm of the Er^{3+} (erbium) ion. The fiber is optically pumped at either 980 nm or at 1480 nm, by a suitable solid-state laser diode. Light emission by electronic transitions between the $^4I_{3/2}$ and $^4I_{5/2}$ levels is stimulated by the light signal at 1.55 μm and transfers power to that signal. To construct the erbium OFA, the fiber core is codoped with Er^{3+} at levels up to about 300 ppm, in addition to the index-adjusting materials (for example, germania). A major challenge is to obtain uniform gain (amplification) across a wide band of wavelengths, such as is required for wavelength division multiplexing (WDM) at 1.5 and 1.6 μm. Some methods for achieving this use separate gain-leveling devices.

Nd- (neodymium-) doped fibers have been investigated for operation within the 1.31-μm communications band, but have not yet been commercially successful. For amplifier operation at those wavelengths, non-silica-based fibers may be of advantage, leading to hybrid (mixed) glass fiber systems.

6.3 GLASS MAKING I—GLASS MELTING

6.3.1 Introduction and General Nature

The term *glass melting* as generally used applies collectively to all the steps used to convert raw materials into a molten mass that can be subsequently formed as an object. The process of preparing a quality melt from which glass products are to be made consists of several stages: *Batch* preparation (raw material selection, weighing and mixing), batch melting (conversion of the batch raw materials into a viscous liquid essentially free of any crystalline material), *fining* (the removal of bubbles), *homogenizing* (the removal of chemical and thermal variations within the melt, often occurring simultaneously with fining, the two processes together sometimes being called refining), and *conditioning* (bringing the melt to the uniform temperature required for whatever forming process will be used to make the product).

Each of these stages is performed more or less in sequence, either at one location, as in a crucible, or at a progression of locations, as in a continuous glass melting tank consisting of several, or many, zones. The various types of melters will be described in Sec. 6.3.3. Here we will describe glass-melting steps in more detail.

6.3.2 Steps in Glass Melting

6.3.2.1 Glass Batch Considerations. Rarely does a commercial process start with an all-oxide batch. This is in part because the expense of the materials would be too great, but mostly because oxides melt at much higher temperatures than the salts of the corresponding metallic elements, thus requiring longer times at higher temperatures to complete the chemical reactions. Many different combinations of raw materials can yield the same final glass composition. Final choice of raw materials is based on factors such as chemical composition, the level of impurities tolerated, particle size, particle size distribution, and the precision to which these characteristics are controlled (maintained) by the vendor, and price.

Batch materials. We cannot for space reasons discuss all the batch materials used in glass manufacturing, but will discuss several of the most relevant to give a feeling for some of the key considerations.

SILICA (SiO_2)

- Quartz sand, crushed quartzite, or beneficiated sandstone.
- For sandstone, a combination of quartz sand and clay, beneficiation consists of crushing, washing, and froth flotation to remove refractory heavy metal oxides.
- In the United States—shipped and handled dry; in Europe—wet.
- Generally more than 99 percent SiO_2; often more than 99.5 percent with $Fe_2O_3 < 0.03$ percent (by weight).
- Generally 40 to 140 mesh (coarser is harder to melt; finer leads to "dusting" effects). Also, finer particles may melt too fast and raise the melt viscosity before air trapped in the batch can escape.
- Cost tradeoffs include iron content and particle size distribution.
- Chemical analysis of raw materials, either in-house or by supplier, is important.

LIMESTONE/CALCITE ($CaCO_3$)

- Either high calcium ($CaCO_3$) or dolomitic (less than 46 percent $MgCO_3$).
- Dolomite is $CaMg(CO_3)_2$.
- Sometimes the oxide (CaO) is used (lime, quicklime, burned lime, or dolomitic quick-lime)
- Sometimes aragonite, a different mineral form of $CaCO_3$ is used.
- Limestone generally greater than 96% $CaCO_3$, with SiO_2 and $MgCO_3$ as major impurities

SODA ASH (Na_2CO_3)

- Sources for the United States and most of world are trona deposits in Wyoming (trona—a hydrated sodium carbonate sodium bicarbonate ore, $Na_2CO_3 \cdot NaHCO_3 \cdot 2H_2O$)
- The ore is calcined and treated to remove insoluble impurities, generally achieving better than 99.5 percent Na_2CO_3.

- Na_2CO_3 is also made by the Solvay process (react salt with limestone to get $CaCl_2$ as a by-product); Solvay is still used a source in Europe and other parts of the world.
- Hydration of the raw materials at temperatures below 110°C is a problem, so materials are often supplied as the monohydrate ($Na_2CO_3 \cdot H_2O$).

ALUMINA (Al_2O_3)

- Alumina is a very refractory material, slow to dissolve, so it is generally batched as a mixed-oxide mineral.
- The source is generally feldspar or nepheline syenite (minerals containing 60 to 70 percent silica, 18 to 23 percent alumina, calcia, magnesia, soda, potassia, and iron oxide (less than 0.1 percent).
- Since alumina is generally a minor batch component, the accompanying oxides can usually be easily assimilated in the composition.
- Accurate chemical analysis is important.
- It is relatively expensive, but when refined from the ore bauxite, it is even more expensive—often too expensive.

BORATES

- Obtained mostly from California or Turkey.
- Borax ($Na_2O \cdot 2B_2O_3 \cdot 5H_2O$), sometimes called *5 mol borax*.
- Boric acid (H_3BO_3 or $B_2O_3 \cdot 3H_2O$)
- Colemanite ($Ca_2B_6O_{11} \cdot 5H_2O$ or $2CaO \cdot 3B_2O_3 \cdot 5H_2O$), from Turkey.
- The mixed sodium-calcium borate minerals ulexite and probertite are used in the fiberglass industry.
- Anhydrous borax ($Na_2O \cdot 2B_2O_3$), also known as anhydrous sodium tetraborate ($Na_2B_4O_7$) is generally not used because it absorbs water. The fully hydrated form of borax ($Na_2O \cdot 2B_2O_3 \cdot 10H_2O$), on the other hand, is generally not used because it loses water, decomposing to 5 mol borax at temperatures above 60°C. Such changes in water content make batch calculations and weighing somewhat uncertain.
- Anhydrous B_2O_3 is too hygroscopic and too expensive to be a good commercial batch material.

OTHERS

- Litharge (PbO) and red lead (Pb_3O_4) are being replaced as batch materials by various lead silicates, which are safer to handle.
- Salt cake (Na_2SO_4) is used as a melting accelerator (forms eutectic with Na_2CO_3) and fining agent.
- Gypsum ($CaSO_4 \cdot 2H_2O$)—melting accelerator, fining agent.
- Sodium nitrate (Na_2NO_3)—oxidizing agent, stabilizes color.

CULLET Waste or broken glass softens readily in glass melters to bring batch particles together, thereby increasing batch reaction rates, often immensely. This batch material is referred to as cullet. There are many economic and environmental factors favoring use of cullet in batch melting operations.

Sources include:

In-house cullet, generally of known composition, usually the same as the glass being produced, therefore few special batch adjustments are required (exceptions are laminated and clad glass).

Foreign cullet, from sources other than the manufacturing plant (other plants, customers, other manufacturers, postconsumer).

Postconsumer cullet is increasing in importance as recycling expands. It must be carefully processed to remove metal, ceramic, and other detrimental contaminants. Transparent glass-ceramics mixed in with the glass cullet are a concern for container manufacturers, especially in Europe.

Cullet can be used in any proportion, generally 30 to 60 percent is considered most effective. Sizes coarser than the raw materials seem to work best; sometimes cullet is added as chunks. It can be added in the mixer, at the fill (doghouse), under, over, or layered with the batch. It must be added in a continuous enough manner to maintain melting stability.

Batch formulation. A combination of batch materials is selected according to the desired glass composition and oxidation state in combination with manufacturing process requirements (including those of mixing, melting, fining, etc.) and product cost. The quantities of each component are calculated to give the required weight of oxide after the volatile components and reaction products, such as water, carbon dioxide, sulfur dioxide, and nitrogen oxides, are lost to the atmosphere.

Raw Materials Handling

TRANSPORTATION AND STORAGE Raw materials that are used in large quantities are often delivered by railroad car and stored in large vertical silos or moderate-sized storage bins. A conveyor or elevating mechanism is used for loading the silos. Lesser batch components are delivered and stored in bags or other containers.

COLLECTING AND WEIGHING The trend in large manufacturing operations is to automate these steps as much as possible. Batch components can be weighed in hoppers at individual silos or storage bins and conveyed to the mixing location. More often the batch components are fed into a single scale for weighing. The scales themselves must be accurate and regularly calibrated. The weight sensors are often electronic, with digital read-out and modern computer interfacing and control. Such electronic weighing systems can be sensitive to 1 part in 4000 (250 ppm).

MIXING A wide variety of mixers are used. Most are of rotary (like a cement mixer) or pan-type construction. A variety of paddle and mixer blade designs are used. The trend is to mix the batch at a location very close to the melting furnace to minimize opportunity for batch segregation (see below) to occur.

FILLING OR BATCH FEEDING A variety of filling devices or machines are used. They often involve a hopper and a mechanism such as an auger or mechanical vibrator to feed the batch into the furnace via a chute or tube. Multiple feeders are generally used to supply batch to large melters. Reciprocating feeders whereby a pile of batch is deposited on a shelf extending the full width of the melter entrance and then pushed into the melter by a bar are used for large container and float-glass furnaces. This reciprocating action results in a sequence of batch "logs" being fed into the tank. The resulting undulating batch surface improves the melting process by allowing rapidly melted batch to run downhill, exposing fresh batch to the heat.

Many variations are possible for all the operations described above. In smaller factories and hand-shops the automation tends to be less, but care and accuracy remain important.

Batch Segregation. The term *batch segregation* refers to some batch components becoming spatially separated from the rest on some relatively large scale. (It can also refer to a separation of different particle sizes of the same batch component.) It is a type of demixing, which is problematic because different regions of segregated batch may then melt to produce glasses of different compositions. Some regions may not melt at all. The resulting inhomogeneities must be removed later in the process. Segregation can occur inside the mixing machine, as the mixed batch is being transported to the melter, or as it is being fed into the melter. Forces causing demixing operate whenever moving streams of particles are present. Often, they rapidly create steady-state patterns of segregation under constant flow conditions. These patterns are reproducible.

Factors affecting batch segregation are:

- Size difference is the main contributing factor. (A size difference ratio of as little as 5 percent can lead to measurable demixing.)
- Nominal grain size and density differences are lesser factors.
- Other much lesser contributing factors include particle shape, lubricity, and surface charge.

Methods for controlling batch segregation include:

- Use multiple discharge silos.
- Use raw materials having a narrow size distribution.
- Match their particle size and size distribution.
- Do not mix too long.
- Minimize the movement of mixed batch (locate the mixer at the furnace, not in the batch house).
- Wet the batch.

Wetting the batch helps reduce batch segregation by suppressing the free-flowing characteristics of the batch. (It provides a thin liquid coating on each particle.) Wetting also helps decrease dusting and batch carryover into the exhaust system. Generally water or a 50 percent NaOH solution is used. Of course, wetting complicates the batch handling system and adds expense. The technique must be used with care when hydrateable batch components are present, since they can absorb water, which may lead to "setting up" of the batch.

Batch Preheating. Several manufacturing groups are currently investigating the advantages of preheating of batch using heat from the furnace exhaust gases. The goals are at least twofold: Improve the efficiency of the batch melting step and recover waste heat. This will, of course, complicate the process and add some expense.

6.3.2.2 Processes Occurring within the Melter. *Batch melting* involves heat transfer from a source of heat energy, for example, fuel combustion in a burner or electric resistance (Joule) heating, and complex chemical reactions among the batch components. Since a formulated batch often contains water (moisture) and many batch components, such as boric acid, contain chemically combined water, the first step of melting consists of drying and dehydrating the powdered raw materials. Many chemical reactions among the dry batch

materials occur, some simultaneously. Solid-state reactions between batch components occur, sometimes leading to molten phases, other times to new crystalline phases. This is followed or accompanied by melting the salts and other low-melting-temperature ingredients (fluxes); decomposing some of the fluxes, producing gases; reacting silica sand and other refractory materials with the melted fluxes (for example, reacting sodium carbonate with silica sand); and dissolving the remaining refractory batch components (e.g., silica, zirconia) into the melt.

Fining involves the removal of the bubbles generated during batch melting. Such bubbles consist of air that was trapped between grains of batch and gases such as CO_2, SO_2, and H_2O generated by the reactions of the batch materials; e.g., decomposition of sodium carbonate releases CO_2 gas. Gases can also be generated by reaction of the melt with materials composing the melter, i.e., the container and electrodes. The bubbles tend to rise to the surface of the melt, driven by buoyant forces according to Stokes's law. This is often referred to as *Stokes fining*. If the bubbles are small, say 0.2 mm diameter or less, this can be a very slow process. To aid the fining the temperature of the melt is often increased, so as to decrease the viscosity of the melt and accordingly decrease the viscous drag on the rising bubbles. Occasionally, pressure changes above the melt may also be utilized to aid in fining.

During fining, gases produced by further chemical reactions in the melt enlarge the bubbles. Generally, the glass composition is designed to contain chemical compounds, known as *fining agents*, which release these additional gases during fining. Examples of such fining agents are As_2O_5, Sb_2O_5, and Na_2SO_4. The elements As, Sb, and S can exist in the glass in different oxidation states. [See "Oxidation State (Redox)" below.] depending on the temperature and oxygen activity of the glass. If the glass temperature is raised above that at which the glass was melted, these elements become more reduced, giving off oxygen (O_2) or sulfur dioxide (SO_2) gas, according to the following equations:

$$As_2O_5 \rightarrow As_2O_3 + O_2(gas)$$
$$Sb_2O_5 \rightarrow Sb_2O_3 + O_2(gas)$$
$$2Na_2SO_4 \rightarrow 2Na_2O + 2SO_2(gas) + O_2(gas)$$

The gases generated by the above equations remain dissolved within the glass in their molecular state until supersaturation becomes sufficient to nucleate bubbles of gas. However, if bubbles are already present, the dissolved gas molecules diffuse to those bubbles, thereby enlarging them in size. The enlarged bubbles then rise to the surface of the melt and break. Bubbles not reaching the surface dissolve when the melt is allowed to cool from the fining temperature. This dissolution process is aided by the reverse action of the fining agents.

Sometimes, during batch melting and fining, the gas bubbles do not burst when they reach the melt surface, but rather create a foam layer. Such foaming adversely affects heat transfer into the melt and can lead to glass defects, and so should be avoided by whatever means is effective.

Homogenization. Sources of inhomogeneity in the melt include the physical segregation of chemical components during batch mixing or batch melting, preferential volatilization of certain chemical components from the melt surfaces, and reaction of the melt with the furnace wall refractories. Mechanisms operating to improve homogeneity are composition-gradient-driven mass diffusion in combination with stirring (forced or thermally driven convection). Stirring serves to reduce the diffusion distances required for homogenization.

Thermally driven convective motion in melters serves several functions. It increases the melting rate by moving hot molten glass under the floating batch layer (called the *batch blanket*), supplying it with a new source of heat. Upward convection part way along the

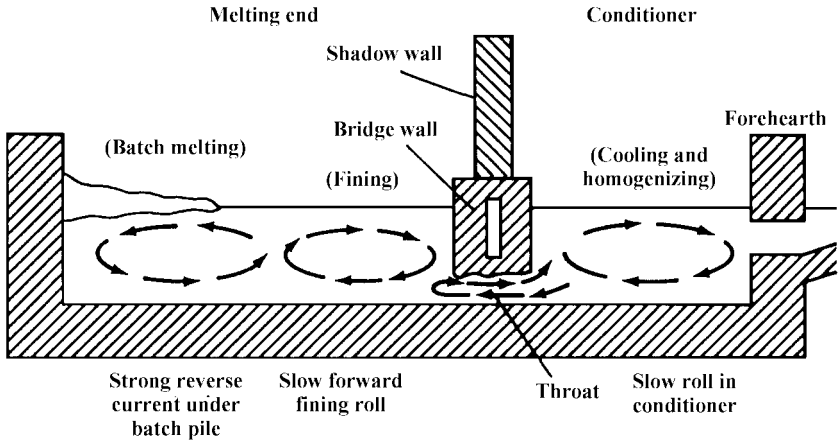

FIGURE 6.9 Major convection flows in a fuel-fired tank furnace. (*From F. E. Woolley, Ref. 7.*)

tank can serve to help separate the batch melting and fining sections of the melter. Simple patterns of convective motion in a large tank-type melter are illustrated in Fig. 6.9. Sometimes a row of bubblers is built into the tank bottom to release large air bubbles that forcefully rise to the top, aiding the convective motion. And, as described above, convection helps to mix and homogenize the melt.

Conditioning and Delivery. For a molten glass to be processed into a product by any of the many commercial forming processes, it must first be adjusted to the temperature required for that process. In general all the glass being delivered from the tank must be at that same temperature. This is referred to as *conditioning* (or *thermal conditioning*) of the glass. Conditioning is usually done either in a final zone of the glass-melting tank or in a separate unit, called a *forehearth*, attached to the exit of the melter. Heat input and heat losses are adjusted to yield glass of uniform temperature. To achieve the needed balance, the forehearth is often heated electrically or by fossil-fuel burners. Mechanical stirrers are often placed in the forehearth to improve the chemical and thermal homogeneity.

The forehearth often has more than one exit from which molten glass is delivered; thereby several different forming machines can be fed from one melter. Forehearth exit configurations vary depending on the forming process that follows. They can be simple single or multiple circular orifices of refractory material, an orifice containing a flow controlling needle, a tube or pipe, or a horizontal lip over which the glass flows. When the forming process requires delivery of discrete gobs of molten glass, automated metallic shears are generally used to cut the stream of glass into sections as it exits the melter. Often motion of a needle or plunger within the delivery orifice is synchronized with the shearing action to better control the gob weight and shape. One common type of gobbing feeder is illustrated in Fig. 6.10.

Oxidation State (Redox). When a glass is melted a chemical equilibrium is approached between the glass composition and that of the surrounding atmosphere. If there are polyvalent ions present within the glass, their average oxidation state is influenced by the partial pressure of oxygen in the atmosphere above the melt. Thus a glass melted in a fuel-fired furnace, where the atmosphere has been depleted of oxygen by the combustion process, tends to be more reduced than one that has been electrically melted in a standard atmosphere containing about 20 percent oxygen. The degree to which a glass is oxidized is often

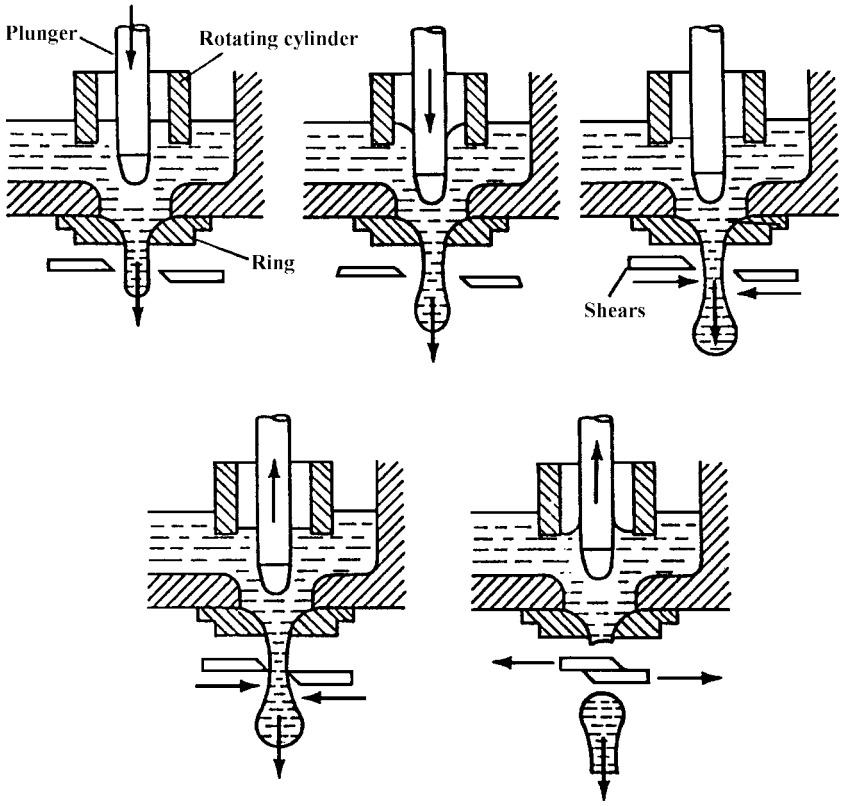

FIGURE 6.10 A typical Gob feeder process. (*From H. J. Stevens, Ref. 7.*)

referred to as its *oxidation state*. The fining equations listed above describe reversible oxidation-reduction reactions, called *redox* reactions. Thus the oxidation state of a glass is sometimes referred to as its redox state.

When the temperature of a glass melt is decreased below its melting temperature during glass manufacture, it generally has insufficient time to equilibrate with the atmospheres it encounters at the various steps. Consequently, it tends to retain the overall oxidation state that it established during melting. However, as the glass cools different multivalent elements (for example, iron and manganese) compete with each other for the available oxygen. The relative oxidation states (percent oxidized) of those elements can change with respect to each other during cooling of the glass. Thus properties such as glass color can change as a glass melt cools. In photosensitive or photochromic glasses, the photosensitivity is affected by the oxidation state of the melt, and in some cases of the solid glass.

The oxidation state of the molten glass also strongly affects the rates of melting and fining.

For redox control, sulfates (salt cake and gypsum) and nitrates are sometimes used as oxidizing agents and carbon or calumite (a reduced calcium-aluminum silicate slag from steel manufacture containing carbon and sulfides) as reducing agents. Of course, the use

of cullet that contains polyvalent coloring ions and impurities can also alter the oxidation state of a melt. Oxygen sensors, usually in the form of galvanic cell probes inserted into the melt, are being used with increasing success as devices for monitoring and controlling redox sate.

Melter-Created Glass Defects. Despite best efforts to generate a perfectly uniform glass melt, within any melter there are naturally occurring processes that oppose those efforts. These include refractory corrosion (dissolution), electrode corrosion, and preferential volatilization of some species from the melt surface. These produce localized and sometimes more global deviations from the desired glass composition. Localized composition deviations lead to inhomogeneities in the product, called cord and striae.

Other glass defects originating in the melter are solid inclusions, called *stones*. These may be particles of nonmelted batch or pieces of eroded furnace refractory. Devitrification (crystallization of the melt resulting from it having been cooled to temperatures below its thermodynamic liquidus temperature and held there for extended periods of time; see Sec. 5.2.2) is another source of solid inclusions, generally called *devit*. Bubbles and blisters may result from incomplete fining or from *reboil* (the exsolution of bubbles in an otherwise bubble-free melt, generally the result of thermally driven chemical or electrochemical reactions). Such reboil occurs either homogeneously within the melt or heterogeneously at a melt-refractory interface.

The selection rate (percentage of "good" ware) and the profitability and competitiveness of a glass manufacturing operation often depend on how successfully these melting-related defects are avoided. The design of the melter and its method of operation are key factors for success.

6.3.3 Types of Melters

6.3.3.1 General. Glass can be melted on greatly different scales, ranging from a few grams in a laboratory experiment to hundreds of tons per day in a large-scale manufacturing operation. A great deal of glass is melted on a scale somewhere in between. It is important to distinguish between continuous and discontinuous melting of glass. In a discontinuous process, the batch is placed in a container, such as a crucible, pot, or a tub-like vessel, and heated according to a prescribed time-temperature cycle to carry the contents through the melting stages described above, namely batch melting, fining, and conditioning. Homogenization may be enhanced by mechanical stirring. The vessels may be constructed of metal, refractory ceramic blocks, or cast fireclay; the stirrers generally are made of metal, fireclay, and high-density ceramic refractories, occasionally with platinum cladding.

In a continuous process, batch materials are continually fed into a melter at one location and molten glass is continually withdrawn from the melter at another location. All the steps required for melting take place approximately sequentially as the molten mass progresses through the melter, either vertically or horizontally. Large glass melters, or tanks, are generally constructed so that the melt passes through them horizontally, with melting, fining, homogenizing, and conditioning occurring progressively as the melt passes through. In some tank designs attempts are made to confine the process steps to zones separated from each other by physical walls or partial walls, or by thermal convective patterns within the melt itself.

Examples of simple discontinuous melters include crucibles of various sizes and configurations and pot melters. Crucibles are generally made of refractory ceramic materials, such as alumina, or refractory metals, such as platinum alloys. If small, the crucibles can be inserted and removed from a heated furnace and the glass delivered to a suitable forming

operation by the simple means of tipping the crucible and pouring the glass. Larger crucibles are generally fixed in position and molten glass delivered, after it has been suitably homogenized, by the means of an orifice, or tap, at the bottom of the crucible. Large crucible and tub-like containers operated discontinuously are sometimes referred to as *day tanks*.

Pot melters generally consist of single or multiple refractory ceramic pots located in a single furnace. The pots are shaped something like tall bee hives with an opening at the top front through which batch or cullet (broken glass) can be inserted and molten glass withdrawn by a ladle or blow pipe. Such pots have been used for hand glassmaking operations, for both artistic and utilitarian products, for centuries and are still used for such purposes today.

Fuel-fired continuous melters, often called *tank melters*, or simply *glass tanks*, generally consist of large refractory swimming-pool-shaped tanks, heated from above the melt by gas or oil flames from multiple burners. The top of the melter is covered by a refractory superstructure consisting of walls and a self-supporting roof called a *crown*. In the simplest version, the so-called direct-fired furnace, the gas flames pass across the top of the melt and the melt is heated by radiation from the flames and from the hot crown of the furnace. The combustion gases are then exhausted from the furnace and dispersed, generally via a tall stack and often after passing through electrostatic bag precipitators to reduce particulate emissions and chemical scrubbers to remove acidic vapors.

Such fuel-fired continuous melters can be very large. For example, a soda-lime-silica float glass melter may contain as much as 2000 tons of molten glass and deliver it at a rate of 800 T/day. The top surface area of the glass in the melter could be more than 5000 ft^2. Large container glass melters can deliver 100 to 300 tons of glass per day with melt surface areas between 600 and 2000 ft^2. Because of the rather slow forward motion of the glass, in combination with the convection-driven mixing effects, it is not unusual to expect an average of 3 to 7 days residence time for the glass in such large melters.

6.3.3.2 Heat Recovery—Regenerative and Recuperative Furnaces. Historically the heat energy required for melting glass was produced by wood or coal fires. Today the heat is generally provided by burning natural gas or oil, or by immersed electrodes utilizing electric resistance (Joule) heating.

Obviously, not all of the heat generated by a flame is transferred to the glass. Some of it is used to heat the nitrogen gas contained in the combustion air fed to the burners (which is about 80 percent nitrogen by volume) and much is carried away by the nitrogen and by the gaseous products of combustion (H_2O and CO_2) as they go up the stack. For economic reasons, especially in operating large melting tanks, it is important to recover some of the exhausted heat. This is generally done by using the exhaust gases to preheat the incoming combustion air, either regeneratively or recuperatively, in rather massive refractory heat exchangers.

In a cross-fired regenerative glass furnace, of the type first developed by Siemens toward the end of the nineteenth century (see Fig. 6.11), the furnace is fired for a period of time by a row of burners along one sidewall, while the hot gases are exhausted from the opposite wall and passed through large chambers, called *regenerators*. The regenerators consist of stacks of firebrick in open three-dimensional checkerboard patterns called *checkers*, which absorb heat. When the checkers have become suitably heated, the burners are shut down. A set of burners on the opposite side of the furnace is then fired and fed with combustion air drawn in through the hot regenerators. The combustion gases are now exhausted from the opposite side of the furnace through another set of regenerators. This process is reversed about every 15 to 20 minutes.

In a *recuperative* furnace, the burners are fired continuously and heat is exchanged continuously in the exhaust system, where the exhaust gases flow outward through a central tube or tubes with the incoming air channeled along the outside of the tubes.

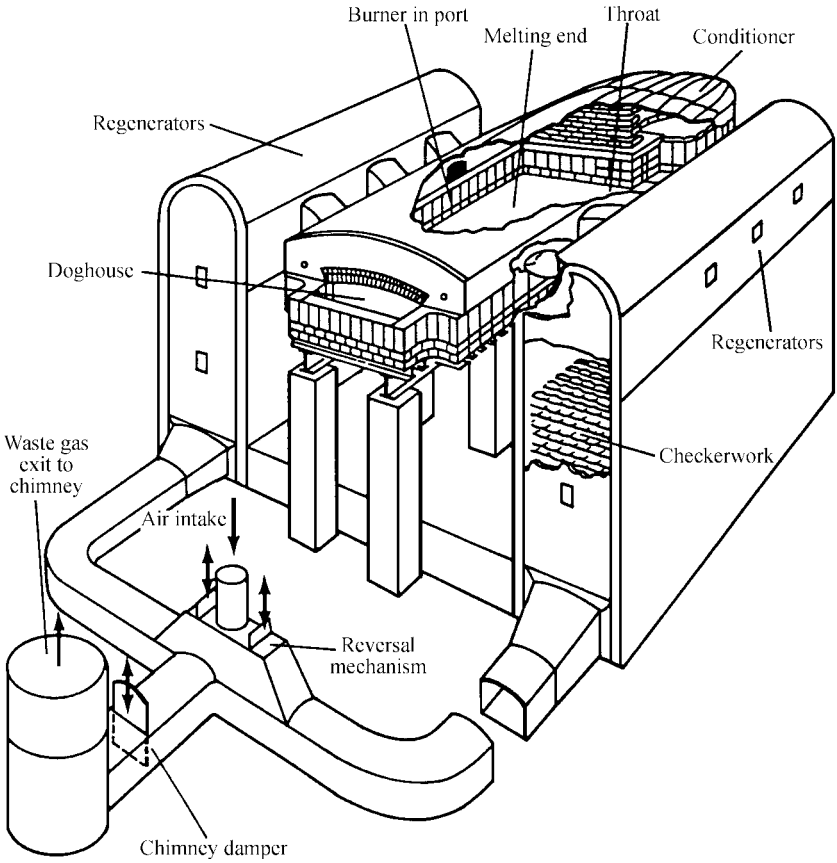

FIGURE 6.11 Cross-fired regenerative-type furnace construction typical of container glass melters. [*From F. E. Woolley, Ref. 7; reference W. Trier, Glass Furnaces (Design, Construction and Operation), trans., K. L. Loewenstein, Society of Glass Technology, Sheffield, England, 1987.*]

6.3.3.3 Construction Materials/Refractories. The refractory materials serve three purposes: They contain the glass melt, provide thermal insulation and heat transfer as needed, and act as key structural elements of the tank. The refractories are generally held in place by an open steel framework, but much of the mechanical load is born by the refractory materials themselves. Crowns are often self-supported refractory structures. The refractories must withstand or resist high temperatures, heavy loads, abrasion, and corrosion.

Types of oxide refractories used in glass melters are:

1. Clay refractories (generally used for insulation)

- Fireclay: kaolinite ($Al_2O_3 \cdot 2\ SiO_2 \cdot 2H_2O$) plus minor components; classified as low-, medium-, high-, or superduty; (25 to 45 percent Al_2O_3)
- High alumina (50 to 87.5 percent Al_2O_3)

2. Nonclay refractories (generally used for glass contact or furnace superstructure)

- Magnesia (MgO)
- Silica (cristobalite and trydimite)
- Stabilized zirconia
- Extra-high alumina (more than 87.5 percent)
- Mullite ($3Al_2O_3 \cdot 2SiO_2$)
- AZS (alumina-zirconia-silica) containing 30 to 42 percent zirconia
- Zircon ($ZrO_2 \cdot SiO_2$)
- Chrome-magnesite and magnesite-chrome (combinations of Cr_2O_3 and MgO)

Classification based on method of manufacture (in order of increasing density):

- Bonded
- Sintered (sometimes densified by cold isostatic pressing before firing)
- Fusion-cast (cast as blocks from arc-melted raw materials); also referred to as *fused* or *fused cast*

Many factors affect the choice of refractory for a particular application. These include melting temperature, thermal conductivity, mechanical strength, creep resistance, resistance to corrosion and spalling, to name a few. Generally, different refractories are used in different regions of a glass-melting tank, because the requirements are different. However, *the ultimate design consideration* is resistance to corrosion by molten glass and by the hot gas atmosphere within the melter. Corrosion determines tank lifetimes and affects the rates at which certain glass defects (such as stones) are generated. In selecting a refractory the considerations are, in order, (1) glass quality, (2) tank lifetime, and (3) initial cost.

Many different corrosion mechanisms operate within a melter. The types and severity depend on the glass composition, the composition and microstructure of the refractory, and the temperature. Corrosion rates tend to increase dramatically with temperature. This is an important reason why different refractories are often selected for different portions of the melter. It is also an important reason why the harder (higher melting temperature) glasses are generally more expensive to manufacture. Corrosion types include:

- *Front surface attack* (frontal attack). This is direct attack at the glass/refractory interface. Its mechanisms include alkali diffusion into the refractory with consequent fluxing and dissolution of the refractory crystals. Porous refractories are generally more susceptible.
- *Melt line corrosion* (attack where glass surface, air and refractory meet). Corrosion at this location is enhanced by localized convection currents and fluctuations in glass level within the melter.
- *Upward drilling*. This form of corrosion occurs where bubbles form under horizontal refractory surfaces, such as throat cover blocks or submerged horizontal refractory joints. Corrosive vapor species concentrate in the bubbles. As with melt line corrosion, the greatest corrosive activity is believed to take place where the vapor, refractory, and glass touch.
- *Downward drilling*. This type of corrosion results when droplets of molten metal settle on the bottom of the tank. Sources of metal can be contaminants in batch raw materials or cullet, chemical reduction of certain glass components (such as lead oxide), and even tools or metal parts accidentally dropped into the tank.

Glass Contact Refractories. The most common glass contact refractories include:

Fused AZS (alumina-zirconia-silica). This is the most common today (41 percent ZrO_2 in high-wear areas and electrode blocks, as opposed to the less expensive 34 percent variety). The oxidation state is critical (the refractory contains a residual glassy phase which, if produced in reduced condition, will oxidize in use, swell, and exude from the brick).

Dense sintered zircon (ZrO_2-SiO_2). Used in some low-expansion borosilicate melters.

Clay, fused alumina, bonded AZS, and dense sintered alumina. Used for lower-melting specialty glasses.

Typical glass contact refractories used for melting various glass types are:

- *Container glass*. Fused AZS, life 8 to 10 years; also, fused α-β alumina. Finer bottoms are sometimes bonded AZS, zircon, and clay.
- *Float glass.* Fused AZS in melting zones; fused alumina in conditioner zones. Life 10 to 12 years.
- *Hard borosilicates.* Fused AZS and zirconia, sometimes dense sintered zircon.
- *Fiberglass wool.* Highly corrosive, melted electrically in fused chrome-AZS or fused alumina-chrome refractories (coloration due to chromium is of little consequence in this application).
- *E glass (textile fiber).* Less corrosive, melted in dense sintered chrome oxide.
- *Lead crystal.* Tendency to electric melting in AZS.

Several refractory side wall design considerations are based on corrosion concerns. First, the thicker the wall, the less heat lost and the lesser the energy consumed. But thicker walls create a smaller temperature gradient, allowing chemical attack to penetrate more deeply into the refractory. Thus the design thickness of a wall must be a compromise between heat loss and wear. To give all sections of the wall approximately equal lifetimes, thickness and type of refractory are often varied from location to location. These techniques are sometimes referred to as *zoning by thickness* and *zoning by type*.

To avoid melt infiltration of horizontal refractory seams and the consequent increased opportunity for upward drilling of corrosion, glass contact wall refractories are often large, full-height blocks arranged adjacent to each other in a "soldier" course fashion. However, if multiple courses are required, close-fitted diamond-ground horizontal joints can help minimize melt infiltration. Similarly, to avoid horizontal joints, the paver blocks composing the top layer of the tank bottom are butted up against the side blocks, not placed under them.

Superstructure and Crown Refractories. The superstructure, which includes all furnace walls above the melt line and the crown, is subject to corrosion by aggressive vapor species such as NaOH, KOH, PbO, and HBO_2, batch dust particles, liquid condensates and liquid reaction products running down from refractories higher up. Superstructure temperatures in fuel-fired furnaces are often 60 to 100°C hotter than the glass. Typically, walls and ports are made of fused AZS from the back wall (where the batch enters) to the hot spot; fused β-alumina is used downstream. But these are not hard and fast rules. Crowns typically consist of sintered silica block. Although silica crowns are attacked by alkali vapors, the drips are homogenized into melt. Crown life is more of a concern. This is especially true with gas-oxy firing (more aggressive vapors, see Sec. 6.3.3.5), in which case more costly refractories may be justified. Silica and alumina blocks should never be in

direct contact—for example, at the joint where the crown and superstructure walls meet (they will react); zircon is used as a buffer.

Regenerative Heat Exchanger Refractories. Special refractory considerations are needed because of the large temperature gradient (top-bottom) within the checker chambers and the corrosive nature of the exhaust gases. As the gases cool, a temperature is reached where the corrosive vapors condense on the refractory surfaces, enhancing the corrosion. Fine batch particles carried over with the exhaust gases also tend to react with and corrode the regenerator refractories. High thermal conductivity and heat capacity are also important characteristics. Checker construction for a typical soda-lime-silica melting tank consists of top third—bonded 95 to 98 percent MgO bricks; middle third—lower magnesia content bricks; bottom third (where alkali vapors condense)—sintered chrome (chromic oxide) or magnesium-chrome bricks.

A relatively new approach to checker construction, especially in Europe, is with special interlocking shapes (cruciforms) of AZS or high-alumina fused cast refractories.

6.3.3.4 Electric Boosting and All-Electric Melting. Crucibles, pots, and day tanks for glass melting can be heated in electric furnaces where the heat is generated by resistance heating in windings or bars. In come cases heat is produced by the flow of electricity through the metal crucible itself and in others by the flow of electricity through the molten glass, which is a moderately good ionic conductor at high temperatures, between submerged electrodes.

These principals are applied to varying degrees in large continuous melters as well. In some fuel fired furnaces, electrodes are installed in the walls below the glass line so as to provide a source of heat below the batch layer, thus the batch is actively melted from below as well as above. By such means the melting rate for the tank can be increased, or boosted, leading to the term *electric boosting*. Resistance heating by external windings or bars is often used to control temperatures at the orifice or delivery tube by which the molten glass leaves the melter.

Sometimes all the heat required for melting is supplied electrically within the molten glass. In this case, electrodes are positioned as plates at the walls of the furnace, or as water-cooled metal rods extending upward through the bottom of the furnace. The electric current passes from electrode to electrode, through the glass, the amount of heat generated depending on the applied voltages, the shape and spacing of the electrodes, and, very importantly, the electrical resistivity of the molten glass. In this case of all-electric melting, the batch components are melted solely by heat flow up from below. It is possible, and desirable, to maintain a continuous layer of batch across the top of the melt, eliminating the need for a refractory roof or crown to contain and reflect the heat. However, in many cases the crown is there for other reasons, but is cold. Hence, all-electric melting in this manner is sometimes referred to as *cold-top* or *cold-crown* melting.

It should be noted that the electrical resistivity of a pile of nonmelted batch, or even a glass melt at temperatures well below 1000°C, is too great to allow for efficient heat generation. Consequently, all-electric melters are started in a more or less traditional way by fossil-fuel burners and a hot crown. Once the molten glass has reached sufficient temperature, the burners and sometimes the crown are removed.

Cold-top melting is valuable for two reasons. First, the batch layer acts as a thermal insulating blanket (the batch blanket), which helps reduce heat loss out the top of the melter (thus enabling it to operate cold-top). Second, the top layers of the batch blanket, being much cooler than the molten glass below, act to condense volatile vapor species which might otherwise escape into the atmosphere. This is especially valuable for fiberglass and other specialty glass melting where the compositions contain fluorides and other very volatile, and sometimes unhealthy, components.

Electrodes are made of materials such as carbon, tin oxide, molybdenum, and platinum, the choice depending on the temperature of operation and the composition of the glass being melted. Melt temperatures, temperature gradients and convection currents are greater at and near the electrodes, therefore better refractories (higher temperature, more corrosion resistant) are required at these locations.

6.3.3.5 Oxygen for Combustion. Over the past decade, there has been a trend toward the use of oxygen, instead of air, in combination with natural gas, to heat fuel-fired furnaces. This is called *oxy-fuel firing*. It has several advantages. First, since one is not using air with its 80 percent nitrogen content, much less polluting NO_x gases are produced. In the face of increasingly stringent air quality legislation, this factor alone is often sufficient to justify conversion to oxy-fuel firing. Second, since there is not the large volume of nitrogen to heat and expel from the furnace, much less waste heat is generated than with gas-air. Some operations have been able to eliminate the massive, costly regenerators as a consequence. Third, higher flame temperatures are possible. Fourth, as claimed by some manufacturers, more stable furnace operation with an associated improvement in glass quality is achieved. This is especially the case when regeneration, with its inherent periodic reversals of gas and heat flow, is eliminated.

There are some disadvantages to oxy-fuel firing. One is the need for liquid oxygen storage or oxygen generation on site. A second is that, without the large volumes of air moving through the furnace, the concentrations of water vapor (a product of combustion) and corrosive volatile species from the melt are much higher, in some cases leading to increased deterioration of the refractory superstructure.

6.3.3.6 Furnaces for Specific Applications

- *Container glass*—typically cross-fired regenerative; maximum melt temperatures about 1600°C; large, up to 500 T/day
- *Float glass*—typically cross-fired regenerative; no bridge wall, but rather an open-surfaced narrow region called a "waist" to keep inhomogeneities running parallel to the surface of the glass sheet; maximum melt temperatures about 1600°C; larger, up to 800 T/day
- *Fiberglass*—smaller gas-fired recuperative or all-electric
- *Lead crystal*—small electric-boosted or all-electric
- *Hard borosilicates*—tending to all electric or heavily boosted regenerative; melt temperatures above 1600°C
- *Aluminosilicate glass-ceramics*—regenerative gas-fired; temperatures near 1700°C required for efficient fining
- *Optical glass*—small fuel-fired or electric heated; fining and conditioning often done in platinum tubes to avoid refractory contact and resulting inclusions and inhomogeneity

With the advent of oxy-fuel, or more specifically, gas-oxygen firing, many of the above listed regenerative and recuperative furnaces have been converted to use this new technology. However, at this writing, float glass manufacturing is just beginning to convert to gas-oxygen firing.

Trends. As is typical of most industry, new designs are aimed at lower overall cost of operation (the calculation of which includes initial cost, melter lifetime, and costs of repairs as well as the daily operating costs), less energy consumption, and less overall environmental impact. Lower cost almost always must be achieved in combination with improved glass quality and less adverse environmental impact.

6.4 GLASSMAKING II—GLASS FORMING

The term *forming* collectively refers to all the processes of glass making used to form a solid object or product from the molten glass. Historically, all glass objects were formed by hand with relatively simple implements. Over time, the techniques were modified, automated, and scaled up. While there are several glass-forming methods in use today that have no precedent in early glass history, most still bear important resemblance to their forebears. Because of space limitations here, this section will describe only processes used in today's manufacturing plants, and the early hand-forming operations, when relevant. Little attention will be paid the many processes that have intervened. We will first discuss processes involving molds.

6.4.1 Blowing

By far containers (bottles and like products) account for the largest volume of glass production. Almost all these products are manufactured by some form of a blowing process.

Historically, glass containers have been blown to shape by gathering a gob of molten glass on the end of a hollow iron pipe, the blowpipe or blowing iron, and blowing a puff of air into the soft glass to form a bubble, which is gradually expanded and worked into shape by the combined effects of gravity and the forces of tools pressed against it. Generally the blowing iron, with the soft glass attached, is rotated to balance the effects of gravity and provide an axial symmetry to the product. While useful containers of remarkably repeatable shapes and dimensions can be created in this manner, for rapid and precise production it is preferable to use a two step process. First, a hollow preform, called a *parison*, is prepared by a simple blowing process. Second the parison is blown to the final shape in a mold.

This process has been automated to a very high degree in modern times to the point where more than a dozen containers per minute can be generated from each mold. Generally, rotating split molds are used for shapes involving bodies of revolution whenever visible seam lines from the molds are undesirable, such as for light bulbs or high quality drinkware. Stationary split molds must be used for containers having handles, flutes, or other nonrotationally symmetric shapes. The rotating split molds are generally paste molds, called that because their molding surface is coated with a thin layer of cork or similarly permeable substance which is saturated with water after each molding cycle. When the mold surface is contacted by hot, molten glass, a steam layer results which provides a low-friction layer between glass and mold, giving the product a highly polished appearance, without seam lines.

The stationary molds are generally hot iron molds. These metal molds are operated at a temperature hot enough to keep the molten glass from being chilled so quickly that surface cracks or "checks" result, but cold enough to quickly extract heat from the glass and allow it to become rigid before removal. Any metal mold surface defects as well as the mold seam lines are transferred to the ware, but production rates can be much faster than with paste molds. Also on the plus side, intentional designs such as a logo can be molded or embossed into the glass surface.

When blowing by a hand-type operation, the final product must be separated from the blowing iron, usually by cracking it off. This leaves a rough surface that must be properly finished by grinding or by *fire polishing*, a process step that involves locally reheating the glass to a point where it will flow to a smooth surface under the influence of surface tension. In modern automated container production, free gobs of glass are handled in the molds so separation from a blowing iron is not required. Two common processes are called

blow-and-blow and *press-and-blow*, depending on the method used to form the parison. Blow- and-blow is generally used for narrow-neck containers such as beverage bottles. The parison is blown in one mold in a way that forms the neck, then, held by the relatively cold newly formed neck, is transferred into a second mold to blow the body of the container. One of the more common machines featuring these operations is Hartford Empire's, now Emhart Corporation's, IS (individual section) machine which may have as many as 12 sections driven in tandem by a cam with overlapped timing, or more recently, by electronically synchronized operation, each section operating on as many as four gobs. Processing takes about 10 seconds per section. In addition to speed, an advantage of the IS machine (as opposed to a rotating turret machine) is that the machine can be programmed to run the remaining sections while one is being repaired. The operation of a single two-mold IS section is shown in Fig. 6.12.

Press forming of the parison before blowing to final shape is used for wide mouthed containers such as food jars. Press forming will be described in the next section. For container manufacture, although pressing of the parison is complicated by the need for an additional tool, the plunger, this disadvantage is offset by the a product's more uniform wall thickness, hence more efficient utilization of glass and lighter weight, than could be made by blow-and-blow.

A very high-speed process for blowing light bulb envelopes and the like, known as the *ribbon machine*, was developed in the 1920s by Corning Glass Works (now Corning Incorporated) and is still in use worldwide. In this machine a stream of molten glass is continuously fed between a set of rollers, one flat, the other with pocket-like indentations. These rollers form a ribbon of glass several inches wide containing regularly spaced circular mounds of glass down the centerline. The parison for each light bulb is formed by inserting a synchronously moving blow head (analogous to a blowpipe) into each mound of glass and blowing it through a synchronously moving orifice plate. As the ribbon travels horizontally along the machine, it is enclosed in an also synchronously moving rotating paste mold and the blowing process is completed. The moving molds open and swing away to allow the finished glass envelope to be cracked off the ribbon at the machine exit. The operation of the ribbon machine is illustrated in Fig. 6.13. Incandescent lamp envelopes, for example, A-19 60-watt bulbs, can be made at speeds in excess of 1200 per minute, on a single machine, by this technique. Small automotive and other specialty lighting bulbs can be made at rates exceeding 2000 per minute.

6.4.2 Pressing

In simplest terms, pressing, or press forming, of glass involves placing a gob of molten glass in a hot metal mold and pressing it into final shape with a plunger. Sometimes a ring is used, as illustrated in Fig. 6.14, to limit the flow of glass up the side of the mold and produce a rim of well-controlled shape. The process steps can be performed entirely by hand, or be fully automated. It produces more accurate and controllable wall thickness distributions than blowing, but is generally limited to open, moderately shallow articles such as dinnerware, cups, baking dishes, sealed-beam headlamp lenses, and television panels and funnels, or for solid objects. Pressing is capable of generating intricate and accurate patterns in the glass surface, such as found in sealed beam spotlight, floodlight, and automotive headlamp lenses and in street and traffic light refractors and lenses.

Large objects, such as 27- and 35-in (diagonal) color television bulb panels weighing more than 25 pounds can be made by automatic pressing equipment.

Glass is generally pressed at a viscosity between 2000 and 3000 P with an applied pressure of about 100 lb/in^2 of article surface area. For large television panels, the total force on the plunger can exceed 20 tons. Temperature control of the molds and plunger

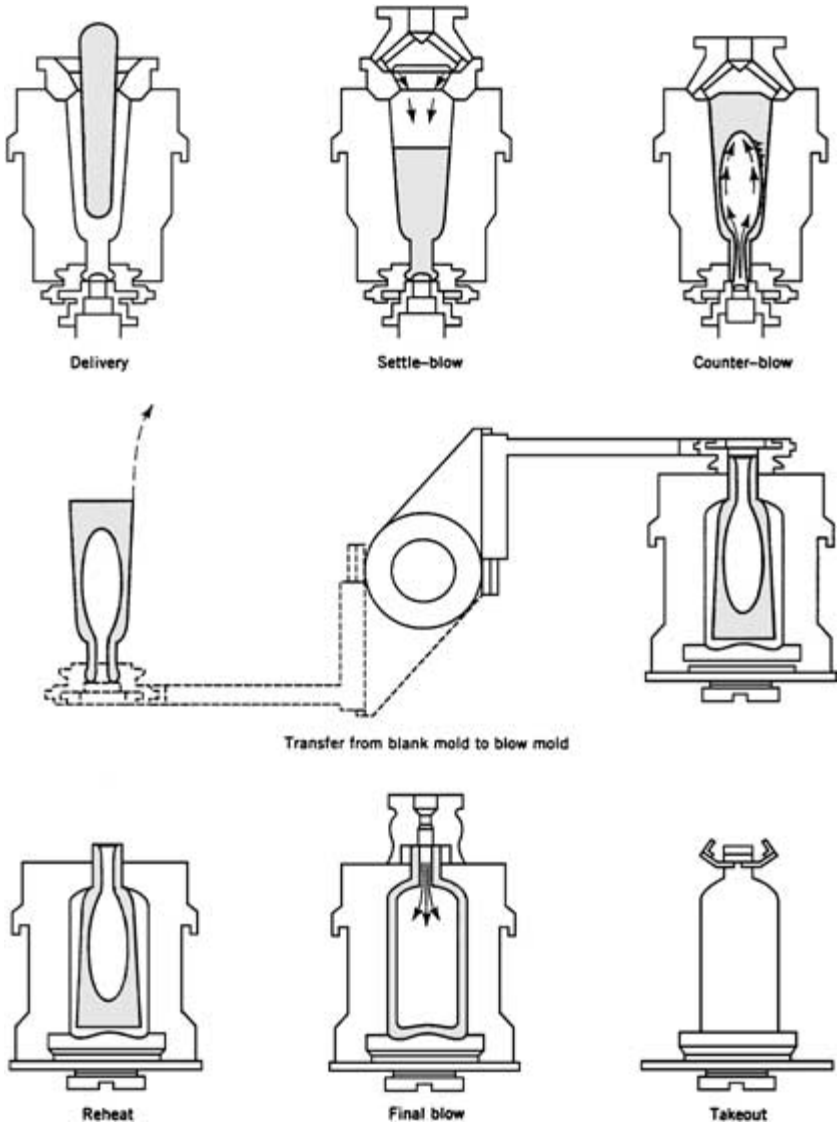

FIGURE 6.12 The H.E. individual section blow-and-blow machine. The gob is delivered into a blank mold, settled with compressed air, and then preformed with a counter-blow. The parison or preform is then inverted and transferred into the blow mold where it is finished by blowing. (*From* "Glass," D. C. Boyd, P. S. Danielson, and D. A. Thompson, in *Kirk-Othmer Encyclopedia of Chemical Technology, 4th ed., vol. 12*, John Wiley & Sons, New York. 1994, p. 602; reference W. Giegerich and W. Trier, *Glass Machine Construction and Operation of Machines for the Forming of Hot Glass*, trans. N. J. Kreidl, Springer-Verlag, Berlin, 1969.)

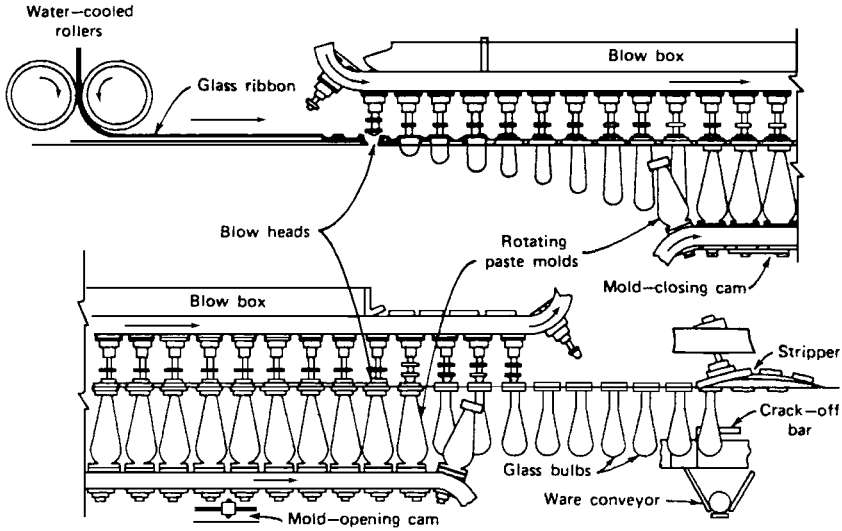

FIGURE 6.13 The "ribbon machine" used for light bulb–envelope manufacture. [*U.S. Patent 1,790, 397 (Jan. 27, 1931), W. J. Woods and D. E. Gray. Courtesy of Corning Incorporated.*]

is crucial: Too cold leads to brittle fracture of the glass under the pressing forces; too hot leads to sticking of the glass to the mold surface, requiring it to be physically broken free. Vents within the mold body, through which cooling air or water may flow, are often used to maintain uniform temperature distribution across the mold surface.

6.4.3 Casting

Casting is a relatively little used process, found mostly in hand shops and in the production of very large pieces of glass such as glass sculptures and astronomical telescope mirrors. For the large pieces, glass is poured into hot ceramic refractory molds (often sand with a small amount of binder) that are slowly cooled after the mold is completely filled. Alternatively, chunks of rigid glass may be placed in a cold mold and together raised in temperature until the glass is sufficiently fluid to flow and fill the mold. This latter method is more susceptible to entrapment of bubbles. Generally, slow cooling and long annealing times are required. The mold can be used only once. The glass surfaces in contact with the mold are generally rough.

6.4.4 Centrifugal Forming

Centrifugal forces have often been utilized by the glassmaker. A glass bubble on the end of a blowing iron can be elongated by swinging the iron back and forth to aid gravity in elongating the bubble to generate the parison. A thick-walled bubble on the end of a rod can be cut open at the point opposite to the rod, and the rod rotated to generate sufficient centrifugal force to open the bubble and spin it into a relatively flat, circular sheet of glass. This is one of the earliest flat glass manufacturing methods, the crown process. Glass made this way

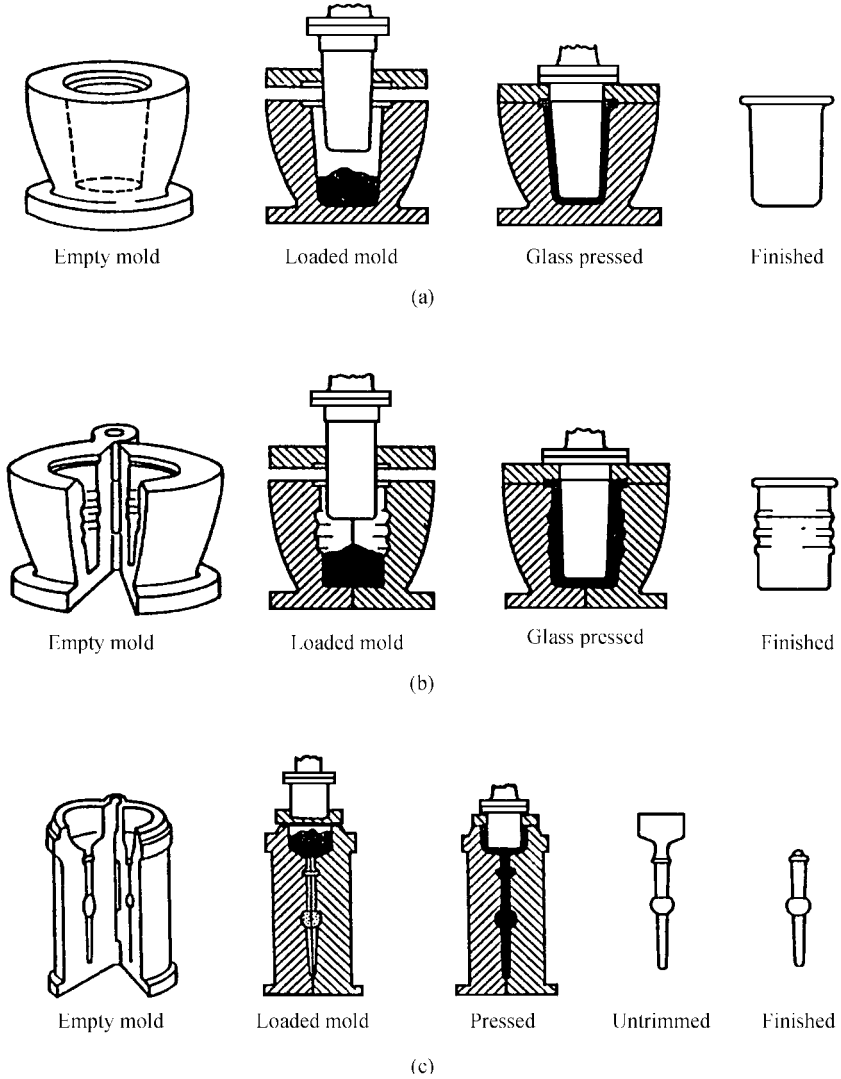

FIGURE 6.14 Pressing glass with mold, plunger, and ring. ("Glass," J. R. Hutchins, III, and R. V. Harrington, in *Kirk-Othmer; Encyclopedia of Chemical Technology, 2d ed., vol. 10*, John Wiley & Sons, New York, 1966, p. 558; reference E. B. Shand, *Glass Engineering Handbook*, McGraw-Hill, New York, 1958, p. 164.)

is often found in old European churches. A droplet of very fluid glass placed at the center of a rotating turntable will also spread under centrifugal force: a process utilized in spin coating or spin casting. The latter is sometimes simply called *spinning*.

If molten glass partially fills a rotating container such as a mold or a crucible, the molten glass will tend to climb the walls propelled by the centrifugal forces, giving the glass surface

the shape of a paraboloid of revolution. This method, called centrifugal casting, is used to form the parabolic shapes for thin astronomical telescope mirrors. It has also been used to spin, rather than press, large, deep television tube funnels and glass-ceramic missile radomes. Six- to eight-meter diameter mirror blanks are spun at about 10 r/min, a television bulb funnel at about 200 r/min. In the 1960s Corning Glass Works used this spinning process to make large, 56-in-diameter glass hemispheres of 1.5-in wall thickness for use in undersea exploration.

A continuous centrifugal process of forming tubing from very short (steep viscosity) glasses or easily devitrifiable glasses has been devised. It is somewhat analogous to the Danner tubing process (see below) except that the stream of glass is fed into the open end of an inclined, rapidly rotating pipe. The very fluid entering glass is flattened against the wall and the adjacent layer of previously deposited glass and is maintained in position by centrifugal forces until it is cooled to sufficient rigidity to be withdrawn from the end of the pipe.

6.4.5 Rod and Tube Drawing

Drawing is the term for a process in which a preshaped blank, or glass flowing from an orifice, is elongated (stretched) in one dimension while diminishing in orthogonal dimensions without losing its cross-sectional characteristics.

The above statement is exactly true for the drawing of cane (rods) or fiber. It is not so for tubing or sheet, where the ratios of inside to outside diameter or width to thickness are not the same as they were at the root. (The solid section of the blank or the glass at the orifice is often referred to as the "root.")

Redrawing is the specific case of drawing from a solid preform (or blank), rather than from a melt. This involves reheating the end of the blank to provide glass sufficiently fluid to be stretched and attenuated. In a continuous process, the blank is replaced at the volume rate it is used up by gradually feeding it into the hot zone of the redraw furnace.

In a steady-state process the volume flow per unit time, the quantity Q, is constant and equals A (area) times v (velocity) at any point in the process. As we will show, A is a very important parameter in the tube drawing process.

Tube Drawing Processes. In a hand process, a gob of glass is gathered on the end of a blow pipe, a bubble is blown within the glass, and an assistant attaches a rod to the side of the gob opposite the blow pipe (or grabs the gob with a pair of tongs) and walks across the room to stretch out the glass and the bubble within it. The final diameter of the resulting tubing, and its wall thickness, depend on several factors including how fast the assistant walks (compared to how rapidly the glass cools) and how much pressure the blower maintains in the bubble. If faster cooling is needed, a second assistant may fan the tubing as it is drawn out. After the drawing step is completed, the hollow glass tubing is cut away from the bulky pieces at each end. The air pressure resists tubing collapse from the draw forces and surface tension. There is only about 10 to 20 percent glass utilization. The rest of the glass remains on the blowpipes or is of unusable dimensions and is generally recycled as cullet. The process is highly labor intensive.

The Danner process, named after its inventor Edward Danner, was developed by the Libbey Glass Company. It is one of the oldest continuous tubing drawing processes still in use today and is the common method for forming fluorescent lamp tubing. The process is unique in the manner of preparing the root of glass from which the tubing is drawn. See Fig. 6.15. A ribbon-shaped stream of glass is fed onto a slowly rotating (about 10 r/min) hollow clay (or metal) mandrel, inclined downward perhaps 15° from horizontal. The glass stream flows onto the mandrel at a viscosity about 1000 P, wraps around the mandrel and overlaps itself to form a cylinder, which is smoothed by the forces of gravity

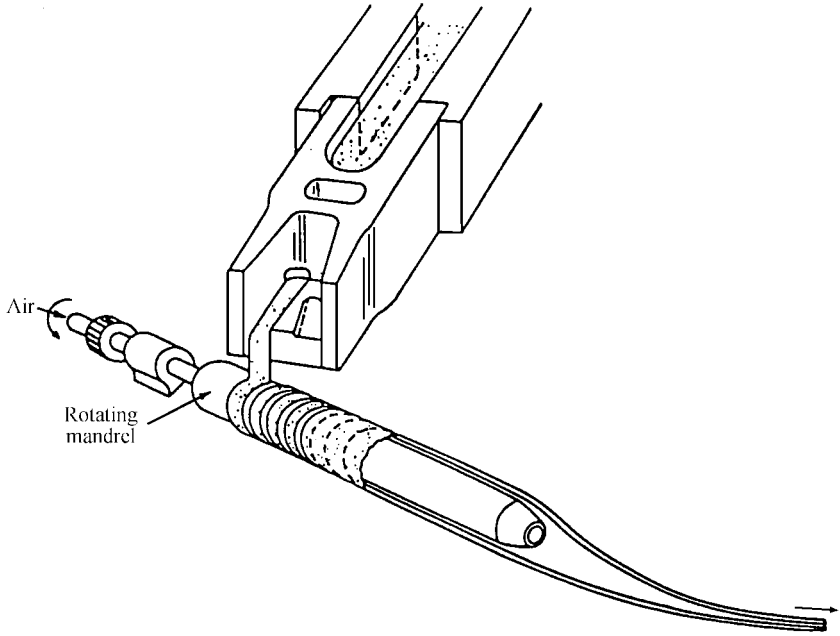

FIGURE 6.15 Rotating mandrel used in Danner tube drawing process.

and surface tension. The glass cools (to a viscosity of about 50,000 P) as it moves along the mandrel and is drawn off the mandrel end in a horizontal direction, forming a catenary. Air is fed through the mandrel, so the latter acts somewhat like a hand blow pipe with a continually replenished supply of glass. The tubing is drawn (stretched to smaller dimensions) by a tractor device, located many feet from the mandrel, and is cut into lengths after it passes through the tractor.

The Danner process is capable of drawing 1/16-to 2.5- in-diameter tubes. Because of temperature nonuniformity, coupled with gravity effects, Danner tubes often exhibit some ovalness and wall thickness (called *siding*) variations. Solid rods of similar diameters can be drawn by stopping the airflow through the mandrel, or even drawing a slight vacuum. Composition variations can produce hairpin-shaped cord defects.

The *Vello* process, after inventor Sanchez Vello, was developed by Corning Glass Works and dates back to the early part of this century. Here the glass is delivered from the glass-melting furnace at about 100,000-P viscosity, through an annular orifice created by the spacing between a conical bowl and a bell-shaped blowpipe, called the *bell*, centered within the bowl. See Fig. 6.16. The drawn tubing first extends vertically downward then turns horizontally, following a catenary curve as it stretches under its own weight, then is transported on a runway of V rollers, often several hundred feet long, as the glass cools. As with Danner, the tubing is cut into lengths after it passes through the tractor at the end of the runway.

The Vello process allows drawing of precision-bore tubing, such as for thermometers and burettes. It is fast (for example, eight hundred 52-in sticks/min at a 2000 lb/h flow rate) and can draw tubing of diameters up to 3 in without significant oval.

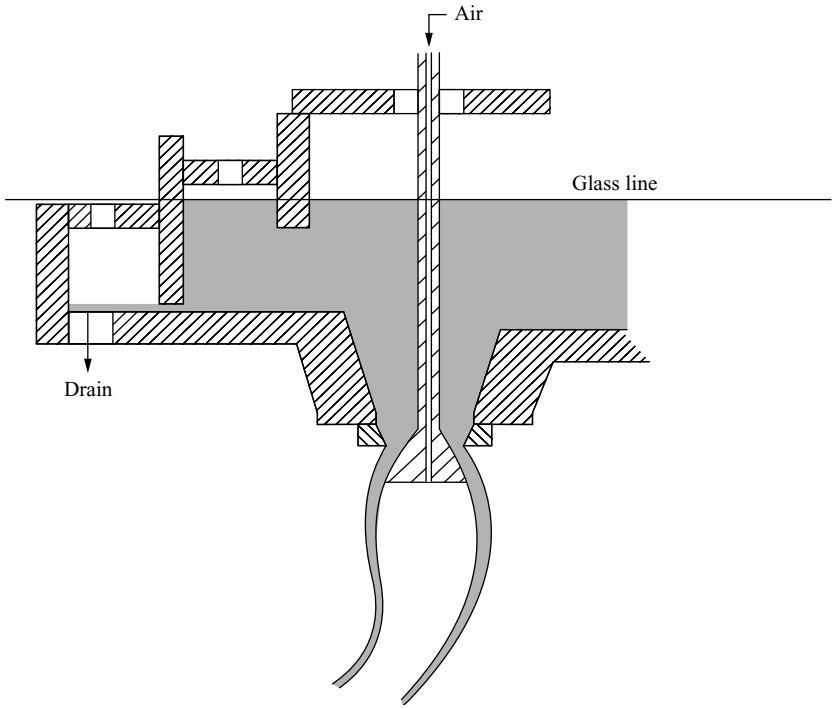

FIGURE 6.16 Bell and bowl arrangement used in Vello tube drawing process. (*From lecture notes. E. H. Wellech, Corning Glass Works, 1963, courtesy of Corning Incorporated.*)

Control of diameter and wall thickness is based on a mathematical equation relating volume flow of glass, tubing velocity, and tubing cross-sectional area, which determines how fast one must run the tractor pulling the tubing to give the requires cross-sectional area of the glass in the tubing. This area is given by

$$Q/v = A = \pi w(D - w)$$

where Q = volume flow of glass from the melter
v = speed of the tractor
w = wall thickness
D = outer diameter of the tubing

Only in the case of a rod, where $w = D/2$, is the diameter uniquely determined by the pulling speed. In all other cases, the diameter and wall thickness interact, and their ratio is maintained within specification by the pressure of the air flowing through the tubing, just as with hand drawing.

The *downdraw* tubing process is essentially a vertical Vello. The glass tubing is cut off one or more floors below the draw. It is useful for tubing too large in diameter or wall thickness to be successfully turned horizontally (i.e., without breaking or deforming from cylindrical shape). For example, Corning has drawn 6-in-diameter, $^3/_8$-in-wall borosilicate

tubing for Pyrex™ brand pipe by this process. Molds and dies can be added to give controlled cross-sectional shapes.

The *updraw* tubing process is analogous to the updraw processes, flat or cylinder, used to manufacture sheet glass, which will be described in the next section. The air pressure needed to keep the tube bore open is supplied from below through a refractory cone positioned in the melt just beneath and on axis with the drawn tubing. The height of the cone helps control the tubing wall thickness.

Continuous updraw of thermometer tubing with enclosed colored glass ribbons is only slightly more complicated.

6.4.6 Sheet Drawing

Sheets of glass can be drawn either upward or downward from a bath of molten glass by a tractive mechanism, provided a method can be found to maintain the root of the draw in a fixed position at constant dimensions. For a downdraw process, the root is essentially a rectangular slot in the bottom of the melter. Molten glass flows from this slot under the force of gravity as a wide, thick sheet. Below the melter the sheet is cooled to become rigid, after which its weight is supported by pairs of horizontal rollers. As the glass is cooled by radiation beneath the slot-shaped orifice, the rollers stretch it to the desired final thickness. The sheet also tends to become narrower in width during stretching, but this effect can be minimized by the judicious use of edge coolers and edge rollers to pull the edges of the sheet outward. These edgewise forces, while maintaining the desired sheet width, also help maintain its flatness. One is essentially pulling on a stretched membrane. The formed sheet is lowered through a heated annealing zone (annealer) and cut into separate sheets below, often in a subbasement or a specially excavated pit.

A disadvantage of the process is that any nonuniformities in the slot, such as might be caused by erosion, or corrosion, lead to vertical streaks in the glass surface. In part to overcome this difficulty, and in part to have better thickness control over the resulting sheet, Corning Glass Works (now Corning Incorporated) developed its fusion downdraw process. In this process molten glass is fed into one end of a slightly inclined refractory trough at a viscosity of about 40,000 P and allowed to overflow both sides, as shown in Fig. 6.17. (Sometimes this trough is called the *overflow pipe*, for obvious reasons.) The outside of the trough tapers to a line at the bottom where the two layers of overflowing liquid meet and fuse together forming the root of the draw, hence the name *fusion*. The outside surfaces of the glass are generated from within the interior of the melt and are therefore never subsequently in contact with other materials; thus they are pristine and defect-free. A key element of Corning's initial patent for this process is the mathematical design of the tapering cross-sectional profile of the trough, which, in combination with the incline of the top of the trough, assures that the volume flow of glass over the pipe is uniform along its length. Along with a method to precisely control the temperature along the root of the draw, this assures uniform sheet thickness across its width.

Below the root, the process is somewhat similar to a downdraw from a slot. One notable difference is that the glass at the root is far more viscous. Having been cooled to a viscosity of 500,000 P or more as it descends the tapered lower refractory of the trough, it must be pulled downward with greater tensile stress. The pulling forces are provided by the weight of the sheet and edge rollers only, so the glass surface is not subject to roller marking. A wide range of thickness may be made, ranging from less than a millimeter to greater than a centimeter. This process is currently used to manufacture thin flat glass of exceptional

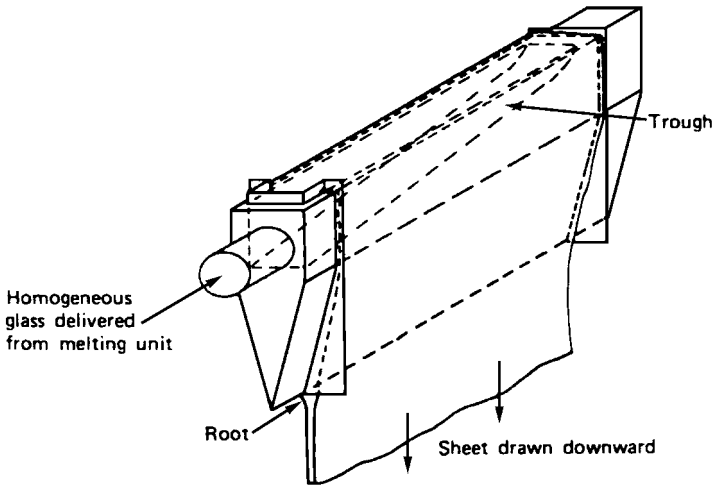

FIGURE 6.17 Illustration of Corning's "fusion" overflow sheet drawing process. [U.S. Patent 3, 338, 696 (Aug. 29, 1967). *Courtesy Corning Incorporated.*]

quality for active-matrix liquid crystal displays (AMLCDs) for flat-panel computer screens and televisions.

A variety of updraw processes have also evolved. The *Fourcault* process, invented in 1910 by the Belgian Emile Fourcault, uses a partially submerged refractory block, containing a long machined slot, to form the root of the draw. This block is called the *debiteuse*. The molten glass that forms the root of the draw is forced up through the slot by the buoyant force of gravity. The draw is started by lowering a metal mesh, called the bait, to the slot, then, once it is wetted by the glass, drawing it upward to form the sheet. Once the process has been started, the sheet of glass is pulled upward by pairs of horizontal rollers, through an annealing zone, and cut into separate sheets above. The bath of molten glass is held at temperatures providing a viscosity of about 100,000 P. Water cooled edge rollers, located somewhat above the melt surface, help prevent the sheet from narrowing in width as it is pulled upward. This process is still in use many places throughout the world for the manufacture of window glass. Process disadvantages include vertical streaks, called *peignage* or "music" lines, caused by erosion of the slot in the debiteuse.

The Pennvernon process, developed by PPG, uses a fully submerged draw bar to control the location and straightness of the root. Viscous forces confine the drawn sheet to a position over the center of the bar. In the Colburn-LOF process, the soft glass is bent 90° over a roller a short distance above the melt surface. This roller, along with water-cooled edge rollers, serves to keep steady the position at which the glass is drawn from the melt surface. In all these updraw processes, the pulling rollers and the bending rollers, when used, tend to mar the glass. Another disadvantage of updraw is that, whenever the sheet breaks in the rolls, the broken glass falls back into the machine and into the melt. The updraw processes are more difficult to restart than are the downdraw processes. With the possible exception of Fourcault, these updraw processes are in relatively little use today, primarily because they have been superseded by the float process (see Sec. 6.4.8).

6.4.7 Rolling

Rolling can be used to manufacture thin or thick sheets of glass. In the simplest form, a puddle of glass can be poured on a metal table and a metal roller is used to spread it to a constant thickness. Generally parallel spacer bars are used to limit the thinness to which the roller can spread the glass. In a continuous process a stream of glass is fed between a pair of counterrotating water-cooled metal rollers. The spacing between the rollers determines the thickness of the resulting sheet; the width is controlled by the amount of glass fed to the rollers. The sheet is generally rolled vertically downward, or at a sufficient incline that a puddle of molten glass can be maintained at the entrance to the rollers. The speed of the operation and the diameter of the rolls must be sized to the thickness of the sheet being rolled. The glass enters the rolls relatively fluid, but must be considerably less fluid when it leaves in order to maintain its shape. The thicker the glass, the more heat that must be removed by the rollers. A generally thick sheet requires large rollers, maybe 4 to 10 feet in diameter, and forming rates of only a few feet per minute. Very thin ribbon can be made with small rollers, a few inches in diameter, at rates of several feet per second. After rolling, the continuous sheet is transported horizontally through a heated annealer.

The surface finish quality and thickness uniformity is generally insufficient for mirror, automotive, and architectural applications. Prior to the development of the float process, described below, rolled glass sheet was ground and polished on both sides, sometimes simultaneously, to meet these requirements. These products were known as *plate* glass. The process was inherently wasteful and expensive.

Patterned glass is made by applying texture to one or both glass surfaces by suitably embossed rollers. Applications include shower doors, furniture tops, room dividers, and windows. There is even an application for roller-applied Fourcault-type sheet texture for use in restorations of nineteenth century homes.

As a variation, *wired* glass, such as used in fire doors and building skylights, can be manufactured by continuously feeding wire mesh between the rollers along with the molten glass.

6.4.8 The Float Process

Grinding and polishing of rolled glass was a very expensive, labor-intensive, materials-wasteful process. In the 1950s and 60s the Pilkington company in England developed a much more economical process based on floating a continuous ribbon of molten glass on a bath of molten tin as the glass cooled and solidified. This process is illustrated in Fig. 6.18. A detailed description of the process and the difficulties that were overcome in its development lie outside the intent of this handbook, but some key points should be made. The glass product, known as *float* glass, has excellent surface properties, the upper surface having flowed freely without contact with rollers or any other forming devices before its solidification, the lower surface similarly having only been in contact with a flat smooth liquid metal surface incapable of marring it. The product also has exceptionally uniform thickness.

Regarding thickness, a freely spreading puddle of glass suspended on molten tin (by buoyant forces in a gravity environment) will reach an equilibrium thickness determined by the tin and glass densities and the various surface and interfacial tensions. For soda-lime-silica glass, on tin in the earth's gravity, this thickness is between 6 and 7 mm, approximately that of traditional plate glass. Several techniques have evolved to make thinner and thicker float glass. These essentially involve pulling the glass off the bath at a rate faster or slower than would maintain the above defined equilibrium thickness, and doing so in a manner that

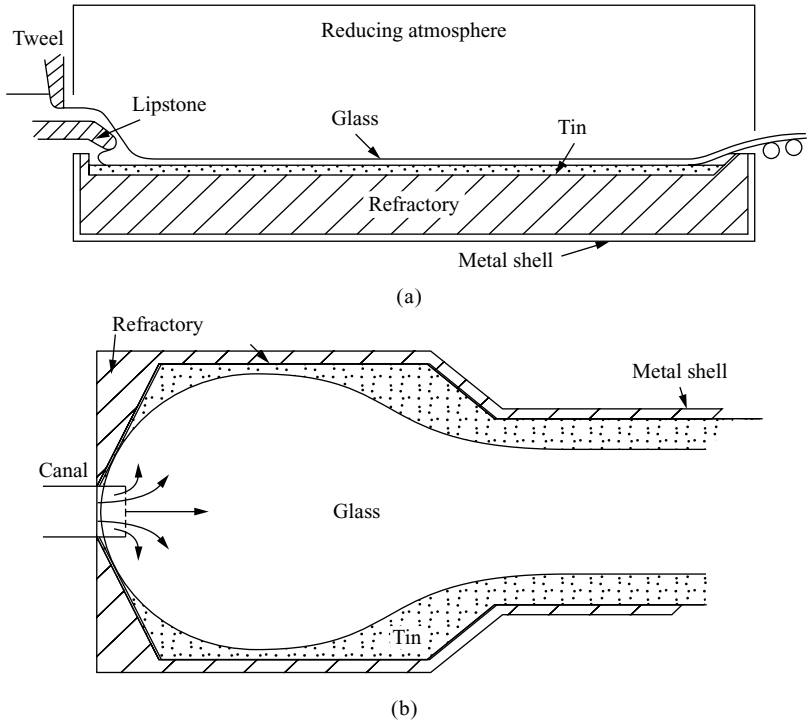

FIGURE 6.18 Pilkington type tin bath: (*a*) side view; (*b*) top view. (*From R. A. McCauley, "Float Glass Production: Pilkington vs. PPG," The Glass Industry, April 1980*, pp. 18–22.)

preserves the thickness uniformity. Several techniques for stretching the glass in this manner have evolved. All employ gripping the edge of the spreading glass puddle on its top surface with knurled rollers to assist, restrict, or redirect the glass flow. One method is illustrated in Fig. 6.19.

It should be noted that many early references to the float process describe the glass sheet as being formed by rolling between two rollers before it is fed onto the tin bath. This approach was tried initially by Pilkington, but it proved unsuccessful. (It led to surface defects in the glass.) In the commercialized processes, the molten glass is fed onto the tin bath by flowing it over a refractory block. The Pilkington and PPG designs differ in how this is done.

The Pilkington and PPG float process have proved so effective and so economical that they have virtually replaced all plate glass manufacture (ground and polished rolled sheet) throughout the world, and most of the drawn sheet products as well. Most of the flat glass producers in the world have been licensed to use the float process. Today's largest float glass plants can produce about 1000 tons of finished glass per day at widths up to about 12 ft, and thickness between about 2 and 25 mm. The overall length of the production line, including melter, tin bath, and annealing lehr can exceed 700 ft, with the tin bath itself occupying between 100 and 200 of those feet.

Specially designed float lines can produce glass less than 1 mm thick. While initially developed for the manufacture of soda-lime-silica glass, several manufactures

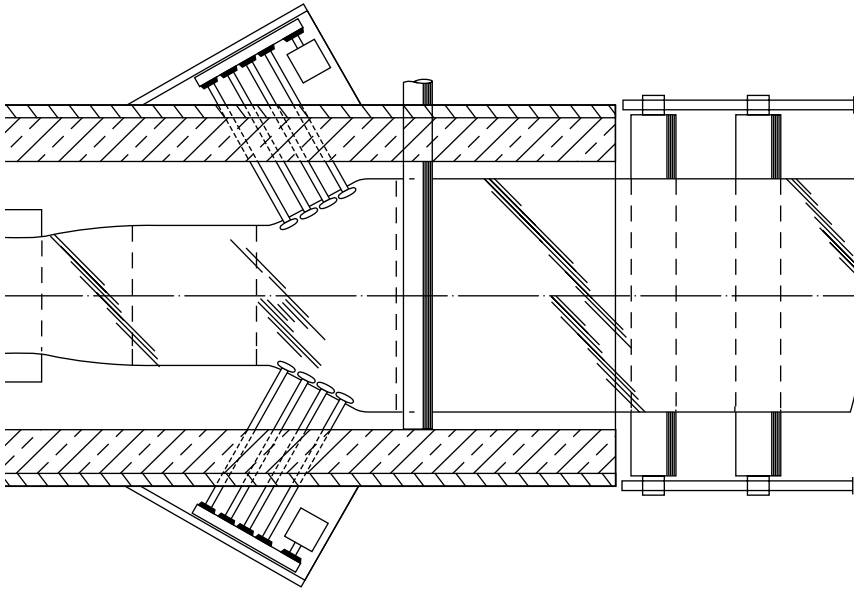

FIGURE 6.19 Decreasing the thickness of float glass by both lateral and longitudinal stretching, with knurled wheels pressing on the edges of the ribbon. (*From Michael Cable, "Mechanism of Glass Manufacture," J. Am. Ceram. Soc., vol. 82, pp. 1093–1112; reference Ford Motor Co., "Float Method of Manufacturing Glass," Br. Pat. No. 1,085,010, 1967.*)

have successfully applied the techniques to borosilicate glasses. However, because of temperature limitations of the tin bath, and its required chemically reducing atmosphere, not all commercially useful glass compositions can be manufactured by the float process.

6.4.9 Fritting

Techniques used for making glass *frit* (granules) include *dry gauging* or *dry gaging* (drizzling or pouring a stream of molten glass into cold water) and rolling as very thin ribbon, followed by particle attrition or comminution (size reduction) processes. These techniques involve a rapid quenching of the melt and can be used to vitrify (make glass from) compositions that tend to crystallize readily. Cooling the glass quickly, directly from the melter, creates high thermal stresses, which shock and often break the glass into small pieces suitable for charging into a ball mill. Dry gauging sometimes forms clinker-like pieces that are difficult to mill and may require an intermediate process step. Thin rolled ribbon often provides the better, more uniform mill feed.

6.4.10 Spheres, Marbles, and Microspheres

Glass spheres can range in size from a few nanometers in diameter to a meter or more. They can be solid, porous, or hollow, at all but the smallest sizes. Applications range from the extremely small solid precursor particles used in Types III, IV, and V fused silica manufacture

and the small hollow spheres used to contain fuel in inertial confinement nuclear fusion research through the small (less than 0.2 mm) microspheres used in reflective signs and projection screens or as fillers in plastics and elastomeric composites and the approximately half-inch marbles used in games, to fish net floats, to deep ocean submersible vessels of military interest.

Because of the wide range of size, and the need for solid, porous, or hollow products, manufacturing techniques necessarily vary. Directing a high-temperature, high-velocity flame across a vertically descending stream of molten glass can generate small solid spheres. If the glass is sufficiently fluid, strands of glass are formed, which quickly break apart into droplets. These droplets spheroidize under the forces of surface tension and cool as they leave the flame. The resulting particle size distribution is not easily controlled. Similarly, molten droplets can form and detach from an orifice at the bottom of a crucible or glass-melting tank. If the droplets have sufficiently low viscosity, and are released from a great enough height, they will spheroidize and cool before reaching the ground, where they are collected. Particle size control is better.

Microspheres (less than 0.2 mm diameter) of controlled size and composition can also be prepared by fritting, sieving, and injecting into a heated region to remelt, spheroidize, and cool, somewhat as described above. The precursor particles can be fed into the top of a tall column having a thermal gradient decreasing downward and collected at the bottom, or can be injected into an upward-directed flame, whereby the molten droplets are drafted to cooler higher altitudes and collected.

To mass produce *marbles* (solid spheres about 1/2 in in diameter), a more viscous stream of glass is delivered from the melter and mechanically cut (sheared) into minigobs having the required volume. The soft gobs fall into the space between two counterrotating cylinders in which there are machined opposing spiral grooves. The gobs of glass are simultaneously rolled into spheres and cooled to temperatures near their annealing point as they are transported down the length of the rolls. Streams of different-colored glass can be partially mixed together before gobbing to give a variegated appearance. Less spherically perfect marbles can be generated by dropping the minigobs into cylindrical holes in vibrating molds, sometimes mounted on a conveyor belt. Steady vibration, maintained until the gobs have been well cooled, generates near-spherical shapes. Of course, decorative marbles of varying sizes can be created as novelties or works of art by studio or hand-shop techniques.

Perfectly spherical spheres of a wide variety of sizes with optical finish can be produced from near-spherical starting blocks by grinding and lapping on optical finishing machines.

Hollow spheres of moderate size can be hand-blown freely or in molds, but the location where the blowpipe is separated after forming is seldom perfect. Hemispheres can be pressed and then pairs fused together. Very large, thick-walled spheres can be made from pairs of centrifugally cast hemispheres.

At the other end of the size spectrum, very small hollow glass spheres such as those used in inertial confinement nuclear fusion (ICF) research, are also prepared by a variety of techniques, all relying on generating small volumes of precursor materials, which are injected into a hot zone. The surface of the precursor particle melts or otherwise reacts to generate a viscous liquid layer. As the interior material heats, it evolves gases that serve to blow the hollow sphere. Solid precursors can be formed as small aggregates of batch material, sometimes by spray drying or sol-gel techniques; alternatively, the required chemical species can be dissolved in an aqueous or organic solution with precursor droplets of the required size being generated by an appropriate means such as an ultrasonic nebulizer.

Porous spheres can be prepared by leaching one glassy phase from a two-phase spherical product, or by processes similar to those used for hollow microspheres whereby the surface layer never forms in a fully continuous manner, i.e., the blowing bubbles are exposed at the surface.

6.5 ANNEALING AND TEMPERING

6.5.1 Development of Permanent Stresses in Glass

Stresses in an unconstrained elastic solid develop only if there is a nonlinear temperature gradient across the body. Such stresses are temporary, or transient; they exist as long as the temperature gradient exists. Liquids, on the other hand, can not sustain shear stresses for any finite length of time; such stresses relax by viscous flow. Glasses behave like a liquid on heating into the liquid state; i.e., all stresses relax because of viscous flow. However, on cooling through the glass transition range into the solid state, stresses are likely to develop within the body, which no longer relax in the absence of a viscous flow. The various mechanisms for such permanent stress development are as follows:

1. Cooling from the outside results in a "frozen" temperature gradient with a higher temperature in the interior (Fig. 6.20). Inner layers continue to relax from fluid flow while the outer layers gradually freeze. In effect, the stress-free state is a solid with a temperature gradient. The need to shrink the inside more relative to the outside at room temperature and the enforcement of the elastic compatibility criteria between the layers cause the appearance of compression on the outside and tension on the inside. *The magnitude of the stresses so developed is related to the linear expansion coefficient of the solid*. This mechanism is also called the *viscoelastic mechanism*.
2. The outside layers cool at a rate faster than that of the inside layers during normal cooling. Hence, the outside layers tend to possess a faster-cooled structure having a higher volume in the free state (see Fig. 5.1). *This, in principle, is a permanent structural heterogeneity*. Again, the enforcement of the elastic compatibility criteria causes the outside layers to develop compression and the inside layers to develop tension. *The magnitude of the*

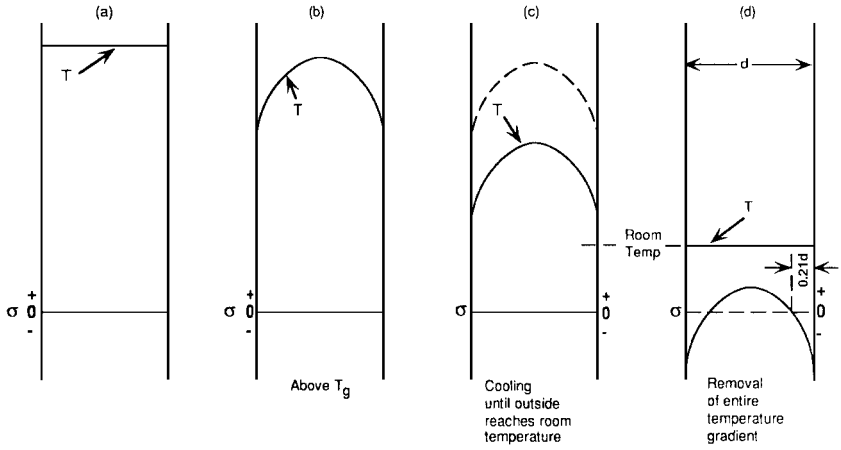

FIGURE 6.20 Simplified concept of permanent stress production in glass due to a "frozen temperature gradient." (*a*) Glass with no temperature gradient well above the transition region has no stress. (*b*) Temperature gradient develops on cooling; however, no stress develops because of rapid relaxation while the glass remains well above T_g. (*c*) Cooling to below T_g while maintaining the same "frozen temperature gradient" produces no stress yet. (d) Final removal of the temperature gradient produces stresses that are now permanent. T is the temperature, d is the glass thickness, σ is the stress. $A + \sigma$ implies tension and a $-\sigma$ implies compression. (*From "Glass Transition Range Behavior" in Fundamentals of Inorganic Glasses by A. K. Varshneya, copyright© 1994 by Academic Press, reproduced by permission of the publisher.*)

stresses so developed is related to the difference between the volumes of the fast-cooled and the slow-cooled solids.

3. The fact that the various layers travel through the glass transition range at different instants of time causes the development of a "frozen fictive temperature gradient." *This is a transient structural heterogeneity*. As in (1), the removal of the transient fictive temperature gradient causes the appearance of compression on the outside and tension on the inside. *The magnitude of the stresses so developed is related to the configurational (or the structural) contribution to the linear expansion coefficient of the supercooled liquid* (= linear expansion coefficient of the liquid − the linear expansion coefficient of the solid).

During glass forming, various regions of glass indeed go through varying cooling rates because of the nonuniform applied heating/cooling and the usually nonuniform thickness; hence, stress generation is likely. There is little chance of fracture while the glass remains somewhat viscous fluid, but once the material starts solidifying, stresses begin to accumulate. For a common soda-lime silicate glass product cooled through the glass transition region at "normal" cooling rates, nearly 60 percent or so of the total stress is due to mechanisms (1) and (2). Warping may result to relieve uneven bending moments across the body of a glass product. In turn, the warping generates bending stresses, some of which end up being tensile on an outer surface. This then poses a potential risk for glass fracture during the manufacture and, worse yet, during service. There is additionally a longer-term risk for property and dimensional changes due to the continuing stabilization of glass. (Optical glass components, particularly those that are space-based, need to have minimized refractive index and dimensional changes.) Glass products are, therefore, customarily reheated in the proximity of the glass transition range to allow the release of any internal stresses that might have developed, and cooled at a rate slow enough that prevents their rebuilding. This procedure is termed *annealing*. An additional objective of annealing is to homogenize the thermal history across the body. *Tempering* (also called *toughening* as a misnomer in this case), on the other hand, implies strengthening, and is accomplished by introducing surface compression into the glass. Since flaws that cause strength degradation usually occur on the surface, the introduction of surface compression strengthens a glass product. Unless the volume-temperature diagram for the glass at hand is somewhat unusual (like that of fused silica), one expects to have some degree of temper obtained by normal cooling through the glass transition, which is clearly beneficial for ordinary handling of glass products.

6.5.2 Stress Profiles in a Symmetrically Cooled Glass Plate during Annealing and Tempering

If a glass plate is cooled symmetrically from both sides, then the temperature distribution across the section is a parabola (for low cooling rates); see Fig. 6.21. The magnitude of the temperature difference ΔT between the outside and the inside layers of glass is given by $\Delta T = d^2R/2\kappa$, where d is the half-thickness of the section, κ is the thermal diffusivity, and R is the cooling rate. (A typical value of κ for soda-lime-silica glass is 0.0084 cm^2/s.) The outside surface compression σ_c is proportional to $2\,\Delta T/3$, and is approximately given by

$$\sigma_c = \frac{E\alpha d^2 R}{\kappa(1-\nu)} \tag{6.1}$$

where E is the Young's modulus and ν is the Poisson's ratio of the glass. (Note that the calculations assume that the room temperature stress is the inverse of that established during the

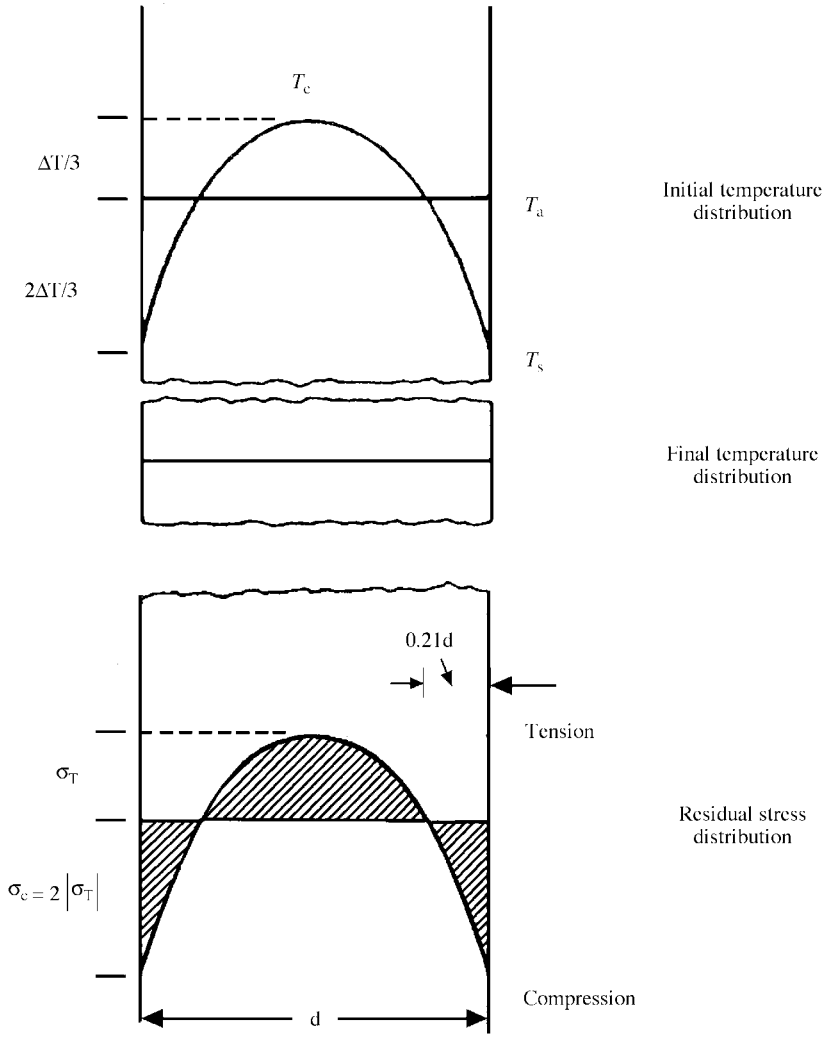

FIGURE 6.21 A parabolic temperature gradient produces surface compression that is twice the interior tension in magnitude; d is the glass thickness. (*From "Glass Transition Range Behavior" in Fundamentals of Inorganic Glasses by A. K. Varshneya, copyright© 1994 by Academic Press, reproduced by permission of the publisher.*)

fluid state when the thermal expansion coefficient was roughly 3 times that in the solid state.) *The center tension is proportional to $\Delta T/3$ (= half of the surface compression magnitude) and is, therefore, given by a half of the above quantity*. The above equation may also be used to calculate a constant cooling rate that would give rise to a specified center tension at room temperature. For instance, for a soda-lime-silicate glass with $\alpha = 90 \times 10^{-7}$/°C, $E = 70$ GPa, $\kappa = 0.0084$ cm^2/s, $\nu = 0.2$, and $d = 0.3$ cm, a 2.8°C/min cooling rate will give rise to a center tension of about 0.2 MPa.

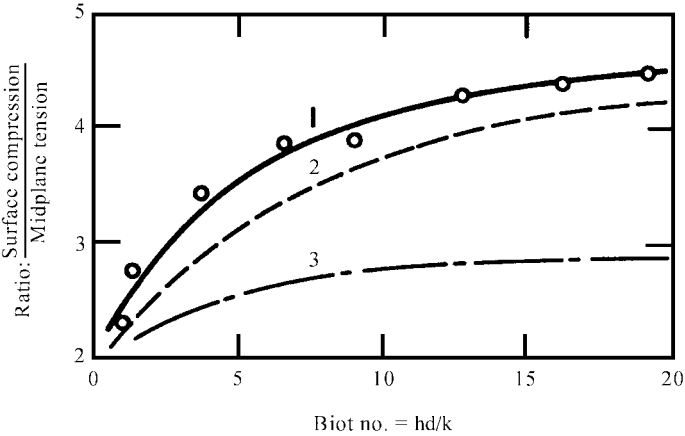

FIGURE 6.22 Ratio of "Plateau level" surface compression to midplane tension as function of Biot number. Curve 1, experimetal results; 2, predictions by Indenbom's theory; 3, predictions by Bartenev's theory. (Boguslavskii et al., 1964.) (*From "Thermal Tempering of Glass" by R. Gardon in Glass: Science and Technology, Vol. 5, Elasticity and Strength of Glass, edited by D. R. Uhlmann and N. J. Kreidl, copyright© 1980 by Academic Press, reproduced by permission of the publisher.*)

For glass tempering, a high cooling rate is deliberately employed in order to introduce a level of surface compression in the glass. Because of the high cooling rates, the tempering stress profile is often not a rectangular parabola of the form $y = ax^2$, but may be approximated by $y = ax^n$. It can be shown that the ratio of the magnitude of the surface compression to that of the midplane tension is simply n. Depending on the Biot number (= hd/k, where h = heat transfer coefficient and k = thermal conductivity), n values as high as 4.5 have been obtained (see Fig. 6.22). Most commonly, n = 2.2 to 2.4. For a rectangular parabolic distribution of stress, the zero stress ("neutral") line is about one-fifth the glass thickness below the surface from each side (see Fig. 6.21) . The thickness of the compression layer from the surface up to the nearest neutral line is called *case depth*. Thus a 6-mm plate may have surface compression layers roughly 1.2 mm thick on each side, which represents a significant depth of protection.

One of the fascinating examples of tempered glass is the *Prince Rupert drop*. Teardrops, generally 4 to 10 mm diameter, of molten soda-lime-silicate glass with a tail are allowed to fall into water. The high degree of surface compression that develops into the teardrop allows hammering on it. The drop explodes into flying fine powder of glass when the tail is snapped. (Caution: This demonstration should be carried out under protective wrapping, or behind a protective shield.)

6.5.3 Standards of Annealing

Commercial glass products are generally called *annealed* if the center tension is no greater than about 500 lb/in^2. In a stress-birefringence setup (see Sec. 6.5.9), and with the assumption that the stress-optical coefficient is 3 brewsters, this stress would roughly correspond to a retardation of 100 nm per centimeter of light path. For most optical glasses, the optical birefringence in the middle should be no more than 5 nm/cm, or even better yet, roughly 2.5 nm/cm.

6.5.4 Annealing Practices

Coarse annealing may be accomplished, particularly in a laboratory setting, by following these guidelines:

1. Hold the glass product isothermally in a box furnace at a temperature within the annealing range. The holding time t may be estimated by the KWW relaxation formula:

$$\sigma_t = \sigma_o \exp\left[-(Gt/\eta)^{1/2}\right] \tag{6.2}$$

   where σ_t = stress at time t and η and G are the viscosity and shear modulus of the glass at the holding temperature, respectively. The stress σ_t is normally taken as 5 percent of σ_o, the initial stress, and the high-temperature value of G is taken as 20 to 25 percent lower than that at room temperature. Thus, at the annealing temperature, where viscosity is 10^{13} P, one needs to hold for 10 to 15 minutes. However, as much as 6 to 8 hours are needed for a comparable relaxation at the strain point ($\eta = 10^{14.5}$ P).

2. Cool the furnace usually at 5°C/min, which can be accomplished by simply turning the box furnace off to cool overnight.

On an industrial scale, a continuous belt lehr is often employed for annealing. One of the several suggested heat treatment schedules for the annealing of glass products is shown in Fig. 6.23. In region *A*, the glass is rapidly heated or cooled to about 5°C above the rated annealing point, depending on whether the product is hot coming out of the forming machine or is cold coming out of storage. It is held at that temperature for a time period t (region *B*), after which it is slowly cooled to a temperature $a°$ below the strain point (region *C*). Once the glass is well below the strain point, any risk of rebuilding permanent stresses is small and the glass may be cooled faster (regions *D* and *E*). The limiting consideration for the

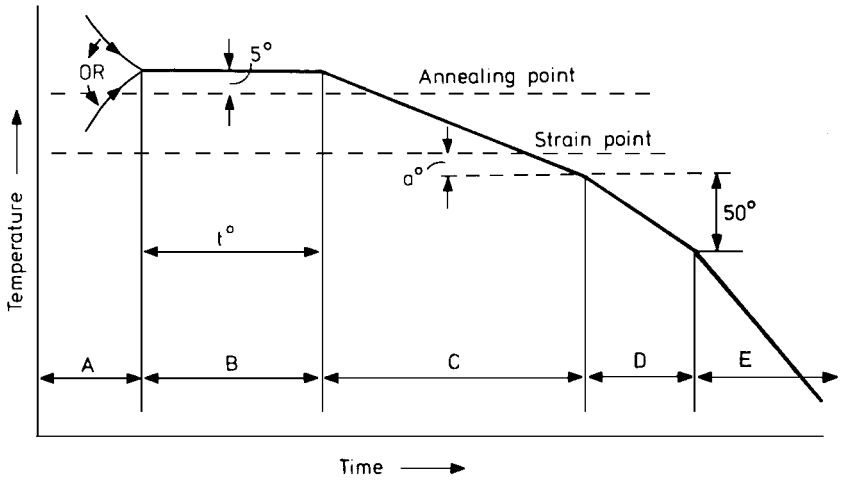

FIGURE 6.23 Suggested schedules for commercial annealing of soda-lime-silica glassware. (*Courtesy of Corning Incorporated.*)

cooling rate in the two regions is the avoidance of thermal shock. The recommended schedule for the various regions is:

A (heating rate) $= 500/\alpha d^2$ °C/min
B (holding time) $= 15z$ min for cooling from one side
C (slow cool) $= 42.6/\alpha d^2$ °C/min
$a°$ (°C/min below the strain point) = 5°C for 0.3-cm-thick plate
= 10°C for 0.6-cm-thick plate
= 20°C for 1.3-cm-thick plate
D (fast cool) = 2 times the slow cool
E (final cool) = no more than 10 times the slow cool,

where α is the thermal expansion coefficient in 10^{-7}/°C units, z is the glass thickness (cm), and $d = z$ when heated/cooled from one side only, $= z/2$ when heated/cooled symmetrically from both sides. Computations for a few glasses with different plate thickness and cooling conditions are tabulated in Table 6.20. The total time for the completion of a commercial-quality annealing is expected to be about 20 minutes.

6.5.5 Standards of Temper

According to ASTM C1048, *Kind FT* (fully tempered) glass shall have a surface compression no less than 69 MPa (10,000 lb/in^2) or an edge compression of not less than 67 MPa (9700 lb/in^2). Such a glass is up to 5 times as strong as a normally annealed product of the same thickness and configuration. It is often recommended that a fully tempered glass should have roughly 100 MPa (14,500 lb/in^2) surface compression. This corresponds to roughly 45 MPa (about 6400 lb/in^2) midplane tension, or about 1350 nm/cm birefringence in the midplane. Glass should meet American National Standards Institute (ANSI) standard Z97.1 or Consumer Product Safety Commission (CPSC) standard 16CFR1201. The ANSI standard specifies that a tempered automotive glass must withstand the impact of a 1/2-lb steel ball and an 11-lb shot-filled bag, both dropped from specified heights. In the ball drop test, 10 out of 12 specimens must remain unbroken. The drop height is then increased till all the specimens have broken. On initiation of the fracture, the stored mechanical energy is released virtually instantly, causing rapid bifurcation of advancing crack fronts. This then yields a dicing behavior, where the pieces do not have acute-angled corners and, hence, are not expected to cause serious injury by sharp cuts. The higher the midplane stress, the smaller the pieces. For the glass to be acceptable, none of the diced pieces may weigh more than 0.15 oz (4.3 g) for a 6-mm-thick glass. The dependence of the break pattern on midplane stress is shown in Fig. 6.24.

Kind HS (heat-strengthened) glass has a surface compression between 24 and 52 MPa (3500 to 7500 lb/in^2) for a thickness of 6 mm. Such a glass may be up to 3 times as strong as a normally annealed product of the same thickness and configuration.

The U.S. Food and Drug Administration (FDA) requires that all eyewear (prescription or otherwise) sold in the United States pass safety ball drop tests for impact resistance described by ANSI Z80.1-1995 and ANSI Z80.3-1996. This testing requires a fully finished and edged glass lens to survive impact testing with a 16-mm-diameter steel ball, dropped in free fall from a height not less than 1.27 m, onto the central 16-mm-diameter area of the outer surface of the horizontally placed lens. Certain specialty lenses are exempt from this test, as are plastic lenses. Industrial safety glasses must pass a more severe test. Both thermal tempering and ion-exchange strengthening are used to meet these impact requirements.

TABLE 6.20 Suggested Annealing Schedules for Glass Products*†

Expansion coefficient of glass, per °C	Thickness of glass, mm	Cooling on one side						Cooling on two sides					
		Heat rate, °C/min	Time *t*, min	Temp. *a*,°C	Cool rate, °C/min			Heat rate, °C/min	Time *t*, min	Temp. *a*,°C	Cool rate, °C/min		
		A	*B*	*C*	*C*	*D*	*E*	*A*	*B*	*C*	*C*	*D*	*E*
33×10^{-7}	3	130	5	5	12	24	130	400	5	5	39	78	400
	6	30	15	10	3	6	30	130	15	10	12	24	130
	13	8	30	20	0.8	1.6	8	30	30	20	3	6	30
50×10^{-7},	3	85	5	5	8	16	85	260	5	5	26	52	260
	6	21	15	10	2	4	21	85	15	10	8	16	85
	13	5	30	20	0.5	1.0	5	21	30	20	2	4	21
90×10^{-7}	3	50	5	5	4	8	50	140	5	5	14	28	140
	6	11	15	10	1	2	11	50	15	10	4	8	50
	13	3	30	20	0.3	0.6	3	11	30	20	1	2	11

*After G. M. McLellan and E. B. Shand, *Glass Engineering Handbook*. McGraw-Hill, New York, 1984.
†Annealing period: *A,* heating to 5°C above annealing point. *B*, hold temperature for time *t*. *C*, initial cooling to a° below strain point. *D*, cooling, next 50°C. *E*, final cooling.
Source: Reference 8.

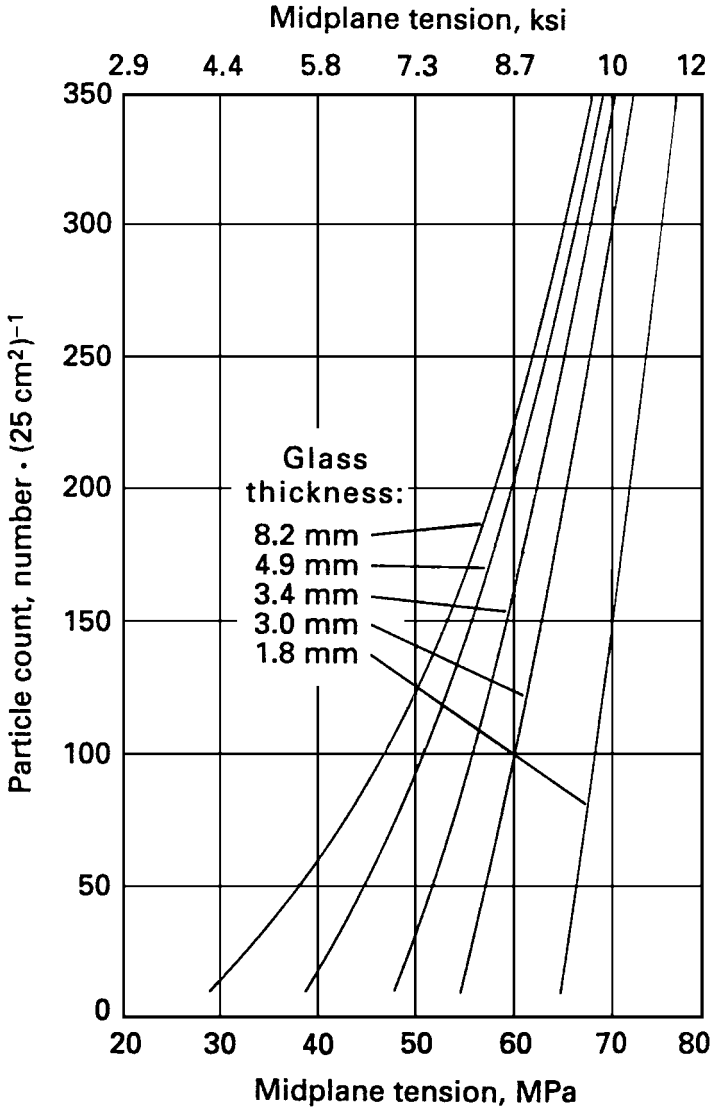

FIGURE 6.24 Dependency of break pattern on midplane stress. Exit temperature, 660°C(122°F). (*R. A. McMaster et al., Ref. 7.*)

6.5.6 Commercial Tempering Practices

Tempering is usually accomplished by heating the glass product, generally to a viscosity of about $10^{9.5}$ to 10^{10} P for a short while, and then quenching symmetrically from both sides with forced-air jets. For a typical soda-lime-silicate glass plate, these viscosity values correspond to about 640 to 620°C. The normal practice is to run a thinner glass hotter;

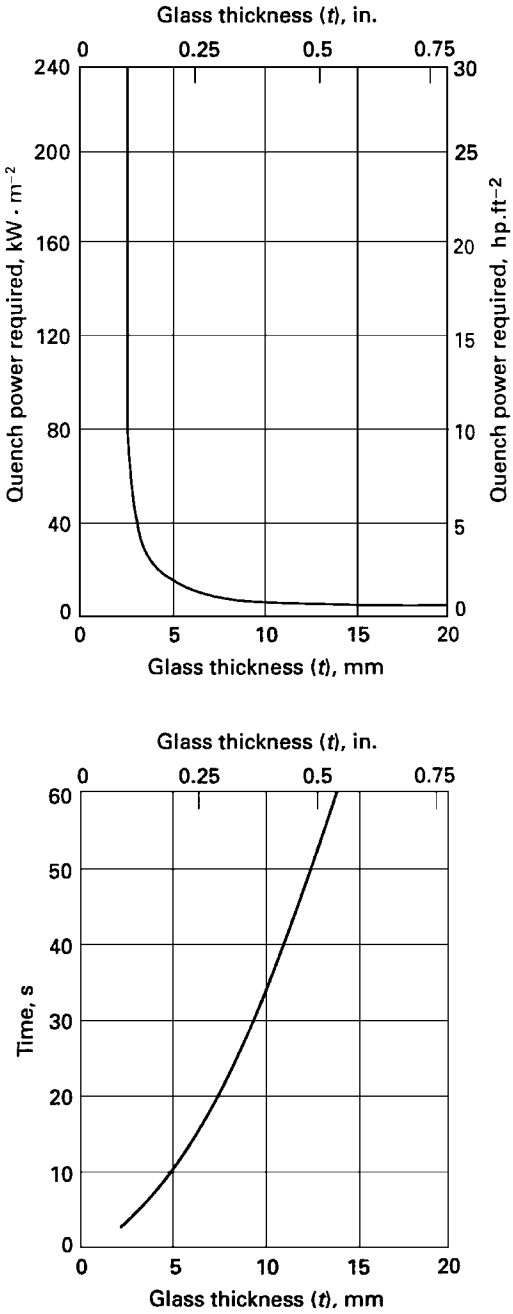

FIGURE 6.25 Effect of glass thickness on (*a*) air power and (*b*) quenching time required for full temper. Exit temperature, 620°C (1150°F). (*R. A. McMaster et al., Ref. 7.*)

however, it must be remembered that higher temperatures bring about noticeable optical distortion. Air power requirement is roughly 40 kW/m^2 for a 3-mm plate and is only about 12 kW/m^2 for a 6-mm plate. The quenching to a viscosity below $10^{14.5}$ P takes roughly 5 seconds for a 3-mm plate and about 12 seconds for a 6-mm-thick plate (see Fig. 6.25). Cooling to room temperature occurs over longer periods. A typical tempering furnace is about 40 m long, and the heating zone may be about 20 m long, the quenching zone about 5 m long, and the slower-cooling zone about 15 m long. With a width of about 1.5 m, the furnace can deliver about 15 tons of fully tempered glass per day.

6.5.7 Limitations of Thermal Tempering

The most important drawbacks of the thermal tempering process are:

1. Surface compression magnitudes much higher than about 140 MPa (about 20,000 lb/in^2) are accompanied by a center tension of about 65 MPa. At this magnitude of tension, a defect such as a stone in the interior could cause the glass product to fail spontaneously.
2. It is difficult to exceed cooling rates of about 100°C/s through the glass transition by forced-air jets. Equation (6.2) suggests that plates thinner than about 1 mm develop no more than about 24 MPa of surface compression, which is not much of a protection.
3. Because of the lack of symmetry in achievable cooling, glass tubes, containers, and other complex-shaped products can not be meaningfully tempered by thermal means.

6.5.8 Chemical Strengthening of Glass

The exchange of large alkali ions from an external source such as a molten salt bath with comparatively smaller host alkali ions in a glass at low temperatures leaves the glass in a state of surface compression, which is an effective means of strengthening the glass. *The level of strengthening achieved could be 2 to 10 times that of an unstrengthened product*. Large ions are essentially stuffed in glass network interstitial spaces occupied previously by the small ions (Fig. 6.26). Stress generation is closely linked to the kinetics of the interdiffusion and the difference in the size of the exchanging ions. Although the diffusion rates increase exponentially with temperature, the rate of stress buildup as the exchange temperature approaches the glass transition temperature is actually reduced by stress relaxation arising from glass fluidity and perhaps some network plasticity. Hence, *chemical strengthening of glass must be carried out at temperatures well below the glass transition range*. A typical ion penetration and stress profile in a glass is shown in Fig. 6.27. Surface compression, of the order of 100 to 1000 MPa (14,500 to 145,000 lb/in^2), can be generated by this technique in many glasses having wall thickness as small as about 1 mm. For consumer glass products, a minimum case depth of about 30 μm is generally recommended to provide an effective protection from the surface flaws. This unfortunately means that *a successful ion exchange strengthening process would usually involve 2 to 100 hours of diffusion, which does not encourage a large-scale continuous process*. Nonetheless, some commercial glass products are ion-exchange-strengthened; windshields for aircrafts, borosilicate glass syringes, ophthalmic products, and large-capacity returnable beverage containers are some examples.

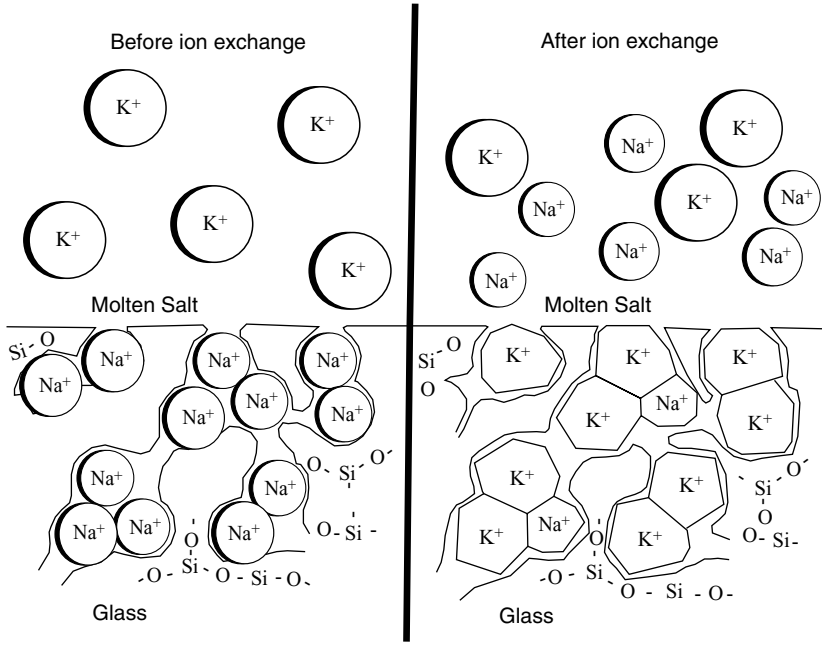

FIGURE 6.26 Crowding from low-temperature exchange of K^+ for Na^+ ions. (*After W. H. Dumbaugh and P. S. Danielson, Ref. 5.*)

Ion-exchange strengthening of glass is typically carried out by immersion of the glass in a bath of molten salt. For instance, a common commercial soda-lime-silicate glass would be strengthened by immersion in a bath of molten KNO_3 at temperatures higher than 328°C (melting point of KNO_3) but lower than about 480°C (the onset of glass transition). Lithium aluminosilicate glass is strengthened by immersion in $NaNO_3$ similarly. The alkali aluminosilicate glasses are the best candidates for ion exchange; the soda-lime-silica glasses do not strengthen well because of rapid relaxation processes despite the rather large alkali content in the host glass. Low-alkali-content glasses, such as the alkali borosilicates of the Pyrex type make even poorer candidates for ion-exchange strengthening.

As the glass ions are continuously rejected into the bath, the concentration of this contaminant builds up. This usually has deleterious consequences on the percent surface exchange even at very low levels of contamination. Hence, the salt bath requires careful control of the contamination level.

The strength is commonly measured in a four-point bending mode or a ring-on-ring method using a mechanical tester on suitably sized test coupons with or without surface abrasion. (It is strongly recommended that edge-independent techniques be employed.) Steel ball drop tests for ophthalmic lenses and bird impact tests for aircraft windshields are also carried out.

To measure stresses in a chemically strengthened glass, one needs to obtain a thin slice across the wall thickness, which has been ceramographically prepared to have sharp square edges at the surface. The observed stresses in such a thin slice must be divided by $(1 - \nu)$

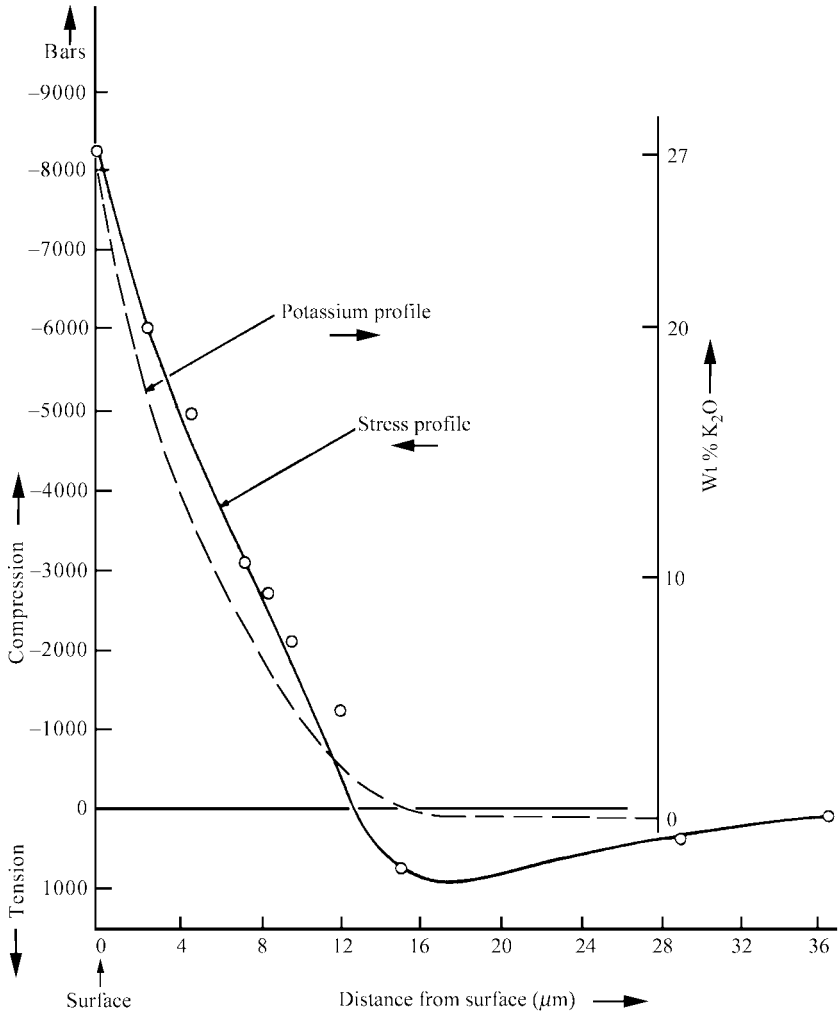

FIGURE 6.27 Stress profile in a sodium borosilicate glass sample after ion exchange at 400°C for 12 h. (*From Fundamentals of Inorganic Glasses by A. K. Varshneya, copyright© 1994 by Academic Press, reproduced by permission of the publisher.*)

to obtain stresses in the unsliced plate. It may also be possible to employ techniques such as the differential surface refractometer (DSR), grazing angle surface polarimeter (GASP) to measure surface compression, and laser scatter to measure internal tension without the need of slicing (see Sec. 6.5.9, "Examination of Stresses in Glass").

Although immersion in molten salt is the more popular technique of ion exchange, there are other techniques that have been tried. Examples of these are pastes using mixtures of inert clays and vapor phase, electrical-field-assisted, multistep (such as thermal and chemical or two-step chemical), sonic-assisted, and plasma-assisted ion exchange.

6.5.8.1 Standards of Chemical Strengthening. Chemically strengthened glass is sold on the consumer's expectation for the improvement of strength; however, it is believed that the varying conditions of application, such as the level of abrasion to be tolerated and the edge conditions, make it difficult to classify the products on the basis of strength. For this reason, the ASTM's recent standard C1422-99 for chemically strengthened flat glass products is based on the measurement of surface compression as well as case depth. These are:

Surface compression σ_c:

7 MPa (1000 lb/in^2) $< \sigma_c <$ 172 MPa (25,000 lb/in^2)	Level 1
172 MPa (25,000 lb/in^2) $< \sigma_c <$ 345 MPa (50,000 lb/in^2)	Level 2
345 MPa (50,000 lb/in^2) $< \sigma_c <$ 517 MPa (75,000 lb/in^2)	Level 3
517 MPa (75,000 lb/in^2) $< \sigma_c <$ 690 MPa (100,000 lb/in^2)	Level 4
690 MPa (100,000 psi) $< \sigma_c$	Level 5

Case depth δ:

< 50 μm (0.002 in)	Level A
50 μm (0.002 in) $< \delta <$ 150 μm (0.006 in)	Level B
150 μm (0.006 in) $< \delta <$ 250 μm (0.010 in)	Level C
250 μm (0.010 in) $< \delta <$ 350 μm (0.014 in)	Level D
350 μm (0.014 in) $< \delta <$ 500 μm (0.020 in)	Level E
500 μm (0.020 in) $< \delta$	Level F

Thus a glass plate which has 60,000-lb/in^2 surface compression and a case depth of 70 μm will be termed Level 3B chemically strengthened glass.

6.5.9 Examination of Stresses in Glass

Stresses in glass are best examined by photoelastic techniques. In the absence of external forces, a well-annealed and homogeneous specimen of glass is isotropic. However, when a nonhydrostatic stress is applied to the glass or when unannealed internal stresses are present, perpendicular vibrations of an unpolarized wave of light travel at different velocities along planes of principal stresses. Glass develops two refractive indices, a phenomenon termed *double refraction* or *birefringence*, which is discussed in Chap. 5. The magnitude of the stress birefringence is measured by one of several methods and related to the stress by using the stress-optic Eq. (5.8.1).

In a simple polariscope setup, light rays from a lamp are first allowed to pass through a polarizer whose sole function is to allow vibrations along only one plane. When an analyzer is oriented such that its plane of allowed vibrations is at 90° to that of the polarizer, all of the light intensity is cut off, leading to a field of view that is dark (i.e., the analyzer is "crossed" with respect to the polarizer to achieve extinction). A stressed glass specimen

is now inserted between the polarizer and the analyzer. The principal stress axis of the specimen is to be at 45° to that of the polarizer. The light rays entering the specimen may be considered to be composed of two equal-intensity, in-phase, mutually perpendicular vibrations. The vibrations travel with different velocities through the specimen, and recombine on exiting. Depending on the path difference δ (or the phase difference $\phi = 360° \delta/\lambda$) that is introduced between the two vibrations while traveling through glass, the recombination yields some intensity along the 90° plane of the analyzer. Consequently, the field of view is no longer dark. For instance, a phase difference of full 360°, i.e., a path difference of λ, brings the two vibrations into the same relationship that they had on entering, with the result that the analyzer cuts off that particular wavelength λ (i.e., extinction is achieved for λ).

When a white light source is used, the particular λ will be missing from the field of view. The balance color of light, therefore, may be judged to estimate δ from a *Michelle-Levy chart*, and the use of the stress-optic relation gives the particular stress responsible for it. Sensitivity is greatly increased if a "full wave" retardation plate (*sensitive tint* plate for $\lambda = 565$ nm) is introduced between the specimen and the analyzer. With a zero-stress specimen, the analyzer cuts off only the 565-nm wavelength, which is between the green and yellow color of the spectrum. The absence of this light causes the balance reds and blues to form a magenta color. Introduction of stress that adds to 565 nm will cause wavelengths at the red end to be cut off, yielding a bluish field of view. On the other hand, a stress that subtracts from 565 nm will cause bluish light to be cut off, thus changing the field of view to orange-red colors. Since the human eye is most sensitive to changes about 565 nm, even small magnitudes of stresses can give noticeable color change. The identification of tensile or compressive stresses by the shift of the color from the magenta tint to either side of the green-yellow line in the white spectrum is the essence of *strain viewing* in glass. The appearance of colors with and without the sensitive tint plate is shown in Table 6.21.

More precise measurements of stress in glass are possible with the use of stress (actually birefringence) compensators. When a compensator is introduced between the specimen and the analyzer, its function is to introduce a retardation that is exactly the same

TABLE 6.21 Colors in Strained Glass When Observed in a Polariscope

Without Tint Plate		With Tint Plate (565 mμ retardation)		
Phase difference or retardation, mμ	Color	Phase difference or retardation, mμ	"Blue" position, Color rising	"Orange" position, Color falling
50	Iron-gray	0	Violet-red	Violet-red
200	Grayish-white	23	Violet-blue	Reddish-violet
300	Yellow	46	Blue	Reddish-orange
425	Orange	69	Greenish-blue	Orange
530	Red	92	Bluish-green	Yellowish-orange
565†	Violet-red	115	Yellowish-green	Gold-yellow
640	Blue	150	Deep green	Gold-yellow
675	Blue-green	180	Green	Yellow
740	Green	220	Pale green	Pale yellow
840	Yellowish-green	290	Greenish-yellow	White
880	Yellow	330	Pale yellow	

*1mμ = 10^{-6} mm = 10 A = 1 nm.
†Color with tint plate of 565 mμ retardation.
Source: J. H. Partredge and W. E. S. Turner, *Glass-to-Metal Seals*, Society of Glass Technology, Sheffield, England, 1949, p. 123.

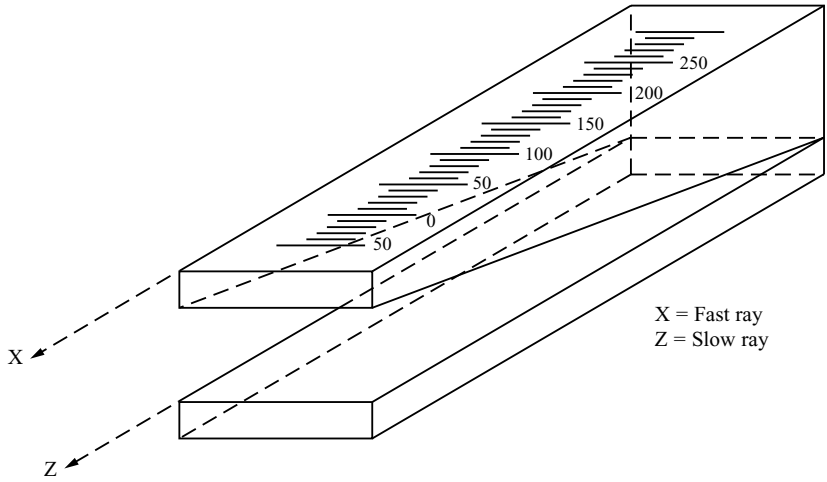

FIGURE 6.28 Combination wedge with wedge-shaped quartz section above and mineral plate below. (*A. G. Pincus and T. R. Holmes, Annealing and Strengthening in the Glass Industry, 2d ed., Ashlee Publishing, New York, 1987, p. 246.*)

in magnitude but opposite in sign to that introduced by the specimen. A precalibration of the compensator readily yields the unknown value of δ. Popular compensators are quartz wedges (or a stretched polymer wedge), Babinet, Babinet-Soleil, Berek, and Sénarmont.

6.5.9.1 Wedge Compensator. Quartz crystal is a naturally birefringent material. It is cut into a slightly tapered wedge such that the directions of the fast and the slow rays are along and perpendicular to the grade of the wedge. (Alternatively, a transparent epoxy resin is stretched while warm and frozen into solid form.) The compensator is introduced such that its fast and slow axes are lined up with that of the specimen (and at 45° to the polarizer or the analyzer). Light rays of a particular wavelength are "compensated" by the thickness of the quartz wedge at a particular location, giving a field that comprises the balance of the spectrum. In the presence of a properly oriented stressed specimen, the colored bands are shifted. The shift is precalibrated in terms of δ by using a monochromatic light without the stressed specimen. The field of view in such a case would be a series of bands that represent exactly one wavelength path difference from each other.

A more useful version of the quartz wedge, shown in Fig. 6.28, comprises a graduated wedge and a flat mineral plate having the opposite sign of the optical birefringence. The path difference created by one is exactly compensated by that created by the other at the "zero" mark.

6.5.9.2 The Babinet Compensator. The Babinet compensator (Fig. 6.29) comprises two quartz wedges with opposite grades; one of the wedges is fixed, the other is movable. At the location where the two wedges have equal thickness, the retardation introduced by one is cancelled by the other, giving rise to a black line ("zero" mark on the movable wedge dial). On either side of the black line, the net retardation increases. The black line will, therefore, be displaced either to the left or to the right depending on the sign of birefringence of the specimen, i.e., whether the stress is tensile or compressive. The movable wedge is then moved to bring the black line back to its original location, and the dial is read to obtain the corresponding retardation. Again, the compensator is calibrated by using a monochromatic source that yields equispaced black lines corresponding exactly to one wavelength path difference.

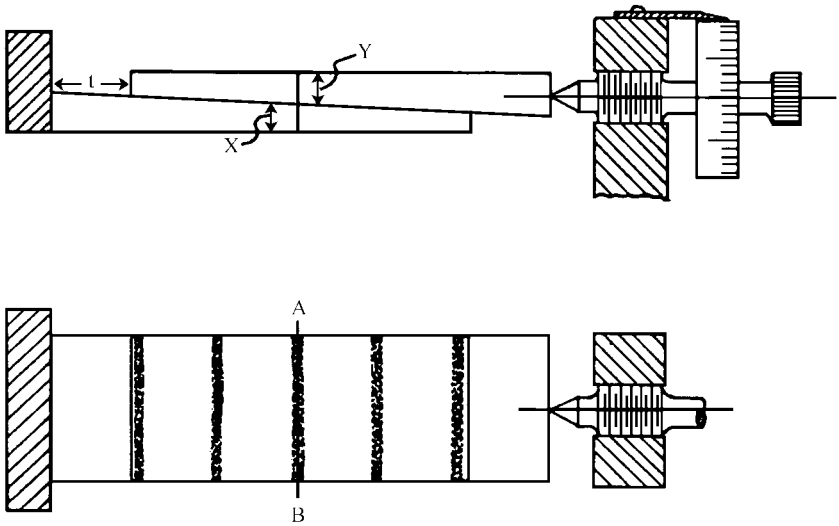

FIGURE 6.29 Arrangement of wedges in the Babinet compensator. (*A. G. Pincus and T. R. Holmes, Annealing and Strengthening in the Glass Industry, 2d ed., Ashlee Publishing, New York, 1987, p. 247.*)

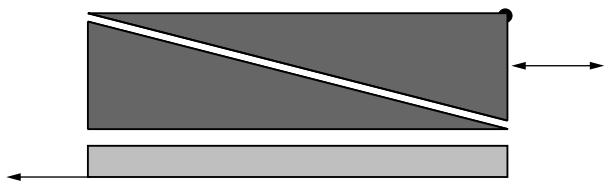

FIGURE 6.30 Arrangement of the optical elements of a Babinet-Soleil compensator. (*H. W. McKenzie and R. J. Hand, Basic Optical Stress Measurement in Glass, Society of Glass Technology, Sheffield, England 1999, p. 33.*)

6.5.9.3 The Babinet-Soleil Compensator. The Babinet-Soleil compensator comprises two quartz wedges with parallel optic axes, one of the wedges being fixed, the other movable, plus a fixed quartz plate with perpendicular optic axes (Fig. 6.30). The double wedge combination adds a constant retardation all across the field of view. Dial rotation causes the upper wedge to move, producing a change in the uniform total thickness of the double wedge. Thus, instead of seeing black and colored bands as in the Babinet compensator, one views a uniform colored field corresponding to the net retardation. In essence, the Babinet-Soleil compensator acts as a variable retardation plate.

6.5.9.4 The Berek Compensator. The Berek compensator (shown in Fig. 6.31) is a calcite (naturally birefringent crystal) plate, cut perpendicular to the optic axis, about 0.1 mm thick, that can be tilted about $\pm 20°$ by a graduated dial motion. In the null position (generally the 30° reading on the dial), the plate is horizontal and introduces no net retardation. A tilt, however, introduces a net retardation between the perpendicular vibrations of light. When viewing a stressed specimen, the user rotates the dial on either

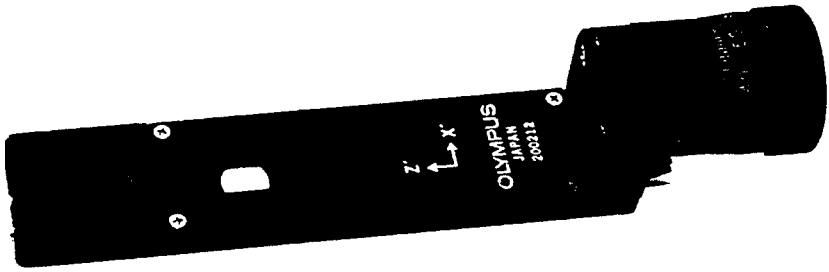

FIGURE 6.31 Berek compensator. (*Photo by A. K. Varshneya.*)

side of the 30° null position to bring the black line back to the center of the crosshairs. It should be noted that the Berek can only compensate one sign of birefringence: The specimen may have to be rotated by 90° for compensation to occur. Nonetheless, Berek is a very widely used instrument, primarily because of its compactness, and also because the compensator can be designed (procured) to measure a range of birefringence magnitudes such as 0 to $\lambda/10$, 0 to λ, and 0 to 10λ.

6.5.9.5 The Sénarmont Compensator

A Sénarmont compensator utilizes a quarter-wave plate introduced between the specimen and the analyzer (Fig. 6.32). Its fast axis is lined up with that of the polarizer. When a stressed glass specimen is introduced (with its axes at 45°), the field of view appears bright in the presence of stresses. The analyzer is rotated by an angle $\theta°$ to achieve extinction. The phase difference introduced by the specimen is $2\theta°$, which implies that the path difference introduced is $2\lambda\theta°/360°$. If $\lambda = 540$ nm, then the path difference introduced by the specimen is 3θ nm. The direction of rotation gives the sign of the birefringence. Thus, tension and compression can both be measured without changing the orientation of the specimen. However, the maximum permissible rotation is 180°, hence the Sénarmont compensator is limited to measuring a maximum of λ nm retardation. The usefulness of the Sénarmont compensator lies in the high level of accuracy with which small retardations can be measured.

6.5.9.6 Measurement of Surface Stresses

An instrument that allows surface stresses to be measured *individually* is the differential surface refractometer (DSR), shown in Fig. 6.33. It is quite useful for surface compression measurements in strengthened glass windows. A specially designed prism rests on the flat glass specimen. The refractive index of the prism glass must be higher than that of the glass specimen in order to allow a total internal reflection at the glass surface. Optical contact between the prism and the glass is assured by using a few drops of an intermediate-refractive-index oil. Some of the incoming light vibrations punch through the glass surface and are internally reflected back (with mirage-like bending), exiting out of the prism at critical angles corresponding to the two refractive indices of the stressed glass. Since the critical angles for the two polarized transverse vibration components (one perpendicular, the other parallel to the test glass surface) are different in general, the exiting rays come out in two slightly shifted bundles, which are then focussed by a telescope. The shift between the two (see Fig. 6.33*b*) is measured and calibrated in terms of the optical retardation. For the surface, velocity of the vertical vibration corresponds to refractive index of the glass in a stress-free condition (since the normal stress component must be zero). Thus, the entire measured optical retardation

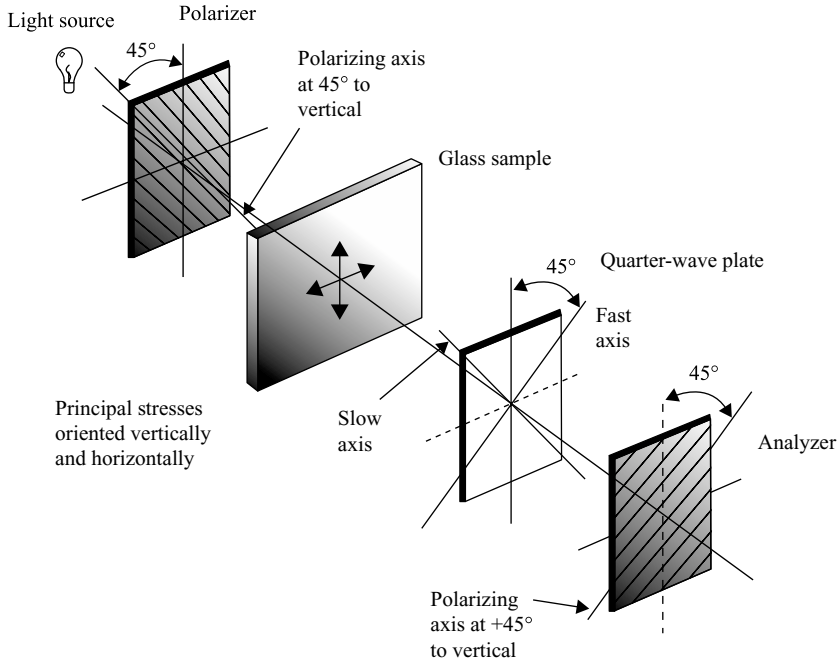

FIGURE 6.32 Polariscope arrangement for Sénarmont compensation. (*H. W. McKenzie and R. J. Hand, Basic Optical Stress Measurement in Glass, Society of Glass Technology, Sheffield, England, 1999, p. 41.*)

corresponds to the in-plane stress (normal to the plane of incidence) in the test glass. Compression or tension may be identified by the direction of the shift relative to the neutral beam. The DSR requires specific prisms for various glass compositions. It is also a common experience that measurements on a float glass are possible only on the tinned side—the refractive index increases with depth on the air side, causing the light rays to bend more into the depth instead of being bent mirage-like to exit. Nonetheless, the DSR requires little sample preparation, and is essentially nondestructive.

Another instrument that enables the measurement of surface stresses is the grazing angle surface polarimeter (GASP), Fig. 6.34. The GASP instrument is much like the DSR, except that a polarized light beam is incident on the glass at a critical angle. Thus, the beam of light travels in the surface and is continuously attenuated and refracted back into the prism; the longer the travel, the larger its optical retardation. The optical retardation in these rays is compared with the main beam of light, which has been specularly reflected by the top surface, by using a Babinet compensator. The no-stress fringe pattern of the Babinet compensator rotates—the rotation is related to the optical retardation due to the in-plane stress normal to the plane of incidence. The sign of stress may be deduced from the direction of the rotation. Again, the instrument can be used only on the tin-side of a float glass; however, it requires no specimen preparation. The GASP instrument is more sensitive than a DSR, since traveling on the surface over a path length t allows a greater amount of optical retardation to be accumulated by multiple refractions.

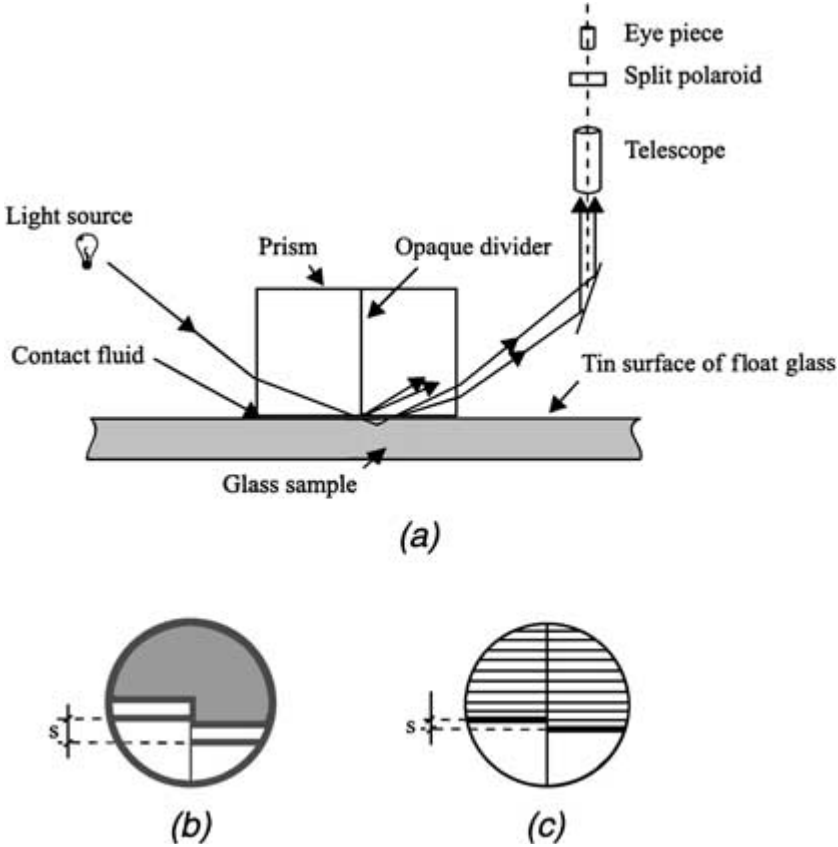

FIGURE 6.33 Optical arrangement for differential surface refractometer and diagrammatic representation of fringes for thermally and chemically toughened glass. (*H. W. McKenzie and R. J. Hand, Basic Optical Stress Measurement in Glass, Society of Glass Technology, Sheffield, England, 1999, p. 64.*)

6.5.9.7 Measurement of Internal Stresses. In tempered glass products, the measurement of the magnitude of center tension is often desired. This can be achieved by a laser light scattering method, as shown in Fig. 6.35. A laser beam that has been polarized to have its intensity vector at 45° to the midplane of the glass is allowed to enter glass from the edge, making sure that propagation of the beam occurs through the central plane. Two transverse vibrations propagate—one parallel to the midplane, the other perpendicular to it—generally at different velocities because of the difference in the stress magnitudes along these planes. Because of the gradual development of phase difference between the two with continuing propagation, there will be a location when the vibrations develop exactly one wavelength retardation. This means that the original vector of vibrations will be reconstituted (which is oriented at 45° to the midplane). When the scattered light is viewed from a point outside along this vector, no intensity will be observed (since light rays may not have longitudinal vibrations). At locations corresponding to a half-wavelength

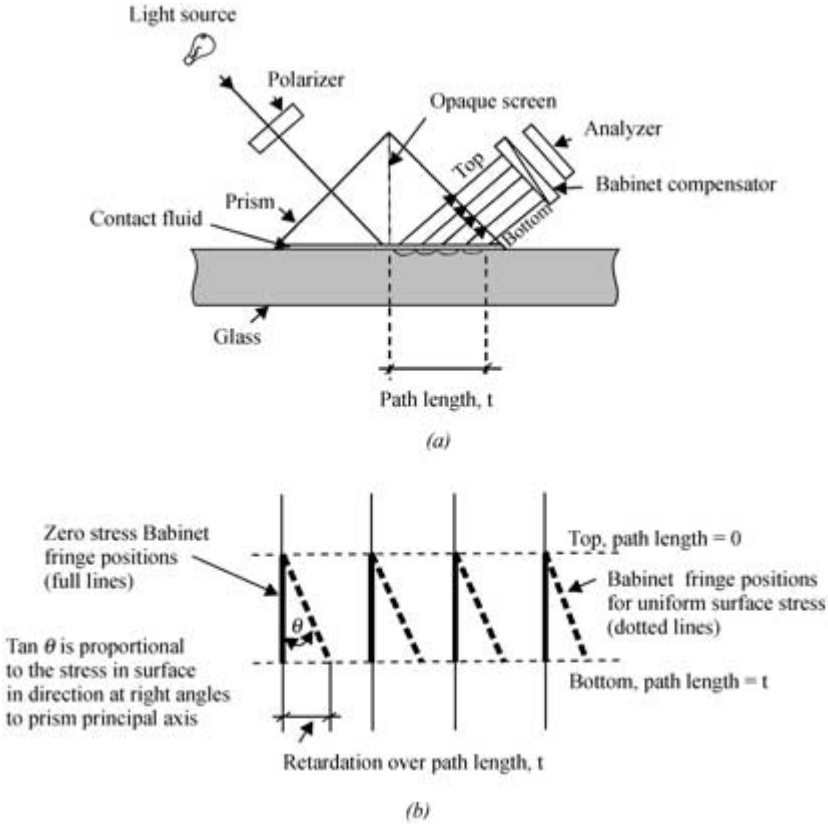

FIGURE 6.34 Optical arrangements and fringe pattern for surface polarimetry. (*H. W. McKenzie and R. J. Hand, Basic Optical Stress Measurement in Glass, Society of Glass Technology, Sheffield, England, 1999, p. 67.*)

retardation, the reconstituting vector makes a 90° angle to the original vector, and one will observe maximum scattered intensity (allowed transverse vibration) when viewing along the original vector. Thus, one observes an interference pattern consisting of 10 to 20 bright bands of light separated by dark bands. The center-to-center distance between two adjacent fringes is measured (by averaging over several fringes) and related to stress by the stress-optic equation, where $\delta = \lambda$ nm. The laser light scattering method is useful where the stress field does not change greatly, for instance, in the midplane region of a chemically strengthened glass. Small, 10- to 20 m-W output, portable polarized light lasers are well-suited for the purpose.

6.5.9.8 Practice and Limitations of the Through-Transmission Photoelastic Techniques. *Light transmission through a glass product in order to view birefringence is greatly aided by (and often necessary) immersion in a matching refractive index oil*. Suitably sized rectangular immersion cells of clear glass plates (not plastic plates) should be

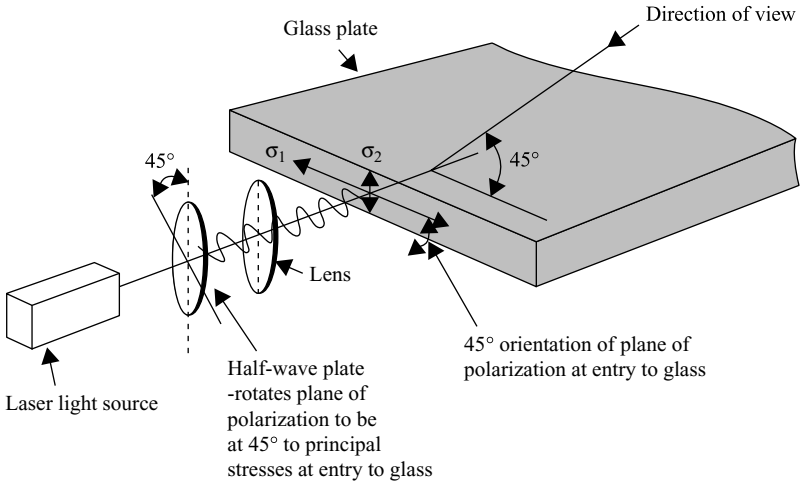

FIGURE 6.35 Optical arrangement for scattered light measurements in thin glass plates. (*H. W. McKenzie and R. J. Hand, Basic Optical Stress Measurement in Glass, Society of Glass Technology, Sheffield, England, 1999, p. 60.*)

constructed. (The corners may be joined by an epoxy.) The matching refractive index allows rectilinear propagation of light without bending at curved surfaces of the glass product. Occasionally, it may be desired to view birefringence through the wall thickness of the glass. In such a case, slices or ring sections having parallel surfaces containing the wall should be sawed out of the glass by a slow-speed diamond wheel saw. (*A considerable amount of experimental skill is needed to obtain wall sections with well-preserved edges.*) The flat surfaces may be smoothed by a fine abrasive slurry on a ceramographic grinding/polishing wheel. Again, use of a drop of a matching refractive index oil on both surfaces sandwiched between a microscope slide or a glass cover slip helps photoelastic measurements.

In a laboratory environment, photoelastic measurements are often made with a commercially available transmission type polarizing microscope. Care should be taken in procuring strain-free optics. For most measurements, it will be necessary to remove the condenser mechanism to allow incidence of light rays on the specimen in a collimated manner.

It should be readily realized that only transparent glasses can be subjected to photoelastic techniques. Darkly colored glasses or sintered glasses are not amenable to these techniques.

A serious problem in the measurement of stresses in glass is the fact that the stress field is rarely uniaxial. One usually needs to consider the effect of a biaxial stress field perpendicular to the direction of light propagation (*a stress component along the direction of light propagation has no effect*). The stress-optic relation has to be modified to read

$$\sigma_{33} - \sigma_{11} = \delta/Bd \tag{6.3}$$

This means that only the difference of principal stresses integrated along the light path d can be estimated by the through-transmission techniques. Since fracture in glass occurs mostly perpendicular to the maximum principal tension, no information about stress magnitudes or sign is obtained in a random stress field. Individual stress components can be separated only at a surface where the normal stress component must be zero, or the second component adds to zero over the light path d. The integration over d also implies that a

biaxial stress field, which varies along the light path, would be impossible to resolve. The sign of the observed birefringence changes if the specimen is rotated by 90°. Hence, even if one of the stress components is zero, the type of the stress (tension or compression) can be mixed up because of an "unknown" orientation. It is strongly advised that a stressed-glass standard be used to calibrate a polarized light microscope setup.

Having extinction at some location does not always imply absence of stresses. It may also mean that the principal stress axes are lined up with the polarizer axes.

Finally, most polarization equipment rarely provides a spatial resolution better than about 100 μm. Glass-to-metal seals often require stress information on a scale of 10 μm or better. Nonetheless, photoelastic methods of measuring stresses in glass remain the most useful means of glass product quality control and assurance.

6.6 GLASS FIBER

This and the following section (6.7) discuss a variety of types of glass fiber, including discontinuous filament glass "wool" used for thermal insulation, continuous filament fiber used for textiles, and the very technically sophisticated optical fiber used for modern high-data-rate, long-distance communications. The compositions and manufacturing processes used for each application differ from each other and from the more common glass manufacturing processes described in Sec. 6.4. For these reasons we are discussing fiber applications, compositions, and manufacturing together in two separate main chapter sections.

In this section (6.6) we will describe manufacture of the continuous and discontinuous fiber used for textiles, reinforcement, insulation, and filter media. All of these materials are often referred to by the one word *fiberglass*. This section also discusses traditional (non-communication) fiber optics. Optical communications fiber is discussed in Sec. 6.7.

6.6.1 Discontinuous Fiberglass (Wool and Textile)

Terminology. Wool is a fluffy mass of discontinuous fibers, generally held together by an organic binder.

Brief History. Glass fibers have been manufactured for insulation and other purposes since the nineteenth century. In the earliest forms, natural mineral compositions, like basalt, and slag from iron-smelting blast furnaces were melted and fiberized (fibrillated) by directing a jet of steam or air perpendicularly across a falling stream of molten glass (Fig. 6.36). The shear forces from the vapor jet would disrupt the glass stream into droplets and attenuate some droplets into fiber. Whether the molten material remained as droplets or was attenuated into fiber, and whether the attenuated fiber remained as such (or disintegrated into arrays of smaller droplets) depended on the size of the droplets, the shear forces exerted by the jet, and the rates of cooling. Many small unusable droplets of glass, called *shot*, often as much as 50 vol% of the melt, were produced, resulting in rather poor process efficiency. The range of fiber diameter produced in any given operation was quite broad. (*Note:* This same type of process, adjusted differently, was described above for the manufacture of glass microspheres.)

Dramatic improvements to the process were made in the 1930s. In modern steam-blown fiberglass manufacture, the molten glass is delivered through multiple holes in the bottom of a heated platinum trough. Each hole is a millimeter or so in diameter and delivers glass at the rate of a few pounds per hour. Pairs of downward-directed blowers, one on each side of the trough, impinge on the streams of glass, attenuating them into thin fiber (3 to 6 μm

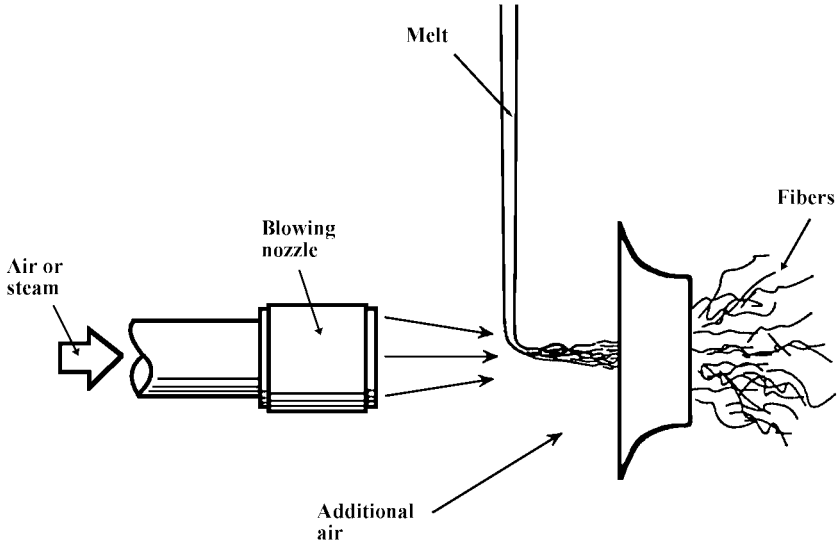

FIGURE 6.36 Fiber-blowing process used to make refractory ceramic fibers. [*Man-Made Vitreous Fibers: Nomenclature, Chemical and Physical Properties, Nomenclature Committee of TIMA Inc., p. 16 (NAIMA—North American Insulation Manufacturers Assoc.).*]

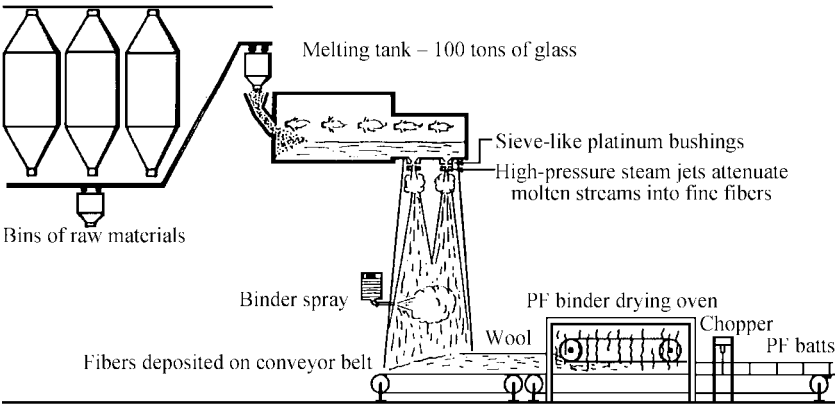

FIGURE 6.37 Steam-blowing (Owens) process for making fiberglass. (*J. G. Mohr and W. P. Rowe, Fiber Glass, Van Nostrand Reinhold, New York, 1978, p. 9.*)

diameter, 3 to 10 cm length). The percentage of shot or nonfiberized glass is still significant. This process, illustrated in Fig. 6.37, continues to be used to varying extent throughout the world. In the United States it is used primarily for specialized fiber applications, but has generally been replaced for building insulation by the rotary process that is described in the next paragraph.

Centrifugal fiber forming processes date back to the 1920s when the Hager process was invented, whereby a stream of molten glass is fed onto a horizontal rotating disk, from which

it is flung off as strands or fibers by centrifugal force. Hager fibers were rather coarse and not as well controlled as steam-blown fiber. In the 1930s, St.-Gobain in Europe and Owens-Corning Fiberglas in the United States developed the rotary (or modern centrifugal) process whereby molten streams of glass are delivered by centrifugal force through multiple fine orifices in the wall of a shallow rotating cylinder, called a *spinner*. An annular downward-directed burner, concentric with and exterior to the rotating cylinder, attenuated the glass streams into fine fibers. A later version, due to Owens-Corning, uses an annular burner to heat the cylinder and an annular steam blower to attenuate the fiber. Variations on these two processes, with spinners up to 2 ft in diameter and containing many thousands of holes (orifices) are now used throughout the world to produce hundreds of thousands of tons of product annually. The rotary process is illustrated in Fig. 6.38.

Applications. Major applications are thermal and acoustical insulation, filtration media, and staple fiber for textiles.

Common Compositions

- *A glass.* This soda-lime-silica composition, with little or no B_2O_3, related to container and window glass, was used in early glass wool manufacture and because of its relatively low cost, is still in use in some parts of the world. However, for many applications, its relatively poor chemical durability leads to mechanical failure due to stress corrosion. For example, when it was used as thermal insulation in refrigerated railroad cars, condensed moisture and constant mechanical vibration often led to fiber fracture, crumbling of the wool, and settling of the insulation at the bottom of the insulating panels. (Because of the small fiber diameter and consequent high surface-to-volume ratio, fibers are much less resistant to water attack than are bulk glasses.)
- *T glass.* Thermal glass (T glass) was developed in the 1930s to supersede A glass. It contained less silica, less alkali, and more lime than A glass; B_2O_3 was added to improve acid and water durability and to lower viscosity. It was more expensive because of the boron content. It was manufactured by the Owens steam-blowing process; however, because of a relatively low liquidus viscosity, it was unsuitable for manufacture by the high-throughput rotary process developed in the 1950s.
- *Modern wool fiberglass compositions.* These stem from Welsh's patent (U.S. Patent 2,877,124, September 25,1955). They tend to contain even more B_2O_3 than T glass. (It should be noted that some authors refer to these modern compositions as T2 glass, calling the earlier compositions T1 glass.)
- *Rock wool and slag wool.* These materials are still manufactured to varying degrees throughout the world. The raw materials are basalt, basalt in combination with limestone, and blast furnace slag.

Composition ranges and typical physical properties for wool-type fiberglass compositions (including rock wool and slag wool) are shown in Tables 6.22 and 6.23.

Manufacturing Processes Summarized

1. Steam or air blowing (Owens process, Fig. 6.37)
   - Blows high-pressure steam or air downward to entrain a stream of glass
   - Produces fibers and lots of unwanted glass droplets, called shot
   - Advantage: high-viscosity and high-liquidus-temperature glasses such as rock wool and slag wool can be fiberized this way

TABLE 6.22 Fiberglass Compositions, wt%

Glass identification		SiO_2	Al_2O_3	B_2O_3	Li_2O	Na_2O	K_2O	MgO	CaO	BaO	ZnO	F	Other	References
Continuous fiberglass														
A glass	Ranges	63–72	0–6	0–6		14–16	~Na+K	0–4	6–10			0–0.4	TiO_2 = 0–0.6; Fe_2O_3 = 0–0.5	Hofmann[17]
C glass	Ranges	64–68	3–5	4–6		7–10	~Na+K	2–4	11–15	0–1			Fe_2O_3 = 0–0.8	Hofmann[17]
	Typical	65	4	5.5		8.5	~Na+K	3	14					Aubourg & Wolf[5]
D glass	Ranges	72–75	0–1	21–24		0–4	~Na+K		0–1				Fe_2O_3 = 0–0.3	Hofmann[17]
E glass	Ranges	52–62	12–16	0–10		0–2	~Na+K	0–5	16–25			0–1	TiO_2 = 0–1.5; Fe_2O_3 = 0–0.8	Aubourg & Wolf[5], Aubourg et al.[7]
	Typical	54	14	10				4.5	17.5					Boyd et al.[9]
	Advantex	X	X	None				X	X				X	Owens Corning
E CR glass	Ranges	54–62	9–15			0–1	~Na+K	0–4	17–25		0–5		TiO_2 = 0–4; Fe_2O_3 = 0–0.8	Hofmann[17], Aubourg et al.[7]
	Typical													
AR glass	Ranges	55–75	0–5	0–8	0–1.5	11–21	~Na+K		1–10			0–5	TiO_2 = 0–12; ZrO_2 = 0–18; Fe_2O_3 = 0–5	Hofmann[17]
R glass	Ranges	55–65	15–30			0–1	~Na+K	3–8	9–25			0–0.3		
S glass	Ranges	64–65	24–25			0–0.3	~Na+K	10–11	0– 0.1				Fe_2O_3 = 0–0.2	Hofmann[17]
	Typical	65	25					10						Aubourg & Wolf[5], Aubourg et al.[7]

TABLE 6.22 Fiberglass Compositions, wt% (Continued)

Glass identification		SiO_2	Al_2O_3	B_2O_3	Li_2O	Na_2O	K_2O	MgO	CaO	BaO	ZnO	F	Other	References
Wool fiberglass	Ranges	55–70	0–7	3–12		13–18	0–2.5	0–5	5–13	0–3		0–1.5	TiO_2 = 0–0.5; Fe_2O_3 = 0.1–0.5; S = 0–0.5	Aubourg et al.[7], TIMA/NAIMA
Welsh's patent (1995)	Ranges	50–65	0–8	5–15		10–20	~Na+K	0–10	3–14	0–8	0–2		TiO_2/ZrO_2 = 0–8; Fe_2O_3 = 0–12; MnO = 0–12	Aubourg & Wolf[5]
	Typical	58.6	3.2	10.1		15.1	~Na+K	4.2	8					Aubourg & Wolf[5]
T_2 glass	Typical	59	4.5	3.5		11	0.5	5.5	16					Boyd et al.[9]
SF glass	Typical	59.5	5	7		14.5						N.A.	ZrO_2 = 4; TiO_2 = 8	Boyd et al.[9]
Rock wool														
Basalt (glass furnace)	Ranges	45–48	12–13.5			2.5–3.3	0.8–2	8–10	10–12				TiO_2 = 2.5–3; FeO = 5–6; S = 0–0.2	Aubourg et al.[7], TIMA/NAIMA
Basalt + limestone (cupola)	Ranges	41–43	6–14			1.1–3.5	0.5–2	6–16	10–25				TiO_2 = 0.9–3.5; FeO = 3–8; S = 0–0.2	Aubourg et al.[7], TIMA/NAIMA
Slag wool (cupola)	Ranges	38–52	5–15			0–1	0.3–2	4–14	20–43				TiO_2 = 0.3–1; FeO = 0–2; P_2O_5 = 0–0.5; S = 0–2	TIMA/NAIMA

Note: X = Specific composition unavailable from manufacturer.

TABLE 6.23 Fiberglass Properties

Glass identification		Density, g/cm^3	CTE, 0–300°C, 10^{-7}/°C	Strain point, °C	Annealing point, °C	Softening point, °C	At 10^3 P, °C	Liquidus, °C	Young's modulus, GPa	Tensile strength, GPa (23°C)	Refractive index	References
Textile fiberglass												
A glass	Typical	2.44				705			68.9	3.3	1.538	Hartman[18]
C glass	Typical	2.56	63	552	588	750			70	3.3	1.537	Aubourg et al.[7]
D glass	Typical	2.11		477	521	771			51.7	2.4	1.465	Hartman[18]
E glass	Ranges	2.52–2.62	54	600–630	640–675	830–860			76–78	3.1–3.8	1.547–1.562	Owens Corning
	Typical	2.62	54	615	657	846			72.3	3.4	1.562	Aubourg et al.[7]
	Advantex	2.62	60	691	736	916			80–81	3.1–3.8	1.560–1.562	Owens Corning
E CR glass	Ranges	2.66–2.68	59			880			80–81	3.1–3.8	1.576	Owens Corning
	Typical	2.76				882			81.3	3.4	1.583	Aubourg et al.[7]
AR glass	Typical	2.7				773			73.1	3.2	1.562	Hartman[18]
R glass	Typical	2.54				952			85.5	4.1	1.546	Hartman[18]
S glass	Ranges	2.46–2.49	29	766	816	1056			88–91	4.6–4.8	1.523–1.525	Owens Corning
	Typical	2.50	16	760	810	970			88.9	4.6	1.525	Aubourg et al.[7]
Wool fiberglass	Ranges	2.40–2.55				650–700	915–1085	880–955	55–62	2.4	1.51–1.54	Aubourg et al.[7], TIMA/NAIMA
Welsh's patent	Ranges							870–980				Aubourg & Wolf[5]
	Typical						1015	925				Aubourg & Wolf[5]
T_2 glass	Typical	2.54	80			715					1.541	Boyd et al.[9]
SF glass	Typical	2.57	75			675					1.537	Boyd et al.[9]
Rock wool												
Basalt (electric furnace)												
Basalt + limestone (cupola)												
Slag Wool (cupola)												

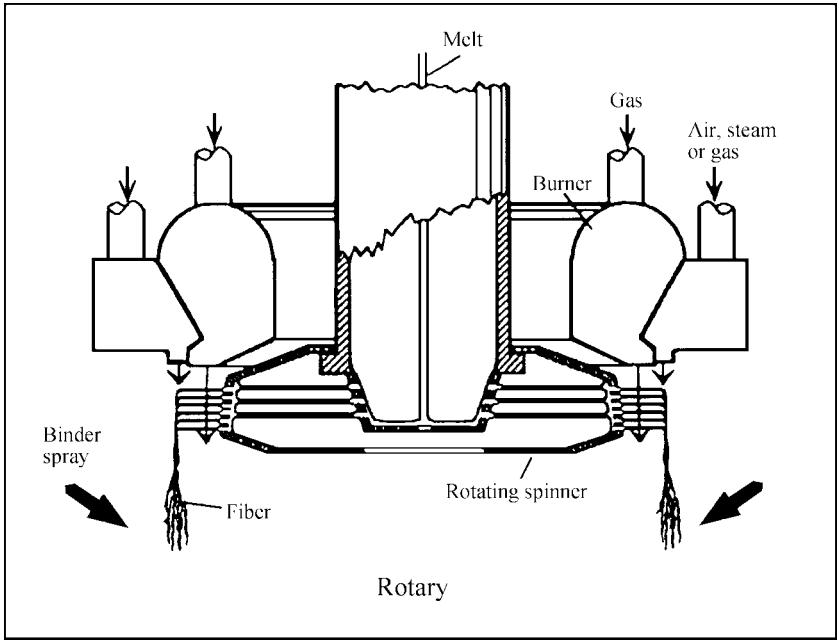

FIGURE 6.38 Rotary fiberglass wool-forming process. [*Man-Made Vitreous Fibers: Nomenclature, Chemical and Physical Properties, Nomenclature Committee of TIMA Inc.* (*Courtesy of NAIMA—North American Insulation Manufacturers Assoc.*).]

2. Rotary process (Fig. 6.38)

- Most commonly used process
- Free of shot
- Molten glass fed into rotating cylinder (spinner cup) with many holes in the sidewall
- Centrifugal force extrudes glass laterally
- High-velocity gas stream (air, steam, combustion gases) entrain and attenuate fiber
- Disadvantage: viscosity and liquidus temperature must be low enough for spinning (rock wool and slag wool liquidus temperatures too high to be made by this process)

Other processes:

3. Mechanical attenuation (see Fig. 6.39)

- Also called the rock wool, wheel centrifuge, cascade, or mechanical spinning process
- Stream of glass falls on rotating disks or series of rotating wheels/drums
- Produces unwanted shot

4. Flame attenuation

- 1-mm (approximate diameter) primary fibers drawn from bushings
- Aligned and passed through burner jet to elongate

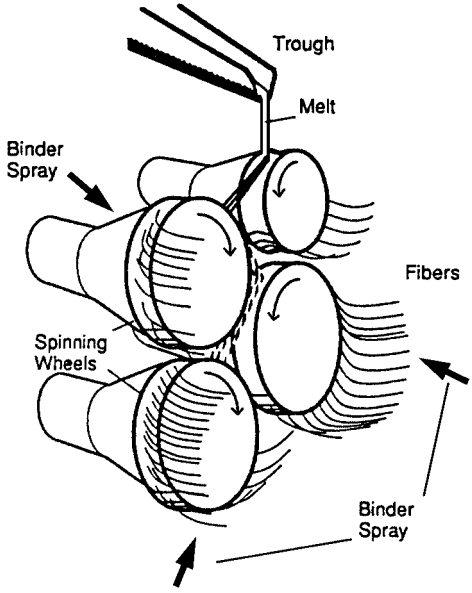

FIGURE 6.39 Mechanical attenuation method for making rock wool and slag wool. [*Man-Made Vitreous Fibers; Nomenclature Chemical and Physical Properties, Nomenclature Committee of TIMA Inc., p. 17 (Courtesy of NAIMA—North American Insulation Manufacturers Assoc.).*]

- Passed through binder spray and collected
- Very fine fibers are possible (less than 0.1- to 8-μm diameter)

Thermal insulation and filter media are manufactured continuously following fiberization. The glass may be fiberized by any of the processes described above. As the fiber falls after fiberization, it is sprayed with a binder, which increases its volume by 5 to 15 percent. The sprayed fiber is then collected as a wool mat on a conveyor belt, compressed by rollers, cured in an oven, and cut into lengths. This is illustrated for the steam-blowing process in Fig. 6.37. The velocity of the conveyor and the height of the roller control mat density. It ranges about 0.5 to 5 lb/ft^3.

Fiber diameters for insulating materials range between 0.2 and 30 μm, with specific surface areas of 0.1 to 0.2 m^2/g. Upper use temperature for glass wool is about 550 to 600°C.

Staple textile yarn (a yarn composed of overlapping discontinuous fibers) can be produced on small scale by collecting discontinuous fiber on a rotating, perforated vacuum drum, then cutting it loose and carding it (somewhat like animal wool and cotton) and finally twisting (spinning) it into strands and yarns. The product is generally of a lower quality and strength than those made by continuous fiber processes (to be described next) because of diameter variations and short fiber length.

Nonwoven mats are formed by collecting the fiber on a continuous suction belt.

6.6.2 Continuous Fiber (Textile and Reinforcement)

Textile Terminology

- Filament (single fiber)
- Strand (made up of many filaments)
- Size or sizing (protective lubricant; may also be a coupling agent)
- Yarn (twisted and/or plied from strands)
- Roving (strands bundled together, but not twisted or plied)
- Textured (strands with fiber spacing opened/varied)

Brief History. Glass fiber in long strands has been produced by hand since ancient times, the length of fiber being determined pretty much by how far and fast two people could run apart while stretching a rapidly cooling gob of glass.

Continuous yarns of glass fiber needed for weaving of textiles can be produced from discontinuous fiber, as described in the previous section. Such yarn has significant strength limitations and the disadvantage of many abrasive fiber ends at the yarn's surface. The goal of yarn made from continuous fiber of arbitrary length was realized in the 1930s through a joint effort by Owens-Illinois Glass Company and Corning Glass Works, which led to the formation of Owens-Corning Fiberglas Corporation. The process consists of simultaneously drawing continuous filaments (fiber) from multiple (up to about 4000) electrically heated precious-metal orifices (called *bushings*), spraying these filaments with a lubricating sizing as they cool, combining into a single multifilament strand, and gathering by winding onto a spool. The wound product is referred to as spun cake. This is sometimes referred to as the bushing fiberizing process. It is shown schematically in Fig. 6.40. The melter supplying the molten glass either melts batch, as described in Sec. 6.4 (direct melt), or remelts glass marbles (15 to 20 mm diameter) produced at a different location (marble melt)

Applications

1. *Woven*—electrical insulation, fabrics (drapes, clothing), screening, battery separator mats, fiber-reinforced composites
2. *Nonwoven*—mats, tire cord, gaskets, fiber-reinforced composites
3. *Chopped fiber*—reinforced composites

Useful physical properties of textile fiberglass include a linear stress-strain relationship up to the yield stress (3400 MPa for E glass and 4500 MPa for S glass; approximately 5 percent deformation), heat resistance and lack of flammability.

Common Compositions. Several different glass composition types are currently manufactured as continuous-filament fiber. The choice of type depends primarily on the intended application. Traditionally, each type has been given a letter name indicative of its original intended application. The names and some key characteristics follow.

- *A glass*—composition discussed in Sec. 6.6.1.
- *E glass*—a calcium aluminosilicate with less than about 2 wt% alkali; developed in the 1930s for electrical insulation applications. It has good electrical resistivity because of its low alkali content. Because of its excellent mechanical properties, its use has spread, particularly for glass-reinforced plastics. (Over 90 percent of all continuous-filament fiber is E glass.) However, it has poor acid durability.

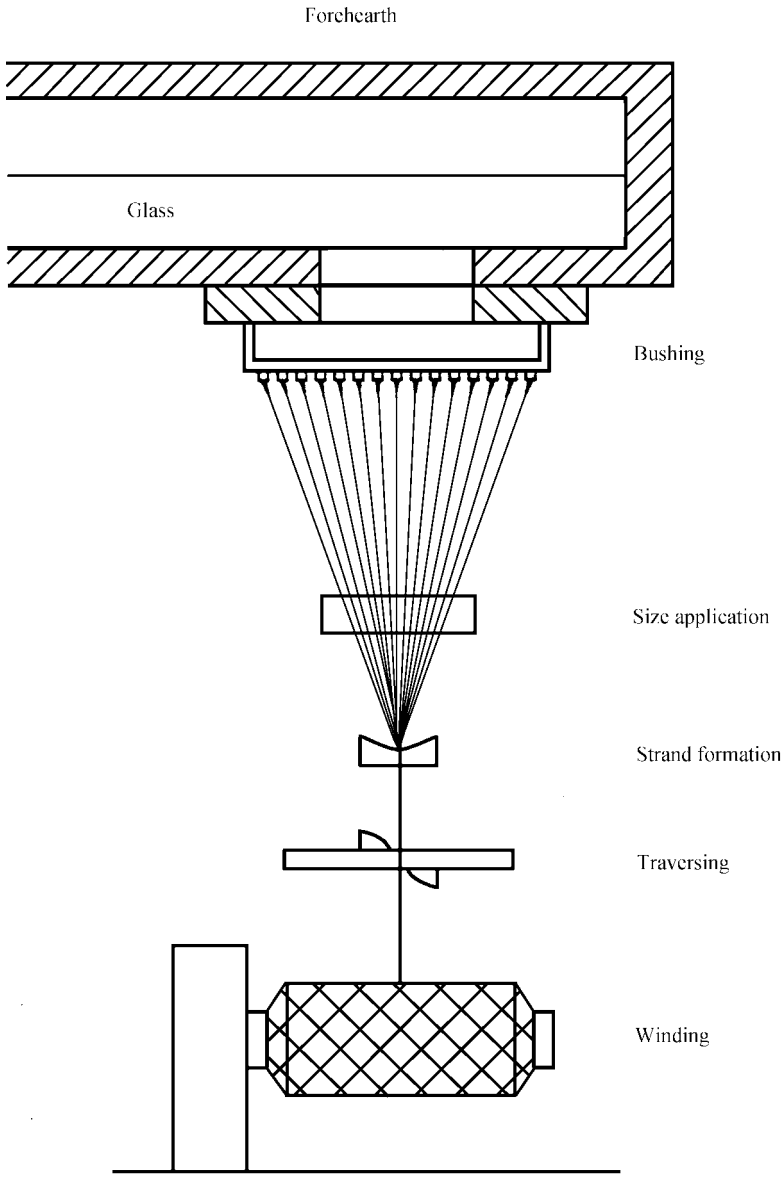

FIGURE 6.40 Continuous filament fiberglass drawing process. (*From P. F. Aubourg and W. W. Wolf, Ref. 5.*)

- *E-CR glass* (CR indicates corrosion resistant)—similar to E glass, but alkali and B_2O_3 are each less than 1 percent. It has improved acid durability.
- *C glass* (C indicates chemically stable)—soda-lime borosilicate; good chemical stability in corrosive environments; used in highly acid environments (e.g., reinforcement of acid-carrying vessels) and other special applications.
- *S glass* (S indicates strong)—essentially pure magnesium aluminosilicate; high-strength/weight ratio and high-use temperature; used especially as reinforcement of containers having high internal pressure.
- *R glass* compositions showing high tensile strength in combination with resistance to acid corrosion.
- *Advantex*™—a boron-free E glass that, according to manufacturer (Owens-Corning), combines the advantages of E and E-CR glasses and has higher temperature capability.
- *Other*—AR (alkali-resistant, used to reinforce cement); L glass (lead, for radiation shielding); D glass (dielectric); M glass (high modulus).

Typical compositions and glass properties for most of these types are given in Tables 6.22 and 6.23. The tabulated ranges have been taken from several sources. The precise compositions used by any single manufacturing plant often depend on their specific manufacturing process and the available raw materials. The fiberglass manufacturers publish few compositions and, with the exception of E glass, there are no published standards for composition.

Bushing Fiberizing Manufacturing Process Summarized

- Melt and deliver glass
- Draw from bushings (Pt-Rh alloy, electrically heated) containing 200 to 4000 orifices (nozzles), each 0.8- to 3.0-mm diameter, at speeds to 180 mi/h (80 m/s)
- A single filament is formed from each bushing
- Cool by air or water to form fiber (solid, continuous, 3- to 25-μm diameter.)
- Apply sizing (for abrasion resistance, may be designed for final application)
- Gather into strand (bundle)
- Wind on reel as spun cake (alternatively, rather than collecting it on a spool, the strand can be directly processed into rovings, continuous strand mats, or chopped strands)

During the fiber draw, the melt is highly deformed by attenuation under relatively high stress, the attenuation (area reduction) ratios being about 40,000:1. The elongated filaments are cooled under load; consequently, internal structural changes induced by the deformation are quenched in. Hence, the internal structure and physical properties of the fiberglass can differ from those of annealed glass of the same composition.

Glass Processing Requirements

1. A high-quality melt

- Few inclusions—could block bushing orifices or act as stress concentrators in fibers, leading to fiber breakage during draw and consequent process interruption (breakage of a single filament between the bushing nozzles and the winder generally causes breakage of others)
- Homogeneous (uniform viscosity)—same reasons

2. As low a temperature as possible, to limit deformation and wear of bushings (typically fiberize at about 500 to 1500 P; for E glass that requires temperatures of about 1250°C)

3. A low liquidus temperature (must operate the process at temperatures above the liquidus temperature to avoid devitrification in the bushing)

Other Manufacturing Methods. Continuous single filaments of glass fiber can of course be drawn upward from the surface of a melt, downward from an orifice at the bottom of a glass melting tank or a crucible, or in almost any direction off the heated end of a solid glass rod. For some applications, such single fibers are useful and the production methods efficient. But for most applications, the simultaneous downdrawing of multiple filaments, as described above, is preferred.

For composite reinforcement applications such as fiber-reinforced polymers (FRPs), also known as glass-fiber-reinforced plastic (GRP), the fiber can be supplied as chopped strands (at several standard lengths, from 3 to 12 mm) or continuous roving, which can be chopped at the point of composite manufacture. It can also be supplied as milled fiber, with lengths of about 0.2 mm. Roving can be woven into a wide variety of two-dimensional and three-dimensional shapes for polymer impregnation. The relationships between the various process steps and the resulting types of reinforcement fiber products are shown in Fig. 6.41.

Fiber Dimensions. For textile products such as textile yarns and plied yarns, filament diameters range from 5 to 13 μm. For plastic reinforcement, such as mats, rovings, and chopped strands, the diameters range from 9 to 25 mm.

6.6.3 Traditional Fiber Optics

Principles of Operation. With optical fibers, light is transmitted within the fiber, along its length, without losing a significant fraction of its energy through the walls of the fiber. This behavior is due to a principle called *total internal reflection*, which can be explained with reference to Fig. 6.42, recalling that, as discussed in Secs. 5.20.1 and 5.20.2, refraction and reflection at an interface between two transparent media behave according to Snells's law and Fresnel's equations.

For light traveling through a fiber surrounded by air (refractive index equal 1), or clad by a polymer or glass medium of refractive index less than that of the fiber core, there will be at the wall a maximum internal angle of incidence α_c, called the *critical angle*, for which the angle of refraction α' becomes 90°. For angles less than critical, some light is transmitted through the wall; at all greater angles the light is totally internally reflected. α_c can be calculated by Snell's law. By that same law, the entrance angle into the fiber (relative to the axis of the fiber), θ_c (corresponding to the angle of total internal reflection, α_c), is determined. All light entering the fiber at angles less than this critical entrance angle will be transmitted through the fiber. Correspondingly, light entering the fiber at angles greater than this critical angle will eventually, after multiple reflections, be lost through the walls of the fiber. The sine of this angle is called the *numerical aperture* (NA) of the fiber. The higher the numerical aperture, the greater the light-gathering power of the fiber. An NA = 1 means that all light incident on the face of the fiber will be conducted or "piped" through the fiber. These same definitions and terminology apply to the optical communications fiber discussed in Sec. 6.7.

It should be pointed out that a simple unclad glass rod or fiber would channel light as described above. The maximum possible NA for a given glass composition results when it is surrounded by air or vacuum. However, for that case, any damage to the fiber surface, such as abraded scratches, disrupts the reflection conditions and allows light to leak (scatter)

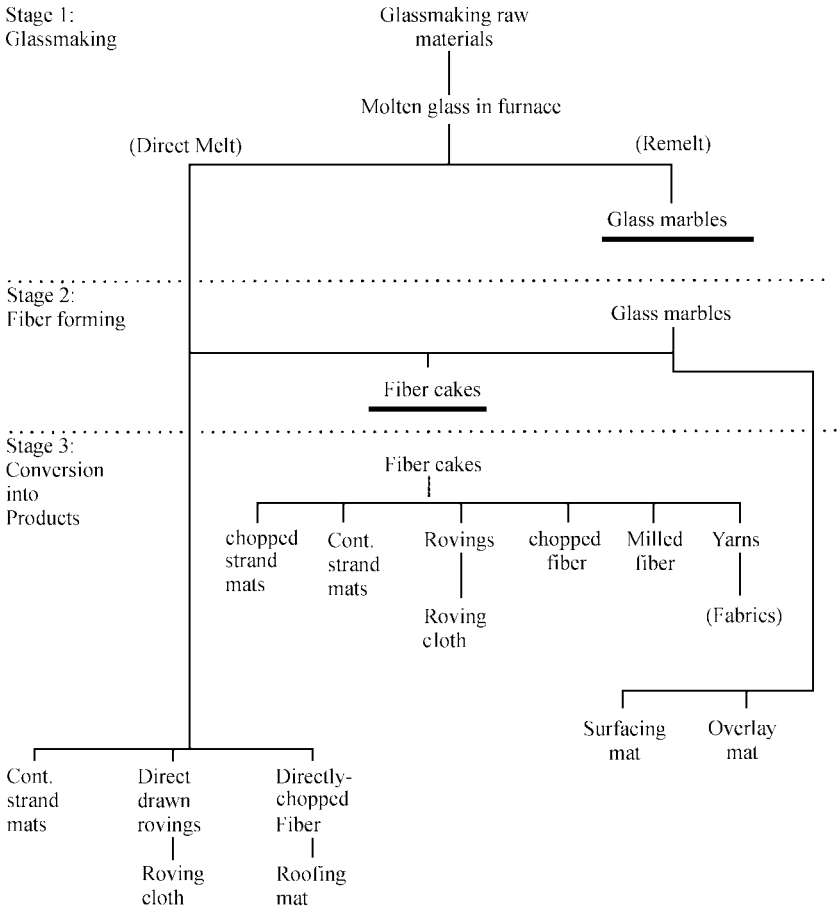

FIGURE 6.41 Flowchart of glass fiber products manufacture. Some products appear in more than one sequence; this is because they are made by both the remelt and the direct-melt processes. (*From K. L. Loewenstein, The Manufacturing Technology of Continuous Glass Fibers, 3d ed., Elsevier, New York, 1999, p. 23.*)

out of the fiber. Hence, the surface of the fiber generally requires protection by a lower-index glass or polymer cladding. Also, if unclad fibers are packed close to each other, some of the light traveling in one fiber may cross over into the adjacent fiber. This is undesirable in applications where images are to be transmitted coherently by the fiber bundle.

Traditional fiber optics such as those described in this section can be designed to transmit images, or illuminating light, or both. They consist either of flexible bundles of fibers, or arrays of fibers stacked and fused together along their length. The latter are appropriately called *fused fiber optics*. Either type may be used to transmit light of various wavelengths and intensities.

Either type (fused fiber optics or flexible bundles fused at each end, called *coherent bundles*) may also be used to transmit images. Since each fiber carries information (light

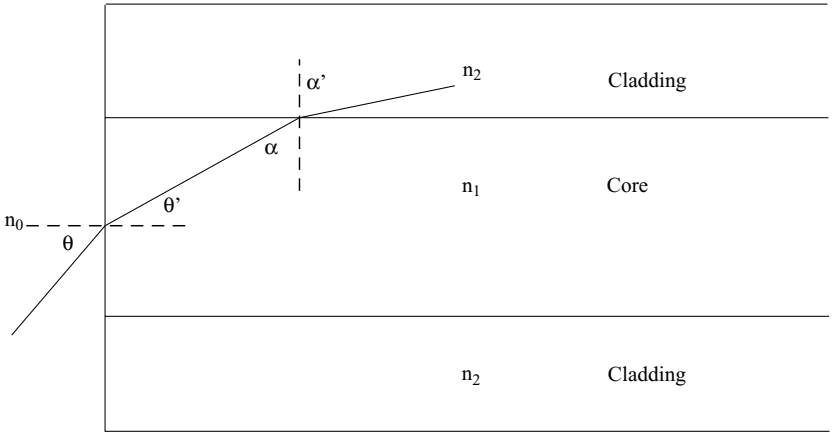

From Snell's Law:

$$n_1 \sin \alpha = n_2 \sin \alpha'$$
$$n_0 \sin \theta = n_1 \sin \theta'$$
$$\text{Sin } \theta = \frac{n_1}{n_0} \sin \theta' = \frac{n_1}{n_0} \cos \alpha = \frac{n_1}{n_0} \sqrt{1 - \sin^2 \alpha}$$
$$\text{Sin } \alpha = \frac{n_2}{n_1} \sin \alpha'$$

For critical α and θ :

$$\alpha' = 90^\circ$$
$$\sin \alpha_c = \frac{n_2}{n_1}$$
$$\sin \theta_c = \frac{n_1}{n_0} \sqrt{1 - \left(\frac{n_2}{n_1}\right)^2} = \frac{1}{n_0} \sqrt{n_1^2 - n_2^2} \equiv \text{NA}$$

FIGURE 6.42 Reflection relationships in clad fiber optics.

intensity) related to one geometric element of an image (a single pixel), the fiber size must be made smaller than the finest detail to be resolved; core diameters are often as small as 10 μm, and cladding is sometimes less than 0.5 μm thick.

Special Capabilities. Flexible fiber optics can transmit light and images around bends and in controlled paths. They can also scramble and unscramble images. Fused fiber optics can magnify, demagnify, rotate, and invert images.

Applications

Illumination

- Medical (diagnostics and surgery)
- Scientific instrumentation
- Automobile and aircraft instrument panels

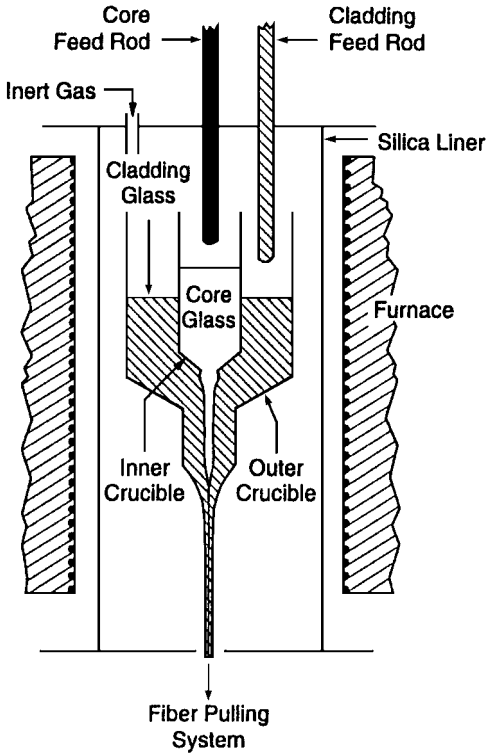

FIGURE 6.43 Schematic representation of a double crucible fiberization system. (*From A. J. Bruce, in Infrared Fiber Optics, J. S. Sanghera and J. D. Aggarwal, eds., CRC Press, Boca Raton, Fa. 1998, p. 35.*)

- Flat panel display back lighting
- Future automotive lighting (interior and driving lights)

Image transmission, magnification, and inversion

- Medical (diagnostic, surgery; endoscopes and the like)
- Technical (e.g., chimney, pipeline, chemical system inspection; remote sensing)
- Optoelectronic devices (including vacuum-tight electron tube faceplates for TV cameras and CRTs; advantages include flat fields and greater image intensity)

Process. Single filaments of clad fiber may be made by redraw of rod in tubing or, alternatively, by a double-crucible method, which is essentially a Vello-type delivery system, where a second glass, rather than air, is delivered through the center of the bell. A version of the latter method is illustrated in Fig. 6.43.

A flexible fiber optic is formed by bundling together many of these clad filaments or monofibers. Often the entrance and exit to the bundle are made more mechanically strong by locally fusing the fibers together, either by heating under pressure, with or without a glass sealing frit as a binder, or with a suitable organic polymer. The fused ends can then be polished to a smooth optical surface. Scrambling and unscrambling devices may be made by disarraying the fibers at some location along the length of the bundle, fusing them together at that location, then cutting the bundle at the fused point.

Fused fiber optic devices are formed by stacking together in parallel alignment hundreds of individual monofibers, then fusing them together under heat and pressure. These fused multifiber stacks are redrawn (to smaller cross-sectional dimensions) cut, stacked, fused, and redrawn again. This process is repeated until the target core diameter (or number of fibers per unit area) is achieved. The final multifiber elements are then cut, stacked and fused (but not redrawn) to give whatever size device is required. Sometimes an extra-mural absorbing (EMA) cladding is used to improve image contrast. This prevents leakage of light from one fiber core to another and attenuates light that enters the fiber stack through the cladding; a light-absorbing second cladding can be made part of the original (first-draw) fibers. More often, absorbing (black) glass rods are substituted for some of the fibers in the first stacking, in either a random or designed pattern. This is often sufficient to provide the extra-mural absorption needed for contrast enhancement.

Fused fiber-optic tapers can be used to magnify (or demagnify) images. Tapers are made by locally heating the central region of a length of fused fiber optic and stretching it to form an hourglass shape. From this hourglass, two tapered sections can be cut. Each section is capable of transferring an image from one surface to the other, the magnification being determined by the ratios of the two diameters (assuming a circular cross section). Image rotators or inverters are made by rotating one end of the hourglass with respect to the other as it is being drawn; not much necking is required.

Near-optical-quality glass is generally required for both core and cladding glasses. Example combinations of refractive index combinations and the corresponding fiber characteristics are:

$$n_1 = 1.700; \quad n_2 = 1.512; \quad \text{NA} = 0.78; \quad \theta_c = 51°$$
$$n_1 = 1.650; \quad n_2 = 1.560; \quad \text{NA} = 0.54; \quad \theta_c = 32°$$

The thermal expansions of core and cladding glasses must be designed to match from the set point of the softer glass to room temperature.

6.7 OPTICAL COMMUNICATIONS FIBER

6.7.1 Introduction

The subjects of optical communication of information and the associated applications of glass are discussed in Chap. 7. Because the invention, manufacture, and application of low-loss optical communications fiber have been so important to the development of worldwide telecommunications and computer networking for the past three decades, and promise to remain so well into the new century, we devote the final section of this chapter to the materials and techniques used to manufacture low-loss optical fiber.

The use of glass as the medium for long distance communication of information by optical signals was pioneered by Corning Glass Works (now Corning Incorporated) and AT&T Bell Telephone Laboratories (now Lucent Technologies). It was Corning that first

demonstrated in the early 1970s that optical fiber could be made with an optical signal loss rate less than 20 dB/km (approximately 1 percent of the input light transmitted through 1 kilometer of fiber), the upper limit imposed by the practicalities of telecommunications system design. This was done by using fiber made from titania-doped synthetic silica glass of otherwise extremely high purity. Each company, Corning and AT&T, proceeded to develop different approaches to manufacturing the fiber and soon others entered the business, sometimes with new techniques as well. In this section we will describe the various key methods of optical fiber manufacture.

6.7.2 Materials

As discussed in Chaps. 5 and 7, silica glass is the material of choice for long-distance optical communications applications. A significant reason is that silica is one of the few optically transmitting materials that can be made with sufficient purity that light absorption in the near-IR spectral region can be kept at an acceptably low level. The silica glass for optical communications fiber is not manufactured by the traditional melting approaches used for most other oxide glasses, but rather by methods based on those described in Sec. 6.2.9 for Types III, IV, and V fused silica.

Other glass composition types, such as fluorides, oxynitrides, and chalcogenides, have been considered, mainly because of their ability to transmit even longer infrared wavelengths, but they are not now manufactured in great volume for long-distance communication, partly because of difficulties in obtaining the extremely high purity needed for low optical loss, and partly because of manufacturing obstacles yet to be overcome.

6.7.3 Types of Optical Fiber Design

There are basically two types of optical communications fiber design, each having many variations. The first type, called *step-index* fiber, is similar in construction to that described in Sec. 6.6 for traditional fiber optics, with several key differences: (1) Communications fiber dimensions are generally much smaller. (The outside diameter is now a standard 125 μm; the core diameter can be as small as about 8 μm.) (2) The refractive index difference (Δn) between core and cladding is much smaller, on the order of 1 percent, or less. (3) Much greater precision is required for the critical dimensions, including core concentricity within the fiber.

The second type is called *graded index* (sometimes *GRIN*) fiber. Here the refractive index is varied from the central axis location gradually out into the cladding. Often the index gradient is parabolic in shape, highest at the axis, decreasing outwardly toward the cladding, but sometimes it is more complex in profile. The core region occupies about 50 to 70 μm of the fiber diameter; the outside diameter is generally, again, 125 μm.

Light propagates through an optical communications fiber as electromagnetic waves, similar to the way microwave energy propagates through a hollow microwave waveguide. Consequently, optical fibers are sometimes referred to as *optical waveguides* and fiber types are correspondingly classified according to whether they are single-mode or multimode.This waveguide terminology refers to the manner in which the light energy is transmitted down the fiber, in particular how the energy is distributed in space, not to how many different signals the fiber can carry. In fact, a single-mode fiber can carry information at much higher rates over a given distance than can a multimode fiber. These aspects of optical fiber communication are explained more fully in Chap. 7.

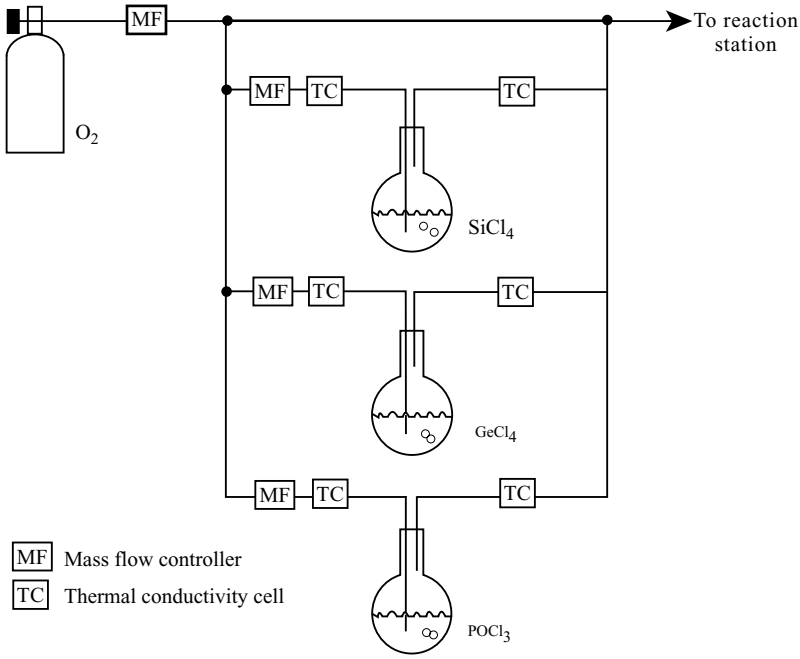

FIGURE 6.44 Reactant delivery system for vapor-phase techniques. (*From "Optical Fiber Waveguides" by R. M. Klein in Glass: Science and Technology, Vol. 2, Processing, edited by D. R. Uhlmann and N. J. Kreidl, copyright© 1983 by Academic Press, reproduced by permission of the publisher.*)

6.7.4 Manufacturing Processes

The manufacturing techniques for all the above types of fiber are generally similar. We list the key steps here as:

1. Vapor generation
2. Preform preparation (silica deposition, including refractive-index-adjusting elements)
3. Blank preparation (glass rod with required index gradient)
4. Fiber drawing
5. Coating
6. Testing

Step 1. As discussed previously, extremely high purity chemical precursors are required and used, even better than semiconductor manufacturing quality. The precursor for silica is often liquid $SiCl_4$. The refractive-index-controlling dopants, germania and fluorine are provided by $GeCl_4$ and SiF_4, respectively. (Other precursor chemicals can be used; there is a trend away from the chlorides, partly for environmental reasons.) These liquids are converted to the vapor phase by bubbling a carrier gas through the liquids at controlled temperatures, as illustrated in Fig. 6.44. Alternatively, the needed chemicals may be sublimed from the surface of a solid in the presence of a carrier gas. In either case, the materials

must have a high vapor pressure at reasonable process temperatures. This requirement actually limits the dopants that can be incorporated easily into the silica. During preform preparation, the ratio of the mix of chemical precursors is varied over time to control the eventual refractive index gradient within the fiber.

Steps 2 and 3. In these steps, the glass blank, the material that eventually will be drawn into fiber, is generated. It is here that the two major approaches to optical fiber manufacture first differ in a very significant way.

The first approach is called the *outside process*. In step 2, preform preparation, the chemical precursors are reacted in the flame of a specially designed gas-oxygen burner, the combustion gas being either natural gas or hydrogen, just as for all the Type III synthetic silicas described in Sec. 6.2.9.1 above. The doped silica is generated as a fine white amorphous (molten glass) soot that is progressively deposited on a rotating bait rod, as shown in Fig. 6.45*a*. The deposition begins with the material that will eventually lie at the axis of the fiber core, and ends with the material that will form the outside of the cladding. In other words, in the outside process, the preform is created from the inside outward. The resulting preform, inherently containing the desired chemical gradient, is porous and moderately fragile.

In order to consolidate this porous preform into a solid glass, in Step 3 the bait rod is removed and the remaining preform heated to temperatures near the softening point of fused silica to allow sintering of the soot via viscous flow. To ensure that air does not become trapped in interstices and thereby create bubbles in the glass, the preform is consolidated in a helium gas atmosphere. The rapid diffusion of helium through the silica glass assures that all voids shrink to zero dimensions under the forces of surface tension. As mentioned also in Sec. 6.2.9.1, Type III silicas contain water in their structure, in the form of OH bonds. Light absorption by such OH is extremely detrimental to communications optical fiber performance, so it is removed from the glass by flowing chlorine (Cl_2) gas through the preform at high temperatures just prior to consolidation.

This outside process is sometimes referred to as OVD (outside vapor deposition). This is somewhat a misnomer, because the glass is not deposited directly from the vapor phase, but rather by the progressive aggregation of submicroscopic particles that were themselves created from the vapor phase. The process has also been called radial flame hydrolysis (RFH).

In a variation of the outside process, called the *axial process*, the soot is deposited at the end of the rotating preform as it is gradually pulled away (withdrawn) from the burners, as illustrated in Fig. 6.45*c*. The preform is thus created from the end, the core and cladding materials being deposited essentially simultaneously. This process is sometimes referred to as vapor axial deposition (VAD), axial vapor deposition (AVD) or even axial flame hydrolysis (AFH).

In the second major approach, the so-called *inside process*, the preform is built up on the inside of a silica glass tube, beginning with the materials that will compose the bulk of the fiber cladding, and ending with what will become the innermost region of the core. (So, for the inside process, the preform is generated from the outside inward.) In this process, the heat-providing burner traverses the outside of the rotating silica tube and the reactive gases travel down the inside, as shown in Fig. 6.45*b*. The gases inside the tube react to form silica soot in the space within the tube. The soot migrates to the walls under thermophoretic forces (diffusion down a temperature gradient). The inner surface of the glass tube is sufficiently hot that the soot particles immediately flow and consolidate into a void-free molten layer (just as in Type III and Type IV synthetic fused silica manufacture). The water vapor generated by the gas-oxygen burner never reaches the inside of the tube, so the deposited glass is very dry, requiring no further drying steps. After the deposition is complete, in process step 3, the resulting thick-walled tubing is collapsed under heat and vacuum to form a solid rod. The outside silica layer (the starting tube) is left in place and becomes part of the cladding.

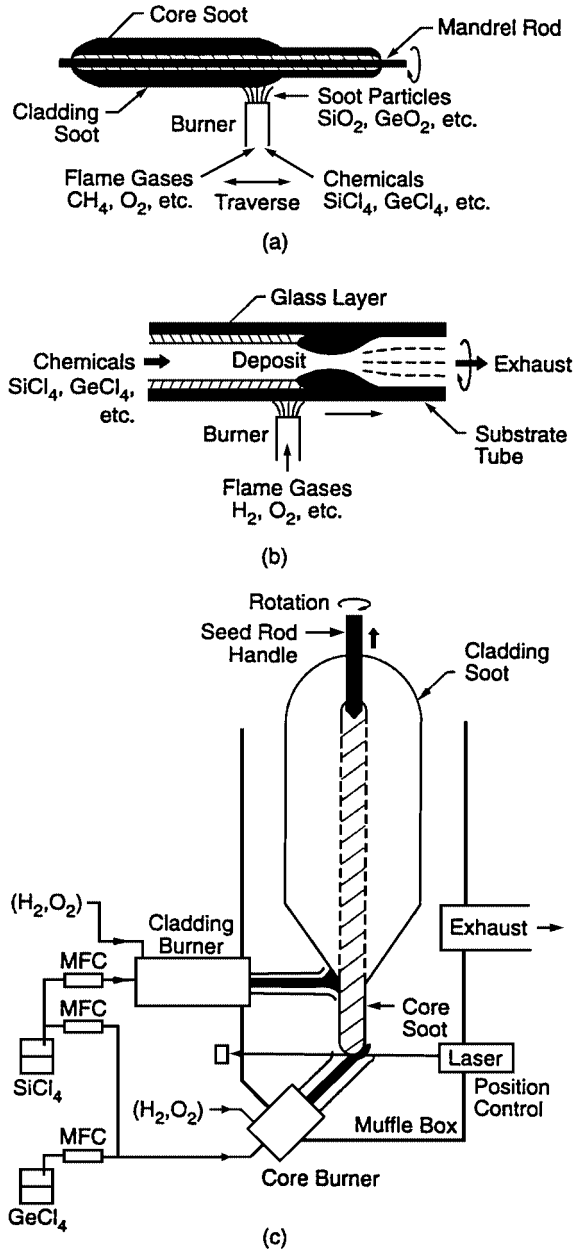

FIGURE 6.45 Schematic representation of (*a*) OVD, (*b*) MCVD, and (*c*) VAD preform fabrication routes. (*From A. J. Bruce, Ref. 10.*)

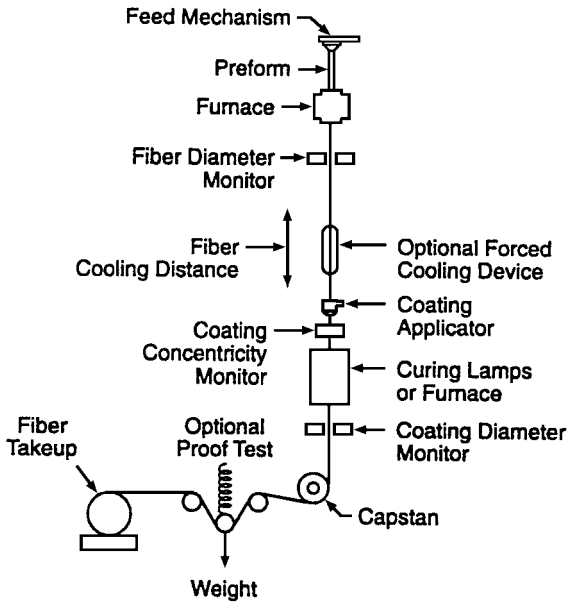

FIGURE 6.46 Schematic representation of a draw tower for high-silica preforms. (*From A. J. Bruce, Ref. 10.*)

The inside process is sometimes called inside vapor phase oxidation (IVPO) or inside vapor deposition (IVD). However, it is perhaps most commonly referred to as modified chemical vapor deposition (MCVD). In one variation, perhaps not currently in commercial use, an argon/oxygen plasma is generated within the tube by microwave radiation to provide the thermal energy for the chemical reaction, instead of relying on heat from a burner outside the tube.

Another technique proposed for the inside process is plasma chemical vapor deposition (PCVD). In this version of the process, a low-pressure plasma is generated inside the tube that does not lead to soot generation, but rather allows a heterogeneously nucleated chemical reaction to occur at the inner surface of the tube, so that the glass is built up in molecular-scale layers. This is a true chemical vapor deposition (CVD) process. More layers are required than with soot, but the process can be controlled more precisely. Unfortunately, the process has not yet proved commercially economical.

Step 4. Fiber drawing from the preform follows the general procedures described in Sec. 6.4.5 (redrawing). Notable differences may be higher temperatures, greater cleanliness, greater speed, and more precise dimensional control. Large commercial draw towers can be 20 m high. Process preforms of dimensions exceeding 10 cm diameter and 2 m length draw at speeds exceeding 10 m/s and produce more than 50 km of fiber from a single preform. A fiber draw tower is illustrated schematically in Fig. 6.46.

Step 5—Coating. To protect the fiber's freshly created (pristine) glass surface and thus preserve its inherent strength, the fiber is coated on the draw tower with a polymeric layer as soon as it is cool enough. Often, dual UV-curable coatings are used: a soft inner coating and a hard outer coating. Sometimes thin hermetic coatings (metal, ceramic, or amorphous carbon) are applied by special equipment just prior to applying the polymeric coatings.

Step 6—Testing. Often the coated fiber is continuously proof-tested for strength on the draw tower or as it is rewound onto other spools. Optical testing is also critically important. For multimode fibers the tests include attenuation, bandwidth, numerical aperture, and core diameter; for single mode they include such additional characteristics as chromatic dispersion, cutoff wavelength, and mode field diameter.

6.8 NOTES

1. Glass manufacturers generally do not sell bulk quantities of glass—that is, chunks of glass by the pound—but rather they sell glass products, for example, beverage bottles, electric lamp envelopes, television bulbs, optical lens blanks, and telescope mirror blanks. However, some specialty glass manufacturers sell glass in limited forms such as sheet, tubing, rod, frit, and bars of optical glass. Often these items are not stocked in inventory and must be special ordered. There are several specialty glassmakers that will melt glasses and fabricate shapes to customer's specifications, within the range of their capabilities.

2. Glass manufacturers generally specify their glass types and products by their physical and chemical properties; it is the properties they control and sell, not the compositions (although careful composition control is needed to assure the desired properties). Often the same properties can be produced by compensated variations in composition, i.e., increase of one alkaline earth ion at the expense of another. Such choices are often made on the basis of batch component cost or availability. For these reasons, many manufacturers do not disclose the compositions of their products. In other cases, the compositions are considered proprietary. Thus, in handbooks such as this one, compositions for some glass types are not known, not given, or only approximately given; others are known only because of independent chemical analysis, sometimes by competitors, and sometimes by scientific researchers.

6.9 ACKNOWLEDGMENTS

One of the authors (T.P.S) wishes to acknowledge that much of his perspective on glass forming processes came through working with several Corning Incorporated process engineers: G. Clinton Shay, Stuart Dockerty, Richmond Wilson, Leonard Anderson, William Lentz, William Pardue, and Frank Coppola. Similarly, his thinking about glass composition has been strongly influenced by close working relationships with Corning researchers Roger J. Araujo, Nicholas F. Borrelli, George H. Beall, and George B. Hares.

6.10 REFERENCES

1. R. W. Douglas and Susan Frank, *A History of Glassmaking,* G. T. Foulis & Co. Ltd., Henley-on-Thames, England, 1972.
2. D. R. Uhlmann and N. J. Kreidl, eds., *Glass: Science and Technology*, vol. 2, *Processing I*, Academic Press, Orlando, 1983.

2a. D. R. Uhlmann and N. J. Kreidl, eds., *Glass: Science and Technology*, vol. 5, *Elasticity and Strength of Glasses*, Academic Press, Orlando, 1980.

3. E. B. Shand and G. W. McLellan, *Glass Engineering Handbook,* 3d ed., McGraw Hill, New York, 1984.

4. F. V. Tooley, ed., *The Handbook of Glass Manufacture,* vols. I and II, Books for the Glass Industry Division, Ashlee Publishing Co., New York, 1984.
5. D. C. Boyd and J. F. MacDowell, eds., *Advances in Ceramics,* vol. 18, *Commercial Glasses*, The American Ceramic Society, Columbus, Ohio, 1986.
6. N. P. Bansal and R. H. Doremus, *Handbook of Glass Properties,* Academic Press, Orlando, 1986.
7. S. J. Schneider, Jr., vol. chairman, *Engineered Materials Handbook*, vol. 4, *Ceramics and Glasses,* ASM International, Materials Park, Ohio, 1991.
8. A. K. Varshneya, *Fundamentals of Inorganic Glasses,* Academic Press, San Diego, 1994.
9. D. C. Boyd, P. S. Danielson, and D. A. Thompson, "Glass," in *Kirk-Othmer Encyclopedia of Chemical Technology,* 4th ed, vol. 12, John Wiley and Sons, New York, 1994.

9a. J. R. Hutchins, III and R. V. Harrington, "Glass," in *Kirk-Othmer: Encyclopedia of Chemical Technology,* 2d ed., vol. 10, John Wiley and Sons, New York, pp. 533–604, 1966.

10. J. S. Sanghera and I. D. Aggarwal, eds., *Infrared Fiber Optics,* CRC Press, Boca Raton, Fla., 1998.
11. H. Bach and N. Neuroth (eds.), *The Properties of Optical Glass,* Springer-Verlag, Berlin and New York, 1998.
12. J. McGaughey, Libbey Inc., personal communication, 1999.
13. T. R. Kozlowski and G. A. Chase, "Parameters of Chemical Strengthening and Impact Performance of Corning Code 8361 (White Crown) and Corning Code 8097 (Photogray®) Lenses," *Am J. of Optometry and Archives of Am. Academy of Optometry,* vol. 50, 1973, pp. 273–282.
14. Y. Nakao, "Next-Generation Glass Substrate," presented at Electronic Display Forum 98, Yokohama, Japan, April 29, 1998.
15. W. Holand, "Materials Science Fundamentals of the IPS Empress 2 Glass Ceramic," *Ivoclar-Vivident Report,* no. 12, December 1998, Ivoclar Aktiengesellschaft, Schaan, Liechtenstein.
16. Y. Abe, "Glass-ceramics based on calcium phosphates—artificial dental crown and microporous glass-ceramics," *Glastech. Ber. Glass Sci. Technol.,* vol. 73, no. CI, 2000.
17. D. Hoffman, Owens Corning Science and Technology Center, private communication, April 1999.
18. D. R. Hartman, "Evolution and Application of High Strength Fibers," *The GlassResearch: Bulletin of Glass Science and Engineering,* vol. 4, no. 2, Winter 1995, NSF Industry-University Center for Glass Research, Alfred University, Alfred, N.Y.
19. G. Hetherington, K. Jack, and M. W. Ramsay, "The high-temperature electrolysis of vitreous silica: Part I. Oxidation, ultra-violet induced fluorescence, and irradiation color," *Phys, Chem Glasses,* vol. 6, 1965, pp. 6–15.
20. R. Bruckner, "Properties and Structure of Vitreous Silica, I," *J. Non-Cryst. Solids,* vol. 5, 1970, pp. 123–175.
21. H. W. McKenzie and R. J. Hand, *Basic Optical Stress Measurements in Glass,* Society of Glass Technology, Sheffield, England, 1999.
22. A. G. Pincus and T. R. Holmes, *Annealing and Strengthening in the Glass Industry,* 2d ed., Ashlee Publishing Co., New York, 1987.
23. G. H. Beall, "Chain silicate glass-ceramics," *J. Non-Cryst. Solids*, vol. 129, 1991, pp. 163–173.

6.11 BIBLIOGRAPHY

Bamford, C. R., *Color Generation and Control in Glasses,* Elsevier Scientific, New York, 1977.

Cable, M., "A Century of Developments in Glassmelting Research," *J. Am. Ceram. Soc*. vol. 81, no. 5, pp.1083–1094 (1998).

Cable, M., "Mechanization of Glass Manufacture," *J. Am. Ceram. Soc.* vol. 82, no. 5, pp. 1093–1112 (1999).

De Jong, B. H. W. S., J. W. Adams, B. G. Aitken, J. E. Dickinson, and G. J. Fine, "Glass-Ceramics," in *Ullmann's Encyclopedia of Industrial Technology,* vol. A12, VCH Verlagsgesellschaft mbH, Weinheim, Germany, 1989, pp. 433–448.

De Jong, B. H. W. S., "Glass," in *Ullmann's Encyclopedia of Industrial Technology,* vol . A12, VCH Verlagsgesellschaft mbH, Weinheim, Germany, 1989, pp. 365–432.

Doremus, R. H., *Glass Science,* John Wiley & Sons., New York, 1973.

Giegerich, G. and W. Trier, *Glass Machines* (English translation), Springer, Berlin-Heidelberg, Germany, 1969.

Kleinholz, R. and H. Tiesler, "Glass Fibers," in *Ullmann's Encyclopedia of Industrial Technology,* vol. A11, VCH Verlagsgesellschaft mbH, Weinheim, Germany, 1989, pp. 11–27.

Kurkjian, C. R. and W. R. Prindle, "Perspectives on the History of Glass Composition," *J. Am. Ceram. Soc*. vol. 81, no. 4, pp. 795–813 (1998).

Loewenstein, K. L., *The Manufacturing Technology of Continuous Glass Fibers,* 3d ed., Elsevier, NewYork, 1993.

Morey, G. W., *The Properties of Glass,* 2d ed., Reinhold, New York, 1954.

McMillan, P. W., *Glass-Ceramics,* 2d ed., Academic Press, London, 1979.

Nakahara, T., M. Hoshikawa, T. Sugawa, and M. Watanabe, "Fiber Optics," in *Ullmann's Encyclopedia of Industrial Technology,* vol. A10, VCH Verlagsgesellschaft mbH, Weinheim, Germany, 1989, pp. 433–450.

Perkins, W. W., ed., *Ceramic Glossary*, 2d ed., American Ceramic Society, Columbus, Ohio (1984).

Pilkington, L. A. B., "The float glass process," *Proc. Roy. Soc. Lond. A.,* vol. 314, pp. 1–25, 1969.

Pilkington, Alastair, "Flat glass: evolution and revolution over 60 years," *Glass Technology,* vol. 17, no. 5, pp. 182–193, 1976.

Rawson, H., *Inorganic Glass-Forming Systems,* Academic Press, London, 1967.

Standard Terminology of Glass and Glass Products, ASTM Standards 1995, ASTM C162-94c, vol. 15.02, pp. 27–41.

Weyl, W. A., *Colored Glasses,* Society of Glass Technology, Sheffield (Reprinted by Dawson's of Pall Mall, London) 1951.

Wachtman, J. B., Jr., ed., *Ceramic Innovations in the 20th Century,* American Ceramic Society, Westerville, Ohio, 1999.

CHAPTER 7
ADVANCED APPLICATIONS OF GLASS

Venkata Bhagavatula
Corning Incorporated
Corning, N.Y.

Francis P. Fehlner
Consultant to Corning Incorporated
Corning, N.Y. 14831

The emphasis in glass applications has gradually changed over the centuries from decorative, domestic, and industrial to optical and electronic uses. This chapter highlights the latest advances in the last two categories, optical waveguides, and electronic displays.

7.1 OPTICAL WAVEGUIDES IN COMMUNICATIONS

The next millennium is expected to be the age of communications. This revolution is fueled by the growth of optical communication networks and the Internet. The backbone of optical networks is the optical fiber. Optical communications and optical fiber have a rich history. The idea of light transmission in dielectric waveguides dates back to the mid-nineteenth century. John Tyndell[1] and Alexander Graham Bell[2] who invented a light communication system more than a century ago may be called the forefathers of the optical communications revolution. The more recent impetus for optical communications came with the development in the early '60s of light-emitting sources based on semiconductors and the breakthrough achievement of 20 dB/km glass optical fiber in 1970.[3] The current state of the technology can be attributed to a large extent to the enormous advances made in materials, in particular glasses and semiconductors, and the processing techniques developed for these applications. The low attenuation and high information-carrying capacity made optical waveguides the medium of choice for communications.

In the following sections, a brief summary of the fundamentals of optical fibers and waveguides will be given. The basic principles involved in the various components that make up the optical communications system will be discussed. In addition to optical communications, optical fibers and waveguides have unique characteristics that make them

suitable for important and emerging roles in a number of areas including sensors, signal processing, and optical computing. The status and future outlook in these diverse areas will be indicated.

7.1.1 Waveguide Introduction and Fundamentals

In the next few sections, some of the fundamentals of optical waveguides and fibers will be given. The basic principle on which the optical waveguide works is total internal reflection.[4] This is the phenomenon where light is perfectly reflected at the boundary of two dielectric materials with different refractive indices. It occurs only when light is incident at the dielectric interface from the higher index material. Figure 7.1 shows the incident ray, reflected ray, and refracted ray at the interface between two dissimilar dielectric materials in the geometrical optical approximation. This approximation is valid when the wavelength of light is significantly smaller than the physical size of the objects under consideration. The relation between the incident light ray, reflected light ray, and refracted light ray is given by Snell's Law:

$$n_1 \sin \theta_1 = n_2 \sin \theta_2 \tag{7.1}$$

where n_1 is the higher-index medium. From this relationship, one notes that for a particular value of θ_1, θ_2 becomes 90°. This incident angle is called the *critical angle* θ_c. The angle of incidence beyond this value leads to total internal reflection and no refracted ray is present. By this mechanism, one gets truly 100 percent reflection, unlike the reflections from metallic mirrors. From Eq. (7.1), the value of the critical angle is given by the simple equation

$$\sin \theta_c = n_2/n_1 \tag{7.2}$$

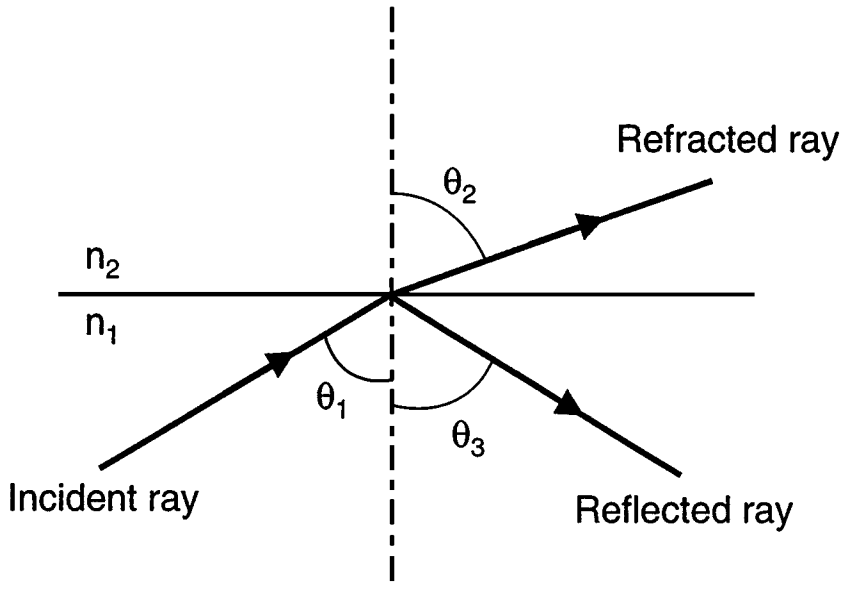

FIGURE 7.1 Reflection and refraction of a light ray at a dielectric interface.

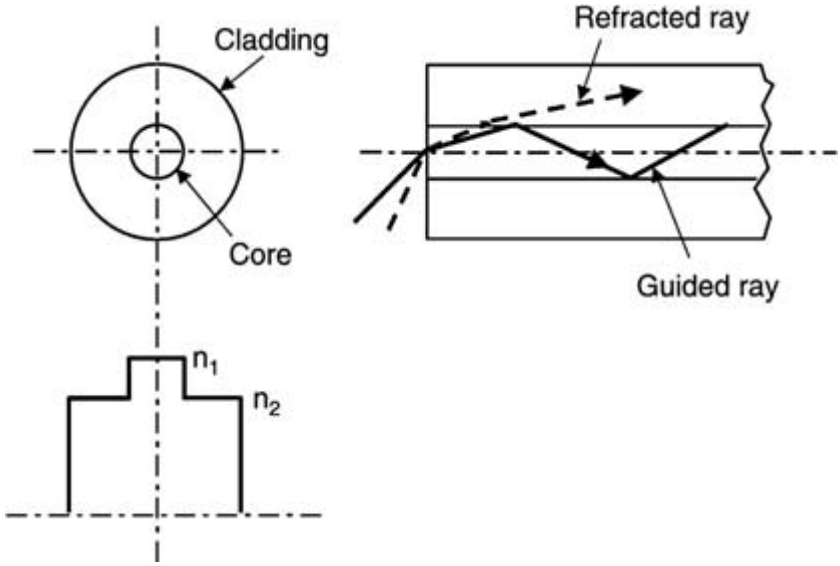

FIGURE 7.2 Structure and principle of an optical waveguide.

Because of this complete, i.e., 100 percent, reflection, the total internal reflection phenomenon can be used to guide and propagate light over unlimited distances provided there are no other loss mechanisms.

A simple structure that allows such guiding of the light is the so-called step-index waveguide shown schematically in Fig. 7.2. It consists of a central core of refractive index n_1, surrounded by a cladding material whose refractive index is n_2. For total internal reflection to occur, n_2 must be lower than n_1. All the light rays undergoing total internal reflection are called *guided rays* and in principle can propagate for unlimited distances in an ideal fiber. In real fibers and optical communication systems, a number of loss mechanisms and pulse dispersion mechanisms exist that limit the propagation distances. Some of the these issues will be discussed in Sec. 7.1.1.2.

The relationships given above are valid when the physical size of the object under consideration is much larger than the wavelength of the light. In the case of waveguides and fibers, the geometrical approximation works well when the size of the core is much larger than the light wavlength. Such waveguides are called *multimode waveguides* or *fibers*. When the size of the core is of the same order of magnitude as the wavelength of light, geometrical optics are not valid and the wave nature of light has to be taken into account. Single-mode fibers fall into this category. For multimodes, where geometrical optics are valid, some of the important characteristics of the fiber can be derived by using the simple equations given above. One such variable is the numerical aperture (NA) which represents the light-collecting efficiency of the fiber. As can be seen from Fig. 7.2, when light is being collected, i.e., coupled, into the fiber from a light source located outside the fiber, there is a maximum angle of the light cone θ_{max}, beyond which the light ray is no longer guided. Using Snell's law and the condition for total internal reflection, the sine of this angle can be easily derived and is called the *numerical aperture*. The larger the NA, the larger the acceptance light cone angle, so more light is coupled into the fiber.

$$\sin\ \theta_{max} = \left(n_1^2 - n_2^2\right)^{1/2} \tag{7.3}$$

Another important fiber parameter is the refractive index difference between the core and cladding, i.e., $n_1 - n_2$. Generally it is represented in normalized fashion and is referred to as the *relative index difference* Δ:

$$\Delta = (n_1 - n_2)/n_1 \tag{7.4}$$

A parameter that depends on core radius a and the relative index difference Δ can be used to distinguish between single-mode fibers and multimode fibers. This parameter, referred to as the *V number* or the *normalized frequency*, is given by

$$V = \frac{2\pi a\left(n_1^2 - n_2^2\right)^{1/2}}{\lambda} \tag{7.5}$$

where λ is the wavelength of light. For step-index fibers, when the V number is less than 2.405, the guide is referred to as *single-mode*. For values larger than 2.405, the guide can support more than one mode. From this relationship it can be seen that to get single-mode fibers at any given wavelength, small core radii and small index differences are needed. Typically, multimode fibers have a core radius of 25 μm and relative index difference of 0.01 (1 percent). In contrast, single mode fibers have relative index differences in the range 0.003 to 0.005 and core radii values of 2 to 4 μm.

7.1.1.1 Waveguide Compositions. Currently, commercial low-loss optical fibers for long-distance applications are based on silica compositions where losses of 0.2 dB/km are found for 1.55-μm operation. Extensive research has been done on finding other compositions and processes that produce low-loss optical fibers. However, none of these efforts produced results anywhere near the low losses obtained with silica compositions made by vapor deposition processes. A brief review of these processes as used for fiber fabrication will be given in Sec. 7.1.2.

Early attempts at making low-loss fiber were based on multicomponent compositions. Research was done on such novel processes as the double-crucible[5] technique. The best loss result obtained with such attempts was in hundreds of dB/km. Some of these techniques, although not useful for long-distance fiber applications, have been shown to be useful for specialty applications such as amplifier fibers that are doped with rare earth elements.

Materials with two different indices are needed for waveguide applications, one to make the higher-index core structure and the other for the lower-index cladding. For this purpose, silica is modified with a variety of dopants to change its refractive index. These dopants must be compatible with silica and capable of low loss at wavelengths of interest. That implies that the dopants should be compatible with the vapor deposition approach. Even after 30 years of research, only a handful of such dopants have been found. The main ones used in commercial fiber fabrication are fluorine and oxides of germanium, boron, and phosphorus. Germania is the main dopant used for raising the index above silica values and is the most commonly used material for doping the core in commercial fibers. This is particularly so in the case of single-mode fibers. P_2O_5 is another material that raises the refractive index. It also reduces the softening point of the glass when doped into silica. P_2O_5 in silica, even in small amounts, facilitates the processing of the fiber blanks and is used mainly in the fabrication of multimode fibers. The use of P_2O_5 in single-mode fibers is limited by its absorption characteristics in the 1.55-μm window. Because of its glass-forming characteristics, P_2O_5 is used in specialty fiber applications where very low loss is not critical, an example being erbium-doped fibers for optical amplification. Clustering of the rare earth ions in high concentrations is reduced by P_2O_5. Alumina is another dopant used for

such applications. Similarly, these dopants are used quite extensively in planar wave-guide fabrication by planar CVD techniques.

Of the dopants mentioned so far, only fluorine and boron are able to depress the refractive index below that of silica. In certain fiber fabrication techniques, such as modified chemical vapor deposition (MCVD), where the clad and core glasses are deposited on the inside of a silica tube,[6] it is necessary to reduce the softening point of the deposited glasses to below that of the silica tube. This is to reduce the distortion of the blank while the tube is collapsed into a solid blank. In such cases, the cladding compositions include materials such as silica, fluorine, and P_2O_5, which reduce the softening temperature while at the same time keeping the refractive index of the deposited cladding layers equal to or below that of the outside silica tube. Otherwise, the deposited cladding layers would act as another set of waveguides with respect to the outside silica tube and degrade the performance of the fiber. Like P_2O_5, boron also exhibits excess loss in the 1.55-μm range. Hence, for low-loss single-mode fiber applications where operation in the 1.55-μm window is important, fluorine is the preferred dopant for depressing the index below silica values. Dopants that can depress the index below that of silica are becoming more and more important for future single-mode applications where advanced fibers with complex refractive index profiles are needed. Hence, research in finding dopants that can depress the index below silica is going to be very important in the future. Also, it is necessary to develop fluorine doping processes that can be applied effectively with the vapor deposition techniques used for making fibers.

In addition to the compositions described above, extensive research has been conducted with fluoride-based glasses and heavy metal oxide–based glasses.[7] The original objective of this research was to produce ultralow-loss compositions for fiber applications. With fluoride compositions, in which the infrared absorption edge is pushed out beyond the 5- to 10-μm range, attenuation values as low as 0.01 dB/km are theoretically possible. But to date, such performance has not been achieved in practice. This research has led to compositions that have found applications in other areas, in particular for fiber amplifiers.[8]

7.1.1.2 Fiber Loss Mechanisms. The two main functional parameters for optical fibers are the loss or attenuation and the information-carrying capacity. In the following sections, these two aspects of the fibers will be discussed. Normally attenuation α expressed in units of dB/km is defined as:

$$\alpha = -[10 \log_{10} (P_{out}/P_{in})]/L \tag{7.6}$$

where P_{in} is the input power to the fiber, P_{out} is the power at the output of the fiber, and L is the length of the fiber in km.

As indicated above, low-loss fibers are fabricated from silica-based compositions doped with materials such as germania and fluorine. In such fibers, there are a number of loss mechanisms that contribute to their total attenuation. These loss mechanisms can be classified as absorption, scattering, and geometric defects. Some of these are intrinsic because they are based on the material compositions and some are extrinsic, depending on the process used for fabrication and other external variables.

Absorption losses caused by electronic transitions and molecular vibrations are examples of intrinsic mechanisms. For silica, the electronic transitions are in the ultraviolet (UV) wavelengths, whereas the molecular vibrations are in the infrared (IR). The tails of these transitions bracket the useful range of low loss between the visible and the near-infrared wavelengths. Impurity absorption losses are examples of extrinsic mechanisms. The main impurities in fibers made by vapor deposition techniques are the transition metal ions and OH ions. Impurities such as iron cause absorption in the UV and visible wavelengths. Their concentrations need to be reduced to the few parts per billion range to reduce their contributions to

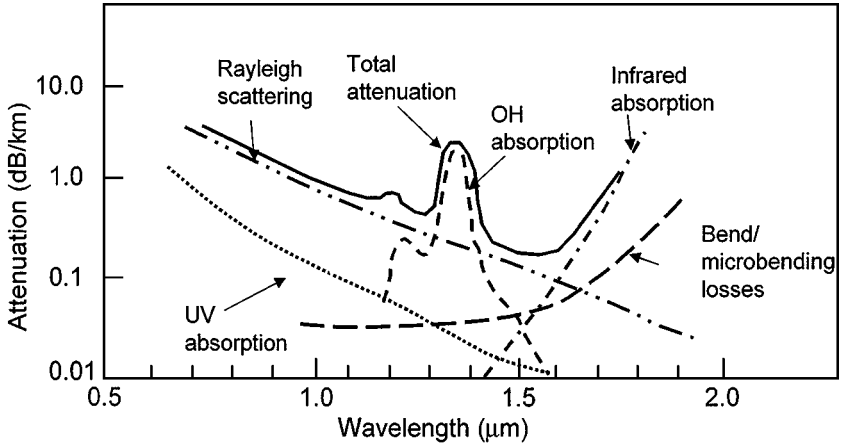

FIGURE 7.3 Loss mechanisms in optical fibers.

the fiber losses to insignificant values in the operating wavelength range. In vapor deposition techniques such as outside vapor deposition (OVD), where core and clad glasses are deposited on a bait rod, and modified chemical vapor deposition (MCVD), these impurities have been reduced to levels where they do not interfere with applications of the fibers.

The main impurity absorption that shows its effect in current commercial fibers is the OH absorption. The OH vibration band has its main absorption wavelength at 2.7 μm, outside the wavelength range of interest. But its overtones and combination bands occur at wavelengths of 0.95, 1.23, and 1.38-μm. To limit the excess loss due to OH absorption to less than 0.5 dB/km at the 1.38-μm wavelength, the OH levels in the fiber must be reduced to a few parts per billion. Using special drying techniques[9] during the blank-making process, OH concentrations have been reduced to such small levels. As a result, the excess loss due to OH absorption tails falls below 0.01 dB/km levels at wavelengths above 1.48 μm. This allows for a very low loss window from 1.48 to 1.63 μm as shown in Fig. 7.3. In the future, one can expect that these levels would be further reduced to levels where they do not contribute any significant loss over the entire wavelength window from 1.0 to 1.65 μm.

Another extrinsic absorption mechanism in fibers is due to atomic defects. For example, irradiation of the fiber with UV or x-rays induces defects in the glass that lead to excess attenuation. A particular example of this is the UV sensitivity of germania-doped silica compositions.[10] This effect, while needing to be minimized for low-loss fiber applications, is used to fabricate a number of useful devices in fibers and waveguides and is a very active area of research. More about this phenomenon will be presented in Sec. 7.1.3.3.

With extrinsic absorption losses minimized, the main mechanism limiting the loss values of the fiber is Rayleigh scattering, an intrinsic mechanism. Glass is an amorphous material with random molecular locations frozen into the structure. This causes local variations of density and leads to refractive index variations. The physical scale of these refractive index variations is smaller than the wavelength of light, and scattering caused by such fluctuations is called *Rayleigh scattering*. This scattering mechanism has a λ^{-4} dependence. Hence, the Rayleigh scattering loss decreases very rapidly at longer wavelengths. For silica-based glasses, Rayleigh scattering losses become as low as 0.16 dB/km at 1.55 μm. Since the Rayleigh scattering is due to density and related refractive index fluctuations, normally multicomponent glasses increase the Rayleigh scattering losses. With germania-doped glasses, this

phenomenon has been studied in detail and the increase in scattering losses with germania concentration can be represented by the following relationship:[11]

$$\alpha_s = a/\lambda^4 \tag{7.7}$$

where a is the Rayleigh scattering coefficient. It is approximately equal to $0.63 + 0.05C$ where C is the germania dopant level in silica by weight percent. As can be seen from this coefficient, the lowest scattering loss is obtained with a pure silica composition and any addition of germania only increases the scattering loss. This has implications for the single-mode fiber design. The lowest losses in single-mode to date have been achieved with fibers having a silica core and fluorine-doped cladding.[12] In such designs, most of the light power in the fiber travels in the low-scattering-loss silica core, leading to very low total losses. Theoretically, this is an attractive option, but in practice making silica core fiber is difficult and doesn't lend itself easily to the fabrication of advanced non-step-index profiles.

Additional losses in a fiber are introduced by geometric effects. Examples of such loss mechanisms are bending and microbending phenomena. In single-mode fibers, these phenomena lead to wavelength-dependent losses.[13] A schematic of the various loss mechanisms described here are shown in Fig. 7.3. In current single-mode fibers, total attenuation, which is a combination of all the loss mechanisms, has low-loss windows in the 1.3- and 1.55-μm ranges, separated by the OH absorption peak at 1.38 μm. The low-loss window in the 1.55 wavelength range is about 100 to 140 nm wide with the lowest loss equal to 0.018 dB/km. The low-loss window in the 1.3-μm wavelength range is about 40 to 50 nm wide and the lowest loss in that window is 0.33 to 0.35 dB/km. With reduced OH levels, the entire range from 1.28 to 1.62 μm can be useful, but still the loss at the 1.55-μm window will be substantially lower.

7.1.1.3 Information-Carrying Capacity and Dispersion. As the name suggests, step multimode fibers guide a number of modes in the core. The larger the V number [defined in Eq. (7.5)]; i.e., the larger the core diameter or the index difference, the larger the number of modes supported. In a qualitative way, one can think of these modes as different paths that the light can take to propagate through the core and still satisfy the optical laws. Hence, in a multimode, the light coupled into the core can travel down the fiber in different paths. The portion of the light traveling down the shortest path arrives at the end of the fiber earlier than the portion of light taking the longer optical path. When a sharp pulse of light is incident on such a multimode fiber, as shown in Fig. 7.4, a portion of the pulse energy will arrive at the destination sooner than the other portions and the pulse starts spreading in time. Thus, the various modes of the fiber can be considered to have different propagation velocities. Now if a series of pulses separated in time are incident on the fiber, after a certain propagation distance, the pulse spreading causes the energy from one pulse to mix with the light from another pulse and smear out the whole pulse train. Since information is sent through the fiber as coded on/off pulses of light, smearing of the pulses leads to loss of information. This limits the information-carrying capacity of the fiber. The phenomenon of pulse spreading due to the different propagation velocities of the modes is called *intermodal dispersion*. In step-index multimodes, the propagation velocity differences are quite large and hence the information-carrying capacity is quite limited. For example, with such fibers, the information-carrying capacity is limited to about 10 MHz · km. The relationship between MHz and Mb/s is dependent on the pulse-coding format. Generally, each MHz · km converts to ~2 (Mb/s) · km. Such representation of the information-carrying capacity allows system designers to estimate the distances over which information of a certain data rate can be sent. For example, if information is sent at the rate of 1 Mb/s, a step-index multimode with 10 (Mb/s) · km information-carrying capacity can send that information over 10 km without loss of information.

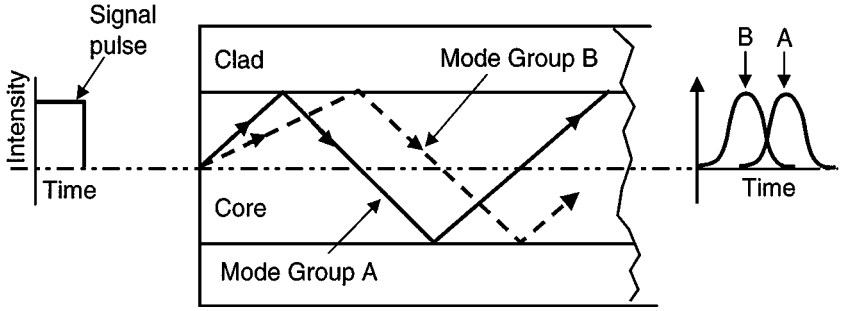

FIGURE 7.4 Intermodal dispersion in a step index multimode fiber.

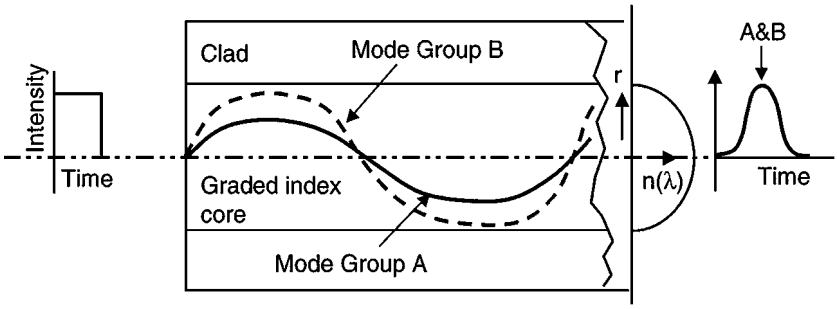

FIGURE 7.5 Intermodal dispersion in an optimally graded index profile.

Proper index profiling of the core significantly reduces the intermodal dispersion. Such profiles, termed *graded-index profiles*, as shown in Fig. 7.5, have been developed[14] for this purpose. These graded-index profiles can be expressed as follows:

$$\begin{aligned} \Delta r &= \Delta(0)[1-(r/a)^{\alpha}] \quad \text{for } 0 < r \le a \\ &= 0 \qquad\qquad\qquad\quad \text{for } r > a \end{aligned} \tag{7.8}$$

where r is the radial distance from the center of the fiber, a is the core radius, and α is the gradient profile parameter.

The most common multimode fiber for high bandwidth applications has an index profile characterized by the above equation with $\alpha \approx 2$ and is referred to as a *parabolic-index profile*. The propagation paths of the different modes in such a fiber are schematically shown in Fig. 7.5, where the optical paths of two different mode groups are shown. Mode Group A travels shorter distances but through a higher-index portion of the waveguide, whereas Mode Group B travels through a longer path, but a significant part of that path is at a lower refractive index. Since optical path is determined by the product of the physical path and the refractive index, in this case the longer physical path length of Mode Group B is compensated by the lower refractive index. For profiles with $\alpha \approx 2$, the optical paths of all the mode groups are equal. Hence, the intermodal dispersion for a parabolic fiber is eliminated under ideal conditions. In practice, the intermodal dispersion is never

completely eliminated because of the imperfections in the profiles, but multimode fibers with information-carrying capacity as high as 1000 to 2000 (Mb/s) · km are routinely made commercially.

Single-mode fibers, which by definition contain only one mode, do not have any intermodal dispersion. For that reason, the information-carrying capacity of single-mode fibers is extremely high. But the information capacity is not infinite, and other dispersion phenomena limit the capacity of single-mode fibers. The main dispersion phenomenon limiting the single-mode fiber capacity is chromatic dispersion. Chromatic dispersion comes about because different spectral components of the light source travel at different velocities. There are two components to the chromatic dispersion: the material dispersion and the waveguide dispersion. The glass materials used to make the fibers have refractive indices that vary with wavelength. This leads to variations in the propagation velocities of the light pulse with a spreading of spectral components. Since this pulse spreading comes about as a result of a material property, it is called *material dispersion*. Dispersion in single-mode fibers is expressed in units of picoseconds per km · nm. This quantity indicates the pulse width increase in picoseconds after traveling through a kilometer length of fiber when the light pulse spectral width is 1 nm.

The material dispersion curve for silica is shown in Fig. 7.6. It depends on the second derivative of the refractive index with respect to wavelength. As can be seen, the material dispersion for silica is zero at a wavelength near 1.3 μm. This implies that a light pulse near 1.3 μm will travel through a block of silica without any pulse spreading and hence would have a very high information-carrying capacity. But single-mode fibers are not slabs of glass. They have waveguide structure. This structure itself leads to pulse spreading as a function of wavelength, contributing to the dispersion called *waveguide dispersion*. Waveguide dispersion comes about because of the change in effective index of the mode with wavelength, and leads to propagation velocity differences in the spectral components. The schematic shown in Fig. 7.7 indicates why the effective index of a single-mode changes

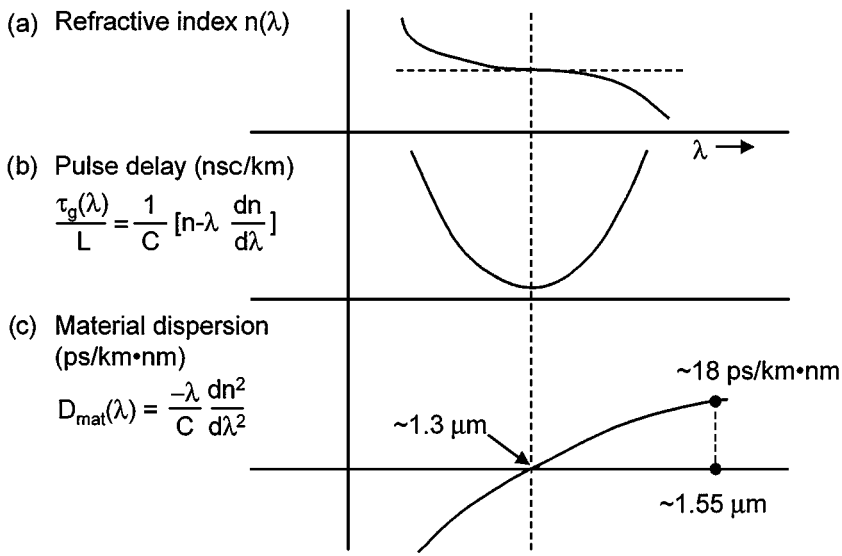

FIGURE 7.6 Material dispersion of silica where τ is the pulse delay, L material length, c velocity of light, and n refractive index.

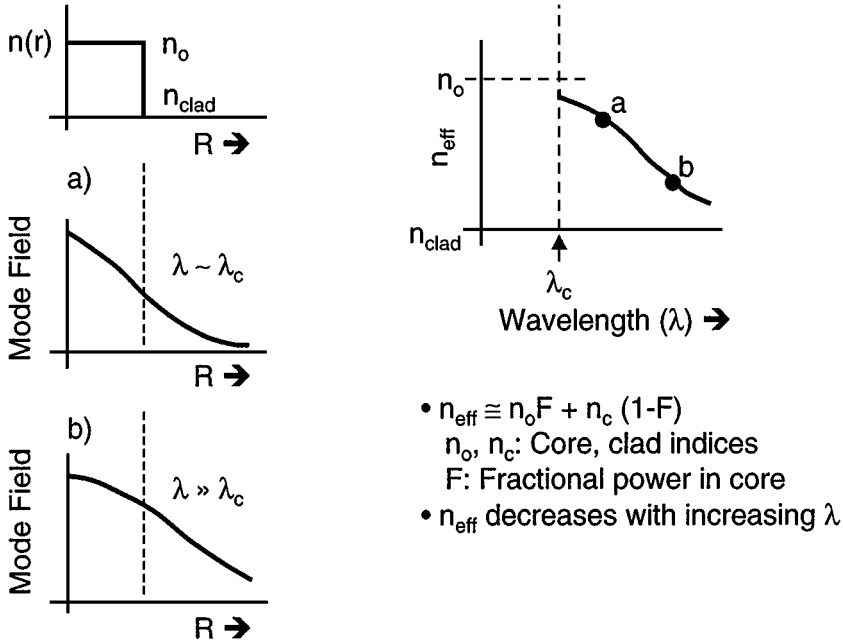

FIGURE 7.7 Effective index and waveguide dispersion in single-mode fibers where λ_c is the cutoff wavelength and R is the radial position from the fiber axis.

with wavelength. Light propagation in single-mode fibers is not completely described by ray optics, and the wave nature of light has to be taken into account. For this reason, the light pulse is not completely confined to the core and part of the mode power is in the cladding. As the wavelength increases, more and more power of the mode spreads out into the cladding, as shown in Fig. 7.7. Since the cladding index is smaller than the core index, when more of the power spreads into cladding, the average or effective index of the mode becomes smaller. This reduction in effective index as the wavelength increases leads to waveguide dispersion.

Generally, in step-index single-mode fibers with low index differences, the waveguide dispersion is not very high. The total dispersion of single-mode fibers that are designed to operate around 1.3 μm is a sum of the material and waveguide dispersions but is mainly determined by the material dispersion. The total dispersion in such a case is shown schematically in Fig. 7.8, where the total dispersion curve passes through the zero value near 1.31 μm and has the highest information capacity in that wavelength range. Many commercial systems use such fibers. However, silica-based fibers have their lowest loss in the 1.55-μm range. So there is a mismatch between the wavelength range where the loss is the lowest and where the information capacity is highest. This mismatch can be eliminated if the zero value of the total dispersion is also moved to the 1.55-μm range. Since the material dispersion zero is not changed much with any dopants with low loss, the only recourse currently available to shift the total dispersion is to use waveguide dispersion to accomplish it. As can be seen in Fig. 7.8, the waveguide dispersion and material dispersion are nearly equal and of opposite sign in the 1.55-μm region. Waveguide dispersion is directly proportional to the relative index difference and is strongly dependent on the core structure.

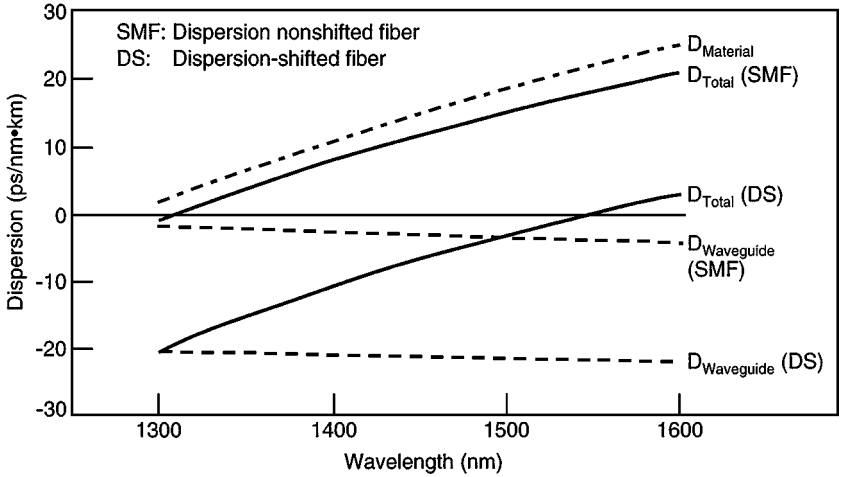

FIGURE 7.8 Total dispersion for dispersion nonshifted (SMF) and dispersion-shifted (DS) single-mode fibers. D_{material} is the same for both types of fiber. Only $D_{\text{wavelength}}$ changes.

Using these design tools, single-mode fibers with zero dispersion, wavelength-shifted to the 1.55-μm window, were developed and commercialized in the mid-'80s. Single-mode fibers optimized for the 1.3-μm window are referred to as *dispersion nonshifted fibers* (SMF) and those optimized for the 1.55-μm window are referred to as *dispersion-shifted* (DS) fibers. An example of a dispersion-shifted fiber profile[15] is shown in Fig. 7.9. Recently, for multiple wavelength channel transmission, dispersion-shifted fibers have been optimized to have finite but low dispersion in the 1.53- to 1.56-μm range. These fibers are referred to as *nonzero dispersion-shifted fibers*. Such fibers are attracting more attention currently for at least two reasons. First, erbium-doped fiber amplifiers (see Sec. 7.1.3.1) operate in the 1.55-μm window, allowing economical multiwavelength transmission over longer distances. The other reason is that the available low-loss window is much wider in the 1.55-μm window than in the 1.3-μm window, allowing more wavelength channels over longer distances. These two factors plus the need for more and more capacity to meet the demands of the Internet revolution are driving optical networks to use the 1.55-μm window in the majority of new installations.

7.1.2 Fiber and Waveguide Fabrication Techniques

A number of fabrication techniques have been developed for the fabrication of low-loss optical fibers. Early work with multicomponent glasses was mainly focused on glass-melting approaches. The approach that is noteworthy is the double-crucible technique.[16] In this technique, high-purity raw materials of the glass composition are melted and processed into rods using high-purity silica or platinum crucibles. To make a fiber, the core glass rod is remelted in the inner crucible and the clad composition in the outer crucible. The crucibles are designed such that core and clad glasses come together at the bottom of the outer crucible to form the waveguide structure. This molten composite structure is pulled into a fiber. By the nature of the process, it is easier to make simple step-index fiber with this technique. With some modifications to generate interdiffusion between the core and cladding

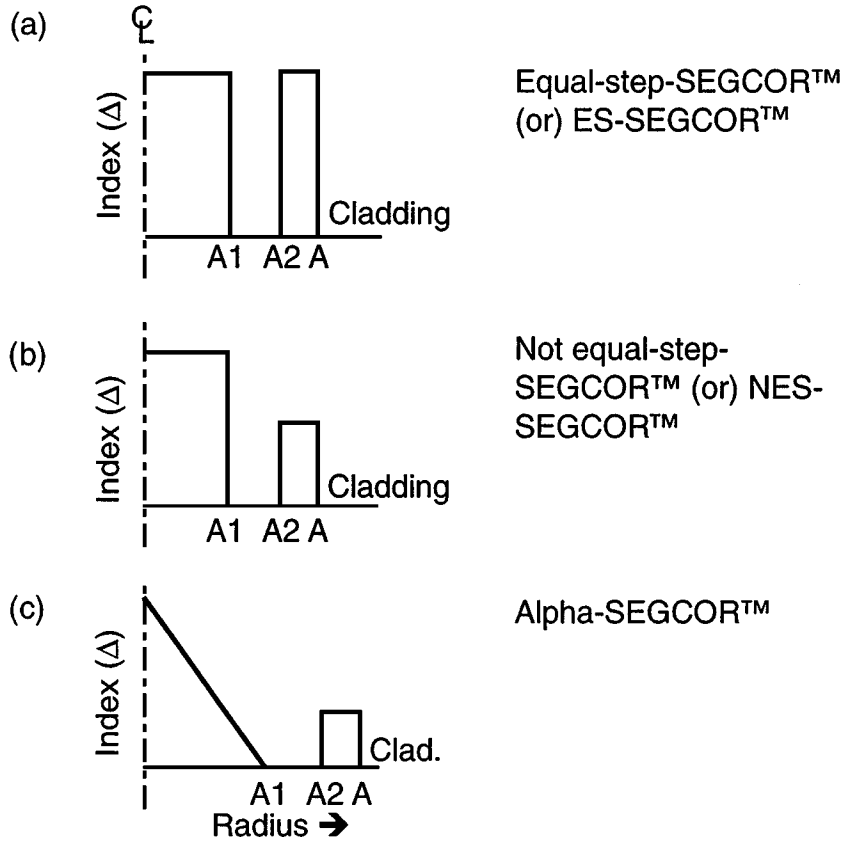

FIGURE 7.9 Index profiles of a dispersion-shifted fiber design starting at the centerline.

glasses, graded profiles have also been fabricated. The best attenuation value achieved with this technique was only in the hundreds of dB/km. The main reason is that with the glass-melting techniques, it was not possible to eliminate the impurities such as transition metals. For this reason, alternate fabrication techniques based on chemical vapor deposition (CVD) were adopted.

A number of vapor deposition techniques have been developed and commercialized.[17–19] The main techniques are the outside vapor deposition (OVD), inside vapor deposition (IVD), and vapor axial deposition (VAD). The IVD process is also known as *modified chemical vapor deposition* (MCVD). In these techniques, high-silica glasses are formed by vapor-phase reaction. A schematic of the OVD process is shown in Fig. 7.10. In this process, silicon-containing liquid material with a high vapor pressure, e.g., silicon tetrachloride, is used. The high vapor pressure of silicon tetrachloride compared to the vapor pressures of impurities such as transition metal chlorides permits purification through distillation. The chemical vapors are delivered through the deposition burner along with oxygen and methane. In the burner, the chemicals undergo flame hydrolysis, depositing the glass soot containing oxides of silica and various dopants on a target (bait) rod. The burner

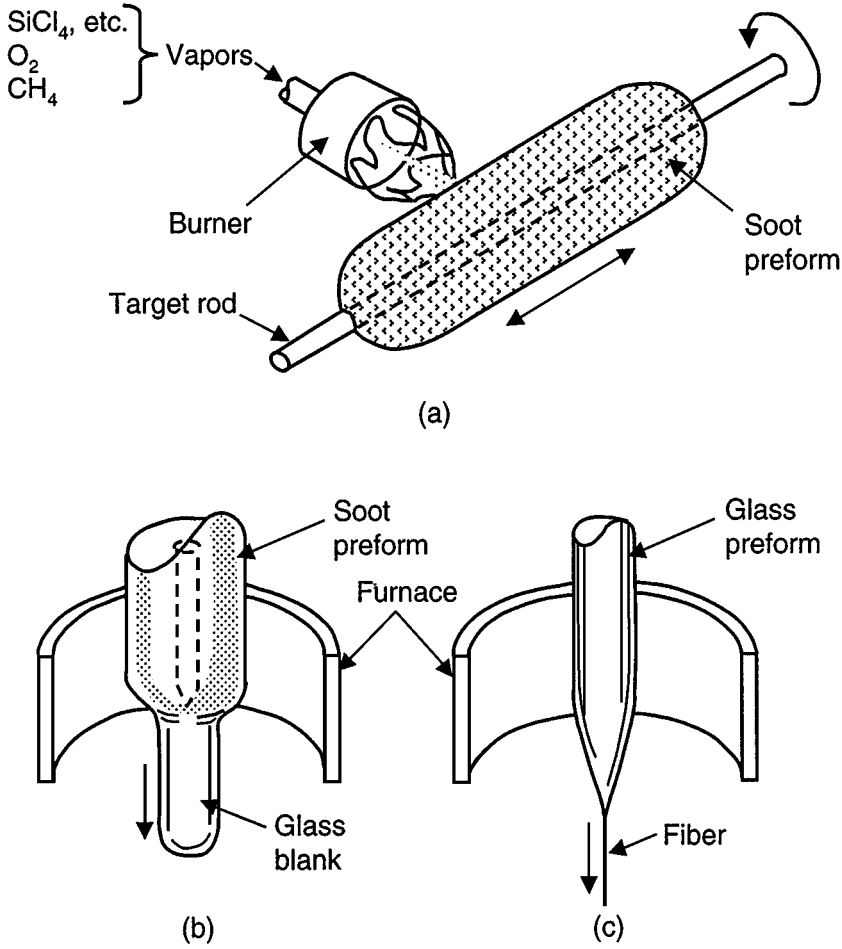

FIGURE 7.10 Outside vapor deposition (OVD) fiber fabrication technique.

is moved back and forth to deposit the soot uniformly over the target rod. The composition of the vapors delivered to the burner can be changed to fabricate various profiles as the soot builds up radially. Next, the target rod is carefully removed and the powdery soot blank is sintered into a clear glass blank in a consolidation furnace. To eliminate the water content incorporated into the soot blank, chlorine is used in the furnace during the consolidation. This consolidated glass blank is next drawn into a fiber in a vertical furnace, coated with a polymer protective layer, and then wound on a reel. The process makes very low-loss multimode and single-mode fibers, with losses for the latter as low as 0.19 dB/km. Other processes that utilize a flame to initiate the hydrolysis reaction have also shown similar low-loss performance. Another noteworthy fabrication process is the plasma CVD process, where the energy source for the chemical reaction is a microwave plasma. Some of the processes mentioned above have been used not only for making fibers, but also for making planar optical components.[20]

7.1.3 Optical Amplification

7.1.3.1 Fundamentals. One of the significant events in the optical communications revolution has been the practical realization of optical amplifiers, in particular, the erbium-doped fiber amplifier (EDFA).[21] The availability of such an optical building block has changed the installation and economics of optical networks. Previous to the availability of the optical amplifiers, fiber systems were mainly point-to-point systems and had to be converted from the optical domain to the electrical domain once every 30 to 60 km to boost and regenerate the signals. Since there was only a limited dynamic range between the light source and receiver, there was little freedom for inserting optical components such as a wavelength-division multiplexer (WDM). This severely limited the number of channels and network architecture options. The advent of the optical amplifier compensated for the loss of the optical elements and allowed a number of network options to become practical. For example, unlike electrical regenerators, optical amplifiers not only amplify, but can also be used to upgrade from one bit rate to a higher bit rate. The same is true with signal format.

Currently, there are three approaches to optical amplifiers. The main approach is the rare-earth-doped fiber amplifier, EDFA being an example. The second approach is the semiconductor amplifier, which is somewhat similar to the semiconductor laser except that the end faces are made nonreflective. The third option, one that is becoming increasingly attractive, is the Raman amplifier. The fundamental mechanism for the rare-earth-doped and semiconductor amplifiers is stimulated amplification. Raman amplification on the other hand is based on a nonlinear phenomenon, stimulated Raman scattering.

A brief description of the operation of the EDFA is given below. As shown in Fig. 7.11, erbium ions in silica glass can be considered a three-level system for the purpose of explaining its operation. Each level is a band of energy levels. In each band, there is a distribution of the population with more ions in the lower parts of the bands as shown in the figure. In the EDFA, ions in the ground level are excited by light at 980 nm to the excited levels of band 3. They relax from band 3 to band 2 by a fast nonradiative decay process. The decay time is of the order of a microsecond. If the radiative transition rate from band 2 to band 1 is slow, there is buildup of population in band 2. In the case of erbium, that radiative decay time from band 2 to band 1 is approximately 10 ms. As pointed out above, the ions in band 2 redistribute within the band by thermalization in such a way that there are more ions in

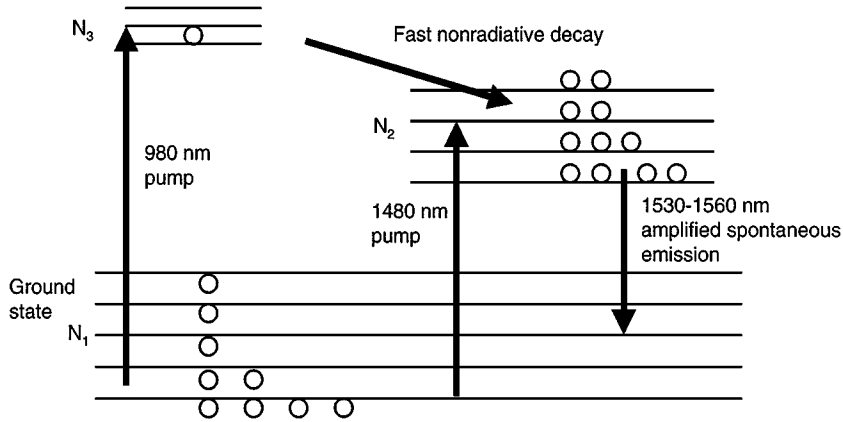

FIGURE 7.11 Schematic of the erbium ion energy level structure for optical amplification.

the bottom levels of the band. When this happens, it can lead to more ions in the bottom levels of band 2 than in the upper levels of band 1, provided there is sufficient pump power at 980 nm. This nonequilibrium condition is called *population inversion*. With population inversion, the stimulated emission is greater than the absorption leading to amplification.

The sequence of processes explained above is based on a pump at the 980-nm wavelength. EDFA also operates with ground-state pumping at other wavelengths. Pumps at 1480 nm have been extensively used. Figure 7.11 shows how a 1480-nm pump works with the EDFA system. In this case the excitation is from lower levels of band 1 to upper levels of band 2. With redistribution within the bands, population inversion occurs between lower levels of band 2 and upper levels of band 1. Since the pumping and stimulated emission is between adjacent bands, performance characteristics such as quantum efficiency and noise will be different from those with 980-nm pumps. Fiber losses are low at 1480 nm compared to the losses at 980 nm, so that 1480-nm pumps may have some advantage for remote pumping. However, for discrete amplifiers, 980 nm seems to be the preferred pump wavelength.

In early EDFA systems based on a silica host, the amplification wavelength region was from 1530 nm to 1560 nm. This wavelength band is referred to as the C band. It coincides with the low-loss transmission window of silica-based optical fibers. Convergence of the low loss with the availability of optical amplification provides a significant advantage for optical networks and has accelerated the growth of optical networks in the last few years. More recently, the amplification band has been expanded even further.[22] Currently, EDFA systems with amplification in the wavelength range from 1570 nm to 1620 nm are being commercialized. This wavelength range is referred to as the L band.

7.1.3.2 Optical Amplifier Material Systems As indicated above, erbium amplifiers with an operating window between 1530 and 1560 nm have been commercialized. This 30-nm window is small compared to the low-loss window possible with silica-based single-mode fibers. To fully utilize the wavelength window, it would be nice to have amplifiers available over the entire wavelength range from 1.28 to 1.62 μm. There is extensive research work going on to achieve this goal. In fact, this extension can be done with the erbium system itself. Some of the recent efforts in optimizing EDFA designs coupled with higher pump power has led to extending the amplification window to cover the range from 1530 to 1620 nm.

There are also a number of efforts to increase the wavelength bands by using hosts other than silica. One such promising system utilizes tellurite-based EDFAs.[23] This system provides optical amplification in the wavelength range from 1460 to 1520 nm. It is also possible to extend the amplification windows to the 1.3-μm wavelength region.[23] Silica hosts do not seem to be the right choices for this application. Heavy-metal oxide or fluoride (e.g., ZBAN) compositions seem to be much better suited. However, the progress in 1.3-μm amplifier research is slow going and requires some breakthroughs to become competitive with 1.55-μm amplifiers based on EDFA.

One of the important features of an amplifier for wideband applications is the flatness of the gain over the wavelength window. The usefulness of the amplifier is increased if the amplification is the same over the wavelength range of interest. Such amplifiers can be cascaded in an optical chain without degrading performance. This characteristic of the fiber, known as *gain flatness*, is a very important variable in the system performance. There are a number of ways to achieve gain flatness in fiber amplifiers. Some of the techniques are based on filtering techniques, but gain flatness can also be achieved by using a materials approach. For example, codopants such as alumina have been shown to improve the gain flatness. However, alumina is a difficult material to dope into silica and fabricate by vapor deposition techniques. For good gain flatness in the 1530- to 1560-nm window, alumina

doping levels of a few percent are needed. At such doping levels, the excess loss in the fibers is high. Further research in process development is needed in this area to reduce excess loss due to alumina doping at useful concentrations. Another approach has been to use fluoride glass hosts.[23] Such materials seem to improve the gain flatness. But the practical issues of handling these glass compositions and integrating them with silica-based fibers are still not completely resolved and research continues in these areas.

Alumina also seems to serve the function of reducing clustering in EDFA systems. When the concentration of erbium is higher than a few hundred parts per million, erbium ions seem to cluster in silica host glasses. This clustering causes reduction in radiative transition times between bands 1 and 2. This leads to unfavorable conditions for obtaining population inversion and optical gain. If large concentrations of erbium can be doped in glass fibers without the clustering issues, then compact planar optical amplifiers become feasible. Such devices could potentially reduce the cost of amplifiers drastically and also may lead to integration of amplification with a number of optical functions. Such a building block would be extremely useful but significant research and progress in alternative host glasses is needed to make this prospect a reality.

Alternative techniques for amplification are semiconductor and Raman amplifiers.[24] The main advantage of semiconductor amplifiers is that they can operate at any wavelength in the low-loss fiber window. They also are quite compact and compatible with optoelectronic integration. But the main drawback is the noise characteristics caused by reflections at the semiconductor end facets and also from gain dynamics. Semiconductor amplifier materials have very fast radiative decay times compared to rare earth amplifiers. Hence, the gain can fluctuate with rapidly changing signal pulses leading to pulse distortions and noise. Another issue is the polarization sensitivity of the semiconductor amplifiers. Nevertheless, significant progress has been made with such devices and they are finding applications not only as amplifier blocks but as elements in cross-connect switches and wavelength converters.

Raman amplifiers are also capable of working as amplifiers at any wavelength provided a high power pump of appropriate wavelength is available. Raman amplifiers are based on nonlinear scattering phenomenon. Hence, high-intensity pump powers and long interaction lengths are needed for high efficiency. Also, Raman amplifiers can benefit from materials research that increases the nonlinear coefficients. Figure 7.12 indicates the various wavelength windows and the corresponding amplifier options. As can be seen from the available options, the prospects for covering the entire low-loss window from 1.28 to 1.62 μm are quite good.

7.1.3.3 Optical Networks and Optical Components. Optical fiber is the backbone of the optical network. But to have a functional optical network, a number of optical and optoelectronic components and subsystems are needed. A variety of active and passive devices are being developed and fabricated with complex geometries and functions to address these emerging applications. The optical amplifier is a very good example of a critical optoelectronic subsystem. However, to build an amplifier, it is insufficient to simply have the amplification media discussed above. In addition to the pump source and erbium fiber, one needs a coupler that combines the pump light and the signal, an isolator to prevent the reflected light in the amplifier from causing laser oscillations, a tap to monitor the power levels, and gain-flattening filters to flatten the gain. A brief overview of some of these components will be covered in the next few paragraghs.

Single-mode and multimode couplers are usually based on one of two phenomena. The first approach is a proximity coupler,[25] shown in Fig. 7.13*a*. In this case, power is coupled between propagating modes and undergoes a periodic transfer from one guide to another. The minimum distance for complete power transfer is called the *coupling length*, and

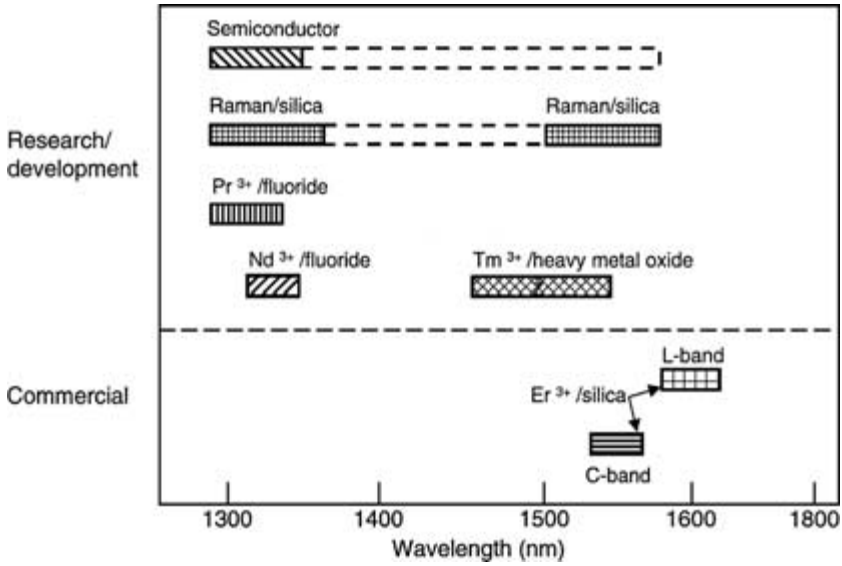

FIGURE 7.12 Amplifier windows and amplifier options.

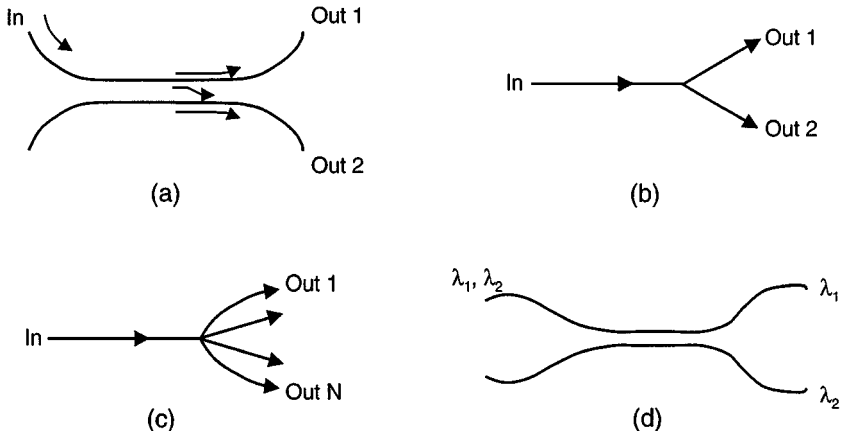

FIGURE 7.13 Coupling phenomena in (*a*) proximity coupler, (*b*) *Y*-junction coupler, (*c*) $1 \times N$ or tree coupler/combiner, and (*d*) wavelength division multiplexer (WDM).

depends on the waveguide parameters, the physical separation, and the operating wavelength. As a result, these devices typically are wavelength dependent and may also be dependent on the launch conditions in multimode operation. In devices made by proximity coupling, the coupling phenomenon is quite sensitive to any perturbations that change the waveguide parameters or optical field distributions. For example, bending a proximity coupler can change the split ratio or the wavelength characteristics of the device.

The second general method for making couplers, shown in Fig. 7.13*b*, is based on splitting a single guide into two or more additional guides. This often is referred to as a Y-junction splitter.[26] Generally, this type of coupler is wavelength independent. Also, the coupling is generally independent of the launch conditions in a multimode coupler. These devices are most often fabricated on planar substrates with pigtail fiber connections.

On the basis of the principles explained above, a variety of couplers have been made. A basic coupler type is a $1 \times N$ splitter shown in Fig. 7.13*c*, which splits a single channel into N different output channels. Similarly, this type of coupler can be used to combine N inputs into one output. Of particular importance is the 1×2 coupler, which is used in systems that transmit and receive over the same fiber. The most important configuration for systems being investigated today is the 3 dB coupler—one that splits the input light equally. However, there are a number of subsystems, such as amplifiers that use taps with a variety of split ratios. An extension of the $1 \times N$ coupler is the $M \times N$ coupler. In this case, a signal input on any of the M input fibers is split equally to all of the N output fibers. Such splitters are used in optical networks to broadcast the information from a source to all the other nodes on the network.

Another important class of devices is the wavelength-division multiplexer (WDM) or demultiplexer, which is used to separate or combine signals of different wavelengths. Such devices, shown in Fig. 7.13*d*, are found in optical systems where different-wavelength sources are used to transmit over the same fiber or where one wavelength is used to transmit and another is used to receive. Narrowband WDM networks are becoming very important in high-bit-rate long-haul systems with erbium-doped fiber amplifiers. These systems utilize multiple-wavelength transmission with separations as small as 0.4 nm. In such dense wavelength-division multiplexed (DWDM) systems, the wavelength stability of the channels is very critical for proper performance. There are a number of techniques that are used to fabricate these DWDM devices. Of particular interest is the fiber grating approach.[27] In this approach, photosensitivity of germania-doped glasses is used to imprint periodic perturbations of refractive index in the single-mode fiber. This is another area of research that is being pursued by a number of groups worldwide, and rapid advances are being made.

7.1.4 Future Developments

Optical fibers and optical communications have made tremendous progress in the last few years. With accelerating growth of optical communications, research into new components and new ways of making existing devices, progress will continue in the foreseeable future. Optical systems with higher powers, higher bit rates, and more WDM channels can be expected. With such trends, the nonlinear effects in fibers are already becoming the bottlenecks for further improvements. These limitations are leading to research to reduce the nonlinear effects on one hand and make use of them on the other. Soliton transmission[28] is a good example of the latter trend. In this case, the high powers and nonlinearities are put to beneficial use to achieve higher-bit-rate transmission over longer distances. This in turn will lead to new fibers optimized for such applications.

Another area of future development will be photonic crystal fibers and waveguides.[29] These waveguides have potential for making novel devices in which photons can be made to go around 90° bends with no losses, leading to significant advances in integrated optics. The main bottleneck for such devices is the ability to fabricate the complex periodic structures with submicrometer features and high refractive index differences. Research into novel materials and processing techniques is needed to overcome these obstacles.

Photosensitivity in fibers[30] has already produced a number of useful devices such as Bragg grating devices for DWDM applications. Commercialization of this technology is

in its infancy. One can expect increasing use of this technology in the future. To realize this potential, significant developments in the area of new materials with higher sensitivities and higher refractive index modulations are needed.

Development of the optical amplifier led to the most recent spurt in the growth of optical communications. This is only a start. Already efforts are underway to increase the wavelength range over which such amplification is possible. In addition to rare-earth-doped fiber amplifiers, one can expect to see more activity in the area of Raman amplifiers. In the next few years, explosive growth of optical networks is expected.[31,32] The size and complexity of these networks make it imperative that devices that can optically switch light signals and convert signal wavelengths become available. Such devices, once developed, can find applications, not only in optical communications, but in areas like optical computing, optical signal processing, and optical sensors.

7.2 ELECTRONIC DISPLAYS

Electronic displays are the connection between human beings and communication systems. Glass has played a key role in the development of such displays, first with vacuum-based cathode-ray tubes (CRTs) and then with solid-state flat panel displays (FPDs).

7.2.1 Vacuum-Based Displays

7.2.1.1 Rastered-Beam Displays. The glass envelope that made television possible had its origins in the experimental apparatus used to study electrical discharges in vacuum. This work was being carried out during the mid-1800s and was the precursor to developments in electric light bulbs. Fabrication of early glass devices was carried out in the laboratories of scientists who experimented with discharge tubes and incandescent lamps. However, Edison in his development of electric light bulbs moved from lab models to commercial samples with the first order for glass envelopes. The order was received by Corning Glass Works in 1879.[33] Bulbs were blown from a soft glass whose coefficient of thermal expansion was compatible with the platinum used to make glass-to-metal seals. Radio tubes and experimental electron-beam tubes evolved, becoming cathode-ray tubes for oscilloscopes in the 1920s and then radar tubes for use during World War II. In the CRT, the electron beam is rastered across the face of the tube. Where light emission is desired from the phosphor, the beam is turned on. Otherwise, it is off.

In a parallel effort, the glass bulbs were modified in composition and shape so that more complex devices could be accommodated. This led to television (TV), which became a commercial reality in 1939. Early broadcasts were in black and white. These were transformed into full color during the 1960s. This progression of events is outlined in Ref. 34.

The cross section of a CRT envelope[35a] for oscilloscope or TV use is shown in Fig. 7.14. The bulb consists of a faceplate, funnel, neck, and base. Originally, the neck, funnel, and faceplate were blown as a single bulb as discussed below. Eventually, the three-part bulb was developed: panel-funnel-neck with base added. The base contains the glass-to-metal seals that support electron emitters and focusing electrodes. A metallized phosphor screen is deposited on the panel. The neck and funnel hold these two sections at the correct distance. Critical properties of the assembled bulb are: mechanical strength to support internal parts and the pressure differential due to a vacuum, capability of maintaining a vacuum of 10^{-8} torr, a faceplate that is both transparent to visible light and a barrier to x-ray radiation

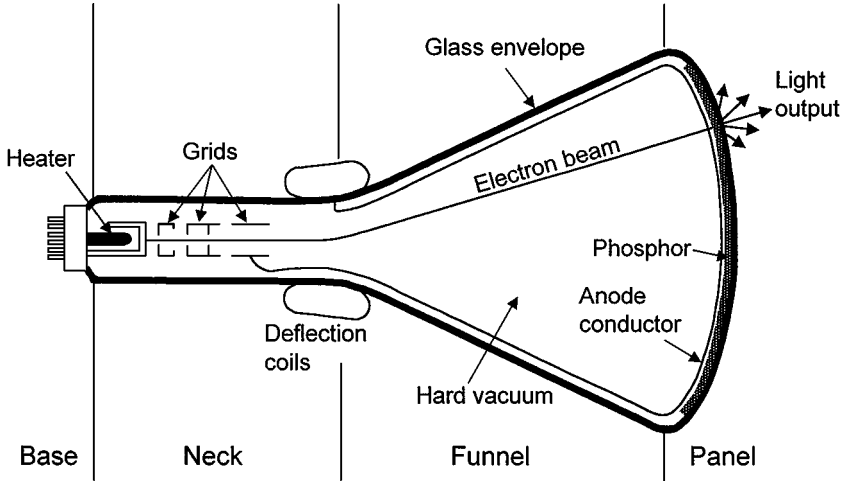

FIGURE 7.14 Cross section of a cathode ray tube using electrostatic focus and magnetic deflection.

generated by electrons accelerated at voltages up to 30 kev, and electrical isolation of the conductors in the base and faceplate. The logarithm to the base 10 of the volume resistivity should be close to 10 at 250°C. Current methods of manufacturing the various components of the bulb are tube drawing for the neck, pressing or centrifugal casting for the funnel, and pressing followed by polishing for the faceplate (panel). An example of the tolerances to which CRT parts must be held is a 36 in diagonal pressed panel. The precision of the inside is critical for mounting internal components of the tube. Hence, deviation from the nominal contour for the inside of the panel is ±0.014 in. The polished exterior has a more relaxed specification of ±0.060 in. The base, with its glass-to-metal seals, requires a special pressing process.

Evolution of the glass compositions and manufacturing processes used for CRT and TV bulbs proceeded with the development of related technologies. Early one-piece round bulbs were blown from hard glasses such as Corning codes 7720 and 7740, whose properties are given in Table 7.1. They resembled Ehrlemeyer flasks and had poor quality face plates. An important improvement was made in the 1940s when the two-part and three-part bulbs were introduced. It was then possible to press the panels and funnels from soft glass of soda-lime, lead, or barium silicate compositions, e.g., codes 906[2] and 0138 respectively in Table 7.2. The lead and barium in the glass were required to block x-rays produced by the 10 kev electron beam used in black-and-white tubes. Electrical sealing made it possible to assemble the thick glass parts into a complete bulb. The high temperatures encountered in the process were acceptable for black-and-white tubes since the phosphor screen was deposited after assembly. Electrical sealing was later replaced by the use of devitrifying solder glass for color TV bulbs. The lower sealing temperature of 450°C was needed so that the red-blue-green phosphor screen could be applied photolithographically to the panel before assembly of the tube.

The RCA metal funnel was developed during the next decade as a response to the 12 in diagonal size limitation of the all-glass bulbs. However, it never delivered expected cost savings. Developments in glass manufacture completely bypassed the metal tube. The key development was centrifugal casting. In this process, glass is introduced into the bottom of a spinning mold. A distributor in the center guides the glass up the sides of the mold so that

TABLE 7.1 Composition in Weight Percent and Properties of Selected Glasses

Oxide	Tungsten sealing, code 7720	General purpose, code 7740	Lamp bulbs code 0080	Electronic substrates, code 7059	Fused sillica, code 7940*
SiO_2	74	81	73	49	100
Al_2O_3	1	2	1	10	—
B_2O_3	15	13	—	15	—
Na_2O	4	4	17	—	—
MgO	—	—	4	—	—
CaO	—	—	5	—	—
BaO	—	—	—	25	—
PbO	6	—	—	—	—
As_2O_3	—	—	—	1	—
Coefficient of thermal expansion (0–300°C), 10^{-7}/°C	36.0	32.5	93.5	46.0	5.6
Strain point, °C	484	510	473	593	956
Density, g/cm^3	2.35	2.23	2.47	2.76	2.20

*Contains 0.1 weight percent H_2O.

TABLE 7.2 Glass Composition in Weight Percent for Color TV Bulbs

Oxide	Nonlead panel, code 9082	Lead panel, code 9062	Funnel, code 0138	Neck, code 0149	Base, code 0120
SiO_2	60	62	54	48	56
Al_2O_3	2	2	2	2	2
Na_2O	8	7	6	<1	4
K_2O	7	9	8	12	9
MgO	<1	<1	2.5	0	0
CaO	1	2	3.5	0	0
SrO	9	9	<1	3	0
BaO	9	6	<1	3	0
PbO	0	2	23	31	29
ZrO_2	2	0	0	0	0
ZnO	0	0	0	1	0
TiO_2	0.5	0.5	0.5	0	0
CeO_2	0.4	0.2	0.3	0	0
Sb_2O_3	0.4	0.4	0.2	0.6	0.5
Co, Ni	Trace	Trace	Trace	0	0
Coefficient of thermal expansion (0–300°C), 10^{-7}/°C	97.2	98.8	97.0	97.5	89.5
Strain point, °C	483	463	435	428	395
Density, g/cm^3	2.788	2.743	2.980	3.275	3.050

deep color-tube funnels can be made in large diameters. The development of rectangular tubes required the adaptation of the process to this new format. See Chap. 6 for further discussion of the various methods that have been used to form bulb parts.

The need for a deep tube was eventually obviated by changing the deflection angle of the electron beam from 90 to 110°. It was again possible to press the funnel as well as

the faceplate. Sizes of 40+in diagonal are currently available commercially although sizes up to 50+in diagonal have been demonstrated.

One other material besides glass is used for funnels. Tektronix developed a ceramic unit in 1963. This proved useful for low-volume applications of a few hundred a year. Glass funnels serve commercial demands which are a thousand times larger.

Special problems are associated with the glass used in the faceplate of CRT and TV bulbs. This glass must, of course, block x-rays generated inside the tube. Hence, lead glass has been a preferred choice for the application as discussed in Chap. 6. A major problem encountered with such glass is electron browning, especially in color TV tubes where 25 to 30 kev electrons impinge on the phosphor. The problem is less serious in black-and-white tubes, which use 10 to 12 kev accelerating voltages. The electrons bombard the glass, giving rise to a charge separation layer at the surface.[36] A portion of the separated cations are reduced to the metallic state, giving rise to optical absorption in the visible spectrum. The lead ion is the one most susceptible to reduction by this process. Thus, lead-containing glasses darken the most. Sodium and potassium ions can also undergo the same reaction but to a lesser extent. The addition of cerium to the glass minimizes darkening.

A second problem with lead glasses is disposal of obsolete tubes. Today, such tubes either must be remanufactured or the glass in them recycled. Disposal in land fills is too expensive.[37] Fortunately, changes in glass composition have allowed lead oxide in glass to be replaced by a mixture of strontium, barium, and zirconium oxides.

Examples of the different glasses[38] used in forming parts for a color TV bulb are given in Table 7.2. These compositions are representative of the standard products available from the manufacturers listed in Table 7.3. Compositions for black and white and projection bulb parts are given in Ref. 39. A background discussion of glass composition can be found in Chaps. 5 and 6. The neck of the bulb is formed from a high-lead glass, e.g., code 0149 (31 wt% lead oxide plus 3 wt% strontium oxide and 3 wt% barium oxide). The funnel glass, e.g., code 0138, has less lead oxide, only 23 wt%, and <1 wt% strontium and barium oxides. Two versions of panel glass are available. The first, code 9062 glass, has 9 wt% strontium oxide and 6 wt% barium oxide but only 2 wt% lead oxide. Low lead content and the presence of cerium minimizes electron browning of the glass. The second, code 9082, is lead-free, substituting 2 wt% zirconium oxide for the lead oxide. This glass is preferred for environmental reasons. The coefficients of thermal expansion for all the parts used to make a CRT bulb are close to the value of 98×10^{-7}/°C except for the code 0120 base glass. Its expansion is 90×10^{-7}/°C, making it compatible with the Dumet ™ wire used for glass-to-metal seals

TABLE 7.3 Manufacturers of CRT Glass

Major:
Nippon Electric Glass (NEG)
Asahi
Samsung Corning
Others:
Philips
Hitachi
Chinese suppliers
Thomson
Corning Asahi Video (CAV)
Schott
Techneglas
Indian suppliers
American Video

located in the base of the tube. An anode button is also sealed into the funnel to provide contact to the phosphor screen metallization.

Another problem encountered with the faceplate of a TV tube is glare from ambient light.[40] Since both the glass surface and the phosphor screen are reflective, ambient light reflects back to the viewers' eyes. This reduces image contrast, leading to viewer fatigue. Two partial solutions have been used to overcome this problem. In the first, the panel is tinted neutral gray by the addition of nickel and cobalt oxides in the ppm concentration range to the glass batch. The image-generating light passes through the panel once while the ambient light must traverse the glass twice. Thus, more of the ambient light is absorbed and contrast of the image is enhanced. However, there is a trade-off between loss of image intensity and elimination of ambient light reflection. As a result, the amount of colorant added to the glass batch is varied with the CRT application.

A second approach to the glare problem avoids this trade-off, although this solution is more expensive than simply coloring the glass. The surface of the faceplate is coated with an antireflection or scattering film. This decreases the intensity of ambient reflected light without materially affecting image intensity, although the scattering film tends to defocus the image. Again, contrast ratio is improved. Some of the newest antireflection films include a transparent conducting layer, which dissipates static charge from the glass surface.

The strength of the finished tube assembly is critical for the safety of viewers. Atmospheric pressure of 14.6 lb/in^2 can lead to implosion of weak structures. An early safety measure was to add a plastic shield to the front of the panel to contain glass fragments resulting from an implosion. A better solution was found in the use of a steel band around the skirt of the panel. This band puts the glass into compression, thus limiting the possibility of failure.[41]

The glass composition and design used to construct a CRT must withstand high-temperature processing. During assembly, frit sealing occurs at 450°C, and for evacuation a temperature of almost 400°C is required. Rates of heating and cooling, and thus speed of production, are inversely proportional to the glass thickness and size. Differential glass shrinkage is also a concern. The larger bulbs offer the greatest challenge to the manufacturing engineer.

7.2.1.2 Flat Panel CRT Displays. The form factor of the CRT has long been a detriment to its versatility. Gradually over the years the depth of the tube was reduced by increasing the deflection angle of the electrons. However, a truly flat device, say, 2 in or less in thickness, was desired. Many experimental models of the flat CRT have come and gone.[42] The latest flurry of activity ended in 1997 when Matsushita and Philips declined to produce their prototype models.

7.2.1.3 Matrix Displays. The method of addressing each pixel in the matrix of a flat panel display differs from that for a CRT. With the matrix, a grid of *x* and *y* addressing lines forms crossover points, which are called pixels (picture elements). Thus, each pixel can be addressed by activating the correct *x* and *y* lines with, say, half the voltage needed to turn a pixel on. The matrix can be either a simple passive matrix or an active one with a switch at each crossover point.

The vacuum fluorescence (VF) tube is a modification of the CRT in which the rastered electron beam is replaced by a hot cathode addressable for each pixel. It has proved to be the most useful of the flat CRTs,[35*b*] a bright, rugged, inexpensive display preferred for automobile applications. The cold-cathode version of the VF display is called the *field emission display* (FED). Prototype models have been recently shown at Display Works 98.[43] The glass used in these flat displays is similar to that used in conventional CRTs (Table 7.2).

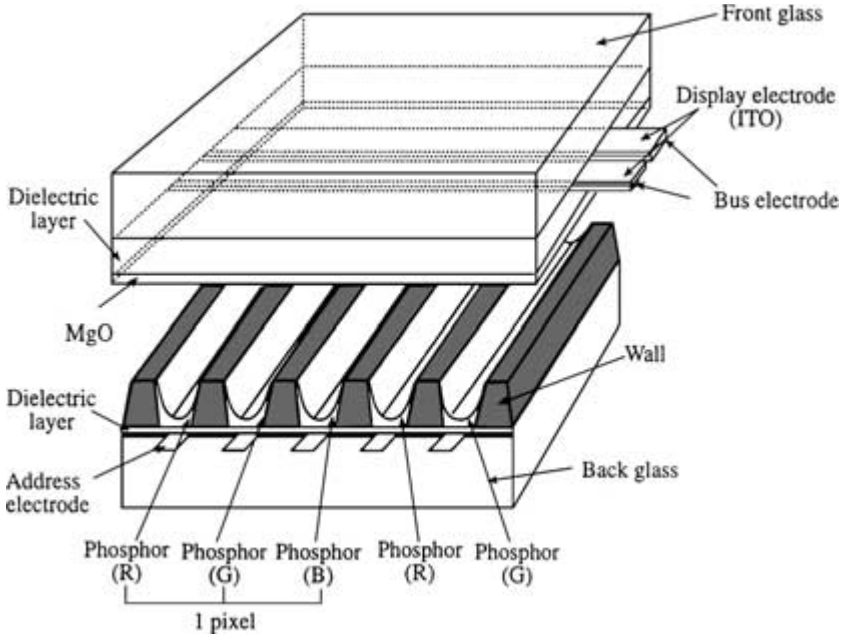

FIGURE 7.15 Exploded view of a Fujitsu ac memory plasma panel showing orthogonal address and sustain electrodes, red-green-blue phosphors, and the separated evacuated channels. (*Courtesy Society for Information Display*.)

Plasma discharge panels (PDPs), one of which is shown in Fig. 7.15, are an example of flat panel displays.[35c] They operate without the electron beam present in other vacuum displays. Instead, a plasma is generated by a voltage differential between electrodes in a noble gas at reduced pressure. This can either be viewed directly or used to generate UV light. The UV light in turn activates colored phosphors, giving the required red, blue, and green emissions required for a full-color display. The advent of full-color capability has made this technology a candidate for large (40 in diagonal or larger) panels useful as hang-on-the-wall TVs. The first glass used in PDPs was a soda-lime-silicate with a strain point approximately 40°C higher than code 0080 glass shown in Table 7.1. The PDP glass was manufactured by the float process. No final polishing was required. Glasses with an even higher strain point of 610°C and a thermal expansion of 83×10^{-7}/°C are now being developed to alleviate problems of shrinkage and sag during temperature exposure up to 600°C.

7.2.2 Soild-State Displays

Vacuum-based displays ultimately were unable to fulfill the growing needs of the computer industry for a lightweight, low-power portable display that was less than an inch thick. It took the solid-state revolution in electronic materials to identify candidates that could truly fill the needs of such devices. An early effort in electroluminescence was translated into light-generating matrix displays such as the one shown in Fig. 7.16. The matrix itself is an array of pixels, each of which is a capacitor structure built of thin films vacuum-deposited

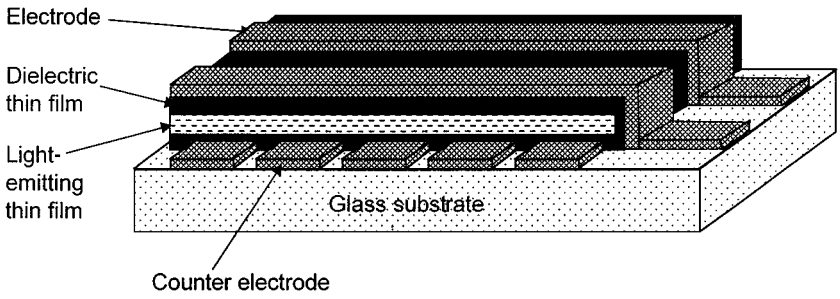

FIGURE 7.16 Three-dimensional view of an ac thin-film electroluminescent structure. (*Courtesy Society for Information Display*.)

onto a glass plate. Nominally sodium-free glasses such as code 7059 (Table 7.2) were initially used as the transparent mechanical support. These have been replaced with the higher-strain-point flat glasses developed for liquid crystal displays (LCDs) as discussed below.

Brody et al. in the late 1960s invented the active version of the matrix display.[44] In his work, a switch was included at each crossover point to increase the nonlinearity of the output response. The switches were thin-film transistors (TFTs) fabricated by using a compound semiconductor film. Both electroluminescent and liquid crystal displays were demonstrated. Brody's seminal work proved to be key to development of the dominant FPD technology of the 1990s, the active-matrix liquid crystal display (AMLCD). Liquid crystals are a special state of matter,[45] physically acting like liquids but giving an x-ray diffraction pattern that is characteristic of a crystalline solid. The optical and electrical properties of these materials make them useful in display applications. They are ideal for optimizing response functions since the almost unlimited ability of synthetic organic chemistry to modify compounds allows versatile combinations of properties to be created. Simple liquid crystal displays are useful for alphanumeric and passive display applications, e.g., watches, calculators, and computers. However, when it comes to full-color and video-rate FPDs, it is necessary to go to the active-matrix version. The structures of these two types of display are shown in Fig. 7.17.

7.2.2.1 Passive-Matrix LCDs. The contrast of an FPD is based on the ability of an observer to discriminate between individual pixels. When a particular pixel is turned on by applying voltages to the suitable x and y lines, it is important that adjacent pixels remain off. However, stray voltages do appear across these pixels in an actual display. Hence, it is important that the display element have a nonlinear output. In other words, a threshold voltage must be applied to a pixel in order to observe the desired response. Electroluminescent and liquid crystal displays have this characteristic up to a point, as illustrated in Fig. 7.18. Thus, the early matrix FPDs were passive matrices. Their small size was an advantage for this format. The glass used in such displays was soda-lime float. This glass was introduced in displays for early portable calculators because of its low cost compared to borosilicates. However, a major problem had to be solved before success was achieved with LCDs. The earliest versions of the display were hermetically sealed with glass frit at elevated temperatures. This protected the interior of the display from moisture. As display size increased, firing of the frit seal became more difficult because of warpage of the flat glass. An epoxy seal was substituted for the glass frit to lower the sealing temperature, but a new problem arose. Moisture entered the liquid

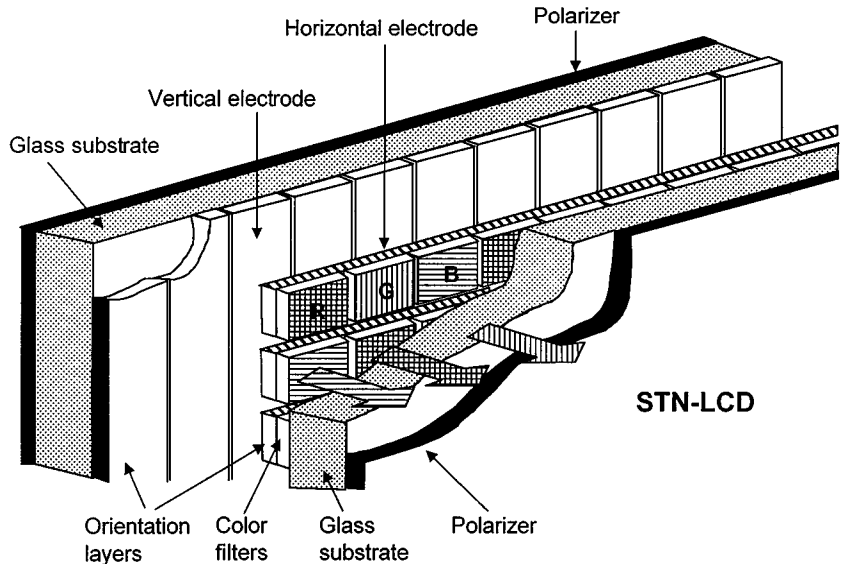

(a)

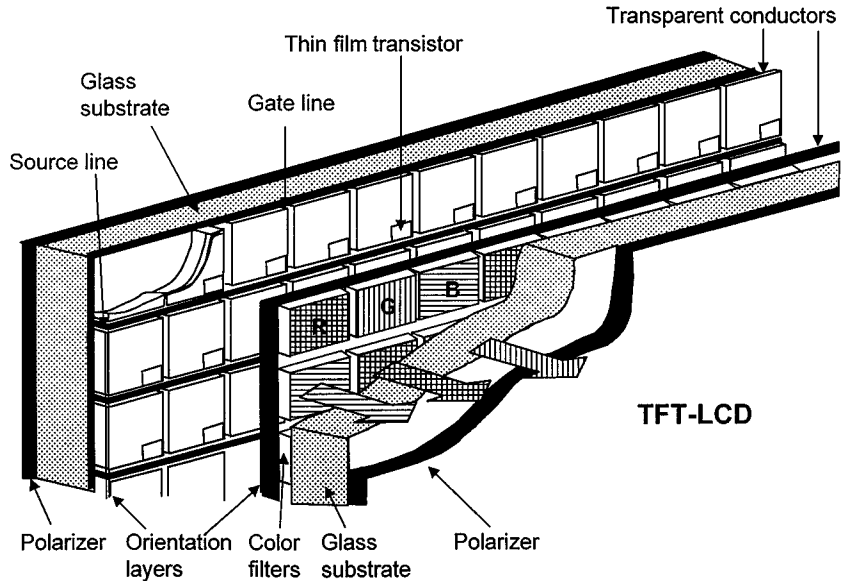

(b)

FIGURE 7.17 Electrode layout and physical cross section for (*a*) passive and (*b*) active matrix liquid crystal displays. (*Courtesy Society for Information Display.*)

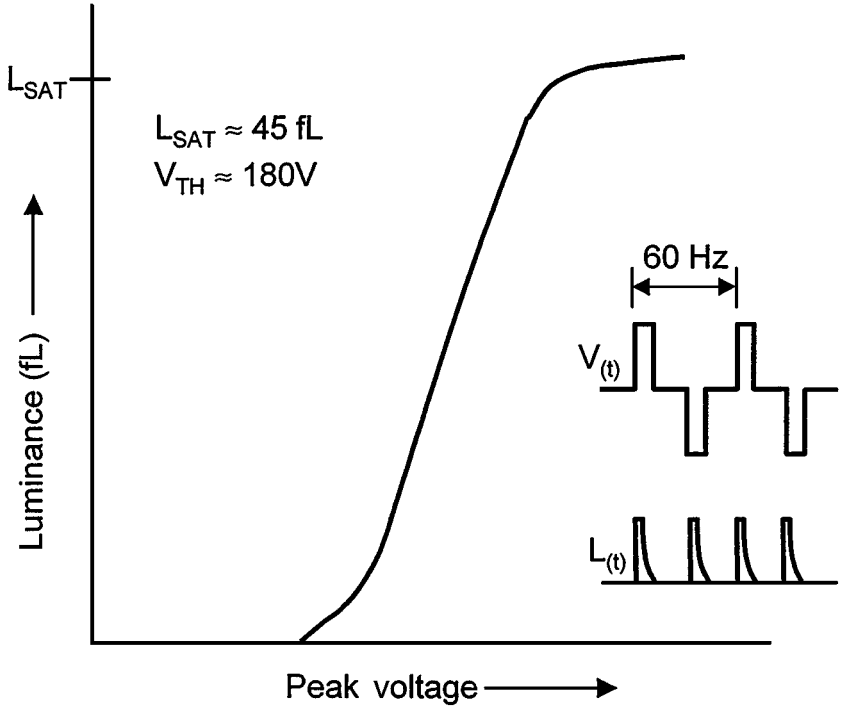

FIGURE 7.18 Threshold response for light emission from an electroluminescent pixel driven by a 60 Hz square-wave voltage train. (*Courtesy Society for Information Display*.)

crystal and caused display degradation during operation. The films in the display were slowly destroyed by electrolysis. It was hypothesized that hydrogen ions from moisture in the display were exchanging with sodium ions in the glass, thus creating mobile ions in the liquid crystal. These ions were then promoting electrolysis of the films. The solution to the problem was based on another film. Soda-lime glass was coated with a 100-nm-thick layer of silica to block the interchange of hydrogen for sodium ions. Such films are produced both on line and off line by manufacturers of float glass. The float process, as discussed in Chap. 6, forms a continuous ribbon of flat glass on a molten tin bath. The sheet is about 3 m wide with thickness variations of ±0.1 mm, negligible warp, and stria (microcorregations) less than 0.1 μm in height.[46] This glass can be used directly in passive LCDs based on twisted nematic (TN) or supertwisted nematic (STN) liquid crystals provided glass defects such as stria are less than 20 to 30 nm when the spacing between the glass plates is 5 to 10 μm.[47] Otherwise, manufacturing defects on the glass cannot be accommodated and the glass must be polished. Major manufacturers of float soda-lime glass for passive LCDs are listed in Table 7.4. Direct application of films to hot float glass while it is still on the tin bath has greatly expanded the usefulness of this technology. The application of the film creates a new product. Examples are barrier layers of silica for LCDs, transparent conductors like fluorine doped tin oxide (FTO) for displays and architectural windows, and black absorbing films for architectural glass.

TABLE 7.4 Manufacturers of Soda-Lime Sheet Glass for Display

Asia:
Asahi Glass
Nippon Electric Glass (NEG)
Nippon Sheet Glass (NSG)
Hoya
Europe:
Pilkington Glass
Schott Glass
Saint Gobain
Glaverbell
Flachglas
United States:
Libby Owens Ford (LOF)

TABLE 7.5 TFT Processes for AMLCDs

Semiconductor	Max. process temp,°C	Electron mobility, $cm^2/(V \cdot s)$	Suitable* glasses (code no.)
α-Si:H	400	1	Annealed 7059 As-formed 1737
Poly-Si thermally recrystallized	600	10–50	Annealed 1737
Poly-Si laser recrystallized	450	100	As-formed 1737

*See also Tables 7.1 and 7.6.

7.2.2.2 Active-Matrix LCDs. Increase in FPD size along with demand for video response equivalent to the CRT made it necessary to avoid the high level of cross talk between adjacent pixels in passive displays. The nonlinear response of the liquid crystals was no longer sufficient and it became apparent that a switch was needed at each pixel. In principle, several switching technologies could be utilized since they all could be fabricated with films and photolithography. Metal-insulator-metal (MIM) devices, diodes, and transistors have all been tried. Thin-film transistors (TFTs) have performed the best and as a result have been adopted for most active-matrix applications.

The early work of Brode on compound semiconductor TFTs led to the current active matrices based on silicon TFTs. A low-temperature process utilizes amorphous silicon films (α-Si:H) as the semiconductor, while higher-temperature versions are based on better performing polycrystalline silicon films (poly-Si). Table 7.5 compares the various approaches and gives an example of glass needed for use with each. Electronic mobility may be taken as a figure of merit for TFT performance, the higher the better.

Sodium contamination in a TFT can lead to instability. For this reason, soda-lime glass is avoided for active-matrix displays. Even with a silica barrier, it is possible for sodium to escape from this glass into adjacent films at elevated processing temperatures. The borosilicate glasses are much better, and it has been shown[48] that these can perform the role of a getter for sodium, purifying a silica barrier layer deposited on them. Of course, the sodium-free, high-temperature glass-fused silica would be ideal for AMLCDs, but it is currently too expensive in sheet form for wide use. Some thought has also been given to the use of transparent glass-ceramics as high-temperature substrates to substitute for fused silica.

TABLE 7.6 Glasses Manufactured for Use in AMLCDs

Manufacturer code no.	Corning code 1737F	NHTechno NA35	NEG 0A10	Asahi AN100
Strain point °C	666	650	651	670
Anneal point °C	721	700	703	720
Density, g/cm^3	2.54	2.48	2.51	2.51
Coefficient of thermal expansion (0–300°C), 10^{-7}/°C	37.8	36.5	36.6	35.5
Young's modulus, (10^6 lb/in^2)	10.15	9.98	10.08	11.31

The float process developed for soda-lime glass accounts for the major tonnage of flat glass products sold worldwide. It was thought that borosilicates required a different process to turn them into quality sheet glass without polishing. Hence, the fusion down-draw process was developed by Corning Incorporated.[38,49] This process, described in Chap. 6, produces a glass sheet that solidifies from the melt so that its surfaces do not contact any solid or liquid material. These pristine glass surfaces are smoother than polished glass by a factor of 2.

Code 7059 glass (Table 7.1) made by the fusion process was the only suitable glass available during the first decade of AMLCD manufacture. Later on, code 1737F glass was produced. Eventually though, the float process was adapted to borosilicate production so that several glasses are available for poly-Si TFTs. A final polishing is needed to make float glass suitable for AMLCD manufacturing. As a result, both the fusion and float processes supply the needs of the FPD industry as shown in Table 7.6.

Certain glass properties are critical for their use in AMLCDs.[50,51] These are summarized below.

Use temperature (25°C below the strain point). Determines the TFT process choice as outlined in Table 7.5 and shown in Fig. 7.19.

Dimensional stability. Shrinkage of less than 1 ppm for a 1-hour heat treatment at the TFT maximum process temperature (in the absence of photomask stepper compensation of up to 40 ppm) is critical to alignment in the photolithographic process for TFT manufacture. It is related to use temperature.

Density. Relates to manufacturing efficiency and weight of final product. A smaller value is better.

Chemical durability. Resistance to attack by photolithographic etchants.[52] Relates to chemical bath contamination.

Coefficient of thermal expansion (CTE). A match to silicon at 35×10^{-7}/°C is desired for chip-on-glass mounting of peripheral circuits. It also offers decreased thermal shock resistance compared to soda-lime glass.

Young's modulus. A higher modulus results in less glass sag during processing. The sag problem becomes more important as processed glass size increases from 550×650 mm to 600×720 mm while at the same time thickness decreases from 1.1 to 0.7 mm.

Surface smoothness. Streak (stria) of no more than 0.02 μm peak-to-valley over 1 mm (less than 3.5 μm variation over 25 mm).

Sheet flatness. Warp less than 0.5 mm over 400 mm.

Thickness of sheet. Nominal dimension within 10 percent with tolerance of less than 50 μm over 400 mm.

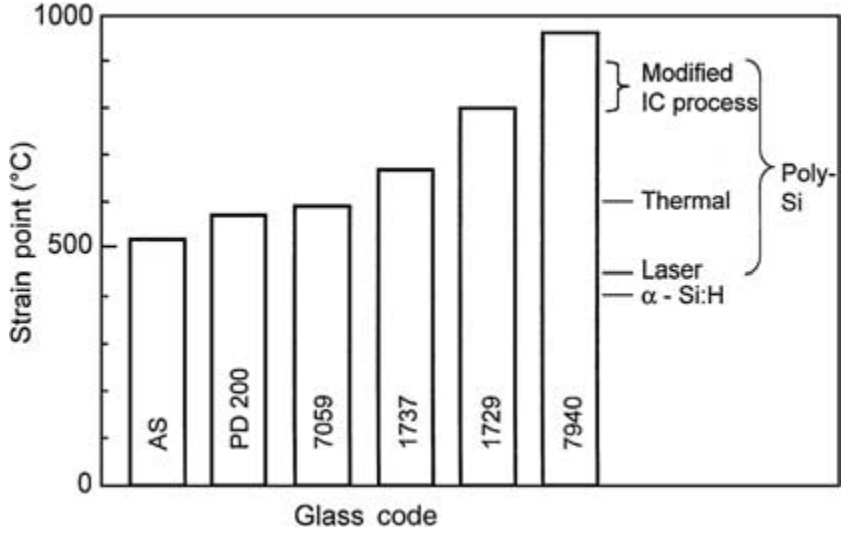

FIGURE 7.19 Comparison of Thermal capability (strain point) of commercial LCD glasses with TFT processing temperatures.

Defects. Internal bubbles and stones must be no larger than 0.1 mm; surface scratches and stains must be invisible under 1.5 to 10 klux illumination, depending on the quality of the substrate.

Strength. Failure is due to defects. Scoring of the glass[53] prior to breaking creates many edge defects. Fewer defects are found in boroaluminosilicates used for AMLCDs than in soda-lime glass used for passive LCDs.

7.2.2.3 Electroluminescent Display. Electroluminescent (EL) displays based on inorganic or organic thin films emit light directly from pixels rather than modulating reflected or transmitted light as occurs in LCDs. The inorganic version has been in existence for many years but is still limited by low efficiency of the blue phosphor. More recently, displays[54] based on organic light emitting diodes (OLEDs) have been developed to complement LCDs. They are current controlled devices as contrasted with voltage controlled LCDs. An OLED uses recombination of holes and electrons in various dye layers to generate red, blue, and green light. Both passive and active versions of OLEDs are useful, similar to LCDs discussed above. As a result, the same glasses have been adopted as substrates for both types of display, although only one instead of two layers of glass are usually required in the case of OLEDs.

7.2.2.4 Peripheral Circuits. The drive and address circuitry that operates a flat panel display is approximately equal in both cost and importance to the display panel itself. It is for this reason that the use of mass produced 10- to 20- volt integrated circuits (ICs) to drive and address LCDs and OLEDs makes these displays so competitive versus other technologies, which require 125- to 150-volt circuitry, e.g., plasma panels and inorganic electroluminescent displays.

Early LCDs had the drive-address circuitry mounted on a separate printed circuit board (PCB). This arrangement required that every conductor line on the display panel be connected by a wire to the PCB. The multitude of interconnects caused two major problems: the expense of making individual connections, each one in a space only 100 μm wide, and the decreased reliability of the finished display due to failure of interconnects.

The next evolution of the circuitry technology was to mount the drive-address IC chips on the glass substrate itself. Toward this end, the new generation of LCD glass, e.g., code 1737, had a TCE that matched that of silicon. The IC chips were mounted by either flip-chip or tape-automated bonding (TAB) techniques. This hybrid approach led to a more compact display morphology.

The ideal solution to the drive-address circuitry is to incorporate it directly into the thin-film structure on the glass. TFTs can be fabricated for the active matrix and the drive-address circuitry at the same time. This is already being done commercially for projection LCDs, where the small size and 1000×1000-line matrix restricts the number of connections that can be made to the substrate. A 950 to 1000°C process utilizing fused silica substrates (Table 7.1) is used to make the high-performance polysilicon transistors. Larger- area displays utilize the lower-cost flat glass shown in Table 7.6 where the strain point is far below that of fused silica. In this case, a laser recrystallization process is used to create high-mobility silicon films for developmental displays.

The future of FPDs lies in the ability to successfully integrate the display panel with the drive-address electronics. This increases reliability, decreases fabrication costs, and will lead to the extension of large-area electronics to applications other than displays, e.g., optical sensors or microelectromechanical devices (MEMs).

REFERENCES

1. J. Tyndell, *Proc. Royal Institution,* vol. 1, p. 446 (1854).
2. A. G. Bell, *Proc. Am. Assoc. Advancement Science,* vol. 29, p. 115 (1880).
3. F. P. Kapron, D. B. Keck, and R. D. Maurer, *Appl. Phys. Lett.,* vol. 17, p. 423 (1970).
4. M. Born and E. Wolf, *Principles of Optics,* Pergamon Press, New York, 1975, sec. 1.5, p. 36.
5. J. E. Midwinter, *Optical Fibers for Transmission,* John Wiley and Sons, New York, 1979.
6. J. B. McChesney, R. E. Jeager, D. A. Pinnow, F. W. Ostermayer, T. C. Rich, and L. G. Van Uitert, *Appl. Phys. Lett.,* vol. 23, p. 340 (1973).
7. T. Miyashita and T. Manabe, *IEEE J. Quantum Electronics,* QE-18, p. 1432 (1982).
8. D. Tran, G. Sigel, and B. Bendow, *J. Lightwave Technol.,* vol. 5, 1219 (1987).
9. M. G. Blankenship and C. W. Deneka, *IEEE J. Quantum Electronics,* vol. QE-18, p. 1418, (1982).
10. K. O. Hill, Y. Fujii, D. C. Johnson, and B. S. Kawasaki, *Applied Physics Letters,* vol. 32, pp. 647, 649 (1978).
11. R. D. Maurer, *J. Chem. Phys.,* vol. 25, p. 1206 (1956).
12. H. Yokata, H. Kanamori, Y. Ishiguro, G. Tanaka, H. Takada, M. Watanam, S. Suziki, K. Yana, M. Hoshikawa, and H. Shimba, in *Technical Digest on Optical Fiber Communication,* 1986, Post Deadline Paper PDP3.
13. D. Marcuse, *Applied Optics,* vol. 23, p. 1082, (1984).
14. D. Gloge and E. A. J. Marcatelli, *Bell Syst. Tech J.,* vol. 52, p. 1563 (1973).
15 V. A. Bhagavatula, M. S. Spotz, and D. E. Quinn, *Proceedings of Conference on Optical Fiber Communication,* 1984, Paper MG2, p. 20.
16. K. J. Beales, C. R. Day, A. G. Dunn, and S. Partington, *Proc. IEEE,* vol. 68, pp. 1191–1194 (1980).

17. D. B. Keck and P. C. Schultz, U.S. Patent 3,711,262, 1973.
18. K. Inada, *IEEE J. Quant. Elec.,* vol. QE-18, p. 1424 (1982).
19. S. Nagel, J. B. McChesney, and K. Walker, *IEEE J. Quant. Elec.,* vol. 18, p. 459 (1982).
20. T. Miyashita, M. Kawachi, and M. Kobayashi, *Optical Fiber Communications Conference,* New Orleans, 1988, Paper THJ3, p. 173.
21. J. F. Massicott, J. R. Armitage, R. Wyatt, B. J. Ainslie, and S. P. Craig-Ryan, *Elec. Lett.,* vol. 26, p. 1645 (1990).
22. Y. Sun, J. W. Sulhoff, A. K. Srivatsava, J. L. Zyskind, T. A. Strasser, J. R. Pedazzani, C. Wolf, J. Zhou, J. B. Judkins, R. P. Espindola, and A. M. Vengsarkar, *Elec. Lett.,* vol. 33, p. 1965 (1997).
23. C. Chen, I. Kim, O. Mizuhara, T. Nguyen, K. Ogawa, R. Tench, L. Tzeng, and P. Yeates, *Optical Fiber Communication Conference,* 1999, Post Deadline Paper PD7, p. PD7-1.
24. R. H. Stolen and E. P. Ippen, *Applied Phys Lett.,* vol. 22, p. 276 (1973).
25. B. S. Kawasaki and K. O. Hill, "Low-Loss Access Coupler for Multimode Optical Fiber Distribution Networks," *Appl. Optics,* vol. 16, pp. 1794–1795 (1977).
26. T. Tamir, *Guided-wave Optoelectronics,* Springer-Verlag, New York, 1988.
27. I. Bennion, D. C. J. Reid, C. J. Rowe, and W. J. Stewart, "High Reflectivity Monomode-Fiber Grating Filters," *Elec. Lett.,* vol. 341, p. 342 (1986).
28. A. Hasegawa and Y. Kodama, *Proc. IEEE,* vol. 69, p. 1145 (1981).
29. S. Barkou, J. Broeng, and A. Bjarklev, *Technical Digest on Optical Fiber Communication,* 1999, Paper FG5-1, p. 117.
30. R. Kashyap, *Fiber Bragg Gratings,* Academic Press, San Diego, 1999.
31. R. Ramaswami and K. N. Sivarajan, *Optical Networks: A Practical Perspective,* Morgan Kaufmann, San Francisco, 1998.
32. C. Brackett, A. Acampora, J. Sweitzer, G. Tangonan, M. T. Smith, W. Lennon, K. Wang, R. H. Hobbs, *J. Lightwave Tech.,* vol. 11, p. 736 (1993).
33. R. L. Mathew, "50 Years of CRT Bulbs at Corning," *Information Display,* September 1993, p. 8.
34. P. A. Keller, *The Cathode-Ray Tube,* Palisades Press, New York, 1991.
35. L. E. Tannas, Jr., *Flat Panel Displays and CRTs,* Van Nostrand Reinhold, New York, 1985, (*a*) p. 4; (*b*) pp. 208–209, 228–229; (*c*) pp. 332–414.
36. J. L. Lineweaver, "Oxygen Outgassing Caused by Electron Bombardment of Glass," *J. Appl. Phys.,* vol. 34, 1786–1792 (1963).
37. J. S. Collentro, "CRT Disposal: Recycle or Pay the Cost," *Information Display,* 1993, pp. 9–11.
38. D. C. Boyd, P. S. Danielson, and D. A. Thompson, "Glass," in *Kirk-Othmer Encyclopedia of Chemical Technology,* 4th ed., vol. 12, John Wiley&Sons, New York, 1994, pp. 574–579.
39. J. H. Connelly and D. J. Lopata, "CRTs and TV Picture Tubes," in *Engineering Materials Handbook,* vol. 4, *Ceramics and Glass,* ASM, 1991, pp. 1038–1044.
40. K. Compton, "CRT Glass—Not Just Sand," *Information Display,* November 1990, pp. 10–13.
41. R. L. Mathew, "Without Glass, It's Not a Tube," *Information Display,* June 1988, pp. 18–21.
42. J. Whitaker, "Display System Applications," in *Active Electronic Component Handbook,* By C. A. Harper and H. C. Jones (eds.), 2d ed., McGraw-Hill, New York, 1977, pp. 8.1–8.63.
43. "Program Directory and Product Guide for Display Works 98," *SID*, San Jose, Calif, 1998.
44. T. P. Brody, J. A. Asars, and G. D. Dixon, *IEEE Trans. on Electron Devices,* vol. ED-20, p. 995 (1971).
45. C. Khoo, *Liquid Crystals,* John Wiley and Sons, New York, 1995.
46. J. C. Lapp, P. L. Bocko, and J. W. Nelson, "Advanced Glass Substrates for Flat Panel Displays," *SPIE Proc.,* vol. 2174, pp. 129–138 (1994).

47. W. H. Dumbaugh, P. L. Bocko, and F. P. Fehlner, "Glasses for Flat-Panel Displays," in *High Performance Glasses,* M. Cable and J. M. Parker (eds.) Blackie, London, 1992, pp. 86–101.

48. R. J. Araujo and F. P. Fehlner, "Sodium Redistribution between Oxide Phases," *J. Non-Crys. Solids,* vol. 197, pp. 154–163 (1996).

49. L. Greasley, "Display Substrates: a Challenge to Glassmakers," *Information Display,* October 1991, pp. 20–23.

50. J. C. Lapp, "Glass Substrates for LCD Applications: Properties and Implications," *SPIE Proc.,* vol. 3014, pp. 2–9 (1997).

51. W. C. O'Mara, *Liquid Crystal Flat Panel Displays,* Van Nostrand Reinhold, New York, 1993.

52. P. L. Bocko and R. K. Whitney, "Information Displays," *Engineering Materials Handbook,* vol. 4, *Ceramics and Glass,* ASM, 1991, pp. 1045–1049.

53. T. L. Muir, "(A Proposal Regarding) Specifications for Precision Scribed and Broken Glass," *SID '92 Digest,* pp. 813–818.

54. G. Gu and S. R. Forrest, "Design of Flat-Panel Displays Based on Organic Light-Emitting Devices," *IEEE J. of Selec. Topics in Quantum Elec. vol. 4*, pp. 83–99 (1998).

CHAPTER 8
CERAMICS AND GLASSES IN MICROELECTRONICS*

Dana L. Hankey
Consultant

Aziz S. Shaikh
S. Vasudevan
Chandra S. Khadilkar
Ferro Corporation
Ferro Electronic Materials Division
Vista, California

8.1 INTRODUCTION

During the past several decades, the progressive development of complex integrated circuits has resulted in demanding requirements such as increased device densities, higher signal speeds, higher operating frequencies, miniaturization, increased reliability, and reduced costs. This has presented a great challenge to materials scientists who must accelerate development of materials and associated processes to keep pace with the rapidly changing environment. These materials include both active and passive components such as conductors, resistors, dielectrics (capacitors and insulators), varistors, filters, substrates, and sensors.[1–3] This chapter will focus on the basic technology for thick film materials with an emphasis on composition, design, processing, properties, test measurement methods, and structure/property relationships. The primary topics include conductors, resistors, and dielectrics. Ceramics and glasses are critical materials, especially in thick-film microelectronics.

8.2 THICK-FILM CONDUCTORS

8.2.1 Background

Materials classified as thick-film conductors play a major role in hybrid microelectronics, electronic packaging, components, displays, and photovoltaic applications. Generally speaking, the functionality of thick film conductors is analogous to wiring in predecessor technologies.

*See also Chap. 4.

However, the current material requirements are much more demanding. These challenges, as identified in the introduction, are further intensified when one considers the broad number of processing conditions to which conductors may be subjected as well as the compositional variations of other circuit elements that require compatible interfacing. The net result requires optimization of conductor properties and related processing parameters for specific applications.

The primary function of a thick-film conductor is to provide an electrically conducting path from one location on the circuit to another. Examples in basic hybrid circuitry include signal traces, crossover connections, and interconnection of one level to another or to an external device. However, conductor materials perform a wide variety of additional functions in microcircuitry, packaging, and component applications. These include the following:

1. Terminations for thick-film resistors, capacitors, and inductors
2. Electrodes/terminations for multilayer and disk capacitors as well as other fine ceramics such as varistors, thermistors, sensors, filters, and inductors
3. Low-value resistors, typically less than 10 Ω/cm^2 (sheet resistivity) for applications such as surge arrestor circuitry
4. Wire bond attachment
5. Die bond attachment
6. Discrete component attachment
7. Base for electroplating
8. Shielding materials
9. Metallizations for photovoltaic materials (solar cells)
10. Electrodes for flat panel displays

The above list is not all-inclusive but is a reasonable representation of most high-volume applications.

Thick-film conductors consist of three basic phases: (1) a metallic conductive or functional phase (i.e., gold, silver, copper); (2) a permanent inorganic binder phase (i.e., high-temperature glass and/or oxide phase); and (3) an organic vehicle for dispersion and application to the substrate.

The properties of thick-film conductors that are typically specified in order to determine formulation selection for a given application include the following:

1. Resistivity
2. Solderability and solder leach resistance
3. Line resolution
4. Physicochemical compatibility with other components such as resistors, dielectrics, and, most important, the substrate
5. Long-term stability in hostile environments such as heat, humidity, and thermal cycling (e.g., resistance to adhesion degradation)
6. Migration resistance
7. Cost
8. Wire and die bondability

Although many properties of conductor formulations are dependent on the bulk properties of the specific metallurgy and inorganic binder compositions, numerous techniques exist for property modification. These include formation of binary and ternary metal alloys, process

modifications, and alternative material selections for such tasks as soldered-lead/device attachments and wire bonding. The physicochemical compatibility of thick film conductors with other circuit elements and various substrate types is one of the most critical parameters in formulation development. As a result of emerging technologies and more stringent packaging requirements, alternative substrates such as aluminum nitride (AlN), porcelainized steel, low-temperature cofired ceramics (LTCC) of various compositions, low-temperature glass (displays), and silicon (photovoltaics) present challenges for material formulators. The ensuing sections will address the numerous topics presented in this introductory section.

8.2.2 Basic Constituents

The basic constituents of a thick-film conductor can be divided into three distinct phases:

1. A metallic, conductive phase (or functional phase) that typically consists of finely divided metal powders or alloys, such as gold (Au), silver (Ag), copper (Cu), silver–palladium (Ag–Pd), aluminum (Al), and nickel (Ni)
2. A permanent binder phase which is inorganic in nature and typically consists of a mixture of glass powders and/or oxides
3. An organic medium, or vehicle, which acts as the carrier agent for the inorganic constituents and provides the rheology appropriate for the deposition technique utilized in application of the pastes on respective substrates

The constituents of polymeric thick film conductors exhibit variations to the above description. These type conductors typically consist of a silver, carbon (C), or Ag and C mixture functional phase dispersed in a thermoplastic or thermosetting polymer and solvent.[4] In the case of polymeric thick film conductors, the polymer serves as an insulative binder and adhesive for the functional phase.

Metallurgy. The conductive (or functional) phase in thick-film conductors consists of elements as described in Table 8.1[5–7] which are categorized into noble and base metals. These metals are utilized in the form of powders which can have different morphological characteristics. The particle sizes range from submicrometer to several micrometers, and the selection of size, distribution, surface chemistry, and shape depends on the application and interfacing materials. Most metal powders are prepared by precipitation from various solutions. Powder morphology and agglomeration state are determined by the processing conditions. These powder characteristics determine packing efficiency and subsequent sintering kinetics which determine fired film densities. These sintering mechanisms will be discussed later.

As can be seen from Table 8.1, there is a broad spectrum of basic properties in the various metals. Those of utmost importance in material selection for a specific application include resistivity, melting point, and relative cost. Metals exhibiting high electrical conductivity, or low resistivity, come from Group IB [gold (Au), Ag, Cu] in the periodic table and have a valence of 1. Metals with valences of 2 or 3 (Groups II and III in the periodic table) cannot attain electrical conductivity values of Group I metals. However, these metals, which include Pd, platinum (Pt), Ni, tungsten (W), and Al (not in Table 8.1), are also good conductors and are widely utilized in conductor formulations. Sheet resistivity, a parameter that is typically specified, is a material property that is independent of film geometry. The derivation of sheet resistivity as specified for a given thickness is presented later in the section on resistors. The values in Table 8.1 are theoretical sheet resistivities which are not fully attained in practice because of impurities and inability to achieve 100 percent dense structures. Polymeric materials, not included in Table 8.1, have sheet resistivities in the range of 0.01 to 0.08 Ω/sq. The melting points of several of the metals in Table 8.1 are high relative to standard thick film processing temperatures, which range from 500 to 1000°C,

TABLE 8.1 Elements Used in Thick-Film Conductors

Element	Density, g/cm^3	Electrical resistance, $\mu\Omega \cdot$ cm at 25°C	Sheet resistivity, mΩ/sq/25 μm	Melting point, °C	Linear thermal expansion coefficient, ppm/°C	Thermal conductivity, W/m · K	Relative cost
			Noble Elements				
Ag	10.5	1.6	0.64	961	19.7	429	1
Au	19.3	2.3	0.92	1063	14.2	317	70
Pt	21.4	10.5	4.2	1769	9.0	72	100
Pd	12	10.8	4.3	1552	11.7	72	30
			Base Elements				
Cu	8.96	1.7	0.68	1083	16.5	401	0.02
Mo	10.2	5.2	2.04	2610	5.1	138	0.07
W	19.3	5.6	2.24	3410	4.6	174	0.06
Ni	8.9	6.8	2.72	1453	13.3	91	0.03

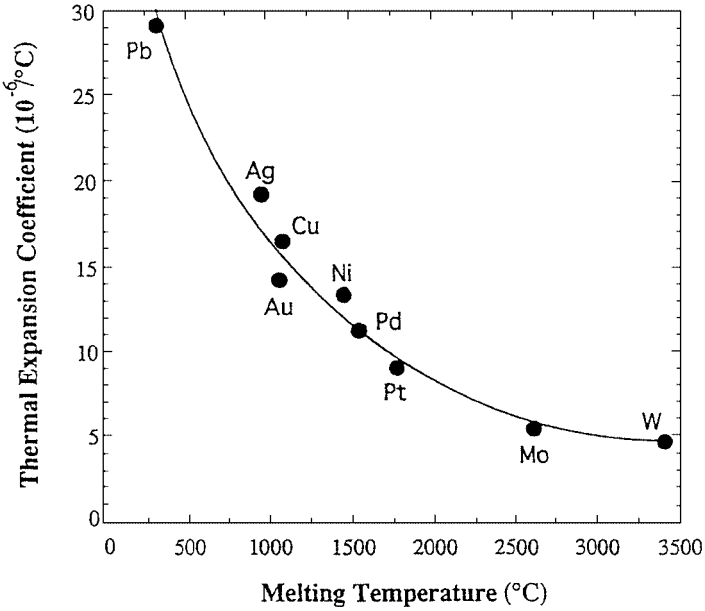

FIGURE 8.1 TCE versus melting temperature of various metals.

depending on the substrate material and application. The noble metals as well as Cu and Ni can be utilized for standard thick-film processing, while W and molybdenum (Mo) are utilized in high-temperature processes (1100 to 1800°C) such as cofired processing of alumina (Al_2O_3) and AlN packages.

Metals with strong bonding characteristics exhibit high melting temperatures, as shown in Figure 8.1.

The thermal coefficient of expansion (CTE) varies inversely with melting temperature of metals.[8,9] Except for W and Mo, the materials exhibit thermal expansion coefficients that greatly exceed the expansion coefficients of substrate materials on which they are deposited. This will create thermal stresses which develop during the cooling segment of the firing profile. Brittle materials such as ceramics would experience severe tensile forces which can lead to brittle fracture. However, in more ductile materials such as metals, the thermal stresses can be eliminated or relieved by plastic deformation. Resultant interfacial shear stresses can lead to metallization delaminations and even cracking in applications where there is repetitive temperature and/or mechanical cycling.[9,10] The wide variations in thermal conductivity of the metals could become important in applications where significant heat is generated, such as power hybrid circuits. This property can also be utilized for selection of heat dissipation in applications where thermal vias are employed.

The final general characteristic to be discussed from Table 8.1 is cost. In many small volume, high-reliability applications, cost is not an issue and Au-based materials may be selected. However, high-volume consumer and commercial applications will generally utilize Ag and Ag–Pd based materials as well as certain base metal conductors. One aspect of cost not factored into Table 8.1 is the associated processing costs of base metals. Refractory base metals such as W and Mo not only require specific controlled atmospheres, but also high temperatures and, therefore, significantly more power consumption. Base metals such as

TABLE 8.2 Solubility of Precious Metals in Molten Tin at 250°C

Metal	Solubility, wt%
Au	15.0
Ag	6.0
Pd	~0.5
Pt	1.0

Cu can be processed at more conventional temperatures, but the costs associated with controlled atmospheres, such as nitrogen, for processing and storage are still significant.

Table 8.2[11] compares the solubility of various precious metals prior to solid phase precipitation in molten tin at 250°C. Au and Ag exhibit the highest solubilities, while Pd and Pt have very limited solubility. These inherent characteristics affect solderability, leach resistance, and film degradation.

Conductor Compositions. Materials selection is a complex issue that is driven by the basic properties of various metals (as noted above), processes, substrate materials, the specific application, and required performance characteristics. The following discussion will review the various metallurgies and applications in more detail. Table 8.3[5] compares attributes of the various conductor system metallurgies.

Similarly, Table 8.4 compares sheet resistivity, leach resistance, and adhesion of various conductor types based on in-house experience. The adhesion values are stated in general terms because there are numerous adhesion tests and soldering methods which can produce a variety of results and discrepancies. Tables 8.1 through 8.4 can be referred to throughout the following sections.

8.2.2.1 Noble Metal Conductors

Gold and Gold Alloys. Pure Au conductor formulations exhibit high conductivity, excellent resistance to corrosion and migration, and are generally nonreactive when interfaced with other materials. Gold also exhibits good to excellent wire bondability with Al and Au, while also demonstrating the ability to be die-bonded with both eutectic and organic materials. Therefore, Au is suitable for applications in military and telecommunication circuits requiring high-reliability interconnections, resistor terminations, complex multilayer configurations, high-frequency stripline configurations, and pads for both wire and die attachments. However, factors such as cost and the inability to withstand commonly used tin–lead (Sn–Pb) solders[2,12] limits the applications of pure Au. Special solders such as Au–Sn alloys or indium (In) compounds must be used when soldering pure Au.[13] Since Pt is even more costly than Au and has an electrical resistivity almost 5 times that of Au, it is typically only used in its pure form for high-temperature applications such as electrodes for sensors and high-fire multilayer ceramic capacitors (MLC). However, additions of Pt to Au conductor formulations can result in materials with excellent solderability and leach resistance at the expense of conductivity.[14] Typical Au–Pt resistivity values are 30 to 50 mΩ/sq at 12.7 μm fired thickness. Gold–platinum conductors are utilized widely in high-reliability applications where discrete components are attached with solder or where circuit complexity requires frequent component replacement. Although initial bond strengths of Au–Pt compositions tend to be slightly lower than those of Ag–Pd alloys, they tend to have greater resistance to solder bond strength degradation.[15] However, the cost issue severely limits applications of Pt-containing golds to those requiring high reliability and solderability.

TABLE 8.3 Attributes of Various Conductor System Metallurgies (Thick Film)

Material	Die bondability			Wire bondability		Solderability	Corrosion resistance
	Eutectic	Solder	Organic	Gold	Aluminum		
Au	Good	Poor	Excellent	Excellent	Good	Poor/good*	Excellent
Pt–Au	NG	Good	Excellent	Fair to poor	Fair	Excellent	Excellent
Pd–Au	NG	Fair	Excellent	Fair to poor	Good	Good	Excellent
Ag	NG	Good	Excellent	Good	NG	Good	NG
Pt–Ag		Good	Excellent	Good	NG	Good	Good
Pd–Ag		Good	Excellent	Good	Good	Good	Good
Pd–Pt–Ag		Good	Excellent	Good	Good	Good	Good
Cu	NG	Good	Excellent	NG	Fair	Excellent	Poor
Ni	NG	NG	Excellent	NG	NG	NG	Excellent
Polymeric	NG	NG	Excellent	NG	NG	NG	Good
W or Mo–Mn	NG	NG	Excellent	NG	NG	NG	Good

NG: Not good.
*Depending on solder type.

TABLE 8.4 Typical Properties of Various Thick-Film Conductors

Conductor type	Resistivity*	Leach resistance†	Initial adhesion‡	Aged adhesion
Gold	3–5	Use In solder	Fair	Fair
Gold/platinum	30–50	Excellent	Good	Fair
Gold/palladium	5–7	Use In solder	Fair	Fair
Gold/via fill	20–40	Poor	Poor	Poor
Silver	3–5	Use 62 Sn–36 Pb–2 Ag	Good	Good
Silver–platinum	4–6	Fair	Excellent	Good
Silver–palladium:				
25 Ag–1 Pd	4–7	Poor	Good	Good
6 Ag–1 Pd	12–16	Fair	Good	Good
4 Ag–1 Pd	15–20	Good	Good	Good
Copper	2–4	Good	Good	Fair
Nickel (air-fired)	40–70	Not solderable	Fair	Fair

*mΩ/sq based on fired thickness of 0.5 mils (12.7 μm).

†Based on results with 60 Sn–40 Pb solder at 230°C. If another solder type is recommended, it means that results in 60 Sn–40 Pb are generally poor.

‡Al_2O_3 substrate.

Addition of Pd to Au compositions results in properties similar to those of Pt additions while reducing the cost. These compositions provide some economical solutions to situations where military specifications exclude the use of Ag because of migration issues. The solder leach resistance and aging of these alloys are somewhat inferior to those of Au/Pt compositions. Although Al wire bonds can be made to Au conductors, bond strengths degrade after aging at 150°C or higher.[12] The degradation is due to the formation of intermetallic compounds such as Al_2Au_5 and $AlAu_4$. This formation leads to Kirkendall void formation within the Au because of diffusion. The addition of a few percent of Pd to Au reduces the susceptibility to wire bond strength degradation.

This is the result of a reduced concentration of Au and a high concentration of Pd at the leading edge of Al. Instead of void formations, a stable Al–Pd–Au intermetallic phase is formed which has high electromechanical integrity. Therefore, Au–Pd alloys are typically employed for Al wire bonding applications and can be die-bonded under suitable conditions (organic).

In addition to binary Au alloys, ternary alloys are sometimes utilized to optimize properties of interest. For example, Au–Pt conductors do not typically fire to high densities and tend to crack, or fissure, in high temperature processing. Small amounts of Pd to form a Au–Pt–Pd alloy usually increase the density of the fired film, reduce the tendency to fissure, and improve solder leach resistance.

Silver and Silver Alloys. Of the noble metals, Ag has the lowest resistivity (Tables 8.1 and 8.4) and is the most economical. Although Ag is readily wetted by molten Sn–Pb solders, its leach resistance is quite poor. Modifications to the solder composition, such as adding 2 percent Ag, improve the leach resistance significantly. Pure Ag is the material of choice for numerous applications including conductors for plasma displays, metallizations for solar cells, terminations and/or electrodes for multilayer and disk capacitors or other fine ceramics, and high-volume hybrid applications where environmental conditions are not corrosive. However, the primary concern with Ag is its inherent tendency to migrate in the presence of an electrolyte, such as molten glass or water, and an applied electric field. The migration can occur very rapidly, as one can witness in a simple water drop test in

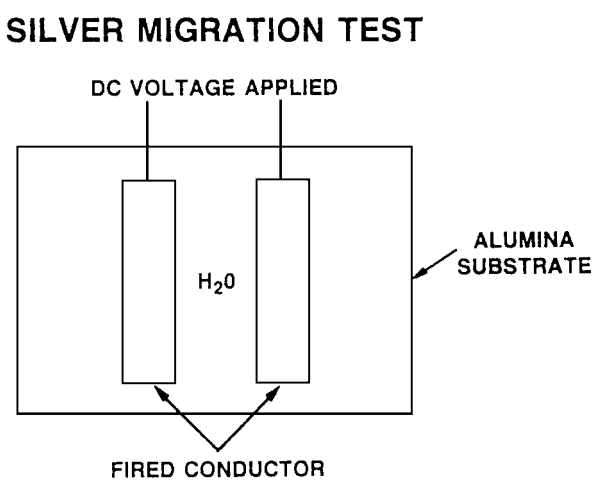

FIGURE 8.2 Electromigration test configuration.

which two Ag electrodes (250 μm apart) are subjected to droplets of distilled water and 5 V (Fig. 8.2). Electromigration results in Ag dendrite growth between the two electrodes, causing a short circuit. Research has also shown that Ag can readily migrate through thick film dielectrics during the firing cycle because of its high solubility in many molten glass compositions.[16] Numerous molten glass compositions can dissolve up to 2 wt% of Ag at peak firing temperatures of 850°C by dissolution, migration in the molten glass electrolyte, and absorption/reprecipitation at the surface of the second electrode. This not only produces dendritic growth, but it also produces the release of gases (such as oxygen) and resultant bubble/blister formation.

Proper design of thick-film dielectric materials, such as crystallizing formulations with optimized remnant glass subsequent to firing, can greatly reduce the tendency for Ag migration in multilayer configurations.[17–19] The referenced work presents data for both thick-film multilayer and low-temperature cofired tape formulations based on crystallizing glass formulations. Cross-sectional analyses using energy dispersive spectroscopy (EDS) for elemental Ag detection coupled with 2000-h bias humidity tests (85°C, 85 percent relative humidity, 30-V bias) suggest little or no Ag migration with specific dielectric compositions. Similarly, capacitance and insulation resistance measurements remained stable, supporting the idea that Ag migration is absent. Work by Alexander and Shaikh[18] suggests that buried Ag can be interfaced with surface Au compositions to eliminate surface migration problems and enhance wire bondability. When material selection is limited, Ag migration can also be reduced by proper circuit design and the use of special encapsulants. Significant technical advances are in progress to reliably enhance the use of Ag to take advantage of its cost and conductivity.

Binary Ag alloys are used extensively in the manufacture of thick film hybrids and electronic components. The most commonly used alloy is Ag–Pd. As illustrated in Fig. 8.3,[6] Ag and Pd exhibit complete solid solubility. These two metals can be prealloyed prior to preparation of the formulation or can be added as two distinct metallic components which alloy during the ensuing firing cycle. X-ray diffraction analysis[20] can be utilized to determine whether one has a true alloy prior to firing. Similarly, this technique can be utilized to determine if complete solid solutions have been formed during the firing cycle.

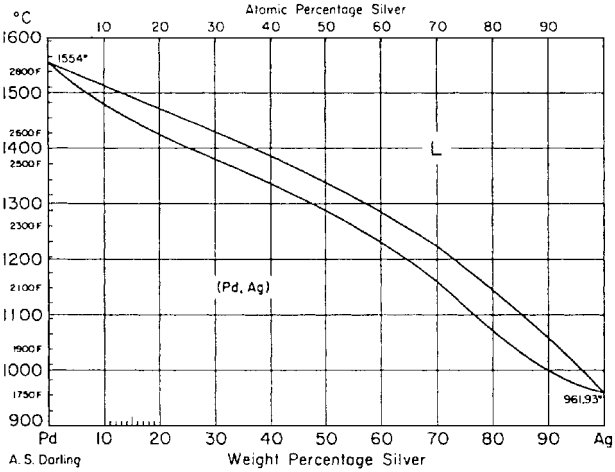

FIGURE 8.3 Ag–Pd phase diagram. (*From Metallography, Structures and Phase Diagrams; courtesy of A. S. Darling.*)

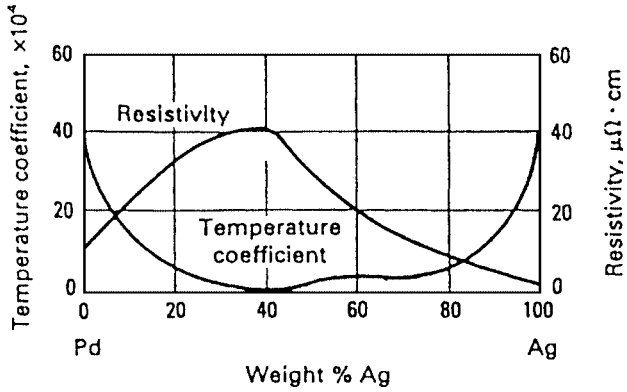

FIGURE 8.4 Electrical resistivity and temperature coefficient of resistance of Ag–Pd alloys. (*From Electronic Materials Handbook.*)

The addition of Pd to pure Ag improves solder leach resistance and reduces the tendency of Ag to migrate because of solid solution formation. These formulations are typically used for terminating resistors in network applications. Also, Ag–Pd conductors with low Pd content generally have good gold and aluminum wire bonding capability[21] (Table 8.3), although they are not suitable for eutectic die bonding. However, the addition of Pd introduces several undesirable attributes. The first significant issue is illustrated in Fig. 8.4[5] and Table 8.4, which show the substantial electrical resistivity increase with increasing Pd amounts. The maximum resistivity of approximately 40 $\mu\Omega \cdot$ cm occurs near the composition of 40 wt% Ag–60 wt% Pd. This coincides with the temperature coefficient of resistance approaching zero which is useful in the design of low value resistors (less than 10 Ω/sq) for numerous

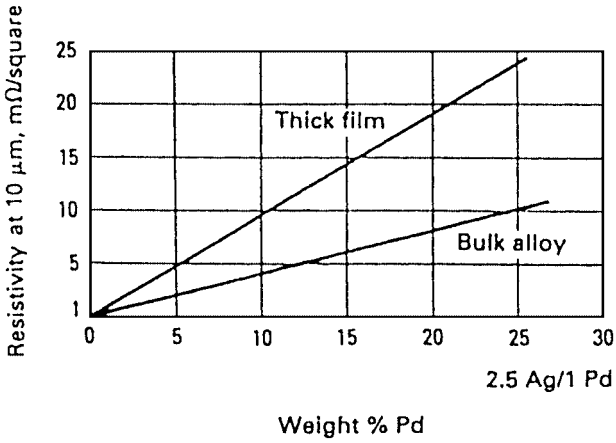

FIGURE 8.5 Effect of binder content on Ag–Pd alloys. (*From Electronic Materials Handbook.*)

applications, particularly in telecommunication and power hybrid circuits. The conductivity of Ag–Pd compositions can be further diluted if additional inorganic binder is necessary in order to achieve full densification as Pd content increases[5] (Fig. 8.5).

The second consideration surrounding Pd additions to Ag is the oxidation potential and kinetics of Pd, which is uncommon for noble metals. The reaction for palladium oxidation can be written as follows:[22]

$$\mathrm{Pd(s)} + \frac{1}{2}\mathrm{O_2(g)} \Leftrightarrow \mathrm{PdO(s)} \tag{8.1}$$

where s indicates a solid and g indicates a gas. The oxygen (O) partial pressure (P_{O_2}) can be expressed by the following equation:[22,23]

$$P_{O_2}^{-1/2} = \exp\left(-\Delta G_f^0 / RT\right) \tag{8.2}$$

where ΔG_f^0 is the standard free energy of formation of one mole of PdO from Eq. (3.1), T is the absolute temperature in kelvin, and R is the gas constant. Standard thermodynamic data compilations[23] illustrate that if $P_{O_2} = 0.21$ atm (the value for air), the calculated temperature is 802°C. Therefore, although Pd metal is the stable phase above 802°C in air, palladium oxide is the stable phase below 802°C, which means that PdO will form on the surface of the conductor during cooling from a typical firing cycle. This can result in reduced conductivity and solderability.

The above analysis assumes unit activity for pure Pd. In a Ag–Pd alloy, the activity of Pd will be reduced and the temperature for Pd oxidation will depend on Pd content. Rapid cooling of the composition during firing can reduce the amount of PdO formation by reducing the oxidation kinetics. As discussed earlier, Ag–Pd formulations can utilize either prealloyed powders or individual constituents that can alloy in situ. Palladium oxidation can inhibit the solid solution process as illustrated by Vest,[22] where 80% Ag–20% Pd (by weight) did not completely form a solid solution even after 24 h at 850°C. In this study, an

equivalent degree of solid solution was attained after 20 min at 450°C when an atmosphere of nitrogen (N_2) containing less than 1 ppm O_2 was utilized. Although one apparent solution would be to use prealloyed compositions, finely dispersed alloy powders are not always readily available or suitable for specific applications.

Although silver to palladium ratios of 3:1, 4:1, and 6:1 are commonly used in hybrid applications, thrifted versions utilizing Pd contents less than 5% have been shown to have good leach resistance in 62% Sn–36% Pb–2% Ag solders.[24,25] Table 8.4 compares properties of various Ag:Pd ratios. These materials meet the requirements of high-conductivity materials needed for circuits with higher speeds and densities. Similar performance can be met by small additions of platinum to silver (1:100).[26] The leach resistance of a 1% Pt addition is shown to be equivalent to a 10 percent Pd addition with minimum effect on conductivity. However, Ag migration such as dendritic growth and diffusion into resistors or capacitors when used as a termination material is still an issue with only minor Pd or Pt additions.

The soldered adhesion of silver conductors, particularly Ag–Pd compositions, appears to undergo more degradation on thermal aging than their Au counterparts. Numerous articles have been written on the subject of intermetallic formation leading to mechanical failure during thermal or power cycling[27–31] after application of tin–lead solders. The last article,[31] by Chiou et al., focuses on intermetallic formation at Ag–Pd conductor interfaces. The research concluded that the formation of intermetallic compounds such as Pd_3Sn_2, Pd_2Sn, Pd_3Sn, PdSn, Ag_5Sn, and Ag_3Sn results in adhesion degradation above 130°C for times exceeding 40 h. Tin diffusion also causes conductor swelling due to volumetric changes of intermetallic phases.

8.2.2.2 Base Metal Conductors. Copper conductors have gained some acceptance over the past decade because of their relatively low metal cost, low resistivity, good adhesion on Al_2O_3 substrates, excellent solder leach resistance, and low migration tendency. Advances in compatible thick film dielectric formulations have resulted in significant use of Cu in multilayer interconnect boards, primarily for military applications. Also, uses of Cu conductor materials have included power hybrid and microwave-related applications. Their applications in more complex systems and networks have been limited by the availability of state-of-the-art nitrogen-firable resistor systems. However, there are additional factors that complicate the widespread usage of this versatile material.

Because of copper's strong oxidation potential, this material must be processed in nitrogen atmospheres containing very low partial pressures of oxygen (typically less than 10 ppm O_2). The cost of processing and storage in nitrogen can be considerable because of the high gas flow rates necessary to prevent oxidation. Most important, however, there are a number of deleterious effects associated with processing in a controlled atmosphere that must be addressed. These include complex phase equilibria scenarios at elevated temperatures for processing Cu (900 to 1000°C) and the difficulty of organic removal in a nonoxidizing atmosphere. The thermodynamics of processing Cu in various atmospheres was studied in detail by Vest[7] as well as by Palanisamy and Sarma.[32] Figure 8.6 is a phase stability diagram[7] for various elements critical to thick film technology as derived from theory and thermodynamic data from Turkdogan[23] and Gaskell.[33] Since the free energy of formation becomes more negative as the oxygen partial pressure decreases [Eq. (8.2)], the more stable oxides at elevated temperatures include alkaline earth materials, while oxides of bismuth (Bi) and lead (Pb) are significantly less stable. Referring to a peak firing temperature of 900°C and O_2 partial pressure of 1 to 10 ppm O_2, it would appear that C would oxidize in this region and Cu metal would be the stable phase. In actuality, cuprous oxide (Cu_2O) is stable in this region.[7,32] Bright metallic films are produced in this region, however, because of the extremely slow copper oxidation

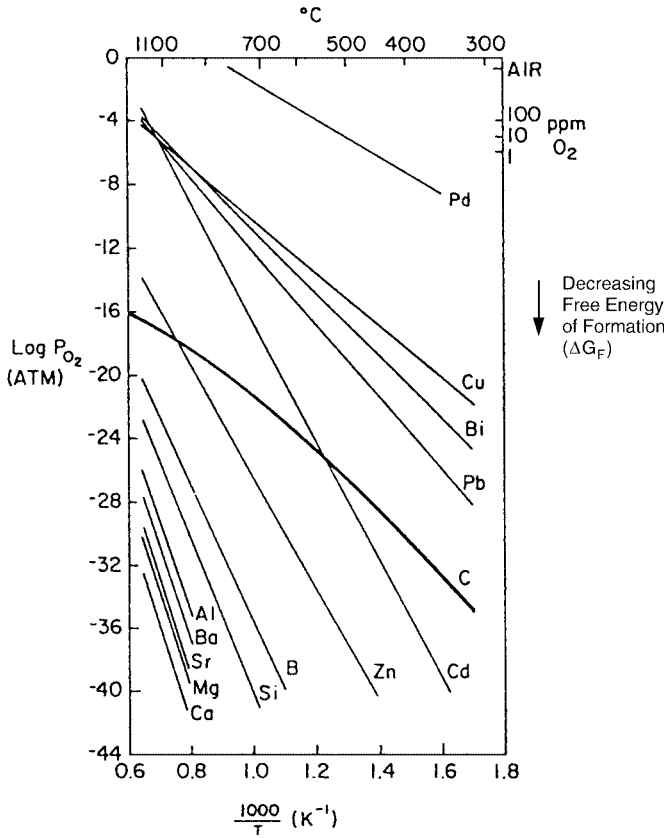

FIGURE 8.6 Phase stability diagram. (*From Ceramics Materials for Electronics.*)

rate at 900°C compared to the rapid diffusion rate of O_2 into Cu. The presence of copper oxide on copper particles during the initial firing stage actually promotes adhesion. It would also appear that lead oxide (PbO) and bismuth trioxide (Bi_2O_3) would remain stable at the 900°C firing range in 1 to 10 ppm O_2. However, lack of complete organic removal leads to localized reducing atmospheres (C line in Fig. 8.6) and subsequent reduction to the metallic phase.

Research by Pitkanen et al.[34,35] concluded that the presence of Cu_2O in copper conductor and dielectric films produced blistering phenomena. Lund[36] proposed that Cu_2O can be reduced to a copper precipitate that forms protuberances that eventually lead to a shorting phenomenon. Additional research has also suggested that reduction of lead and bismuth oxides leads to vaporization/condensation of these metals in furnaces and onto substrates creating cosmetic as well as functional problems. Reduction of Bi_2O_3 can also lead to grain boundary penetration into Cu conductors and subsequent formation of brittle alloys.[37] From a design standpoint, the ideal situation is to eliminate lead- and bismuth-containing oxides or glasses from all formulations to be processed in nitrogen. However, they have numerous benefits and cannot always be eliminated.

Although Cu exhibits excellent leach resistance and good solderability, the most severe limitation is the deterioration of adhesion on Al_2O_3 substrates when it is soldered with Sn–Pb alloys and subjected to thermal aging and/or temperature cycling. The formation of various copper/tin intermetallic compounds[38] such as Cu_3Sn and Cu_6Sn produces a thermal expansion mismatch at the conductor-substrate interface. The degradation is accelerated by voids in the solder and conductor porosity. This has prevented Cu from being accepted into the automotive industry where corrosive environments abound and acceptable thermal shock and power-cycling behavior is imperative.

In addition to Cu, other base metals not requiring high firing temperatures include Ni and Al. As seen in Table 8.4, Ni compositions are typically modified for firing in air and exhibit sheet resistivities in the 40 to 70 mΩ/sq range (12.7 μm fired thickness). These compositions are generally not solderable and have fair adhesion values on Al_2O_3 substrates. However, Ni and/or Ni-containing compounds such as nickel borides and silicides are utilized in many nonhybrid applications such as end terminations for capacitors and electrodes for gas discharge display devices.[39] Similarly, Al compounds have found nonhybrid applications as back metallizations for photovoltaic devices. The requirements are quite different than those for traditional thick film conductors. Nickel and aluminum requirements in these applications will be discussed in more detail in a later section.

Refractory Metals. Refractory metals, such as W, Mo, and molybdenum–manganese (Mo–Mn), have been used for many years in high-temperature packaging applications. Although Mo–Mn compositions can be used as postfired metallizations on particular substrate types such as Al_2O_3, AlN, and beryllium oxide (BeO), the majority of the W and Mo paste consumption is in high temperature multilayer cofired applications. These conductors, as seen in Table 8.1, exhibit high-resistivity values compared to Au, Ag, or Cu. As a result of their high melting points, high-temperature processing is necessary for production of dense fired films. These materials are also nonsolderable and must be plated with a solderable metal or alloy such as Ni prior to soldering. They require processing in moist, reducing atmospheres. Refractory metallizations are typically utilized in high-volume commercial areas such as automotive applications (i.e., ignition module, voltage regulators).

Polymeric Conductive Formulations. The conductive systems used in polymeric formulations include C, Ag, Ni, Cu, and various mixtures. Table 8.5 illustrates typical sheet resistivities for various metal powders and flakes. Silver flakes produce the most conductive system, since silver oxide remains conductive and exhibits slow oxidation kinetics, resulting in wide processing latitude with respect to curing cycles. Base metals oxidize in air and, therefore, require very limited curing profiles. As seen in Table 8.3, polymeric conductors have reasonable corrosion resistance and can be used for organic die attachment applications. However, wire bonding and solderability are typically poor for these systems.

TABLE 8.5 Typical Sheet Resistivity of Conductive Fillers

Conductor	Resistivity for 25-μm film, Ω/sq
Silver	0.01–0.1
Silver mixture	0.1–1.0
Nickel–copper	1.0–10.0
Carbon	10.0–100+

8.2.3 Inorganic Binders

Thus far the discussions have focused on thick-film conductor formulations from a metallurgical standpoint. This section addresses inorganic binder compositions and their importance in property development of thick-film conductors, particularly adhesion. These inorganic binder systems are typically composed of glass compositions and oxide additives.

Glass compositions are primarily utilized in thick-film formulations for two reasons: (1) to promote and develop adhesion to the substrate and (2) to affect the sintering kinetics and mechanisms of the composite. General requirements for glass compositions include the following properties:[7] good dielectric and mechanical strength; low dielectric loss; corrosion resistance, particularly with respect to moisture and acids; high electrical resistivity; thermal shock resistance; abrasion resistance; and low dielectric constants except in the case of capacitor dielectrics. In addition to the above general properties, additional physical properties of the glass that will be relevant to the particular application and substrate type include thermal expansion coefficient, viscosity as a function of temperature, glass transition temperature, surface-tension/temperature relationship, and compatibility with each material with which the glass will interface.

Typical thick-film glasses include a variety of borosilicate compositions ranging from Pb and Bi borosilicate compositions to alkaline earth borosilicate systems including barium (Ba), calcium (Ca), and magnesium (Mg). Although alkali ions serve as excellent fluxes in glass, their content should remain low in thick-film glass compositions in order to minimize electrical conductivity and dielectric loss. During the firing cycle, the glass must exhibit an optimum change in viscosity with temperature in order to control the sintering kinetics of the metal powders. This will lead to optimum densification of the fired film without bubble entrapment, blister formation, capillary movement of excessive amounts of glass to the fired film surface, and exaggerated grain growth of the conductive phase. The glass must also wet the substrate in order to penetrate the ceramic to a certain extent to provide mechanical and chemical bonding to enhance adhesion. This is accomplished by mechanical interlocking with substrate surface grains augmented by interdiffusion of ions. Typical weight percentages of glass additions range from 1 to 10 percent. The glass should penetrate the functional phase or metallic network as well as the substrate. Processing conditions and glass viscosity/temperature relationships must be optimized in order to prevent a continuous glass film formation between metal and substrate. This can result in brittle fracture and crack propagation at the interface under conditions of thermal and power cycling or relatively low mechanical stresses. The chemical composition of the glass is not only critical to the above requirements, but determines the chemical compatibility with the substrate in question.

The majority of thick-film research in the past has been conducted on alumina substrates. However, rapidly changing technology has introduced new substrate materials which require utilization of alternative glass compositions. For example, typical lead/bismuth borosilicate compositions compatible with alumina are rapidly reduced when processed on aluminum nitride substrates, as seen in Fig. 8.7.[40] Therefore, alternate compositions such as alkaline earth borosilicates with lower thermal expansion coefficients must be developed to optimize compatibility with the substrate.[41–43]

A scanning electron micrograph illustrates a cross section of an AlN-compatible glass in Fig. 8.8.[43] A topographic scanning electron micrograph (Fig. 8.9) illustrates the fracture surface of a conductor containing the compatible glass on AlN.[43] This micrograph shows the excellent mechanical interlocking of the referenced glass composition by the presence of fractured glass structures still adhering to the substrate after a pull test. Figure 8.10[43] shows a cross section of an optimized Ag–Pd thick film formulation on AlN.

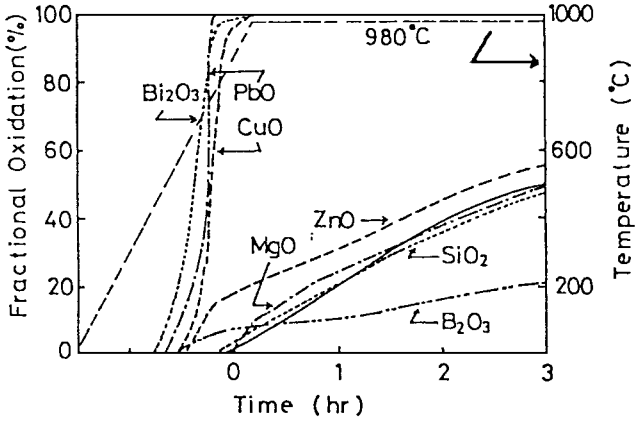

FIGURE 8.7 Effect of 5 mol% oxide additions on the oxidation of AlN (solid line: oxidation of pure AlN). (*From Proceedings of IMC.*)

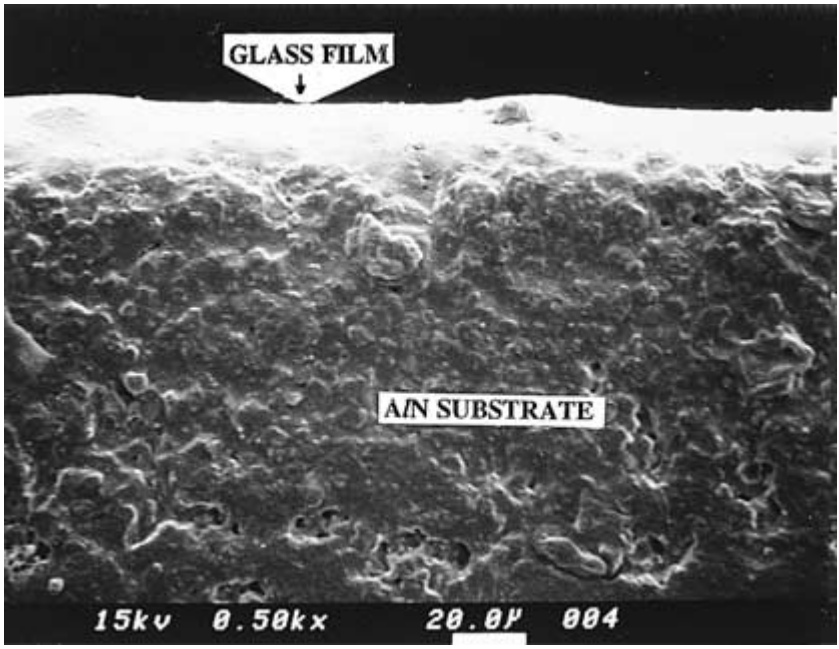

FIGURE 8.8 Cross section of compatible glass film on AlN substrate.

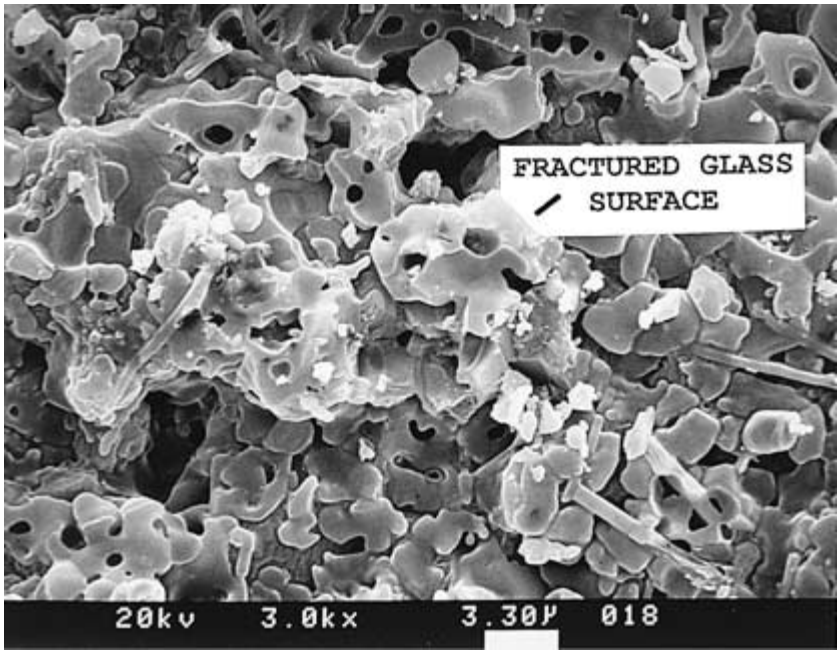

FIGURE 8.9 Fracture surface underneath conductor film illustrating bonding with AlN substrate.

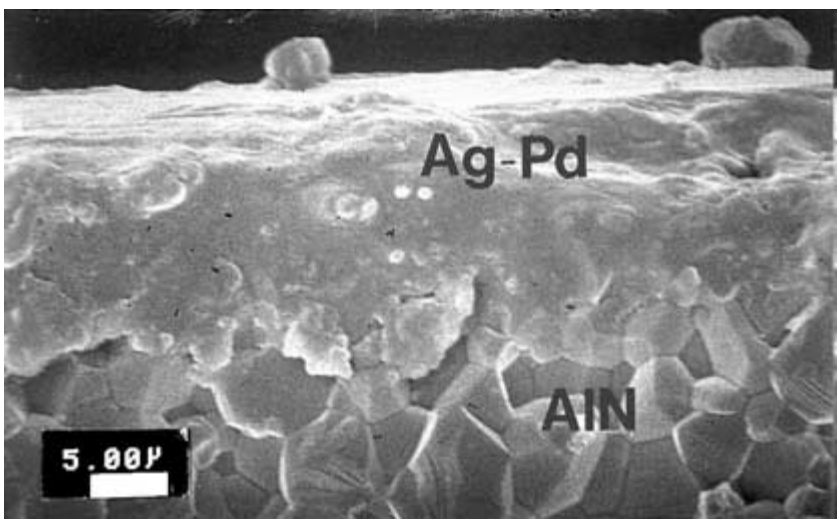

FIGURE 8.10 Cross section of Ag–Pd conductor on AlN.

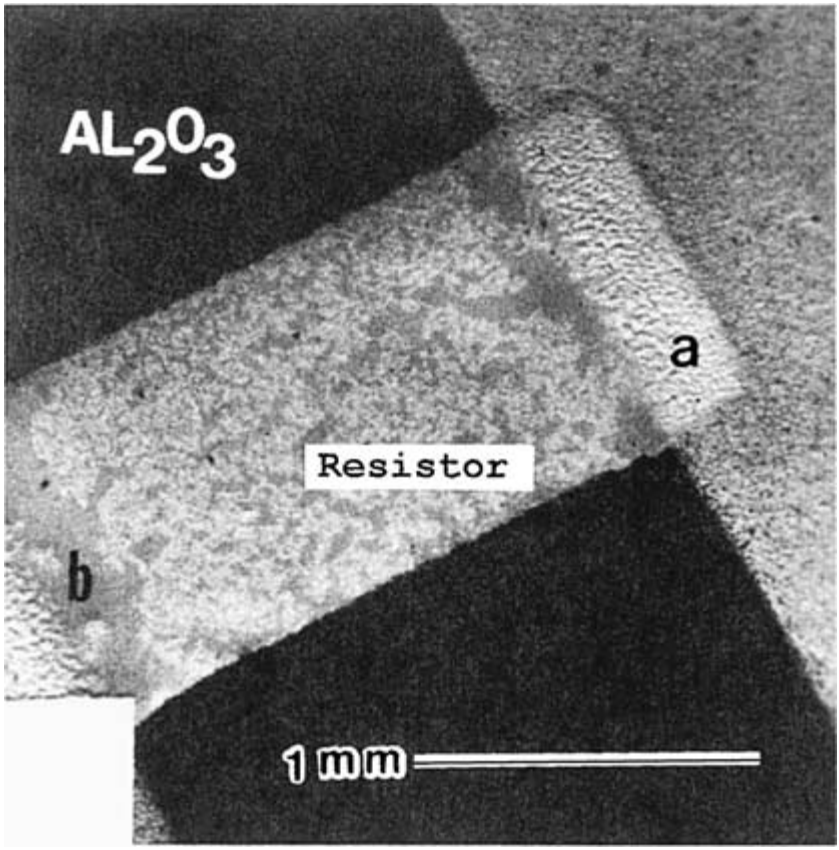

FIGURE 8.11 SEM photomicrograph of incompatible conductor–resistor interface and conductive phase thinning.

Similar research has been necessary to optimize formulations for applications on alternative substrate types such as BeO, low-temperature tape, and nonhybrid substrates such as glass substrates for displays, silicon (Si) for photovoltaic applications, and various ceramic bodies for component applications such as titanates for MLCs, zinc oxide varistors, and zirconia sensors. In each application, not only will the chemistry vary, but the particle size, surface area, and volume percentage of the respective glass compositions will also vary.

As previously mentioned, the glass composition is also critical to compatibility of thick-film conductors with other thick film materials such as resistors and dielectrics. This requires additional considerations when the formulation is designed. Figure 8.11[44] shows conductor/resistor incompatibilities at the interface resulting in cosmetic as well as performance-related issues. Glass chemistry selection is also very dependent on the firing atmosphere, as discussed earlier in the section on Cu conductors.

The second class of inorganic binders includes oxide additives that perform various functions. Numerous oxides such as copper oxide and cadmium oxide promote adhesion on

alumina substrates by formation of spinel compounds[23] such as copper aluminate ($CuAl_2O_4$). This type of bonding mechanism is a chemical or reactive bond. Reactive oxides are typically present in concentrations of less than 2 wt%. The benefit of this type of adhesion promoter is the absence of deleterious effects on wire bonding and solderability. Other oxide additions, such as Bi_2O_3, have been found to flux many glass systems and aid in wetting the substrate and enhancing adhesion. This is called *flux bonding* and typically utilizes additions of less than 5 wt% of the respective oxides. M. Hrovat and D. Kolar[45] investigated the Bi_2O_3–Al_2O_3–CuO system and concluded that, although no ternary compounds exist in this system, numerous binary compounds exist that melt incongruently at various temperatures and assist in adhesion promotion. Thick-film conductor compositions are, therefore, commonly regarded as having three different types of bonding mechanisms to the substrate:

1. Frit bonding, which is totally dependent on the glass-substrate interaction
2. Reactive bonding, which depends on the chemical reaction between oxide addition and the substrate
3. Flux bonding, which is a result of oxide additions to flux mixed-bonded conductors typically containing all of the above components

Reactive-bonded conductors offer the best bond between noble metals and the substrate, which is an oxygen-metal bond. Frit-bonded systems offer surprisingly strong bonds via mechanical interlocking mechanisms, but remain dependent on appropriate firing conditions. Excessive interactions can significantly reduce the strength of mechanical bonds. Mixed-bonded systems offer unique solutions for good adhesion by combining the above mechanisms.

Organic Vehicles. Organic vehicles, which act primarily as the transfer medium in thick-film compositions, consist of one or more high molecular weight polymers, such as ethyl cellulose, and low vapor pressure solvents, such as terpineol or glycol ethers. The vehicle also usually contains rheology modifiers such as surfactants and thixotropes. The composition of an organic vehicle for a given formulation depends on the following: (1) the concentration, densities, and morphological characteristics of the metallic and inorganic binder phases; (2) the method of paste manufacturing; (3) the deposition method (screen printing, dipping, spraying); and (4) the subsequent processing environment such as drying and firing profiles and atmospheres. Rheology is a very complex issue and is discussed later in the chapter as a separate topic.

8.2.4 Microstructure Development

Microstructural development of the thick-film compact during the firing process is critical since the resultant microstructure will largely determine the respective properties of this material. The relationship between processing, microstructure, and properties is extremely important in the production of all materials, especially in complex systems such as thick film composites which involve metals, ceramics, and polymers. The physicochemical properties of the raw materials will affect green packing densities, sintering kinetics and mechanisms, and the resultant material properties.

Initially, the particles in a given system, as printed and dried, are in intimate point contact prior to the specific firing cycle. As the temperature is raised during the firing cycle, however, several forces and resultant processes arise that lead to densification of the compact. This process is referred to as *sintering.*

The principal driving forces that are responsible for material transport and sintering are capillary-type forces that are a result of surface and interfacial tensions. Subsequently, these tensions or forces produce stresses that are related to the curvatures of the respective surfaces and interfacial areas. The pressure difference ΔP produced across curved surfaces of two different particles or grains can be represented as[46]

$$\Delta P = \gamma\left(\frac{1}{r_1}+\frac{1}{r_2}\right) \tag{8.3}$$

where γ is the surface tension and r_1 and r_2 are the radii of curvature of the surfaces. This pressure difference, for example, causes liquids to rise in capillaries. This equation is usually presented with stress σ replacing ΔP and is called the *LaPlace equation*.[47]

Similarly, there is a free energy difference ΔG across a curved grain boundary represented by[46]

$$\Delta G = \gamma \overline{V}\left(\frac{1}{r_1}+\frac{1}{r_2}\right) \tag{8.4}$$

where γ is the boundary energy, $\overline{V}$ is the molar volume, and r_1 and r_2 are the principal radii of curvature as above.

This free energy difference applied to material on two sides of a grain boundary is the driving force that moves a boundary toward the center of curvature and leads to densification and grain growth. Therefore, material transfer, on a microscopic scale, is related to both the pressure differences [Eq. (8.3)] and changes in free energy [Eq. (8.4)] across a curved surface. The free energy change that gives rise to densification processes in materials is the lowering of the surface free energy and respective surface areas. This results in elimination of higher energy solid-vapor interfaces by the formation of lower energy solid-solid interfaces.

Although sintering is typically divided into three stages, the major focus is on the initial stage of sintering where vapor pressure differences between the neck area and particle surface results in transfer of material, resulting in neck formation[46] (Fig. 8.12). In the case of solid-state sintering, a general equation for isothermal neck growth between two spheres can be expressed as[48]

$$\left(\frac{x}{r}\right)^N = Bt \tag{8.5}$$

where x = neck radius
r = particle radius
N = constant dependent on the sintering mechanism
B = constant
t = time

The small negative radius of curvature ρ at the neck produces a vapor pressure that is significantly lower than that of the particle. This results in the driving force for material transport.

Material transport during the initial stages of solid-state sintering can occur by a number of mechanisms, as displayed in Table 8.6.[46] If the material is transferred from the surface to the neck by surface, lattice, or vapor transport, there is no resultant shrinkage of the compacted material or decrease in porosity. However, if the matter source is in the bulk material—grain

TABLE 8.6 Alternative Paths for Matter Transport during the Initial Stages of Sintering

Transport path	Source of matter	Sink of matter
Surface diffusion	Surface	Neck
Lattice diffusion	Surface	Neck
Vapor transport	Surface	Neck
Boundary diffusion	Grain boundary	Neck
Lattice diffusion	Grain boundary	Neck
Lattice diffusion	Dislocations, neck	

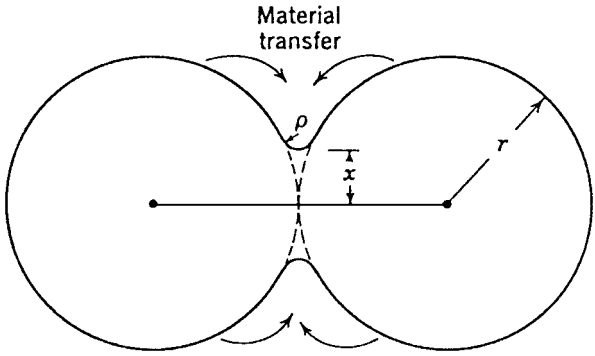

FIGURE 8.12 Neck formation during initial stages of sintering. (*From Introduction to Ceramics.*)

boundaries or dislocations, for example, then shrinkage and pore elimination occur. Figure 8.13 illustrates some of these mechanisms.

Thick-film formulations exhibit different types of dominant sintering mechanisms, depending on their composition. For example, thick-film conductors can sinter like solid-state metal particles or spheres, while sintering of resistors and dielectrics is more complex and largely dependent on glass sintering behavior.

Nordstrom and Yost[48] studied the sintering behavior of thick-film reactively bonded Au films and concluded that surface diffusion is the controlling mechanism in these systems, as in prior findings about sintering of high-purity Au spheres[49] and pure Au wires.[50] Intermediate and final stage sintering was controlled by volume or grain boundary diffusion mechanisms. However, most thick-film conductor formulations include low temperature glasses and fluxes to aid in the densification process at relatively modest time/temperature profiles. This can result in additional sintering mechanisms, referred to as *vitrification* and *reactive liquid sintering*. Vitrification is densification with the aid of a viscous liquid phase which results in microrearrangement by viscous flow of material into the pore regions. Kingery[46] defined the initial neck growth rate by this type of mechanism by the following equation:

$$\frac{x}{r} = \left(\frac{3\gamma}{2\eta l}\right)^{1/2} t^{1/2} \tag{8.6}$$

where η is the viscosity of the viscous component.

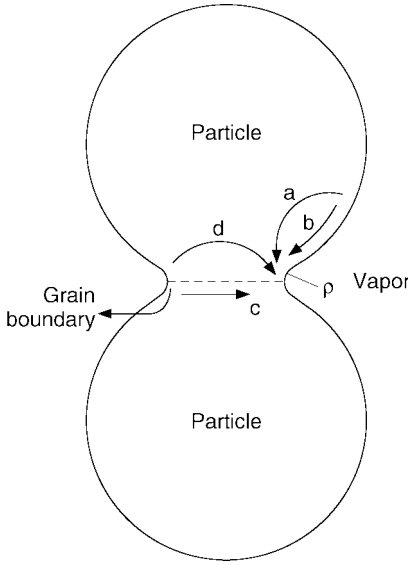

FIGURE 8.13 Material transport mechanisms during initial stage of solid-state sintering: (*a*) volume diffusion, (*b*) surface diffusion, (*c*) grain-boundary diffusion, and (*d*) volume diffusion from grain boundary.

Sintering with a reactive liquid refers to a process in which the solid phase has limited solubility in the liquid at the sintering temperature. During this sintering process, the solid phase dissolves in the glass at the high-energy region and is transported to the low-energy neck region where reprecipitation of the solid phase results in increased grain size and densification. Densification rates depend on the amount of liquid phase, the solid phase solubility in the liquid, and the solid phase wettability.

Cole[51] reported significant increases in sintering rates of Ag/Pd compositions attributable to the solution/reprecipation process described above. As it is important to control the viscosity of the respective glasses for optimum densification in the above processes, control of heating rates, peak firing temperature, and glass compositions are critical parameters for attainment of optimum densification. Sintering mechanisms for thick-film resistors and dielectrics which have high concentrations of glass constituents are addressed by Vest.[52]

The sintering process is undoubtedly very complex and various mechanisms compete and occur simultaneously for a given system. Sintering of thick-film conductors typically involves all of the mechanisms described above. Variables such as composition, particle size, surface area, packing efficiency (green density), glass viscosity, surface tension, wettability, impurity levels, atmosphere, time, and temperature all affect the sintering rates and mechanisms. Figure 8.14[5] is an example of the type of data that can be generated for a specific metal system to understand processing latitude of selected variables. In this figure, the preferred particle size can be determined in order to achieve optimum green density and maximum sintered density. Generally speaking, particle size increases result in decreases in surface area and associated surface energy. Green density is determined by these factors as well as interparticle forces that can control the degree of agglomeration. The final level of densification is controlled by many factors, including the green density and related particle/pore structure as well as sintering profiles.

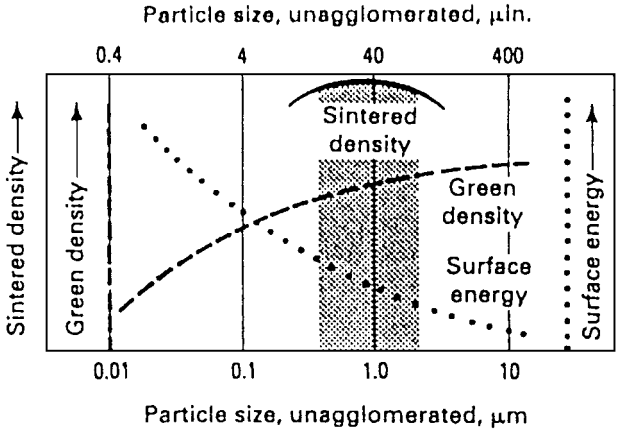

FIGURE 8.14 Effect of particle size on green and sintered densities. (*From Electronic Materials Handbook.*)

Wu and Vest[53] conducted research on Ag conductor systems with varying amounts of glass frit. For compositions containing 2 percent glass frit, initial porosities were approximately 50 percent, which is comparable to theoretical values (48%) for simple cubic packing of spheres. As glass frit content increased, initial porosities increased because of inefficient packing. With respect to particle size of Ag, relative shrinkages of conductors with particle sizes less than 1 μm were much higher (as expected) than conductors with Ag particle sizes greater than 8 μm. These studies illustrate the significance of optimization of all sintering parameters for achieving maximum densification. An example of complete densification can be seen in Fig. 8.10, noted earlier. The relationship between microstructure of fired thick films and various properties will be addressed in later sections for conductors, resistors, and dielectrics.

8.2.5 Conductor Properties and Test Methods

The combination of several factors including bulk material properties, conductor composition (i.e., metallurgy and glass content), substrate type, and the various processing steps (i.e., deposition process and firing profile) will determine the properties of the fired conductor. In most cases, the testing configuration depends on the conductor type and the specific customer requirements, which usually depend on the application. In this section, the basic tests and various factors that can affect test results will be addressed.

Test Pattern. The basic conductor properties can be measured using a single test pattern, as illustrated in Fig. 8.15. These include resistivity, print definition and film thickness, film density, solder leach resistance, wettability, adhesion, and wire bondability. Each property will be discussed individually with reference to Fig. 8.15. Many applications require functional use tests which usually require specific test patterns and even multilayer construction processes. Similarly, numerous applications require standard conductor tests on thick-film dielectrics instead of the bare substrate.

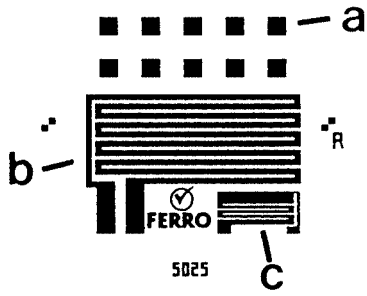

FIGURE 8.15 Conductor test pattern serving various functions: (*a*) pads for adhesion, wettability, solder leach resistance, and wire bondability; (*b*) serpentine pattern for measuring print thickness and resistivity; and (*c*) pattern for print resolution.

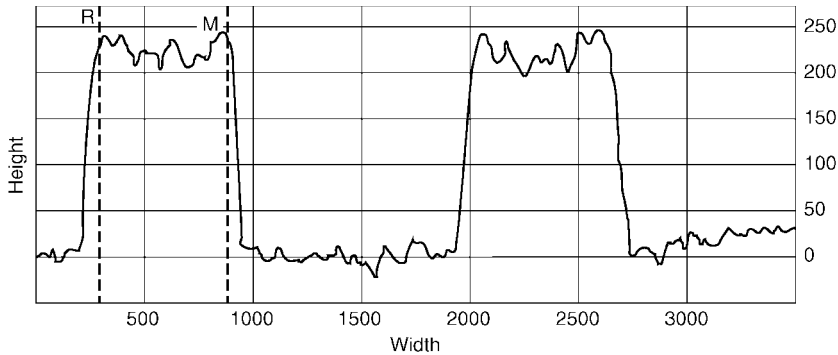

FIGURE 8.16 Surface profilometer tracing of thick film conductor. Dashed lines represent width of line at peak height.

Fired-film thicknesses can be measured by a number of instruments such as light-section microscopes and surface profilometers. Thickness uniformity is an important parameter, since variations can affect properties such as resistivity, adhesion, and solder leach resistance. Print definition is usually measured with surface profilometers and provides a measure of print quality, since it relates to both printing conditions and paste rheology. Undesirable conditions such as excessive line spreading and splining (commonly referred to as *drying lines*) can be detected. Figure 8.16 illustrates a data printout from a surface profilometer. The data were collected on the conductor test pattern in Fig. 8.15 by profiling a line perpendicular to the serpentine pattern (*b*). The trace illustrates the print definition as well as the actual thickness and uniformity of the print. A similar profile could be utilized on pattern (*c*) to study line definition. In this particular pattern, line widths and spaces down to 125 μm are utilized to determine print resolution. Microscopy techniques can also be used to study print resolution.

Conductivity. The conductivity for various metallurgy types varies significantly, as discussed in earlier sections. This property is especially important for applications requiring rapid signal speed. Electrical conductivity can be defined by the following relationship:[46]

$$\sigma = \frac{j}{E} \tag{8.7}$$

where j is the electric current density (charge transported through a unit area in unit time) and E is the electric field strength.

In practice, the figure of merit for conductors is resistivity, which is the inverse of conductivity. Resistivity is the ability of a material to resist the passage of current (units are ohm-centimeters for bulk resistivity, as illustrated for metals in Table 8.1). Surface resistance or line resistance is expressed in ohms. The common expression for thick film conductors is sheet resistivity (expressed in milliohms per square), which is the electrical resistance measured across opposing sides of a square for a normalized thickness.

Resistivity is measured by utilizing a four-point probe ohmmeter and very low currents. As illustrated in Fig. 8.15*b,* a serpentine pattern of 200 to 400 squares in length is usually employed for this measurement. The pattern in Fig. 8.15*b* is 360 squares. Resistivity depends on the metallurgy, composite formulation, fired density, and thickness.

Wettability. Wettability is defined as the extent to which a metal surface is clean and free of oxides so that metal contact can be made between solder and the metal. This term is used interchangeably in hybrid microelectronics with *solderability*. Various conductor systems exhibit different degrees of solder acceptance, as illustrated in Table 8.3. The tests for wettability in the past have been largely subjective and qualitative and have been based on visual observations. Most solderability tests involve dipping a fired metallized substrate into a particular solder system with a specified flux, time, and temperature. After the substrate is cleaned with solvent, the solderability is qualitatively determined by the degree of coverage and evidence of dewetting and/or voiding. Moderate differences can be readily visualized, but subtle differences cannot be determined from this qualitative approach. This visual test can be done on the pads on Fig. 8.15*a*.

Solderability or wettability depends on the wetting characteristics of a solid surface by a liquid or molten solder. The angle θ between a solid surface and the tangent to the liquid surface at the contact point specifies the conditions for minimum energy according to the following equation:[46]

$$\gamma_{LV} \cos\theta = \gamma_{SV} - \gamma_{SL} \tag{8.8}$$

where γ_{SV}, γ_{SL}, and γ_{LV} are the interfacial energies between the phases present in a particular system. The boundary condition between wetting and nonwetting is $\theta = 90°$. If we review Fig. 8.17,[46] we can see the various conditions for wetting, nonwetting, and complete spreading of a liquid on a solid.

The above principles were utilized to develop a more quantitative solder-wetting test within the North American Rockwell Electronics Group.[11] Engineers developed a formula for calculating a spreading factor based on the weight and density of the solder as well as the height of the solder after spreading on a fired substrate surface. Cooper and Monahan[54] also utilized these principles to characterize solder wetting forces using a meniscograph.

More recently, precision wetting balances have been developed to provide qualitative wetting force values that arise from interfacial energies developed by solders on fired metallized substrates. The apparatus consists of a precision microbalance and electromechanical dipping device that executes preset substrate immersion and emersion rates. The test substrate should be fully metallized on both sides and should be standardized with respect to size. During the test, the metallized substrate is suspended from the microbalance and is stationary while the pot containing molten solder is raised and subsequently lowered to produce constant immersion and emersion rates. Figure 8.18 illustrates a typical wetting balance curve for a solderable material.[55] The zero wetting force line must first be calculated

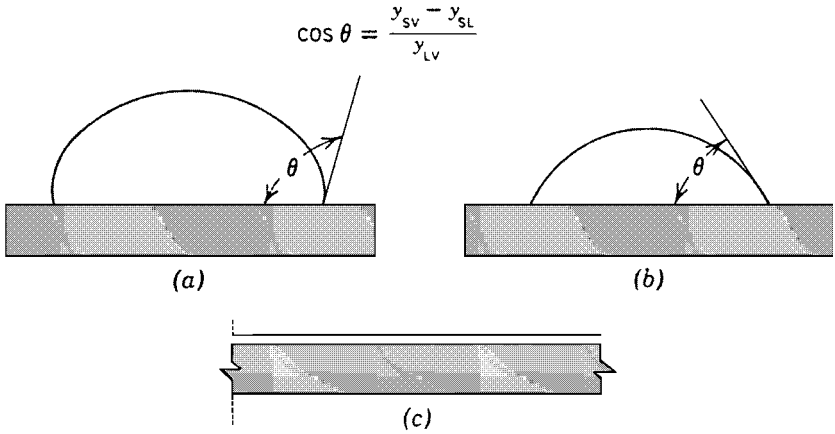

FIGURE 8.17 Illustration of (a) nonwetting ($\theta > 90°C$), (b) wetting ($\theta < 90°C$), and (c) spreading ($\theta = 0$) of liquid on a solid.

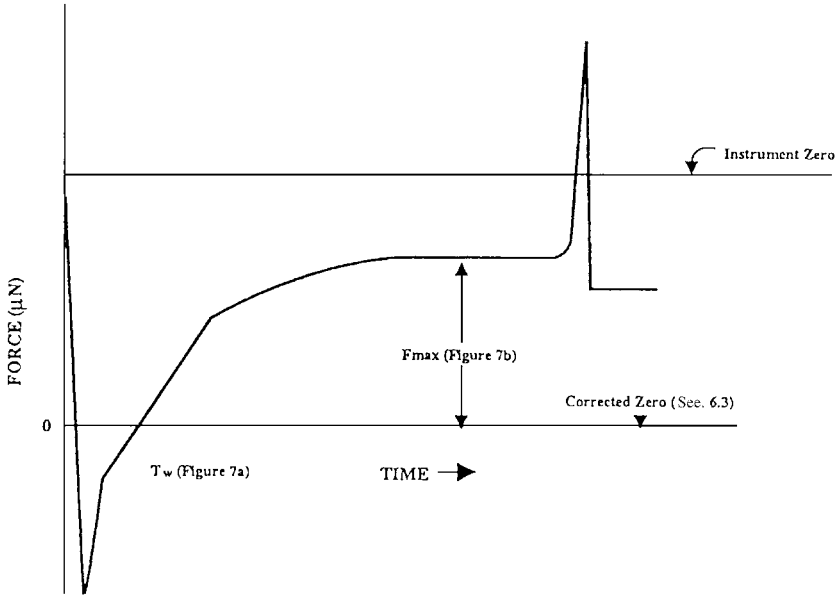

FIGURE 8.18 Wetting balance curve. (*From Joint Industry Standard.*)

to make corrections for buoyancy forces produced during the immersion phase. This force depends on solder density and coupon volume. The time to commence wetting is designated by T_W on Fig. 8.18, while F_{max} is the maximum wetting force of the solder on the substrate. For materials that are nonsolderable, such as bare ceramic, the net wetting forces are rarely significant enough to exceed the buoyancy force.

Pinch and Sjostak[56] utilized this type of equipment to characterize solderability of various Cu pastes on ceramic circuit boards. This type of test is particularly useful in distinguishing minor performance variations in materials that typically exhibit good solderability. There are numerous suppliers for this type of wetting balance test apparatus.[55]

Adhesion. Adhesion measurements provide a figure of merit for the degree of conductor bonding to the substrate. The various mechanisms for bonding to the substrate are composition-dependent and were discussed in Sec. 8.2.3 under "Inorganic Binders." This property is one of the most difficult to measure in terms of reproducibility and correlation. This is a result of the many factors that affect adhesion test results. These include, but are not limited to, the following: specific conductor formulation, substrate, test pattern, test preparation, wire attachment method, solder type, and adhesion test method.

Although adhesion mechanisms have already been discussed, it should be noted that the relative concentrations and combinations of adhesion promoters in the formulation will have a significant effect on relative adhesion values.

Substrate variables that affect adhesion include bulk and surface chemistry, surface roughness, thickness, size, and shape. For example, increased surface roughness results in an increase in the respective surface area. The net result is increased conductor adhesion due to the additional area for mechanical and chemical bonding as well as the fact that adhesion test loading will not always be perpendicular to the potential fracture surface.[57] In this situation the delamination forces produced by the adhesion test may result in nonplanar interfacial stresses that are less than those in the planar direction because of stress relaxation arising from plastic flow behavior. The fracture mechanics of this type of behavior is discussed by Anderson et al.[58] In addition to substrate type (i.e., Al_2O_3 versus AlN) and the resultant effect on reactivity with various bonding agents, the intergranular strength and chemistry of the substrate can affect the adhesion strength.

When specifying the results of a particular adhesion test, it is important to also specify the details of the test pattern being utilized. These parameters should include the size, shape, quantity, and arrangement of the test pads as well as the recommended and actual thickness of the fired conductor. An example is the test pattern illustrated in Fig. 8.15, which utilizes 80×80-mil square test pads in a double-row configuration. Individual paste suppliers will provide the recommended fired thickness targets.

The wire attachment process involves a number of variables that must also be considered. Wire considerations include metallurgy, shape, size (diameter), and finish. Preparation processes prior to wire attachment could include a pad burnishing operation to remove oxides from the surface, a pretinning step, and cleaning or fluxing operations that employ various flux compositions. The attachment process can utilize various solder compositions that require different solder times and temperatures. Methods of wire attachment include hand soldering, solder reflow such as belt reflow and vapor phase reflow, and solder dipping. Each of these methods involves specific processing variables with respect to time, temperature, and solder type. These variables have a profound effect on the solder leaching characteristics of the metallization and, therefore, have an impact on adhesion values. Williams[59] concluded that the solder dip test is an easy and rapid test for generating comparative adhesion values. However, this study also concluded that total pad lift should be attained to fully understand true adhesion values and mechanisms. Hand soldering methods were determined to be the most appropriate for this approach. Undoubtedly, aging of the soldered test coupon or assembly prior to testing also has an effect on the final value.

As noted earlier and readily seen by the complexity of variables, adhesion testing is a very inexact science. Many tests have been devised in order to characterize the adhesion property. These include both qualitative and quantitative test methods. Examples of qualitative tests are the Scotch tape test and razor blade tests which certify that the adhesion exceeds some

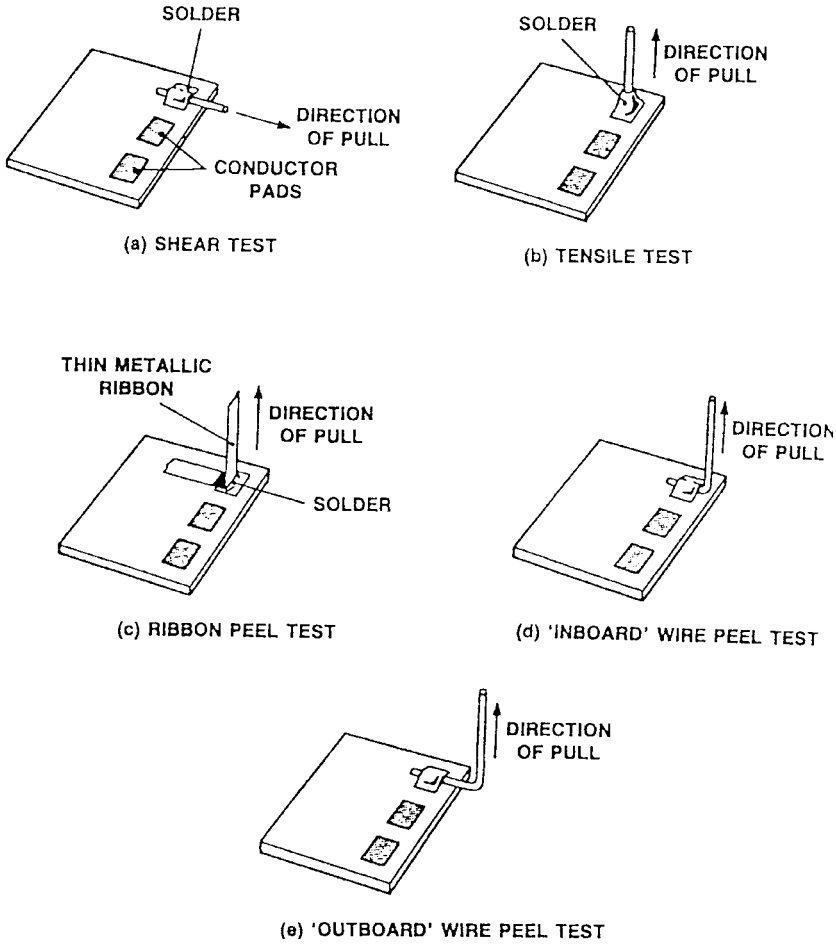

FIGURE 8.19 Quantitative adhesion test configurations. (*a*)–(*e*) (*From Handbook of Thick Film Technology.*)

arbitrary threshold strength. These tests are not recommended and are not discussed further here. The quantitative tests typically used are not ideal either in terms of generating complete adhesion information or their dependence on operator experience, technique, etc. However, they do provide a quantitative comparison for a particular material type, substrate, and process that can be utilized to determine differences or changes in the adhesion performance. These tests can also indicate the robustness of a particular material and process with respect to adhesion performance.

Some of the quantitative adhesion test configurations are illustrated in Fig. 8.19.[15] These include shear, tensile, and various wire peel tests. The shear test (Fig. 8.19*a*) involves pulling a wire in a direction that is parallel to the substrate. The primary drawback of this test is

that the failure mode is typically within the substrate, which prevents testing the true strength of the conductor-substrate interface. Reported adhesion values of this test are very high and are reported as load values in kilograms. The tensile test (Fig. 8.19*b*) employs a wire or nail with a small head which is attached to the center of a conductor pad. The nail head should extend to the edges of the pad in order to render the test insensitive to the amount of solder used to produce the joint. These values are often inaccurate if tensile failure occurs only in the center of the pad. Adhesion values of tensile tests are typically lower than those from shear tests.

Peel tests are a combination of tensile and shear forces and more accurately simulate the types of forces that are encountered during actual circuit assembly and operation.

The ribbon peel test, shown in Fig. 8.19*c,* is not a popular test. It requires soldering a thin metal ribbon (e.g., Cu) to a conductor pad, followed by application of a force perpendicular to the pad. Ensuring solder uniformity is difficult and test results can therefore be variable. The most popular test employed is the wire peel test (Fig. 8.19*d* and *e*). This test involves attaching a wire (which may be prebent to form a 90° angle) across one or more conductor pads in a row and pulling the wire in a direction perpendicular to the substrate surface. This test is sensitive to the pull rate, solder method, position of the wire bend, and pad configuration. Peeling or twisting the lead against the soldered conductor produces failures at much lower forces than normal tension or shear tests because of the enhanced stresses at the rather brittle conductor-substrate interface.

A detailed description of one form of this test can be found in Chap. 5 of Ref. 11. Figure 8.20[11,57] illustrates various detailed aspects of the peel test. Figure 8.20*a* shows bending of the wire lead, positioning of the bend with respect to the substrate, and the ideal solder fillet geometry over the conductor pad. Figure 8.20*b* shows a popular pad configuration which utilizes three 80 × 80-mil pads in a linear geometry. Figure 8.20*c* illustrates a popular lead attachment method to the back end of the substrate, known as the *shepherd's crook* method. Although test configurations must be standardized, many variations are acceptable. Figure 8.15*a* shows a test pad configuration that utilizes the shepherd's crook on two rows of five pads.

Adhesion values for the peel test method are generally lower compared to tensile and shear test methods. As noted earlier, Williams[59] concluded that the hand solder test combined with the wire peel test for a specified pull rate produces the most significant data for an adhesion test, since it generally results in total pad lift from the substrate. After adhesion values have been measured, close observation can reveal the true failure mode and provide accurate conclusions regarding the limiting factors. As many of these tests require room temperature aging of the soldered fixture at some specified condition prior to the peel test, adhesion values versus time should not be overlooked. There is usually an increase in value over a given time, resulting from an annealing process in the solder which renders it more ductile. The net result is a more uniform load distribution over the conductor pad. Although soldered peel tests are not usually done on Au conductors due to their solubility in Sn–Pb solders, work has been done using indium-containing alloys.[60]

Although not usually thought of as an adhesion test method, the wire bond test can measure the adherence of a film. Thermocompression bonding of even 1-mil wires can result in visible film separation of conductors with poor adhesion. The test severity can be increased by increasing the diameter of the wires utilized in the bonding test. However, the failure mode must be analyzed because the concentrated load often results in breakdown of the cohesive forces of the fired film. The appearance of this type of failure indicates tearing of the intergranular particles or layers of the film. This type of failure is most often noted in Au films. The wire and die bondability as a function of conductor metallurgy was discussed earlier in this chapter. Additional discussions will occur in Sec. 8.2.6, "Structure-Property relations."

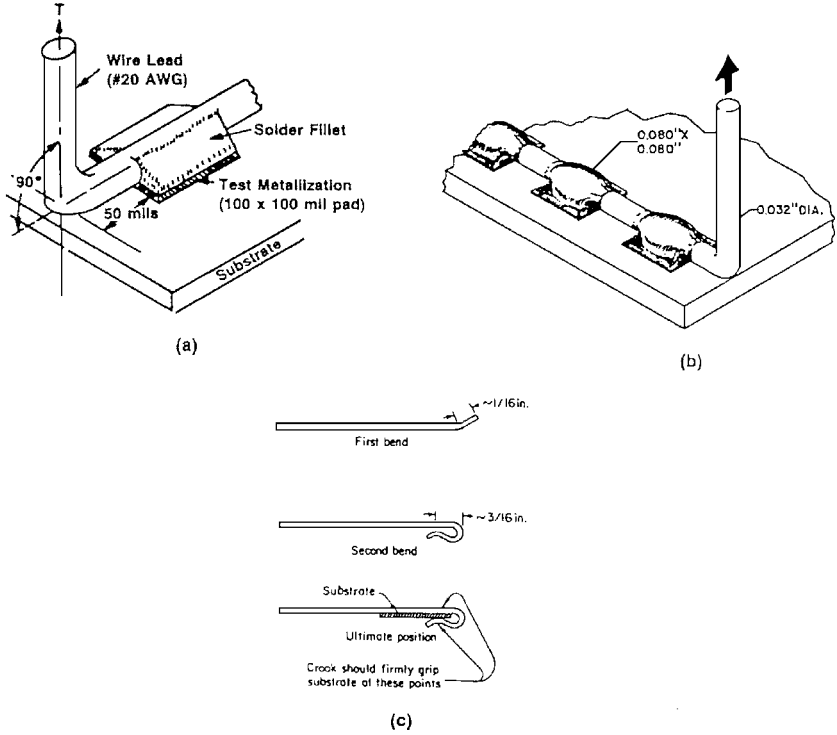

FIGURE 8.20 Detailed aspects of wire peel test. (*a*) Wire bend and solder fillet configuration. (*b*) Specific pad geometry configuration. (*c*) Shepherd's crook lead attachment method.

Aging Characteristics. The most severe tests that ultimately limit the number of applications for thick film conductors are aging tests, including storage at elevated temperatures as well as thermal and power cycle tests. Specific conditions are usually determined by the application. Typical storage temperatures exceed 100°C, with 150°C being the most common. Storage times can extend to 1000 or 2000 h, although most quality control tests specify 48 h. Figure 8.21[11] illustrates adhesion aging of several thick film conductors. Since property degradation is basically exponential with time, most of the change is often seen within the first 48 h. However, this can be misleading, since it is possible for the degradation to continue to completion (zero adhesion). Thermal cycle tests that monitor adhesion as a function of time measure the thermomechanical stability of the conductor-substrate interface. The test parameters vary with respect to the end-point temperatures and dwell and excursion times. A typical profile could include end point temperatures of −55°C and 150°C coupled with excursion and dwell times on the order of 10 min. This type of test is imperative for the automotive industry because of the variable environmental conditions both external to the car and under the hood.

Adhesion degradation under these conditions results from various phenomena. The diffusion of tin (Sn) from the solder into the interfacial regions and subsequent formation of intermetallic compounds is the primary failure mechanism. This was discussed earlier for Ag, Ag–Pd, and Cu formulations. Formation of these compounds creates interfacial stresses as a result of thermal expansion mismatches of the various phases. The result is mechanical

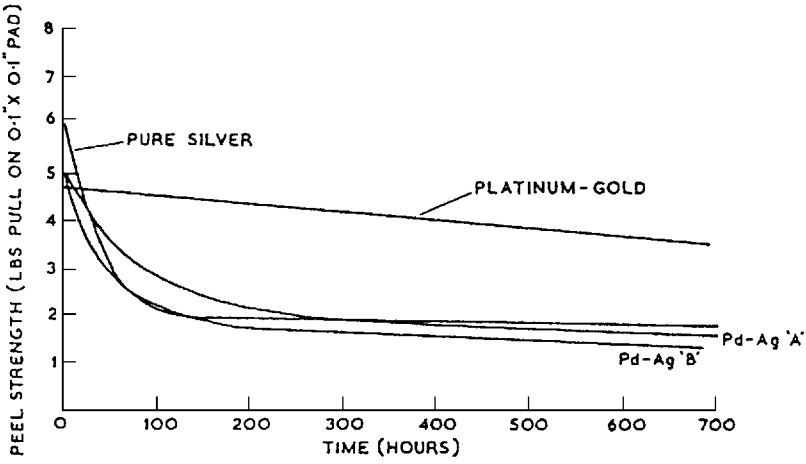

FIGURE 8.21 Aging of thick film conductors at 125°C. (*From Handbook of Thick Film Technology*.)

failure during thermal and power cycling. Another mechanism proposed by Crossland and Hailes[61] suggests that Sn diffuses more rapidly into the conductor than Ag diffuses outward during thermal aging. The net effect is growth of the composite and fracture of the glass network resulting in adhesion loss. In general, Au-containing conductors exhibit less adhesion loss during aging than Ag-bearing conductors. The use of low Sn solders (i.e., 10 Sn–90 Pb) can reduce this degradation.

Solder Leach Resistance. Solder leach resistance can be defined as the ability of a specific conductor to withstand the attack of molten solders and resulting dissolution of the fired film. The solder leach characteristics of various precious metals and conductor metallurgy systems were discussed earlier. The solder leach test typically involves immersion of a test coupon with conductor pads and/or lines into a molten solder for a specified time. Visual and/or microscopic observations are utilized to determine the extent of solder leaching. The variables include the solder composition, solder temperature, immersion rate, time of immersion, and number of immersions. The test was originally conducted by single immersions for long time periods. However, the solder adjacent to the immersed metal area would attain saturation and reduce the severity and sensitivity of the test. Therefore, this test was replaced by tests involving multiple dips for relatively short times. For example, one form of the test requires that 80 percent of a 20-mil line or 80-mil-square pad remains after 20 successive 1-s dips into a specified solder. The integrity of the conductor line or pad should be observed after each immersion. The observer should also look for breaks in the line or discontinuities in the pad. Backlighting the substrate can be useful in this type of observation. Mild conditions are utilized for Ag conductors such as 62 Sn–36 Pb–2 Ag solders at 215°C with a mildly active flux, while more durable compositions such as Au–Pt conductors may utilize an active flux with a 63 Sn–37 Pb solder at 250°C. The severity of this test is usually determined by the specific application.

Microstructure. As the microstructure of the fired conductor dictates many of the performance characteristics, various techniques can be employed to assess different features. Macroscopic features such as blistering, leaching, and line spreading can often be seen by visual observations. Metallurgical microscopes can be utilized to see finer features not discernible with the naked eye. Backlighting the substrate provides information regarding the

density of the film and continuity of fine lines. Toplighting of the substrate can provide information regarding the surface of the film and the print resolution, as well as more detail on visual observations described above. Compatibility of the conductor with the substrate, resistors, dielectrics, etc., can be initially assessed with microscopic examination. Advanced microscopic techniques such as dark field or bright field imaging can provide more detailed information such as elemental diffusion, phase separation, and internal porosity. The photomicrographs in Fig. 8.22 were prepared using dark field-imaging techniques and compare two Cu multilayer systems (cross sections), with Cu diffusion or "blushing" being visible in Fig. 8.22*b*. The use of polarization techniques can provide additional microstructural data.

More complex characterization tools can be employed in research or troubleshooting. Scanning electron microscopy (SEM) provides detailed microstructural information by topographic and cross-section examination. Topographic features are best characterized by secondary electron imaging (SEI), while cross-section features can be studied using SEI or backscattered electron imaging (BEI), which provides atomic number contrast for elemental or phase distinction. Figures 8.9 and 8.11 provide examples of SEI and BEI, respectively. Energy dispersive spectroscopy is utilized to determine elemental diffusion across critical interfaces such as the substrate–conductor, resistor–conductor, or dielectric–conductor interfaces. Surface analytical techniques can be utilized to determine the elemental composition of the first several atomic layers of an exposed surface. These techniques include Auger electron spectroscopy (AES) and elemental spectroscopy for chemical analysis (ESCA). The latter technique can produce actual phase information, while AES is limited to elemental information. Finally, x-ray diffraction (XRD) analysis provides phase information such as the extent of solid solution formation of an Ag–Pd composition (described earlier) or the crystallizing phase in a particular glass composition. Numerous examples of the above techniques will be discussed in the section on structure–property relations.

8.2.6 Structure–Property Relations

Although some examples of structure–property relations have been alluded to in the text, this section will focus on more specific examples.

In the study by Nordstrom and Yost,[48] the sintering behavior of thick film Au conductors was monitored by electrical resistance measurements and scanning electron microscopy. Initial-stage sintering kinetic equations coupled with resistance/neck area correlations were used to develop a relationship between resistance R and sintering time T:

$$\frac{1}{R} = Ct^{2/n} \tag{8.9}$$

where C is a constant and n depends on the sintering mechanism. Resistance changes were correlated with structural changes during the initial and intermediate stages of sintering. This leads to a good understanding of the relationship between resistivity and densification. The sintering or firing profile can be optimized to maximize the fired density and resultant performance with respect to resistivity, solderability, leach resistance, and bondability.

Pinch and Sjostak[56] studied the effects of surface structure and processing parameters of Cu conductors on solderability. They utilized AES to study the differences in the distribution of oxide components on the surface as they relate to solderability. The formation

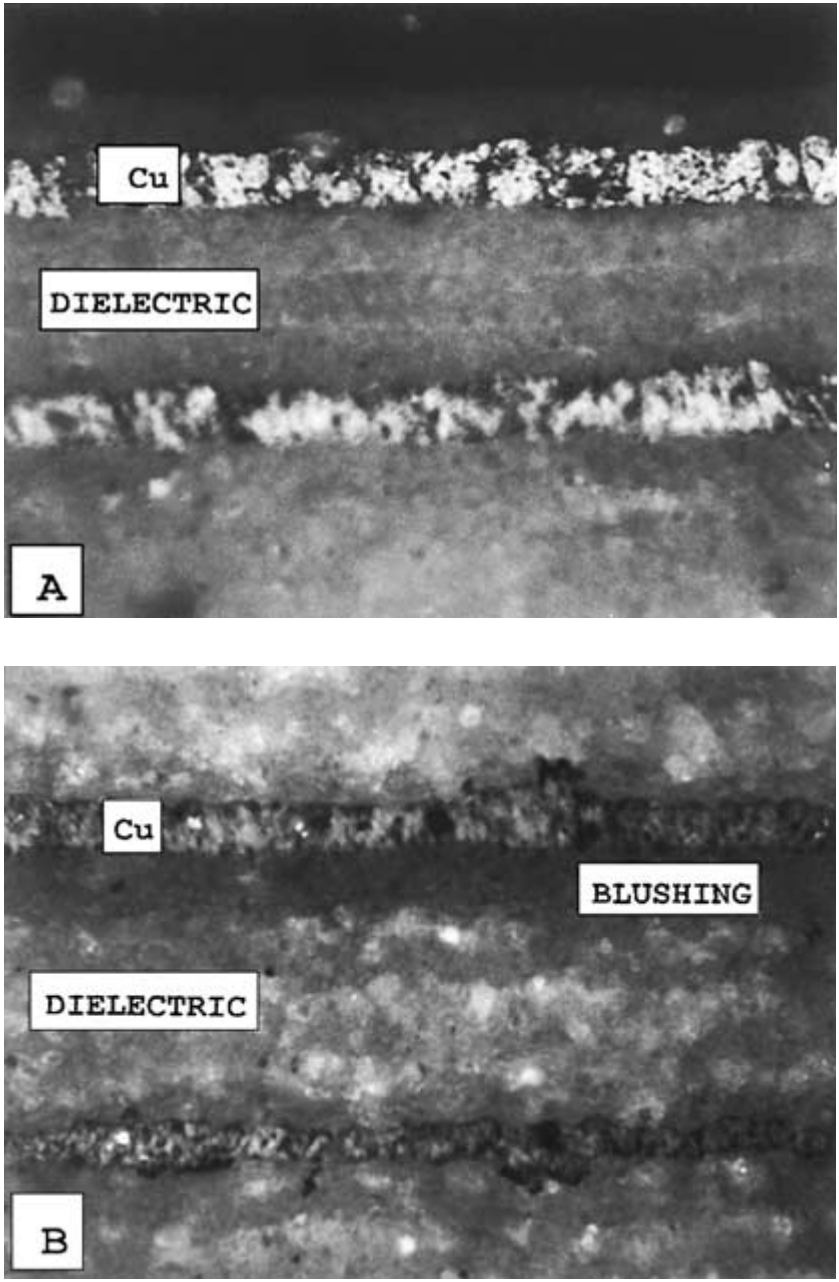

FIGURE 8.22 Photomicrographs of Cu multilayer cross sections using dark field imaging microscopy. (*A*) No diffusion of Cu into dielectric; (*B*) excessive Cu diffusion into dielectric, termed *blushing*.

of very thin layers of surface oxides due to local fluctuations in the oxygen content of the furnace atmosphere adversely affected the solder acceptance of the fired Cu conductor. A similar study by Webb[62] utilized AES and SEM to study the effects of firing conditions on solderability and adhesion of Cu conductors. Adhesion of Cu films was increased when nitrogen flow rates or the partial pressure of the oxygen in the nitrogen gas was increased. This is due to the greater copper oxide concentration at the conductor–substrate interface under these conditions, resulting in spinel compound formation. Adhesion was also increased when multiple firings were employed because of the reduction of residual carbon at the interface. However, soldering to the conductor became increasingly more difficult under these conditions as thin oxide layers formed on the surface. Soldering to Cu becomes difficult when the oxygen concentration in the nitrogen gas exceeds 15 ppm. Adhesion degradation mechanisms for Cu- and Ag-bearing conductors due to intermetallic formation were also observed.

The surface of the fired conductor is critical to the success of bonding wire and die. The surface should be clean of oxides and metal-rich, smooth, and dense. Overfiring of a conductor or the use of glasses in the formulation that are not appropriate for a specific firing profile can result in capillary forces that cause migration of the molten glass to the conductor surface. The firing atmosphere can also lead to oxide formation on the surface of the fired film. Similarly, mishandling of processed parts can produce the same result. Figure 8.23 illustrates an oxide-containing surface as verified by AES. The black region is glass that has penetrated the surface by capillary action. Wire bonds to a fired film with glassy regions and/or oxides on the surface are not acceptable, since the metal bonding process cannot be

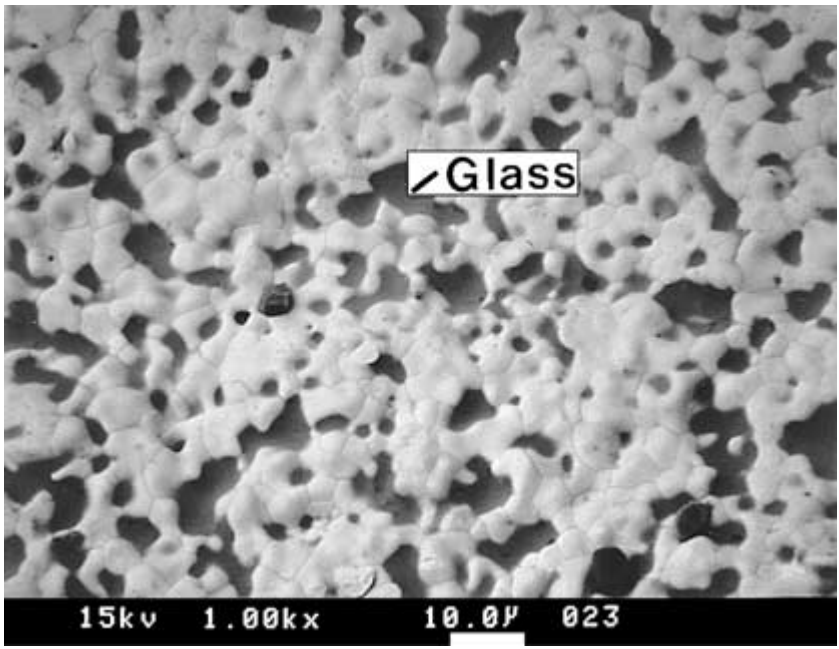

FIGURE 8.23 SEM photomicrograph of Au conductor surface illustrating presence of oxides in form of glass.

completed, resulting in little or zero adhesion of the wires. A brief acid etch of the surface results in acceptable bond characteristics by removing the oxide layer.

The design of thick-film components must take into account the compatibility of other materials being considered. As discussed earlier, Ag migration is a major concern in the presence of an electrolyte and an applied voltage. Many thick film glasses act as electrolytes in their molten state, with up to 2 percent solubility of Ag. These glass formulations cannot be utilized in dielectric compositions that interface with Ag. With proper design, however, the dielectric can accommodate the use of Ag in multilayer configurations. Figure 8.24 illustrates the energy dispersive spectra (elemental mapping of Ag) of multilayer cross sections of Ag electrodes and dielectric before and after 1000 h of bias humidity testing.[19] The ratio of Ag concentration at the center of the Ag conductor to the concentration at the center of the Ag dielectric remains essentially constant after the stringent test for Ag migration. The statistical count at the center of the dielectric corresponds with the background noise in this configuration. Capacitance measurements for this simple capacitor structure also suggest that there is no migration of the Ag, as there is little change in capacitance or insulation resistance values following the bias humidity test up to 2000 h. Proper design of the materials system can eliminate or control phenomena that can typically lead to failure during circuit testing or operation. In this situation, the design of a crystallizing glass with very low Ag solubility provided a stable environment for the use of Ag and its beneficial properties. The utilization of formulations and processing knowledge to engineer micro-structures and the resultant properties is critical for meeting the performance challenges in today's electronics industry.

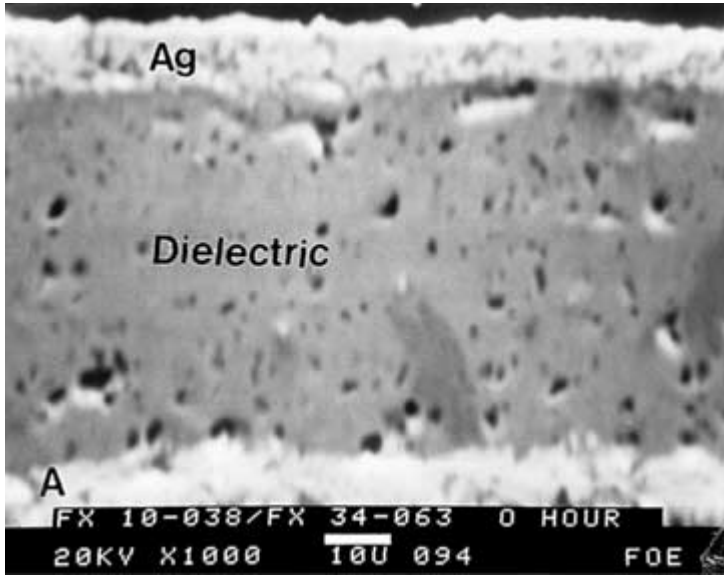

FIGURE 8.24 Cross sections of Ag–Pd multilayer structure. (*A*) SEM photomicrograph; (*B*) Energy dispersive spectroscopy (EDS) Ag elemental map of as-fired structure; (*C*) EDS Ag elemental map after 1000-h humidity bias test.

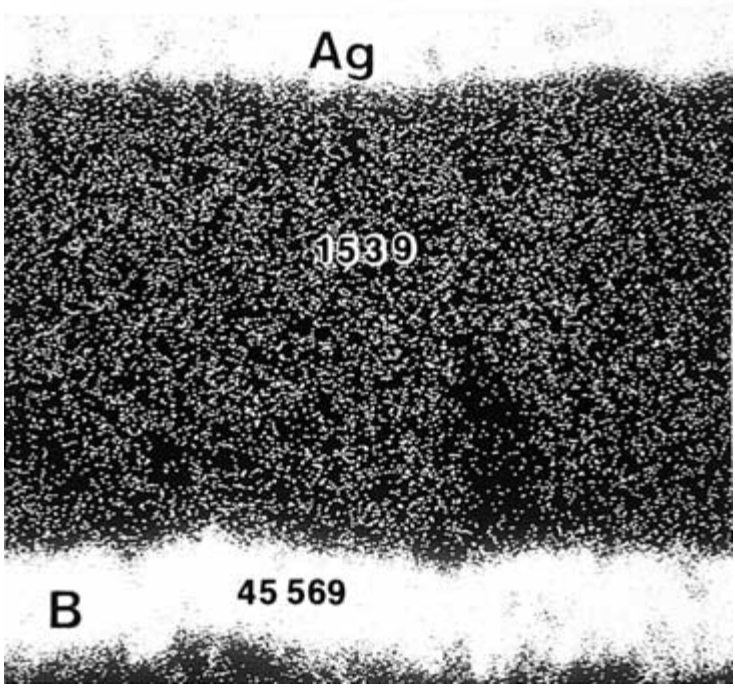

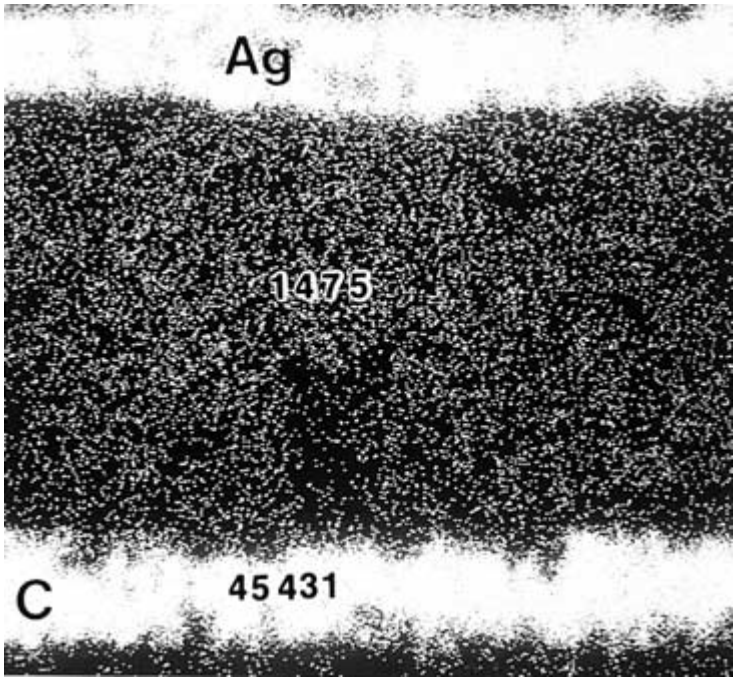

FIGURE 8.24 (*Continued*)

8.3 THICK-FILM DIELECTRICS

8.3.1 Introduction

Thick-film dielectrics are used in a variety of hybrid microelectronics applications. The most common functions of thick-film dielectrics are to:

1. Provide electrical insulation
2. Provide mechanical and environmental protection
3. Store electric charge as a capacitor

Dielectrics used to satisfy the first and the second requirements are electric insulators with relatively low dielectric constants (less than 15). Capacitor dielectrics with dielectric constants greater than 20 are used as charge storage devices. Thus, thick-film dielectric formulations can be broadly categorized as either insulator or capacitor dielectrics. Insulator dielectric materials can be further categorized as sealing glasses, crossover dielectrics, and multilayer dielectrics.

Sealing glasses are used for environmental, chemical, and mechanical protection. Key properties for sealing glasses are:

1. Coefficient of thermal expansion
2. Sealing temperature
3. Hermeticity
4. Chemical resistance
5. Compatibility with other materials
6. Stability at high temperature and humidity
7. Electrical insulation resistance

The substrate material, environmental conditions, and firing temperature limitations determine the sealing glass selection for a particular application.

Crossover dielectrics are used as electrical insulation layers between two conductor traces. The requirements for sealing glasses also apply to crossover dielectrics. Additional requirements include dielectric strength and interactions with conductor materials. Unlike sealing glasses, crossover dielectrics are typically fired at the same temperature as the conductor material. Interactions between the dielectric and conductor materials influence their respective properties.

Multilayer dielectric materials are used to build three-dimensional interconnect structures, whereby vias provide connectivity in the direction perpendicular to the substrate between several layers of signal conductor traces, voltage planes, and ground planes. The requirements listed for crossover dielectrics are applicable to multilayer dielectrics. Additional requirements complicate design of multilayer dielectrics. During multilayer construction, dielectric and conductor materials are subjected to multiple firings. The chemical interaction between dielectric and conductor materials in a multilayer configuration should be minimized. The CTE of the dielectric material should be closely matched with that of the substrate and should be stable on refiring to prevent warpage of the substrate.[63,64] Since multilayer dielectric layers contain vias, the printability of multilayer dielectric materials is critical. The dielectric paste, when printed, should retain via holes, which are as small as 8 mils in diameter, and should level quickly to fill in the pinholes created by

the printing process. These two characteristics require opposing rheological properties and require an optimum rheology.

For high-speed multilayer circuitry, low dielectric constant (K) materials are required. Furthermore, the impedance along the signal traces needs to be tightly controlled, which requires uniform thickness of the dielectric layers over the entire printed area. The compatibility of multilayer dielectrics with conductor materials is also a critical parameter. Gold, Ag, and Cu are the most commonly used conductor materials. Gold is the least reactive of the three materials. Since Cu must be processed in an inert atmosphere, the dielectric materials used for Cu-based multilayer interconnect boards (MIBs) must also be stable in an inert atmosphere. The temperature-dependent sintering kinetics should be conducive to the removal of organics from these materials during the firing process.

The key properties of thick-film capacitor materials are

1. Dielectric constant
2. Temperature coefficient of dielectric constant
3. Insulation resistance
4. Dielectric strength
5. Dielectric loss
6. Stability of the dielectric properties in humid environments
7. Laser trimmability
8. CTE

Thick-film capacitor dielectric materials provide a cost-effective and high-performance alternative to externally mounted discrete monolithic chip capacitors.

8.3.2 Dielectric Compositions

8.3.2.1 Insulator dielectrics. An insulator glass is the major component of any insulator dielectric formulation. The use of glass by itself does not provide adequate mechanical strength to prevent submerging of the conductor film at high temperatures encountered in the firing process. To achieve this strength, refractory oxides such as Al_2O_3, zirconia (ZrO_2), silica (SiO_2), and titania (TiO_2) are added to the glass. These thick-film dielectric formulations are referred to as *glass filled with ceramic* thick-film dielectrics. Crystallization of the glass after full densification can also provide high-temperature strength. These formulations are referred to as *crystallizing dielectrics*.

8.3.2.2 Ceramic-Filled Glasses. These dielectric compositions consist of glass and one or more refractory oxides. During firing of these materials, the glass melts and the ceramic oxide partially dissolves in the glass. The glasses used in these formulations have low alkali content, high insulation resistance, high dielectric strength, and excellent resistance to property changes in humid environments. The glass in the dielectric forms a hermetic structure. The ceramic oxide provides high temperature strength and also acts as a CTE modifier. Table 8.7 lists the properties of some of the commercially available dielectrics of this type.

The chemistry of glasses used in thick-film dielectrics covers a broad range of formulations. Barium aluminosilicate or lead borosilicate glasses have reportedly been used in these formulations.[65,66] Figure 8.25 is a differential thermal analysis (DTA) trace of a noncrystallizing glass used in a thick-film dielectric. The glass transition temperature is about 670°C and no exothermic peak associated with crystallization of the glass can be seen.

TABLE 8.7 Typical Properties of Ceramic Filled Glass Dielectrics

Properties	Typical values
Dielectric constant	7–11
Dissipation factor, %	<0.2
Insulation resistance, Ω	$>10^{12}$
Breakdown voltage, V/mil	>500
Hermeticity, $\mu A/cm^2$, as measured by leakage current test	<1

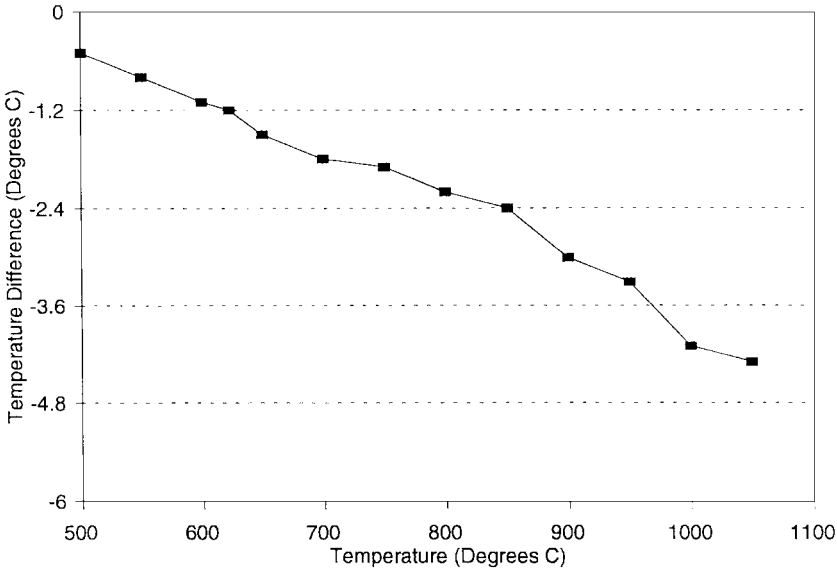

FIGURE 8.25 DTA trace of glass used in a glass-filled ceramic thick film dielectric.

The endothermic step at about 750°C is due to the glass fusion. The oxide fillers partially dissolve in the fluid glass and increase the viscosity of the glass, thereby providing mechanical support to the film. Glasses filled with refractory ceramics are normally recommended to be used with Au-based conductors. Silver is chemically more reactive than Au and typically dissolves in glasses to a certain extent, which leads to poor dielectric properties. Also, interaction of glasses in the dielectric with Ag-based conductors may affect the solderability of these conductors[66] as well as basic properties of interfacing resistors. Crystallizing dielectrics offer solutions to some of these problems.

8.3.2.3 Crystallizing Dielectrics. The major constituents of crystallizing dielectrics are a crystallizable glass and crystallization agents. The crystallization agents are added to control the crystallization behavior of the base glass. Generally, fine powder of the phase being

TABLE 8.8 Typical Properties of Crystallizing Dielectrics

Properties	Typical values
Dielectric constant	7–10
Dissipation factor, %	<0.2
Insulation resistance, Ω	$>10^{12}$
Breakdown voltage, V/mil	>500
Hermeticity, $\mu A/cm^2$	<20

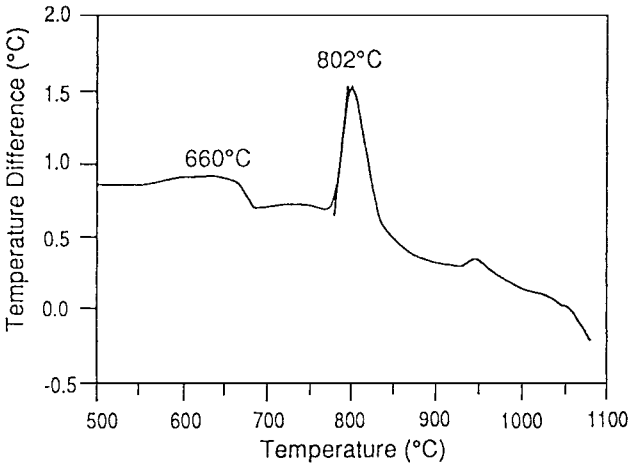

FIGURE 8.26 DTA trace of a crystallizing dielectric.

crystallized is used as a seed crystal. The amount of crystallization and type of phase affects the densification and CTE of the dielectric. Figure 8.26 is a DTA trace of a typical crystallizing dielectric. The glass transition temperature of the dielectric glass is about 660°C, and the onset of crystallization occurs at 802°C. The crystallization is completed by 850°C. Glass densification occurs mostly between the glass transition temperature and the onset of the crystallization. Crystallization of the dielectric minimizes the interaction of the dielectric with other components (e.g., conductor, resistors, etc.) at standard thick-film peak firing temperatures of 850°C. Table 8.8 lists a range of properties of some commercially available crystallizing dielectrics.

8.3.2.4 Specialty Dielectrics

Low-K dielectrics. For high-speed digital circuitry, insulator dielectrics with low dielectric constants are needed. In general, there are three types of low *K* dielectrics: polymeric dielectric, porous dielectric, and glass ceramic dielectric materials. Table 8.9 lists dielectric constants and CTEs of various ceramic materials.

Fused silica has the lowest *K* among ceramic materials. The dielectric constants of polymeric materials are in the range of 2.7–3.7. Thick-film dielectric materials based on fused silica filled with quartz, cordierite, sol-gel silica, and other proprietary glass ceramic formulations

TABLE 8.9 CTE and *K* Values for Various Ceramic Materials

Material	CTE, ppm/°C	*K*
Quartz (crystalline)	10	4.5
Fused silica	0.55	3.78
Spinel ($MgAl_2O_4$)	6.6	7.5
Mullite (Al_2SiO_5)	4.3–5	6.2–6.38
Steatite ($MgSiO_3$)	7.8–10.4	5.9–6.1
Forsterite (Mg_2SiO_4)	10.6	5.8–6.7
Cordierite ($Mg_2Al_4Si_5O_{18}$)	2.3	4.1–5.4
Wollastonite ($CaSiO_3$)	7.0	6.6

TABLE 8.10 Typical Properties of Low *K* Thick Film Dielectrics

Properties	Typical values
Dielectric constant	3.9–5.2
Dissipation factor, %	<0.3
Insulation resistance, Ω	$>10^{11}$
Breakdown voltage, V/mil	>1000
Hermeticity, $\mu A/cm^2$	<1

have been developed.[68,69] Table 8.10 summarizes properties of low *K* dielectric materials reported in the literature.

Attempts have been made to lower the dielectric constant of thick-film dielectrics below 4 by introducing controlled porosity. Porous thick-film dielectrics with *K* values as low as 2.5 have been reported.[70–72] Thus far, use of these low *K* dielectric materials has not been very successful in the production of complex hybrids.[73] These dielectric materials are not stable during refiring. For example, the materials based on fused silica crystallize a quartz phase during refiring, leading to significant changes in thermal expansion and subsequent cracking. Materials based on controlled entrapped porosity tend to exhibit growth of porosity during multiple firings.

Nitrogen-Firable Dielectric Materials. Copper has been considered an alternative conductor material to precious metals for more than a decade. Conductivity, solderability, solder leach resistance, and microwave properties of Cu make it a very desirable material for building MIBs and radio frequency (rf) circuitry. In addition to performance advantages, Cu is less expensive than precious metals. However, Cu conductors need to be processed in a nitrogen atmosphere. Special dielectric materials need to be used for nitrogen processing. Glasses used in these dielectric materials must be stable in reducing atmospheres. Sintering kinetics of these dielectrics should be rigorously controlled so that a hermetically dense film is formed that still permits removal of organics under the reducing conditions. Furthermore, special glass compositions must be carefully selected to minimize reactivity of Cu with the dielectric material. Incomplete pyrolysis of organics, copper–dielectric interactions, and porosity in the dielectric film are the leading causes of failures of Cu-based MIBs. These problems have been the topic of numerous technical articles.[34–37,74–79] These problems can be addressed by selecting a crystallizing nitrogen-firable dielectric with a high temperature glass softening point. Figure 8.27 is a DTA trace of a crystallizing dielectric.

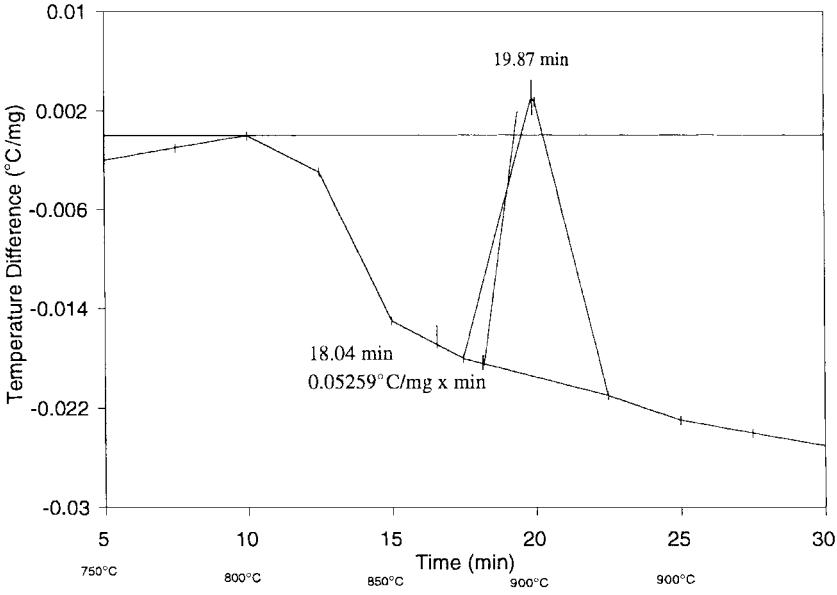

FIGURE 8.27 DTA trace of a nitrogen-firable crystallizing dielectric.

Glass fusion begins above 830°C, which allows complete pyrolysis and organic removal as well as total densification during a standard 900°C N_2 firing profile. Glass densification occurs between 830 and 880°C. The glass crystallizes at the recommended peak firing temperature of 900°C. Glass crystallization reduces the interaction with copper conductors during firing. The crystallization kinetics are carefully controlled to obtain a dense microstructure (Fig. 8.28).

Table 8.11 lists typical properties of commercially available nitrogen-firable dielectrics.

Thick-Film Dielectrics for Other Applications. So far the information presented in this section has dealt with thick-film dielectric materials for Al_2O_3 substrates. Other substrate materials used in the hybrid industry include beryllia (BeO), AlN, and porcelainized steel substrates. The display industry uses a variety of glass substrates. These other substrate materials all require the design and development of specific formulations because of their chemical and mechanical differences.[41–43,80,81]

The CTE of BeO (8 ppm/°C) is close to that of alumina (7.3 ppm/°C).[67] Thus, dielectric materials for alumina substrates have been used on BeO substrates, although chemical compatibility and adhesion issues often surface as problems.

Aluminum nitride is a nonoxide ceramic material. The CTE of AlN (4.5 ppm/°C) is substantially lower than that of alumina. Early attempts to use thick-film dielectric materials designed for alumina substrates on AlN were unsuccessful.[80] Many of the glasses used in thick-film formulations designed for alumina substrates are chemically incompatible with AlN. Furthermore, the CTE differences between dielectrics designed for alumina and AlN substrates lead to cracking. Special thick-film dielectric formulations have been developed for use on AlN substrates.[23] Table 8.12 shows properties of a typical thick-film dielectric on AlN substrates.[41–43]

TABLE 8.11 Typical Properties of N_2-Fireable Dielectrics

Properties	Typical values
Dielectric constant	6–9
Dissipation factor, %	<0.5
Insulation resistance, Ω	$>10^{12}$
Breakdown voltage, V/mil	>500
Hermeticity, $\mu A/cm^2$	1–1000

TABLE 8.12 Typical Properties of an AlN-Compatible Dielectric

Properties	Typical values
Dielectric constant	<7
Dissipation factor, %	<0.4
Insulation resistance, Ω	$>10^{12}$
Breakdown voltage, V/mil	>750
Hermeticity, $\mu A/cm^2$	<1
CTE, ppm/°C	4.4

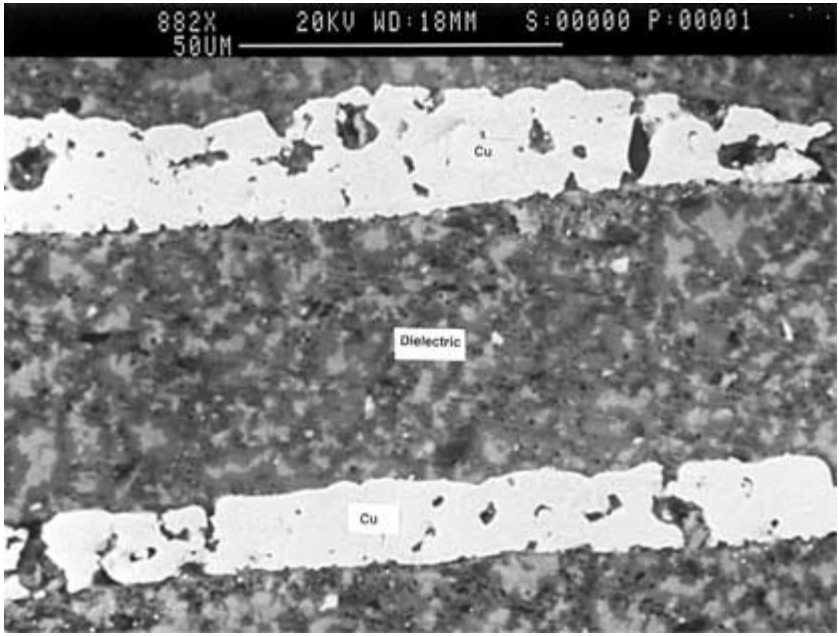

FIGURE 8.28 Cross section of a hermetic dielectric and copper conductors in a multilayer configuration.

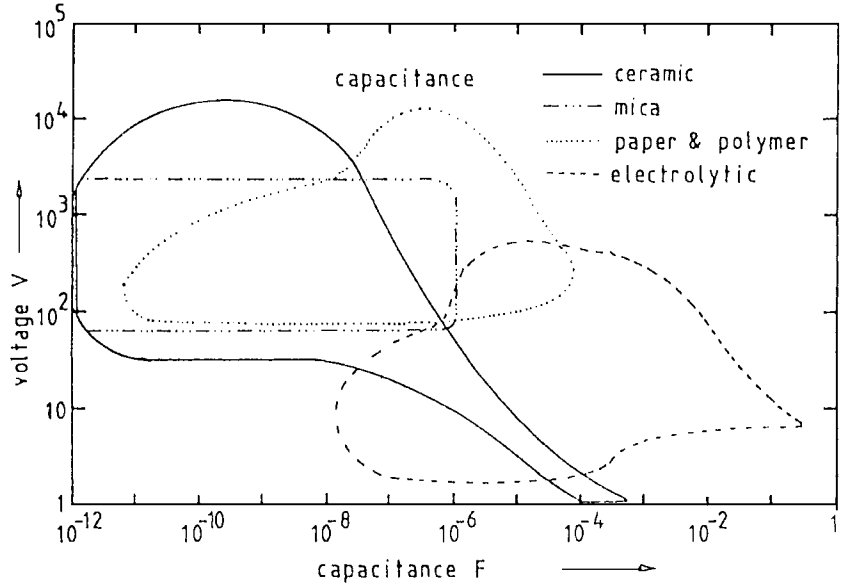

FIGURE 8.29 Working voltage and capacitance ranges of various types of dielectric materials. (*From Ceramic Dielectrics and Capacitors.*)[67]

Displays are produced with soda-lime-silica or other types of glasses. These glasses have softening points of less than 650°C. Thus, dielectric formulations with a CTE matched to display glass panels and fireable at temperatures less than 600°C have been developed.

8.3.3 Thick-Film Capacitor Dielectrics

Figure 8.29[67] shows working voltage-capacitance areas for the principle types of capacitors. Polymer dielectrics have low dielectric constants and a limited capacitance range. Electrolytic capacitors have high dissipation factors at high frequencies due to high series resistance of electrode materials, which limit their use in applications requiring low dielectric loss. Ceramic dielectrics offer high capacitance per unit volume, low losses, and a controlled temperature coefficient of capacitance. There are several challenging issues in the development of thick-film capacitor materials fireable at commonly used temperatures for thick-film processing. Ferroelectric materials such as barium titanate ($BaTiO_3$) and lead titanate ($PbTiO_3$) possess high dielectric constants. The temperature dependence of K can be altered by numerous additives.[82–84] These materials sinter at temperatures of 1350 to 1400°C. The sintering temperature can be lowered by sintering aid additions which lead to a dramatic decrease in the dielectric constant. Other materials known as *relaxor ferroelectric materials* sinter at relatively low temperatures, but they are extremely process and composition sensitive. Resultant compositional modifications to match TCE also lower K and create additional undesirable effects. Although there are ceramic materials with dielectric constants in excess of 15,000, only capacitor dielectric thick-film materials with dielectric constants of less than 1500 are commercially available.[85–87]

TABLE 8.13 Typical Properties of High-*K* Thick-Film Dielectrics

Properties	Typical values
Dielectric constant	25–2000
Dissipation factor, %	<5
Insulation resistance, Ω	$>10^9$
Breakdown voltage, V/mil	>200

Thick-film capacitor materials with *K* values of 500 to 1000 have been produced by mixing ferroelectric phases such as barium titanate, lead titanate, strontium titanate and their solid solutions with sintering aids. Most commonly used sintering aids are cadmium borosilicate glass, bismuth oxide, or lead-based glasses.[88–91] Thick film capacitor formulations with *K* values of 400 to 800 which crystallize high dielectric constant phases such as barium titanate, lead bismuth titanate, and barium bismuth titanate have also been developed.[92–94] More recently, thick-film capacitor dielectrics based on relaxor dielectric materials such as lead iron tungstate/niobate were synthesized. Dielectric constant values of 1600 to 4300 have been achieved.[95–97] Table 8.13 shows typical properties of commercially available high *K* thick-film dielectrics.[98,99]

A typical thick-film capacitor dielectric material with *K* of approximately 25 has a dissipation factor less than 1 percent, insulation resistance greater than 10^{12}, and breakdown voltage greater than 500 V/mil. In contrast, thick-film capacitor materials with *K* of 2000 have dissipation factors as high as 5 percent, insulation resistance greater than 10^9, and low breakdown voltages (about 200 V/mil).

8.3.4 Microstructure Development

Microstructural features of dielectric materials include the chemical composition and structure of the various phases as well as porosity and its distribution. These microstructural features, coupled with macroscopic defects such as pinholes, mesh marks, foreign matter, and interaction with conductor materials, determine dielectric properties. Very little information is published about composition of thick-film dielectrics, which are complex materials systems. The following section is a general discussion of dielectric microstructure development.

Insulator Dielectrics. Microstructure development of insulator thick-film dielectrics may be divided into three stages: (1) organic removal, (2) sintering, and (3) crystallization or ceramic dissolution.

Dielectric paste is a mixture of organic vehicle, glass powders, and oxide powders. Most commonly used ethyl cellulose–based resins are completely removed in air before 550°C. Figure 8.30 is a thermogravimetric analysis of a dielectric paste. The organic removal in the dielectric paste appears to be a two-step process. The weight loss prior to 200°C is associated with solvent removal and that between 250 and 550°C is related to binder removal.

It is important that the organic removal be completed prior to any appreciable sintering of the dielectric. Since the glass transition temperature of typical glasses used in air-fireable dielectrics is greater than 600°C, organic entrapment in these dielectrics is not a major concern. However, low-temperature sealing glasses or overglazes often use glasses with glass transition temperatures in the range of 350 to 400°C. Copper-compatible dielectrics must be processed in a nitrogen atmosphere in which ethyl cellulose–based binders are not completely removed until 800°C. This problem can be solved by using an acrylic-based binder system. However, these binders do not exhibit the good screen printing characteristics of

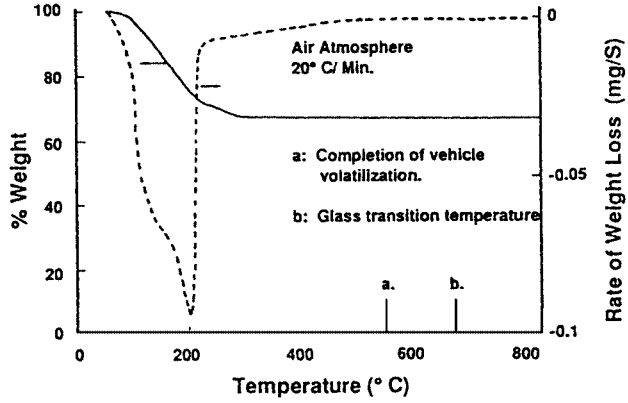

FIGURE 8.30 Thermogram of dielectric paste.

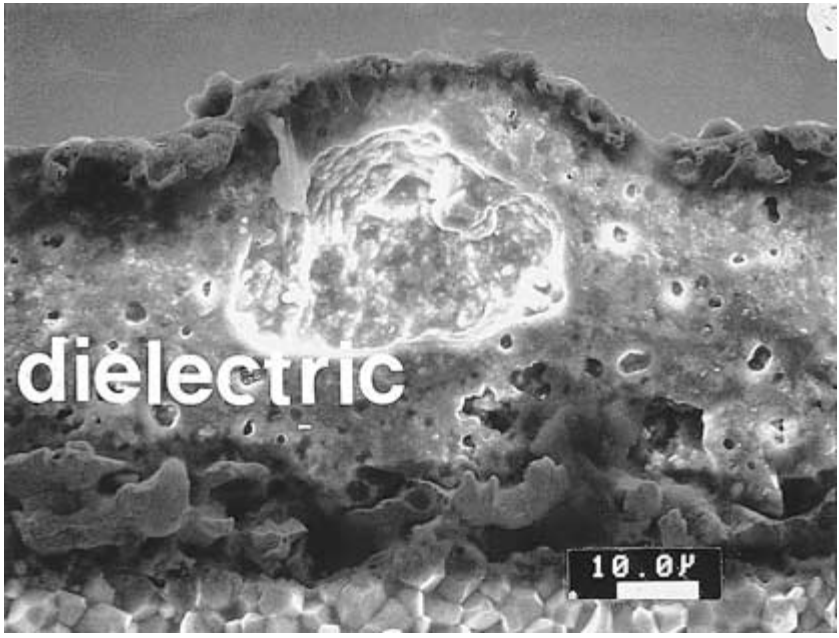

FIGURE 8.31 Blistering of dielectric related to organic entrapment. Solid curve = % weight. Broken curve = rate of weight loss. (*a*) T (°C) for complete vehicle volatization. (*b*) T (°C) at which glass transition occurs.

ethyl cellulose–based binder systems. Thus, for nitrogen-fireable dielectrics, glasses with high glass transition temperatures are desired. Incomplete removal of organics prior to sintering may lead to organic entrapment resulting in porosity and blistering (Fig. 8.31). Some of these issues have also been discussed in Sec. 8.2, "Thick-Film Conductors."

Sintering of dielectrics is dominated by the glass phase. Glasses undergo sintering by viscous flow. Initial sintering kinetics as measured by volumetric shrinkage are given by the following equation:[46]

$$\frac{\Delta V}{V} = \frac{9\gamma t}{4\eta r} \tag{8.10}$$

where $\Delta V/V$ is the volume shrinkage, γ is surface energy of glass, η is the viscosity of the glass, r is the radius of glass particles, and t is time. The sintering kinetics of glass-ceramic materials are governed by viscosity and surface energy as well as their temperature dependencies. As temperature increases, the glass viscosity decreases and the amount of densification increases. In the final stages of sintering, the glass contains isolated pores. The final densification of glass occurs as a result of surface tension forces and is given by the following expression:[46]

$$\frac{d\rho}{dt} = \frac{3\gamma}{2r_0\eta}(1-\rho) \tag{8.11}$$

where ρ is the relative density of the glass (the bulk density divided by the true density) and r_0 is the initial radius of glass particles.

Crystallization of glasses has been well researched for a variety of glass compositions used for houseware. The basic research on crystallization of thick-film dielectrics is not well published. However, the nucleation and growth theories regarding crystallization of other glass ceramics apply to crystallizing thick film dielectrics. A book by Z. Strand[100] describes the crystallization of glass ceramic materials in great detail. Crystallization processes are governed by the free energy of the liquid-to-solid transformation, the interfacial energy of the solid-liquid interface, and other kinetics-related parameters. For diffusion-controlled crystallization processes, the rate of crystallization of glasses is inversely proportional to the viscosity of glasses. Sintering and crystallization processes compete with each other during the microstructure development of thick-film crystallizing dielectrics. As viscosity of the glass decreases, the extent of sintering and crystallization may increase. Crystallization of the glass reduces the amount of liquid phase and retards the sintering process. Crystallization of the dielectric prior to densification can lead to an interconnected porosity in the fired structure.

Crystallization of dielectric materials also reduces the interaction with conductor materials and diffusion of conductor materials into the dielectric. Some of these interactions have been discussed in Sec. 8.2, "Thick-Film Conductors."

The crystallization temperature must be carefully controlled to reduce interactions with the conductor material and still attain full densification of the dielectric. Particle size of the glass powders and the amount and type of nucleation agents in the dielectric formulation affect the crystallization temperature and the structure of the crystallized phases.

In the case of glass-filled ceramics, the rate of dissolution of the filler oxide increases as the viscosity of the glass decreases. Dissolution of refractory oxides in the glass increases the viscosity, thereby reducing reactivity with conductor materials.

Capacitor Dielectrics. Capacitor dielectrics contain barium titanate and its solid solutions, which possess high dielectric constants. The melting point of these materials is over 1600°C. Sintering additives are often used to lower the sintering temperature to 850 to 1000°C. The liquid phase formed by reaction between sintering aids and refractory

dielectrics controls the sintering kinetics. For rapid and complete densification the following are necessary:[46]

1. An appreciable amount of liquid phase
2. Appreciable solubility of the solid in the liquid
3. Wetting of the solid by the liquid

The driving force for densification is the capillary pressure of the liquid phase located between the solid particles.

The liquid phase, on solidification, has a much lower dielectric constant than the ferroelectric phase. For good densification, complete wetting of the ferroelectric phase by the liquid phase is desired. On the contrary, to achieve high dielectric constants, the amount of liquid phase should be minimized and the liquid phase should not completely surround the ferroelectric phase. The composition of capacitor dielectrics is arrived at by a compromise between sintered density and the respective dielectric constant.

8.3.5 Dielectric Properties

This section describes the important properties of dielectric materials, structure–property relationships, and property measurement techniques.

Dielectric Constant. The dielectric constant K of a material is the ratio of dielectric permittivity ε of the material to the permittivity ε_0 of a vacuum:

$$K = \frac{\varepsilon}{\varepsilon_0} \quad \text{or} \quad \varepsilon = K\varepsilon_0 \tag{8.12}$$

Most often, the K of a material is obtained from capacitance measurements of a parallel plate capacitor made from thick-film dielectric and conductor materials. The electrical capacitance C of a parallel plate capacitor with electrode area A and dielectric thickness d may be expressed as follows:

$$C = \frac{\varepsilon A}{d} \tag{8.13}$$

Substituting Eq. (8.13) into Eq. (8.12) gives

$$C = \frac{K\varepsilon_0 A}{d} \tag{8.14}$$

where $\varepsilon_0 = 8.85$ pF/m. Rearranging Eq. (8.14) to solve for K gives

$$K = \frac{Cd}{\varepsilon_0 A} \tag{8.15}$$

Equation (8.15) does not take into account the effect of fringing fields shown in Fig. 8.32. The effect of a fringing field is significant under the following conditions:

1. The dielectric constant K_m of the material is close to that of the medium (generally air) in which the measurement is being made.

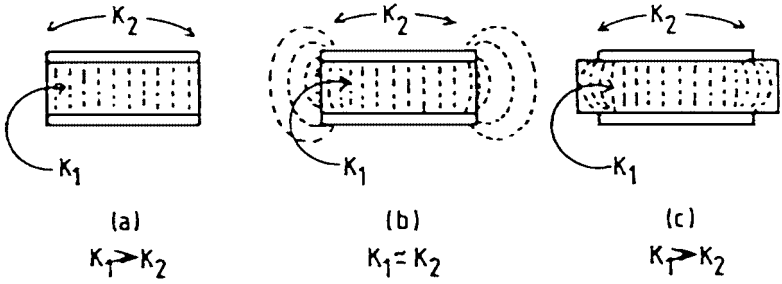

FIGURE 8.32 Fringing fields across various capacitors.[67]

2. The separation d of electrodes is comparable to the area A of electrodes.

3. Electrodes do not extend to the edge of the dielectric.

The effect of the fringing field can be taken into account as an increase in the electrode area, δA, as expressed by the following equation:

$$\delta A = XUd \tag{8.16}$$

where X is a factor dependent on the ratio K_m/K and capacitor structure and U is the perimeter of the electrode material. The factor X has a maximum value of 0.3 when $K = K_m$ and the electrode covers the entire dielectric area. However, $X = 0$ when $K >> K_m$ and the electrode covers the entire area.

For a square electrode geometry with sides w, the ratio of capacitance due to fringing, C_f, to that due to area between the electrode, C_e, is given by

$$\frac{C_f}{C_e} = \frac{\delta A}{w^2} = \frac{4dX}{w} \tag{8.17}$$

Normally $d/w << 0.1$. In this case, the correction due to fringing fields is insignificant.

Effects of Material Structure on Dielectric Constant. Electrical capacitance is the ability of a material to store an electric charge. When an electric field E is applied to a material, charges within the material are realigned in such a way as to neutralize part of the applied electric field (Fig. 8.33). The realignment of charges in the dielectric is referred to as *polarization.* Equation (8.18) shows the relationship of polarization P of the dielectric, the dielectric constant K, and the electric field E:

$$P = \varepsilon_0(K-1)E \tag{8.18}$$

Equation (8.18) is valid for linear dielectric materials (i.e., polarization is directly proportional to electric field). Ferroelectric materials used in high-K capacitor dielectric materials are nonlinear. Figure 8.34 illustrates the relationships between polarization, electric field, and dielectric constant for a ferroelectric material as given by the following equation:

$$\frac{\Delta P}{\Delta E} = \varepsilon_0(K-1) \tag{8.19}$$

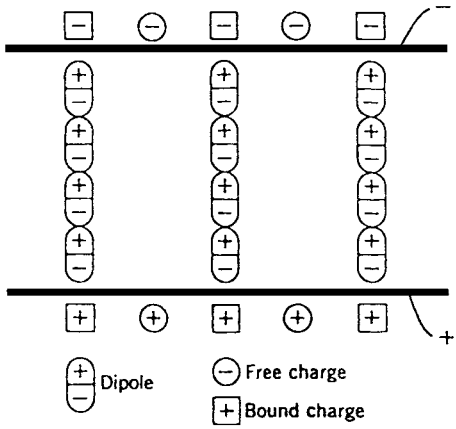

FIGURE 8.33 Schematic of rearrangement of charges within a capacitor body.

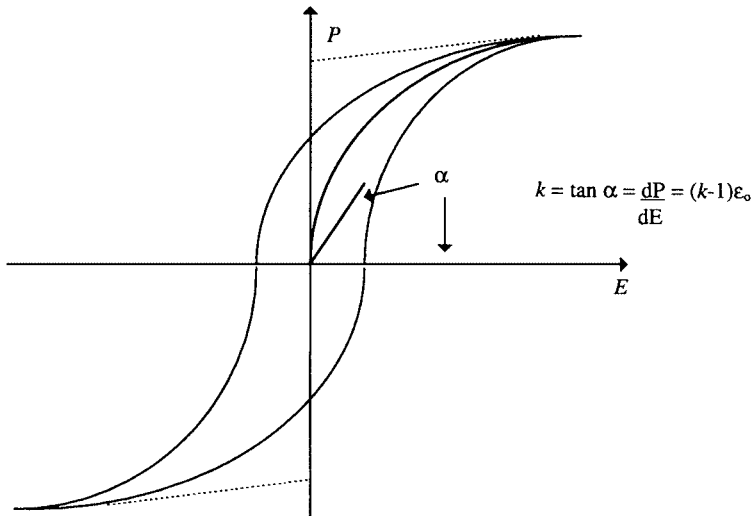

FIGURE 8.34 Polarization versus electric field behavior of a nonlinear dielectric material.

In the case of ferroelectric materials which have not been subjected to a polarizing dc field, K is the slope of the P versus E curve at the origin, as shown in Fig. 8.34. The K of ferroelectric materials is dependent on the prior electric field history, the frequency of the electrical signal used for the measurements, the DC bias voltage applied across the sample, and temperature. Figure 8.35 shows polarization mechanisms contributing to K. Figure 8.36 shows frequency ranges in which these mechanisms operate. Electric polarization is a result of the shift of the center of gravity of the negatively charged electronic cloud in relation to the positively charged nucleus in an atom. Electronic polarization is common to

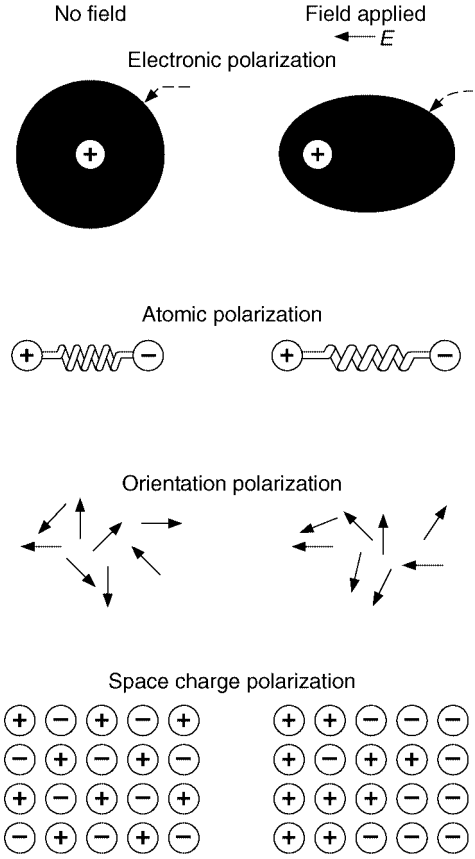

FIGURE 8.35 Schematic of polarization mechanisms. (*From Introduction to Ceramics.*)

all dielectric materials. Movement of anions and cations under an electric field leads to ionic polarization. Some materials are classified as polar materials. The charge distribution in polar materials is nonuniform, which gives rise to a permanent electric dipole even in the absence of an electric field. When an electric field is applied to such materials, the dipoles are aligned in the direction of the electric field, resulting in orientation polarization. Water is a polar material. In a macroscopic sense, ferroelectric materials are considered to contain permanent electric dipoles. However, the most fundamental theories of ferroelectricity are based on lattice vibration modes (phonons). The total polarization is a sum of contributions from various mechanisms.

Insulator Dielectrics. Insulator thick film dielectrics are multiphase materials. The electronic, ionic, and interfacial polarization mechanisms all contribute to the dielectric constant of glass–ceramic materials. Electronic polarization is directly proportional to the density of electrons in the glass–ceramic. Thus, dielectrics based on glasses containing oxides of high atomic number elements (e.g., lead) or high density exhibit high dielectric constants.

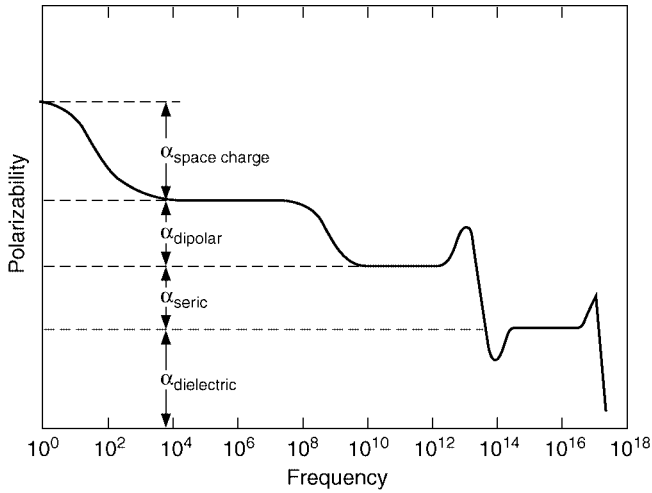

FIGURE 8.36 Polarization mechanisms for the full spectrum of frequencies. (*From Introduction to Ceramics.*)

The electronic contribution to dielectric constant, K_e, can be calculated from the refractive index n as shown in the following equation:

$$K_e = n^2 \tag{8.20}$$

The ionic contribution to the dielectric constant also can be calculated using the physics of lattice vibrations. Reference 46 shows a method of calculating ionic contribution to the dielectric constant. Since low K glass ceramics do not contain permanent dipoles, the contribution of orientation polarization is not significant in these thick-film dielectrics. However, if glasses contain mobile alkali ions, these mobile ions can jump between the two sites in an open network structure of glasses. This leads to an increase in dielectric constant at low frequencies. The dielectric constant of a multiphase glass ceramic material may also increase at low frequencies due to accumulation of space charges at the interface between phases with different electrical conductivity.

Capacitor Dielectrics. For capacitor dielectrics, dielectric constant and its temperature dependence are critical properties. Capacitor dielectric materials contain ferroelectric materials with high dielectric constants and sintering additives which have low dielectric constants. Barium titanate and its solid solutions are the most commonly used ferroelectric materials in capacitor dielectrics. At the Curie temperature, barium titanate also undergoes a cubic to tetragonal structural transformation. The cubic form of barium titanate is paraelectric, whereas the tetragonal form of barium titanate is ferroelectric. Tetragonal barium titanate changes to the orthorhombic phase at a lower temperature. Both structural transformations lead to an increase in the dielectric constant. Figure 8.37 shows the temperature dependence of K for barium titanate and barium strontium titanates. The addition of strontium titanate to barium titanate decreases the Curie temperature, thereby increasing the room temperature dielectric constant. A similar effect is produced by addition of barium stannate, barium zirconate, or rare earth oxides to barium titanate.[67] Table 8.14 shows the effect of various additives on the phase transition temperature of barium titanate.

TABLE 8.14 Effect of Additives on the Phase Transition Temperature of Barium Titanate

		Substitution site		Amount of substitution	
Class	Modifier ions	Ba	Ti	Partial	Complete
IA	Pb^{2+}, Sr^{2+}	X			X
IB	Zr^{2+}, HF^{4+}, Sn^{4+}		X		X
IIA	MG^{2+}, Ca^{2+}, Cd^{2+}, Zn^{2+}	X		X	
IIB	Th^{4+}, Ce^{4+}, Si^{4+}, Ge^{4+}		X	X	
IIIA	La^{3+}, Ce^{3+}, Gd^{3+}, Tb^{4+}, Sc^{3+}, Y^{3+}, Pr^{3+}, Nd^{3+}, Sm^{3+}, Eu^{3+}, Dy^{3+}, Ho^{3+}, Er^{3+}, Bi^{3+}	X	X	X	
IIIB	Nb^{5+}, Ta^{5+}, Sb^{5+}, W^{6+}, Mo^{6+}		X	X	
IVA	Na^{+}, K^{+}, Rb^{+}, Cs^{+}		X	X	
IVB	Fe^{3+}, Co^{3+}, Ni^{3+}, Mn^{3+}, Cr^{3+}, Rh^{3+}, Tm^{3+}, Yb^{3+}, Lu^{3+}		X	X	

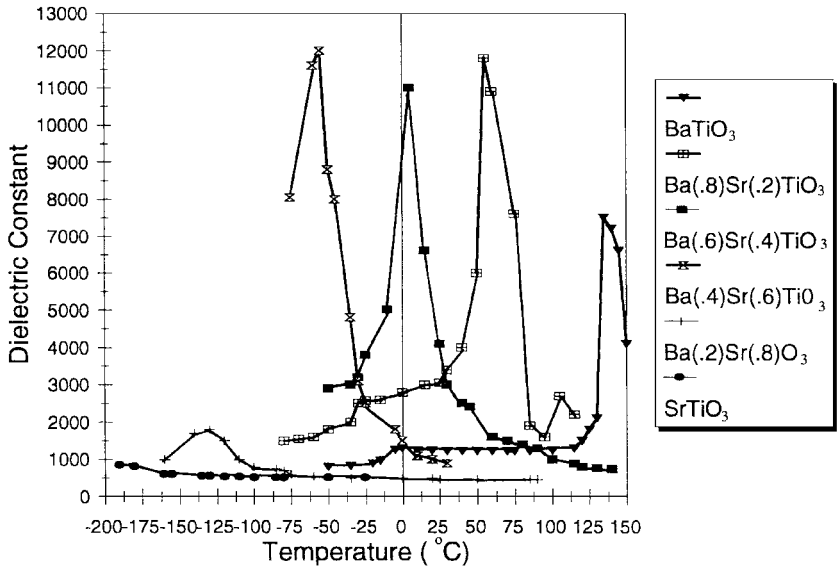

FIGURE 8.37 Temperature dependence of the dielectric constant of $BaTiO_3$–$SrTiO_3$ solid solutions.

Other materials that possess high dielectric constants are relaxor materials such as lead magnesium niobates. The structure of relaxor materials is extremely sensitive to stoichiometry and processing. Small changes in processing conditions or stoichiometry lead to formation of undesirable paraelectric phases and a resultant low dielectric constant. The extreme sensitivity of these materials has limited their use in capacitor dielectrics.

The fired microstructure of a thick film dielectric contains ferroelectric phases and other phases produced by sintering additives or modifiers. The dielectric constant of this complex mixture of phases can be estimated by using various mixture rules.[46] For example, one of the mixture rules used in estimating the dielectric constant of a mixture is

$$K = \frac{V_m k_m \left(\frac{2}{3} + \frac{k_d}{3k_m}\right) + V_d k_d}{V_m \left(\frac{2}{3} + \frac{k_d}{3k_m}\right) + V_d} \tag{8.21}$$

where V_m is the volume fraction of the matrix phase, k_m is the dielectric constant of the matrix, V_d is the volume fraction of the dispersed phase, and k_d is the dielectric constant of the dispersed phase.

Dielectric Loss. Ideal dielectric materials store electrical energy without dissipating energy in the form of heat. In reality, however, part of the electrical energy supplied to the dielectric material is lost in the form of heat. The dielectric loss factor is an indicator of the amount of this lost energy.

To understand dielectric loss, the current flowing through a capacitor and the voltage applied across a capacitor should be treated as vectors. Figure 8.38 is an electric phase diagram, a graphical representation of current and voltage across a capacitor.

The component of the current which is in phase with the voltage that causes the resistive heating is called the loss current I_l. The component of the current which leads the voltage by 90° is called the charging current I_c. The details of derivations of equations for

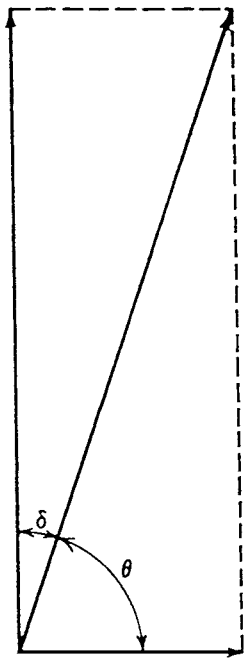

FIGURE 8.38 Electric phase diagram for a lossy capacitor.

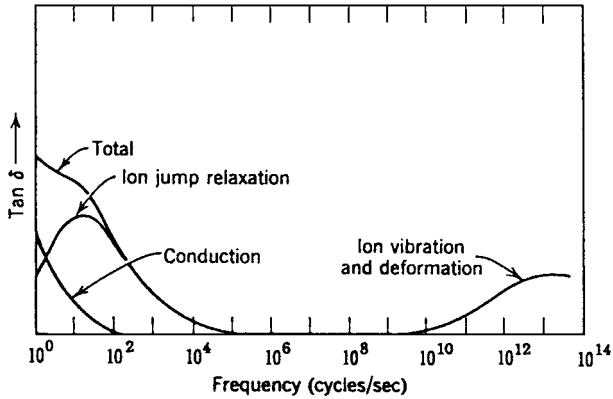

FIGURE 8.39 Dielectric loss mechanisms as a function of frequency.

charging current and loss current can be found in textbooks.[46] The following equation is commonly used to measure dielectric loss:

$$\text{Loss tangent}(\tan\delta) \text{ or dissipation factor} = \frac{I_L}{I_c} = \frac{\varepsilon''}{\varepsilon'} \tag{8.22}$$

where ε'' is absolute dielectric loss and ε' is dielectric permittivity. For high frequency applications, the quality factor is used as a figure of merit:

$$\text{Quality factor} = \frac{1}{\tan\delta} \tag{8.23}$$

Figure 8.39 shows various loss mechanisms over a spectrum of frequencies.

Dielectric losses at lower frequencies are associated with movement of ions, which generates heat. Mobile alkali ions or free charge carriers in glass–ceramic materials can drift when a DC electric field is applied. The movement of ions under an AC electric field ceases above a certain frequency. Thus, the contribution to dielectric losses from the conduction of ions is negligible at frequencies greater than 1 kHz.

Glasses possess an open structure in which ions such as silicon and boron form a network and monovalent or bivalent ions are randomly distributed in the network. Under an electric field, the randomly distributed bivalent or monovalent ions can jump from site to site in the open network. These ionic jumps also contribute to dielectric loss at frequencies up to 1 MHz. The ions are unable to follow the electric field at frequencies greater than 1 MHz. Ionic jumps are also possible in crystalline ceramic materials. Crystalline ceramics possess lattice defects which act as sites for ionic jumps.

The presence of porosity in ceramic materials can also lead to an increase in the dielectric loss. The surfaces of pores contain large numbers of crystalline defects. These surface defects can provide sites for the hopping of ions. Further absorption of moisture in the pore and subsequent leaching of the ions in the ceramic by adsorbed moisture can lead to increases in dielectric loss.

In capacitor dielectrics containing ferroelectric materials, movement of domain walls near and below the Curie temperature leads to additional dielectric losses. At frequencies

greater than 10^{10} Hz, ion deformation or movement of the electronic cloud surrounding atoms leads to absorption of energy, which results in dielectric losses.

Resistance of the electrode material and stray impedance of leads attached to the capacitors also cause the dielectric loss to increase at high frequencies. The part of the dissipation factor attributable to resistance of the electrode is given by[67]

$$(\tan\delta)_s = 4\pi f C\left(\frac{\rho_e}{t_e}\right)\left(\frac{L}{w}\right) \tag{8.24}$$

where $(\tan\delta)_s$ = contribution to the dissipation factor due to series resistance
f = frequency
C = capacitance
ρ_e = resistivity of the electrode
f_e = thickness of the electrode
L = overlapping length of the electrode
w = width of the electrode

Insulation Resistance. In ceramic materials, electrical charge may be carried by electrons, electron holes, or ions. The total electrical conductivity is the sum of the contributions of the conductivities due to various charge carriers:

$$\sigma = \sum \mu_i (n_i z_i e) \tag{8.25}$$

where n_i is the concentration of charge particle i, μ_i is the mobility of the particle, and $z_i e$ is the charge on the particle. Electrical resistivity is the inverse of electrical conductivity. Alkali metal ions or free electrons or holes show high electronic mobility. Glasses containing high amounts of alkali metal oxides or semiconducting oxides show low insulation resistance or high conductivity. Figure 8.40 shows the effect of various oxides used in typical thick film dielectric glasses on electrical resistivity. Glasses containing CaO, BaO, PbO, and MgO exhibit higher resistivity than those containing alkali metal oxides. Therefore, insulator dielectrics are predominantly free of alkali metal oxides and semiconducting oxides.

Capacitor dielectric formulations contain mixtures of ferroelectric and nonferroelectric phases. The ferroelectric phases are complex oxides with crystal defects. The crystalline defects in ferroelectric phases may create highly mobile electrons or holes for charge balance. Furthermore, some of the crystalline defects are charged and quite mobile. Thus, insulation resistance of capacitor dielectric materials is lower than insulator thick-film dielectrics.

As mentioned in the discussion of dielectric loss, the presence of porosity in dielectric materials can lower the insulation resistance because of absorption of moisture and crystalline defects at the surfaces of pores. The migration of electrode material into the dielectric during firing can lower the insulation resistance. Migration of metals or other conducting ions through interconnected porosity in a humid atmosphere can also cause loss of insulation resistance.

Dielectric Strength. The intrinsic dielectric strength of insulator dielectric materials is very high. However, observed dielectric strength of thick-film dielectric materials is 10 to 60 V/μm. Dielectric breakdown is generally caused by localized defects which increase the intensity of the local electric field to a level as high as the intrinsic breakdown strength. The largest flaw determines the breakdown strength of the material. As the electrode area or dielectric thickness increases, the probability of finding a critical flaw in the material also increases and the resultant breakdown strength decreases. Mesh marks, pinholes

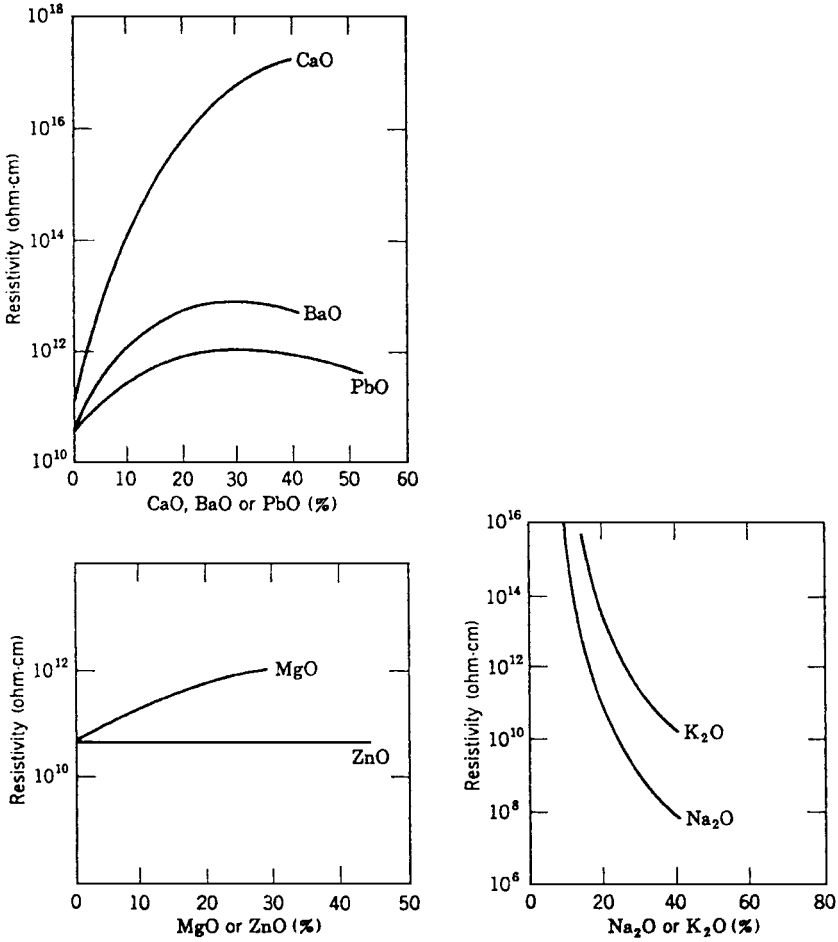

FIGURE 8.40 Effect of glass composition on insulation resistance.

related to printing, porosity, and nonuniformity of the electrode increase electric field concentration and promote reduction of the breakdown strength. Intrinsic dielectric breakdown occurs when the electric field levels are sufficient to cause a field emission of electrons into the dielectric. These electrons experience additional acceleration due to the electric field. Accelerated electrons possess enough energy to generate additional electrons on collision with the material and initiate electron avalanches.

Dielectric materials may also undergo thermal breakdown. Application of an electric field for an extended period of time may cause localized heating. Dielectric materials with high dissipation factors may increase the local temperature even further. This increase in temperature generates additional charge carriers which increase the dissipation factor and accelerate the temperature rise, ultimately leading to localized melting of the ceramic.

Coefficient of Thermal Expansion. The coefficient of thermal expansion is one of the most important thermomechanical properties of the dielectric. The CTE is determined by

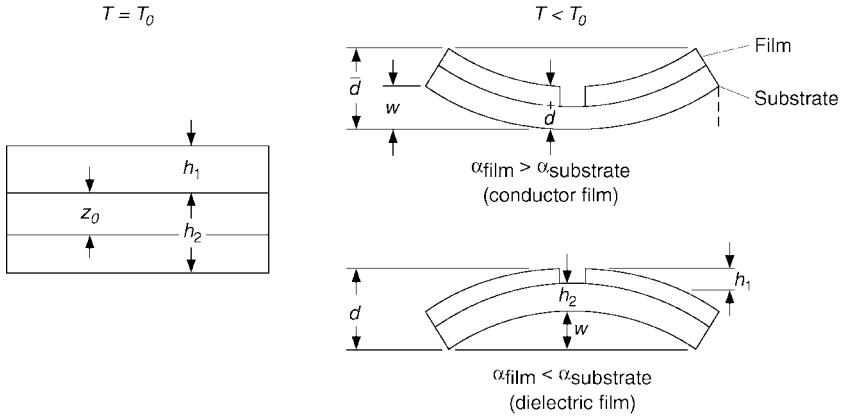

FIGURE 8.41 Warpage of substrate due to thermal stress created by CTE mismatch.[185]

the CTEs of the individual phases present in the dielectric. An empirical relationship for the CTE of a ceramic composite containing multiple phases is[46]

$$\alpha_c = \frac{\sum \frac{\alpha_i K_i F_i}{P_i}}{\sum \frac{K_i F_i}{P_i}} \tag{8.26}$$

where α_c = CTE of the composite
α_i = CTE of the individual phases
F_i = weight percent of individual phases
K_i = bulk modulus of individual phases
P_i = density of individual phases

The mechanical stresses created by CTE differences between the substrate and the dielectric cause bowing of the substrate and, in extreme cases, cracking of the dielectric. Strobeck et al.[185] proposed a model for substrate bowing using the theory of plates. Figure 8.41 illustrates bowing of the substrate under various conditions. The degree of bowing w is given by:

$$w = \frac{3}{16}(a^2 + b^2)\left(\frac{D}{C}\right)(\Delta T) \tag{8.27}$$

where ΔT is $T_0 - 25°C$ and T_0 is the temperature below which thermal stresses in the dielectric are not relieved.

$$D = -E_1\alpha_1(h_1 + z_0)^2 + E_2\alpha_2(h_2 - z_0)^2 + (E_1\alpha_1 - E_2\alpha_2)z_0^2 \tag{8.28}$$

and

$$C = E_1(h_1 + z_0)^3 + E_2(h_2 - z_0)^3 + (E_2 - E_1)z_0^2 \tag{8.29}$$

z_0 is the position of a generalized neutral axis and is given by

$$z_0 = \frac{h_1}{2}\left(\frac{E_2 h_2^{\,2}}{E_1 h_1^{\,2}} - 1\right) \Bigg/ \left(\frac{E_2 h_2}{E_1 h_1} + 1\right) \tag{8.30}$$

where E_1 = Young's modulus of the dielectric
E_2 = Young's modulus of the substrate
α_1 = CTE of the dielectric
α_2 = CTE of the substrate
h_1 = thickness of the dielectric film
h_2 = thickness of the substrate

If the CTE of the dielectric is less than that of the substrate, the dielectric film is under compressive stress and the substrate is under tensile stress after cooling during the firing process. Since ceramics are typically brittle, it is desired to place them under compression. Excessive tensile stresses in the substrate can produce unacceptable warpage. Since the thickness of the substrate is much larger than the thickness of the dielectric film, tensile stresses created in the substrate due to thermal expansion mismatch seldom exceed the fracture strength of the substrate. If the CTE of the dielectric is greater than that of the substrate, the dielectric material is under tension. These tensile stresses often exceed the fracture strength of the dielectric, resulting in dielectric cracking. Ideally, the CTE of the dielectric should be slightly less than that of the substrate and the CTE should be stable on refiring. Figure 8.42 shows a comparison of the CTE of a dielectric designed for an AlN substrate and that of the substrate. The resultant warpage is shown in Fig. 8.43.

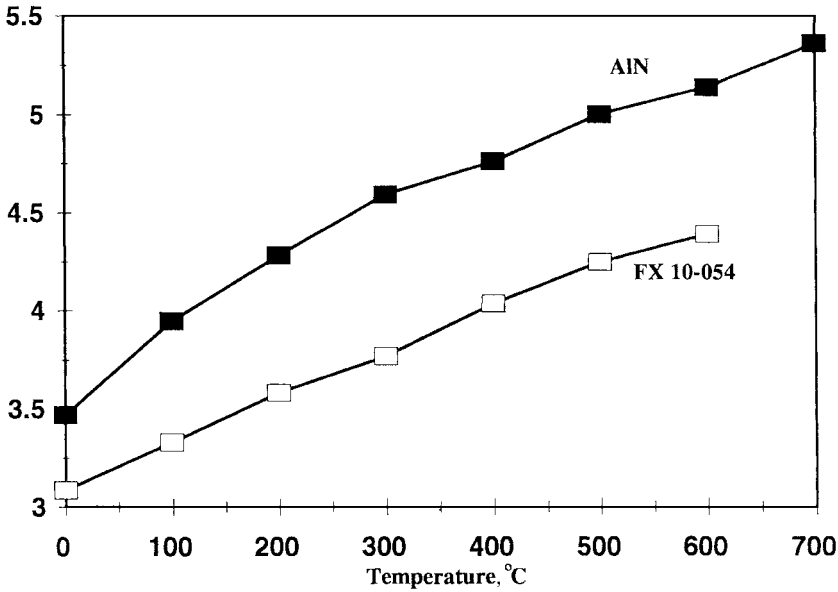

FIGURE 8.42 Comparison of CTE of a thick-film dielectric and AlN substrate.

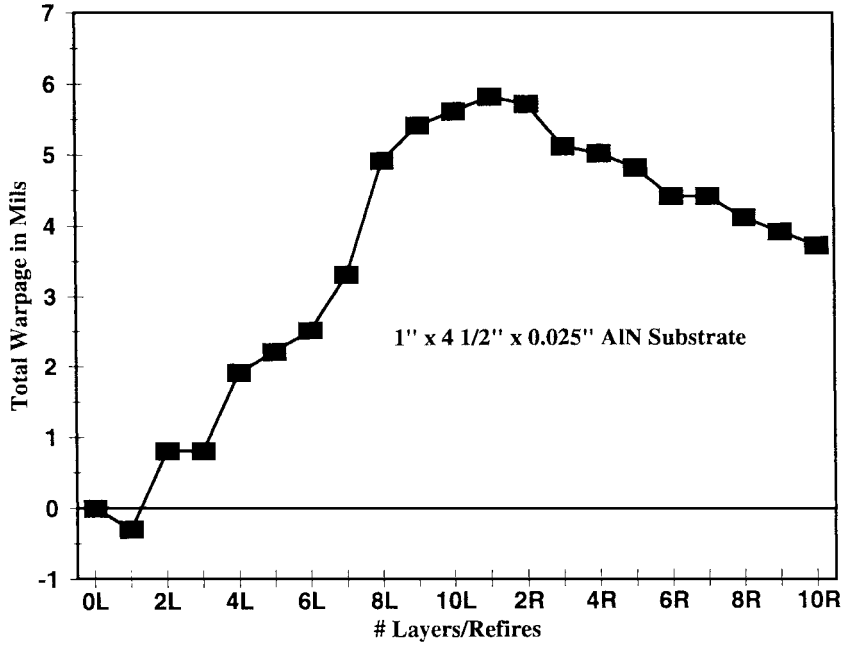

FIGURE 8.43 Warpage of an AlN substrate caused by CTE mismatch.

Hermeticity and Stability in Humid Environments. Hermeticity of a dielectric depends on its ability to seal and form a dense glass–ceramic body. Reliability of dielectrics in a humid environment is a function of hermeticity and inherent stability of the glasses. Interconnected porosity in the fired structure can provide paths for ion migration. The migration of ions under an electric field ultimately leads to the formation of a metallic film in the interconnected pores and results in an electrical failure. The correlation between hermeticity and failures in the humidity bias test is proposed by C. R. S. Needes.[76] For a copper–dielectric system, a leakage current value in an electrolytic hermeticity test of less than 20 μA/cm^2 is considered acceptable for prevention of failures in a humidity bias test. The electrolytic leakage current test does not take into account the stability of glasses in humid environments. Certain glasses are soluble in water. In general, glasses containing high amounts of boric oxide and strontium oxide are susceptible to failure in moist environments even though they may pass a hermeticity test.

8.3.6 Property Measurements

Dielectric Constant and Dielectric Loss. Impedance measurement bridges are the most commonly used instruments for dielectric constant and dielectric loss measurements for frequencies up to 10 MHz. A capacitor structure is built as a bottom electrode, top electrode, and two or more separation layers of dielectric material. Figure 8.44 shows a typical electrode pattern. The outside guard ring on the top electrode pattern prevents measurement errors due to fringe effects. Dielectric constant and dielectric loss measurements at frequencies

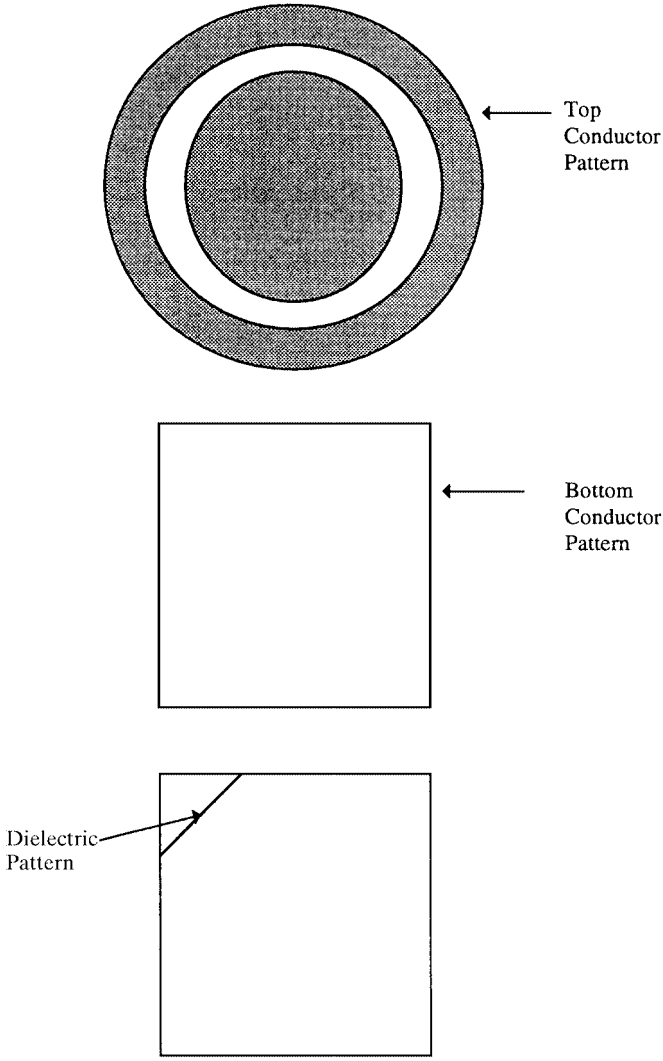

FIGURE 8.44 Patterns used for dielectric property measurements.

higher than 10 MHz are much more difficult and require special equipment and measurement techniques.

Figure 8.45 shows various dielectric property measurement techniques over a broad frequency range. Details of these measurement techniques are available in various references.[102,103]

Dielectric Strength. Dielectric strength is measured by applying an AC or DC electric field across a capacitor structure. The voltage across the capacitor is increased incrementally

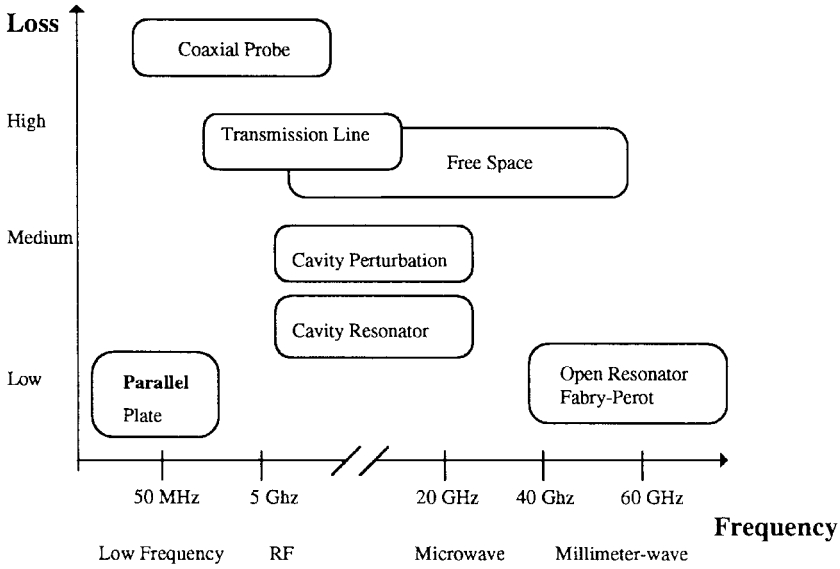

FIGURE 8.45 Dielectric property measurement techniques used for various frequency ranges.

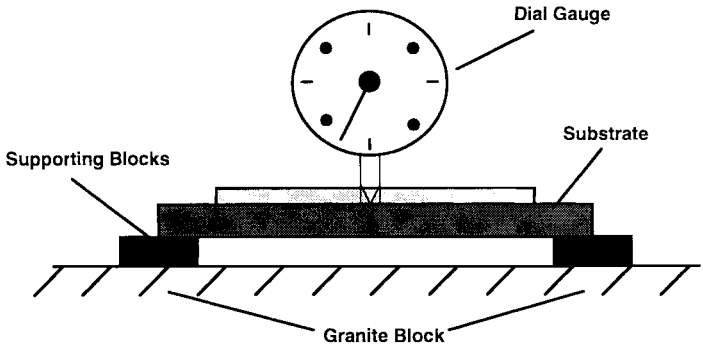

FIGURE 8.46 Warpage test configuration.

until dielectric breakdown occurs. Dielectric strength under a DC electric field is lower than that under an AC electric field. Sample preparation, the rate of increase of electric field, and the environment surrounding the sample all affect dielectric strength measurements.

Warpage. Warpage of the substrate is determined using several methods which involve measurement of distortion of the substrate due to deposition, firing, and refiring of dielectric layers. Generally, a flat granite block and spherometer or dial gauge with a stylus is used for warpage measurements. The substrate is kept on two supporting pieces on the granite block and the position of the center of the substrate with respect to the flat granite block is measured with the dial gauge (Fig. 8.46). More than 95 percent of the substrate area is covered with dielectric except for a small area at the center of the substrate, which is left open for the dial gauge measurements (Fig. 8.47).

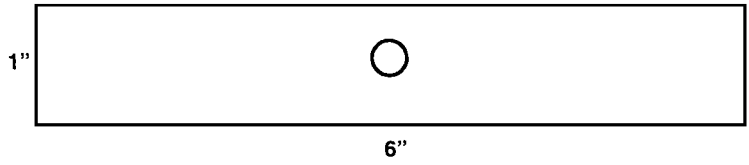

FIGURE 8.47 Warpage test pattern.

Hermeticity. Hermeticity of thick-film dielectrics is evaluated by an electrolytic leakage current test. This test measures leakage current through the fired dielectric printed on an electrode pad when 10 V is applied between a Pt foil anode and an electrode. A saline solution of 1 normal concentration is used as the electrolyte. Details of the leakage current test can be found in Refs. 101 and 104. Figure 8.48*a* illustrates a test coupon used for this test. Figure 8.48*b* illustrates the test configuration. Since a single print defect can lead to very high leakage current, the leakage current test results exhibit very high degrees of scatter. Sample preparation and interaction between the dielectric and the conductor can strongly influence leakage current values.

Life Tests. The high humidity bias test is the most commonly used test to determine reliability of a conductor/dielectric system. The most commonly used test conditions are 85 percent relative humidity, 85°C, and 10- or 30-V bias voltage. Typically, the test is run for 1000 h. This test simulates more than 20 years' life at average ambient conditions.

For a quick evaluation of the stability of materials in humid environments, an accelerated humidity bias test is conducted in a pressure cooker. The test coupons shown in Fig. 8.49 are subjected to atmospheric pressure of water vapor and 10- or 30-V bias voltage.

8.3.7 Effects of Processing Conditions on Dielectric Properties

Printing. The screen printing process for dielectric materials should be carefully controlled to eliminate print defects. Print defects such as pinholes, mesh marks, and foreign matter can reduce the breakdown strength of the dielectric and, in extreme cases, lead to shorts. As discussed in Sec. 8.5, "Rheology and the Screen Printing Process," the rheology of the inks and printing parameters affect print quality. In an automated production line, printing defects can lead to substantial yield loss if the process is not properly controlled.

Drying. Drying parameters are not known to have a significant effect on dielectric properties. However, in the case of copper-conductor-based multilayers, drying can affect the oxidation of copper conductors. The oxidized copper conductor may interact with the dielectric. In certain instances these interactions can result in dielectric blistering.

Firing. Firing is the most critical process. It can be broken into three segments: heating, isothermal hold, and cooling. The organic removal process is completed during the early part of the heating cycle. The heating rate and airflow rates influence organic removal. Very high heating rates and insufficient airflows can lead to organic entrapment, which can cause blistering and porous microstructure development.

The heating rate between the glass transition temperature and peak firing temperature and the isothermal hold temperature govern sintering and crystallization of the glasses. Thus, CTE and hermeticity of dielectrics are greatly affected by this region of the firing cycle. In return, warpage and leakage current are greatly affected by the firing cycle. The isothermal hold temperature and time also affect the conductor–dielectric interactions. In general, higher temperatures lead to increased blistering or dissolution of the conductor into the dielectric. These interactions can lead to reductions in insulation resistance and breakdown strength as well as increases in the dissipation factor.

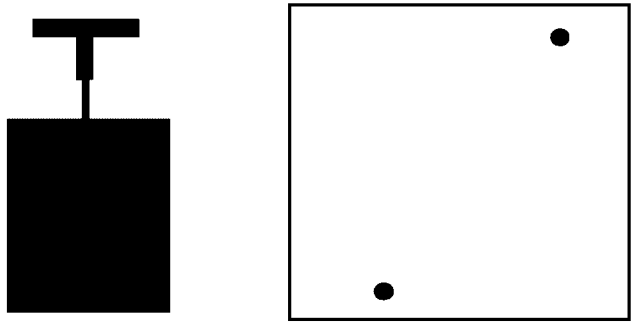

a) Conductor Test Pattern b) Dielectric test Pattern

FIGURE 8.48*a* Test patterns used for the leakage current test. Conductor test pattern; dielectric test pattern.

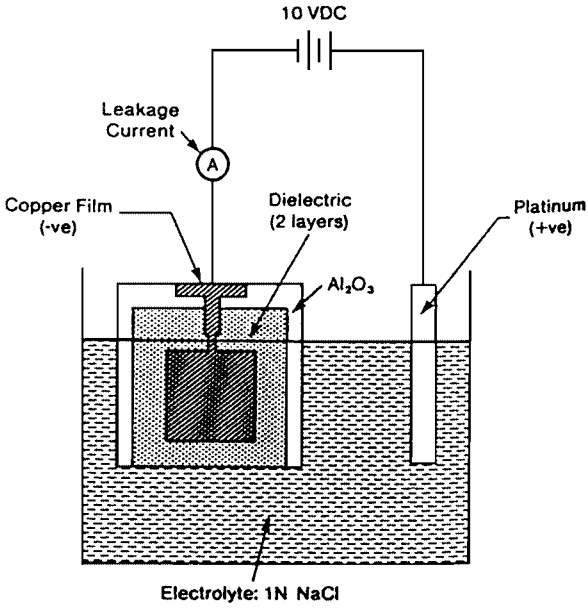

FIGURE 8.48*b* Leakage current test configuration.

8.4 RESISTOR MATERIALS AND PROCESSING

8.4.1 Introduction

The developments and technological advancements in the area of thick-film resistors have played a major role in establishing thick film as a viable technology. The term *thick-film resistor* is a generic name applied to a wide variety of resistive materials presently used in hybrid microcircuits and other electronic applications.[15] A thick-film resistor is a complex

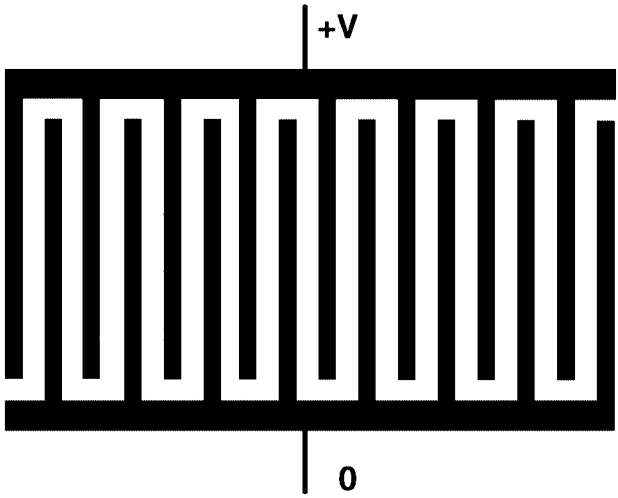

FIGURE 8.49 A test pattern for humidity bias testing.

nonequilibrium system made up of at least one conductive phase in an insulating glass matrix. Resistor inks generally contain, as a minimum, an insulating glass frit, an electrically conducting powder, and an organic screening agent. In addition, commercial formulations invariably contain small amounts of additives in order to improve certain electrical properties such as temperature coefficient of resistance (TCR), stability, and voltage handling characteristics. A thick-film resistor is processed by screen printing the resistor ink or paste onto a ceramic substrate. The firing process removes organic constituents and fuses the glass frit in order to bond the resistor to the substrate and produce the required microstructure. The two most important features that make thick-film resistor technology unique are its ability to vary sheet resistance by adjusting the volume fraction of the conductive phase and the low TCRs it produces. The sheet resistance of a thick-film resistor can be varied by at least 6 orders of magnitude (from 10 to 10^7 Ω/sq) by adjusting the volume fraction of the conductive phase. State-of-the-art thick film resistors will exhibit TCR values of less than ±100 ppm/°C. However, there are several resistor systems now commercially available which exhibit very low TCR values of ±50 ppm/°C for limited sheet resistance ranges. Advances in thick-film resistor materials have paralleled thick-film technology progress to date. Thick-film resistors enjoy applications in every phase of the electronics industry ranging from consumer electronics to space exploration.

8.4.2 Background

In the 1950s, work with palladium conductors led to the development of resistors formulated with mixtures of Ag, Pd, and glass powder.[105] Electrical properties were controlled by adjusting the ratios of Ag–Pd solid solutions, palladium oxide (PdO), and glass.[106] These materials were successfully used in SLT (solid logic technology) modules by IBM in the late 1960s for the model 360 computer and by other hybrid circuit manufacturers. However, the materials required stringent process controls by the end user. Silver–palladium resistors were designed to fire at 760°C, which is below the palladium oxide reduction temperature (800°C).[107] Palladium oxide is thermodynamically stable below 800°C and reduces to palladium metal[108] above this temperature.

The kinetics influencing the amount of PdO in the fired film and the resulting electrical properties are controlled by the amount of Ag. This system is chemically dynamic and reproducibility of sheet resistance from part to part is very difficult to achieve. Processing limits of time and temperature are very narrow. The shortcomings of this technology resulted in wide variations in sheet resistance due to slight changes in furnace conditions, limited sheet resistance ranges (10 to 500 kΩ/sq), and high TCR values (between 250 and 500 ppm/°C). Because of the deficiencies of Ag–Pd technologies, researchers actively pursued alternative conductive phases to be used in resistors.[109]

Since the late 1960s and early 1970s, several conductive phases, such as bismuth and lead ruthenates ($Bi_2Ru_2O_7$, $Pb_2Ru_2O_7$), ruthenium dioxide (RuO_2), and iridium dioxide (IrO_2), have been successfully utilized in thick-film resistor formulations.[109] The sheet resistance of these resistor systems can be varied from 10 to 10^7 Ω/sq by adjusting the volume fraction of the conductive phase. Although conductive phase developments created significant advancements in resistor technology, the importance of glass chemistry and its influence on resistor properties cannot be overlooked.

Studies of glass chemistry and its influence on microstructure,[52] interaction of the glass and conductive phases, and interdiffusion of substrates and resistor glasses have provided understanding of these complex systems. This led to the development of resistor systems with excellent performance and properties. Similarly, studies of thermal expansion coefficients of resistor composites relative to substrate materials has led to development of resistors with excellent laser trim stability.[110] A high-performance resistor can be formulated by appropriate control of particle size of the conductive phase and the design of glass chemistry. Currently, component and hybrid manufacturers use RuO_2 as the conductive phase for low sheet resistance values (10 Ω/sq to 100 kΩ/sq) and pyrochlore-type ruthenates ($Bi_2Ru_2O_7$, etc.) for values exceeding 100 kΩ/sq. This optimizes the inherent properties of each resistor system. Recently, silver–palladium resistor inks, consisting of Ag–Pd powder and glass powder, have been developed for surge protection applications.[111] They are typically formulated for lower sheet resistance ranges (0.1 to 10 Ω/sq) and utilize long serpentine resistor designs to achieve the desired resistance. Through appropriate control of particle size of silver and palladium powders and Ag/Pd ratios, TCR values of less than ±100 ppm/°C can be readily achieved.

8.4.3 General Requirements

Thick-film resistors are extensively used in hybrid microcircuits because they can meet design requirements such as high sheet resistance, good power dissipation, high voltage handling capabilities, and desirable response at high frequencies. These design functions are difficult or impossible to achieve with silicon monolithic integrated circuits. The most important electrical property of a thick film resistor is the attainable sheet resistance range. Figure 8.50 shows a typical variation of sheet resistance with volume fraction of RuO_2 conductive phase.

Electrical resistance R of materials is expressed as

$$R = \rho \frac{L}{A} \tag{8.31}$$

where ρ is resistivity, L is the current carrying length, and A is the current carrying cross-sectional area. Sheet resistivity of thick film resistors is generally expressed in terms of ohms per square, as shown in the following equations:

$$R_s = \frac{R}{n} = \frac{R}{L/W} \tag{8.32}$$

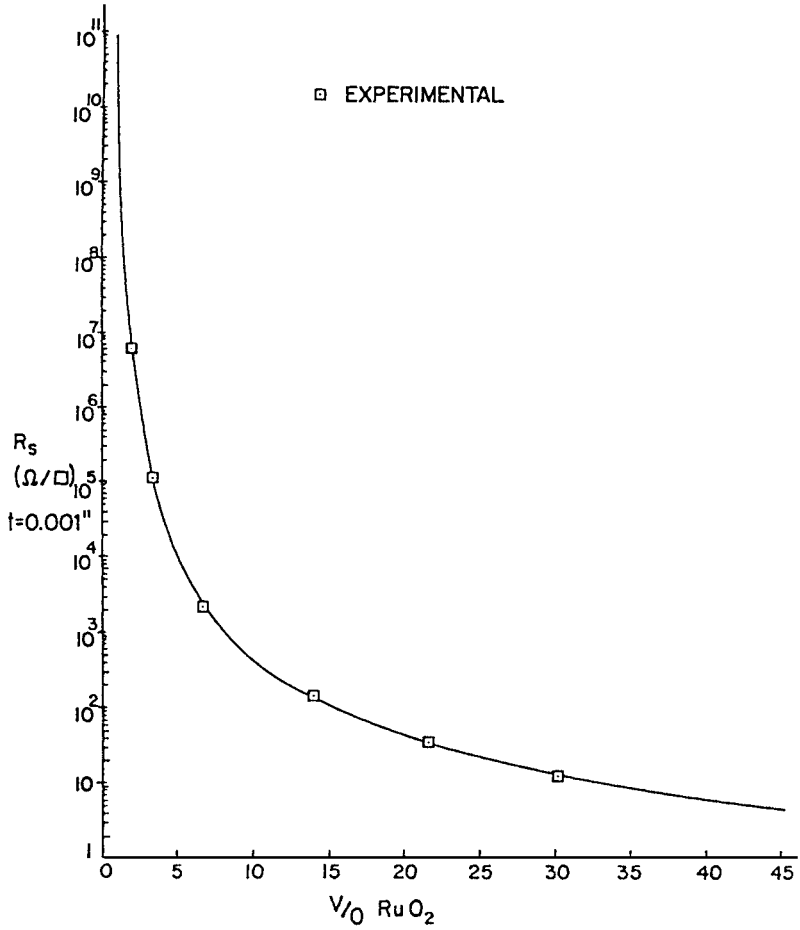

FIGURE 8.50 Variation of sheet resistance with volume fraction of conductive phase.

where R_s is the sheet resistance and n is the number of squares, which is the aspect ratio (length/width) of the resistor. Substituting Eq. (8.31) into Eq. (8.32) results in the following:

$$R_s = \frac{\rho(L/A)}{L/W} \tag{8.33}$$

The current-carrying cross-sectional area A is equal to W times thickness t. Substituting for A in Eq. (8.33) gives

$$R_s = \frac{\rho(L/Wt)}{L/W} \tag{8.34}$$

and

$$R_s = \frac{\rho}{t} \tag{8.35}$$

Therefore, sheet resistivity at a desired thickness can be calculated using Eq. (8.35). For example, the sheet resistivity at 25 μm is given by:

$$R_s(\text{at } 25\ \mu) = \frac{R_s(\text{measured}) \times t}{25} = \frac{\rho}{25} \tag{8.36}$$

Resistance of thick-film resistors of any geometry can then be predicted by the following equation:

$$R = R_s n \tag{8.37}$$

The above analysis assumes that the thickness of the resistors is uniform and a linear relationship exists between the resistance and the thickness of a resistor. This assumption is not always true.

From the above equations, the sheet resistivity of the fired paste can be calculated for a given resistor size. In the same way, the ratio of length to width, or aspect ratio, of a resistor for a required resistance value can theoretically be determined for a paste of known resistance.

Another important parameter which describes the electrical characteristics of thick-film resistors is the temperature coefficient of resistance. The TCR can be defined most rigorously as

$$\text{TCR} = \frac{1}{R}\frac{dR}{dT} \tag{8.38}$$

where T is the temperature and dR and dT are incremental changes in resistance and temperature, respectively.

Taking into consideration dimensional changes in the resistor due to temperature changes, one can write:

$$\frac{1}{R}\frac{dR}{dT} = \frac{1}{\rho} = \frac{d\rho}{dT} + \frac{1}{L}\frac{dL}{dT} - \frac{1}{t}\frac{dt}{dT} - \frac{1}{W}\frac{dW}{dT} \tag{8.39}$$

Over a limited temperature range where ρ equals resistivity between T_1 and T_2, TCR values can also be approximated as follows:

$$TCR_{(T_1-T_2)} = \frac{R_{T_2} - R_{T_1}}{R_{T_1}(T_1 - T_2)} \tag{8.40}$$

where R_T is the resistance of the resistor at temperature T. Since TCR is very small in magnitude, the right side of the above equation is generally multiplied by 10^6 and the result is expressed in parts per million per degree Celsius, ppm/°C.

The temperature coefficient of resistance is usually defined as

$$\text{TCR} = \frac{R_T - R_{25}}{R_{25}(T-25)} \times 10^6 \text{ ppm/°C} \tag{8.41}$$

where R_T is the resistance measured at some temperature T (°C) and R_{25} is resistance at room temperature. In industrial practice, two standard TCR values are typically specified: (1) hot TCR (HTCR), where $T_2 = 125$°C and $T_1 = 25$°C; and (2) cold TCR (CTCR), where $T_2 = -55$°C and $T_1 = 25$°C. A standard thick-film resistor should exhibit both hot and cold TCR values of less than ±100 ppm/°C and preferably less than ±50 ppm/°C. It is also quite common for specific applications to require some predetermined TCR value over expected circuit operating temperature ranges (i.e., ±50 ppm/°C between 0 and 70°C). Later discussions will focus on formulation changes to control TCR values.

Thick-film resistor performance is also measured by the voltage coefficient of resistance (VCR), which can be defined as follows:

$$\text{VCR} = \frac{1}{R_{V_1}} \frac{R_{V_2} - R_{V_1}}{V_2 - V_1} \times 10^6 \text{ ppm/°C} \tag{8.42}$$

where V is the applied voltage and R_{V_2} and R_{V_1} are the resistances measured at the respective voltages of V_2 and V_1. These voltages are typically 50 V (V_2) and 5 V (V_1). Permanent changes in resistance with application of voltage are characterized by the short-term overload voltage (V_{STOL}). The short-term overload voltage is the voltage required at 5 s duration to produce a 0.1% permanent change in resistance at 25°C. The short-term overload voltage of a thick-film resistor should be maximized. Resistor stability under applications of high voltage transforms to good power handling characteristics of the resistor, as power is directly proportional to voltage squared. Resistor power rating can be defined by the following equation:

$$P_R = \frac{(V_{\text{SW}})^2}{R} \tag{8.43}$$

where P_R is the maximum power rating and V_{SW} is the standard working voltage. V_{SW} is defined as 0.4 times V_{STOL}. Another resistor property of importance is current noise I_n, which should be minimized. The current noise is measured in terms of noise index. It is the decibel equivalent of the root mean square noise voltage to DC bias voltage ratio in a decade of frequency.

$$\text{Noise index} = 20 \log \left(\sqrt{V^2 / V_{\text{DC}}} \right) \text{dB} \tag{8.44}$$

where current noise $\sqrt{V^2}$ is the rms current noise voltage measured in microvolts and V_{DC} is the DC applied voltage across the resistor measured in volts. By this definition, 1 μV of current noise at 1-V DC bias would give a noise index of zero decibels.

Resistor stability is a key parameter for fired resistor performance criteria. In addition to tests already described, changes in resistance are typically monitored as a result of hot column testing, thermal aging, thermal cycling, humidity and bias voltage aging, as well as stability following laser trimming. These will be discussed later.

8.4.4 Resistor Compositions

Cermet Resistors. The name *cermet* is generally applied to materials which result in a fused structure of conductive phase in a vitreous, nonconductive binder. Resistor inks contain an electrically conducting powder, an insulating glass powder, and an organic screening agent. In addition, commercial resistor inks contain small amounts of various additives added to adjust specific electrical properties. The conducting phase used in thick film resistor formulations should satisfy the following requirements: (1) stability at the peak firing temperature, (2) small but finite solubility in the glass at the firing temperature, and (3) ability to be readily wet by the glass. These requirements limit the choice of the conductive phase for air-fireable resistor systems to a few binary metallic oxides such as RuO_2 and IrO_2. Both RuO_2 and IrO_2 are thermodynamically stable in air at the typical thick-film processing temperature of 850°C. More complex conductive materials commonly used in commercial thick film resistors are $Bi_2Ru_2O_7$, $Pb_2Ru_2O_6$, and Ag-Pd-PdO. These conductive materials exhibit a positive temperature coefficient of resistance and have resistivities somewhat higher than those of metals. Examples of resistivities for various conductive phases are shown in Table 8.15.

In the case of nitrogen firing, typical conductive phases are tin oxide (SnO_2), indium oxide (In_2O_3), strontium ruthenate ($SrRuO_3$), lanthanum hexaboride (LaB_6), titanium disilicide ($TiSi_2$), and tantalum nitride (TaN).

TABLE 8.15 Resistivity Values of Various Oxides

Oxide	ρ at 300 K, $\Omega \cdot$ cm
Rutile	
RuO_2	3.5×10^{-5}
IrO_2	4.9×10^{-5}
Rh_2O_3	$<10^{-4}$
Pyrochlore	
$BiRu_2O_7$	2.3×10^{-2}
$Ri_2Rh_2O_{6.8}$	3.2×20^{-3}
$Bi_2Ir_2O_7$	1.5×10^{-3}
$PbRu_2O_6$	2.0×10^{-2}
$Pb_2Ru_2O_{6.5}$	5.0×10^{-4}
$Pb_2Rh_2O_7$	6.0×10^{-1}
$Pb_2IrO_{6.5}$	1.5×10^{-4}
$Pb_2Os_2O_7$	4.0×10^{-4}
$Ti_2Ru_2O_7$	1.5×10^{-2}
$Tilr_2O_7$	1.5×10^{-3}
$Ti_2Rh_2O_7$	6.0×10^{-4}
$Ti_2Os_2O_7$	1.8×10^{-4}
Perovskite	
$LaRuO_3$	4.5×10^{-3}
$La_{0.5}Sr_{0.5}RuO_3$	5.6×10^{-3}
$CaRuO_3$	3.7×10^{-3}
$SrRuO_3$	2.0×10^{-3}
$BaRuO_3$	1.8×10^{-3}

Insulating glass frits generally utilized are lead borosilicate glasses. Glass chemistry plays a major role in the resistor ink formulation. Electrical performance such as voltage handling and properties such as laser trim stability and environmental stability are mainly dependent on the glass chemistry. Flow properties of the glass such as the glass softening point and viscosity of the glass at the firing temperature are critical to the final resistor properties. In this chapter the discussions are limited to air-fireable resistor inks.

Low-Ohm Resistor Inks. Resistor inks having sheet resistances lower than 10 Ω/sq are generally classified as *low-ohm thick-film resistors.* These resistors generally consist of Ag-Pd solid solutions and an insulating glass matrix. Low ohm resistors are mostly used in the telecommunications industry for surge protectors. These are typically thick-film resistor networks used to protect electronic devices against lightning strikes and power crosses. Recent advances in telecommunications for lightning strike and voltage protection requires resistors having low sheet resistance and excellent stability under an applied electric surge.[112] These applications also demand resistors with low TCR (less than ±100 ppm/°C) and sheet resistance as low as 100 mΩ/sq. The TCR values of ±100 ppm/°C can typically be controlled by optimizing the Ag/Pd ratio and the particle sizes of the glass and metal powders. Further requirements of these resistors include: good stability on life testing such as humidity aging and thermal cycling, good laser trimmability, and stability during multiple refirings. There are several publications[112,113] which describe the use of low-ohm thick-film resistors for surge protection in telecommunications.

The typical composition of a low-ohm resistor paste is given in Table 8.16.

Thick film inks are generally screen-printed onto a 96 percent alumina substrate and fired through a furnace at a peak firing temperature of 850°C for 10 min. The typical profile used to fire low-ohm resistors is given in Fig. 8.51.

Glass softening point and viscosity of the glass at the peak firing temperature affect the final resistor properties.[114] The proper selection of glass and metal powders can aid in complete sintering of the resistor with a dense, pore-free resistor microstructure. A representative scanning electron micrograph of a dense, as-fired resistor cross section is shown in Fig. 8.52.

Figure 8.53 shows the effect of metal content on the sheet resistance of low-ohm resistors for various cooling rates. As metal content increases, the sheet resistance of the ink decreases for a given cooling rate.

Typical properties of high performance, low-ohm resistors are presented in Table 8.17.

Mid/High-Range Resistors. Midrange to high-range resistors include those with sheet resistance values exceeding 10 Ω/sq. The inks for these resistors contain an electrically conducting oxide such as RuO_2, Bi_2RuO_7, or Pb_2RuO_7, insulating glass powder, and an organic screening agent. They contain dopants in order to alter one or more of the electrical characteristics of the ink. The most common dopants are TCR modifiers and stabilizers. TCR values

TABLE 8.16 Typical Composition of a Low-Ohm Resistor Paste

Material chemistry	Function	Sample
Metal powders	Conductive phase	Ag and Pd powders
Glass powders	Binder	Borosilicate powder
Resin	Rheology (binder to improve green strength)	Ethyl cellulose
Solvent	Carrier for the ingredients	Terpinoel, butyl, carbital, etc.
Surfactant	Dispersion	Proprietary

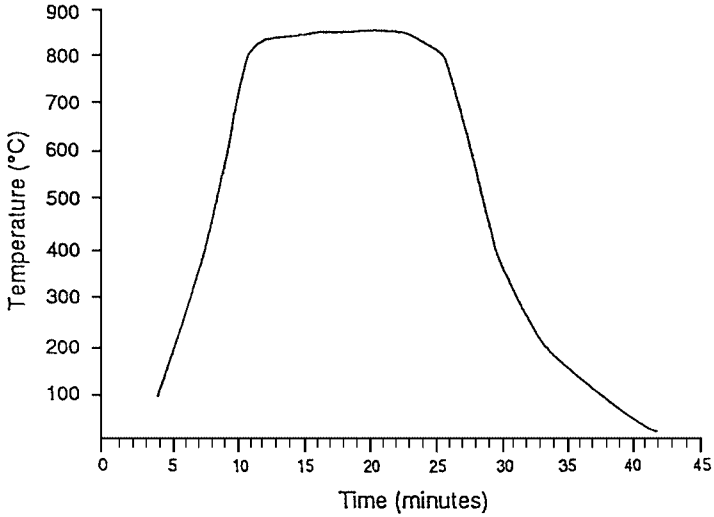

FIGURE 8.51 Typical firing profile used to process thick film resistors.

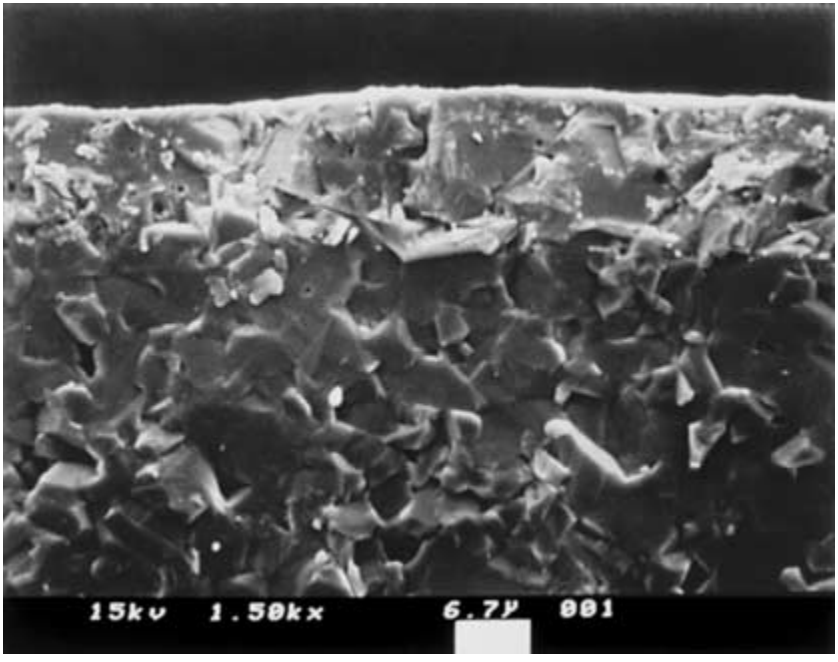

FIGURE 8.52 Scanning electron micrograph of a low ohm resistor cross section.

TABLE 8.17 Typical Properties of High Performance Low Ohm Resistors

Properties	Typical values
Sheet resistance, Ω/sq	0.2–10.0
Tolerance, %	±10
TCR, ppm/°C:	
Hot TCR	±100
Cold TCR	±100
Drift after electrostatic discharge (ESD) at 2000 V, %	<0.1
Drift after thermal aging (150°C for 1000 h), %	<0.1
Drift after thermal cycling (5 cycles), %	<0.5
Drift after humidity aging (85°C/85% for 1000 h), %	<0.5
Drift after overglazing (low temperature overglaze), %	<0.1
Drift under lightning surge (10×1000 μs, 200 pulses at 970 V),%	<0.1

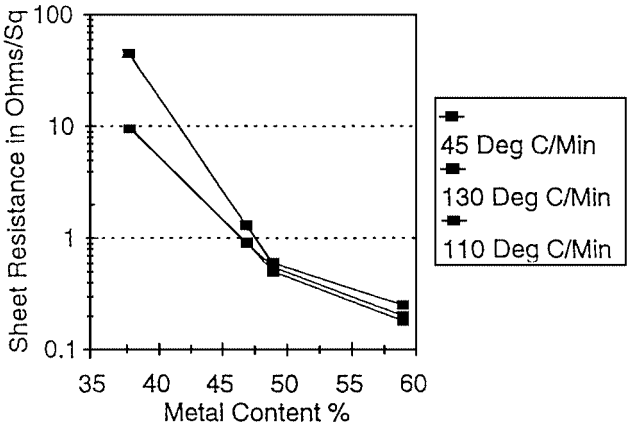

FIGURE 8.53 Effect of metal content on sheet resistance of low ohm resistors for different cooling rates. (*From The International Society for Hybrid Microelectronics, Dallas, TX.*)

are typically ±100 ppm/°C and are controlled by varying the type and amount of TCR modifiers in the ink. Semiconducting oxides such as manganese dioxide (MnO_2), cobalt oxide (Co_2O_3), titanium dioxide (TiO_2), niobium pentoxide (Nb_2O_5), ferric oxide (Fe_2O_3), rhodium sesquioxide (Rh_2O_3), and vanadium pentoxide (V_2O_5) are added to shift the TCR values in a negative direction. These are all called *negative TCR modifiers*. Metal oxides such as

TABLE 8.18 Chemical Composition of Typical Lead Borosilicate Glass

Oxide	Weight %
PbO	55.5
B_2O_3	22.0
SiO_2T	10.5
Al_2O_3	12.0

TABLE 8.19 Physical Properties of Typical Lead Borosilicate Glass

Density	4.31 g/cm^3
Coefficient of linear thermal expansion (25–200°C)	6.03 ppm/°C
Strain point	464°C
Annealing point	469°C
Deformation point	490°C

cuprous oxide (Cu_2O) and silver oxide (Ag_2O) are added to the inks to shift TCR values in a positive direction. These are called *positive TCR modifiers*. Oxides such as Al_2O_3, SiO_2, and ZrO_2 are added to improve resistor stability and reduce sensitivity to variations in processing conditions. These are called *stabilizers.* Ruthenium dioxide (RuO_2) based thick-film resistors are one of the most commonly used commercial thick-film resistors. Properties of RuO_2-based thick-film resistors will be discussed in detail.

Both sheet resistance and TCR are a function of particle[115–117] size of the respective conductive and glass powder phases. Several studies have been done to understand the effect of conductive phase particle size on electrical properties of resistors. Ruthenium dioxide powder is commercially available in a range of particle sizes from 5 to 100 nm. Since RuO_2 particles are very small, the powders tend to agglomerate. The particle size is a function of the surface area of the powder, which is the key property typically specified for resistor conductive phases. The glass powder generally used is lead borosilicate. A typical composition and properties of a lead borosilicate glass are listed in Tables 8.18 and 8.19, respectively. Physical properties of lead borosilicate glasses have been well studied by Vest et al.[52] In addition to particle size, glass chemistry plays a significant role in controlling the electrical properties such as *R*, TCR, ESD shift, voltage handling, laser trim properties, and stability of the resistor.

A typical microstructure of a RuO_2-based thick-film resistor is shown in Fig. 8.54. The microstructure consists of networks of conductive phase in an insulating glass matrix. Electrical properties of thick-film resistors are a function of these conductive chains in the glass. Formation of the conductive chains and their distribution is a function of particle sizes of both conductive phase and glass, the physicochemical properties of the glass, and thermophysical conditions during firing. Typical properties of resistors ranging from 10 Ω/sq to 10 MΩ/sq are listed in Table 8.20.

Thermistors. Thick-film thermistors are generally used for temperature compensation in various electronic circuits. They are a special class of thick-film resistors, designed to

TABLE 8.20 Typical Properties of Thick Film Resistors

	Resistor value						
Property	10 Ω	100 Ω	1 kΩ	10 kΩ	100 kΩ	1 MΩ	10 MΩ
Sheet resistance, Ω/sq	10	100	1 k	10 k	100 k	1 M	10 M
Tolerance, %	±10	±10	±10	±10	±10	±10	±20
TCR hot/cold, ppm/°C	±100	±100	±100	±100	±100	±100	±200
Drift on ESD (2000 V), %	<0.1	<0.1	<0.1	<0.1	<0.1	<0.1	<0.1
Drift on thermal aging, %	<0.1	<0.1	<0.1	<0.1	<0.1	<0.5	<0.5
Drift on thermal cycling, %	<0.5	<0.5	<0.5	<0.5	<0.5	<0.5	<0.5
Drift on thermal shock, %	<0.5	<0.5	<0.5	<0.5	<0.5	<0.5	<0.5
Drift on humidity aging, %	<0.1	<0.1	<0.1	<0.1	<0.1	<0.5	<0.5
Short-term overload voltage, V/mm	8	25	75	250	380	370	
Power dissipation, mW/mm^2	900	600	800	1000	230	22	
Tech noise, dB	<–30	<–30	<–20	<–15	<–10		

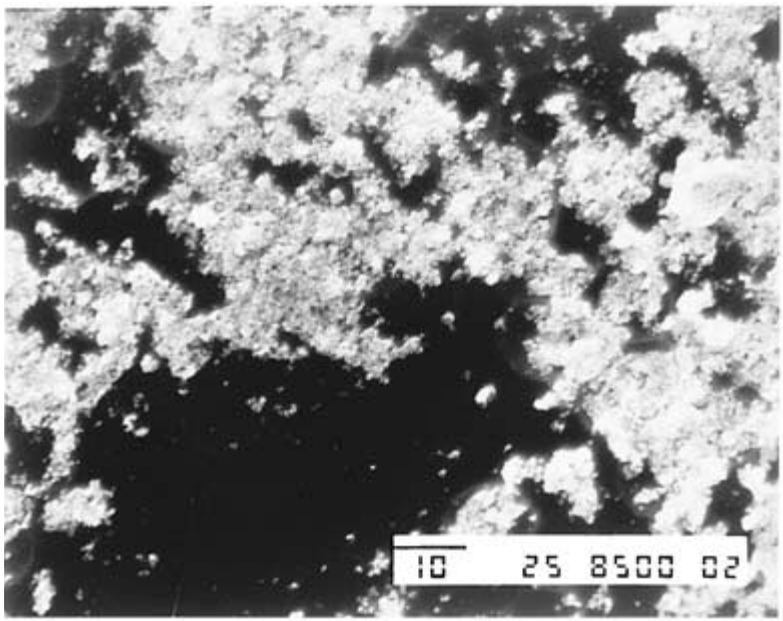

FIGURE 8.54 Typical microstructure of an RuO_2-based thick film resistor.

have a very large and controlled change in resistance with temperature. These materials can be classified into two systems: (1) sensor materials made of glass doped with metal oxides and (2) thermistor materials made of spinel type oxides and conductive oxides embedded in a glassy matrix. Sensor materials can exhibit a TCR which is low and fairly constant over the entire operating temperature range of –55°C to 125°C. The response curve, resistance

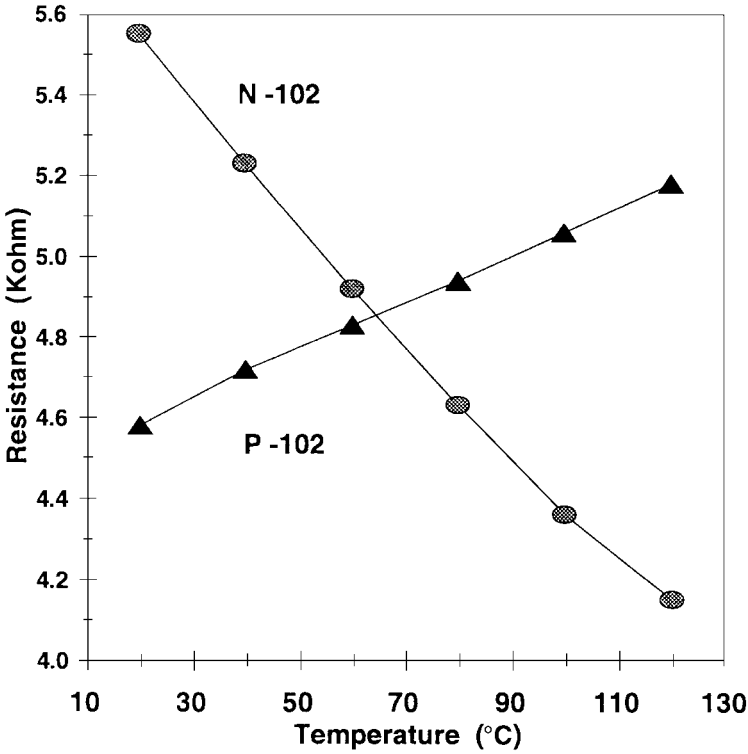

FIGURE 8.55 Resistance versus temperature behavior of sensohm type thermistors.

vs. temperature, can be described by the following relationship:

$$R(T) = R_0(1 + \alpha\Delta T) \tag{8.45}$$

where R_0 is sheet resistance at 25°C and α is the temperature coefficient of resistance. Typical measured α values are +1300 ppm/°C for positive type materials and −3000 ppm/°C for negative type materials. The resistance versus temperature behavior of these materials is shown in Fig. 8.55.[118]

Spinel-based inks exhibit a different response curve, more frequently associated with thermistors:

$$R(T) = R_0 \exp\left(\frac{ß}{T}\right) \tag{8.46}$$

where T is expressed in degrees Kelvin, R_0 is the sheet resistance at 25°C, and ß is the thermistor constant. Temperature dependence is controlled by the parameter ß, and the magnitude of resistance is controlled by the preexponential term R_0.

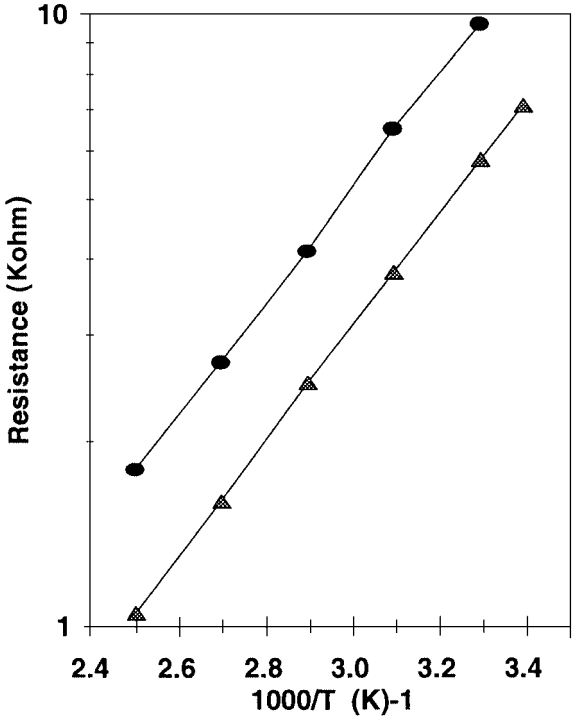

FIGURE 8.56 Resistance versus temperature behavior of spinel type NTC thermistors.

Negative temperature coefficient (NTC) thermistors are resistors that have an inverse relationship between their electrical resistance and their body temperature. As the body temperature increases, the electrical resistance decreases, and vice versa. This resistance–temperature (*R–T*) characteristic is predictable and reproducible. Electrical resistance change per degree Celsius is typically −4 to −6 percent, which provides a significant signal response to changes in temperature. Because of the large signal change with temperature, long lead lengths have virtually no effect on the accuracy of NTC thermistors. The *R–T* behavior of NTC thermistors is shown in Fig. 8.56.[118]

The materials used in thermistor inks are typically a mixture of doped transition metal oxides, RuO_2, and glass.[119] The metal oxides include Mn, cobalt (Co), Ni, iron (Fe), and Cu. Two-glass systems, each glass having different softening points, combined with compositions in the Cu–Mn–O and Co/Mn/O systems, were found to have good control of ß to ±50 over the range of 1000 to 250.[120] It is a common practice to add a conductive phase such as RuO_2 to lower R_0. A wide range of R_0 can be achieved (from 500 to 10,000 Ω/sq) by varying the RuO_2 content. Thick-film resistors with a high positive TCR are also useful as thermistors or temperature sensors. The spinel type thermistors exhibit a 25 percent tolerance in sheet resistance values, while sensor type materials exhibit a tolerance of around 10 percent.[118] Sensor-type materials are quite stable during aging at 120°C in air. Spinel-type oxides exhibit a large initial increase in resistance at relatively short times followed by a more stable response.[118]

Strain Gauge Resistors. Thick-film resistors experience a resistance value change with the application of stress. This piezoelectric property of thick-film resistors has been utilized in several pressure and strain gauge sensor applications. Thick-film resistors utilized for strain gauge applications must show a reversible relative change in resistance ($\Delta R/R$) with strain ε.[121] Strain is defined as fractional change in length ($\Delta L/L$). The relative resistance change is directly proportional to the applied strain ε and, therefore, the gauge factor GF is defined as

$$\mathrm{GF} = \frac{\Delta R/R}{\varepsilon} \tag{8.47}$$

An ideal strain gauge should exhibit a high piezoresistive effect combined with a negligible thermoresistive effect. More precisely, a high gauge factor (greater than 10) is associated with a low TCR and TCGF, where TCGF is ΔGF/GF and is called the *temperature coefficient of gauge factor*[122] and ΔT is the temperature range where ΔR and ΔGF are considered. The resistance and gauge factor should remain stable with time under operating conditions. Figure 8.57 shows the relative change of resistance under compressive and tensile stress of highly strain sensitive thick-film resistors.[123]

Commercially available strain gauges use semiconductor or metal film resistors. The former are characterized by high GF, but also high TCR and TCGF. Thick-film resistors

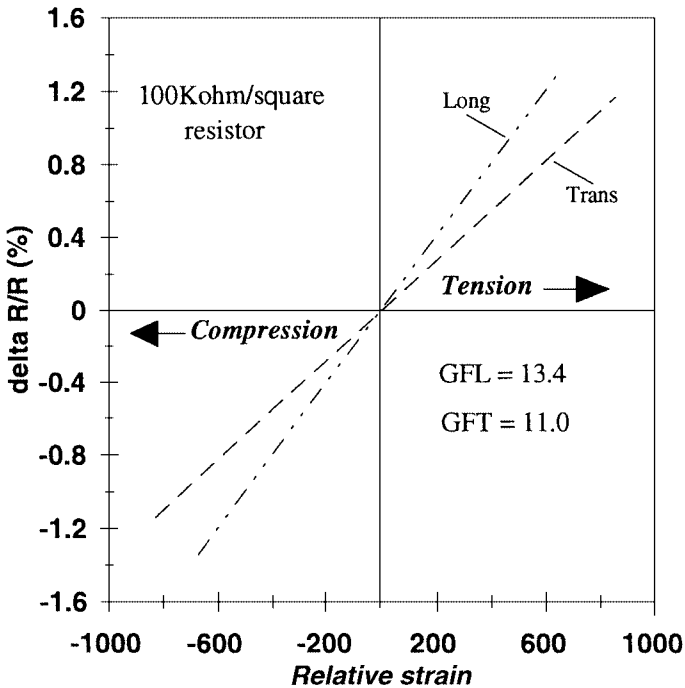

FIGURE 8.57 Relative change of resistance under compressive and tensile stress of a highly strain sensitive thick film resistor.

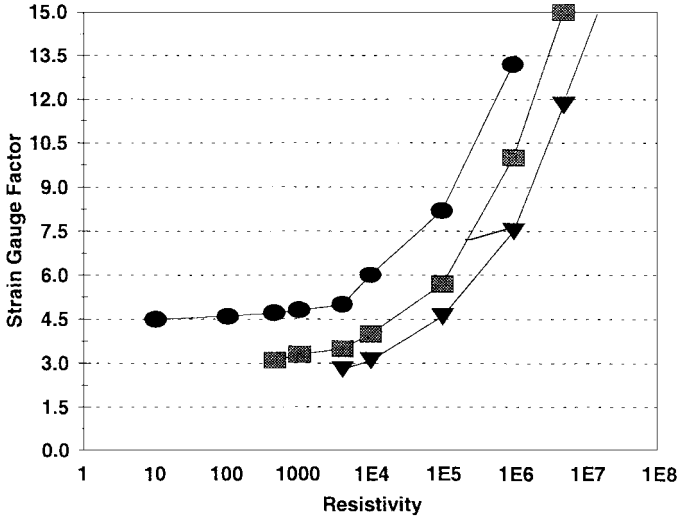

FIGURE 8.58 Effect of RuO_2 particle size on gauge factor for various resistivities.

used in strain applications must be extremely stable. A minimum in the temperature versus resistance curve near room temperature is a typical property of high GF, stable thick-film resistors. There is no scientific basis to explain this phenomenon. However, this behavior is used to identify a new thick-film resistor with improved gauge factors. The low TCR values of thick-film resistors make them more attractive as thick-film pressure sensors than semiconductor sensors. The semiconductor sensors have very high gauge factors, but their TCR values are very high, typically, ±1500 ppm/°C. Generally, the large gauge factor in thick-film resistors is due to the large particle size of glass and RuO_2 powders. Modifiers do not typically improve the gauge factor. Figure 8.58 shows that resistors with larger RuO_2 particle sizes have higher gauge factors.[124]

Resinates. Precious metal resinates are organometallic compounds in which the metal atom is attached to a sulfur or oxygen atom linked to a carbon atom.[125] When these compounds are thermally decomposed, a film is deposited on the substrate. The thermal decomposition process takes place between 250 and 500°C. Under these conditions, noble metal compounds deposit metallic films while other precursor materials deposit metal oxide films. Ruthenium resinates can be used to formulate thick-film resistors. Ruthenium resinates decompose during firing and form an RuO_2 conductive phase. Thick and thin film ruthenium resinate-based resistors are extensively used in thermal printhead applications.[126,127]

8.4.5 Resistor Properties

Microstructure Development. Thick-film resistors are prepared by formulating pastes consisting of submicrometer size conductive phase particles and micrometer size glass particles. Since conductive particles are of submicrometer size, complete mixing of conductive phase particles and glass powder is difficult to achieve because the smaller

particles tend to agglomerate to a certain extent. During screen printing and drying, conductive particles/agglomerates can segregate at the interstices of glass powder because of the density differences. Also, the smaller conductive particles can fill interstices of the glass particles. A segregated microstructure is formed even prior to firing thick-film resistors because of these factors. Although some of the conductive phase agglomerates coat the surface of the glass particles, a higher concentration of the small conductive phase agglomerates can be seen[128] in the interstices of the large glass particle matrix. During firing, the conductive phase particles rearrange themselves to form a continuous network of electrically conducting chains. These preexisting chains of conductive phase can undergo further development or degradation, depending on the thermophysical conditions during firing.

Networks of conductive phases have frequently been observed by many investigators.[128–130] Electrical conduction occurs through the networks of electrically conducting chains embedded in the glass matrix. The formation and connectivity of these conducting networks determine the microstructural development and resultant electrical properties. Thick-film resistors are very complex nonequilibrium systems whose microstructure is a nontrivial function of various materials' properties and processing parameters.

Extensive investigations have been conducted in order to develop a comprehensive model for microstructural development of RuO_2-containing thick film resistors.[52,128,129] The various stages of microstructure development and the respective sintering kinetics were studied. The important processes were determined to be glass sintering, glass wetting and infiltration, conductive phase rearrangement, and conductive phase network formation.

Resistor Noise. The random motion of current carriers causes spontaneous fluctuations in electric current, termed *electrical noise*. Current noise in thick-film resistors is called *excess noise*, as it is considered the excess noise over thermal noise. Thermal noise is predictable and is a function of resistance and temperature, whereas current noise has no definite relationship. Noise in thick-film resistors depends on the sheet resistance value, thickness of the resistor print, and geometry of the resistor. Figure 8.59[131] shows a typical plot of measured noise versus resistor area for a 200-kΩ/sq resistor. Current noise decreases as resistor area increases. Resistor noise also depends on processing conditions. Generally, noise decreases with an increase in peak firing temperature. The typical noise value for commercial thick-film resistors is shown in Table 8.20.

Sheet Resistance. The sheet resistance can be adjusted by altering the conductive phase concentration. Figure 8.60[132] illustrates the variation of sheet resistivity as a function of conductive phase concentration for various systems. The relationship between volume fraction and electrical properties of a heterogeneous system consisting of a conducting phase and an insulating phase was studied by several people, including Avogadro, Faraday, Lorents Clausias, Lorentz, and Maxwell. Various theoretical models such as percolation theory, effective medium theory, and perturbation theory have attempted to explain the variation of sheet resistivity of thick-film resistors in terms of conductive phase concentration. The theoretical models developed by Pike,[133] Smith and Anderson,[134] and Ewen and Robertson[135] all assume a fixed idealized microstructure for thick-film resistors. Pike developed a bond percolation model to explain the connectivity in thick-film resistors, commencing with a small volume fraction of the conductive phase. According to his model, the larger size glass particles are closely packed and the smaller size conductive particles occupy the interstices. The conductive particles form partial bonds in a lattice of connecting interstices. Smith and Anderson[134] developed a model based on effective medium theory. In their model, they considered the size difference between conductive phase and glass particles. They developed an equation for resistivity in terms of volume fraction, particle size ratio, resistivity of a

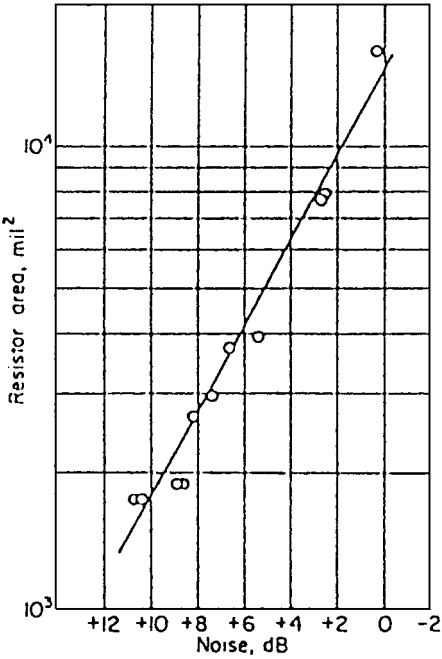

FIGURE 8.59 Measured noise versus resistor area for a 200-kΩ/sq resistor.

representative unit in the network, and a probability parameter related to the distribution of conductive phase particles.

Ewen and Robertson[135] developed a site percolation model to explain the variation of resistance as a function of conductive phase concentration. In their model, they used a packing fraction for glass and conductive phase particles and an empirical parameter which explains how effectively the conductive phase particles fill the random lattice.

Statistical loading curve models have been proposed that take into account the segregated nature of thick-film resistors. A systematic microstructure development study has been conducted by Vest[52] for RuO_2 model thick-film resistors. Vest[136] proposed a statistical loading curve to explain the sheet resistivity variation as a function of volume fraction of the conductive phase and particle sizes of both the conductive phase and glass. Several theoretical models have been developed to explain the variation of resistivity as a function of volume fraction of the conductive phase. A comprehensive model to explain the sheet resistivity variation in thick-film resistors in terms of composition and physicochemical properties of powders over the entire resistance range has not been developed to date.

Temperature Coefficient of Resistance. The TCR of a thick-film resistor is typically less than ±100 ppm/°C. The TCR of the conducting oxide used in the resistor formulation is typically several thousand ppm/°C (the TCR of RuO_2 is 5760 ppm/°C).

Lead borosilicate glass has an extremely large negative TCR, with its resistivity showing an exponential temperature dependence. The typical temperature dependence of resistance behavior for a thick-film resistor is shown in Fig. 8.61. This behavior has led to

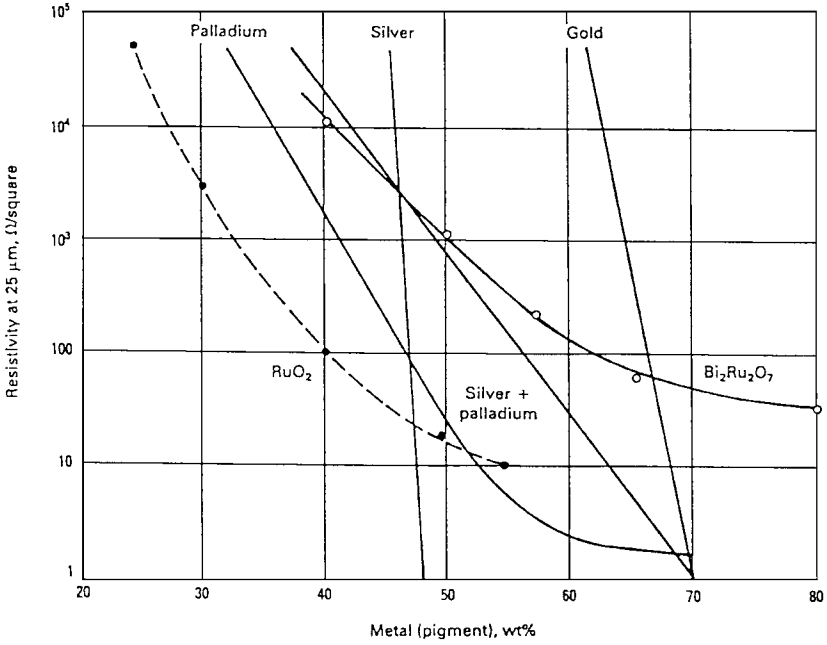

FIGURE 8.60 Variation of sheet resistivity as a function of conductive concentration for different conductive phases.

the development of large numbers of diverse explanations and resultant models to explain this behavior. The R versus T curve typically shows a minimum in sheet resistance near room temperature. The TCR of a thick-film resistor is not a constant because the resistance is not a linear function of temperature. The more commonly observed behavior is a shallow minimum in resistance at some temperature as shown in Fig. 8.61. As a result of this behavior, TCR values of thick-film resistors are low. The variation of resistance with temperature is determined by the microstructure and charge transport mechanisms of thick-film resistors. The temperature dependence of resistance is a function of the arrangement of conducting chains in the insulating matrix and the charge transport through these chains. Variables such as material parameters and processing conditions can, therefore, influence the microstructure development and resultant temperature dependence of resistance and TCR values of thick-film resistors.

Charge transport through the conductive particle is metallic conduction. Resistance to charge transport through the conducting chains is due to particle and grain boundary resistance. However, charge transport through the insulating glass is very different and has to be explained by charge transport mechanisms that occur in insulating films.

Voltage Stability. Thick-film resistors are required to be stable under an applied voltage. Voltage stability of resistors depends on the microstructure of thick-film resistors, glass chemistry, and conductive phase types used to formulate the resistors. Recent trends in hybrid microelectronics require resistors with higher voltage stability. The power handling characteristics of commercial thick-film resistors are shown in Table 8.20.

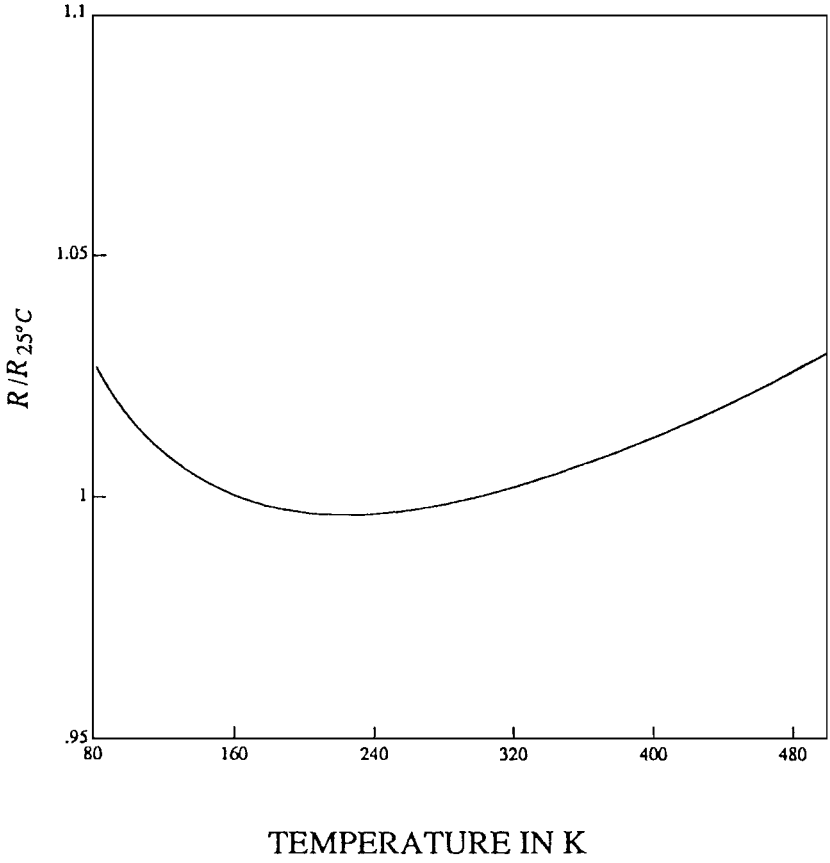

FIGURE 8.61 Typical temperature dependence of resistance behavior for an RuO_2 thick film resistor.

Surge Properties. Fractional ohm resistors are commonly used in telecommunications for surge protection applications. The resistors used in this application require excellent stability under electric surge with low sheet resistance and TCR. Voltage surges due to lightning and switching are very short and typically subside within microseconds. Such pulses can be extremely destructive, since surge currents can produce intense heat. Any thick-film resistor used in a protective circuit should withstand instantaneous current and effectively dissipate the heat generated. During this process, the resistor should remain stable. Generally, these resistors are tested for stability against repetitive pulses.

During lightning strikes, very high voltages can be transmitted through telephone lines. It is very hard to predict the magnitude of the voltage and type of voltage pulse that may be produced during lightning strikes. There are several standards, such as those of the U.S. Federal Communications Commission (FCC), Underwriters Laboratories (UL), the Institute of Electrical and Electronics Engineers (IEEE), and Bellcore, which specify the exact shape of a pulse or its wave form and the number of pulses to be used for testing.

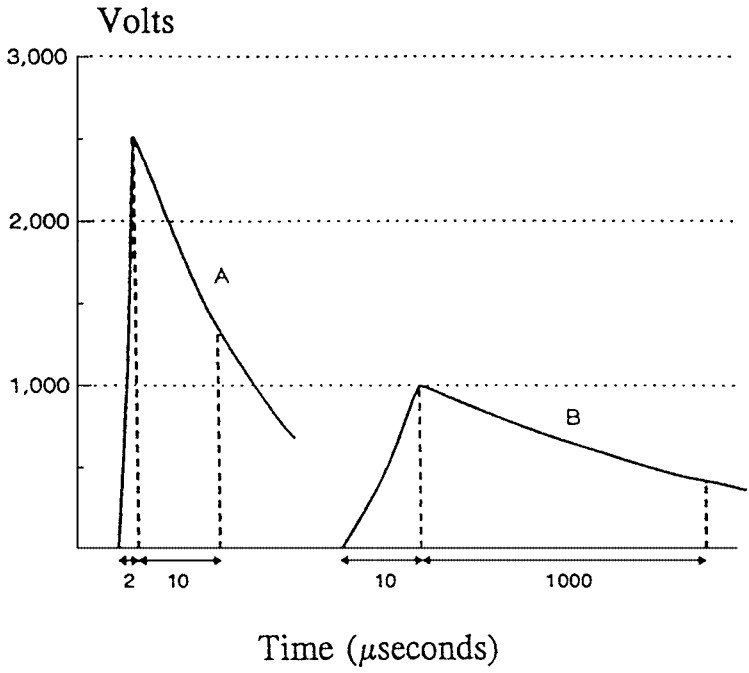

FIGURE 8.62 Various surge waveforms used to test resistors.

Wave shapes that are typically used to test the surge resistor are shown in Fig. 8.62. The surge handling capability of resistors is considered excellent when the drift due to repetitive voltage pulsing of different shapes is low as shown in Table 8.17. These low drift values are typical of state-of-the-art thick-film resistors for surge applications.

Thermal Stability. After laser trimming and overglazing, resistors are generally tested for shift in resistance in thermal aging, thermal shock, and hot column tests. Typically, commercial thick-film resistors change less than 0.5 percent in resistance after these tests. Thermal aging is done by storing parts at 150°C for 1000 h. Typical change in resistance due to thermal aging for stable resistors from 10 Ω/sq to 1 MΩ/sq is less than 0.1 percent. (The relative change in resistance as function of storage time at 125°C is shown in Fig. 8.63 for 1 kΩ/sq resistors.)

Hot column stability testing is done by placing the test substrate with resistors on a hot stage at 400°C for 5 min, with a subsequent quench to room temperature. The shift in resistance values is then recorded. Stable resistors experience minimum change from this test. Stability of resistors after thermal shock is shown in Fig. 8.64. The stability of resistors can also be tested by subjecting them to a thermal cycle test which consists of 5 cycles of 5 min at −65°C, transfer within 10 s to +150°C, and a dwell of 5 min before transfer back to −65°C. The stability of commercial thick film resistors is considered acceptable if changes in resistance of less than ±0.2 percent result from this test.

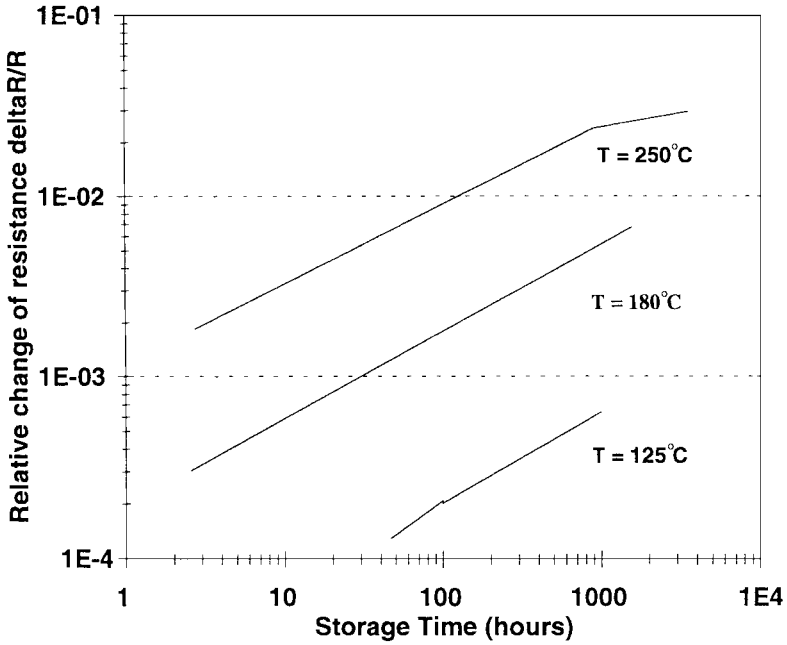

FIGURE 8.63 Relative change in resistance as a function of storage time for 1-kΩ/sq resistors.

8.4.6 Effects of Variables on Electrical Properties

Peak Firing Temperature. The effect of peak firing temperature on resistance of different decade value resistors is shown in Fig. 8.65. Sheet resistance values decrease with an increase in peak firing temperature for high-value resistors. As firing temperature increases, the glass viscosity is reduced. The primary way in which glass affects the electrical properties is by controlling the formation of three-dimensional conductive phase networks. As temperature increases, the conductive particles rearrange to form an increased number of conductive chains, which can result in decreased sheet resistances. The effect of peak firing temperature on TCR values of resistors is shown in Fig. 8.66. TCR values typically become more positive for high-value resistors as temperature increases. However, for low-value resistors, the increase in firing temperature results in an increase in the resistance and more negative TCR values. The peak firing temperature has a different effect on the microstructure formation of low-value resistors because of the low glass concentrations; glass may flow better at higher temperatures and form thin barriers around conductive phase particles.

Firing Time at Peak Firing Temperature. An increase in firing time at peak temperature produces conductive phase rearrangement, which alters the number of three-dimensional conducting chains. If this rearrangement can increase the number of conducting chains, the resistance will decrease and TCR values will become more positive. The effect of firing time on R and TCR at peak firing temperature is shown in Fig. 8.67. As in most

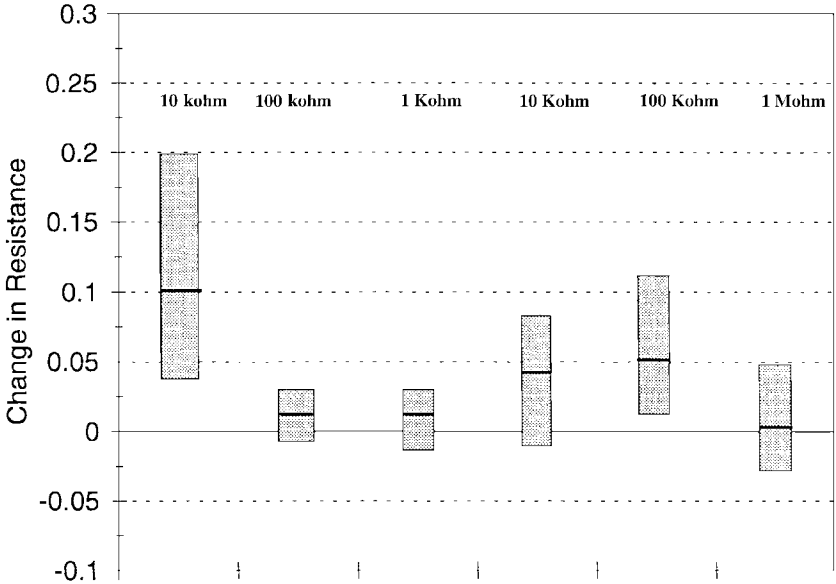

FIGURE 8.64 Stability of thick-film resistors subjected to thermal shock test.

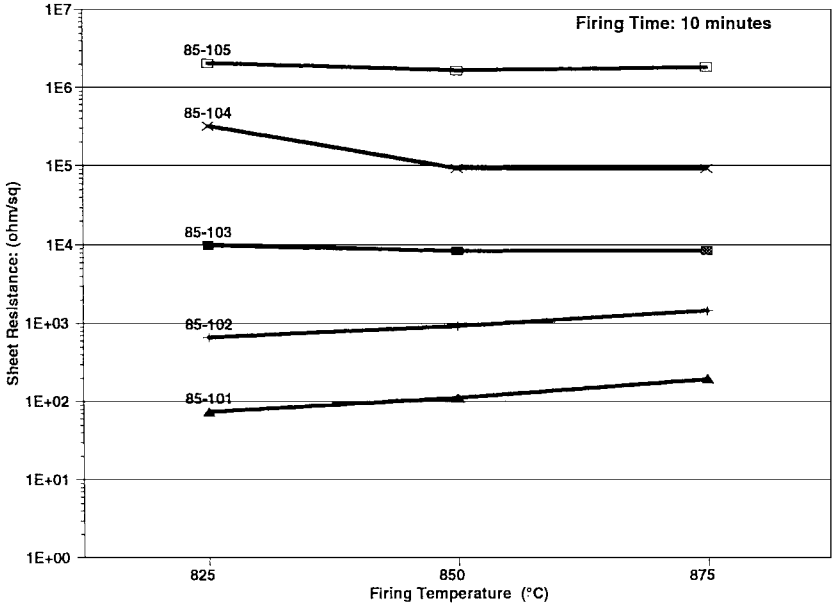

FIGURE 8.65 Effect of peak firing temperature on sheet resistance for decade value resistors.

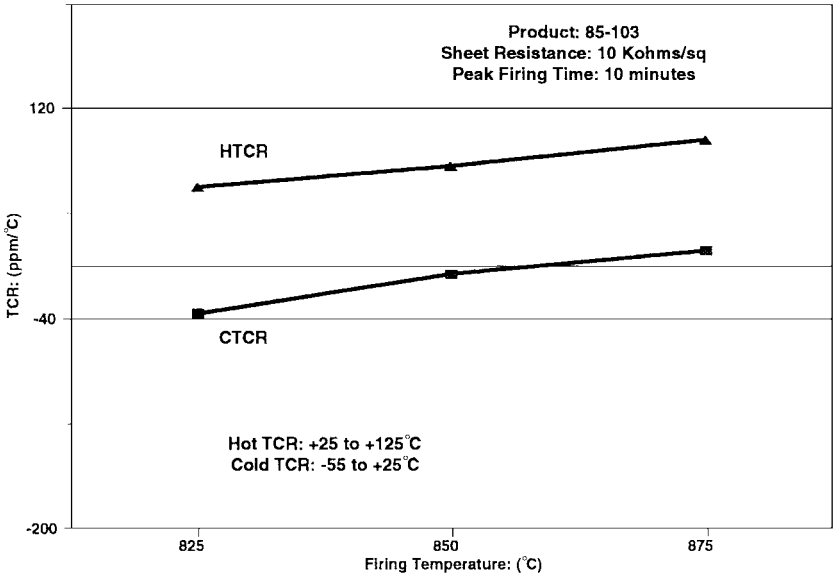

FIGURE 8.66 Effect of peak firing temperature on TCR values of a 10-kΩ/sq resistor.

kinetic processes, temperature has a greater impact on properties than time and must be more tightly controlled.

Particle Size and Electrical Properties. The effect of glass particle size on sheet resistance of a model thick-film resistor is shown in Fig. 8.68[137] for various conductive phase concentrations. The effects of glass particle size are more pronounced at low conductive phase concentrations. The effect of conductive phase particle size on electrical properties of thick-film resistors was studied by several researchers.[115–117,137] For a given volume fraction of conductive phase, smaller particle sizes will decrease the sheet resistance and render the TCR more positive.

Termination Effects. Sheet resistance can be affected by the type of conductor material used to terminate the resistor. Several techniques have been developed to demonstrate the interaction between conductor and resistor at the termination interface. Figure 8.69[138] illustrates the observed resistance as a percent of total resistance when the profile point is moved from one termination interface to another. This technique shows that the resistance value and interaction between conductor and resistor can be studied by observing the nonlinearities in the resistance vs. length curve. The region very close to the conductor shows a nonlinear relationship between length and resistance because of conductor–resistor interfacial interactions.

The ideal geometry of a terminated resistor is shown in Fig. 8.70*a*. The resistor overlap area will always be thicker since the resistor is typically printed on top of the fired conductor. If the current flux is uniform throughout the resistor and conductor–resistor interface, there are no geometry effects. However, if there is conductor bleed-out during resistor firing, then the current flux will not be uniform and current crowding can lead to hot spots at the edge of the conductor, as shown in Fig. 8.70*b*. A change in resistance due

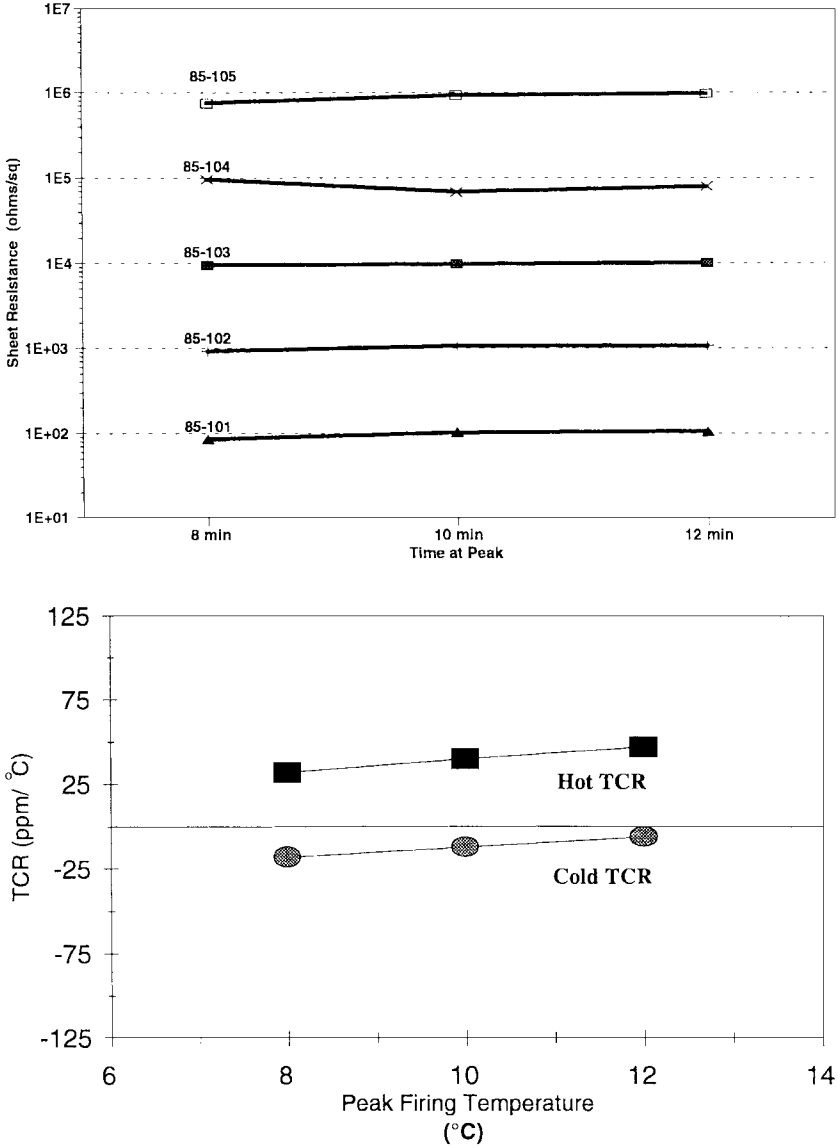

FIGURE 8.67 Effect of firing time at peak firing temperature (850°C) on electrical properties of (10-kΩ/square) resistors.

to a local increase in temperature will occur at the hot spots. This will result in a nonuniform resistance at the conductor–resistor interface.

The observed variation in resistance along resistor length is due to chemical interactions at the conductor–resistor interface. The ideal voltage distribution along the length of a resistor is shown in Fig. 8.71 for low- and high-resistance values. The diffusion of

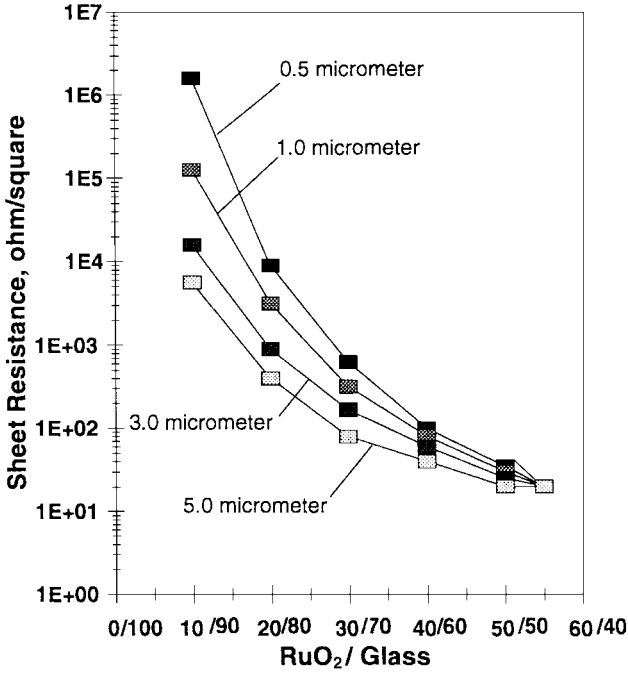

FIGURE 8.68 Effect of glass particle size on sheet resistance of model thick-film resistors.

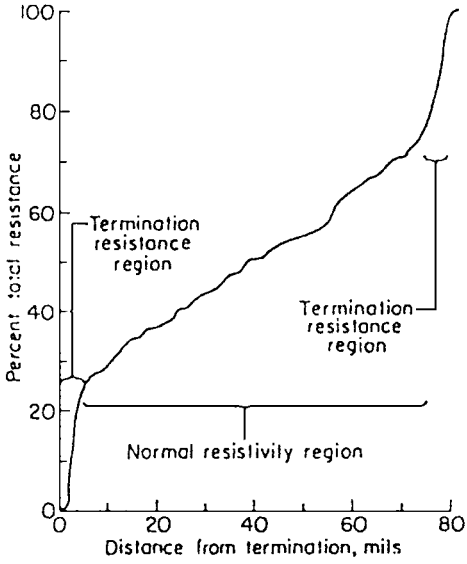

FIGURE 8.69 Effect of resistance as a function of length of a thick-film resistor.

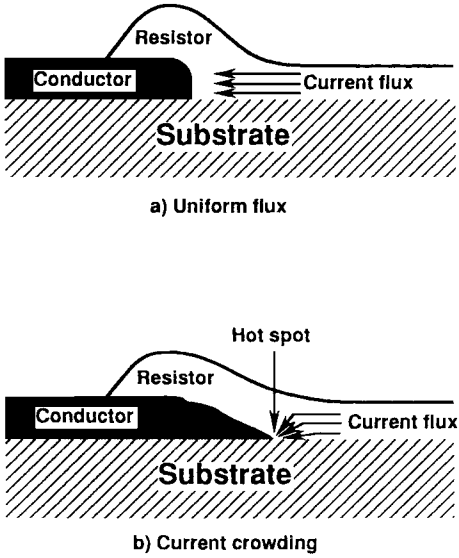

FIGURE 8.70 Current flux at the resistor–conductor interface.

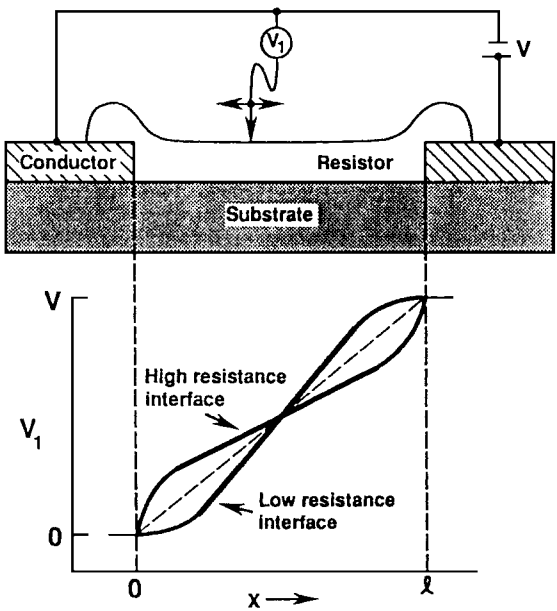

FIGURE 8.71 Ideal voltage distribution along the length of a resistor.

conductor material into the resistor during resistor firing will result in low resistance. This is most commonly observed in conductors which contain silver. This correlates well with the diffusion rates of metals. The chemical interactions between resistor and conductor materials can change the microstructure of the resistor near the interface and will result in higher resistance in that region. This can also increase current noise in thick-film resistors. The effect of various types of conductor terminations on sheet resistance and TCR is shown in Fig. 8.72.

Another technique used to demonstrate conductor–resistor interactions is the determination of aspect ratio. The aspect ratio variations for both an ideal resistor and a resistor experiencing interfacial interactions are shown in Fig. 8.73. The data presented in these figures are very useful for the design engineer, who must account for all geometry effects as well as termination effects for thick-film resistor design. The effect of resistor length and geometry on resistance of thick-film resistors is shown in Fig. 8.74*A* and 8.74*B*.

8.4.7 Conduction Mechanisms

A considerable amount of research has been done in attempts to understand conduction mechanisms in thick-film resistors. However, there is no common agreement among researchers in explaining these mechanisms. Pike and Seager[133] proposed a tunneling barrier model to explain the small activation energy associated with the shallow minimum in resistance

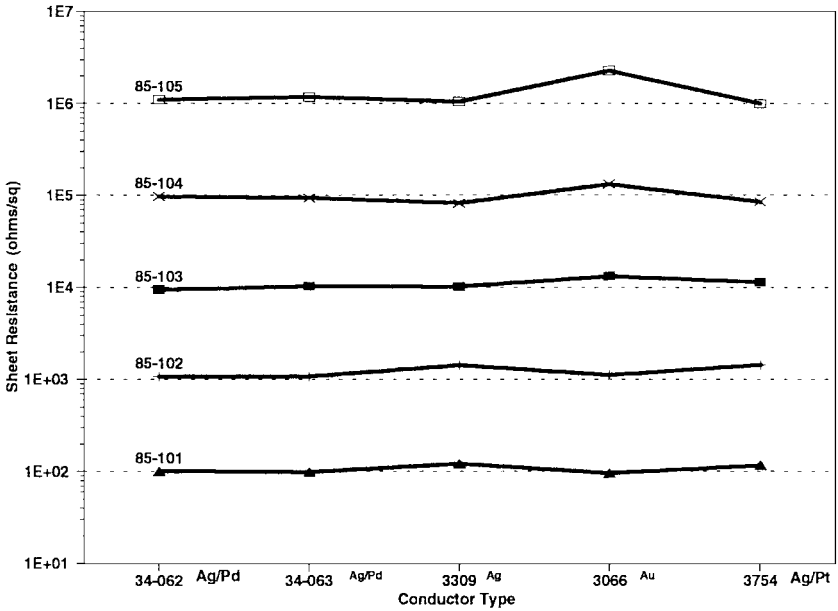

FIGURE 8.72 Effect of conductor termination on electrical properties of resistors.

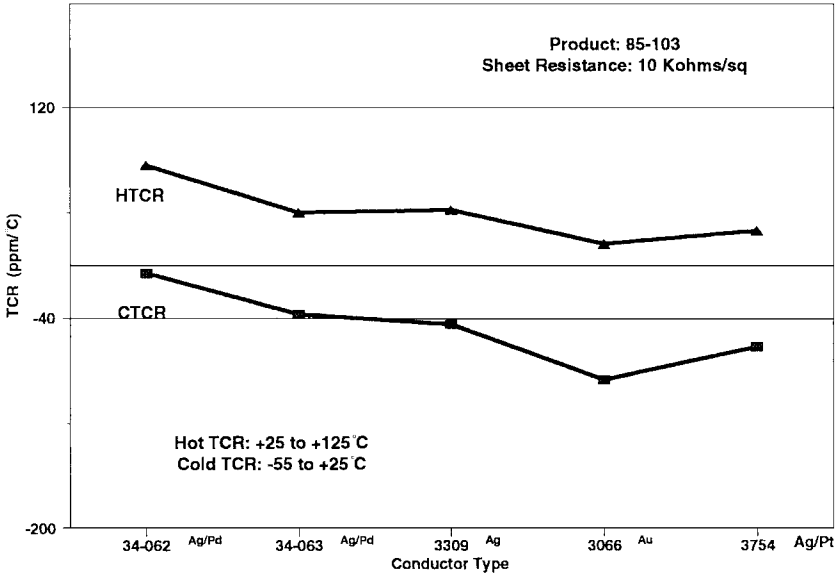

FIGURE 8.72 (*Continued.*)

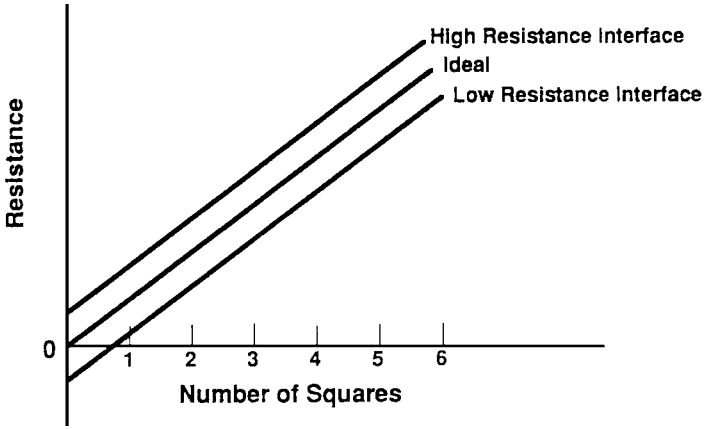

FIGURE 8.73 Aspect ratio variations for both ideal and typical resistors.

versus temperature behavior of thick-film resistors. In explaining the conduction mechanism, they assumed a simple metal–insulator–metal (MIM) unit as the typical microstructure of thick-film resistors, and concluded that the conduction mechanism through the insulating glass is thermally activated tunneling. According to their model, the small activation energy is associated with electrostatic charging of the fine conductive particles.

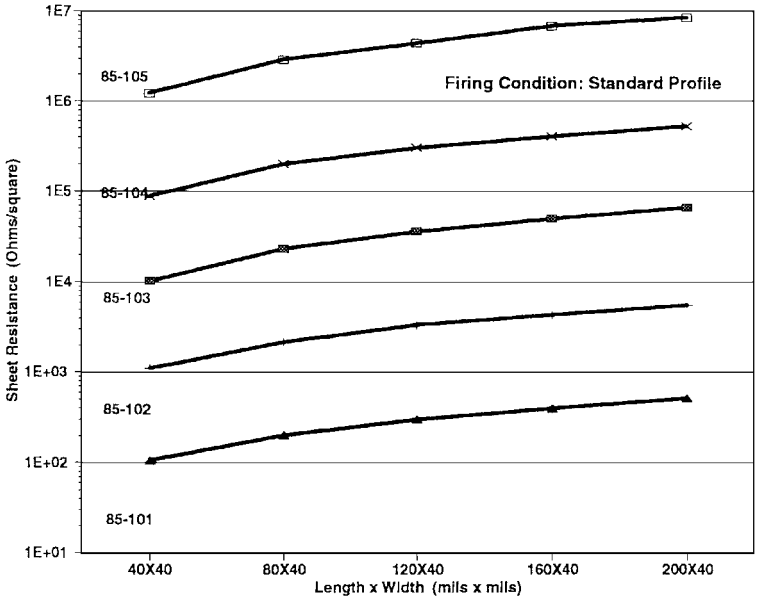

FIGURE 8.74*A* Effect of resistor length on sheet resistance of resistors.

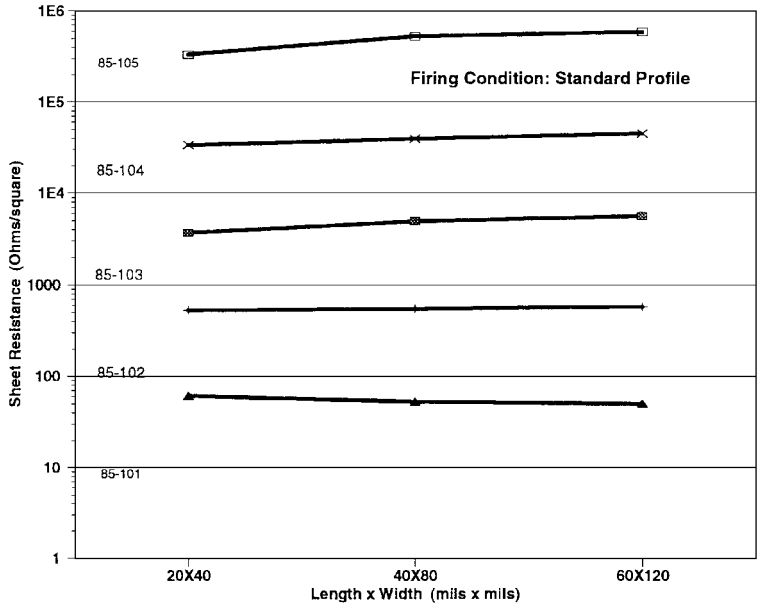

FIGURE 8.74*B* Effect of resistor geometry on sheet resistance of resistors.

The model also assumed that the presence of impurities within the tunnel barrier can act as resonant centers to increase the barrier transmission coefficient. Hill[139] proposed an alternative model with the assumption that doping impurities in the glass interface form narrow bands. Smith and Anderson[140] developed another model by combining the tunneling barrier and narrow band models and concluded that both mechanisms occur together. Halder[141] proposed that the electron transport in thick-film resistors is due to both tunneling and hopping mechanisms. Prudenziati et al.[142] proposed a model with a temperature-dependent tunneling barrier height and width without taking into account the resistance of the conductive phase. Vest[143] proposed a multipath model for thick-film resistors in which the dominant carrying paths were viewed as a series of parallel resistors, each having a parallel path consisting of resistors with different numbers of sintered and nonsintered contacts. The equivalent resistance of these paths and their temperature dependence is a function of the number of sintered and nonsintered contacts, the geometry of the contacts, and the respective conduction mechanism.

It has been demonstrated that, by considering simple resistor microstructures and utilizing the multipath model, conduction mechanisms with very high activation energies (0.5 eV) can be used to explain the temperature dependence of resistors which exhibit very low activation energies.[144] However, no single quantitative model developed thus far completely explains the conduction mechanism of thick-film resistors.

8.4.8 Laser Trimming

Hybrid thick-film resistors are required to meet tight tolerances of ±0.1 percent. Because of the complex nature of thick-film resistors, they cannot be consistently fired to a predetermined resistance value with the required tolerances. Therefore, the resistors are laser-trimmed to the target value by removing part of the resistor material with a laser. The material removal process in thick-film resistors is called *laser trimming*. Generally, design engineers will choose resistance values for a given circuit such that the as-fired distribution will remain below the final target value. The resistors can then be trimmed to the target value by decreasing the effective width of the resistor, which in turn increases the resistance value.

In laser trimming, materials are actually removed by short duration, high intensity, coherent light pulses. The material absorbs the light energy, which causes it to heat rapidly and vaporize. The typical volume of thick-film resistor removed by a single laser pulse is on the order of several cubic micrometers (μm^3). A laser cut is produced by a succession of overlapping laser pulses as shown in Fig. 8.75.[145]

For thick-film resistor trimming, a neodymium-doped yttrium aluminum garnet (Nd: YAG) laser operating at 1.06-μm wavelength is typically utilized. There are several important parameters in laser trimming. Q rate is defined as the number of laser pulses issued per second. Byte size is the amount of incremental material affected by each laser pulse. Kerf width is the outer width of the cut. Trim speed is the rate of materials removed in inches per second. The laser operation is typically in the Q-switch mode and the laser beam pulses are focused by galvanometer mirrors. The resistance is continuously monitored and as soon as the desired resistance values are obtained, a closed-loop control system shuts off the laser power. Because of the complexities and variations of laser cut parameters, the combination of byte size, Q-rate, and laser power which can produce an optimum laser cut for a particular material must be experimentally determined. High throughput, trim accuracy, and stability are goals of these experiments for ultimate trim parameter recommendation.

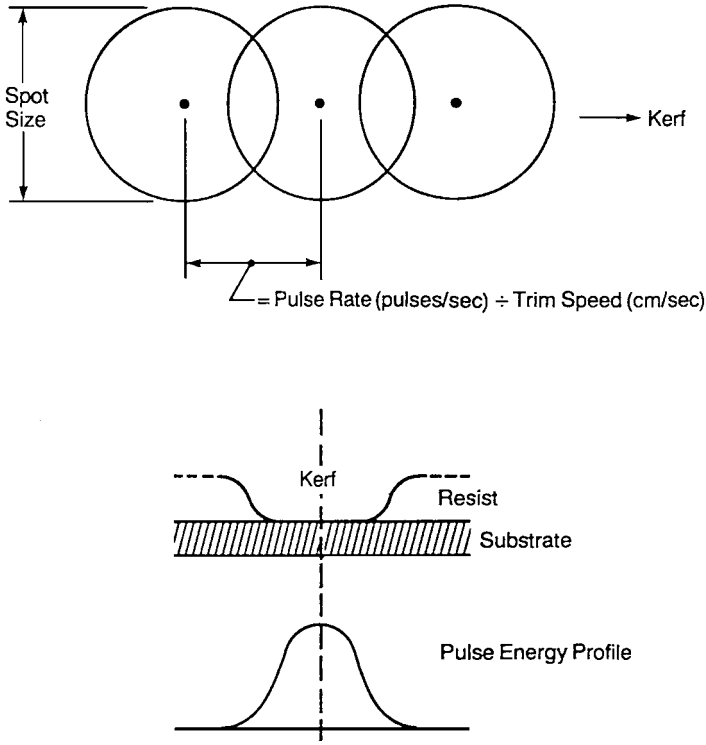

FIGURE 8.75 Overlapping of successive laser pulses which produce a laser cut.

Types of Cuts. Laser trims made on thick-film resistors can be categorized into three major groups: plunge cuts, L cuts, and double cuts.

PLUNGE CUTS The fastest cut that can be used to trim a resistor is the plunge cut. It also provides the lowest amount of laser exposure to the resistor. The disadvantage of this type of cut is that resistors with high accuracy cannot be achieved because of rapid change in the resistance value as the cut approaches the other side of the resistor. The increase in resistance with laser cut length is shown in Fig. 8.76. In general, if the initial value of the resistor prior to trimming is close to the target value, then reasonable control and accuracy can be achieved.

L CUTS L cuts are used to avoid the problem of rapid resistance change which is inherent in the plunge cut. First, the resistor is trimmed linearly toward the opposite side of the resistor until the resistance begins to change rapidly. The laser trim direction is subsequently changed to run along the length of the resistor for more accurate control. The laser cut, however, exposes the resistor to a greater amount of laser damage. Studies suggest that the L cut produces a narrow distribution of resistance about the target and maintains a low current noise after trimming. The lower noise index in thick-film resistors is achieved

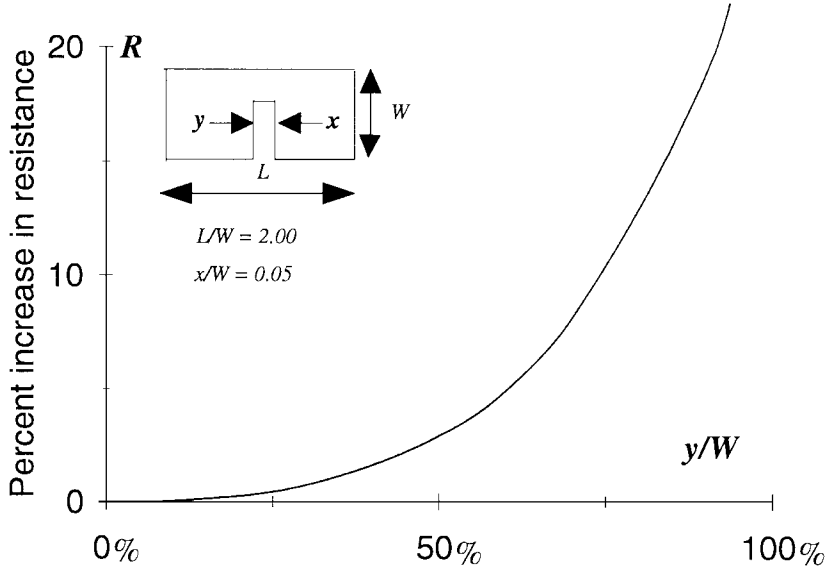

FIGURE 8.76 Increase in resistance with laser cut length.

by removing resistor material parallel to the current flow, which retains uniform flux lines. In the case of the L cut, the length of the laser cut and trim times are longer. Also, a larger amount of resistor material remains. If the L cut extends too far into the other side of the resistor, microcracks will form and propagate and cause large variations in resistance after completion of the laser trim.

DOUBLE PLUNGE CUTS Double plunge cuts are also used to avoid rapid resistance changes during trimming. During the first cut the resistor is trimmed to a specified resistance value (e.g., 80 percent of total trim target), which permits the second cut to trim the resistor at a slower rate. The second cut works in the "shadow" of the first laser cut. In order to make this method effective, the second cut should be shorter than the first cut. Laser damage due to double cuts is less than that of the L cut because microcracks perpendicular to the kerf do not cause the resistor to open. Double cuts also have less laser trim length than L cuts.

SERPENTINE CUTS The serpentine cut is very similar to a double cut except that it is used to increase the resistance by a large amount. It consists of a series of short plunge cuts on opposite sides of the resistor. This is done by increasing the length of the current path. The increase in the length of current path is a function of the depth of cuts and their locations.

Drift Due to Trimming. Laser trimming produces a very severe thermal shock in thick-film resistors and can lead to microcracking in the neighborhood of the kerf. These microcracks can cause resistance drift during storage at elevated temperatures.

Thick film resistors with tight tolerance values can be predetermined by calculating the drift due to trimming and subsequent processes prior to setting target values. This is possible only if the resistor drift is both predictable and repeatable.

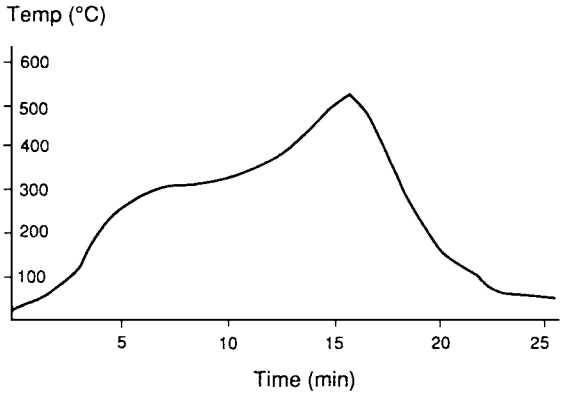

FIGURE 8.77 Typical firing profile (505°C) used to fire overglaze.

8.4.9 Overglazing of Resistors

Thick-film resistors are often overcoated with a glaze material to protect against the environment, chemical attack, and mechanical abrasion. The typical material used is lead borosilicate glass, which usually fires at or below 550°C. When thick-film resistors are refired, there is a drift in sheet resistance associated with this process. Overglazes are typically designed to fire at lower temperatures in order to minimize this drift. The color of overglazes is generally green to facilitate laser trimming of resistors; the laser energy absorption of green material is excellent because of the wavelength matching with Nd:YAG laser light. The thermal expansions of the glazes are matched to that of the substrate to avoid any cracks due to thermal stresses.

A typical firing profile for processing an overglaze is shown in Fig. 8.77. Low-temperature firing of overglazes can also serve as an annealing treatment for both resistors and glazes to avoid any stress buildup in the resistor.

8.5 RHEOLOGY AND THE SCREEN PRINTING PROCESS

8.5.1 Introduction

Rheology is the study of flow and deformation of materials. It is sometimes confused with the viscosity of a material. The viscosity of a material is its resistance to flow. Viscosity is but one aspect of rheology. The study of rheology includes viscous as well as viscoelastic response of the material, the ability to thin and thicken with increasing stress, and the concept of yield point, i.e., the point at which material begins to flow.

Thick film preparation and applications involve flow phenomena. The control of rheological behavior of thick-film inks is important for the screen printing operation. Print thickness and print resolution are directly affected by paste rheology. Paste viscosity is used as a quality control tool by circuit manufacturers. For the paste manufacturer, understanding the correlation between the paste formulation and rheology is important for reproducible product manufacturing and new product development.

A number of excellent books and review articles are available on rheology.[146–153] In this section, rheology concepts and examples related to the manufacture of thick-film inks and paste flow behavior during and after screen printing will be examined.

8.5.2 Viscosity

The viscosity of a liquid is the property that defines resistance of the liquid to flow. The viscous nature of the liquid is due to the molecular attraction that offers resistance to flow. To understand the concept of viscosity, consider the model illustrated in Fig. 8.78. Two parallel plates are separated by a distance x and the space between the plates is filled with a viscous liquid. The bottom plate is held stationary. A force F is applied to the top plate, of area A, in a tangential direction so that the top plate moves with a constant velocity V in the y direction, parallel to the bottom plate. A thin layer of liquid adjacent to the plate will move with the same velocity as the plate. This is the *no-slip* assumption and holds true for most liquids. Thus, the liquid molecules near the top plate surface will move with a specific velocity V, while velocity at the bottom plate will be zero. Molecules in the liquid layers between these two plates will move at an intermediate velocity.

The tangential force acting per unit area is called the shear stress σ and is given by the following equation:

$$\sigma = \frac{F}{A} \tag{8.48}$$

The units of shear stress are N/m^2 or dyn/cm^2.

The shear rate $\dot{\gamma}$ is related to the velocity gradient (dV/dx) across the gap. Shear rate is defined by the following equation:

$$\dot{\gamma} = \frac{dV}{dx} \tag{8.49}$$

The units of shear rate are (m/s)/m, i.e., 1/s or s^{-1}.

Viscosity η of the liquid can be defined in terms of two measurable quantities, i.e., shear stress and shear rate, as follows:

$$\eta = \frac{\sigma}{\dot{\gamma}} \tag{8.50}$$

The International System of Units (SI) unit of viscosity is the pascal-second or $N/m^2 \cdot s$. A commonly used centimeter-gram-second (cgs) system unit of viscosity in the thick film industry is poise ($dyn/cm^2 \cdot s$). The following relation exists between various units:

1 Pa · s (pascal-second) = 10 poise (P) = 1000 centipoise (cP)
= 1000 millipascal-second (mPa · s)

For example, the viscosity of water at 20.2°C is 1 cP or 1 mPa · s.

8.5.3 Classification of Rheological Behavior

Thick-film pastes are two-phase mixtures of solid particles dispersed in a continuous organic phase. If the particle size of the solid phase is smaller than 1 μm, the two-phase mixture is called a *colloidal dispersion*. For suspensions, the solid particle size is greater than 1μm. The rheological properties of the dispersion are dependent on the nature of the

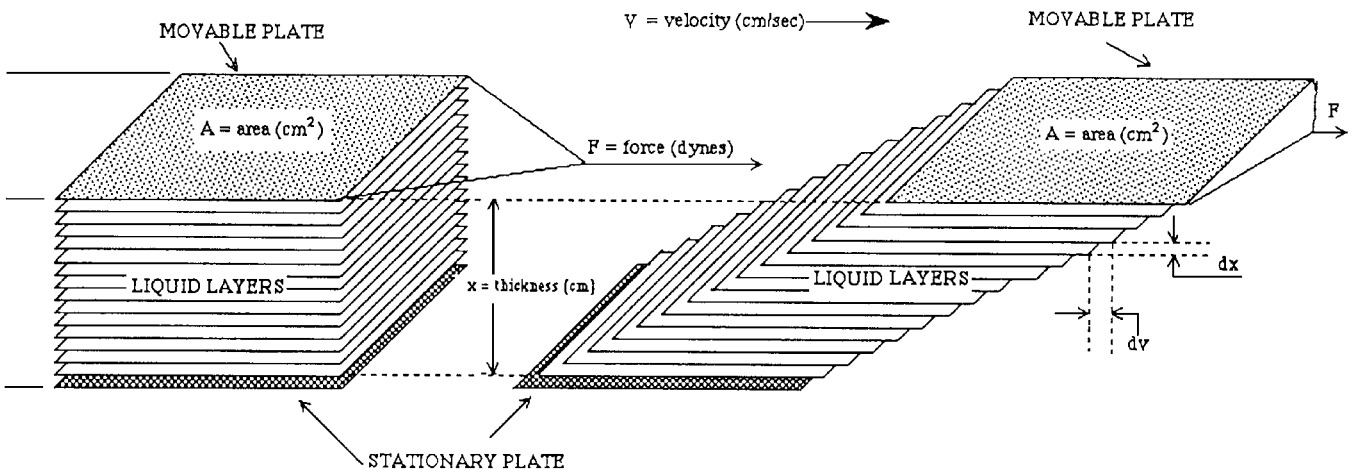

FIGURE 8.78 Schematic diagram illustrating the flow behavior of a newtonian liquid in a parallel plate arrangement.

components and also on the interactions between these two phases. Dispersions can be classified into two broad categories based on rheological behavior: (1) newtonian and (2) nonnewtonian.

Newtonian Flow. Newtonian flow behavior is characterized by a linear relation between the shear stress and shear rate. In this case, the viscosity is independent of the applied shear rate or stress and is a material constant. Materials exhibiting shear-independent viscosity are called *newtonian* fluids. Newtonian flow behavior is generally exhibited by solvents, dilute polymer solutions, and dispersions. Thick-film pastes rarely show newtonian flow behavior, although the concept is sometimes used in the theoretical analysis of screen printing behavior.

Nonnewtonian Flow. Materials which do not strictly follow newtonian flow behavior are called *nonnewtonian fluids*. For nonnewtonian materials, it is convenient to define an apparent viscosity, η_a,

$$\eta_a = \frac{\sigma}{\dot{\gamma}} \tag{3.51}$$

where η_a is a function of $\dot{\gamma}$ .Thus, it is not sufficient to characterize materials by measuring viscosity at a single shear rate. The material is characterized by describing the relationship between the shear stress and shear rate. This type of plot is referred as a *flow diagram*. Nonnewtonian materials also show time-dependent flow behavior, whereby the viscosity is a function of shear stress or rate and time.

Dispersions can behave either as pure viscous substances or viscoelastic materials. In the case of viscous substances, the deformation does not recover after the stress has been removed. Part of the deformation can be recovered after the removal of shear stress for viscoelastic materials. Thick-film pastes may exhibit both time-dependent and viscoelastic flow behavior. The classification of flow behavior is shown in Table 8.21. Various types of flow behavior are shown in Fig. 8.79. This figure shows the plots of shear stress versus shear rate and corresponding plots of viscosity versus shear rate.

Shear Thinning Flow. Dispersions showing a decrease in viscosity with shear rate (or shear stress) are described as *shear thinning* or *pseudoplastic*. Shear thinning behavior is generally produced by the reversible breakdown of suspension structures or alignment of anisotropic particles due to shear.

TABLE 8.21 Classification of Fluid Flow Characteristics

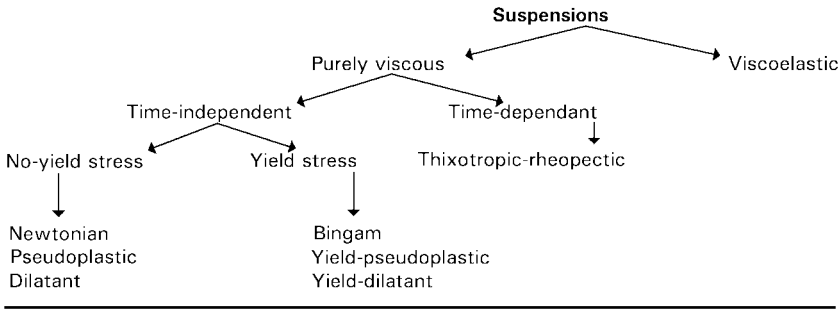

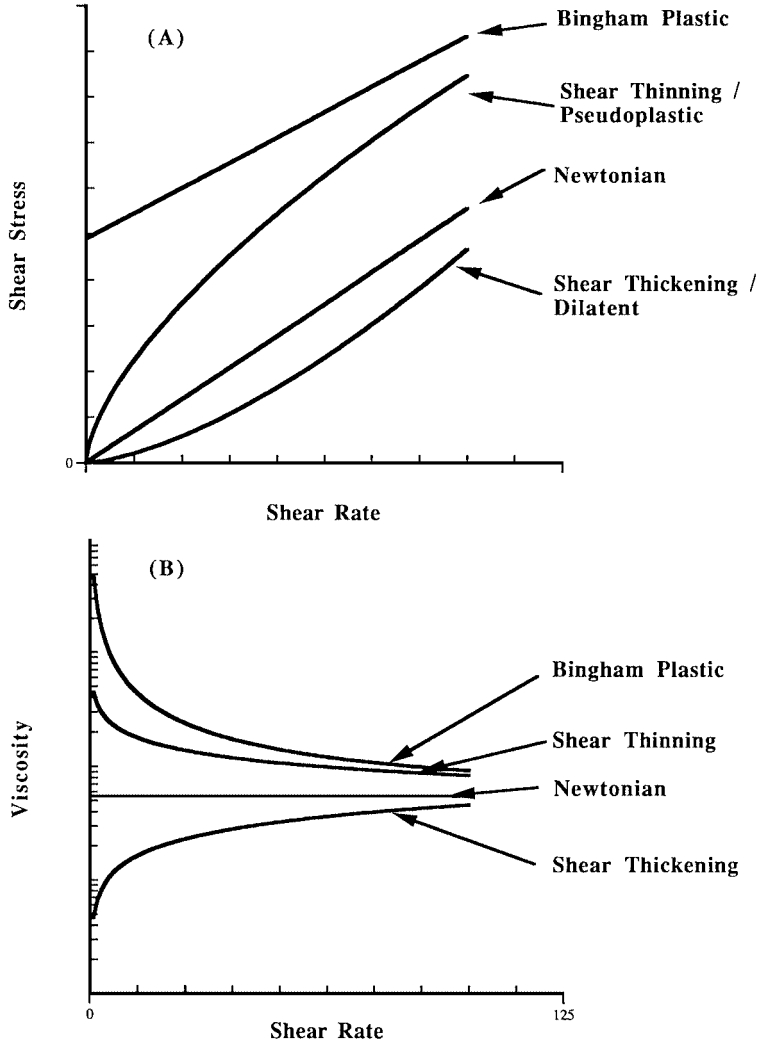

FIGURE 8.79 Plots of (A) shear stress versus shear rate and (B) viscosity versus shear rate for various types of flow behavior.

Shear Thickening. Dispersions showing an increase in viscosity with increasing shear rate are called *shear thickening* or *dilatant* materials. This type of flow behavior is usually exhibited by dispersions of rigid particles at high concentrations. Thick-film pastes rarely show this type of flow behavior.

Bingham Plastic. Bingham plastic dispersions exhibit a yield stress σ_y, the minimum shear stress that must be exceeded to initiate flow. Below the yield stress it is generally assumed that the material behaves as an elastic solid (i.e., it can deform but it does not flow). The presence of a yield stress indicates strong interactions between the particles

and the presence of a suspension structure. Once the yield stress is reached, flow starts and the Bingham plastic dispersion behaves as a newtonian dispersion; i.e., the excess shear stress is proportional to the shear rate. The slope of this straight line is called the plastic viscosity η_p.

After the yield point, dispersion may show yield shear thinning or yield shear thickening flow behavior. Thick-film pastes often show a yield point. The importance of yield point in paste flow behavior will be discussed later.

Thixotropy. For the dispersions discussed above, it was assumed that for a given shear stress there is only one associated shear rate (or viscosity). Thus, it was assumed that the measured viscosity is independent of other factors such as shear history and time.

Dispersions showing time-dependent flow behaviors are called *thixotropic* dispersions. There is a gradual decrease in viscosity with time when a constant shear stress (or shear rate) is applied. After removal of the stress, the viscosity gradually increases. Thixotropic materials generally show shear thinning behavior. The origin of shear thinning and thixotropic behavior is in the breakdown of the suspension structure. The suspension structures arise due to attractive interactions between the particles. In the case of shear thinning materials, the rate of structure breakdown is the same as structure rebuilding at a given shear rate. For a thixotropic material the suspension structure gradually breaks down when the stress is applied.

The presence of thixotropy can be detected either by measuring shear stress at a constant shear rate as a function of time or by studying ascending and descending shear stress–shear rate curves under certain programmed conditions as shown in Fig. 8.80. A thixotropic dispersion under such conditions will produce a hysteresis loop in the shear stress versus shear rate plot. If the program conditions are kept constant, the hysteresis can be related to the degree of thixotropy.[154]

Thick-film pastes often show thixotropic flow behavior. The shear history must be taken into account during paste viscosity measurements in order to explain the paste rheology and printing correlation.

8.5.4 Measurement Instruments

To measure viscosity, a sample is placed in a specified measuring geometry to produce a steady simple shear. Most of the viscometers depend on rotational motion to induce a simple shearing flow. Three types of geometries are commonly used: concentric cylinder, cone and plate, and parallel plate. The shear rate is calculated from the applied or induced angular speed and the measuring geometry. The shear stress is determined by the applied or induced torque and the measuring geometry utilized. From the known value of shear stress or shear rate, the viscosity can be calculated. The dependence of shear stress, shear rate, and viscosity on measuring geometry is shown in Table 8.22.

Instruments used to measure the flow behavior of pastes can be broadly classified into two categories: (1) stress-controlled and (2) strain-controlled viscometers. In the strain-controlled machines, the shear rate is varied with a suitable drive motor and the induced shear stress is measured. The strain-controlled equipment can be further divided into two categories: (1) instruments where the applied shear rate and the induced shear stress are measured on the same member of the measuring geometry (Brookfield, HAAKE-RV, and Ferranti Shirley viscometers are examples of this type) and (2) instruments where the drive is applied on one member of the measuring geometry, e.g., outer cylinder, and the resulting torque is measured on the other member, e.g., inner cylinder (Weissenberg and Rheometrics rheogoniometers and HAAKE CV-100 systems are examples of this type).

In the stress-controlled viscometer, the torque is applied to the material and the resulting deformation is measured. The torque and resulting rate of rotation are measured on the same

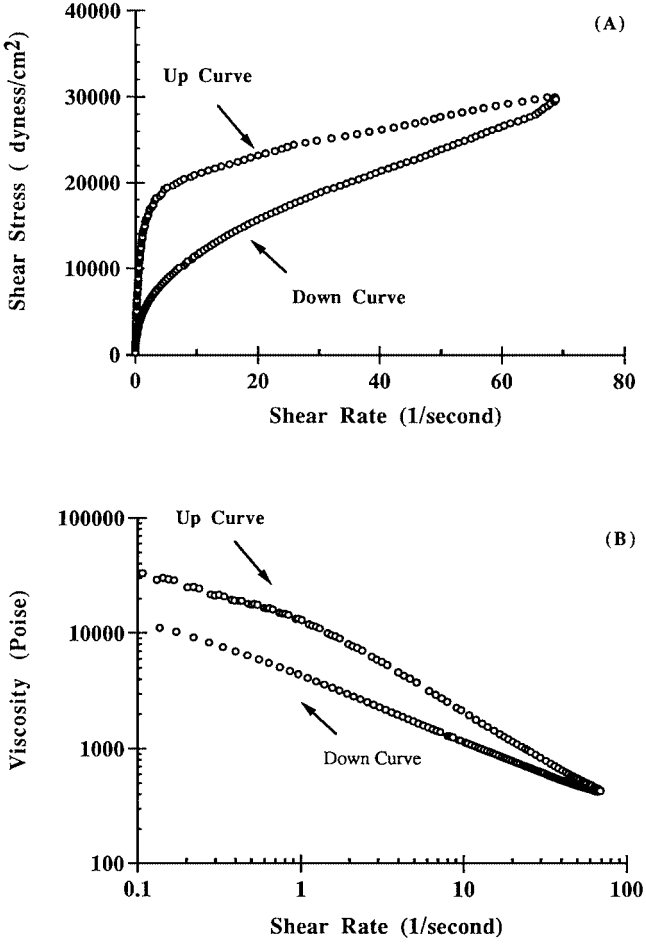

FIGURE 8.80 Thixotropic flow behavior of a thick-film paste illustrating the thixotropic loop.

member of the measuring system. Carri-Med, Physica, Rheometrics, DSR, and Bohlin are stress-controlled viscometers. Stress-controlled viscometers are useful in characterizing stress-controlled phenomena encountered in coating applications such as sagging and leveling of coatings and the sedimentation of particles. The "true" yield point of the paste can be measured using stress-controlled viscometers. The viscosity shear rate behavior over several decades of shear rates can also be measured.

The type of viscometer used to characterize a thick-film paste depends on the information required. To measure viscosity accurately, viscometers should be routinely calibrated with a newtonian viscosity standard. The viscosity of the standard should be similar to that of the sample being measured. Viscometers should be properly leveled and the sample temperature should be carefully controlled. The shear and temperature history during storage and

TABLE 8.22 Dependence of Viscosity Parameters on Measuring Geometry

Geometry	Measured quantity	Maximum shear stress	Maximum shear rate	Newtonian flow equation
Concentric cylinder	Torque M, angular velocity ω	$\sigma = \frac{M}{2\pi a^2 L}$	$\dot{\gamma} = \frac{\omega_a^2 a^2 b^2}{a^2(b^2 - a^2)}$	$\eta = \frac{M}{4\pi L \omega a}\left(\frac{1}{a^2} - \frac{1}{b^2}\right)$ a = radius of inner circle b = radius of outer circle L = length of cylinder
Cone, plate	Torque, angular velocity	$\sigma = \frac{3M}{2\pi a^3}$	$\dot{\gamma} = \frac{\omega a}{\alpha}$	$\eta = \frac{3\alpha M}{2\pi \omega a^3}$ a = radius of core α = angle between cone, plate ($\approx 1°$)
Parallel plate	Torque, angular velocity	$\sigma = \frac{3M}{2\pi a^3}$	$\dot{\gamma} = \frac{\omega a}{h}$	$h = \frac{3Mh}{2\pi a^4 \omega}$ h = gap between parallel plates

shipping of a sample should be closely monitored to obtain consistent results for thixotropic samples. Enclosed measuring systems are preferred to avoid solvent loss during measurements. Brookfield viscometers with the cone and plate geometry are commonly used for checking the lot-to-lot reproducibility of a paste. A single point viscosity measurement is generally not sufficient to correlate viscosity to printing characteristics of a paste. To characterize paste flow behavior over a broader shear rate range, research type viscometers are required.

8.5.5 Measurement Methods

Flow Curves. In this type of testing, shear stress or shear rate is changed as a function of time and resulting shear rate or shear stress is measured. This type of test is generally used to survey flow behavior over one to two orders of magnitude of shear rate range. Thixotropic behavior of pastes can be determined from the hysteresis in shear stress–shear rate plots. There are several phenomenological models available to curve-fit the experimental data.[150] Flow curves for various thick-film pastes are shown in Fig. 8.81.

Creep Test. In a creep test, a constant shear stress is applied to a sample for a certain period of time and the resulting deformation is monitored. This type of test is used to characterize viscoelastic properties of the paste. Creep tests can also be used to measure paste viscosity at very low shear rates (approximately 10^{-3} to 10^{-6} s^{-1}). In a strain test, a step shear rate is applied to the sample and the resulting stress relaxation is measured. Examples of creep tests for thick film pastes are shown in Fig. 8.82.

Oscillation Test. During an oscillation test, a cyclic shear strain is applied to the sample and resulting shear rate response and time lag of response are measured. From these measurements, viscous and elastic properties of the material can be separated. The elastic modulus G' measures the amount of energy stored, whereas the loss modulus G'' measures the energy loss due to viscous dissipation. Figure 8.83 is an illustration of G', G'', and η as a function of frequency for a Ag paste. The viscoelastic properties of materials are further

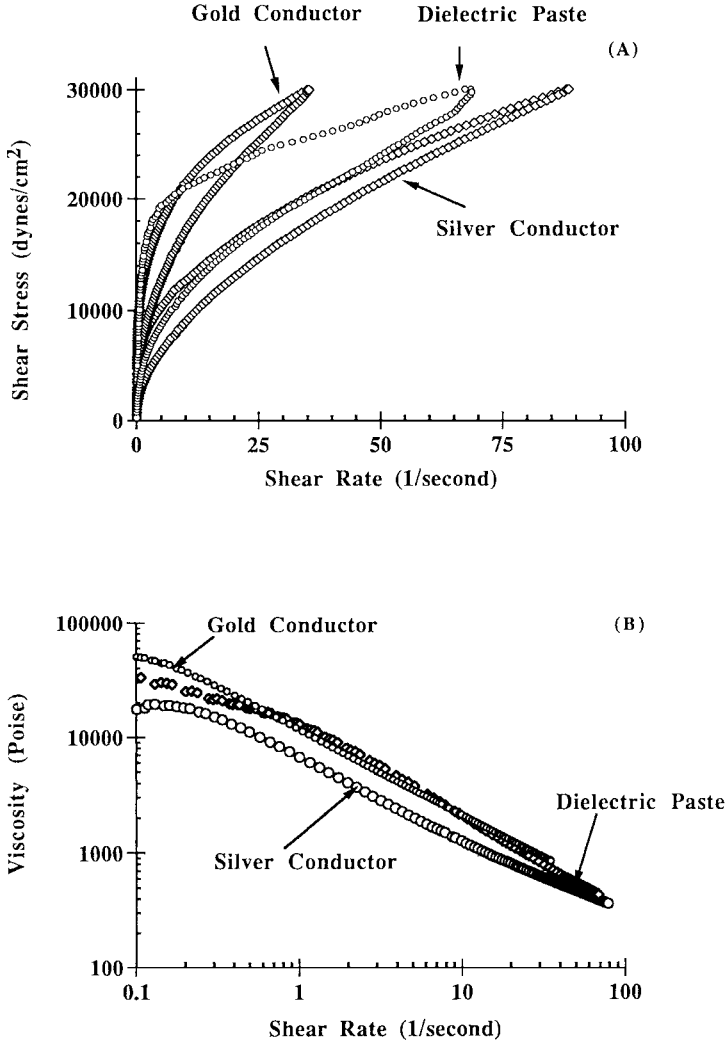

FIGURE 8.81 Plot of (*A*) shear stress versus shear rate and (*B*) viscosity versus shear rate for various thick-film pastes.

characterized by measuring the frequency, amplitude, time, and temperature dependence of the elastic and loss modulus.

The rheological response of a material during either measurement or use depends on the ratio of the characteristic time of the material τ, to the characteristic time T of the deformation process being observed. This ratio is called a *Deborah number*, D_e,[146] where

$$D_e = \frac{\tau}{T} \tag{8.52}$$

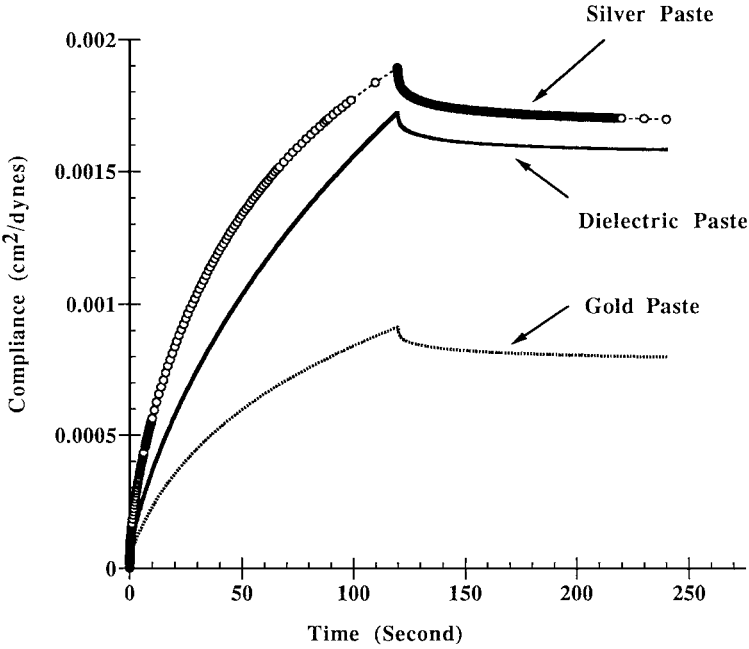

FIGURE 8.82 Creep flow behavior of various thick film pastes.

The time τ is infinite for an elastic solid and zero for a newtonian viscous liquid. Low Deborah numbers indicate liquidlike behavior and high Deborah numbers indicate solidlike behavior. Thus, the normally viscous material will behave as a viscoelastic material if the characteristic time of the process is very small (e.g., ink entry into the rollers).

8.5.6 Interparticle Forces

Thick-film pastes are mixtures of solid particulates (metal powders, frit, etc.) suspended in polymeric solutions. The rheological properties of the paste are directly influenced by the relative amounts of each ingredient and interactions between the solid, polymer, and solvent. Additives such as dispersants/surfactants and rheology modifiers are also commonly added to the paste to improve paste performance. The average particle size of the powders is in the range of approximately 0.1 to 10 μm for most thick-film pastes. In this size range, the specific surface area is large (several m^2/g to 100 m^2/g) and the interparticle interactions are dominated by the solid–liquid interface characteristics or surface chemistry of the system.

The main factors that affect the rheological behavior of a suspension are brownian motion, hydrodynamic interactions, and the interparticle forces of attraction and repulsion. In the colloidal particle size range (1 nm to 1 μm), gravitational forces on the particle are not very important and particles are moving randomly in a dispersion medium because of thermal energy. Particle encounters due to brownian motion can lead to formation of either doublets or particle aggregates, or particles can remain as individual units depending on the particle interactions. In the absence of any repulsive interactions, these random collisions can lead to aggregation of particles to reduce the free energy of the system.

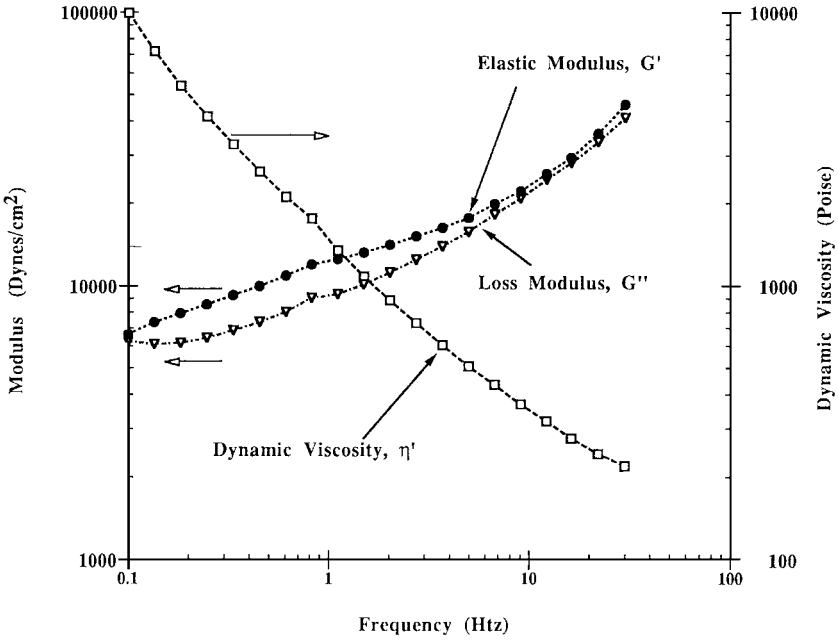

FIGURE 8.83 Loss modulus G'', elastic modulus G', and dynamic viscosity η' as a function of frequency for a silver paste.

The origin of attractive interactions between particles is the van der Waals attraction between atoms of the colloidal particles. This attraction energy is short range, since it is inversely proportional to the sixth power of distance of separation between atoms, but the total interaction energy between colloidal particles (i.e., for a collection of a large number of atoms), is quite large and of long-range order. The energy of attraction V_a between two colloidal particles can be quantified by the following relations:

$$V_a = -\Lambda(A)H(G) \tag{8.53}$$

where $\Lambda(A)$ is the Hamaker constant of the material and $H(G)$ is determined by the geometry of the system. The Hamaker constant for the medium (i.e., solvent used) and absorption of the polymer at the solid-liquid interface will modify the attraction between the particles.[155] Two mechanisms are available to overcome the attraction between particles: (1) electrostatic interactions and (2) interactions of absorbed polymer.

If the collided particles can develop an electric charge and if all particles have the same sign of charge, then particles will repel one another during approach. Surface charge can be developed in the case of simple oxides by surface group dissociation or by preferential absorption of ionic dispersants. The charge on the solid surface contributes to the distribution of counterions in the solution. This model of the charged interface is often called the *electrical double layer*. The total interaction energy between two particles described by the DLVO theory (for Deryagin, London, Verwey, and Overbeek) is calculated by summation of van der Waals attraction and electrostatic repulsion as shown in Fig. 8.84.[156] The repulsive interaction energy as a function of the distance of separation of particles between two

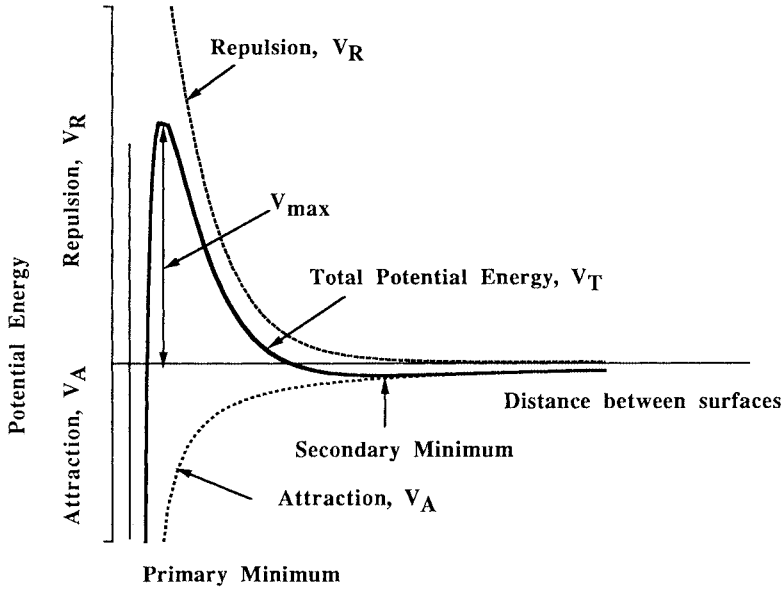

FIGURE 8.84 The potential energy of interaction as a function of distance of separation for electrostatic interactions.

spheres is controlled by the ionic strength of the solution, surface potential (related to charge density on the surface), and the radii of the particles. When the electrostatic repulsive potential barrier is sufficiently large (10 kT), a stable dispersion can be obtained. If the potential barrier is low, the particles will be flocculated due to the van der Waals attraction. Electrostatic interactions are important, for example, during milling of glass flakes in water.

The second method to modify interparticle interactions is by absorption of polymer at solid–liquid interfaces.[157] The absorbed polymer increases the stability by increasing the electrostatic repulsion between particles and/or by decreasing the van der Waals attraction. The absorbed polymer can also impart stability due to an additional steric component of repulsion. In this case, the overlap of absorbed polymer layers gives rise to repulsive interactions. Figure 8.85 illustrates the potential energy of interaction between two particles with an absorbed polymer layer. This protective action due to the absorbed polymer is often called *steric stabilization*. The phenomenon of steric stabilization has a thermodynamic basis. The absorbed polymer should completely cover the particle surface to prevent bridging flocculation. The thickness of the absorbed polymer layer should be sufficient to overcome the van der Waals attraction. The solvent used should be such that the overlap of polymer segments leads to repulsion during particle encounters.

If ionic dispersants are used in paste preparation, then steric as well as electrostatic interactions can occur during particle encounters. There is competition for the particle surface between solvent, binder, dispersant, rheology additives, etc., and complete quantitative understanding regarding dispersion stability of pastes is not possible.

The third type of force important in paste rheology is hydrodynamic in nature. Viscous force arises from the relative motion of particles with respect to the suspending medium (i.e., localized velocity difference). Since viscosity is a measure of resistance to flow, or the localized energy dissipation rate, presence of particles leads to disturbance in the fluid

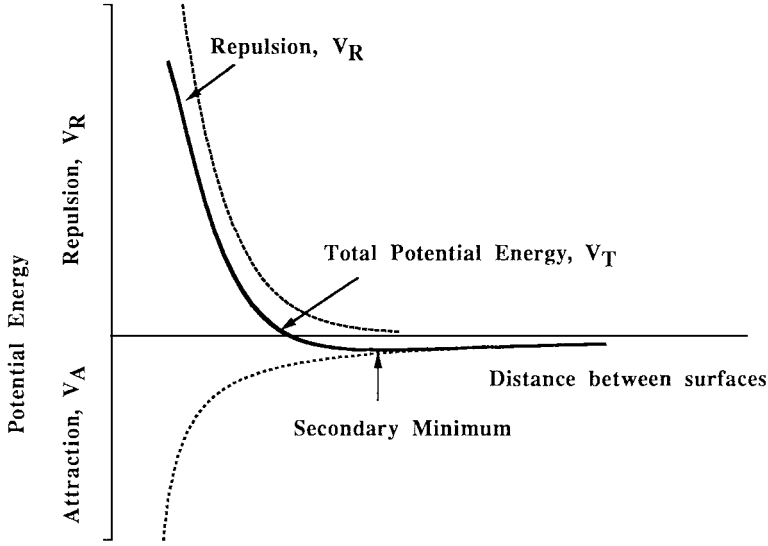

FIGURE 8.85 Potential energy of interaction as a function of distance of separation for steric stabilization.

flow lines and an increased rate of energy dissipation. Hence, the viscosity of the suspension is larger than the suspending fluid. The effect of the suspending liquid is normalized by dividing the suspension viscosity with solution viscosity to get the relative viscosity η_{relative} of a suspension:

$$\eta_{\text{relative}} = \frac{\eta_{\text{suspension}}}{\eta_{\text{solution}}} \tag{8.54}$$

From this equation, it is evident that control of solution or vehicle viscosity is important to control the paste flow behavior. The solution viscosity can be controlled by adjusting polymer molecular weight, solvent selection, and polymer concentration.[158]

8.5.7 Suspension Structure

The above-described interparticle interactions lead to formation of suspension structures at rest. The type of suspension structure formed depends on whether the interparticle forces are attractive or repulsive in nature. With strong repulsive interactions, solid crystalline structures can be formed.[159] The attractive interaction appears to be more common with paste materials. The flow behavior of the suspension is strongly affected by the nature of the suspension structure. The extreme cases are the formation of chainlike structures or formation of spherically shaped clusters of particles. The two shapes are the extreme simplifications of the real structures and are often used as structural models. The type of suspension structure developed depends on interparticle interactions, the shape and size of solid particles, solid surface characteristics, particle concentration, mixing conditions, shear history, etc. The basic flow units, called *flocs*, are formed by random packing of primary particles. At low shear or at rest, the flocs group into clusters of flocs called *aggregates*, as shown in

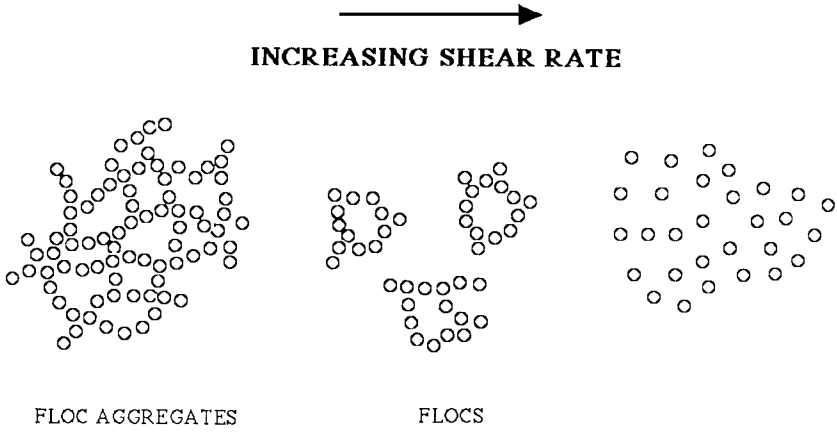

FIGURE 8.86 Schematic of paste structure.

Fig. 8.86. These aggregates may form a network which can fill the entire volume of the dispersion and control its plastic or structural properties.[160] Another method to obtain the suspension structure is through the vehicle phase. In paste formulations, rheology additives (generally organic in nature) can form a gel type structure at low shear rates. The observed yield point and viscoelastic response of the materials are indicative of a suspension structure above a critical volume fraction of the solid phase.[161]

When a shear stress is applied, the suspension structure is broken down into smaller units. The vehicle entrapped within the floc aggregates is released. This leads to a decrease in viscosity with increasing shear rate. If the rate of structure breakdown due to shear is equal to the rate of structure buildup due to brownian motion, shear thinning or pseudoplastic flow behavior is observed. The equilibrium floc is generally spherical in shape and the size distribution is narrow.[162]

If the rate of structure buildup is slower than the rate of breakdown due to shear, thixotropic flow behavior is observed. Breakdown of the suspension structure can be reversible and the suspension structure is slowly recovered. The rate of structural breakdown and rebuilding is important to obtain optimum print quality during screen printing of thick film pastes.

There are several phenomenological models available to correlate the rate dependence of suspension viscosity.[146–150] The Cross model described below is a general model that requires four parameters to describe the dependence of viscosity on the shear rate of a suspension:

$$\frac{\eta - \eta_0}{\eta_0 - \eta_\infty} = \frac{1}{1 + K\dot{\gamma}^m} \tag{8.55}$$

where η_0 and η_∞ are asymptotic values of viscosity at very low and very high shear rates and K and m are constants. These parameters are shown in Fig. 8.87. With the Cross model, the shear rate dependence of paste viscosity can be described over a wide shear rate range. The Cross model can be reduced to power law, Sisko, and Bingham model equations with certain approximations:[146]

Power law model: $$\eta = K_2\dot{\gamma}^{m-1} \tag{8.56}$$

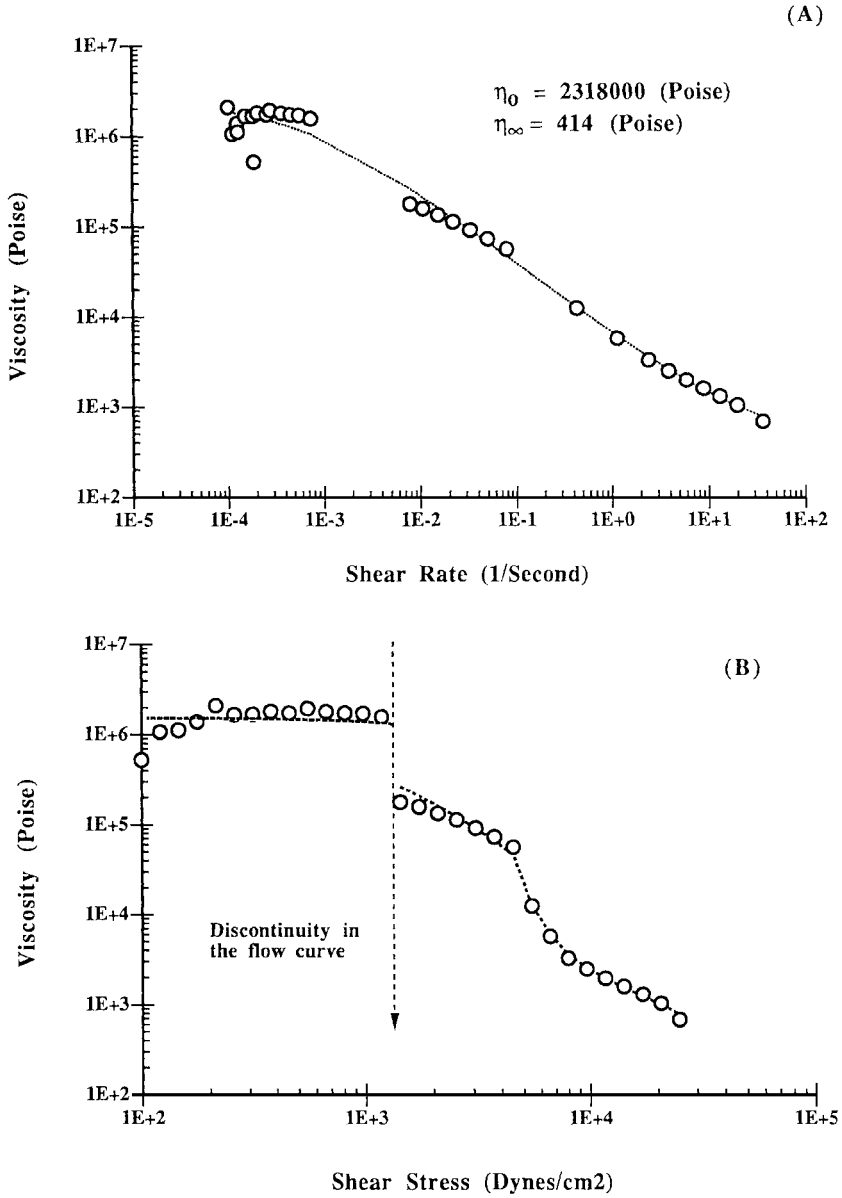

FIGURE 8.87 Plots of (*A*) viscosity versus shear rate and (*B*) viscosity versus shear stress for a dielectric paste.

where m is called the *power law index* and K_2 is called the *consistency.*

Sisko model: $$\eta = \eta_\infty + K_2 \dot{\gamma}^{m-1} \tag{8.57}$$

Bingham model: $$\sigma = \sigma_y + \eta_p \bar{\gamma} \tag{8.58}$$

where σ_y is the yield stress and η_p is the plastic viscosity. Another model used in the paint and coatings industry is called the Casson equation:

$$\sqrt{\sigma} = \sqrt{\eta_\infty}\sqrt{\dot{\gamma}} + \sqrt{\sigma_y} \tag{8.59}$$

The yield point described by the above models is a calculated value. The true yield point of the material is difficult to measure and depends on the sample shear history and measurement technique.[163] It is sometimes more useful to describe low shear paste behavior by the zero shear viscosity using the Cross model. Still, yield point is of practical importance in describing certain engineering applications.

8.5.8 Effects of Paste Formulation on Paste Rheology

The rheological behavior of thick-film pastes depends on its composition and the chemical nature of the ingredients. In this section, we will illustrate the effect of some of the compositional variables on paste rheology. It should be noted that each component of the paste (e.g., solid, solvent, dispersant, etc.), has an effect on paste rheology, while interactions between various components can also exhibit a strong effect on paste rheology. The effect of various components is summarized in Table 8.23.[149,153]

The solid constituents of a paste are selected according to the functional requirements of the final products (e.g., metal powders for conductor inks, etc.). Frit is generally added to improve the densification of the film during firing. Most paste formulations generally involve more than one type of solid powder with different densities and particle characteristics such as average particle size, size distribution, and specific surface area. The rheological properties of the paste are influenced by the fraction of the paste volume occupied by the suspending phase. The volume fraction of the phase is defined by the following:

$$\phi = \frac{\text{volume of the phase}}{\text{total volume of the suspension}} \tag{8.60}$$

As we have seen, hydrodynamic forces influence paste rheology. Hydrodynamic forces act on the surface of particles or aggregates of particles and are generally independent of particle density. The weight percent solids in the paste is sometimes reported by the paste manufacturer. From the known density and weight percent of each ingredient, it is straightforward to convert this information to a volume fraction basis. It is important to understand that the rheological behavior is most influenced by the volume fraction of a particular phase. Addition of similar amounts of diluent thinner can have different effects on a high density conductor paste versus a low-density dielectric paste.

Effects of Solid Concentration. Einstein showed that for a dilute dispersion of solid particulates the viscosity of the suspension increases linearly with the solid phase volume fraction:

$$\eta_{\text{rel}} = \frac{\eta_0}{\eta_{\text{solution}}} = 1 + 2.5\phi \tag{8.61}$$

TABLE 8.23 Effect of Paste Components on Paste Rheology

Thick-film paste component	Effect on rheological properties
	Solid Phase
Volume concentration of solid, ϕ	Influences hydrodynamic interactions between particles, flocculation and aggregate characteristics.
Particle size, particle size distribution, and particle shape	Influences rheological properties over entire range of shear rates and viscoelastic properties of paste. The particle size, etc., affects the particle concentration per unit volume and the rate of flocculation.
Chemical compositions	Influences the interaction force between particles.
	Continuous Phase
Viscosity η_0	Directly proportional to the paste viscosity.
Chemical constitution, polarity	Influences viscosity through the effect on potential energy of interaction between particles, solubility of resin, and viscosity.
	Surface Active Agent
Chemical constitution	Solubility in continuous phase, absorption behavior at solid–liquid interface.
Concentration	Coverage of the surface, viscosity of the continuous phase, η_0
Absorbed layer at interface	Thickness influences the effective particle dimensions and viscosity; it also influences interparticle interactions.
	Additives
Thixotropes, wetting agents, etc.	Modify the interparticle interactions through effect on surfaces of particles, gel formation in vehicle, etc.; can also modify hydrodynamic interactions.

where η is the suspension viscosity, η_0 is the viscosity of suspending media, and ϕ is the volume fraction of particles. The above equation is valid for rigid, uncharged, spherical particles at very low particle concentrations where hydrodynamic interactions between particles can be ignored.

The dependence of viscosity on volume fraction solids is shown in Fig. 8.88. At high particle concentrations, viscosity of the suspension increases more rapidly than predicted by the above equation due to interparticle interactions. Several empirical equations are available to relate viscosity to the solid concentration behavior of suspensions.[149] As the volume fraction of solids is increased further, a stage will be reached where the particles will be interlocked and no flow will occur (i.e., viscosity approaches infinity). The volume fraction of solids at which this occurs is called the *maximum packing fraction* ϕ_m, and its value will depend on the particle packing, size distribution, shape, etc.

The effect of solids concentration on dielectric paste viscosity at a shear rate of 9.6 s^{-1} is shown in Fig. 8.89. These pastes were prepared using the same vehicle with varying solids concentrations from 66 to 76 wt%. A flow test was used in which the shear stress was increased to a maximum value in 2 min and then decreased to zero in 2 min. The viscosity was measured at 25°C using a cone and plate geometry. As shown in Fig. 8.89, a sharp increase in the up curve viscosity with solids loading was observed. The difference in the up curve and down curve viscosity also increased, indicating a higher degree of thixotropy.

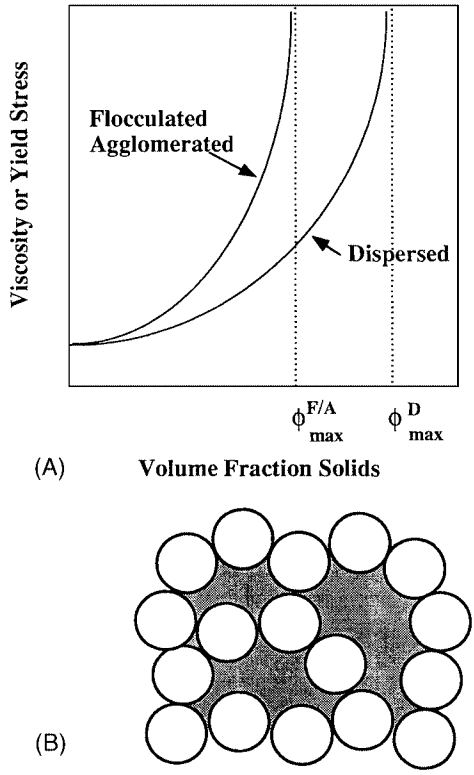

FIGURE 8.88 (A) Schematic of viscosity versus volume fraction of solids in the suspension. (B) schematic of a flocculated suspension.

The measured yield point of the paste also increased with increasing solids loading, as shown in Fig. 8.90. The yield measurements were conducted by increasing the shear stress from zero to 5000 dyn/cm^2 in 2 min. The reported yield stress indicates the stress at which flow was detected. The measurement of yield stress is sometimes difficult and there is some controversy regarding the existence of yield point.[146,163] Figure 8.91 shows the effect of solids concentration on zero-shear viscosity. The low shear flow behavior was determined by applying a constant shear stress to the sample until a constant or "equilibrium" strain rate was obtained. From the known shear stress and shear rate, an equilibrium viscosity at a given shear rate was calculated. The above procedure was repeated again on the same sample at higher shear stresses.

From Fig. 8.91, it is clear that these pastes show a constant (newtonian) viscosity at low shear rates. This viscosity is called *zero-shear viscosity*. The zero-shear viscosity was then calculated from viscosity shear rate data using the Cross equation. The sharp decrease in viscosity with increasing shear stress above a critical shear stress indicates the presence of strongly flocculated suspension structures. As shown in Fig. 8.92, the zero-shear viscosity increases exponentially with increasing solids concentrations. An increase in elastic modulus G' and the loss modulus G'' was also observed for these pastes with increasing solids concentration.[164]

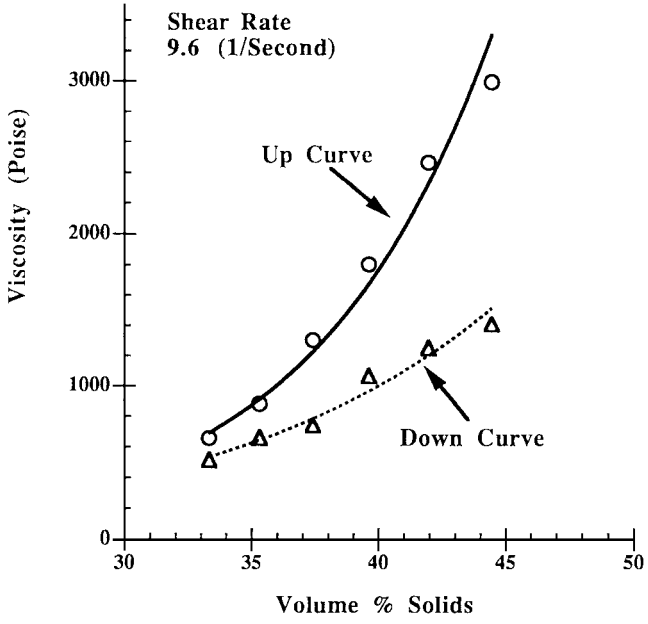

FIGURE 8.89 Viscosity versus vol% solids for a dielectric paste.

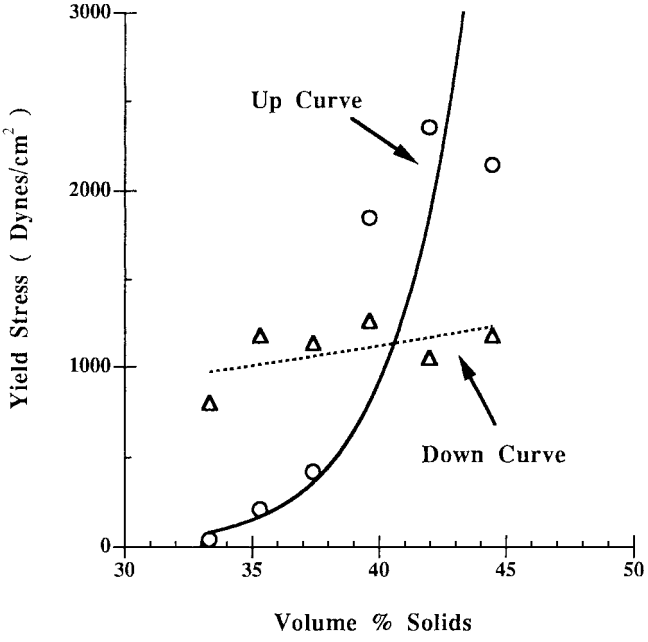

FIGURE 8.90 Yield stress versus vol% solids for a dielectric paste.

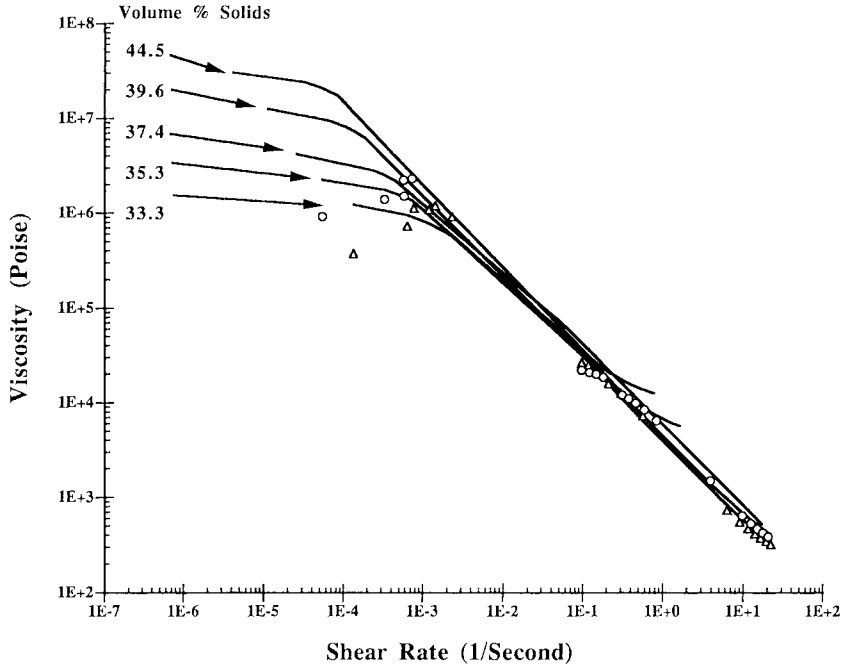

FIGURE 8.91 Effect of solids concentration on viscosity versus shear rate.

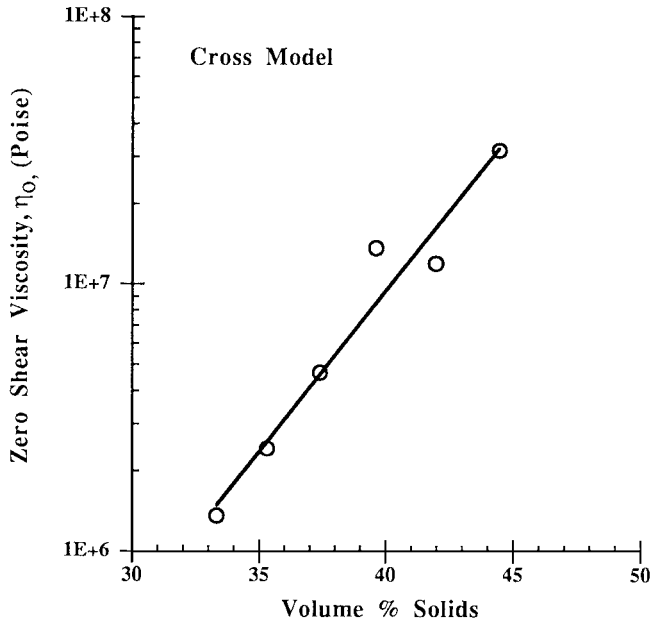

FIGURE 8.92 Zero-shear viscosity versus vol% solids as calculated from the Cross model.

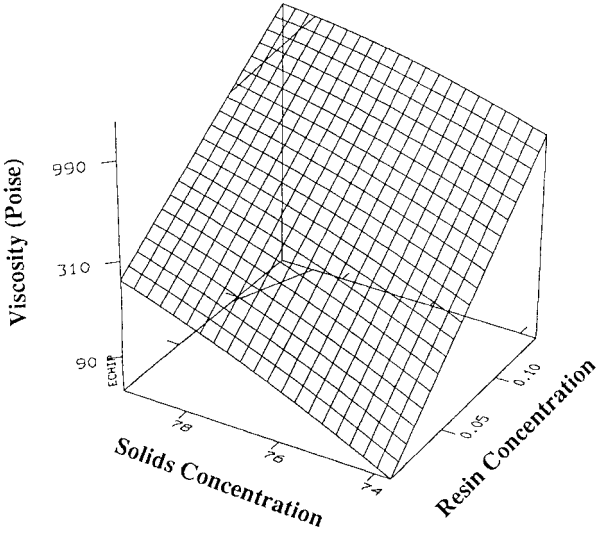

FIGURE 8.93 Effect of solids concentration and resin concentration on dielectric paste viscosity.

Effects of Vehicle Viscosity. The paste viscosity is directly proportional to the vehicle viscosity as defined by Eq. (8.60). Vehicle viscosity is controlled by the chemical nature, average molecular weight, molecular weight distribution, and concentration of the resin. The resin concentration and type are generally optimized for paste rheology as well as the green strength of the dried film.[158,165] Solvent viscosity and solvent resin interactions also influence vehicle viscosity. The effect of resin concentration on a crystallizing dielectric paste viscosity at a shear rate of 9.6 s^{-1} is shown in Fig. 8.93.

In the concentration range investigated, paste viscosity essentially increased exponentially (note the log scale for the viscosity) with increasing resin concentration. The increase in viscosity can also be due to absorption of polymer at the solid–liquid interface and an increase in hydrodynamic volume of each particle.[166]

Effects of Dispersants and Other Additives. As described earlier, the rheological behavior of suspensions is strongly influenced by interparticle interactions which are either electrostatic or steric in nature. These interactions are predominantly determined by the solid–liquid interface properties and absorption behavior of the surface active agent at the interface.

Dispersants are added to thick-film pastes to improve the dispersion of particulates in the vehicle. The type and amount of dispersant are generally optimized to obtain a stable paste with dense green and fired microstructures. Dispersants are classified into three categories:

1. Anionic, where the dispersant molecule has a negative charge
2. Cationic, where the dispersant molecule has a positive charge
3. Nonionic, where the dispersant molecule is electrically neutral

Surface active agents also decrease surface tension of the paste and can help wet the screen mesh during printing. The reduced surface tension of the ink will help to wet the substrate.

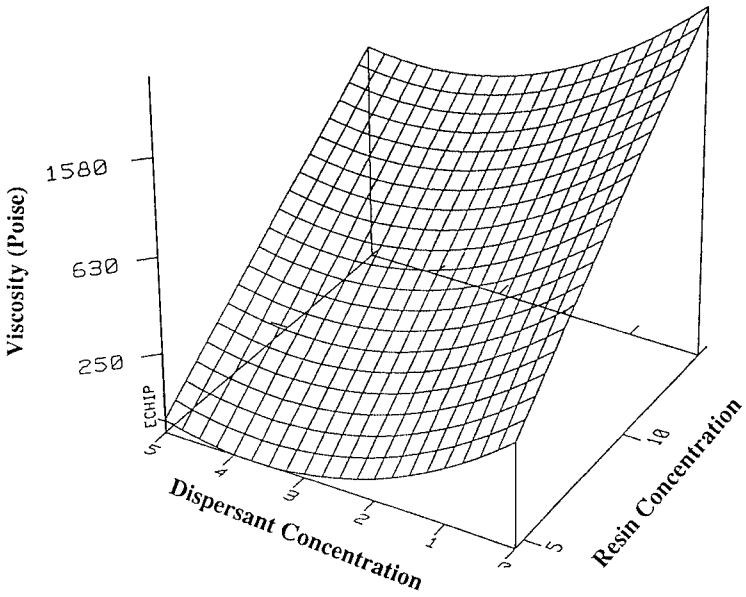

FIGURE 8.94 Effect of dispersant and resin concentration on dielectric paste viscosity.

Dispersants also tend to interact with rheological additives and reduce paste viscosity. Excessive amounts of dispersant should be avoided.

Figure 8.94 illustrates the effect of dispersant concentration on paste viscosity at a shear rate of 9.6 s^{-1}. As expected, viscosity decreases with increasing dispersant amounts.

Other additives (i.e., rheology modifiers) are often added to thick film formulations to adjust paste rheology. The interaction between various ingredients is important in understanding paste rheological behavior. Since numerous ingredients are commonly used, statistical techniques must be employed to understand these interactions.

8.5.9 Rheology and Thick-Film Screen Printing Correlation

The properties of thick-film printed circuits, such as print thickness, fine line definition, via resolution, and surface smoothness, depend on the screen printer setup and ink rheology. A large number of variables can affect the screen printing process.[167,168] Analysis of shear stresses or shear rates during the screen printing process is important to establish a correlation between the print properties and rheology. The machine setup parameters such as squeegee hardness, squeegee speed, squeegee angle, screen mesh properties, snap-off distance, and the force that presses the squeegee against the screen and substrate affect the shear rates experienced by the ink. Hydrodynamic analysis of the screen printing process during ink transfer from the screen to the substrate is available.[169–174]

During the screen printing process, a roll of ink is formed in front of the squeegee. Movement of the ink caused by the squeegee generates hydrostatic pressure within the ink. The ink is pumped through the screen opening by the pressure difference and attaches to the substrate by wetting and cohesion between the ink and substrate. The screen emulsion

TABLE 8.24 Approximate Shear Rate Ranges Experienced by Thick-Film Inks

Operation	Shear rate range, s^{-1}
Paste manufacture, three-roll mill	10^3–10^4
Paste storage	10^{-4}–1
Stirring and transfer to stencil screen	10^{-2}–1
Rolling of ink in front of squeegee	1–10^4
Ink flow through screen	10^3–10^4
Ink leveling after deposition	10^{-2}–10^{-1}

should provide a sealed gasket to avoid spreading of ink due to hydraulic pressure in order to obtain a high definition print.[171] The hydrostatic pressure developed is maximum in the vicinity of the squeegee edge in contact with the screen. Theoretical analysis shows that the hydrostatic pressure generated on the screen and on the squeegee increases with increasing squeegee speed and ink viscosity. This means that the force required to move the ink in front of the squeegee increases with increasing ink viscosity and squeegee speed. The maximum pressure is generated at an angle equal to $\alpha/3$, where α is the squeegee angle. The squeegee angle can decrease during screen printing, depending on the squeegee hardness.[170] The hydrostatic force acting on the squeegee surface can lift the squeegee off the screen and hydroplaning can occur with high-viscosity inks at high printing speeds.

As described above, the ink undergoes a complex shear history during the screen printing operation. The estimates of shear rates are shown in Table 8.24.

First we will look at the shear rates involved during the screen printing process. When the ink is stirred and transferred to the screen the shear rate is approximately 10^{-2} to 1 s^{-1}. The shear rates near the vicinity of the squeegee edge are difficult to estimate. These estimates of shear rate are 1 to 10^4 s^{-1}.[169,170,175] In practice, it is difficult to measure the high shear rate viscosity of thick-film inks (greater than 500 s^{-1}) because of cohesive failure of the paste.

Shear rate for the flow of ink into the screen mesh can be estimated by the Hagen-Poiseville relation:

$$Q = \frac{\Delta p \pi R^4}{8\eta L} \tag{8.62}$$

where Q = volume of the liquid that flows across the cross section in unit time (i.e., flow rate)
R = radius of the tube
I = length of the tube
Δp = pressure gradient
η = viscosity of a newtonian fluid.

The maximum shear rate $\dot{\gamma}_{max}$ occurs near the tube wall and is given by the following equation:

$$\dot{\gamma}_{max} = \frac{\Delta p R}{2\eta L} \tag{8.63}$$

The relationship between ink viscosity and squeegee speed can be analyzed using Eq. (8.61).

The volume of ink filled in the wire mesh is related to the fabric thickness L and the diameter of the mesh opening, D (approximately $2R$)

$$\text{Volume of ink in the mesh} \approx D^2 L \tag{8.64}$$

where $D = 1/(M - d_w)$
M = mesh count per unit length
d_w = wire diameter of the mesh
L = thickness of the fabric $\approx 2d_w$

The time t to fill the ink into the mesh is related to the squeegee speed V by

$$t = \frac{D}{V} \tag{8.65}$$

Substitution of Eqs. (8.64) and (8.65) into Eq. (8.66) yields the relationship between the screen printer setup and the newtonian ink viscosity to fill the screen mesh:

$$V_\eta \le \frac{\Delta p D^3}{128 L^2} \tag{8.66}$$

Thus, for a given screen (D^3/L^2) and the squeegee angle (related to Δp), the product of squeegee speed and ink viscosity is constant. Smaller screen openings and thicker emulsions need lower-viscosity inks and slower printing speeds. A similar equation has been used[169] to explain the emptying of a mesh where Δp is atmospheric pressure. The subtle difference is whether poor printing is due to improper filling of the mesh or the release of ink from the screen mesh. The above equations are modified if the flow behavior is nonnewtonian. Thick-film pastes often show yield stress (or very high viscosity at very low shear rate). If a yield stress is present, then no flow will occur into the mesh if

$$\Delta p < \frac{4 L \sigma_y}{D} \tag{8.67}$$

where σ_y is the static yield stress of the paste. The above equation can help to explain why the ink needs to be worked on before the printing operation is started. The applied shear breaks down the paste structure and the yield stress is decreased. The pressure developed by the squeegee is then sufficient to cause flow into the mesh. The initial few strokes also help to wet the screen with ink.

During the flow of ink through the wire mesh, separation of vehicle and solid can occur. The particles are deflected toward the center of the mesh, and vehicle-rich region is formed on the surface of the mesh. This was experimentally confirmed by measuring the solids concentration of ink left on a screen.[169]

The next event that occurs is adhesion of the ink column to the substrate. At this stage, it is important to have a sealed gasket formed by emulsions so that ink does not flow out to degrade the print quality. The squeegee movement above the screen wipes off the excess ink. After depositing the ink, the screen must separate from the substrate immediately behind the squeegee to deposit ink columns, as shown in Fig. 8.95.

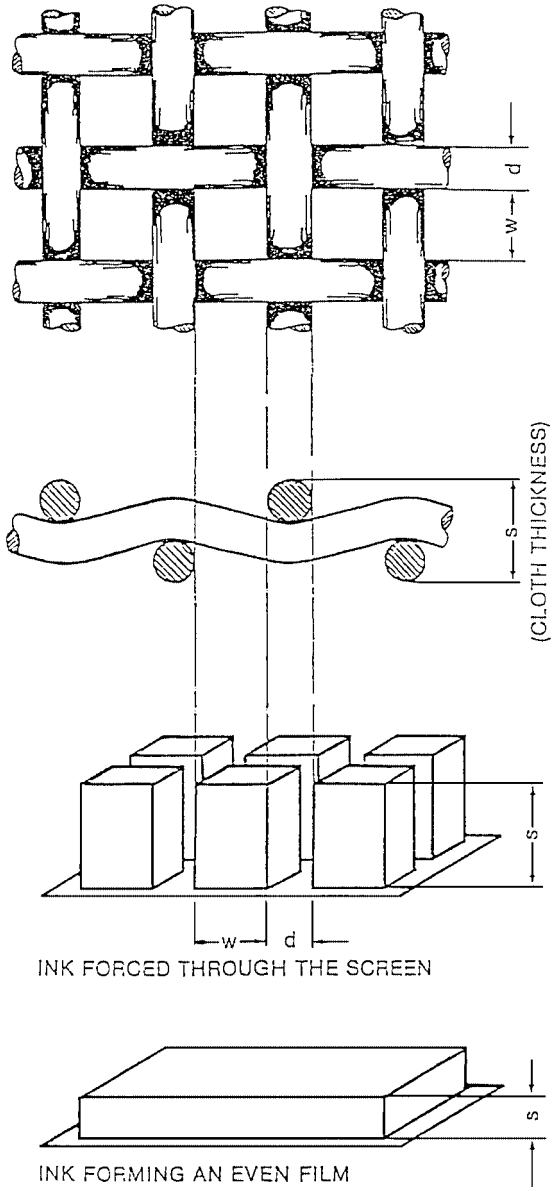

FIGURE 8.95 Schematic of paste columns deposited during screen printing.[168]

The screen wires are under tension and the pulling force F is determined by the tension in the wire. The pulling force should overcome the viscous resistance of the ink. The situation can be visualized as moving a wire through a viscous fluid. From the definition of viscosity, the following relation can be written:

$$\frac{F}{A} = \sigma = \eta\dot{\gamma} \tag{8.68}$$

The shear rate can be approximated by the velocity gradient in the mesh:

$$\dot{\gamma} \approx \frac{V_a}{D/2} \tag{8.69}$$

where V_a is the snap-off velocity and D is the mesh opening. Substituting Eq. (8.69) into Eq. (8.68) yields

$$\frac{F}{A} \approx 2\eta\frac{V_a}{D} \tag{8.70}$$

If the tension in the screen is not sufficient to overcome viscous drag, the screen is slowly released from the substrate. This leads to formation of a *cling* zone which will degrade the print resolution. The snap-off speed V_a is related to the squeegee speed and snap-off distance. The screen tension needs to be increased for faster printing of a high-viscosity paste. Smaller mesh openings will also need higher screen tension. The tension in the screen should be less than the elastic limit of the wires to prevent permanent elongation and distortion of the screen. Near the end of the squeegee stroke, the lifting force decreases because of geometric factors. This can lead to an increase in the width of the cling zone and the degradation of print quality.

It is generally observed that all of the ink inside the wire mesh is not transferred to the substrate.[171] Near the end of screen release from the deposited ink, the upward movement of wires in the paste applies tensile stresses to the paste. The applied tensile stress can lead to cavitation within the ink. The tensile stress required to cavitate the paste can be low because of the presence of particles and dissolved bubbles which can act as nuclei.[176] If the rate of separation of wires from the ink is sufficiently high, the paste can develop high internal stresses that exceed the cohesive strength of the paste and the paste can fracture like a brittle solid.

8.5.10 Wetting and Screen Print Resolution

The release of ink from the mesh and wetting of the substrate depend on the proper surface energy relationships of ink, screen, and substrate.[177,178] Wetting behavior was described earlier in Sec. 8.2, "Thick-Film Conductors."

A high surface energy substrate is most easily wet with a low surface tension liquid. In order to obtain good print resolution, the ink should not excessively wet the screen substrate and emulsion. The screen material can be treated to modify the surface energy so that the ink does not wet the screen.[177] If the ink wets the screen but the ink cohesive forces are sufficiently strong to overcome ink–screen adhesion, well-defined ink columns are deposited. Ceramic substrates used in thick-film applications have sufficiently high surface energy and the ink wets the substrate. An excessive amount of surfactant can lower

the surface tension of the paste and promote excessive wetting and loss of print resolution. Generally, the surface energy of the paste is approximately 30 to 40 dyn/cm. Improved print resolution was observed for an ink printed on low surface energy Teflon compared to that on an Al_2O_3 substrate.

After the ink columns have been deposited on the substrate, low shear rate processes come into effect. The viscosity of the paste begins to increase immediately. The forces acting on the ink are due to gravity, surface tension, and temperature.

8.5.11 Leveling of the Printed Part

The time to achieve good leveling is given by the following equation:

$$t = K\left(\frac{\eta}{\dot{\gamma}}\right)\frac{(\lambda^4)}{(x^3)}\log\left(\frac{A_0}{A_t}\right) \tag{8.71}$$

where λ = wavelength of the mesh marks
A_0 = depth of the mesh mark at time $t = 0$
A_t = depth of the mesh mark at time t
K = numerical constant
x = print thickness

The terms are defined in Fig. 8.96.

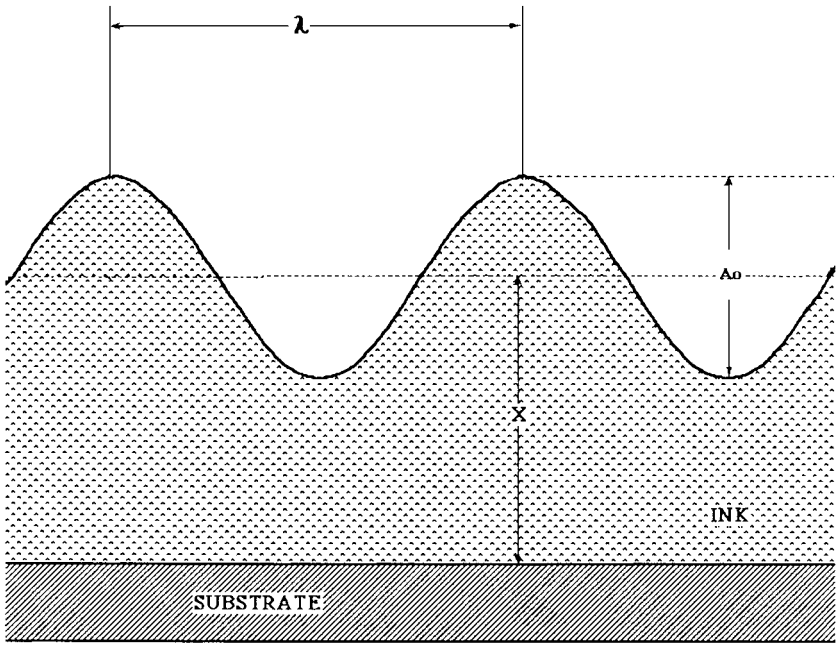

FIGURE 8.96 Schematic of mesh marks.

TABLE 8.25 Parameters Affecting Leveling Time

Mesh count, M/in	Mesh count, M/cm	λ, μm	Initial roughness $A_0 = \frac{1}{2} d_0$, μm	Leveling time, s	Min. roughness A_{ty} with yield stress, μm
400	160	63	13	61	0.55
325	130	77	14	38	0.98
250	100	100	18	118	2.15
200	80	125	20	298	4.19

Assumptions: γ is 30 dyn/cm, A_t is 1 μm, x is 25-μm print thickness, η is 10^6 P, d_0 is wire diameter in μm, and yield stress is 2000 dyn/cm^2.

The suspension structure of a thixotropic paste is broken down during screen printing. It is important to achieve leveling before the structure can rebuild. To achieve a smooth surface finish, A_0 should be on the order of 1 μm. From the above equation, it is clear that leveling behavior is strongly affected by the wavelength of the mesh marks, which is related to the mesh count M. The leveling time is significantly reduced by using smaller mesh openings, as shown in Table 8.25.

If the paste develops yield stress during leveling, then the leveling stops when the stress due to surface tension becomes equal to the yield stress:[180]

$$A_{ty} = \frac{\sigma_y \lambda^3}{4\pi^3 \dot{\gamma} x} \tag{8.72}$$

The mesh mark depth due to the presence of yield is also shown in Table 8.25. It should be noted that mesh marks will also be affected by drying conditions. During drying, the viscosity of paste can decrease due to a decrease in the vehicle viscosity. The viscosity will increase because of solvent evaporation. Eventually, the solvent loss will overcome the effect of high temperature on vehicle viscosity and the leveling will be completed. If the sample is left at room temperature for drying, then the evaporative cooling and solvent loss will increase the paste viscosity and the yield stress. During firing of the ink, some of the mesh marks are further eliminated.

8.5.12 Via Retention and Line Resolution

The rheological behavior required to keep vias open during printing and leveling can be analyzed using a viscous sintering analogy.[181,182] The driving force is the surface tension acting on the surface of a via. The pressure gradient Δp on a via of radius r can be given by the following Laplace equation:

$$\Delta p = \frac{\gamma}{r} \tag{8.73}$$

where γ is the surface tension of the paste.

The pressure gradient will produce shear stresses in the material, and, subsequently, the vias will close. If the material behaves as a Bingham plastic body, then the yield stress will prevent via closure.

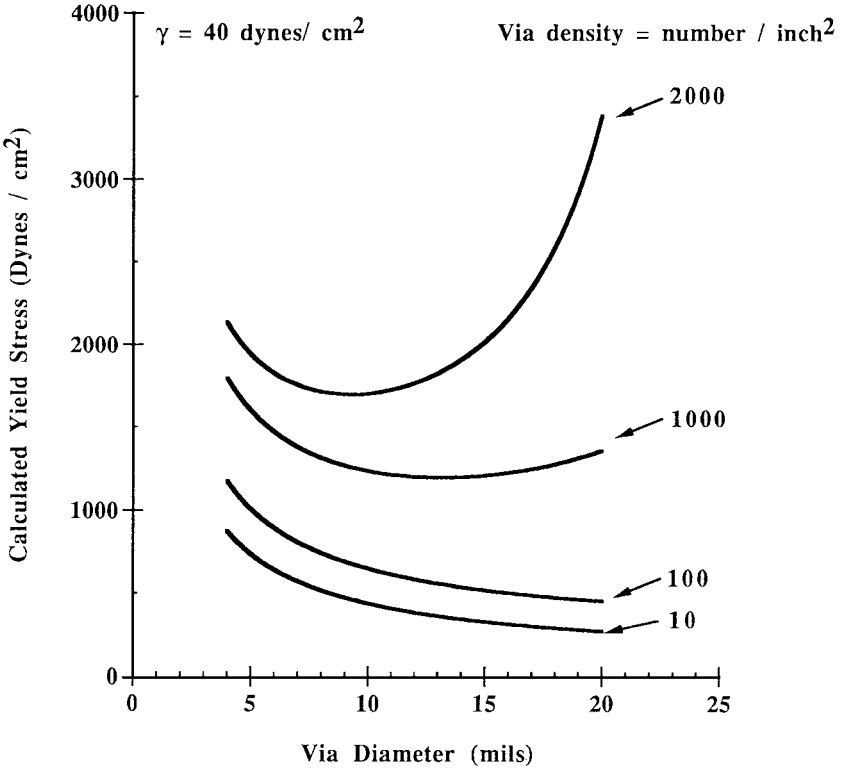

FIGURE 8.97 Calculated yield stress as a function of via diameter and via density using viscous sintering model.[181]

For a via, the condition to prevent via closure is given by the following equation:[181]

$$\sigma_c > \frac{\gamma}{2r_1 \ln(r_2/r_1)} \tag{8.74}$$

where r_2 is related to the number of vias per unit area. The effect of via diameter and density on the necessary yield stress to prevent via closure is shown in Fig. 8.97. From this figure it is clear that a higher yield stress is required with decreasing via diameter and increasing via density. The paste yield stress needs to be optimized with respect to leveling and via closure. An excessively high yield stress will result in mesh marks on the printed part. If the paste does flow below the yield point and exhibits creep flow as observed in many thick-film pastes, the zero or low shear rate viscosity should be utilized to predict via closure behavior. The rate of via closure will be slower with higher zero shear rate viscosity pastes. The concept of zero shear rate viscosity or yield stress is also important to predict long-term storage stability of pastes. The weak network structure can retard sedimentation and hard packing of particles during storage.

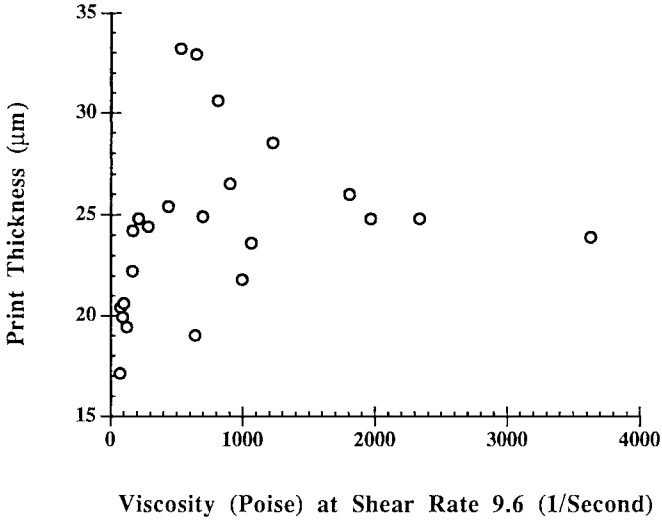

FIGURE 8.98 Dry print thickness versus dielectric paste viscosity.

8.5.13 Examples of Paste Rheology Printing Performance

In this section, examples of correlation between ink rheology and printing characteristics will be illustrated. The effect of ink viscosity on the wet print thickness is shown in Fig. 8.98, a plot of print thickness versus paste viscosity. Twenty dielectric pastes were prepared from the same dielectric powder. The relative amounts of solids, vehicle, dispersant, and rheology additive were varied. The paste viscosity was modified from approximately 70 to 7500 P at a shear rate of 9.6 s^{-1} with formulation changes. All parts were printed with a similar printer setting. All pastes were screen printable except one paste sample with a viscosity of approximately 7500 P and a yield stress of approximately 4800 dyn/cm^2. This paste sample did not wet the screen and the paste roll could not be formed. The paste with an up curve viscosity of approximately 3600 P and yield stress of 2900 dyn/cm^2 was screen printable. From Fig. 8.98 it is clear that the viscosity requirements for ink transfer from the screen to the substrate are quite broad. No systematic relation between the wet and fired thickness and the ink viscosity at moderate shear rates was observed. Statistically, significant correlation between the fired print thickness and the solids and dispersant concentration was observed, as shown in Fig. 8.99. The fired thickness increased with increasing solids concentration in the paste. This is expected since the higher solids concentrations or particle packing density results in reduced shrinkage on drying and firing. The effect of dispersant on the fired thickness was more significant at lower solids concentrations. At lower particle concentrations, the better packing of particles can lead to increased densification and more shrinkage.[183]

The effect of ink viscosity on the fired microstructure is shown in Fig. 8.100. Pastes with low viscosities formed a dense sintered microstructure with a low leakage current. Samples which yielded thicker fired layers had significant internal porosity and high leakage current. The zero-shear viscosity of the high leakage current sample was approximately 1×10^8 P whereas the dense sample had a zero shear viscosity of approximately 1×10^4 P. Very high viscosities at low shear rates prevent the dense packing of particles. A lower green density

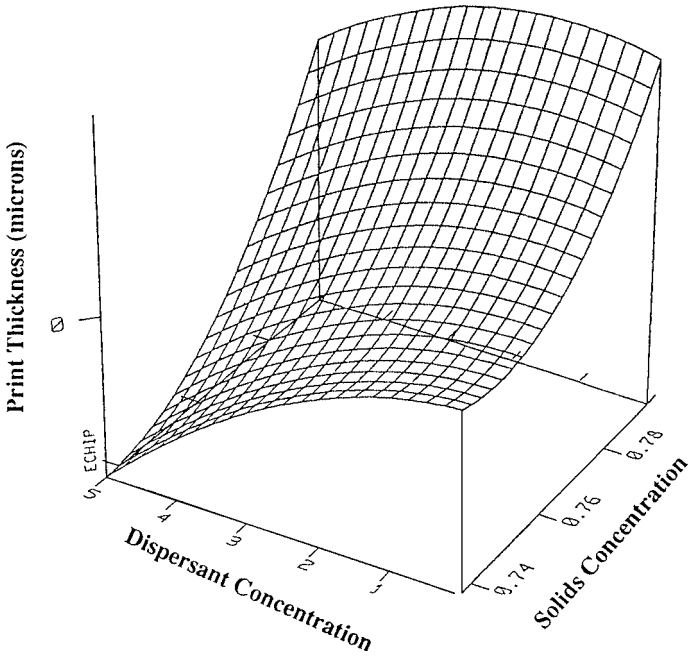

FIGURE 8.99 Print thickness as a function of paste solids and dispersant concentration for dielectric pastes.

retards densification.[183] From these photomicrographics, it is clear that the paste rheology not only affects printing performance but also the properties of the fired films.

The correlation between via retention and ink rheology is shown in Fig. 8.101. The paste samples were prepared using the same powder lot. These pastes had a different inorganic composition from the pastes described above. Figure 8.101 shows a plot of paste yield stress versus paste viscosity at a moderate shear rate of 9.6 s^{-1}. At a given viscosity level, increasing yield stress improved via retention consistent with the previous equations. With a further increase in viscosity but constant yield stress, the paste produced vias with a noncircular cross section (i.e., poor acutance). Similar correlation between the yield stress and improved resolution was observed for conductor patterns. The yield stress measured in these experiments was a static yield stress. In actual screen printing, yield stress development with time after high shear mixing will be more appropriate. Nevertheless, high yield stress indicates a higher degree of suspension structure which helps to prevent excessive flow and via closure.

Figure 8.102 shows the importance of characterizing paste rheological behavior over various shear rates. This figure shows viscosity versus shear rate plots for two pastes prepared using the same powder. The viscosity/shear rate behavior was nearly identical at shear rates of 10^{-1} to 10 s^{-1} which are commonly measured in the quality control of pastes. The poor via resolution could not be explained with high shear viscosity data. The low shear paste viscosity was approximately 10 times more for a paste with good via retention than the paste with poor resolution. Thus the rheological tests which simulate shearing conditions during ink use will have a better chance of establishing correlation between the paste rheology and print resolution.

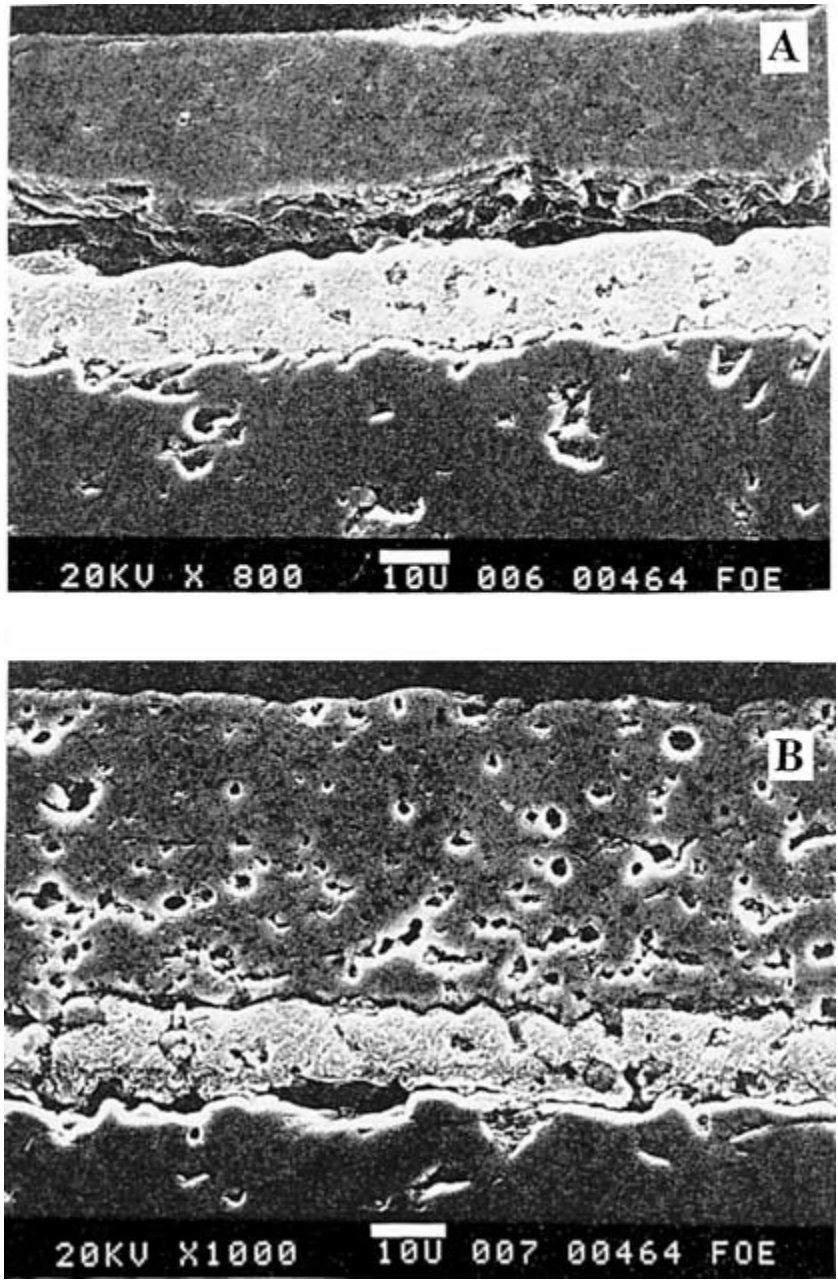

FIGURE 8.100 The effect of paste rheology on fired microstructure.

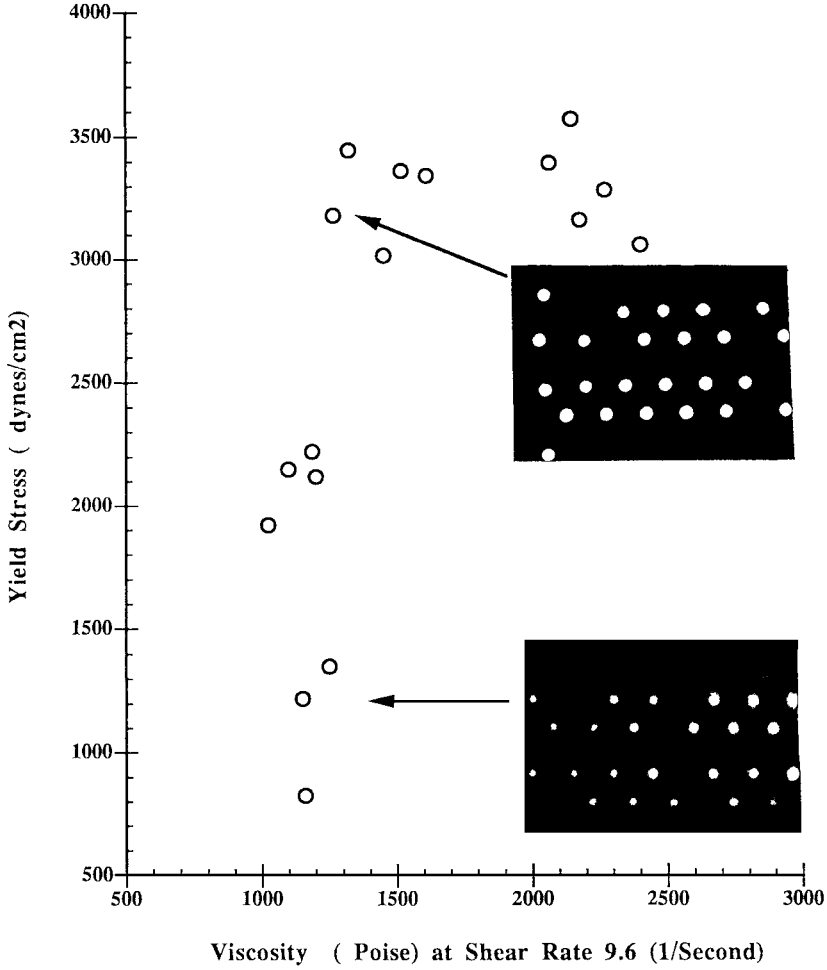

FIGURE 8.101 Measured yield stress versus viscosity for various dielectric paste samples.

8.6 QUALITY CONTROL AND MANUFACTURING PROCESSES

8.6.1 Raw Material and Paste Characterization

Control of the raw material constituents is critical to the reproducibility and ultimate performance of thick-film products. Traceability of each of the components and the intermediates is imperative for the quality control function in order to comply with the high standards of ISO-9000 and continuous improvement programs. Routing equipment calibration programs, vendor audits, and utilization of statistical process control techniques are also necessary to

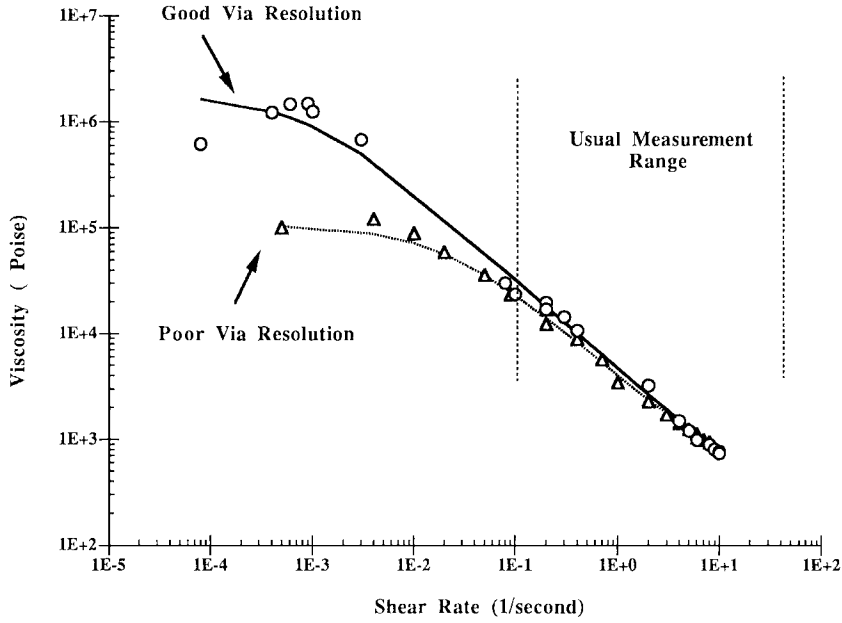

FIGURE 8.102 Viscosity versus shear rate for two dielectric pastes.

ensure maintenance of high standards of quality. The raw material constituents can be either produced in-house or purchased. In either case, specifications must be determined and satisfied for each raw material in order to reproducibly sustain the relationships between processing, microstructure, and the resultant fired properties.

The properties typically specified for metal or conductive oxide powders may include particle size and size distributions, surface area, tap and/or bulk densities, critical impurity levels, loss on ignition, and morphological characteristics. Metal powders can be utilized in various shapes, including spheres, flakes, and combinations of both. Their particle sizes can range from submicrometer to 20 μm. In the case of conductive oxides such as ruthenium oxide used in resistor formulations, the surface areas can approach 100 m^2/g, which translates to a particle size of less than 10 μm. The state of agglomeration becomes particularly important for these types of powders.

Glass powders can be more difficult to characterize because of their criticality to the densification process. Properties typically specified for glass powders include particle size and size distribution, surface area, purity, TCE, softening point, glass transition temperature, and onset of crystallization. Glass powders are made by high-temperature melting of the appropriate mixture of oxides, carbonates, or hydroxides, followed by subsequent quenching of the melt from the peak temperature into a liquid medium such as water or onto cooled rolls. The glass melting conditions must be controlled in order to ensure reproducibility. These parameters include the peak temperature, time, crucible composition, and quench rates. Since the glass must be subjected to particle reduction processes such as ball milling, these parameters must also be controlled, including mill and media composition, milling medium, time, speed, and impurity introductions from the process. The melting process should occur in high purity crucibles such as those made of Pt to produce crystallizing formulations that are very sensitive to minor impurity levels.

The organic constituents are also very important and must be tested to ensure purity, molecular weight, viscosity, and loss-on-ignition characteristics. Utilization of electronic grade products where feasible will improve the tolerance and reproducibility of molecular weight distributions of the critical polymers. The thick-film paste manufacturer must determine the critical characteristics for each raw material in the respective formulations and consistently monitor these for each lot of raw material.

8.6.2 Paste Production and Characterization

The raw material components are weighed out individually and blended prior to three-roll milling by selected blending processes such as planetary mixing or shaking using conventional paint shakers. After the initial blending, or *wetting-out*, phase, the mixture is typically submitted to a three-roll milling process during which the paste is homogenized and coarse particles and agglomerates are reduced in size. Other milling processes can be employed for paste production, although these tend to be proprietary in nature. In the case of three-roll milling, the pastes are subjected to a specific number of passes at specified pressures or milled to a fineness-of-grind specification. This is evaluated by the use of a fineness-of-grind gauge that involves drawing a paste over calibrated grooves that continuously get shallower. The appearance of specks or streaks in the paste defines the upper limit of the paste with respect to particle size. The milling process is continued until the specification is met (e.g., smaller than 10 μm).

The pastes are also tested for conformance to a predetermined viscosity specification. Test methods and the relationship between viscosity (rheology) and screen printing have been addressed in detail in Sec. 8.5, "Rheology and the Screen Printing Process." The percent solids in a paste is typically specified as well, particularly for conductor formulations. The primary purpose of this test is detection of gross weighing errors. This test involves a standard loss-on-ignition test and is described in detail elsewhere.[11] After confirming that the paste meets the preliminary specifications, the materials are subjected to screen printing, drying, firing, and characterization processes as described in Secs. 8.2, 8.3, and 8.4.

8.6.3 Screen Printing

The most commonly used process for thick-film deposition is screen printing, although stenciling, dipping, spraying, spin coating, etc., can also be utilized. The specific deposition process, materials performance requirements, and circuit design will determine the necessary rheological characteristics of the paste. Section 8.2, "Rheology and the Screen Printing Process," addressed the paste rheological requirements and also provided a detailed discussion of rheology and screen printing correlations. The important process variables in screen printing were also identified; they include screen printer setup parameters, squeegee parameters, and screen details. Examples of some of these variables include snap-off distance, squeegee hardness, speed, pressure, wire diameter, mesh opening size, emulsion chemistry and thickness, and screen tension.

Vest,[7] Harper,[11] and Holmes and Loasby[15] all provide additional information on the basics of the printing process which supplements our detailed discussions on rheology in this text.

8.6.4 Drying

Thick-film pastes are normally dried prior to firing. The drying process evaporates the solvents from the printed films. Most commonly used solvents in thick-film inks have boiling points in the range of 180 to 250°C. Because of the high ratio of surface area to volume of deposited films, drying at 80 to 160°C for a period of 10 to 30 min is adequate to remove

most of the solvents from wet films. Box furnaces utilizing convection-type heating or belt-type infrared furnaces are commonly used as dryers. Box-type space dryers are suitable for batch processes and are used for small- to medium-production volumes.

Belt furnaces provide ease of process automation. Some automated production lines utilize a dryer and firing furnace with a common belt. Airflow rates inside the dryer, drying temperature, and time influence the drying process.

9.6.5 Firing

Figure 8.51 shows a typical furnace profile used for thick-film materials firing. The heating rate is typically determined by organic removal requirements. The peak firing temperature or isothermal hold temperature is determined by the composition of the thick-film materials. The cooling rate influences thermal shock stresses in the substrate and is determined by the substrate material, its dimensions, and the production rate.

Belt furnaces are commonly used for firing thick films. Belt furnaces have several zones through which a belt travels at a constant speed. The zone temperatures and speed of the belt can be controlled independently. By adjusting the zone temperature and the belt speed, a variety of time versus temperature profiles can be achieved. Typically, belt furnaces utilize resistive heating elements. In muffleless belt furnaces, the heating elements directly provide the heat for the firing process. In belt furnaces with a muffle, the heating elements are wrapped around a metallic muffle which transfers the heat to the substrates being fired. Firing processes in which a controlled firing atmosphere is required utilize belt furnaces with a muffle. Since the muffle increases the thermal mass of the furnace, the response time of this type furnace to the changes in the temperature set points of the furnace zones is sluggish. Prototype facilities in which furnace profiles are often changed employ belt furnaces without muffles. During air firing, the atmosphere inside belt furnaces is typically controlled by adjusting the flow rates of the respective gases. Special furnace designs are utilized to control the furnace atmosphere during the firing of copper conductors and compatible materials.[184]

Thick-film metallizations for solar cells are processed in infrared-heated furnaces. These furnaces utilize infrared lamps as the source of heat. With infrared furnaces, it is possible to maintain very short dwell times at peak firing temperatures.

8.7 NONHYBRID APPLICATIONS

In addition to the numerous traditional hybrid applications mentioned throughout the text, there are several other applications of thick-film materials that are worth discussing. These include thick-film materials for solar cells, fine ceramics, and the display industry.

An interesting niche application which has emerged for thick-film metallizations is in the mass production of single and polycrystalline silicon solar cells. These devices convert incoming solar radiation directly into electrical current with typical conversion efficiencies of 10 percent to 18 percent. The typical uses of commercially produced photovoltaics are in cost-sensitive markets where electricity is required in locations that are isolated from the conventional power grid. The commercial solar cell is a device similar to that pictured in Fig. 8.103. The most widely used technique for metallizing the *n*-doped layer that faces the sun involves the screen printing of a grid type pattern of thick-film Ag ink to make contact with the silicon. This metallization must be highly conductive at the Ag–silicon interface. Various dopants are added to this formulation to enhance the efficiency of the cell.

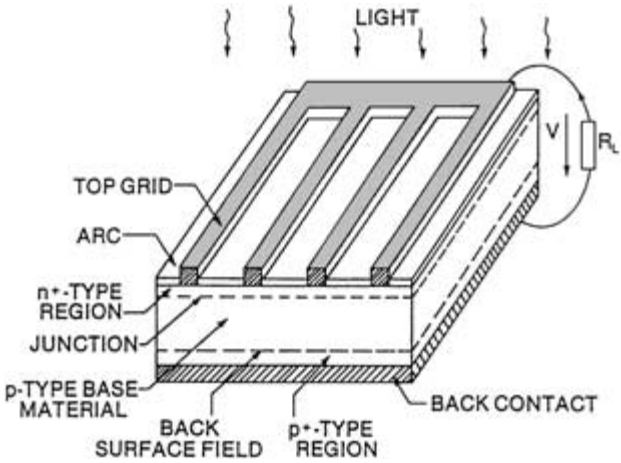

FIGURE 8.103 Schematic representation of a typical silicon solar cell.

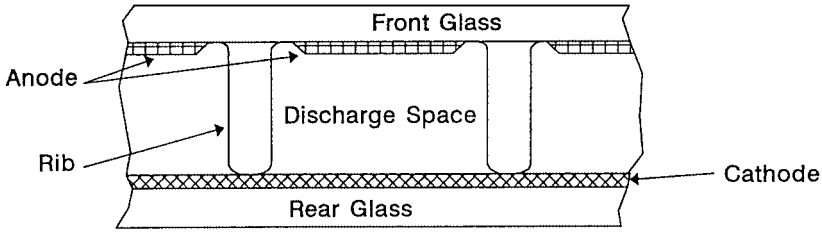

FIGURE 8.104 Cross section of plasma display discharge pixel.

The requirements of this metallization also include low contact resistance at the interface, good solderability, and fine line resolution. The back contact or metallization of the solar cell can be configured in a variety of geometries. Because the back side of the cell is usually coated with an *n*-doped layer, back contacts are usually Ag–Al mixtures. The back contact may be in a grid pattern or may completely coat the entire surface. The Al ensures electrical penetration through the *n*-doped layer. Some back contacts are pure or fritted Al which reflects stray charge carriers back toward the *n-p* junction. The technical feasibility of thick-film phosphorus diffusion sources and screen-printable antireflective coatings based on oxides of tantalum and titanium has been demonstrated, although they are not used in large volume production.

One of the fastest growing categories of electronic devices is flat panel displays. Although there are a number of competing technologies, there is potential for the use of high volumes of thick-film materials in the display market. Plasma displays, as depicted in Fig. 8.104, utilize thick-film components including air-fired Ni for electrodes, dielectric pastes as barrier ribs (partitioning pixel elements), insulating dielectrics for separation of electrodes, and sealing glass pastes for joining the glass panels. In the liquid crystal display area, thick-film opportunities include glass sealing pastes and Ag or Au inks for the driver circuitry and chip mounting. Other display technologies also utilize thick films for

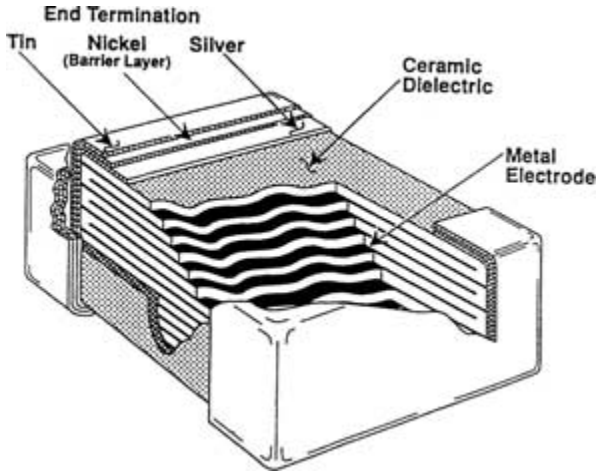

FIGURE 8.105 Cross section of monolithic ceramic chip capacitor.

sealing panels or driver circuitry. As this technology matures, it is likely that other opportunities for these versatile materials will emerge.

The final applications discussed here are electrodes and metallizations for fine ceramics. This includes ohmic contact pastes for varistors and thermistors as well as materials for complex multilayer components. Figure 8.105 illustrates a cross-sectional view of a ceramic chip capacitor. The internal electrode can be Pt, Pd, or Ag–Pd depending on the type of ceramic formulation and its respective firing temperature. The end termination may be Ag or Ag–Pd and is typically required to be platable. The technical requirements of these materials are extremely challenging.

REFERENCES

1. R. R. Tummala, "Ceramic and Glass-Ceramic Packaging in the 1990's," *J. Am. Cer. Soc.,* vol. 74, no. 5, pp. 895–908, 1991.
2. R. W. Vest, "Materials Science of Thick Film Technology," *Am. Cer. Soc. Bull.,* vol. 64, no. 4, pp. 631–636, 1986.
3. R. R. Tummala and E. Rymaszewski, *Microelectronics Packaging Handbook,* Van Nostrand Reinhold, New York, 1989.
4. R. Keeler, "Polymer Thick Film Multilayers: Poised for Takeoff," *Elect. Pack. and Prod.,* pp. 35–38, August 1987.
5. *Electronic Materials Handbook,* vol. 1, *Packaging,* ASM International, Materials Park, Ohio, pp. 106–109, pp. 339–353, 1989.
6. *Metals Handbook,* vol. 8, *Metallography, Structures and Phase Diagrams,* ASM International, Materials Park, Ohio, 1973.
7. R. C. Buchanan (ed.), *Ceramic Materials for Electronics,* 2d ed., Marcel Dekker, New York, 1991.
8. *Metals Handbook,* 10th ed., ASM International, Materials Park, Ohio, 1990.
9. B. S. Rawal et al., "Factors Responsible for Thermal Shock Behavior of Chip Capacitors," *Proc. 37th Elect. Comp. Tech. Conf.,* Boston, pp. 145–156, 1987.

10. R. O. Carlson et al., "Thermal Expansion Mismatch in Electronic Packaging," *Proc. Matls. Res. Soc. Symp.,* vol. 40, pp. 177–190, 1985.
11. C. A. Harper (ed.), *Handbook of Thick Film Hybrid Microelectronics,* McGraw-Hill, New York, 1974.
12. J. R. Larry et al., "Thick Film Technology: An Introduction to the Materials," *IEEE Trans. on Comp. Hybrids and Mfg. Tech.,* vol. CHMT-3, no. 2, pp. 211–225, 1980.
13. D. T. Novick and A. R. Kroehs, "Gold Scavenging Characteristics of Bonding Alloys," *Solid State Tech.,* vol. 17, no. 6, pp. 43–47, 1974.
14. J. C. Fu, "A Study of Structure of Gold-Platinum in Thick Film Conductors," *Precious Metal,* E. D. Zysk and J. A. Bonucci (eds.), pp. 469–483, 1985.
15. P. J. Holmes and R. G. Loasby, *Handbook of Thick Film Technology,* Electrochemical Publishers, Scotland, 1976.
16. J. Savage, "Silver Transfer Through Thick Film Insulants," *Joint Conf. on Hybrid Microelec.,* IERE, Canterbury, pp. 335–340, 1973.
17. J. H. Alexander et al., "A Low Temperature Cofiring Tape System Based on a Crystallizing Glass," *Proc. Intl. Symp. Microelec.,* Orlando, pp. 414–417, 1991.
18. J. H. Alexander and A. S. Shaikh, "The Use of Silver and Silver Plus Gold Conductors with the Ferro Low Temperature Tape," *Proc. 43d ECC Conf.,* Orlando, pp. 888–892, 1993.
19. G. Sarkar et al., "High Reliability Silver-Based Multilayer System," addendum to *Proc. IEMT Symp.,* Japan, 1991.
20. B. D. Cullity, *Elements of X-Ray Diffraction,* 2d ed., Addison-Wesley, Reading, Mass., 1978.
21. L. R. Lichtenberg and M. J. Roll, "Palladium-Silver as an Alternative Metal for Wire Bonding Metallization," *Proc. Intl. Symp. Microelec.,* pp. 229–233, 1988.
22. R. W. Vest, "Materials Interactions During Firing of PdAg Conductors," *Proc. ASM Conf. on Thick Films,* Atlanta, 1988.
23. E. T. Turkdogan, *Physical Chemistry of High Temperature Technology,* Chap. 1, Academic Press, New York, pp. 1–26, 1980.
24. Y. Kudoh et al., "Investigations of Resistance to Solder Leaching of 4 Pd 96 Ag Thick Film Conductors with Ag/Sn/Pd Solders," *Proc. Intl. Symp. Microelec.,* Minneapolis, pp. 51–56, 1987.
25. P. S. Tong and C. E. Falleta, "Silver Palladium Conductors with Excellent Leach Resistance and Solderability but Containing Less Than 1% Palladium," *Proc. Intl. Symp. Microelec.,* Minneapolis, pp. 8–10, 1987.
26. W. Borland et al., "High Conductivity Materials Systems for Advanced Hybrids," *Proc. ECC Conf.,* Houston, pp. 704–713, 1989.
27. G. D. O'Clock, Jr., et al., "PbSn Microstructure: Potential Reliability Indicator for Interconnects," *IEEE Trans. CHMT,* vol. 10, pp. 82–88, 1987.
28. P. W. Dehaven, "The Reaction Kinetics of Liquid 60/40 SnPd Solder with Copper and Nickel: A High Temperature X-Ray Diffraction Study," *Proc. Matls. Res. Soc. Symp.,* vol. 40, pp. 123–128, 1985.
29. D. S. Dunn et al., "Dependence of CuSn and Cu_6OSn_4OPb Solder Joint Strength on Diffusion Controlled Growth of Cu_3Sn and Cu_6Sn_5," *Proc. Matls. Res. Soc. Symp.,* vol. 40, pp. 120–138, 1985.
30. C. W. Allen et al., "A Study of Intermetallic Compound Development in Nickel-Tin Interfacial Zones," *Proc. Matls. Res. Soc. Symp.,* vol. 40, pp. 139–144, 1985.
31. B. S. Chiou et al., "Intermetallic Formation on the Fracture of SnPb Solder and PdAg Conductor Interface," *IEEE Trans. CHMT,* vol. 13, no. 2, pp. 267–274, 1990.
32. P. S. Palanisamy and D. H. R. Sarma, "Thermodynamics of Processing Copper Thick Film Systems in a Reactive Atmosphere," *Hybrid Circuits,* no. 13, pp. 13–20, May 1987.
33. D. R. Gaskell, *Introduction to Metallurgical Thermodynamics,* McGraw-Hill, New York, 1973.

34. D. E. Pitkanen et al., "Materials Compatibility and Processing Relationships for Copper Thick Film Hybrids," *Intl. J. Hybrid Microelec.,* vol. 2, no. 2, pp. 45–51, 1979.

35. D. E. Pitkanen et al., "Part II—Materials Compatibility and Processing Relationships for Copper," *Intl. J. Hybrid Microelec.,* vol. 3, no. 1, pp. 1–6, 1980.

36. R. F. Lund, "Circuit Shorting Mechanisms in Copper Multilayer Systems," *Proc. Intl. Symp. Microelec.,* Anaheim, Calif., pp. 463–471, 1985.

37. P. L. Toch et al., "Failure Mechanism and Process Control Requirements in the Production of Copper Multilayer Interconnect Boards," *Proc. 36th Elect. Comp. Tech. Conf.,* pp. 602– 608, 1986.

38. D. H. R. Sarma et al., "An Accelerated Lot Acceptance Test for Adhesion Degradation of Soldered Copper Thick Films in Temperature Cycling," *Proc. Intl. Symp. Microelec.,* Minneapolis, pp. 554–561, 1987.

39. F. N. Patterson, "Conductor Compositions Compressing Nickel Borides," U.S. patent no. 3,943,168, March 9, 1976.

40. M. Kageyama and T. Yamaguchi, "Mechanism of Reaction Between AlN and Glasses," *Proc. 5th Intl. Microelec. Conf.,* Tokyo, pp. 161–164, 1988.

41. K. Allison et al., "Thick Film Materials for Application on Aluminum Nitride Substrates," *Proc. 5th Intl. Microelec. Conf.,* pp. 153–160.

42. K. Allison et al., "Thick Film Conductor Compositions for Use with an Aluminum Nitride Substrate," U.S. patent no. 5,089,172, February 18, 1992.

43. A. Shaikh, "Thick Film Pastes for AlN Substrates," *Advancing Microelec.,* vol. 21, no. 1, pp. 18–21, 1994.

44. D. L. Hankey et al., "Scanning Electron Microscopy Techniques for Thick Film Microstructural Characterization," *Advances in Ceramics,* vol. 11, *Processing for Improved Productivity,* K. M. Nais (ed.), ACS, Columbus, Ohio, pp. 117–130, 1984.

45. M. Hrovat and D. Kolar, "Investigation in the Al_2O_3–Bi_2O_3–CuO System," *J. Matl. Sci. Letters,* vol. 3, pp. 659–662, 1984.

46. W. D. Kingery et al., *Introduction to Ceramics,* 2d ed., John Wiley & Sons, New York, 1976.

47. *Metals Handbook,* 9th ed., *Powder Metallurgy,* vol., ASM, Metals Park, Ohio, 1984.

48. T. V. Nordstrom and F. G. Yost, "Sintering Behavior of a Reactively Bonded Thick Film Gold Ink," *J. Elec. Matls.,* vol. 7, no. 1, pp. 109–122, 1978.

49. D. W. Pashley et al., "The Growth and Structure of Gold and Silver Deposits Formed by Evaporation Inside an Electron Microscope," *Philosophy Mag.,* vol. 10, pp. 127–158, 1965.

50. R. M. German and Z. A. Munin, "Identification of the Initial Stage Sintering Mechanism Using Aligned Wires," *J. Matl. Sci.,* vol. 11, pp. 71–77, 1976.

51. S. S. Cole, "The Sintering Mechanism in a Silver-Palladium Film," *Proc. Intl. Symp. Microelec.,* Washington, paper 2A1, 1972.

52. R. W. Vest, "Conduction Mechanics in Thick Film Microcircuits," final technical report, grant nos. DAHC-15-70-G7 and DAHC-15-73-G8, ARPA, December 1975.

53. H. Z. Wee and R. W. Vest, "Densification and Adhesion of Silver Thick Film Conductors," *Intl. J. Hybrid Microelec.,* vol. 10, no. 4, pp. 20–24, 1987.

54. R. O. Cooper and E. M. Monahan, "The Characterization of the Solderability of Thick Film Conductors Using a Meniscograph," *Proc. Intl. Symp. Microelec.,* Dallas, pp. 8–12, 1984.

55. "Solderability Tests for Printed Boards," Joint Industry Standard, EIA/IPC, ANSI/J-STD-003, pp. 11–15, April 1992.

56. H. L. Pinch and D. J. Sjostak, "Solderability, Chemical Composition, and Surface Characterization of Fritless Copper Thick Film Inks," *Proc. Intl. Symp. Microelec.,* Seattle, pp. 398–404, 1988.

57. T. T. Hitch, "Adhesion Measurements on Thick Film Conductors," Adhesion Measurement of Thin Films, Thick Films, and Bulk Coatings, ASTM STP 640, K. L. Mittal (ed.), ASTM, pp. 211–232, 1978.

58. G. P. Anderson et al., "The Influence of Loading Direction upon the Character of Adhesive Bonding," *J. Coll. and Interface Sci.,* pp. 600–609, 1974.

59. K. J. Williams, "Adhesion Test Methods for Solderable Thick Film Conductors," Brazing and Soldering, no. 15 (autumn), pp. 10–18, 1988.

50. R. H. Zeien, "Characterization of Thick Film Fritless Metallization," *Proc. Intl. Symp. Microelec.,* Boston, pp. 7–15, 1974.

51. W. A. Crossland and L. Hailes, "Thick Film Conductor Adhesion Reliability," *Solid State Tech.,* vol. 14, no. 2, pp. 42–47, 1971.

62. E. A. Webb, "Effects of Copper Thick Film Processing on Adhesion and Bondability," *Proc. 6th Euro. Microelec. Symp.,* Bournemouth, U.K., pp. 128–135, June 1987.

63. R. Senkalski et al., "Large-Area Non-Warp Dielectric for Multilayer Structures," *Proc. Intl. Symp. Microelec.,* Atlanta, pp. 132–135, 1986.

64. E. Liang et al., "Thick Film Materials System for Air and Nitrogen Firing Applications," *Proc. IEEE 36th Elec. Comp. Conf.,* pp. 493–500, 1986.

65. J. Barrett and P. Moran, "Laser Drilling of Vias in Unfired Thick Film Dielectrics," *Proc. Intl. Symp. Microelec.,* Dallas, pp. 1–7, 1984.

66. A. Shaikh et al., "Thick Film Interfacial Interactions and Resultant Effects on Fired Film Properties," *Proc. Intl. Symp. Microelec.,* Baltimore, pp. 568–576, 1989.

67. J. M. Herbert, *Ceramic Dielectrics and Capacitors,* Gordon and Beach, 1985.

68. A. Shaikh et al., "A Hermetic Low *K* Dielectric for Alumina Substrate," *Proc. Intl. Symp. Microelec.,* pp. 189–194, 1988.

69. S. J. Stein et al., "Interconnection and Packaging of Advanced Electronic Circuitry," *Proc. Intl. Symp. Microelec.,* Orlando, pp. 130–134, 1991.

70. Gary P. Shorthouse et al., "A Hermetic Very Low *K* High Resolution Thick Film Dielectric for High Speed High Density Interconnections," *Proc. Intl. Symp. Microelec.,* pp. 528–532, 1991.

71. A. Shaikh et al., "New Materials for High Speed Multilayer Circuits," *Proc. 8th Euro Hybrid Microelec. Conf.,* Rotterdam, 1991.

72. D. Kellerman, "The Development and Characterization of a Low Dielectric Constant Thick Film Material," *Proc. 37th Elec. Comp. Conf.,* Boston, pp. 316–327, 1987.

73. M. K. Rao et al., "Effects of Infra-Red Firing on the Properties of Low *K* Thick Film Dielectrics Compositions," *Proc. Intl. Symp. Microelec.,* Atlanta, pp. 119–123, 1986.

74. C. M. Val et al., "Copper-Dielectric Interactions—A Comprehensive Study," *Proc. Intl. Symp. Microelec.,* pp. 37–48, 1980.

75. V. P. Suita and R. J. Bacher, "Firing Process-Related Failure Mechanisms in Thick Film Copper Multilayers," *Proc. 36th Elec. Comp. Conf.,* Seattle, pp. 471–480, 1986.

76. C. R. S. Needs, "The Accelerated Life Testing of Copper Thick Film Multilayer Materials," *Proc. Intl. Symp. Microelec.,* Atlanta, pp. 840–847, 1986.

77. R. Gardner et al., "Materials Science Aspect of a Thick Film Copper/Dielectric System," *Proc. Intl. Symp. Microelec.,* pp. 285–294, 1990.

78. R. R. Sutherland et al., "A Comparison of Reliability of Copper and Palladium Silver Thick Film Crossovers," *Proc. 35th Elec. Comp. Conf.,* pp. 498–504, 1985.

79. S. S. Tamhankar and R. Keusseyan, "Optimization of Atmosphere Doping for Firing Photoformable Copper Thick Film Materials," *Proc. Intl. Symp. Microelec.,* Chicago, pp. 8–83, 1990.

80. E. S. Dettmer et al., "Hybrid Design and Processing Using Aluminum Nitride Substrates," *Proc. Intl. Symp. Microelec.,* pp. 545–553, 1988.

81. S. Chitale et al., "ESL Thick Film Materials for AlN," *J. of Adv. Microelec.,* vol. 22, no. 1, pp. 21–23, 1994.

82. V. Komarov et al., "Classification of Dopants for Barium Titanate," *Izv. Akad. Nauk SSSR, Ser. Fiz.,* vol. 29, pp. 1873–1875, 1975.

83. O. I. Prokopalo et al., "Classification of Modifier for Barium Titanates," *Izv. Akad. Nauk SSSR, Ser. Fiz.* (English trans.), vol. 33, pp. 1075–1079, 1969.
84. Leppavuori et al., "Electrical Properties of Thick Film Capacitor Based on Barium Titanate Glass Formulation," *Thin Solid Films,* vol. 86, pp. 287–295, 1981.
85. A. Ikegami, "Thick Film Capacitor Materials of the Powder-Glass Binary Systems and Their Dielectric Properties," *Electrocom. Sci. and Tech.,* vol. 9, pp. 147–152, 1981.
86. L. C. Hoffman and T. Nakayama, "Screen Printed Capacitor Dielectrics," *Microelec. and Reliability,* Paragon Press, vol. 7, pp. 131–135, 1968.
87. K. Abe et al., "Development of the Thick Film Capacitor and Its Application for Hybrid Circuit Modules," *Proc. 29th Elec. Comp. Conf.,* pp. 277–285, 1979.
88. J. V. Biggers et al., "Thick Film Glass Ceramic Capacitor," *Solid State Tech.,* pp. 63–66, 1970
89. R. A. Delaney et al., *IBM J. of R&D,* vol. 11, pp. 511–519, September 1967.
90. J. P. Holden, *Radio Electron. Eng.,* pp. 381–387, December 1968.
91. R. L. Stermer, *IEEE Intl. Conv. Rec.,* vol. 12, pt. 9, pp. 47–53, 1964.
92. H. Stetson et al., "Development of a High *K* Thick Film Capacitor with Copper Electrodes for Nitrogen Firing," *Proc. 36th IEEE Elec. Comp. Conf.,* pp. 488–492, 1986.
93. J. W. Asher and C. R. Pratt, *Proc. Electron. Comp. Conf.,* pp. 239–245, 1968.
94. M. Anliker et al., *Helv. Phys. Acta.,* vol. 27, pp. 99–124, 1954.
95. Shen-Li Fu and Gung Fu Chen, "Low Temperature Firing Thick Film Dielectrics in the System $Pb(Fe_{2/3}W_{1/3})_x(Fe_{1/2}Nb_{1/2})_{0.86-x}Ti_{0.14}O_3$–$Bi_2O_3$–$Li_2O$," *Am. Cer. Soc. Bull.,* vol. 66, no. 9, pp. 1397–1400, 1987.
96. S. L. Fu and G. F. Chen, "Low Firing $Pb(FeW)(FeNb)TiO_3$ Based Thick Film Capacitor Materials," *Proc. Intl. Symp. Microelec.,* Anaheim, Calif., pp. 48–51, 1985.
97. T. C. Reiley et al., "A Low Temperature Firing Thick Film Capacitor Material Based on Lead Iron Niobate Tungstate," *Matl. Res. Bull.,* vol. 19, no. 12, pp. 1543–1549, 1984.
98. S. J. Stein et al., "High Reliability Thick Film Capacitor Dielectrics," *Proc. Intl. Symp. Microelec.,* Dallas, pp. 433–440, 1984.
99. J. Steinberg, "Materials and Applications for Thick Film *RC* Networks," *Proc. Intl. Symp. Microelec.,* Chicago, pp. 276–283, 1990.
100. Z. Strand, *Glass-Ceramic Materials,* Elsevier, New York, 1986.
101. C. R. S. Needs and D. P. Button, "Reliability Testing of Thick Film Multilayer Materials," *Proc. Elec. Comp. Conf.,* pp. 505–511, 1985.
102. Hewlett-Packard, "Basics of Measuring the Dielectric Properties of Materials," HP application note 1217-1, HP lit. no. 5091-3300E, February 1992.
103. IEC, "Recommended Method for the Determination of the Permittivity and Dielectric Dissipation Factor of Electrical Insulating Materials at Power, Audio and Radio Frequencies Including Meter Wavelengths," IEC pub. no. 250.
104. MIL-M-28787 C Test Method, app. B, par. 40.8.3.7, January 29, 1988.
105. M. E. Deunesnil, "Resistor and Resistor Composition," U.S. pat. no. 3052573, September 4, 1962.
106. E. M. Davis et al., "Solid Logic Technology Versatile High Performance Microelectronics," *IBM J. of R&D,* vol. 8, no. 2, pp. 102–114, 1964.
107. E. H. Melan and A. H. Mones, "The Glaze Resistor—Its Structure and Reliability," *Proc. IEEE Comp. Conf.,* p. 76, 1964.
108. E. H. Melan, "Stability of Palladium Oxide Resistive Glaze Films," *Microelec. Reliability,* vol. 6, p. 53, 1967.
109. P. R. Van Loan, "Conductive Ternary Oxides of Ruthenium and Their Use in Thick Film Resistor Glazes," *Amer. Cer. Bull.,* vol. 51, no. 3, pp. 231–234, 1972.

110. R. E. Cote et al., "Factors Affecting Laser Trim Stability of Thick Film Resistors," *Proc. Intl. Symp. Microelec.,* Vancouver, pp. 128–137, 1976.

111. S. Vasudevan and A. Shaikh, "Structure Property Modeling of Low Ohm Thick Film Resistors," *Proc. Intl. Symp. Microelec.,* Dallas, pp. 685–694, 1993.

112. D. Bender and R. Lathroy, "Novel High Performance Resistor Design for Telecommunications A-C Surge Protection," *Proc. ISHM Adv. Matl. Tech. Conf.,* Orlando, 1989.

113. C. Y. Kuo, "Thick Film Circuits," *Engineered Materials Handbook,* vol. 4, *Ceramics and Glasses,* ASM, 1991.

114. B. S. Lee and R. W. Vest, "Peak Temperature Glass Viscosity Effects on the Properties of Thick Film Resistors," *Cer. Trans.,* vol. 11, pp. 405–416, 1990.

115. S. Vasudevan and R. W. Vest, "The Effect of Conductive Particle Size on the Temperature Dependence of Resistance in Thick Film Resistors," *Proc. Am. Cer. Soc. Symp.,* pp. 417–428, Indianapolis, 1989.

116. Osamu Abe et al., "The Effect of Various Factors on the Resistance and TCR of RuO_2 Thick Film Resistors," *Active and Passive Elec. Comp.,* vol. 13, pp. 67–83, 1988.

117. P. F. Garcia et al., "Particle Size Effects in Thick Film Resistors," *J. Appl. Phys.,* vol. 53, no. 7, pp. 5282–5287, 1982.

118. B. Morten et al., "Thick Film Technology and Sensors," *Sensors and Actuators,* vol. 16, p. 109, 1983.

119. L. Golonka et al., "Influence of Composition and Construction Parameter on the Basic Properties of Thick Film Thermistors," *Hybrid Cir.,* no. 28, pp. 9–12, 1992.

120. P. Palanisamy and K. E. Ewing, "Self Sealing Thermally Sensitive Resistor and Method of Making Same," U.S. patent no. 4,452,726, June 5, 1984.

121. Jayanth S. Shah, "Strain Sensitivity of Thick Film Resistors," *IEEE Trans. CHMT,* vol. 3, no. 4, pp. 554–564, 1980.

122. M. Prudenziati and B. Morten, "Piezoresistive Properties of Thick Film Resistors: An Overview," *Hybrid Cir.,* vol. 10, pp. 20–25, 1986.

123. M. Purdenziati et al., "Very High Strain Sensitivity in Thick Film Resistors: Real and False Super Gauge Factors," *Sensors and Actuators,* vol. 19, pp. 401–414, 1989.

124. P. R. Garcia et al., "Electrical Conduction and Strain Sensitivity in RuO_2 Thick Film Resistors," *J. Appl. Phys.,* vol. 54, no. 10, pp. 6002–6008, 1983.

125. R. T. Hopper, "How to Apply Noble Metals to Ceramics," *Cer. Ind.,* June 1963.

126. K. Bab et al., "Formation of Thin Film Resistors By Use of Metallo-Organic Deposition Method and its Application for Thermal Print Head," *Proc. Intl. Symp. Microelec.,* Seattle, pp. 381–386, 1988.

127. S. Taguchi and T. Watanabe, "The Development of Thick Film Resistors for Thermal Print Head," *Proc., Intl. Symp. Microelec.,* Minneapolis, pp. 221–230, 1987.

128. S. M. Chitale and R. W. Vest, "Critical Relationships Between Particle Size, Composition, and Microstructure in Thick Film Resistors," *IEEE Trans. CHMT,* vol. 11, no. 4, pp. 604–609, 1988.

129. A. N. Prabu and R. W. Vest, "Investigation of Microstructure Development in RuO_2 Lead Borosilicate Glass Thick Film," *Matl. Sci. Res.,* vol. 10, pp. 399–401, 1978.

130. A. Kushy, "Chains of Conducting Particles that Determine the Resistivity of Thick Resistive Films," *Thin Solid Films,* vol. 121, p. 263, 1984.

131. Mathey Biship, Inc., *Application Data Index,* EMG 2.2, June 1972.

132. M. V. Coleman, "Evaluation Methods for the Examination of Thick Film Materials," *Radio and Electronic Engineer,* vol. 45, no. 3, pp. 121–130, 1975.

133. G. E. Pike and C. H. Seager, "Electrical Properties and Conduction Mechanisms of Ru-Based Thick Film (Cermet) Resistors," *J. Appl. Phys.,* vol. 48, pp. 5122–5168, 1977.

134. D. P. H. Smith and J. C. Anderson, "Electrical Conduction in Particulate Thick Films," *Philosophy Mag. B,* vol. 43, no. 5, p. 811, 1981.

135. P. J. S. Ewen and J. M. Robertson, "A Percolation Model of Conduction in Segregated Systems of Metallic and Insulating Materials: Application to Thick Film Resistors," *J. Appl. Phys.,* vol. 14, pp. 2253–2268, 1981.

136. R. W. Vest, "A Model for Sheet Resistivity of RuO_2 Thick Film Resistors," *IEEE Trans. CHMT,* vol. 14, no. 2, pp. 396–406, 1991.

137. Toshio Inokuma et al., "The Microstructure of RuO_2 Thick Film Resistors and the Influence of Glass Particle Size on Their Electrical Properties," *IEEE Trans. CHMT,* vol. 7, no. 2, pp. 166–175, 1984.

138. J. A. Loughran and R. A. Sigsbee, "Termination Anomalies in Thick Film Resistors," *Proc. Intl. Symp. Microelec.,* 1969.

139. R. M. Hill, *Proc. IEEE Conf. 402,* London, 1977.

140. D. P. H. Smith and J. C. Anderson, "Electrical Conduction in Thick Film Paste Resistors," *Thin Solid Films,* vol. 71, p. 79, 1980.

141. N. C. Halder, "Electron Tunnelling and Hopping Possibilities in RuO_2 Thick Films," *Electro. Comp. Sci. and Tech.,* vol. 110, pp. 21–34, 1983.

142. M. Prudenziati, "Electrical Transport in Thick Film (Cermet) Resistors," *Electro. Comp. Sci. and Tech.,* vol. 10, pp. 285–293, 1983.

143. R. W. Vest et al., "The Dependence of Charge Transport on Microstructure in Thick Film Resistors," *Proc. 5th Euro. Hybrid Microelec. Conf.,* Italy, pp. 406–412, 1985.

144. S. Vasudevan, "Charge Transport Mechanisms in Thick Film Resistors," Ph.D. dissertation, Purdue Univ., Ind., 1990.

145. David E. Hayes and Donald R. Emmons, "Laser Pulse Measurements for Safe and Proper Trimming System Alignment," *Hybrid Circuit Tech.,* pp. 35–40, November 1987.

146. M. A. Barnes et al., *An Introduction to Rheology,* Elsevier, 1989.

147. F. R. Eirich (ed.), "Rheology—Theory and Applications," vol. 3, Academic Press, 1960.

148. F. R. Eirich (ed.), "Rheology—Theory and Applications," vol. 4, Academic Press, 1960.

149. P. Sherman, *Industrial Rheology,* Academic Press, 1960.

150. K. M. Oesterle and M. B. Palmer, "Viscometry of Coating Material," *Treatise on Coatings,* vol. 2, Marcel Dekker, New York, pp. 123–248.

151. T. R. Tadros, "Control of the Properties of Suspensions," *Colloid and Surfaces,* vol. 18, pp. 137–173, 1986.

152. J. W. Goodwin, "The Rheology of Dispersions," *Colloid Sci.,* vol. 2, The Chemical Society, pp. 246–293, 1975.

153. T. C. Patton, "Paint Flow and Pigment Dispersion," 2d ed., Wiley Interscience, 1979.

154. W. H. Bauer and E. A. Collins, "Thixotropy and Dilatancy," *Rheology—Theory and Applications,* vol. 4, Academic Press, pp. 423–466, 1960.

155. R. J. Hunter, "Foundations of Colloid Science," vol. 1, Clarendon Press, 1987.

156. J. Th. G. Overbeck, *Adv. Colloid Interface Science,* vol. 15, p. 251, 1982.

157. T. Sato, *Coatings Tech.,* vol. 65, no. 825, pp. 113–121, 1983.

158. G. Y. Onoda, Jr., *Ceramic Processing Before Firing,* John Wiley and Sons, p. 235, 1978.

159. J. N. Israelachvili and B. W. Ninham, *J. Colloid Interface Science,* vol. 58, p. 14, 1977.

160. A. S. Michaels and J. C. Bolger, *Ind. Eng. Chem. Fund.,* vol. 1, no. 3, p. 153, 1962.

161. R. Buscall et al., "Scaling Behaviour of the Rheology of Aggregate Networks Formed from Colloidal Particles," *J. Chem. Soc., Faraday Trans. 1,* vol. 84, no. 12, pp. 4249–4260, 1988.

162. R. C. Sunntag and W. B. Russel, *J. Colloid Interface Science,* vol. 17, p. 33, 1987.

163. D. C.-H. Cheng, "Yield Stress: A Time-Dependent Property and How to Measure It," *Rheolog. Acta,* vol. 25, pp. 542–554, 1986.

164. C. S. Khadilkar, unpublished work.

165. R. M. Stanton, *Proc. Intl. Symp. Microelec.,* pp. 419–432, 1976.

166. C. S. Khadilkar and M. D. Sacks, "Effects of Poly (Vinyl Alcohol) on the Properties of Model Silica Suspensions," *Cer. Trans.,* vol. 1, pt. A, *Cer. Powder Sci.,* pp. 397–409, 1988.

167. D. R. Kobs and D. R. Voight, "Parametric Dependencies in Thick Film Screening," *Solid State Tech.,* pp. 34–41, February 1971.

168. C. Missels, *Hybrid Circuit Tech.,* pp. 11–13, May 1985.

169. D. E. Riemer, "The Theoretical Fundamentals of the Screen Printing Process," *Hybrid Cir.,* vol. 18, pp. 8–17, January 1989.

170. J. A. Owczarek and F. L. Howland, "A Study of the Off-Contact Screen Printing Process," pts. I and II, *IEEE Trans. CHMT,* vol. 13, no. 2, pp. 358–375, June 1990.

171. D. E. Riemer, "Ink Hydrodynamics of Screen Printing," *Proc. Intl. Symp. Microelec.,* Anaheim, Calif., pp. 52–58, 1985.

172. D. E. Riemer, "The Shear Flow Experience of Ink During Screen Printing," *Proc. Intl. Symp. Microelec.,* Minneapolis, pp. 335–340, 1987.

173. D. O. Brown, "Screen Printing—An Integrated System," *Proc. Intl. Symp. Microelec.,* Atlanta, pp. 582–590, 1986.

174. M. Chi Rang et al., "A Model for Deposition of Thick Films by the Screen Printing Technique," *Proc. Intl. Symp. Microelec.,* Dallas, pp. 604–609, 1984.

175. R. E. Trease and R. L. Dietz, "Rheology of Pastes in Thick Film Printing," *Solid State Tech.,* vol. 1, pp. 39–43, 1972.

176. A. C. Zettlemoyer and R. R. Myers, "The Rheology of Printing Inks," *Rheology,* vol. 3, Academic Press, pp. 145–188, 1960.

177. J. R. Larry, "Influence of Surface Energies on Line Resolution in Screen Printing," *Solid State Tech.,* pp. 48–58, June 1972.

178. K. Gilleo, "Rheology and Surface Chemistry for Screen Printing," *Screen Printing,* pp. 128–132, February 1989.

179. S. Wu, "Rheology of High Solids Coatings," "Analysis of Combined Sagging and Leveling," *J. Appl. Polymer Sci.,* vol. 22, pp. 27–83, p. 2791, 1978.

180. H. L. Beeferman and D. Bergren, "Practical Applications of Rheology in the Paint Industry," *J. Paint Tech.,* vol. 38, no. 492, January 1966.

181. J. D. Mackenzie and R. Shuttleworth, "Phenomenological Theory of Sintering," *Proc. Phys. Soc.,* London, vol. 62, no. 12B, pp. 833–852, 1949.

182. G. Scherer and T. Garino, "Viscous Sintering on Rigid Substrate," *J. Am. Cer. Soc.,* vol. 68, no. 4, pp. 216–220, 1980.

183. M. D. Sacks and T. Y. Tseng, "Preparation of SiO_2 Glass from Model Powder Compacts," "Sintering," *J. Am. Cer. Soc.,* vol. 67, no. 8, pp. 532–537, 1984.

184. J. P. Bradley, "Copper Thick Film Nitrogen Atmosphere Furnace Design and Firing Process Considerations," *Proc. Intl. Symp. Microelec.,* pp. 435–453, 1985.

185. I. Strobeck et al., "Substrate Bowing of Multilayer Thick Film Circuits," *Hybrid Circuits,* no. 11, pp. 21–23, 1986.

CHAPTER 9
INDUSTRIAL DIAMOND

Mark P. D'Evelyn
GE Corporate Research and Development
Schenectady, New York

Human fascination with diamond as a hard gemstone dates back several millennia,[1,2] while the use of diamond for industrial manufacturing and processing is much more recent and has grown considerably since the development of high-pressure/high-temperature (HPHT) methods for synthesis of diamond and cubic boron nitride (cBN). After a brief historical overview, this chapter will describe the industrial diamond and cBN products in widespread use today and the applications for which they are so well suited.[3]

9.1 INTRODUCTION AND HISTORICAL OVERVIEW

The discovery by Lavoisier and Tennant in the late 1700s that diamond was a form of carbon stimulated a number of attempts to synthesize diamond from graphite (obviously a cheaper and much more plentiful form of carbon). Because natural diamonds were formed deep within the earth, it was natural for scientists to assume that conditions of elevated temperatures and pressures would be required. Various attempts were made during the 1800s and early 1900s, but none were successful.[2]

During the 1940s, three factors converged to pave the way for a successful synthesis a decade later: new experimental capability, a heightened sense of need, and theory. Professor Percy Bridgman of Harvard University, later to win a Nobel Prize, began pioneering studies on the production of pressures in the 1 to 100 kbar range (1 kbar = 1010 atm = 0.1 GPa). During the 1940s, with support from an industrial consortium, Bridgman performed HPHT experiments aimed at converting graphite to diamond. Although pressures of 40 kbar and temperatures up to 3000°C were reached, no diamond was produced and the experiments were abandoned.

With the end of World War II and the beginning of the Cold War, industry in the West found that it had become dependent on diamond for processing of advanced materials: grinding cemented tungsten carbide cutting tools; sawing and drilling hard rock and concrete; and polishing. The main sources of industrial-grade diamond (South Africa, the Soviet Union) were of uncertain long-term reliability, and the need for a domestic, manufactured source of industrial diamond was felt keenly, particularly in the United States.

Careful experiments on the thermodynamics of graphite and carbon, notably by Rossini and Jessup at the U.S. National Bureau of Standards, led to a prediction by Leipunskii that pressures of 40 to 60 kbar would be required for diamond synthesis at temperatures of 1000 to 1700°C.[4] The Rossini-Jessup-Leipunskii phase diagram turned out to slightly underestimate the pressure required for the stability of diamond, and was particularly important as a guide for experimentalists. The phase diagram of Berman and Simon,[5] proposed shortly after diamond synthesis was successful, has been verified by a number of careful experiments.

In 1951 the General Electric Company took up the challenge to develop a manufacturing process for industrial diamond, committing a significant level of resources. The team spent considerable effort on high-pressure equipment, refining Bridgman's designs, culminating in Hall's "belt" apparatus. The belt comprises a series of tensioned steel rings that radially load a tungsten carbide die. An oblique angle between the tungsten carbide punches and the die, together with an appropriate gasket material (e.g., pyrophyllite), provides confinement so that pressures beyond the yield point of tungsten carbide can be accessed. During 1954 the team experimented with various catalysts to facilitate the tranformation from graphite to diamond. Finally, Hall tried iron sulfide—which serendipitously included some elemental iron—and, on December 16, 1954, successfully grew some grayish-green and yellow diamond crystals. The experiments were carefully repeated, and the GE team published the results[6] and filed patent applications. Successful diamond synthesis was quickly reproduced at a number of labs across the world. Ironically, an effort led by von Platen and Lundblad at ASEA in Sweden had synthesized diamond at HPHT more than a year earlier, in February 1953, but ASEA did not publish or patent its results until after the GE announcement. By 1957 GE had successfully begun commercial manufacturing of diamond, followed several years later by De Beers.

Virtually all commercial HPHT synthesis of diamond uses iron, nickel, cobalt, manganese, chromium, and their alloys as catalyst-solvents. However, many other metals can catalyze graphite-to-diamond formation at higher temperatures and pressures, as can water, silicates, and other minerals that are more akin to the environment in which natural diamonds grow in the earth.

During the next 15 years there were a number of additional innovations in the application of HPHT technology to the synthesis of industrial superabrasives, virtually all of which were pioneered by GE—the Superabrasives[7] business working in close collaboration with the Corporate Research and Development laboratory. In 1956, Wentorf synthesized cubic boron nitride (cBN).[8] Boron nitride does not exist in nature, but the hexagonal form of BN, which has a structure very similar to that of graphite, was a well known synthetic material. The second-hardest material known, cBN has much better abrasion resistance with ferrous alloys and oxidation resistance than diamond. The best catalyst-solvents for cBN synthesis are alkali- and alkaline-earth nitrides and related inorganic salts. GE introduced cBN commercially in 1969 under the tradename Borazon* cBN.

In 1971, GE researchers Wentorf and Rocco developed a process for synthesis of polycrystalline diamond (PCD, introduced with the commercial name Compax* Diamond), in which cobalt was added to diamond powder as a sintering aid and subjected to HPHT treatment. The resultant compact is about 85 percent diamond, with the balance cobalt, depending on the grain size of the starting material. PCD is normally supplied directly bonded to tungsten carbide, and is extremely effective in machining nonferrous metals, in woodworking, and as a dresser of aluminum oxide and silicon carbide grinding wheels. GE introduced PCD wire dies in 1974 and PCD drilling products in 1976. The original process for manufacturing PCD has been significantly refined by GE and others, leading to significant improvements in performance.

---

* Names marked with an asterisk are trademarks of the General Electric Company.

Also in 1971, GE researchers Wentorf and Rocco developed a process for synthesis of polycrystalline cubic boron nitride (PCBN, introduced with the commercial name BZN* Compacts), in which cobalt was added to cBN powder as a sintering aid and subjected to HPHT treatment. GE introduced PCBN commercially in 1975. Other forms of PCBN followed, including ceramic-sintered and TiN-filled composites.

In the late 1960s GE developed a temperature-gradient method for growing large single crystals ("gems"), but never introduced them as a regular commercial product. Large single-crystal synthetic diamond is currently available from De Beers and Sumitomo Electric and is mainly used in wire die and heat sink applications.

There are currently a large number of manufacturers of industrial diamond and cBN worldwide, and the overall market for industrial superabrasives is approximately $1 billion U.S. per year and growing. Depending on size and grade, mesh and micron superabrasives sell for approximately $0.20 to $5.00 per carat (1 carat = 0.2 gram).

9.2 MESH DIAMOND

Ceramics, cermets such as tungsten carbide, hard stone such as granite, and glasses have become increasingly important as industrial materials during the past several decades. In many cases diamond is the abrasive of choice for sawing, grinding, and polishing these materials. Mainly because of diamond's extreme hardness, the material removal rates achievable with diamond tools are sufficiently high that the overall processing cost is considerably reduced relative to tools made with conventional abrasives such as alumina or silicon carbide.

GE's initial grade of commercial mesh diamond, Type A, introduced in 1957, was designed for grinding cemented tungsten carbide. These first tiny sand-like grains quickly established a clear edge over natural diamond for performance and consistency. Within the first ten years of commercial production, operations and engineering developments were refined, and three families of mesh diamond were created for specific applications using resin, metal, electroplated, or vitrified-bond grinding wheels and saw blades.

The first of these families was RVG* diamond, for grinding in resin or vitreous bond systems, which replaced Type A diamond. RVG diamond was designed for use in grinding wheels made with resin or vitreous bond systems, especially for grinding tungsten carbide tools. RVG crystals are elongated, irregular in shape, with rough edges to ensure good retention in the bond. The particles are polycrystalline and contain many metallic inclusions, rendering them highly friable, and are shown in Fig. 9.1. This friability provides a key advantage over natural industrial diamond in grinding. When mined diamond wears, the crystal edges become dull and grinding becomes inefficient. RVG diamond, by contrast, microfractures during grinding, continuously generating fresh, sharp edges that continue to grind efficiently. For the grinding industry, this translates to cost savings via faster grinding, longer-life grinding wheels, and less downtime for wheel changeovers. In 1966, new grades of RVG diamond with nickel or copper coatings were introduced. The metal coatings yielded superior retention in resin bond systems that reached high operating temperatures. Today, nickel-coated RVG diamond is used primarily for wet grinding of cemented tungsten carbide, while copper-coated RVG diamond is used mainly in dry grinding of carbide-steel composites.

During the early 1960s, GE researchers found that by decreasing the diamond growth rate, mesh-sized single crystals could be produced rather than polycrystals, with much higher toughness. This breakthrough made it possible to offer two new classes of products, optimized for new applications: MBG* metal-bond grinding diamond products and MBS* metal-bond saw diamonds. Both MBG and MBS crystals have predominantly cubo-octahedral,

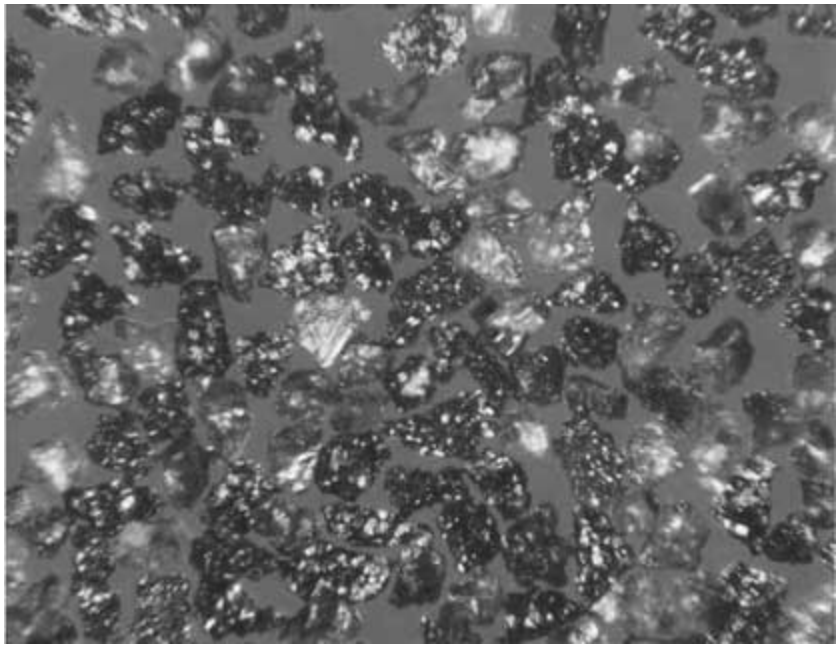

FIGURE 9.1 Resin-bond grinding (RVG*) diamond crystals—irregularly shaped, friable.

blocky shapes resulting from well-formed (100) (square or octagonal) and (111) (hexagonal or triangular) facets, as shown in Fig. 9.2. MBG diamonds are used predominantly for grinding cemented carbides, glass, alumina, and other ceramics, and for electrolytic grinding. MBS diamonds are used in metal bond systems for sawing granite, concrete, tile, marble, other stone, and a variety of masonry and refractory materials and for exploratory core-drilling, and production mining. In some applications adhesion of the diamond crystals to the metal bond is performance limiting, and coatings of TiC or CrC were developed that greatly improve adhesion and crystal retention.

9.2.1 Properties and Characterization

The properties of diamond, cubic boron nitride, and conventional hard materials are summarized in Table 9.1. In addition to being the hardest known substance, diamond is chemically inert to essentially all environments below a temperature of about 500°C and is therefore uniquely qualified for many applications. Diamond has a cubic structure, with each carbon atom bonded to four nearest neighbors. Cleavage normally occurs on one of four (111) planes. In addition to its intrinsic brittleness, diamond has two important limitations. Diamond begins to oxidize and/or graphitize rapidly at temperatures above 600–700°C in air or an oxidizing atmosphere. Diamond readily dissolves in and can be graphitized by ferrous metals such as iron, steels, nickel, and nickel-based superalloys, and therefore abrasion resistance with these metals is poor.

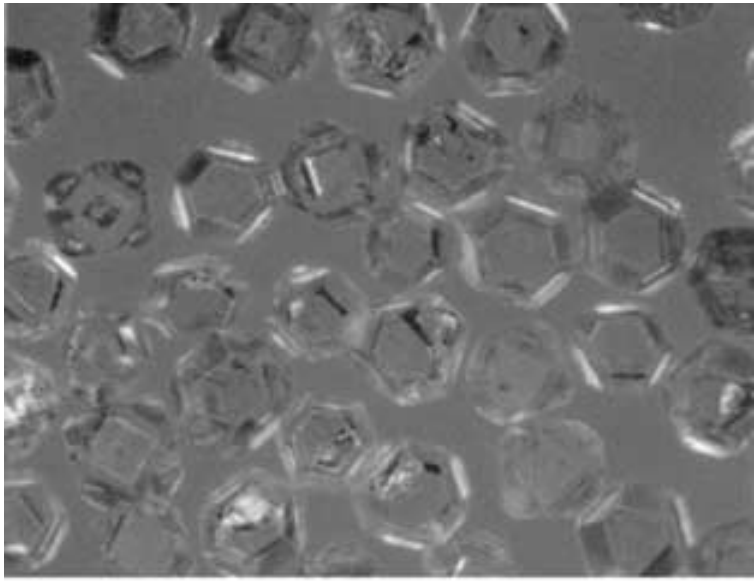

(a)

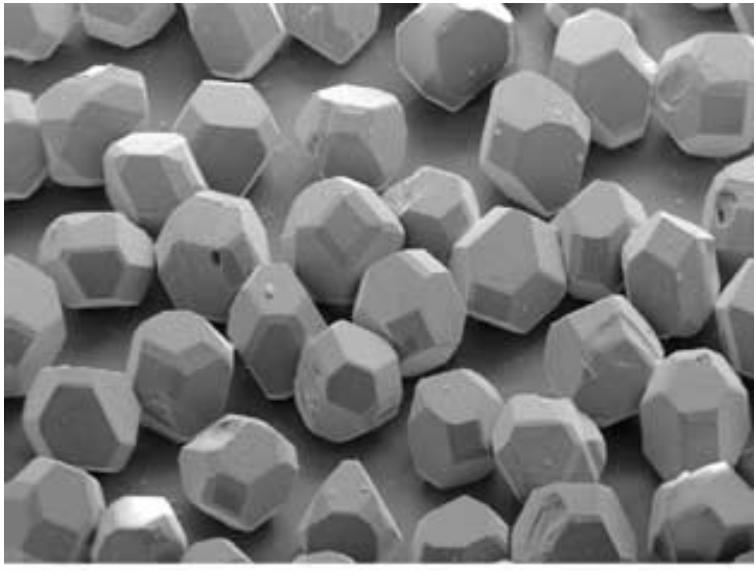

(b)

FIGURE 9.2 Metal-bond saw (MBS*) diamond crystals—well-crystallized and tough—(a) optical; (b) scanning electron micrographs.

TABLE 9.1 Summary of Properties of Superabrasive and Conventional Abrasive Materials

Property	Diamond	Cubic boron nitride	Silicon carbide	Alumina	Tungsten carbide
Knoop hardness,† GPa	70–100	50	25	22	20
Young's modulus,† GPa	1143	909	410	366	570
Poisson's ratio†	0.07	0.12	0.14	0.22	0.22
Density, g/cm^3	3.52	3.48	3.21	3.92	15.0
Thermal conductivity, W/(m · K)	2100	1400	380	40	105
Coefficient of thermal expansion (10^{-6} °C^{-1})	4.8	5.6	4.5	8.6	4.5

†Orientational average.

All grades of industrial diamond have, to first approximation, the same hardness. However, the size, the toughness or friability, the strength and thermal stability, the shape, and impurity contents of the crystals vary greatly and are key metrics for predicting performance in various applications. The ability to *control* these properties constitutes a principal advantage of synthetic diamond over natural diamond for industrial applications.

Commercial-grade diamonds are not pure—they contain dissolved nitrogen, which conveys a yellow or yellow-green color, metallic and oxide inclusions, hydrogen, and other trace impurities. If the metallic inclusions are magnetic they may be quantified via the magnetic susceptibility of the material. The total noncarbon content may be assayed by ashing the diamonds in air and weighing. Nitrogen, oxygen, and hydrogen contents may be quantified by inert gas fusion methods. For saw-grade diamond the ash content typically lies in the range of 0.02 to 1 percent; in resin-grade diamond it is considerably higher, causing the crystals to appear black to the eye. For saw-grade diamond the nitrogen and oxide contents are typically in the ranges of 80 to 300 ppm and 10 to 500 ppm, respectively.

Crystal *size* is very important for determining suitability in an application: larger crystals typically remove workpiece material faster but leave a rougher finish. Relatively coarse crystals are normally used for sawing applications and finer crystals for grinding, as noted above. Crystal sizing is traditionally performed by using sieves, with U.S. mesh being the most common standard. U.S. mesh sizes are summarized in Table 9.2. Crystals with a range of sizes may be separated (classified) by placing them onto a stack of sieves, with the width of the openings decreasing down the stack, and vigorously shaking. The size of crystals may then be specified by the marginal mesh size through which they did and did not pass. For example, −40/+45 (or 40/45, for short) crystals pass through a 40-mesh sieve but not through a 45-mesh sieve. From Table 9.2, these crystals have a median diameter of about 385 μm.

Perhaps the single most important property of mesh diamond is *toughness* (or its converse, friability). In the most commonly applied test, crystals of a fixed mesh size are placed within a steel capsule along with a single ball bearing. The capsule is then vigorously shaken, at a controlled amplitude and frequency for a specified period of time, and the diamonds are removed. The diamonds are then placed on a sieve that is one size smaller than their nominal size, and the weight fraction that does not pass through the sieve is measured. Some manufacturers, including GE, report this weight fraction of essentially unbroken crystals as the toughness index (TI), while other manufacturers report the length of time required to break down a fixed fraction of the crystals. In the most aggressive saw-blade applications, tougher crystals perform better, but in many other applications there is an optimum level of toughness, i.e., a significant degree of friability.

TABLE 9.2 Standard Sizes of Superabrasive Grit

ANSI[§] mesh size	FEPA[†] Size (D = diamond; B = cubic boron nitride)	Median aperture size, μm	Crystal count per carat[‡]
25/30	D/B 711	650	450
30/35	D/B 601	545	750
35/40	D/B 501	460	1,250
40/45	D/B 426	385	2,150
45/50	D/B 356	325	3,600
50/60	D/B 301	275	6,000
60/70	D/B 251	230	10,000
70/80	D/B 213	195	16,900
80/100	D/B 181	165	28,200
100/120	D/B 151	140	47,500
120/140	D/B 126	115	80,000
140/170	D/B 107	97	136,000
170/200	D/B 91	81	230,000
200/230	D/B 76	68	390,000
230/270	D/B 64	58	640,000
270/325	D/B 54	49	1,100,000
325/400	D/B 46	41	1,800,000

[†]Fédération Européenne de Produits Abrasifs.
[‡]For reference only; based on ideal cubo-octahedral particles. 1 carat = 0.2 grams.
[§]American National Standards Institute.

The toughness test has the advantage of being able to test a large number of crystals quickly and cost-effectively, but has the disadvantage of only testing (breaking) the weakest crystals in a distribution. No quantitative information is gained about the strength of the stronger crystals, only that they survived the treatment. Some manufacturers report the results of single-crystal crush tests, in which a crystal is placed between two plates and the load (weight) increased until the crystal breaks. Many crystals are broken in this way, and the mean and standard deviation of the crush strength are reported. This test is rather tedious and does not mimic the type of loading of the diamond crystals that occurs in actual applications.

GE developed a strength test—denoted compressive fracture strength (CFS)—that cost-effectively measures the strength of each crystal and also simulates the dynamic impact loading conditions that are experienced by crystals in an abrasive tool. The test is illustrated schematically in Fig. 9.3. Crystals are dropped one-by-one into the narrow region between two spring-loaded, counter-rotating tungsten carbide wheels. As each crystal "catches," the wheels move apart to accommodate its diameter, increasing the force on the crystal until it breaks. The maximum force on each crystal (measured by a linear voltage displacement transducer) is recorded electronically, so that the mean, standard deviation, or the entire histogram of crystal strengths can be reported.

Fabrication of abrasive tools containing mesh diamonds, particularly with metal bonds, involves processing at temperatures of up to 900°C or even higher. The *thermal stability* of the crystals is therefore very important for such applications. The most common way to characterize thermal stability is to perform a toughness measurement after a high-temperature exposure—for example, 1100°C for 10 minutes in an inert atmosphere—yielding a thermal toughness index (TTI). The thermal stability of diamonds is mainly determined by the

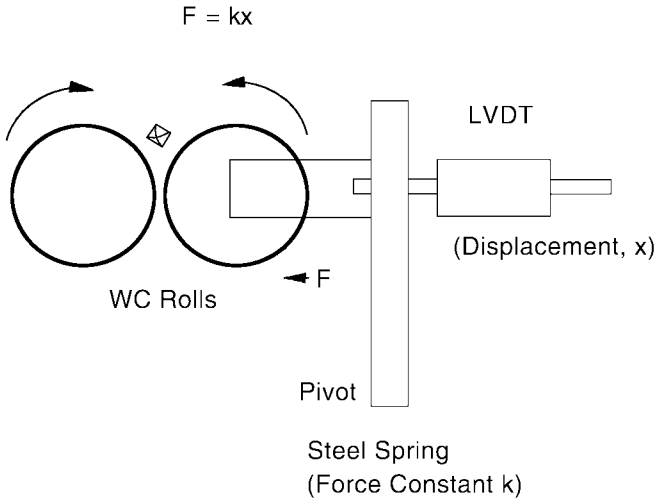

FIGURE 9.3 Schematic of roll-crusher apparatus for measuring compressive fracture strength.

internal concentration of inclusions—catalyst metal and other impurities. Back-conversion of diamond to graphite around the inclusion may occur on heating, and in addition the thermal expansion coefficient of most inclusions is higher than that of diamond. Both effects will contribute to the generation of internal stresses that weaken the crystals.

The *shapes* of diamond crystals turn out to be very important to their strength and toughness and ease of retention in a bond. The highly irregular shape of resin-grade crystals (Fig. 9.1) contributes to their high friability as well as improving bond retention. Even with well-faceted saw-grade crystals (Fig. 9.2), the shape can range from octahedral to cubo-octahedral to cubic, as illustrated in Fig. 9.4, and the eccentricity (ratio of maximum and minimum diameters) can deviate significantly from 1. Diamond manufacturers have known for many years that the crystal shape is sensitive to growth conditions—higher temperatures generally produce more octahedral crystals—and therefore have found it important to control shape. Historically, assessing crystal shape has been performed visually. However, in 1994 GE developed an automated image analysis system that can quantitatively determine crystal shape. Referring to Fig. 9.4, imagine a line running from the center of the top face of the cube circumscribing the crystal to its corner along the diagonal. The shape parameter τ is defined as the ratio of the distances from the center of the top face to (1) the edge of the facet and (2) to the corner of the "reference" cube.[9] Thus, $\tau = 0$ for an octahedron and 1 for a cube.

Although more difficult to quantify, the *fracture characteristics* of diamond crystals can greatly affect overall performance. The fracture characteristics may be assessed by examination of fractured crystals—for example, the debris produced by toughness or strength tests—including the size and shapes of the fragments. Tough (high-strength) diamonds break down via splintering of the crystal edges, producing large and medium fragments and splinters. Many blocky crystals with smooth facets remain. Friable diamonds, by contrast, fracture more completely, producing few large fragments and many small pieces with a rough, irregular texture. The fracture characteristics are affected by many factors, including crystal morphology and shape and the type, content, and distribution of inclusions.

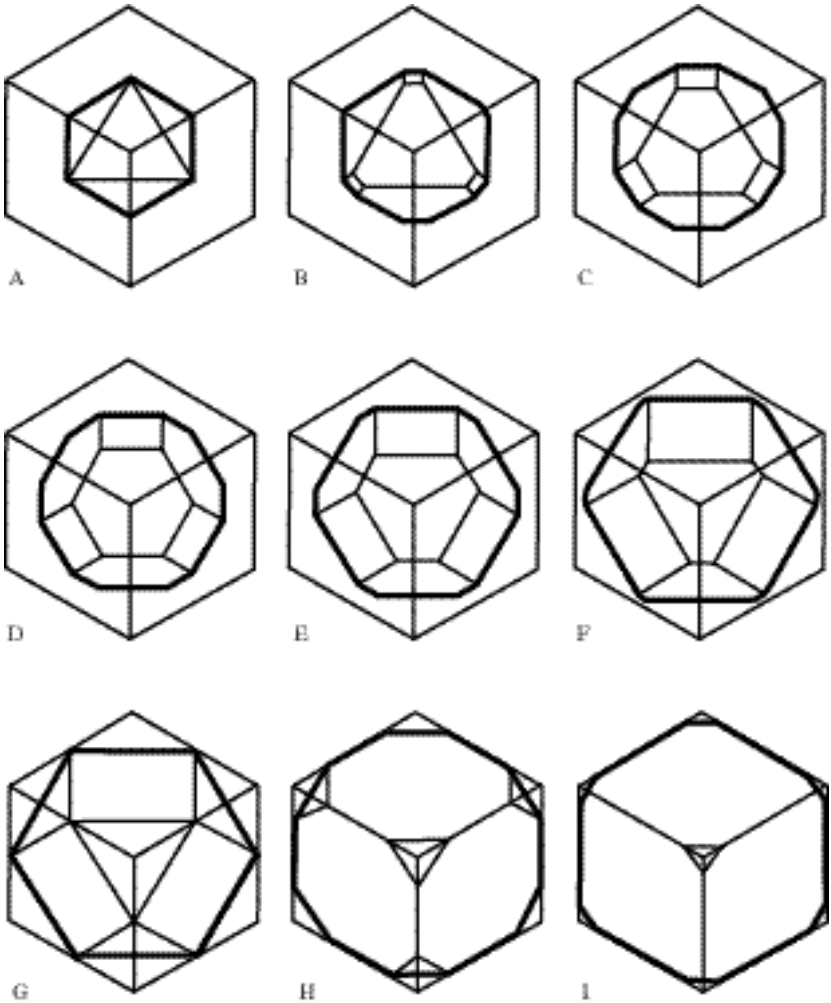

FIGURE 9.4 Shapes of cubo-octahedral crystals.

9.2.2 Bond Systems and Tool Fabrication

To fabricate a diamond tool, diamond crystals are blended with a matrix material, normally in the form of a powder, pressed into a shape, and cured or hot-pressed at elevated temperature.[10] Each tool manufacturer has their own techniques, and most of the details are held as trade secrets. The diamond content is specified by the *concentration*, which in the diamond tool industry refers to 4 times the volume fraction of superabrasive. A tool with concentration 100 therefore comprises 25 vol% diamond. The matrix must be capable of dispersing and supporting the diamond, distributing impact and load as the diamond attacks the workpiece, providing controlled wear while allowing crystal protrusion, and holding

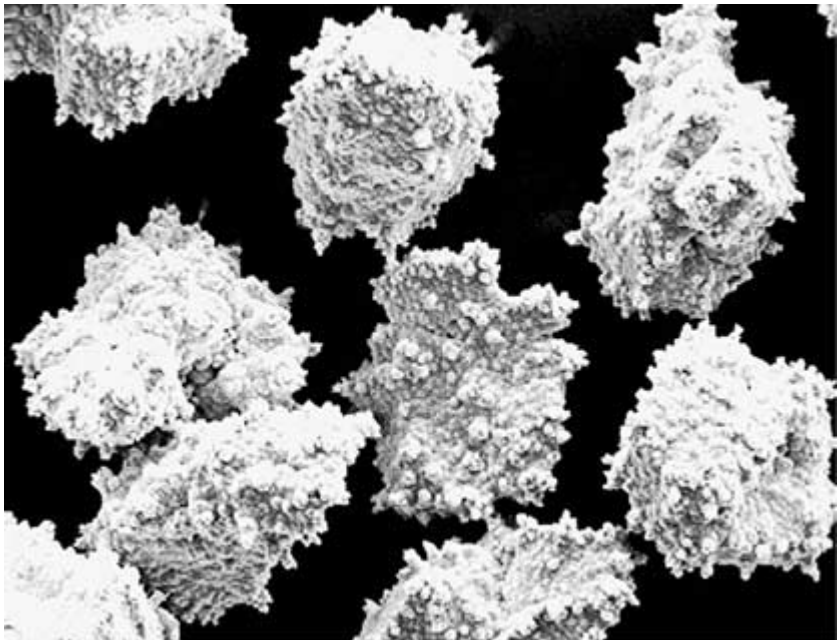

FIGURE 9.5 A spiked-nickel coating on resin-bond diamond increases tool life in many wet grinding applications. Increased life comes from greater mechanical crystal retention in the bond matrix due to the increased surface area created by spikes on the coating surface.

the diamond sufficiently tightly to prevent premature pullout. The matrix may also need to carry away much of the heat generated by abrasion, particularly if no coolant is provided (*dry* rather than *wet* cutting).

In *resin bond* tools the matrix consists of a polymeric resin, for example, a phenolic or polyimide resin, and the curing is typically performed at a relatively mild temperature, around 150–300°C. Because of the limited thermal conductivity and thermal stability of resin bonds, the diamonds used in these applications are most commonly coated with 30 to 70 wt% metal, typically copper or nickel. The metal coatings aid in diffusing the heat generated during the grinding operation to a larger area, minimizing decomposition of the matrix. In addition, the surface of the relatively thick coating is often considerably rougher than that of the diamond, increasing the interfacial area with the matrix and improving retention. GE offers a grade of diamond (RVG-WS60) whose nickel coating has a distinct spiky morphology, as shown in Fig. 9.5. Resin bond tools typically contain diamond at concentrations between 50 and 125 (12.5 to 37.5 vol%).

In *vitreous bonds* the matrix consists of a glassy material, high in silica. Hot pressing requires considerably higher temperatures than with resin bonds, but the thermal conductivity and thermal stability of the matrix are much higher. The porosity of the finished tool is typically much higher, 10 to 25 percent, versus less than 2 percent in most resin or metal bonds, simplifying wheel surface conditioning. Because of the high temperatures required for processing and the inferior thermal stability of diamond relative to cubic boron nitride, vitreous bonds are employed mainly with the latter. Vitreous bond tools typically contain superabrasives at concentrations between 50 and 200.

In *metal bonds* the matrix consists of a metal powder, of which cobalt is the most common. After blending and compaction the green body is hot pressed to achieve densification, typically at temperatures in the range of 750 to 900°C. The thermal stability of the diamond is obviously important in metal bonds. Low-temperature bonds, consisting of cobalt, nickel, bronze, and/or iron (in low concentrations), or a combination of these metals, preserve the strength of the diamond crystals best. In addition, if not managed properly the metal in the bond can catalyze back-conversion of the surface of the diamond to graphite, weakening retention in the bond. In many cases bond retention can be improved by the use of diamonds with coatings, particularly titanium or chromium. In contrast to coatings for resin bonds, coatings for metal bonds are quite thin, less than 1 μm, and form chemical bonds with both the diamond (as the metal carbide) and the metal matrix. Other bonding materials do not sinter well at temperatures below 900°C, and in these cases the bond can be cold pressed and then infiltrated with molten metal (braze alloy) or hot pressed above 1000°C. If temperatures are too high or exposure times too long, the diamond impact strength will be reduced.

In *electroplated* bonds a single layer of diamond crystals is attached to a grinding wheel by means of a layer of metal, typically nickel, that is electroplated on top of the diamonds. The thickness of the electroplated layer is typically about one-third to one-half the diameter of the crystals. Single-layer tools can also be produced by *brazing*. It is essential for the braze to achieve good wetting of the crystals when melted to develop a strong bond. The thickness of the braze layer is typically 15 to 30 percent of the diameter of the crystals.

9.2.3 Applications

Applications for mesh diamond generally fall into the categories of *grinding*, *sawing*, and *drilling*. As noted above, diamond is frequently the abrasive material of choice for processing concrete and hard stone, ceramics, cermets, and glasses. For hard, brittle workpiece materials such as tungsten carbide, technical ceramics, and polycrystalline diamond or cBN, grinding is often carried out most effectively with a friable grade of diamond (e.g., RVG*) in a resin bond.[10] In such an application, grinding of the workpiece occurs via an impact mode involving rubbing, plowing, and chipping. As the bond matrix erodes during grinding, friable diamond crystals undergo controlled fracture, constantly generating sharp new cutting edges. In such applications tough diamond crystals become dull instead of fracturing and polish rather than grind the workpiece. As noted above, in most resin bond applications the diamond crystals are coated with 50 to 60 wt% nickel or copper, which helps dissipate heat and also creates a rougher interface with the bond, increasing the adhesion strength.

For other types of materials, grinding wheels containing a tougher grade of diamond in metal bonds perform better. For example, granite, which has become very popular as an architectural material and as a kitchen counter surface, is too tough to be effectively ground by friable diamond. And for fabricating fine features, e.g., by pencil grinding, resin bonds are not strong enough and wear too fast to hold a sharp edge. Examples of applications of metal-bonded diamond grinding tools, together with recommended grades of MBG* diamond, are summarized in Table 9.3.

Sawing and drilling, primarily of concrete, granite, and other hard stone building materials, have become the largest applications of industrial diamond, and metal bonds are normally employed. Diamond tools are used throughout the concrete industry in new construction, renovation, demolition, and road and runway construction and resurfacing. Types of cutting include flat sawing, wall sawing, wire sawing, core drilling, dry sawing, and grinding and grooving. Applications in the stone industry range from quarrying and slabbing to trimming, calibrating, and finishing, as summarized in Table 9.4. Saw-grade diamond is also used for

TABLE 9.3 Application Guidelines for Metal-Bond Grinding (MBG*) Diamond, Listed by Preferred Product[†]

MBG 660	MBG 640	MBG 620	MBG 610	MBG 600	MBG 300
Glass Pencil edging Fluting crystal stems	Glass Pencil edging Seaming Engraving crystal Cutoff wheels	Glass Pencil edging Beveling	Glass Seaming Mirror edging Bevel polishing	Glass Mirror edging Bevel polishing	
Granite Beveling/edging Trimming Polishing	Granite Midstage polishing	Granite Trimming	Granite Polishing	Granite Polishing	Granite Finish polishing
Marble/limestone Trimming		Marble/limestone Trimming/polishing	Marble Polishing	Marble Polishing	Marble Polishing
Ceramic tiles Trimming Rough polishing		Tungsten carbide Burr grinding	Ceramic Dental burrs Cutoff wheels	Ceramic Dental burrs	Ceramic tiles Finish polishing
Ferrite Grinding motor cores	Ferrite Grinding motor cores	Cast iron Honing cylinder liners			

[†]The toughness of the crystals decreases from MBG 660 to MBG 300.

TABLE 9.4 Application Guidelines for Metal-Bond Saw (MBS*) Diamond, Listed by Preferred Product[†]

MBS 970	MBS 960-950	MBS 950-940	MBS 930-920	MBS 920-910
Concrete/asphalt Reinforced Tough aggregates	Concrete/asphalt Reinforced All aggregates	Concrete/asphalt Nonreinforced Medium, light aggregates	Concrete/asphalt Hand-held equipment	Concrete/asphalt Hand-held equipment Do-it-yourself-cutters
Granite Wire sawing Multiblade slabbing Large blade slabbing Trimming	Granite Wire sawing Multiblade slabbing Large blade slabbing Trimming	Granite Trimming Calibrating	Granite Polishing	
Marble/limestone Belt sawing		Hard marble/limestone Wire sawing Frame sawing Trimming Calibrating	Soft marble/limestone Wire sawing Frame sawing Trimming	Marble/limestone/softstone Wire sawing Frame sawing Polishing
Exploration/mining Core drilling				Natural diamond replacement

[†]The toughness of the crystals decreases from MBS 970 to MBS 910.

FIGURE 9.6 Diamond saw blades, wire saws, and core drills are extremely useful in a range of applications with concrete, granite, and other hard stone materials.

drilling hard and medium rock formations. Various tools fabricated with saw-grade diamond are illustrated in Fig. 9.6.

Diamonds used in sawing and drilling normally range in size from 20 to 80 mesh (about 850 to 175 μm). The size of the crystal determines the protrusion from the bond during abrasion, which in turn affects the depth of cut and material removal rate. In general, larger crystals are used for cutting softer materials. The mesh size also determines the number of cutting points, for a given concentration. Mesh size and concentration must be balanced for the best performance in a given application. Retention of the crystals in the bond can often be significantly enhanced by Ti or Cr coatings. Either coating performs well in Co-, Ni-, and WC-based bonds. Cr coatings are typically recommended for Co-bronze bonds with less than 10 percent bronze and low-Fe bonds. Ti coatings typically perform better in Fe-Ni bonds and Co-bronze bonds with more than 10 percent bronze.

For diamond saws, crystals are mixed with metal powder at typical concentrations of 15 to 40 and hot pressed to form curved segments. The segments are then brazed to the outer diameter of a metal disk to form a saw blade, with slots separating the segments, as shown in the lower right corner of Fig. 9.6. Diamond saw blades can be used either individually or with many blades spaced along a single spindle, allowing many slabs to be cut in a single operation. Saw blades can be quite large, 5 m in diameter! Core drills have a related geometry, with segments that are curved perpendicular to the cutting direction and brazed to the end of a tube, as shown in Fig. 9.6. For some applications, for example, quarrying, cutting very large slabs of stone, or cutting concrete where space is limited, wire saws provide the best solution. Wire saws comprise diamond/metal-matrix beads strung over a steel wire and separated by spacers, as shown in Fig. 9.6. The wire saw is placed around the workpiece or through holes in it, supported by pulleys as needed, and driven by a motor.

The abrasion mechanism in sawing hard stone has received considerable attention because of its importance. There is considerable evidence that the primary mechanism by

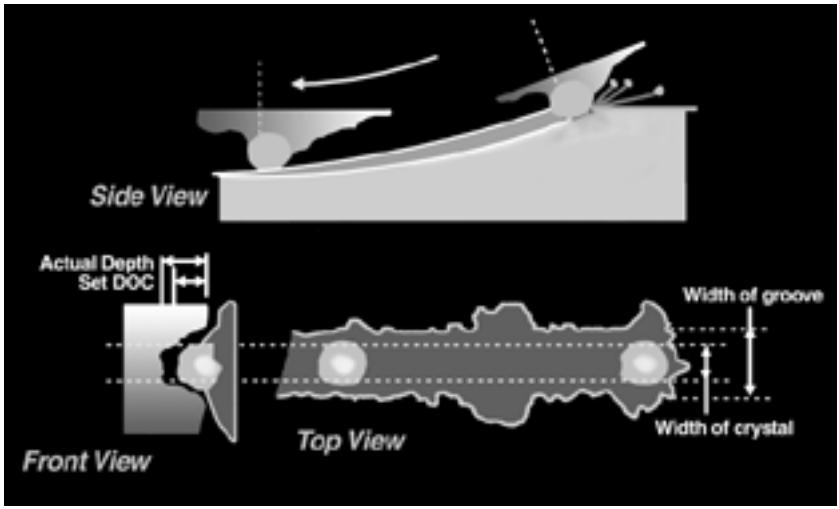

FIGURE 9.7 Schematic illustration of the cutting mechanism of diamond with hard materials.

which diamond removes workpiece material is *spalling*. Blunt grit particles compressively load protrusions in the workpiece, which then microcrack and spall out when the load is removed. This process is illustrated schematically in Fig. 9.7. As an individual diamond crystal is exposed by wear of the overlaying matrix, it begins to impact the workpiece. Depending on the toughness of the diamond and of the workpiece and of the loading (surface speed, depth of cut, concentration of cutting points), the crystal begins to wear by microfracture and/or polishing. Polishing is undesirable, as it increases the power necessary to drive the blade, and can be minimized by increasing the cutting rate and thereby the sawing forces on each crystal. After the crystal has accumulated substantial microfracture damage, it typically macrofractures. Once too little diamond is left in the bond for adequate adhesion, the crystal pulls out. The optimum type of crystal for a given application is determined by the relationship between the compressive fracture strength of the diamond and the toughness of the material, because optimal cutting performance is achieved when the sawing force per crystal is just below the failure point of the crystal. Tougher workpiece materials demand stronger/tougher diamond crystals.

9.3 CUBIC BORON NITRIDE (cBN)

The invention of cBN was actually part of an attempt by GE to develop a material harder than diamond. Of course, cubic boron nitride turned out to be the second hardest known material (Table 9.1). However, cBN is considerably superior to diamond in precisely the two areas where diamond's performance is poor: its abrasion resistance with ferrous alloys, such as steels, and its oxidation resistance. The former property enables it to effectively grind steels, nickel-based superalloys, and cast iron, whereas diamond works best with nonmetals and nonferrous metals. The oxidation resistance is important in high-temperature applications in air or a similar oxidizing environment.

Two grades of cBN were introduced commercially by GE in 1969—Borazon* Type I and Type II. Type I Borazon cBN comprises black (from inclusions), uncoated crystals, with a blocky but irregular shape and moderate strength/friability. Type II is similar, but with a 60 wt% coating of nickel. In 1975 GE introduced so-called 500 grade, comprising brownish-gold crystals that are considerably tougher than Type I. An additional grade, type 400, was introduced in 1996, comprising tan-colored crystals that are almost as tough as type 500 but are considerably more angular in shape, often requiring lower power during grinding. Finally, a microcrystalline grade of cBN, introduced by GE in 1981 as Borazon* 550 cBN and synthesized by direct conversion of the hexagonal BN precursor, has the highest toughness and thermal stability of any grade on the market. Metal-coated grades of each type of cBN crystal are also available (420, 510, 520, 560), particularly for use in resin or metal bonds.

9.3.1 Properties

Cubic boron nitride has the same atomic structure as diamond, with boron or nitrogen replacing every other carbon atom, but the additional complexity of two atomic constituents significantly complicates the possible crystal morphologies. The growth facets are normally (111) and (110) rather than (111) and (100) as in the case of diamond. In addition, the (111) facets are polar—either B- or N-terminated—and so there are (111)-B and (111)-N (or $(\bar{1}\,\bar{1}\,\bar{1})$) facets. Finally, twinning during growth is more prevalent with cBN than diamond. The overall consequence is a much wider range of possible crystalline morphologies for cBN, as illustrated in Fig. 9.8, than for diamond (Figs. 9.2, 9.4). Cleavage in cBN occurs on

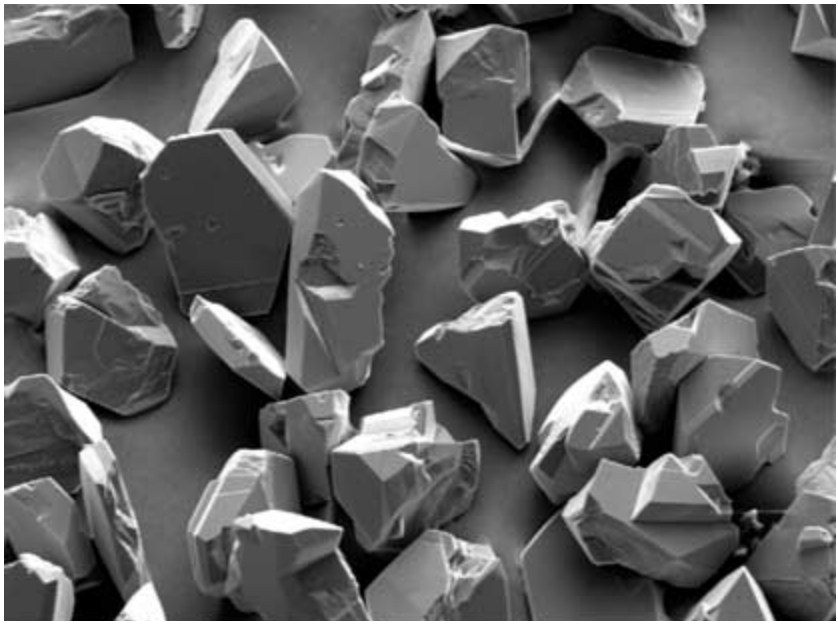

FIGURE 9.8 Scanning electron micrograph of cBN crystals (type 400), showing angular crystals with a non-cubo-octahedral facet geometry.

the (110) planes, of which there are six, making cBN intrinsically more friable than diamond [which has four (111) cleavage planes].

The standard characterization methods applied to cBN are similar to those applied to diamond, particularly toughness and thermal stability (cf. Sec. 9.2.1). As noted above, the various grades of cBN differ in their toughness and thermal stability; these properties must be optimized for each application.

As compared to diamond morphologies (Fig. 9.4), cBN has a different facet structure and is frequently more angular (Fig. 9.8). The heterogeneity in the shape of cBN crystals of all grades is considerably larger than the case of diamond, due to the more complex growth morphologies, and quantitative image analysis is so far not possible.

9.3.2 Bond Systems

The bond systems used with cBN are the same as those with diamond—resin, vitreous, metal, and single layer (electroplated or brazed)—but the relative prevalence is different. The most popular bond systems with cBN are vitreous and single layer, the reverse of the situation with diamond. In many cases the lifetime, finish, and grinding efficiency of vitreous bond cBN wheels are superior to those of corresponding resin bond wheels. Factors contributing to the performance of vitreous bonds are hardness, thermal conductivity and stability, and higher porosity (which simplifies wheel surface conditioning) than resin bonds.

Uncoated cBN of all grades is most commonly employed in vitreous or single-layer bonds. In phenolic or polyimide resin bonds, cBN with a thick coating of nickel is the recommended choice, as the coating improves crystal retention and heat dissipation. In metal bonds, Ti-coated monocrystalline cBN or microcrystalline cBN are typically used. Recommended concentrations are between 50 and 125 for resin bonds, 50 and 200 for vitreous bonds, and 50 and 100 for metal bonds.

9.3.3 Applications

Mesh cBN is used predominantly in grinding applications, typically in the form of an abrasive wheel.[10] Whereas mesh diamond is most commonly used with nonmetals (stone, concrete, ceramics, glass), cBN is used mainly with ferrous metals such as tool steels, hardened steels, cast iron, and nickel-based superalloys, including Iconel, René 77 and 95, Hastelloy, and Stellite. These workpiece materials are much less brittle than the nonmetals, and careful attention must be paid to grinding wheel conditioning to achieve optimum performance. In general, wheel conditioning includes *trueing* and *dressing*. Trueing involves the restoration of accurate wheel geometry (e.g., the flatness of the wheel surface) and sharpening of dull abrasive crystals, if necessary. Dressing refers to the removal of surface matrix material immediately surrounding the crystals to improve workpiece chip flow during grinding. Dressing is more important in resin and metal bonds than in vitreous bonds because of the much lower porosity in the former. Trueing is typically performed with diamond tools (since diamond is considerably harder than cBN) and dressing is commonly performed by dry blasting with alumina grit.

Grinding wheels are manufactured for a wide variety of applications, and the type of cBN crystal that is optimum varies. A summary of typical applications for cBN, together with use guidelines, is given in Table 9.5.

In many grinding applications, the abrasive tool itself constitutes less than 10 percent of the total cost. Thus, although cBN-based tools may cost more than conventional alumina- or silicon carbide–based tools by a factor of 2 to 20, they commonly demonstrate performance

TABLE 9.5 Typical Applications, Bond Systems, and Recommended Grades for Cubic Boron Nitride

		Borazon* cBN Product choice by bond system			
Application	Workpiece material	Resin	Vitreous	Single layer	Metal
Cutting tools, dies, punches, shears, knives, saw blades	Tool steels > R_C 40, case-hardened alloy steels	Type II, 420, 520, 560	Type I, 400, 500/510, 550	400, 500/510[†]	500/510, 550
Bearing rings, needles, rollers, spacers, balls	52100, M50, alloy steels > R_C 40	Type II, 420, 520	Type I, 400, 500/510, 550	400, 500/510[†]	
Pump, compressor parts	Nodular iron, alloy steel	Type II, 420, 520	Type I, 400, 500/510, 550	500/510,[†] 400	
Engine, transmission parts	Alloy steels > R_C 40, chilled iron, nodular iron		Type I, 400, 500/510, 550	500/510,[†] 400	
Gas turbine parts (vanes, blades, nozzles, seals)	Superalloys, stainless steels > R_C 40		Type I, 400, 500/510, 550	500/510,[†] 400, 570	
Surgical tools	Alloy steels > R_C 40, stainless steels > R_C 40	Type II, 420, 520	Type I, 400, 500/510, 550	400, 500/510,[†] 570	
Honing, superfinishing	Alloy steels, gray iron, nodular iron, thermal sprays		Type I, 400, 500/510, 550	500/510,[†] 400, 570	550, 510/500
Roll grinding: steel and paper mills	Chilled iron, high-Cr and tool steels	Type II, 420, 520	Type I, 400, 500/510, 550		
Miscellaneous	Soft steels, thermal spray coatings		Type I, 400, 500/510, 550	400, 500/510,[†] 570	550, 510/500

[†]Vacuum braze process.

advantages of 10 to 300 times and deliver overall savings of 30 to 40 percent or more. In addition to the superabrasive grinding wheel itself lasting considerably longer than a conventional wheel, the edge life of cutting tools that have been ground with cBN often last 50 percent longer than alumina-ground tools because of better heat dissipation and sharper cutting points within the grinding wheel. The relatively "cold" working process achieved with cBN grinding tends to leave the surface of the workpiece in neutral or compressive stress, which promotes its durability. Additional benefits of cBN grinding include better part accuracy and repeatability, due to less wear of the wheel, and environmentally friendly processes, due to less swarf and lower coolant consumption.

9.4 POLYCRYSTALLINE DIAMOND AND cBN

The third family of superabrasive materials, polycrystalline diamond and cBN, was introduced by GE in the 1970s for machining of nonferrous and ferrous metal alloys, wire drawing, and drilling. Polycrystalline superabrasives are synthesized by sintering diamond or cBN micron powders at high pressure and high temperature and, in many cases, integrally bonding the compact to a tungsten carbide disk or ring for support. The orientation of the diamond/cBN grains is random, making for a uniform tool surface that wears evenly in all directions. In addition, the propensity for cleavage is greatly reduced in polycrystalline materials relative to a single crystal. Cracks may initiate [along (111) planes for diamond or (110) planes for cBN] but are likely to be arrested at grain boundaries, producing local chipping but not catastrophic failure. Tool blanks are finished in various sizes and shapes by specialized techniques for cutting, grinding, lapping, and polishing. Cutting tools *separate* workpiece material, producing shavings, instead of *pulverizing* it as with sawing or grinding brittle materials.

Polycrystalline diamond (PCD) machining products (Compax* Diamond) were introduced commercially in 1973, tailored for nonferrous metals. PCD offers the hardness, strength, and abrasion resistance of single-crystal diamond without the susceptibility to fracture. PCD wire dies were offered in 1974 for the first time, revolutionizing the copper wire industry by providing longer die life, improved productivity, consistent surface finish, and better dimensional control. PCD blanks for geological drilling applications were introduced in 1976 (Stratapax* drill blanks). Similar in form to machining blanks but smaller in diameter and with thicker diamond tables and tungsten carbide supports, these tools are attached to bit bodies used in drilling wells on land and offshore. GE introduced Geoset* drill diamond, a thermally-stable, free-standing form of PCD, in 1981 for use as a surface cutting element capable of being bonded in a matrix-type bit.

Most polycrystalline diamond contains cobalt as a sintering aid, with a volume fraction of about 5 to 12 percent. Cobalt performs well as a sintering aid, as it is a good diamond-to-graphite conversion catalyst and a good carbon solvent. However, its presence in PCD has the disadvantage of limiting the thermal stability to less than about 700°C, as it catalyzes back-conversion to graphite and generates stresses because of a differential thermal expansion coefficient at elevated temperatures. Manufacturers have addressed this limitation in two ways. PCD can be sintered with other materials, such as silicon carbide, that do not catalyze back-conversion to graphite. However, there is very little diamond-to-diamond bonding in SiC-sintered PCD and the abrasion resistance is normally considerably inferior to that of Co-sintered PCD. Alternatively, nearly all the cobalt in Co-sintered PCD can be leached out, dramatically increasing the thermal stability while retaining excellent abrasion resistance, albeit at the cost of introducing some porosity.

Polycrystalline cBN (PCBN) machining products—for ferrous metals—were introduced by GE in 1975 (BZN* Compacts). The initial series of products (BZN 6000) were Co-sintered and bonded to tungsten carbide supports. Like most grades of PCD, this material is electrically conductive because of the metallic binder phase. A family of ceramic-sintered, freestanding PCBN blanks (7000S) was introduced in 1991, which is electrically insulating. Although cBN is considerably more inert than diamond while abrading ferrous alloys, it is more reactive than some conventional hard materials. Composites of cBN and TiN, sintered at high pressure and high temperature and integrally bonded to tungsten carbide (e.g., BZN 8200) have proved to be useful in a number of high-speed applications with hardened steel.

9.4.1 Properties

Specification of the properties of polycrystalline superabrasives is more complex than with mesh, because of the greater complexity of the material itself and the range of parameters that enter the manufacturing process. As a starting point, key characteristics of polycrystalline superabrasives include the grain size of the superabrasive in the compact, the volume percent of superabrasive, and the composition of the binder. A number of macroscopic properties can be readily determined, for example, the hardness and the elastic constants. Summary properties of GE polycrystalline diamond and cBN are listed in Table 9.6.

However, other features of PCD and PCBN that are not so readily specified are also critical to performance. For example, the identity and concentration of impurities, the size distribution of binder-filled pores, the microstructure of the superabrasive/WC interface, and stress distributions, particularly near the interface with the tungsten carbide support, are all crucial. As yet there are no industry standard tests that can satisfactorily predict abrasion resistance, surface finish, etc., in specific applications. Each manufacturer is therefore forced to maintain strict quality standards for the manufacturing process and to empirically determine the relationship between manufacturing process, material properties, and performance in various applications.

Supported PCD or PCBN tool or die blanks, bonded to a tungsten carbide, are typically stable up to about 700°C in an inert atmosphere. The stability of self-supported blanks, from

TABLE 9.6 Summary of Properties of Commercial GE Polycrystalline Diamond and Cubic Boron Nitride

	Diamond			Cubic boron nitride		
Property	PCD-1600	PCD-1300	PCD-1500	BZN-6000	BZN-7000S	BZN-8200
Volume % superabrasive	90	92	94	90	82	65
Mean particle size, μm	4	5	25	2	15	2
Binder phase	Co	Co	Co	Co	Ceramic	TiN
Knoop hardness, GPa	≈70	≈70	≈70	28	32	36
Young's modulus, GPa	920	945	970	740	710	660
Poisson's ratio	0.10	0.10	0.11	0.16	0.15	0.18
Density, g/cm^3	4.1	4.0	3.9	4.0	3.4	4.1

FIGURE 9.9 Polycrystalline diamond (PCD) tool blanks and finished cutting tools.

which most of the metal has been removed, extends up to 1200°C. Some examples of finished PCD and PCBN cutting tools are shown in Figs. 9.9 and 9.10, respectively. A diagram of a Stratapax blank on a tungsten carbide blank is in Fig. 9.11.

9.4.2 Processing and Tool Fabrication

Residual metal in Co-sintered diamond and cBN causes the compacts to be electrically conductive, which allows convenient cutting of the blanks by electric discharge machining (EDM). Particularly useful are EDM machines using a traveling wire. Guidelines for performing EDM with PCD and PCBN products are available from GE and other superabrasive manufacturers. Electrically-insulating grades of PCD and PCBN are typically cut with a laser.

PCD or PCBN blanks integrally bonded to tungsten carbide are normally attached to cutting tools such as inserts by brazing via the carbide. The carbide may be thinned, if necessary, but should be left thicker than the superabrasive layer. Silver-based braze alloys, with flow points between 600 and 920°C are generally used. High-temperature braze alloys (860 to 920°C) can be used for tools that will experience high temperatures during machining and where high shear strengths are required. Low-temperature alloys (600 to 700°C) are typically useful for modest depths of cut, where high temperatures will not be generated. Low-temperature braze alloys are specifically recommended for attachment to steel shanks because of the mismatch in thermal expansion coefficient between tungsten carbide and steel. Brazing may be performed with a torch, in a furnace, or inductively.

After brazing, the edges of PCD or PCBN tools must be prepared by grinding. Grinding is typically performed with a resin- or vitreous-bond superabrasive wheel with a concentration near 100. In some cases the edge is honed to strengthen its resistance to chipping. Some additional aspects of edge preparation are specific to the application and are described briefly in the next section. Further details are available from GE and other superabrasive manufacturers.

FIGURE 9.10 Polycrystalline cubic boron nitride (PCBN) blanks and workpiece materials.

The central hole in a PCD wire die is normally prepared by EDM, laser drilling, or needle methods. Final polishing, for the finest surface finish, is performed with diamond micron powder.

9.4.3 Application and Use Guidelines

In general, PCD works well for machining of nonferrous metals, including high-silicon aluminum, copper and copper alloys, tungsten carbide, and metal matrix composites. PCD is also very well suited for machining nonmetals such as natural wood and wood composites, fiber-reinforced plastics, ceramics, and graphite-epoxy composites. Machining manufactured wood or PC board products with diamond may seem like overkill, but the plastic laminates and resins used in these materials are extremely abrasive. PCD tools are capable of

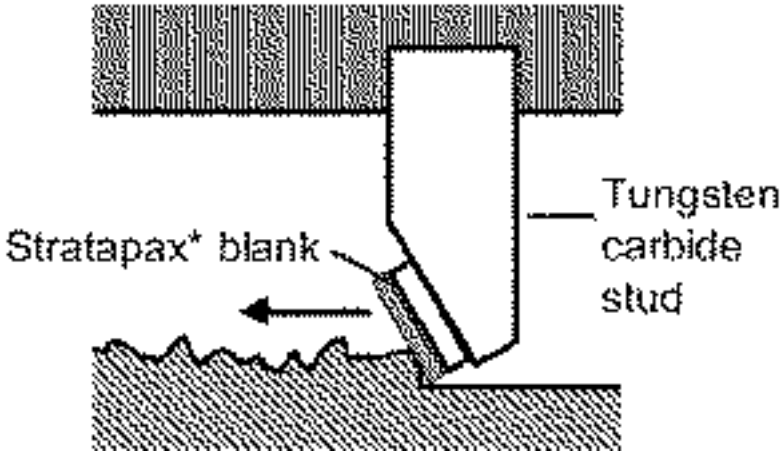

FIGURE 9.11 Schematic of Stratapax* drilling blank cutting rock.

high material removal rates in production boring, turning, and milling operations while providing consistently fine surface finishes. In addition, the high thermal conductivity of the polycrystalline diamond layer allows greater heat dissipation in rough and finish machining of a wide range of materials. PCD with coarse grains is normally preferred for severe interrupted cuts, rough machining, and with highly abrasive high-silicon aluminum metal composite alloys. Medium-grained PCD is optimal for fine machining of highly abrasive alloys, and fine-grained PCD is specified for less-abrasive materials such as wood, wood materials, and copper alloys.

PCD tool blanks perform best with a sharp edge. A positive rake angle (5 to 7°), with the largest possible nose radius, is preferred. Machining may be performed wet or dry, but flood coolant is recommended whenever possible. Application guidelines for PCD tool blanks, listed by workpiece material, type of operation, and recommended product, are given in Table 9.7.

PCD wire dies deliver stellar performance in drawing wire of nonferrous alloys, including copper, aluminum and its alloys, bronze, tungsten, and molybdenum, with a relative performance 3 to 15 times that of natural diamond and 50 to 500 times that of tungsten carbide. Perhaps surprisingly, PCD wire dies also perform well with ferrous alloy wire, including stainless steel, carbon steel, and nickel, roughly 15 to 100 times better than tungsten carbide. Coarse-grained wire dies (25 to 50 μm) have the highest abrasion resistance, and fine-grained wire dies (0.7 to 5 μm) deliver the finest surface finish.

Tool performance is particularly critical in oilfield and geological drilling applications because of the time and expense associated with changing bits; PCD products have been widely accepted in many applications because of their long life and fast penetration rates in soft- to medium-hard rock formations. Suitable types of rock include salt, anhydrites, limestone, dolomite, claystones, mudstones, marl, shales, and chalk. Supported blanks are typically used as drag cutting elements attached to bits in drilling and mining applications, as shown schematically in Fig. 9.11. As the blank wears during the drilling operation, sharp new crystals are exposed, maintaining a sharp edge through the life of the blank. Fine-grained blanks are used most commonly, striking a field-proven balance between abrasion resistance and toughness. Coarse-grained blanks trade superior abrasion resistance for inferior impact resistance and generally perform best in rock formations with a consistently

TABLE 9.7 Compax* Diamond Tool Application Guidelines

Material	Operation	Grade	Surface speed, m/min	Depth of cut, mm	Feed rate, mm/revolution
Aluminum and its alloys					
<12% Si	Rough turning	1300/1500	1000–3000	0.1–3.0	0.1–0.4
>12% Si		1300/1500	300–800	0.1–3.0	0.1–0.4
<12% Si	Finish turning	1600/1300/1500	1000–3000	0.1–1.0	0.1–0.2
>12% Si		1600/1300/1500	300–800	0.1–1.0	0.1–0.2
<12% Si	Milling	1300/1500	1500–3500	0.1–3.0	0.1–0.3/tooth
>12% Si		1300/1500	400–900	0.1–3.0	0.1–0.3/tooth
Copper/zinc/brass	Rough turning	1300/1500	600–1000	0.5–2.0	0.1–0.4
	Finish turning	1600/1300	700–1200	0.1–0.5	0.1–0.4
	Milling	1300/1500	700–1200	0.1–3.0	0.1–0.3/tooth
Reinforced plastics	Rough turning	1300/1500	200–800	1.0–2.0	0.1–0.4
	Finish turning	1600/1300	300–1500	0.1–2.0	0.1–0.4
	Milling	1300/1500	300–1500	0.1–3.0	0.1–0.3/tooth
Sintered tungsten carbide	Rough turning	1300/1500	20–40	0.1–0.5	0.1–0.3
	Finish turning	1600/1300	20–40	0.1–0.2	0.1–0.3
Manufactured wood	Sawing, routing	1600	2000–5000		0.5–1.5/tooth

TABLE 9.8 BZN* Compacts Application Guidelines

Material	Operation	Grade	Surface speed, m/min	Feed rate, mm/revolution	Depth of cut, mm
Pearlitic gray cast iron	Turning, milling	6000/7000S	600–1200	0.15–0.60	0.10–2.5
Hard cast iron (>45 R_C)	Turning, milling	7000S	75–150	0.13–0.65	0.20–2.5
Hardened steel (>45 R_C)	Rough turning	7000S	65–120	0.10–0.50	0.50–2.5
	Rough milling	6000	65–120	0.10–0.50	0.50–2.5
Alloy steels	Finish turning	8200	100–150	0.10–0.15	0.10–0.5
Tool and die steels	Finishing	8100/8200	90–110	0.10–0.15	0.10–0.5
Hard facing alloys	Turning, milling	6000	300–700	0.10–0.25	0.10–1.5
Powder metals	Turning milling	6000	90–180	0.10–0.25	0.10–1.3
Superalloys (<35 R_C)	Turning	6000	150–250	0.10–0.30	0.10–2.5

high level of abrasiveness. PCD drill blanks are often used with water-based drilling fluids, but performance in certain shales is improved with oil-based fluids. PCD drill blanks commonly drill twice as fast and last three times as long as conventional carbide insert roller cone bits or natural diamond bits in high-speed drilling, slim hole (<7″ diameter) drilling, and some coring applications.

Unsupported (Geoset*) drill diamond was introduced to replace surface set mined diamond in matrix-type bits. The most common geometry is a triangular prism; these PCD bits are then fixed within a hard metal bond and attached to the end of a drill bit. Typical applications involve drilling through sandstone, limestone, dolomite, soft granite, quartzite, siltstone, claystone, and shale. The polycrystalline nature of these materials conveys a resistance to fracture (no cleavage planes) and self-sharpening properties which allows them to consistently outperform mined diamond crystals in matrix drill bits.

PCBN machine tools perform well with hardened steels, pearlitic gray cast iron, hard cast iron, powder metal materials, hard facing alloys, and high-temperature, nickel-based superalloys. Tool blanks should be prepared with a negative rake angle (5 to 7°) and large lead angles whenever possible. Chamfered edges minimize chippage on interrupted cuts. Coolant is recommended for long cut operations but not for severe interrupted cuts. The machining system needs to be rigid, with sufficient power. A summary of machining parameter guidelines is given in Table 9.8, by workpiece material and recommended product.

9.5 MICRON DIAMOND AND cBN

Diamond micron powder (DMP) has been in commercial use for polishing for a very long time, because of diamond's unique hardness. Until the advent of HPHT technology, of course, all DMP was natural, produced by milling or grinding larger diamonds and as a by-product of the cutting and shaping of gem-grade diamond.

Micron powders of diamond and cBN also occur as by-products of HPHT manufacturing of mesh materials, and have become increasingly important in their own right as their availability increased. Of course, cubic boron nitride micron powder (BMP) did not exist before 1957. Particles smaller than about 50 to 80 μm are normally considered "micron," although there is some overlap with finer sizes of mesh grinding products. It becomes difficult

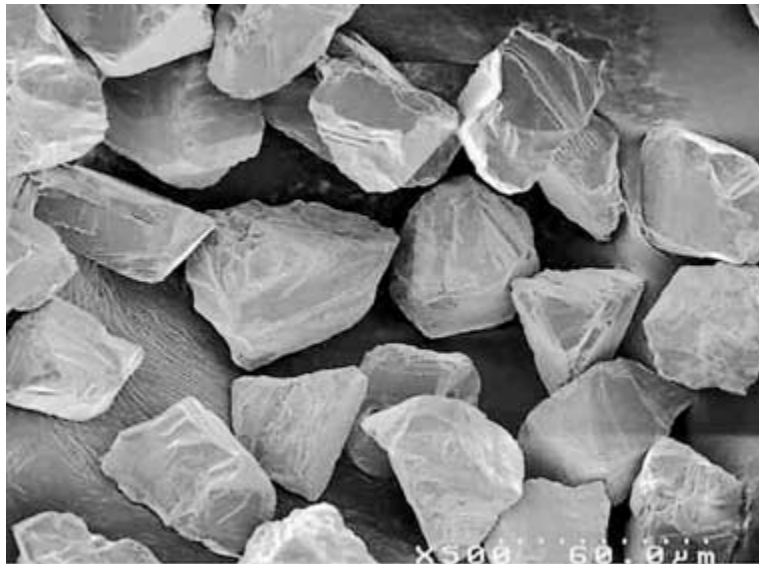

FIGURE 9.12 Diamond micron powder.

to grow well-faceted crystals at HPHT for sizes smaller than 50 to 80 μm, and "micron" diamond and cBN are mainly produced by milling of larger crystals and is therefore have an irregular surface morphology. An example of DMP is shown in Fig. 9.12; BMP has essentially the same morphology.

Diamond and cBN powders produced by milling are essentially monocrystalline and dominate the market. However, *polycrystalline* diamond powder can also be produced by shock synthesis. Under suitable conditions, shock waves produced by explosively driven projectiles can produce HPHT conditions in confined volumes for a sufficient duration to achieve partial conversion of graphite into nanometer-sized diamond grains which can also sinter into micrometer-sized, polycrystalline particles.[11] This process was commercialized by DuPont to produce a polycrystalline DMP (trade name Mypolex*) that is more friable than monocrystalline DMP and is well suited to fine polishing applications. Hexagonal (graphite-like) BN will also react under shock-synthesis conditions, but the dense, nanometer-sized particles that are produced are of the wurtzite phase (wBN) rather than the cubic phase. So far, nano-wBN has not achieved much commercial importance.

9.5.1 Characterization

For monocrystalline DMP and BMP, the first important characteristic is the *source material*—the type of diamond or cBN that was milled into powder. GE manufactures two grades of diamond micron powders—MBM* and RVM*, produced by milling metal-bond grade and resin-bond grade diamond, respectively. Properties of the source material—inclusions, impurities, other defects—will of course define the properties of the micron powder. Fracture during the milling process occurs preferentially at inclusions and other internal flaws, so in general the impurity content of micron powder is less than that of the source material from which it came.

A second important property is the *particle size distribution* (PSD). The effectiveness of sieving diminishes as particles become smaller than 50 μm, and micron materials are generally classified by using wet techniques such as static and dynamic sedimentation. Particle sizes can be measured by a range of techniques, but the standard in the superabrasive industry for particles down to a few micrometers in diameter is based on the Coulter principle. In this technique particles suspended in an electrolyte solution are drawn through an orifice through which a small electrical current is passed. Particles traversing the orifice displace electrolyte, increasing the electrical resistance through the orifice by an extent that is proportional to the particle volume. Commercial instruments collect a histogram of particle volumes, which are then converted to an effective diameter by assuming spherical particles. Milled particles are not spherical, of course, and to maintain continuity with historical particle size standards based on microscopy the nominal diameter of DMP or BMP particles is approximately 1.5 times the mean spherical diameter measured using the Coulter technique. Finer particles must be characterized by other methods, including laser light scattering, photon correlation spectroscopy, and electron microscopy.

All samples of micron particles contain a range of sizes, of course, since no classification technique is perfect. Ideally the PSD is "clean," e.g., a log-normal distribution with a narrow width and neither oversized particles or superfines, and in fact the PSD constitutes one critical measure of quality. The presence of oversized particles will generate scratches in the workpiece being polished, while superfines often adversely affect wetting and dispersion and the stability of suspensions. Micron sizes are traditionally specified by a set of ranges, as summarized in Table 9.9.

A further important property of DMP or BMP is the distribution of *shapes*. Milled particles are not faceted, of course. However, the aspect ratio, the ratio of maximum and minimum diameters as viewed under a microscope, can vary substantially. Blocky particles have an aspect ratio near 1, while shardlike particles can have an aspect ratio of 2 or more. The polishing behavior of these types of particles is rather different, so it is also important to control shape. Shape distributions can be measured quantitatively by image analysis techniques and used to control the overall process.

Finally, *surface cleanliness* is critical to proper dispersion of micron particles in slurry vehicles and mixing and retention with bond components. The identity and concentration of surface impurities can be determined by surface spectroscopic and bulk elemental analysis techniques down to the part-per-million level.

9.5.2 Applications

Superabrasive micron powders are widely used in grinding, lapping, polishing, texturing, and superfinishing of a variety of materials. DMP works best with nonferrous metals, ceramics, glasses, semiconductor materials, stone (e.g., granite) and, of course, superabrasives. cBN micron powder is recommended for superfinishing of bearing surfaces and honing of larger components and lapping, polishing, centerless grinding, and precision grinding of hardened steels, superalloys, and other hardened ferrous materials.

Micron powders are often used in the form of a paste, particularly for polishing. However, *slurries* are used in a wider range of applications. Slurries perform several functions, including dispersing the superabrasive particles; transporting and evenly distributing particles across the workpiece, and ensuring that fresh abrasive particles are always available; providing lubrication and cooling; and removing swarf (material abraded from the workpiece) from the work area. Slurry vehicles are commercially available that are water-based, oil-based, or emulsion formulations. Slurry systems function best when optimized for a given application, including the PSD, concentration, and zeta potential of the superabrasive particles and the pH, viscosity, lubricity, wetting characteristics, and rinseability of the slurry.

TABLE 9.9 Micrometer Size Equivalents (All Diameters Are Given in μm)

Nominal size designation	Target mean size[†]	Approximate equivalent mesh size
Fine:		
0–1/10	0.08	
0–1/4	0.18	
0–1/2	0.28	60,000
0–1	0.42	28,000
0–2	0.9	14,000
1–2	1.2	13,000
Medium:		
1–3	1.6	12,000
2–4	2/6	8,000
3–6	4.5	5,000
4–8	6.0	3,000
5–10	7.5	2,200
6–12	9.0	1,800
Coarse:[‡]		
10–15	12.5	1,400
10–20	15.0	1,200
12–22	17.0	1,100
15–20	17.5	1,100
15–25	20.0	1,000
20–30	25.0	800
22–36	30.0	700
30–40	35.0	600
36–54	45.0	500
40–50	45.0	500
54–80	67.0	325/400
60–100	80.0	270/325

[†]Diameter includes shape factor (≈1.5).

[‡]Most coarse sizes are also available from GE with a 56 weight % nickel coating.

For *lapping* of flat parts, the abrasive is typically fed to the surface of a cast iron lap as a slurry with a water-soluble glycol solution. To provide uniform material removal, each workpiece is pressed against the lap face by a fixed load and rotated by a fixture while the lap is turning. In fine grinding applications, the diamond particles are incorporated into metallic, phenolic resin or vitreous bonds to form the edge of grinding wheels. The wheel edges can be either flat or shaped so that the tool imparts a curved or contoured surface to the workpiece. Diamond particles are also electroplated, electroformed, or co-deposited with electroless nickel onto certain tools such as precision slicing blades.

ACKNOWLEDGMENTS

The author thanks Bob DeVries, for a careful reading of the manuscript, and his many colleagues at GE Corporate Research and Development and GE Superabrasives for teaching him about HPHT diamond and cBN, especially Bob Giddings, Bob DeVries, Steve Hayden,

Dong-Sil Park, Ric Klug, Minyoung Lee, Tim Dumm, Tom Anthony, Steve Webb, Chris Long, Yue Meng, Jim McHale, and Eoin O'Tighearnaigh. He thanks GE Superabrasives for ongoing support of his work.

REFERENCES

1. Jeremiah 17:1, *The Bible* (some translations).
2. For an excellent and very readable introduction to the history of diamond synthesis, see R. M. Hazen, *The New Alchemists: Breaking Through the Barriers of High Pressure,* Times Books, New York, 1993.
3. T. J. Clark and R. C. DeVries, "Superabrasives and Ultrahard Tool Materials," *ASM Metals Handbook,* vol. 2, 10th ed., pp. 1008–1018, 1990.
4. F. D. Rossini and R. S. Jessup, *J. Res. Natl. Bur. Stand,* vol. 21, p. 491, 1938; O. I. Leipunskii, Uspekhi Khim, vol. 8, p. 1519, 1939.
5. R. Berman and F. E. Simon, *Z. Electrochemie,* vol. 59, p. 333, 1955.
6. F. P. Bundy, H. T. Hall, H. M. Strong, and R. H. Wentorf, Jr., "Man-Made Diamonds," *Nature,* vol. 176, pp. 51–55, 1955; H. P. Bovenkerk, F. P. Bundy, H. T. Hall, H. M. Strong, and R. H. Wentorf, Jr., "Preparation of Diamond," *Nature,* vol. 184, pp. 1094–1098, 1959; H. P. Bovenkerk, F. P. Bundy, R. M. Chrenko, P. J. Codella, H. M. Strong, and R. H. Wentorf, Jr., "Errors in Diamond Synthesis" (Erratum), *Nature,* vol. 365, p. 19, 1998.
7. www.AbrasivesNet.com.
8. R. H. Wentorf, Jr., "Cubic Form of Boron Nitride," *J. Chem. Phys.,* vol. 26, p. 956, 1957.
9. τ is closely related to the shape parameter $\alpha = \sqrt{3}$ times the ratio of the growth rates in the [100] and [111] directions) that has been used widely in the context of CVD diamond. In particular, $\tau = (3/\alpha - 1)/2$.
10. S. F. Krar and E. Ratterman, *Superabrasives—Grinding and Machining with cBN and Diamond,* McGraw-Hill, New York, 1990.
11. P. S. DeCarli and J. C. Jamieson, "Formation of diamond by explosive shock," *Science,* vol. 133, p. 1821, 1966; L. F. Trueb, "Microstructural study of diamond synthesized under conditions of high temperature and moderate explosive shock conditions," *J. Appl. Phys.,* vol. 42, p. 503, 1971.

APPENDIX

GUIDE TO CERAMIC MATERIALS

For more than 70 years, the leading ceramic industry magazine, ***Ceramic Industry***, has published an annual extensive guide to all of the great multitude of materials used in and with ceramics. With permission from the magazine, and much credit to it, this appendix is an abbreviated listing from the *2000 Materials Handbook*, listing materials related to the contents of this ***Handbook of Ceramics, Glasses, and Diamonds***. Special thanks is extended to Christine Grahl, editor of ***Ceramic Industry***, for her much appreciated assistance. The reader will find this appendix useful for, first, defining and explaining these materials and, secondly, identifying leading suppliers of these materials.

Recommendation is made to the reader to subscribe to ***Ceramic Industry***, 6075 B Glick Road, Powell, Ohio 43065. Editor Christine Grahl can be reached at (248) 244-1294, or grahlk@bnp.com.

ALUMINUM CARBIDE. Al_4C_3. Mol. wt. 143.88; m.p. 2800°C; density, 2.99 g/cm^3. Yellow-green with hexagonal crystal structure, it decomposes in dilute acid and decomposes to produce CH_4 in cold water. The material is stable up to 1400°C.

ALUMINUM FLUORIDE. AlF_3. Mol. wt. 83.97; m.p. 1040°C; density 3.07 g/cm^3. Triclinic crystal structure, soluble in water but insoluble in acids and alkalis.

ALUMINUM NITRIDE. AlN. Mol. wt. 40.99; density 3.26 g/cm^3; CTE 4.6 × 10^{-6}/°C; m.p. 2200°C under 4 atm. N_2, sublimes at 1 atm. White, hexagonal crystal structure. Powder hydrolyzes on contact with water or water vapor. Water-resistant powders that allow aqueous processing are commercially available. Stable against acids, slightly reacts with bases. Made by reacting aluminum metal with nitrogen, by reduction of aluminum oxide with carbon in the presence of nitrogen or ammonia, or by decomposition of the product of reaction between aluminum trichloride and ammonia. Powder may be sintered to full density above 1800 in 1 atm N_2 with the addition of sintering aids such as Y_2O_3 or CaO. Thermal conductivity in excess of 200 W/mK can be achieved in sintered parts, which is five times that of aluminum oxide. Dielectric strength is 1.5 times, and electrical resistivity and mechanical strength are comparable to that of aluminum oxide. Dielectric constant is about half that of aluminum oxide. Major applications include thermally conductive substrates and heat sinks for semiconductors, automotive and transit power modules, mobile communications and multichip modules.

ALUMINUM NITRIDE WHISKERS. (AlN_w). Single-crystal, acicular particles of aluminum nitride, with a diameter of 1 micron, and aspect ratios ranging from 5:1 to 20:1. AlN_w have been reported to form from both vapor-solid and vapor-liquid-solid mechanisms. The resulting product is often pure from both metallic and oxygen contamination. AlN_w exhibit improved stability against hydrolysis compared to AlN powders. Properties of interest include high thermal conductivity, good mechanical strength and chemical compatibility with a wide range of materials. Potential applications include improved thermally conductive fillers for polymers; improved mechanical reinforcements for light metals; reinforcement for AlN ceramics, for use as dense materials (structural) or porous materials

(filters, separators, etc.); and reinforcement for intermetallic materials such as nickel aluminide and titanium aluminide.

ALUMINUM NITRIDE, SILICA COATED. Developed to provide improved thermal management for today's smaller, faster electronic devices, silica coated aluminum nitride is a highly thermally conductive filler material used in semiconductor molding compounds. Molding compounds filled with this material provide the potential to improve reliability when compared to standard and non-metal-enhanced packages. Silica coated aluminum nitride also provides the potential to enhance functionality, power, heat dissipation and performance, while lowering system costs.

Grades with a finer particle size distribution are available. The finer particle sizes provide improved heat dissipation in standard packages, as well as in smaller and thinner packages in which metal is usually not a cost-effective solution.

ALUMINUM OXIDE. (Corundum.) Al_2O_3. (See ALUMINA.)

ALUMINUM OXIDE SUPPLIERS

ALFA AESAR, A JOHNSON MATTHEY COMPANY
30 Bond St.
Ward Hill, MA 01835-8099 U.S.A.
(800) 343-0660 Fax: (800) 322-4757
Email: info@alfa.com
Website: www.alfa.com

ELECTRO ABRASIVES CORP.
701 Willet Rd.
Buffalo, NY 14218 U.S.A.
(716) 822-2500; (800) 284-4748
Fax: (716) 822-2858
Email: info@electroabrasives.com
Website: www.electroabrasives.com

EXOLON-ESK CO.
1000 E. Niagara St., P.O. Box 590
Tonawanda, NY 14151-0590 U.S.A.
(716) 693-4550 Fax: (716) 693-0151
Email: info@exolon.com
Website: www.exolon.com

ALUMINUM SILICATE. $Al_6O_4Si_2O_4$. Mol. wt. 345.94; density 3.15 g/cm^3. Colorless and very slightly soluble in water. Decomposes when heated to 1810°C.

ALUMINUM SILICATE, CALCINED. Consists of up to 95% mullite crystals. Made from pure kaolins. Chemical and physical properties are those of mullite. (See MULLITE, KYANITE, CLAY.)

ALUMINUM TITANATE. Al_2O_3-TiO_2. Stable from 1260–1865°C, while instability from 860–1260°C is reduced by minor amounts of iron or magnesium titanate. Made by reacting Al_2O_3 and TiO_2 for 12 hr at 1300°C. CTEs along the three major crystal axes: (a) 8.3×10^{-6}/C; (b) 18.7 and (c) 2.8. CTE of the aggregate (25–1000°C) decreases with increasing temperature, reaching -2×10^{-7}/C after aging at 1650–1700°C. Aluminum titanate shows an expansion hysteresis loop due to internal fractures caused by anisotropy of the expansion coefficients.

Fired aluminum titanate is easy to machine. This characteristic, combined with extremely high heat resistance, makes it an attractive candidate for such thermal shock-resistant applications as catalytic converter and diesel engine components.

ANTIMONY OXIDE. Sb_2O_3. Mol. wt. 291.52; sp. gr. 5.2-5.7; very slightly soluble in water. Derived principally from stibnite, which is mined in western United States, China, Mexico and Bolivia. The oxide also is produced by the oxidation of antimony metal or as a byproduct in the refining of antimonial-lead alloys.

Antimony oxide's most important ceramic industry application is in the **porcelain enameling** industry, where it is used as an opacifier, both in the raw batch and in combination with other oxides as a mill addition opacifier. It also is often added as sodium antimonate. Antimony finds its chief use in leadless cast iron enamels and a few colored sheet steel enamels. Its opacifying efficiency in these types of enamels has been markedly increased over the years.

When used in lead-bearing enamels, a yellow color may be produced by the formation of lead antimonate. Also, antimony oxide does not give as good opacity in lead-bearing enamels as it does in the leadless types.

Since the development of titania white enamels, the importance of antimony or sodium antimonate as a P/E opacifier for sheet steel has been greatly reduced. Nevertheless, there are still numerous applications where antimony-based white enamels cannot be replaced by titania enamels.

Antimony-bearing, light-colored ground coat enamels are, however, still of importance where cobalt-nickel ground coats have to be replaced.

The formation of lead antimonate, referred to above, is sometimes deliberately encouraged in low-temperature pottery glazes, where a compound of lead oxide and antimony oxide, known as Naples yellow, is used. Antimony is not often used as an opacifier in glazes, but is used in the **pottery** industry as a yellow body stain, usually in combination with rutile or titanium dioxide.

Antimony oxide, when applied to red-burning clay, will chemically bleach the clay surface to a buff color. The **brick** industry uses this techinque to produce interesting colors. Application is by spraying in a water or oil suspension. In **glasses**, antimony is used as a decolorizing and fining agent. The decolorizing action appears to be the result of oxidation of the iron to its ferric state by the action of pentavalent antimony. To ensure the development of pentavalent antimony, for either decolorizing or fining, an oxidizing agent—usually sodium nitrate—is commonly used together with the antimony oxide. Antimony has a special advantage in that glasses decolorized with it do not change color upon solarization as do glasses decolorized with arsenic oxide. It has a substantially lower vapor pressure than arsenic oxide and is less subject to volatilization losses in the early stages of melting.

Antimony oxide is important as a fining agent, especially in optical glass batches and in ruby red compositions.

Antimony trioxide, without an accompanying oxidizing agent, is used for the stabilization of emerald green glass, in which case it is a glass former and very soluble.

ANTIMONY OXIDE SUPPLIERS

ALFA AESAR, A JOHNSON MATTHEY COMPANY
30 Bond St.
Ward Hill, MA 01835-8099 U.S.A.
(800) 343-0660 Fax: (800) 322-4757
Email: info@alfa.com
Website: www.alfa.com

ARLINGTON INTERNATIONAL, INC.
85 Arlington St.
Asheville, NC 28801 U.S.A.
(828) 254-8811; (828) 251-0981 Fax: (828) 254-6437; (828) 251-0983
Email: arlingtonintl@mindspring.com

BARIUM TITANATE. $BaTiO_3$ M.p. >1500°C. Pure form undergoes abrupt phase change from tetragonal to cubic at 130°C, the Curie temperature. Barium titanate is usually produced by the solid-state reaction of barium carbonate and titanium dioxide. Has widespread use in the **electronics** industry because of its high dielectric constant, and piezoelectric and ferroelectric properties. The high dielectric constant of $BaTiO_3$ and the ease with which its electrical properties can be modified by combination with other materials make it exceptionally suitable for miniature capacitors.

The dielectric constant of barium titanate ranges from 1200–1600 at 1 kHz and 25°C, increasing to ~10,000 as the Curie temperature is approached. Under these same conditions, the power factor is a maximum of 1.5%. Because of the large variation of its dielectric properties with temperature and voltage, barium titanate is not, except in rare instances, used as a dielectric without modification. Dielectric properties can be easily modified, however, by combination

with zirconates, stannates and other titanates, for example, to form solid solutions, defect structures or mixtures. Modified barium titanates can be produced with a wide variation in dielectric properties—from those which are comparatively insensitive to voltage and temperature and have a low dissipation factor, to those which show a significant variation with temperature and voltage and have a high dissipation factor.

Dielectric and piezoelectric properties of $BaTiO_3$ can be affected by stoichiometry, microstructure and additive ions that can enter into solid solution. With excess Ba^{+2}, generally a fine textured matrix with <5 μm grain is obtained. With excess Ti^{+4}, grain growth is rather extreme, and at comparable firing temperatures, results in coarse grains of 50–100 μm. Nonstoichiometry originating from the $BaO:TiO_2$ ratio or additional impurities may result in semiconductive ceramics upon firing. The transition temperature of barium titanate can be shifted and depressed. Sr^{+2}, Zr^{+4}, Sn^{+4} and Hf^{+4} may shift it downward to room temperature and below. Bi^{+3} and Pb^{+2} substitution may result in a shift to higher temperatures. Dielectric permittivity of barium titanate at room temperature is usually claimed to be ~2000 which may vary from ~1500–3500, depending upon purity and microstructure. Barium titanate PTC ceramics have been shown to exhibit twin lamellae lying on the {111} plane in crystallites. This condition is necessary for anomalous grain growth.

Since anything that will affect the crystal lattice of barium titanate will alter its dielectric properties, it is important that impurities (SiO_2, Al_2O_3, etc.) be controlled and maintained at comparatively low levels, not only in the as-received material but also throughout subsequent processing operations. Barium titanate is produced by solid-state reaction of $BaCO_3 + TiO_2$ or precipitation from an intermediate such as the oxalate.

There are three basic steps involved in preparing barium titanate bodies for capacitors and other dielectric applications: preparation of the dielectric composition (usually involves mixing, sometimes calcination and milling); forming of the dielectric unit (pressing, extrusion, punching or, in the case of multilayer capacitors, tape casting); and thermal treatment and densification. Depending on the composition, barium titanate bodies can be fired to vitrification at temperatures between 1900 and 2600°F. The multilayer ceramic capacitor process, which is the most popular method of making monolithic capacitors, may include mixing of powder with organic binder in water or a solvent-based system, tape casting (thickness: ~l25 μm), silk screening of electrode, stacking of tape, cutting of laminated tape into individual capacitors, binder burn-out, firing, termination and encapsulation.

Barium titanate ceramic products are used for applications in underwater sonar, guided missiles, acoustic mines, ultrasonic cleaning, measuring instruments (flaw detection, liquid level sensing, thickness gauges), accelerometers, sound reproduction, filters, ultrasonic therapy, ultrasonic machining and vibration detection and, most important, for ceramic capacitors of disk, tube and multilayer designs. Multilayer capacitors are the single highest user of barium titanate.

BARIUM TITANATE SUPPLIERS

CABOT CORPORATION
144 Holly Rd.
Boyertown, PA 19512-1607 U.S.A.
(610) 367-1500 Fax: (610) 369-8259
Website: www.cabot-corp.com/cpm

BAUXITE. Generally nonplastic but with variable physical characteristics, a mineral raw material used to produce the alumina from which aluminum metal is made, as well as alumina-based aluminum oxide for ceramic and chemical applications; Major domestic deposits are in Arkansas.

Physical properties of bauxites vary widely, depending on type, nature of deposit and tectonic history. In texture, some bauxites are soft, friable and structureless; some

are hard, dense and pisolitic; still others are porous but strong, or are stratified. Color may be pink, cream, red, brown, yellow or gray, depending upon the amount of impurities, particularly iron oxide.

The alumina constitutents in the various types of bauxite have been identified as gibbsite (trihydrate), boehmite and diaspore (monohydrates), alone or in mixtures. The clay minerals kaolinite, hermatite, magnetite, geothite, siderite and quartz may be present as common impurities. Residual minerals may include rutile, anatase and zircon.

The specific gravity of bauxite varies, with type and composition, from 2.45–3.25. Bauxites fuse at 1800°C or higher. Trihydrate bauxites start to lose combined water at about 500°C. Any boehmite present will lose water at about 500°C. Combined water is driven off in two main stages: trihydrate converts at about 250°C to monohydrate with loss of 2 moles of water, and most of the remainder is driven off around 550°C. Practical dehydration is attained at about 950°C.

The amounts of silica, iron and alkalies present in bauxite control its value for use in refractories, abrasives and cements.

Bauxite is an excellent material for **refractories** provided adequate attention is given to initial calcining to take care of the tendency of bauxite with residual moisture to shrink at the temperatures at which the refractories are used. Bauxite refractories have adequate strength when cold and at working temperatures. They resist cracking, spalling, and chemical and physical reaction with furnace charges.

Mullite refractory raw material is produced by the sinter-bonded method from mixtures of bauxite and silica sand or quartz, and by the electrically fused-cast method from bauxite-derived alumina.

The chief uses of **bauxite-containing refractories** are: linings in rotary kilns for the manufacture of Portland cement, dolomite and lime; combustion chamber linings for boilers; in the ceramic industry as glass tank blocks, furnace parts, regenerator walls and checkers; in the steel ladles metals industry for center walls of zinc distillation furnaces, bottoms of malleable iron furnaces, water-cooled ports of basic open-hearth furnaces, walls and floors of aluminum holding furnaces and in other types of furnaces where the ash is highly corrosive to brick.

Bauxite has been used in increasing quantities for the manufacture of special quick-hardening high-alumina cements. These cements are prepared in blast furnaces, rotary kilns or electric furnaces by the fusion of bauxite and limestone. The resulting product consists of a mixture of calcium aluminates and calcium-aluminum silicates with some iron oxide and possibly some calcium silicates.

Bauxite abrasives are prepared by fusion of a mixture of calcined bauxite, coke and iron turnings in an electric arc furnace at temperatures above 2000°F. Massive corundum crystals containing 94–95% aluminum oxide result. These are crushed, ground and separated into various grit or grain sizes, which are then manufactured into such products as grinding wheels, abrasive stones, abrasive cloths and papers, and grinding and polishing powders. The fused alumina grinding wheels used extensively in the metals industries are made of this material.

BAUXITE SUPPLIERS

ALU CHEM INC.
One Landy Lane
Reading, OH 45215 U.S.A.
(513) 733-8519 Fax: (513) 733-3123
Email: aluchem@fuse.net
Website: www.aluchem.com/

AMSAT, DIV. OF FLUID ENERGY
P.O. Box 95
East Greenville, PA 18041 U.S.A.
(215) 679-5984; (215) 679-5983
Fax: (215) 679-5985
Email: epipe@fluidenergy.com

INTERNATIONAL MINERALS, INC.
333 Rouser Rd., Bldg. 4

Corapolis, PA 15108 U.S.A.
(412) 299-9300 Fax: (412) 299-9329
JERSEY MINERAL PROCESSING CO., LTD.,
REFRACTORIES AND MINERALS DIV.
RM B-13B, Triumphal Arc Mansion, 66 Nanjing Rd.
Tianjin, 300042, P.R. China
86-22-23133086 Fax: 86-22-23133085
Email: cmptjmax@shell.jtvan.com.cn

BERYL. $3BeO\text{-}Al_2O_3$. Mineral silicate of beryllium and aluminum containing 12–14% BeO. It is at present the only commercial source of either beryllium oxide or the metal itself and, therefore, is of prime importance. Forms green, blue, yellow or white hexagonal crystals and occurs as an accessory mineral in some pegmatites, usually those found with commercial feldspar deposits. Chief producing centers are Brazil, South Africa, Madagascar and India, with smaller quantities from South Dakota, Colorado and the New England states. Brazil produces best volume but available supply is nonuniform.

Phenacite analyzing as much as 40% Be has been found in a helvite-containing deposit in New Mexico. This may be a future source of beryllium.

In a number of ceramic bodies, it is not feasible to use beryl to obtain the benefits of beryllium oxide because: (1) impurities, such as alkalies, are always present; (2) eight to nine times as much beryl as BeO must be used to obtain an equivalent effect; and (3) some formulas will not stand the addition of alumina or silica, which are always present in beryl.

Beryl has long been advocated for use in certain **spark plug porcelains** where it gives high electrical resistance even at high temperatures, sometimes improving dielectric strength by as much as 16%. It requires very careful treatment in firing, however, because of the short maturing range. In such bodies it also lowers firing shrinkage, increases impact resistance, increases transverse strength and greatly improves resistance to thermal shock. Under certain conditions, BeO in small amounts will bring about recrystallization in alumina. It is an active flux and has been used in high-temperature electrical porcelain and crucible bodies.

Due to the eutectic that forms between feldspar and beryl, the direct substitution of beryl for feldspar will seriously harden a glaze.

A dull matte beryl glaze can be compounded to mature at cone 11 or 12, suitable for coating low-expansion, thermal shock-resisting bodies containing talc. Such a glaze reduces the crazing ordinarily exhibited on talc bodies by glossy glazes.

In colored **glazes**, beryl offers an unusual property—the ability to produce high-temperature chrome greens. The simple formula:

Beryl	36.6%
Whiting	15.3%
Clay	11.3%
Flint	36.8%

When tinted with small amounts of chromium oxide or specially prepared chromium stains, a bright glaze with extremely pleasing colors will be produced at cone 14. Beryl glazes are highly fluid and of rather short firing range. Unless care is taken to properly design them, paying close attention to firing time and temperature, excessive crystallization is likely to occur. The crystals that result are mainly cristobalite and mullite.

A patent has been issued for a glass composition in which 1.4 parts of beryllium carbonate are fused with 4.3 parts of lithium carbonate and 18.5 parts of boric acid to produce a borate glass suitable for X-ray tube windows. This glass has a high coefficient of expansion, very high permeability to ultraviolet rays, is quite tough and easily worked. Note: Inhalation of particles of any BeO-containing material should be avoided because of their toxicity.

BERYLLIUM OXIDE. BeO. (Beryllia.) M.p. 2650°C; density 3.03 g/cm^3. Beryllium compounds are toxic and should be used

only under the guidance of the supplier and according to local, state and federal regulations. Impervious beryllia ceramics are now almost exclusively of 99.4% purity with higher purity material (up to 99.9% BeO) used to satisfy special requirements. Lower purity is rarely considered because thermal conductivity drops appreciably as the impurity level rises.

BeO powder is available in three particle size ranges: (1) submicron to 1–2 μm, used for fabricating both ceramic components and BeO-UO_2 nuclear fuel elements; (2) 2–8 μm, used primarily for fabricating beryllia bodies of 96–99.5% purity; and (3) ultrahigh density grains of specific size distribution for ad-mixing with resins and other organics to provide very high thermal conductivity coatings and/or potting compounds.

Beryllia ceramics have these characteristics: extremely high thermal conductivity, particularly in the lower temperature range; excellent dielectric properties; outstanding resistance to wetting and corrosion by many metals and nonmetals; mechanical properties only slightly less than those of 96% alumina ceramics; valuable nuclear properties, including an exceptionally low thermal neutron absorption cross section; and ready availability in a wide variety of shapes and sizes. Like alumina and some other ceramics, beryllia is readily metallized by a variety of thick and thin film techniques.

Although beryllia usually is selected for a desirable combination of properties, key to most applications is the material's comparatively high thermal conductivity. Even at the highest temperatures, its thermal conductivity is four times that of dense alumina; and from room temperature to 500°C, seven to eight times greater. BeO's thermal conductivity is quite dependent on purity. For example, increasing purity from 99% to 99.8% results in a 10–15% rise in conductivity.

Physical Properties

Specific gravity	3.008
Melting point, °C	2650
Softening temperature, °C	>2000
Thermal conductivity, Btu/h/ft^2/F/ft	150
CTE, 10^{-6}/F, at...	
212°F	5.4
932°F	7.4
1832°F	8.9

Mechanical Properties

Tensile strength, 10^3 psi, at...	
Room temperature	18–20
1000°C	5
Compressive strength, 10^3 psi, at...	
Room temperature	200
2000°F	60
Transverse strength, 10^3 psi	35
Modulus of elasticity, 10^6 psi	40–45

Beryllia ceramic components are formed by hot pressing in graphite molds in induction furnaces, by slip casting, conventional dry pressing and extrusion.

Major markets for BeO ceramics are: microwave tube parts such as cathode supports, envelopes, spacers, helix supports, collector isolators, heat sinks and windows; substrates, mounting pads, heat sinks and packages for solid-state electronic devices; and bores or plasma envelopes for gas lasers.

Other uses: klystron and ceramic electron tube parts, radiation and antenna windows, and radar antennae. Beryllia's exceptional resistance to wetting (and thus corrosion) by many molten metals and slags makes it suitable for crucibles for melting uranium, thorium and beryllium.

Beryllia's high general corrosion resistance has helped it capture new applications in the chemical and mechanical fields. And other uses in aircraft, rockets and missiles are predicted.

BeO is tapped for nuclear reactor service because of its refractoriness, high thermal conductivity and ability to moderate (slow down) fast neutrons. The "thermal" neutrons that result are more efficient in causing fusion of U^{235}. Nuclear industry uses for beryllia include reflectors and the matrix material for fuel elements. When mixed with suitable nuclear poisons, BeO may be a new candidate for shielding and control rod assembly applications.

The market for electrically insulating, heat conductive encapsulants based on beryllia grain-polymer mixtures is both small and restricted. While these composites have thermal conductivities 10–20 times higher than those of other filled plastics, the handling restrictions necessitated by the presence of beryllia limit their use.

BERYLLIUM OXIDE SUPPLIERS

ALFA AESAR, A JOHNSON
MATTHEY COMPANY
30 Bond St.
Ward Hill, MA 01835-8099 U.S.A.
(800) 343-0660 Fax: (800) 322-4757
Email: info@alfa.com
Website: www.alfa.com

BINDERS. Substances which serve to hold low green-strength ceramic materials and bodies together and give them sufficient bonding for handling and machining in all prefiring stages of manufacture. Their use reduces loss of ware and, in many cases, makes fabrication possible. Binders make possible the use of otherwise difficult clays; improve products made of heretofore unsatisfactory raw materials and bind powders that contain no natural plasticizers at all.

According to Thumuer, a satisfactory binder should have a combination of attributes such that it would impart high strength, be nonabrasive, be free of noncombustible residual matter, burn out readily at low temperatures, not stick to die parts, not pick up atmospheric moisture and be readily dispersible as solution or emulsion. Another criterion is that it should not unduly add to final product cost.

Materials being used for binders include clays, magnesium-aluminum silicate, natural gums, dextrine, pitch, asphalt, wax of several types, sodium silicate, alginates, glues, starches, lignin, microcrystalline cellulose, cellulose derivatives and thermoplastic resins. These are used in varying percentages, but most do not exceed 5% of batch weight.

The sodium salt of pentachlorophenal, when added to water solutions of certain organic binders, prevents bacterial decomposition. (Material is acutely toxic so must be handled carefully and with full knowledge of its toxic properties.)

Abopon. Viscous water-white liquid approximating the chemical composition of sodium borophosphate. When 100 cm^3 of 1:1 solution is added on the basis of 100 lb of frit, the set of porcelain enamel is reduced and the bisque is hardened in a nature similar to that produced by gums. Tends to give a yellowish dirty color to titania-opacified cover coat enamels.

Ammonium alum. $Al_2(SO_4)_3$-$(NH_4)_2$-SO_4-$24H_2O$. Soluble in water. Not in common usage because of its tendency to decompose during drying, thus imparting variable film strength. Tends to cause shorelining and scumming but has been used in porcelain enamel in amounts of 0.5% to increase set in sheet-iron ground coats and acid resisting cover coats. It has no effect on the acid resisting properties of the enamel.

Dextrin. Cream-colored powder or granules formed by heating some form of starch with a little acid. Is used in ceramics chiefly as a binder. In matte glazes, practically the entire glaze is fritted and would settle to a cement-like mass if a flotative were not used. Dextrin also has proved of value in increasing the plasticity of clays, improving the working properties of porcelain bodies and promoting the adhesion of engobes and glazes to ware.

Lignosulfonates (Lignin). Derivatives of the bisulfite pulping process, lignosulfonates are anionic, surface active polyelectrolytes. The lignin polymer with branched polyaromataic chains can be modified to vary by cation, degree of sulfonation and purity, and average molecular size. Lignin processing technology has developed aqueous-based dispersants and binders for various ceramic applications, including structural clays, whitewares, technical ceramics, refractories, and related areas of cement, concrete and gypsum board.

As effective clay modifiers, lignin dispersants can improve tile and casting slip rheology, reduce free water for brick extrusion, and provide lubricity and plasticity for both extruded and dry-press ceramics. As a binder, lignin may increase both green and dry strengths of ceramic pieces with less than optimum body compositions.

Lignin addition rates of 0.10–0.15% for fine grain and 0.20–2.0% for coarse ceramic materials will improve handling in prefiring stages of ceramic manufacturing. (See BINDERS.)

Tannic acid. Long used for increasing the plasticity of clays, it is not as effective as lignin extract in increasing the dry strength of clays or in deflocculant action.

Magnesium-aluminum silicate. As supplied for ceramic binder purposes, it is the refined product of a naturally occurring smectite mineral. At least two such materials are commercially available.

One has this analysis: 48.7% SiO_2, 25.5% MgO, 0.6% Al_2O_3, 6.3% CaO, 1.8% Na_2OK_2O, 13.0% LOI.

Best bonding properties with these binders are developed by dispersing the material into the preparation water. When added dry, it develops some bonding ability but is more effective as a lubricant.

Magnesium-aluminum silicate binders consist of flat, plate-like flakes, which readily break down into submicron particles when agitated in water. Useful concentrations range from about 0.5–5.0%. Working and dry strength properties increase with increasing concentrations.

These materials do not migrate on drying so that the properties imparted to the ceramic body are uniform from internal to external surfaces. As film formers, they add to surface hardness, but to a lesser degree than most other binders.

Advantages in processing are ease in cleaning of equipment and no inherent tendency to cause corrosion of metal parts. It should be expected that magnesium-aluminum silicate will take part in ceramic body reactions and that it can influence fired properties.

Paraffin. Ordinary paraffin, with a small percentage of carnauba wax for increased rigidity, is a good binder in some cases and can be molded cold with a consequent reduction in molding time. Material has been used in the manufacture of porcelain barriers in telephone transmitters. Requirements as to the strength of the molded part, sharpness of outline and dimensional tolerances chiefly determine the type of binder employed in each case.

Starch. Henderson has reported the use of 0.3% ordinary laundry starch in a glaze very low in plastic content which settled and crawled badly. The starch acted as a floater and eliminated the crawling.

On the negative side, starch sours on standing.

Cellulose gum. (CMC.) Synthetic gum with excellent properties as a protective colloid for suspending, film-forming and binding.

In whitewares it is used in both bodies and glazes, increasing plasticity and strength. It fires out readily and completely in the kiln. (See SODIUM CARBOXY-METHYL-CELLULOSE.)

Methylcellulose. Synthetic gum proven effective as a temporary binder for refractories, structural clay products, whiteware and abrasives. In addition, it functions as a lubricant, wetting agent and plasticizer. As a film former, it toughens unfired glazes and improves bonding. It has been used to thicken and suspend glaze slips, and fired ware has been observed to possess a smoother finish. Trade named Methocel, the material has an extremely low ash content, does not melt, is nontoxic and does not deteriorate in storage. Manufactured under controlled conditions, its uniformity represents an important advantage. The material has a mild deflocculating effect varying with type (low, medium and high viscosity). Advantage can be taken of this effect to select the correct viscosity grade to give the necessary deflocculation.

Microcrystalline cellulose. Ultrapure crystalline form of cellulose that's clean

burning (<50 ppm ash), nontoxic, very uniform and does not deteriorate in storage. Functions as a binder/lubricant (dry or wet mixing) in press powder compacts. When used as a binder/extrusion aid in extruded bodies, it controls shrinkage. Particle size range: 20–100 μm. Allows formation of porous or high-density fired bodies. Green and fired strengths enhanced significantly.

Colloidal grades of microcrystalline cellulose, coproduced and dried with cellulose gum, function as nonmigrating binders and suspending agents in glaze slips. Performs as efficient binder/lubricants and extrusion aids in aqueous systems.

Polyethylene emulsions. Utilized as combination binders and lubricants.

Polyethylene glycols (PEGs). PEGs are widely used in ceramic processing. They are soluble in water and a variety of organic solvents, such as alcohols, ketones and chloroethylenes. Low molecular weight PEGs are viscous liquids and are used as internal or external lubricants and plasticizers. High molecular weight forms are waxy solids and are used as a binder in addition to being good lubricants and plasticizers. PEGs burn out over a temperature range of 175–350°C in air and 250–475°C in nitrogen. The ash content is low (<0.05%).

PEG Compound 20M is a modified form of polyethylene glycol. It is made by chemically joining 2 mols of linear PEG-8000 with the help of a linker. It has most of the properties of linear PEGs, but is amorphous in nature and is a stronger binder than an equivalent molecular weight linear PEG.

Polyvinyl alcohol. Used for rendering certain glazes hard in the dry state so that they resist rub-off while being placed on kiln cars. The equivalent of 0.25% dry powder gives a very hard coating to glazes. It does not change on standing nor ferment, but cannot be used in borax frits due to salting out.

Sodium silicate. Many grades are available with differences in their characteristics. Best results are obtained by consulting with the manufacturer.

When used properly as a deflocculant, sodium silicate eases the drying of a body in that there is less strain in the ware due to the absence of much water. Ware dries hard and tough which decreases loss in the green state.

Sodium metasilicate. Used as a mill addition in enamels for aluminum. Improves working properties and gives higher gloss values.

Wax emulsions. Widely used as binders and lubricants because they permit easy dispersion of water-insoluble waxes throughout ceramic mixes. Wax emulsions act as lubricants in wet bodies and impart strength to the formed piece after drying. A major application is dust-pressing of steatite and other nonplastic bodies. Dust pressing originated with the use of organic binders and is the only ceramic forming method that does not depend on the plasticity of the body to form the article. The chief advantage of this method is that dimensional tolerances are more easily maintained. Emulsions also are offered for use in extrusion mixes.

Special emulsions are used in glazes to aid suspension, improve coverage and firing characteristics, and impart rub-off resistance (an area in which they're particularly outstanding). Emulsions also have proved most effective as a green strength binder in floor and wall tile.

A wax emulsion has been used as an adhesive for applying underglaze decals to semivitreous dinnerware. The emulsion replaces a starch size and varnish adhesive, and a moderate heat treatment prior to glazing is substituted for the harden-on fire formerly needed.

Petroleum wax emulsions are easily removed from a ceramic body or glaze upon firing in an oxidizing atmosphere and leave no residue to adversely affect the properties of the ceramic article.

BINDER SUPPLIERS

BAYER CORPORATION,
POLYURETHANES DIV.
100 Bayer Road

Pittsburgh, PA 15205-9741 U.S.A.
(412) 777-2000 Fax: (412) 777-4889
Website: www.bayer.com/polymers-usa
FRASER PAPERS INC., LIGNIN PRODUCTS
P.O. Box 340
Park Falls, WI 54552-0340 U.S.A.
(715) 762-5228 Fax: (715) 762-5299
Email: tomczakb@pf.fraserpapers.com
LIGNOTECH USA
100 Hwy. 51 S.
Rothschild, WI 54474-1198 U.S.A.
(715) 355-3603 Fax: (715) 355-3674
Email: misc@ltus.com
Website: www.ltus.com
ROHM AND HAAS COMPANY
100 Independence Mall W.
Philadelphia, PA 19105 U.S.A.
(800) 206-0101 Fax: (610) 437-5212
Website: www.rohmhaas.com
R. T. VANDERBILT, CO. INC.
P.O. Box 5150
Norwalk, CT 06856-5150 U.S.A.
(203) 853-1400 Fax: (203) 853-1452
Email: rjohnson@rtvanderbilt.com
Website: www.rtvanderbilt.com

BORAX. (Sodium tetraborate.) Na_2O-$2B_2O_3$-$10H_2O$. Mol. wt. 381.4; sp. gr. 1.73 (25°C); hardness 2.0–2.5 Mohs; begins to melt in its own water of crystallization at 60.8°C. Soluble in water, acids, glycol, glycerol and other solvents. Practically all American borax comes from California. The mineral tincal is mined in the Mohave Desert and is processed and marketed as borax. Borax also is prepared by evaporation and purification of brines from Searles Lake.

Theoretical composition of borax: 16.25% sodium oxide, 36.51% boric acid, 47.24% water of crystallization. The water of crystallization is eliminated during fusion with other ceramic raw materials, leaving 52.76 wt% sodium and boric oxides to form part of the ceramic composition. Purity of ordinary commercial borax is guaranteed 99.5% min; original impurities being largely clay or other soluble salts. Borax is obtainable in large crystal, powder and granular form, the last being regarded as the most practical and economical for ceramic use.

The 10 molecules (47.24%) of water of crystallization in borax are subject to a small normal variation, the mineral losing water slowly during storage. In cases where considerable accuracy of batch composition is desired, it is necessary to determine and make proper adjustment for the actual water content immediately prior to use. This determination is accomplished by fusion or titration, the latter method being preferred.

Sodium tetraborate pentahydrate. Na_2O-$2B_2O_3$-$5H_2O$. Mol. wt. 286.6; sp. gr. 1.815 (25°C). Typical composition: 21.6–21.8% sodium oxide, 48.6–48.8% boric oxide. An economical replacement for borax. Theoretically 76.4 lb are equivalent to 100 lb of regular borax. The commercial product has about 4.75 rather than 5 mol of water of crystallization.

Anhydrous borax. (Fused borax.) Na_2O-$2B_2O_3$. Mol. wt. 201.27; sp. gr. 2.36; m.p. 742°C; soluble in water. Its rate of solubility is considerably slower than that of borax at 20°C but about the same at 60°C. Theoretical composition: 30.8% sodium oxide, 69.2% boric oxide.

Theoretically, anhydrous borax contains no water of crystallization, and actual analyses show less than 0.5% water. It may be substituted for ordinary borax, approximately 53 lb being equivalent to 100 lb of hydrated material. Unlike borax, it does not puff or swell to a light fluffy mass during melting, and, therefore, its use minimizes segregation and loss, particularly in furnaces operated under strong drafts. In cases where relatively large amounts of boric oxide are required in the finished product, the substitution of anhydrous borax for ordinary borax can substantially increase production. Due to its concentrated form, larger yields are possible and less time is required for melting, the water content having previously been eliminated and there being no insulating action due to the absence of the

light, porous stage which is evident in the melting of ordinary borax. Anhydrous borax saves fuel, involves the handling and storage of less material and, in general, makes for a smoother and more complete process.

Borates in glazes. Borax is widely used as a flux for glazes on earthenware, artware and other types of ceramic bodies. Boric oxides share with silica the property of combining with bases to form glassy compounds after fusion. The readiness with which boric oxide combines with bases finds application in the production of pottery colors from metallic oxides; the shades obtained often vary according to the amount of boric oxide used. It also has an important function in reducing viscosity of glazes; by the addition of a little borax, the most viscous glaze can be made to heal better. Borax also tends to produce higher gloss in a glaze and lowers the maturing temperature. In raw porcelain glazes, borax may advantageously be added in small amounts. An excess, however, induces defects such as crazing, blistering, injury to underglaze colors, injury to the stability of the glaze and thickening of the glaze to an unworkable jelly-like state. Borax is largely used in glazes where it is required to keep the amount of lead as low as possible and yet produce a glaze of moderately low melting point.

By decreasing the boric acid content, where it is included in the glaze formula, and substituting an equivalent amount of silica, a glaze is made harder, more brilliant and more durable. The introduction of boric acid into the glaze as a substitute for silica, however, decreases the coefficient of expansion. Thus, the relative amounts of boric acid and silica may be proportioned to achieve the best possible fit between body and glaze.

Borates in enamels. Borax is one of the principal ingredients of porcelain enamels. The amount of borax in the frit batch for sheet-steel ground-coat enamels varies from 20–45%, for sheet-steel cover coats from 15–40%, and for dry-process ground coats from 20–45%. About one-third of the amounts indicated represent boric oxide itself. In enamels, borax is one of the most active of all the fluxes used. It has a comparatively low melting point and vigorously attacks other ingredients, thus accelerating the rate at which the enamel is brought to a uniform molten state. Borax also imparts important thermal properties necessary to assure proper fit of the enamel to the base metal.

Borax imparts high luster, strength, toughness and durability, and assists in obtaining deep brilliant colorings, though it shortens the firing range of most enamels. Increasing the boric oxide content of a mill liquor decreases the scumming of an enamel caused by firing at too low temperatures. Better mobility and yield values of an enamel are attained by the use in the slip of hard water with 0.4–0.7% borax. Pitting caused by crystallization of borax on the surface of an enamel during drying will burn out in firing. Borax helps to prevent crazing, but excessively large amounts will cause tearing and crawling and will reduce the efficiency of mill-added opacifiers.

Borates in glass. Borax is indispensable to the manufacture of heat-resisting glass, fiber glass and other special glasses in which the presence of boric oxide, in relatively large percentages, is essential to obtain thermal durability, corrosion resistance and other important properties.

In general, those glasses containing the greatest amount of boric oxide show a minimum expansion, a property which is of great importance in obtaining thermal durability.

For this purpose, the thermal properties of the glass are not of primary importance and smaller quantities are employed to gain other desirable results. With the average batch, the boric oxide content of the resultant glass will run about 0.6–1.5%. In these amounts borax has been found to facilitate melting and refining to a considerable degree; increases in production capacity of 20–50% have been reported. In the event increased melting capacity cannot be employed, it is usually possible to decrease the melting

temperature required to produce normal requirements with consequent savings in fuel and wear and tear on melting equipment. Since borax generally decreases the viscosity of glass, its use should be accompanied by lower temperatures in the working end of the furnace. Borax also tends to shorten the working range and is, therefore, advantageous in connection with the use of high-speed machines.

In addition to its beneficial effects in melting, the presence of small amounts of borax in ordinary soda-lime-silica glass (resulting from use of borax in the batch) imparts greater brilliance, strength, durability and thermal shock resistance. It also decreases the tendency for glass to devitrify or crystallize.

With large melting units, the rate of production of good seed-free glass does not necessarily increase in direct proportion to the borax content of the batch, but probably reaches a maximum efficiency in glasses containing about 1.0–1.5% B_2O_3. Use of borax in such batches usually narrows the setting range, thus permitting greater speeds for the automatic fabrication of ware on bottle machines.

Boric oxide in the glass composition has been found to increase both the impact and tensile strength of glass containers. It also decreases the coefficient of expansion and increases rate of heat transfer and strength, all of which play important roles in thermal endurance. The use of 1% B_2O_3 often results in a better distribution and less checking in machine-made ware, besides the other advantageous properties mentioned above.

The presence of boric oxide in glass considerably improves its appearance, making the glass more brilliant and of better color, while the surface appears smoother and freer from minute imperfections. Boric oxide itself has no effect on color, but as the rate of melting is increased, less decolorizer is needed. This is true only for those batches in which moderate amounts of boric oxide are used. In heat-resisting glasses, high in boric acid, only neodymium functions satisfactorily as a decolorizer. (See RARE EARTHS.)

The effect of replacing soda and silica with boric oxide in a Fourcault glass sheet has been investigated. The glass composition: 72.5% SiO_2, 1.05% Al_2O_3, 10.69% CaO, 15.67% Na_2O. The substitution of boric oxide for silica increased both the melting and refining rates, while the substitution of boric oxide for soda decreased the melting rate only when amounts exceeded 5%.

From the foregoing it seems evident that moderate amounts of borax (60–120 lb/ton sand batch) will facilitate melting, allow increased fabricating speeds and improve the quality of the resultant glassware.

The extent to which melting is facilitated and quality is improved depends largely on the general composition of the batch employed and the specific operating conditions in each individual glass plant. However, it may be assumed that the amount of borax used in the batch bears a close relationship to the results obtained. When particularly large increases in melting rate are desired (durability, thermal properties, etc. of secondary importance) the borax may be used directly to replace sand. When durability and thermal properties are most important, the borax is substituted for soda.

BORAX SUPPLIERS

BORAX
26877 Tourney Rd.
Valencia, CA 91355 U.S.A.
(661) 287-5400; (800) 553-5232
Fax: (661) 287-5455; (800) 673-6183
Email: Telex: 371-6120
Website: www.borax.com

BORON CARBIDE. B_4C. Mol. wt. 55.26; m.p. 2450°C; b.p. 3500°C; density 2.52 g/cm^3. Black or dark gray, sooty when fine powder, glassy when dense. Theoretical boron content 78.3 wt%.

Boron carbide is the third hardest material known—after diamond and cubic boron

nitride (CBN)—and the hardest among mass-produced materials. Above 1300°C, boron carbide is even harder than diamond and CBN. This light ceramic material is very strong, with a 4-point flexural strength of 50,000–70,000 psi and a compressive strength of 414,000 psi (strength depends strongly on densification method and microstructure). The high strength-weight ratio makes B_4C especially attractive for armor and aerospace applications. Low thermal conductivity (29–67 W/mK) combined with a large Seebeck coefficient (200–300 μmV/K) makes B_4C an efficient p-type thermoelectric, especially at elevated temperatures. Electrical resistivity ranges from 0.1–10 ohm-cm, and is sensitive to hydrostatic pressure.

Different commercial grades of B_4C are available, based on boron content and particle size. Technical grades (55–75% B) are usually sold as coarse grit while nuclear (76.5% B min) and high-purity (75–80% B) grades can be obtained with sizes ranging from grit (5–20 mesh) to submicron powder.

Boron carbide parts are fabricated by hot pressing, sintering and sinter-HIPing. Industrially, densification is carried out by hot pressing (2100–2200°C, 20–40 MPa) in argon. The best properties are obtained when pure fine powder is densified without additives. Pressureless sintering to high density is possible using ultrafine powder with additives (notably carbon). Less expensive than hot pressing, sintering also can be used for more complex shapes.

Special part formulations include bonding B_4C with fused sodium silicate, borate frits, glasses, plastics or rubbers to lend strength, hardness or abrasion resistance. Boron carbide-based cermets and metal matrix composites (especially Al/B_4C, Mg/B_4C, Ti/B_4C), and ceramic matrix composites (e.g. TiB_2/B_4C) have unique properties that make these materials suitable for highly specialized applications. Superior ballistic performance, high-temperature strength, light weight, corrosion resistance and hardness make these composites especially attractive. Boron carbide shapes can be reaction bonded using silicon carbide as the bonding phase. B_4C-carbon mixtures are formed, then reacted with silicon to create the silicon carbide bond. SiC also can be used as a sintering aid for boron carbide and vice versa.

As an abrasive, B_4C is used for fine polishing and ultrasonic grinding and drilling, either as a loose powder or as a slurry. Tendency to oxidize at workpiece temperatures precludes its use in bonded abrasive wheels. Abrasion-resistant parts made from boron carbide include spray and blasting nozzles, bearing liners and furnace parts. Boron carbide's refractory properties, in addition to its abrasion resistance, are of value in the latter application.

Boron carbide is chemically inert, although it reacts with oxygen at elevated temperatures and with white hot or molten metals of the iron group, and certain transition metals. B_4C reacts with halogens to form boron halides—precursors for the manufacture of most nonoxide boron chemicals. B_4C also is used in some reaction schemes to produce transition metal borides. Boronizing packings containing B_4C are used to form hard boride surface layers on metal parts.

Boron carbide and elemental boron are used for nuclear reactor control elements, radiation shields and moderators.

BORON CARBIDE SUPPLIERS

CERADYNE INC.
3169 Redhill Ave.
Costa Mesa, CA 92626 U.S.A.
(714) 549-0421 Fax: (714) 549-5787
Email: sales@ceradyne.com
Website: www.ceradyne.com
CERCOM INC.
991 Park Center Dr., P.O. Box 70
Vista, CA 92083 U.S.A.
(760) 727-6200 Fax: (760) 727-6209
ELECTRO ABRASIVES CORP.
701 Willet Rd.
Buffalo, NY 14218 U.S.A.

(716) 822-2500; (800) 284-4748
Fax: (716) 822-2858
Email: info@electroabrasives.com
Website: www.electroabrasives.com
WACKER ENGINEERED CERAMICS, INC.
3301 Sutton Rd.
Adrian, MI 49221-9397 U.S.A.
(800) 833-7608 Fax: (517) 264-8137
Email: wec.info@wacker.de
H.C. STARCK GMBH & CO. KG
P.O. Box 25 40
D-38615 Goslar Germany
+49/53 21/7 51-1 45 Fax: +49/53 21/7 51-1 93
Email: bettina.essmann.be@hcstarck.de
Website: www.hcstarck.com
H.C. STARCK INC.
45 Industrial Place
Newton, MA 02161-1951 U.S.A.
(617) 630-5916 Fax: (617) 630-5919
Email: elisabeth.james.b@bayer.com
Website: www.hcstarck.com
UK ABRASIVES, INC.
3045 Mac Arthur Blvd.
Northbrook, IL 60062 U.S.A.
(847) 291-3566 Fax: (847) 291-7670
Email: sales@ukabrasives
Website: www.ukabrasives.com
WASHINGTON MILLS ELECTRO MINERALS CORP.
P.O. Box 423, 1801 Buffalo Ave.
Niagara Falls, NY 14302 U.S.A.
(716) 278-6600 Fax: (716) 278-6650
Email: sales@washingtonmills.com
Website: www.washingtonmills.com

BORON NITRIDE. BN. A highly refractory material with physical and chemical properties similar to carbon. Graphite-like (g-BN), wurzite (w-BN) and zinc blende (z-BN) are known polymorphs of BN corresponding to the graphite (hexagonal) and diamond (cubic) structures. Transformation of g-BN to w-BN occurs at pressures above 12 GPa at relatively low temperature (230°C). Transformation of w-BN to z-BN occurs above 1300°C and pressures above 5.5 GPa. Zinc blende (z-BN) is stable above 5.5 GPa and from 1100 to 1500°C.

All forms of BN are good electrical insulators, possessing band gaps of several eV; electrical resistance of the hexagonal form varies from 1.7×10^{13} ohm-cm at 25°C to 3×10^4 ohm-cm at 1000°C and is little affected by frequency. The dielectric constant of hexagonal BN is 3 with the electric vector parallel to the basal plane and 5 perpendicular to the plane. Consistent with the short interatomic distances and light atomic weights, all forms of BN are very good thermal conductors. Boron nitride is chemically inert in most environments, resisting attack by mineral acids or wetting by glasses, slags and molten oxides; cryolite and fused salts; and most molten metals including aluminum. Its rate of oxidation in air is negligible below 1100°C.

Hexagonal boron nitride is commonly synthesized as a fine powder. Powders will vary in crystal size, agglomerate size, purity (including % residual B_2O_3) and density. BN powders can be used as mold release agents, high temperature lubricants, and additives in oils, rubbers and epoxies to improve thermal conductance of dielectric compounds. Powders also are used in metal- and ceramic-matrix composites to improve thermal shock and modify wetting characteristics.

Hexagonal boron nitride may be hot pressed into soft (Mohs 2) and easily machinable, white or ivory billets having densities 90–95% of theoretical (2.25 g/ cm^3). Thermal conductivities of 17–58 W/ mK and CTEs of $0.4–5 \times 10^{-6}$/C are obtained, depending on density, orientation with respect to pressing direction and amount of boric oxide binder phase. Because of its porosity and relatively low elastic modulus (50–75 GPa), hot pressed boron nitride has outstanding thermal shock resistance and fair toughness. Pyrolytic boron nitride, produced by chemical vapor deposition on heated substrates, also is hexagonal; the process is used to

produce coatings and shapes having thin cross sections.

Uses for hexagonal boron nitride shapes include crucibles, parts for chemical and vacuum equipment, metal casting fixtures, boron sources for semiconductor processing and transistor mounts.

Cubic boron nitride is second in hardness only to diamond. It is used for high-performance tool bits and in special grinding applications. Cubic BN tooling typically outlasts alumina and carbide tooling and is preferred in applications where diamond is not appropriate, such as grinding of ferrous metals.

BORON NITRIDE SUPPLIERS

ADVANCED CERAMICS CORP.
P.O. Box 94924
Cleveland, OH 44101 U.S.A.
(216) 529-3900; (800) 822-4322
Fax: (216) 529-3954
Email: info@advceramics.com
Website: www.advceramics.com

CARBORUNDUM CORPORATION, BORON NITRIDE
168 Creekside Dr.
Amherst, NY 14228 U.S.A.
(716) 691-2051 Fax: (716) 691-2090
Email: sales@carbobn.com
Website: www.carbobn.com

CERCOM INC.
991 Park Center Dr., P.O. Box 70
Vista, CA 92083 U.S.A.
(760) 727-6200 Fax: (760) 727-6209

WACKER ENGINEERED CERAMICS, INC.
3301 Sutton Rd.
Adrian, MI 49221-9397 U.S.A.
(800) 833-7608 Fax: (517) 264-8137
Email: wec.info@wacker.de

SHS CERAMICAS
Poligono Industrial "Las Vinas," P.O. Box 28
37500 Ciudad Rodrigo, Salamanca Spain
34-923-46.11.39 Fax: 34-923-48.10.60
Email: jag@mina.enusa.es

H.C. STARCK GMBH & CO. KG
P.O. Box 25 40
D-38615 Goslar Germany
+49/53 21/7 51-1 45 Fax: +49/53 21/7 51-1 93
Email: bettina.essmann.be@hcstarck.de
Website: www.hcstarck.com

H.C. STARCK INC.
45 Industrial Place
Newton, MA 02161-1951 U.S.A.
(617) 630-5916 Fax: (617) 630-5919
Email: elisabeth.james.b@bayer.com
Website: www.hcstarck.com

BOROSILICATE. A material which has BO_3 planar triangles and SiO_4 tetrahedra linked to form networks; produces glasses with lower fusion temperatures and a longer working viscous range.

CALCIUM-ALUMINUM SILICATE. Specially processed and refined product derived from preselected and blended blast furnace slag. Normally sold on both chemical and physical specifications to manufacturers of various types of glass. Chemically, it offers four major oxides: calcia, magnesia, alumina and silica. Physically, calcium-aluminum silicate is classified as a 16-mesh product.

Typical average composition of Calumite calcium-aluminum silicate slag is: 31.6% SiO_2, 15.7% Al_2O_3, 0.25% Fe_2O_3, 34% CaO, 15.5% MgO, 0.25% MnO, 0.8% sulfur, 0.55% alkali; fusion point, 2350°F.

Use of calcium-aluminum silicate was originally confined to reduced amber and green glasses where large amounts can be added. Because of its reducing nature, the quantities of slag used in reduced colored glasses are much greater than those used in oxidized glasses. The material is added to solve glass stability problems. It is believed that the reducing action of slag helps liberate retained gases from the glass, a major cause of seeds, blisters and limitations on production pulls. Increased production rates are said to result from the elimination of soluble sulfates and by the formation of a eutectic with silica, which reduces the time and temperature required for melting. Reductions in

furnace temperature of as much as 150°F have been reported. Also, a slag batch is usually lower in cost and easier to melt.

Upon introduction into an amber glass batch, most or all of the alumina requirement and approximately half the diabasic oxide requirement can be fulfilled. In certain cases, the number of basic batch components can be reduced. Some commercial glass is being produced with only sand, soda, an oxidant and slag, plus a colorant.

The material contributes in several ways to the manufacture of amber glass. One of the most important is that the alumina and lime requirements are initially combined, resulting in less batch segregation than when these constituents are used individually. The product is amorphous (partially premelted) when introduced into the batch. In the production of amber, the slag's reducing components provide a more controllable color formation.

Calumite slag also is being used in production of oxidized glasses because of its excellent fining properties. The amount added: 2–4 wt%.

Potential applications include plate glass, textile and other special glasses, and certain ceramic applications.

CALCIUM ALUMINUM SILICATE SUPPLIERS

BPI INC. (BY-PRODUCT INDUSTRIES)
612 S. Trenton Ave.
Pittsburgh, PA 15221 U.S.A.
(412) 371-8554 Fax: (412) 371-9984
Email: info@bpiminerals.com
Website: www.bpiminerals.com

R. T. VANDERBILT, CO. INC.
P.O. Box 5150
Norwalk, CT 06856-5150 U.S.A.
(203) 853-1400 Fax: (203) 853-1452
Email: rjohnson@rtvanderbilt.com
Website: www.rtvanderbilt.com

CALCIUM CARBONATE. Precipitated calcium carbonate, in low-micrometer sizes, is used as an inorganic filler in basing cements. These cements consist of a two-stage phenol-formaldehyde resin, calcium carbonate filler and enough hexamethylenetetramine to catalyze the reaction of the resin with heat. Various organic dyes are sometimes added. Material also can be used for insulating coatings for ceramic capacitors and printed circuits. (See LIME and WHITING.)

CALCIUM CARBONATE SUPPLIERS

ALFA AESAR, A JOHNSON MATTHEY COMPANY
30 Bond St.
Ward Hill, MA 01835-8099 U.S.A.
(800) 343-0660 Fax: (800) 322-4757
Email: info@alfa.com
Website: www.alfa.com

GLOBAL STONE CORPORATION
10898 Crabapple Rd., #101
Roswell, GA 30075 U.S.A.
(770) 992-1268 Fax: (770) 992-0488
Website: www.oglebaynorton.com

SOLVAY PERFORMANCE CHEMICALS
3333 Richmond Ave.
Houston, TX 77098 U.S.A.
(713) 525-6700 Fax: (713) 525-7804
Email: sandy.wilson@solvay.com
Website: www.solvay.com/na/smi

CARBIDE. A binary compound of carbon with other elements; cemented or compacted mixture of carbides used for metal-cutting and machining tools.

CARBON AND GRAPHITE. Carbon boasts high resistance to thermal shock, and a strength that increases with temperature. It is chemically inactive, not wet by most molten metals and resists abrasion and erosion. Graphite, in addition, has high thermal conductivity, low thermal expansion, high electrical conductivity, is relatively pure and is easily machinable.

This unique combination of physical and chemical properties has resulted in numerous applications. Among them: lighting carbons; carbon-graphite and metal-graphite brushes for motors and generators; welding

carbon products; electrodes for electrometallurgical and electrochemical industry use; carbon, graphite and impervious carbon and graphite pipe, fittings, valves, pumps, towers, heat exchangers, Raschig rings, tubes, brick, tile and special structural shapes for handling and processing corrosive materials; and porous carbon and graphite products for filtration and gas dispersion. Activated carbon is used for solvent recovery and absorption of odors and vapors.

In addition, carbon and graphite products have many important metallurgical applications. These include carbon linings for hearth and wall sections of blast furnaces and ferroalloy furnaces; phosphorus furnaces; aluminum pot linings; cinder notch liners; liners for run-out troughs and pickling tanks; carbon and graphite ingot mold plugs and tool inserts; and graphite fluxing tubes for purification of metals; thermocouple sheaths; riser rods for steel castings; molds for ingots, billets, centrifugally cast bushings, static cast rods and other simple castings; core rods; sintering boats and trays; crucibles for induction and resistance melting; and skimmer floats.

Special applications of carbon and graphite include switch and circuit breaker contacts; rheostat disks; steam turbine packing; piston rings; stuffing box packing; thrust rings for automobile clutches; back plates, diaphragms and granular carbon for telephones; anodes and grids for electronic devices; and, in the form of pure graphite powder, a lubricant and constituent of lubricating grease. Graphite also is used as rudder vanes for guided missiles, nozzles for rocket motors and tooling for the manufacture of thermosetting and thermoplastic composite parts.

Carbon and graphite electrodes have made possible the electric arc furnace. Graphite anodes have been an important factor in the development of electrolytic processes.

Nuclear grades of graphite are used as moderators, thermal columns, reflectors, and shields in nuclear reactors.

Specialty grades of graphite are used in many highly technical applications, including semiconductor processing, mechanical heart valves, electrical discharge machining and electrochemical cells.

CARBON AND GRAPHITE SUPPLIERS

ALFA AESAR, A JOHNSON MATTHEY COMPANY
30 Bond St.
Ward Hill, MA 01835-8099 U.S.A.
(800) 343-0660 Fax: (800) 322-4757
Email: info@alfa.com
Website: www.alfa.com

ASBURY GRAPHITE MILLS INC.
405 Old Main St.
Asbury, NJ 08802 U.S.A.
(908) 537-2155 Fax: (908) 537-2908
Email: ntmares@asbury.com
Website: www.asbury.com

GRAPHITE DIE MOLD, INC.
18 Airline Park
Durham, CT 06422-1000 U.S.A.
(860) 349-4444 Fax: (860) 349-0136
Email: sales@graphitediemold.com
Website: www.graphitediemold.com

JERSEY MINERAL PROCESSING CO., LTD.,
REFRACTORIES AND MINERALS DIV.
RM B-13B, Triumphal Arc Mansion, 66 Nanjing Rd.
Tianjin, 300042, P.R. China
86-22-23133086 Fax: 86-22-23133085
Email: cmptjmax@shell.jtvan.com.cn

POCO GRAPHITE INC.
1601 S. State St.
Decatur, TX 76234 U.S.A.
(940) 627-2121; (877) 762-6747 (US)
Fax: (940) 393-8366
Email: sales@poco.com
Website: www.poco.com

STRATMIN GRAPHITE INC., HEAD OFFICE
630 Rene-Leveque Blvd. W., Ste. 2660
Montreal, PQ Canada H3B 1S6

(514) 866-8467 Fax: (514) 866-8725
Email: info@stratmin.com
Website: www.stratmin.com
TIMCAL AMERICA INC.
29299 Clemens Rd. 1-L
Westlake, OH 44145 U.S.A.
(440) 871-7504 Fax: (440) 871-6026
Email: westlake@us.timcal.com
Website: www.timcalamerica.com

CLAY. Product of the decomposition and alteration of feldspathic rocks. Consists of a mixture of particles of different sizes and widely differing physical, chemical and mineralogical properties. The nonplastic portion consists of altered and unaltered rock particles of which the most common and abundant substances are quartz, micas, feldspars, iron oxides, and calcium and magnesium carbonates. Organic matter usually is also present in greater or lesser amounts, and frequently plays an important role in determining clay properties. The essential constituents of clays are hydrated silicates of aluminum, of which there are several, but the most important and widespread are the kaolinite group, Al_2O_3-$2SiO_2$-$2H_2O$, and montmorillonite group, (Mg,Ca)O-Al_2O_3-$5SiO_2$-H_2O. Bentonite belongs to the montmorillonite group.

Clays may be designated as residual or secondary, according to their geologic history. Residual clays are those occurring in the same location as originally formed by weathering. English china clays and North Carolina kaolin are the most important residual clays. Secondary clays are those that have been transported by water, ice or wind, and redeposited, alteration usually occurring during the transportation process typified by the middle Georgia Fall Line area.

The typical clay minerals—kaolinite, montmorillonite, etc.—have microscopic plate-like structures which are believed to be chiefly responsible for their plasticity (formability) when wetted with water. Other important properties: (1) hardening when dried and permanency when fired; (2) shrinkage during drying and firing; (3) variety of colors obtainable when fired; (4) refractoriness, or resistance to softening at high temperatures; (5) heat, sound, and electrical insulation; and (6) decolorizing and clarifying action (particularly fuller's earths, which are used for refining oils).

An extremely high content of fine particles is characteristic of very plastic clays. The finest fraction, which also is quite small, contains the clay suspensoids or colloids which are responsible for the plasticity. Most of the material consists of granular matter. Too high a content of so-called clay substances can make the material excessively plastic, which renders it sticky and difficult to work.

Other important factors in plasticity are the amount, size, relative proportion of sizes, shape and other characteristics of the granular material, and the amount and character of soluble salts (electrolytes) and organic material present.

The fineness of a clay's grain influences not only its plasticity but also such properties as drying performance, drying shrinkage, warping, and tensile, transverse and bonding strength.

For example, the greater the proportion of fine material, the slower the drying rate, the greater the shrinkage, and the greater the tendency to warp and crack during this stage. Clays with a high fines content usually are mixed with coarser materials to avoid these problems.

For two clays having different degrees of plasticity, the more plastic one will require more water to make it workable, and water loss during drying will be more gradual because of its more extensive capillary system. The high-plasticity clay also will shrink more and will be more likely to crack.

The most important clays in the pottery industry are the ball clays and china clays (kaolin). (See CLAY, BALL and KAOLIN.) The following paragraphs focus on special-purpose clays.

Enamel clays. In general, are very clean with minimal impurities, selected for their ability to hold the finely ground enamel frit particles in water suspension so they will dip and spray evenly. Clay also aids the opacity of the fired coating. Amounts of clay ranging from 2–15%, based on dry weight of frit, have been added to the mill; the usual amount, however, is about 7%. Enamel clays are usually of ball clay characteristics, although somewhat lighter in color. The well-known Vallendar clay of Germany had been used in the United States enameling industry for many years and was popular because of its exceptional freedom from carbonaceous material. Blended domestic clays also can be made satisfactory by means of purifying methods and extreme pulverization. Bentonite also is used in some plants for suspension of frit particles. (See BENTONITE.)

Glaze clays. Are introduced into the glaze batch to serve as suspending and binding agents in the unfired state, and as an intrinsic part of the finished glaze.

It may be concluded that fine-grained ball clays of exceptional purity, which contain appreciable quantities of colloidal organic matter, are desirable glaze clays. Apparently, the fine clay provides suspending power and dried film strength, and its organic content prevents undue changes in slip consistency from leached out flocculating and deflocculating ions.

Fine-grained china clays are used where exceptional purity is required, together with high suspending qualities. Hoever, such clays are sensitive to soluble salt effects, and usually must be modified with gum additions or deflocculants. The coarser china clays are low in film strength and suspending power but tend to release water more readily than the finer kaolins. For high film strengths, the china clays normally require binder additions.

Sagger clays. Open-firing refractory clays of suitable uniformity with resistance to repeated heating and cooling. They are used wholly or in part for forming and making a refractory container, known as a sagger, in which articles are protected from dirt, furnace gases, uneven heating and thermal shock during heating in their manufacture.

Clays that are plastic and used in making **stoneware** (heavier ceramics such as jugs, pots and other containers) are found in New York, New Jersey, Missouri, Maryland, Texas, Ohio, Minnesota, Illinois, Pennsylvania and Indiana. Many brick clays and refractory clays can also be made into stoneware. Other products made from these clays are called **yellowware**, **artware**, **earthenware** and **terra cotta**. **Tableware** has also been made from these clays and is classified as semiporcelain. The products may be any color, glazed or unglazed, and the body can be modified with other ceramic materials. A tensile strength of 125 psi or higher is desirable, and the clay should show low firing shrinkage.

Wad clays. Low grades of fire clay, used for closing the joints between saggers when they are set up in the kiln. A wad clay should be inexpensive, should not soften so much that it will stick to the saggers, and should be free from pyrite, ferrous carbonate and other objectionable materials. It should have good strength and low shrinkage. Ball clays are sometimes used in this application.

CLAY SUPPLIERS

IONE MINERAL & REFRACTORIES
8631 Hwy. 124
Ione, CA 95640 U.S.A.
(209) 274-2471 Fax: (209) 274-4102

KALEMADEN ENDUSTRIYEL HAMMADDELER SAN. VE TIC. A.S., HEADQUARTERS
Semedeli Koyu, Can
Canakkale Turkey
(90 286) 4341330 Fax: (90 286) 4371340
Email: can@kalemaden.com.tr
Website: www.kalemaden.com.tr

KALEMADEN ENDUSTRIYEL HAMMADDELER SAN. VE TIC. A.S., EXPORT & MARKETING MANAGEMENT

Eski Uskudar Yolu, Bodur Is Merkezi, No. 8, Kat 6
Daire: 23-24, Icerenkoy, Istanbul
Turkey
(90 216) 3844999; (90 216) 3844748
Fax: (90 216) 3725548
Email: ist@kalemaden.com.tr
OLD HICKORY CLAY COMPANY
P.O. Box 66
Hickory, KY 42051-0066 U.S.A.
(270) 247-3042 Fax: (270) 247-1842
Email: psp@oldhickoryclay.com
Website: www.oldhickoryclay.com
RESCO PRODUCTS INC., CEDAR HEIGHTS CLAY
P.O. Box 295
Oak Hill, OH 45656 U.S.A.
(740) 682-7794 Fax: (740) 682-6438
Website: www.rescoproducts.com
SHEFFIELD POTTERY, INC.
U.S. Rte. 7, P.O. Box 399
Sheffield, MA 01257 U.S.A.
(413) 229-7700; (888) 774-2529
Fax: (413) 229-0200
Email: sales@sheffield-pottery.com
Website: www.sheffield-pottery.com
H. C. SPINKS CLAY CO. INC.
P.O. Box 820
Paris, TN 38242 U.S.A.
(901) 642-5414 Fax: (901) 642-5493
Email: hcspinks@worldnet.att.net
Website: www.spinksclay.com
UNIMIN CORP.
258 Elm St.
New Canaan, CT 06840 U.S.A.
(203) 966-8880; (800) 243-9004
Fax: (203) 972-1378; (800) 243-9005
R. T. VANDERBILT, CO. INC.
P.O. Box 5150
Norwalk, CT 06856-5150 U.S.A.
(203) 853-1400 Fax: (203) 853-1452
Email: rjohnson@rtvanderbilt.com
Website: www.rtvanderbilt.com
WBB PACIFIC CLAYS PTE. LTD.
1 Philip St., #13-00
Singapore, 048692 Singapore
+65 538 0355 Fax: +65 536 6182
Email: clay@wbbpacific.com
Website: www.wbb.co.uk

CLAY, CHINA. (See KAOLIN.) The terms *kaolin* and *china clay* are used interchangeably to describe a type of clay which fires to a white color and has a PCE of 34–35.

The name kaolin comes from the two Chinese words kao-ling, meaning high ridge, and was originally a local term used to describe the region from which the clay was obtained. The term kaolin was originally used in the United States to refer to certain residual clays of a white- or nearly white-burning character. In recent years, however, it has been stretched to cover certain white sedimentary clays like those obtained in South Carolina and Georgia. The present terminology differentiates between the two types of deposits by designating as primary or residual kaolins those white-burning clays formed by the weathering, in place, of feldspathic rocks, pegmatite dikes, granites, and the like, and found in the location of the parent rock. Secondary or sedimentary kaolins are those that were formed by weathering, then carried by water and redeposited in another area. Thus, the secondary kaolins of South Carolina and Georgia were deposited in lagoons and embayments at or near the old shoreline of the Atlantic in an area later uplifted to form the Atlantic Coastal Plain. Secondary kaolins were also deposited in the lone formation in Northern California.

Most of the domestic supply of residual kaolin is obtained from western North Carolina, and most of the sedimentary clay comes from Georgia, South Carolina and Northern California. The South Carolina kaolins are widely used in the refractory and elastomeric industries. Although some of the South Carolina kaolin deposits have a naturally occurring large particle size which makes them excellent casting clays, most

are finer particle-sized than the Georgia kaolins, and both can be fractionated into casting clays. Lone kaolins are widely used in casting sanitaryware, ceramics and refractories.

Kaolin (Al_2O_3-$2SiO_2$-$2H_2O$) usually contains less than 2% alkalies and smaller quantities of iron, lime, magnesia and titanium. Because of its purity, kaolin has a high fusion point and is the most refractory of all clays.

Georgia china clay is one of the most uniform kaolins to be found. Generally speaking, there are two types of Georgia-sourced kaolin, both of which are widely used for casting and other processes. One type imparts unusually high strength and plasticity, and is used for both casting and jiggering where a high degree of workability is required. The other type typically is a fractionated, controlled particle size clay that also behaves well in casting, dries uniformly and reduces cracking of ware.

Both china clay and kaolin are often used in place of alumina in continuous fiberglass applications, due to their low alkali and iron contents.

CLAY, CHINA SUPPLIERS

HAMMILL & GILLESPIE INC.
154 S. Livingston Ave.
Livingston, NJ 07039 U.S.A.
(973) 994-3650 Fax: (973) 994-3847
Email: hamgilinc@aol.com
Website: www.hamgil.com

IONE MINERAL & REFRACTORIES
8631 Hwy. 124
Ione, CA 95640 U.S.A.
(209) 274-2471 Fax: (209) 274-4102

KENTUCKY-TENNESSEE CLAY COMPANY, AND K-T FELDSPAR CORPORATION
1441 Donelson Pike
Nashville, TN 37217 U.S.A.
(615) 365-0852 Fax: (615) 365-0842
Email: mdonovan@k-tclay.com
Website: www.k-tclay.com

R. T. VANDERBILT, CO. INC.
P.O. Box 5150
Norwalk, CT 06856-5150 U.S.A.
(203) 853-1400 Fax: (203) 853-1452
Email: rjohnson@rtvanderbilt.com
Website: www.rtvanderbilt.com

WBB GROUP
Park House, Courtenay Park
Newton Abbot, Devon England, U.K. TQ12 4PS
+44 (0)1626 332345 Fax: +44(0)1626 332344
Email: clay@wbb.co.uk
Website: www.wbb.co.uk

WBB DEVON CLAYS LTD.
Park House, Courtenay Park
Newton Abbot, Devon England, U.K. TQ12 4PS
+44 (0)1626 332345 Fax: +44 (0)1626 332344
Email: sales@wbb.co.uk
Website: www.wbb.co.uk

WBB FUCHS GMBH & CO KG
Postfach 347
D-56223 Ransbach-Baumbach Germany
49 (2623) 83-0 Fax: 49 (2623) 83-40
Email: info@wbbfuchs.com
Website: www.wbb.co.uk

COPPER OXIDE. (Cuprous oxide.) Cu_2O. Mol. wt. 143.08; density 6.0 g/cm^3; m.p. 1235°C. Cubic red crystals insoluble in water, soluble in HCl, NH_4Cl and NH_4OH. Prepared by the oxidation of copper, by the addition of bases to cuprous chloride or by the action of glucose on cupric hydroxide.

(Cupric oxide or black copper oxide.) CuO. Mol. wt. 79.54; sp. gr. 6.4; decomposes at 1026°C. Insoluble in water and soluble in acids and NH_4Cl. Derived by the ignition of copper carbonate or copper nitrate, copper hydrate, or oxidation of lower oxides.

Both copper oxides are used in ceramics —cupric oxide is generally preferred in **glazes** and cuprous oxide in **glasses**. Copper ores from which these oxides are derived are mined in Arizona, Utah, Montana and

Nevada in the United States; and in Africa, Chile, Canada, Russia and Japan.

Cupric oxide, when used in glazes, has a wide range of color. It may be used either as the raw oxide in a raw glaze, as the raw oxide in a fritted glaze, or as part of the frit itself. It is used equally well in any of these cases, but when mixed with the frit there is a loss of color strength under certain conditions due to volatilization of the oxide, and it is not so satisfactory above cone 4 when operations are carried out under oxidizing conditions.

The color of the glaze will depend upon these conditions: (1) amount of copper oxide in the glaze, (2) whether atmosphere is reducing or oxidizing and fast or slow, (3) RO group relation, (4) Al_2O_3 group relation, (5) SiO_2 group relation and (6) degree of fineness of the copper oxide used.

Copper oxide is the only individual pigmentary oxide in common use which in practically every combination and under ordinary conditions produces clear green colors. In combinations with tin oxide and other opacifying agents it gives turquoise or blue-greens when the glaze is alkaline.

The amount of copper oxide in the glaze for light shades of green will be 0.03–0.06 equivalents, and for darker shades 0.6–1.0 equivalents. The actual amount will depend almost entirely upon composition of the RO group. In glazes containing PbO in fairly large amounts, smaller than normal amounts of copper oxide are used.

Crystal effects may be produced in copper glazes by means of the firing process in conjunction with variations of the RO group. For instance, this glaze is said to give very bright crystals on a green background: 27.385 zinc oxide, 7.382 potassium nitrate, 13.700 borax, 7.200 whiting, 4.466 boric acid, 0.600 cupric oxide, 39.603 flint.

This total glaze should be fritted and dextrin used to thicken it after grinding to pass 120 mesh if possible. Fire from cone 04–02 in 8.25 hr, hold at cone 02 for approximately 45 min, drop to cone 010 and hold for about 3 hr, natural cool.

In producing green glazes, if the fire is oxidizing and the rate of temperature increase is the same in every case, the color will be the same. There are some copper glazes where the color will vary because of slow firing and little soaking. The best color will be obtained by a quick regular fire and little soaking.

Cupric oxide is subject to color changes depending upon the six factors listed previously. CaO is not likely to affect the color of copper in a glaze. In a cone 02 glaze similar to that used on decorative ware, K_2O changes the color to a yellowish tint, and when CuO is used in combination with either Na_2O or PbO, the K_2O should not exceed 0.15 equivalent. Copper oxide in a glaze containing barium oxide and zinc oxide gives a decidedly blue shade when combined with sodium or potassium oxide, but with lead oxide has more of a black-green color. A copper oxide glaze with calcium and magnesium oxides produces a green color very different from that produced with lead oxide. Cupric oxide is slightly affected by the use of zinc oxide in combination with lead oxide and others of the RO group.

If tin oxide is incorporated in a green copper glaze of moderate intensity, the color will be changed from green to turquoise or robin's egg blue, and will vary with the amount of tin used. The firing must remain oxidizing, and a quick fire is recommended to obtain best results. The addition of small amounts of titanium oxide (rutile) to a copper glaze with or without tin will sometimes create very beautiful, unusual effects. Generally, small brown specks and blotches will appear in the glaze by this addition.

When reducing conditions prevail in the kiln, a red color is produced. In the well-known sang deboeuf and rouge flambe, the glaze should be rich in alkalies and contain but little copper oxide—only about 0.10–0.15 equivalent for dark red and 0.05–0.10 for light red tinge. This glaze, if fired to cone 5–7, reducing until 900°C and oxidizing

to maturity, will give a good copper red:

$$\left.\begin{array}{l}0.25\ CaO\\0.05\ MgO\\0.14\ K_2O\\0.12\ Na_2O\\0.32\ PbO\\0.05\ ZnO\\0.07\ CuO\end{array}\right\}\left\{\begin{array}{l}.18\ Al_2O_3\\0.12\ B_2O\end{array}\right\}\left\{\begin{array}{l}2.40\ SiO_2\\0.05\ SnO_2\end{array}\right.$$

The purple colors, which are a mixture of copper in its blue-green oxidized and red reduced forms, appear most frequently in glazes high in lime. Similar effects may be obtained in more fusible glazes by an earlier period of oxidation and by a neutral firing condition in the latter stages of firing. High lime and alumina produce purple splotches. The purple color becomes uniform if the calcium content is supplied by colemanite. Increased soda content shifts the color toward red.

Red copper oxide may be used as an underglaze, being best produced by very thin sprays of copper oxide underneath a soft soda glaze.

There is a tendency to leave the body and diffuse into the glaze unless both color and glaze are applied thinly. The most reliable underglazes contain at least 0.2% soda. The firing is the same as that for the red glazes. This is a reliable batch: 35% calcined clay, 25% copper oxide, 20% tin oxide, 20% following glaze.

$$\left.\begin{array}{l}0.123\ Na_2O\\0.734\ CaO\\0.143\ K_2O\end{array}\right\}0.394\ Al_2O_3\left\{\begin{array}{l}0.123\ SiO_2\\3.710\ B_2O_3\end{array}\right.$$

In the enameling industry, copper is widely used in making black enamels where the black is produced in the smelter. Small quantities added to cobalt oxide, manganese dioxide and/or nickel oxide also serve to improve adherence of ground coat enamels.

Copper oxide is used to make copper ruby glass. The red color is produced by precipitation of the metallic colloid by means of sodium cyanide in the batch.

It is difficult to make copper ruby glass which will be transparent in thicknesses as great as 1/8 in. It is therefore generally flashed as a thin layer on a much thicker layer of colorless or opaque glass. The color ordinarily develops more rapidly and is more intense in lead glasses, and increased silica tends to reduce the rate of color development. Tin oxide and additional reducing agents such as cream of tartar are always necessary.

Cuprous oxide produces blue or green glass. From 5–10 lb of oxide per ton of batch gives a desirable range of colors. Nitrate should be present during melting. Copper oxide and cobalt oxide mixed give a very delightful blue shade. When green glasses are required, copper oxide must be mixed with iron oxide, chromium oxide or both. An emerald green results from a mixture with iron oxide, and a deep green when chromium oxide is used in conjunction with copper oxide. The addition of 2–3% borax with the nitrate to the batch improves brightness.

COPPER OXIDE SUPPLIERS

ALFA AESAR, A JOHNSON MATTHEY COMPANY
30 Bond St.
Ward Hill, MA 01835-8099 U.S.A.
(800) 343-0660 Fax: (800) 322-4757
Email: info@alfa.com
Website: www.alfa.com

AMERICAN CHEMET CORP.
400 Lake Cook Rd., Box 437
Deerfield, IL 60015 U.S.A.
(847) 948-0800 Fax: (847) 948-0811
Email: rklattII@aol.com
Website:www.chemet.com

CORDIERITE. $2MgO\text{-}2Al_2O_3\text{-}5SiO_2$. Sp. gr. 2.6–2.7; hardness 7.0–7.5 Mohs. There are no known large deposits of natural cordierite, and it probably is never available for introduction in ceramic bodies. A body having the theoretical composition of

cordierite may consist of 39.6% talc, 47.0% clay and 13.4% alumina. Bodies of this composition, however, have so short a vitrification range that they cannot be fired in industrial kilns. The addition of 20–30% zirconium silicate to a body of cordierite composition increases the firing range. The thermal shock properties of such bodies are excellent, even though they contain no more than 60% cordierite crystals (the balance being chiefly zirconium silicate). A wider vitrification range also has been obtained by recalcining flux ingredients, which consist chiefly of alkaline earth oxides. The dielectric losses of cordierite bodies are low, making them very suitable for high-frequency insulators. Cordierite bodies are quite difficult to glaze because of their low thermal expansion coefficient, which is hard to match in a glaze.

Commercial, electronic ceramic-type cordierites range in color from off-white to light brown. Cordierite crystals can be developed in certain bodies; for example, about 30% talc in a kaolin body produces cordierite as the chief crystalline compound in the fired piece.

The spalling resistance of ordinary stoneware bodies may be improved by adding magnesium oxide to promote the formation of cordierite. Cordierite porcelain is pure white and somewhat translucent, while bodies darker in color and opaque are considered stoneware. Care must be taken to assure firing at a high enough temperature to bring the reactions to completion, otherwise cristobalite will be retained in the body, preventing attainment of the desired low expansion characteristic. Instead of using talc, it also is possible to make cordierite bodies by firing magnesite with clay and quartz.

Cordierite setters have been used in the firing of vitreous china dinnerware. The process appears successful but modifications were needed to overcome some warpage which appeared after five or six burns, up to cone 6.

Cordierite-type compositions have been used for insulation in motors, radar and other mechanisms which operate at high temperatures. Another application is as a high-temperature flux for bonding large grains of aluminum oxide. Uses being studied include thermal barriers and abradable seals in gas turbine engines.

Cordierite also is available as a fused synthetic product.

CORDIERITE SUPPLIERS

MASON COLOR WORKS, INC.
250 E. Second St., Box 76
East Liverpool, OH 43920 U.S.A.
(330) 385-4400 Fax: (330) 385-4488
Email: mcwinc@valunet.com
Website: www.ceramics.com/mason

R. T. VANDERBILT, CO. INC.
P.O. Box 5150
Norwalk, CT 06856-5150 U.S.A.
(203) 853-1400 Fax: (203) 853-1452
Email: rjohnson@rtvanderbilt.com
Website: www.rtvanderbilt.com

CRYOLITE. (Sodium fluoaluminate, sodium-aluminum fluoride.) Na_3AlF_6. Mol. wt. 210; m.p. 1000°C; density (room temperature) 2.95–3.00 g/cm^3; density of liquid at melting point 2.1 g/cm^3; hardness 2.5 Mohs; CTE 2.2×10^{-7}/°C (glass) and 2.5×10^{-7}/°C (enamels); water solubility (room temperature) 0.4 g/L. Other properties: index of refraction 1.34; heat of fusion 76 cal/g; transition point 565°C; composition 32.9% Na, 12.8% Al, 54.3% F; weight factors $Na_3AlF_6 = 1.00$ or $Na_2O = 0.4429$, $Al_2O_3 = 0.2429$, $F = 0.5435$. Crystal is monoclinic at room temperature and changes to isometric, or possibly cubic, at elevated temperatures.

Natural cryolite, which occurs in the monoclinic form, is comparatively rare. The only commercial deposit is located at Ivigtut, Greenland, where it constitutes a large bed in a granite vein in a gray gneiss. Small amounts of cryolite are found at Pike's Peak, Colorado, and near Miask (Ilmen Mountains) in the former USSR. Pure cryolite is colorless and translucent.

Refined natural cryolite is known to the ceramic industry as Kryolith, a white, finely divided powder. A typical analysis: 99.4% Na_3AlF_6, 0.3% other fluorides (mostly CaF_2), 0.2 SiO_2, 0.07% Fe (as Fe_2O_3), 0.026% H_2O.

Important amounts of cryolite are used in the ceramic industry, the greatest consumption occurring in the manufacture of opal glass and enamels. Less widely known is cryolite's extensive use as a filler for abrasive wheels, especially the resin- and rubber-bonded types. Another application is in flux coatings for welding rods, particularly those used to join aluminum.

Cryolite has two main functions as a constituent of enamel and opal glass batches. It is a powerful flux because it has a relatively low melting point, is an excellent solvent for (or reacts strongly with) such oxides as SiO_2, Al_2O_3 and CaO, and it forms low-melting eutectics with various compounds. Opacification is cryolite's second function. It is a primary opacifier for opal glass and a secondary opacifier for enamels.

Although there has been some disagreement concerning the identity of the crystalline or opacifying phase, glasses or enamels made from cryolite-containing batches contain NaF as a crystalline phase, or, if appreciable amounts of calcium are present, both NaF and CaF. Some crystalline form of silica also may be present. Cryolite is considered to be the most stable form of fluoride addition to glass and enamel batches, probably because of its aluminum content.

Most of the cryolite used in enamels goes into white cover-coat formulations, where it generally constitutes 5–15 wt% of the batch. However, use of cryolite is not as prevalent now that titanium enamels have replaced zircon enamels as the volume frits. Cryolite has also been used in boron- and lead-free enamels; much work on which was done in Germany in response to shortages of boron- and lead-containing materials. The cryolite contents of the B- and Pb-free enamel batches ranged from 2–13 wt%. Some jewelry enamel and ground-coat formulations also include cryolite.

Cryolite is generally used either alone or with fluorspar in opal glass manufacture. Amounts in the batch vary from 4–13 wt%. In addition to acting as a flux and opacifier, cryolite aids in fining the glass and serves as an easily meltable source of Al_2O_3, which is an extremely important constituent of opal glass.

The amount of cryolite added to opal glasses depends primarily on the other opacifiers present, and may be as high as 30 lb per 100 lb of batch when used alone. Other factors include: (1) type of batch used; (2) whether melting is done in a closed pot, day tank or continuous tank; (3) temperature and type of fire used in melting; (4) whether ware is to be pressed or blown; (5) whether the article is to be thick- or thin-walled; (6) if the glass is to be pressed, whether it is pressed by hand or by machine; and (7) the character and degree of opacity required.

Cryolite is an efficient medium for the introduction of fluorides to glass batches. Being tied up with aluminum, the fluorine in cryolite does not as readily attack tank blocks as do many other fluorine fluxes. Cryolite, due to its high aluminum content, acts potentially in supplying alumina in an easily meltable form.

High-grade illuminating ware generally has a high cryolite content, as this seems to be a good way to control light transmission. In batches where feldspar and fluorspar are used, cryolite is beneficial as it tends to intensify the opal. Cryolite opals do not burn out as easily as do fluorspar opals. Cryolite is said to be one of the best known materials for eliminating bloom often found in highly alkaline glass. It also aids durability and is thought to be the best possible means of adding alumina to the batch without introducing "cords." As with other fluorides, cryolite increases homogeneity and aids in fining.

Cryolite's fluxing power has been used to accelerate the melting of clear glass batches,

in which it also serves as a source of sodium and aluminum. Small amounts of fluorine (about 0.5%) cause a remarkable lowering of the viscosity of glass and aid in the fining operation. Fluorides were reported as fairly common fining agents in European practice with cryolite among the more common fluorine substances used.

Decolorization of glass by fluorine-containing substances is attributed to the formation of iron-fluorine complexes, perhaps FeF_6.

Applications of cryolite to ceramic fields other than enamels or glass, such as an abrasive wheel filler and welding-rod flux constituent, have already been mentioned. Still other uses include: a mineralizer for quartzite, alumina, mullite and (with aluminum chloride) spinel; an auxiliary flux for whiteware bodies; glazes and an ingredient in special glazes for crucibles; an insolubilizer for sodium silicate coatings on roofing granules; and a mineralizer constituent of dental cements. Small amounts of cryolite are used in light bulbs to prevent and retard blackening by tungsten, and in "getter" formulations that remove trace amounts of oxygen from light bulbs.

CRYOLITE SUPPLIERS

WASHINGTON MILLS ELECTRO MINERALS CORP.
P.O. Box 423, 1801 Buffalo Ave.
Niagara Falls, NY 14302 U.S.A.
(716) 278-6600 Fax: (716) 278-6650
Email: sales@washingtonmills.com
Website: www.washingtonmills.com

DIAMOND, INDUSTRIAL. The bulk of industrial or synthetic diamond is made by subjecting hexagonal carbon (graphite) to high pressures (approx. 5 GPa) and high temperatures (approx. 1500°C) with large special-purpose presses. By the simultaneous application of heat and pressure, hexagonal carbon can be transformed into a hard cubic form.

Diamond is chemically inert to inorganic acids, but reacts upon heating with carbide forming elements such as iron, nickel, cobalt, tantalum, tungsten, titanium, vanadium, boron, chromium, zirconium, and hafnium. The thermal conductivity of diamond can be as high as five times that of copper at room temperature. In terms of electrical conductivity, diamond is an electrical insulator. Diamond is the hardest material known, but is also a brittle material, which breaks on impact. The toughness, or its inverse, the friability, can be varied considerably for industrial diamonds. The conversion from graphite to diamond is reversible at elevated temperatures (approx. 750°C in air) and can impose critical limitations on the use and fabrication of bonded diamond tools.

Synthesized diamond is available in the size range from submicron to about one centimeter. Submicron and micron size diamond is used as loose abrasive in pastes and slurries for lapping and polishing applications. Depending on the needs of the application, diamond powders can be provided in several types that differ in aggressiveness or sharpness of cutting points, in shape, and in toughness.

Diamond is by far the hardest and strongest of all abrasives available. As such, it is the superior abrasive of choice for grinding ceramics, glasses, concretes, natural stones, cemented carbides and other nonferrous metals. Critical in the development of an abrasive bond system for a specific area of application is the bondability of the surfaces of the abrasive. Diamonds have relative inert surfaces, and as such are retained in the grinding wheel almost solely by the mechanical strength of the bond system. Relatively weak, resilient resin bonds are used widely to grind technical ceramics. Because of the low-strength bond, even irregularly shaped, friable diamonds are lost from the surface of the wheel after undergoing only sight wear. Wheel life is relatively short. To alleviate this problem, thick metal coatings for friable diamonds were introduced. Significant advantages are, among others, that grinding heat is buffered from the degradable resin and that larger

surface areas increase the bonding strength over the uncoated diamond. These advantages translate into grinding wheel life improvements, which are easily two to three times that of wheels with uncoated diamonds.

DIAMOND, INDUSTRIAL SUPPLIERS

GE SUPERABRASIVES
6325 Huntley Rd.
Worthington, OH 43085 U.S.A.
(614) 438-2000 Fax: (614) 438-2829
Email: terry.kane@gepex.ge.com
Website: www.ge.com/superabrasives

DIAMOND POWDER COMPOUNDS.

Diamond powders in various micrometer sizes are dispersed in a paste or carrier for finishing ceramic parts. Slurry diamond compounds that are spray-applied also are used for lapping and other finishing applications.

The two major reasons for using diamond are the rapid stock removal and excellent finishes obtained. Diamond also can produce true flatness, and cause far less surface damage than other abrasives. And diamond properly used will keep dissimilar materials, one of which is a ceramic, at the same height. By selecting the proper diamond size and lap, a surface suitable for almost any application can be produced.

Many diamond-finished ceramic parts are used in electronic and aerospace applications. Other diamond-finished ceramic components include seals, thread guides, drawing dies and gyro bearing races. Many of these parts have tolerances down to 0.001 micro-in. Diamond is the only abrasive capable of producing the required tolerance-surface finish combination.

A diamond-finishing operation normally has as many as three steps, with a different grade of diamond used in each. Most stock removal is performed in step 1 and/or 2. The required surface finish is produced in step 2 and/or 3. In the case of seals, where the ceramic component is finished on a ceramic lap, a single grade of diamond will usually do the job.

DIAMOND POWDER COMPOUND SUPPLIERS

G E MICRON PRODUCTS
1111 W. Newport Center Dr.
Deerfield Beach, FL 33442-7732 U.S.A.
(954) 481-1800; (800) 327-8982
Fax: (954) 481-1804
Email: ralph.alea@gepex.com
Website: www.ge.com/micronproducts
UK ABRASIVES, INC.
3045 Mac Arthur Blvd.
Northbrook, IL 60062 U.S.A.
(847) 291-3566 Fax: (847) 291-7670
Email: sales@ukabrasives
Website: www.ukabrasives.com
WARREN DIAMOND POWDER COMPANY
1401 E. Lackawanna St., Box 177
Olyphant, PA 18447-0177 U.S.A.
(570) 383-3261 Fax: (570) 383-3218
Email: info@warrendiamond.com
Website: www.warrendiamond.com

DIATOMACEOUS EARTH.

(Diatomaceous silica, diatomite, Kieselguhr.) A highly siliceous mineral derived from skeletons of diatoms (microscopic organisms). Density 0.8–1.2 g/cm^3; fusion point 1715°C. The material's closed cells and high porosity provide a low density and low thermal conductivity. Diatomaceous earth is mined in California, Nevada and Arizona. A typical analysis: 85.3% silica, 5.4% alumina, 1.1% Fe_2O_3, 1.1% calcium carbonate, 5.6% moisture.

Three insulating brick products are made from this material:

1. Brick cut directly from the diatomaceous earth deposit can be used at temperatures up to 1500°F without shrinking.

2. For higher temperature use, brick cut from the deposit are prefired at 1500–1950°F, which causes them to shrink.

3. Brick made by dust pressing and firing at 2500°F. This product is called tridymite brick. However, firing at temperatures above 1950°F leads to spalling caused by the formation of cristobalite. To avoid this

objectionable form of SiO_2, 1–3% lime as a catalytic agent, plus grog, spar and clay, are added to the batch.

DOLOMITE. $CaMg(CO_3)_2$. Sp. gr. 2.9; hardness Mohs 3.5–4.0. A rock intermediate in composition between limestone ($CaCO_3$) and magnesite ($MgCO_3$). True dolomite is composed of 54% $CaCO_3$ and 46% $MgCO_3$. Other materials containing appreciable amounts of magnesium carbonate, but less than the 46% found in true dolomite, are commonly called dolomitic limestones, and also are used in the ceramic industry.

In the raw state, dolomite may be white, light buff, pink, yellow to brown and gray to blue. Its physical structure may be either crystalline or amorphous. Fired material is white. At about 1650°F, all CO_2 is expelled and the material burns to dolomite lime (CaOMgO). In the presence of lower melting fluxes of acid character, dolomite frequently decomposes at even lower temperatures.

Commercial deposits of dolomite are found in many regions of the planet. The most important U.S. deposits of dolomite and dolomitic limestone are located in northwestern Ohio, New York, Connecticut, California, northwestern Pennsylvania, Missouri, Texas and Kansas. Important offshore deposits are found in England and Germany. The compositions shown in the table are typical.

Typical Dolomite Compositions, %*

	A1	A2	B	C	D
CaO	31.60	30.60	30.57	31.15	30.48
MgO	20.60	21.52	19.42	20.57	21.77
Al_2O_3	0.08	0.28	0.20	0.15	0.02
Fe_2O_3	0.12	Trace	0.10	0.16	0.04
SiO_2	0.50	—	—	—	0.30
LOI	47.10	47.70	45.11	47.08	47.54

*Key: A, from California; B, Connecticut; C, England; D, northwestern Ohlo.

The manufacture of dolomitic quicklime includes selection and sizing of raw material, burning or calcination to drive off the carbon dioxide, inspection of the kiln product, size gradation and removal of impurities. Vertical kilns are designed to provide several distinct steps in the burning process. The first is preheating of kiln feed, in which the cold stone is gradually brought up to calcination temperature (~1900°F) by contact with the hot gasses from the burning zone. Product is then held in the burning zone long enough for most or all of the CO_2 to be driven off. (Recovery of the carbon dioxide has been tried but with little commercial success.)

In another manufacturing process, preparation of rotary kiln feed includes a heavy-media separation step to remove most siliceous impurities.

Rotary kilns are commonly used to produce granular sintered dolomite (dead-burned dolomite) at temperatures >1700°C. This dense product is pressed into brick which are used to line steelmaking vessels and cement kilns.

The rotary kiln has become extremely important in lime processing, and is used to burn a large portion of dolomitic quicklime production. More than half of all industrial quicklime is made in rotary kilns. The rotary is particularly useful for making the "hard burned" grade of quicklime that must contain a minimum amount of unburned limestone.

Dolomitic quicklime is the form of dolomite used by many **glass** plants. Dolomitic hydrate is made from the quicklime by adding ~20% H_2O. It furnishes H_2O at 600–700°F, boosting melting speed. However, little dolomitic hydrate is used in ceramics.

The raw material is dry-milled and air-floated to uniform fineness for **pottery** applications, although a granulated form is more commonly used in the glass trade. The pottery grade is specified 100% through 100 mesh, 99.9% through 200 mesh and 99.1% min through 325 mesh. Glass plants prefer a quicklime that is 100% through 10 mesh and substantially all on 100 mesh.

Davidson, Hodkin and Turner examined a series of soda-magnesia trisilicate glasses and found that small amounts of magnesia tend to produce glasses with a rapid melting

rate. Large quantities of magnesia, however, result in a glass that's hard to melt. Also, high-magnesia glasses have a viscosity much greater than that of corresponding lime glasses, and they exhibit tendencies to stringiness and cordiness not found in lime-containing glasses.

When magnesia replaces lime molecularly in a soda-lime glass, meltability and workability initially improve. Thus, a glass containing 9.26% calcium oxide will have a slower melt rate and be harder to work than one with 4.43% CaO and 2.58% MgO (or any intermediate glass). Beyond this point, however, the benefits of further additions of magnesia decrease. When the two oxides are present in equimolecular proportions, as is the case when dolomite is used alone, the glass is not as easy to melt as lime glass and somewhat less workable. This indicates that best results are to be obtained when pure dolomite is substituted for only a part of the lime. However, northwestern Ohio dolomites are not strictly pure but contain lime and magnesia in the desirable 3:2 ratio and, therefore, they are often used as the only source of lime in commercial glass batches. Magnesia also improves the working properties of lime-containing glass and lessens the tendency toward devitrification.

Jones also has noted the advantage of easier melting as magnesia replaces lime up to a certain point in soda-lime-silica glasses. Beyond the relationship of about 2.6% MgO:6.5% CaO, the increased viscosity at high temperatures becomes detrimental. As MgO replaces CaO molecularly, there is a marked decrease in the setting rate near the temperature at which glassware is formed, thus increasing the working range. Annealing also is made easier, as the temperature required for annealing falls to a value lower than that for either a straight "lime" or a straight "magnesia" glass. The addition of MgO also gives a reduction in thermal expansion, and makes the glass more resistant to the corrosive effects of water.

The great majority of glass container manufacturers are using only dolomite, either raw or burned, as the lime source. The ratio 4CaO:6MgO is usually used. The properties of the batch are often modified by the use of small quantities of borax to lower the melting point still further, and alumina, in the form of nepheline syenite or feldspar, is often added to improve permanence. Only in the sheet glass industry is there still a tendency to mix calcite and dolomite as liming sources.

The use of dolomite is beneficial to a glass in that it is said to prevent "soda bloom" and to add luster to the ware. Dolomite has a powerful fluxing action and a glass containing dolomite is said to fine quicker than one using lime from another source. Dolomite tends to increase the modulus of rupture of glass, and it is possible to use dolomite containing as much as 30% $MgCO_3$ in window glasses.

Dolomite has often been criticized because of its relatively high iron oxide content, compared with other commercial glass batch materials. This iron content, however, offers no serious obstacle in colored glasses, and commercial producers have recently made notable strides in reducing the iron oxide content, so that more general use of dolomite in colorless glasses also is indicated. The northwestern Ohio dolomite, being very low in iron, produces, when burned, a lime of unusual whiteness which adds no color to the glass batch. Ohio dolomites commonly average 0.04–0.07% Fe_2O_3 in the raw state, and suppliers of burned dolomite customarily hold iron oxide content to 0.07–0.14%.

In general, dolomite may be substituted for nearly any other type of lime flux in pottery bodies and glazes when other batch constituents are properly compensated. In ceramic bodies it promotes a glassy bond by reacting with feldspar, flint and clay in the range of cone 1–12 to form a lime glass. This property is of particular value in promoting maturing speed, especially under rapid firing schedules. The amount to be used varies with the vitrification desired and firing temperature, but the range of 0.5–8%,

based on dry body weight, covers most vitreous and semivitreous bodies. Frequently a reduction in feldspar, with compensating increase in flint, seems to be possible. When dolomite is used to replace whiting, the safe firing range is widened by 1 or 2 cones. In combination with other fluxes, dolomite is effective as low as cone 03–04 and is in use as an auxiliary in those clays which carry variable amounts of alkaline earths. In such bodies, it acts as a stabilizing flux and tends to widen as well as lower the firing range.

DOLOMITE SUPPLIERS

UNIMIN CORP.
258 Elm St.
New Canaan, CT 06840 U.S.A.
(203) 966-8880; (800) 243-9004
Fax: (203) 972-1378; (800) 243-9005

FELDSPAR. The most common mineral in crystalline rocks. Hardness 6.0–6.5 Mohs. Usually occurs as small grains intimately associated with other minerals, but commercial deposits are obtained from pegmatites. Feldspars form a group of which the principal types are potash spar (orthoclase, microcline), soda spar (albite), lime spar (anorthite), and lime-soda spar (oligoclase, andesine, labradorite and bytownite). They are aluminum silicates of potassium, sodium and calcium.

Feldspars exhibit uneven fracture, and have a vitreous to pearly luster. Colors are generally white, cream and pink, but also milky, clear, buff, brown, red, gray, green and bluish. Property ranges for the major types of feldspar are: sp. gr. 2.56–2.63; m.p. 1110–1532°C; refractive index 1.524–1.584.

None of the minerals in the feldspar group is found pure. Potash feldspars always contain some albite (soda spar) and soda feldspars always contain some anorthite (lime spar). Feldspar is found in practically all igneous rocks throughout the United States and Canada. Chief commercial sources are in North Carolina, South Dakota and Georgia. European deposits are located in Norway, Sweden, Finland, France, Italy and the former USSR. Other foreign sources include Brazil, Mexico, South Africa and India. Cornwall stone is a feldspathic rock containing feldspar, quartz, and also alumina in excess of the feldspar ratio. It occurs in large deposits at Cornwall, England.

General empirical formulas for the common feldspars used in ceramics are: microcline (K_2O-Al_2O_3-$6SiO_2$), albite (Na_2O-Al_2O_3-$6SiO_2$) and anorthite (CaO-Al_2O_3-$2SiO_2$).

Most commercial feldspars also contain iron oxide (0.04–0.15%) and traces of magnesia. The amount of free quartz varies considerably, with figures for commercial shipments ranging from 0.4–40.0%.

Free quartz acts as a diluent in feldspar and decreases the fluxing power. In unburned ceramic bodies, feldspar acts as an antiplastic the same as sand does. Soda feldspar and quartz mixtures deform much more rapidly after deformation begins than do the potash feldspars or any of their mixtures with quartz. High-soda content in general indicates low deformation temperature. The fusion point of a feldspar depends upon the alkalies present, and becomes lower as soda content increases and potassium oxide content decreases. Some spars fuse as low as cone 4, others as high as cone 10, but the average is cone 8–9.

With the possible exception of clay, feldspar is the most essential ceramic material in the **whiteware** industry. It is the universal flux used in all types of ceramic bodies, and should be ground very fine. The fluxing effect of feldspar may be noted in a whiteware body as low as cone 09. As temperature increases, the feldspar becomes more active, dissolving first the clay substance and finally the flint particles. Above cone 10, mullite begins to crystallize in the glassy matrix formed by the feldspar; at cone 12, it is present in sufficient quantities to improve ware properties. It affects practically all fired body properties, including even translucency, resonance and expansion. In some cases, the

alkalinity introduced by feldspar alters the casting and working properties of pottery slips.

The amounts of feldspar used in common types of pottery bodies are: sanitaryware, 25–35%; hotel china, 15–35%; chemical porcelain, 15–30%; electrical porcelain, 30–50%; whiteware, 15–30%; floor and wall tile, 10–55%.

The softening range of the body decreases, and refractoriness increases with increased K_2O, at the expense of NaO and CaO, in the feldspar used. With semivitreous bodies which do not contain any CaO, soda feldspar compositions mature slightly sooner than potash feldspar. When lime is added the situation is reversed. The reason: lime causes a sharp increase in the fusibility of potash feldspar but not of soda spar. The glassy content of the body produced with soda feldspar is less viscous than that produced by potash spar, and thus the soda spar bodies deform more readily.

Unfortunately, there is no pronounced eutectic in the flint-feldspar system. However, approximately 20% quartz can be added to a pure potash feldspar and 10% to a pure soda spar without materially raising the melting points. Feldspars of different potash-soda ratios are sometimes interchangeably reduced. The development of leucite crystals in melting, which accounts for the high viscosity of molten feldspar, depends upon the amount of potash spar present. Translucency is best with potash spar bodies; thermal expansion is highest for bodies with high soda spar content.

Ware containing soda feldspar is generally weaker (in terms of modulus of rupture) than that containing potash. High soda feldspar bodies soften at temperatures about 45°C lower than similar potash bodies.

The role of feldspar in **glazes** is similar to that in bodies. It again is used for its fluxing action and should be ground very finely, preferably to 200 mesh, for more uniform and thorough reaction with other ingredients. Both potash and soda feldspars are used in glazes. The potash spar is desirable because it dissolves the silica more readily and makes a more durable glaze.

Feldspar has been used in opal and alabaster **glass** for many years, but also has become widely adopted by the entire industry as an economical and dependable source of alumina. Glass spar is used in a coarse granular state, usually in the neighborhood of 20 mesh. Important chemical considerations are the alumina and iron oxide contents and the ratio between the soda and potash contents. Alumina is very beneficial to glass and is the main reason for the use of feldspar. Feldspar also is a source of alkalies and reduces the quantity of soda ash required in the batch. Iron oxide, of course, enters as an impurity and discolors the glass, so it must be held to a minimum. Glassmakers usually specify a maximum iron oxide content of 0.08% when buying feldspar.

The effects of feldspar on commercial glass batches may be summarized as: increased resistance to scratching, increased resistance to breaking due to both bending and impact, improved thermal endurance, increased chemical durability, and decreased tendency to devitrify. In view of these benefits, it is advisable to add an amount of feldspar which will leave from 1–3% alumina in the resultant glass, with 2% the approximate optimum. Some glass container manufacturers, however, are making milk and beer bottles with as much as 7–8% alumina.

The effect of feldspar on the workability of glass is very similar to that of lime, although the addition of feldspar to a lime-soda glass increases the viscosity range without lowering resistance of the glass to acids, alkalies and weathering. Glass containing feldspar is especially well adapted to pressing because its skin sets quickly, thus keeping plungers from registering deeply on the ware. Feldspar does not increase the annealing temperature, but it helps improve appearance of the ware by adding brilliance. (See ALUMINA.)

Feldspar is of great importance in **porcelain enamels** and constitutes from 25–50% of most batches. It is the principal means of

introducing alumina into the batch; it adds potassium at a lower price than is possible with any other material; and it brings in silica in a form that is readily fusible. Alumina is particularly desirable in P/E batches because it has relatively high expansion, allowing good fit to the base metal. Feldspars used in enamel must become white upon burning and can contain only a very small amount of iron oxide.

Excessive amounts of feldspar may produce a tendency to craze. Too high a content also may lower gloss and unduly increase refractoriness. Feldspar increases an enamel's viscosity at any given temperature as well as its resistance to chemical action.

The ease with which feldspar enters into solution during smelting depends upon its fineness; 120–140 mesh material is common in the enamel industry. Potash spar almost always is used. Soda spars frequently cause fishscaling in enamels that are entirely satisfactory when made with potash. Such impurities as garnet, hornblende, tourmaline and biotite mica cannot be tolerated. They maintain their identity throughout smelting, rise to the surface of the milled enamel and appear as black or brown specks in the finished product. Muscovite mica, a potassium-aluminum silicate, on the other hand, readily enters into solution and, therefore, is not particularly harmful.

FELDSPAR SUPPLIERS

AVALON VENTURES
111 Richmond St. W., Ste. 1116
Toronto, ON Canada M5H 2G4
(416) 364-4938 Fax: (416) 364-5162
Email: info@avalonventures.com
Website: www.avalonventures.com

HAMMILL & GILLESPIE INC.
154 S. Livingston Ave.
Livingston, NJ 07039 U.S.A.
(973) 994-3650 Fax: (973) 994-3847
Email: hamgilinc@aol.com
Website: www.hamgil.com

KALEMADEN ENDUSTRIYEL HAMMADDELER SAN. VE TIC. A.S., HEADQUARTERS
Semedeli Koyu, Can
Canakkale Turkey
(90 286) 4341330 Fax: (90 286) 4371340
Email: can@kalemaden.com.tr
Website: www.kalemaden.com.tr

KALEMADEN ENDUSTRIYEL HAMMADDELER SAN. VE TIC. A.S., EXPORT & MARKETING MANAGEMENT
Eski Uskudar Yolu, Bodur Is Merkezi, No. 8, Kat 6
Daire: 23-24, Icerenkoy, Istanbul
Turkey
(90 216) 3844999; (90 216) 3844748 Fax: (90 216) 3725548
Email: ist@kalemaden.com.tr

KENTUCKY-TENNESSEE CLAY COMPANY, AND K-T FELDSPAR CORPORATION
1441 Donelson Pike
Nashville, TN 37217 U.S.A.
(615) 365-0852 Fax: (615) 365-0842
Email: mdonovan@k-tclay.com
Website: www.k-tclay.com

NORTH CAPE MINERALS AS
P.O. Box 45
Rud N-1309 Norway
011-47 67 15 2200 Fax: 011-47 67 15 2201

PACER CORP.
P.O. Box 912
Custer, SD 57730 U.S.A.
(800) 568-2492 Fax: (605) 673-4459
Email: pacer@rapidnet.com
Website: www.ceramics.com/pacer

UNIMIN CORP.
258 Elm St.
New Canaan, CT 06840 U.S.A.
(203) 966-8880; (800) 243-9004
Fax: (203) 972-1378; (800) 243-9005

ZEMEX INDUSTRIAL MINERALS, INC.
(FELDSPAR CORP.)
1040 Crown Pointe Pkwy., Ste. 270
Atlanta, GA 30338 U.S.A.

(770) 392–8660 Fax: (770) 392–8670
Email: minerals@zemex.com
Website: www.zemex.com/minerals

FORSTERITE. $2MgO\text{-}SiO_2$. Synthetic-fused material typically containing 56% magnesia and 43% silica. Higher purity, fine-particle-size material used extensively in electronic ceramic formulations and ceramic-metal seals because its high CTE matches that of some metals. Higher purity materials require higher maturing temperatures.

FORSTERITE SUPPLIERS

MASON COLOR WORKS, INC.
250 E. Second St., Box 76
East Liverpool, OH 43920 U.S.A.
(330) 385-4400 Fax: (330) 385-4488
Email: mcwinc@valunet.com
Website: www.ceramics.com/mason

FRIT. Mixture of inorganic substances fused together in a furnace and quenched rapidly by either a water bath or water-cooled metal rolls.

Frit is a complex combination of oxides. Its purpose is to render solubles and hazardous components insoluble by combining them with silica and other oxides.

The fritting is done either on a continuous basis by introducing raw batch into a properly heated furnace or on a batch basis in crucibles or a rotary furnace. Frit then is used in combination with clay and possibly other suspending agents to produce a coating material for whiteware, which is applied, dried and fired to produce the glassy deposit called a glaze.

Frit also is used with clay and electrolytes for coating steel, aluminum, cast iron and other metals. This coating—called porcelain enamel—is used on major household appliances, sanitaryware, cast iron and aluminum cookware and architectural panels.

The coating may be applied by wet spraying or dipping. Frit is wet milled with clay and electrolytes. Drying and firing follow application. Dry application of powdered frit to pretreated metal by electrostatic spraying also is possible. Frit is milled with organic components. The drying step is eliminated.

Use of frit is not only beneficial from the standpoint of stabilizing hazardous materials and controlling solubles, but it also helps develop a more uniform coating that generally fires at lower temperatures, all of which results in increased surface and color uniformity and better process control.

Frit also may be used as a component for bonding grinding wheels, as a body flux to lower vitrification temperatures and as a flux for glass-decorating enamels. Frit can be used as a mold lubricant in continuous casting of steel, as a lubricant for metal extrusion, and as coatings for jet engine parts, rocket components, auto exhaust systems and solar heating panels. High-temperature paints and stabilizers for nuclear waste are other applications.

FRIT SUPPLIERS

CERDEC CORP., CONSTRUCTION CERAMICS
West Wylie Ave., P.O. Box 519
Washington, PA 15301 U.S.A.
(724) 223-5900 Fax: (724) 228-3170
Website: www.cerdec.com

FERRO CORPORATION, CERAMIC DIV., NORTH AMERICA
4150 East 56th St., P.O. Box 6550
Cleveland, OH 44101 U.S.A.
(216) 641-8580 Fax: (216) 441-4330
Website: www.ferro.com

FUSION CERAMICS INC.
P.O. Box 127
Carrollton, OH 44615 U.S.A.
(330) 627-2191 Fax: (330) 627-2082

GENERAL COLOR & CHEMICAL CO. INC.
P.O. Box 7, 604 Valley St.
Minerva, OH 44657 U.S.A.
(330) 868-4161 Fax: (330) 868-5880
Email: info@generalcolor.com
Website: www.generalcolor.com

JOHNSON MATTHEY CERAMICS INC., JOHNSON MATTHEY COLORS & COATINGS DIVISION

498 Acorn Ln.
Downingtown, PA 19335 U.S.A.
(610) 873-3200 Fax: (610) 873-3255
Website: www.cmd.matthey.com
PEMCO CORP.
5601 Eastern Ave.
Baltimore, MD 21224
(410) 633-9550 Fax: (410) 631-4354
Email: pat.pawlicki@us.pemco-intl.com

GLASS ENAMEL. (Vitrifiable glass colors.) Fine-powder mixtures of low melting flux and calcined ceramic pigment, usually produced in a 9:1 flux: pigment ratio. The enamels may be mixed with suitable vehicles, applied to glass articles and fired to a smooth, hard enamel coating at temperatures below the deformation point of the ware. A glass enamel must have an expansion coefficient closely matching that of the base glass; a low enough fusion point to permit development of a good glass at a permissible temperature; and a sufficient degree of chemical resistance to materials to which the article may be exposed. The preparation of glass enamels has become a highly complex art.

Enamels are compounded for maximum acid, alkali and detergent resistance. Firing temperatures range from 1000-1250°F. Colors and transparent colors in satin etch, matte and full gloss finishes are available. Special enamels are offered for use on Pyrex and low-coefficient glass. Applications for glass enamels include: containers, dinnerware, drinking ware, lighting goods, building exterior and interior panels, chalk boards and signs.

GLASS ENAMEL SUPPLIERS

GENERAL COLOR & CHEMICAL CO. INC.
P.O. Box 7, 604 Valley St.
Minerva, OH 44657 U.S.A.
(330) 868-4161 Fax: (330) 868-5880
Email: info@generalcolor.com
Website: www.generalcolor.com
JOHNSON MATTHEY CERAMICS INC., JOHNSON MATTHEY COLORS & COATINGS DIVISION
498 Acorn Ln.
Downingtown, PA 19335 U.S.A.
(610) 873-3200 Fax: (610) 873-3255
Website: www.cmd.matthey.com

GRAPHITE. (Carbon.) C. A natural and synthetic mineral. Graphite sublimes at 3500°C and 1 atm.; m.p. ~3700°C and 816 atm. Graphite will begin to oxidize at temperatures as low as 335°C, and oxidizes readily above 800°C. Ceramic coatings have been developed to reduce this oxidation characteristic.

Natural graphite is widely distributed throughout the world with the best sources being Ceylon, the People's Republic of China, Brazil, Canada, Germany, Madagascar, Mexico and Korea. Graphites have a sp. gr. of 2.1–2.5 as mined, but purified material is close to the theoretical value of 2.26. Ideally, graphite should behave as a metalloid in two directions and a ceramic in the third. Thus, for flake graphite or other polycrystalline graphites in which crystals are well oriented, the thermal and electrical conductivities are high in two directions and low in the other. However, such material as Ceylon chunk graphite consists of disordered crystals and has nearly isotropic properties.

Natural graphites are unctuous and soft (hardness 0.5–1.5 Mohs), burn slowly, are chemically inert and have a sublimation temperature >3500°C. Graphite has excellent weathering properties, is hydrophobic, and tends to form water in oil-type emulsions. It is used in clay-bonded refractories and may be glazed to prevent oxidation.

Synthetic graphite can be made in large pieces with properties which can be varied over wide ranges. Sp. gr. varies from 1.2–2.0 for normal commercial graphites and from 1.2–2.26 for pyrolytic graphites.

Thermal conductivity for normal commercial graphite at room temperature is about 0.3 cal/(cm·s·C). For pyrolytic graphites, the values in two directions can vary over the 5.0–0.5 cal/(cms·C) range, and in the third, from 0.004–0.008 cal/(cm·s·C).

Electrical resistivity for commercial graphite is 700 μOhm-cm at room temperature. In the high-conductivity directions, the resistivity of pyrolytic graphite can be varied from 60–4000 μOhm-cm; in the high-resistance direction, from 0.6–0.1 Ohm-cm.

The tensile strength of commercial graphite increases with temperature from ~1700 psi at room temperature to 3400 psi at 2450°C. Pyrolytic graphite has an ultimate tensile strength in the strong orientations of 20,000 psi at room temperature and 60,000 psi at 2750°C. In the weak orientation, strength is 1500 psi from room temperature to 1000°C.

Graphite, which is found in the mineral form, is said to be "nature's best refractory." Desirable properties of graphite **refractories** include high thermal conductivity, high electrical conductivity, low thermal expansion, high resistance to molten metal and flux attack, excellent heat shock resistance, increased strength at high temperatures, resistance to wetting by molten substances and high refractoriness.

All types of mineral graphite are used in refractories. Madagascar flake, for example, is used almost exclusively in crucibles. Mexican, Ceylon and flake dusts are used for the foundry facings that prevent mold sand from adhering to metal castings. Other graphite-containing refractories include stopper heads and nozzles, retorts, tubes, rods and stirrers, brick, slabs and special shapes, refractory cements, and plastic linings for ladles, runners, etc.

Mineral graphite of the microcrystalline type, often referred to as amorphous graphite, is found in most of the ramming mixes used by the steel industry. Graphite is mixed with fireclay to produce plastic patch material, unburned brick and mortar. It also is used with high-alumina clay for plastic material and unburned high-alumina brick. The amount of graphite used in various refractories varies from 10–60%, except in foundry facings where pure graphite may be used.

Graphite also is used to moderate high-velocity neutrons in nuclear energy applications. It boasts a low neutron-capture cross section.

Manufactured forms of graphite, referred to as synthetic graphite, resist attack by all materials except oxidants. It is unreactive with many metals (zinc, aluminum, magnesium, copper and their alloys) and metal-producing slags at their melting points.

A special form of synthetic graphite, pyrolytic graphite is unusually nonreactive and can be made into long-lasting crucibles for molten silicon and many of the more reactive elements. Average threshold oxidation temperatures for most commercial graphites are 400°C in air, 700°C in steam and 900°C in CO_2. Corresponding values for pyrolytic graphite are ~200°C higher.

Graphite is well known for its lubricity, and is an important ingredient in most lubricants for glass molds, particularly for the blank molds used in container manufacturing.

Because of its outstanding high-temperature strength, graphite is often chosen for molds used in hot pressing of advanced ceramics.

It is also outstanding for the ultrahigh temperatures encountered in guided missiles and electric arc furnaces.

GRAPHITE SUPPLIERS

ASBURY GRAPHITE MILLS INC.
405 Old Main St.
Asbury, NJ 08802 U.S.A.
(908) 537-2155 Fax: (908) 537-2908
Email: ntmares@asbury.com
Website: www.asbury.com

GRAPHITE DIE MOLD, INC.
18 Airline Park
Durham, CT 06422-1000 U.S.A.
(860) 349-4444 Fax: (860) 349-0136
Email: sales@graphitediemold.com
Website: www.graphitediemold.com

NANSHU GRAPHITE CORP., TZ
PLANT (ISO-9002) NANSHU
PLANT (ISO-9002)
301 Bridge Plaza N.
Fort Lee, NJ 07024 U.S.A.
(201) 947-6228 Fax: (201) 585-0698
Email: ligraphite@aol.com

POCO GRAPHITE INC.
1601 S. State St.
Decatur, TX 76234 U.S.A.
(940) 627-2121; (877) 762-6747 (US)
Fax: (940) 393-8366
Email: sales@poco.com
Website: www.poco.com
STRATMIN GRAPHITE INC., HEAD OFFICE
630 Rene-Leveque Blvd. W., Ste. 2660
Montreal, PQ Canada H3B 1S6
(514) 866-8467 Fax: (514) 866-8725
Email: info@stratmin.com
Website: www.stratmin.com
SUPERIOR GRAPHITE CO.
10 S. Riverside Plaza, Ste. 1600
Chicago, IL 60606 U.S.A.
(312) 559-2999 Fax: (312) 559-9064
Website: www.graphitesgc.com
TIMCAL AMERICA INC.
29299 Clemens Rd. 1-L
Westlake, OH 44145 U.S.A.
(440) 871-7504 Fax: (440) 871-6026
Email: westlake@us.timcal.com
Website: www.timcalamerica.com

GRAPHITE, STRUCTURAL. Plates and shapes fabricated from laminated graphite cloth. Sp. gr. 1.2–1.8. Structural sections can be tailored to achieve required tensile and flexural properties in specific orientations.

GRAPHITE FIBERS AND FABRICS. Tensile strengths exceed 15,000 psi. On a 26×26 square-weave cloth, tensile strength is 10–20 lbf/in., with an electrical resistance of 0.5 Ohm/in^2.

INDIUM OXIDE. $In2O_3$. Mol. wt. 277.64; sp. gr. 7.179; m.p. 1910°C. An n-type semiconductor finding use as a resistive element in integrated circuits. Resistivity values from 100 ohm/sq to megohms per square can be tailored. The screen printed mix consists of high-purity indium oxide, dopants and borosilicate glass flux. Firing temperature: 900–1000°C. Temperature coefficients of resistivity of such systems have been measured at <500 ppm/C from room temperature to 100°C.

INDIUM OXIDE SUPPLIERS

ALFA AESAR, A JOHNSON MATTHEY COMPANY
30 Bond St.
Ward Hill, MA 01835-8099 U.S.A.
(800) 343-0660 Fax: (800) 322-4757
Email: info@alfa.com
Website: www.alfa.com
ARCONIUM
50 Sims Ave.
Providence, RI 02909 U.S.A.
(401) 456-0800; (800) 343-0282
Fax: (401) 421-2419
Website: www.arconium.com
GFI ADVANCED TECHNOLOGIES INC.
379 Winthrop Rd.
Teaneck, NJ 07666 U.S.A.
(201) 833-8530 Fax: (201) 833-9156
Email: gfiadvtech@attmail.com
INDIUM CORPORATION OF AMERICA
34 Robinson Rd.
Clinton, NY 13323 U.S.A.
(315) 853-4900; (800) 446-3486
Fax: (315) 853-1000;
(800) 221-5759
Email: askus@indium.com
Website: www.indium.com

INTERMETALLIC COMPOUNDS. Includes the borides, hydrides, nitrides, silicides and aluminides of the transition metal elements of Groups V and VI in the periodic table, combined with semimetallic elements of small diameter. More than 1000 possible compounds fit this definition, with approximately 200 of them having melting points above 1500°C.

Methods of preparation for silicides and aluminides are very similar to those used for carbides, nitrides and borides: (1) synthesis by fusion or sintering, (2) reduction of the metal oxide by silicon or aluminum, (3) reaction of the metal oxide with SiO_2 and carbon, (4) reaction of the metal with silicon halide or (5) fused salt electrolysis. The simplest preparation method consists of

mixing the metal powders in proper ratio, and then heating the mixture in vacuum or inert atmosphere to the temperature where reaction begins. At that point, the exothermic reaction furnishes the heat needed to drive it to completion.

The best forming methods are hot pressing and vacuum sintering. Some intermetallic compounds—ZrB_4 with $MoSi_2$, Mo_2NiB_2, Mo_2CoB, for example—are as hard as tungsten carbide. Borides of zirconium or titanium added in small amounts to Al_2O_3, BeO, ZrO_2 or ThO_2 improve their resistance to heat checking. Nitrides of aluminum, titanium, silicon and boron are used as refractory materials.

Fibers and whiskers of intermetallic materials also are being considered for strength-enhancing fillers in metal- and ceramic-matrix composites.

KAOLIN. (China clay.) Al_2O_3-$2SiO_2$-$2H_2O$). The terms *kaolin* and *china clay* are used interchangeably to describe a type of clay which fires to a white color and has a PCE of 34–35.

The name kaolin comes from the two Chinese words kao-ling, meaning high ridge, and was originally a local term used to describe the region from which the clay was obtained. The term kaolin was originally used in the United States to refer to certain residual clays of a white- or nearly white-burning character. In recent years, however, it has been stretched to cover certain white sedimentary clays like those obtained in South Carolina and Georgia. The present terminology differentiates between the two types of deposits by designating as primary or residual kaolins those white-burning clays formed by the weathering, in place, of feldspathic rocks, pegmatite dikes, granites, and the like, and found in the location of the parent rock. Secondary or sedimentary kaolins are those that were formed by weathering, then carried by water and redeposited in another area. Thus, the secondary kaolins of South Carolina and Georgia were deposited in lagoons and embayments at or near the old shoreline of the Atlantic in an area later uplifted to form the Atlantic Coastal Plain.

Most of the domestic supply of residual kaolin is obtained from western North Carolina, and most of the sedimentary clay comes from Georgia and South Carolina. The South Carolina kaolins are widely used in the refractory and elastomeric industries. Although some of the South Carolina kaolin deposits have a naturally occurring large particle size which makes them excellent casting clays, most are finer particle sized than the Georgia kaolins and both can be fractionated into casting clays.

Kaolin usually contains less than 2% alkalies and smaller quantities of iron, lime, magnesia and titanium. Because of its purity, kaolin has a high fusion point and is the most refractory of all clays. Lone kaolins are widely used in casting sanitaryware, ceramics and refractories.

Georgia china clay is one of the most uniform kaolins to be found. Generally speaking, there are two types of Georgia-sourced kaolin, both of which are widely used for casting and other processes. One type imparts unusually high strength and plasticity, and is used for both casting and jiggering where a high degree of workability is required. The other type typically is a fractionated, controlled particle size clay that also behaves well in casting, dries uniformly and reduces cracking of ware. Fired color is an important secondary parameter for Georgia kaolin, also due to its low Fe_2O_3 and TiO_2 content.

KAOLIN SUPPLIERS

ALBION KAOLIN COMPANY,
HEPHZIBAH SITE
1 Albion Rd.
Hephzibah, GA 30815
(706) 592-9121 Fax: (706) 592-9824
Email: sales@albionkaolin.com
Website: www.albionkaolin.com

ALBION KAOLIN COMPANY,
MCINTYRE SITE
P.O. Box 595

McIntyre, GA 31054 U.S.A.
(912) 946-8960 Fax: (912) 946-2992
Email: sales@albionkaolin.com
Website: www.albionkaolin.com
DRY BRANCH KAOLIN CO.
Route 1, Box 468-D
Dry Branch, GA 31020 U.S.A.
(912) 750-3500 Fax: (912) 750-3808
ECC INTERNATIONAL INC., CERAMICS & SPECIALTIES
100 Mansell Ct. E., Ste. 300
Roswell, GA 30076 U.S.A.
(770) 645-3411; (800) 843-3222
Fax: (770) 645-3384
Email: ceramics@ecc.com
Website: www.ecci.co.uk
FUSION CERAMICS INC.
P.O. Box 127
Carrollton, OH 44615 U.S.A.
(330) 627-2191 Fax: (330) 627-2082
IONE MINERAL & REFRACTORIES
8631 Hwy. 124
Ione, CA 95640 U.S.A.
(209) 274-2471 Fax: (209) 274-4102
KALEMADEN ENDUSTRIYEL HAMMADDELER SAN. VE TIC. A.S., HEADQUARTERS
Semedeli Koyu, Can
Canakkale Turkey
(90 286) 4341330 Fax: (90 286) 4371340
Email: can@kalemaden.com.tr
Website: www.kalemaden.com.tr
KALEMADEN ENDUSTRIYEL HAMMADDELER SAN. VE TIC. A.S., EXPORT & MARKETING MANAGEMENT
Eski Uskudar Yolu, Bodur Is Merkezi, No. 8, Kat 6
Daire: 23-24, Icerenkoy, Istanbul Turkey
(90 216) 3844999; (90 216) 3844748
Fax: (90 216) 3725548
Email: ist@kalemaden.com.tr
KENTUCKY-TENNESSEE CLAY COMPANY, AND K-T FELDSPAR CORPORATION
1441 Donelson Pike
Nashville, TN 37217 U.S.A.
(615) 365-0852 Fax: (615) 365-0842
Email: mdonovan@k-tclay.com
Website: www.k-tclay.com
R. T. VANDERBILT, CO. INC.
P.O. Box 5150
Norwalk, CT 06856-5150 U.S.A.
(203) 853-1400 Fax: (203) 853-1452
Email: rjohnson@rtvanderbilt.com
Website: www.rtvanderbilt.com
WBB GROUP
Park House, Courtenay Park
Newton Abbot, Devon England, U.K. TQ12 4PS
+44 (0)1626 332345 Fax: +44(0)1626 332344
Email: clay@wbb.co.uk
Website: www.wbb.co.uk
ZEMEX INDUSTRIAL MINERALS, INC., (FELDSPAR CORP.)
1040 Crown Pointe Pkwy., Ste. 270
Atlanta, GA 30338 U.S.A.
(770) 392-8660 Fax: (770) 392-8670
Email: minerals@zemex.com
Website: www.zemex.com/minerals

KYANITE. (Cyanite.) $3Al_2O_3$-$3SiO_2$. This mineral has the same chemical composition as andalusite and sillimanite, but differs in crystal structure and physical properties. Kyanite ore has a specific gravity of 3.5–3.7 and a variable hardness, 4–5 parallel to the long direction of its blades and 6–7 across them.

It is found in India, Africa, Sweden and the Appalachian region of the United States. Deposits in Dillwyn, Va., and Cullen, Va., have been worked for some years and are turning out many thousands of tons annually for use in refractories, ceramics and other associated fields.

The American kyanite has an approximate analysis (in %) of: 54–60 alumina, 37–43 silica, 0.16–1.0 ferric oxide, 1.20 titanium oxide, 0.5 alkalies.

The PCE runs 36–38. At about 2750°F, pure kyanite decomposes into mullite and silica with an accompanying decrease in specific gravity to about 2.9–3.2. The effect

of this volume change on the finished product depends largely on the grain size of the kyanite and upon the physical properties of the bond used. The larger the grain, the greater the expansion.

Kyanite from India is different in character from American kyanite in that its native occurrence is as surface boulders, while domestic kyanite is associated with quartz, from which it must be separated after grinding down to a workable mesh. In consequence, domestic Kyanite is not offered in grain sizes larger than 35 mesh, while Indian material can be calcined in lump form. Large grain sizes make an excellent grog.

Although pure kyanite runs theoretically 63% Al_2O_3, good Indian kyanite will at times show about 62% due to the presence of free corundum in this ore. In general, Indian kyanite shows greater variation in consistency than domestically produced mineral. African kyanite, while resembling the Indian variety in that the ore is fairly pure in its native state, is far more inconsistent in quality, etc.

American kyanite is offered raw and calcined to mullite, in grain sizes −35, −48, −100, −200 and 325 mesh. While the mullite form is quite stable as to volume change under heat, the raw form shows definite and substantial expansion, depending upon grain size and temperature. This property permits the use of raw kyanite as a balance against clay shrinkages in refractory bodies and it is, therefore, widely used in high-performance cements, ramming mixes, gunning mixes, monolithics, specialities and mortars. Domestic kyanite also goes into insulating brick, firebrick, kiln furniture and refractory shapes.

While American kyanite's first inroads into the clay products field took place in super-refractories (owing to its resistance to extreme temperatures), it is now making great headway in ceramic bodies not even subject to heat at all, after their original firing in course of manufacture. This is due to the well-known interlocking property of the crystal which gives much added mechanical strength to all ceramic compositions, even when fired at low heats during manufacture. The result has been a rapidly increasing use of kyanite in sanitary porcelains, wall tile, precision casting molds, brake disks, electrical porcelains and filters.

MAGNESIUM OXIDE. (Periclase.) MgO. Mol. wt. 40.32. Cubic crystals with density of 3.65 g/cm^3; slightly soluble in water and soluble in acids. M.p. 2800°C.

A synthetic mineral produced in electric arc furnaces or by sintering of amorphous powder. Specific gravity of pure crystal is 3.53 and Mohs hardness is 6–6.5.

Made in varying degrees of purity, depending on raw material. Both natural and synthetic magnesites are used with higher purity fused products derived primarily from synthetic material.

Refractory applications consume a large quantity of MgO. Both brick and shapes are fabricated at least partially of sintered grain for use primarily in the metal processing industries.

Heating unit insulation is another major application for periclase. High purity levels have always been important in this industry, but types of impurities are of equal importance. For many years the industry standard was a product made from Indian magnesite (95%). Recently, however, a trend toward higher purity magnesite (99.5%) has been noted. Some seawater magnesite also is used.

Principal advantages of periclase in this application are its thermal conductivity and electrical resistivity at elevated temperatures.

Others include its cubic crystal structure, its crushability during compaction and its relatively low cost compared with other possible materials.

Specialty crucibles and shapes also are fabricated from MgO. These are used in pyrometallurgical and other purifying processes for specialty metals. Both slip casting and pressing techniques are employed to manufacture shapes.

Thermocouple insulation comprises still another outlet for periclase. Since most of

these go into nuclear applications, a high purity product is required. Both grain and preformed bushings are used to load the tubing. Densification is obtained by diameter reduction processes similar to those used in heating element manufacture. MgO is an important glaze constituent. (See **magnesium carbonate**.)

Single crystals of MgO have received attention due to their use in ductile ceramic studies. Extreme purity is required in this area. Periclase windows are also of potential interest in infrared applications due to their transmission characteristics.

MAGNESIUM OXIDE SUPPLIERS

AMERICAN MINERALS, INC.
901 E. Eighth Ave., Ste. #200
King of Prussia, PA 19406 U.S.A.
(610) 337-8030 Fax: (610) 337-8033
Email: dsoderlund@aol.com
Website: www.ceramics.com/american

AMSAT, DIV. OF FLUID ENERGY
P.O. Box 95
East Greenville, PA 18041 U.S.A.
(215) 679-5984; (215) 679-5983
Fax: (215) 679-5985
Email: epipe@fluidenergy.com

EXOLON-ESK CO.
1000 E. Niagara St., P.O. Box 590
Tonawanda, NY 14151-0590 U.S.A.
(716) 693-4550 Fax: (716) 693-0151
Email: info@exolon.com
Website: www.exolon.com

MUSCLE SHOALS MINERALS
4820 Honey Grove Dr.
Antioch, TN 37013 U.S.A.
(256) 370-7102; (615) 385-5367
Fax: (256) 370-7770; (615) 292-7710
Email: lmkrieg@aol.com

PRED MATERIALS
INTERNATIONAL, INC.,
THE LINCOLN BUILDING
60 E. 42nd St., Ste. 1456
New York, NY 10165 U.S.A.
(212) 286-0068 Fax: (212) 286-0072
Email: predmatsp@aol.com
Website: www.predmaterials.com

WASHINGTON MILLS ELECTRO MINERALS CORP.
P.O. Box 423, 1801 Buffalo Ave.
Niagara Falls, NY 14302 U.S.A.
(716) 278-6600 Fax: (716) 278-6650
Email: sales@washingtonmills.com
Website: www.washingtonmills.com

MANGANESE DIOXIDE. MnO_2. Mol. wt. 87; sp. gr. 5. It is converted into Mn_2O_3 at 535°C. Is insoluble in water and HNO_3 and soluble in HCl. It occurs in nature as the blue-black mineral pyrolusite, which is mined in the former USSR, Gabon, Ghana, Morocco, South Africa, India, Brazil, Mexico, and in small quantities in several U.S. states, including Tennessee, Montana and New Mexico.

In **glass**, manganese dioxide is used as a colorant and decolorizer, though the latter use has now been practically abandoned in favor of selenium.

As a coloring oxide in lead potash glasses, manganese produces an amethyst color, while in soda glass a reddish-violet is produced.

Manganese suitable for such purposes should contain at least 85% MnO_2 and not more than 1% iron oxide.

In potash-lime glasses containing manganese, the coloring properties of manganese are more far reaching than in other glass batches. A reported red-violet batch is: 1000 sand, 300 potash, 620 red lead, 26 manganese dioxide, 50 niter.

A smoky flame or organic matter in glass tanks will reduce manganese dioxide to a manganese salt, and as such it will lose its coloring power.

The so-called burning out of manganese, which produces a green glass, may be said to be akin to the changes in valency of the manganese radicals. In a batch containing 40 lb Mn/1000 lb sand, it was found that the manganese content could be cut down to 10 lb by adding an oxidizing agent such as niter.

Manganese is sometimes used in combination with powder blue to form colors; for example, powder blue in glass containing

3–6% cobalt oxide. In a glass batch containing 200 lb sand, 80 lb soda ash and 23 lb burned lime, 32 oz manganese and 1 oz powder blue are said to give a dark red at 1325°C.

In the manufacture of amber glasses, especially the dark red-browns, manganese is used as a coloring agent in conjunction with iron. This, however, is more the practice in Europe, and in this country is only used to a limited extent.

In **whiteware** bodies, manganese oxide (added as dioxide) may act as a mineralizer when added to alumina in some high-temperature electrical porcelain mixes. When spinel is thus formed, a dark red-brown color is imparted to the porcelain.

In the **pottery** industry manganese oxide is used to give red, brown, purple and black colors to bodies and glazes. One of its most important properties is that of stability. It is often used to make a purple- or plum-colored speckled effect in pottery bodies and glazes. Granulated manganese oxide is frequently used to achieve speckled effects in buff-burning brick. Air-floated, it is used as a gray background in brick.

Manganese should never be fritted if it is possible not to do so.

A finer and brighter purple color can be obtained by the use of this oxide without fritting.

In crystal **glass**, it is said that the combination of copper and manganese hydroxide serves to give very beautiful crystalline formations.

Manganese is used in ground-coat **enamels** in combination with cobalt. This combination seems to have a peculiar property of bonding with the iron base—1.5% manganese oxide in a ground-coat batch is said to be sufficient. Too much manganese in an enamel ground coat will make it very brittle and destroy the bonding power.

Manganese dioxide is a strong oxidizing agent and its use in enamels is primarily due to this fact. When used in an enamel batch, it disintegrates during smelting into manganous oxide and oxygen; and the latter, besides helping to fuse the enamel, changes some of the ingredients to the highest possible oxide. Manganese oxide is especially desirable in ground coats which must bear an excessively hot treatment, such as in sign work, and it reduces the possibility of overburning.

Manganese dioxide cannot be used in white enamels in more than minute quantities as it will color the cover coat an amethyst purple. Because of its coloring property, it is used in many colored enamels.

In enamels, the use of manganese oxide with nickel and cobalt oxides will practically eliminate reboiling, according to Clayford and King.

MANGANESE DIOXIDE SUPPLIERS

AMERICAN MINERALS, INC.
901 E. Eighth Ave., Ste. #200
King of Prussia, PA 19406 U.S.A.
(610) 337-8030 Fax: (610) 337-8033
Email: dsoderlund@aol.com
Website: www.ceramics.com/american

THE PRINCE MFG. CO.
P.O. Box 1009
Quincy, IL 62306 U.S.A.
(217) 222-8854 Fax: (217) 222-5098
Email: prince@princemfg.com
Website: www.princemfg.com

METALLIZING. The application of a metallic coating to a ceramic to permit subsequent brazing to a mating part. Various techniques are used, but the basic steps follow the common practices of ceramic decorating—except that materials must be carefully chosen. A description of the process and materials follows:

Metallizing Systems

Metals: Reactivity being desirable, most metal powders are purchased as –325 mesh to ensure a high surface-to-volume ratio. Only the elemental powders will be listed with the assumption that the oxide, or other combining forms, may be alternatively used with possible adjustments in firing conditions.

Copper: May be mixed, as flake, with coarse glass particles which melt and seal to the ceramic preserving the integrity of the flake. This continuous electrical path through

the glass seal is useful in the manufacture of spark plugs. Copper, as the oxide, will bond to a ceramic under precise firing conditions and, when mixed with silver, may be used as a metallizing preparation.

Gold: Frequently combined with reactive glass for uses in the air-fired paste and solder category.

Iron: Reactive material originally combined with tungsten by Pulfrich. Very common additive for sintered powder process.

Manganese: Reactive material combined with molybdenum in early work with sintered powder process at General Electric. Very common additive.

Molybdenum: Most used as basic metal for sintered powder metallizing. Oxidation potential allows control of oxidation state in controlled atmosphere furnace. Coefficient of expansion of the metal and its reaction products favorable.

Palladium: Similar to platinum and sometimes added to platinum-frit mixtures for air firing.

Platinum: Used with reactive glasses in air-fired metallizing.

Silver: Basic metal for many air-fired pastes. Mixed as granular or flake material with a reactive glass; e.g., borosilicate.

Tin: Basis for direct chemical bonding to numerous ceramics and high-temperature metals. Primary work, done by Intrater and Bertoldo, found significant wetting of tin-based pastes and preforms which contained minor additions of transition metals when fired in a CO-containing atmosphere at 800–950°C. Ohmic contact is observed without accompanying diffusion. Tin metallization has been patented by Advanced Technology Inc. under the trade name Intragene™.

Titanium: Basis of the active metals process. May be used as powder or foil prior to braze alloying. Original work by Kelley and Bondley of General Electric. Titanium-bearing brazes will wet and flow over ceramic; in vacuum, almost as well as solder over copper. Frequently applied as the hydride, which dissociates at <800°C, providing nascent hydrogen which tends to scour the surface to be wetted. May be added to sintered powder compositions to promote reaction.

Tungsten: Similar in metallizing properties to molybdenum. Basis of original metallizing work by Pulfrich.

Zirconium: Performs similarly to titanium, but with less activity. Has lower coefficient of expansion. Infrequently used in industry.

Miscellaneous Reactive Powders

Many companies have evolved proprietary sintered powder metallizing systems which may be very complicated. Some of the likely additives to these compositions are: aluminum, barium, boron, cadmium, magnesium, rare earths and silicon. Most of these would be added as an oxide.

Glass Compositions: Most metallizing suppliers purchase glass-bearing metallizing compositions from commercial vendors. The glass compositions are regarded as proprietary and are not generally known. No attempt will be made to categorize the varieties of glass used in the area of air-fired pastes.

Binders: Binders are fugitive materials which are required to increase viscosity and density of the vehicles developed for suspending metal powders during application of the ceramic. They must leave no deleterious residue following the firing operation and must hold the metal *in situ* until the particles become somewhat adherent. Typical binders are represented by: acrylic polymers, commercial binders, nitrocellulose and pyroxyline resins.

Solvents: Are required to dissolve the binder material and usually have a high vapor pressure, so they are effectively lost before firing of the metallizing begins. These materials, with the binders, constitute the vehicle. The best vehicles allow a smooth application with controlled thickness, and dry to a dense abrasion-resistant layer prior to firing. Solvents are selected typically from the following families: acetates, alcohols, commercial solvents, ethers and ketones.

Application Methods

Pastes, when used, are prepared by selecting the metal powders and blending with

additives in a ball mill. Acetone is frequently used as the carrier during the milling operation. Attention is given to the desired degree of particle size reduction. The milled material is removed, dried, pulverized and combined with the chosen binder and solvent. This preparation may be milled further to ensure complete blending. The paste is then ready to be applied to the ceramic.

Many methods of application are in use. They vary depending upon size of the order, configuration of the part, the precision required and operating economy.

Brushing: A paintable slurry is prepared and applied by brush to the desired area of the ceramic. Useful for small lots or unusual configurations.

Decalcomania: Commercial sources offer patterns prepared for transfer to ceramic.

Dipping: Applicable where complete coverage is permissible or where subsequent methods of recovering a pattern are feasible.

Evaporation: Vacuum evaporation of metals offers a readily controllable metal thickness for thin film and other applications not requiring high strength.

Printing: Banding or printing equipment may be successfully used with certain pastes. Limitations result from ink thickness requirements.

Screening: A slurry is forced through a fine-mesh screen by a squeegee. This technique yields excellent patterns on cylindrical or flat surfaces.

Solution Metallizing: A liquid solution of the desired metal is applied to the ceramic, subsequently dissociated and then reduced to provide a metallic coating.

Spraying: Paint-spray techniques are adapted to metallizing. Masking is usually required on the part. High-volume production may be maintained.

Tapes: Metallizing compositions manufactured as a tape of controlled thickness are being offered commercially. The tape may be applied to the ceramic, adhered by solvent action and fired.

Vapor Deposition: Reduction of chemical vapors, e.g. nickel carbonyl, produces a uniform metallic layer on the ceramic. Deposition can be conventional or electrostatic firing.

Air Furnaces: Useful for glass-fritted pastes containing noble metal powders. Firing temperatures vary up to ~1000°C.

Controlled Atmosphere Furnaces: Hydrogen or cracked ammonia atmospheres, with dew point and temperature controls, are typically used to react sintered-powder metallized coatings with ceramic. These furnaces operate at 1300–1700°C.

Vacuum Furnaces: Vacuum of 10^{-4} torr, or less, is required for metallizing and sealing by the active metals method. Vacuum evaporators operating in the 10^{-3}–10^{-10} torr range are presently in use, experimentally, for studies of ultrapure metals deposited for two-dimensional circuitry requirements.

Others: While not yet of full commercial significance, work in plasma-jet technology and electron beam machining should be mentioned. A significant potential is recognized for these new fields.

Electroplating: Following firing, the active metal assembly hardware may be electroplated for ease of installation by user. Air-fired silver may be electroplated to improve solderability. Sintered-powder metallized ceramics must ordinarily be electroplated to allow wetting by solders or brazes. Many methods of electroplating are in use. Barrel plating is more economical than rack plating and is the preferred method. The thickness, purity and type of electroplated metal has a significant effect upon the effective strength of sintered-powder metallizing.

Etching: A chemical process used in conjunction with a masking system to create fine lines.

MICA. Synthetic mica has recently been put into commercial production and is available in various powdered forms in organically bonded paper sheets; in a three-dimensional, hot-pressed, machinable synthetic mica ceramic; and in sheet form of limited area. Synthetic mica has unusually high thermal

stability. For example, a synthetic fluorphlogopite can be safely used at temperatures up to 1800°F, whereas muscovite mica, the most common commercial variety, is limited to temperatures <1100°F.

Of considerable interest to the refractories field is vermiculite, a form of mica that, on rapid heating, expands 16 times accordion-fashion to form a light and inert material suitable for use as a grog in refractories or as an aggregate for the production of lightweight casting refractory concretes.

An investigation now under way promises to produce a flexible synthetic mica with excellent electrical properties, high heat resistance and flexibility at elevated temperatures. (See GLASS-CERAMIC COMPOSITE.)

MICA SUPPLIERS

PACER CORP.
P.O. Box 912
Custer, SD 57730 U.S.A.
(800) 568-2492 Fax: (605) 673-4459
Email: pacer@rapidnet.com
Website: www.ceramics.com/pacer

MICROSPHERES, HOLLOW. Hollow microspheres are derived from the hollow fraction of fly-ash, and sometimes are also refered to as cenospheres. Typical compositions are 27–37 wt% aluninas and are 55–65 wt% silica. Cenospheres are a lightweight aggregate consisting of closed-cell, nonporous spheres. They have an average true density of between 0.6–0.8g/cc. an average bulk density of between 0.35–0.45g/cc and a very low surface area to volume ratio. With an average crush strength of 2000 psi, systems with good strength-to-weight ratios can be achieved. Appliations include insulating refractory brick, lightweight castable products, gunning mixes, and lightweight tumbling media.

MICROSPHERES, HOLLOW SUPPLIERS

TRELLEBORG FILLITE, INC.
1856 Corporate Dr., Ste. 135
Norcross, GA 30093-2925 U.S.A.
(770) 729-8030 Fax: (770) 729-1820

MULLITE. $3Al_2O_3$-$2SiO_2$. M.p. 1810°C; softens at 1650°C. Can be synthesized by calcining Alabama bauxite of correct Al_2O_3:SiO_2 ratio or blending and calcining alumina and kaolin in proper ratio. Pre-compacting of feed materials is required.

Currently being offered in both calcined and fused forms with this analysis (in %): 71.7–76.2 Al_2O_3, 23.0–23.6 SiO_2, 0.11–3.0 TiO_2, 0.13–1.17 Fe_2O_3, 0.04–0.06 CaO, 0.05–0.06 MgO, 0.05–0.44 alkalies. Sp. gr. 3.156

Mullite occurs in nearly all ceramic products containing alumina and silica but, with the exception of refractories, is seldom introduced as such except as calcined kyanite. Mullite is rare in nature, one locality being the Isle of Mull, Scotland, where argillaceous sediments have been fused by igneous intrusion. The compound was formerly thought to be synthetic sillimanite (a name that still persists in some quarters). Mullite is very refractory, breaking up into corundum and liquid silica at 1810°C.

In the manufacture of refractory and porcelain bodies, the desirable mullite is formed from the chemically similar minerals andalusite, kyanite and dumortierite, which decompose into mullite and silica at cone 13, cone 12 and cone 6, respectively. To break up sillimanite in the same way, cone 20 is required. Sintered and electrofused synthetic mullites (including zirconium mullite) are used in kiln furniture and refractories for the glass and steel industries. The theoretical chemical analysis (wt%) of mullite and five typical mullite materials are as follows:

	A	B	C	D	E	F
SiO_2	28.20	31.98	36.37	22.0	37.30	26.60
Al_2O_3	71.60	68.02	62.63	77.0	59.20	69.20
Corundum	—	1.50	1.39	trace	—	—
TiO_2	—	1.77	—	0.05	2.11	2.77
Fe_2O_3	—	—	—	0.12	1.13	1.22
$Na_2O \cdot K_2O$				0.35	0.11	0.12

Mullite bodies show a uniform rate of thermal expansion and are resistant to spalling and deformation under load. Their

strength is due to the interlocking of long, needle-like crystals. Some authorities have stated that to get long crystals there must be present impurities which will promote their growth, but a mullite body with short, interlocking crystals is more stable to load-deformation at high temperatures.

Mullite porcelains are used in spark plugs and laboratory ware.

MULLITE SUPPLIERS

IONE MINERAL & REFRACTORIES
8631 Hwy. 124
Ione, CA 95640 U.S.A.
(209) 274-2471 Fax: (209) 274-4102
JERSEY MINERAL PROCESSING CO., LTD.,
REFRACTORIES AND MINERALS DIV.
RM B-13B, Triumphal Arc Mansion, 66 Nanjing Rd.
Tianjin, 300042, P.R. China
86-22-23133086 Fax: 86-22-23133085
Email: cmptjmax@shell.jtvan.com.cn
KEITH CERAMIC MATERIALS LTD.
Fishers Way, Belvedere
Kent England, U.K. DA17 6BN
44 (020) 8311 82 99 Fax: 44 (020) 8311 82 38
Email: info@kcm.co.uk
Website: www.kcm.co.uk
NABALTEC GMBH, ALUMINA & ALUMINIUM HYDROXIDE
Alustrasse 50–52
D-92409 Schwandorf Germany
49 (0) 9431 53 457 Fax: 49 (0) 9431 61 557
Email: mail@nabaltec.de
Website: www.nabaltec.de
U.S. ELECTROFUSED MINERALS INC., T/A ELFUSA - U.S.A.
6905 A San Tomas Rd., Rt. 100 Business Park
Baltimore, MD 21227
(410) 796-8823 Fax: (410) 796-8826
Email: info@usminerals.com
Website: www.elfusa.com.br
WASHINGTON MILLS ELECTRO MINERALS CORP.
P.O. Box 423, 1801 Buffalo Ave.
Niagara Falls, NY 14302 U.S.A.
(716) 278-6600 Fax: (716) 278-6650
Email: sales@washingtonmills.com
Website: www.washingtonmills.com

NEODYMIUM OXIDE. Nd_2O_3. Mol. wt. 336.5; sp. gr. 7.2. Soluble in acids and very slightly soluble in water.

An oxide of a rare earth element, it occurs in monazite and bastnasite. It is marketed as the oxide or as other salts, such as oxalate, carbonate or chloride salts. Technical grade products contain more or less amounts of praseodymium and some lanthanum and other rare earths.

Neodymium materials are available in purities of 38–99.99%.

Neodymium oxide is used in glass in concentrations of 3–6% to give a beautiful violet color, red-violet in artificial light and blue-violet in daylight. It also is used to suppress the transmission of yellow (sodium) light in technical glasses. On the other hand, in heat-resisting glasses high in boric oxide, neodymium oxide functions better than any other known decolorizer. Neodymium-doped glass finds applications in the manufacture of lasers. Neodymium oxide is used extensively in the multilayer capacitor field to produce NPO capacitors. In combination with barium titanate, it produces a capacitor with no change in coefficient of capacitance over –100–300°F temperature range. It also is perfect for high temperature glazes, having a m.p. of 2270°C, and can be used as both a main component and as a dopant.

NEODYMIUM OXIDE SUPPLIERS

ALFA AESAR, A JOHNSON MATTHEY COMPANY
30 Bond St.
Ward Hill, MA 01835-8099 U.S.A.
(800) 343-0660 Fax: (800) 322-4757
Email: info@alfa.com
Website: www.alfa.com

MELDFORM RARE EARTHS LTD.
York Way
Royston, Herts SG8 5HJ England, U.K.
44 (0) 1763 248915 Fax: 44 (0) 1763 249312
Email: rare.earths@meldform.com
Website: www.meldform.com
PACIFIC INDUSTRIAL DEVELOPMENT CORP.
900 Victors Way, #300
Ann Arbor, MI 48108 U.S.A.
(734) 930-9292 Fax: (734) 930-9293
Email: rareearth@pidc.com
Website: www.pidc.com
PRIMET CORPORATION
1450 E. American Ln., Ste. 1860
Schaumburg, IL 60173 U.S.A.
(847) 517-8620 Fax: (847) 517-8625
Email: rareearth@primetcorp.com
TIANJIAO INTERNATIONAL TRADING CO. (USA), INC.
1818 Gilbreth Rd., Ste. 223
Burlingame, CA 94010 U.S.A.
(888) 661-1668; (650) 259-9618
Fax: (650) 259-9608
Email: baotoure@aol.com
Website: www.baotou.com

OPACIFIERS. Opacifiers are those materials used in enamels, glazes, and colorless glass batches to produce an appearance usually called opaque, although they really possess translucency rather than opacity. According to Andrews, the opacity is caused by the phenomena of reflection, refraction and diffraction of light by particles embedded in the matrix of glass. The light falls on the enamel in diffused rays, and by means of these phenomena the rays are diffused in all directions, destroying the transparency of the enamel.

Opacity produced by particles of a different index of refraction than the parent glass may be divided into (1) insoluble particles, (2) crystallites, (3) immiscible constituents and (4) gas bubbles. Insoluble particles of opacifier added to the frit and milled to a fine state of dispersion represent the insoluble type. In fusing the enamel, glass or glaze, these particles are suspended in the glass in a finely divided form. In the second type of opacity, the particles are formed by devitrification, or crystallization. Arsenic oxide is one of the opacifiers that works in this way, crystallizing on cooling. The same is sometimes true of zirconium silicate or titanium oxide when used as the opacifier in the frit batch. With antimony oxide, opacity is developed during smelting by oxidation of the antimony trioxide to antimony pentoxide. In sodium antimonate, the production of uniformly high opacity is more certain. If immiscible melts are formed in smelting, the third type of opacity results. When minute gas bubbles are left in the enamel, opacity of the fourth type is produced, although this type is undesirable since the bubble structure gives poor resistance to scratching and abrasion. Few enamelers depend upon one material alone to develop opacity and it is very likely that all four types are developed in many enamels.

Enamel glass composition has a marked effect on the nature of the crystalline compounds causing opacity. Unless the enamel and the opacifier are compatible, reaction between the two may take place during firing. Color development and low opacity often result from such chemical action.

Patented mill addition opacifiers for vitreous enamels and glazes are sold under many trade names.

A number of scientific instruments have been developed for determining the opacity and color of enamel coatings, but the principle of all is the same and involves ultimate comparison with a block of magnesium oxide which is taken as the standard of 100% whiteness. The comparisons are made at different wavelengths throughout the visible spectrum to determine what color is predominant.

Opacity is developed in glass and glazes by the same methods employed for enamels. The use of tin oxide as a primary opacifier

has virtually disappeared in commercial ceramic glazes, although it still finds use as a glaze color stabilizer. Zirconium silicate is the dominant glaze opacifier in fritted and raw glazes for almost all applications.

The indices of refraction of various materials used as primary or secondary opacifiers, according to Andrews, are:

Titanium oxide.....2.52–2.76
Zinc sulfite.....2.37
Calcium fluoantimonate 2.20
Zirconium oxide 2.13–2.20
Lead arsenate.....2.14
Antimony trioxide 2.09
Tin oxide 2.04
Zirconium silicate.....2.00
Zinc spinel 1.90
Enamel glasses 1.50–1.55
Calcium fluoride.....1.44
Cryolite.....1.34
Sodium fluoride.....1.33
Arsenic trioxide 1.13

OPACIFIER SUPPLIERS

CONTINENTAL MINERAL PROCESSING INC.
11817 Mosteller Rd.
Cincinnati, OH 45262 U.S.A.
(513) 771-7190 Fax: (513) 771-9153
Email: continentalmineral@fuse.net

ELF ATOCHEM NORTH AMERICA INC.
2000 Market St., 22nd Floor
Philadelphia, PA 19103-3222 U.S.A.
(215) 419-7000 Fax: (215) 419-7415

FERRO CORPORATION, CERAMIC DIV., NORTH AMERICA
4150 East 56th St., P.O. Box 6550
Cleveland, OH 44101 U.S.A.
(216) 641-8580 Fax: (216) 441-4330
Website: www.ferro.com

JOHNSON MATTHEY CERAMICS INC., JOHNSON MATTHEY COLORS & COATINGS DIVISION
498 Acorn Ln.
Downingtown, PA 19335 U.S.A.
(610) 873-3200 Fax: (610) 873-3255
Website: www.cmd.matthey.com

PASTES. Conductor, resistor, dielectric, seal glass, polymer and soldering compositions are available in paste or ink form. They are used to produce hybrid circuits, networks and ceramic capacitors. The materials are often called thick film compositions.

Conductor pastes consist of metallic elements and binders suspended in an organic vehicle. Primarily, precious metals such as gold, platinum, palladium, silver, copper and nickel are used singularly or in combination as the conductive element. The adhesion mechanism to the substrate is provided by either a frit bond, reactive bond or mixed bond. During drying, usually at ~125°C, the vehicle is removed. Further processing is done through free-air-flowing tunnel kilns at 550–1000°C. Fired film thickness is 2–20 μm. Important properties of conductor pastes include wire bondability, conductivity, solderability, solder leach resistance and line definition.

Thick-film resistor pastes are composed of a combination of glass frit, metal and oxides. Resistor pastes are available in values ranging from 0.2 ohm/sq to 10 M ohm/sq. Firing temperatures: 600–850°C. Temperature coefficient of resistance can vary from 40–150 ppm/C. These pastes are used in microcircuits, voltage dividers, resistor networks, chip resistors and potentiometers.

Dielectric compounds are used as insulators for the fabrication of multilayer circuits, crossovers or as protective coverings.

Solder pastes are one of the more common component attach products. They consist of finely divided solder powders of all common alloys of tin, lead, silver, gold, etc., suspended in a vehicle-flux system. The fluxes may be nonactivated or completely activated. The most popular is RMA (rosin, mildly activated).

PASTE SUPPLIERS

CERDEC CORP., CONSTRUCTION CERAMICS
West Wylie Ave., P.O. Box 519
Washington, PA 15301 U.S.A.

(724) 223-5900 Fax: (724) 228-3170
Website: www.cerdec.com

PHOSPHORS. The properties of phosphors may be divided into two groups: (1) luminescent properties, such as the color of the fluorescence and phosphorescence, persistence and light output; and (2) other physical properties relating to the behavior of the phosphors during processing. Some phosphors used in porcelain enamels and the fluorescent colors they produce are: zinc sulfide (green); zinc sulfide, copper-activated (phosphorescent green); uranium oxide (yellow-green); molybdic acid (yellow); wollastonite (violet); willemite (green).

PHOSPHOR SUPPLIERS

PACIFIC INDUSTRIAL
DEVELOPMENT CORP.
900 Victors Way, #300
Ann Arbor, MI 48108 U.S.A.
(734) 930-9292 Fax: (734) 930-9293
Email: rareearth@pidc.com
Website: www.pidc.com

PIEZOELECTRIC. A ceramic material, such as barium titantate, which generates mechanical force when electrical force is applied.

PIEZOELECTRIC SUPPLIERS

MORGAN ELECTRO CERAMICS
232 Forbes Rd.
Bedford, OH 44146 U.S.A.
(440) 232-8600 Fax: (440) 232-8731
Email: sales@morganelectroceramics.com
Website: www.morganelectroceramics.com

PIGMENTS. Solid powders used to give black, white or other color to bodies and coatings by reflecting the light of certain wavelengths and absorbing the light of other wavelengths.

PIGMENTS SUPPLIERS

GENERAL COLOR & CHEMICAL
CO. INC.
P.O. Box 7, 604 Valley St.
Minerva, OH 44657 U.S.A.
(330) 868-4161 Fax: (330) 868-5880
Email: info@generalcolor.com
Website: www.generalcolor.com
MASON COLOR WORKS, INC.
250 E. Second St., Box 76
East Liverpool, OH 43920 U.S.A.
(330) 385-4400 Fax: (330) 385-4488
Email: mcwinc@valunet.com
Website: www.ceramics.com/mason

PLASTER OF PARIS. (Calcined gypsum.) $CaSO_4$-$0.5H_2O$. A white, gray or pinkish-colored powder prepared by heating gypsum ($CaSO_4 2H_2O$) to remove 75% of its water of crystallization. Available in various types of products having specific, controlled properties. When mixed with water and allowed to rehydrate to the dihydrate ($CaSO_4$-$2H_2O$), there is no apparent action at first, but soon a slight stiffening takes place and shortly after that it "sets" to a solid mass. As set progresses the mass begins to heat and expand, and final set is not reached until the evolution of heat has ceased and expansion is complete.

Through changes in the manufacturing process, the time of set can be varied widely (from a few minutes to many hours), and linear setting expansion also is controllable from 0.05%–2.0%. The normal linear setting expansion of pottery plasters is ~0.20% in all directions if the cast is unconfined, but under conditions of confinement, all the setting expansion may take place in one direction only. Under conditions of partial confinement, warping, twisting, or slight crushing of surface or internal structures can develop. The stresses set up by the setting expansion forces are usually relieved rapidly by cold flow in the set plaster before drying. When this occurs, the magnitude of expansion is not accurately predictable and must be obtained by measurement.

Plasters are used in a variety of ceramic industry applications:

1. In a limited way, as chemical additives to glazes, supplying neutral, slightly soluble calcium and sulfate sulfur.

2. As a **glass** batching material to replace part or all of the salt cake when combined with soda ash in proper proportions. Here, use of plaster eliminates salt water scumming, retaining the desirable fluxing property of salt cake. It appears that gypsum is going to be widely used as a source of sulfur. The basic problem here is to obtain an inexpensive material (as compared with barium sulfate) that will furnish sulfur dioxide upon decomposition. Apparently, SO_2 gas aids in clearing up the glass and in giving added brilliance.

3. As a bedding and leveling agent in grinding and polishing plate glass, plaster cements the glass to the grinding bed during the operation while also being easy to remove from the glass surface. Its soft crystal is not abrasive to glass surfaces.

4. Optical glass mounting. Used to retain optical glass, lenses, prisms and oculars in position while surfaces are formed to the desired curves by grinding and polishing. Also used in setting levels and bubble glasses in position where permanent positioning is desired.

5. Model making. Used in the **ceramic** industry generally for preparing original models. Remains permanently without dimensional change or surface corrosion. Set blocks of plaster have a grain-free structure which permits carving or cutting in any direction without difficulty, and advantage may be taken of the plastic period prior to set for template forming. Various types of models are used for foundry patterns directly, for master patterns, for diemaking operations in metals, etc.

6. **Metal** mold making. When suitably compounded with refractory substances, molds for the casting of nonferrous alloys, such as white metal, brass, aluminum alloys, etc., are made with plaster.

7. Low-density insulation. Used to provide green strength to mixtures of clays, nonplastic refractories and organics.

8. Potter mold and die making. This use constitutes the principal ceramic application of plasters. Newer plasters are commercially available, which, while having identically the same chemical composition as other plasters, require much lower amounts of mixing water to form a pourable mix. This characteristic is due to the manufacturing processes that differ from those used for ordinary plasters. Two types of these super-strength gypsum plasters are commercially known. One type is made by calcination under steam pressure, while the other is calcined in a chemical solution. The steam calcined material requires approximately 25% more mixing water than the chemically calcined gypsum to yield a pourable mix. As a result of this property, the chemically calcined material gives a much stronger, denser cast. A number of products are made with these materials, the important characteristics of which are high compressive strength, resistance to wear and low expansion in the finished mold. These super-strength plasters are called alpha gypsum to differentiate them from regular plasters (beta gypsum), which have a somewhat different crystal structure in the calcined state.

Regardless of the plaster used, 100 lb of HEMI hydrate ($CaSO_4$-$0.5H_2O$) requires just 18.6 lb of water to react to dihydrate ($CaSO_4$-$2H_2O$).

Water in excess of the chemical requirement is always necessary to obtain fluidity, however, and when this is removed by drying, numerous empty pores result. The effects of the decrease in density accompanying increasing water additions are reductions in compressive strength, hardness and wear resistance. Decrease in density does, however, result in greater water absorption in the mold, and the minimum permissible absorption usually governs the water-to-plaster ratio used. In general, working molds should be made with the lowest water-to-plaster ratio (consistency) that is compatible with plant conditions. It is important to note that at a given density the hardness, strength and abrasion resistance of a mold are greatly reduced by the presence of free water. Compressive strength, for

example, is usually about half as much for a damp mold as for the same mold when dry.

The requirements for a block-mold material are somewhat similar to those of a model material because carving is often essential. Since the block mold is generally used to make a few check casts in clay, it must be sufficiently durable and absorbent to lend itself to this use.

Case Molds: In the production of case molds, the principal requisites of a good material are: (1) extremely low setting expansion to prevent binding in or warpage of the block mold; (2) a low normal consistency that will provide a hard, smooth surface and high strength (possession of these characteristics makes sizing easier, prevents excessive case mold wear, prevents sticking of the working mold to the case mold and results in well-fitting working molds); (3) a low normal consistency so that fine detail may be duplicated accurately without the necessity of sacrificing strength to obtain high fluidity; (4) a sufficiently long period of plasticity to enable the mold maker to trim the mold exterior before final set occurs; and (5) dimensional stability throughout a long storage period without loss of surface perfection.

Jigger and Casting Molds: The requirements of a working jigger or casting mold are that it accurately reflects the model, produces good ware having uniform density and neither pinholes nor high spots, and provides long, economical service. The specific demands made on a plaster for working molds are: (1) low normal consistency so that slurries for the densest molds may be easily mixed and poured without pinholes or loss of details; (2) moderate but uniform expansion so that, while the working mold will free itself from the case mold easily, it will not bind or warp, will fit the jigger ring, and will attain an accurate, predetermined size and shape; (3) sufficiently long and uniform period of plasticity to enable the mold maker to complete pourings without haste and to plan work with the assurance that the length of the plastic period will not change from mix to mix; (4) sufficient regularity in physical properties of the calcined gypsum that many molds may be made over a period of years without significant variations in mold characteristics; and (5) the ability to make molds that wear slowly and evenly, absorb water uniformly and, at the same time, have sufficient strength to resist ordinary abuse.

In practical mold making, uniformity and careful control of procedures by the user are of the greatest importance for best performance of any plaster. Factors that must be standardized and kept nonvarying are: consistency (water-to-plaster ratio); mixing (time and method); and clay shop handling methods, environment and conditions of use.

Chemical Action of Clay on Mold: When sodium silicate and carbonate of soda are used in the slip, the mold will effloresce. There is no absolutely certain way of preventing this, as it is due to the reaction between the sodium carbonate (soda ash) or silicate with the gypsum in the mold itself, forming insoluble calcium carbonate and calcium silicate and soluble sodium sulfate. This sulfate of soda is carried to the surface of the mold by the water absorbed from the slip. As it reaches the surface, it evaporates, leaving behind the sulfate as a white powder, the efflorescence. Wherever such chemicals are used in the slip, efflorescence is bound to occur. This can be remedied somewhat by placing the mold during drying in such a position that the evaporation will take place from the back of the mold. The soluble salts are thus drawn, by capillarity, away from the face of the mold. The use of organic dispersing agents in place of sodium silicate or carbonate will obviate this trouble.

For maximum mold life, deflocculants should be used in the minimum quantity required to obtain proper slip characteristics. Also, when sodium carbonate and sodium silicate are employed in combination as a deflocculant, the amount of carbonate should be reduced to the absolute minimum permissible. Silicate in general has a less eroding effect on mold surface

than carbonate, and indications are that 50% greater mold life is obtainable with sodium silicate as compared with carbonate.

PLASTER OF PARIS SUPPLIERS

G-P GYPSUM
133 Peachtree St., N.E.
Atlanta, GA 30303 U.S.A.
(888) Plaster Fax: (404) 588-3833
Email: gpgind@gapac.com
Website: www.gp.com/plaster

PYROLYTIC GRAPHITE. A high purity form of carbon (C) produced by thermal decomposition of carbonaceous gases.

The commercial manufacture of pyrolytic graphite products is a relatively new division of the graphite industry. Though this material has been known for some 50 years (glance coal, deposited carbon in gas retorts, etc.), it is only within the last 10–15 years that the necessary production techniques have been developed.

The manufacturing process essentially consists of bringing a relatively cold, carbonaceous gas into contact with a heated surface (mandrel) and thus extracting the carbon, in the form of graphite, directly from the gas. This process is not to be confused with the pyrolysis of resins and pitches which is involved in the manufacture of the more common bulk or polycrystalline graphites.

The formation of pyrolytic graphite directly from a hydrocarbon gas results in a structure which is distinctly different from other commercial forms of this element. While polycrystalline graphites consist of at least two solid phases (binder and filler) and are porous to varying degrees, pyrolytic graphite consists of a single phase (no binder) and is essentially impervious to gases.

By properly designing furnace hardware and controlling the deposition process, pyrolytic graphite can be manufactured commercially as solid plate, cones, tubes and other free-standing shapes. Because the deposition process relies, in part, on diffusion of the hydrocarbon gas to the heated mandrel, it also is possible to densify porous structures of carbon or graphite by infiltration with pyrolytic graphite. This infiltration procedure is presently the basis for considerable commercial activity.

As with other materials, pyrolytic graphite can be manufactured with a variety of different properties. By employing deposition temperatures of 1000–2500°C, it is possible to generate pyrolytic graphites with densities of 1.2–2.20 g/cm^3 or higher. Further heat treatments and pressure annealing can increase the density to values approaching the theoretical density of graphite (2.26 g/cm^3). Deposits formed at lower temperatures are generally referred to as pyrolytic carbons and are relatively isotropic and of low density. High temperature deposits of pyrolytic graphite are of higher density and are very anisotropic.

The anisotropy of well-ordered pyrolytic graphite is attributable to the fundamental structure of graphite. A simple analogy can be drawn between a piece of pyrolytic graphite and a deck of cards. Each card, or plane of graphite, is composed of a two-dimensional network of carbon atoms bonded together in the form of hexagons. Within these planes (called basal planes), the carbon-carbon bond strength exceeds that in diamond. However, there is no equivalent bonding between the planes or sheets of carbon atoms and, in fact, the stack of planes is held together primarily by the rather weak, van der Waals' forces of attraction.

With this layered structure, the thermal and electrical conductivity of pyrolytic graphite is very high parallel to the planes but much lower in the direction perpendicular to the planes. This directionality is so great that a well-ordered pyrolytic graphite may have a thermal conductivity equal to copper in the planar (a-b) direction, while it is essentially an insulator in the direction perpendicular to the planes (the c direction). Advantage is taken of this anisotropy when pyrolytic graphite is employed for rocket nozzles, missile nose cones and other applications where conductive anisotropy is desirable.

The structure of pyrolytic graphite also accounts for the fact that this material can exhibit tensile strengths of 20,000 psi in the a-b direction, while in the c direction the tensile strength is about 1500 psi. As with other graphites, the pyrolytic form displays higher strengths at elevated temperatures, does not melt under normal pressures and sublimes above 3500°C.

Pyrolytic graphite is much more resistant to oxidation than ordinary polycrystalline graphites because the attack by oxygen occurs at the edges of the basal planes, which comprise less of the surface of a piece of pyrolytic graphite. In addition, pyrolytic graphite is essentially impervious to oxygen and, therefore, internal oxidation is minimized.

The commercially available forms of pyrolytic graphite include plate stock, tubes and free-standing shapes. In addition, pyrolytic graphite is used commercially to densify porous structures such as carbon felts, fabrics, composites of carbon/graphite yarns and that can withstand the deposition temperature and are compatible with pyrolytic graphite. It also is used to coat conventional (bulk) graphites where increased resistance to oxidation and chemical attack are desired.

In the past, pyrolytic graphite has been used primarily in those areas where its high cost was offset by the unique properties of this material. Today, however, as this technology comes of age, pyrolytic graphite is being used in an increasing number of applications within industry.

PYROLYTIC GRAPHITE SUPPLIERS

POCO GRAPHITE INC.
1601 S. State St.
Decatur, TX 76234 U.S.A.
(940) 627-2121; (877) 762-6747 (US)
Fax: (940) 393-8366
Email: sales@poco.com
Website: www.poco.com

QUARTZ. SiO_2. M.p. 1713°C. (See FLINT, SILICA, SAND.)

QUARTZ SUPPLIERS

CHARLES B. CHRYSTAL CO., INC.
30 Vesey St.
New York, NY 10007 U.S.A.
(212) 227-2151 Fax: (212) 233-7916
KALEMADEN ENDUSTRIYEL HAMMADDELER SAN. VE TIC. A.S., HEADQUARTERS
Semedeli Koyu, Can
Canakkale Turkey
(90 286) 4341330 Fax: (90 286) 4371340
Email: can@kalemaden.com.tr
Website: www.kalemaden.com.tr
KALEMADEN ENDUSTRIYEL HAMMADDELER SAN. VE TIC. A.S., EXPORT & MARKETING MANAGEMENT
Eski Uskudar Yolu, Bodur Is Merkezi, No. 8, Kat 6
Daire: 23-24, Icerenkoy, Istanbul
Turkey
(90 216) 3844999; (90 216) 3844748
Fax: (90 216) 3725548
Email: ist@kalemaden.com.tr
OGLEBAY NORTON INDUSTRIAL SANDS INC.
P.O. Box 1000
Zanesville, OH 43702-1000 U.S.A.
(740) 452-2822 Fax: (740) 452-2775
Email: mchalcraft@oglebay.onco.com
Website: www.oglebaynorton.com
UNIMIN CORP.
258 Elm St.
New Canaan, CT 06840 U.S.A.
(203) 966-8880; (800) 243-9004
Fax: (203) 972-1378; (800) 243-9005

SILANE COUPLING AGENTS. Polymer materials based on $Si(OR_3)$, vinyl or amino groups that are used as a pretreatment for reinforcing fibers. Provides strong bonding between the fiber and matrix.

SILANE COUPLING AGENT SUPPLIERS

GELEST INC.
612 William Leigh Dr.
Tullytown, PA 19007 U.S.A.
(215) 547-1015 Fax: (215) 547-2484
Website: www.gelest.com

SILICA. SiO_2. Melting points up to 1713°C; softening temperatures 600–800°C. Silica, when foamed, is 99% SiO_2 with a bubble structure that is nonconnecting. (See FLINT.)

Silicon, next to oxygen, is the most abundant element found in nature. Silica occurs in the crystalline forms quartz, tridymite and cristobalite; in cryptocrystalline forms such as chert, flint and chalcedony; and in hydrated forms such as opal. In combination with many of the basic oxides, it forms a very large group of minerals known as the silicates.

Silica occurs in a number of crystal forms, the nature and stability ranges of which have been extensively studied. This study has been difficult, partly due to the slow rate at which the changes occur, and the low thermal conductivity of silica and silicates, which tends to mask the results and prevent precise determinations.

While tridymite and cristobalite may exist for indefinite periods of time at room temperature, the low-temperature alpha-quartz is believed to be the form of silica truly stable at these temperatures. A considerable expansion accompanies the conversion of α-cristobalite to β-cristobalite at 220–275°C, and a sudden expansion of ~2.2% occurs during the inversion of α-quartz at 573°C. The conversion of quartz to tridymite at 870°C is accompanied by an expansion of ~15%.

These volume changes cause strains in a ceramic body containing free silica. All forms of silica, when heated to sufficiently high temperatures, fuse and form amorphous silica glass or fused silica. If the heating is very rapid, quartz may fuse without appearing to pass through the intermediate stages. When fused silica is very slowly cooled, the reactions taking place are the reverse of those occurring during heating, and a quartz will ultimately be produced.

In the ceramic industry, SiO_2 is known as sand, silica, quartz and flint. As silica or sand, it is used in the enameling and glass industries, particularly the latter. As ground quartz, or quartz, as it's termed, SiO_2 is used in some forms of pottery. As ground silica or ground sand, it's known as flint and used in the pottery, enamel and terra cotta industries. It is used as fused quartz and crystalline quartz in the electronic ceramic industry.

Glass Sands: For the purpose of glass manufacture, however, it is necessary that quartz be not only an essential constituent of the silica rock, but it must be practically the only constituent present. Sand deposits and sandstones are found in nature that analyze >99% silica.

In the present-day manufacture of glass, nearly pure quartz sands are used almost exclusively as the source of silica, which is the major constituent of all common varieties of glass. Ordinary soda-lime glasses, such as bottle, common tableware, plate and window glasses, contain 65–75% silica. Glass sands occur in nature either in the form of loose, unconsolidated sediments or in deposits in which the individual grains have been bound together by some cementing agent so as to form sandstone. While deposits of sand and sandstones are abundantly distributed, deposits that are sufficiently free of other constituents, particularly iron oxide, are comparatively rare.

West Virginia, Illinois, Pennsylvania, New Jersey and Missouri supply 80–90% of all glass sand used in the U.S. In Pennsylvania and West Virginia, the bulk of the glass sand produced is derived from Oriskany quartzite. For almost a century, the most important source of silica for the production of glass has been the Oriskany quartzite deposits in the eastern United States. In Illinois and Missouri, practically all of the glass sand is derived from the St. Peter sandstone. In New Jersey, glass sands occur as horizontal beds of unconsolidated sand, sometimes 90 ft thick and capped by 1–15 ft of gravel, sand and loam. Silica of the purity required for the manufacture of glass and ceramics is found in south-central Oklahoma in the Oil Creek quartzite of the Ordovician Age. Located in the heart of the Southwest, this deposit is fast becoming a major source for Western glass and ceramic manufacturers.

In California, sand is mined from sedimentary sandstone formations of early tertiary age (namely Paleocene deposits south of Mission Viejo, in the Trabuco Canyon area of Orange County) and Eocene deposits near Ione in Amador County and Oceanside in San Diego County. These deposits are essentially feldspathic sands containing clays and heavy minerals. In most cases, glass sand on the West Coast is recovered only after beneficiation. Oriskany and St. Peter sandstones remain the two major sources of glass sand in the United States.

Uniformity in grain size is perhaps of more importance in a glass sand than the actual size of the grains themselves. If the sand grains are too fine, the first reaction will take place so rapidly that the large volumes of carbon dioxide liberated will cause the batch to foam badly and, in case of a tank furnace, excessive amounts of material will be carried into the checkers of the regenerators and into the flues. Too fine a sand also may be responsible for the formation of a fine, persistent seed in the glass.

The coarser the sand used, the greater is the tendency for the formation of batch scum. A sand containing only a few percent of coarse grains is more likely to cause scum, stones and cords than a sand in which all the grains are uniformly coarse. If sand grains are uniform in size, the attack on them will be approximately uniform and consequently they will decrease in size at a uniform rate. On the other hand, if the sand is composed of a few percent of large grains and the remainder relatively small grains, the solution of the small grains will be completed before the large grains have decreased but very little in size.

The finer portions of a glass sand are apt to contain a large part of the undesirable iron-bearing minerals of the sand, such as magnetite and ilmenite. If the sand grains are coated with small amounts of limonite or hematite, the finer sand, on account of its greater surface area in proportion to its weight, will contain the highest percentage of iron.

The silica (actually ground silica) used in the **pottery** industry is called flint. The addition of flint affects warpage very little. Bleininger and Stull found that porosity decreased more in high flint bodies than in high clay bodies.

In ceramic bodies, potters' flint or pulverized quartz or sand is the constituent which reduces drying and burning shrinkage and assists promotion of refractoriness. Flint has an important bearing on the resistance of bodies to thermal and mechanical shock, because of the volume changes which accompany crystal transformation. In the unburned body, it lowers plasticity and workability, lowers shrinkage and hastens drying. A coarse crystalline form of quartz, called macrocrystalline quartz, is more often used for potters' flint than the cryptocrystalline form.

Cryptocrystalline flint will show more cristobalite development under heat treatment than will quartz flint. This property has an important bearing on thermal shock resistance of whiteware bodies, allowing more resistant bodies to be made using quartz flint. Impurities in the flint and the fineness to which it is ground have a decided effect on the behavior of the body; this effect is probably of more commercial importance than that caused by the type of flint used. The maturing temperature of a body is now lowered materially by the use of cryptocrystalline flint, but overfiring will take place more rapidly than in bodies where quartz flint is used.

Purdy and Potts found that with any mixture of flint and feldspar, or even when added at the expense of flint, clay slightly increases rather than decreases the coefficient of expansion. Up to 45% flint added to any constant clay-to-feldspar ratio slightly decreases the coefficient of expansion and tends to reduce crazing.

Silica is used in all **glazes** as the chief, and often the only, acid radical (RO_2 group). It may be adjusted to regulate the melting temperature of the glaze. In common glazes, the ratio of silica to bases (RO group) is never less than 1:1 nor more than 3:1. By varying

the relative proportions of the RO group and balancing the group against any desired silica content, the maturing temperature of a glaze may be quite closely controlled. In other words, the fusibility of the glazes used in the presence of equal proportions of fluxes depends on their relative silica contents.

In porcelain **enamels**, it may be taken as a general rule that, other things remaining constant, the higher the percentage of silica, the higher will be the melting point of the enamel and the greater its acid resistance. Silica has a low coefficient of expansion and increasing it in an enamel lowers the coefficient of expansion of that enamel. One method of regulating an enamel coating is to increase the silica content when the enamel is inclined to split off in cooling. Silica in the form of flint or quartz is used in both ground-coat and cover-coat enamels, and it has the same effect in either type.

The temperature required for melting an enamel is materially affected by the fineness of the silica. Cryolite, antimony and tin oxide give their maximum value as opacifiers with minimum heat treatment in the smelter. The form and fineness of the silica should, therefore, be carefully watched and allowed for in compounding the batch. All forms of silica may be used with good results, but experience has shown that, in the same enamel, a smaller quantity of sand than of powdered quartz is necessary. Similarly, less sand than flint should be used, but the difference in this case is less than in the former. High SiO_2 tends to harden the enamel. The lower limit established in the usual run of enamels is 1.1 equivalents.

In the manufacture of semiconductors, monolithic circuits and integrated circuits for the electronics industry, the use of fused quartz is widespread for plumbing and diffusion furnace muffles. The need to prevent product contamination makes this choice mandatory.

SILICA SUPPLIERS

BADGER MINING CORP.
409 S. Church St., P.O. Box 328
Berlin, WI 54923-0328 U.S.A.
(920) 361-2388; (800) 285-0038
Fax: (920) 361-2826
Email: bolmen@badgerminingcorp.com
Website: www.badgerminingcorp.com

MUSCLE SHOALS MINERALS
4820 Honey Grove Dr.
Antioch, TN 37013 U.S.A.
(256) 370-7102; (615) 385-5367
Fax: (256) 370-7770; (615) 292-7710
Email: lmkrieg@aol.com

OGLEBAY NORTON INDUSTRIAL SANDS INC.
P.O. Box 1000
Zanesville, OH 43702-1000 U.S.A.
(740) 452-2822 Fax: (740) 452-2775
Email: mchalcraft@oglebay.onco.com
Website: www.oglebaynorton.com

SILICA RESOURCES, INC./SRI
4553 Hammonton Rd.
Marysville, CA 95901 U.S.A.
(530) 741-0290 Fax: (530) 741-3457
Email: sri@otn.net

U.S. SILICA CO.
P.O. Box 187
Berkeley Springs, WV 25411 U.S.A.
(304) 258-2500; (800) 243-7500
Fax: (304) 258-8295
Email: sales@u-s-silica.com
Website: www.u-s-silica.com

UNIMIN CORP.
258 Elm St.
New Canaan, CT 06840 U.S.A.
(203) 966-8880; (800) 243-9004
Fax: (203) 972-1378; (800) 243-9005

ZEMEX INDUSTRIAL MINERALS, INC., (FELDSPAR CORP.)
1040 Crown Pointe Pkwy., Ste. 270
Atlanta, GA 30338 U.S.A.
(770) 392-8660 Fax: (770) 392-8670
Email: minerals@zemex.com
Website: www.zemex.com/minerals

SILICA, FUSED. (Quartz.) The desired property of this material is its low coefficient of thermal expansion. It is primarily used in refractories for kiln and furnace walls, and as a shell material for molds in

investment casting. Used in the electronics industry as an inert, low expansion filler for epoxy resins. Each chip or microcircuit is packaged in a blend of fused silica and epoxy for protection. One additional use is windows for spacecraft and other high temperature applications.

Successful **refractories** have been made by adding fused silica to the body. Quartz in itself, after it is fused, has a very low coefficient of expansion and actually assists in bringing out a good heat resistant type of body. A danger of recrystallization of quartz is possible if reheated too high and too many times which, of course, would destroy the low coefficient of expansion.

Silica refractories are made from gannister and quartz rock. These refractories are very commonly used in roofs of glass tanks and open hearth furnaces.

The rock is ground to a specified size range. The silica then is mixed with a binder, sometimes even molasses, and then shaped into form either by dry pressing or by a drop press. Silica is fired to ~2700°F for the final formation.

Lime sometimes is used as the binder and also acts as a flux.

Two types of silica refractories are made: (1) the common variety and (2) a very low-alumina variety. Alumina up to ~4% acts as a flux, lowering the service temperature of the silica brick.

SILICA, FUSED SUPPLIERS

BPI INC. (BY-PRODUCT INDUSTRIES)
612 S. Trenton Ave.
Pittsburgh, PA 15221 U.S.A.
(412) 371-8554 Fax: (412) 371-9984
Email: info@bpiminerals.com
Website: www.bpiminerals.com
PEMCO, INC.
MPO Box 8
Niagara Falls, NY 14302 U.S.A.
(716) 284-2482 Fax: (716) 284-2483

SILICON CARBIDE. SiC. Mol. wt. 40.07; sp. gr. 3.22. Commercial SiC is produced in an electric furnace from a mixture of coke and silica sand (>99.4% SiO_2), which sometimes also contains sawdust and salt or another binder. An electric current passed between permanent electrodes located at both ends of the furnace, and through a graphite core, produces a temperature higher than 2200°C, at which point crystals of silicon carbide form from the sand-coke charge. Beta-SiC (cubic) forms at 1400-1800°C and alpha-SiC (hexagonal) forms at temperatures >1800°C. If used, the sawdust burns out, keeping the mass porous, and the salt assists in the removal of impurities through a formation of volatile chlorides. A furnace run takes ~36 hr. Another method used to form SiC pieces is by vapor deposition of silicon onto a heated graphite or carbon surface. SiC has been found in nature in meteoric iron and in diamond mineral assemblages in South Africa and the former USSR.

SiC is extremely hard (Mohs 9.1 or 2500 Knoop); has high thermal conductivity (100 W/mK); and high strength at elevated temperatures (at 1000°C, SiC is 7.5 times stronger than Al_2O_3). SiC has a modulus of elasticity of 410 GPa, with no significant decrease in strength up to 1600°C, and it does not melt at normal pressures but instead dissociates at >2815.5°C. The material is a semiconductor, exhibiting 0.1 Ohm-cm resistance in porous recrystallized form, and is capable of rectification and electroluminescence. SiC oxidizes very slowly in air, and is serviceable to 2800–3000°F for many uses. It is not attacked by acids, but reacts readily with fused caustic, halogens and certain metal oxides at high temperatures. SiC's CTE is 5.2×10^{-6}/C (25–1500°C); Weibull modulus is 10; Poisson's ratio is 0.16.

Three main types are produced commercially. Green SiC is an entirely new batch composition made from a sand and coke mixture, and is the highest purity of the three. Green is typically used for heating elements. Black SiC contains some free silicon and carbon and is less pure. A common use is as

bonded SiC refractories. The third grade is metallurgical SiC, and is not very pure. It typically is used as a steel additive. Typical green and black SiC compositions (in %) are compared in the table.

Ingredient	Green	Black
SiC	98.6	97.5
Free Si	0.15	0.5
Free C	0.36	0.6
SiO_2	0.63	0.8
Fe	0.08	0.2
Al	0.08	0.2
Ca	0.05	0.05
Mg	0.03	0.05

Silicon carbide is manufactured in many complex bonded shapes, which are utilized for super-refractory purposes such as setter tile and kiln furniture, muffles, retorts and condensors, skid rails, hot cyclone liners, rocket nozzles and combustion chambers, and mechanical shaft seals. It is also used for erosion- and corrosion-resistant uses, such as check valves, orifices, slag blocks, aluminum die-casting machine parts and sludge burner orifices. Electrical uses of SiC include lightning arrestors, heating elements and nonlinear resistors.

Silicon carbide materials also offer superior friction and wear characteristics when used in mechanical seals and pump bearings. High hardness, strength, and thermal conductivity make them excellent mating components for all types of high-performance applications.

There are different families of materials, including reaction-bonded materials, which contain free silicon metal; sintered materials, which offer superior chemical resistance; chemical vapor deposited materials, which offer enhanced tribological properties; and composites of silicon carbide, which can contain graphite (for lubricity) and/or porosity (to improve marginal lubrication situations). These materials are typically run against carbon-graphite materials or against themselves, depending on the application requirements.

Silicon carbide refractories are classified on the basis of the bonds used. Associated-type bonds are oxide or silica, clay, silicon oxynitride and silicon nitride, as well as self-bonded. The dense materials contain 85–99% SiC; the clay-bonded contain 75–80% SiC; and the semisilicon carbides are still lower in SiC content.

Properties vary according to the types and amounts of bond used. Generally speaking, SiC **refractories** exhibit properties that warrant their use in kiln furniture applications, structural members, chemical and municipal incinerators, coal handling equipment, recuperator tubes, muffles, retorts, crucibles and pyrometer protection tubes. Added to plastic fireclays, silicon carbide imparts high thermal emissivity and conductivity to the refractory and extends the useful application of this material. Silicon carbide also finds application as refractory cements for laying SiC brick or shapes, ramming or patching linings, and washes. These cements or mortars are sized for each specific application. Bonds generally of a phosphate- or clay-type impart a thermal working range to the particular cement and mature at predetermined temperatures.

In addition, SiC is used in the manufacture of **grinding wheels** and coated **abrasives**. Large tonnages are used in cutting granite with wire saws and as a metallurgical additive in the foundry and steel industries. About 700,000 tons are produced per year, of which 33% is used as a metallurgical additive and 50% is used in the abrasives industry.

The remainder is used in the refractory and structural ceramic industries. As an abrasive, silicon carbide is best used on either very hard materials such as cemented carbide, granite and glass, or on soft materials such as wood, leather, plastics, rubber, etc.

The specific electrical resistivity of SiC single crystals depends on purity. Values at room temperature range from 2.1–0.4 Ohm-cm. Single crystals formed by the traveling solvent method have the higher purity needed for rectifier applications in

the 10 A range and operating temperatures up to 500°C. Low power injection lasers are possible with SiC. Electronic applications include thermistors, varistors and attenuator material for microwave devices.

SILICON CARBIDE SUPPLIERS

BPI INC. (BY-PRODUCT INDUSTRIES)
612 S. Trenton Ave.
Pittsburgh, PA 15221 U.S.A.
(412) 371-8554 Fax: (412) 371-9984
Email: info@bpiminerals.com
Website: www.bpiminerals.com

CERADYNE INC.
3169 Redhill Ave.
Costa Mesa, CA 92626 U.S.A.
(714) 549-0421 Fax: (714) 549-5787
Email: sales@ceradyne.com
Website: www.ceradyne.com

CERCOM INC.
991 Park Center Dr., P.O. Box 70
Vista, CA 92083 U.S.A.
(760) 727-6200 Fax: (760) 727-6209

ELECTRO ABRASIVES CORP.
701 Willet Rd.
Buffalo, NY 14218 U.S.A.
(716) 822-2500; (800) 284-4748
Fax: (716) 822-2858
Email: info@electroabrasives.com
Website: www.electroabrasives.com

WACKER ENGINEERED CERAMICS, INC.
3301 Sutton Rd.
Adrian, MI 49221-9397 U.S.A.
(800) 833-7608 Fax: (517) 264-8137
Email: wec.info@wacker.de

EXOLON-ESK CO.
1000 E. Niagara St., P.O. Box 590
Tonawanda, NY 14151-0590 U.S.A.
(716) 693-4550 Fax: (716) 693-0151
Email: info@exolon.com
Website: www.exolon.com

INTERMINERAL USA, INC.
333 Rouser Rd., Bldg. 4
Corapolis, PA 15108 U.S.A.
(412) 299-7700 Fax: (412) 299-7835
Email: joem2@ix.netcom.com

INTERNATIONAL MINERALS, INC.
333 Rouser Rd., Bldg. 4
Corapolis, PA 15108 U.S.A.
(412) 299-9300 Fax: (412) 299-9329

JERSEY MINERAL PROCESSING CO., LTD.,
REFRACTORIES AND MINERALS DIV.
RM B-13B, Triumphal Arc Mansion, 66 Narjing Rd.
Tianjin, 300042, P.R. China
86-22-23133086 Fax: 86-22-23133085
Email: cmptjmax28@shell.jtvan.com.cn

NANCHUAN MINERALS GROUP, SALES OFFICE
P.O. Box 3205
Stamford, CT 06905-0205 U.S.A.
(203) 253-1699 Fax: (203) 323-6711
Email: wgholroyd@prodigy.net
Website: www.nanchuanminerals.com

POCO GRAPHITE INC.
1601 S. State St.
Decatur, TX 76234 U.S.A.
(940) 627-2121; (877) 762-6747 (US)
Fax: (940) 393-8366
Email: sales@poco.com
Website: www.poco.com

ROHM AND HAAS COMPANY, ADVANCED MATERIALS
185 New Boston St.
Woburn, MA 01801 U.S.A.
(781) 933-9243 Fax: (781) 933-5142
Email: cvdsales@rohmhaas.com
Website: www.cvdmaterials.com

H.C. STARCK GMBH & CO. KG
P.O. Box 25 40
D-38615 Goslar Germany
+49/53 21/7 51-1 45 Fax: +49/53 21/7 51-1 93
Email: bettina.essmann.be@hcstarck.de
Website: www.hcstarck.com

H.C. STARCK INC.
45 Industrial Place
Newton, MA 02161-1951 U.S.A.
(617) 630-5916 Fax: (617) 630-5919
Email: elisabeth.james.b@bayer.com
Website: www.hcstarck.com

SUPERIOR GRAPHITE CO.
10 S. Riverside Plaza, Ste. 1600
Chicago, IL 60606 U.S.A.
(312) 559-2999 Fax: (312) 559-9064
Website: www.graphitesgc.com
UK ABRASIVES, INC.
3045 Mac Arthur Blvd.
Northbrook, IL 60062 U.S.A.
(847) 291-3566 Fax: (847) 291-7670
Email: sales@ukabrasives
Website: www.ukabrasives.com
WASHINGTON MILLS ELECTRO MINERALS CORP.
P.O. Box 423, 1801 Buffalo Ave.
Niagara Falls, NY 14302 U.S.A.
(716) 278-6600 Fax: (716) 278-6650
Email: sales@washingtonmills.com
Website: www.washingtonmills.com

SILICON CARBIDE FIBERS. There are two forms of SiC fibers, neither of which is available commercially. One consists of a pyrolytic deposit (CVD) of SiC on an electrically conductive, usually carbon, continuous filament. Fiber diameter is about 140 μm. This technology has been used to make filaments with both graded and layered structures, including surface layers of carbon which provide a toughness-enhancing parting layer in composites having a brittle matrix (silicon nitride, for example).

The other form of filamentary SiC is still in the development stage. Fibers are extruded from sinterable SiC powder, and allowed to sinter during free fall from the extruder. Commercialization is not yet possible because the fibers produced to date are too large: 0.005-0.010 in. in diameter.

SILICON CARBIDE PLATELETS. Single crystals of alpha-phase hexagonal crystal structure. Four size ranges currently are produced: –100, +200 mesh (100–300 μm in diameter, 5–15 μm thick); –200, +325 mesh (50–150 μm in diameter, 1–10 μm thick); –325 mesh (5–70 μm in diameter, 0.5–5 μm thick) and –400 mesh (3–30 μm in diameter, 0.5–3 μm thick). The finest size is a research product and additional development work is being conducted to produce an even smaller diameter platelet in the 0.5 μm range, which would be an ideal reinforcement material for ceramic-matrix composites.

In addition to reinforcing ceramics, silicon carbide platelets also are used to increase the strength, wear resistance and thermal shock performance of aluminum matrices, and to enhance the properties of polymeric matrices. Because platelets are very free-flowing, they can be processed in the same manner as particulates.

SILICON CARBIDE WHISKERS. Silicon carbide whiskers are single crystals of either α or β-phase crystal structure. The SiC whiskers tend to exhibit a hexagonal, triangular or rounded cross section and may contain stacking faults.

SiC whiskers can be fabricated by the reaction of silicon and carbon to form a gaseous species that can be transported and reacted in the vapor phase. This type of formation is referred to as a vapor-solid reaction and occurs by the following multistep process: 1) $SiO_2 + C\text{-}SiO + CO$ and 2) $SiO + 2C\text{-}SiC + CO$. Although the raw materials used in these carbothermal processes vary widely, nearly all of the commercial and high-volume SiC whisker products are formed by this method. These reactions occur at temperatures greater than 1400°C and in an inert or nonoxidizing atmosphere. In addition, a catalyst is added to assure the formation of whiskers rather than particulate during the reaction.

SiC whiskers range from 0.1–5.0 μm in average diameter and from 5–100 μm in average length. Although SiC whiskers can be coated with several different materials, such as carbon, to enhance their performance, the as-produced SiC whiskers generally contain a 5–30 SiO_2 coating, which forms during synthesis.

SiC whiskers are added to a variety of matrices to increase the toughness and high-temperature strength of these materials. The elastic modulus for SiC whiskers is

400–500 GPa and the tensile strength ranges from 1–5 GPa. A variety of ceramic matrices, such as Al_2O_3, Si_3N_4, $MoSi_2$, AlN, mullite, cordierite and glass ceramics, are combined with SiC whiskers to increase the overall mechanical properties of the resulting composite. For example, the wear resistance, toughness and thermal shock of Al_2O_3 is increased by the addition of SiC whiskers. The resulting composite has been used for such applications as high-performance cutting tool inserts. The addition of SiC whiskers to an alumina matrix can double the fracture toughness of the resulting composite, depending on whisker content and processing conditions.

SiC whiskers also can be combined with metals to increase the high-temperature strength of the material as well as provide a comparable substitution for heavier traditional materials, such as steel. Metal-matrix composites (MMCs) are being tested for such applications as piston ring grooves, cylinder block liners, brake calipers and aerospace components. MMCs can be fabricated by infiltrating an SiC whisker preform with aluminum or by the addition of SiC whiskers to molten aluminum.

Polymer matrix composites combine the strength and impact resistance of polymers with the thermal conductivity fatigue and wear resistance of the whiskers. Whisker-reinforced polymers have strong potential to replace traditional plastics in automotive, aerospace and recreational applications.

SILICO N CARBIDE WHISKER SUPPLIERS

ADVANCED REFRACTORY TECHNOLOGIES, INC., WORLD HEADQUARTERS
699 Hertel Ave.
Buffalo, NY 14207 U.S.A.
(716) 875-4091 Fax: (716) 875-0106
Email: chailand@art-inc.com
Website: www.art-inc.com

SILICON NITRIDE. Si_3N_4. Mol. wt. 140.28; sp. gr. 3.19. Dissociates in air at 1800°C and at 1850°C under 1 atm N_2. Two crystal structures: alpha (1400°C) and beta (1400–1800°C), both hexagonal. Hardness approximately 2200 on Knoop K100 scale. Excellent corrosion and oxidation resistance over a wide temperature range. Typical applications: molten-metal-contacting parts, wear surfaces, special electrical insulator components and metal forming dies. Under evaluation as gas turbine and heat engine components as well as antifriction bearing members.

Pure silicon nitride powders are produced by several processes, including direct nitridation of silicon, carbothermal reduction—$C + SiO_2 + N_2$ yields Si_3N_4 (gas atmosphere)—and chemical vapor deposition—$3SiH_4 + 4NH_3$ yields $Si_3N_4 + 12H_2$. Reacting SiO_2 with ammonia, or silanes with ammonia will also produce silicon nitride powders. It is found that the highest purity powders come from gas-phase reactions. Polymer pyrolysis at 600–1200°C using trimethylsilane will produce high-purity powder. Example: 90% alpha-phase Si_3N_4 with a mean particle size of 0.7–10 μm. (Powders having other levels of alpha phase also can exhibit a similar particle size.) Pure Si_3N_4 powders are very difficult to sinter, and in pure form cannot be formed into shapes nor densified to a pore-free state, since atomic mobility in the material is low and Si_3N_4 vaporizes at very high temperatures. Descriptions of two main types of silicon nitride follow:

Sinterable/Hot Pressed/Hot Isostatically Pressed Silicon Nitrides. (SSN, HPSN and HIPSN, respectively.) Used mainly in higher performance applications. Powdered additives, known as sintering aids, are blended with the pure Si_3N_4 powder and allow densification to proceed via the liquid state. Pore-free bodies can be so produced by sintering or hot pressing. Of course, the properties of the material and dense pieces are dependent on the chemical nature of the sintering aid(s) employed.

Sinterable silicon nitrides are a more recent innovation, and allow more flexibility

in shape fabrication than does HPSN. Highly complex shapes can be die pressed or isostatically pressed. Densification can be performed by either sintering or hot isostatic pressing (HIP). Properties of the dense piece are dependent on the additives, but in general the strength below 1400°C, as well as oxidation resistance of HPSN and SSN, far exceed those properties for RBSN. For example, a commercially available HPSN has a density of 3.2 g/cm^3, CTE of 3.2×10^{-6}/C, thermal conductivity of 32 W/mK, modulus of elasticity of 46×10^6 psi, and MOR of 143,000 psi at room temperature and 60,000 psi at 1375°C (type NC). Hardness is 2200 (Knoop K100). HPSN has typical values of: specific heat, 0.17 cal/gC; toughness, 6.6 MPam; and mean Weibull modulus, 12.

More common today is **Reaction Bonded Silicon Nitride** (RBSN). Silicon powder is pressed, extruded or cast into shape then carefully nitrided in a N_2 atmosphere at 1100–1400°C, so as to prevent an exothermic reaction that might melt the pure silicon.

The properties of RBSN are usually lower than those of HPSN or SSN, due mainly to the fact that bodies fabricated in this manner only reach 85% of the theoretical density of silicon nitride and no secondary phase between grains is present. Sp. gr. is 2.5 g/cm^3; hardness is 900–1000 kg/mm^2 (VHN, 0.5 kg load); Charpy impact energy is 2.0 ft-lbf/in.^{2}; tensile strength is 145 MPa; and compressive strength is 1000 MPa. The thermal conductivity of RBSN at room temperature is 8–12 W/mK; CTE is 3.2×10^{-6}/C; Poisson's ratio is 0.27; and Weibull modulus is 10–15. Commercial RBSN of type NC350 has a density of 2.4 g/cm^3 and an MOR of 40,000 psi at room temperature and 50,000 psi at 1375°C.

SILICON NITRIDE SUPPLIERS

CERADYNE INC.
3169 Redhill Ave.
Costa Mesa, CA 92626 U.S.A.
(714) 549-0421 Fax: (714) 549-5787
Email: sales@ceradyne.com
Website: www.ceradyne.com

CERCOM INC.
991 Park Center Dr., P.O. Box 70
Vista, CA 92083 U.S.A.
(760) 727-6200 Fax: (760) 727-6209
PERMASCAND AB, CERAMICS
P.O. Box 42
S-840 10 Ljungaverk Sweden
+46 (0)691 355 00 Fax: +46 (0)691 330 40
Email:
ann-christin.persson@permascand.se
Website:
www.permascand.com/ceramic
PRED MATERIALS INTERNATIONAL, INC.,
THE LINCOLN BUILDING
60 E. 42nd St., Ste. 1456
New York, NY 10165 U.S.A.
(212) 286-0068 Fax: (212) 286-0072
Email: predmatsp@aol.com
Website: www.predmaterials.com
SHS CERAMICAS
Poligono Industrial "Las Vinas,"
P.O. Box 28
37500 Ciudad Rodrigo, Salamanca
Spain
34-923-46.11.39 Fax: 34-923-48.10.60
Email: jag@mina.enusa.es
H.C. STARCK GMBH & CO. KG
P.O. Box 25 40
D-38615 Goslar Germany
+49/53 21/7 51-1 45 Fax: +49/53 21/7 51-1 93
Email: bettina.essmann.be@hcstarck.de
Website: www.hcstarck.com
H.C. STARCK INC.
45 Industrial Place
Newton, MA 02161-1951 U.S.A.
(617) 630-5916 Fax: (617) 630-5919
Email: elisabeth.james.b@bayer.com
Website: www.hcstarck.com

SPINEL. $MgO\text{-}Al_2O_3$ or $MgAl_2O_4$. Mol. wt. 142.26; sp. gr. 3.6–3.9; m.p. 2135°C. A mineral found in small deposits. It is formed by solid-state reaction between MgO and Al_2O_3 and is an excellent refractory showing high resistance to attack by slags, glass, etc.

High-purity spinel is a chemically derived spinel powder made by the co-precipitation of magnesium and aluminum complex sulfates, with subsequent calcination to form the oxide compound. Purities range from 99.98–99.995%. Since it is chemically derived, the stoichiometries can be adjusted for virtually any $MgO:Al_2O_3$ ratio. The ceramic powders prepared by this process can be hot pressed into transparent window materials with exceptional IR transmission range.

Properties of 1:1 spinel:

Crystal system: cubic
Phase purity: 100% spinel
Mohs hardness: 8
Melting point: 2135°C
Crystal density: 3.57 g/cm^3
Optical transmission: 0.25–6 μm
Refraction index: 1.718–1.723
Average particle size, chemically prepared ceramic powder: 3 μm
CTE: 8.9×0^{-6}

The name spinel also has more general usage, designating a structural group: XY_2O_4. A unit cell of this structure contains a face-centered cubic arrangement of 32 oxygen atoms which has 96 interstitial sites: 64 tetrahedral and 32 octahedral. Of these, only 24 are occupied: 16 octahedral and 8 tetrahedral. Five types of spinels are reported, characterized by the valence distribution of the constituent cations:

1. $X^2 + Y^3 + 2O_4$ (e.g. $TiMg_2O_4$).
2. $X^4 + Y^2 + 2O_4$ (e.g. $MgAl_2O_4$; $FeFe_2O_4$; $ZnFe_2O_4$).
3. $X + Y^3 + 0.5Y_2O_4$ (e.g. $(LiAl)_{0.5}Al_2O_4$; $(LiFe)0.5Fe_2O_4$).
4. $X^6 + Y + 2O_4$ (e.g. Li_2MoO_4; Ag_2MoO_4).
5. $g - Y^3 + 2O_3$ (e.g. g-Al_2O_3; g-Fe_2O_3).

Spinels containing S= for O= also have been synthesized.

In these general forms, two types of cation distributions are present: the normal and the inverse. The normal configuration has for the spinel unit cell ($Mg^2 + 8Al^3 + 5D 16O_{33}$), the Mg^{2+}cations in the 8 tetrahedral sites and the Al^{3+} cations in the 16 octahedral sites. The inverse configuration has for the magnetite unit cell ($Fe^2 + 8Fe^3 + 16O_{32}$) 8 of the 16 Fe^{3+} cations filling the 8 tetrahedral sites with the remaining 8 Fe^{3+} cations and the 8 Fe^{2+} cations filling the 16 octahedral sites in a random manner. The gamman oxides are special cases of this inverse configuration with, on the average, 2/3 vacant octahedral sites per unit cell.

The major ceramic applications for spinels are the magnetic ferrospinels (ferrites), chromite brick and spinel colors (see table). Magnetic recording tape coated with α-Cr_2O_3 is a relatively recent development. Also used as a porous protective coating in oxygen sensors for automotive emission controls.

Spinel Colors

Spinel	Crystal Color	Under Porcelain Glaze	Under Lead Glaze	In a Parian Body
$CoAl_2O_4$	dk. blue	dk. blue	brt. bl.	blue
$CuAl_2O_4$	lt.gr.	gr. grn.	green	gray-gr.
$MnAl_2O_4$	tan	tan	tan	brown
$NiAl_2O_4$	sky blue	green	yel-gr.	gray-gr.
$BaCr_2O_4$	dk. gr.	lt.gr.	lt. gr.	green
$CyCr_2O_4$	dk. gr.	lt.gr.	lt. gr.	green
$CoCr_2O_4$	bl. gr.	bl.gr.	bl.gr.	bl. gr.
$MgCr_2O_4$	dk. gr.	green	scummed	yel-gr.
$MnCr_2O_4$	dk. brn.	tel-gr.	scummed	tan
$NiCr_2O_4$	lt. gr.	gr. grn.	mottled	dk. gr.
$SrCr_2O_4$	dk. gr.	green	mottled	lt. br.
$ZnCr_2O_4$	gr. green	brown	mottled	lt. br.
$BaFe_2O_4$	med. gray	gray	brown	brown
$CaFe_2O_4$	med. gray	gray	tan	tan
$CoFe_2O_4$	black	gray	gray	gray
$CuFe_2O_4$	black	gray	gray	tan
$MgFe_2O_4$	or. brown	brown	tan	brown
$MnFe_2O_4$	dk. gray	brown	brown	brown
$NiFe_2O_4$	black	gray	gray	brown
$SrFe_2O_4$	med. gray	gray	tan	brown
$ZnFe_2O_4$	dk. gray	gray	or. br.	brown

Available as fused spinel in special refractory applications and also in a special particle shape and distribution for flame and plasma-arc spraying. The magnetic spinels are of special importance because of the widespread interest and application of the ceramic ferrospinels (ferrites).

Two classes of ferrospinels occur: the magnetic and nonmagnetic. The magnetic are related to the inverse structure and the nonmagnetic to the normal structure.

SPINEL SUPPLIERS

AMSAT, DIV. OF FLUID ENERGY
P.O. Box 95
East Greenville, PA 18041 U.S.A.
(215) 679-5984; (215) 679-5983
Fax: (215) 679-5985
Email: epipe@fluidenergy.com
BAIKOWSKI INT'L. CORP.
325 Westinghouse Blvd.
Charlotte, NC 28273 U.S.A.
(704) 587-7100 Fax: (704) 587-7106
Email: sales@baikowski.com
BPI INC. (BY-PRODUCT INDUSTRIES)
612 S. Trenton Ave.
Pittsburgh, PA 15221 U.S.A.
(412) 371-8554 Fax: (412) 371-9984
Email: info@bpiminerals.com
Website: www.bpiminerals.com
EXOLON-ESK CO.
1000 E. Niagara St., P.O. Box 590
Tonawanda, NY 14151-0590 U.S.A.
(716) 693-4550 Fax: (716) 693-0151
Email: info@exolon.com
Website: www.exolon.com
JERSEY MINERAL PROCESSING CO., LTD.,
REFRACTORIES AND MINERALS DIV.
RM B-13B, Triumphal Arc Mansion,
66 Nanjing Rd.
Tianjin, 300042, P.R. China
86-22-23133086 Fax: 86-22-23133085
Email: cmptjmax@shell.jtvan.com.cn
PRED MATERIALS INTERNATIONAL, INC.,
THE LINCOLN BUILDING
60 E. 42nd St., Ste. 1456
New York, NY 10165 U.S.A.
(212) 286-0068 Fax: (212) 286-0072
Email: predmatsp@aol.com
Website: www.predmaterials.com
U.S. ELECTROFUSED MINERALS INC., T/A ELFUSA - U.S.A.
6905 A San Tomas Rd., Rt. 100 Business Park
Baltimore, MD 21227
(410) 796-8823 Fax: (410) 796-8826
Email: info@usminerals.com
Website: www.elfusa.com.br
WASHINGTON MILLS ELECTRO MINERALS CORP.
P.O. Box 423, 1801 Buffalo Ave.
Niagara Falls, NY 14302 U.S.A.
(716) 278-6600 Fax: (716) 278-6650
Email: sales@washingtonmills.com
Website: www.washingtonmills.com

STEATITE. A mineral with a m.p. >1300°C. Refers almost entirely now to electrical insulators made from talc. Formerly, the term referred to the massive type of talc mineral which could be machined to close tolerances then fired. Due to a decreasing market and a shortage of supply, this terminology is rarely used. Powdered talc has been successfully bonded with materials such as magnesium oxychloride or phosphoric acid cement so as to form dense machinable blocks. Specific gravity and hardness are the same as for foliated talc. Steatite contains only about 3.75–4.75% combined water, so that firing shrinkage of the mineral is only about 1%. Thus, articles can be machined of crude steatite nuggets that are much more exact in dimensions than those made of porcelain mixes, which have a greater firing shrinkage. The natural mineral may be machined to close tolerances to make ware from mined blocks, or it may be crushed into a powder and dry pressed, using a small amount of binder such as sodium silicate or clay.

In general, massive steatite is used for articles requiring adherence to low dimensional

tolerances, or where the volume of production is too small to warrant the expense of dies for pressing or extrusion processes. Compounded steatite bodies can be produced having electrical properties superior to those of massive steatite, and now supply most requirements for radio insulation. Ample supplies of steatite for this purpose are produced in California, Nevada and Montana.

TALC. $3MgO\text{-}4SiO_2\text{-}H_2O$. Talc is a hydrous magnesium silicate, with the composition 63.4% SiO_2, 31.9% MgO and 4.7% H_2O when found in pure form. It is an extremely soft mineral with a Mohs hardness of 1, has a platy structure and it is naturally hydrophobic. Talc occurs as a relatively pure massive mineral in Montana, Australia and China. Elsewhere it occurs in conjunction with magnesite (Vermont, Quebec, Ontario and Finland), with tremolite and serpentine in New York and with chlorite in France and Austria. In many ceramic applications, the presence of non-talc minerals such as chlorite and tremolite are beneficial.

Talc products of greatest use in ceramics are mined in Texas, New York and Montana. Typical chemical analyses of these ores are shown on the table.

	New York	California	China
Magnesia	30.7	30.5	32.54
Calcia	6.2	1.6	0.20
Silica	55.9	59.7	51.00
R_2O_3	1.3	1.2	8.60
LOI	5.9	7.0	7.30
Total	100.0	100.0	99.64

Talc used in ceramics is usually mined, sorted, crushed, and milled to 95–99% -200 mesh. Milling is done in roller mills for softer massive ores while ball mills are used for harder tremolitic products. Products are shipped as a dry powder, mostly in 50 pound bags but the use of supersacks is increasing and larger customers use bulk rail or truck. Some product is calcined prior to shipping and this will usually improve dry pressing characteristics.

The major applications for talc in North America are tile and hobbyware bodies, cordierite catalyst supports, kiln furniture and electrical porcelains. There are minor applications in electronic packaging, sanitaryware, dinnerware and glazes.

In traditional tile and hobbyware bodies, bodies containing 30 to 60% talc are fired at low temperatures (below cone 2), and long cycles (>12 hours) to form porous bodies, which are then glazed and refired. Talc products containing tremolite are preferred for their better pressing and permeability characteristics. White firing New York and Texas talc dominate this market and some calcined product is also used. If purer or platier talc products are used, wollastonite has to be added to improve pressing and permeability. The tile industry today is moving to fast fire technology, and this is reducing talc to a minor component in these single fire formulations.

Cordierite bodies can be formed from pure talc (44%), plastic kaolin (41%) and alumina (15%) or from 50/50 mixtures of kaolin and chlorite. Cordierite has very low coefficients of thermal expansion (CTE), which accounts for its use in kiln furniture and automotive catalysts supports. Firing temperatures have to be much higher for the pure talc containing bodies. The talc based body is preferred for automotive catalyst supports; although it is more expensive, it is possible to get better control of minor elements such as iron and calcium which have a major impact on CTE. For kiln furniture, chlorite-based bodies are preferred because of their lower cost and better high temperature creep resistance. In kiln furniture modified with mullite to improve shock resistance, French sourced chloritic talc is utilized.

For steatite bodies used in electrical insulating applications, pure talc along with about 10% plastic kaolin and 10% barium carbonate is fired at cone 12–13 to form low loss bodies. Low calcium and alkali metal levels are critical, so only high purity Montana talc is used. Consistency is also critical, since

many parts have high tolerances and shrinkage requires close control.

Talc is used as a flux for high alumina ceramics, sanitaryware and dinnerware. It is a low cost source of magnesium in these applications and helps to produce less porous bodies at lower firing temperatures.

TALC SUPPLIERS

H. C. SPINKS CLAY CO. INC.
P.O. Box 820
Paris, TN 38242 U.S.A.
(901) 642-5414 Fax: (901) 642-5493
Email: hcspinks@worldnet.att.net
Website: www.spinksclay.com
UNIMIN CORP.
258 Elm St.
New Canaan, CT 06840 U.S.A.
(203) 966-8880; (800) 243-9004 Fax: (203) 972-1378; (800) 243-9005
R. T. VANDERBILT, CO. INC.
P.O. Box 5150
Norwalk, CT 06856-5150 U.S.A.
(203) 853-1400 Fax: (203) 853-1452
Email: rjohnson@rtvanderbilt.com
Website: www.rtvanderbilt.com
ZEMEX INDUSTRIAL MINERALS, INC., (FELDSPAR CORP.)
1040 Crown Pointe Pkwy., Ste. 270
Atlanta, GA 30338 U.S.A.
(770) 392-8660 Fax: (770) 392-8670
Email: minerals@zemex.com
Website: www.zemex.com/minerals

TITANIUM DIOXIDE. TiO_2. Mol. wt. 80; sp. gr. 3.9–4.2; m.p. ~3370°F; refractive index 2.52–2.76. Insoluble in water, dilute acids, organic acids, dilute alkalis. Soluble in hot concentrated sulfuric acid and hydrofluoric acid. Manufactured mainly by digesting ilmenite, the principal ore, in concentrated sulfuric acid; separating hydrous titanium dioxide obtained through thermal hydrolysis; then purifying, treating and calcining the hydrous oxide to titanium dioxide, which is finally milled. In addition to ilmenite, rutile ore and titanium slag obtained from the electric furnace smelting of titaniferous iron ore also are starting materials.

Another method for manufacturing titanium dioxide is the chloride process wherein natural rutile ore is chlorinated to form titanium tetrachloride, which is purified, vaporized and reacted with oxygen at elevated temperature to form the dioxide.

The great bulk of the titanium dioxide of commerce is in the form of the strongest white pigment known. Unsurpassed opacity of this pigment is mainly the result of optimum particle size and refractive index higher than that of any other white pigment substance. Titanium dioxide pigment is available in two primary classes according to the two crystal structures of anatase and rutile and, in addition, in different types according to use. Pigment having the rutile crystal structure has generally 20–40% greater opacity than the anatase form.

Average refractive indices for these two classes are 2.72 for rutile and 2.52 for anatase.

Titanium dioxide is a most important ceramic finish coat for sheet metal products. The opacity of this enamel imparted by titanium dioxide has lowered film thickness of these finishes to the range of organic coatings while retaining the durability of porcelain. These enamels are self-opacified. That is, titanium dioxide is not dispersed as an insoluble suspension during smelting nor is it added at the mill. Rather, titanium dioxide is taken into solution during smelting of the batch and is held in supersaturated solution through fritting. Upon firing the enamel, titanium dioxide crystallizes or precipitates from the glassy matrix. Composition of these enamels and their processing is so controlled as to provide the proper particle size and particle size distribution to make the high refractive index of titanium dioxide most effective. Thus far, in titania enamels having the most desirable properties, the precipitated titanium dioxide is anatase. While the rutile crystal structure is preferred in titanium pigments for many different nonceramic compositions, in titania enamels appreciable rutile gives rise to objectionable color.

Care must be exercised in selecting TiO_2 because pigment qualities are not characteristic of nonpigmentary titanium dioxide made especially for titania porcelain enamels. This grade flows freely in the dry state and eliminates sticking and balling up that often characterizes titanium dioxide pigments. It also has maximum TiO_2 content, being free from additives and harmful colorants used in pigments. As a result, nonpigmentary titanium dioxide is preferred for titania porcelain enamels.

The addition of small amounts of titanium dioxide pigment to the enamel mill is not for primary opacification, but usually to increase hiding power of the enamel slip or to regulate and stabilize reflectance of certain compositions.

Prior to the advent of titania porcelain enamel, the chief ceramic use of manufactured titanium dioxide was in dry process enamels for cast iron. In these, titanium dioxide, carried in solution in the glass, provided resistance to household acids and other acidic substances with opacity gained from other opacifiers, such as antimony oxide.

Thus, for these enamels, nonpigmentary grade titanium dioxide pigment is preferred. Contrasted with self-opacified titania enamels in which titnaium dioxide is often 20 wt% of the batch, dry process enamels carry only 4–8 wt%.

Titanium dioxide pigment is, however, used primarily as an opacifier, added at the mill, for glass enamels and for porcelain enamels for aluminum. In both these enamels, nonpigmentary titanium dioxide is smelted into the composition to produce acid and chemical resistance.

Titanium dioxide is used in glazes to affect acid resistance, color and texture. In certain fritted glazes maturing at about cone 2, unusual semimatte and textured finishes are secured through adding pigmentary titanium dioxide at the mill. Crystals of sphene ($CaO\text{-}SiO_2\text{-}TiO_2$) resulting from the added titanium dioxide and the calcium and silica of the frit, account for these effects. Much research is being conducted on glazes analogous to titania porcelain enamels self-opacified by titanium dioxide.

To glass, nonpigmentary titanium dioxide imparts interesting properties, including high refractive index for optical and other glass, such as reflective beads. It also intensifies and brightens colored transparent glasses, especially those utilizing ceria as colorant. Can shrink the fibers of fiberglass. Where whiteness and sharp clean tints are not important, mineral or natural rutile finds use in some of the above applications, such as dry process enamels for cast iron and fiberglass. This titanium dioxide mineral, largely because of impurities, is used in minor amounts to color certain bodies and glazes.

Dielectric applications. Available in three mineral forms: rutile, anatase and brookite; distinguished from each other by differences in crystal modification, index of refraction, density, etc. Only the rutile form, which decomposes at 1640°C, is used for dielectric purposes.

Rutile bodies are used in either the pure form or with minor additions of various materials for: capacitors (substitutes for mica, paper and electrolytics), temperature compensating (tc) capacitors, trimmer condensers, bypass condensers, filter and power circuits, and as fillers for resins and low melting glasses.

Manufacture involves dry mixing or tempering with water (up to 10%), dry pressing at 5000–10,000 psi or extrusion; or, for complex parts, slip casting (deflocculate with 1% ethylene diamine or 1% tannic acid with 10% NH_4OH) followed by firing the parts to vitrification with approximately a 2 hr soak at peak temperature (2400–2450°F). Results have shown that in firing titanium dioxide bodies, a particular fired structure yields the best all-around dielectric properties and may be obtained in a body having a porosity of zero or nearly zero.

As a capacitor, pure rutile has a dielectric constant of 173 parallel to the principal axis and 89 perpendicular to this axis. Most polycrystalline bodies produced commercially have a value of 85–96 at room temperature

when measured statically or in the trequency range of 60 Hz to 3000 MHz. Bodies are characterized by a fairly large negative coefficient of dielectric constant 750–800 (25–86°C), which may be made less negative by the addition of other compounds, such as magnesium titanate or zirconium dioxide (though with a decrease in dielectric constant).

Power factor is ~0.5–0.7% at 60 Hz, dropping off rapidly to 0.05% at 10 kHz and remaining at that figure to 100 MHz. Resistivity (25°C) is approximately 1014 ohm-cm for commercial grade TiO_2 and 1016–1018 ohm-cm for extremely pure TiO_2. Ordinary dielectric strength is 150–200 V/mil, but proper design of the test piece can raise this to 600–700 V/mil for commercially pure TiO_2 and about 50% higher for very pure TiO_2.

Temperature compensating capacitors based on TiO_2 have dielectric constants varying from 15–85 and temperature coefficients varying from +120 ppm/C through zero to −750 ppm/C (most negative body has highest TiO_2 content). The compensators are necessary in all radio receivers where the exact frequency of resonance of the resonant circuit changes slightly with changes in temperature. These undesirable changes are corrected by introducing a reactive component having a temperature coefficient of the opposite sign and of such a value as to offset the undesired change with temperature. Extraordinary duplicable and close tolerances are available, in some cases as accurate as 3–5 ppm. Capacitances range from 1–1100 pF.

Trimmers or trimmer condensers employing TiB_2 bodies are used for minute adjustments of capacitance. Normally the rotor consists of a TiO_2 body. Parts are made with extreme accuracy, and are usually supplied in one of three temperature coefficient types. The base is a low loss ceramic composition.

Mechanical and physical properties of TiO_2 include relatively low strength (MOR 18,000–22,000 psi; tensile strength 6000–8000 psi), low thermal conductivity (0.14 cal/cm/s/C) and a CTE (for rutile) of $7–9 \times 10^{-6}$/°C.

Rutile (TiO_2) can be prepared in the form of single crystals by the Verneuil (flame fusion) technique. Slightly reduced rutile is an n-type semiconductor with an energy gap of 3.05 eV and electron mobilities of ~1.0 cm^2/Vs at room temperature.

TITANIUM DIOXIDE SUPPLIERS

ALFA AESAR, A JOHNSON MATTHEY COMPANY
30 Bond St.
Ward Hill, MA 01835-8099 U.S.A.
(800) 343-0660 Fax: (800) 322-4757
Email: info@alfa.com
Website: www.alfa.com

ARLINGTON INTERNATIONAL, INC.
85 Arlington St.
Asheville, NC 28801 U.S.A.
(828) 254-8811; (828) 251-0981
Fax: (828) 254-6437; (828) 251-0983
Email: arlingtonintl@mindspring.com

CPM INDUSTRIES
5803 Kennett Pike
Wilmington, DE 19807 U.S.A.
(302) 656-3200 Fax: (302) 656-5798
Email: info@cpmindustries.com
Website: www.cpmindustries.com

KRONOS, INC.
P.O. Box 700
Hightstown, NJ 08520-1007 U.S.A.
(281) 423-3300; (800) 866-5600;
(609) 443-2249 Fax: (281)
423-3258; (609) 443-2496
Email: kronos_marketing@nli.e-mail.com
Website: www.kronosti02.com

VERMICULITE. $(MgFe)_3(SiAlFe)_4O_{10}$-$4H_2O$. A hydrated biotite mica that has undergone alteration by further hydration. It possesses the peculiar property of exfoliating from 16–20 times its original size on heating.

It can be used as a grog for lightweight refractory brick, or as an aggregate for cast refractories, being resistant to fairly high temperatures.

VERMICULITE SUPPLIERS

ZIRCONIA SALES (AMERICA) INC.
1000 Cobb Place Blvd., Bldg. 100,
Ste. 190
Kennesaw, GA 30144 U.S.A.
(770) 590-7970 Fax: (770) 590-0239
Website: www.amverco.com

WOLLASTONITE. $CaSiO_3$. A naturally occurring calcium metasilicate. Wollastonite imparts low moisture expansion, reduced drying and firing shrinkage, higher fired strength, improved heat shock, faster firing, easy pressing, better bonding, and superior electrical properties to bodies, glazes, porcelain enamels and frits. Wollastonite applications in the ceramic industry can be classified in two general groups: (1) a replacement for flint and limestone and (2) a material for producing bodies and glazes of superior properties.

Wollastonite is mined in various locations throughout the world. The oldest mined sites are located in New York state. Wollastonite is a natural mineral and has almost the chemical formula of theoretical calcium silicate. Its most outstanding characteristics are its brilliant whiteness, its chemical and physical uniformity, and its acicular nature, which is easily controlled by mechanical means from a granular material to acicular crystals. Because it is relatively new in the minerals field, all its uses are not known, but already it has proven successful in making brighter and smoother glazes, better low-loss dielectric bodies, a good flux for stronger welding rod coatings, an excellent material for semivitreous bodies of the wall tile type and in applications where good thermal shock properties are of primary importance.

Among the many other ceramic applications in which wollastonite can be used are: glazed porous ceramics of nearly every kind, dinnerware, ovenware, artware, structural clay products, terra cotta, sanitaryware, chemical stoneware, ceramic-bonded abrasives, refractories, high alumina bodies, spark plugs, electrical porcelains, frits and investment castings.

Wollastonite Properties

Specific gravity	2.9
PH, 10% slurry	9.9
Weight, solid gal, lb	24.2
Apparent density, loose; lb/ft^3	45–52
Coefficient of expansion, 100% $CaSiO_3$, 10^{-6}/°C	6.5
Mohs hardness	4.5
Melting Point, °C	1540
Solubility in H_2O, g/100ml	0.0095
PCE cone	18
Molecular weight	116

Typical Chemical Analyses of Wollastonite

	A	B
SiO_2	50.9	50.20
CaO	46.90	46.10
DeO	0.5	0.15
Al_2O_3	0.25	0.21
MnO	0.10	—
MgO	0.10	—
TiO_2	0.0	—
Na_2O	—	0.94
LOI	0.90	0.22
Total	99.75	99.64

WOLLASTONITE SUPPLIERS

BPI INC. (BY-PRODUCT INDUSTRIES)
612 S. Trenton Ave.
Pittsburgh, PA 15221 U.S.A.
(412) 371-8554 Fax: (412) 371-9984
Email: info@bpiminerals.com
Website: www.bpiminerals.com
NANCHUAN MINERALS GROUP, SALES OFFICE
P.O. Box 3205
Stamford, CT 06905-0205 U.S.A.
(203) 253-1699 Fax: (203) 323-6711
Email: wgholroyd@prodigy.net
Website: www.nanchuanminerals.com
NYCO
#500, 205 Ninth Ave., S.E.
Calgary, AB Canada T2G 0R4
(403) 260-8102 Fax: (403) 263-7923
Email: roland_beck@nyco.fording.ca
Website: www.nycominerals.com

R. T. VANDERBILT, CO. INC.
P.O. Box 5150
Norwalk, CT 06856-5150 U.S.A.
(203) 853-1400 Fax: (203) 853-1452
Email: rjohnson@rtvanderbilt.com
Website: www.rtvanderbilt.com

ZINC OXIDE. White powder. Mol. wt. 81.4; sp. gr. 5.6; sublimes at 1800°C. Insoluble in water, soluble in strong alkali solutions and in acids.

The rubber industry is the largest consumer of zinc oxide, accounting for more than 50% of the market. Zinc oxide is most effective as an activator of accelerators in the vulcanization process.

The chemical industry has been opening new markets for zinc oxide. Examples are lubricating oil additives, water treatment and catalysts. For photocopying, photoconductivity is a unique electronic property of zinc oxide.

The paint and coatings industry used to be the second largest consumer of zinc oxide. But shipments declined as the industry switched from linseed oil exterior house paints to latex paints. Since 1950, however, that situation has been changing, and more zinc oxide-containing latex paints are available.

In the ceramic industry, zinc oxide is used in the manufacture of glasses, glazes, frits, porcelain enamels and magnetic ferrites. Here, the largest consuming plants are in the tile industry.

There are two production types of zinc oxide, namely the French process and the American process. In the French process, zinc metal is vaporized in large containers by external heating. In an adjoining off-take pipe or combustion chamber, the vapor is burned off in the air to fine zinc oxide powder. In the American process, oxidized ores of roasted sulfide concentrates are mixed with anthracite coal and smelted in a Wetherill-type flat bed furnace. The coal, plus the products of partial combustion, particularly CO, reduce the ore to metallic zinc, which issues as a vapor. In the off-take pipe, the vapor, together with the gases from the coal, is burned under controlled conditions and piped to the bag house where the oxide is collected. American process material contains sulfur compounds of zinc and provides a slower cure rate that is preferred by some rubber manufacturers.

One ceramic grade of zinc oxide has these properties: sp. gr. 5.6; apparent density 1201 kg/m^3; weight 5595.5 kg/m^3. Typical chemical analysis (in %): 99.5 ZnO, 0.05 Pb, 0.02 Fe, 0.01 Cd, 0.02 S (total), 0.10 HCl (insoluble), 5 ppm magnetic iron.

In **glass**, zinc oxide reduces the coefficient of thermal expansion, thus making possible the production of glass products of high resistance to thermal shock. It imparts high brilliance of luster and high stability against deformation under stress. As a replacement flux for the more soluble alkali constituents, it provides a viscosity curve of lower slope. Specific heat is decreased and conductivity increased by the substitution of zinc oxide for BaO and PbO.

A 1% addition of zinc oxide to tank window glass lowers the devitrification temperature and improves chemical resistivity while maintaining good workability for drawing. It is used consistently in high-grade fluoride opal glass, in which it greatly increases opacity, whiteness and luster by inducing precipitation of fluoride crystals of optimum number and size. Apparently, zinc oxide makes its contribution to opacity through reduction of the primary opacifiers. It is used in optical glasses of high barium content to reduce their tendency to crystallize on cooling. The resistance of phosphate glasses to chemical attack is improved by the presence of zinc oxide. About 10% zinc oxide assists in the development of the characteristic color of cadmium sulfoselenide ruby glass, although its exact function is obscure.

Zinc oxide is used in many types of **glazes**, its function varying according to the particular composition in which it is included. In general, it provides fluxing power, reduction of expansion, prevention of crazing, greater gloss and whiteness, a

favorable effect on elasticity, increased maturing range, increased brilliance of colors and correction of eggshell finish. It is useful in preventing volatilization of lead by partial substitution for CaO, since high CaO tends to satisfy SiO_2, leaving PbO in a more volatile form. Glaze crawling, when attributable to the action of zinc oxide in the glaze, is due to shrinkage and can be avoided through the use of calcined zinc oxide. Calcined zinc oxide, by virtue of its greater density and decreased bulkiness, allows for less prefire shrinkage of the glaze.

In Bristol glazes for earthenware products, zinc oxide in combination with alumina produces both opacity and whiteness to a fair degree, provided the lime content is low. The use of zinc oxide in wall tile glazes is very general; the zinc oxide content of certain types being 10% or more. Small amounts are used in gloss or bright tile, while higher percentages are used where it is desired to develop a highly pleasing matte finish. Crystalline glazes are produced by loading to supersaturation with zinc oxide. Zinc compounds crystallize when the solution reaches a critical fluidity and, if cooled rapidly after formation, the crystals are held in suspension. These crystals may be tinted if various pigmentary oxides are incorporated in the glaze composition. The more homogenous a zinc crystalline glaze is, the more perfectly the crystals will separate out. The value of zinc oxide in crystalline glazes lies in its unusual property of crystallizing as a silicate instead of an oxide. In semiporcelain glazes zinc oxide forms opaque silicates. It reduces the melting point of the mass and tends to reduce boiling of the glaze during firing. It increases the firing range, improves resistance to crazing and generally makes the glaze more flexible. It has no opacifying power when used in borosilicate glazes. In general, zinc oxide has a beneficial effect upon colored glazes, but should be used with caution because of its adverse effect with certain coloring agents. It alters the colors obtained with underglaze decorations, destroying some and improving others. It lightens normally strong blues and greens. With the light greens of copper, it produces cleaner, more brilliant colors.

Zinc oxide is commonly used in dry-process cast iron **porcelain** enamels in amounts of 0.5–1% to 14%. In general, low lead content implies high zinc and vice versa. Its specific functions are to increase fusibility, improve luster, contribute to opacity and whiteness, reduce expansion and increase extensibility. It is probably a little stronger as a flux than is lime, but does not produce the sudden fluidity characteristic of lime. Gloss may be decreased by using an excessive amount of zinc oxide or by attempting to introduce it into a composition not adapted to its use. It is thought that loss of gloss is due to the crystallization of zinc compounds, which in turn are due to the state of balance of the enamel ingredients. Of great benefit to producers of cast iron enamels is the relative nontoxicity of zinc oxide.

A recent use for zinc oxide is its application to the manufacture of **magnetic ferrites**, which have been developed over the past 25–30 years. They usually are composed of ferric oxide in combination with zinc oxide (of high chemical purity) and any one or more of several other oxides of bivalent metals. The amount of zinc oxide used varies from 10–35%, depending upon the characteristics desired in the finished magnetic ferrite. Having as their prime properties high permeability and low hysteresis, they are used in the field of electronics for such devices as high frequency transformer cores for television receivers.

Zinc oxide crystals can exhibit strong piezoelectric properties. Normally recognized as an n-type semiconductor, it has a resistivity less than 103 ohm-cm. When doped with lithium, resistivity rises to 1012 ohm-cm and it exhibits piezoelectricity about four times that of quartz.

ZINC OXIDE SUPPLIERS

AMERICAN CHEMET CORP.
400 Lake Cook Rd., Box 437

Deerfield, IL 60015 U.S.A.
(847) 948-0800 Fax: (847) 948-0811
Email: rklattII@aol.com
Website: www.chemet.com

ARLINGTON INTERNATIONAL, INC.
85 Arlington St.
Asheville, NC 28801 U.S.A.
(828) 254-8811; (828) 251-0981 Fax: (828) 254-6437; (828) 251-0983
Email: arlingtonintl@mindspring.com

CMM INC., CONSIDAR METAL MARKETING INC.
70 York St., Ste. 720
Toronto, ON Canada M5J 1S9
(416) 601-9550 Fax: (416) 362-3542
Email: info@considarmm.com
Website: www.considarmm.com

EAGLE ZINC CO., T. L. DIAMOND & CO. INC.
30 Rockefeller Plaza
New York, NY 10112 U.S.A.
(212) 582-0420 Fax: (212) 582-3412

ZINC CORPORATION OF AMERICA
300 Frankfort Rd.
Monaca, PA 15061-2295 U.S.A.
(724) 774-1020 Fax: (724) 773-2217

INDEX

Page numbers followed by an *f* or *t* indicate the term is from a figure or table.